THE OLIVO-CEREBELLAR SYSTEM

EDITED BY: Egidio D'Angelo, Elisa Galliano and Chris I. De Zeeuw
PUBLISHED IN: Frontiers in Neural Circuits

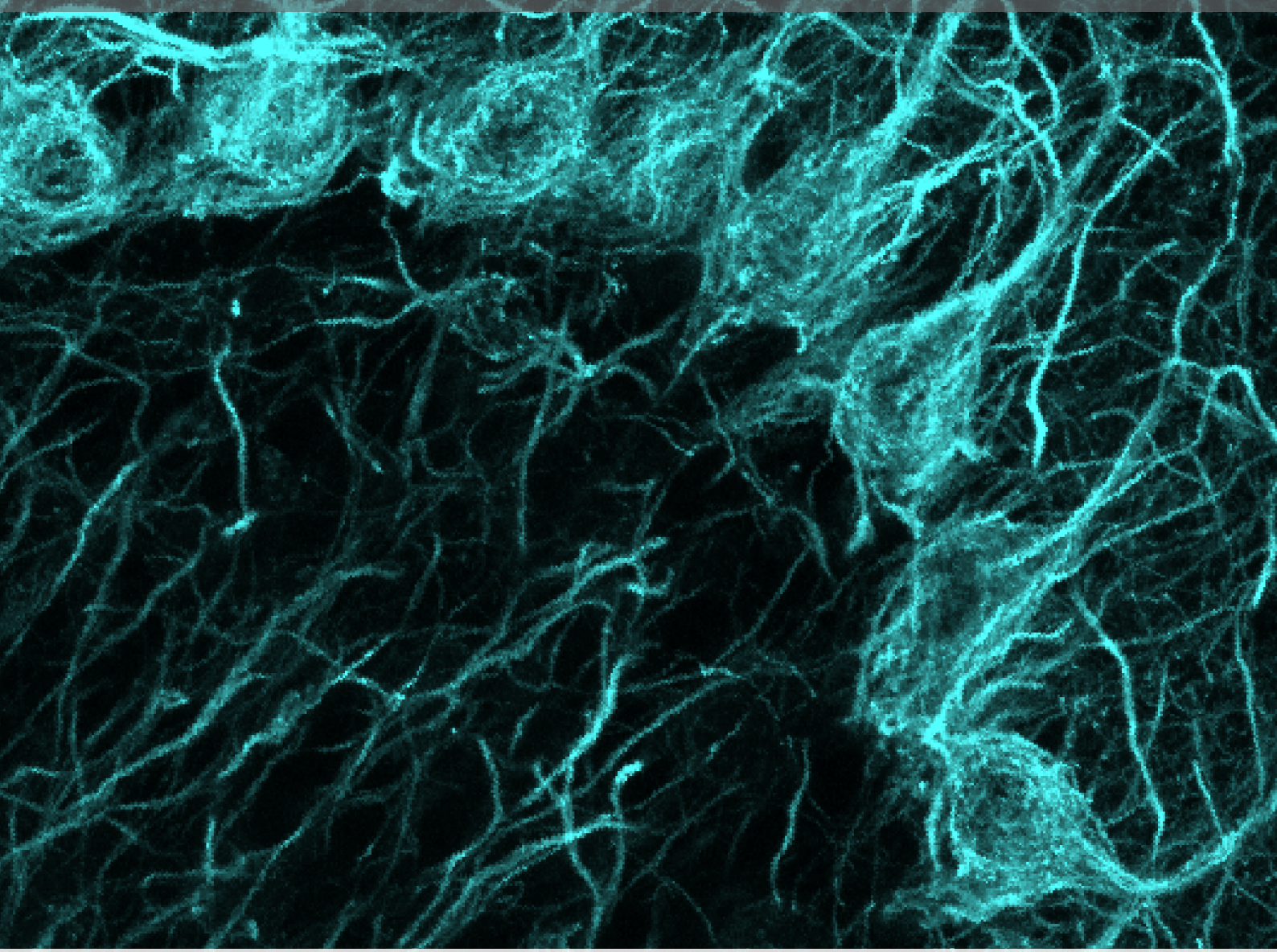

frontiers Research Topics

frontiers

ISSN 1664-8714
ISBN 978-2-88919-826-9
DOI 10.3389/978-2-88919-826-9

About Frontiers

Frontiers is more than just an open-access publisher of scholarly articles: it is a pioneering approach to the world of academia, radically improving the way scholarly research is managed. The grand vision of Frontiers is a world where all people have an equal opportunity to seek, share and generate knowledge. Frontiers provides immediate and permanent online open access to all its publications, but this alone is not enough to realize our grand goals.

Frontiers Journal Series

The Frontiers Journal Series is a multi-tier and interdisciplinary set of open-access, online journals, promising a paradigm shift from the current review, selection and dissemination processes in academic publishing. All Frontiers journals are driven by researchers for researchers; therefore, they constitute a service to the scholarly community. At the same time, the Frontiers Journal Series operates on a revolutionary invention, the tiered publishing system, initially addressing specific communities of scholars, and gradually climbing up to broader public understanding, thus serving the interests of the lay society, too.

Dedication to Quality

Each Frontiers article is a landmark of the highest quality, thanks to genuinely collaborative interactions between authors and review editors, who include some of the world's best academicians. Research must be certified by peers before entering a stream of knowledge that may eventually reach the public - and shape society; therefore, Frontiers only applies the most rigorous and unbiased reviews.

Frontiers revolutionizes research publishing by freely delivering the most outstanding research, evaluated with no bias from both the academic and social point of view.

By applying the most advanced information technologies, Frontiers is catapulting scholarly publishing into a new generation.

What are Frontiers Research Topics?

Frontiers Research Topics are very popular trademarks of the Frontiers Journals Series: they are collections of at least ten articles, all centered on a particular subject. With their unique mix of varied contributions from Original Research to Review Articles, Frontiers Research Topics unify the most influential researchers, the latest key findings and historical advances in a hot research area! Find out more on how to host your own Frontiers Research Topic or contribute to one as an author by contacting the Frontiers Editorial Office: **researchtopics@frontiersin.org**

THE OLIVO-CEREBELLAR SYSTEM

Topic Editors:
Egidio D'Angelo, University of Pavia, Italy
Elisa Galliano, King's College London, UK
Chris I. De Zeeuw, Erasmus Medical Center, Netherlands

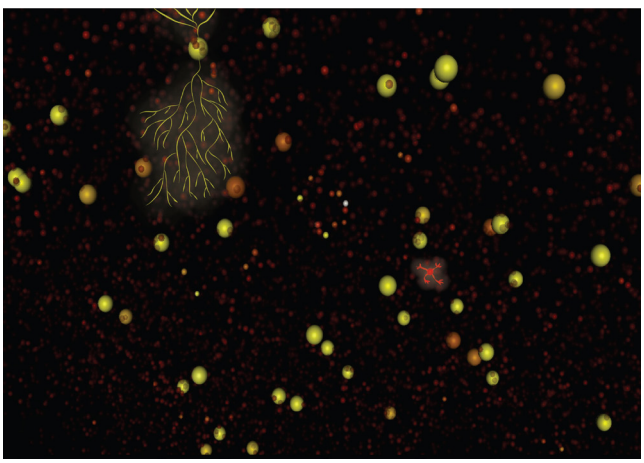

The figure captures the activity state of the granular layer in a realistic simulation, during which a cluster of granule cells is activated over a background noisy activity. The large elements are Golgi cells, the small elements are granule cells. The simulation, which involved about 400000 neurons, was run in the Human Brain Project framework on a blue-gene-II supercomputer (Casali S., VanGeit W., Masoli S., Rizza M., D'Angelo E., unpublished).
Image by Elisa Galliano

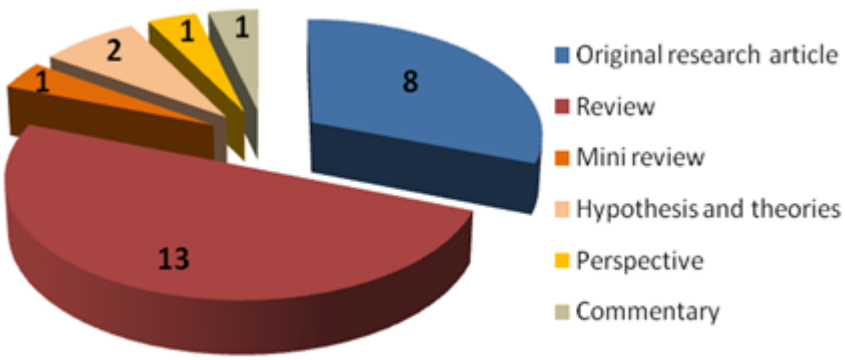

During the last decades, investigations on the olivo-cerebellar system have attained a high level of sophistication, which led to redefinitions of several structural and functional properties of neurons, synapses, connections and circuits. Research has expanded and deepened in so many directions and so many theories and models have been proposed that an ensemble review of the matter is now needed. Yet, hot topics remain open and scientific discussion is very lively at several fronts.

One major question, here as well as in other major brain circuits, is how single neurons and synaptic properties emerge at the network level and contribute to behavioural regulation via neuronal plasticity. Other major aspects that this Research Topic covers and discusses include the development and circuit organization of the olivo-cerebellar network, the established and recent theories of learning and motor control, and the emerging role of the cerebellum in cognitive processing.

By touching on such varied and encompassing subjects, this Frontiers Special Topic aims to highlight the state of the art and stimulate future research. We hope that this unique collection of high-quality articles from experts in the field will provide scientists with a powerful basis of knowledge and inspiration to enucleate the major issues deserving further attention.

Citation: D'Angelo, E., Galliano, E., Zeeuw, C. I. D., eds. (2016). The Olivo-Cerebellar System. Lausanne: Frontiers Media. doi: 10.3389/978-2-88919-826-9

Cover Image:
A forest of Purkinje cells, stained with an antibody against SMI-32.
Image by Elisa Gallian

Table of Contents

Network patterns

Theories of learning and control

Cerebellum as an integrated system for sensorimotor control and cognition

frontiers in Neural Circuits

EDITORIAL
published: 12 January 2016
doi: 10.3389/fncir.2015.00066

Editorial: The Olivo-Cerebellar System

Egidio D'Angelo[1,2]*, *Elisa Galliano*[3,4] *and Chris I. De Zeeuw*[4,5]*

[1] *Neurophysiology Unit, Department of Brain and Behavioral Sciences, University of Pavia, Pavia, Italy,* [2] *Brain Connectivity Center, Neurophysiology, IRCCS C. Mondino Neurological Institute, Pavia, Italy,* [3] *MRC Centre for Developmental Neurobiology, King's College London, London, UK,* [4] *Department of Neuroscience, ErasmusMC, Rotterdam, Netherlands,* [5] *Department of Cerebellar Coordination and Cognition, Netherlands Institute for Neuroscience, Amsterdam, Netherlands*

Keywords: cerebellum, inferior olive, synaptic plasticity (LTP/LTD), purkinje cell, granular layer, deep cerebellar nucleus

The Editorial on the Research Topic

The Olivo-Cerebellar System

Studies on the olivo-cerebellar system have rapidly advanced over the past decade, leading to new insight in the structural and functional properties of its synapses, neurons, intrinsic circuits, and connectivity with the rest of the brain. As in many other fields of neuroscience, it is becoming more and more appropriate to try to bring our understanding at the level of individual synapses and neurons to that of ensemble activity, circuits, and behavior. This Editorial aims to facilitate this process by ordering the 26 contributions of this special issue of Frontiers in Brain Microcircuits Series from studies on the development and structure of synaptic contacts to those on the function of local microcircuits and network plasticity as well as the olivo-cerebellar system as a whole. More specifically, we highlight here the main points of the chapters on development, circuit organization and structural plasticity of various types of neurons in the olivo-cerebellar system (A); the chapters on their basic activity and synaptic plasticity (B); the chapters on the relevance of the emerging network patterns in the olivo-cerebellar system (C); the chapters on current high-level theories of motor learning (D); and the chapters on the overall role of the olivo-cerebellar system in the integration of sensorimotor control and cognition (E).

OPEN ACCESS

Edited and reviewed by:
Rodolfo R. Llinas, New York University School of Medicine, USA

***Correspondence:**
Egidio D'Angelo
dangelo@unipv.it;
Chris I. De Zeeuw
c.dezeeuw@erasmusmc.nl

Received: *28 May 2015*
Accepted: *12 October 2015*
Published: *12 January 2016*

Citation:
D'Angelo E, Galliano E and De Zeeuw CI (2016) Editorial: The Olivo-Cerebellar System. Front. Neural Circuits 9:66. doi: 10.3389/fncir.2015.00066

(A) DEVELOPMENT, CIRCUIT ORGANIZATION, AND STRUCTURAL PLASTICITY OF THE OLIVO-CEREBELLAR SYSTEM

The development and architecture of the olivo-cerebellar afferents, the climbing fibers, are described in great detail by Reeber and colleagues and Fujita and Sugihara. Indeed, attempts to relate the climbing fiber branching patterns to the development of cerebellar compartmentalization and lobulation will help us to untangle the organization of the cerebellar cortex at the functional level. Interestingly, the climbing fiber system is not only highly plastic during development, but also following degeneration of Purkinje cells and/or their afferents. Grasselli and Strata highlight how this process depends on the growth-associated protein GAP-43 in olivary neurons, while Mishina and colleagues show how postsynaptic GluRδ2 plays a pivotal role in territory control of the Purkinje cell spines by the parallel fibers versus that of the climbing fibers through trans-synaptic interaction with presynaptic neurexins (NRXNs) and cerebellin 1. The compartmental restriction in sagittal zones, which is evident in the climbing fiber system, apparently also provides a framework for both the excitatory and inhibitory interneurons in the cerebellar cortex in that

their axons mostly remain within the same zonal boundaries (Consalez and Hawkes). However, in terms of direct appositions there is a clear distinction between the interneurons in the granular layer, which do not show direct contact with climbing fibers, and those in the molecular layer, which do show adjacent climbing fiber varicosities (Galliano et al.).

(B) NEURONAL ACTIVITY AND SYNAPTIC PLASTICITY

The activity at the input stage of cerebellum plays an important role in determining the spatiotemporal patterns of simple spike activity that are ultimately generated by Purkinje cells. Gandolfi and colleagues show how resonance in the granular layer can be sustained at the theta-frequency range by K slow (M-like), KA, and Na-persistent currents and thereby improve spike timing at the millisecond time-scale. In addition, the same lab illustrates how the Golgi cells can fine-tune the spatiotemporal organization of granular layer activity by generating dense center-surround clusters of granule cell activity and implementing combinatorial operations on multiple mossy fiber inputs (D'Angelo et al.), regulating transmission gain and cut-off frequency, controlling spike timing and burst transmission, and determining the intensity and duration of mossy fiber to granule cell plasticity.

Importantly, van Beugen and colleagues were the first to show in awake behaving mammals that the high instantaneous firing frequency of mossy fiber bursts can be reliably transferred to individual granule cells (up to about 800 Hz) and from there via the parallel fibers to Purkinje cells, inducing a heterogeneous short-lived facilitation to ensure signaling within the first few spikes. To what extent the activity in the parallel fibers will be subsequently depressed or potentiated in the Purkinje cells depends on the temporal relation with the climbing fiber activity, implying a non-Hebbian form of spike-timing-dependent plasticity (Piochon et al.). If parallel fiber EPSPs are elicited in Purkinje cells before activation by the climbing fibers, long-term depression (LTD) will be induced; instead, when they are evoked after climbing fiber activity long-term potentiation (LTP) will occur. As all climbing fibers originate in the inferior olive, this means that the precise timing of activation of olivary neurons is critical. Bazzigaluppi and colleagues did whole-cell recordings of olivary neurons in vivo and showed that the number of wavelets riding on top of their action potentials is related to the amplitude of their subthreshold oscillations as well as the level of electronic coupling between them. The pattern of simple spikes and complex spikes that are generated in the Purkinje cells following various forms of plasticity ultimately converge onto a smaller set of neurons in the cerebellar and vestibular nuclei. Importantly, here these patterns can evoke rebound firing and trigger movements, especially when the timing with respect to the activity of mossy fiber and/or climbing fiber collaterals is optimal (Witter et al.).

(C) NETWORK PATTERNS

As discussed above, the olivo-cerebellar modules form a unique control system and their specific wiring allows fine temporal control and rhythmicity. Oscillatory and synchronous activities are generated, sustained, and modulated throughout the network, in order to create the appropriate spatiotemporal code necessary to drive behavior.

In his review Rodolfo Llinas focuses on rhythmicity in the olive (Llinas) and he underlies that it is indeed the combination of strong and rather stereotyped intrinsic electrical properties with electrical coupling that allows the synchronous activation of clusters of olivary neurons. Feedback inhibition provides the dynamic variance of the membership of such coupled clusters, and the cluster's activity phase can be resetted by an incoming stimulus or by inputs arising from outside the olivo-cerebellar system.

Geborek and colleagues show that olivary excitability is suppressed during different phases of movement and a relay through the cuneate nucleus is a possible gateway (Geborek et al., Geborek et al.). Elaborating even further on the topic of external inputs providing modulation to system's rhythmicity, Libster and Yarom provide a detailed review of neuromodulators acting on DCN, IO, and PCs and they advocate for the importance of cerebellar neuromodulation, which is necessary to produce a wide range of behavioral response appropriate in the context of the general behavioral state of the animal.

Going back to internal source of rhythmic activity in the olivo-cerebellar system, Person and Ramon contribute with a very comprehensive review on PC-DCN convergence and coding. They underline that disruption to such finetuned code, both in terms of timing and rate, can lead to motor dysfunctions.

Finally, rhythmic activity is not only essential at the input (IO) and output (DCN) stages of the system. Courtemanche and colleagues provide an overview on oscillatory activity of the cerebellar cortex. Slow oscillations (4–25 Hz) organize spatial patterns of synchronization and communication with and within the granular layer. Fast oscillations (150–300 Hz) in PCs have a more direct influence on DCN, neighboring modules and motor output, and are found to be more pronounced in pathological scenarios such as Angelman disease.

(D) THEORIES OF LEARNING AND CONTROL

Central to all theoretical models of cerebellar learning is the instructive role played by the IO signals carried via CF to PCs. One of the original proposers of such role, Masao Ito, here elaborates about the apparent dichotomy between sensory (feedforward control) and motor (feedback control) errors carried by CFs to PCs, and pinpoints that such an error dichotomy persists throughout vertebrate phylogeny (Ito). Najafi and Medina focus on the nature of such error signals, and argue that the all-or-nothing idea is being separated. They support this position by underlining that CF burst size has been shown to be tightly regulated and informative, but that it can modulate calcium channels on PC dendrites. A graded CF instructive signal activating PCs can thus be effectively encoded via pre- or post-synaptic modulation. The Otis laboratory confirmed that such

signal not only is graded, but is also not univocally received by PCs, but also by MLIs via spillover mechanisms (Otis et al.). Schweighofer et al. discuss the implication of electrical coupling strength in the IO on the error signal effectiveness. They argue that intermediate coupling strength is best, because it leads to chaotic resonance and increase information transfer of the error signal.

Beside the recognized role of supervised plasticity at the PF-CF-PC node, the impact of distributed cerebellar plasticity on cerebellar adaptive behaviors remains to be clarified. This problem would be hard to tackle unless distributed plasticity mechanisms are integrated into a fully interconnected sensory-motor control system operating in closed-loop during behavior. This challenge has been taken by the Ros' and D'Angelo's laboratories (Garrido et al.), who elaborated on a robotic controller, embedding a computational model of the whole olivo-cerebellar system. The model was endowed with multiple distributed forms of synaptic plasticity. During a closed-loop load manipulation task, parallel fiber—Purkinje cell LTP and LTD rapidly acquired sensory-motor contingencies under climbing fiber guidance but then plasticity was slowly transferred into the DCN. This two-rate process proved critical to allow the system to dynamically adjust its gain when the load was changed. Distributed plasticity beyond parallel fiber LTD was therefore required to efficiently generate rapid, stable and self-adapting behavioral learning and control.

(E) CEREBELLUM AS AN INTEGRATED SYSTEM FOR SENSORIMOTOR CONTROL AND COGNITION

After the fundamental recognition of its involvement in sensorimotor coordination and learning, the olivo-cerebellar system is now also believed to take part in cognition and emotion. D'Angelo and Casali have reviewed a broad spectrum of observations and argue that a similar circuit structure in all olivo-cerebellar sections may cope with the different cerebellar operations using a common underlying computational scheme. It is proposed that the different roles of the cerebellum depend on the specific connectivity of cerebellar modules and that motor, cognitive and emotional functions are (at least partially) segregated in different cerebro-cerebellar loops. In a multi-level conceptual framework, cellular/molecular and network mechanisms would generate computational primitives (timing, learning, and prediction) that could operate in high-level cognitive processing and finally control mental function and dysfunction. It is proposed that the cerebellum operates as a general-purpose co-processor, whose effects depend on the specific brain centers to which individual modules are connected. Abnormal functioning in these loops could eventually take part in the pathogenesis of major brain pathologies including not just ataxia but also dyslexia, autism, schizophrenia, and depression.

The Apps laboratory highlights anatomical and physiological evidence gathered in monkeys, cats, and rats, indicates that survival circuits structures such as the peri-acquaductal gray are connected with cerebellum and olive (Watson et al.). Additionally, the Rondi-Reig laboratory calls for a key role of the cerebellum in spatial navigation (Rochefort et al.). They argue that the cerebellum is a necessary regulator of spatial representation and integrates multisource self-motion information, transforming such reference frame into vestibular signals and distinguishing between self and externally generated vestibular signals.

OPEN QUESTIONS AND DEBATES

While much progress has been made during the last decades in trying to elucidate how the olivo-cerebellar network might work, several questions still remain open. Some of the questions raised by the articles contributing to this special issue concern the genetic and molecular mechanisms during development that generate olivo-cerebellar compartmentalization and determine which behavior is encoded in each cerebellar zone. Another fundamental question is how spatio-temporal patterns elaborated in local microcircuits are integrated into meaningful engrams under the coordination of oscillation and resonance phenomena. At the front of synaptic plasticity there are several open issues. Do we know all existing forms of plasticity in the cerebellum? How do these plasticities contribute to cerebellar learning? How important is structural plasticity in adults and how does this interact with synaptic and intrinsic plasticity mechanisms? How are all the different forms of rhythmicity and plasticity affected by neuromodulators? Taken together, it is becoming clear that understanding how the cerebellum works eventually depends on how its activity is integrated into large-scale loops in the whole brain. A major challenge will be therefore to determine the precise anatomy and behavioral correlates of cerebellar-telencephalic connections in different species, as well as the impact of cerebellar temporally patterned activity onto the cerebral cortex. Tackling such important questions will be the challenge that the field will face in the years ahead of us.

ACKNOWLEDGMENTS

This work was supported by grants of European Union to ED (CEREBNET FP7-ITN238686 to ED and CDZ, REALNET FP7-ICT270434, Human Brain Project HBP-604102 to ED) and ERC-advanced and ERC-POC to CDZ. EG is supported by a Sir Henry Wellcome Fellowship.

Conflict of Interest Statement: The authors declare that the research was conducted in the absence of any commercial or financial relationships that could be construed as a potential conflict of interest.

frontiers in
NEURAL CIRCUITS

REVIEW ARTICLE
published: 02 January 2013
doi: 10.3389/fncir.2012.00115

Architecture and development of olivocerebellar circuit topography

Stacey L. Reeber[1,2], Joshua J. White[1,2], Nicholas A. George-Jones[1,2] and Roy V. Sillitoe[1,2]*

[1] Department of Pathology and Immunology, Baylor College of Medicine, Jan and Dan Duncan Neurological Research Institute of Texas Children's Hospital, Houston, TX, USA
[2] Department of Neuroscience, Baylor College of Medicine, Jan and Dan Duncan Neurological Research Institute of Texas Children's Hospital, Houston, TX, USA

Edited by:
Chris I. De Zeeuw, Erasmus MC, Netherlands

Reviewed by:
Edward S. Ruthazer, Montreal Neurological Institute, Canada
Iris Salecker, MRC National Institute for Medical Research, UK

***Correspondence:**
Roy V. Sillitoe, Department of Pathology and Immunology, Baylor College of Medicine, Jan and Dan Duncan Neurological Research Institute of Texas Children's Hospital, 1250 Moursund Street, Suite 1325, Houston, TX 77030, USA.
e-mail: sillitoe@bcm.edu

The cerebellum has a simple tri-laminar structure that is comprised of relatively few cell types. Yet, its internal micro-circuitry is anatomically, biochemically, and functionally complex. The most striking feature of cerebellar circuit complexity is its compartmentalized topography. Each cell type within the cerebellar cortex is organized into an exquisite map; molecular expression patterns, dendrite projections, and axon terminal fields divide the medial-lateral axis of the cerebellum into topographic sagittal zones. Here, we discuss the mechanisms that establish zones and highlight how gene expression and neural activity contribute to cerebellar pattern formation. We focus on the olivocerebellar system because its developmental mechanisms are becoming clear, its topographic termination patterns are very precise, and its contribution to zonal function is debated. This review deconstructs the architecture and development of the olivocerebellar pathway to provide an update on how brain circuit maps form and function.

Keywords: inferior olive, circuitry, topography, climbing fibers, cerebellum, zones

INTRODUCTION

It is well established that brain circuits are organized into spatial maps that control behavior (Hubel and Wiesel, 1979; Johnston, 1989; Friedman and O'Leary, 1996; Logan et al., 1996; Bozza et al., 2002; Huffman and Cramer, 2007; Leergaard and Bjaalie, 2007; Li and Crair, 2011; Suzuki et al., 2012). Yet, we have a limited understanding of how precise functional connections form during map development. Neural circuit connectivity is intensely studied in the cerebellum because its cellular networks are well understood and its developmental mechanisms are experimentally tractable. Cerebellar circuits have an established role in motor control and they are now also implicated in higher order functions such as cognition and emotion (Sacchetti et al., 2009; Strata et al., 2011). Two main types of afferents transmit information to the cerebellum: climbing fibers and mossy fibers. Climbing fibers arise only from neurons of the inferior olivary nucleus in the brainstem (**Figure 1**) and monoinnervate adult Purkinje cells (**Figure 2A**) whereas mossy fibers originate from numerous brain and spinal cord nuclei to innervate granule cells. Each climbing fiber elicits powerful Purkinje cell responses that sculpt cerebellar function (**Figures 2C,D**). Here, we discuss the development, organization, and function of the olivocerebellar projection and highlight the mechanisms that make this pathway an attractive model for understanding topographic brain circuitry.

CEREBELLAR SAGITTAL ZONES

The adult cerebellum is anatomically divided into distinct folds called lobules (**Figure 3A**; Larsell, 1952). Mammals and birds have 10 lobules that are separated from one another by a series of fissures. Because each fissure extends to a specific depth in the cerebellum, each lobule develops with a unique shape (**Figure 3A**). The invariance of lobule structure and their conservation across species support the idea that lobule/fissure formation is spatially and temporally controlled by complex morphogenetic programs (Sudarov and Joyner, 2007).

Strikingly, each lobule in the cerebellum is further compartmentalized along the medial-lateral axis into sagittal zones (**Figure 3**). Each set of zones is clearly delineated by the patterned expression of genes and proteins (Apps and Hawkes, 2009). The most comprehensively studied zonal marker is zebrin II (Brochu et al., 1990; **Figures 3B,C**, **4D**), an antigen on the aldolase C protein (Ahn et al., 1994; Hawkes and Herrup, 1995). Zebrin II is expressed by alternating subsets of Purkinje cells (zebrin II+ adjacent to zebrin II−), thus forming complementary rows of biochemically distinct Purkinje cells (**Figures 3B,C**, **4D**). The zonal organization of zebrin II is symmetrical about the cerebellar midline, highly reproducible between individuals, and conserved across species (Brochu et al., 1990; Sillitoe et al., 2005; Apps and Hawkes, 2009). The pattern of zebrin II has an intricate relationship to the expression of several other Purkinje cell proteins. For example, phospholipase Cβ3 (PLCβ3), sphingosine kinase 1a (SPHK1a), and excitatory amino-acid transporter 4 (EAAT4; Hawkes et al., 1985; Hawkes and Leclerc, 1987; Dehnes et al., 1998; Terada et al., 2004; Sarna et al., 2006) are all co-expressed with zebrin II. In contrast, phospholipase C β4 (PLCβ4; Armstrong and Hawkes, 2000; Sarna et al., 2006) is expressed selectively in zebrin II− zones. In addition to the complementary and corresponding relationships between zones, proteins such as neurofilament heavy chain (NFH) divide individual zebrin II zones into smaller sagittal units (Demilly et al., 2011).

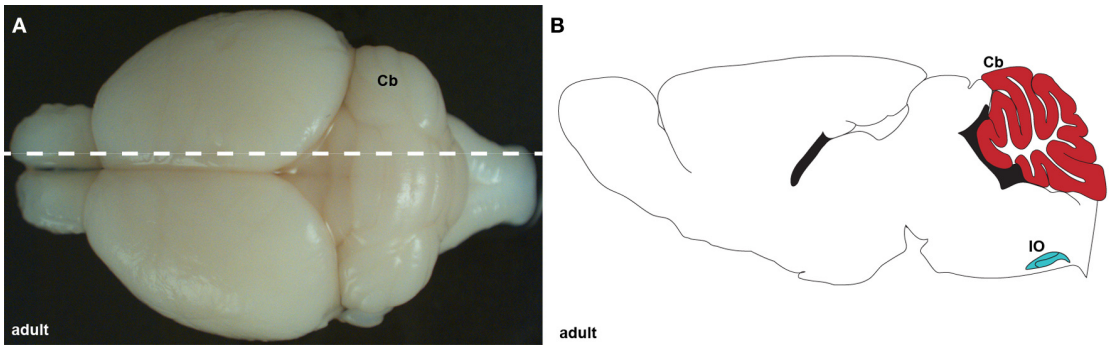

FIGURE 1 | (A) Wholemount image of an adult brain showing the cerebellum (Cb) from a dorsal view. The dotted line indicates the level of the tissue section schematic in **(B)**. **(B)** Schematic of sagittal section cut through an adult cerebellum showing the cerebellum (red) and inferior olive (IO; blue).

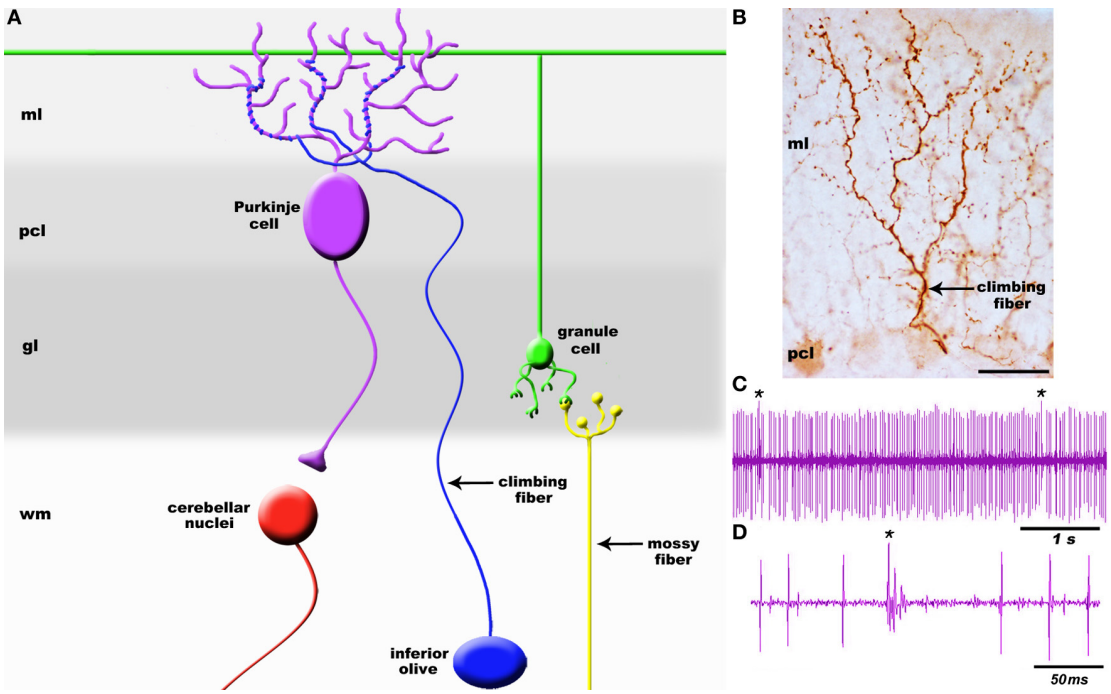

FIGURE 2 | (A) Schematic of a simplified cerebellar microcircuit illustrating the two major sensory afferent pathways that project to the cerebellum: climbing fibers and mossy fibers. Climbing fibers (blue projection) terminate directly onto Purkinje cells whereas mossy fibers (yellow projection) terminate on granule cell dendrites (green). Granule cell axons called parallel fibers contact Purkinje cells (purple). Purkinje cells are the sole output of the cerebellar cortex and transmit signals to the cerebellar nuclei (red). **(B)** High power image of a climbing fiber expressing cocaine-and amphetamine-regulated transcript (CART) peptide [arrow; staining was performed according to Reeber and Sillitoe (2011)]. The target Purkinje cell is weakly immunoreactive for CART. **(C)** Example Purkinje cell spike train recorded *in vivo*. Recordings were performed in Ketamine/Xylazine anesthetized mice using 2–5 M Ohm Tungsten electrodes (Thomas Recording, Germany). Signals were band-pass filtered at 300–5000 Hz, amplified with an ELC-03XS amplifier (NPI, Germany), and recorded with Spike2 (CED, England). **(D)** Higher power view of the recording trace illustrating the clear distinction between a climbing fiber complex spike (cs) and simple spike (ss) responses in Purkinje cells. Asterisk in panel **(C)** indicates a complex spike. The layers of the cerebellum are indicated as molecular layer (ml), Purkinje cell layer (pcl), granular layer (gl), and white matter (wm). The cerebellar nuclei are located in the white matter. Scale bar in **(B)** = 25 μm.

Cumulatively, molecularly defined zonal compartments divide the cerebellar cortex into hundreds of reproducible units with each one containing up to several hundred Purkinje cells (Apps and Hawkes, 2009).

Purkinje cell zones may be used to divide the cerebellum into four transverse domains in the anterior–posterior axis (Ozol et al., 1999). For example, in the vermis zebrin II expression reveals a specific pattern in lobules I–V and VIII/IX (**Figures 3B,C**, **4D**). In contrast, expression of the small 25 kDa heat shock protein HSP25 delineates distinct zonal patterns in lobules VI/VII and IX/X, which express zebrin II in all Purkinje cells (Armstrong et al., 2000). Afferent termination patterns mirror the topography

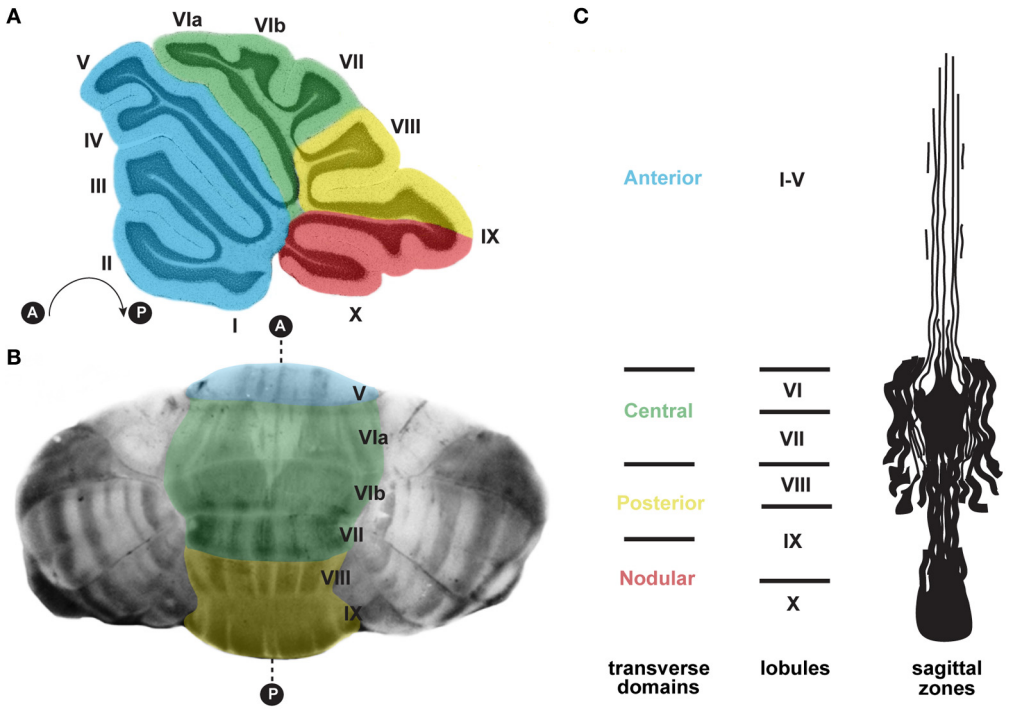

FIGURE 3 | (A) Schematic of a sagittal section cut through the cerebellar vermis revealing the stereotypical foliation pattern, which consists of 10 lobules [adapted with permission from White and Sillitoe (2013)]. The cerebellum can be further divided along the anterior–posterior axis into four transverse domains: anterior (blue; lobules I–V), central (green; lobules VI and VII), posterior (yellow; lobules VIII and anterior IX), and nodular (red; lobules posterior IX and X) (Ozol et al., 1999). **(B)** In the adult cerebellum, zebrin II/aldolase C expression, which is revealed using wholemount staining (Sillitoe and Hawkes, 2002; White et al., 2012), delineates zones of Purkinje cells. The transverse zones are color coded according to panel **(A)**. **(C)** A schematic representation of an unfolded vermis illustrating the full pattern of zebrin II zones (adapted with permission from Sillitoe and Joyner, 2007). Lobule numbers are indicated by Roman numerals. Anterior and posterior axes are denoted by A and P.

of Purkinje cell zones (**Figures 4B,E**). As a result, each transverse domain is innervated by a specific combination of functionally distinct afferent fibers. For instance, spinocerebellar mossy fibers project to lobules I–V and VIII/IX (Arsenio Nunes and Sotelo, 1985; Brochu et al., 1990; Sillitoe et al., 2010), whereas the vestibulocerellar mossy fibers project mainly to lobules IX and X (Jaarsma et al., 1997; Maklad and Fritzsch, 2003). In mouse, climbing fibers that express cocaine- and amphetamine-related transcript peptide (CART) terminate selectively in lobules VI/VII and IX/X (Reeber and Sillitoe, 2011), and corticotrophin releasing factor (CRF) expressing climbing fibers are expressed in a striking array of zones in lobules I–V and VIII/IX (**Figures 4C,E**) (Sawada et al., 2008).

The efferent side of the cortical circuit also respects the zonal topography. Sugihara and collaborators have mapped the trajectories of Purkinje cell axons from specific cerebellar cortical compartments onto the three sets of cerebellar nuclei. They revealed a close correspondence between adolase C expressing Purkinje cell terminals with subdivisions of cerebellar nuclei (Sugihara and Shinoda, 2007). Together, Purkinje cell zones, afferent topography, and Purkinje cell efferent projections to the cerebellar nuclei define the cerebellar module, the functional unit of the cerebellum (Apps and Hawkes, 2009; Ruigrok, 2011).

ANATOMICAL AND FUNCTIONAL ORGANIZATION OF OLIVOCEREBELLAR ZONES

Fine topological mapping using anterograde tracers injected into specific sub-nuclei of the inferior olive and the tracing of climbing fiber collateral projections labeled from injections into the cerebellar cortex of birds, rodents, and primates have shown that there is a strict and precise association between climbing fiber topography and zebrin II Purkinje cell zones (Voogd et al., 2003; Sugihara and Shinoda, 2004; Voogd and Ruigrok, 2004; Sugihara and Quy, 2007; Pakan and Wylie, 2008; Sugihara et al., 2009; Fujita et al., 2010). In addition, several studies have used climbing fiber markers to link the architecture of chemically distinct subsets of climbing fiber afferents to the adult pattern of Purkinje cell zones (**Table 1**). For example, CRF, an amino acid peptide, is expressed in a subset of climbing fibers that corresponds to specific Purkinje cell zones (Sawada et al., 2001, 2008) (**Figures 4C,E**). In addition, we recently showed that the expression of the CART 55–102 peptide (**Figure 2B**) is intricately patterned into a complex topographic map that respects HSP25 (mouse) and zebrin II (rat) Purkinje cell zone boundaries (Reeber and Sillitoe, 2011). The class III intermediate filament protein peripherin is also expressed in a subset of climbing fibers that are organized into parasagittal compartments, although it is not clear how peripherin labeled climbing fibers relate to Purkinje

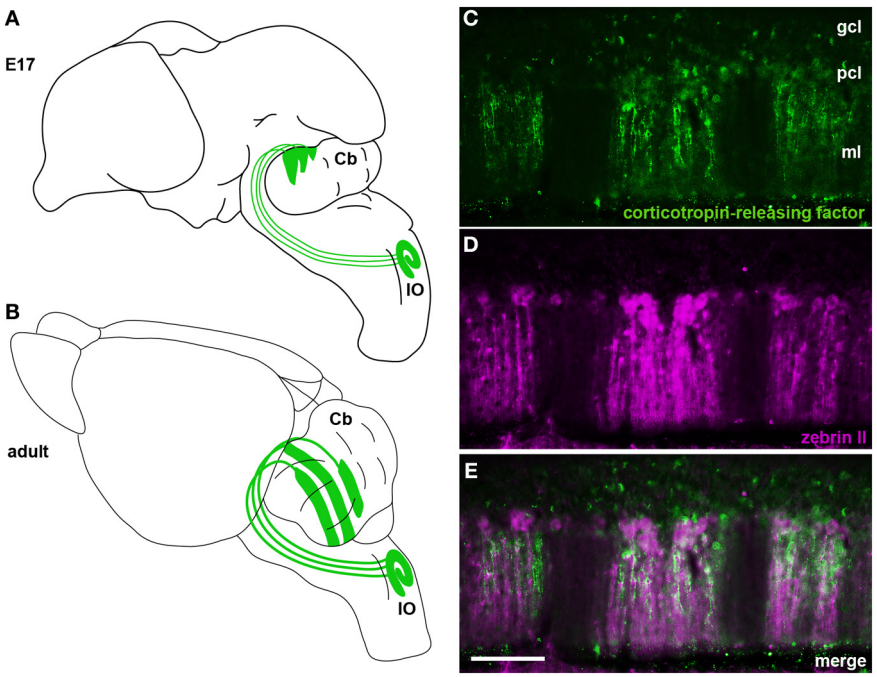

FIGURE 4 | (A) Schematic illustrating climbing fibers projecting from the inferior olivary nucleus (IO) to the cerebellum (Cb) and their organization into a crude zonal pattern at E17. **(B)** A schematic of the adult brain showing climbing fibers projecting from the inferior olive (IO) to well-defined Purkinje cell zones in the cerebellum. **(C–E)** In the adult cerebellum corticotropin-releasing factor (CRF) is expressed in subsets of climbing fibers that align with zebrin II Purkinje cell zones. Panels **(C)** and **(D)** show individual channels of CRF and zebrin II expression and panel **(E)** is a merged image showing the corresponding relationship between the two patterns. The staining pattern of CRF and its relationship to zebrin II zones was previously described (Sawada et al., 2008). CRF and zebrin II staining was carried out exactly as previously described (Sawada et al., 2008). Scale bar in **(E)** = 100 μm (applies to **C–D**).

cell zones (Errante et al., 1998). The precise topography of the olivocerebellar pathway raises the tantalizing possibility that zonal circuits may be functionally relevant. In this regard, two pressing questions have yet to be fully answered: (1) what is the functional significance of zones? and (2) what role do topographic circuits play during behavior?

Previous electrophysiological mapping studies suggested that parasagittal zones could be related to cerebellar function (Armstrong et al., 1974; Ekerot and Larson, 1980; Llinas and Sasaki, 1989; Chockkan and Hawkes, 1994; Sugihara et al., 1995; Chen et al., 1996; Hallem et al., 1999). However, it was only recently that modern optical imaging and electrophysiological approaches were exploited to uncover potential links between functional cerebellar circuits and zonal architecture (Ebner et al., 2012; Graham and Wylie, 2012). In their seminal paper, Wadiche and Jahr (2005) used molecular physiology approaches to demonstrate that synaptic plasticity may vary between zones. Accordingly, the level of glutamate that is released at climbing fiber terminals is zone dependent (Paukert et al., 2010) and climbing fiber inputs initiate synchronous firing in zones of Purkinje cells (Sasaki et al., 1989; Lang et al., 1999; Blenkinsop and Lang, 2006; Wise et al., 2010). These studies support the notion that there are fundamental differences in the physiology of Purkinje cell zones and suggest the possibility that climbing fibers contribute to the functional specificity of the zones.

The behavioral significance of zones remains elusive. However, surgically induced lesions and localized delivery of pharmacological agents into the inferior olive have provided some evidence that cerebellar zones may facilitate behavior (Watanabe et al., 1997; Seoane et al., 2005; Pijpers et al., 2008; Horn et al., 2010; Cerminara and Apps, 2011). For example, Llinas and collaborators found that when the neurotoxin 3-acetylpyridine (3AP) is injected intraperitoneally, the inferior olive is rapidly destroyed and severe ataxia emerges (Llinas et al., 1975). Similarly, injecting another neurotoxin called trans-crotononitrile (TCN) into rats inactivates the olive and induces profound motor deficits (Seoane et al., 2005; Cerminara and Apps, 2011). Ruigrok and colleagues used yet a different approach to inactivate the olive (Pijpers et al., 2008). They injected cholera toxin b conjugated to saporin into individual cerebellar cortical zones, which retrogradely transported the neurotoxin into the olive and induced dysfunction of specific modules. By targeting distinct modules they were able to demonstrated specific defects in the step phase-dependent modulation of cutaneously induced reflexes during locomotion (Pijpers et al., 2008; Cerminara and Apps, 2011). Moreover, inactivating specific olivary subdivisions in cats with the glutamate receptor blocker, CNQX, produced a series of unique motor deficits that were dependent on the particular sub-nucleus that was lesioned (Cerminara, 2010; Horn et al., 2010). What is far from clear is whether each zone encodes specific behaviors (or distinct aspects of a behavior), or

Table 1 | Molecular and genetic markers for studying olivocerebellar topography.

Transient expression in subsets of climbing fibers	
CGRP (zones in rat E16-P20)	Chedotal and Sotelo, 1992; Morara et al., 1992
Parvalbumin (zones in rat ∼P0–P10)	Wassef et al., 1992; Chedotal and Sotelo, 1993
Topographic climbing fiber projections	
Calretinin (zones in cat)	Yan and Garey, 1996
CART (zones in mouse and rat)	Reeber and Sillitoe, 2011
CRF (zones in mouse and opossum)	Cummings et al., 1989; Sawada et al., 2008
DNPI/VGLUT2 (zones in mouse)	Paukert et al., 2010
NPY (zones in rat)	Ueyama et al., 1994
Peripherin (zones in rat)	Errante et al., 1998
Compartmentalization of the inferior olive	
BEN	Chedotal et al., 1996
Brn3a	Xiang et al., 1996
Brn3b	Xiang et al., 1996
CART	Reeber and Sillitoe, 2011
Cdh6	Suzuki et al., 1997
Cdh8	Suzuki et al., 1997; Redies et al., 2011
Cdh11	Suzuki et al., 1997
CRF	Yamano and Tohyama, 1994
Cx36	Belluardo et al., 2000; Weickert et al., 2005
Cx45	Van Der Giessen et al., 2006
Cx47	Weickert et al., 2005
Cx57	Zappala et al., 2010
DCC	Bloch-Gallego et al., 1999
EphA3	Nishida et al., 2002
EPHA4	Hashimoto et al., 2012
EphA5	Nishida et al., 2002
EphA6	Nishida et al., 2002
EPHA7	Hashimoto et al., 2012
ER81	Zhu and Guthrie, 2002; Hashimoto et al., 2012
FOXP2	Hashimoto et al., 2012
NPY	Ueyama et al., 1994; Morara et al., 1997
Nr-CAM	Backer et al., 2002
Pannexin1	Weickert et al., 2005
Pdh7	Redies et al., 2011
Pdh10	Redies et al., 2011
Unc-5H2	Bloch-Gallego et al., 1999
Unc-5H3	Bloch-Gallego et al., 1999
DNPI/VGLUT2	Hisano et al., 2002
Genetic markers for the inferior olive and/or climbing fibers	
CART-Cre	Madisen et al., 2010
CRF-Cre	Martin et al., 2010
Cx36-LacZ	Degen et al., 2004
Cx45-lacZ	Van Der Giessen et al., 2006
Npy-GFP	Nishiyama et al., 2007
Parvalbumin-Cre	Tanahira et al., 2009
Parvalbumin-CreER	Taniguchi et al., 2011

Note that the markers in each subsection are organized in alphabetical order and molecules of the same family are grouped together. The names of proteins are upper case and not italicized. mRNAs and transgenic mouse lines are italicized.

whether multiple zones interact during motor control. Perhaps one way to unravel what zones do is to uncover how they form. Indeed, developmental studies have raised two critical questions that are ultimately relevant to cerebellar behavior: (1) what are the cellular and molecular mechanisms that control Purkinje cell zone development? and (2) how do climbing fiber projections invade, recognize, and connect to their targets?

GENETIC LINEAGE, MIGRATION, AND AXONOGENESIS OF INFERIOR OLIVE CELLS

Several landmark studies have used the regulatory sequences of developmentally expressed genes to design genetic tools for tracking the fate of cerebellar and inferior olive cells from embryogenesis to adulthood (Rodriguez and Dymecki, 2000; Hoshino et al., 2005; Machold and Fishell, 2005; Pascual et al., 2007). Genetic fate-mapping studies using *Atonal homolog 1* (*Atoh1*, formerly known as *Math1)* and *Wnt1* regulatory elements revealed that inferior olive neurons emerge from a distinct progenitor pool in the lower rhombic lip of the hindbrain (Rodriguez and Dymecki, 2000; Landsberg et al., 2005; Wang et al., 2005; Nichols and Bruce, 2006). In accordance with these findings, genetic fate-mapping using a *pancreas specific transcription factor 1a-Cre* ($Ptf1a^{Cre/+}$) allele to drive *lacZ* reporter gene expression in *R26R* [$Gt(ROSA)26Sor^{tm1sor}$; Soriano, 1999] mice revealed that inferior olivary neurons are derived from a distinct *Ptf1a* domain (Hoshino et al., 2005; Yamada et al., 2007). Hoshino and colleagues determined that *Ptf1a* is required for the proper development of inferior olive neurons, because the inferior olivary complex is severely altered in *Ptf1a* null mutants (Yamada et al., 2007). Without *Ptf1a*, some inferior olive neurons do not differentiate while others migrate inappropriately. Moreover, a large number of apoptotic cells were observed in the *Ptf1a* mutants, and the fate of *Ptf1a*-dependent lineages adopted mossy fiber neuron characteristics (Yamada et al., 2007). Although *Ptf1a* appears to control the development of most, if not all, olivary neurons, it is not clear what upstream or downstream molecular pathways might be responsible for generating the sub-nuclei. Studies by Bloch-Gallego and colleagues provide some insight into this question. The authors determined that the absence of Rho-guanine exchange factor Trio impairs the organization of the inferior olivary nucleus into distinct lamellae (Backer et al., 2007). Additionally, in a recent elegant study, quail-chick chimaeras were used to provide evidence that each inferior olive sub-nucleus originates from

specific rhombomeres, developmental hindbrain units that are each restricted in their lineages (Hidalgo-Sanchez et al., 2012). It is intriguing that climbing fiber zones, which arise from distinct olivary sub-nuclei, may be specified early by rhombomere specific cues.

Inferior olive neurons are born dorsally in the lower rhombic lip and migrate circumferentially around the edges of the brainstem to their final location near the ventral midline (Altman and Bayer, 1987; Sotelo, 2004; Sotelo and Chedotal, 2005) (**Table 2**). Tritiated thymidine labeling (Altman and Bayer, 1987) and HRP axonal tracing *in vitro* (Bourrat and Sotelo, 1988, 1990b) revealed that inferior olivary neurons migrate along the lateral edges of the brainstem in a unique "submarginal stream" (Altman and Bayer, 1987; Bourrat and Sotelo, 1988, 1990b; Sotelo and Chedotal, 2005). Interestingly, the somata of olivary neurons do not cross the floor plate, whereas their axons do cross and project exclusively to the contralateral cerebellum (Altman and Bayer, 1987; Altman, 1997). The restriction of olivary neurons to one side of the midline is controlled by both chemoattractive and chemorepellent molecules (e.g., netrin-1/DCC and Slit/Robo; Bloch-Gallego et al., 1999; Causeret et al., 2002; de Diego et al., 2002; Marillat et al., 2004). Marillat et al. (2004) showed that Rig-1/Robo3 plays an essential role in controlling the migration of precerebellar neurons and the projection of axons across the midline. In *Rig1/Robo3* deficient mice, inferior olive neurons incorrectly send axons to the ipsilateral cerebellum in addition to sending the normal contralateral projection (Marillat et al., 2004).

The first climbing fibers arrive in the developing cerebellum at ∼embryonic day (E) 14/15 in the mouse (Paradies and Eisenman, 1993) (**Table 2**) and are already organized in a crude zonal map at ∼E15/16 (Sotelo et al., 1984; Chedotal and Sotelo, 1992; Paradies and Eisenman, 1993; Paradies et al., 1996), which is approximately when Purkinje cells begin to express parasagittal markers (e.g., *engrailed1/2* and *L7/Pcp2*) (Hashimoto and Mikoshiba, 2003; Wilson et al., 2011). By ∼E17 in mice, olivocerebellar topography strongly corresponds with the nascent architecture of Purkinje cell zones (Paradies et al., 1996; **Figure 4A**).

FORMATION OF OLIVOCEREBELLAR ZONES

The almost perfect overlap between climbing fiber terminal field topography and Purkinje cell zones suggests that the spatial and temporal targeting of cerebellar afferent pathways is closely coordinated with Purkinje cell development. Purkinje cells become postmitotic between ∼E10 and ∼E13 and form symmetrical

Table 2 | Timeline of olivocerebellar development.

Developmental stage	Developmental event	References
∼E12/13 rat (E10/11 mouse)	Inferior olive neurons are born	Pierce, 1973; Bourrat and Sotelo, 1990a, 1991; Sotelo, 2004
∼E14/15 mouse	Climbing fibers arrive in cerebellum	Paradies and Eisenman, 1993
∼E16–E18 rat (E14–16 mouse)	Inferior olive neurons settle in final position adjacent to the floor plate	Bourrat and Sotelo, 1990a; Sotelo, 2004
∼E16 rat (E14 mouse)	Transient biochemical compartmentation of inferior olive and Purkinje cells (arising independently)	Wassef et al., 1992; Larouche et al., 2006
∼E15/16 mouse	Climbing fibers organize into crude parasagittal clusters	Paradies and Eisenman, 1993
∼E17 mouse	Climbing fiber topography corresponds clearly with nascent Purkinje cell zone	Paradies et al., 1996
∼P0–P5 rat (P0–P3 mouse)	Olivocerebellar projections resolve into precise sagittal zones similar to the adult	Sotelo et al., 1984
∼P0 rat (P0 mouse)	Creeper stage starts	Watanabe and Kano, 2011
∼P0–P10 rat (P0–P8 mouse)	Critical period for olivocerebellar plasticity	Sherrard et al., 1986
∼P3 mouse	Discrete climbing fiber mediated EPSCs recorded in Purkinje cells (all fibers induce similar amplitudes in perinatal Purkinje cells)	Hashimoto and Kano, 2003
∼P5 rat (P3 mouse)	Pericellular nest stage starts	Watanabe and Kano, 2011
∼P5 mouse	Development of climbing fiber terminal structure	Mason and Gregory, 1984
∼P7 mouse	"Winner" climbing fiber is strengthened	Hashimoto and Kano, 2003
End of the first postnatal week	Climbing fiber complex spikes are first detected	Woodward et al., 1969
∼P9 rat (P7 mouse)	Capuchon stage	Watanabe and Kano, 2011
∼P12 rat (P10 mouse)	Dendritic stage commences	Watanabe and Kano, 2011
∼P7–11 rat (P5–9 mouse)	Climbing fiber pruning and perisomatic synpase elimination: the early phase	Watanabe and Kano, 2011
∼P12–17 rat (P10–15 mouse)	Climbing fiber pruning and perisomatic synpase elimination: the late phase	Watanabe and Kano, 2011

zonal "clusters" by ∼E14 (Hashimoto and Mikoshiba, 2003; Hoshino et al., 2005; Sillitoe et al., 2009; Namba et al., 2011; Sudarov et al., 2011). Climbing fiber neurons are also born at ∼E10/11 (Sugihara and Shinoda, 2007). Interestingly, when they arrive in the developing cerebellum they immediately project into clusters of Purkinje cells (Paradies and Eisenman, 1993). The predictable termination of climbing fibers into Purkinje cell zones suggests that the Purkinje cells may play an active role in instructing the pattern of olivocerebellar targeting.

Sotelo and collaborators postulated that the cerebellum and the inferior olive might have matching gene expression domains that establish bidirectional signaling to generate the olivocerebellar map (Sotelo and Wassef, 1991; Sotelo and Chedotal, 1997, 2005). Support for this hypothesis was first provided by using a combination of markers that labeled zones of Purkinje cells (calbindin, GMP-cyclic dependent protein kinase, Purkinje cell-specific glycoprotein, and PEP-19) and also marked corresponding subsets of inferior olive cells along with their projections [calbindin, parvalbumin, and calcitonin gene-related peptide (CGRP); **Table 1**]. The precision and reproducibility of zonal boundaries defined by these markers suggested the possibility that inferior olivary neurons might target Purkinje cell zones by recognizing positional cues (Sotelo and Wassef, 1991; Sotelo and Chedotal, 1997, 2005).

Eph/ephrin genes play a major role in establishing brain topography (Flanagan and Vanderhaeghen, 1998; Cang et al., 2008a,b; Allen-Sharpley and Cramer, 2012). In the cerebellum, eph/ephrin are expressed in distinct parasagittal domains (Karam et al., 2000, 2002). Nishida and coworkers (2002) provided compelling evidence for the involvement of eph/ephrin signaling in controlling the molecular matching between climbing fibers and Purkinje cells during olivocerebellar circuit formation (Nishida et al., 2002). They showed that altering ephA receptor and ephrin-A ligand expression in chick hindbrain explant cultures disrupted the anterior–posterior targeting of olivocerebellar axons. However, this study did not address whether eph/ephrin signaling controls the development of olivocerebellar zones (Nishida et al., 2002; Hashimoto and Hibi, 2012). Regardless, because specific ephA/ephrin-A manipulations can disrupt the global targeting of olivocerebellar axons, there is a possibility that other eph/ephrins and/or additional molecules likely cooperate to establish precise Purkinje cell-afferent interactions during map formation. Besides the eph/ephrins, possible candidates are the type-II classic cadherin and δ-protocadherin cell–cell adhesion molecules, which are expressed in a striking array of Purkinje cell sagittal zones (Suzuki et al., 1997; Neudert et al., 2008; Redies et al., 2011) and in specific subdivisions of the inferior olive (Suzuki et al., 1997; Neudert et al., 2008; Redies et al., 2011). Despite these clues, we still do not have a clear picture of what genes control the topographic connectivity of olivocerebellar zones nor do we understand the detailed mechanisms that initiate and maintain the physical interaction between specific Purkinje cells and climbing fibers. However, recent work demonstrates that starting from birth, inferior olive neurons spontaneously organize into clusters that fire synchronous Ca^{2+} transients in *in vitro* brain slice preparations (Rekling et al., 2012). Curiously, during early postnatal development spontaneous waves travel along chains of axon collaterals that connect sagittal rows of Purkinje cells (Watt et al., 2009). Both phenomena were suggested as likely mechanisms contributing to the development of cerebellar compartments. However, whether the spontaneous waves of Purkinje cell activity are linked to the spontaneous activity of inferior olive neurons awaits further analysis. It will also be interesting to determine whether cerebellar spontaneous activity interacts with developmental gene function in a zone specific fashion.

POSTNATAL REMODELING OF CLIMBING FIBERS

Following the establishment of the crude zonal map, climbing fibers undergo extensive morphological changes and proceed through different stages of fiber remodeling to form functionally mature connections (Watanabe and Kano, 2011) (**Table 2**). The first phase of remodeling is the "creeper" stage (∼P0 in rat) when climbing fibers are very thin and form transient synapses on immature Purkinje cell dendrites (Chedotal and Sotelo, 1993; Sugihara, 2005; Watanabe and Kano, 2011). Then, climbing fibers enter a "transitional" stage and exhibit characteristics that are intermediate between those of the creeper and nest stages (Sugihara, 2005). The "pericellular nest' stage (∼P5) is defined by the dense terminal arbors ("nest") that surround Purkinje cell somata (Cajal, 1911; O'Leary et al., 1971; Mason et al., 1990; Sugihara, 2005; Watanabe and Kano, 2011). During this stage, each Purkinje cell receives polyneuronal input from more than five different climbing fibers. Climbing fibers are progressively displaced onto the developing dendritic stems of maturing Purkinje cells ("capuchon stage"; starting at ∼P9). As the dendritic arbors develop, the climbing fibers leave their perisomatic and capuchon positions to occupy peridendritic positions (after ∼P12; referred to as dendritic stage; Chedotal and Sotelo, 1992; Watanabe and Kano, 2011). During this period, climbing fibers translocate up the Purkinje cell dendrite to find their ultimate location within the basal two thirds of the molecular layer (Crepel et al., 1976; Mariani and Changeux, 1981; Hashimoto and Kano, 2005; Kano and Hashimoto, 2009; Watanabe and Kano, 2011).

The monoinnervation of adult climbing fibers onto Purkinje cells is achieved through massive pruning of climbing fibers during postnatal development. Previous studies have revealed systematic changes occurring in the relative synaptic strength of multiple climbing fibers when they polyinnervate a single Purkinje cell during postnatal development. These studies revealed that climbing fiber mediated excitatory postsynaptic currents (EPSCs) recorded in Purkinje cells have similar amplitudes until ∼P3. In the second postnatal week, multiple EPSCs differentiate into one large EPSC and a few small EPSCs (Hashimoto and Kano, 2003). These results suggest that climbing fiber synaptic strengths are similar to one another during early postnatal development, and a single climbing fiber, the "winner," is selectively strengthened during the second postnatal week (∼P7; Hashimoto and Kano, 2003; Bosman et al., 2008). Following these studies, Kano and colleagues used electrophysiological and morphological techniques to determine that competition between multiple climbing fibers occurs at the soma before climbing fibers form synapses with Purkinje cell dendrites (Hashimoto et al., 2009). Notably, the "winner" climbing fiber undergoes translocation to the dendrites

and simultaneously maintains synapses on the soma, while the weaker climbing fibers remain around the soma forming "pericellular nests" with the "winner" synapses (Hashimoto et al., 2009). After the strengthening of a single "winner" climbing fiber, pruning and perisomatic synapse elimination occur in two distinct phases: the early phase (∼P7–11), which is independent of parallel fiber synapses and the late phase (∼P12–17), which depends on activity between parallel fibers and Purkinje cells (Watanabe and Kano, 2011).

In three different mutant mice, *weaver*, *staggerer*, and *reeler*, Purkinje cells develop in the absence of granule cells but are permanently innervated by multiple climbing fibers (Crepel and Mariani, 1976; Mariani et al., 1977; Crepel et al., 1980; Mariani and Changeux, 1980; Steinmayr et al., 1998). Similarly, studies using experimentally-induced "hypogranular" cerebella (Woodward et al., 1974; Crepel and Delhaye-Bouchaud, 1979; Bravin et al., 1995; Sugihara et al., 2000) revealed that the presence of intact granule cells, normal parallel fiber-Purkinje cell synapses, and activity all play a role in climbing fiber synapse elimination.

The process of fiber elimination is mediated by several molecules including metabotropic glutamate receptor mGluR1, PLCβ4, Ca(v)2.1 P/Q-type Ca^{2+} channel, glutamate receptor Glurδ2, precerebellin (or Cbln1), and the GABA synthesizing enzyme GAD67 (Kano et al., 1995, 1997, 1998; Kashiwabuchi et al., 1995; Offermanns et al., 1997; Sugihara et al., 1999; Ichikawa et al., 2002; Miyazaki et al., 2004, 2010; Hirai et al., 2005; Uemura et al., 2007; Hashimoto et al., 2011; Nakayama et al., 2012; Uesaka et al., 2012). Mutations that alter the function of these proteins cause severe defects in climbing fiber synapse development and elimination (Kano et al., 1995, 1997, 1998; Kashiwabuchi et al., 1995; Offermanns et al., 1997; Sugihara et al., 1999; Ichikawa et al., 2002; Miyazaki et al., 2004, 2010; Hirai et al., 2005; Uemura et al., 2007; Hashimoto et al., 2011; Nakayama et al., 2012; Uesaka et al., 2012). Interestingly, Kano and colleagues developed an organotypic co-culture preparation to recapitulate *in vivo* climbing fiber remodeling and with this system identified neuroligin-2 as a key player of climbing fiber elimination in Purkinje cells (Uesaka et al., 2012). Thus, synaptogenesis in the olivocerebellar projection starts relatively early during brain circuit formation, occurs over a protracted period of time, and requires both genetic control and neural activity (Chedotal and Sotelo, 1992; Sotelo, 2004). However, it is not clear whether developmental remodeling plays a role in generating climbing fiber compartments: although one can imagine that the precise zonal boundaries emerge as supernumerary axons are pruned away.

PLASTICITY OF OLIVOCEREBELLAR ZONE CONNECTIVITY

In contrast to the adult central nervous system which has a limited capacity for axonal regeneration, the immature central nervous system is capable of some axonal regrowth (Nicholls and Saunders, 1996). However, regrowth during development frequently occurs through an alternative pathway that is distinct from the normal one. The olivocerebellar pathway is an excellent example of a system in which regrowth establishes a new pathway. Various groups have used the pedunculotomy approach to stimulate transcommissural olivocerebellar reinnervation to determine the temporal properties of afferent-target interactions during development (Angaut et al., 1985; Sherrard et al., 1986; Zagrebelsky et al., 1997; Sugihara et al., 2003; Dixon et al., 2005; Willson et al., 2007). Following unilateral early postnatal transection of an inferior cerebellar peduncle (which carries the climbing fibers), the contralateral inferior olive degenerates and new axons, arising from the remaining inferior olive, grow into the denervated hemicerebellum (Zagrebelsky et al., 1997). The innervation of these transcommissural axons precisely aligns with Purkinje cell expression zones and mirrors the distribution of the "unaltered" projections on the intact side (Zagrebelsky et al., 1997). Sugihara and colleagues (2003) have shown that the newly formed projections develop normal climbing fiber arborizations and form functional synapses onto Purkinje cells. Remarkably, olivocerebellar reinnervation can compensate for motor deficits (Dixon et al., 2005) and rescue the cerebellums influence over spatial learning (Willson et al., 2007). Similar to what might occur during normal development, reinnervation may be regulated by position-dependent cues that mediate the precise connectivity between climbing fibers and Purkinje cells (Dixon and Sherrard, 2006; Willson et al., 2008).

NOVEL TOOLS TO STUDY OLIVOCEREBELLAR DEVELOPMENT, CONNECTIVITY, AND FUNCTION

Neuronal tracing using viruses and genetically encoded fluorescent reporters are now widely used for unraveling circuit connectivity (Wickersham et al., 2007; Marshel et al., 2010; Wall et al., 2010). Retrograde transneuronal infection of rabies virus reveals the organization of multi-synaptic neuronal networks (Coulon et al., 1989; Ugolini, 1995; Kelly and Strick, 2000; Graf et al., 2002). Genetically modified viruses have also allowed control over which cells are initially infected, extent of viral spread, and direction of the spread (Callaway, 2008). Recently, the use of a deletion-mutant rabies virus allowed the spread of the virus to be restricted to monosynaptic connections for selectively revealing first-order presynaptic neurons (Wickersham et al., 2007, 2010; Marshel et al., 2010; Rancz et al., 2011). Using the rabies virus tracing approach, communication networks between the cerebral cortex, basal ganglia, and cerebellum have been resolved (Kelly and Strick, 2003; Bostan et al., 2010; Coffman et al., 2011; Suzuki et al., 2012). More recently, Ruigrok and colleagues also used viral tracing to show that cerebrocerebellar connectivity respects cerebellar zonal organization (Suzuki et al., 2012). Combining viral tracing with transgenic targeting of recombinant viruses (Weible et al., 2010) will allow for unparalleled resolution of circuit topography in the olivocerebellar pathway.

In the past, lesioning, electrical stimulation, and chemical activation/deactivation have unveiled essential functions of the cerebellum and inferior olive (Llinas et al., 1975; McCormick and Thompson, 1984; Bradley et al., 1991; O'Hearn et al., 1993; O'Hearn and Molliver, 1993; Willson et al., 2007; Pijpers et al., 2008; Strick et al., 2009; Horn et al., 2010; Cerminara and Apps, 2011). However, these manipulations are limited by the lack of cell type specificity and/or the by the tissue damage that occurs. Optogenetics methods offer an ideal solution to these shortcomings as they provide an avenue for targeting induced

neural activity to specific cells *in vivo*, without damaging the circuit (Deisseroth et al., 2006; Zhang et al., 2006; Hira et al., 2009; Tsubota et al., 2011). These light-activated ion channels, which include channelrhodopsin-2 (ChR2) and halorhodopsin (eNpHR), have fast temporal kinetics to efficiently activate or inhibit the firing of action potentials (Boyden et al., 2005; Zhang et al., 2006; Adamantidis et al., 2007; Arenkiel et al., 2007; Abbott et al., 2009). Importantly, by using cell type specific promoters one can drive the expression of these light-responsive proteins in selective neuronal populations (e.g., using the *L7/Pcp2* Purkinje cell specific promoter; Oberdick et al., 1990). Indeed, a recent study used *L7/Pcp2-Cre* mice to target ChR2 and eNpHR expression to examine the role of Purkinje cells in controlling cardiovascular function (Tsubota et al., 2011). It will now be interesting to develop optogenetic methods for manipulating neuronal activity within specific inferior olivary nuclei in order to determine the contribution of olivocerebellar zones to motor and nonmotor functions *in vivo*.

SUMMARY

It is well established that the cerebellum is divided into a complex map of functional zones. Much progress has been made in delineating the zonal topography between the inferior olivary nucleus, cerebellar cortex, and the cerebellar nuclei. However, there are several important questions that remain unanswered. For example: (1) Are the olivocerebellar cells that project to each cerebellar zone born at different times and/or are they derived from different genetic lineages? (2) What are the molecular mechanisms that guide olivocerebellar projections into zonal compartments? and (3) What behaviors are encoded into each zone? In future studies, it will be interesting to combine modern anatomical tracing techniques with high-resolution imaging, sophisticated genetic approaches and electrophysiology to answer such questions.

ACKNOWLEDGMENTS

We would like to thank Lionel D. Vázquez-Figueroa (SMART Program student, Baylor college of Medicine) for his contribution to the cerebellar circuitry schematic. All animal work was carried out under an approved IACUC animal protocol at Baylor College of Medicine (Houston, TX). Roy V. Sillitoe is supported by the Caroline Wiess Law Fund for Research in Molecular Medicine, a BCM IDDRC Project Development Award, and start-up funds from Baylor College of Medicine and Texas Children's Hospital (Houston, TX). This work was also supported by BCM IDDRC Grant Number 5P30HD024064 from the Eunice Kennedy Shriver National Institute of Child Health and Human Development.

REFERENCES

Abbott, S. B., Stornetta, R. L., Socolovsky, C. S., West, G. H., and Guyenet, P. G. (2009). Photostimulation of channelrhodopsin-2 expressing ventrolateral medullary neurons increases sympathetic nerve activity and blood pressure in rats. *J. Physiol.* 587, 5613–5631.

Adamantidis, A. R., Zhang, F., Aravanis, A. M., Deisseroth, K., and de Lecea, L. (2007). Neural substrates of awakening probed with optogenetic control of hypocretin neurons. *Nature* 450, 420–424.

Ahn, A. H., Dziennis, S., Hawkes, R., and Herrup, K. (1994). The cloning of zebrin II reveals its identity with aldolase C. *Development* 120, 2081–2090.

Allen-Sharpley, M. R., and Cramer, K. S. (2012). Coordinated Eph-ephrin signaling guides migration and axon targeting in the avian auditory system. *Neural Dev.* 7:29. doi: 10.1186/1749-8104-7-29

Altman, J., and Bayer, S. A. (1987). Development of the precerebellar nuclei in the rat: IV. The anterior precerebellar extramural migratory stream and the nucleus reticularis tegmenti pontis and the basal pontine gray. *J. Comp. Neurol.* 257, 529–552.

Altman, J. B. S. (1997). *Development of the Cerebellar System in Relation to its Evolution, Structure, and Functions.* New York, NY: CRC.

Angaut, P., Alvarado-Mallart, R. M., and Sotelo, C. (1985). Compensatory climbing fiber innervation after unilateral pedunculotomy in the newborn rat: origin and topographic organization. *J. Comp. Neurol.* 236, 161–178.

Apps, R., and Hawkes, R. (2009). Cerebellar cortical organization: a one-map hypothesis. *Nat. Rev. Neurosci.* 10, 670–681.

Arenkiel, B. R., Peca, J., Davison, I. G., Feliciano, C., Deisseroth, K., Augustine, G. J., et al. (2007). *In vivo* light-induced activation of neural circuitry in transgenic mice expressing channelrhodopsin-2. *Neuron* 54, 205–218.

Armstrong, C. L., and Hawkes, R. (2000). Pattern formation in the cerebellar cortex. *Biochem. Cell Biol.* 78, 551–562.

Armstrong, C. L., Krueger-Naug, A. M., Currie, R. W., and Hawkes, R. (2000). Constitutive expression of the 25-kDa heat shock protein Hsp25 reveals novel parasagittal bands of purkinje cells in the adult mouse cerebellar cortex. *J. Comp. Neurol.* 416, 383–397.

Armstrong, D. M., Harvey, R. J., and Schild, R. F. (1974). Topographical localization in the olivo-cerebellar projection: an electrophysiological study in the cat. *J. Comp. Neurol.* 154, 287–302.

Arsenio Nunes, M. L., and Sotelo, C. (1985). Development of the spinocerebellar system in the postnatal rat. *J. Comp. Neurol.* 237, 291–306.

Backer, S., Hidalgo-Sanchez, M., Offner, N., Portales-Casamar, E., Debant, A., Fort, P., et al. (2007). Trio controls the mature organization of neuronal clusters in the hindbrain. *J. Neurosci.* 27, 10323–10332.

Backer, S., Sakurai, T., Grumet, M., Sotelo, C., and Bloch-Gallego, E. (2002). Nr-CAM and TAG-1 are expressed in distinct populations of developing precerebellar and cerebellar neurons. *Neuroscience* 113, 743–748.

Belluardo, N., Mudo, G., Trovato-Salinaro, A., Le Gurun, S., Charollais, A., Serre-Beinier, V., et al. (2000). Expression of connexin36 in the adult and developing rat brain. *Brain Res.* 865, 121–138.

Blenkinsop, T. A., and Lang, E. J. (2006). Block of inferior olive gap junctional coupling decreases Purkinje cell complex spike synchrony and rhythmicity. *J. Neurosci.* 26, 1739–1748.

Bloch-Gallego, E., Ezan, F., Tessier-Lavigne, M., and Sotelo, C. (1999). Floor plate and netrin-1 are involved in the migration and survival of inferior olivary neurons. *J. Neurosci.* 19, 4407–4420.

Bosman, L. W., Takechi, H., Hartmann, J., Eilers, J., and Konnerth, A. (2008). Homosynaptic long-term synaptic potentiation of the "winner" climbing fiber synapse in developing Purkinje cells. *J. Neurosci.* 28, 798–807.

Bostan, A. C., Dum, R. P., and Strick, P. L. (2010). The basal ganglia communicate with the cerebellum. *Proc. Natl. Acad. Sci. U.S.A.* 107, 8452–8456.

Bourrat, F., and Sotelo, C. (1988). Migratory pathways and neuritic differentiation of inferior olivary neurons in the rat embryo. Axonal tracing study using the *in vitro* slab technique. *Brain Res.* 467, 19–37.

Bourrat, F., and Sotelo, C. (1990a). Early development of the rat precerebellar system: migratory routes, selective aggregation and neuritic differentiation of the inferior olive and lateral reticular nucleus neurons. An overview. *Arch. Ital. Biol.* 128, 151–170.

Bourrat, F., and Sotelo, C. (1990b). Migratory pathways and selective aggregation of the lateral reticular neurons in the rat embryo: a horseradish peroxidase *in vitro* study, with special reference to migration patterns of the precerebellar nuclei. *J. Comp. Neurol.* 294, 1–13.

Bourrat, F., and Sotelo, C. (1991). Relationships between neuronal birthdates and cytoarchitecture in the rat inferior olivary complex. *J. Comp. Neurol.* 313, 509–521.

Boyden, E. S., Zhang, F., Bamberg, E., Nagel, G., and Deisseroth, K. (2005). Millisecond-timescale, genetically targeted optical control

of neural activity. *Nat. Neurosci.* 8, 1263–1268.

Bozza, T., Feinstein, P., Zheng, C., and Mombaerts, P. (2002). Odorant receptor expression defines functional units in the mouse olfactory system. *J. Neurosci.* 22, 3033–3043.

Bradley, D. J., Ghelarducci, B., and Spyer, K. M. (1991). The role of the posterior cerebellar vermis in cardiovascular control. *Neurosci. Res.* 12, 45–56.

Bravin, M., Rossi, F., and Strata, P. (1995). Different climbing fibres innervate separate dendritic regions of the same Purkinje cell in hypogranular cerebellum. *J. Comp. Neurol.* 357, 395–407.

Brochu, G., Maler, L., and Hawkes, R. (1990). Zebrin II: a polypeptide antigen expressed selectively by Purkinje cells reveals compartments in rat and fish cerebellum. *J. Comp. Neurol.* 291, 538–552.

Cajal, R. Y. (1911). *Histologie du Systeme Nerveux de l'homme et des Vertebres*. Vol. II. Paris: Maloine.

Callaway, E. M. (2008). Transneuronal circuit tracing with neurotropic viruses. *Curr. Opin. Neurobiol.* 18, 617–623.

Cang, J., Niell, C. M., Liu, X., Pfeiffenberger, C., Feldheim, D. A., and Stryker, M. P. (2008a). Selective disruption of one Cartesian axis of cortical maps and receptive fields by deficiency in ephrin-As and structured activity. *Neuron* 57, 511–523.

Cang, J., Wang, L., Stryker, M. P., and Feldheim, D. A. (2008b). Roles of ephrin-as and structured activity in the development of functional maps in the superior colliculus. *J. Neurosci.* 28, 11015–11023.

Causeret, F., Danne, F., Ezan, F., Sotelo, C., and Bloch-Gallego, E. (2002). Slit antagonizes netrin-1 attractive effects during the migration of inferior olivary neurons. *Dev. Biol.* 246, 429–440.

Cerminara, N. L. (2010). Cerebellar modules: individual or composite entities? *J. Neurosci.* 30, 16065–16067.

Cerminara, N. L., and Apps, R. (2011). Behavioural significance of cerebellar modules. *Cerebellum* 10, 484–494.

Chedotal, A., Pourquie, O., Ezan, F., San Clemente, H., and Sotelo, C. (1996). BEN as a presumptive target recognition molecule during the development of the olivocerebellar system. *J. Neurosci.* 16, 3296–3310.

Chedotal, A., and Sotelo, C. (1992). Early development of olivocerebellar projections in the fetal rat using CGRP immunocytochemistry. *Eur. J. Neurosci.* 4, 1159–1179.

Chedotal, A., and Sotelo, C. (1993). The 'creeper stage' in cerebellar climbing fiber synaptogenesis precedes the 'pericellular nest'–ultrastructural evidence with parvalbumin immunocytochemistry. *Brain Res. Dev. Brain Res.* 76, 207–220.

Chen, L., Bao, S., Lockard, J. M., Kim, J. K., and Thompson, R. F. (1996). Impaired classical eyeblink conditioning in cerebellar-lesioned and Purkinje cell degeneration (pcd) mutant mice. *J. Neurosci.* 16, 2829–2838.

Chockkan, V., and Hawkes, R. (1994). Functional and antigenic maps in the rat cerebellum: zebrin compartmentation and vibrissal receptive fields in lobule IXa. *J. Comp. Neurol.* 345, 33–45.

Coffman, K. A., Dum, R. P., and Strick, P. L. (2011). Cerebellar vermis is a target of projections from the motor areas in the cerebral cortex. *Proc. Natl. Acad. Sci. U.S.A.* 108, 16068–16073.

Coulon, P., Derbin, C., Kucera, P., Lafay, F., Prehaud, C., and Flamand, A. (1989). Invasion of the peripheral nervous systems of adult mice by the CVS strain of rabies virus and its avirulent derivative AvO1. *J. Virol.* 63, 3550–3554.

Crepel, F., and Delhaye-Bouchaud, N. (1979). Distribution of climbing fibres on cerebellar Purkinje cells in X-irradiated rats. An electrophysiological study. *J. Physiol.* 290, 97–112.

Crepel, F., Delhaye-Bouchaud, N., Guastavino, J. M., and Sampaio, I. (1980). Multiple innervation of cerebellar Purkinje cells by climbing fibres in staggerer mutant mouse. *Nature* 283, 483–484.

Crepel, F., and Mariani, J. (1976). Multiple innervation of Purkinje cells by climbing fibers in the cerebellum of the weaver mutant mouse. *J. Neurobiol.* 7, 579–582.

Crepel, F., Mariani, J., and Delhaye-Bouchaud, N. (1976). Evidence for a multiple innervation of Purkinje cells by climbing fibers in the immature rat cerebellum. *J. Neurobiol.* 7, 567–578.

Cummings, S. L., Young, W. S. 3rd., Bishop, G. A., De Souza, E. B., and King, J. S. (1989). Distribution of corticotropin-releasing factor in the cerebellum and precerebellar nuclei of the opossum: a study utilizing immunohistochemistry, *in situ* hybridization histochemistry, and receptor autoradiography. *J. Comp. Neurol.* 280, 501–521.

de Diego, I., Kyriakopoulou, K., Karagogeos, D., and Wassef, M. (2002). Multiple influences on the migration of precerebellar neurons in the caudal medulla. *Development* 129, 297–306.

Degen, J., Meier, C., Van Der Giessen, R. S., Sohl, G., Petrasch-Parwez, E., Urschel, S., et al. (2004). Expression pattern of lacZ reporter gene representing connexin36 in transgenic mice. *J. Comp. Neurol.* 473, 511–525.

Dehnes, Y., Chaudhry, F. A., Ullensvang, K., Lehre, K. P., Storm-Mathisen, J., and Danbolt, N. C. (1998). The glutamate transporter EAAT4 in rat cerebellar Purkinje cells: a glutamate-gated chloride channel concentrated near the synapse in parts of the dendritic membrane facing astroglia. *J. Neurosci.* 18, 3606–3619.

Deisseroth, K., Feng, G., Majewska, A. K., Miesenbock, G., Ting, A., and Schnitzer, M. J. (2006). Next-generation optical technologies for illuminating genetically targeted brain circuits. *J. Neurosci.* 26, 10380–10386.

Demilly, A., Reeber, S. L., Gebre, S. A., and Sillitoe, R. V. (2011). Neurofilament heavy chain expression reveals a unique parasagittal stripe topography in the mouse cerebellum. *Cerebellum* 10, 409–421.

Dixon, K. J., Hilber, W., Speare, S., Willson, M. L., Bower, A. J., and Sherrard, R. M. (2005). Post-lesion transcommissural olivocerebellar reinnervation improves motor function following unilateral pedunculotomy in the neonatal rat. *Exp. Neurol.* 196, 254–265.

Dixon, K. J., and Sherrard, R. M. (2006). Brain-derived neurotrophic factor induces post-lesion transcommissural growth of olivary axons that develop normal climbing fibers on mature Purkinje cells. *Exp. Neurol.* 202, 44–56.

Ebner, T. J., Wang, X., Gao, W., Cramer, S. W., and Chen, G. (2012). Parasagittal zones in the cerebellar cortex differ in excitability, information processing, and synaptic plasticity. *Cerebellum* 11, 418–419.

Ekerot, C. F., and Larson, B. (1980). Termination in overlapping sagittal zones in cerebellar anterior lobe of mossy and climbing fiber paths activated from dorsal funiculus. *Exp. Brain Res.* 38, 163–172.

Errante, L., Tang, D., Gardon, M., Sekerkova, G., Mugnaini, E., and Shaw, G. (1998). The intermediate filament protein peripherin is a marker for cerebellar climbing fibres. *J. Neurocytol.* 27, 69–84.

Flanagan, J. G., and Vanderhaeghen, P. (1998). The ephrins and Eph receptors in neural development. *Annu. Rev. Neurosci.* 21, 309–345.

Friedman, G. C., and O'Leary, D. D. (1996). Retroviral misexpression of engrailed genes in the chick optic tectum perturbs the topographic targeting of retinal axons. *J. Neurosci.* 16, 5498–5509.

Fujita, H., Oh-Nishi, A., Obayashi, S., and Sugihara, I. (2010). Organization of the marmoset cerebellum in three-dimensional space: lobulation, aldolase C compartmentalization and axonal projection. *J. Comp. Neurol.* 518, 1764–1791.

Graf, W., Gerrits, N., Yatim-Dhiba, N., and Ugolini, G. (2002). Mapping the oculomotor system: the power of transneuronal labelling with rabies virus. *Eur. J. Neurosci.* 15, 1557–1562.

Graham, D. J., and Wylie, D. R. (2012). Zebrin-immunopositive and -immunonegative stripe pairs represent functional units in the pigeon vestibulocerebellum. *J. Neurosci.* 32, 12769–12779.

Hallem, J. S., Thompson, J. H., Gundappa-Sulur, G., Hawkes, R., Bjaalie, J. G., and Bower, J. M. (1999). Spatial correspondence between tactile projection patterns and the distribution of the antigenic Purkinje cell markers anti-zebrin I and anti-zebrin II in the cerebellar folium crus IIA of the rat. *Neuroscience* 93, 1083–1094.

Hashimoto, K., Ichikawa, R., Kitamura, K., Watanabe, M., and Kano, M. (2009). Translocation of a "winner" climbing fiber to the Purkinje cell dendrite and subsequent elimination of "losers" from the soma in developing cerebellum. *Neuron* 63, 106–118.

Hashimoto, K., and Kano, M. (2003). Functional differentiation of multiple climbing fiber inputs during synapse elimination in the developing cerebellum. *Neuron* 38, 785–796.

Hashimoto, K., and Kano, M. (2005). Postnatal development and synapse elimination of climbing fiber to Purkinje cell projection in the cerebellum. *Neurosci. Res.* 53, 221–228.

Hashimoto, K., Tsujita, M., Miyazaki, T., Kitamura, K., Yamazaki, M., Shin, H. S., et al. (2011). Postsynaptic P/Q-type Ca2+ channel in Purkinje cell mediates synaptic competition and elimination in developing cerebellum. *Proc. Natl. Acad. Sci. U.S.A.* 108, 9987–9992.

Hashimoto, M., and Hibi, M. (2012). Development and evolution of cerebellar neural circuits. *Dev. Growth Differ.* 54, 373–389.

Hashimoto, M., Ito, R., Kitamura, N., Namba, K., and Hisano, Y. (2012). Epha4 controls the midline crossing and contralateral axonal projections of inferior olive neurons. *J. Comp. Neurol.* 520, 1702–1720.

Hashimoto, M., and Mikoshiba, K. (2003). Mediolateral compartmentalization of the cerebellum is determined on the "birth date" of Purkinje cells. *J. Neurosci.* 23, 11342–11351.

Hawkes, R., Colonnier, M., and Leclerc, N. (1985). Monoclonal antibodies reveal sagittal banding in the rodent cerebellar cortex. *Brain Res.* 333, 359–365.

Hawkes, R., and Herrup, K. (1995). Aldolase C/zebrin II and the regionalization of the cerebellum. *J. Mol. Neurosci.* 6, 147–158.

Hawkes, R., and Leclerc, N. (1987). Antigenic map of the rat cerebellar cortex: the distribution of parasagittal bands as revealed by monoclonal anti-Purkinje cell antibody mabQ113. *J. Comp. Neurol.* 256, 29–41.

Hidalgo-Sanchez, M., Backer, S., Puelles, L., and Bloch-Gallego, E. (2012). Origin and plasticity of the subdivisions of the inferior olivary complex. *Dev. Biol.* 371, 215–226.

Hira, R., Honkura, N., Noguchi, J., Maruyama, Y., Augustine, G. J., Kasai, H., et al. (2009). Transcranial optogenetic stimulation for functional mapping of the motor cortex. *J. Neurosci. Methods* 179, 258–263.

Hirai, H., Pang, Z., Bao, D., Miyazaki, T., Li, L., Miura, E., et al. (2005). Cbln1 is essential for synaptic integrity and plasticity in the cerebellum. *Nat. Neurosci.* 8, 1534–1541.

Hisano, S., Sawada, K., Kawano, M., Kanemoto, M., Xiong, G., Mogi, K., et al. (2002). Expression of inorganic phosphate/vesicular glutamate transporters (BNPI/VGLUT1 and DNPI/VGLUT2) in the cerebellum and precerebellar nuclei of the rat. *Brain Res. Mol. Brain Res.* 107, 23–31.

Horn, K. M., Pong, M., and Gibson, A. R. (2010). Functional relations of cerebellar modules of the cat. *J. Neurosci.* 30, 9411–9423.

Hoshino, M., Nakamura, S., Mori, K., Kawauchi, T., Terao, M., Nishimura, Y. V., et al. (2005). Ptf1a, a bHLH transcriptional gene, defines GABAergic neuronal fates in cerebellum. *Neuron* 47, 201–213.

Hubel, D. H., and Wiesel, T. N. (1979). Brain mechanisms of vision. *Sci. Am.* 241, 150–162.

Huffman, K. J., and Cramer, K. S. (2007). EphA4 misexpression alters tonotopic projections in the auditory brainstem. *Dev. Neurobiol.* 67, 1655–1668.

Ichikawa, R., Miyazaki, T., Kano, M., Hashikawa, T., Tatsumi, H., Sakimura, K., et al. (2002). Distal extension of climbing fiber territory and multiple innervation caused by aberrant wiring to adjacent spiny branchlets in cerebellar Purkinje cells lacking glutamate receptor delta 2. *J. Neurosci.* 22, 8487–8503.

Jaarsma, D., Ruigrok, T. J., Caffe, R., Cozzari, C., Levey, A. I., Mugnaini, E., et al. (1997). Cholinergic innervation and receptors in the cerebellum. *Prog. Brain Res.* 114, 67–96.

Johnston, A. (1989). The geometry of the topographic map in striate cortex. *Vision Res.* 29, 1493–1500.

Kano, M., and Hashimoto, K. (2009). Synapse elimination in the central nervous system. *Curr. Opin. Neurobiol.* 19, 154–161.

Kano, M., Hashimoto, K., Chen, C., Abeliovich, A., Aiba, A., Kurihara, H., et al. (1995). Impaired synapse elimination during cerebellar development in PKC gamma mutant mice. *Cell* 83, 1223–1231.

Kano, M., Hashimoto, K., Kurihara, H., Watanabe, M., Inoue, Y., Aiba, A., et al. (1997). Persistent multiple climbing fiber innervation of cerebellar Purkinje cells in mice lacking mGluR1. *Neuron* 18, 71–79.

Kano, M., Hashimoto, K., Watanabe, M., Kurihara, H., Offermanns, S., Jiang, H., et al. (1998). Phospholipase cbeta4 is specifically involved in climbing fiber synapse elimination in the developing cerebellum. *Proc. Natl. Acad. Sci. U.S.A.* 95, 15724–15729.

Karam, S. D., Burrows, R. C., Logan, C., Koblar, S., Pasquale, E. B., and Bothwell, M. (2000). Eph receptors and ephrins in the developing chick cerebellum: relationship to sagittal patterning and granule cell migration. *J. Neurosci.* 20, 6488–6500.

Karam, S. D., Dottori, M., Ogawa, K., Henderson, J. T., Boyd, A. W., Pasquale, E. B., et al. (2002). EphA4 is not required for Purkinje cell compartmentation. *Brain Res. Dev. Brain Res.* 135, 29–38.

Kashiwabuchi, N., Ikeda, K., Araki, K., Hirano, T., Shibuki, K., Takayama, C., et al. (1995). Impairment of motor coordination, Purkinje cell synapse formation, and cerebellar long-term depression in GluR delta 2 mutant mice. *Cell* 81, 245–252.

Kelly, R. M., and Strick, P. L. (2000). Rabies as a transneuronal tracer of circuits in the central nervous system. *J. Neurosci. Methods* 103, 63–71.

Kelly, R. M., and Strick, P. L. (2003). Cerebellar loops with motor cortex and prefrontal cortex of a nonhuman primate. *J. Neurosci.* 23, 8432–8444.

Landsberg, R. L., Awatramani, R. B., Hunter, N. L., Farago, A. F., DiPietrantonio, H. J., Rodriguez, C. I., et al. (2005). Hindbrain rhombic lip is comprised of discrete progenitor cell populations allocated by Pax6. *Neuron* 48, 933–947.

Lang, E. J., Sugihara, I., Welsh, J. P., and Llinas, R. (1999). Patterns of spontaneous purkinje cell complex spike activity in the awake rat. *J. Neurosci.* 19, 2728–2739.

Larouche, M., Che, P. M., and Hawkes, R. (2006). Neurogranin expression identifies a novel array of Purkinje cell parasagittal stripes during mouse cerebellar development. *J. Comp. Neurol.* 494, 215–227.

Larsell, O. (1952). The morphogenesis and adult pattern of the lobules and fissures of the cerebellum of the white rat. *J. Comp. Neurol.* 97, 281–356.

Leergaard, T. B., and Bjaalie, J. G. (2007). Topography of the complete corticopontine projection: from experiments to principal Maps. *Front. Neurosci.* 1:1. doi: 10.3389/neuro.01.1.1.016.2007

Li, H., and Crair, M. C. (2011). How do barrels form in somatosensory cortex? *Ann. N.Y. Acad. Sci.* 1225, 119–129.

Llinas, R., and Sasaki, K. (1989). The functional organization of the olivocerebellar system as examined by multiple Purkinje cell recordings. *Eur. J. Neurosci.* 1, 587–602.

Llinas, R., Walton, K., Hillman, D. E., and Sotelo, C. (1975). Inferior olive: its role in motor learing. *Science* 190, 1230–1231.

Logan, C., Wizenmann, A., Drescher, U., Monschau, B., Bonhoeffer, F., and Lumsden, A. (1996). Rostral optic tectum acquires caudal characteristics following ectopic engrailed expression. *Curr. Biol.* 6, 1006–1014.

Machold, R., and Fishell, G. (2005). Math1 is expressed in temporally discrete pools of cerebellar rhombic-lip neural progenitors. *Neuron* 48, 17–24.

Madisen, L., Zwingman, T. A., Sunkin, S. M., Wook Oh, S., Zariwala, H. A., Gu, H., et al. (2010). A robust and high-throughput Cre reporting and characterization system for the whole mouse brain. *Nat. Neurosci.* 13, 133–140.

Maklad, A., and Fritzsch, B. (2003). Partial segregation of posterior crista and saccular fibers to the nodulus and uvula of the cerebellum in mice, and its development. *Brain Res. Dev. Brain Res.* 140, 223–236.

Mariani, J., and Changeux, J. P. (1980). Multiple innervation of Purkinje cells by climbing fibers in the cerebellum of the adult staggerer mutant mouse. *J. Neurobiol.* 11, 41–50.

Mariani, J., and Changeux, J. P. (1981). Ontogenesis of olivocerebellar relationships. I. Studies by intracellular recordings of the multiple innervation of Purkinje cells by climbing fibers in the developing rat cerebellum. *J. Neurosci.* 1, 696–702.

Mariani, J., Crepel, F., Mikoshiba, K., Changeux, J. P., and Sotelo, C. (1977). Anatomical, physiological and biochemical studies of the cerebellum from Reeler mutant mouse. *Philos. Trans. R. Soc. Lond. B Biol. Sci.* 281, 1–28.

Marillat, V., Sabatier, C., Failli, V., Matsunaga, E., Sotelo, C., Tessier-Lavigne, M., et al. (2004). The slit receptor Rig-1/Robo3 controls midline crossing by hindbrain precerebellar neurons and axons. *Neuron* 43, 69–79.

Marshel, J. H., Mori, T., Nielsen, K. J., and Callaway, E. M. (2010). Targeting single neuronal networks for gene expression and cell labeling *in vivo*. *Neuron* 67, 562–574.

Martin, E. I., Ressler, K. J., Jasnow, A. M., Dabrowska, J., Hazra, R., Rainnie, D. G., et al. (2010). A novel transgenic mouse for gene-targeting within cells that express corticotropin-releasing factor. *Biol. Psychiatry* 67, 1212–1216.

Mason, C. A., Christakos, S., and Catalano, S. M. (1990). Early climbing fiber interactions with Purkinje cells in the postnatal mouse cerebellum. *J. Comp. Neurol.* 297, 77–90.

Mason, C. A., and Gregory, E. (1984). Postnatal maturation of cerebellar mossy and climbing fibers: transient expression of dual features on single axons. *J. Neurosci.* 4, 1715–1735.

McCormick, D. A., and Thompson, R. F. (1984). Cerebellum: essential involvement in the classically conditioned eyelid response. *Science* 223, 296–299.

Miyazaki, T., Hashimoto, K., Shin, H. S., Kano, M., and Watanabe, M. (2004). P/Q-type Ca2+ channel alpha1A regulates synaptic competition on developing cerebellar Purkinje cells. *J. Neurosci.* 24, 1734–1743.

Miyazaki, T., Yamasaki, M., Takeuchi, T., Sakimura, K., Mishina, M., and Watanabe, M. (2010). Ablation of glutamate receptor GluRdelta2 in adult Purkinje cells causes multiple innervation of climbing fibers by inducing aberrant invasion to parallel fiber innervation territory. *J. Neurosci.* 30, 15196–15209.

Morara, S., Marcotti, W., Provini, L., and Rosina, A. (1997). Neuropeptide, Y (NPY) expression is up-regulated in the rat inferior olive during development. *Neuroreport* 8, 3743–3747.

Morara, S., Rosina, A., and Provini, L. (1992). CGRP as a marker of the climbing fibers during the development of the cerebellum in the rat. *Ann. N.Y. Acad. Sci.* 657, 461–463.

Nakayama, H., Miyazaki, T., Kitamura, K., Hashimoto, K., Yanagawa, Y., Obata, K., et al. (2012). GABAergic inhibition regulates developmental synapse elimination in the cerebellum. *Neuron* 74, 384–396.

Namba, K., Sugihara, I., and Hashimoto, M. (2011). Close correlation between the birth date of Purkinje cells and the longitudinal compartmentalization of the mouse adult cerebellum. *J. Comp. Neurol.* 519, 2594–2614.

Neudert, F., Nuernberger, K. K., and Redies, C. (2008). Comparative analysis of cadherin expression and connectivity patterns in the cerebellar system of ferret and mouse. *J. Comp. Neurol.* 511, 736–752.

Nicholls, J., and Saunders, N. (1996). Regeneration of immature mammalian spinal cord after injury. *Trends Neurosci.* 19, 229–234.

Nichols, D. H., and Bruce, L. L. (2006). Migratory routes and fates of cells transcribing the Wnt-1 gene in the murine hindbrain. *Dev. Dyn.* 235, 285–300.

Nishida, K., Flanagan, J. G., and Nakamoto, M. (2002). Domain-specific olivocerebellar projection regulated by the EphA-ephrin-A interaction. *Development* 129, 5647–5658.

Nishiyama, H., Fukaya, M., Watanabe, M., and Linden, D. J. (2007). Axonal motility and its modulation by activity are branch-type specific in the intact adult cerebellum. *Neuron* 56, 472–487.

O'Hearn, E., Long, D. B., and Molliver, M. E. (1993). Ibogaine induces glial activation in parasagittal zones of the cerebellum. *Neuroreport* 4, 299–302.

O'Hearn, E., and Molliver, M. E. (1993). Degeneration of Purkinje cells in parasagittal zones of the cerebellar vermis after treatment with ibogaine or harmaline. *Neuroscience* 55, 303–310.

O'Leary, J. L., Inukai, J., and Smith, J. M. (1971). Histogenesis of the cerebellar climbing fiber in the rat. *J. Comp. Neurol.* 142, 377–391.

Oberdick, J., Smeyne, R. J., Mann, J. R., Zackson, S., and Morgan, J. I. (1990). A promoter that drives transgene expression in cerebellar Purkinje and retinal bipolar neurons. *Science* 248, 223–226.

Offermanns, S., Hashimoto, K., Watanabe, M., Sun, W., Kurihara, H., Thompson, R. F., et al. (1997). Impaired motor coordination and persistent multiple climbing fiber innervation of cerebellar Purkinje cells in mice lacking Galphaq. *Proc. Natl. Acad. Sci. U.S.A.* 94, 14089–14094.

Ozol, K., Hayden, J. M., Oberdick, J., and Hawkes, R. (1999). Transverse zones in the vermis of the mouse cerebellum. *J. Comp. Neurol.* 412, 95–111.

Pakan, J. M., and Wylie, D. R. (2008). Congruence of zebrin II expression and functional zones defined by climbing fiber topography in the flocculus. *Neuroscience* 157, 57–69.

Paradies, M. A., and Eisenman, L. M. (1993). Evidence of early topographic organization in the embryonic olivocerebellar projection: a model system for the study of pattern formation processes in the central nervous system. *Dev. Dyn.* 197, 125–145.

Paradies, M. A., Grishkat, H., Smeyne, R. J., Oberdick, J., Morgan, J. I., and Eisenman, L. M. (1996). Correspondence between L7-lacZ-expressing Purkinje cells and labeled olivocerebellar fibers during late embryogenesis in the mouse. *J. Comp. Neurol.* 374, 451–466.

Pascual, M., Abasolo, I., Mingorance-Le Meur, A., Martinez, A., Del Rio, J. A., Wright, C. V., et al. (2007). Cerebellar GABAergic progenitors adopt an external granule cell-like phenotype in the absence of Ptf1a transcription factor expression. *Proc. Natl. Acad. Sci. U.S.A.* 104, 5193–5198.

Paukert, M., Huang, Y. H., Tanaka, K., Rothstein, J. D., and Bergles, D. E. (2010). Zones of enhanced glutamate release from climbing fibers in the mammalian cerebellum. *J. Neurosci.* 30, 7290–7299.

Pierce, E. T. (1973). Time of origin of neurons in the brain stem of the mouse. *Prog. Brain Res.* 40, 53–65.

Pijpers, A., Winkelman, B. H., Bronsing, R., and Ruigrok, T. J. (2008). Selective impairment of the cerebellar C1 module involved in rat hind limb control reduces step-dependent modulation of cutaneous reflexes. *J. Neurosci.* 28, 2179–2189.

Rancz, E. A., Franks, K. M., Schwarz, M. K., Pichler, B., Schaefer, A. T., and Margrie, T. W. (2011). Transfection via whole-cell recording *in vivo*: bridging single-cell physiology, genetics and connectomics. *Nat. Neurosci.* 14, 527–532.

Redies, C., Neudert, F., and Lin, J. (2011). Cadherins in cerebellar development: translation of embryonic patterning into mature functional compartmentalization. *Cerebellum* 10, 393–408.

Reeber, S. L., and Sillitoe, R. V. (2011). Patterned expression of a cocaine- and amphetamine-regulated transcript peptide reveals complex circuit topography in the rodent cerebellar cortex. *J. Comp. Neurol.* 519, 1781–1796.

Rekling, J. C., Jensen, K. H., and Jahnsen, H. (2012). Spontaneous cluster activity in the inferior olivary nucleus in brainstem slices from postnatal mice. *J. Physiol.* 590, 1547–1562.

Rodriguez, C. I., and Dymecki, S. M. (2000). Origin of the precerebellar system. *Neuron* 27, 475–486.

Ruigrok, T. J. (2011). Ins and outs of cerebellar modules. *Cerebellum* 10, 464–474.

Sacchetti, B., Scelfo, B., and Strata, P. (2009). Cerebellum and emotional behavior. *Neuroscience* 162, 756–762.

Sarna, J. R., Marzban, H., Watanabe, M., and Hawkes, R. (2006). Complementary stripes of phospholipase Cbeta3 and Cbeta4 expression by Purkinje cell subsets in the mouse cerebellum. *J. Comp. Neurol.* 496, 303–313.

Sasaki, K., Bower, J. M., and Llinas, R. (1989). Multiple Purkinje cell recording in rodent cerebellar cortex. *Eur. J. Neurosci.* 1, 572–586.

Sawada, K., Fukui, Y., and Hawkes, R. (2008). Spatial distribution of corticotropin-releasing factor immunopositive climbing fibers in the mouse cerebellum: analysis by whole mount immunohistochemistry. *Brain Res.* 1222, 106–117.

Sawada, K., Sakata-Haga, H., Hisano, S., and Fukui, Y. (2001). Topological relationship between corticotropin-releasing factor-immunoreactive cerebellar afferents and tyrosine hydroxylase-immunoreactive Purkinje cells in a hereditary ataxic mutant, rolling mouse Nagoya. *Neuroscience* 102, 925–935.

Seoane, A., Apps, R., Balbuena, E., Herrero, L., and Llorens, J. (2005). Differential effects of trans-crotononitrile and 3-acetylpyridine on inferior olive integrity and behavioural performance in the rat. *Eur. J. Neurosci.* 22, 880–894.

Sherrard, R. M., Bower, A. J., and Payne, J. N. (1986). Innervation of the adult rat cerebellar hemisphere by fibres from the ipsilateral inferior olive following unilateral neonatal pedunculotomy: an autoradiographic and retrograde fluorescent double-labelling study. *Exp. Brain Res.* 62, 411–421.

Sillitoe, R. V., Gopal, N., and Joyner, A. L. (2009). Embryonic origins of ZebrinII parasagittal stripes and establishment of topographic Purkinje cell projections. *Neuroscience* 162, 574–588.

Sillitoe, R. V., and Hawkes, R. (2002). Whole-mount immunohistochemistry: a high-throughput screen for patterning defects in the mouse cerebellum. *J. Histochem. Cytochem.* 50, 235–244.

Sillitoe, R. V., and Joyner, A. L. (2007). Morphology, molecular codes, and circuitry produce the three-dimensional complexity of the cerebellum. *Annu. Rev. Cell Dev. Biol.* 23, 549–577.

Sillitoe, R. V., Marzban, H., Larouche, M., Zahedi, S., Affanni, J., and Hawkes, R. (2005). Conservation of the architecture of the anterior lobe vermis of the cerebellum across mammalian species. *Prog. Brain Res.* 148, 283–297.

Sillitoe, R. V., Vogel, M. W., and Joyner, A. L. (2010). Engrailed homeobox genes regulate establishment of the cerebellar afferent circuit map. *J. Neurosci.* 30, 10015–10024.

Soriano, P. (1999). Generalized lacZ expression with the ROSA26 Cre reporter strain. *Nat. Genet.* 21, 70–71.

Sotelo, C. (2004). Cellular and genetic regulation of the development of the cerebellar system. *Prog. Neurobiol.* 72, 295–339.

Sotelo, C., Bourrat, F., and Triller, A. (1984). Postnatal development of the inferior olivary complex in the rat. II. Topographic organization of the immature olivocerebellar projection. *J. Comp. Neurol.* 222, 177–199.

Sotelo, C., and Chedotal, A. (1997). Development of the olivocerebellar projection. *Perspect. Dev. Neurobiol.* 5, 57–67.

Sotelo, C., and Chedotal, A. (2005). Development of the olivocerebellar system: migration and formation

of cerebellar maps. *Prog. Brain Res.* 148, 1–20.

Sotelo, C., and Wassef, M. (1991). Cerebellar development: afferent organization and Purkinje cell heterogeneity. *Philos. Trans. R. Soc. Lond. B Biol. Sci.* 331, 307–313.

Steinmayr, M., Andre, E., Conquet, F., Rondi-Reig, L., Delhaye-Bouchaud, N., Auclair, N., et al. (1998). staggerer phenotype in retinoid-related orphan receptor alpha-deficient mice. *Proc. Natl. Acad. Sci. U.S.A.* 95, 3960–3965.

Strata, P., Scelfo, B., and Sacchetti, B. (2011). Involvement of cerebellum in emotional behavior. *Physiol. Res.* 60(Suppl. 1), S39–S48.

Strick, P. L., Dum, R. P., and Fiez, J. A. (2009). Cerebellum and nonmotor function. *Annu. Rev. Neurosci.* 32, 413–434.

Sudarov, A., and Joyner, A. L. (2007). Cerebellum morphogenesis: the foliation pattern is orchestrated by multi-cellular anchoring centers. *Neural Dev.* 2:26. doi: 10.1186/1749-8104-2-26

Sudarov, A., Turnbull, R. K., Kim, E. J., Lebel-Potter, M., Guillemot, F., and Joyner, A. L. (2011). Ascl1 genetics reveals insights into cerebellum local circuit assembly. *J. Neurosci.* 31, 11055–11069.

Sugihara, I. (2005). Microzonal projection and climbing fiber remodeling in single olivocerebellar axons of newborn rats at postnatal days 4–7. *J. Comp. Neurol.* 487, 93–106.

Sugihara, I., Bailly, Y., and Mariani, J. (2000). Olivocerebellar climbing fibers in the granuloprival cerebellum: morphological study of individual axonal projections in the X-irradiated rat. *J. Neurosci.* 20, 3745–3760.

Sugihara, I., Fujita, H., Na, J., Quy, P. N., Li, B. Y., and Ikeda, D. (2009). Projection of reconstructed single Purkinje cell axons in relation to the cortical and nuclear aldolase C compartments of the rat cerebellum. *J. Comp. Neurol.* 512, 282–304.

Sugihara, I., Lang, E. J., and Llinas, R. (1995). Serotonin modulation of inferior olivary oscillations and synchronicity: a multiple-electrode study in the rat cerebellum. *Eur. J. Neurosci.* 7, 521–534.

Sugihara, I., Lohof, A. M., Letellier, M., Mariani, J., and Sherrard, R. M. (2003). Post-lesion transcommissural growth of olivary climbing fibres creates functional synaptic microzones. *Eur. J. Neurosci.* 18, 3027–3036.

Sugihara, I., and Quy, P. N. (2007). Identification of aldolase C compartments in the mouse cerebellar cortex by olivocerebellar labeling. *J. Comp. Neurol.* 500, 1076–1092.

Sugihara, I., and Shinoda, Y. (2004). Molecular, topographic, and functional organization of the cerebellar cortex: a study with combined aldolase C and olivocerebellar labeling. *J. Neurosci.* 24, 8771–8785.

Sugihara, I., and Shinoda, Y. (2007). Molecular, topographic, and functional organization of the cerebellar nuclei: analysis by three-dimensional mapping of the olivonuclear projection and aldolase C labeling. *J. Neurosci.* 27, 9696–9710.

Sugihara, I., Wu, H., and Shinoda, Y. (1999). Morphology of single olivocerebellar axons labeled with biotinylated dextran amine in the rat. *J. Comp. Neurol.* 414, 131–148.

Suzuki, L., Coulon, P., Sabel-Goedknegt, E. H., and Ruigrok, T. J. (2012). Organization of cerebral projections to identified cerebellar zones in the posterior cerebellum of the rat. *J. Neurosci.* 32, 10854–10869.

Suzuki, S. C., Inoue, T., Kimura, Y., Tanaka, T., and Takeichi, M. (1997). Neuronal circuits are subdivided by differential expression of type-II classic cadherins in postnatal mouse brains. *Mol. Cell. Neurosci.* 9, 433–447.

Tanahira, C., Higo, S., Watanabe, K., Tomioka, R., Ebihara, S., Kaneko, T., et al. (2009). Parvalbumin neurons in the forebrain as revealed by parvalbumin-Cre transgenic mice. *Neurosci. Res.* 63, 213–223.

Taniguchi, H., He, M., Wu, P., Kim, S., Paik, R., Sugino, K., et al. (2011). A resource of Cre driver lines for genetic targeting of GABAergic neurons in cerebral cortex. *Neuron* 71, 995–1013.

Terada, N., Banno, Y., Ohno, N., Fujii, Y., Murate, T., Sarna, J. R., et al. (2004). Compartmentation of the mouse cerebellar cortex by sphingosine kinase. *J. Comp. Neurol.* 469, 119–127.

Tsubota, T., Ohashi, Y., Tamura, K., Sato, A., and Miyashita, Y. (2011). Optogenetic manipulation of cerebellar Purkinje cell activity *in vivo*. *PLoS ONE* 6:e22400. doi: 10.1371/journal.pone.0022400

Uemura, T., Kakizawa, S., Yamasaki, M., Sakimura, K., Watanabe, M., Iino, M., et al. (2007). Regulation of long-term depression and climbing fiber territory by glutamate receptor delta2 at parallel fiber synapses through its C-terminal domain in cerebellar Purkinje cells. *J. Neurosci.* 27, 12096–12108.

Uesaka, N., Mikuni, T., Hashimoto, K., Hirai, H., Sakimura, K., and Kano, M. (2012). Organotypic coculture preparation for the study of developmental synapse elimination in mammalian brain. *J. Neurosci.* 32, 11657–11670.

Ueyama, T., Houtani, T., Nakagawa, H., Baba, K., Ikeda, M., Yamashita, T., et al. (1994). A subpopulation of olivocerebellar projection neurons express neuropeptide Y. *Brain Res.* 634, 353–357.

Ugolini, G. (1995). Specificity of rabies virus as a transneuronal tracer of motor networks: transfer from hypoglossal motoneurons to connected second-order and higher order central nervous system cell groups. *J. Comp. Neurol.* 356, 457–480.

Van Der Giessen, R. S., Maxeiner, S., French, P. J., Willecke, K., and De Zeeuw, C. I. (2006). Spatiotemporal distribution of Connexin45 in the olivocerebellar system. *J. Comp. Neurol.* 495, 173–184.

Voogd, J., Pardoe, J., Ruigrok, T. J., and Apps, R. (2003). The distribution of climbing and mossy fiber collateral branches from the copula pyramidis and the paramedian lobule: congruence of climbing fiber cortical zones and the pattern of zebrin banding within the rat cerebellum. *J. Neurosci.* 23, 4645–4656.

Voogd, J., and Ruigrok, T. J. (2004). The organization of the corticonuclear and olivocerebellar climbing fiber projections to the rat cerebellar vermis: the congruence of projection zones and the zebrin pattern. *J. Neurocytol.* 33, 5–21.

Wadiche, J. I., and Jahr, C. E. (2005). Patterned expression of Purkinje cell glutamate transporters controls synaptic plasticity. *Nat. Neurosci.* 8, 1329–1334.

Wall, N. R., Wickersham, I. R., Cetin, A., De La Parra, M., and Callaway, E. M. (2010). Monosynaptic circuit tracing *in vivo* through Cre-dependent targeting and complementation of modified rabies virus. *Proc. Natl. Acad. Sci. U.S.A.* 107, 21848–21853.

Wang, V. Y., Rose, M. F., and Zoghbi, H. Y. (2005). Math1 expression redefines the rhombic lip derivatives and reveals novel lineages within the brainstem and cerebellum. *Neuron* 48, 31–43.

Wassef, M., Chedotal, A., Cholley, B., Thomasset, M., Heizmann, C. W., and Sotelo, C. (1992). Development of the olivocerebellar projection in the rat: I. Transient biochemical compartmentation of the inferior olive. *J. Comp. Neurol.* 323, 519–536.

Watanabe, M., and Kano, M. (2011). Climbing fiber synapse elimination in cerebellar Purkinje cells. *Eur. J. Neurosci.* 34, 1697–1710.

Watanabe, Y., Kinoshita, K., Koguchi, A., and Yamamura, M. (1997). A new method for evaluation of motor deficits in 3-acetylpyridine-treated rats. *J. Neurosci. Methods* 77, 25–29.

Watt, A. J., Cuntz, H., Mori, M., Nusser, Z., Sjostrom, P. J., and Hausser, M. (2009). Traveling waves in developing cerebellar cortex mediated by asymmetrical Purkinje cell connectivity. *Nat. Neurosci.* 12, 463–473.

Weible, A. P., Schwarcz, L., Wickersham, I. R., Deblander, L., Wu, H., Callaway, E. M., et al. (2010). Transgenic targeting of recombinant rabies virus reveals monosynaptic connectivity of specific neurons. *J. Neurosci.* 30, 16509–16513.

Weickert, S., Ray, A., Zoidl, G., and Dermietzel, R. (2005). Expression of neural connexins and pannexin1 in the hippocampus and inferior olive: a quantitative approach. *Brain Res. Mol. Brain Res.* 133, 102–109.

White, J. J., Reeber, S. L., Hawkes, R., and Sillitoe, R. V. (2012). Wholemount immunohistochemistry for revealing complex brain topography. *J. Vis. Exp.* 62:e4042. doi: 10.3791/4042

White, J. J., and Sillitoe, R. V. (2013). Development of the cerebellum: from gene expression patterns to circuit maps. *WIREs Dev. Biol.* 2, 149–164.

Wickersham, I. R., Lyon, D. C., Barnard, R. J., Mori, T., Finke, S., Conzelmann, K. K., et al. (2007). Monosynaptic restriction of transsynaptic tracing from single, genetically targeted neurons. *Neuron* 53, 639–647.

Wickersham, I. R., Sullivan, H. A., and Seung, H. S. (2010). Production of glycoprotein-deleted rabies viruses for monosynaptic tracing and high-level gene expression in neurons. *Nat. Protoc.* 5, 595–606.

Willson, M. L., Bower, A. J., and Sherrard, R. M. (2007). Developmental neural plasticity and its cognitive benefits: olivocerebellar reinnervation compensates for spatial function in the cerebellum. *Eur. J. Neurosci.* 25, 1475–1483.

Willson, M. L., McElnea, C., Mariani, J., Lohof, A. M., and Sherrard, R.

M. (2008). BDNF increases homotypic olivocerebellar reinnervation and associated fine motor and cognitive skill. *Brain* 131, 1099–1112.

Wilson, S. L., Kalinovsky, A., Orvis, G. D., and Joyner, A. L. (2011). Spatially restricted and developmentally dynamic expression of engrailed genes in multiple cerebellar cell types. *Cerebellum* 10, 356–372.

Wise, A. K., Cerminara, N. L., Marple-Horvat, D. E., and Apps, R. (2010). Mechanisms of synchronous activity in cerebellar Purkinje cells. *J. Physiol.* 588, 2373–2390.

Woodward, D. J., Hoffer, B. J., and Altman, J. (1974). Physiological and pharmacological properties of Purkinje cells in rat cerebellum degranulated by postnatal x-irradiation. *J. Neurobiol.* 5, 283–304.

Woodward, D. J., Hoffer, B. J., and Lapham, L. W. (1969). Postnatal development of electrical and enzyme histochemical activity in Purkinje cells. *Exp. Neurol.* 23, 120–139.

Xiang, M., Gan, L., Zhou, L., Klein, W. H., and Nathans, J. (1996). Targeted deletion of the mouse POU domain gene Brn-3a causes selective loss of neurons in the brainstem and trigeminal ganglion, uncoordinated limb movement, and impaired suckling. *Proc. Natl. Acad. Sci. U.S.A.* 93, 11950–11955.

Yamada, M., Terao, M., Terashima, T., Fujiyama, T., Kawaguchi, Y., Nabeshima, Y., et al. (2007). Origin of climbing fiber neurons and their developmental dependence on Ptf1a. *J. Neurosci.* 27, 10924–10934.

Yamano, M., and Tohyama, M. (1994). Distribution of corticotropin-releasing factor and calcitonin gene-related peptide in the developing mouse cerebellum. *Neurosci. Res.* 19, 387–396.

Yan, X. X., and Garey, L. J. (1996). Calretinin immunoreactivity in the monkey and cat cerebellum: cellular localisation and modular distribution. *J. Hirnforsch.* 37, 409–419.

Zagrebelsky, M., Strata, P., Hawkes, R., and Rossi, F. (1997). Reestablishment of the olivocerebellar projection map by compensatory transcommissural reinnervation following unilateral transection of the inferior cerebellar peduncle in the newborn rat. *J. Comp. Neurol.* 379, 283–299.

Zappala, A., Parenti, R., La Delia, F., Cicirata, V., and Cicirata, F. (2010). Expression of connexin57 in mouse development and in harmaline-tremor model. *Neuroscience* 171, 1–11.

Zhang, F., Wang, L. P., Boyden, E. S., and Deisseroth, K. (2006). Channelrhodopsin-2 and optical control of excitable cells. *Nat. Methods* 3, 785–792.

Zhu, Y., and Guthrie, S. (2002). Expression of the ETS transcription factor ER81 in the developing chick and mouse hindbrain. *Dev. Dyn.* 225, 365–368.

Conflict of Interest Statement: The authors declare that the research was conducted in the absence of any commercial or financial relationships that could be construed as a potential conflict of interest.

Received: 28 September 2012; accepted: 12 December 2012; published online: 02 January 2013.

Citation: Reeber SL, White JJ, George-Jones NA and Sillitoe RV (2013) Architecture and development of olivocerebellar circuit topography. Front. Neural Circuits ***6****:115. doi: 10.3389/fncir.2012.00115*

frontiers in
NEURAL CIRCUITS

REVIEW ARTICLE
published: 04 February 2013
doi: 10.3389/fncir.2013.00003

Branching patterns of olivocerebellar axons in relation to the compartmental organization of the cerebellum

Hirofumi Fujita [1,2] ***and Izumi Sugihara*** [1]*

[1] *Department of Systems Neurophysiology, Tokyo Medical and Dental University Graduate School, Tokyo, Japan*
[2] *Systems Neurobiology Laboratories, The Salk Institute for Biological Studies, La Jolla, CA, USA*

Edited by:
Chris I. De Zeeuw, Erasmus Medical Center, Netherlands

Reviewed by:
Troy Margrie, National Institute for Medical Research, UK
Graham W. Knott, University of Lausanne, Switzerland

***Correspondence:**
Izumi Sugihara, Department of Systems Neurophysiology, Tokyo Medical and Dental University Graduate School, 1-5-45 Yushima, Bunkyo-ku, Tokyo 113-8519, Japan.
e-mail: isugihara.phy1@tmd.ac.jp

A single olivocerebellar (OC) axon gives rise to about seven branches that terminate as climbing fibers (CFs). Branching patterns of an OC axon, which are classified into local, transverse, and longitudinal types, are highly organized, in relation to the longitudinal molecular (aldolase C or zebrin II) compartmentalization and the transverse lobulation of the cerebellum. Local branching is involved in forming a narrow band-shaped functional subarea within a molecular compartment. On the other hand, transverse and longitudinal branchings appear to be involved in linking mediolaterally separated molecular compartments and rostrocaudally separated lobular areas, respectively. Longitudinal branching occurs frequently between equivalent molecular compartments of specific combinations of lobules. These combinations include lobule V-simple lobule and crus II-paramedian lobule in the pars intermedia and hemisphere, and lobules I–V and lobule VIII in the vermis. The longitudinal branching pattern not only fits with mirror-imaged somatosensory double representation of the body in the pars intermedia, but it also suggests a general rostrocaudal link exists for the whole cerebellum across the putative rostrocaudal boundary in lobule VIc-crus I. Molecular compartments of the cerebellar cortex originate from the Purkinje cell (PC) clusters that appear in the late embryonic stage, when the immature OC projection is formed. Some clusters split rostrocaudally across crus I during the development of cortical compartments, which would result in longitudinal branching of OC projection across crus I. Supposing that the branching pattern of OC axons represents an essential organization of the cerebellum, longitudinal branching suggests a functional and developmental links between the rostral and caudal cerebellum across lobule VIc-crus I throughout the cerebellar cortex.

Keywords: climbing fibers, collaterals, aldolase C, zebrin, lobules, compartments, somatotopical representation

INTRODUCTION

The cerebellar cortex is subdivided two ways: transversely by its lobular folding and longitudinally by PC subset compartments that are defined by the expression patterns of certain molecules, such as aldolase C or zebrin II (Brochu et al., 1990; Ahn et al., 1994). While the lobular and compartmental organizations are complex, a concrete functional localization is founded on these organizations in the cerebellar cortex (Nieuwenhuys et al., 2008).

Involvement of a cerebellar subarea in specific functions is thought to be largely dependent on regional differences in afferent and efferent connectivity. Climbing fiber (CF) afferents, which originate exclusively from the inferior olive (IO) as the OC projection, are particularly well-organized in a topographic sense. CFs that arise from a specific IO subdivision form synapses onto PCs in a particular aldolase C compartment that are about 0.1–0.5 mm in mediolateral width but elongated in the longitudinal direction (Voogd et al., 2003; Sugihara and Shinoda, 2004). In turn, PCs located within each compartment provide a highly convergent projection to specific regions of the cerebellar and vestibular nuclei (Voogd and Bigaré, 1980; Buisseret-Delmas and Angaut, 1993; Apps and Garwicz, 2005; Sugihara et al., 2009).

While the PC projection from the cortex is highly convergent, afferent projections to the cortex, CFs as well as mossy fibers (MFs), are characterized by their divergent branching patterns (Sugihara et al., 1999, 2001, 2009; Wu et al., 1999). Since CFs and MFs are the two main afferents of the cerebellar cortex, the branching patterns of CF and MF axons (in other words, the positional relationships between CF and MF terminals that originate from a single axon) are supposed to be tightly involved in the functional organization of the cerebellum. Since a CF is supposed to significantly affect the activity of an individual PC by its one-to-one innervation, topographic organization of the olivocerebellar (OC) projection, including the branching pattern of individual axons, is particularly critical in determining the functional organization of the cerebellum.

The branching patterns of cerebellar afferent and efferent axons have been analyzed clearly by reconstructing single axons as well as by other methods, which we review in this article, mainly focusing on OC axons.

BRANCHING OF INDIVIDUAL OC AXONS

The fact that the number of IO neurons is smaller than that of PCs (1:7 in the rat, Schild, 1970) implies a branching of OC axons, since a CF, terminal portion of the OC axon, generally projects to a PC in one-to-one relationship (Ramón y Cajal, 1911). Local branching of an OC axon in the cerebellar cortex has been shown in Golgi staining preparation in monkey (Fox et al., 1969). Local branching of an OC axon has also been demonstrated by electrophysiological recording of the "climbing fiber reflex" between lobule III and V in the cat (Faber and Murphy, 1969). Later, single axonal reconstruction has shown that an OC axon gives rise to several types of branches in the rat (Sugihara et al., 1999). One OC axon gives rise to about seven "thick" branches that terminate as CFs, and about nine "thin" collaterals that terminate mainly in the granular layer and the deep cerebellar nucleus (DCN) in the rat (Van der Want et al., 1989). Granular layer collaterals terminate in a similar cortical area where some thick branches terminate in the molecular layer as CFs. Nuclear collaterals terminate in a topographically related small area in the cerebellar nuclei (reviewed in Sugihara, 2011). We will focus on "thick" branches that terminate as CFs in the rest of this article.

CLASSIFICATION OF SPATIAL PATTERN OF BRANCHING: LOCAL, TRANSVERSE, AND LONGITUDINAL BRANCHING

LOCAL BRANCHING

We classify branching patterns of OC axons into local, transverse, and longitudinal types in this article (**Figure 1**). Multiple CFs that originate from an OC axon terminate in a single lobule or neighboring lobules. These CFs are often distributed in a narrow longitudinal band-shaped area (0.1–0.3 mm wide in rats). We designate this type of branching as local branching. CF termination of local branching of OC axons that originate from a small subarea in the IO share the same narrow longitudinal band-shaped area (**Figures 2A** and **B**). This narrow band-shaped area usually occupies a small sub-compartment within a single longitudinal compartment defined by the aldolase C expression pattern (**Figures 2C** and **D**; refer to (Voogd et al., 2003; Sugihara and Shinoda, 2004; Sugihara, 2011) for aldolase C compartments). Twenty-two out of thirty-four reconstructed OC axons had only local branching (Sugihara et al., 2001).

TRANSVERSE BRANCHING

Transverse branching of an OC axon was first noticed by electrophysiological recording of somatosensory responses between C1

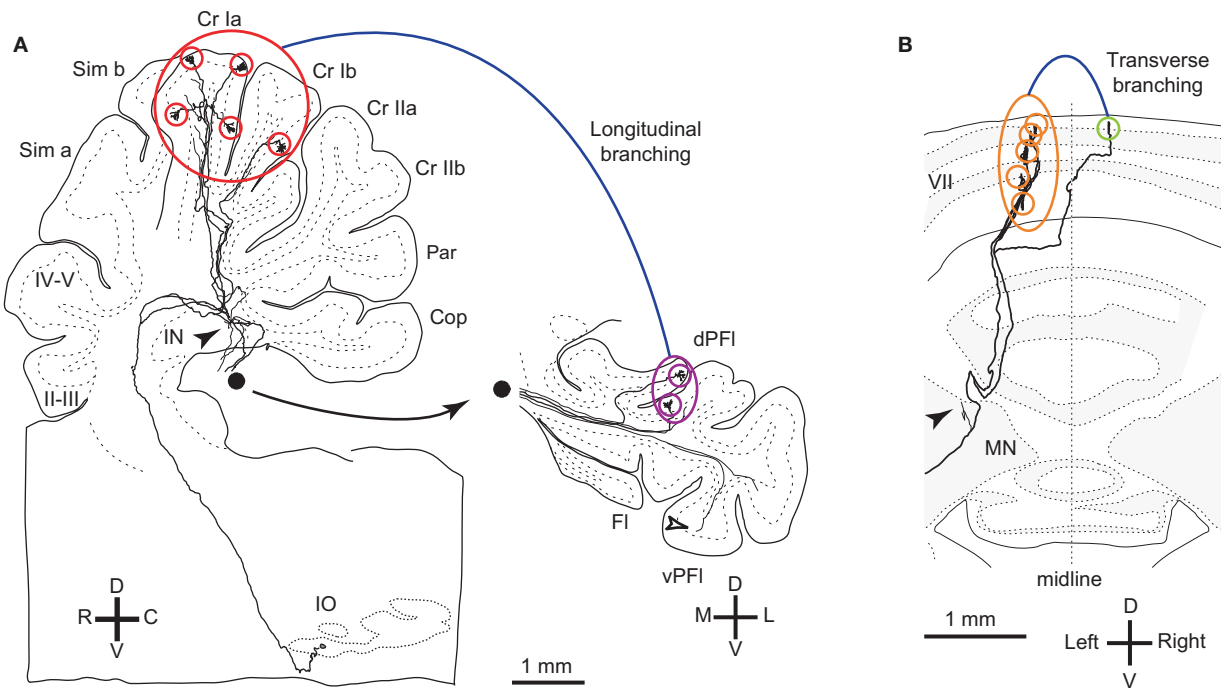

FIGURE 1 | Reconstructed OC axons showing different types of branching. (A) Reconstructed rat OC axon that terminated in crus I and paraflocculus with five (red circles) and two (purple circles) CFs, respectively, indicating longitudinal and local branching. This axon also had thin collaterals terminating in the granular layer (open arrowheads) and cerebellar nuclei (filled arrowheads). This axon was reconstructed in our previous study (Sugihara et al., 1999). Filled circle shows continuation of axons from the white matter of the paraflocculus. **(B)** Reconstructed rat OC axon that terminated mainly in the left lobule VII (orange circles) but also had a transcommissural transverse branch (yellow-green circle) (same axon as shown in Figure 4B of Sugihara et al., 1999). Abbreviations in this and subsequent figures, I–X, lobules I–X; a-d, sublobules a-d; AIN, anterior interposed nucleus; C, caudal; CF, climbing fiber; Cop, copula pyramidis; Cr I, crus I of ansiform lobule; Cr II, crus II of ansiform lobule; D, dorsal; das, dorsal acoustic stria; DCN, deep cerebellar nuclei; dPFl, dorsal paraflocculus; Fl, flocculus; fp, floccular peduncle; IN, interposed nucleus; IO, inferior olive; L, lateral; LN, lateral cerebellar nucleus; M, medial; MN, medial cerebellar nucleus; p, sublobule p; Par, paramedian lobule; PC, Purkinje cell; pf, primary fissure; PIN, posterior interposed nucleus; R, rostral; Sim, simple lobule; V, v–, ventral; vPFl, ventral paraflocculus.

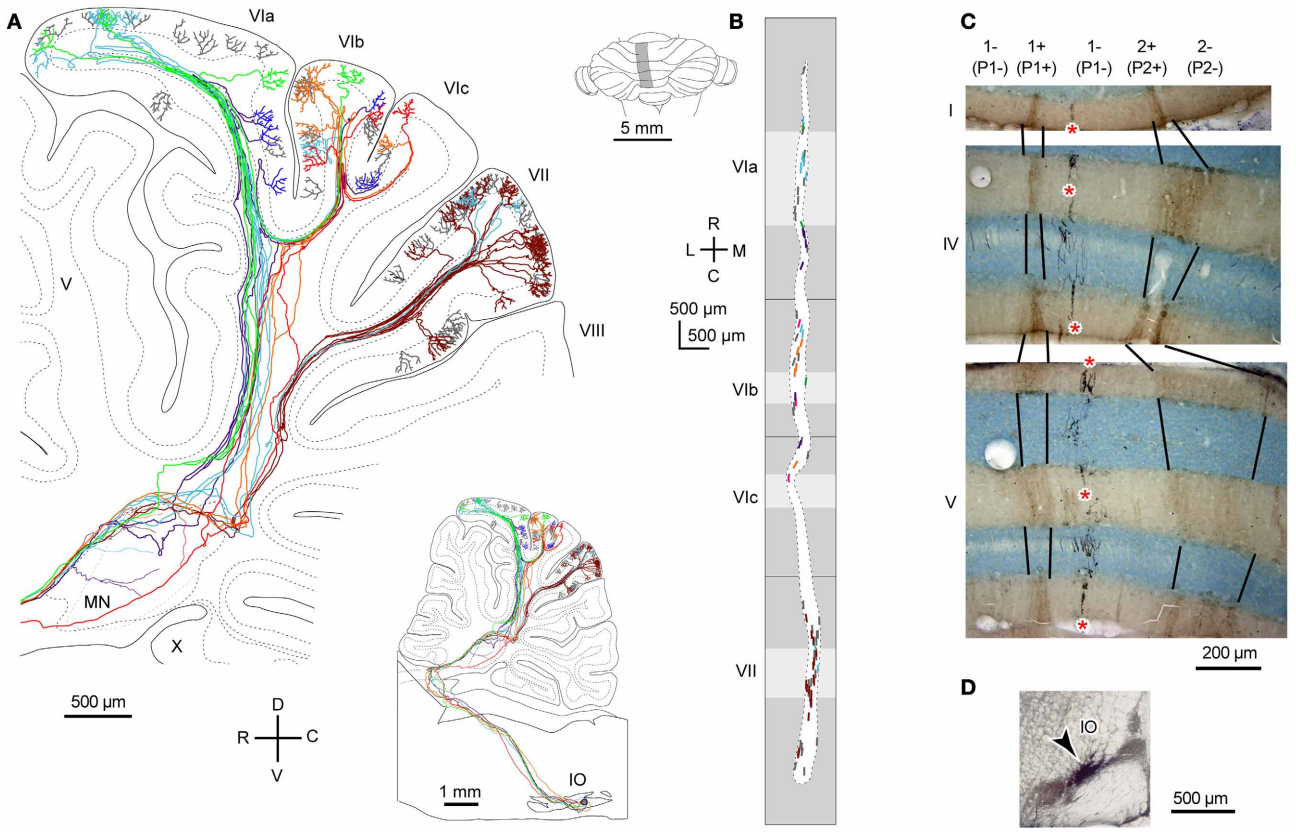

FIGURE 2 | Local branching terminating in a narrow longitudinal band-shaped area. (A) Six axons that were labeled with a small injection of biotinylated dextran amine to the IO were reconstructed. The inset shows the entire trajectory of these axons. **(B)** Distribution of labeled CFs of axons in **(A)** (six colors) and other axons that were not reconstructed (gray) were plotted on the unfolded cerebellar cortex. Light and dark gray areas indicate apical and fissural parts of the lobule. **(C)** Double labeling of CFs (in black, asterisks) and aldolase C (brown) in cerebellar sections. CFs labeled by a localized injection of biotinylated dextran amine to the IO were distributed in a narrow band-shaped area that occupied a portion of a single aldolase C compartment. **(D)** Injection site of biotinylated dextran amine in the rat IO. **(A)** and **(B)** are cited from Sugihara et al. (2001). **(C)** and **(D)** are based on the data in Sugihara et al. (2004). 1+, 1−, 2+, names of aldolase C compartments according to the nomenclature of Sugihara and Shinoda (2004), which are equivalent to "P1+," "P1−," and "P2+" as often used in ligature (Brochu et al., 1990; Apps and Hawkes, 2009).

and C3 zones, which correspond to aldolase C-negative (including lightly-positive) compartments in the medial and lateral pars intermedia, respectively, in lobule V in cats (Ekerot and Larson, 1982). However, CF labeling by tracer uptake from CF terminals of the same axon (designated retro-anterograde labeling, **Figure 3A** inset) has also shown transverse branching of OC axons between C1 and C3 zones in lobules III–V in rats (Voogd et al., 2003). We observed transverse branching of OC axons in multiple aldolase C-negative stripes in the vermis and pars intermedia in retro-anterograde OC axon labeling in the marmoset cerebellum (**Figure 3A**, orange). We define typical transverse branching as branching between unilateral and mediolaterally distinct compartments in the same or adjacent lobules. Although we did not see typical transverse branching in our samples of reconstructed single axons in rats ($n = 34$ axons, Sugihara et al., 2001), results from a prior study suggested that it, in fact, occurs (Sugihara and Shinoda, 2004). Following a small injection of biotinylated dextran amine in the IO labeled CFs often appeared in multiple mediolaterally separate compartments in the lateral vermis and pars intermedia (seen in roughly in half cases, Figures 5B,C, 6B, and 7A,B of Sugihara and Shinoda, 2004), suggesting transverse branching (**Figure 3B**).

OC axon branching between the nodulus and flocculus (Takeda and Maekawa, 1989; Sugihara et al., 2004) may also be considered an example of transverse branching. Transcommissural transverse branching, in which a branch terminates in the opposite side about the midline, has been observed in the vermis less frequently (**Figure 1B**; Sugihara et al., 1999).

LONGITUDINAL BRANCHING

Here we define longitudinal branching as branching to non-contiguous lobules in the cerebellar cortex. Longitudinal branching was first demonstrated with the CF reflex between lobule V and the paramedian lobule in the cat pars intermedia (Armstrong et al., 1973). A double retrograde labeling study has also shown longitudinal branching between lobule V and the paramedian lobule (Rosina and Provini, 1983). Branching is formed between C1 zones in lobule V and paramedian lobule, which are physiologically equivalent areas that both receive forelimb cutaneous inputs (Apps, 2000). Single axon reconstruction

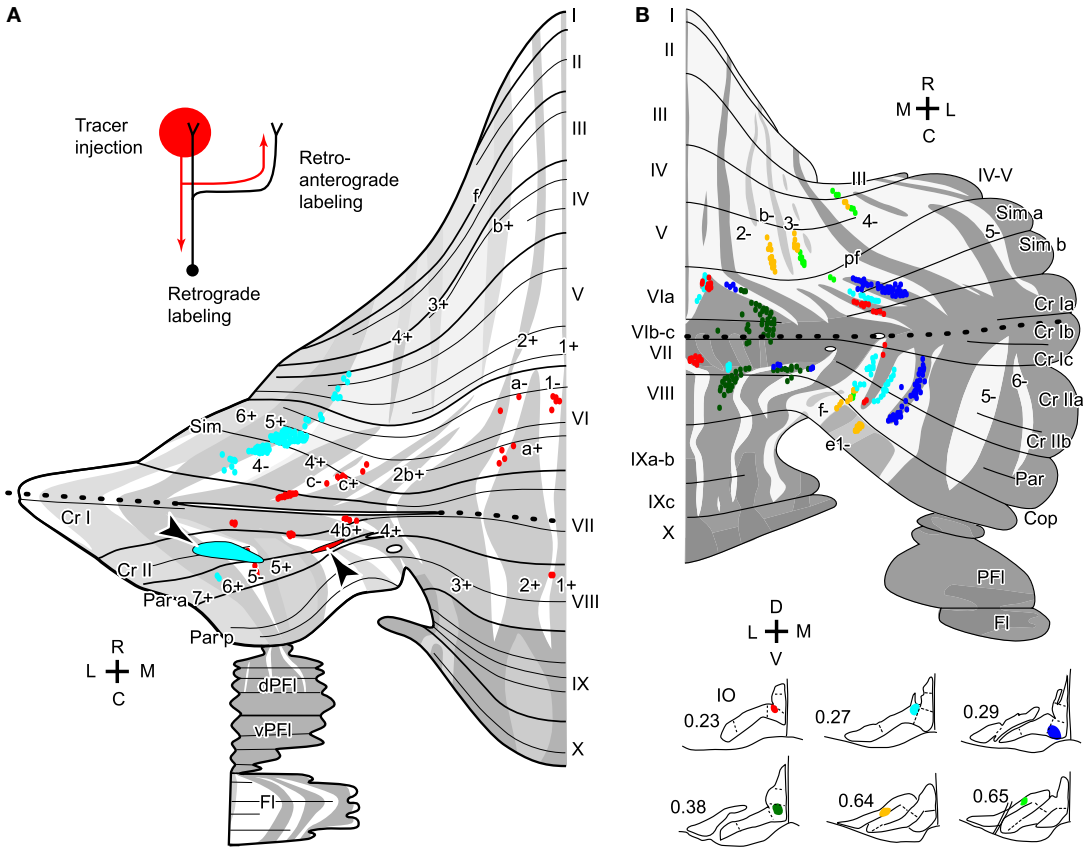

FIGURE 3 | Transverse branching of olivocerebellar axons. (A) Mapping of CFs that were labeled retro-anterogradely by a biotinylated dextran amine injection in the cerebellar cortex in marmosets (arrowheads). While an injection in crus II in pars intermedia (red) labeled CFs in transversely separate compartments, indicating transverse branching, an injection in crus II in the hemisphere (cyan) labeled CFs only in the longitudinally separate areas, indicating presence of longitudinal branching but absence of transverse branching. Inset in the top left-hand corner illustrate retro-anterograde labeling. **(B)** Mapping of labeled CFs labeled by a small injection of biotinylated dextran amine into the mouse IO, mapped in the scheme of aldolase C compartments in the cerebellar cortex. Cases in which CFs were labeled in multiple mediolaterally separate compartments are summarized here, suggesting transverse branching. CFs are also distributed in longitudinally separate areas, suggesting longitudinal branching. Single axons were not reconstructed. **(A)** and **(B)** are based on the data in Fujita et al. (2010) and Sugihara and Quy (2007), respectively. Dotted lines indicate the rostrocaudal boundary.

has shown that longitudinal branching occurs frequently (in 12 out of 34 axons) not only in the pars intermedia but also in the vermis and hemisphere (**Figure 4A**; Sugihara et al., 2001). Mediolateral positions of the termination areas of longitudinal branching are usually similar (Sugihara et al., 2001). Longitudinal branching is usually distinguished easily from local branching, which targets single or neighboring lobules, in terms of morphology of axonal trajectories (**Figure 1A**).

Molecular compartmentalization of the cerebellar cortex, which is visualized by immunostaining of aldolase C or some other molecules (Brochu et al., 1990), has an ultra-tight relationship with the longitudinal branching of OC axons (Voogd et al., 2003; Sugihara and Shinoda, 2004). The aldolase C expression pattern shows mediolateral merging and lateral shift in vermal lobule VIc and crus I, appearing to be a landmark for the center between the rostral and caudal cerebellum (designated as "rostrocaudal boundary," Sugihara and Shinoda, 2004). Longitudinal branches often terminate in aldolase C compartments that have similar expression levels of aldolase C and are located at a similar mediolateral distance from the midline in the rostral and caudal cerebellum (**Figure 4B**; Sugihara and Shinoda, 2004; Sugihara and Quy, 2007). Even if these aldolase C compartments are not really continuous, targeting of longitudinal branches of an axon to these compartments indicates that they are paired or linked compartments (see Table 1 of Sugihara and Shinoda, 2004).

In regards to target lobules, the most typical pairs of lobules that receive longitudinal branches include (1) simple lobule and caudal lobule V vs. crus II and paramedian lobule in the pars intermedia and hemisphere, (2) lobules II–V vs. copula pyramidis in the pars intermedia, and (3) lobules II–V and lobule VIII in the vermis (Sugihara and Shinoda, 2004). These longitudinal branching patterns are consistent with the mirror-image organization about the "rostrocaudal boundary" positioned on crus I (Sugihara and Shinoda, 2004; Sugihara and Quy, 2007). Other longitudinal branching has been seen between

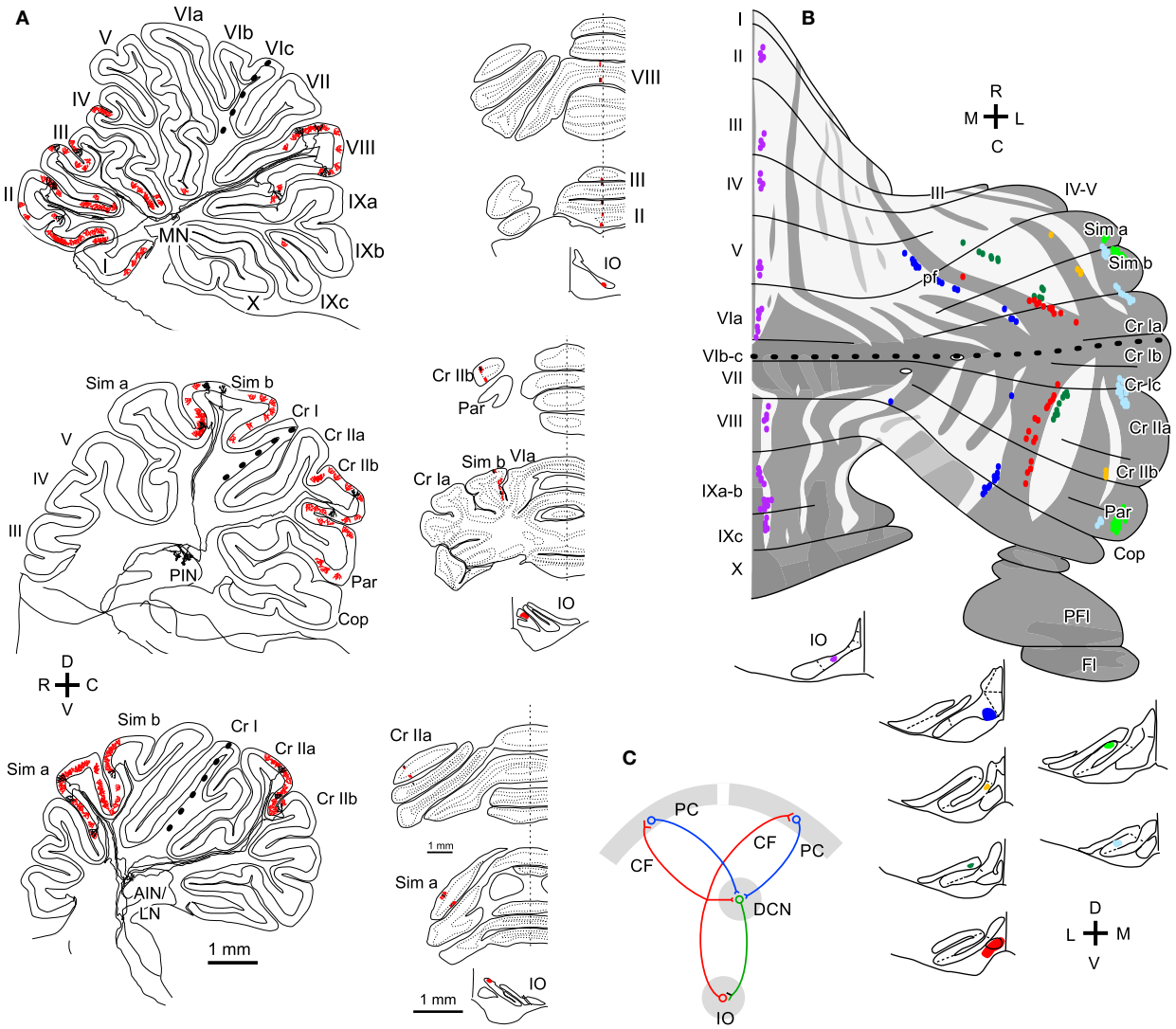

FIGURE 4 | Longitudinal branching of olivocerebellar axons. (A) Reconstructed axon depicted with all other CFs labeled by a small injection of biotinylated dextran amine into the IO in three rats. Drawings of labeled CFs in coronal sections and injection sites in the IO were also shown (right-hand insets). Red color indicates labeled CFs that did not belong to the reconstructed axon. **(B)** Mapping of labeled CFs labeled by a small injection of biotinylated dextran amine into the mouse IO, mapped in the scheme of aldolase C compartments in the cerebellar cortex. Cases in which CFs were labeled only in longitudinally separate pair of equivalent compartments are summarized here, suggesting longitudinal branching. **(A)** and **(B)** are based on the data in experiments in Sugihara et al. (2001) and Sugihara and Quy (2007), respectively. **(C)** Schematic of the closed-loop-shaped modular organization between the IO, cerebellar cortex and DCN modified by the longitudinal branching of the OC axon.

lobule VIa-b and lobule IX in the vermis, between crus I and the paraflocculus in the hemisphere, and between the most lateral part of crus I and the flocculus (Sugihara et al., 2004). Thus, the longitudinal branching occurs not randomly but in specific pairs of lobules. This reflects the basic organization of the cerebellum.

PROJECTION PATTERNS OF PC AXONS

To relate branching patterns of single OC axons to cerebellar function requires looking at efferent PC projection patterns. A major question is whether PCs that receive branches of a single OC axon converge in their output projection. In relation to the local branching that terminates in a narrow band-shaped area, an electrophysiological study has shown that PCs located in such an area (one of the five subzones in "zone B" in the lateral vermis) generally project and converge to a distinct neuronal group in the lateral vestibular nucleus (Andersson and Oscarsson, 1978), which is equivalent to the DCN in receiving PC projections. An anatomical labeling study of multiple PCs indirectly supported the convergent PC projection from a band-shaped area (Sugihara et al., 2009). Furthermore, PCs that slightly separate in the mediolateral direction (but still in the same molecular compartment) terminate in slightly mediolaterally separate areas in the DCN. Therefore, the narrow longitudinal band-shaped area

in the cerebellar cortex may represent the basic operational units of the cerebellum.

Concerning transverse branching of OC axons, Apps and Garwicz (2000) have shown that corticonuclear projections from C1 and C3 zones in lobule V, which receive forelimb cutaneous inputs, converge to the same area in the anterior interposed nucleus (AIN). Furthermore, depending on the receptive field (ulnar, radial, and ventral side of the forelimb), the projections from C1 and C3 zones converge on slightly different areas in the AIN. Retrograde PC labeling by localized injections of retrograde tracers in the AIN supports convergence of PC projections from C1 and C3 zones (Pijpers et al., 2005). In other areas, projections of PCs that receive transverse branches of OC axons have not been fully studied yet.

Concerning the longitudinal branching, PCs in separate lobules of the rostral and caudal cerebellum are simultaneously labeled by a localized injection of retrograde tracers in the DCN, indicating convergence of PC projections (Pijpers et al., 2005; Sugihara et al., 2009). Anterograde PC labeling has also shown that PCs located in the same (or paired) aldolase C compartment(s) in adjacent (crus IIa and IIb) or separate lobules (simple lobule and crus II) in the cerebellar cortex project to the same small area in the DCN (Sugihara et al., 2009).

In sum, experimental data generally support the idea that PCs that receive local, transverse, and longitudinal branches of a single OC axon make a convergent projection to the same small area in the DCN. It should be noted that the target area of nuclear collaterals of OC axons generally coincides with the target area of the PCs that are innervated by these OC axons (Sugihara, 2011). Thus, there is generally a closed-loop-shaped modular organization between small subareas within the IO, DCN, and cerebellar cortex connected by the topographic OC and corticonuclear projections (Pijpers et al., 2005; Sugihara, 2011), and by the nucleoolivary projection (Ruigrok and Voogd, 1990; Marshall and Lang, 2009). If branching divergence in the projections of OC axons and convergence in the corticonuclear PC projection are taken into account, the closed-loop-shaped modular organization needs to be modified; the loop is divided into multiple parallel loops in the cerebellar cortex (**Figure 4C**).

BRANCHING OF MOSSY FIBER AXONS

Although this article is focused on OC axons that terminate as CFs, we have also briefly looked at the MFs that constitute the other main afferent system in the cerebellar cortex. Axonal branching patterns of MF axons (Wu et al., 1999; Quy et al., 2011) are clearly different from that of OC axons or from PC axons. Basically, the stem MF axon runs transversely in the deep cerebellar white matter, giving rise to several branches at different mediolateral locations. While classifying branches into definite types can be difficult, many branches generally have secondary, tertiary, and further branches that can be of transverse, longitudinal, or local types (Quy et al., 2011) As a whole, rosette-shaped terminals of a MF axon (about 100 per axon, Wu et al., 1999; Quy et al., 2011) are distributed in many band-shaped or patch-shaped areas in multiple lobules. Although there is still some topographical pattern in each MF projection originating from a specific subarea of the precerebellar nuclei, it is not generally simple to relate branching patterns of MF axons to that of OC axons or from PC axons (Quy et al., 2011).

RELATIONSHIP TO THE FUNCTIONAL ORGANIZATION OF THE CEREBELLUM

LOCAL BRANCHING

OC axons originating from IO neurons located in close vicinity to each other project to the same or an overlapping narrow longitudinal band-shaped area (0.1–0.3 mm wide) with their local branches (Sugihara et al., 2004). We speculate that these neighboring IO neurons share input and thus have a similar responsiveness to stimuli and, consequently, PCs in a narrow longitudinal area have a similar responsiveness in their complex spike activity. Indeed, such band-shaped areas, also called "microzones," have been shown to be present in the vermal B zone (Andersson and Oscarsson, 1978) and in the paravermal C1 and C3 zones (Ekerot and Larson, 1982), both of which receive somatosensory information. Neighboring IO neurons also have synchronized activity through electrotonic coupling, which results in synchronous complex spike activity in PCs arranged in a narrow longitudinal area (Sasaki et al., 1989; Lang et al., 1999). These PCs may also have synchronized simple spike activity (Wise et al., 2010). A similar organization is thought to be present throughout the cerebellar cortex and to represent the basic operational unit of the cerebellum (Apps and Hawkes, 2009). Since PCs in a narrow longitudinal band-shaped area project to the same target area in the DCN (above), some DCN neurons should receive input from multiple PCs that are synchronized. Synchronous input from PC axons causes time-locked activity in DCN neurons (Person and Raman, 2011). Thus, local branching of OC axons contributes to longitudinal functional organization of the cerebellar cortex.

TRANSVERSE BRANCHING

Transverse branching seems to occur only in particular areas, mainly in the pars intermedia and vermis (above). Thus, the transverse branching does not seem to represent the general projection pattern of OC axons. Transverse branching of OC axons makes multiple longitudinal narrow areas that are separated mediolaterally, receive the same OC input, and project to the similar subarea in the DCN. Functional significance of this organization has not been much clarified. Further studies, including comparative ones, may be required to better characterize the transverse branching.

LONGITUDINAL BRANCHING

The most frequently observed category of longitudinal branching is the one across crus I in the pars intermedia and hemisphere. Branching between lobule V and paramedian lobule in C1 zone in cats (above) belongs to this category. Branching between lobules II–V and the copula pyramidis and branching between the simple lobule and the crus II-paramedian lobule, which are the most common pattern in the rat (Sugihara et al., 2001), also belong in this category. We think these branching patterns are not essentially different between cats and rats, since the copula pyramidis in the rat is equivalent with the caudal part of the paramedian lobule in the cat. This type of longitudinal branching fits well with the double localization of forelimb and hindlimb

representation in the rostral and caudal pars intermedia in a classic study of evoked field potentials (Snider, 1950). A human imaging study also located arm and leg representation in lobules III–VI and in lobules VII–VIII in the pars intermedia and hemisphere (Timmann et al., 2009). CF input as well as MF input are involved in forming these representations. These rostral and caudal somatosensory areas are involved in different aspects of movement control (Timmann et al., 2009).

Furthermore, the longitudinal branching across crus I or lobule VIc represents a general organization of the entire cerebellar cortex, since longitudinal branching is seen in not only the somatosensory-responsive areas in the pars intermedia including C1 and C3 zones, but also in the rest of the cerebellum. MF axons also often make longitudinal branching across crus I and lobule VIc, projecting to both the rostral and caudal cerebellum simultaneously (Quy et al., 2011). Therefore, there seems to be general divergent organization in the afferent projection between the rostral and caudal cerebellum across crus I and lobule VIc. Thus, corresponding areas in the rostral and caudal cerebellum can belong to the same module. Yet, beyond generating a somatosensory double representation, the functional significance of the longitudinal branching remains unclear. Moreover, functional significance of the somatosensory double representation itself remains unclear, besides the fact that the

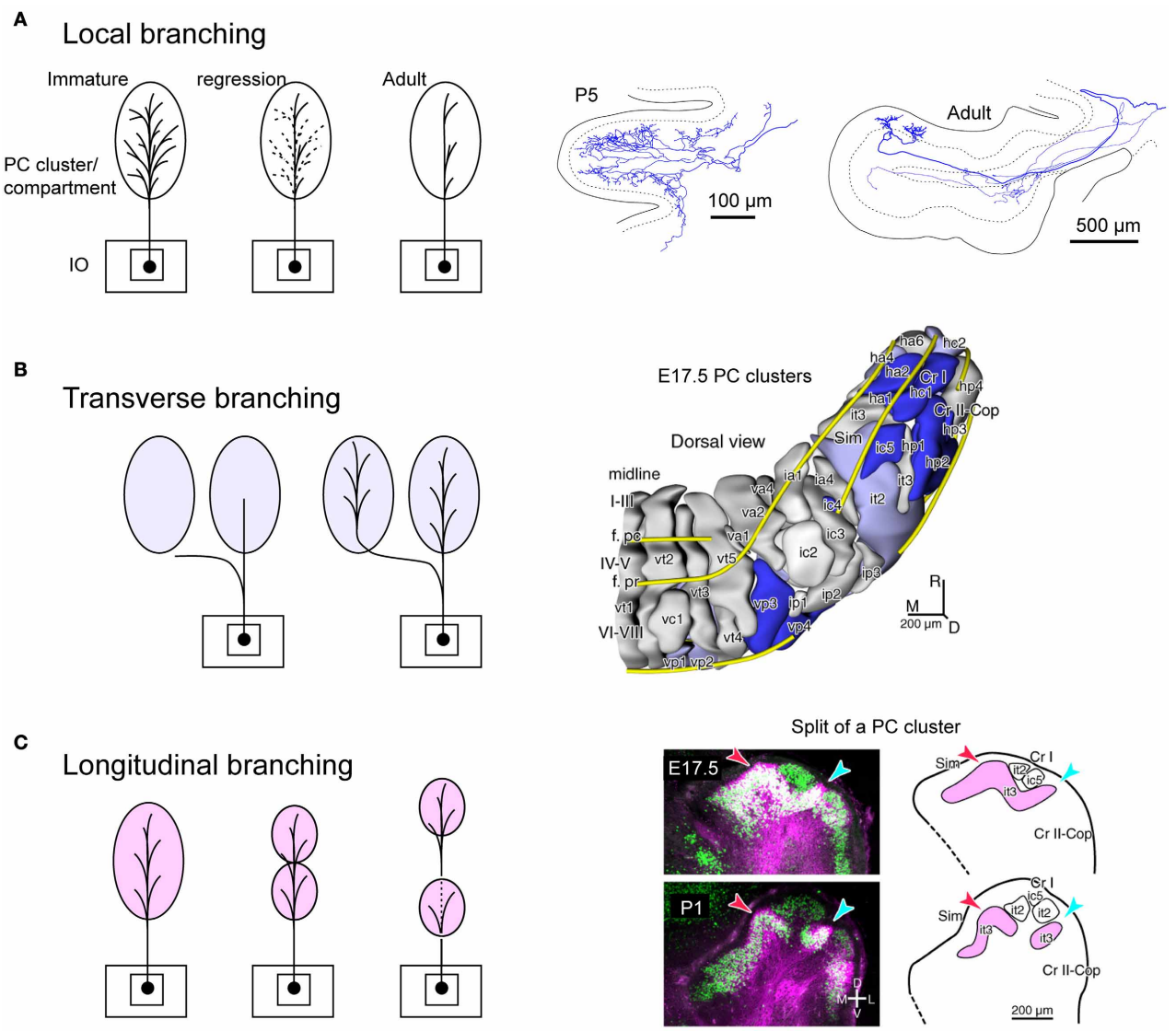

FIGURE 5 | Speculative illustration of formation of OC branching patterns. (A) Projection by local branches to a narrow band-shaped subarea within a single aldolase C compartment may be formed in accordance with regression of exuberant branches. Right-hand insets show exuberant local branches in immature OC axons at P5 (cited from Sugihara, 2006). **(B)** Some transverse branching may be formed by branching of growing axon toward multiple clusters of PCs. Right-hand inset shows PC clusters in the E17.5 cerebellum (cited from Fujita et al., 2012). **(C)** Some longitudinal branching may be formed by longitudinal separation of a target compartment. Right-hand inset shows the longitudinal split of a PC cluster in the developing cerebellum (cited from Fujita et al., 2012). E17.5, embryonic day 17.5; P1 postnatal day 1; it2, ic5, it3, etc.; names of embryonic PC clusters.

rostral and caudal areas have different activities in somatosensory tasks (Timmann et al., 2009).

DEVELOPMENTAL BASIS FOR BRANCHING PATTERNS OF OC AXONS

Projections of CF and MFs begin to form in the late embryonic stages around embryonic days 14–18 (E14–E18) in the mouse (Sotelo et al., 1984; Ashwell and Zhang, 1992; Paradies and Eisenman, 1993). Although these projections have compartment-specific topography in adult (Sugihara and Shinoda, 2004, 2007; Quy et al., 2011), and the CF projection seems to have adult-like topography at P5 (Sugihara, 2005), it is not clear how precise a topography the immature climbing and MF projections have in the late embryonic stage. PCs are arranged in multiple clusters in the immature cerebellar cortex at this stage (Altman and Bayer, 1997). We have recently shown that the number of recognizable PC clusters is as large as 54 (Fujita et al., 2012). Therefore, we speculate that these PC clusters, which have different expression profiles of molecules, may form proper topographic connections in the cerebellar cortex through molecular matching between PCs and afferent axons during development (Sotelo, 2004). Neuronal clustering may be essential in the development of compartmentalization for topographic afferent and efferent connections as seen in the spinal cord (Sürmeli et al., 2011).

We speculate that branching patterns of OC axons is hinted in the cluster organization of the immature cerebellar cortex. Each PC cluster has its own molecular expression profile (Wilson et al., 2011; Fujita et al., 2012), i.e., some molecules are expressed only in particular clusters of PCs. Eph receptors and cadherin family molecules are among these molecules (Nishida et al., 2002; Neudert et al., 2008; Hashimoto et al., 2012). Thus, these molecules are presumably involved in establishing correct OC connections. This may indicate that the embryonic OC projection, including all branches, may have precision to the level of clusters. A cluster is basically equivalent to a single molecular compartment in adulthood, since each embryonic PC cluster basically develops into single molecular compartment (Fujita et al., 2012). Immature OC axons have superabundant number of branches, which regress in the early postnatal period (Mariani and Changeux, 1981; Sugihara, 2005). It may be speculated that this regression process is involved in restricting the final local branching distribution to the microzone range, which is much narrower than a single molecular compartment (**Figure 5A**). Concerning transverse branching, supposing two mediolaterally separate clusters have similar molecular expression profiles, an OC axon may project to these two clusters by mediolateral branching (**Figure 5B**).

In relation to the longitudinal branching across crus I (see above), our analysis of PC cluster development has shown some clusters are "split" into rostral and caudal clusters underneath other clusters in crus I (Fujita et al., 2012). Supposing the initial cluster receives multiple branches of an OC axon, the splitting of this cluster would explain the final longitudinal branching pattern of OC axons and hence general mirror-image organization of the OC projection across crus I (**Figure 5C**). Thus, we hypothesize that crus I is the key lobule that determines the rostro-caudal arrangement of the cerebellum. Further studies on the development of PC clusters in the embryonic cerebellum will be required to clarify whether splitting of embryonic clusters can also explain other types of longitudinal and/or transverse branching.

CONCLUSION

Branching patterns of OC axons can be classified into local, transverse, and longitudinal types. These branching patterns of OC axons are tightly related with the functional organization of the cerebellar cortex. The local branching is in accordance with the microzonal organization of the cerebellar cortex. The transverse and longitudinal branching patterns are in accordance with the compartmental organization of the cerebellar cortex and related to the lobular organization. The longitudinal branching, in particular, is a basis of the mirror-imaged double somatotopic representation of the body in the cerebellum. Attempts to relate the OC branching patterns to development of cerebellar compartmentalization and lobulation may be helpful in untangling the complicated compartmental and lobular organization of the cerebellar cortex.

ACKNOWLEDGMENTS

This work was supported by the Grants-in-Aid for Scientific Research (23.5291 to Hirofumi Fujita) from the Japan Society for the Promotion of Science (JSPS). Hirofumi Fujita is a research fellow of JSPS. Authors thank Dr. Eric Lang and Ms. Michelle Lee for reading the manuscript.

REFERENCES

Ahn, A. H., Dziennis, S., Hawkes, R., and Herrup, K. (1994). The cloning of zebrin II reveals its identity with aldolase C. *Development* 120, 2081–2090.

Altman, J., and Bayer, S. A. (1997). *Development of the Cerebellar System in Relation to its Evolution, Structure, and Functions*. Boca Raton, FL: CRC Press.

Andersson, G., and Oscarsson, O. (1978). Climbing fiber microzones in cerebellar vermis and their projection to different groups of cells in the lateral vestibular nucleus. *Exp. Brain Res.* 32, 565–579.

Apps, R. (2000). Rostrocaudal branching within the climbing fibre projection to forelimb-receiving areas of the cerebellar cortical C1 zone. *J. Comp. Neurol.* 419, 193–204.

Apps, R., and Garwicz, M. (2000). Precise matching of olivo-cortical divergence and cortico-nuclear convergence between somatotopically corresponding areas in the medial C1 and medial C3 zones of the paravermal cerebellum. *Eur. J. Neurosci.* 12, 205–214.

Apps, R., and Garwicz, M. (2005). Anatomical and physiological foundations of cerebellar information processing. *Nat. Rev. Neurosci.* 6, 297–311.

Apps, R., and Hawkes, R. (2009). Cerebellar cortical organization: a one-map hypothesis. *Nat. Rev. Neurosci.* 10, 670–681.

Armstrong, D. M., Harvey, R. J., and Schild, R. F. (1973). The spatial organization of climbing fibre branching in the cat cerebellum. *Exp. Brain Res.* 18, 40–58.

Ashwell, K. W., and Zhang, L. L. (1992). Ontogeny of afferents to the fetal rat cerebellum. *Acta Anat. (Basel)* 145, 17–23.

Brochu, G., Maler, L., and Hawkes, R. (1990). Zebrin II: a polypeptide antigen expressed selectively by Purkinje cells reveals compartments in rat and fish cerebellum. *J. Comp. Neurol.* 291, 538–552.

Buisseret-Delmas, C., and Angaut, P. (1993). The cerebellar olivocorticonuclear connections in the rat. *Prog. Neurobiol.* 40, 63–87.

Ekerot, C.-F., and Larson, B. (1982). Branching of olivary axons to innervate pairs of sagittal zones in the cerebellar anterior lobe of the cat. *Exp. Brain Res.* 48, 185–198.

Faber, D. S., and Murphy, J. T. (1969). Axonal branching in the climbing fiber pathway to the cerebellum. *Brain Res.* 15, 262–267.

Fox, C. A., Andrade, A., and Schwyn, R. C. (1969). "Climbing fiber branching in the granular layer," in *Neurobiology of Cerebellar Evolution and Development*, ed R. Llinás (Chicago, IL: American Medical Association), 603–611.

Fujita, H., Morita, N., Furuichi, T., and Sugihara, I. (2012). Clustered fine compartmentalization of the mouse embryonic cerebellar cortex and its rearrangement into the postnatal striped configuration. *J. Neurosci.* 32, 15688–15703.

Fujita, H., Oh-Nishi, A., Obayashi, S., and Sugihara, I. (2010). Organization of the marmoset cerebellum in three-dimensional space: lobulation, aldolase C compartmentalization and axonal projection. *J. Comp. Neurol.* 518, 1764–1791.

Hashimoto, M., Ito, R., Kitamura, N., and Hisano, Y. (2012). EphA4 controls the midline crossing and contralateral axonal projections of inferior olive neurons. *J. Comp. Neurol.* 520, 1702–1720.

Lang, E. J., Sugihara, I., Welsh, J. P., and Llinás, R. (1999). Patterns of spontaneous complex spike activity in the awake rat. *J. Neurosci.* 19, 2728–2739.

Mariani, J., and Changeux, J.-P. (1981). Ontogenesis of olivocerebellar relationships. I. Studies by intracellular recordings of the multiple innervation of Purkinje cells by climbing fibers in the developing rat cerebellum. *J. Neurosci.* 1, 696–702.

Marshall, S. P., and Lang, E. J. (2009). Local changes in the excitability of the cerebellarcortex produce spatially restricted changes in complex spike synchrony. *J. Neurosci.* 29, 14352–14362.

Neudert, F., Nuernberger, K. K., and Redies, C. (2008). Comparative analysis of cadherin expression and connectivity patterns in the cerebellar system of ferret and mouse. *J. Comp. Neurol.* 511, 736–752.

Nieuwenhuys, R., Voogd, J., and Van Huijzen, C. (2008). *The Human Central Nervous System, Fourth Edn*. Berlin: Springer.

Nishida, K., Flanagan, J. G., and Nakamoto, M. (2002). Domain-specific olivocerebellar projection regulated by the EphA-ephrin-A interaction. *Development* 129, 5647–5658.

Paradies, M. A., and Eisenman, L. M. (1993). Evidence of early topographic organization in the embryonic olivocerebellar projection: a model system for the study of pattern formation processes in the central nervous system. *Dev. Dyn.* 197, 125–145.

Person, A. L., and Raman, I. M. (2011). Purkinje neuron synchrony elicits time-locked spiking in the cerebellar nuclei. *Nature* 481, 502–505.

Pijpers, A., Voogd, J., and Ruigrok, T. J. H. (2005). Topography of olivo-cortico-nuclear modules in the intermediate cerebellum of the rat. *J. Comp. Neurol.* 492, 193–213.

Quy, P. N., Fujita, H., Sakamoto, Y., Na, J., and Sugihara, I. (2011). Projection patterns of single mossy fiber axons originating from the dorsal column nuclei mapped on the aldolase C compartments in the rat cerebellar cortex. *J. Comp. Neurol.* 519, 874–899.

Ramón y Cajal, S. (1911). *Histologie du Systeme Nerveux de l'Homme et des Vertébrés, Vol. II*. Paris: Maloine.

Rosina, A., and Provini, L. (1983). Somatotopy of climbing fiber branching to the cerebellar cortex in cat. *Brain Res.* 289, 45–63.

Ruigrok, T. J. H., and Voogd, J. (1990). Cerebellar nucleo-olivary projections in rat. An anterograde tracing study with Phaseolus vulgaris leucoagglutinin (PHA-L). *J. Comp. Neurol.* 298, 315–333.

Sasaki, K., Bower, J. M., and Llinás, R. (1989). Multiple Purkinje cell recording in rodent cerebellar cortex. *Eur. J. Neurosci.* 1, 572–586.

Schild, R. F. (1970). On the inferior olive of the albino rat. *J. Comp. Neurol.* 140, 255–260.

Snider, R. S. (1950). Recent contributions to the anatomy and physiology of the cerebellum. *Arch. Neruol. Psychiatry* 64, 196–219.

Sotelo, C. (2004). Cellular and genetic regulation of the development of the cerebellar system. *Prog. Neurobiol.* 72, 295–339.

Sotelo, C., Bourrat, F., and Triller, A. (1984). Postnatal development of the inferior olivary complex in the rat. II. Topographic organization of the immature olivocerebellar projection. *J. Comp. Neurol.* 222, 177–199.

Sugihara, I. (2005). Microzonal projection and climbing fiber remodeling in single olivocerebellar axons of newborn rats at postnatal days 4–7. *J. Comp. Neurol.* 487, 93–106.

Sugihara, I. (2006). Organization and remodeling of the olivocerebellar climbing fiber projection. *Cerebellum* 5, 15–22.

Sugihara, I. (2011). Compartmentalization of the deep cerebellar nuclei based on afferent projections and aldolase C expression. *Cerebellum* 10, 449–463.

Sugihara, I., Ebata, S., and Shinoda, Y. (2004). Functional compartmentalization in the flocculus and the ventral dentate and dorsal group y nuclei: an analysis of single olivocerebellar axonal morphology. *J. Comp. Neurol.* 470, 113–133.

Sugihara, I., Fujita, H., Na, J., Quy, P. N., Li, B. Y., and Ikeda, D. (2009). Projection of reconstructed single Purkinje cell axons in relation to the cortical and nuclear aldolase C compartments of the rat cerebellum. *J. Comp. Neurol.* 512, 282–304.

Sugihara, I., and Quy, P. N. (2007). Identification of aldolase C compartments in the mouse cerebellar cortex by olivocerebellar labeling. *J. Comp. Neurol.* 500, 1076–1092.

Sugihara, I., and Shinoda, Y. (2004). Molecular, topographic, and functional organization of the cerebellar cortex: a study with combined aldolase C and olivocerebellar labeling. *J. Neurosci.* 24, 8771–8785.

Sugihara, I., and Shinoda, Y. (2007). Molecular, topographic and functional organization of the cerebellar nuclei: analysis by three-dimensional mapping of the olivonuclear projection and aldolase C labeling. *J. Neurosci.* 27, 9696–9710.

Sugihara, I., Wu, H.-S., and Shinoda, Y. (1999). Morphology of single olivocerebellar axons labeled with biotinylated dextran amine in the rat. *J. Comp. Neurol.* 414, 131–148.

Sugihara, I., Wu, H.-S., and Shinoda, Y. (2001). The entire trajectories of single olivocerebellar axons in the cerebellar cortex and their contribution to cerebellar compartmentalization. *J. Neurosci.* 21, 7715–7723.

Sürmeli, G., Akay, T., Ippolito, G. C., Tucker, P. W., and Jessell, T. M. (2011). Patterns of spinal sensory-motor connectivity prescribed by a dorsoventral positional template. *Cell* 147, 653–665.

Takeda, T., and Maekawa, K. (1989). Olivary branching projections to the flocculus, nodulus and uvula in the rabbit. II. Retrograde double labeling study with fluorescent dyes. *Exp. Brain Res.* 76, 323–332.

Timmann, D., Konczak, J., Ilg, W., Donchin, O., Hermsdörfer, J., Gizewski, E. R., et al. (2009). Currrent advances in lesion-symptom mapping of the human cerebellum. *Neuroscience* 162, 836–851.

Van der Want, J. J. L., Wiklund, L., Guegan, M., Ruigrok, T. J. H., and Voogd, J. (1989). Anterograde tracing of the rat olivocerebellar system with *Phaseolus vulgaris* leucoagglutinin (PHA-L). Demonstration of climbing fiber collateral innervation of the cerebellar nuclei. *J. Comp. Neurol.* 288, 1–18.

Voogd, J., and Bigaré, F. (1980). "Topographical distribution of olivary and cortico nuclear fibers in the cerebellum: a review," in *The Inferior Olivary Nucleus, Anatomy and Physiology*, eds J. Courville, C. de Montigny, and Y. Lamarre (New York, NY: Raven Press), 207–234.

Voogd, J., Pardoe, J., Ruigrok, T. J. H., and Apps, R. (2003). The distribution of climbing and mossy fiber collateral branches from the copula pyramidis and the paramedian lobule: congruence of climbing fiber cortical zones and the pattern of zebrin banding within the rat cerebellum. *J. Neurosci.* 23, 4645–4656.

Wilson, S. L., Kalinovsky, A., Orvis, G. D., and Joyner, A. L. (2011). Spatially restricted and developmentally dynamic expression of engrailed genes in multiple cerebellar cell types. *Cerebellum* 10, 356–372.

Wise, A. K., Cerminara, N. L., Marple-Horvat, D. E., and Apps, R. (2010). Mechanisms of synchronous activity in cerebellar Purkinje cells. *J. Physiol.* 588, 2373–2390.

Wu, H. S., Sugihara, I., and Shinoda, Y. (1999). Projection patterns of single mossy fibers originating from the lateral reticular nucleus in the rat cerebellar cortex and nuclei. *J. Comp. Neurol.* 411, 97–118.

Conflict of Interest Statement: The authors declare that the research was conducted in the absence of any commercial or financial relationships that could be construed as a potential conflict of interest.

Received: 10 September 2012; accepted: 08 January 2013; published online: 04 February 2013.

Citation: Fujita H and Sugihara I (2013) Branching patterns of olivocerebellar axons in relation to the compartmental organization of the cerebellum. Front. Neural Circuits 7:3. doi: 10.3389/fncir.2013.00003

frontiers in
NEURAL CIRCUITS

PERSPECTIVE ARTICLE
published: 21 February 2013
doi: 10.3389/fncir.2013.00025

Structural plasticity of climbing fibers and the growth-associated protein GAP-43

Giorgio Grasselli*[1] *and* ***Piergiorgio Strata*[2]**

[1] *Department of Neurobiology, University of Chicago, Chicago, IL, USA*
[2] *National Institute of Neuroscience-Italy, University of Turin, Turin, Italy*

Edited by:
Chris I. De Zeeuw, Erasmus MC, Netherlands

Reviewed by:
David Linden, Johns Hopkins University, USA
Patricia C. Salinas, University College London, UK

****Correspondence:***
Giorgio Grasselli, Department of Neurobiology, University of Chicago, 947 E. 58th Street, MC0928, Chicago, IL 60637, USA.
e-mail: ggrasselli@uchicago.edu

Structural plasticity occurs physiologically or after brain damage to adapt or re-establish proper synaptic connections. This capacity depends on several intrinsic and extrinsic determinants that differ between neuron types. We reviewed the significant endogenous regenerative potential of the neurons of the inferior olive (IO) in the adult rodent brain and the structural remodeling of the terminal arbor of their axons, the climbing fiber (CF), under various experimental conditions, focusing on the growth-associated protein GAP-43. CFs undergo remarkable collateral sprouting in the presence of denervated Purkinje cells (PCs) that are available for new innervation. In addition, severed olivo-cerebellar axons regenerate across the white matter through a graft of embryonic Schwann cells. In contrast, CFs undergo a regressive modification when their target is deleted. *In vivo* knockdown of GAP-43 in olivary neurons, leads to the atrophy of their CFs and a reduction in the ability to sprout toward surrounding denervated PCs. These findings demonstrate that GAP-43 is essential for promoting denervation-induced sprouting and maintaining normal CF architecture.

Keywords: climbing fiber, GAP-43, sprouting, atrophy, branching

INTRODUCTION

Structural plasticity is limited in the central nervous system (CNS) of adult mammals, constituting a significant impediment to recovery from injuries such as those caused by trauma, stroke, and neurodegenerative and demyelinating diseases (Duffau, 2006; Wieloch and Nikolich, 2006; Landi and Rossini, 2010). Nevertheless, a relatively high degree of structural plasticity is retained by certain areas of brain, such as the cerebellum (Carulli et al., 2004; Cesa and Strata, 2009).

The cerebellar climbing fiber (CF), the terminal arbor of the olivo-cerebellar axons, has provided the first example, in the mammalian CNS, of individually observed fibers undergoing sprouting after brain injury (Rossi et al., 1991a,b). In 6-weeks-old Wistar rats, CFs normally encompass approximately 1000 μm of dendritic length and bear an average of 544 ± 23 varicosities that express the vesicular glutamate transporter VGLUT2 (Grasselli et al., 2011).

CFs constitute a suitable model that can be used to investigate axonal structural plasticity, based on their significant plastic potential and morphological hallmarks. In fact, they have a one-to-one relationship with their target Purkinje cell (PC). CFs undergo lesion-induced sprouting, activity-dependent remodeling, expansion of their area of innervation in response to an enlarged target territory, and regressive modifications after elimination of their target (Rossi and Strata, 1995; Strata and Rossi, 1998; Cesa and Strata, 2009).

STRUCTURAL PLASTICITY OF CLIMBING FIBERS

Neurons differ widely in regard to their response to axonal injuries (Carulli et al., 2004; Dusart et al., 2005). For example, in the cerebellum, PCs respond to injury with little upregulation of plasticity-related genes in the cell body, no axonal regeneration after axotomy, and weak sprouting; most PCs survive, but they usually do not increase the expression of plasticity-related genes, except when the axotomy occurs near the cell body (Rossi et al., 1995; Bravin et al., 1997; Zagrebelsky et al., 1998; Wehrle et al., 2001; Morel et al., 2002; Gianola and Rossi, 2004). Further, axonal sprouting is limited and might be induced only following proper manipulation of intrinsic and environmental factors (Buffo et al., 1997, 2000; Zagrebelsky et al., 1998; Zhang et al., 2005, 2007).

In contrast, neurons in the inferior olive (IO) respond dramatically to axonal injury. The resection of olivo-cerebellar axons leads to the regression of the remaining stump and the death of many axotomized neurons in the IO during the first few weeks after injury (Buffo et al., 1998). Concurrently, olivary neurons upregulate several intrinsic factors, including nitric oxide synthase (NOS), c-Jun, JunD, the early growth response protein EGR1/Krox-24 (Rossi and Strata, 1995; Bravin et al., 1997; Buffo et al., 1998, 2003; Wehrle et al., 2001).

As a result of this upregulation and the high constitutive levels of growth-associated factors in olivary neurons, such as GAP-43, MARCKS, EGR-1/KROX-24, L1CAM, and PSA-NCAM in the olivary neurons (Kruger et al., 1993; Herdegen et al., 1995; McNamara and Lenox, 1997; Fernandez et al., 1999; Horinouchi et al., 2005), lesioned olivo-cerebellar axons can elongate and innervate their target PCs when an appropriate permissive environment is provided, such as neonatal Schwann cells that have been inserted at the site of axotomy (Bravin et al., 1997). Lesioned olivo-cerebellar fibers can also elongate into a transplant of embryonic cerebellum, where they innervate the

grafted PCs, forming new CFs (Gardette et al., 1988; Rossi et al., 1995).

The constitutive regenerative properties of olivo-cerebellar fibers render them responsive to axotomy and to the expansion or deletion of their target PC territory in the absence of direct cellular lesions. Grafting embryonic cerebellar tissue onto the surface of a non-lesioned host cerebellum leads to the formation of a minicerebellum whose PCs become innervated by collateral sprouting of intact host CFs that elongate across the pial barrier, likely under the influence of target diffusible factors. Consequently, they form new CF-like structures in the minicerebellum (**Figure 1A**) and on PCs that have migrated inside the host cerebellar parenchyma (Rossi et al., 1992) and establish functional synapses (Tempia et al., 1996).

Moreover, CFs can innervate and establish new functional synapses with additional nearby PCs, if the latter are deprived of their original CF innervation due to the neuronal degeneration of part of olivary neurons, selectively among pre-cerebellar nuclei, induced by intraperitoneal administration of the niacinamide analog 3-acetylpyridine (3-AP; **Figure 1B**) (Desclin and Escubi, 1974; Benedetti et al., 1983; Rossi et al., 1991a,b). Further, in neonatal rats (to 7–10 days after birth), olivo-cerebellar axons sprout and form long transcommissural branches to reinnervate the opposite hemicerebellum if it is denervated by transection of its peduncle (Sherrard et al., 1986). This form of transcommissural growth can be induced experimentally after development (30 days after birth) by infusion of exogenous BDNF (Dixon and Sherrard, 2006) or IGF-I (Sherrard and Bower, 2003) into the denervated hemicerebellum.

Conversely, if the target PC is deleted by neurotoxins, the CF arbor becomes atrophic, shrinking, and altering the shape of the varicosities (**Figure 1C**) (Rossi et al., 1993, 1995). Also, on blockade of electrical activity by tetrodotoxin or on inhibition of AMPA glutamate receptors with an infusing NBQX into the cerebellar parenchyma for 7 days, the varicosities of CFs decrease significantly in size, and fewer synaptic contacts are made with the spines of the proximal dendritic domain of PCs (Bravin et al., 1999; Cesa et al., 2007). These changes are attributed to findings that electrical activity mediates in the ongoing competition between the CF and parallel fibers (Cesa and Strata, 2009). Electrical activity of IO neurons also impedes the motility of the transverse branches of the CF that extend perpendicularly to the plane of the major structure of the fiber (Nishiyama et al., 2007).

EXTRINSIC AND INTRINSIC FACTORS IN CF PLASTICITY: THE FUNCTION OF GAP-43

The molecular determinants that induce, guide, and regulate CF elongation and innervation of PCs are only partially clarified. Like most mature CNS neurons, CFs can grow only in limited space that is devoid of extrinsic inhibitory influences, such as the

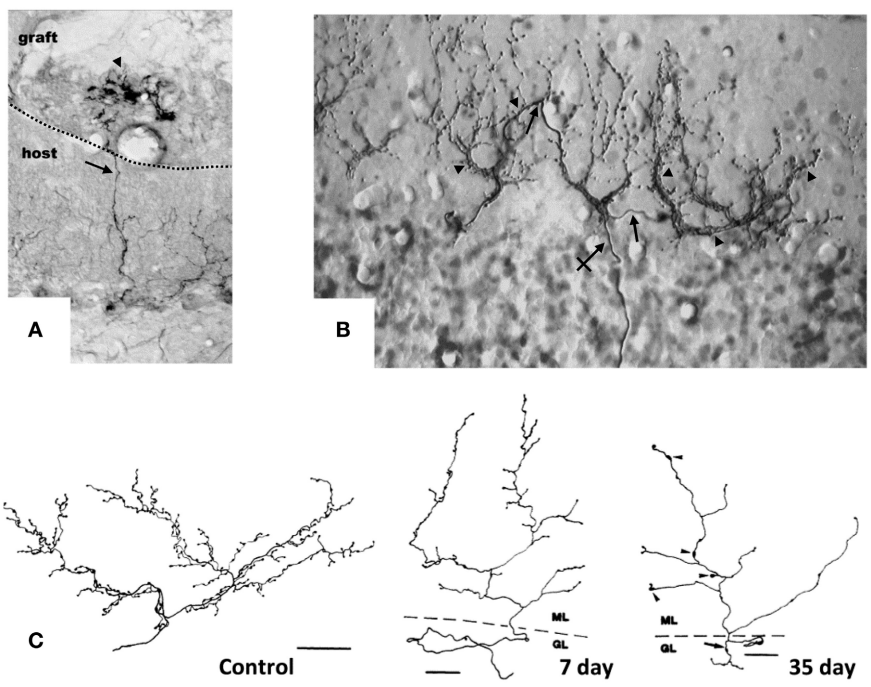

FIGURE 1 | Target-dependent structural plasticity of CFs. (A) Sprouting of adult CFs 7 days following transplantation of embryonic cerebellum on to the surface of the adult cerebellar cortex. The sprouts (arrows) innervate PCs in the graft (arrowheads). Dotted line: host-graft border (Rossi et al., 1994, unpublished). **(B)** CF sprouting and innervation of adjacent PCs previously denervated by a partial lesion of the IO, shown 1 year after the lesion on a sagittal plane. From 1 olivo-cerebellar axon (crossed arrow), a CFs is formed with collateral branches (arrows) giving rise to new CF-like structures (arrowheads) innervating the adjacent PCs (Rossi et al., 1991b). **(C)** A control CF and atrophic modification induced in CFs 7 and 35 days after deletion of PCs. CFs were reconstructed using a camera lucida. GL, granular layer; ML, molecular layer. Scale bar: 30 μm, 25 μm, and 25 μm, respectively, for control, 7 and 35 days (Rossi et al., 1993). CFs were labeled by PHA-l axon tracing, PCs by anti-calbindin immunostaining.

cerebellar molecular layer, which lacks inhibitory myelin growth factors.

More is known about the intrinsic factors that confer highly plastic properties to CFs. The well-characterized plasticity of mature IO neurons is associated with high, constitutive expression of the growth-associated proteins GAP-43, EGR-1/KROX-24, MARCKS, L1CAM, and PSA-NCAM, and with the upregulation of c-Jun, JunD, Krox-24, and NOS in response to axonal lesions. However, the contribution of each factor is still not clear.

GAP-43 was one of the first of these proteins to be studied extensively and described for its abundance in axonal growth cones (Zwiers et al., 1976; Skene and Willard, 1981); thus it is used widely as a marker of axonal sprouting (Oestreicher et al., 1997). GAP-43 (also known as neuromodulin and B-50) mediates axonal growth, branching, and pathfinding during development. Mice that lack this protein have a low survival rate in the early postnatal period (Strittmatter et al., 1995; Maier et al., 1999). In humans, heterozygous chromosomal deletions comprising the locus for *Gap-43* gene (3q13.10–3q13.21) are linked to agenesis of the *corpus callosum* and severe mental retardation (Genuardi et al., 1994; Mackie Ogilvie et al., 1998).

GAP-43 plays a pivotal role not only during development but also in axonal remodeling in the adult brain. Its expression rises in several conditions that induce neuronal rewiring, such as the disruption of the neuronal networks due to pathological or traumatic lesions (Benowitz et al., 1990; Oestreicher et al., 1997; Buffo et al., 2003): it is upregulated in the motoneurons of dystrophin-deficient mice (*mdx* mice), a model of human muscular dystrophy, in which degeneration-regeneration events in muscle fibers are accompanied by remodeling of intramuscular terminal nerve fibers (Verzè et al., 1996), and after the induction of robust neuronal activity, for example due to seizure or electrical stimulation (McNamara and Routtenberg, 1995; Cantallops and Routtenberg, 1996; Miyake et al., 2002; Sharma et al., 2010).

Complex alterations in GAP-43 expression are frequently observed in human neuropathologies and their animal models, suggesting axonal damage or attempts of regenerative axonal sprouting. For instance GAP-43 expression declines in the frontal cortex and certain areas of the hippocampus in Alzheimer patients but is robust in association with senile-like plaques (Bogdanovic et al., 2000). Moreover, GAP-43 levels decrease in most lesions in the white matter of patients with multiple sclerosis and increase in some remyelinated white matter tracts (Teunissen et al., 2006).

In several experimental conditions, GAP-43 overexpression *in vivo* increases axonal sprouting. In transgenic mice that overexpress GAP-43, motoneurons undergo axonal sprouting, even spontaneously in the absence of injuries, and increased sprouting after lesion. These mice experience prominent, spontaneous sprouting of mossy fibers in the dentate gyrus (Aigner et al., 1995). As discussed, when GAP-43 was overexpressed in PCs, their axons sprout profusely along their length and at their stump even at sites that are covered by myelin demonstrating that its overexpression is sufficient to induce sprouting in the absence of any injury and promote lesion-induced sprouting in PCs (Buffo et al., 1997; Gianola and Rossi, 2004). In a recent report, after silencing the expression of GAP-43 in IO neurons of juvenile wild-type rats using shRNA-expressing lentiviral vectors, their CFs were virtually unable to sprout in response to 3-AP-induced denervation of PCs (**Figure 2A**) (Grasselli et al., 2011). The few CFs that were, however, still able to sprout were significantly smaller than control fibers (**Figures 2B,C**). Because IO neurons are heterogeneous with regards to sprouting and gene expression after axotomy (Buffo et al., 2003), a more in-depth examination of the differences in CF morphology and their relationship to gene expression profiles of their neurons should provide greater insight into the function of the factors that regulate CF morphology.

GAP-43 is not only necessary for CF sprouting but plays also a crucial role for normal neuronal morphology in non-traumatic conditions. The mere silencing of GAP-43 destabilizes CF structure in the absence of any insult (**Figures 2D–G**) (Grasselli et al., 2011). Control CFs normally comprises a thick axonal stalk from which many thin collaterals emerge (namely tendrils), forming a net-like structure around the PC dendrite and bearing varicosities (Rossi et al., 1991b; Sugihara et al., 1999). Their structure has been examined quantitatively and a recent complete digital reconstruction shows that tendrils and distal branches are richer in varicosities (Brown et al., 2012).

On silencing GAP-43, CFs alter their structure, extending fewer tendrils along their proximal and distal portions (**Figures 2D–G**), quantified as a significant 17% reduction in the density of varicosities, as defined by their morphology and VGLUT2 expression. Further, the most distal portions of CFs, which have fewer tendrils and a thinner stalk, are affected by GAP-43 silencing, which shortens CF length by 33%. These data have been confirmed in 2–3-months-old mice (Grasselli et al., 2011).

Several lines of evidence support a model in which GAP-43 is needed for proper interaction of the axon with its target neuron and organization of the molecular machinery that supports axonal structures during axonal growth. In GAP-43 knockout mice, the axons of retinal ganglion cells fail to cross the optic chiasm properly (Strittmatter et al., 1995), instead assuming abnormal trajectories in the chiasm (Sretavan and Kruger, 1998). Moreover, these mice fail to form the anterior commissure, hippocampal commissure, and *corpus callosum* (Shen et al., 2002), consistently with the agenesis of the *corpus callosum* observed in patients who bear heterozygous chromosomal deletions comprising the *Gap-43* locus (Genuardi et al., 1994; Mackie Ogilvie et al., 1998).

In the hippocampus of transgenic mice that overexpress an inactive mutant form of GAP-43 that cannot be phosphorylated (with an amino acid substitution S42A), mossy fibers grow ectopically to their normal target layer, innervating the distal *stratum oriens* (Holahan et al., 2010). Notably, similar ectopic growth was observed in mice lacking the neuronal cell adhesion molecule NCAM (Cremer et al., 1997; Bukalo et al., 2004). L1CAM, another adhesion molecule that mediates commissural axon guidance (Kamiguchi et al., 1998; Demyanenko et al., 1999), regulates GAP-43 pathway, acting synergistically with it promoting axon growth and regeneration when overexpressed in PCs *in vivo* (Zhang et al., 2005).

L1CAM and NCAM are expressed at constitutively high levels in the IO (Horinouchi et al., 2005; Quartu et al., 2010), and

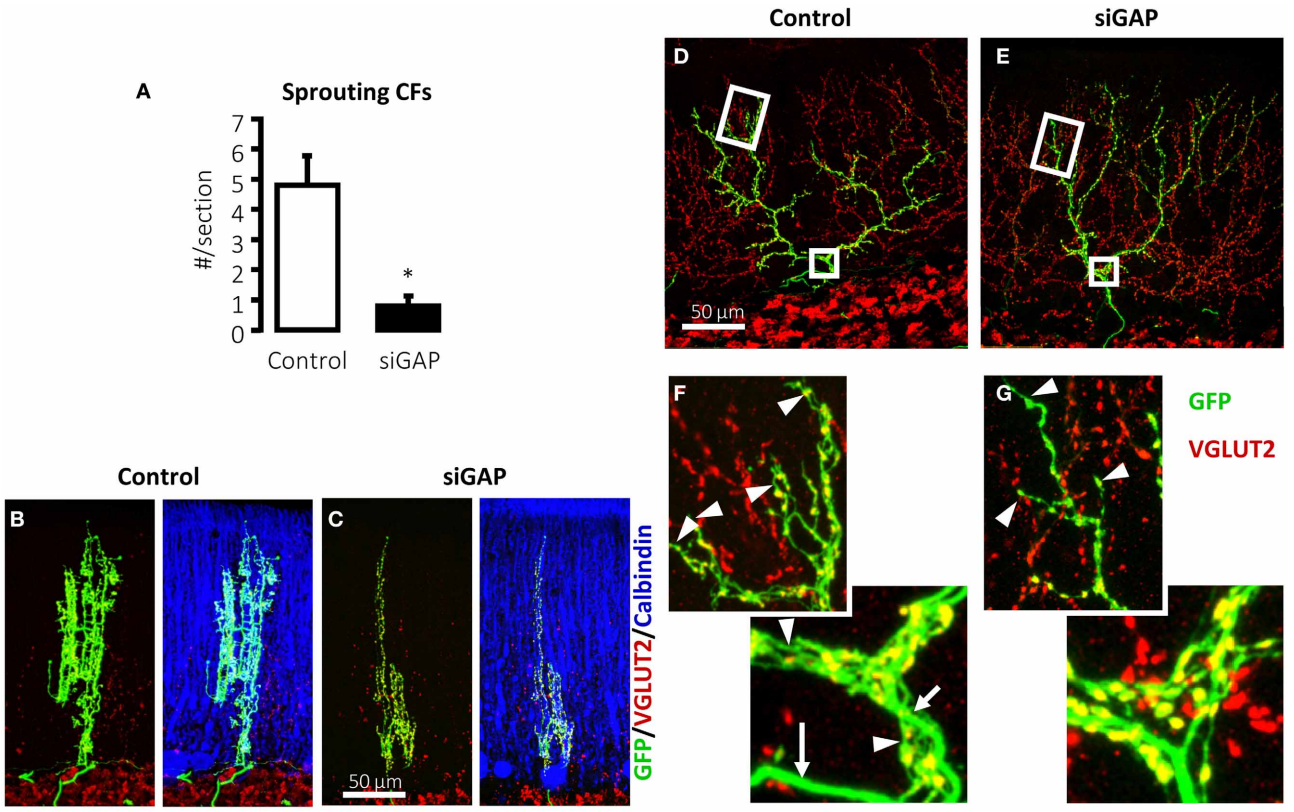

FIGURE 2 | Silencing of GAP-43 in CFs prevents its sprouting and induces atrophy. (A) Sprouting in GFP-positive CFs, induced by a sub-total lesion of the IO, is dramatically reduced to nearly null levels in rats treated with GAP-43-silencing vectors (siGAP) 3 weeks before the lesion compared with controls as observed on coronal sections ($N = 3$ and 5 animals, respectively; $^*p < 0.05$; mean ± SEM). **(B,C)** The total extension of CFs that are still able to grow sprouts following GAP-43 silencing was also significantly reduced as assessed on coronal sections. **(D,E)** Representative confocal images of rat CFs in sagittal sections under normal conditions 3 weeks after treatment with control or silencing vectors. **(F,G)** Details of the most distal segment and first main branching point of CFs shown in **(D,E)**, showing a reduction in number and length of tendrils and consequent decrease in the density of varicosities. Arrows: thick axonal stalks; arrowheads: examples of tendrils [GFP, green; VGLUT2, red; calbindin, blue; modified from Grasselli et al. (2011)].

GAP-43 responds to the NCAM pathway by being phosphorylated by protein kinase C (PKC), ultimately binding the actin filaments and other scaffolding proteins stabilizing their cytoskeletal complexes (Oestreicher et al., 1997; Riederer and Routtenberg, 1999; Mosevitsky, 2005; Denny, 2006; Chakravarthy et al., 2008; Ditlevsen et al., 2008). These findings suggests that, in CFs, GAP-43 synergizes with cell adhesion molecules to transduce target-dependent signals and stabilize the cytoskeleton.

In addition to maintaining of CF structure, GAP-43 might also govern the organization of the presynaptic terminal and, consequently, neurotransmitter release. When GAP-43 is silenced, CF varicosities undergo alteration in morphology, becoming rounder and larger compared with control varicosities (Grasselli et al., 2011), which are often irregularly shaped and smaller, mirroring the phenotype observed after blockade of AMPA receptor (Cesa et al., 2007). These changes might be related to GAP-43 calcium- and PKC-dependent control of the cytoskeleton.

Several studies have also established the involvement of GAP-43 in neurotransmitter release and synaptic plasticity (Dekker et al., 1989; Gianotti et al., 1992; Ramakers et al., 1995, 1999, 2000; Biewenga et al., 1996; Kantor and Gnegy, 1998; Routtenberg et al., 2000; Hulo et al., 2002; Denny, 2006; Powell, 2006; Holahan and Routtenberg, 2008; Holahan et al., 2010), reporting direct calcium-dependent interactions with components of the synaptic machinery, such as SNAP-25, syntaxin, and VAMP (Haruta et al., 1997), and with rabaptin-5, which regulate the recycling of synaptic vesicle (Neve et al., 1998).

Thus, increasing evidence suggest that GAP-43 has a double role in mature CFs in sustaining both injury-induced sprouting and the maintaining their structure under normal conditions, possibly by mediating cytoskeletal reorganization that is triggered by cell adhesion molecules and CFs interactions with their target. In addition GAP-43 appears to regulate the organization of CF presynaptic terminal and neurotransmitter release.

Emerging technologies, such as 2-photon microscopy and laser axotomy, will allow us to monitor cells during injury and repair in live mammalian brains and induce microscopic lesions, enabling us to determine the sequence of structural remodeling events that occur in single fibers after axotomy (Holtmaat and Svoboda, 2009; Allegra Mascaro et al., 2010).

REFERENCES

Aigner, L., Arber, S., Kapfhammer, J. P., Laux, T., Schneider, C., Botteri, F., et al. (1995). Overexpression of the neural growth-associated protein GAP-43 induces nerve sprouting in the adult nervous system of transgenic mice. *Cell* 83, 269–278.

Allegra Mascaro, A. L., Sacconi, L., and Pavone, F. S. (2010). Multiphoton nanosurgery in live brain. *Front. Neuroenergetics* 2:21. doi: 10.3389/fnene.2010.00021

Benedetti, F., Montarolo, P. G., Strata, P., and Tosi, L. (1983). "Collateral reinnervation in the olivocerebellar pathway in the rat," in *Birth Defects Original Article Series*, eds P.-P. J. Haber, B. Hashim, G. Giuffrida-Stella Am (New York, NY: Alan Liss, Inc.), 461–464.

Benowitz, L. I., Rodriguez, W. R., and Neve, R. L. (1990). The pattern of GAP-43 immunostaining changes in the rat hippocampal formation during reactive synaptogenesis. *Brain Res. Mol. Brain Res.* 8, 17–23.

Biewenga, J. E., Schrama, L. H., and Gispen, W. H. (1996). Presynaptic phosphoprotein B-50/GAP-43 in neuronal and synaptic plasticity. *Acta Biochim. Pol.* 43, 327–338.

Bogdanovic, N., Davidsson, P., Volkmann, I., Winblad, B., and Blennow, K. (2000). Growth-associated protein GAP-43 in the frontal cortex and in the hippocampus in Alzheimer's disease: an immunohistochemical and quantitative study. *J. Neural Trans.* 107, 463–478.

Bravin, M., Morando, L., Vercelli, A., Rossi, F., and Strata, P. (1999). Control of spine formation by electrical activity in the adult rat cerebellum. *Proc. Natl. Acad. Sci. U.S.A.* 96, 1704–1709.

Bravin, M., Savio, T., Strata, P., and Rossi, F. (1997). Olivocerebellar axon regeneration and target reinnervation following dissociated Schwann cell grafts in surgically injured cerebella of adult rats. *Eur. J. Neurosci.* 9, 2634–2649.

Brown, K. M., Sugihara, I., Shinoda, Y., and Ascoli, G. A. (2012). Digital morphometry of rat cerebellar climbing fibers reveals distinct branch and bouton types. *J. Neurosci.* 32, 14670–14684.

Buffo, A., Carulli, D., Rossi, F., and Strata, P. (2003). Extrinsic regulation of injury/growth-related gene expression in the inferior olive of the adult rat. *Eur. J. Neurosci.* 18, 2146–2158.

Buffo, A., Fronte, M., Oestreicher, A. B., and Rossi, F. (1998). Degenerative phenomena and reactive modifications of the adult rat inferior olivary neurons following axotomy and disconnection from their targets. *Neuroscience* 85, 587–604.

Buffo, A., Holtmaat, A. J., Savio, T., Verbeek, J. S., Oberdick, J., Oestreicher, A. B., et al. (1997). Targeted overexpression of the neurite growth-associated protein B-50/GAP-43 in cerebellar Purkinje cells induces sprouting after axotomy but not axon regeneration into growth-permissive transplants. *J. Neurosci.* 17, 8778–8791.

Buffo, A., Zagrebelsky, M., Huber, A. B., Skerra, A., Schwab, M. E., Strata, P., et al. (2000). Application of neutralizing antibodies against NI-35/250 myelin-associated neurite growth inhibitory proteins to the adult rat cerebellum induces sprouting of uninjured Purkinje cell axons. *J. Neurosci.* 20, 2275–2286.

Bukalo, O., Fentrop, N., Lee, A. Y., Salmen, B., Law, J. W., Wotjak, C. T., et al. (2004). Conditional ablation of the neural cell adhesion molecule reduces precision of spatial learning, long-term potentiation, and depression in the CA1 subfield of mouse hippocampus. *J. Neurosci.* 24, 1565–1577.

Cantallops, I., and Routtenberg, A. (1996). Rapid induction by kainic acid of both axonal growth and F1/GAP-43 protein in the adult rat hippocampal granule cells. *J. Comp. Neurol.* 366, 303–319.

Carulli, D., Buffo, A., and Strata, P. (2004). Reparative mechanisms in the cerebellar cortex. *Prog. Neurobiol.* 72, 373–398.

Cesa, R., Scelfo, B., and Strata, P. (2007). Activity-dependent presynaptic and postsynaptic structural plasticity in the mature cerebellum. *J. Neurosci.* 27, 4603–4611.

Cesa, R., and Strata, P. (2009). Axonal competition in the synaptic wiring of the cerebellar cortex during development and in the mature cerebellum. *Neuroscience* 162, 624–632.

Chakravarthy, B., Rashid, A., Brown, L., Tessier, L., Kelly, J., and Menard, M. (2008). Association of Gap-43 (neuromodulin) with microtubule-associated protein MAP-2 in neuronal cells. *Biochem. Biophys. Res. Commun.* 371, 679–683.

Cremer, H., Chazal, G., Goridis, C., and Represa, A. (1997). NCAM is essential for axonal growth and fasciculation in the hippocampus. *Mol. Cell. Neurosci.* 8, 323–335.

Dekker, L. V., De Graan, P. N., Oestreicher, A. B., Versteeg, D. H., and Gispen, W. H. (1989). Inhibition of noradrenaline release by antibodies to B-50 (GAP-43). *Nature* 342, 74–76.

Demyanenko, G. P., Tsai, A. Y., and Maness, P. F. (1999). Abnormalities in neuronal process extension, hippocampal development, and the ventricular system of L1 knockout mice. *J. Neurosci.* 19, 4907–4920.

Denny, J. B. (2006). Molecular mechanisms, biological actions, and neuropharmacology of the growth-associated protein GAP-43. *Curr. Neuropharmacol.* 4, 293–304.

Desclin, J. C., and Escubi, J. (1974). Effects of 3-acetylpyridine on the central nervous system of the rat, as demonstrated by silver methods. *Brain Res.* 77, 349–364.

Ditlevsen, D. K., Povlsen, G. K., Berezin, V., and Bock, E. (2008). NCAM-induced intracellular signaling revisited. *J. Neurosci. Res.* 86, 727–743.

Dixon, K. J., and Sherrard, R. M. (2006). Brain-derived neurotrophic factor induces post-lesion transcommissural growth of olivary axons that develop normal climbing fibers on mature Purkinje cells. *Exp. Neurol.* 202, 44–56.

Duffau, H. (2006). Brain plasticity: from pathophysiological mechanisms to therapeutic applications. *J. Clin. Neurosci.* 13, 885–897.

Dusart, I., Ghoumari, A., Wehrle, R., Morel, M. P., Bouslama-Oueghlani, L., Camand, E., et al. (2005). Cell death and axon regeneration of Purkinje cells after axotomy: challenges of classical hypotheses of axon regeneration. *Brain Res. Brain Res. Rev.* 49, 300–316.

Fernandez, A. M., Gonzalez De La Vega, A. G., Planas, B., and Torres-Aleman, I. (1999). Neuroprotective actions of peripherally administered insulin-like growth factor I in the injured olivo-cerebellar pathway. *Eur. J. Neurosci.* 11, 2019–2030.

Gardette, R., Alvarado-Mallart, R. M., Crepel, F., and Sotelo, C. (1988). Electrophysiological demonstration of a synaptic integration of transplanted Purkinje cells into the cerebellum of the adult Purkinje cell degeneration mutant mouse. *Neuroscience* 24, 777–789.

Genuardi, M., Calvieri, F., Tozzi, C., Coslovi, R., and Neri, G. (1994). A new case of interstitial deletion of chromosome 3q, del(3q)(q13.12q21.3), with agenesis of the corpus callosum. *Clin. Dysmorphol.* 3, 292–296.

Gianola, S., and Rossi, F. (2004). GAP-43 overexpression in adult mouse Purkinje cells overrides myelin-derived inhibition of neurite growth. *Eur. J. Neurosci.* 19, 819–830.

Gianotti, C., Nunzi, M. G., Gispen, W. H., and Corradetti, R. (1992). Phosphorylation of the presynaptic protein B-50 (GAP-43) is increased during electrically induced long-term potentiation. *Neuron* 8, 843–848.

Grasselli, G., Mandolesi, G., Strata, P., and Cesare, P. (2011). Impaired sprouting and axonal atrophy in cerebellar climbing fibres following *in vivo* silencing of the growth-associated protein GAP-43. *PLoS ONE* 6:e20791. doi: 10.1371/journal.pone.0020791

Haruta, T., Takami, N., Ohmura, M., Misumi, Y., and Ikehara, Y. (1997). Ca2+-dependent interaction of the growth-associated protein GAP-43 with the synaptic core complex. *Biochem. J.* 325(Pt 2), 455–463.

Herdegen, T., Kovary, K., Buhl, A., Bravo, R., Zimmermann, M., and Gass, P. (1995). Basal expression of the inducible transcription factors c-Jun, JunB, JunD, c-Fos, FosB, and Krox-24 in the adult rat brain. *J. Comp. Neurol.* 354, 39–56.

Holahan, M., and Routtenberg, A. (2008). The protein kinase C phosphorylation site on GAP-43 differentially regulates information storage. *Hippocampus* 18, 1099–1102.

Holahan, M. R., Honegger, K. S., and Routtenberg, A. (2010). Ectopic growth of hippocampal mossy fibers in a mutated GAP-43 transgenic mouse with impaired spatial memory retention. *Hippocampus* 20, 58–64.

Holtmaat, A., and Svoboda, K. (2009). Experience-dependent structural synaptic plasticity in the mammalian brain. *Nat. Rev. Neurosci* 10, 647–658.

Horinouchi, K., Nakamura, Y., Yamanaka, H., Watabe, T., and Shiosaka, S. (2005). Distribution of L1cam mRNA in the adult mouse brain: *in situ* hybridization and Northern blot analyses. *J. Comp. Neurol.* 482, 386–404.

Hulo, S., Alberi, S., Laux, T., Muller, D., and Caroni, P. (2002). A point mutant of GAP-43 induces enhanced short-term and long-term hippocampal plasticity. *Eur. J. Neurosci.* 15, 1976–1982.

Kamiguchi, H., Hlavin, M. L., Yamasaki, M., and Lemmon, V. (1998). Adhesion molecules and

inherited diseases of the human nervous system. *Annu. Rev. Neurosci.* 21, 97–125.

Kantor, L., and Gnegy, M. E. (1998). Protein kinase C inhibitors block amphetamine-mediated dopamine release in rat striatal slices. *J. Pharmacol. Exp. Ther.* 284, 592–598.

Kruger, L., Bendotti, C., Rivolta, R., and Samanin, R. (1993). Distribution of GAP-43 mRNA in the adult rat brain. *J. Comp. Neurol.* 333, 417–434.

Landi, D., and Rossini, P. M. (2010). Cerebral restorative plasticity from normal ageing to brain diseases: a "never ending story." *Restor. Neurol. Neurosci.* 28, 349–366.

Mackie Ogilvie, C., Rooney, S. C., Hodgson, S. V., and Berry, A. C. (1998). Deletion of chromosome 3q proximal region gives rise to a variable phenotype. *Clin. Genet.* 53, 220–222.

Maier, D. L., Mani, S., Donovan, S. L., Soppet, D., Tessarollo, L., McCasland, J. S., et al. (1999). Disrupted cortical map and absence of cortical barrels in growth-associated protein (GAP)-43 knockout mice. *Proc. Natl. Acad. Sci. U.S.A.* 96, 9397–9402.

McNamara, R. K., and Lenox, R. H. (1997). Comparative distribution of myristoylated alanine-rich C kinase substrate (MARCKS) and F1/GAP-43 gene expression in the adult rat brain. *J. Comp. Neurol.* 379, 48–71.

McNamara, R. K., and Routtenberg, A. (1995). NMDA receptor blockade prevents kainate induction of protein F1/GAP-43 mRNA in hippocampal granule cells and subsequent mossy fiber sprouting in the rat. *Brain Res. Mol. Brain Res.* 33, 22–28.

Miyake, K., Yamamoto, W., Tadokoro, M., Takagi, N., Sasakawa, K., Nitta, A., et al. (2002). Alterations in hippocampal GAP-43, BDNF, and L1 following sustained cerebral ischemia. *Brain Res.* 935, 24–31.

Morel, M. P., Dusart, I., and Sotelo, C. (2002). Sprouting of adult Purkinje cell axons in lesioned mouse cerebellum: "non-permissive" versus "permissive" environment. *J. Neurocytol.* 31, 633–647.

Mosevitsky, M. I. (2005). Nerve ending "signal" proteins GAP-43, MARCKS, and BASP1. *Int. Rev. Cytol.* 245, 245–325.

Neve, R. L., Coopersmith, R., McPhie, D. L., Santeufemio, C., Pratt, K. G., Murphy, C. J., et al. (1998). The neuronal growth-associated protein GAP-43 interacts with rabaptin-5 and participates in endocytosis. *J. Neurosci.* 18, 7757–7767.

Nishiyama, H., Fukaya, M., Watanabe, M., and Linden, D. J. (2007). Axonal motility and its modulation by activity are branch-type specific in the intact adult cerebellum. *Neuron* 56, 472–487.

Oestreicher, A. B., De Graan, P. N., Gispen, W. H., Verhaagen, J., and Schrama, L. H. (1997). B-50, the growth associated protein-43: modulation of cell morphology and communication in the nervous system. *Prog. Neurobiol.* 53, 627–686.

Powell, C. M. (2006). Gene targeting of presynaptic proteins in synaptic plasticity and memory: across the great divide. *Neurobiol. Learn. Mem.* 85, 2–15.

Quartu, M., Serra, M. P., Boi, M., Melis, T., Ambu, R., and Del Fiacco, M. (2010). Brain-derived neurotrophic factor (BDNF) and polysialylated-neural cell adhesion molecule (PSA-NCAM): codistribution in the human brainstem precerebellar nuclei from prenatal to adult age. *Brain Res.* 1363, 49–62.

Ramakers, G. M., De Graan, P. N., Urban, I. J., Kraay, D., Tang, T., Pasinelli, P., et al. (1995). Temporal differences in the phosphorylation state of pre- and postsynaptic protein kinase C substrates B-50/GAP-43 and neurogranin during long-term potentiation. *J. Biol. Chem.* 270, 13892–13898.

Ramakers, G. M., Heinen, K., Gispen, W. H., and De Graan, P. N. (2000). Long term depression in the CA1 field is associated with a transient decrease in pre- and postsynaptic PKC substrate phosphorylation. *J. Biol. Chem.* 275, 28682–28687.

Ramakers, G. M., McNamara, R. K., Lenox, R. H., and De Graan, P. N. (1999). Differential changes in the phosphorylation of the protein kinase C substrates myristoylated alanine-rich C kinase substrate and growth-associated protein-43/B-50 following Schaffer collateral long-term potentiation and long-term depression. *J. Neurochem.* 73, 2175–2183.

Riederer, B. M., and Routtenberg, A. (1999). Can GAP-43 interact with brain spectrin? *Brain Res. Mol. Brain Res.* 71, 345–348.

Rossi, F., Borsello, T., and Strata, P. (1992). Embryonic Purkinje cells grafted on the surface of the cerebellar cortex integrate in the adult unlesioned cerebellum. *Eur. J. Neurosci.* 4, 589–593.

Rossi, F., Borsello, T., and Strata, P. (1994). Embryonic Purkinje cells grafted on the surface of the adult uninjured rat cerebellum migrate in the host parenchyma and induce sprouting of intact climbing fibres. *Eur. J. Neurosci.* 6, 121–136.

Rossi, F., Borsello, T., Vaudano, E., and Strata, P. (1993). Regressive modifications of climbing fibres following Purkinje cell degeneration in the cerebellar cortex of the adult rat. *Neuroscience* 53, 759–778.

Rossi, F., Jankovski, A., and Sotelo, C. (1995). Differential regenerative response of Purkinje cell and inferior olivary axons confronted with embryonic grafts: environmental cues versus intrinsic neuronal determinants. *J. Comp. Neurol.* 359, 663–677.

Rossi, F., and Strata, P. (1995). Reciprocal trophic interactions in the adult climbing fibre-Purkinje cell system. *Prog. Neurobiol.* 47, 341–369.

Rossi, F., Van Der Want, J. J., Wiklund, L., and Strata, P. (1991a). Reinnervation of cerebellar Purkinje cells by climbing fibres surviving a subtotal lesion of the inferior olive in the adult rat. II. Synaptic organization on reinnervated Purkinje cells. *J. Comp. Neurol.* 308, 536–554.

Rossi, F., Wiklund, L., Van Der Want, J. J., and Strata, P. (1991b). Reinnervation of cerebellar Purkinje cells by climbing fibres surviving a subtotal lesion of the inferior olive in the adult rat. I. Development of new collateral branches and terminal plexuses. *J. Comp. Neurol.* 308, 513–535.

Routtenberg, A., Cantallops, I., Zaffuto, S., Serrano, P., and Namgung, U. (2000). Enhanced learning after genetic overexpression of a brain growth protein. *Proc. Natl. Acad. Sci. U.S.A.* 97, 7657–7662.

Sharma, N., Marzo, S. J., Jones, K. J., and Foecking, E. M. (2010). Electrical stimulation and testosterone differentially enhance expression of regeneration-associated genes. *Exp. Neurol.* 223, 183–191.

Shen, Y., Mani, S., Donovan, S. L., Schwob, J. E., and Meiri, K. F. (2002). Growth-associated protein-43 is required for commissural axon guidance in the developing vertebrate nervous system. *J. Neurosci.* 22, 239–247.

Sherrard, R. M., and Bower, A. J. (2003). IGF-1 induces neonatal climbing-fibre plasticity in the mature rat cerebellum. *Neuroreport* 14, 1713–1716.

Sherrard, R. M., Bower, A. J., and Payne, J. N. (1986). Innervation of the adult rat cerebellar hemisphere by fibres from the ipsilateral inferior olive following unilateral neonatal pedunculotomy: an autoradiographic and retrograde fluorescent double-labelling study. *Exp. Brain Res.* 62, 411–421.

Skene, J. H., and Willard, M. (1981). Characteristics of growth-associated polypeptides in regenerating toad retinal ganglion cell axons. *J. Neurosci.* 1, 419–426.

Sretavan, D. W., and Kruger, K. (1998). Randomized retinal ganglion cell axon routing at the optic chiasm of GAP-43-deficient mice: association with midline recrossing and lack of normal ipsilateral axon turning. *J. Neurosci.* 18, 10502–10513.

Strata, P., and Rossi, F. (1998). Plasticity of the olivocerebellar pathway. *Trends Neurosci.* 21, 407–413.

Strittmatter, S. M., Fankhauser, C., Huang, P. L., Mashimo, H., and Fishman, M. C. (1995). Neuronal pathfinding is abnormal in mice lacking the neuronal growth cone protein GAP-43. *Cell* 80, 445–452.

Sugihara, I., Wu, H., and Shinoda, Y. (1999). Morphology of single olivocerebellar axons labeled with biotinylated dextran amine in the rat. *J. Comp. Neurol.* 414, 131–148.

Tempia, F., Bravin, M., and Strata, P. (1996). Postsynaptic currents and short-term synaptic plasticity in Purkinje cells grafted onto an uninjured adult cerebellar cortex. *Eur. J. Neurosci.* 8, 2690–2701.

Teunissen, C. E., Dijkstra, C. D., Jasperse, B., Barkhof, F., Vanderstichele, H., Vanmechelen, E., et al. (2006). Growth-associated protein 43 in lesions and cerebrospinal fluid in multiple sclerosis. *Neuropathol. App. Neurobiol.* 32, 318–331.

Verzè, L., Buffo, A., Rossi, F., Oestreicher, A. B., Gispen, W. H., and Strata, P. (1996). Increase of B-50/GAP-43 immunoreactivity in uninjured muscle nerves of MDX mice. *Neuroscience* 70, 807–815.

Wehrle, R., Caroni, P., Sotelo, C., and Dusart, I. (2001). Role of GAP-43 in mediating the responsiveness of cerebellar and precerebellar neurons to axotomy. *Eur. J. Neurosci.* 13, 857–870.

Wieloch, T., and Nikolich, K. (2006). Mechanisms of neural plasticity

following brain injury. *Curr. Opin. Neurobiol.* 16, 258–264.

Zagrebelsky, M., Buffo, A., Skerra, A., Schwab, M. E., Strata, P., and Rossi, F. (1998). Retrograde regulation of growth-associated gene expression in adult rat Purkinje cells by myelin-associated neurite growth inhibitory proteins. *J. Neurosci.* 18, 7912–7929.

Zhang, Y., Bo, X., Schoepfer, R., Holtmaat, A. J., Verhaagen, J., Emson, P. C., et al. (2005). Growth-associated protein GAP-43 and L1 act synergistically to promote regenerative growth of Purkinje cell axons *in vivo*. *Proc. Natl. Acad. Sci. U.S.A.* 102, 14883–14888.

Zhang, Y., Zhang, X., Yeh, J., Richardson, P., and Bo, X. (2007). Engineered expression of polysialic acid enhances Purkinje cell axonal regeneration in L1/GAP-43 double transgenic mice. *Eur. J. Neurosci.* 25, 351–361.

Zwiers, H., Veldhuis, H. D., Schotman, P., and Gispen, W. H. (1976). ACTH, cyclic nucleotides, and brain protein phosphorylation *in vitro*. *Neurochem. Res.* 1, 669–677.

Conflict of Interest Statement: The authors declare that the research was conducted in the absence of any commercial or financial relationships that could be construed as a potential conflict of interest.

Received: 18 September 2012; accepted: 03 February 2013; published online: 21 February 2013.

Citation: Grasselli G and Strata P (2013) Structural plasticity of climbing fibers and the growth-associated protein GAP-43. Front. Neural Circuits 7:25. doi: 10.3389/fncir.2013.00025

frontiers in
NEURAL CIRCUITS

REVIEW ARTICLE
published: 23 November 2012
doi: 10.3389/fncir.2012.00090

Molecular mechanism of parallel fiber-Purkinje cell synapse formation

Masayoshi Mishina[1,2]*, Takeshi Uemura[2], Misato Yasumura[2] and Tomoyuki Yoshida[2]

[1] *Brain Science Laboratory, The Research Organization of Science and Technology, Ritsumeikan University, Shiga, Japan*
[2] *Molecular Neurobiology and Pharmacology, Graduate School of Medicine, The University of Tokyo, Tokyo, Japan*

Edited by:
Egidio D'Angelo, University of Pavia, Italy

Reviewed by:
Yang Dan, University of California, Berkeley, USA
Graziella DiCristo, University of Montreal, Canada

****Correspondence:***
Masayoshi Mishina, Brain Science Laboratory, The Research Organization of Science and Technology, Ritsumeikan University, Nojihigashi 1-1-1, Kusatsu, Shiga 525-8577, Japan.
e-mail: mmishina@fc.ritsumei.ac.jp

The cerebellum receives two excitatory afferents, the climbing fiber (CF) and the mossy fiber-parallel fiber (PF) pathway, both converging onto Purkinje cells (PCs) that are the sole neurons sending outputs from the cerebellar cortex. Glutamate receptor δ2 (GluRδ2) is expressed selectively in cerebellar PCs and localized exclusively at the PF-PC synapses. We found that a significant number of PC spines lack synaptic contacts with PF terminals and some of residual PF-PC synapses show mismatching between pre- and postsynaptic specializations in conventional and conditional GluRδ2 knockout mice. Studies with mutant mice revealed that in addition to PF-PC synapse formation, GluRδ2 is essential for synaptic plasticity, motor learning, and the restriction of CF territory. GluRδ2 regulates synapse formation through the amino-terminal domain, while the control of synaptic plasticity, motor learning, and CF territory is mediated through the carboxyl-terminal domain. Thus, GluRδ2 is the molecule that bridges synapse formation and motor learning. We found that the *trans*-synaptic interaction of postsynaptic GluRδ2 and presynaptic neurexins (NRXNs) through cerebellin 1 (Cbln1) mediates PF-PC synapse formation. The synaptogenic triad is composed of one molecule of tetrameric GluRδ2, two molecules of hexameric Cbln1 and four molecules of monomeric NRXN. Thus, GluRδ2 triggers synapse formation by clustering four NRXNs. These findings provide a molecular insight into the mechanism of synapse formation in the brain.

Keywords: glutamate receptor δ2, motor learning, neurexin, parallel fiber, Purkinje cell, synapse formation

INTRODUCTION

The cerebellum receives two excitatory afferents, the climbing fiber (CF) and the mossy fiber-parallel fiber (PF) pathway, both converging onto Purkinje cells (PCs) that are the sole neurons sending outputs from the cerebellar cortex. Glutamate receptors (GluRs) play central roles in synaptic transmission, synaptic plasticity, learning, memory, and development in the brain. Ionotropic GluRs have been classified into three major subtypes, the α-amino-3-hydroxy-5-methyl-4-isozaxole propionic acid (AMPA), kainate and *N*-methyl-D-aspartate (NMDA) receptors, based on the pharmacological, and electrophysiological properties (Mayer and Westbrook, 1987; Monaghan et al., 1989). We found the δ subtype of GluR by molecular cloning (Yamazaki et al., 1992). With respect to the amino-acid sequence identity, the GluRδ (GluD) subtype is positioned between the NMDA and non-NMDA (AMPA/kainite) subtypes (Yamazaki et al., 1992; Araki et al., 1993; Lomeli et al., 1993; Hollmann and Heinemann, 1994; Mori and Mishina, 1995; Mishina, 2000). GluRδ2, the second member of this subfamily, is selectively expressed in cerebellar PCs (Araki et al., 1993; Lomeli et al., 1993). Interestingly, GluRδ2 is localized at PF-PC synapses in cerebellar PCs, but not at CF-PC synapses (Takayama et al., 1996; Landsend et al., 1997). GluRδ2 knockout mice showed severe impairments of long-term depression (LTD) at the PF-PC synapse, motor learning, and motor coordination (Funabiki et al., 1995; Hirano et al., 1995; Kashiwabuchi et al., 1995; Kishimoto et al., 2001). Furthermore, a significant number of PC spines lack synaptic contacts with PF terminals and multiple CF innervation to PCs is sustained in GluRδ2 mutant mice (Kashiwabuchi et al., 1995; Kurihara et al., 1997; Hashimoto et al., 2001; Ichikawa et al., 2002). Thus, GluRδ2 plays a central role in the synaptic plasticity, motor learning, and neural wiring of cerebellar PCs. Since there is no evidence for GluRδ2 channel activities, although lurcher mutation (Ala639Thr) transformed GluRδ2 to constitutively active channels (Zuo et al., 1997), it remained unknown how GluRδ2 regulates cerebellar wiring and function. Recent findings provided significant insights on the issue.

GluRδ2 REGULATES SYNAPTIC PLASTICITY AND MOTOR LEARNING THROUGH THE C-TERMINAL DOMAIN

Studies with conventional and conditional knockout mice revealed that GluRδ2 is essential for synapse formation, synaptic plasticity, motor learning, and the restriction of CF territory (**Figure 1**). However, the causal relationships of these phenotypes remained to be clarified. The C-terminal cytoplasmic region of GluRδ2 contains at least three domains for protein-protein interactions (Roche et al., 1999; Uemura et al., 2004; Yawata et al., 2006). The postsynaptic density (PSD)-95/Discs large/zona occludens 1 (PDZ)-binding domain at the C-terminal, designated as the T site (Uemura et al., 2007), interacts with PSD-93, PTPMEG, Delphilin, nPIST, and S-SCAM (Roche et al., 1999; Hironaka et al., 2000; Miyagi et al., 2002; Yue et al., 2002; Yap et al., 2003).

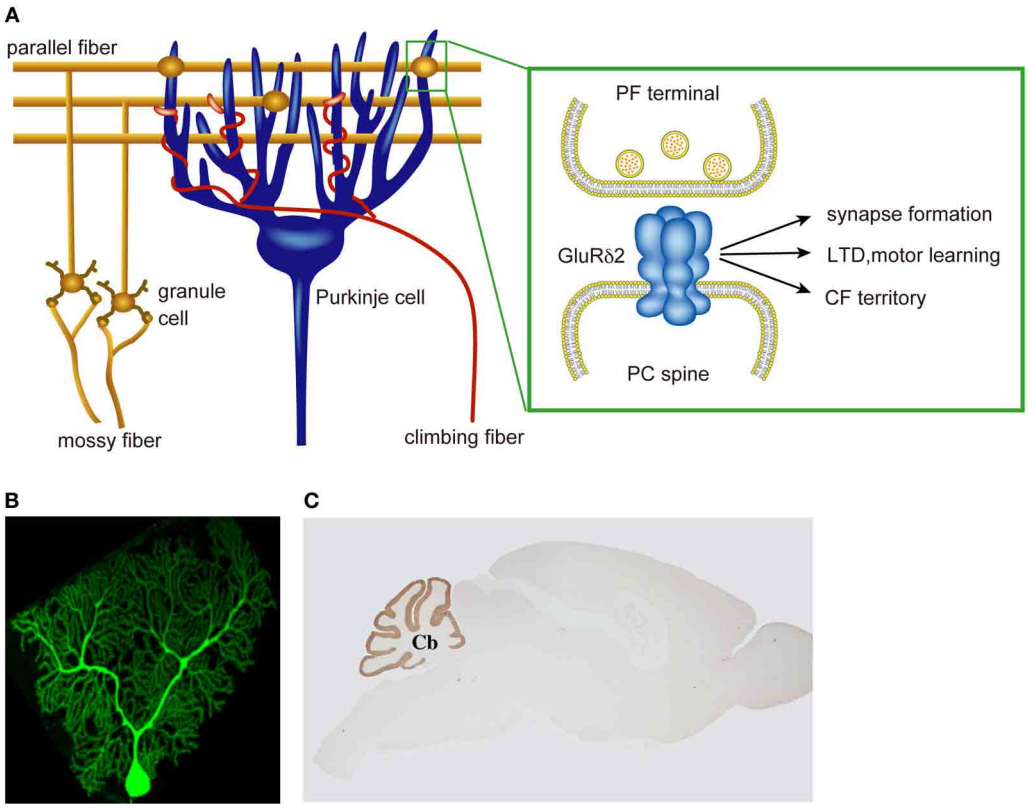

FIGURE 1 | Multiple roles of PC-specific GluRδ2 in cerebellar wiring and function. (A) A cerebellar PC receives a large numbers of PF innervation at distal dendrites and a single CF innervation at proximal dendrites. GluRδ2 is selectively expressed in cerebellar PCs and exclusively localized at the PF-PC synapse. GluRδ2 at the PF synapse regulates PF-PC synapse formation, LTD induction, motor learning, and CF territory. **(B)** A cerebellar PC visualizes by EGFP. **(C)** Immunohistochemical staining of a mouse brain with anti-GluRδ2 antibody.

In the middle of the C-terminal cytoplasmic region, there is the domain that interacts with Shank scaffold proteins, designated as the S segment (Uemura et al., 2004). The membrane-proximal domain of the C-terminal cytoplasmic region of GluRδ2 interacts with PICK1 (Yawata et al., 2006).

We generated GluRδ2ΔT mice carrying mutant GluRδ2 lacking the T site comprising seven amino acids at the C-terminal (Uemura et al., 2007). There were no significant differences in the amount of receptor proteins in the PSD fraction and in the density of GluRδ2 immunogold particles at PF-PC synapses between wild-type and GluRδ2ΔT mice. Thus, the C-terminal truncation exerted little effect on the synaptic localization of receptor proteins. Synaptic connections between PF terminals and PC spines were intact in GluRδ2ΔT mice. However, LTD induction at PF-PC synapses was impaired and the improvement of the performance in the accelerating rotarod test was diminished in the mutant mice. The importance of the GluRδ2 C-terminal in cerebellar LTD and motor learning is consistent with the observations that in PTPMEG mutant mice, LTD at PF-PC synapses was significantly attenuated and rapid acquisition of the cerebellum-dependent delay eyeblink conditioning was impaired (Kina et al., 2007). These results suggest that the C-terminal T site of GluRδ2 is essential for LTD induction and motor learning, but is dispensable for PF-PC synapse formation (Uemura et al., 2007).

Delphilin is selectively expressed in cerebellar PCs except for a slight expression in the thalamus and is exclusively localized at the postsynaptic junction site of the PF-PC synapse (Miyagi et al., 2002). The characteristic expression pattern of Delphilin is reminiscent of GluRδ2. Delphilin knockout mice showed no detectable abnormalities in cerebellar histology, PC cytology, and PC synapse formation (Takeuchi et al., 2008). Delphilin ablation exerted little effect on the synaptic localization of GluRδ2. However, LTD induction was facilitated at PF-PC synapses and intracellular Ca^{2+} required for the induction of LTD appeared to be reduced in Delphilin knockout mice. We further showed that the gain-increase adaptation of the optokinetic response (OKR) was enhanced in the mutant mice. These findings suggest that synaptic plasticity at PF-PC synapses is a crucial rate-limiting step in OKR gain-increase adaptation, a simple form of motor learning (Takeuchi et al., 2008).

GluRδ2 TRIGGERS PF-PC SYNAPSE FORMATION BY *TRANS*-SYNAPTIC INTERACTION WITH NEUREXINS THROUGH Cbln1

We examined the role of GluRδ2 in the adult brain using inducible and cerebellar PC-specific gene targeting on the C57BL/6 genetic background (Takeuchi et al., 2005). When GluRδ2 proteins were

diminished, a significant number of PC spines lost their synaptic contacts with PF terminals. Thus, studies with conventional and inducible knockout mice indicate that the formation and maintenance of PF-PC synapses are critically dependent on GluRδ2 *in vivo* (Kashiwabuchi et al., 1995; Takeuchi et al., 2005). Concomitant with the decrease of postsynaptic GluRδ2 proteins, presynaptic active zones shrank progressively and PSD expanded, resulting in mismatching between pre- and postsynaptic specializations at PF-PC synapse (**Figure 2**). Furthermore, GluRδ2 and PSD-93 proteins were concentrated at the contacted portion of mismatched synapses, while AMPA receptors distributed in both the contacted and dissociated portions. Thus, postsynaptic GluRδ2 is a key regulator of the presynaptic active zone and PSD organization at PF-PC synapses. Based on the direct relationship between the density of postsynaptic GluRδ2 and the size of presynaptic active zones in GluRδ2 mutant mice generated by inducible Cre-mediated ablation, we proposed that GluRδ2 makes a physical linkage between the active zone and PSD by direct or indirect interaction with an active zone component (Takeuchi et al., 2005). Indirect interaction through PSD proteins appears to be less likely since the C-terminal truncation of GluRδ2 has little effect on PF-PC synapse formation, while the mutation impairs cerebellar LTD and motor learning (Uemura et al., 2007).

To identify the key domain responsible for synapse formation, we expressed GluRδ2 in HEK293T cells and cultured the transfected cells with cerebellar granule cells (GCs) (Uemura and Mishina, 2008) (**Figure 3**). Numerous punctate signals for presynaptic markers were observed on the surface of HEK293T cells expressing GluRδ2. The presynaptic specializations of cultured GCs induced by GluRδ2 were capable of exo- and endocytosis as indicated by FM1-43 dye labeling. Replacement of the extracellular N-terminal domain (NTD) of GluRδ2 with that of the AMPA receptor GluRα1 abolished the inducing activity. The NTD of GluRδ2 (GluRδ2-NTD) coated on beads successfully induced the accumulation of presynaptic specializations. These results suggest that GluRδ2 triggers synapse formation by direct interaction with presynaptic component(s) through the NTD (Uemura and Mishina, 2008; Kakegawa et al., 2009; Kuroyanagi et al., 2009; Mandolesi et al., 2009).

To seek for GluRδ2 interacting proteins, the presynaptic differentiation of cerebellar GCs was induced by treatment with GluRδ2-NTD-coated magnetic beads and then

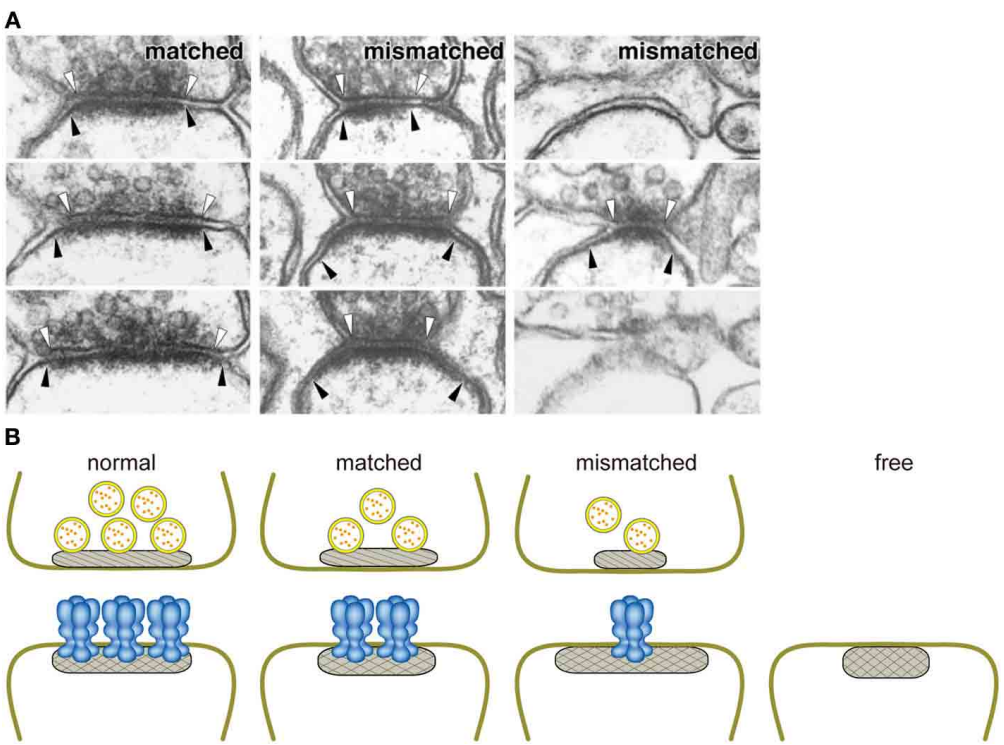

FIGURE 2 | Close relationship between the amount of GluRδ2 protein and the size of the active zone. (A) Ablation of GluRδ2, when induced in the adult brain, resulted in the disruption of synaptic connections with PF terminals in a significant number of PC spines. In addition, some of residual PF-PC synapses show mismatching between pre- and postsynaptic specializations (Takeuchi et al., 2005). White and black arrowheads indicate the edges of active zone and PSD, respectively. **(B)** Schematic presentation of the relationships between the amount of GluRδ2 protein and the sizes of presynaptic active zone (hatched) and PSD (cross-hatched). The length of active zone became shorter in the order of normal, matched, and mismatched synapses according to the decrease of the density of GluRδ2-immunogold labeling at postsynaptic sites (Takeuchi et al., 2005). Based on the direct relationship between the density of postsynaptic GluRδ2 and the size of presynaptic active zones in GluRδ2 mutant mice, we proposed that GluRδ2 makes a physical linkage between the active zone and PSD by interaction with an active zone component. Normal, normal synapse of wild-type mice; matched, matched synapse of induced GluRδ2 KO mice; mismatched, mismatched synapse of induced GluRδ2 KO mice; free, free spine of induced GluRδ2 KO mice.

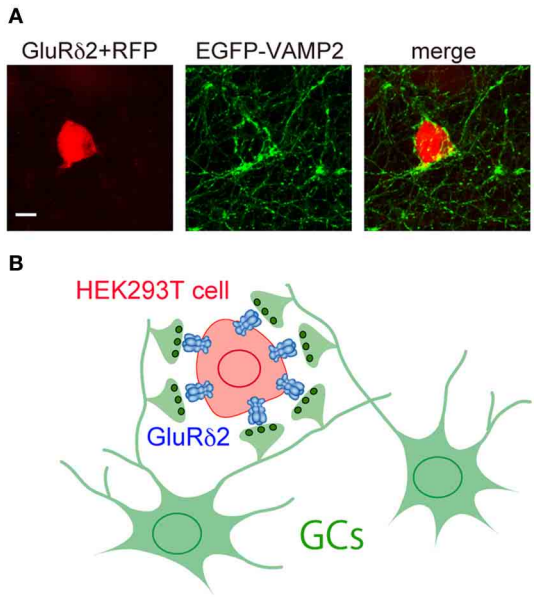

FIGURE 3 | Induction of presynaptic differentiation by GluRδ2. **(A)** HEK293T cells transfected with expression vectors for GluRδ2 and tagRFP (red) were seeded on top of cultured cerebellar neurons transfected with an expression vector for vesicle-associated membrane protein-2 (VAMP-2) fused with EGFP at its N terminus (EGFP-VAMP2) (green). After 2 days of co-culture, cells were immunostained for EGFP. Note that numerous EGFP-VAMP2 signals accumulated on the surface of HEK293T cells expressing GluRδ2. Scale bar represents 10 μm. **(B)** Schematic presentation of the accumulation of GC axon terminals on the surface of HEK293T cells expressing GluRδ2.

surface proteins of cerebellar GC axons were covalently bound to GluRδ2-NTD using non-permeable cross-linker 3,3′-dithiobis(sulfosuccinimidylpropionate). Comparative analysis of the isolated proteins by liquid chromatography-tandem mass spectrometry identified neurexin (NRXN) 1, NRXN2, FAT2, protein tyrosine phosphatase σ (PTPσ), and cerebellin 1 precursor protein (Cbln1) as possible GluRδ2-interacting proteins (Uemura et al., 2010). NRXN1, NRXN2, FAT2, and PTPσ are membrane proteins (Pulido et al., 1995; Nakayama et al., 2002; Südhof, 2008), while Cbln1 is a glycoprotein secreted from cerebellar GCs (Bao et al., 2005). After a series of selections, we found robust binding signals of GluRδ2-NTD on the surface of HEK293T cells transfected with NRXN1β or NRXN2β in the presence of Cbln1. It is known that presynaptic NRXNs bind to postsynaptic neuroligins (NLGNs) forming *trans*-synaptic cell adhesion complexes (Ichtchenko et al., 1995; Scheiffele et al., 2000; Graf et al., 2004) and NLGNs preferentially bind to NRXN variants lacking splice segment 4 (S4) (Boucard et al., 2005; Chih et al., 2005; Comoletti et al., 2006). In contrast to NLGNs, GluRδ2 selectively interacts with NRXN variants containing S4. NRXN variants containing S4 were expressed in the cerebellum but those lacking S4 were hardly detectable except for early stages of development, while both variants were found in the cerebral cortex and hippocampus (Uemura et al., 2010; Iijima et al., 2011).

Direct binding experiments showed that GluRδ2 is a receptor for Cbln1 and NRXN is another receptor for Cbln1 (Uemura et al., 2010). The K_D value of Cbln1 for the NTD of GluRδ2 estimated by surface plasmon resonance binding assays is 16.5 nM and that for the extracellular domain (ECD) of NRXN1β is 0.17 nM. These values suggest high affinity interactions of GluRδ2, Cbln1 and NRXN as compared with K_D values (∼200 to ∼600 nM) reported for the interactions between NLGNs and NRXNs (Comoletti et al., 2003; Koehnke et al., 2008). Matsuda et al. (2010) also reported the interaction between Cbln1 and GluRδ2. Since Cbln1 is a ligand for both GluRδ2 and NRXN, we propose a model in which postsynaptic GluRδ2 interacts with presynaptic NRXN through Cbln1 and this ternary interaction provides a physical linkage between PSD and active zone (Uemura et al., 2010). The synaptogenic activity of GluRδ2 is hindered by knockout of Cbln1 and by small interference RNA-mediated knockdown of NRXNs. Furthermore, the synaptogenic activity of Cbln1 in cerebellar primary cultures and *in vivo* was abolished by the NTD of GluRδ2 and the ECD of NRXN1β (**Figure 4**). These results suggest that the *trans*-synaptic interaction of postsynaptic GluRδ2 and presynaptic NRXNs through Cbln1 mediates PF-PC synapse formation in the cerebellum (Uemura et al., 2010). This model well explains previous observations that the size of the presynaptic active zone shrank progressively concomitant with the decrease of postsynaptic GluRδ2 proteins upon inducible Cre-mediated GluRδ2 ablation (Takeuchi et al., 2005) and that Cbln1 knockout mice phenotypically mimic GluRδ2 knockout mice (Hirai et al., 2005).

ASSEMBLY STOICHIOMETRY OF THE *TRANS*-SYNAPTIC TRIAD

Cumulative evidence indicates the tetrameric assembly of the AMPA/kainate- and NMDA-type GluRs (Laube et al., 1998; Rosenmund et al., 1998; Bowie and Lange, 2002; Sun et al., 2002; Weston et al., 2006). The mobility of GluRδ2 molecules from the membrane fraction corresponded to the size of the tetramer in blue native PAGE. GluRδ2 band collapsed into monomeric and dimeric intermediates by the treatment of 1% SDS. These behaviors were similar between GluRδ2 and AMPA-type GluR. These results suggest that GluRδ2 exists as a tetramer in the membrane. On the other hand, GluRδ2-NTD assembled into a stable homodimer. The NTD of ionotropic GluRs with tetrameric structure assembles as a dimer of dimers (Schorge and Colquhoun, 2003; Tichelaar et al., 2004; Midgett and Madden, 2008; Kumar et al., 2009) and tetrameric iGluRs have 2-fold symmetry rather than 4-fold symmetry (Armstrong and Gouaux, 2000; Sobolevsky et al., 2004, 2009; Nanao et al., 2005).

When incubated with cultured cerebellar GCs, dimeric GluRδ2-NTD exerted little effect on the intensities of punctate immunostaining signals for Bassoon and vesicular glutamate transporter 1 (VGluT1). In contrast, tetrameric GluRδ2-NTD prepared by cross-linking dimeric GluRδ2-NTD-Fc using $F(ab')_2$ of anti-Fc antibody enhanced the accumulation of the active zone and synaptic vesicle proteins in axons of cultured GCs. These results suggest that native GluRδ2 is

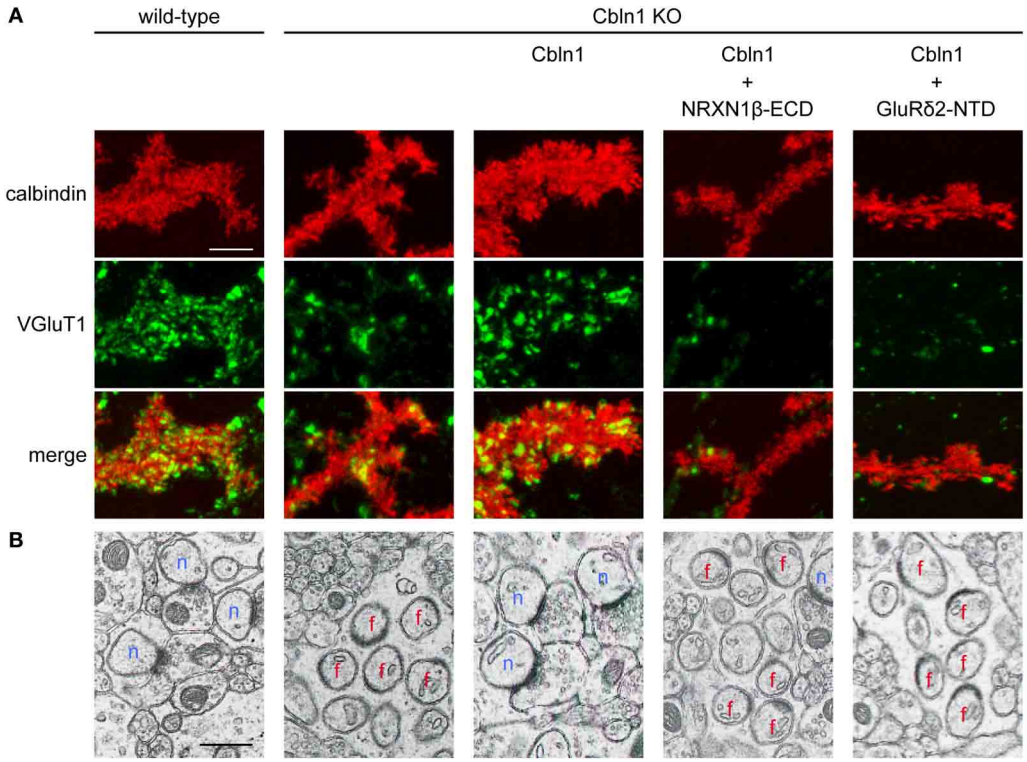

FIGURE 4 | The GluRδ2-Cbln1-NRXN *trans*-synaptic triad mediates synapse formation (modified from Uemura et al., 2010). (A) Suppression of Cbln1 synaptogenic activity by the extracellular domain of NRXN1β (NRXN1β-ECD) and the N-terminal domain of GluRδ2 (GluRδ2-NTD) in cultured cerebellar neurons. In primary cultures of cerebellar neurons, numerous punctate staining signals for VGluT1 were found on the dendrites of PCs from wild-type mice. VGluT1 signals were significantly reduced in PCs from Cbln1 KO mice. Addition of Cbln1 restored the intensity of VGluT1 signals. The restoring activity of Cbln1 was suppressed by addition of NRXN1β-ECD and GluRδ2-NTD. **(B)** Suppression of Cbln1 synaptogenic activity by NRXN1β-ECD and GluRδ2-NTD *in vivo*. Electron micrographs of cerebella from wild-type and Cbln1 KO mice and those from Cbln1 KO mice injected with Cbln1 together with or without NRXN1β-ECD and GluRδ2-NTD. In wild-type mice, all PC spines formed synaptic contacts with PFs. In Cbln1 KO mice, many PC spines lacked synaptic contacts (free spines). Injection of Cbln1 restored PF-PC connections in Cbln1 KO mice. The *in vivo* synatogenic activity of Cbln1 was suppressed by co-injection of NRXN1β-ECD and GluRδ2-NTD. n, normal synapses; f, free spines. Scale bars represent 5 μm in **(A)** and 0.5 μm in **(B)**.

assembled into a tetramer and this tetrameric assembly is essential for GluRδ2 to induce presynaptic differentiation (Lee et al., 2012).

Affinities of a series of Cbln1 mutants for GluRδ2-NTD and NRXN1β-ECD suggest that the binding sites of Cbln1 for GluRδ2 and NRXN1β are differential rather than identical. In addition, no competition was detectable in the binding to Cbln1 between GluRδ2-NTD and the laminin–neurexin–sex hormone-binding globulin (LNS) domain of NRXN1β during triad formation. These results suggest that GluRδ2 and Cbln1 interact with each other rather independently of Cbln1-NRXN1β interaction and vice versa. We thus examined the assembly stoichiometries of GluRδ2-Cbln1 and Cbln1-NRXN1β complexes one by one. Both fast protein liquid chromatography gel-filtration assay and isothermal titration calorimetry analysis consistently showed that dimeric GluRδ2-NTD and hexameric Cbln1 assembled in the molar ratio of one to one, while hexameric Cbln1 and monomeric NRXN1β-LNS assembled in the molar ratio of one to two. Since native GluRδ2 exists as a tetramer in the membrane and the tetramerization is essential for GluRδ2-NTD to stimulate the accumulation of Bassoon and VGluT1 in the axons of cultured GCs, we suggest that the synaptogenic triad is composed of one molecule of tetrameric GluRδ2, two molecules of hexameric Cbln1 and four molecules of monomeric NRXN (Lee et al., 2012).

MECHANISM OF GluRδ2-MEDIATED SYNAPSE FORMATION

During development, axons of immature neurons show a capacity for evoked recycling of synaptic vesicles and clusters of the vesicles along axonal segments, even in the absence of target cells (Ziv and Garner, 2004; Jin and Garner, 2008). However, the synaptic vesicle aggregation, in the absence of a postsynaptic contact, is not stably anchored to a given region of the cell surface. Contacts with postsynaptic sites trigger the stabilization and maturation of synapses. In cultured cerebellar GCs, the majority of varicosities containing presynaptic proteins are not apposed to definite postsynaptic structures (Marxen et al., 1999; Urakubo et al., 2003). Cbln1 is a high-affinity ligand for NRXNs (Uemura et al., 2010; Joo et al., 2011) and is secreted from cerebellar GCs (Bao et al., 2005), suggesting that the interaction between secreted Cbln1 and presynaptic NRXNs takes place before PF-PC synapse formation. However, punctate staining signals for Bassoon were comparable between GC cultures from wild-type and Cbln1 knockout mice. The addition of Cbln1 to GC cultures exerted little effect on the intensity of Bassoon

signals. Thus, the formation of NRXN dimers is not sufficient to induce presynaptic differentiation. Consistently, GluRδ2-NTD dimer that binds to one molecule of Cbln1 failed to induce presynaptic differentiation. In contrast, GluRδ2-NTD tetramer stimulated the accumulation of punctate signals for active zone protein Bassoon and synaptic vesicle protein VGluT1 in cultured cerebellar GCs. Since GluRδ2-NTD tetramer is soluble, it is unlikely that this stimulating effect is due to anchoring presynaptic proteins. Our results suggest that tetrameric GluRδ2-NTD assembles two molecules of Cbln1 and four molecules of NRXNs, whereas dimeric GluRδ2-NTD interacts with one molecule of Cbln1 and two molecules of NRXNs. Thus, clustering of four NRXNs by tetrameric GluRδ2-NTD via two Cbln1 is a key step to trigger presynaptic differentiation (Lee et al., 2012). Taken together, our results suggest the mechanism of PF-PC synapse formation as follows. Cbln1 secreted from cerebellar GCs may interact with presynaptic NRXNs before PF-PC synapse formation. However, Cbln1-induced NRXN dimerization is not sufficient to trigger presynaptic differentiation. When the contact between the PF terminal and PC spine takes place, GluRδ2 triggers synapse formation by clustering four NRXNs through triad formation (**Figure 5**). Since NRXNs interact with synaptotagmin, CASK, Mint and syntenin through its C-terminal (Hata et al., 1993, 1996; Butz et al., 1998; Biederer and Südhof, 2000; Grootjans et al., 2000) and the C-terminal of NRXN is critical for the induction of presynaptic differentiation *in vitro* (Dean et al., 2003), tetramerization of NRXNs may stimulate the clustering of these scaffold proteins leading to the organization of transmitter release machineries (Butz et al., 1998; Maximov et al., 1999; Biederer and Südhof, 2000, 2001).

CONCLUSION

Cerebellar PC-specific GluRδ2 plays essential roles in synapse formation, synaptic plasticity and motor learning. The NTD of GluRδ2 is responsible for synapse formation, whereas the C-terminal domain is essential for LTD induction and motor learning. Thus, GluRδ2 is the molecule that bridges synapse formation and motor learning in the cerebellum.

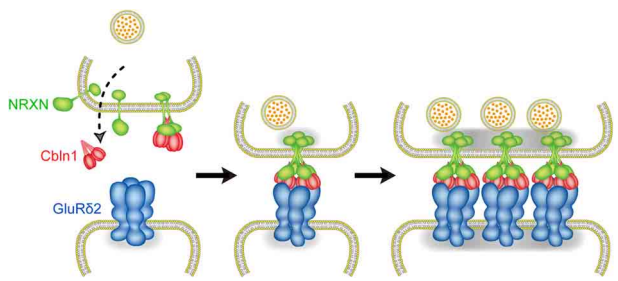

FIGURE 5 | Molecular mechanism of PF-PC synapse formation. Before PF-PC synapse formation, Cbln1 secreted from cerebellar GCs may interact with presynaptic NRXNs. Cbln1-induced NRXN dimerization is not sufficient to trigger presynaptic differentiation. When the contact between the PF terminal and PC spine takes place, GluRδ2 triggers synapse formation by clustering four NRXNs through triad formation.

Synapse formation is the key step in the development of neuronal networks. Precise synaptic connections between nerve cells in the brain provide the basis of perception, learning, memory, and cognition. Although a number of *trans*-synaptic cell adhesion molecules have been identified that play roles in pre- and postsynaptic differentiation of cultured hippocampal neurons, the precise roles of these molecules in synapse formation *in vivo* remain elusive (Scheiffele et al., 2000; Dean et al., 2003; Graf et al., 2004; Waites et al., 2005; Varoqueaux et al., 2006; Dalva et al., 2007; McAllister, 2007; Südhof, 2008; Shen and Scheiffele, 2010; Williams et al., 2010; Siddiqui and Craig, 2011). Our results provide evidence that the *trans*-synaptic interaction of postsynaptic GluRδ2 and presynaptic NRXNs through Cbln1 mediates PF-PC synapse formation *in vivo* in the cerebellum (Uemura et al., 2010). Furthermore, the stoichiometry of synaptogenic GluRδ2-Cbln1-NRXN triad suggests that GluRδ2 triggers presynsptic differentiation by clustering four NRXNs (Lee et al., 2012). It will be essential for the elucidation of synaptogenesis mechanism to investigate how NRXN clustering initiates the formation of presynaptic active zone. Interestingly, approximately half of PF-PC synapses survived in GluRδ2 knockout mice (Kashiwabuchi et al., 1995; Kurihara et al., 1997). There may be at least two types of PF-PC synapses, GluRδ2-dependent and independent synapses. Alternatively, other synaptogenic molecule(s) may partly compensate GluRδ2 deficiency in the knockout mice. It should be noted that the organization and composition of remaining PF-PC synapses in the absence of GluRδ2 appear to be altered, suggesting that GluRδ2 also plays a role as a PSD organizer (Takeuchi et al., 2005; Yamasaki et al., 2011). Further investigation of the structure and function of the GluRδ2-Cbln1-NRXN synaptogenic triad will provide a clue to understand how central synapses are formed, mature, show plastic changes, and mediate learning and memory.

During development, PC circuitry is established through heterosynaptic competition between PFs and CFs (Mariani et al., 1977; Crépel, 1982). GluRδ2 regulates the PC wiring by suppressing invasion of CF branches to the territory of PF innervation and to neighboring PCs (Kashiwabuchi et al., 1995; Hashimoto et al., 2001; Ichikawa et al., 2002; Uemura et al., 2007; Miyazaki et al., 2010). Weakened PF inputs due to the decrease of PF-PC synapses in GluRδ2 mutant mice may result in CF invasion to the PF territory (Hashimoto et al., 2001; Ichikawa et al., 2002). However, the territory of CF innervation expanded distally to spiny branchlets in GluRδ2ΔT mice with intact PF-PC synaptic connections (Uemura et al., 2007). GluRδ2 is localized at PF-PC synapses but not at CF synapses (Takayama et al., 1996; Landsend et al., 1997). Thus, GluRδ2 should suppress the distal extension and ectopic innervation of CF axon terminals by the signaling through the C-terminal T site (Uemura et al., 2007).

ACKNOWLEDGMENTS

This work was supported in part by research grants from the Ministry of Education, Culture, Sports, Science, and Technology of Japan.

REFERENCES

Araki, K., Meguro, H., Kushiya, E., Takayama, C., Inoue, Y., and Mishina, M. (1993). Selective expression of the glutamate receptor channel δ2 subunit in cerebellar Purkinje cells. *Biochem. Biophys. Res. Commun.* 197, 1267–1276.

Armstrong, N., and Gouaux, E. (2000). Mechanisms for activation and antagonism of an AMPA-sensitive glutamate receptor: crystal structure of the GluR2 ligand binding core. *Neuron* 28, 165–181.

Bao, D., Pang, Z., and Morgan, J. I. (2005). The structure and proteolytic processing of Cbln1 complexes. *J. Neurochem.* 95, 618–629.

Biederer, T., and Südhof, T. C. (2000). Mints as adaptors: direct binding to neurexins and recruitment of Munc18. *J. Biol. Chem.* 275, 39803–39806.

Biederer, T., and Südhof, T. C. (2001). CASK and Protein 4.1 support F-actin nucleation on neurexins. *J. Biol. Chem.* 276, 47869–47876.

Boucard, A. A., Chubykin, A. A., Comoletti, D., Taylor, P., and Südhof, T. C. (2005). A splice code for *trans*-synaptic cell adhesion mediated by binding of neuroligin 1 to α- and β-neurexins. *Neuron* 48, 229–236.

Bowie, D., and Lange, G. D. (2002). Functional stoichiometry of glutamate receptor desensitization. *J. Neurosci.* 22, 3392–3403.

Butz, S., Okamoto, M., and Südhof, T. C. (1998). A tripartite protein complex with the potential to couple synaptic vesicle exocytosis to cell adhesion in brain. *Cell* 94, 773–782.

Chih, B., Engelman, H., and Scheiffele, P. (2005). Control of excitatory and inhibitory synapse formation by neuroligins. *Science* 307, 1324–1328.

Comoletti, D., Flynn, R., Jennings, L. L., Chubykin, A., Matsumura, T., Hasegawa, H., et al. (2003). Characterization of the interaction of a recombinant soluble neuroligin-1 with neurexin-1β. *J. Biol. Chem.* 278, 50497–50505.

Comoletti, D., Flynn, R. E., Boucard, A. A., Demeler, B., Schirf, V., Shi, J., et al. (2006). Gene selection, alternative splicing, and post-translational processing regulate neuroligin selectivity for β-neurexins. *Biochemistry* 45, 12816–12827.

Crépel, F. (1982). Regression of functional synapses in the immature mammalian cerebellum. *Trends Neurosci.* 5, 266–269.

Dalva, M. B., McClelland, A. C., and Kayser, M. S. (2007). Cell adhesion molecules: signalling functions at the synapse. *Nat. Rev. Neurosci.* 8, 206–220.

Dean, C., Scholl, F. G., Choih, J., DeMaria, S., Berger, J., Isacoff, E., et al. (2003). Neurexin mediates the assembly of presynaptic terminals. *Nat. Neurosci.* 6, 708–716.

Funabiki, K., Mishina, M., and Hirano, T. (1995). Retarded vestibular compensation in mutant mice deficient in δ2 glutamate receptor subunit. *Neuroreport* 7, 189–192.

Graf, E. R., Zhang, X., Jin, S. X., Linhoff, M. W., and Craig, A. M. (2004). Neurexins induce differentiation of GABA and glutamate postsynaptic specializations via neuroligins. *Cell* 119, 1013–1026.

Grootjans, J. J., Reekmans, G., Ceulemans, H., and David, G. (2000). Syntenin-Syndecan binding requires Syndecan-Synteny and the co-operation of both PDZ domains of Syntenin. *J. Biol. Chem.* 275, 19933–19941.

Hashimoto, K., Ichikawa, R., Takechi, H., Inoue, Y., Aiba, A., Sakimura, K., et al. (2001). Roles of glutamate receptor δ2 subunit (GluRδ2) and metabotropic glutamate receptor subtype 1 (mGluR1) in climbing fiber synapse elimination during postnatal cerebellar development. *J. Neurosci.* 21, 9701–9712.

Hata, Y., Butz, S., and Südhof, T. C. (1996). CASK: a novel dlg/PSD95 homolog with an N-terminal calmodulin-dependent protein kinase domain identified by interaction with neurexins. *J. Neurosci.* 16, 2488–2494.

Hata, Y., Davletov, B., Petrenko, A. G., Jahn, R., and Südhof, T. C. (1993). Interaction of synaptotagmin with the cytoplasmic domains of neurexins. *Neuron* 10, 307–315.

Hirai, H., Pang, Z., Bao, D., Miyazaki, T., Li, L., Miura, E., et al. (2005). Cbln1 is essential for synaptic integrity and plasticity in the cerebellum. *Nat. Neurosci.* 8, 1534–1541.

Hirano, T., Kasono, K., Araki, K., and Mishina, M. (1995). Suppression of LTD in cultured Purkinje cells deficient in the glutamate receptor δ2 subunit. *Neuroreport* 6, 524–526.

Hironaka, K., Umemori, H., Tezuka, T., Mishina, M., and Yamamoto, T. (2000). The protein-tyrosine phosphatase PTPMEG interacts with glutamate receptor δ2 and ε subunits. *J. Biol. Chem.* 275, 16167–16173.

Hollmann, M., and Heinemann, S. (1994). Cloned glutamate receptors. *Annu. Rev. Neurosci.* 17, 31–108.

Ichikawa, R., Miyazaki, T., Kano, M., Hashikawa, T., Tatsumi, H., Sakimura, K., et al. (2002). Distal extension of climbing fiber territory and multiple innervation caused by aberrant wiring to adjacent spiny branchlets in cerebellar Purkinje cells lacking glutamate receptor GluRδ2. *J. Neurosci.* 22, 8487–8503.

Ichtchenko, K., Hata, Y., Nguyen, T., Ullrich, B., Missler, M., Moomaw, C., et al. (1995). Neuroligin 1: a splice site-specific ligand for β-neurexins. *Cell* 81, 435–443.

Iijima, T., Wu, K., Witte, H., Hanno-Iijima, Y., Glatter, T., Richard, S., et al. (2011). SAM68 regulates neuronal activity-dependent alternative splicing of neurexin-1. *Cell* 147, 1601–1614.

Jin, Y., and Garner, C. C. (2008). Molecular mechanisms of presynaptic differentiation. *Annu. Rev. Cell Dev. Biol.* 24, 237–262.

Joo, J.-Y., Lee, S.-J., Uemura, T., Yoshida, T., Yasumura, M., Watanabe, M., et al. (2011). Differential interactions of cerebellin precursor protein (Cbln) subtypes and neurexin variants for synapse formation of cortical neurons. *Biochem. Biophys. Res. Commun.* 406, 627–632.

Kakegawa, K., Miyazaki, T., Kohda, K., Matsuda, K., Emi, K., Motohashi, J., et al. (2009). The N-terminal domain of GluD2 (GluRδ2) recruits presynaptic terminals and regulates synaptogenesis in the cerebellum *in vivo*. *J. Neurosci.* 29, 5738–5748.

Kashiwabuchi, N., Ikeda, K., Araki, K., Hirano, T., Shibuki, K., Takayama, C., et al. (1995). Impairment of motor coordination, Purkinje cell synapse formation, and cerebellar long-term depression in GluRδ2 mutant mice. *Cell* 81, 245–252.

Kina, S., Tezuka, T., Kusakawa, S., Kishimoto, Y., Kakizawa, S., Hashimoto, K., et al. (2007). Involvement of protein-tyrosine phosphatase PTPMEG in motor learning and cerebellar long-term depression. *Eur. J. Neurosci.* 26, 2269–2278.

Kishimoto, Y., Kawahara, S., Suzuki, M., Mori, H., Mishina, M., and Kirino, Y. (2001). Classical eyeblink conditioning in glutamate receptor subunit δ2 mutant mice is impaired in the delay paradigm but not in the trace paradigm. *Eur. J. Neurosci.* 13, 1249–1253.

Koehnke, J., Jin, X., Trbovic, N., Katsamba, P. S., Brasch, J., Ahlsen, G., et al. (2008). Crystal structures of β-neurexin 1 and β-neurexin 2 ectodomains and dynamics of splice insertion sequence 4. *Structure* 16, 410–421.

Kumar, J., Schuck, P., Jin, R., and Mayer, M. L. (2009). The N-terminal domain of GluR6-subtype glutamate receptor ion channels. *Nat. Struct. Mol. Biol.* 16, 631–638.

Kurihara, H., Hashimoto, K., Kano, M., Takayama, C., Sakimura, K., Mishina, M., et al. (1997). Impaired parallel fiber-Purkinje cell synapse stabilization during cerebellar development of mutant mice lacking the glutamate receptor δ2 subunit. *J. Neurosci.* 17, 9613–9623.

Kuroyanagi, T., Yokoyama, M., and Hirano, T. (2009). Postsynaptic glutamate receptor δ family contributes to presynaptic terminal differentiation and establishment of synaptic transmission. *Proc. Natl. Acad. Sci. U.S.A.* 196, 4912–4916.

Landsend, A. S., Amiry-Moghaddam, M., Matsubara, A., Bergersen, L., Usami, S., Wenthold, R. J., et al. (1997). Differential localization of δ glutamate receptors in the rat cerebellum: coexpression with AMPA receptors in parallel fiber-spine synapses and absence from climbing fiber-spine synapses. *J. Neurosci.* 17, 834–842.

Laube, B., Kuhse, J., and Betz, H. (1998). Evidence for a tetrameric structure of recombinant NMDA receptors. *J. Neurosci.* 18, 2954–2961.

Lee, S.-J., Uemura, T., Yoshida, T., and Mishina, M. (2012). GluRδ2 assembles four neurexins into *trans*-synaptic triad to trigger synapse formation. *J. Neurosci.* 32, 4688–4701.

Lomeli, H., Sprengel, R., Laurie, D. J., Köhr, G., Herb, A., Seeburg, P. H., et al. (1993). The rat delta-1 and delta-2 subunits extend the excitatory amino acid receptor family. *FEBS Lett.* 315, 318–322.

Mandolesi, G., Autuori, E., Cesa, R., Premoselli, F., Cesare, P., and Strata, P. (2009). GluRδ2 expression in the mature cerebellum of hotfoot mice

promotes parallel fiber synaptogenesis and axonal competition. *PLoS ONE* 4:e5243. doi: 10.1371/journal.pone.0005243

Mariani, J., Crepel., F., Mikoshiba, K., Changeux, J. P., and Sotelo, C. (1977). Anatomical, physiological and biochemical studies of the cerebellum from Reeler mutant mouse. *Philos. Trans. R. Soc. Lond. B Biol. Sci.* 281, 1–28.

Marxen, M., Volknandt, W., and Zimmermann, H. (1999). Endocytic vacuoles formed following a short pulse of K^+-stimulation contain a plethora of presynaptic membrane proteins. *Neuroscience* 94, 985–996.

Matsuda, K., Miura, E., Miyazaki, T., Kakegawa, W., Emi, K., Narumi, S., et al. (2010). Cbln1 is a ligand for an orphan glutamate receptor δ2, a bidirectional synapse organizer. *Science* 328, 363–368.

Maximov, A., Südhof, T. C., and Bezprozvannv, I. (1999). Association of neuronal calcium channels with modular adaptor proteins. *J. Biol. Chem.* 274, 24453–24456.

Mayer, M. L., and Westbrook, G. L. (1987). The physiology of excitatory amino acids in the vertebrate central nervous system. *Prog. Neurobiol.* 28, 197–276.

McAllister, A. K. (2007). Dynamic aspects of CNS synapse formation. *Annu. Rev. Neurosci.* 30, 425–450.

Midgett, C. R., and Madden, D. R. (2008). The quaternary structure of a calcium-permeable AMPA receptor: conservation of shape and symmetry across functionally distinct subunit assemblies. *J. Mol. Biol.* 382, 578–584.

Mishina, M. (2000). "Molecular diversity, structure, and function of glutamate receptor channels," in *Handbook of Experimental Pharmacology 147*, eds M. Endo, Y. Kurachi, and M. Mishina (Berlin: Springer Verlarg), 393–414.

Miyagi, Y., Yamashita, T., Fukaya, M., Sonoda, T., Okuno, T., Yamada, K., et al. (2002). Delphilin: a novel PDZ and formin homology domain-containing protein that synaptically colocalizes and interacts with glutamate receptor δ2 subunit. *J. Neurosci.* 22, 803–814.

Miyazaki, T., Yamasaki, M., Takeuchi, T., Sakimura, K., Mishina, M., and Watanabe, M. (2010). Ablation of glutamate receptor GluRδ2 in adult Purkinje cells causes multiple innervation of climbing fibers by inducing aberrant invasion to parallel fiber innervation territory. *J. Neurosci.* 30, 15196–15209.

Monaghan, D. T., Bridges, R. J., and Cotman, C. W. (1989). The excitatory amino acid receptors: their classes, pharmacology, and distinct properties in the function of the central nervous system. *Annu. Rev. Pharmacol. Toxicol.* 29, 365–402.

Mori, H., and Mishina, M. (1995). Structure and function of the NMDA receptor channel. *Neuropharmacology* 34, 1219–1237.

Nakayama, M., Nakajima, D., Yoshimura, R., Endo, Y., and Ohara, O. (2002). MEGF1/fat2 proteins containing extraordinarily large extracellular domains are localized to thin parallel fibers of cerebellar granule cells. *Mol. Cell. Neurosci.* 20, 563–578.

Nanao, M. H., Green, T., Stern-Bach, Y., Heinemann, S. F., and Choe, S. (2005). Structure of the kainite receptor subunit GluR6 agonist-binding domain complexed with domoic acid. *Proc. Natl. Acad. Sci. U.S.A.* 102, 1708–1713.

Pulido, R., Serra-Pagès, C., Tang, M., and Streuli, M. (1995). The LAR/PTPδ/PTPσ subfamily of transmembrane protein-tyrosine-phosphatases: multiple human LAR, PTPδ, and PTPσ isoforms are expressed in a tissue-specific manner and associate with the LAR-interacting protein LIP.1. *Proc. Natl. Acad. Sci. U.S.A.* 92, 11686–11690.

Roche, K. W., Ly, C. D., Petralia, R. S., Wang, Y. X., McGee, A. W., Bredt, D. S., et al. (1999). Postsynaptic density-93 interacts with the δ2 glutamate receptor subunit at parallel fiber synapses. *J. Neurosci.* 19, 3926–3934.

Rosenmund, C., Stern-Bach, Y., and Stevens, C. F. (1998). The tetrameric structure of a glutamate receptor channel. *Science* 280, 1596–1599.

Scheiffele, P., Fan, J., Choih, J., Fetter, R., and Serafini, T. (2000). Neuroligin expressed in nonneuronal cells triggers presynaptic development in contacting axons. *Cell* 101, 657–669.

Schorge, S., and Colquhoun, D. (2003). Studies of NMDA receptor function and stoichiometry with truncated and tandem subunits. *J. Neurosci.* 23, 1151–1158.

Shen, K., and Scheiffele, P. (2010). Genetics and cell biology of building specific synaptic connectivity. *Annu. Rev. Neurosci.* 33, 473–507.

Siddiqui, T. J., and Craig, A. M. (2011). Synaptic organizing complexes. *Curr. Opin. Neurobiol.* 21, 132–143.

Sobolevsky, A. I., Rosconi, M. P., and Gouaux, E. (2009). X-ray structure, symmetry and mechanism of an AMPA-subtype glutamate receptor. *Nature* 462, 745–756.

Sobolevsky, A. I., Yelshansky, M. V., and Wollmuth, L. P. (2004). The outer pore of the glutamate receptor channel has 2-fold rotational symmetry. *Neuron* 41, 367–378.

Südhof, T. C. (2008). Neuroligins and neurexins link synaptic function to cognitive disease. *Nature* 455, 903–911.

Sun, Y., Olson, R., Horning, M., Armstrong, N., Mayer, M., and Gouaux, E. (2002). Mechanism of glutamate receptor desensitization. *Nature* 417, 245–253.

Takayama, C., Nakagawa, S., Watanabe, M., Mishina, M., and Inoue, Y. (1996). Developmental changes in expression and distribution of the glutamate receptor channel δ2 subunit according to the Purkinje cell maturation. *Brain Res. Dev. Brain Res.* 92, 147–155.

Takeuchi, T., Miyazaki, T., Watanabe, M., Mori, H., Sakimura, K., and Mishina, M. (2005). Control of synaptic connection by glutamate receptor δ2 in the adult cerebellum. *J. Neurosci.* 25, 2146–2156.

Takeuchi, T., Ohtsuki, G., Yoshida, T., Fukaya, M., Wainai, T., Yamashita, M., et al. (2008). Enhancement of both long-term depression induction and optokinetic response adaptation in mice lacking delphilin. *PLoS ONE* 3:e2297. doi: 10.1371/journal.pone.0002297

Tichelaar, W., Safferling, M., Keinänen, K., Stark, H., and Madden, D. R. (2004). The three-dimensional structure of an ionotropic glutamate receptor reveals a dimer-of-dimers assembly. *J. Mol. Biol.* 344, 435–442.

Uemura, T., Mori, H., and Mishina, M. (2004). Direct interaction of GluRδ2 with Shank scaffold proteins in cerebellar Purkinje cells. *Mol. Cell. Neurosci.* 26, 330–341.

Uemura, T., Kakizawa, S., Yamasaki, M., Sakimura, K., Watanabe, M., Iino, M., et al. (2007). Regulation of long-term depression and climbing fiber territory by glutamate receptor δ2 at parallel fiber synapses through its C-terminal domain in cerebellar Purkinje cells. *J. Neurosci.* 27, 12096–12108.

Uemura, T., and Mishina, M. (2008). The amino-terminal domain of glutamate receptor δ2 triggers presynaptic differentiation. *Biochem. Biophys. Res. Commun.* 377, 1315–1319.

Uemura, T., Lee, S. J., Yasumura, M., Takeuchi, T., Yoshida, T., Ra, M., et al. (2010). *Trans*-Synaptic interaction of GluRδ2 and neurexin through Cbln1 mediates synapse formation in the cerebellum. *Cell* 141, 1068–1079.

Urakubo, T., Tominaga-Yoshino, K., and Ogura, A. (2003). Non-synaptic exocytosis enhanced in rat cerebellar granule neurons cultured under survival-promoting conditions. *Neurosci. Res.* 45, 429–436.

Varoqueaux, F., Aramuni, G., Rawson, R. L., Mohrmann, R., Missler, M., Gottmann, K., et al. (2006). Neuroligins determine synapse maturation and function. *Neuron* 51, 741–754.

Waites, C. L., Craig, A. M., and Garner, C. C. (2005). Mechanisms of vertebrate synaptogenesis. *Annu. Rev. Neurosci.* 28, 251–274.

Weston, M. C., Schuck, P., Ghosal, A., Rosenmund, C., and Mayer, M. L. (2006). Conformational restriction blocks glutamate receptor desensitization. *Nat. Struct. Mol. Biol.* 13, 1120–1127.

Williams, M. E., de Wit, J., and Ghosh, A. (2010). Molecular mechanisms of synaptic specificity in developing neural circuits. *Neuron* 68, 9–18.

Yamasaki, M., Miyazaki, T., Azechi, H., Abe, M., Natsume, R., Hagiwara, T., et al. (2011). Glutamate receptor δ2 is essential for input pathway-dependent regulation of synaptic AMPAR contens in cerebellar Purkinje cells. *J. Neurosci.* 31, 3362–3374.

Yamazaki, M., Araki, K., Shibata, A., and Mishina, M. (1992). Molecular cloning of a cDNA encoding a novel member of the mouse glutamate receptor channel family. *Biochem. Biophys. Res. Commun. 183*, 886–892.

Yap, C. C., Muto, Y., Kishida, H., Hashikawa, T., and Yano, R. (2003). PKC regulates the δ2 glutamate receptor interaction with S-SCAM/MAGI-2 protein. *Biochem. Biophys. Res. Commun.* 301, 1122–1128.

Yawata, S., Tsuchida, H., Kengaku, M., and Hirano, T. (2006). Membrane-proximal region of glutamate receptor δ2 subunit is critical for long-term depression and interaction with protein interacting

with C kinase 1 in a cerebellar Purkinje neuron. *J. Neurosci.* 26, 3626–3633.

Yue, Z., Horton, A., Bravin, M., DeJager, P. L., Selimi, F., and Heintz, N. (2002). A novel protein complex linking the δ2 glutamate receptor and autophagy: implications for neurodegeneration in *lurcher* mice. *Neuron* 35, 921–933.

Ziv, N. E., and Garner, C. C. (2004). Cellular and molecular mechanisms of presynaptic assembly. *Nat. Rev. Neurosci.* 5, 385–399.

Zuo, J., De Jager, P. L., Takahashi, K. A., Jiang, W., Linden, D. J., and Heintz, N. (1997). Neurodegeneration in lurcher mice caused by mutation in δ2 glutamate receptor gene. *Nature* 388, 769–773.

Conflict of Interest Statement: The authors declare that the research was conducted in the absence of any commercial or financial relationships that could be construed as a potential conflict of interest.

Received: 30 August 2012; accepted: 02 November 2012; published online: 23 November 2012.

Citation: Mishina M, Uemura T, Yasumura M and Yoshida T (2012) Molecular mechanism of parallel fiber-Purkinje cell synapse formation. Front. Neural Circuits ***6****:90. doi: 10.3389/fncir.2012.00090*

frontiers in
NEURAL CIRCUITS

REVIEW ARTICLE
published: 22 January 2013
doi: 10.3389/fncir.2012.00123

The compartmental restriction of cerebellar interneurons

G. Giacomo Consalez[1] and Richard Hawkes[2]*

[1] Division of Neuroscience, San Raffaele Scientific Institute, Milan, Italy
[2] Department of Cell Biology and Anatomy, Genes and Development Research Group, Faculty of Medicine, Hotchkiss Brain Institute, The University of Calgary, Calgary, AB, Canada

Edited by:
Egidio D'Angelo, University of Pavia, Italy

Reviewed by:
Leonard Maler, University of Ottawa, Canada
Samuel S. Wang, Princeton University, USA

***Correspondence:**
Richard Hawkes, Department of Cell Biology and Anatomy, Genes and Development Research Group, Faculty of Medicine, Hotchkiss Brain Institute, University of Calgary, 3330 Hospital Drive N.W., Calgary, AB T2N 4N1, Canada.
e-mail: rhawkes@ucalgary.ca

The Purkinje cells (PC's) of the cerebellar cortex are subdivided into multiple different molecular phenotypes that form an elaborate array of parasagittal stripes. This array serves as a scaffold around which afferent topography is organized. The ways in which cerebellar interneurons may be restricted by this scaffolding are less well-understood. This review begins with a brief survey of cerebellar topography. Next, it reviews the development of stripes in the cerebellum with a particular emphasis on the embryological origins of cerebellar interneurons. These data serve as a foundation to discuss the hypothesis that cerebellar compartment boundaries also restrict cerebellar interneurons, both excitatory [granule cells, unipolar brush cells (UBCs)] and inhibitory (e.g., Golgi cells, basket cells). Finally, it is proposed that the same PC scaffold that restricts afferent terminal fields to stripes may also act to organize cerebellar interneurons.

Keywords: Purkinje cell, stripe, zone, Golgi cell, basket cell, stellate cell, unipolar brush cell, granule cell

REVIEW OF CEREBELLAR COMPARTMENTATION

The architecture of the adult cerebellar cortex is built around hundreds of modules ("stripes"), each comprising no more than a few hundred Purkinje cells (PC's: Hawkes et al., 1997; Apps and Hawkes, 2009: **Figure 1**). Along the rostrocaudal axis, the cerebellar cortex is divided into five transverse zones—the anterior zone (AZ: ~lobules I–V), central zone anterior (CZa: ~VI), central zone posterior (CZp: ~VII), posterior zone (PZ: ~VIII–IX), and nodular zone (NZ: ~X). Transverse zones and zonal boundaries are revealed by expression patterns (e.g., Odutola, 1970; Prasadarao et al., 1990; Eisenman and Hawkes, 1993; Millen et al., 1995; Alam et al., 1996; Ozol et al., 1999; Armstrong et al., 2000; Eisenman, 2000; Logan et al., 2002; Marzban et al., 2008; etc.), reflect patterns of cell death in many genetic mutations or toxic insults [reviewed in Sarna and Hawkes (2003)], and coincide with boundaries in the actions of mutations that disrupt cerebellar development and structure (Herrup and Wilczynsk, 1982; Hess and Wilson, 1991; Napieralski and Eisenman, 1993, 1996; Ackerman et al., 1997; Armstrong and Hawkes, 2001; Beirebach et al., 2001; etc.).

Each transverse zone is further subdivided from medial to lateral into stripes. For example, **Figure 1** shows alternating zones and stripes in cerebella immunostained for zebrin II (Brochu et al., 1990 = aldolase C (Aldoc)—Ahn et al., 1994; Hawkes and Herrup, 1996; Sillitoe and Hawkes, 2002) and phospholipase C (PLC)β4—Sarna et al., 2006). Many molecular markers co-localize with either the zebrin II+ or PLCβ4+ stripes [e.g., reviewed in Sillitoe et al. (2011); Sillitoe and Hawkes (2013)]. Furthermore, other markers reveal subdivisions within stripes (e.g., the patterns of afferent terminal fields: Akintunde and Eisenman, 1994; Ji and Hawkes, 1994, 1995; etc.) and additional PC subtypes within the zebrin II+/− families [e.g., heat shock protein (HSP)25: Armstrong et al. (2000)], the *L7/pcp2* transgene (Oberdick et al., 1993; Ozol et al., 1999) and human natural killer cell antigen 1 (HNK1: Eisenman and Hawkes, 1993; Marzban et al., 2004 identify subsets of zebrin II+ PCs.). The pattern of zones and stripes is symmetrical about the midline, highly reproducible between individuals and insensitive to experimental manipulation [see below, and reviewed in Larouche and Hawkes (2006); Apps and Hawkes (2009)]. The implication is that the adult cerebellar cortex of the mouse is highly reproducibly subdivided into several hundred distinct stripes with >10 distinct PC molecular phenotypes (Hawkes, 1997; Apps and Hawkes, 2009).

Transverse zones and parasagittal stripes are important because cerebellar patterning influences all aspects of cerebellar organization and function. The most-studied example is that the terminal fields of both climbing fibers and mossy fibers are aligned parasagittally with stripes of PCs (climbing fibers: Gravel et al., 1987; Voogd and Ruigrok, 2004; Sugihara and Quy, 2007; etc.; mossy fibers: Gravel and Hawkes, 1990; Akintunde and Eisenman, 1994; Ji and Hawkes, 1994; Sillitoe et al., 2003; Armstrong et al., 2009; Gebre et al., 2012; etc.).

The molecular topography of the cerebellar cortex correlates nicely with the functional maps [see Apps and Garwicz (2005); Apps and Hawkes (2009)]. For example, mossy fiber tactile receptive field boundaries correlate well with zebrin II+/− stripe boundaries [Chockkan and Hawkes, 1994; Hallem et al., 1999: see also Chen et al. (1996)]. More recently, Wylie et al. have demonstrated an elegant correlation between PC stripes and complex spike activity boundaries associated with optic flow in the pigeon vestibular zone (e.g., Graham and Wylie, 2012). The reproducible association of function with specific stripes also presents a potential substrate for function-specific adaptations at

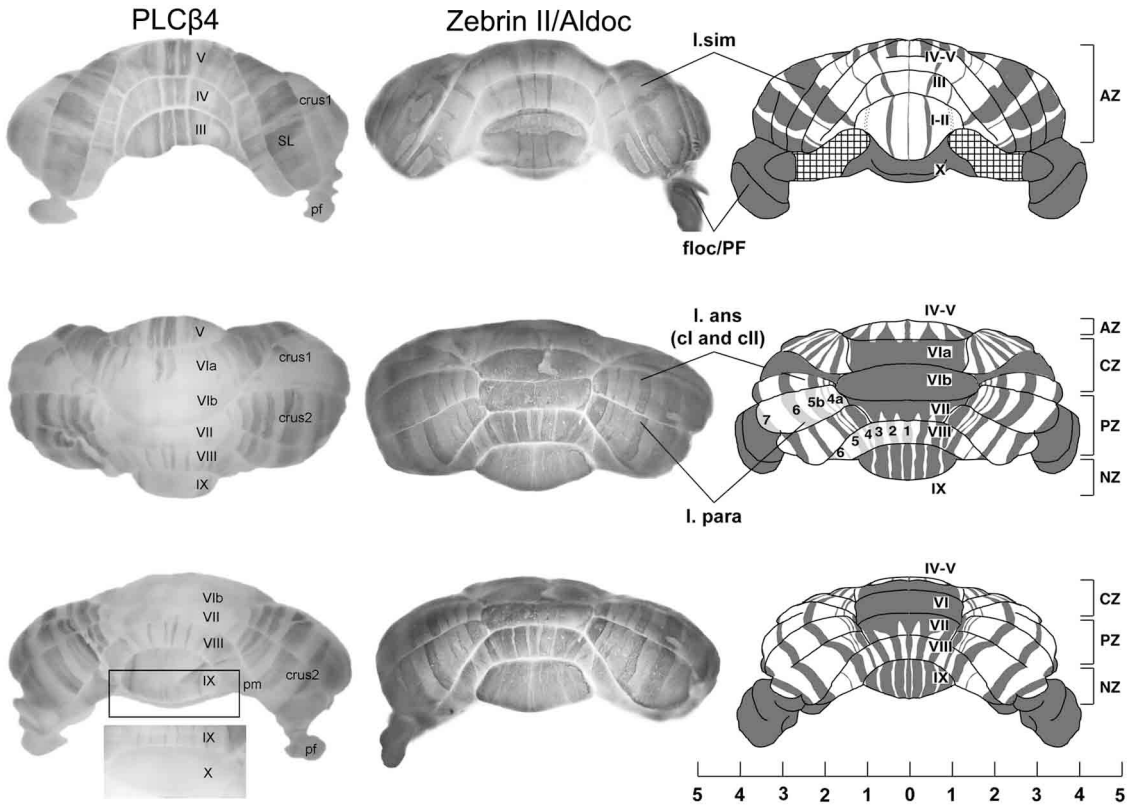

FIGURE 1 | An overview of cerebellar compartmentation. Whole mount views of the complementary stripe arrays revealed by immunoperoxidase-staining for phospholipase cβ4 (PLCβ4) and zebrin II/aldolase C in the adult mouse. (Views: above—anterior; middle—dorsal; lower—posterior). Abbreviations: l. sim, lobulus simplex; floc/PFl, flocculus and paraflocculus; l. ans (c1 and c2), lobulus ansiformis, crus 1 and crus 2; l. para/pm, lobulus paramedianus; SL, lobulus simplex; AZ, anterior zone; CZ, central zone; PZ, posterior zone; NZ, nodular zone; lobules are indicated by Roman numerals (I–X). Scale bar is in mm [Adapted from Sarna et al. (2006) and Sillitoe and Hawkes (2002)].

the molecular level. For instance, many of the molecules thought to mediate synaptic transmission and long-term depression at the parallel fiber-PC synapse show stripe restriction [including metabotropic glutamate receptors (Mateos et al., 2001), excitatory amino acid transporter 4 (Dehnes et al., 1998), PLC (Tanaka and Kondo, 1994; Sarna et al., 2006), protein kinase C (Chen and Hillman, 1993; Barmack et al., 2000), neuroplastin (Marzban et al., 2003), GABA receptors (Chung et al., 2008a), and so on]. Consistent with this hypothesis, electrophysiological studies have confirmed differences in parallel fiber-PC synaptic behavior between stripes (e.g., Wadiche and Jahr, 2005; Paukert et al., 2010; Ebner et al., 2012).

Thus, both patterns of gene expression and functional maps in the cerebellum seem to share a common architecture. The present review considers some of the evidence that PC stripe architecture also restricts the distributions of cerebellar interneurons. We begin with an overview of cerebellar pattern formation during development, then discuss the origins and development of the various cerebellar interneurons, review the evidence that interneurons are restricted to particular zones and stripes, and conclude by proposing the general hypothesis that interactions between interneurons and PCs during development are an important mechanism that restrict interneuron distributions.

Because we argue that much cerebellar patterning is built around a PC zone and stripe scaffold, we begin with a brief review of the origins of PC zones and stripes [reviewed in Herrup and Kuemerle (1997); Armstrong and Hawkes (2000); Larouche and Hawkes (2006); Sillitoe and Joyner (2007); Apps and Hawkes (2009); Dastjerdi et al. (2012); Sillitoe and Hawkes (2013)]. The cerebellar primordium arises from the rostral metencephalon between E8.5 and E9.5 (e.g., Wang et al., 2005; Sillitoe and Joyner, 2007: all timings are for mice). It houses two distinct germinal matrices—the dorsal rhombic lip (RL) and the ventral ventricular zone (VZ) of the 4th ventricle. Genetic fate mapping shows that a *Ptf1a* expressing domain in the VZ gives rise to all PCs (Hoshino et al., 2005; Hoshino, 2006). The *Ptf1a*+ VZ is not homogenous and gene expression differences further subdivide it (including *Ascl1*, *Neurogenin 1/2*, *Lhx1/5,* etc.—Chizhikov et al., 2006; Salsano et al., 2007; Zordan et al., 2008). PCs undergo terminal mitosis in the VZ between E10 and E13 (Miale and Sidman, 1961).

Adult PC zebrin II+/− phenotypes are specified early in development and birthdating studies in mice have identified two PC populations—an early born subset (E10–E11.5) mostly destined to become zebrin II+ and late-born subset (E11.5–E13) destined to become zebrin II—(Hashimoto and Mikoshiba, 2003;

Larouche and Hawkes, 2006; Namba et al., 2011). Many experimental interventions—*in vitro* culture models, cerebellar transplants, afferent lesions, sensory deprivation, etc.—have been used to try to alter adult PC zebrin II+/− phenotypes, but these have always proved ineffective [reviewed in Larouche and Hawkes (2006)]. In fact, the only experimental manipulation known to alter PC subtype identity is deletion of the atypical helix-loop-helix transcription factor *Early B-cell Factor 2* (*Ebf2*), a repressor of the zebrin II+ phenotype (Croci et al., 2006; Chung et al., 2008b).

Postmitotic PCs migrate out of the VZ and stack in the cortical transitory zone with the earliest-born located dorsally and the youngest ventrally. Subsequently, the PCs reorganize to yield a stereotyped array of embryonic clusters with multiple molecular phenotypes [E14–E18: reviewed in e.g., Herrup and Kuemerle (1997)]. Starting at around E18, the embryonic clusters disperse, triggered by Reelin/Disabled-1 (Dab1) signaling (e.g., Armstrong and Hawkes, 2000; Larouche and Hawkes, 2006; Apps and Hawkes, 2009). As the clusters disperse into adult stripes the PCs spread to form a monolayer. Because dispersal occurs primarily in the anteroposterior plane, the clusters string out into long parasagittal stripes (e.g., Marzban et al., 2007).

The embryonic PC clusters are the targets for ingrowing climbing and mossy fiber afferents. Climbing fibers from the contralateral inferior olive enter the cerebellar cortex prenatally (Sotelo, 2004), and contact with PC clusters can be identified from birth (e.g., Mason et al., 1990). It appears that as the PC clusters disperse into parasagittal stripes the climbing fiber terminal fields ride along with them, thereby maintaining the embryonic topographical relationship and assuring a reproducible coupling between specific subnuclei of the inferior olivary complex and specific PC stripes [reviewed in Ruigrok (2011)]. Postnatally, extensive pruning of the climbing fiber projection occurs until each PC receives input from only one cell in the inferior olive, but this does not seem to contribute significantly to the refinement of the topography (Crépel, 1982). A similar sequence of events also patterns the mossy fiber projections, which are found in direct association with embryonic PC clusters from (*circa* E15: Grishkat and Eisenman, 1995; and possibly earlier—e.g., Morris et al., 1988). In the adult cerebellar cortex mossy fibers do not directly contact PCs. Rather, between P0 and P20, as the granular layer matures, mossy fiber afferents detach from the PCs and form new synapses with local granule cells. As a result, mossy fiber terminal fields retain their alignment with the overlying PC stripes (e.g., Gravel and Hawkes, 1990; Matsushita et al., 1991; Akintunde and Eisenman, 1994; Ji and Hawkes, 1994, 1995; Apps and Hawkes, 2009).

The aim of this review is to assess the evidence first that cerebellar interneurons show restriction and secondly to review the hypothesis that the PC architecture is the template around which they organize. This is a straightforward extension of the model previously espoused for the development of cerebellar afferent topography (e.g., Sotelo, 2004). The main classes of cerebellar interneurons are granule cells and unipolar brush cells (UBCs; glutamatergic—excitatory), and Golgi, stellate, and basket cells (GABAergic—inhibitory). In addition, there are several other types of inhibitory interneuron—Lugaro cells, Chandelier cells, etc. [see Schilling et al. (2008)]—but nothing is known of their patterns of restriction and they will not be considered further below.

THE EMBRYOLOGICAL ORIGINS OF CEREBELLAR INTERNEURONS

Upon completion of early cerebellar patterning, neurogenesis begins. Two germinative compartments are established, the VZ and the rostral RL. In the mouse, this second phase of cerebellar development starts between E9 and E11 and proceeds for many days, giving rise to the different classes of cerebellar cells (**Figure 2**). At the onset of neurogenesis, the cerebellar primordium consists of two symmetric bulges extending dorsally and laterally from the midline of rhombomere one. These two halves are fated to eventually fuse at the midline, giving rise to a single dorsal formation spanning, and eventually exceeding, the width of the 4th ventricle. The inner and outer germinal layers of the cerebellar plate constitute the VZ and the RL, respectively (Altman and Bayer, 1997).

A series of studies conducted since 1990 have unveiled the origin of GABAergic and glutamatergic neurons that populate the cerebellar primordium and, eventually, the adult cerebellar cortex. The development of RL-derived progenitors is affected by signals produced by the roof plate (Alder et al., 1999; Millonig et al., 2000; Chizhikov et al., 2006). These progenitors soon become positive for the proneural gene *Atoh1/Math1* (Machold and Fishell, 2005; Wang et al., 2005). Targeted disruption of *Atoh1* virtually ablates the entire repertoire of cerebellar glutamatergic neurons (Jensen et al., 2004; Wang et al., 2005). Progenitor cells originating in the RL first migrate tangentially, dispersing over the dorsal surface of the cerebellar primordium, and then move radially into the cortex or cerebellar nuclei (CN). The first cells to migrate tangentially from the RL (*circa* E10.5) give rise

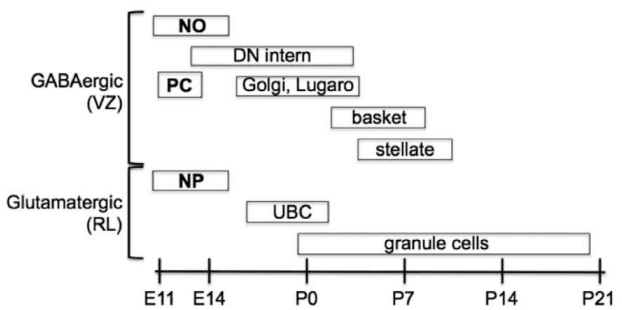

FIGURE 2 | Temporal sequence of birth for the main types of neurons that populate the adult cerebellum. Projection neurons are in boldface, interneurons are in normal text. Projection neurons of the cerebellar nuclei and cortex are the first to be born at the outset of cerebellar neurogenesis. These include glutamatergic nuclear projection neurons (NP) derived from the rhombic lip (RL) and GABAergic nucleo-olivary projection neurons (NO) and Purkinje cells (PC) derived from the ventricular zone (VZ). Local interneurons (of both neurotransmitter phenotypes) are born during late embryonic and early postnatal development. GABAergic interneurons are generated according to an inside-out sequence, occupying the deep nuclei first, and then the granular and molecular layer [Modified from Carletti and Rossi (2008)].

to glutamatergic projection neurons of the CN (Machold and Fishell, 2005). They enter the primordium from just below its surface, giving rise to a transient structure sometimes referred to as nuclear transitory zone (NTZ), which will evolve into the CN. Shortly thereafter (*circa* E11–E14), a second echelon of RL-derived glutamatergic progenitors disperses by tangential migration to populate the external granular layer (EGL). These cells are fated to give rise to granule cell neurons only (Hallonet et al., 1990; Alvarez Otero et al., 1993). Starting shortly before birth, these progenitors undertake a long phase of clonal expansion in the EGL (between E17 and P20), under control of signals secreted by PCs (Smeyne et al., 1995; Dahmane and Ruiz-i-Altaba, 1999; Wallace, 1999; Wechsler-Reya and Scott, 1999; Lewis et al., 2004).

In addition to CN neurons and GCs, a third population of glutamatergic neurons originates in the embryonic cerebellum between E15 and E17: the so-called UBCs. UBCs are glutamatergic interneurons of the granular layer, with small somata, mossy fiber-like axon terminals, and brush-like dendrites (Altman and Bayer, 1977; Mugnaini and Floris, 1994; Diño et al., 1999, 2000, 2001; Nunzi and Mugnaini, 2000; Nunzi et al., 2001, 2002). Like granule cell progenitors, UBCs originate in the RL (Englund et al., 2006), and migrate inwards to invade the white matter of prospective lobule X. From there they disperse, populating the granular layer and extending glutamatergic axons akin to mossy fibers to form synapses with granule cell dendrites.

Unlike glutamatergic neurons, all GABAergic neurons of the cerebellum originate in a ventral germinative epithelium lining the 4th ventricle, called the VZ and recent evidence indicates that, as for granule cell proliferation, VZ progenitor proliferation is also controlled by *sonic hedgehog* (Huang et al., 2010). Projection neurons are generated first and local interneurons are born during late embryonic and early postnatal life (Miale and Sidman, 1961; Pierce, 1975; Altman and Bayer, 1997; Morales and Hatten, 2006). While GABAergic projection neurons only proliferate in the VZ, interneurons derive from progenitors that delaminate from the VZ into the prospective white matter. Projection neurons (PCs and nucleo-olivary neurons) proliferate in the VZ and become committed to their fate at early stages of development, acquiring their mature subtype phenotypes through cell-autonomous mechanisms [for example, see Florio et al. (2012)]. Conversely, interneurons derive from progenitors that delaminate into the prospective white matter, where they develop in an inside-out progression (CN to granular layer to molecular layer) from a single pool of progenitors. While sojourning in the white matter, their fate choices, production rates, and differentiation schedules remain flexible and are largely dependent on stage-specific extracellular cues (Leto et al., 2006, 2009).

In regard to gene expression, all VZ-derived progenitors express *Ptf1a*, a gene encoding a bHLH transcription factor, as shown by targeted inactivation studies (Hoshino et al., 2005; Pascual et al., 2007). *Ptf1a*+ progenitors start regulatory cascades leading to the expression of other proneural genes (Zordan et al., 2008; Dastjerdi et al., 2012; Consalez et al., 2013). Cerebellar *Ascl1/Mash1*+ precursors give rise to PCs and to all GABAergic interneurons (Kim et al., 2008; Grimaldi et al., 2009; Sudarov et al., 2011). Precursors expressing *neurogenin 1* (*Neurog1*) become PCs or cortical GABA interneurons (Kim et al., 2008; Lundell et al., 2009). *Neurog2*+ precursors give rise to PCs and GABAergic CN neurons, including presumptive nucleo-olivary neurons and interneurons (Florio et al., 2012). Two subsets originate from that population. The first, located anteriorly and medially, starts expressing the proneural gene *Neurog1* and gives rise to cortical interneurons of the GL (Golgi, Lugaro) and ML (basket, stellate) (Lundell et al., 2009; Kim et al., 2011). The second group, positive for *Neurog2*, gives rise to CN interneurons (Florio et al., 2012). While the cell surface marker Neph3 is expressed throughout the VZ, including interneuron progenitors, E-cadherin (Cdh1) is differentially expressed, with higher levels found on the surface of mitotic PC progenitors (Mizuhara et al., 2009). To date, it is not clear if some progenitors co-express *Neurog1* and *Neurog2*.

ZONE AND STRIPE BOUNDARIES RESTRICT CEREBELLAR INTERNEURONS

GRANULE CELLS

The most plentiful cerebellar interneuron is the granule cell, which comprises almost all the neurons of the cerebellum. Granule cells receive their input from mossy fibers (mostly directly but in some cases via UBCs), and synapse in the molecular layer as parallel fiber synapses on PC dendrites and inhibitory interneurons. The development of granule cells has been studied extensively [e.g., reviewed in Chédotal (2010); Butts et al. (2011); Hashimoto and Hibi (2012)]. After several proliferative cycles, granule cell precursors located in the outer part of the EGL exit the cell cycle, express differentiation markers, and modify their repertoire of adhesion molecules (e.g., Xenaki et al., 2011). Through these surface molecules, in particular astrotactin (Edmondson et al., 1988), they contact the distal processes of Bergmann glia and undertake a centripetal radial migration in the course of which they begin to populate the granular layer, migrating inwards across the PC layer while extending T-shaped axons (future parallel fibers) orthogonal to their migration path (Altman and Bayer, 1997). Upon their arrival in the granular layer, granule cells receive inputs from mossy fiber presynaptic terminals, and trans-synaptically induce their maturation by secreting *Wnt* family ligands (Hall et al., 2000).

Restriction

Several lines of evidence point to an elaborate parcellation of the granular layer, with evidence of restriction both into transverse zones and parasagittal stripes. Differences in gene expression have revealed multiple granule cell subtypes [e.g., *Otx1/2*—Frantz et al., 1994; nicotinamide adenine dinucleotide phosphate (NADPH)-oxidase—Hawkes and Turner, 1994; fibroblast growth factor (FGF)1—Alam et al., 1996; Eph receptors and Ephrins—Rogers et al., 1999, etc.; reviewed in Hawkes and Eisenman (1997); Ozol and Hawkes (1997)]. Multiple granule cell subtypes can be explained in two broad ways: either they represent granule cell lineages or they are a secondary response to their local environment (for example, the local mossy fibers or PCs). In many cases, we cannot distinguish these possibilities. However, the analysis of murine embryonic stem cell chimeras

FIGURE 3 | Compartmentation of the granular layer. Cell transverse lineage boundaries seen in a β-gal-stained sagittal section through an adult murine embryonic stem cell chimera. The ES-cell-derived granule cells (β-gal+) are concentrated preferentially in the anterior vermis (AZ) with a restriction boundary in lobule VI (AX/CZ: arrow), and in the nodulus with a boundary in the sulcus between lobules IX and X (the PZ/NZ boundary: arrow) [Adapted from Hawkes et al. (1999)].

has revealed two consistent granule cell lineage boundaries, one located close to the AZ/CZ PC boundary and a second to the PZ/NZ boundary (Hawkes et al., 1999: **Figure 3**). An AZ/CZ granule cell boundary can also be seen in the granular layer of several mouse mutants (e.g., *scrambler*—Goldowitz et al., 1997; *disabled*—Gallagher et al., 1998), and studies with *weaver* (*wv/wv*) X +/+ and *M. musculus* X *M. caroli* chimeras also revealed developmental boundaries at these sites (Goldowitz, 1989). Evidence for a distinct AZ compartment in the EGL also comes from analysis of *Unc5h3 X* +/+ (Goldowitz et al., 2000) and (small eye) Sey/Sey$^{\text{Neu X}+/+}$ chimeras (Swanson and Goldowitz, 2011), and from the effects of several mouse mutations (e.g., *rostral cerebellar malformation*—Eisenman and Brothers, 1998; *NeuroD*−/−—Miyata et al., 1999). Finally, patterns of granular layer and/or EGL gene expression show the AZ/CZ (e.g., acidic FGF, receptor protein tyrosine phosphatase—McAndrew et al., 1998; *Otx-1*—Frantz et al., 1994) and PZ/NZ (e.g., *Otx1*—Frantz et al., 1994; *En2*—Millen et al., 1995; *Tlx3*—Logan et al., 2002; *Lmx1a*$^{+}$—Chizhikov et al., 2010) boundaries. Similarly, neuronal nitric oxide synthase (nNOS: NADPH) is expressed by most granule cells but is entirely absent from those of the NZ (Hawkes and Turner, 1994). While epigenetic interactions with PCs may explain differential gene expression, they cannot account for the spatial distribution of genotypes in the chimeras. We therefore conclude that the cerebellar granular layer has multiple lineage histories and derives from multiple distinct precursor pools either side of lineage boundaries within the RL. It has been established by genetic fate mapping that early born granule cell progenitors (E12.5–E15.5), migrate preferentially into the anterior vermis, whereas later born ones distribute more evenly along the AP axis, and only late-born ones (*circa* E17) populate lobule X (Machold and Fishell, 2005).

What determines the location of the granular layer lineage boundaries? While some signals may be intrinsic to early born granule cell progenitors in the RL, the most obvious source of positional information for the developing granular layer (or, more likely, the developing EGL) is the compartmentation of the PCs, and it is therefore noteworthy that the granular layer lineage restriction boundaries roughly align with PC transverse zone boundaries, and suggests that distinct PC compartments may direct the spreading EGL into distinct migratory streams. Consequently, as the EGL comes to cover the cerebellar surface, granule cell lineage discontinuities end up aligned with the PC transverse zone boundaries. Subsequently, both intrinsic differences between granule cell populations and epigenetic interactions between developing granule cells and PCs could contribute to selective patterns of granule cell gene expression. Notably, PCs express extracellular factors during early postnatal development. One of them, Igf-1, is expressed in a pattern very similar to the distribution of zebrin II—PC stripes. Igf-1 acts in an autocrine/paracrine fashion to protect PCs from apoptotic cell death, particularly at birth, and its expression is driven locally by EBF2 expressed by PCs (Croci et al., 2011). Abundant evidence supports a role for Insulin-like growth factor 1 and 2 (IGF1 and IGF2) in central nervous system (CNS) development. IGF1 is predominantly expressed in neurons in a fashion that coincides with outbursts of neural progenitor proliferation, neurite outgrowth, and synaptogenesis (D'Ercole et al., 1996; Bondy and Cheng, 2004; Ozdinler and Macklis, 2006; Fernandez and Torres-Alemàn, 2012). A recent paper indicates that Igf-1, whose levels fluctuate with light-dark cycles, promotes granule cell migration into the GL (Li et al., 2012). Thus, it is conceivable that granule cells in contact with *Igf1*-expressing (zebrin II-) PCs may migrate faster into the GL and thus establish privileged synaptic contacts.

Beyond the restriction of granule cell subtypes to transverse zones, several granule cell markers reveal a much more elaborate parcellation into parasagittal stripes [e.g., in the expression patterns of acetylcholinesterase (Marani and Voogd, 1977; Boegman et al., 1988), cytochrome oxidase (Hess and Voogd, 1986; Leclerc et al., 1990), and nNOS (Yan et al., 1993; Hawkes and Turner, 1994; Schilling et al., 1994)]. It is plausible that this molecular complexity is related to the complex array of somatotopic patches mapped in some cerebellar regions (Welker, 1987; Hallem et al., 1999; Apps and Hawkes, 2009). Finally, perhaps the most curious manifestation of granular layer heterogeneity is the reproducible array of wrinkles in the granular layer ("blebs") that are seen when ethanol-fixed, paraffin-embedded sections are rehydrated (Hawkes et al., 1997, 1998). The structural basis of blebbing is not known, but it points to the possibility that blebs represent individual cytoarchitectonic units and that the mouse granular layer is subdivided into several thousand modules [reviewed in Hawkes (1997)].

Do these granular layer stripes arise through lineage restriction or are they secondary responses to the local environment (e.g., the type of mossy fiber input or the local PCs)? It is not known but it is difficult to imagine a mechanism by which granule cell stripes form through the targeted migration of granule cell subtypes to hundreds of destinations (although raphes between PC clusters do seem to preferentially guide the descent of immature granule cells to the granular layer: e.g., Karam et al., 2000; Luckner et al., 2001), so it is more plausible that stripe molecular phenotypes among granule cells are secondary responses to local cues. One mechanism might be that granule cells adopt

their molecular phenotypes according to the local PC subtype environment through which they migrate (and synapse) during postnatal development (several studies have demonstrated PC influences on granule cell growth and differentiation—e.g., PC-derived sonic hedgehog regulates granule cell proliferation (Wallace, 1999); PC-derived brain-derived neurotrophic factor (BDNF) stimulates granule cell migration—Borghenasi et al., 2002). An alternative mechanism might be that granule cell subtypes are specified by the type of mossy fiber (or UBC) afferent input they receive. As noted earlier (section "Review of cerebellar compartmentation") mossy fiber terminal fields from different sources and of different molecular phenotypes are restricted to parasagittal stripes that align with PC stripes (e.g., somatostatin-immunoreactive—Armstrong et al., 2009; vesicular glutamate transporter immunoreactive—Gebre et al., 2012). Perhaps differential mossy fiber innervation specifies granule cell subtype. In both cases, PC specification or mossy fiber specification of granule cell subtype, granule cell stripes would naturally also align with PC stripes.

This is consistent with the demonstration by Schilling et al. (1994) that ingrowing mossy fibers may downregulate nitric oxide synthase expression and thereby contribute to the generation of granule cell subtypes.

UNIPOLAR BRUSH CELLS

UBCs are glutamatergic interneurons of the granular layer. They receive mossy fiber innervation, in large part from primary vestibular afferents (e.g., Diño et al., 2000, 2001), and project in turn to granule cell dendrites. At least three subtypes of UBC are known, one immunoreactive for calretinin (= CR+ subset), another expressing both the metabotropic glutamate receptor (mGluR1α: Nunzi et al., 2001, 2002) and PLCβ4 (Chung et al., 2009a = the mGluR1α+ subset), and a third expresses PLCβ4 but not mGluR1α (Chung et al., 2009a = the PLCβ4+ subset).

UBCs are born between E15 and P2 (Abbott and Jacobowitz, 1995; Sekerková et al., 2004; Chung et al., 2009b). They appear to have two distinct origins. The majority arise ventrally, possibly in the VZ of the fourth ventricle (e.g., Ilijic et al., 2005) but more likely from the RL since RL ablation in slice cultures significantly reduced the number of UBCs (Englund et al., 2006) and the production of UBCs is decreased in the *Math1* null cerebellum (as mentioned, *Math1* is required for the development of RL derivatives: Machold and Fishell, 2005; Wang et al., 2005). Either way, most UBCs migrate into the developing cerebellar anlage soon after the PCs arrive (E14 onwards: Abbott and Jacobowitz, 1995) and then disperse via the white matter tracts, presumably guided by cues associated with PC axons or afferent projections. In addition, a second, small population of UBCs arises dorsally from the EGL (and presumably the RL) and reaches the granular layer by following the same dorsoventral migratory route as the granule cells (Abbott and Jacobowitz, 1995; Chung et al., 2009b).

Each UBC subset has a characteristic topographical distribution (Braak and Braak, 1993; Floris et al., 1994; Diño et al., 1999; Nunzi et al., 2002; Chung et al., 2008a): all three are concentrated preferentially in the NZ, but mGluRlα+ UBCs are also common throughout the vermis, only occasional CR+ UBCs are seen in the AZ, and the PLCβ4+ subset is very rare in the AZ (Mugnaini and Floris, 1994; Diño et al., 2000; Chung et al., 2009a). Each subset is also loosely restricted to stripes that align with PC stripes (e.g., Chung et al., 2009b: **Figure 4**). This distribution implies that each UBC subset receives afferent input from a different set of mossy fiber inputs. However, it seems unlikely that UBC subtype phenotypes are secondary to mossy fiber input since when they are allowed to mature as dissociated cells *in vitro*, in the absence of extracerebellar mossy fiber cues, the different phenotypes are all expressed (Anelli and Mugnaini, 2001; Chung et al., 2009a). It is therefore plausible that the restricted distributions of UBC

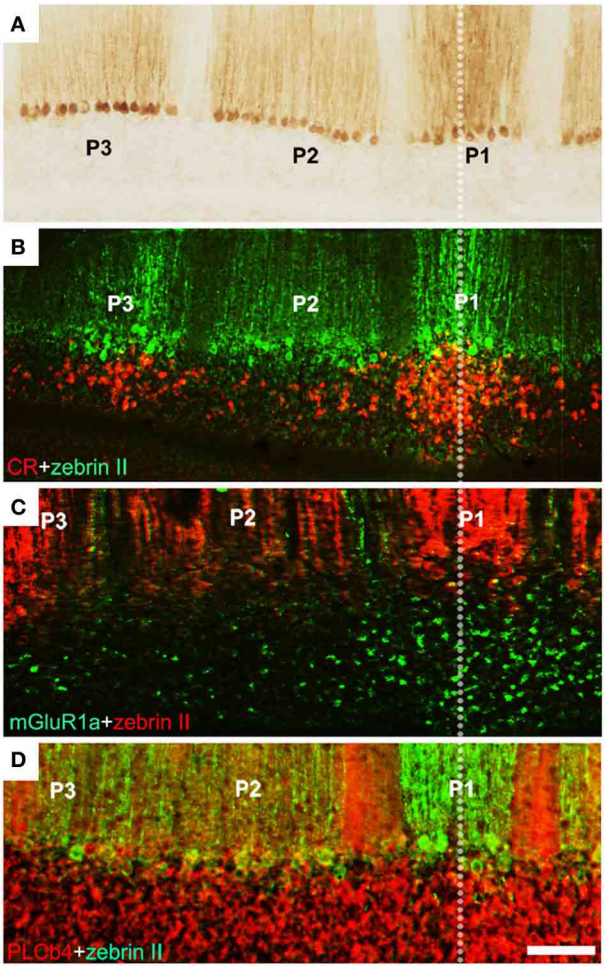

FIGURE 4 | Unipolar brush cells are restricted at stripe boundaries in the adult mouse cerebellum. (A) Cerebellar stripe topography is built around PC subtypes. Immunoperoxidase staining of a transverse section through lobule IX for zebrin II reveals three broad stripes of immunoreactive PCs [P1+ at the midline, P2+ and P3+ laterally on either side: for stripe nomenclature, see Sillitoe and Hawkes (2002)]. **(B)** CR+ UBC clusters (red) in lobule IX align with the zebrin II P1+ and P3+ PC stripes (green). **(C)** mGluR1α+ UBCs (green) in lobule IX cluster beneath the midline P1+ PC stripe (red). **(D)** Double immunostaining with anti-PLCβ4 (red) and anti-zebrin II (green) shows that PLCβ4-immunopositive UBCs are uniformly distributed in cerebellar lobule IX (the combined PLCβ4+ and mGluR1α+ subsets). Scale bars: D = 125 μm **(A–D)** [Adapted from Chung et al. (2009b)].

subtypes comes about because each uses different topographical cues to guide their migrations. Experiments using an *Ebf2*−/− mouse support this inference. When *Ebf2* is deleted, many PCs express abnormal molecular phenotypes (a mixture of zebrin II+ and zebrin II−: Croci et al., 2006; Chung et al., 2008b). Notably, anterior vermis PCs adopt features of the posterior vermis. Interestingly, in these mice, the normal restriction of UBCs to the posterior vermis is also lost, and UBC profiles become plentiful in the anterior lobules (Chung et al., 2009b). Because EBF2 is not expressed by UBCs this suggests that the abnormal topography in the mutant is not cell-autonomous but rather secondary to the abnormal PC transdifferentiated phenotype. This is also consistent with the developmental data showing a close association between PCs and UBCs in the perinatal cerebellum (Chung et al., 2009b). Finally, mutations in the Reelin signaling pathway result in a failure of PC cluster dispersal. This results in a corresponding UBC ectopia. For example, in *scrambler* (a *Disabled1* mutant: Sheldon et al., 1997) UBCs are found in association with specific PC ectopic clusters (Chung et al., 2009b). Taken together, the data support the hypothesis that PCs present topographically organized cues to the growth cones of migrating UBCs and thereby restrict their topography.

BASKET AND STELLATE CELLS

Basket and stellate cells are small inhibitory interneurons of the molecular layer. Whether or not they represent two distinct cell classes or a morphological continuum is unclear (e.g., Schilling et al., 2008): for our purposes we will discuss them together. There is little evidence of distinct subclasses of basket/stellate cells (cyclin D2 expression can distinguish subtypes, but this is amenable to other explanations: Huard et al., 1999). An exception is the study of Chen and Hillman (1993) who showed that a protein kinase Cδ-immunoreactive basket/stellate cell subset in the rat cerebellum is strongly concentrated in the AZ.

All GABA interneuron progenitors transiently activate *Pax2* expression around cell cycle exit. Before homing in on their final location, the young *Pax2*+ interneurons reside for several days in the white matter, progressing in their maturation, and acquiring their final identities. Postmitotic Pax2+ neurons harvested while in the white matter and transplanted heterochronically into a recipient cerebellum invariably give rise to GABA interneurons, but their choice to adopt a CN, granular layer, or molecular layer interneuron fate remains entirely dependent upon the host-specific, extrinsic environment (Leto et al., 2009).

Few inhibitory interneurons are present in the molecular layer at birth. While CN interneurons, are all born between E12 (Florio et al., 2012) and P3, Golgi cells that populate the GL continue to divide until P4 and basket/stellate interneuron progenitors keep proliferating through the second postnatal week [reviewed in Zhang and Goldman (1996); Carletti and Rossi (2008)], according to an inside-out progression (Leto et al., 2006). In rat, the interneurons of the inner molecular layer (= basket cells) are born between P2 and P17 with a peak at P6, while those in the outer molecular layer (= stellate cells) are born between P4 and P19 (peak at P10: Altman, 1972). The morphological evidence of restriction of basket/stellate cell neurites follows a similar continuum. In particular for the cells located deep in the molecular layer (basket) and less so for the more superficial ones (stellate), both the axons and the dendrites tend to be oriented parasagittally. For example, a classic basket cell contacts about 40 PCs. Their terminal fields are ovoid in shape, four times longer than they are wide, and with their long axes aligned parasagittally with the PC stripes (e.g., Eccles et al., 1967; Rakic, 1972; King et al., 1993). This axial ratio is much less for stellate cells. Ever since the work of Szentagothai (1965) it has been recognized that the parasagittal orientation of basket cells represents a substrate for PC lateral inhibition. More recently, and consistent with the morphology, physiological studies both *in vitro* and *in vivo* confirm that the inhibitory fields of basket/stellate cells are confined to a single stripe, with molecular layer inhibition restricted parasagittally (Ekerot and Jörntell, 2001, 2003; Jörntell and Ekerot, 2002; Gao et al., 2006; Dizon and Khodakhah, 2011; etc.: the functional implications of reciprocal inhibition between interneurons within a microzone have recently been reviewed—Jörntell et al., 2010).

How do basket/stellate cells acquire their parasagittal orientations? First, they are born too late to interact with embryonic PC clusters (from P2 to P19: and anyway there is little evidence of subtype specification). However, the parasagittal orientation of basket cell axonal arbors can still be explained by PC rostrocaudal spreading. Molecular layer interneurons invade the immature molecular layer randomly from the white matter. Once in the molecular layer they contact a local cluster of some 40 PCs. In the course of the next 3 weeks, these PCs gradually disperse rostrocaudally, so that the cerebellar cortex extends more than 10-fold in rostrocaudal extent with almost no change in width. As a result, the basket/stellate cell terminal field becomes a short, parasagittal PC stripe (**Figure 5**). It is not clear to what extent the basket/stellate terminal fields are restricted to particular stripes. It could be that there are as yet unrecognized subtypes (as for UBCs, for example), or that secondary pruning refines their arbors, or the restriction could be purely statistical. In any case, PC dispersal would result in a continuum of terminal field shapes: the earliest-born interneurons enter the molecular layer first and therefore develop the most extended parasagittal terminal fields (basket cell); the later-born interneurons have progressively more symmetrical terminal fields (e.g., stellate cells—Sultan and Bower, 1998).

GOLGI CELLS

Golgi cells are large interneurons of the granular layer (Palay and Chan-Palay, 1974). Golgi cell apical dendrites ramify through the molecular layer and are contacted primarily by the axons of granule cells (e.g., Geurts et al., 2003). Their axonal terminals contact granule cell-mossy fiber glomeruli. Five distinct classes of Golgi cell have been identified based on morphology and differential expression patterns (various combinations of glycinergic, gabaergic, mGluR2+/−, and neurogranin+/−: Simat et al., 2007).

The origin of Golgi cells is controversial. On the one hand, Popoff (1896) and Athias (1897) suggested the EGL was the origin of these large neurons. This interpretation was supported by the more recent studies of Hausmann et al. (1985), who used cerebellar transplantation to provide experimental evidence that Golgi cells originate from the EGL. More recently,

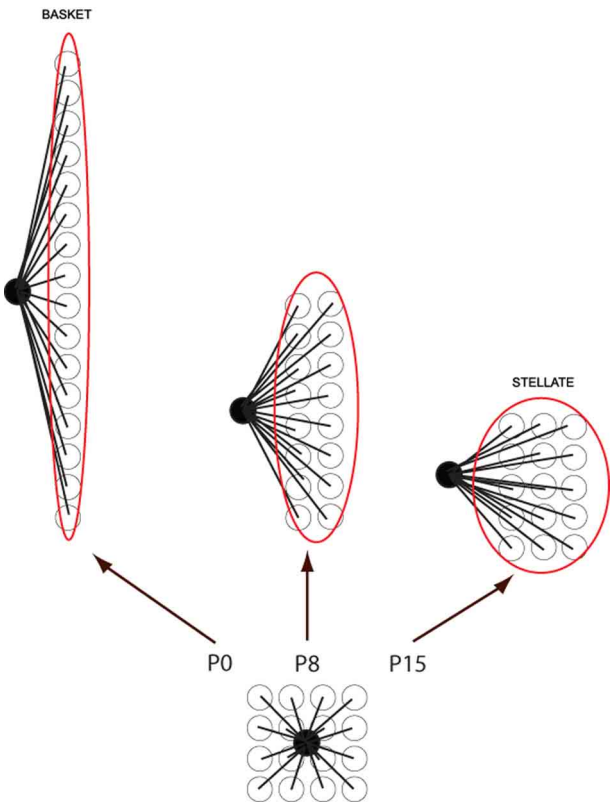

FIGURE 5 | Cartoon to show how basket/stellate cell parasagittal orientations might arise. Newly migrated basket/stellate cells enter the molecular layer and synapse on a small group of PCs. As the PCs extend parasagittally to form adult stripes, the basket/stellate cell arbors extend with them. As a result the shape of the final axonal arbor depends on the time they arrive: the earlier they enter the molecular layer, the more extended the arbor (= basket cell), the later they enter, the less it is extended (= stellate cells).

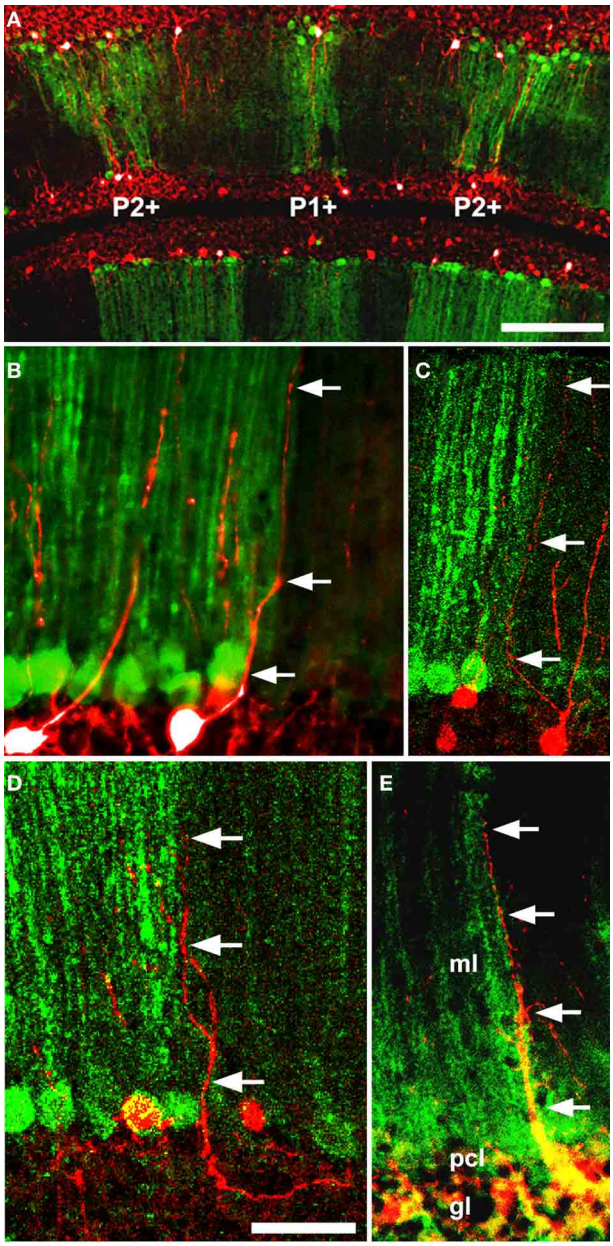

FIGURE 6 | Five examples (A–E) of double immunofluorescence for a GlyT2-EGFP transgene (Golgi cell dendrites: Zeilhofer et al., 2005) and anti-PLCβ4 (PC stripes: Sarna et al., 2006) in the adult mouse cerebellum reveals that Golgi cell dendrites are restricted at Purkinje cell stripe boundaries. Two examples of GlyT2-EGFP+ Golgi cell dendrites (green: arrowheads) in the vicinity of a PLCβ4+/− stripe boundary (red): in 68 cases examined, the dendrite never crossed between stripes. Abbreviations: ml, molecular layer; pcl, Purkinje cell layer; gl, granular layer. Scale bar = 50 μm [From Sillitoe et al. (2008)].

Chung et al. (2011) also identified a small, unique population of ZAC1-immunopositive Golgi cells, restricted to the posterior zone of the cerebellum that appears to derive from the EGL between E13 and E16. On the other hand, Ramon y Cajal (1911) and Altman and Bayer (1977) both concluded that Golgi cells derive from the ventricular neuroepithelium. Zhang and Goldman (1996) reached the same conclusion based on retroviral lineage tracing data. By this view Golgi cells, as all other GABA interneurons of the cerebellum, originate from *Ascl1*+ progenitors that delaminate from the VZ into the prospective white matter, exit the cell cycle, and activate *Pax2*. It seems probable that both explanations are correct, and that two distinct populations of Golgi cells are present in the adult cerebellum.

With the exception of the restriction to the PZ of the ZAC1+ population (Chung et al., 2011) nothing is known of the localization of Golgi cell subtypes to particular transverse zones or lobules. However, a different sort of patterning does occur: the apical dendrites of Golgi cells show restriction at parasagittal PC stripe boundaries (Sillitoe et al., 2008: **Figure 6**). Golgi cell apical dendrites contact the parallel fiber axons of granule cells in the molecular layer. By using different markers of Golgi cell dendrites and a selection of stripe antigens, the apical dendritic arbors of Golgi cells were studied in the vicinity of PC stripe boundaries. The conclusion was clear—fewer than 3% of Golgi cell dendrites cross a PC stripe boundary (Sillitoe et al., 2008).

The mechanisms that restrict Golgi cell dendritic arbors are speculative. They might be prevented from crossing stripe boundaries by structural barriers (such as those reported in the somatosensory cortex—Faissner and Steindler, 1995). However, no such barriers to neurite extension are known and other axons (e.g., parallel fibers) cross parasagittal stripes unhindered. Alternatively, Golgi cell dendritic arbors may be restricted, via adhesion molecules or attractive/repulsive extracellular cues, as they develop in concert with the PC dendrites (e.g., Hekmat et al., 1989; Nagata and Nakatsuji, 1991). In this model, the newly born Golgi cells migrate via the white matter into the embryonic PC clusters (Zhang and Goldman, 1996) where they contact the nascent PC dendrites. Subsequently, as the PC clusters disperse into adult stripes, individual Golgi cell dendritic arbors would automatically become restricted to one side of a boundary Subsequently, as the granule cells mature, the Golgi cell dendrites would displace from the PCs and synapse with local parallel fibers. In this way they would retain their original topographical restriction.

PURKINJE CELL ARCHITECTURE GENERATES INTERNEURON RESTRICTION

We have reviewed the evidence that cerebellar interneurons show anatomical and molecular restriction to zones and stripes. The general hypothesis presented is that these restrictions come about through interactions with the PC architecture. In this light, it is worthwhile to recall briefly the hypothesis to explain how climbing and mossy fiber afferents become aligned with PC stripes. First, the afferent fiber growth cones make direct contacts with specific embryonic PC clusters (e.g., Sotelo and Wassef, 1991; Grishkat and Eisenman, 1995; Chédotal et al., 1997; Sotelo and Chédotal, 2005). Subsequently, the clusters disperse into stripes triggered by Reelin signaling. As a result, the PC layer extends in the rostrocaudal plane, the clusters transform into stripes and, because the afferent terminal fields are carried along, they too form stripes, which are aligned with specific PC stripes. In the case of mossy fibers, as the granular layer matures, the mossy fibers detach from their embryonic PC targets (Mason et al., 1990) and synapse instead on local granule cell dendrites. Hence, although the mossy fibers no longer directly contact PCs their terminal fields remain aligned with specific PC parasagittal stripes.

This hypothesis is straightforwardly adaptable to the interneurons of the cerebellar cortex. First, the developing EGL spreads over the surface of the cerebellar anlage, restricted by cues from the underlying PCs (section "Zone and stripe boundaries restrict cerebellar interneurons"). As a result, different EGL lineages become aligned with boundaries between different PC transverse zones (Ozol and Hawkes, 1997; Hawkes et al., 1999, etc.). The lineage boundaries are also expression boundaries, but it is not clear whether these are also lineage restricted or if they are secondary responses to local PC cues. Developing Golgi cells and most UBCs access the PC clusters via the white matter tracts (Leto et al., 2006, 2009) and associate with specific PC clusters (e.g., Chung et al., 2009b). Therefore, as the PC clusters disperse into stripes the Golgi cells and UBCs move with them, just as for mossy fiber afferent terminal fields, and therefore also become restricted to specific stripes and zones. Subsequently, they mimic the mossy fibers and relocate from the PCs to the granular layer as it matures. This also explains how Golgi cell apical dendrites become restricted to particular PC stripes (Sillitoe et al., 2008). The dispersal of embryonic PC clusters into stripes continues roughly during the first three postnatal weeks (in mice). Although basket/stellate cells are born too late to interact with the embryonic PC clusters they benefit from cluster dispersal to orient their axon arbors parasagittally. Once *in situ*, interneurons differentiate in response to local environmental cues (e.g., granule cell stripes of nNOS—Hawkes and Turner, 1994).

Finally, it is interesting to speculate why parallel fibers appear to be the sole exception: why are parallel fibers not restricted? One possibility is that it is important that they are not. Parallel fibers are several millimeters long (e.g., Brand et al., 1976) and as they run orthogonal to the PC stripes, they necessarily intersect many stripes, of many different subtypes. In a nutshell, if PC boundaries were to restrict parallel fibers there would be no parallel fibers! A subtler question is whether they synapse with all the PC dendritic arbors that they pass through. This issue has not been studied experimentally. One scenario is that parallel fibers have a primary function to distribute MF afferent input widely across multiple neighboring stripes, in which case they might be expected to synapse promiscuously with *all* stripes they encounter, at least initially. How that input is used is another matter. One possibility is that PCs synapse with every PC they intersect but only a subset of those synapses is active: in one study, a large fraction of parallel fiber-PC synapses were found to be silent (Brunel et al., 2004), so sculpting in this fashion is entirely plausible.

ACKNOWLEDGMENTS

These studies were supported by the Canadian Institutes of Health Research (Richard Hawkes), and by Ataxia UK and Fondazione Berlucchi, Italy (G. Giacomo Consalez).

REFERENCES

Abbott, L. C., and Jacobowitz, D. M. (1995). Development of calretinin-immunoreactive unipolar brush-like cells and an afferent pathway to the embryonic and early postnatal mouse cerebellum. *Anat. Embryol. (Berl.)* 191, 541–559.

Ackerman, S. L., Kozak, L. P., Przyborski, S. A., Rund, L. A., Boyer, B. B., and Knowles, B. B. (1997). The mouse rostral cerebellar malformation gene encodes an UNC-5-like protein. *Nature* 386, 838–842.

Ahn, A. H., Dziennis, S., Hawkes, R., and Herrup, K. (1994). The cloning of zebrin II reveals its identity with aldolase C. *Development* 120, 2081–2090.

Akintunde, A., and Eisenman, L. M. (1994). External cuneocerebellar projections and Purkinje cell zebrin II bands: a direct comparison of parasagittal banding in the mouse cerebellum. *J. Chem. Neuroanat.* 7, 75–86.

Alam, K. Y., Frostholm, A., Hackshaw, K. V., Evans, J. E., Rotter, A., and Chiu, I.-M. (1996). Characterization of the 1B promoter of fibroblast growth factor 1 and its expression in the adult and developing mouse brain. *J. Biol. Chem.* 271, 30263–30271.

Alder, J., Lee, K. J., Jessell, T. M., and Hatten, M. E. (1999). Generation of cerebellar granule neurons *in vivo* by transplantation of BMP-treated neural progenitor cells. *Nat. Neurosci.* 2, 535–540.

Altman, J. (1972). Postnatal development of the cerebellar cortex in the rat. I. The external germinal layer

and the transitional molecular layer. *J. Comp. Neurol.* 145, 353–398.

Altman, J., and Bayer, S. A. (1977). Time of origin and distribution of a new cell type in the rat cerebellar cortex. *Exp. Brain Res.* 29, 265–274.

Altman, J., and Bayer, S. A. (1997). *Development of the Cerebellar System in Relation to its Evolution, Structure, and Functions*. Boca Raton, FL: CRC Press.

Alvarez Otero, R., Sotelo, C., and Alvarado-Mallart, R. M. (1993). Chick/quail chimeras with partial cerebellar grafts: an analysis of the origin and migration of cerebellar cells. *J. Comp. Neurol.* 333, 597–615.

Anelli, R., and Mugnaini, E. (2001). Enrichment of unipolar brush cell-like neurons in primary rat cerebellar cultures. *Anat. Embryol. (Berl.)* 203, 283–292.

Apps, R., and Garwicz, M. (2005). Anatomical and physiological foundations of cerebellar information processing. *Nat. Rev. Neurosci.* 6, 297–311.

Apps, R., and Hawkes, R. (2009). Cerebellar cortical organization: a one-map hypothesis. *Nat. Rev. Neurosci.* 10, 670–681.

Armstrong, C., Chung, S.-H., Armstrong, J., Hochgeschwender, U., Jeong, Y.-G., and Hawkes, R. (2009). A novel somatostatin-immunoreactive mossy fiber pathway associated with HSP25-immunoreactive Purkinje cell stripes in the mouse cerebellum. *J. Comp. Neurol.* 517, 524–538.

Armstrong, C. L., and Hawkes, R. (2000). Pattern formation in the cerebellar cortex. *Biochem. Cell Biol.* 78, 551–562.

Armstrong, C. L., and Hawkes, R. (2001). Selective failure of Purkinje cell dispersion in the cerebellum of the *weaver* mouse. *J. Comp. Neurol.* 439, 151–161.

Armstrong, C. L., Krueger-Naug, A. M., Currie, W. C., and Hawkes, R. (2000). Constitutive expression of the 25kDa heat shock protein Hsp25 reveals novel parasagittal stripes of Purkinje cells in the adult mouse cerebellar cortex. *J. Comp. Neurol.* 416, 383–397.

Athias, M. (1897). Recherches sur l'histogenese de l'ecorce du cervelet. *J. Anat. Physiol. Normale* 33, 372–404.

Barmack, N. H., Qian, Z., and Yoshimura, J. (2000). Regional and cellular distribution of protein kinase C in rat cerebellar Purkinje cells. *J. Comp. Neurol.* 427, 235–254.

Beirebach, E., Park, C., Ackerman, S. L., Goldowitz, D., and Hawkes, R. (2001). Abnormal dispersion of a Purkinje cell subset in the mouse mutant *cerebellum deficient folia* (*cdf*). *J. Comp. Neurol.* 436, 42–51.

Boegman, R. J., Parent, A., and Hawkes, R. (1988). Zonation in the rat cerebellar cortex: patches of high acetylcholinesterase activity in the granular layer are congruent with Purkinje cell compartments. *Brain Res.* 448, 237–251.

Bondy, C. A., and Cheng, C. M. (2004). Signaling by insulin-like growth factor 1 in brain. *Eur. J. Pharmacol.* 490, 25–31.

Borghenasi, P. R., Peyrin, J. M., Klein, R., Rubin, J., Carter, A. R., Schwartz, P. M., et al. (2002). BDNF stimulates migration of cerebellar granule cells. *Development* 129, 1435–1442.

Braak, E., and Braak, H. (1993). The new monodendritic neuronal type within the adult human cerebellar granule cell layer shows calretinin-immunoreactivity. *Neurosci. Lett.* 154, 199–202.

Brand, S., Dahl, A. L., and Mugnaini, E. (1976). The length of parallel fibers in the cat cerebellar cortex. An experimental light and electron microscopic study. *Exp. Brain Res.* 26, 39–58.

Brochu, G., Maler, L., and Hawkes, R. (1990). Zebrin II: a polypeptide antigen expressed selectively by Purkinje cells reveals compartments in rat and fish cerebellum. *J. Comp. Neurol.* 291, 538–552.

Brunel, N., Hakim, V., Isope, P., Nadal, J. P., and Barbour, B. (2004). Optimal information storage and the distribution of synaptic weights: perceptron versus Purkinje cell. *Neuron* 43, 745–757.

Butts, T., Chaplin, N., and Wingate, R. J. (2011). Can clues from evolution unlock the molecular development of the cerebellum? *Mol. Neurobiol.* 43, 67–76.

Carletti, B., and Rossi, F. (2008). Neurogenesis in the cerebellum. *Neuroscientist* 14, 91–100.

Chédotal, A. (2010). Should I stay or should I go? Becoming a granule cell. *Trends Neurosci.* 33, 163–172.

Chédotal, A., Bloch-Gallego, E., and Sotelo, C. (1997). The embryonic cerebellum contains topographic cues that guide developing inferior olivary axons. *Development* 124, 861–870.

Chen, G., Hanson, C. L., and Ebner, T. J. (1996). Functional parasagittal compartments in the rat cerebellar cortex: an *in vivo* optical imaging study using neutral red. *J. Neurophysiol.* 76, 4169–4174.

Chen, S., and Hillman, D. E. (1993). Compartmentation of the cerebellar cortex by protein kinase C delta. *Neuroscience* 56, 177–188.

Chizhikov, V. V., Lindgren, A. G., Currle, D. S., Rose, M. F., Monuki, E. S., and Millen, K. J. (2006). The roof plate regulates cerebellar cell-type specification and proliferation. *Development* 133, 2793–2804.

Chizhikov, V. V., Lindgren, A. G., Mishima, Y., Roberts, R. W., Aldinger, K. A., Miesegaes, G. R., et al. (2010). Lmx1a regulates fates and location of cells originating from the cerebellar rhombic lip and telencephalic cortical hem. *Proc. Natl. Acad. Sci. U.S.A.* 107, 10725–10730.

Chockkan, V., and Hawkes, R. (1994). Functional and antigenic maps in the rat cerebellum: zebrin compartmentation and vibrissal receptive fields in lobule IXa. *J. Comp. Neurol.* 345, 33–45.

Chung, S.-H., Kim, C. T., and Hawkes, R. (2008a). Compartmentation of GABA B receptor 2 expression in the mouse cerebellar cortex. *Cerebellum* 7, 295–303.

Chung, S.-H., Marzban, H., Croci, L., Consalez, G. G., and Hawkes, R. (2008b). Purkinje cell subtype specification in the cerebellar cortex: EBF2 acts to repress the zebrin II-negative Purkinje cell phenotype. *Neuroscience* 153, 721–732.

Chung, S.-H., Marzban, H., Aldinger, K., Dixit, R., Millen, K., Schuurmans, C., et al. (2011). Zac1 plays a role in the development of specific neuronal subsets in the mouse cerebellum. *Neural Dev.* 6:25. doi: 10.1186/1749-8104-6-25

Chung, S. H., Marzban, H., Watanabe, M., and Hawkes, R. (2009a). Phospholipase Cbeta4 expression identifies a novel subset of unipolar brush cells in the adult mouse cerebellum. *Cerebellum* 8, 267–276.

Chung, S.-H., Sillitoe, R. V., Croci, L., Baldoni, A., Consalez, G. G., and Hawkes, R. (2009b). Unipolar brush cells use Purkinje cells to restrict their topography. *Neuroscience* 164, 1496–1508.

Consalez, G. G., Florio, M., Massimino, L., and Croci, L. (2013). "Proneural genes and cerebellar neurogenesis in the ventricular zone and upper rhombic lip," in *Handbook of Cerebellum and Cerebellar Disorders*, eds M. Manto, D. Gruol, J. Schmahmann, N. Koibuchi, and F. Rossi (New York, NY: Springer), 23–41.

Crépel, F. (1982). Regression of functional synapses in the immature mammalian cerebellum. *Trends Neurosci.* 5, 266–269.

Croci, L., Barili, V., Chia, D., Massimino, L., van Vugt, R., Maserdotti, G., et al. (2011). Local insulin-like growth factor 1 expression is essential for Purkinje neuron survival at birth. *Cell Death Diff.* 18, 48–59.

Croci, L., Chung, S.-H., Masserdotti, G., Gianola, S., Motti, E., Tonini, R., et al. (2006). A key role for the HLH transcription factor EBF2 (COE2, O/E-3) in Purkinje neuron migration and cerebellar cortical topography. *Development* 133, 2719–2729.

Dahmane, N., and Ruiz-i-Altaba, A. (1999). Sonic hedgehog regulates the growth and patterning of the cerebellum. *Development* 126, 3089–3100.

Dastjerdi, F. V., Consalez, G. G., and Hawkes, R. (2012). Pattern formation during development of the embryonic cerebellum. *Front. Neuroanat.* 6:10. doi: 10.3389/fnana.2012.00010

Dehnes, Y., Chaudry, F. A., Ullensvang, K., Lehre, K. P., Storm-Mathisen, J., and Danbolt, N. C. (1998). The glutamate transporter EAAT4 in rat cerebellar Purkinje cells: a glutamate-gated chloride concentrated near the synapse in parts of the dendritic membrane facing astroglia. *J. Neurosci.* 18, 3606–3619.

D'Ercole, A. J., Ye, P., Calikoglu, A. S., and Gutierrez-Ospina, G. (1996). The role of the insulin-like growth factors in the central nervous system. *Mol. Neurobiol.* 13, 227–255.

Diño, M. R., Nunzi, M. G., Anelli, R., and Mugnaini, E. (2000). Unipolar brush cells of the vestibulocerebellum: afferents and targets. *Prog. Brain Res.* 124, 123–137.

Diño, M. R., Perachio, A. A., and Mugnaini, E. (2001). Cerebellar unipolar brush cells are targets of primary vestibular afferents: an experimental study in the gerbil. *Exp. Brain Res.* 140, 162–170.

Diño, M. R., Willard, F. H., and Mugnaini, E. (1999). Distribution of unipolar brush cells and other calretinin immunoreactive components in the mammalian cerebellar cortex. *J. Neurocytol.* 28, 99–123.

Dizon, M. J., and Khodakhah, K. (2011). The role of interneurons in shaping Purkinje cell responses in the cerebellar cortex. *J. Neurosci.* 31, 10463–10473.

Ebner, T. J., Wang, X., Gao, W., Cramer, S. W., and Chen, G. (2012). Parasagittal zones in the cerebellar cortex differ in excitability, information processing, and synaptic plasticity. *Cerebellum* 11, 418–419.

Eccles, J. C., Ito, M., and Szentágothai, J. (1967). *The Cerebellum as a Neuronal Machine*. Berlin: Springer-Verlag.

Edmondson, J. C., Liem, R. K. H., Kuster, J. C., and Hatten, M. E. (1988). Astrotactin: a novel neuronal cell surface antigen that mediates neuronal-astroglial interactions in cerebellar microcultures. *J. Cell Biol.* 106, 505–517.

Eisenman, L. M. (2000). Anteroposterior boundaries and compartments in the cerebellum: evidence from selected neurological mutants. *Prog. Brain Res.* 124, 23–30.

Eisenman, L. M., and Brothers, R. (1998). Rostral cerebellar malformation (*rcm/rcm*): a murine mutant to study regionalization of the cerebellum. *J. Comp. Neurol.* 394, 106–117.

Eisenman, L. M., and Hawkes, R. (1993). Antigenic compartmentation in the mouse cerebellar cortex: zebrin and HNK-1 reveal a complex, overlapping molecular topography. *J. Comp. Neurol.* 335, 586–605.

Ekerot, C. F., and Jörntell, H. (2001). Parallel fibre receptive fields of Purkinje cells and interneurons are climbing fibre-specific. *Eur. J. Neurosci.* 13, 1303–1310.

Ekerot, C. F., and Jörntell, H. (2003). Parallel fiber receptive fields: a key to understanding cerebellar operation and learning. *Cerebellum* 2, 101–109.

Englund, C., Kowalczyk, T., Daza, R. A., Dagan, A., Lau, C., Rose, M. F., et al. (2006). Unipolar brush cells of the cerebellum are produced in the rhombic lip and migrate through developing white matter. *J. Neurosci.* 26, 9184–9195.

Faissner, A., and Steindler, D. (1995). Boundaries and inhibitory molecules in developing neural tissues. *Glia* 13, 233–254.

Fernandez, A. M., and Torres-Alemàn, I. (2012). The many faces of insulin-like peptide signalling in the brain. *Nat. Rev. Neurosci.* 13, 225–239.

Florio, M., Leto, K., Muzio, L., Tinterri, A., Badaloni, A., Croci, L., et al. (2012). Neurogenin 2 regulates progenitor cell-cycle progression and Purkinje cell dendritogenesis in cerebellar development. *Development* 139, 2308–2320.

Floris, A., Diño, M., Jacobowitz, D. M., and Mugnaini, E. (1994). The unipolar brush cells of the rat cerebellar cortex and cochlear nucleus are calretinin-positive: a study by light and electron microscopic immunocytochemistry. *Anat. Embryol.(Berl.)* 189, 495–520.

Frantz, G. D., Weimann, J. M., Levin, M. E., and McConnell, S. K. (1994). *Otx1* and *Otx2* define layers and regions in developing cerebral cortex and cerebellum. *J. Neurosci.* 14, 5725–5740.

Gallagher, E., Howell, B. W., Soriano, P., Cooper, J. A., and Hawkes, R. (1998). Cerebellar abnormalities in the disabled (mdab1-1) mouse. *J. Comp. Neurol.* 402, 238–251.

Gao, W., Chen, G., Reinert, K. C., and Ebner, T. J. (2006). Cerebellar cortical molecular layer inhibition is organized in parasagittal zones. *J. Neurosci.* 26, 8377–8387.

Gebre, S. A., Reeber, S. L., and Sillitoe, R. V. (2012). Parasagittal compartmentation of cerebellar mossy fibers as revealed by the patterned expression of vesicular glutamate transporters VGLUT1 and VGLUT2. *Brain Struct. Funct.* 217, 165–180.

Geurts, F. J., De Schutter, E., and Dieudonne, S. (2003). Unraveling the cerebellar cortex: cytology and cellular physiology of large-sized interneurons in the granular layer. *Cerebellum* 2, 290–299.

Goldowitz, D. (1989). The *weaver* granuloprival phenotype is due to intrinsic action of the mutant locus in granule cells: evidence from homozygous *weaver* chimeras. *Neuron* 2, 1565–1575.

Goldowitz, D., Cushing, R. C., Laywell, E., D'Archangelo, G., Sheldon, M., Sweet, H. O., et al. (1997). Cerebellar disorganization characteristic of *reeler* in *scrambler* mutant mice despite presence of reelin. *J. Neurosci.* 17, 8767–8777.

Goldowitz, D., Hamre, K. M., Przyborski, S. A., and Ackerman, S. L. (2000). Granule cells and cerebellar boundaries: analysis of Unc5h3 mutant chimeras. *J. Neurosci.* 20, 4129–4137.

Graham, D. J., and Wylie, D. R. (2012). Zebrin-immunopositive and–immunonegative stripe pairs represent functional units in the pigeon vestibulocerebellum. *J. Neurosci.* 12, 12769–12779.

Gravel, C., Eisenman, L. E., Sasseville, R., and Hawkes, R. (1987). Parasagittal organization of the rat cerebellar cortex: a direct correlation between antigenic Purkinje cell bands revealed by mabQ113 and the organization of the olivocerebellar projection. *J. Comp. Neurol.* 263, 294–310.

Gravel, C., and Hawkes, R. (1990). Parasagittal organization of the rat cerebellar cortex: direct comparison of Purkinje cell compartments and the organization of the spinocerebellar projection. *J. Comp. Neurol.* 291, 79–102.

Grimaldi, P., Parras, C., Guillemot, F., Rossi, F., and Wassef, M. (2009). Origins and control of the differentiation of inhibitory interneurons and glia in the cerebellum. *Dev. Biol.* 328, 422–433.

Grishkat, H. L., and Eisenman, L. M. (1995). Development of the spinocerebellar projection in the prenatal mouse. *J. Comp. Neurol.* 363, 93–108.

Hall, A. C., Lucas, F. R., and Salinas, P. C. (2000). Axonal remodeling and synaptic differentiation in the cerebellum is regulated by WNT-7a signaling. *Cell* 100, 525–535.

Hallem, J. S., Thompson, J., Gundappa-Sulur, S., Hawkes, R., Bjallie, J. G., and Bower, J. M. (1999). Spatial correspondence between tactile projection patterns and the distribution of the antigenic Purkinje cell markers anti-zebrin I and anti-zebrin II in the cerebellar folium crus IIa of the rat. *Neuroscience* 93, 1083–1094.

Hallonet, M. E., Teillet, M. A., and Le Douarin, N. M. (1990). A new approach to the development of the cerebellum provided by the quail-chick marker system. *Development* 108, 19–31.

Hashimoto, M., and Hibi, M. (2012). Development and evolution of cerebellar neural circuits. *Dev. Growth Differ.* 54, 373–389.

Hashimoto, M., and Mikoshiba, K. (2003). Mediolateral compartmentalization of the cerebellum is determined on the "birth date" of Purkinje cells. *J. Neurosci.* 23, 11342–11351.

Hausmann, B., Mangold, U., Sievers, J., and Berry, M. (1985). Derivation of cerebellar Golgi neurons from the external granular layer: evidence from explantation of external granule cells *in vivo*. *J. Comp. Neurol.* 22, 511–522.

Hawkes, R. (1997). An anatomical model of cerebellar modules. *Prog. Brain Res.* 114, 39–52.

Hawkes, R., Beierbach, E., and Tan, S.-S. (1999). Granule cell dispersion is restricted across transverse boundaries in mouse chimeras. *Eur. J. Neurosci.* 11, 3800–3808.

Hawkes, R., and Eisenman, L. M. (1997). Stripes and zones: the origins of regionalization of the adult cerebellum. *Perspect. Dev. Neurobiol.* 5, 95–105.

Hawkes, R., Gallagher, E., and Ozol, K. (1997). Blebs in the cerebellar granular layer as a sign of structural inhomogeneity. I. Anterior lobe vermis. *Acta Anat. (Basel)* 158, 205–214.

Hawkes, R., Gallagher, E., and Ozol, K. (1998). Blebs in the cerebellar granular layer as a sign of structural inhomogeneity. II. Posterior lobe vermis. *Acta Anat. (Basel)* 163, 47–55.

Hawkes, R., and Herrup, K. (1996). Aldolase C/zebrin II and the regionalization of the cerebellum. *J. Mol. Neurobiol.* 6, 147–158.

Hawkes, R., and Turner, R. W. (1994). Compartmentation of NADPH-diaphorase activity in the mouse cerebellar cortex. *J. Comp. Neurol.* 346, 499–516.

Hekmat, A., Kunemund, V., Fischer, G., and Schachner, M. (1989). Small inhibitory cerebellar interneurons grow in a perpendicular orientation to granule cell neurites in culture. *Neuron* 2, 1113–1122.

Herrup, K., and Kuemerle, B. (1997). The compartmentalization of the cerebellum. *Annu. Rev. Neurosci.* 20, 61–90.

Herrup, K., and Wilczynsk, S. L. (1982). Cerebellar cell degeneration in the *leaner* mutant mouse. *Neuroscience* 7, 2185–2196.

Hess, D. T., and Voogd, J. (1986). Chemoarchitectonic zonation of the monkey cerebellum. *Brain Res.* 369, 383–387.

Hess, E. J., and Wilson, M. C. (1991). *Tottering* and *leaner* mutations perturb transient developmental expression of tyrosine hydrozylase in embryologically distinct Purkinje cells. *Neuron* 6, 123–132.

Hoshino, M. (2006). Molecular machinery governing GABAergic neuron specification in the cerebellum. *Cerebellum* 5, 193–198.

Hoshino, M., Nakamura, S., Mori, K., Kawauchi, T., Terao, M., Nishimura, Y. V., et al. (2005). Ptf1a, a bHLH transcriptional gene, defines GABAergic neuronal fates in cerebellum. *Neuron* 47, 201–213.

Huang, X., Liu, J., Ketova, T., Fleming, J. T., Grover, V. K., Cooper, M. K., et al. (2010). Transventricular delivery of Sonic hedgehog is essential to cerebellar ventricular zone development. *Proc. Natl. Acad. Sci. U.S.A.* 107, 8422–8427.

Huard, J. M. T., Forster, C. C., Carter, M. L., Sicinski, P., and Ross, M.

E. (1999). Cerebellar histogenesis is disturbed in mice lacking cyclin D2. *Development* 126, 1927–1935.

Ilijic, E., Guidotti, A., and Mugnaini, E. (2005). Moving up or moving down? Malpositioned cerebellar unipolar brush cells in *reeler* mouse. *Neuroscience* 136, 633–647.

Jensen, P., Smeyne, R., and Goldowitz, D. (2004). Analysis of cerebellar development in *math1* null embryos and chimeras. *J. Neurosci.* 24, 2202–2211.

Ji, Z., and Hawkes, R. (1994). Topography of Purkinje cell compartments and mossy fiber terminal fields in lobules II and III of the rat cerebellar cortex: spinocerebellar and cuneocerebellar projections. *Neuroscience* 61, 935–954.

Ji, Z., and Hawkes, R. (1995). Developing mossy fibers terminal fields in the rat cerebellar cortex may segregate because of Purkinje cell compartmentation and not competition. *J. Comp. Neurol.* 359, 197–212.

Jörntell, H., Bengtsson, F., Schonewille, M., and De Zeeuw, C. I. (2010). Cerebellar molecular layer interneurons – computational properties and roles in learning. *Trends Neurosci.* 33, 524–532.

Jörntell, H., and Ekerot, C. F. (2002). Reciprocal bidirectional plasticity of parallel fiber receptive fields in cerebellar Purkinje cells and their afferent interneurons. *Neuron* 34, 797–806.

Karam, S. D., Burrows, R. C., Logan, C., Koblar, S., Pasquale, E. B., and Bothwell, M. (2000). Eph receptors and ephrins in the developing chick cerebellum: relationship to sagittal patterning and granule cell migration. *J. Neurosci.* 20, 6488–6500.

Kim, E. J., Battiste, J., Nakagawa, Y., and Johnson, J. E. (2008). Ascl1 (Mash1) lineage cells contribute to discrete cell populations in CNS architecture. *Mol. Cell. Neurosci.* 38, 595–606.

Kim, E. J., Hori, K., Wyckoff, A., Dickel, L. K., Koundakjian, E. J., Goodrich, L. V., et al. (2011). Spatiotemporal fate map of neurogenin1 (Neurog1) lineages in the mouse central nervous system. *J. Comp. Neurol.* 519, 1355–1370.

King, J. S., Chen, Y. F., and Bishop, G. A. (1993). An analysis of HRP-filled basket cell axons in the cat's cerebellum. II. Axonal distribution. *Anat. Embryol. (Berl.)* 188, 299–305.

Larouche, M., and Hawkes, R. (2006). From clusters to stripes: the developmental origins of adult cerebellar compartmentation. *Cerebellum* 5, 77–88.

Leclerc, N., Doré, L., Parent, A., and Hawkes, R. (1990). The compartmentalization of the monkey and rat cerebellar cortex: zebrin I and cytochrome oxidase. *Brain Res.* 506, 70–78.

Leto, K., Bartolini, A., Yanagawa, Y., Obata, K., Magrassi, L., Schilling, K., et al. (2009). Laminar fate and phenotype specification of cerebellar GABAergic interneurons. *J. Neurosci.* 29, 7079–7091.

Leto, K., Carletti, B., Williams, I. M., Magrassi, L., and Rossi, F. (2006). Different types of cerebellar GABAergic interneurons originate from a common pool of multipotent progenitor cells. *J. Neurosci.* 26, 11682–11694.

Lewis, P. M., Gritli-Linde, A., Smeyne, R., Kottmann, A., and McMahon, A. P. (2004). Sonic hedgehog signaling is required for expansion of granule neuron precursors and patterning of the mouse cerebellum. *Dev. Biol.* 270, 393–410.

Li, Y., Komuro, Y., Fahrion, J. K., Hu, T., Ohno, N., Fenner, K. B., et al. (2012). Light stimuli control neuronal migration by altering of insulin-like growth factor 1 (IGF-1) signaling. *Proc. Natl. Acad. Sci. U.S.A.* 109, 2630–2635.

Logan, C., Millar, C., Bharadia, V., and Rouleau, K. (2002). Onset of Tlx-3 expression in the chick cerebellar cortex correlates with the morphological development of fissures and delineates a posterior transverse boundary. *J. Comp. Neurol.* 448, 138–149.

Luckner, R., Obst-Pernberg, K., Hirano, S., Suzuki, S. T., and Redies, C. (2001). Granule cell raphes in the developing mouse cerebellum. *Cell Tissue Res.* 303, 159–172.

Lundell, T. G., Zhou, Q., and Doughty, M. L. (2009). Neurogenin1 expression in cell lineages of the cerebellar cortex in embryonic and postnatal mice. *Dev. Dyn.* 238, 3310–3325.

Machold, R., and Fishell, G. (2005). Math1 is expressed in temporally discrete pools of cerebellar rhombic-lip neural progenitors. *Neuron* 48, 17–24.

Marani, J., and Voogd, J. (1977). An acetylcholinesterase band-pattern in the molecular layer of the cat cerebellum. *J. Anat.* 124, 335–345.

Marzban, H., Chung, S.-H., Watanabe, M., and Hawkes, R. (2007). Phospholipase Cβ4 expression reveals the continuity of cerebellar topography through development. *J. Comp. Neurol.* 502, 857–871.

Marzban, H., Khanzada, U., Shabir, S., Hawkes, R., Langnaese, K., Smalla, K.-H., et al. (2003). Expression of the immunoglobulin superfamily neuroplastin adhesion molecules in adult and developing mouse cerebellum and their localization to parasagittal stripes. *J. Comp. Neurol.* 462, 286–301.

Marzban, H., Kim, C. T., Doorn, D., Chung, S. H., and Hawkes, R. (2008). A novel transverse expression domain in the mouse cerebellum revealed by a neurofilament-associated antigen. *Neuroscience* 153, 1190–1201.

Marzban, H., Sillitoe, R. V., Hoy, M., Chung, S., Rafuse, V. F., and Hawkes, R. (2004). Abnormal HNK1 expression in the cerebellum of an N-CAM null mouse. *J. Neurocytol.* 33, 117–130.

Mason, C. A., Christakos, S., and Catalano, S. M. (1990). Early climbing fiber interactions with Purkinje cells in the postnatal mouse cerebellum. *J. Comp. Neurol.* 297, 77–90.

Mateos, J. M., Osorio, A., Azkue, J. J., Benítez, R., Elezgarai, I., Bilbao, A., et al. (2001). Parasagittal compartmentalization of the metabotropic glutamate receptor mGluR1b in the cerebellar cortex. *Eur. J. Anat.* 5, 15–21.

Matsushita, M., Ragnarson, B., and Grant, G. (1991). Topographic relationship between sagittal Purkinje cell bands revealed by monoclonal antibody to zebrin I and spinocerebellar projections arising from the central cervical nucleus in the rat. *Exp. Brain Res.* 84, 133–141.

McAndrew, P. E., Frostholm, A., Evans, J. E., Zdilar, D., Goldowitz, D., Chiu, I. M., et al. (1998). Novel receptor protein tyrosine phosphatase (RPTPrho) and acidic fibroblast growth factor (FGF-1) transcripts delineate a rostrocaudal boundary in the granular layer of the murine cerebellar cortex. *J. Comp. Neurol.* 391, 444–455.

Miale, I. L., and Sidman, R. L. (1961). An autoradiographic analysis of histogenesis in the mouse cerebellum. *Exp. Neurol.* 4, 277–296.

Millen, K. J., Hui, C. C., and Joyner, A. L. (1995). A role for *En-2* and other murine homologues of *Drosophila* segment polarity genes in regulating positional information in the developing cerebellum. *Development* 121, 3935–3945.

Millonig, J. H., Millen, K. J., and Hatten, M. E. (2000). The mouse *Dreher* gene Lmx1a controls formation of the roof plate in the vertebrate CNS. *Nature* 403, 764–769.

Miyata, T., Maeda, T., and Lee, J. E. (1999). NeuroD is required for differentiation of the granule cells in the cerebellum and hippocampus. *Genes Dev.* 13, 1647–1652.

Mizuhara, E., Minaki, Y., Nakatani, T., Kumai, M., Inoue, T., Muguruma, K., et al. (2009). Purkinje cells originate from cerebellar ventricular zone progenitors positive for Neph3 and E-cadherin. *Dev. Biol.* 338, 202–214.

Morales, D., and Hatten, M. E. (2006). Molecular markers of neuronal progenitors in the embryonic cerebellar anlage. *J. Neurosci.* 26, 12226–12236.

Morris, R. J., Beech, J. N., and Heizmann, C. W. (1988). Two distinct phases and mechanisms of axonal growth shown by primary vestibular fibres in the brain, demonstrated by parvalbumin immunohistochemistry. *Neuroscience* 27, 571–596.

Mugnaini, E., and Floris, A. (1994). The unipolar brush cell: a neglected neuron of the mammalian cerebellar cortex. *J. Comp. Neurol.* 339, 174–180.

Nagata, I., and Nakatsuji, N. (1991). Rodent CNS neuroblasts exhibit both perpendicular and parallel contact guidance on the aligned parallel neurite bundle. *Development* 112, 581–590.

Namba, K., Sugihara, I., and Hashimoto, M. (2011). Close correlation between the birth date of Purkinje cells and the longitudinal compartmentalization of the mouse adult cerebellum. *J. Comp. Neurol.* 519, 2594–2614.

Napieralski, J. A., and Eisenman, L. M. (1993). Developmental analysis of the external granular layer in the *meander tail* mutant mouse: do cerebellar microneurons have independent progenitors? *Dev. Dyn.* 197, 244–254.

Napieralski, J. A., and Eisenman, L. M. (1996). Further evidence for a unique developmental compartment in the cerebellum of the *meander tail* mouse as revealed by the quantitative analysis of Purkinje cells. *J. Comp. Neurol.* 364, 718–728.

Nunzi, M. G., Birnstiel, S., Bhattacharyya, B. J., Slater, N. T., and Mugnaini, E. (2001). Unipolar brush cells form a glutamatergic projection system within the mouse cerebellar cortex. *J. Comp. Neurol.* 434, 329–341.

Nunzi, M. G., and Mugnaini, E. (2000). Unipolar brush cell axons form

a large system of intrinsic mossy fibers in the postnatal vestibulocerebellum. *J. Comp. Neurol.* 422, 55–65.

Nunzi, M. G., Shigemoto, R., and Mugnaini, E. (2002). Differential expression of calretinin and metabotropic glutamate receptor mGluR1alpha defines subsets of unipolar brush cells in mouse cerebellum. *J. Comp. Neurol.* 451, 189–199.

Oberdick, J., Schilling, K., Smeyne, R. J., Corbin, J. G., Bocchiaro, C., and Morgan, J. I. (1993). Control of segment-like patterns of gene expression in the mouse cerebellum. *Neuron* 10, 1007–1018.

Odutola, A. B. (1970). The topographical localization of acetylcholinesterase in the adult rat cerebellum: a reappraisal. *Histochimie* 23, 98–106.

Ozdinler, P. H., and Macklis, J. D. (2006). IGF-I specifically enhances axon outgrowth of corticospinal motor neurons. *Nat. Neurosci.* 9, 1371–1381.

Ozol, K., Hayden, J. M., Oberdick, J., and Hawkes, R. (1999). Transverse zones in the vermis of the mouse cerebellum. *J. Comp. Neurol.* 412, 95–111.

Ozol, K. O., and Hawkes, R. (1997). The compartmentation of the granular layer of the cerebellum. *Histol. Histopathol.* 12, 171–184.

Palay, S. L., and Chan-Palay, V. (1974). *Cerebellar Cortex: Cytology and Organization*. Berlin, Heidelberg, New York: Springer-Verlag.

Pascual, M., Abasolo, I., Mingorance-Le Meur, A., Martinez, A., Del Rio, J. A., Wright, C. V., et al. (2007). Cerebellar GABAergic progenitors adopt an external granule cell-like phenotype in the absence of Ptf1a transcription factor expression. *Proc. Natl. Acad. Sci. U.S.A.* 104, 5193–5198.

Paukert, M., Huang, Y. H., Tanaka, K., Rothstein, J. D., and Bergles, D. E. (2010). Zones of enhanced glutamate release from climbing fibers in the mammalian cerebellum. *J. Neurosci.* 30, 7290–7299.

Pierce, E. T. (1975). Histogenesis of the deep cerebellar nuclei in the mouse: an autoradiographic study. *Brain Res.* 95, 503–518.

Popoff, S. (1896). Weiterer Beitrag zur Frage über die Histogenese der Kleinhirnrinde. *Biologischer Centralblatt* 16, 462–466.

Prasadarao, N., Tobet, S. A., and Jungalwala, F. B. (1990). Effect of different fixatives on immunocytochemical localization of HNK-12-reactive antigens in cerebellum: a method for differentiating the localization of the same carbohydrate epitope on proteins vs. lipids. *J. Histochem. Cytochem.* 38, 1193–1200.

Rakic, P. (1972). Extrinsic cytological determinants of basket and stellate cell dendritic pattern in the cerebellar molecular layer. *J. Comp. Neurol.* 146, 335–354.

Ramon y Cajal, S. (1911). *Histologie du Système Nerveux de l'Homme et des Vertébrés*. Madrid: Instituto Ramon y Cajal.

Rogers, J. H., Ciossek, T., Menzel, P., and Pasquale, E. B. (1999). Eph receptors and ephrins demarcate cerebellar lobules before and during their formation. *Mech. Dev.* 87, 119–128.

Ruigrok, T. J. (2011). Ins and outs of cerebellar modules. *Cerebellum* 10, 464–474.

Salsano, E., Croci, L., Maderna, E., Lupo, L., Pollo, B., Giordana, M. T., et al. (2007). Expression of the neurogenic basic helix-loop-helix transcription factor NEUROG1 identifies a subgroup of medulloblastomas not expressing ATOH1. *Neuro Oncol.* 9, 298–307.

Sarna, J., and Hawkes, R. (2003). Patterned Purkinje cell death in the cerebellum. *Prog. Neurobiol.* 70, 473–507.

Sarna, J. R., Marzban, H., Watanabe, M., and Hawkes, R. (2006). Complementary stripes of phospholipase Cβ3 and Cβ4 expression by Purkinje cell subsets in the mouse cerebellum. *J. Comp. Neurol.* 496, 303–313.

Schilling, K., Oberdick, J., Rossi, F., and Baader, S. L. (2008). Besides Purkinje cells and granule neurons: an appraisal of the cell biology of the interneurons of the cerebellar cortex. *Histochem. Cell Biol.* 130, 601–615.

Schilling, K., Schmidt, H. H., and Baader, S. L. (1994). Nitric oxide synthase expression reveals compartments of cerebellar granule cells and suggests a role for mossy fibers in their development. *Neuroscience* 59, 893–903.

Sekerková, G., Ilijic, E., and Mugnaini, E. (2004). Time of origin of unipolar brush cells in the rat cerebellum as observed by prenatal bromodeoxyuridine labeling. *Neuroscience* 127, 845–858.

Sheldon, M., Rice, D. S., D'Arcangelo, G., Yoneshima, H., Nakajima, K., Mikoshiba, K., et al. (1997). *Scrambler* and *yotari* disrupt the *disabled* gene and produce a *reeler*-like phenotype in mice. *Nature* 389, 730–733.

Sillitoe, R. V., Benson, M. A., Blake, D. J., and Hawkes, R. (2003). Abnormal dysbindin expression in cerebellar mossy fiber synapses in the mdx mouse model of Duchenne muscular dystrophy. *J. Neurosci.* 23, 6576–6585.

Sillitoe, R. V., Chung, S.-H., Fritschy, J. M., Hoy, M., and Hawkes, R. (2008). Golgi cell dendrites are restricted by Purkinje cell stripe boundaries in the adult mouse cerebellar cortex. *J. Neurosci.* 28, 2820–2826.

Sillitoe, R. V., Fu, Y., and Watson, C. (2011). "The cerebellum," in *The Mouse Nervous System*, eds C. Watson, G. Paxinos, and L. Puelles (Amsterdam: Elsevier), 360–397.

Sillitoe, R. V., and Hawkes, R. (2002). Whole mount immunohistochemistry: a high throughput screen for patterning defects in the mouse cerebellum. *J. Histochem. Cytochem.* 50, 235–244.

Sillitoe, R. V., and Hawkes, R. (2013). "Zones and stripes: development of cerebellar topography," in *Handbook of Cerebellum and Cerebellar Disorders*, eds M. Manto, D. Gruol, J. Schmahmann, N. Koibuchi, and F. Rossi (New York, NY: Springer), 43–59.

Sillitoe, R. V., and Joyner, A. L. (2007). Morphology, molecular codes, and circuitry produce the three-dimensional complexity of the cerebellum. *Annu. Rev. Cell Dev. Biol.* 23, 549–577.

Simat, M., Parpan, F., and Fritschy, J. M. (2007). Heterogeneity of glycinergic and gabaergic interneurons in the granule cell layer of mouse cerebellum. *J. Comp. Neurol.* 500, 71–83.

Smeyne, R. J., Chu, T., Lewin, A., Bian, F., Sanlioglu, S., Kunsch, C., et al. (1995). Local control of granule cell generation by cerebellar Purkinje cells. *Mol. Cell. Neurosci.* 6, 230–251.

Sotelo, C. (2004). Cellular and genetic regulation of the development of the cerebellar system. *Prog. Neurobiol.* 72, 295–339.

Sotelo, C., and Chédotal, A. (2005). Development of the olivocerebellar system: migration and formation of cerebellar maps. *Prog. Brain Res.* 148, 1–20.

Sotelo, C., and Wassef, M. (1991). Cerebellar development: afferent organization and Purkinje cell heterogeneity. *Philos. Trans. R. Soc. Lond. B Biol. Sci.* 331, 307–313.

Sudarov, A., Turnbull, R. K., Kim, E. J., Lebel-Potter, M., Guillemot, F., and Joyner, A. L. (2011). Ascl1 genetics reveals insights into cerebellum local circuit assembly. *J. Neurosci.* 31, 11055–11069.

Sugihara, I., and Quy, P. N. (2007). Identification of aldolase C compartments in the mouse cerebellar cortex by olivocerebellar labeling. *J. Comp. Neurol.* 500, 1076–1092.

Sultan, F., and Bower, J. M. (1998). Quantitative Golgi study of the rat cerebellar molecular layer interneurons using principal component analysis. *J. Comp. Neurol.* 393, 353–373.

Swanson, D. J., and Goldowitz, D. (2011). Experimental Sey mouse chimeras reveal the developmental deficiencies of Pax6-null granule cells in the postnatal cerebellum. *Dev. Biol.* 351, 1–12.

Szentagothai, J. (1965). The use of degeneration methods in the investigation of short neuronal connexions. *Prog. Brain Res.* 14, 1–32.

Tanaka, O., and Kondo, H. (1994). Localization of mRNAs for three novel members (β 3, β 4 and gamma 2) of phospholipase C family in mature brain. *Neurosci. Lett.* 182, 17–20.

Voogd, J., and Ruigrok, T. J. (2004). The organization of the corticonuclear and olivocerebellar climbing fiber projections to the rat cerebellar vermis: the congruence of projection zones and the zebrin pattern. *J. Neurocytol.* 33, 5–21.

Wadiche, J. I., and Jahr, C. E. (2005). Patterned expression of Purkinje cell glutamate transporters controls synaptic plasticity. *Nat. Neurosci.* 8, 1329–1334.

Wallace, V. A. (1999). Purkinje-cell-derived Sonic hedgehog regulates granule neuron precursor cell proliferation in the developing mouse cerebellum. *Curr. Biol.* 9, 445–448.

Wang, V. Y., Rose, M. F., and Zoghbi, H. Y. (2005). Math1 expression redefines the rhombic lip derivatives and reveals novel lineages within the brainstem and cerebellum. *Neuron* 48, 31–43.

Wechsler-Reya, R. J., and Scott, M. P. (1999). Control of neuronal precursor proliferation in the cerebellum by Sonic Hedgehog. *Neuron* 22, 103–114.

Welker, W. (1987). "Spatial organization of somatosensory projections to granule cell cerebellar cortex: functional and connectional implications of fractured somatotopy (summary of Wisconsin studies)," in *New Concepts in Cerebellar Neurobiology*, ed J. S. King (New York, NY: Alan R. Liss Inc.), 239–280.

Xenaki, D., Martin, I. B., Yoshida, L., Ohyama, K., Gennarini,

G., Grumet, M., et al. (2011). F3/contactin and TAG1 play antagonistic roles in the regulation of sonic hedgehog-induced cerebellar granule neuron progenitor proliferation. *Development* 138, 519–529.

Yan, X. X., Yen, L. S., and Garey, L. J. (1993). Parasagittal patches in the granular layer of the developing and adult rat cerebellum as demonstrated by NADPH-diaphorase histochemistry. *Neuroreport* 4, 1227–1230.

Zeilhofer, H. U., Studler, B., Arabadzisz, D., Schweizer, C., Ahmadi, S., Layh, B., et al. (2005). Glycinergic neurons expressing enhanced green fluorescent protein in bacterial artificial chromosome transgenic mice. *J. Comp. Neurol.* 482, 123–141.

Zhang, L., and Goldman, J. E. (1996). Generation of cerebellar interneurons from dividing progenitors in white matter. *Neuron* 16, 47–54.

Zordan, P., Croci, L., Hawkes, R., and Consalez, G. G. (2008). Comparative analysis of proneural gene expression in the embryonic cerebellum. *Dev. Dyn.* 237, 1726–1735.

Conflict of Interest Statement: The authors declare that the research was conducted in the absence of any commercial or financial relationships that could be construed as a potential conflict of interest.

Received: 21 September 2012; accepted: 26 December 2012; published online: 22 January 2013.

Citation: Consalez GG and Hawkes R (2013) The compartmental restriction of cerebellar interneurons. Front. Neural Circuits ***6****:123. doi: 10.3389/fncir.2012.00123*

frontiers in
NEURAL CIRCUITS

ORIGINAL RESEARCH ARTICLE
published: 08 April 2013
doi: 10.3389/fncir.2013.00059

Anatomical investigation of potential contacts between climbing fibers and cerebellar Golgi cells in the mouse

Elisa Galliano[1], Marco Baratella[1], Martina Sgritta[1,2], Tom J. H. Ruigrok[1], Elize D. Haasdijk[1], Freek E. Hoebeek[1], Egidio D'Angelo[2], Dick Jaarsma[1] and Chris I. De Zeeuw[1,3]*

[1] Department of Neuroscience, Erasmus Medical Centre Rotterdam, Rotterdam, Netherlands
[2] Department of Neuroscience and Brain Connectivity Center, University of Pavia and IRCCS C. Mondino, Pavia, Italy
[3] Netherlands Institute for Neuroscience, Royal Netherlands Academy of Arts and Sciences, Amsterdam, Netherlands

Edited by:
Michael Brecht, Humboldt University Berlin, Germany

Reviewed by:
Deborah Baro, Georgia State University, USA
Jens Eilers, University Leipzig, Germany

***Correspondence:**
Chris I. De Zeeuw, Department of Neuroscience, Erasmus Medical Centre, Dr. Molewaterplein 50, NL-3015 GE Rotterdam, Netherlands.
e-mail: c.dezeeuw@erasmusmc.nl

Climbing fibers (CFs) originating in the inferior olive (IO) constitute one of the main inputs to the cerebellum. In the mammalian cerebellar cortex each of them climbs into the dendritic tree of up to 10 Purkinje cells (PCs) where they make hundreds of synaptic contacts and elicit the so-called all-or-none complex spikes controlling the output. While it has been proven that CFs contact molecular layer interneurons (MLIs) via spillover mechanisms, it remains to be elucidated to what extent CFs contact the main type of interneuron in the granular layer, i.e., the Golgi cells (GoCs). This issue is particularly relevant, because direct contacts would imply that CFs can also control computations at the input stage of the cerebellar cortical network. Here, we performed a systematic morphological investigation of labeled CFs and GoCs at the light microscopic level following their path and localization through the neuropil in both the granular and molecular layer. Whereas in the molecular layer the appositions of CFs to PCs and MLIs were prominent and numerous, those to cell-bodies and dendrites of GoCs in both the granular layer and molecular layer were virtually absent. Our results argue against the functional significance of direct synaptic contacts between CFs and interneurons at the input stage, but support those at the output stage.

Keywords: cerebellum, climbing fiber, Golgi cells, synapse, confocal microscopy

INTRODUCTION

Classically, the olivo-cerebellar system is believed to be an online comparator that calculates the difference between a desired and an executed movement via its highly organized and preserved cellular network and forwards the appropriate modification through its projections to the brainstem (Marr, 1969; Albus, 1971). Among the numerous cell types in the cerebellar cortical network, the Purkinje cell (PC) is traditionally thought to be the most important, because it is the only one to directly receive both signals on movement context and signals on sensory feedback (Bloedel and Bracha, 1998; Schmolesky et al., 2002), and because it constitutes the sole output of the cerebellar cortex so as to adjust movements.

Information about the desired and executed behavior reaches the cerebellar cortex via two main types of fibers. These are the so-called climbing fibers (CFs), which all originate from the inferior olivary nucleus (IO), and the mossy fibers (MFs), which can be derived from many other sources in the brainstem (Ramon y Cajal, 1995). The MFs provide inputs on the context of planned and ongoing movements and are connected to the PCs through a di-synaptic pathway via cerebellar granule cells (GCs), which in turn innervate the PCs by their parallel fibers. The CFs on the other hand probably provide the relevant feedback signals for adjusting the amplitude and timing of movements (De Zeeuw et al., 2011; Gao et al., 2012). Single CFs make direct and numerous synaptic contacts with PCs. A classical model of cerebellar functioning postulates that the CFs provide the required error signals encoding the difference between the executed and desired movement and thereby guide motor learning (Marr, 1969; Albus, 1971). More recently, it has been proposed that the CFs do not only evoke their feedback via their direct contacts on the PC dendritic tree, but also through extrasynaptic effects via the molecular layer interneurons (MLIs) (Szapiro and Barbour, 2007; Gao et al., 2012; Mathews et al., 2012). Moreover, in principle it is possible that collaterals of the olivary axons also contact Golgi cells (GoCs), which provide direct inhibition onto the GCs (Galliano et al., 2010). Branches of olivary axons, named Scheibel collaterals (Scheibel and Scheibel, 1954), are known to travel through the densely populated granule cell layer (GL) and thus can approach cell-bodies and/or dendrites of GoCs (Hamori and Szentagothai, 1966a; Palay and Chan-Palay, 1974; Shinoda et al., 2000). Indeed, two electrophysiological studies confirmed an effect of olivary activation on GoC firing, but they were unable to elucidate whether these effects were mono-synaptic or multi-synaptic (Schulman and Bloom, 1981; Xu and Edgley, 2008). Here, we took various morphological approaches to shed light on the question as to what extent CFs may also directly contact GoCs. We injected a fluorescent anterograde tracer in the IO in mutant mice that express eGFP in their glycinergic neurons (GlyT2-eGFP) so as to enable immunofluorescent identification of both

CF terminals and GoCs in the same material and subsequently quantify their appositions. For comparison we also labeled the PCs with Calbindin and the MLIs'cell-bodies with DAPI in combination with VGlut2 staining of CFs terminals, allowing us to compare the density of appositions of CFs onto GoCs with those onto PCs and MLIs.

METHODS

ANIMALS

We used mice of both genders older than 20 days, either inbred C57BL/6 mice provided by Harlan Laboratories (The Netherlands) or transgenic mice that specifically express enhanced green fluorescent protein under the control of the glycine transporter type 2 promoter (GlyT2-EGFP). The GlyT2-EGFP were generated and kindly provided by Dr. Fritschy (Zeilhofer et al., 2005), and all experimental animals were bred at the Erasmus MC breeding facility by backcrossing with C57BL/6. All experiments were performed in accordance with the guidelines for animal experiments of the respective universities and the Dutch national legislation.

OLIVARY INJECTIONS

Injections of the neuro-anatomical tracer biotin dextran amine (BDA) in the IO were performed as previously described in rats (Pijpers et al., 2005). Briefly, mice were anaesthetized (∼1.5% isofluorane in O_2, buprenorphine 0.05 mg/kg subcutaneous, and rymadyl 5 mg/kg, subcutaneous) and placed in a stereotactic head holder. The dorsal side of the head and neck was exposed using a midline incision of the skin (running from lambda to processus spinosus of C2). Neck muscles were split longitudinally and laterally with a spreader. The atlanto-occipital membrane and dura mater were opened to gain a direct view of the caudal part of the medulla oblongata and caudal part of lobule IX of the cerebellum. From this position the IO could be well approached by a micromanipulator driven glass micropipette (tip diameter: 5–10 μm) filled with the neuro-anatomical tracer BDA (10,000 mW) dissolved in 0.5 μl 2% NaCl using stereotactic coordinates. Location of injection was determined by use of a stereotactic mouse atlas (Paxinos and Franklin, 2004) and typical electrophysiological characteristics of the IO neurons (i.e., extracellular action potential consisting of a usually negative-positive going spike that is followed by a negative wave lasting about 5 msec or by several small spikelets and an overall spike frequency of ∼1 Hz; see example trace in **Figure 2A** and Ruigrok et al., 1995). Afterwards, the dura was placed back, the left, and right muscles were attached to each other in layers and the skin was sutured. After 5 days of recovery in their home cage mice were perfused and processed for immunohistochemistry.

IMMUNOFLUORESCENCE

The animals were deeply anesthetized by intraperitoneal administration sodium pentobarbital (Nembutal) and perfused through the ascending aorta with saline followed by 4% paraformaldehyde in 0.12 M phosphate buffer (PB). Brains were removed, immersed in the same fixative for 1.5 h at room temperature, and subsequently cryoprotected in 10% sucrose in PB solution and embedded in a gelatin block (12% in PB). Blocks were post-fixed in 10% paraformaldehyde and 30% sucrose solution for 1.5 h at room temperature; subsequently they were immersed in 30% sucrose overnight at 4°C. Coronal or sagittal sections were cut at 40 μm with a freezing microtome (Leica SM 2000 R), and then collected in PBS. Sections were rinsed in 0.1 M PB and incubated for 2 h in 10 mM Na-citrate at 80°C. After the antigen retrieval the sections were washed with TBS. Free-floating sections were blocked against non-specific antibody binding with a pre-incubation step of 1 h at room temperature, in a TBS buffer containing 10% normal horse serum and 0.5% Triton X-100. Free-floating section were then incubated for 48–72 h at 4°C in a mixture of primary antibodies diluted in TBS buffer containing 2% normal horse serum and 0.4% Triton. Sections were washed and incubated for 1.5–2 h at room temperature in a mixture of secondary antibodies (10 ml buffer: 200 μl AB) coupled to a fluorochrome. Sections were washed again, mounted onto gelatin-coated slides, air-dried, and cover-slipped with a mounting medium for Fluorescence (Vectrashield H-1000). Primary antibodies used were mouse anti-mGluR2 (1:1000, AbCam), Guinea pig anti-VGlut2 (1:1000, Millipore), mouse anti-Calbindin (1:7000, Sigma). We used FITC, Alexa Fluor488, Cy3, and Cy5 conjugated anti-mouse IgG as secondary antibodies (Jackson ImmunoResearch) (Hossaini et al., 2011). To label BDA we used alexa Fluor568 Streptavidin. In case of section from GFP mouse and tracing VGLUT was labeled with Cy5. Generally sections were counterstained with DAPI (1:100,000, Invitrogen).

SELECTION OF APPROPRIATE MARKERS FOR GoCs AND CFs

To study the connectivity between GoCs and CFs we selected two reliable GoC markers: the metabotropic glutamate receptor type 2 (mGluR2), which stains 83.5% of the entire GoC population (Neki et al., 1996; Simat et al., 2007); and the glycine transporter type 2 (GlyT2), which is expressed by 94.5% of GoCs (Simat et al., 2007) and has been coupled with EGFP in a transgenic animal [GlyT2-EGFP animals, (Zeilhofer et al., 2005)]. Together these markers encompass the complete population of GoCs (Simat et al., 2007). CF synaptic terminals in the molecular layer were identified using vesicular glutamate transporter type 2 (VGluT2) immunohistochemistry (Kaneko et al., 2002). In the granular layer, however, VGluT2 immunostaining is not exclusive for CFs, since a subset of MFs also colocalize with VGluT2 staining (Kaneko et al., 2002). To unequivocally identify CFs in the granular layer we injected the IO with the anterograde tracer BDA and, in order to unequivocally prove the presence of a synapse, also stained this tissue for VGluT2. Finally, we used Calbindin staining to identify PCs and DAPI staining to identify cell-bodies of MLIs in the molecular layer.

DATA ANALYSIS

Images (512 × 512 or 1024 × 1024 pixels) were obtained using the confocal laser scanning microscope Zeiss LSM 700 (Zeiss, Jena, Germany) equipped with 10×, 20×, 40×, 63× lenses. All the samples were analyzed making z-stacks with an interval of 0.3–0.45 μm and the presence of CF-GO contact was investigated analyzing each z-plane.

The quantification in 10 μm thick sections was performed in 50 × 50 × 10 mm portions of ML and GL ($n = 30$, $N = 3$ for both layers). Each maximum intensity projection image (aligned configuration) was then processed by rotating 90° clockwise (rotated configuration) or translating 25 pixels to the right (translated configuration) either the VgluT2 channel (ML) or the GlyT2 channel (GL). The resulting 180 images (90 ML and 90 GL) were shuffled, renamed and blindly analyzed in order to quantify the number of colocalizations (i.e., spatial overlap of two or three colors) between VGluT2 + GlyT2/mGluR2 (ML), VGlut2 + BDA + GlyT2, and BDA + GlyT2 (GL). Differences between the three configurations (aligned, rotated, and translated; see scheme in **Figure 4**) were statistically analyzed with a One-Way ANOVA with Tukey *post-hoc* corrections.

Antibody dilutions and settings of the confocal microscopy (CM) were optimized to avoid bleed-through of one fluorophore into the other. Fluorophores with overlapping excitation/emission spectra (e.g., Alexa488 and Cy3) were collected in different tracks. Routinely, confocal stacks were collected in dual tract mode with DAPI and orange/red fluorophore (Cy3, Alexa555, Alexa 568) in one tract (wave lengths 405 and 555, filter settings: $LP = 560$, $SP = 490$) and green (FITC, Alexa) and infra red in the other tract (wave lengths 488 and 639, filter settings: $LP = 640$, $SP = 555$). To avoid false negatives only established markers that produce strong signal were selected. To avoid chromatic aberration the confocal microscope was routinely calibrated for differences in focal lengths.

Offline analysis of both thin and thick sections was performed with LSM Image browser and Image J software packages.

RESULTS

ABSENCE OF CO-LOCALIZATION OF mGluR2 AND VGluT2 IN THE ML

We performed mGluR2 and VGluT2 immunohistochemistry in 3 C57BL/6 adult animals and we analyzed both sagittal and coronal sections. As shown in **Figure 1A**, the mGluR2 antibody reliably stained GoCs (in red, see also **Figure 1A′**) allowing the visualization of the entire dendritic tree. Similarly, VGlut2 staining (in green, see also **Figure 1A″**) revealed a typical CF pattern in the ML and MF rosettes in the GL. High-magnification images of the ML showed a clear mis-match between GoCs dendrites and VGluT2 expression (**Figures 1B–B″**). Occasionally, maximum intensity projections of three-dimensional areas hinted toward a possible co-localization (see inset in **Figure 1B**), but a careful analysis in the z-plane consistently confirmed the supposed co-localization to be a bi-dimensional artifact, because the two colors were never present at the same depth (see montage in **Figure 1C**). In contrast, when we analyzed the number of VGluT2 stained terminals on top of Calbindin stained PCs' dendrites we found consistent and abundant co-localization (**Figures 1D–D″**). Moreover, when we quantified the number of VGluT2 stained terminals on top of DAPI stained cell-bodies of MLI's ($n = 550$) (for examples, see e.g., **Figure 1A**), we found that 61.3% showed a co-localization using the same criteria. In summary, these data did not provide any evidence of synaptic contacts in the ML layer between mGluR2-positive GoCs and VGlut2-containing CFs, whereas they provided robust evidence for appositions of CFs onto PCs and MLIs.

ANTEROGRADE TRACING OF CFs ALSO FAILED TO SHOW CONTACTS ONTO GLYCINERGIC GoCs

Five GlyT2-EGFP adult mice received a BDA injection into their IO (**Figure 2A**, BDA in red), which diffused in the olivary axons all the way up to the cerebellar cortex (**Figure 2B**) where the typical "climbing" character of CFs was clearly identifiable against the "virtual" dendritic trees of PCs (**Figure 2C**). Whereas CFs were stained violet in the ML, which is due to the co-localization of BDA (red) with VGluT2 (blue), in the GL CFs remained bright red (**Figure 2C**). A systematic analysis of such material revealed that any potential triple-localization of the CF (BDA, red), VGluT2 (blue), and GoC dendrites (green) seen in maximum projections (inset in **Figure 2D**) disappeared when the individual images at various depths were studied (**Figure 2E**). In total we traced over 200 CFs and analyzed 800 potential BDA and VGluT2 colocalizations with GlyT2. However, a careful analysis in the z-plane revealed that no BDA-VGluT2 staining occurred at the level of a glycinergic GoC dendrite. Taken together with the results described above, our data argue against a CF-GoC connection in the ML.

CF-GoC SYNAPSES ALSO APPEAR ABSENT IN THE GL

Having found no evidence for a connection in the ML, we proceeded to analyze the GL. We divided it in three subzones (upper third, just below the PCs layer, middle third and lower third). We began focusing on what we believed being the hot-spot for possible CF-GoC contacts due to the presence of the CF "Scheibel" collaterals, i.e., the upper third of the GL (**Figure 3**). As previously reported for the ML, in the tissue collected from the BDA-injected GlyT2-EGFP mice stained for VGlut2 the potential colocalization of the BDA-marked CFs with VgluT2 and GlyT2 were extremely scarce. Twenty-eight locations appeared promising, but again a thin-section analysis showed that none of these locations had triple labeling with GlyT2, excluding synaptic contacts between CFs and GoCs in this upper GL.

Proceeding deeper toward the white matter, we found 7 combined BDA-VGlut2 positive spots in the middle third of the GL and only 1 in the lower third of the GL, but again none co-stained with GlyT2. In addition, we studied 23 GoC somata and their potential co-localization with BDA-stained CFs, but unlike what we observed in the combined CF-PC and CF-MLI stainings described above, we never found VGluT2-expression in these labeled fibers apposed to GoCs. **Figure 3** shows a 3D-representation of the upper GL (**Figure 3A**) and its maximum intensity projection (**Figure 3B**; BDA in red, VGluT2 in blue, and glycinergic GoC in green). Four possible contact points, either on the GoC soma (inset **C**) or at the level of GoC dendrites (insets **D–F**), were analyzed in detail in the z-plane (**Figures 3C–F**). Yet, again, all failed to show a convincing co-localization of the three channels at the same depth. These results argue against a CF-GoC connection in the GL.

QUANTIFICATION IN THICK SECTIONS

Our systematic analysis in the z-plane (optical sections of 0.3–0.4 μm) returned negative results both for both layers. As a final test to confirm that due to the above mentioned thinness of slices we did not miss any contact (i.e., fibers lying just

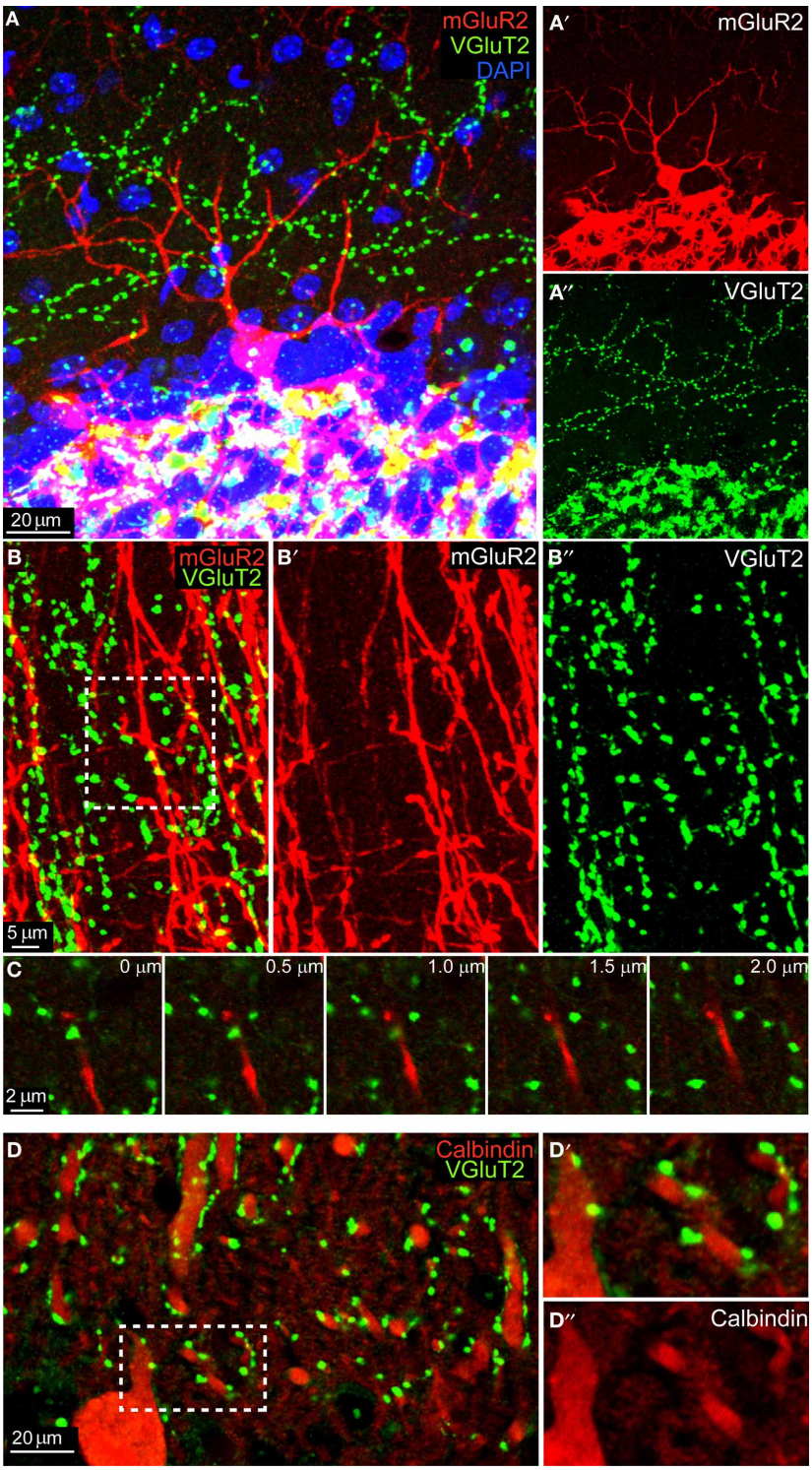

FIGURE 1 | No colocalization between mGluR2-marked GoC and VGlut2 in the ML. (A) Maximum intensity projection of a 20 µm-thick sagittal section of an mGlur2-stained GoC (red) located in the upper GL (identifiable through the extremely dense DAPI staining, in blue). Its dendrite ascends to the ML, where punctuate staining indicates VGlut2. The red and green channels are split and presented separately in, respectively, **(A′)** and **(A″)**. Note the mismatch of the two signals. **(B)** High-magnification of the ML in coronal section (maximum intensity projection of a 2 µm slices), with red GoC dendrites (mGluR2 positive; **B′**) and VGlut2-marked CF endings (green; **B″**). Potential colocalizations are scarce, and when present appear like yellow spots (see arrow). **(C)** Montage in the z-plane with 0.5 µm interval between photographs of the inset indicated in **(B)**. Note how the GoC dendrite (red) and the VGluT2 varicosity (green) lay on different planes, separated by at least 1 µm. **(D)** Maximum intensity projection of a 4.5 µm-thick sagittal section of Calbindin-stained PCs dendrites (red, see detail in **D″**) which abundantly colocalized with VGlut2 (green; **D′**).

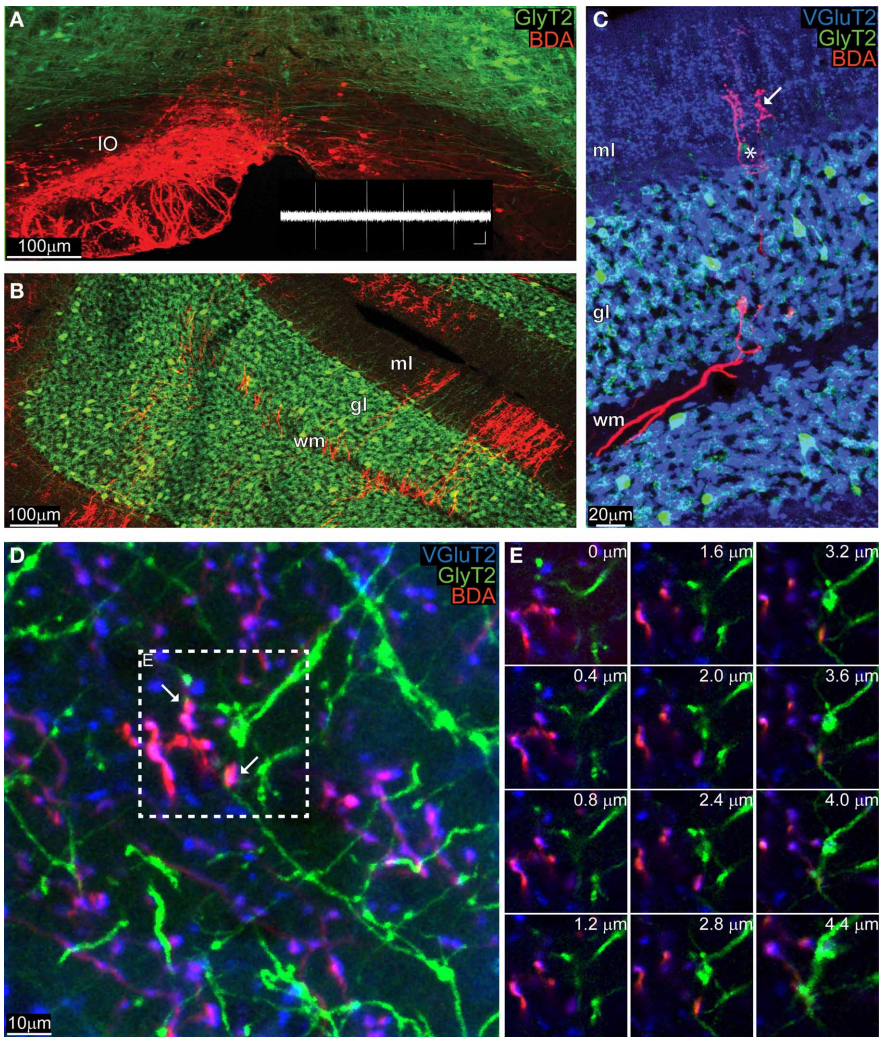

FIGURE 2 | Anatomically marked CFs co-stain with VGlut2 in the ML, but not with GoC dendrites. (A) Maximum intensity projection of a low magnification image (10 μm thick) of the IO of a GlyT2-EGFP mouse, in which all glycinergic neurons (GoC included) are green. The animal was unilaterally injected with BDA in the left IO, and the BDA was visualized with a red fluorochrome. The inset in white reproduces a typical olivary neuron firing pattern (scalebar: 0.5 mV, 500 ms). **(B)** View of the cerebellar cortex of the same GlyT2-EGFP mouse presented in **(A)** (maximum intensity projection of a 10 μm thick slice). The BDA along the olivary axon clearly stained CFs, which entered in the white matter (WM), passed through the GL and reached the ML. **(C)** Example picture (maximum intensity projection, 5 μm thick) gathered from a BDA-injected (CFs in red red) GlyT2-EGFP mouse (GoCs in green) additionally stained for the synaptic marker VGluT2 (blue). The CF in the WM and GL remained bright red, while in the ML it co-localized with VGluT2 and circled around a PC (star) and assumed a violet color (arrow). **(D)** Maximum intensity projection at high magnification of the ML (4.4 μm thick), with abundant double labeling BDA-VGlut2 (red and blue), but not with GlyT2 (green). Two potential triple-labelings are indicated by the arrows. **(E)** Montage in the z-plane of the inset presented in **(D)** containing the potential synapses with 0.4 μm interval between photographs. The red and blue channel appear at the same depth, but not the green one, indicating that the GoC dendrite resides in a different plane than the CF terminal.

above or just below the cell body or dendrite), we performed an additional analysis on maximum projection of thick slices (10 μm). The bidimensional flattening of such volume is due to produce noise, which can be used as a statistical comparison to test for signal (i.e., real connections). Specifically, to confirm the absence of CF-GoC contacts and prove that all the colocalization that we saw in such maximum projections were indeed noise, we rotated and translated one channel while keeping the others fixed and blindly counted the colocalizations in all configurations (aligned, rotated, and translated; see **Figures 4A–C** and Methods). In the ML the number of colocalizations between VGluT2 and GlyT2/mGluR2 identified in the aligned configuration did not differ from the ones identified in the rotated nor in the translated ones (**Figure 4D**; aligned vs. rotated $p = 0.46$, aligned vs. translated $p = 0.62$; One-Way ANOVA with Tukey correction; data normalized to the aligned configuration). In the GL we counted both the triple colocalization VGluT2 + Gly + BDA (which were very scarce) and the double GlyT2 + BDA, and again we found no difference between the three configurations (**Figure 4E**; all $p > 0.93$ One-Way ANOVA with Tukey correction;

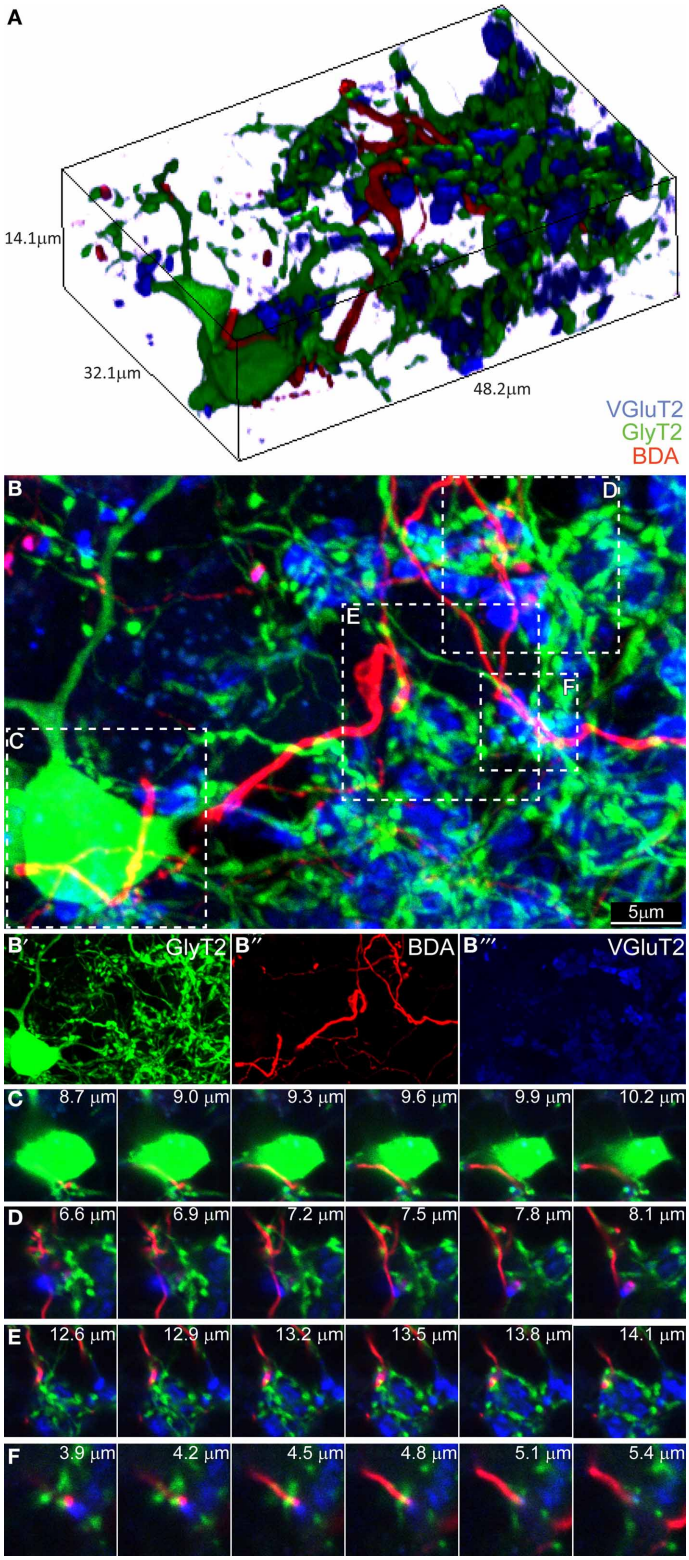

FIGURE 3 | Three-dimensional analysis of the upper GL fails to discover CF-GoC synapses. (A) 3D reconstruction of a portion of the upper GL of a BDA-injected (CF, red) GlyT2-EGFP mouse (GoC, green) co-stained for VGluT2, and containing on GoC soma and numerous dendrites, together with one clearly identifiable CF and the typical MF glomerular rosettes (VGlut2 positive, in blue). **(B)** Maximum intensity projection of the 3D image (14.1 µm thick), with below the three individual channels **(B′–B‴′)**. Five possible triplets are indicated in the insets **(C–F)**. Montages of the five potential synapses analyzed in the z-plane. In all five instances the CF does not co-localize with VGlut2, arguing against the existence of synaptic contacts.

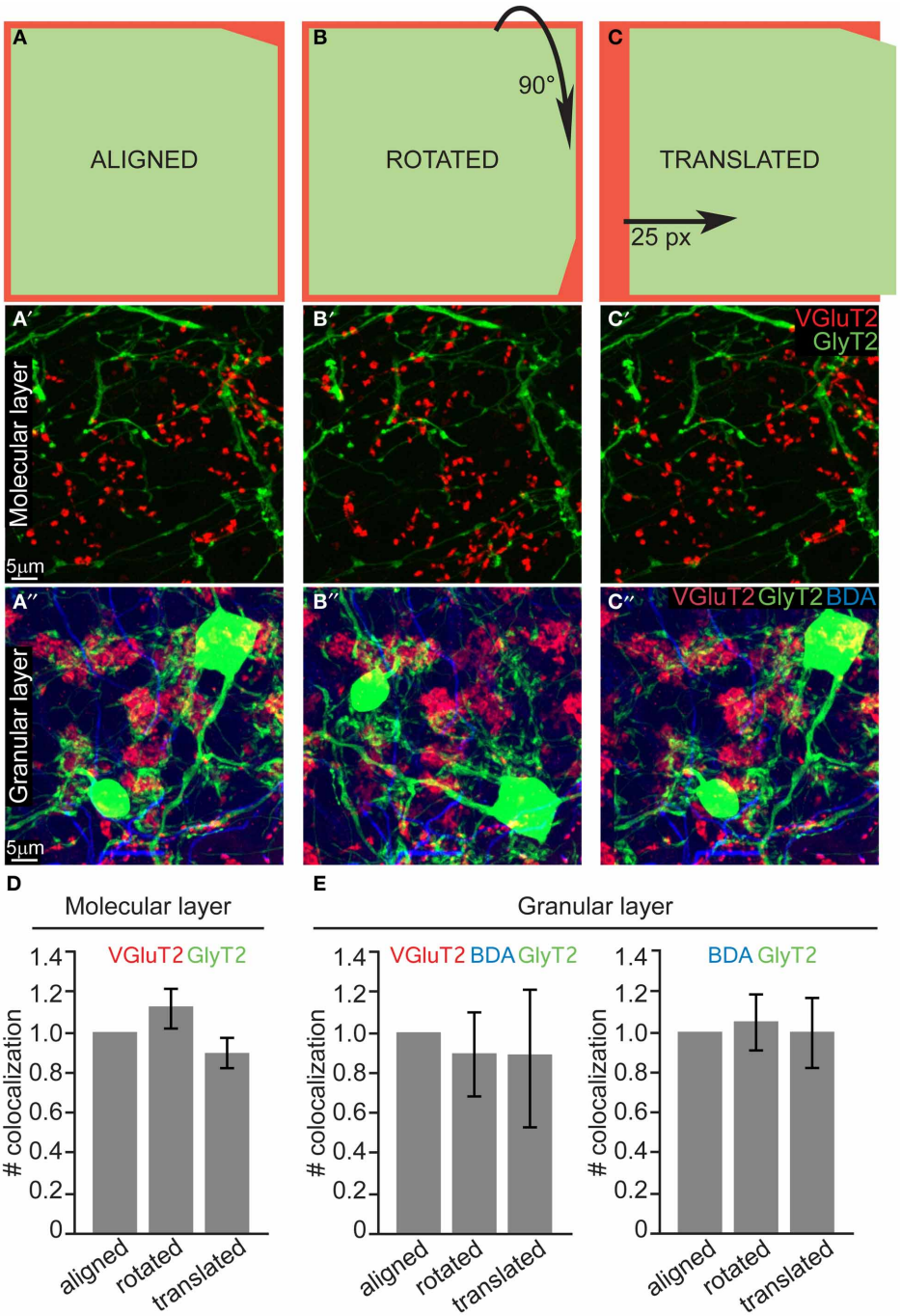

FIGURE 4 | Quantification of potential colocalization in thick slices also returns a negative result. (A) Schematic drawing of the "aligned" configuration, and examples of maximum intensity projections of 10µm slices from both the ML and GL (**A′** and **A″**, respectively). **(B–B″)** Same as **(A–A″)** for the "rotated" configuration, in which one channel was rotated 90° clockwise. **(C–C″)** Same as **(A–A″)** for the "translated" configuration in which one channel was shifted 25 pixels to the right. **(D)** Quantification of the number of colocalization between VGluT2 and mGluR2/GlyT2 found in the ML ($n = 30$, $N = 3$). **(E)** Quantification of the number of colocalization between VGluT2, BDA, and GlyT2 or between BDA and GlyT2 only found in the GL ($n = 30$, $N = 3$). The values are presented in (**D** and **E**) as mean ± s.e.m. and are normalized to the respective aligned configurations for averaging purposes.

data normalized to the aligned configuration). This lack of difference suggests that indeed in tick sections the colocalization are noise, and complements our thin-sections analysis in indicating that there are no connections between CF and GoC.

DISCUSSION

The present study addresses with morphological techniques the long-standing question as to whether olivary CFs contact cerebellar GoCs. Our analyses failed to prove such an

existence in both the molecular layer and granular layer, whereas we found robust evidence for appositions of CFs at PCs in the molecular layer. While we clearly and consistently encountered co-localizations of GoC soma or dendrites with anterogradely traced CFs, these apposition points never also stained positively for the synaptic marker VGluT2 (again, unlike the VGluT2 labeling in the molecular layer onto PCs' dendrites and MLIs' cell-bodies). This observation could potentially explain some of the earlier reports supporting the connection, in which standard light microscopy (LM) techniques were employed to trace CFs without co-staining for synaptic proteins such as VGluT2 (Scheibel and Scheibel, 1954; Sugihara et al., 1999; Shinoda et al., 2000).

Three different laboratories have presented electron microscopic (EM) analysis corroborating the existence of CF-GoC contacts (Hamori and Szentagothai, 1966b; Desclin, 1976; Castejon and Castejon, 2000). While EM is a superior analytical technique compared to the CM that we employed, all three EM studies share the same limitation: neither GoCs nor CFs were marked with immunocytochemical labeling, leaving ample room for interpretation of the micrographs. The inconclusiveness of these studies and the clear necessity of having unequivocally marked presynaptic and postsynaptic elements prompted us to apply CM, and with these stringent conditions we consistently failed to see synaptic connections. While being aware that it is hardly possible to demonstrate the non-existence of any entity, our data strongly suggest the absence of direct CF-GoC contacts.

Our findings reopen the debate about both the nature of the Scheibel collaterals, and, more importantly, the interpretation of the *in vivo* electrophysiological experiments performed by Schulman and Bloom (1981) in the Eighties and recently confirmed by Xu and Edgley (2008). Regarding the first issue, while their existence is undoubted, it is unclear what function such projections might serve. Either they contact cells other than GoCs, or, they might be vestigial "loser" CFs that retracted their synapses from PCs soma during the developmental competition and were not fully degraded to the branching point (Sugihara, 2006). With respect to the *in vivo* results, both studies mentioned above demonstrated that olivary stimulation decreases the firing rate of GoCs, an effect that if not due to a direct contact mediated by the abundantly-expressed mGluR2 receptors (Watanabe and Nakanishi, 2003), has to be derived either from extrasynaptic signaling or from an inhibitory intermediary neuron receiving CF input and projecting onto a GoC (Xu and Edgley, 2008). Which neurons are the candidates for this intermediary role? It is now widely acknowledged that both MLIs and PCs receive functional CF inputs (Ramon y Cajal, 1995; Schmolesky et al., 2002; Szapiro and Barbour, 2007; Mathews et al., 2012). Until recently the MLI would have been considered the best candidate to fulfill the presumptive inhibitory, intermediary role, because it was traditionally thought to project to GoCs (Ramon y Cajal, 1995; Dumoulin et al., 2001). However, a recent physiological study failed to prove a functional connection between MLIs and GoCs (Hull and Regehr, 2012). Maybe, PCs form a better candidate. According to an ultrastructural study by Hamori and Szentagothai (1966a) and a CM study by Frola and colleagues (Frola et al., 2012) axon collaterals of PCs do contact GoC cell-bodies. If this preliminary evidence can be confirmed with paired recordings, they could explain the electrophysiological results *in vivo* and open new scenarios in terms of cerebellar computation and integration at the input stage (D'Angelo and De Zeeuw, 2009).

ACKNOWLEDGMENTS

We are grateful to Dr. J. M. Fritschy for sharing the GlyT2-EGFP mice; to M. Rutteman, E. Goedknegt and S. Venkatesan for technical assistance; and to Dr. B. van Beugen and Dr. Z. Gao for critical discussions. This work was supported by the Dutch Organization for Medical Sciences (ZonMw; Freek E. Hoebeek, Chris I. De Zeeuw), Life Sciences (ALW; Freek E. Hoebeek, Chris I. De Zeeuw), Senter (Neuro-Basic), ERC-adv, CEREBNET, and C7 programs of the EU (Chris I. De Zeeuw).

REFERENCES

Albus, J. S. (1971). A theory of cerebellar function. *Math. Biosci.* 10, 25–61.

Bloedel, J. R., and Bracha, V. (1998). Current concepts of climbing fiber function. *Anat. Rec.* 253, 118–126.

Castejon, O. J., and Castejon, H. V. (2000). Correlative microscopy of cerebellar Golgi cells. *Biocell* 24, 13–30.

D'Angelo, E., and De Zeeuw, C. I. (2009). Timing and plasticity in the cerebellum: focus on the granular layer. *Trends Neurosci.* 32, 30–40.

Desclin, J. C. (1976). Early terminal degeneration of cerebellar climbing fibers after destruction of the inferior olive in the rat. Synaptic relationships in the molecular layer. *Anat. Embryol. (Berl.)* 149, 87–112.

De Zeeuw, C. I., Hoebeek, F. E., Bosman, L. W., Schonewille, M., Witter, L., and Koekkoek, S. K. (2011). Spatiotemporal firing patterns in the cerebellum. *Nat. Rev. Neurosci.* 12, 327–344.

Dumoulin, A., Triller, A., and Dieudonne, S. (2001). IPSC kinetics at identified GABAergic and mixed GABAergic and glycinergic synapses onto cerebellar Golgi cells. *J. Neurosci.* 21, 6045–6057.

Frola, E., Patrizi, A., and Sassoè-Pognetto, M. (2012). *Novel Gabaergic Inputs to Golgi Cells in the Cerebellar Granule Cell Layer, 8th FENS 3782.* (Barcelona), 119.08.

Galliano, E., Mazzarello, P., and D'Angelo, E. (2010). Discovery and rediscoveries of Golgi cells. *J. Physiol.* 588, 3639–3655.

Gao, Z., van Beugen, B. J., and De Zeeuw, C. I. (2012). Distributed synergistic plasticity and cerebellar learning. *Nat. Rev. Neurosci.* 13, 619–635.

Hamori, J., and Szentagothai, J. (1966a). Identification under the electron microscope of climbing fibers and their synaptic contacts. *Exp. Brain Res.* 1, 65–81.

Hamori, J., and Szentagothai, J. (1966b). Participation of Golgi neuron processes in the cerebellar glomeruli: an electron microscope study. *Exp. Brain Res.* 2, 35–48.

Hossaini, M., Cardona Cano, S., van Dis, V., Haasdijk, E. D., Hoogenraad, C. C., Holstege, J. C., et al. (2011). Spinal inhibitory interneuron pathology follows motor neuron degeneration independent of glial mutant superoxide dismutase 1 expression in SOD1-ALS mice. *J. Neuropathol. Exp. Neurol.* 70, 662–677.

Hull, C., and Regehr, W. G. (2012). Identification of an inhibitory circuit that regulates cerebellar Golgi cell activity. *Neuron* 73, 149–158.

Kaneko, T., Fujiyama, F., and Hioki, H. (2002). Immunohistochemical localization of candidates for vesicular glutamate transporters in the rat brain. *J. Comp. Neurol.* 444, 39–62.

Marr, D. (1969). A theory of cerebellar cortex. *J. Physiol.* 202, 437–470.

Mathews, P. J., Lee, K. H., Peng, Z., Houser, C. R., and Otis, T. S. (2012). Effects of climbing fiber driven inhibition on purkinje neuron spiking. *J. Neurosci.* 32, 17988–17997.

Neki, A., Ohishi, H., Kaneko, T., Shigemoto, R., Nakanishi, S., and Mizuno, N. (1996). Metabotropic glutamate receptors mGluR2 and mGluR5 are expressed in two non-overlapping populations of Golgi cells in the rat cerebellum. *Neuroscience* 75, 815–826.

Palay, S. L., and Chan-Palay, V. (1974). *Cerebellar Cortex: Cytology and Organization.* Berlin; Heidelberg; New York: Springer.

Paxinos, G., and Franklin, K. B. J. (2004). *The Mouse Brain in Stereotaxic Coordinates.* San Diego, CA: Academic Press.

Pijpers, A., Voogd, J., and Ruigrok, T. J. (2005). Topography of olivocortico-nuclear modules in the intermediate cerebellum of the rat. *J. Comp. Neurol.* 492, 193–213.

Ramon y Cajal, S. (1995). *Histology of the Nervous System of Man and Vertebrates.* New York, NY: Oxford University Press.

Ruigrok, T. J., Teune, T. M., van der Burg, J., and Sabel-Goedknegt, H. (1995). A retrograde double-labeling technique for light microscopy. A combination of axonal transport of cholera toxin B-subunit and a gold-lectin conjugate. *J. Neurosci. Methods* 61, 127–138.

Scheibel, M. E., and Scheibel, A. B. (1954). Observations on the intracortical relations of the climbing fibers of the cerebellum; a Golgi study. *J. Comp. Neurol.* 101, 733–763.

Schmolesky, M. T., Weber, J. T., De Zeeuw, C. I., and Hansel, C. (2002). The making of a complex spike: ionic composition and plasticity. *Ann. N.Y. Acad. Sci.* 978, 359–390.

Schulman, J. A., and Bloom, F. E. (1981). Golgi cells of the cerebellum are inhibited by inferior olive activity. *Brain Res.* 210, 350–355.

Shinoda, Y., Sugihara, I., Wu, H. S., and Sugiuchi, Y. (2000). The entire trajectory of single climbing and mossy fibers in the cerebellar nuclei and cortex. *Prog. Brain Res.* 124, 173–186.

Simat, M., Parpan, F., and Fritschy, J. M. (2007). Heterogeneity of glycinergic and gabaergic interneurons in the granule cell layer of mouse cerebellum. *J. Comp. Neurol.* 500, 71–83.

Sugihara, I. (2006). Organization and remodeling of the olivocerebellar climbing fiber projection. *Cerebellum* 5, 15–22.

Sugihara, I., Wu, H., and Shinoda, Y. (1999). Morphology of single olivocerebellar axons labeled with biotinylated dextran amine in the rat. *J. Comp. Neurol.* 414, 131–148.

Szapiro, G., and Barbour, B. (2007). Multiple climbing fibers signal to molecular layer interneurons exclusively via glutamate spillover. *Nat. Neurosci.* 10, 735–742.

Watanabe, D., and Nakanishi, S. (2003). mGluR2 postsynaptically senses granule cell inputs at Golgi cell synapses. *Neuron* 39, 821–829.

Xu, W., and Edgley, S. A. (2008). Climbing fibre-dependent changes in Golgi cell responses to peripheral stimulation. *J. Physiol.* 586, 4951–4959.

Zeilhofer, H. U., Studler, B., Arabadzisz, D., Schweizer, C., Ahmadi, S., Layh, B., et al. (2005). Glycinergic neurons expressing enhanced green fluorescent protein in bacterial artificial chromosome transgenic mice. *J. Comp. Neurol.* 482, 123–141.

Conflict of Interest Statement: The authors declare that the research was conducted in the absence of any commercial or financial relationships that could be construed as a potential conflict of interest.

Received: 31 January 2013; accepted: 14 March 2013; published online: 08 April 2013.

Citation: Galliano E, Baratella M, Sgritta M, Ruigrok TJH, Haasdijk ED, Hoebeek FE, D'Angelo E, Jaarsma D and De Zeeuw CI (2013) Anatomical investigation of potential contacts between climbing fibers and cerebellar Golgi cells in the mouse. Front. Neural Circuits 7:59. doi: 10.3389/fncir.2013.00059

frontiers in
NEURAL CIRCUITS

ORIGINAL RESEARCH ARTICLE
published: 10 April 2013
doi: 10.3389/fncir.2013.00064

Theta-frequency resonance at the cerebellum input stage improves spike timing on the millisecond time-scale

Daniela Gandolfi*[1,2], *Paola Lombardo*[1], *Jonathan Mapelli*[2,3], *Sergio Solinas*[3] and *Egidio D'Angelo*[1,3]

[1] *Neurophysiology Unit, Department of Brain and Behavioral Sciences, University of Pavia, Pavia, Italy*
[2] *Department of Biomedical, Metabolic and Neural Sciences, University of Modena and Reggio Emilia, Modena, Italy*
[3] *Brain Connectivity Center, IRCCS Fondazione Istituto Neurologico Nazionale C. Mondino, Pavia, Italy*

Edited by:
Chris I. De Zeeuw, Erasmus MC and Netherlands Institute for Neuroscience, Netherlands

Reviewed by:
Leonard Maler, University of Ottawa, Canada
Attila Szücs, Hungarian Academy of Sciences Hungary

***Correspondence:**
Egidio D'Angelo, Neurophysiology Unit, Department of Brain and Behavioral Sciences, University of Pavia, Via Forlanini 6, 27100 Pavia, Italy.
e-mail: dangelo@unipv.it

The neuronal circuits of the brain are thought to use resonance and oscillations to improve communication over specific frequency bands (Llinas, 1988; Buzsaki, 2006). However, the properties and mechanism of these phenomena in brain circuits remain largely unknown. Here we show that, at the cerebellum input stage, the granular layer (GRL) generates its maximum response at 5–7 Hz both *in vivo* following tactile sensory stimulation of the whisker pad and in acute slices following mossy fiber bundle stimulation. The spatial analysis of GRL activity performed using voltage-sensitive dye (VSD) imaging revealed 5–7 Hz resonance covering large GRL areas. In single granule cells, resonance appeared as a reorganization of output spike bursts on the millisecond time-scale, such that the first spike occurred earlier and with higher temporal precision and the probability of spike generation increased. Resonance was independent from circuit inhibition, as it persisted with little variation in the presence of the $GABA_A$ receptor blocker, gabazine. However, circuit inhibition reduced the resonance area more markedly at 7 Hz. Simulations with detailed computational models suggested that resonance depended on intrinsic granule cells ionic mechanisms: specifically, K_{slow} (M-like) and KA currents acted as *resonators* and the persistent Na current and NMDA current acted as *amplifiers*. This form of resonance may play an important role for enhancing coherent spike emission from the GRL when theta-frequency bursts are transmitted by the cerebral cortex and peripheral sensory structures during sensory-motor processing, cognition, and learning.

Keywords: resonance, cerebellum, granular layer

INTRODUCTION

Brain activity is characterized by complex temporal patterns, which often take the form of coherent oscillations (Buzsaki, 2006). These are organized over defined frequency bands giving raise to the electroencephalographic rhythms. Important among these is the theta-band, which characterizes various functional states encompassing deep sleep, attentiveness, learning, and voluntary movement. In the latter case, the commands generated by the motor cortex are associated with increased power in the theta-band (around 6–9 Hz in humans), which is then transmitted to cortical and subcortical centers (Gross et al., 2005; Schnitzler et al., 2006, 2009). Interestingly, these same frequencies are exploited by the thalamo-cortical circuits to elaborate motor commands and estimate kinematic parameters in behaviors like whisking (Ahissar et al., 2000; Szwed et al., 2003; Kleinfeld et al., 2006; Zuo et al., 2011). But how do these signals interfere with the activity of the receiving networks? One main hypothesis is that the receiving network is tuned over the transmission frequency band through resonance, being therefore more efficiently engaged when the transmitted frequency pattern is recognized (Llinas, 1988). This resonance could emerge both from membrane mechanisms based on specific ionic channels and from the synaptic connectivity of the neuronal circuit involved.

The cerebellum shows theta-band activity correlated with that of the premotor and motor areas during bimanual voluntary tasks in humans (Gross et al., 2005; Schnitzler et al., 2006, 2009). Moreover, single-neuron responses in the cerebellum are correlated with theta-frequency activity in the sensory-motor cortex of awake rats (Ros et al., 2009). Extracerebellar theta-frequency activity (Harish and Golomb, 2010) can be conveyed to the cerebellum through two main pathways. The inferior olive, which also shows self-sustained theta-band oscillations (Marshall and Lang, 2004), can generate theta-frequency spike bursts in climbing fibers (Mathy et al., 2009), and complex spikes in Purkinje cells (Welsh et al., 1995; Van Der Giessen et al., 2008). The granular layer (GRL) could also be entrained into theta-rhythms by extracerebellar activity (Pellerin and Lamarre, 1997; Hartmann and Bower, 1998; Ros et al., 2009).

It has been reported that the interneuron inhibitory network made by Golgi cells shows theta-band resonant properties based on interneuronal connectivity through gap-junctions (Dugue et al., 2009). Moreover, it was shown that neuronal elements of the GRL show intrinsic resonance in the theta-band, as both the granule and the Golgi cells respond maximally to input currents at around 6 Hz (D'Angelo et al., 2001; Solinas et al., 2007a,b). However, it remained unclear whether the GRL resonates to extracerebellar inputs and which mechanisms would be involved. Here we show

that patterned sensory stimulation of the whisker pad causes GRL resonance at 5–7 Hz in the rat cerebellum GRL with marginal involvement of the inhibitory network. Resonance enhanced spike generation in granule cells raising time-precision on the millisecond time-scale. Theta-band resonance in the GRL could play an important role to tune the cerebellar circuit over one of the main frequency band of cerebro-cortical activity during generation of voluntary movement and other central functional states.

MATERIALS AND METHODS

Recordings were performed *in vitro* and *in vivo* and mathematical simulations were done using computational models. Experiments were performed using Wistar rats at postnatal day P20–P24 [internal breeding, Harlan (Indianapolis, IN, USA)] both in acute slices and *in vivo* under anesthesia. All experiments were conducted in accordance with international guidelines from the European Community Council Directive 86/609/EEC on the ethical use of animals.

STIMULATION PATTERNS

In order to investigate the frequency – dependent properties of the GRL response, stimulus trials were repeated at frequencies between 1 and 10 Hz (1 Hz steps). Each trial was composed of 30 bursts and was repeated in a pseudo-random order (10 times *in vivo*, 20 times in both VSD recordings, whole-cell recordings and simulations) to prevent potential effects due to short or long-term adaptation processes and to reduce the effect of response variability. The stimuli *in vitro* consisted of mossy fiber bursts composed of 3 pulses at 300 Hz intra-burst frequency. The stimuli *in vivo* consisted of 30 ms air puffs, which are known to generate short high-frequency bursts of similar frequency in the mossy fibers (Chadderton et al., 2004; Rancz et al., 2007).

RECORDINGS IN ACUTE CEREBELLAR SLICES

Patch-clamp and VSD imaging recordings were obtained from parasagittal cerebellar slices (D'Angelo et al., 1995; D'Errico et al., 2009). Briefly, the rats were deeply anesthetized with halothane (Sigma-Aldrich, Saint Louis, MO, USA) and decapitated. The cerebellum was removed, the vermis isolated and fixed on the vibroslicer stage (Dosaka, Kyoto, Japan) with cyano-acrylic glue. Acute 220 μm thick slices were cut in cold cutting solution containing (in mM): 130 K-gluconate, 15 KCl, 0.2 EGTA, 20 HEPES, and 10 glucose, pH adjusted at 7.4 with NaOH. Slices were incubated at 32°C in oxygenated extracellular Krebs solution containing (in mM): 120 NaCl, 2 KCl, 1.2 $MgSO_4$, 26 $NaHCO_3$, 1.2 KH_2PO_4, 2 $CaCl_2$, 11 glucose (pH 7.4 when equilibrated with 95% O_2 and 5% CO_2), at least 1 h before recordings. In some experiments the solution was implemented with the $GABA_A$ receptor blocker 20 μM gabazine (SR95531; Sigma-Aldrich), which was maintained throughout the recording session. Slices were transferred to the recording chamber on the stage of an upright microscope (Zeiss Axioskop F2S, Oberkochen, Germany) and perfused at 1.5 ml min^{-1} with oxygenated Krebs solution at 32°C with a feed-back Peltier device (TC-324B, Warner Instruments Corp., Hamden, CT, USA). Slices were immobilized with a nylon mesh attached to a platinum Ω-wire.

Patch-clamp recordings

Whole-cell current-clamp recordings were made in whole-cell patch-clamp configuration from granule cells as reported previously (D'Angelo et al., 1995; D'Errico et al., 2009). Recordings were obtained using Multiclamp 700B amplifier (Molecular Devices, Union City, CA, USA) (3-dB; cut-off frequency = 10 kHz). Recordings were subsequently digitized at 20 kHz using pClamp 9 (Molecular Devices) and a Digidata 1322A A/D converter (Molecular Devices). Patch pipettes were pulled from borosilicate glass capillaries (Hilgenberg, Malsfeld, Germany) and filled with the following solution (in mM): 126 K-gluconate, 4 NaCl, 15 glucose, 5 HEPES, 1 $MgSO_4$ * 7 H_2O, 0.1 BAPTA-free, 0.05 BAPTA-Ca^{2+}, 3 ATP, 100 μm GTP; pH was adjusted to 7.2 with KOH. This solution maintained resting free-$[Ca^{2+}]$ at 100 nM and had a resistance of 7–10 MΩ before seal formation. The stability of patch-clamp recordings can be influenced by modifications of series resistance and neurotransmitter release. To ensure that series resistance remained stable during the recordings, passive cellular parameters were extracted in voltage-clamp by analyzing current relaxation induced by a 10 mV step from a holding potential of −70 mV. According to previous reports (D'Angelo et al., 1993, 1995; Silver et al., 1996), the transients were reliably fitted with a monoexponential function yielding membrane capacitance (C_m) of 3.9 ± 0.2 pF ($n = 18$), membrane resistance (R_m) of 2.2 ± 0.3 GΩ ($n = 18$) and series resistance (R_s) of 18.0 ± 0.9 MΩ ($n = 18$). The 3-dB cell plus electrode cut-off frequency was $f_{VC} = (2\pi R_{sCm})^{-1} = 2.3 \pm 0.1$ kHz ($n = 18$) and did not significantly change during recordings attesting their stability. Mossy fibers were stimulated with a bipolar tungsten electrode (Clark Instruments, Pangbourne, UK) via a stimulus isolation unit and stimulation intensity (±4–8 V; 100 μs) was raised until the EPSPs generated spikes in 10–50% of the responses at 1 Hz from a membrane potential between −70 and −60 mV (mean 64.2 ± 2.7 $n = 18$). From a comparison with previous data (D'Angelo et al., 1995; Sola et al., 2004), between one and three mossy fibers were stimulated per granule cell.

VSD imaging

The procedures for VSD imaging were the same as reported in previous papers (Mapelli and D'Angelo, 2007; Mapelli et al., 2010a,b). The slices were incubated for 30 min in oxygenated Krebs solution added with 3% Di-4-ANEPPS stock solution mixed with 50% fetal Bovine Serum (Molecular Probes). The dye (Di-4-ANEPPS, Molecular Probes) was dissolved and stocked in Krebs with 50% ethanol (SIGMA) and 5% Cremophor EL (a Castor oil derivative, SIGMA). Perfusion of standard extracellular solution (2–3 ml/min) maintained at 32°C with a feed-back temperature controller (Thermostat HC2, Multi Channel Systems, Reutlingen, Germany) was performed during the recording session. In a series of experiments, the extracellular solution was implemented with the $GABA_A$ receptor blocker, 20 μM gabazine (SR95531; Sigma-Aldrich), which was maintained throughout the recording session. Mossy fibers were stimulated with a bipolar tungsten electrode (Clark Instruments, Pangbourne, UK) via a stimulus isolation unit using an electronic stimulator (STG 1008, Multi channel systems). The recording chamber was installed on an upright epifluorescence microscope (BX51WI, Olympus, Europa Gmbh, Hamburg,

Germany), equipped with a 20X (XLUM Plan FL 0.95 NA) (see Tominaga et al., 2000). The light generated by a halogen lamp (150W, MHF-G150LR, MORITEX Corp., Tokyo, Japan) was controlled by an electronic shutter (model0, Copal, Co., Tokyo, Japan) and then passed through an excitation filter ($\lambda = 530 \pm 10$ nm), projected onto a dichroic mirror ($\lambda = 565$ nm), and reflected toward the objective lens to illuminate the specimen. Fluorescence generated by the tissue was transmitted through an absorption filter ($\lambda > 590$ nm) to the CCD camera (MICAM Ultima, Scimedia, Brainvision, Tokyo, Japan). The whole imaging system was connected through an I/O interface (Brainvision) to a PC controlling illumination, stimulation, and data acquisition. The final pixel size was 5 μm with 20× objective. Full-frame image acquisition was performed at 1 kHz. The signal-to-noise ratio was improved by averaging 30 consecutive sweeps at the stimulus repetition frequency of 0.2 Hz. Given maximal $\Delta F/F_0 \approx 1\%$ and noise SEM $\approx \pm 0.1\%$ ($n = 12$ slices), the signal-to-noise (S/N) ratio was about 10 times ensuring a reliable measurement of peak response amplitude. Data were acquired and displayed by Brainvision software and signals were analyzed using routines written in MATLAB (Mathworks, Natick, USA). The analysis was performed by evaluating the maximum response of the VSD signal obtained at each tested frequency (1–10 Hz) normalized to the first peak response.

RECORDINGS *IN VIVO*

Extracellular field recordings were performed in the GRL of Crus-IIa in 20–24-days-old Wistar rats (internal breeding, Harlan). The rats were deeply anesthetized with urethane (1.4 mg/kg; Sigma-Aldrich; see Roggeri et al., 2008) dissolved in 0.9% NaCl and injected intraperitoneally. The heart rate (360–420/min) and respiratory rate (100–120/min) of each animal were constantly monitored and remained stable throughout the experiments. Animals were placed on a stereotaxic table (David Kopf Instruments, Tujunga, CA, USA) covered with a heating pad and the body temperature was maintained at 38 ± 0.5°C through a feed-back temperature controller (Fine Science Tools Inc.; Foster City, CA, USA). The exposure of the cerebellar surface was performed following previously reported surgical procedures (Bower and Woolston, 1983; Morissette and Bower, 1996; Lu et al., 2005). Briefly, a craniotomy was made on the right hemisphere (AP −13 mm ML 3 mm). The *dura mater* was carefully removed and extracellular Krebs solution was placed onto the cerebellar surface (Roggeri et al., 2008).

Local field potential (LFP) recordings from the GRL were obtained at the depth of 500 μm with glass borosilicate pipettes (Hilgenberg) filled with NaCl 2 M (0.5–1 MΩ). Insertion of the electrodes was at a 45° angle. Sensory stimulation was performed through a plastic pipette connected to a MPPI-2 Pressure Injector (Applied Scientific Instrumentation, Eugene, OR, USA) and positioned 2–3 mm from the whisker pad. The low-frequency stimulation protocol delivered 30 ms air puffs (40 psi) at 0.1 Hz frequency. Extracellular currents were recorded with Multiclamp 700 A amplifier (Molecular Devices). The signals were band-pass filtered between 100 Hz (high-pass) and 2 kHz (low-pass), digitized at 50 kHz using a Digidata 1322A interface, and stored on a PC using Clampex 9 (Molecular Devices). The same board and software were used to monitor and record body temperature and heart and respiratory rate and to generate stimulation pulses. The $GABA_A$ receptor blocker, 20 μM gabazine (SR95531, Tocris Cookson), was dissolved in Krebs solution, placed in a microliter syringe (Hamilton, Bonadus, Switzerland) and injected 500 μm deep into Crus-IIa of the cerebellar cortex close to recording electrode. Extracellular signals were acquired and processed off-line with the Clampfit 9.2 software (Molecular Devices). The signal-to-noise ratio was improved by averaging 100 consecutive traces and by digital filtering (Gaussian low-pass filter 1 kHz). The LFPs consisted of two main waves, T and C. T was generated by rapid afferences through the trigeminal-cerebellar pathway, C by delayed afferences passing through the thalamo-cortico-ponto-cerebellar pathway (Morissette and Bower, 1996). In order to achieve a precise assessment of the LFP amplitude, only T measures were considered for resonance analysis. LFP peak amplitudes were measured relatively to the preceding 10 ms baseline.

COMPUTATIONAL MODELING

Computational modeling was performed using a reduced version of a large-scale cerebellar GRL network model (Solinas et al., 2010). The granule cell (D'Angelo et al., 2001) and Golgi cell (Solinas et al., 2007a) models contain an explicit representation of ionic conductance mechanisms, which have been extensively tested with respect to large sets of experimental data. In order to generate the several seconds of neuronal activity required for these simulation, the modeling strategy was to use a single granule cell and a single Golgi cell in different combinations. The number of Golgi cells impinging on the granule cell (0–4) was simply simulated by linearly scaling the synaptic weight (see inset to **Figure 6**). The simulations were performed in the Python environment using models written in NEURON and were run on a 144 processors cluster (SiComputer INTEL MFSYS25V2).

In brief, as in the previous network model (Solinas et al., 2010), the synaptic mechanisms included neurotransmission dynamics based on a vesicular release process generating short-term facilitation and depression. Release probability was derived from experimental works showing average values of 0.4 at the mossy fiber – granule cell synapse (Sola et al., 2004; D'Errico et al., 2009) and 0.4 at the Golgi cell – granule cell synapse (Mapelli et al., 2009). Both the excitatory and inhibitory synapse were endowed with spillover mechanisms allowing activation of slow synaptic responses (Sargent et al., 2005). For the sake of simplicity, the synapses of the same kind (either excitatory or inhibitory) were set with identical release probability and postsynaptic receptor density and properties. In order to mimic synaptic noise and generate jitter in spike timing, release at the mossy fiber – granule cell synapse was set in its stochastic version (Arleo et al., 2010) and background activity was generated in the mossy fibers activating the granule cell and the Golgi cell.

The simulations were run by activating a single granule cell in all its 20 different synaptic combinations formed by four mossy fibers and four Golgi cell axon fibers (including the case of no active Golgi cell synapses to simulate inhibition block) (cf. **Figure 8A**). The Golgi cell was connected to the same four mossy fibers impinging of the granule cell plus other four, for a total of eight mossy fibers. All the mossy fibers carried low-frequency (4 Hz) background activity. Then, in each simulation, 1–4 mossy fibers were

activated by a 3 pulses – 300 Hz burst repeated at frequencies between 0.2 and 10 Hz (in 0.2 Hz steps) for 50 times (during the activation bursts, in these mossy fibers the background activity was interrupted). The data relative to membrane potential, membrane conductance, and current were stored and analyzed off-line using Matlab routines (Mathworks Inc.).

The synaptic combinations determining the excitatory/inhibitory (E/I) balance of granule cells (**Table 1**) were considered to give specific relative contributions to the ensemble GRL response. The weight of these contributions was derived from estimates obtained in *in vivo* LFP recordings (Roggeri et al., 2008; Solinas et al., 2010; Diwakar et al., 2011) and from computations of the probability of connection between mossy fibers, Golgi cells, and granule cells (Solinas et al., 2010). These values are reported in **Table 1**.

RESONANCE ANALYSIS

In each experimental series (either LFP, VSD, patch-clamp, or modeling), for each tested frequency, the first five responses in each trial were excluded in order to allow the responses to stabilize. When required, the remaining 25 responses were averaged over all the trial repetitions at the same frequency. Resonance plots from LFP and VSD data were directly obtained by the response amplitude at the different frequencies. The response amplitudes at each frequency f_i were normalized with respect to the value measured at 1 Hz, $y(f_i) = (y(f_i) - y(1\,Hz))/y(1\,Hz)$. Resonance plots for single-neuron responses (either whole-cell recordings or simulations) were obtained by analyzing the frequency-dependent changes in spike count, first spike delay, first spike standard deviation, and average maximum depolarization (*sc, sd, ssd, amd*). In this case we calculated the Resonance Index (RI). At all tested frequencies, *sc, sd, ssd, amd* were measured, normalized between the extreme values for each cell and rescaled between 0 and 1. Thus, RI in a cell approaches one when the number of emitted spikes and membrane average depolarization are maximum and the delay and time-dispersion of the first spike are minimum. Then the four RI parameters (*sc, sd, ssd, amd*), were summed yielding a compound RI ranging from 0 to 4 and representative of resonance in the given cell.

The resonance plots were usually well fitted by a double Lorentz equation $y(f)$ (Siebert, 1986) (OriginPro8.0, Microcal Inc.) of the form:

$$y(f) = y_0 + \sum_{i=1,2} \frac{2A_i}{\pi} \cdot \frac{\omega_i}{4(f - f_{ci})^2 + \omega_i^2} \qquad (1)$$

Table 1 | Cross-table of excitatory and inhibitory inputs to a granule cell.

Exc/Inh (%)	GoC 0	GoC 1	GoC 2	GoC 3	GoC 4	Total
MF 4	0.43	2.16	3.97	3.62	1.66	11.84
MF 3	7.9	12.78	1.17	1.48	0.51	23.84
MF 2	0	2.42	24.84	15	7.22	49.48
MF 1	0	0.97	5.32	6.29	2.26	14.84
Total	8.33	18.33	35.3	26.39	11.65	100

The values indicate the relative contribution of each synaptic combination (from Solinas et al., 2010; Diwakar et al., 2011).

Where, y_0 is a baseline level and, for each ith curve, A_i is the underlying area, f_{ci} is the peak frequency, and ω_i is the width at $y(f_{ci})/2$. Lorentzian fittings allowed to find the resonance frequencies ($RF_{1,2} = f_{c1,2}$) and to determine the relative weight of the two component of resonance plots with respect to their amplitudes $y(RF_2)/y(RF_1)$. Lorentzian fittings allowed also to calculate $RA = y(f_c)/\omega$, which corresponds to the quality factor Q in resonance literature and characterizes a resonator's bandwidth relative to its center frequency. The goodness of fit was assessed with χ^2 statistics and by calculating the squared correlation factor, R^2. In some cases, the identification of peaks did not require fittings so that RF and RA were determined directly from the raw data by using a peak-detection routine (when the two procedures were compared, the data obtained by peak-detection did not significantly differ from those obtained using Lorentzian fitting: e.g., see **Figure 2B**).

STATISTICAL ANALYSIS

Data are reported as mean ± SEM and compared for their statistical significance by paired Student's t-test, unless stated otherwise (a difference was considered significant at $p < 0.05$).

RESULTS

RESONANT RESPONSES EVOKED IN THE CEREBELLAR CORTEX *IN VIVO*

The response of the GRL to sensory inputs was evaluated by using repetitive air-puff stimulation of the whisker pad in urethane anesthetized rats. A single air-puff is known to cause a short spike burst in mossy fibers (Chadderton et al., 2004; Rancz et al., 2007) and to determine the LFPs recorded from the GRL (Roggeri et al., 2008; Diwakar et al., 2011) (**Figure 1A**). In order to investigate the frequency-dependence of LFPs in response to tactile stimulation, stimulus sequences of 30 impulses (30 ms duration) were delivered between 1 and 10 Hz in random order. After allowing responses to stabilize during the first 5 impulses, the amplitude of the average LFP obtained from the remaining 25 impulses was measured (**Figure 1A**). In control recordings, the LFP increased at 5–7 Hz and then decreased again toward 10 Hz. Thus, the response was resonant in the middle of the theta-band, with a peak at 7 Hz (65.6 ± 26.2% increase compared to 1 Hz; $p < 0.01$, $n = 9$) (**Figure 1B**, left).

The resonant properties of the GRL could reside into the intrinsic properties of granule cells (D'Angelo et al., 2001) but could also be shaped by the inhibitory Golgi interneuron network (Solinas et al., 2007b; Dugue et al., 2009). In order to test the role of the inhibitory circuit, the $GABA_A$ receptor blocker, 20 μM gabazine, was microperfused into the GRL. After 5 min from commencing perfusion, the LFP increased by 49.4 ± 8.1% ($n = 9$; data obtained at 0.1 Hz, not shown), as expected from blockage of inhibitory transmission onto granule cells (Roggeri et al., 2008). Then, the stimulus sequence at different frequencies was repeated. The response was resonant in the middle of the theta-band, with a peak at 7 Hz (123.9 ± 4.9% increase compared to 1 Hz; $p < 0.01$, $n = 9$) (**Figure 1B**, right). Apparently, resonance increased with respect to control and became more pronounced at 7 Hz compared to 5 Hz.

Fittings to resonance plots were performed using double Lorentzian functions (see Eq.1) under the hypothesis that two components were present in the data distributions and

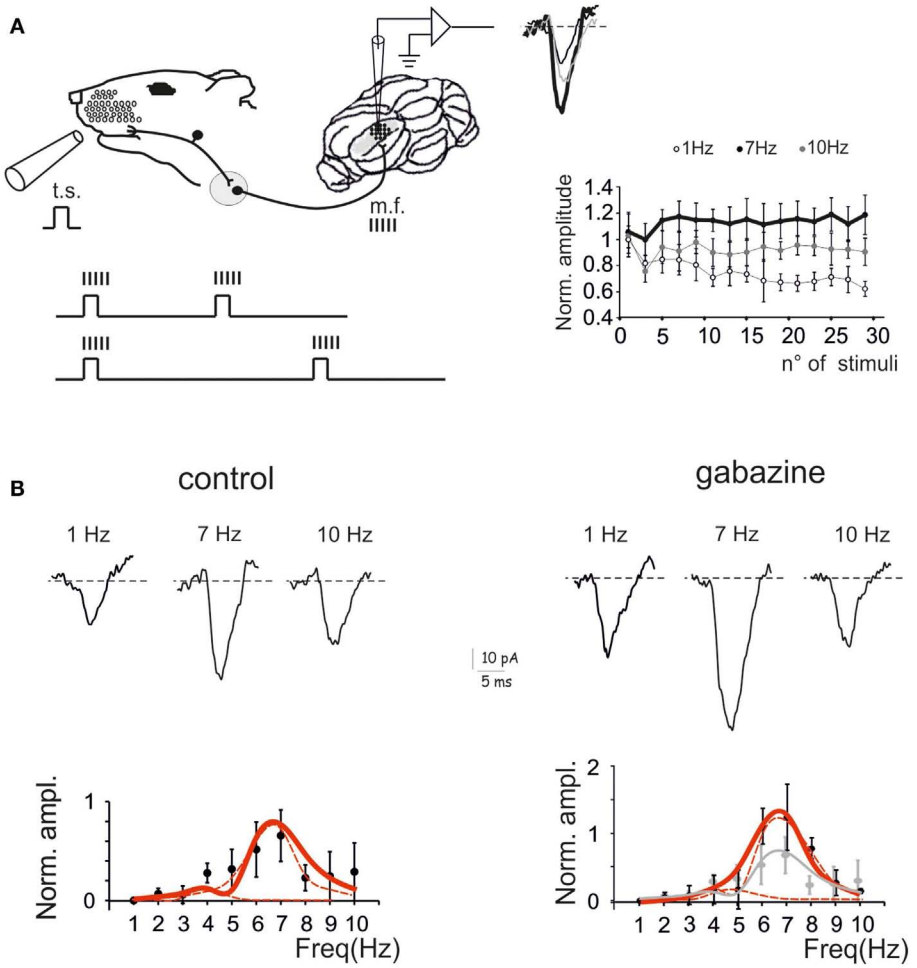

FIGURE 1 | Granular layer (GRL) resonance induced by sensory stimulation. (A). Schematic representation of the recording set-up *in vivo*. The lower inset illustrates that brief air-puff stimuli repeated at different frequencies are expected to generate repeated bursts in the mossy fibers (Chadderton et al., 2004; Rancz and Hausser, 2006; Rancz et al., 2007). By changing the frequency of sensory stimuli the frequency of the bursts is also changed. The GRL response is revealed by local field potential (LFP) recordings. The plot shows the time-course of LFP amplitude in response to subsequent pulses at three different stimulus frequencies. **(B)** LFPs recorded from the GRL at different frequencies of sensory stimulation in control and after intracerebellar microperfusion of gabazine. The normalized maximum LFP amplitude is reported in the plots. Note resonance at 5–7 Hz, which is maintained in the presence of gabazine. Data are reported as mean ± SEM. Red lines fitting the data point represent double Lorentzian functions (broken lines are the two individual component functions) obtained on control and gabazine data, respectively.

that their relative contribution could explain shape changes caused by gabazine application. In control, fittings yielded $RF_1 = 4.4 \pm 0.9$ and $RF_2 = 6.7 \pm 0.3$ with $y(RF_2/y(RF_1) = 2.2$ ($R^2 = 0.86$; $\chi^2 = 0.02$). In the presence of gabazine, fittings yielded $RF_1 = 4.7 \pm 1.6$ and $RF_2 = 6.7 \pm 0.3$ with $y(RF_2)/y(RF_1) = 4.8$ ($R^2 = 0.9$; $\chi^2 = 0.003$). Thus, gabazine application modulated the resonance profile by raising the relative weight of the component peaking around 7 Hz with respect to that peaking around 5 Hz.

RESONANT RESPONSES EVOKED IN ACUTE CEREBELLAR SLICES

Voltage-sensitive dye (VSD) imaging was performed in parasagittal cerebellar slices in order to define the spatial distribution of resonance in the GRL. Mossy fiber stimulation was performed using 3 pulse-300 Hz bursts repeated at frequencies varying between 1 and 10 Hz in random order. The signals generated by mossy fiber stimulation invaded the GRL (**Figure 2A**) reproducing patterns reported previously (Mapelli et al., 2010a,b). In the same slices, 20 μM gabazine application increased the response to mossy fiber stimuli (average $\Delta F/F_0$ increase of 42.7 ± 11%; $p < 0.01$ $n = 4$), as expected from the disinhibitory effect of the drug (Mapelli et al., 2010a,b).

The GRL responses showed maximum $\Delta F/F_0$at input frequencies of 5–7 Hz (**Figure 2A**). This behavior was quantified by constructing resonance curves in ROIs covering limited areas of the GRL (or even single pixels), which showed characteristic profiles peaking in the same 5–7 Hz frequency range (**Figure 2B**). In the presence of gabazine, resonance at 5–7 Hz was still evident.

Resonance maps were constructed by plotting the resonance frequency (RF) measured in each pixel on color-scale (**Figure 3A**).

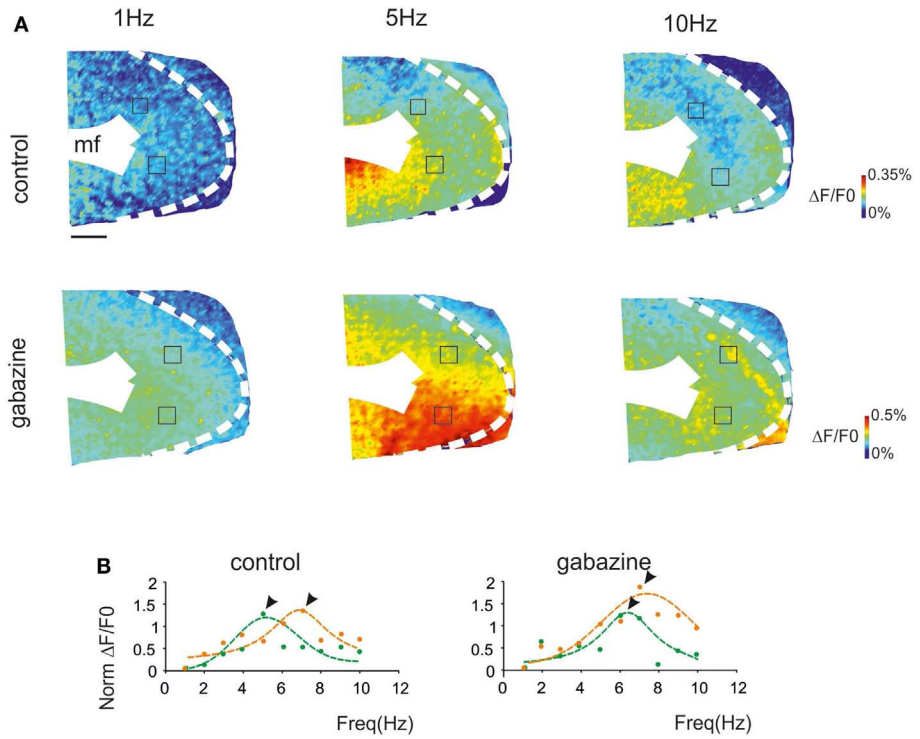

FIGURE 2 | The spatial distribution of resonance in the granular layer (GRL). (A) Optical maps of VSD responses in the GRL evoked by repeated bursts stimulation delivered to the mossy fibers bundle (mf) at three different frequencies. The VSD maps were generated by taking the maximum depolarization for each pixel both in control and after gabazine perfusion. Scale bar 100 μm. **(B)** The panels show the resonance curves corresponding to specific ROIs of the GRL indicated in **(A)** (squares). The data points show maximum responses either at 5 Hz (green) or 7 Hz (orange), both in control and after gabazine perfusion (arrowheads indicate points at the resonance frequency). Broken lines are single Lorentzian functions fitted to the points.

The maps clearly showed that the large majority of single pixel resonance frequencies were in the 5–7 Hz region. After gabazine application, RF appeared still concentrated at 5–7 Hz, although the area covered by 7 Hz RF became prevalent.

The average pattern of changes was evaluated by generating average resonance curves, which were constructed from all single pixel resonance curves in each of 11 slices (**Figure 3B**). The average resonance curve showed two sub-peaks at 5 Hz ($38.6 \pm 9.3\%$ increase vs. 1 Hz) and 7 Hz ($31.1 \pm 7.2\%$ increase vs. 1 Hz), which were both significantly higher than nearest neighbor points ($p < 0.05$, paired t-test). In the presence of gabazine, the average resonance curve increased compared to controls ($137.1 \pm 9.6\%$ increase; $p > 0.4$ t-test paired with nearest neighbors), with a maximum at 7 Hz (**Figure 3B**, right). In control, fittings yielded $RF_1 = 5.0 \pm 0.6$ and $RF_2 = 7.0 \pm 0.6$ with $y(RF_2)/y(RF_1) = 0.7$ ($R^2 = 0.92$; $\chi^2 = 0.04$). In the presence of gabazine, fittings yielded $RF_1 = 4.4 \pm 0.5$ and $RF_2 = 7.0 \pm 0.4$ with $y(RF_2)/y(RF_1) = 1.4$ ($R^2 = 0.99$; $\chi^2 = 0.006$). The ensemble changes caused by gabazine in the resonance curve were to increase the absolute size of the component peaking around 7 Hz and its relative weight with respect to that peaking around 5 Hz, similar to what observed in the LFP *in vivo*.

The extension of 5–7 Hz resonance in the GRL was assessed by counting the number of pixels with the same resonant frequency (**Figure 3C**). On average, 5 Hz resonance occurred in $23.4 \pm 4.7\%$ of the active area and 7 Hz resonance occurred in $13.4 \pm 2.9\%$ of the active area. Overall, the only significant peak was that at 5 Hz ($p < 0.01$; paired t-test with nearest neighbors), suggesting that this was the most represented resonant frequency. In the presence of gabazine, the amount of area showing resonance at 7 Hz was increased compared to that at 5 Hz with a single significant peak at 7 Hz ($31.7 \pm 5.8\%$ of active pixels; $p < 0.01$; paired t-test with nearest neighbors). In order to determine the origin of these differences, we measured resonance in individual pixels (evaluated using resonance amplitude, RA: see Materials and Methods), which showed similar amplitude in control and after gabazine perfusion ($p < 0.00005$, comparison of 50 pixels in control and after gabazine chosen at random). Therefore, since single pixel resonance was not significantly affected by gabazine (see above), the amplification of the resonance curve with gabazine was probably due to the increased area over which resonance occurred.

In aggregate, these results show that the cerebellar GRL in acute slices generates maximum responses when the input bursts conveyed through the mossy fibers are organized in theta-frequency range. The results closely resemble those obtained from LFPs *in vivo*, in that theta-frequency resonance persists but tends to increase at 7 Hz compared to 5 Hz after blocking inhibitory synaptic transmission.

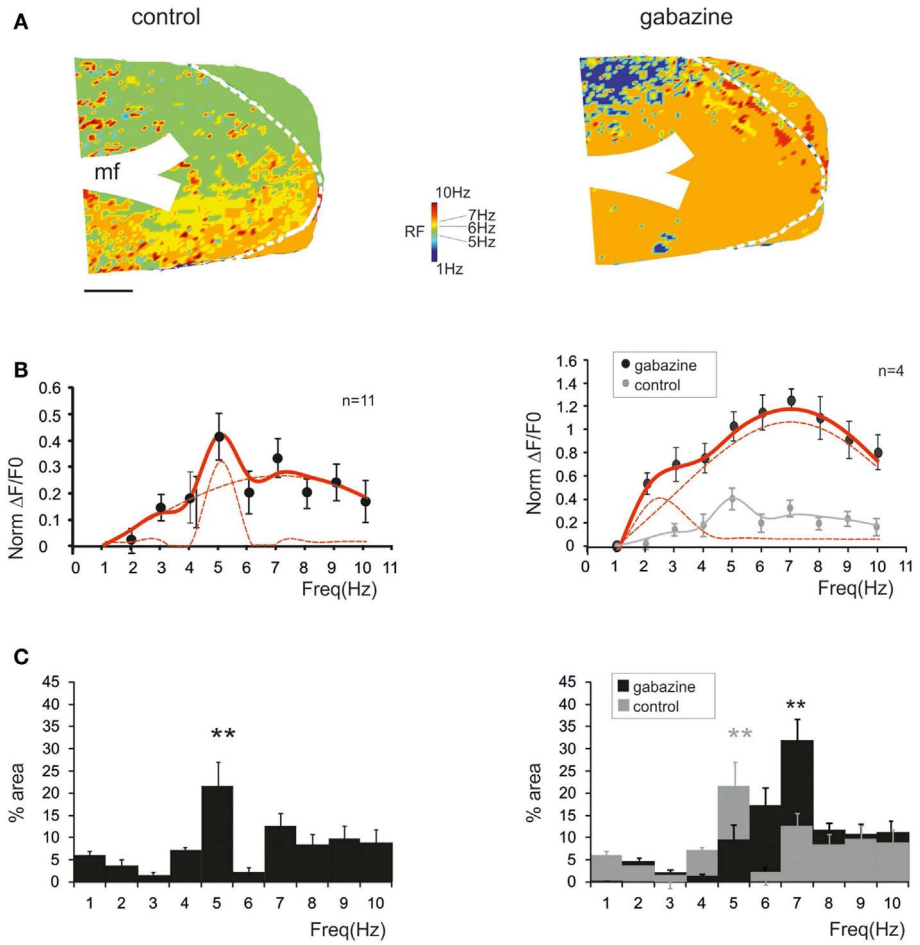

FIGURE 3 | Synaptic inhibition modulates granular layer (GRL) resonance. (A) The maps show the resonance frequency (RF) for each of GRL pixels before and after application of gabazine. The maps reveal a prevalence of areas showing resonance at 5 and 7 Hz and an increase of the 7 Hz area after gabazine. Scale bar 100 μm. **(B)** The resonance profiles obtained by all active GRL pixels and averaged over several recordings ($n = 11$ control and $n = 4$ gabazine) reveal statistically significant peaks in the 5–7 Hz range. The amplitude of the resonance plot increases after gabazine. **(C)** Histograms report the relative areas covered by each RF averaged over several recordings ($n = 11$ control and $n = 4$ gabazine). Note that the main peak in control occurs at 5 Hz but moves to 7 Hz in the presence of gabazine. Data are reported as mean ± SEM. Red lines fitting the data point represent double Lorentzian functions (broken lines are the two individual component functions) obtained on control and gabazine data, respectively.

RESONANT RESPONSES EVOKED IN SINGLE GRANULE CELLS BY PATTERNED SYNAPTIC ACTIVITY

In order to investigate the cellular basis of resonance in the GRL, we performed whole-cell recordings from granule cells in acute cerebellar slices. The granule cells, which showed high input resistance ($R_{in} =$ of 2.2 ± 0.3 GΩ $n = 18$) and low membrane capacitance ($C_m = 3.9 \pm 0.2$ *p*F, $n = 18$), generated repeated spike discharge upon depolarizing current injection (D'Angelo et al., 1995, 2001) (**Figure 4A**, inset). The granule cells were maintained at a holding potential between −60 and −70 mV, from which mossy fiber low-frequency stimulation could elicit spikes in <50% of responses. Then, high-frequency burst patterns were repeated between 1 and 10 Hz in random order and the modifications in synaptic excitation were analyzed (**Figure 4A**; *left*).

In most recordings ($n = 7$), at 5–7 Hz, the burst depolarization increased along with the probability of generating spikes, which also became more precise and occurred with shorter delay (**Figure 4A**; *left*). In order to obtain an estimate of resonance from these measurements we calculated the RI (see Materials and Methods for definition) through the combination of the following parameters: spikes count (*sc*), first spike delay (*sd*), first spike SD (*ssd*), and average maximum depolarization (*amd*). It should be noted that these parameters are strongly correlated, so a stronger depolarization commonly elicited stronger spiking and shorter latency of the First spike (absolute values for *sc* and *ssd* are reported in **Figure 4A**, inset). Interestingly, RI/frequency plots for all the parameters (*sc, sd, ssd, amd*) showed a resonant shape and commonly peaked between 5 and 7 Hz (**Figure 4B**; *left*). The RIs were then summed to obtain a *compound RI* for each cell (**Figure 4C**, *left*). A similar analysis was performed in recordings in which gabazine was applied ($n = 7$). The granule cells became more excitable and made more spikes generating protracted discharges,

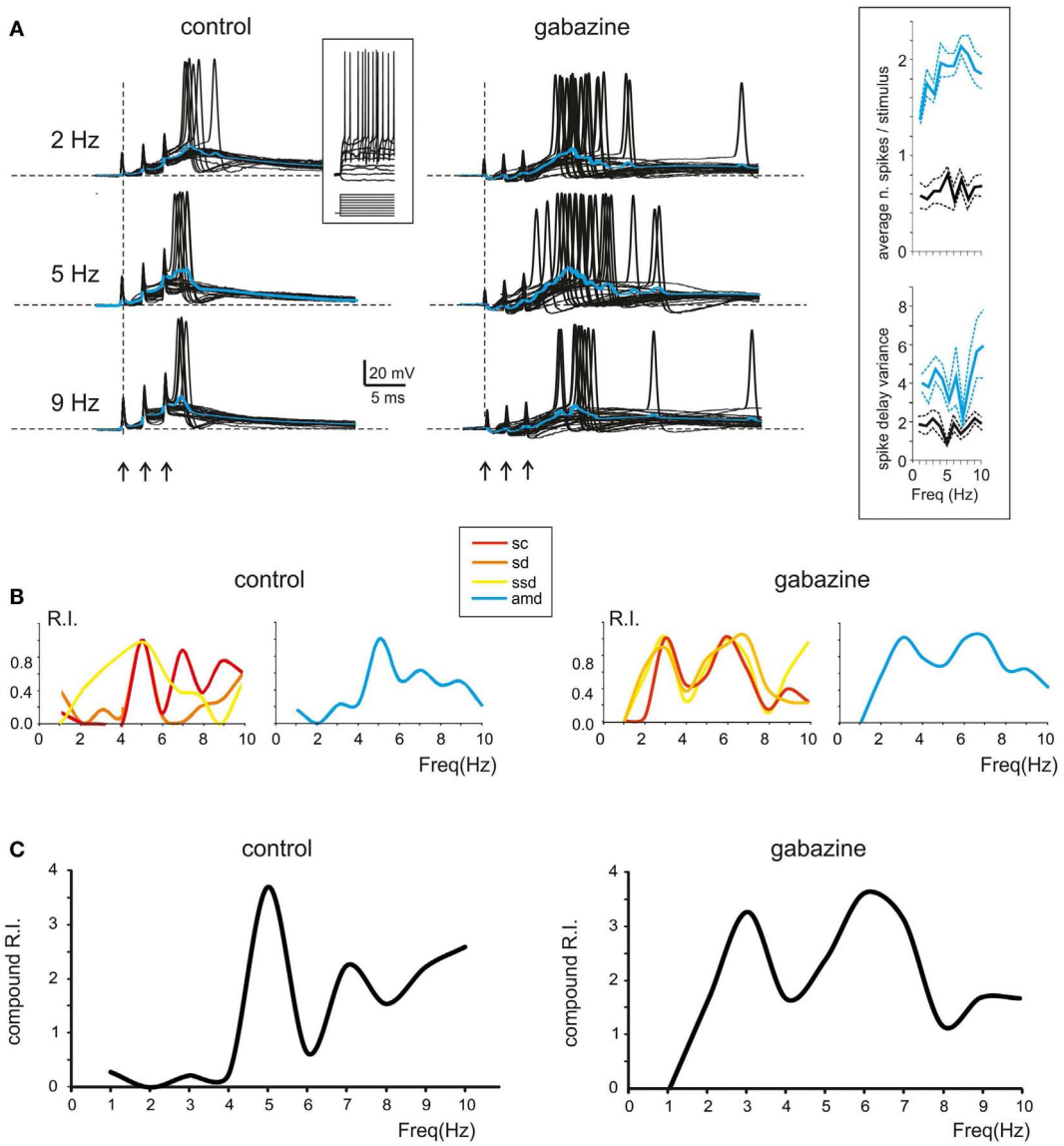

FIGURE 4 | Resonance in spike emission from single granule cells. **(A)** *Left*; Single sweeps from a single granule cell recorded in control solution are shown over imposed at three different frequencies (2, 5, 9 Hz). Note the increased number, shorter delay and higher precision of spikes at 5 Hz. Blue traces show the average depolarization. Note that maximum depolarization is obtained at 5 Hz. *Right;* Single sweeps from a single granule cell recorded in the presence of gabazine are shown over imposed at three different frequencies (2, 5, 9 Hz). Note the increased number, shorter delay, and higher precision of spikes at 5 Hz. Blue traces show the average depolarization. Note that maximum depolarization is obtained at 5 Hz. The inset in the middle shows granule cell responses elicited by 150 ms-2pA current steps. The inset on the right shows the spike count and the spike variance in control and after gabazine perfusion. **(B)** *Left*; In a single granule cell, the Resonance Index (RI) for individual parameters in control (*sc, ssd, sd, amd*) reveal peaks between 5 and 7 Hz. *Right*; In the presence of gabazine RI reveal peaks between 5 and 7 Hz **(C)** Compound RI in the same granule cell in control (*left*) and in the presence of gabazine (*right*).

but the resonance patterns remained unvaried. In most cases, the granule cells generated more spikes and the first spike occurred earlier and with higher precision around 5–7 Hz (**Figure 4A**; *right*) causing a higher maximum average depolarization at the same frequencies (**Figure 4A**; *right*). Accordingly, the RI/frequency plots showed main peaks at 5–7 Hz both for individual parameters (*sc, sd, ssd, amd*) (**Figure 4B**; *right*) and for the compound RI index (**Figure 4C**; *right*).

The probability of observing a given RF for each of the parameters (*sc, sd, ssd, amd*) is reported in **Figure 5A**, which shows that the maximum concentration of resonance frequencies occurs at 5–7 Hz, both in control and in the presence of gabazine. When the probability of occurrence were summed, a clear resonance curve peaking at 5–7 Hz was generated. Another way to represent the behavior of the granule cell population was to average their compound RIs. Also this average compound RI/frequency

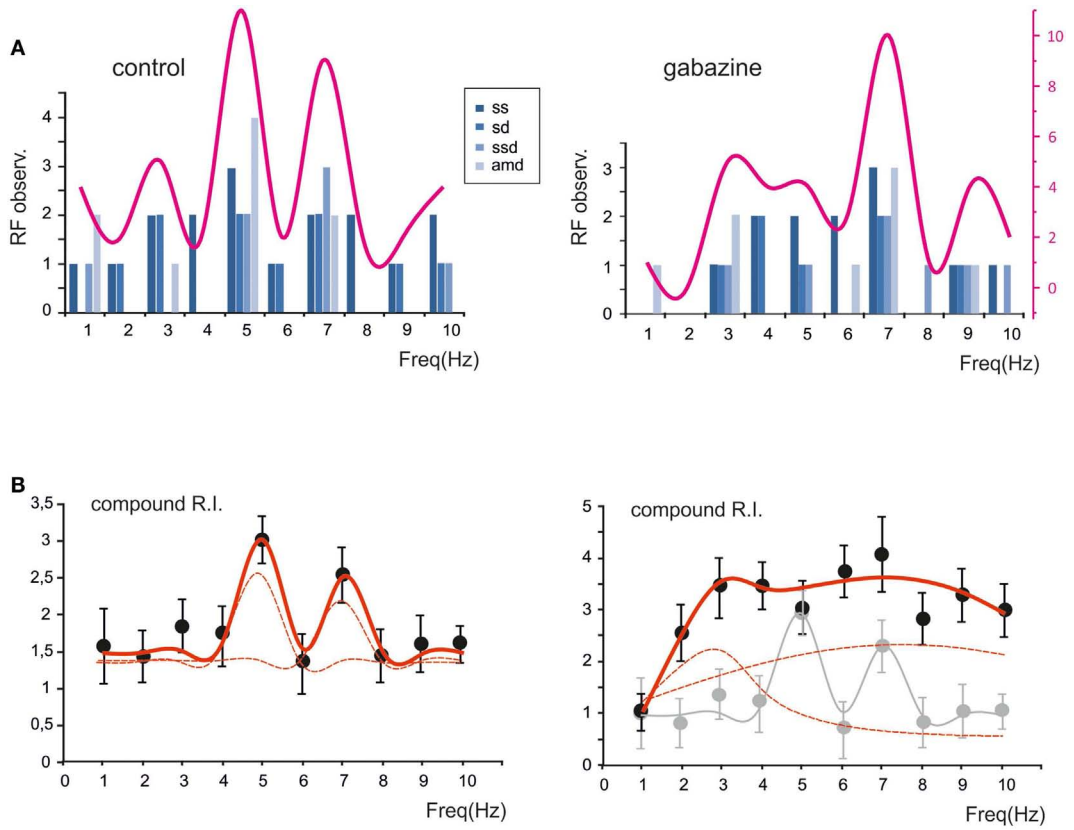

FIGURE 5 | The global effect of resonance on spike emission in the granular layer network. (A) The histogram shows, for each frequency, the probability of observing a certain RF for spike number, spike delay, spike standard deviation and maximum average depolarization ($n = 7$). The superimposed plots show, at each frequency, the sum of observations in individual parameters. Note peaks at 5–7 Hz. **(B)** The plot shows the compound resonance index (RI) calculated from all the neurons recorded in control and in the presence of gabazine. Note peaks at 5–7 Hz. Data are reported as mean ± SEM. Red lines fitting the data point represent double Lorentzian functions (broken lines are the two individual component functions) obtained on control and gabazine data, respectively.

curve showed major peaks at 5–7 Hz (**Figure 5B**). In control, fittings to these plots yielded: $RF_1 = 4.8 \pm 0.3$ and $RF_2 = 7.0 \pm 0.2$ with $y(RF_2)/y(RF_1) = 0.8$ ($R^2 = 0.93$; $\chi^2 = 0.06$). In the presence of gabazine, fittings yielded $RF_1 = 2.7 \pm 0.5$ and $RF_2 = 7.4 \pm 0.6$ with $y(RF_2)/y(RF_1) = 1.1$ ($R^2 = 0.86$; $\chi^2 = 0.1$). Thus, the resonance profile of the ensemble responses obtained from several single granule cells showed that, after the application of gabazine, the relative weight of the component peaking around 7 Hz increased with respect to that peaking around 5 Hz.

In summary, the ensemble of spike-related parameters in granule cells generated resonance compatible with that observed in global network measurements obtained with LFPs (cf. **Figure 1**) and VSD imaging (cf. **Figures 2–3**), suggesting that resonance can be traced to elementary cellular phenomena mostly residing in the granule cells.

MODELING GRANULAR LAYER RESONANCE

The mechanisms underlying circuit resonance were explored by performing simulations with a model derived from a previous large-scale network of the GRL (Solinas et al., 2010). The model included detailed realistic representations of granule cells and Golgi cells and the related synapses (D'Angelo et al., 2001; Nieus et al., 2006; Solinas et al., 2007a,b; Arleo et al., 2010). Similar to what observed experimentally (D'Angelo et al., 1995; Sola et al., 2004), the mossy fiber – granule cell synapses were endowed with stochastic neurotransmission mechanisms, so that simulated granule cell responses were affected by noise and showed jitter in spike generation (**Figure 6A**). Once subjected to input patterns identical to those used in whole-cell recordings, the granule cells in the model generated RI/frequency plots for the resonance parameters (*sc, sd, ssd, amd*) and for compound RI, with main peaks in the 5–7 Hz region (**Figure 6B**), both in control and when simulating the "gabazine" condition (phasic and tonic inhibition blocked; **Figure 6C**).

The granule cells in the model received all the basic combinations of excitatory and inhibitory connections occurring in the real network, amounting to just 20 different combinations (see **Table 1**). Indeed, an active granule cells receives 1–4 excitatory and 0–4 inhibitory synapses, on average (Solinas et al., 2010). The RI/frequency plots of resonance parameters (*sc, sd, ssd, amd*) for all the synaptic combinations are shown in **Figure 7A**. These plots reveal that, due to the different excitatory/inhibitory (E/I)

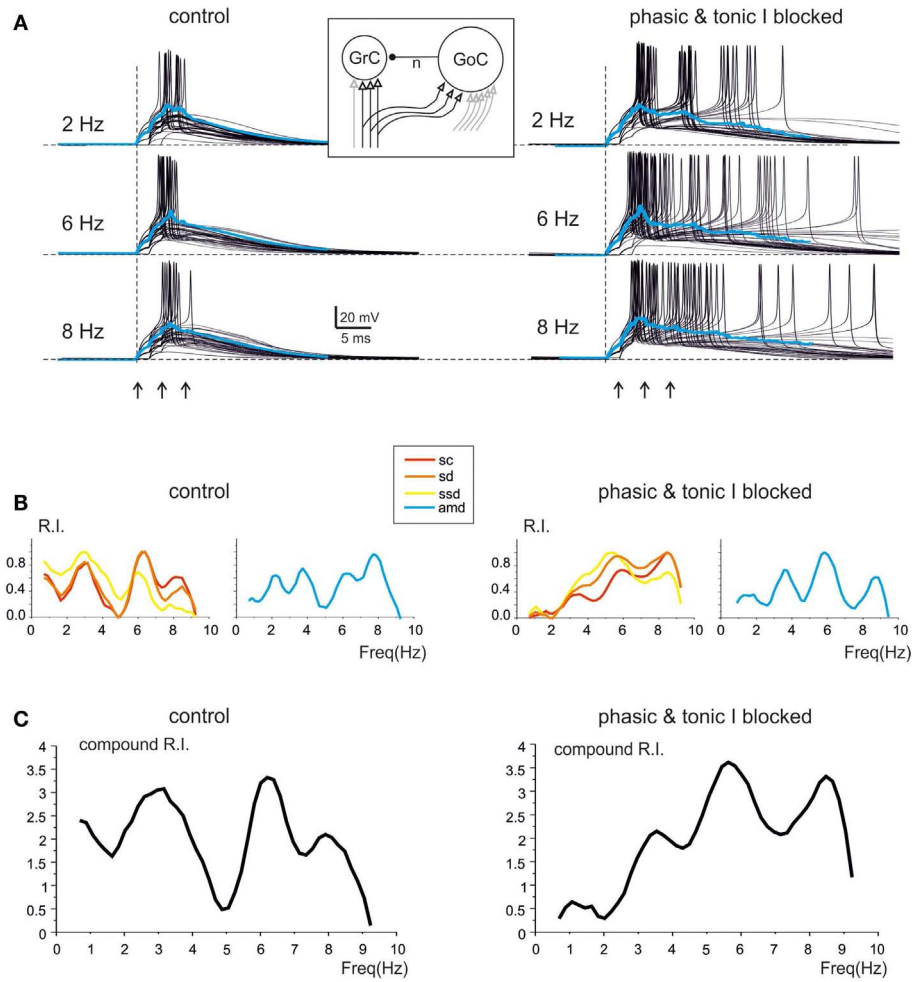

FIGURE 6 | Modeling resonance in spike emission from single granule cells. Resonance in a model granule cell embedded into the granular layer network model. The traces and plots on the left show the case of two excitatory and two inhibitory synapses and simulate a control experimental condition. The traces and plots on the right have two excitatory synapses, while tonic and phasic inhibition are blocked simulating experimental gabazine application. The mossy fibers in the model are activated with patterns homologous to those used for investigating resonance in acute cerebellar slices (3-spike bursts at 300 Hz repeated 50 times at frequencies ranging from 1 to 10 Hz in 0.5 Hz increments). The inset shows a schematic of the model, with afferent fibers carrying background only (gray) or background interrupted by the bursts (black). **(A)** The last 45 of 50 sweeps from a single granule cell in the network model are shown superimposed at three different frequencies. Note the increased number, shorter delay and higher precision of spikes at 6 Hz (control and inhibition blocked) compared to the other two frequencies. The average traces are shown superimposed in color. **(B)** In the same model granule cell as in **(A)**, the R.I. for individual parameters (left: *sc, ssd, sd*; right: *amd*) reveal peaks in the theta range. **(C)** Compound R.I. obtained from the data shown in **(B)**. Both in **(A,B)** the peak around 7 Hz is enhanced after blocking synaptic inhibition.

balance, individual granule cells do not show identical resonant properties, although the RI/frequency plots usually peak in the 5–7 Hz range. Interestingly, resonance was more marked (evaluated using resonance amplitude, RA: see Materials and Methods) and more precisely centered at 5–7 Hz for E/I ≤ 1 (**Figure 7B**). Moreover, when synaptic inhibition was blocked (either in the transient or both in the transient and tonic component), RF shifted toward 7 Hz. These observations provide a possible explanation for the variability in resonance properties of single granule cells measured in whole-cell recordings and suggest that GRL resonance emerges from the statistical distribution of microscopic parameters characterizing granule cells with different E/I.

In order to evaluate how the different E/I balance in granule cells influenced RF and RI/frequency plots, we determined the statistical distribution of these parameters (**Figure 8A**). The probability of observing a given RF for each of the resonance parameters (*sc, sd, ssd, amd*) is reported in **Figure 8A** for two different probability distributions. A uniform distribution, in which the probability of finding the different E/I balances is identical, was compared to the probability distribution reported by Diwakar et al. (2011) from the analysis of LFP recordings *in vivo* and VSD recordings in acute cerebellar slices. In both cases, the highest concentration of resonance parameters was observed at 5–7 Hz, with a higher peak using the Diwakar's distribution.

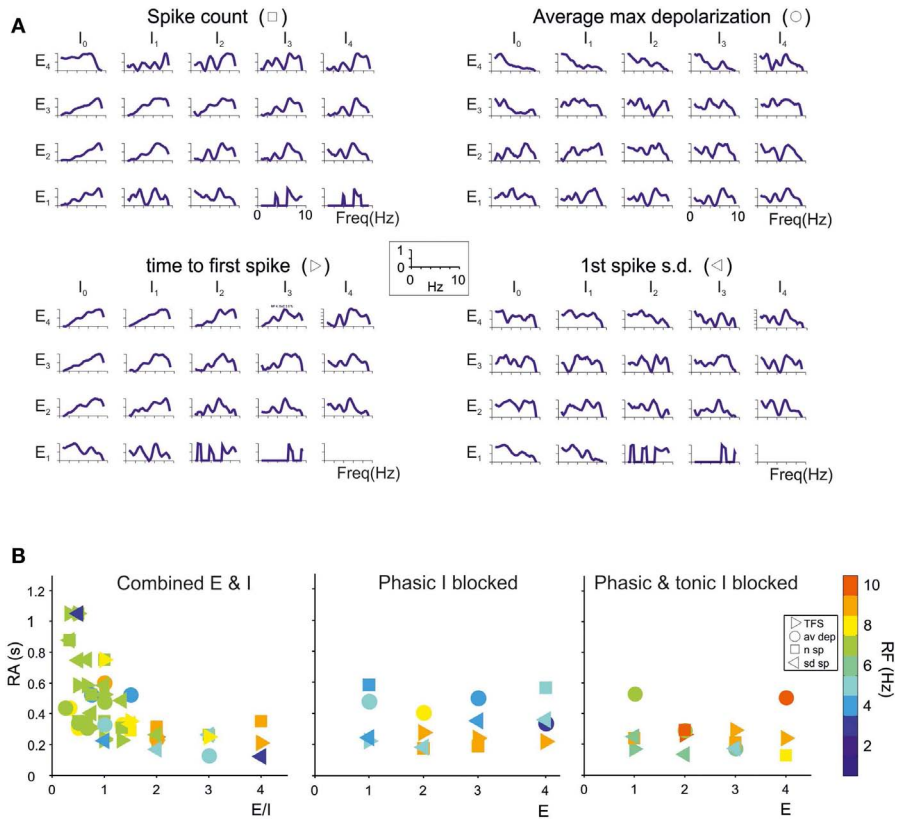

FIGURE 7 | Contribution of different E/I combinations to single-neuron resonance. The impact of the excitatory/inhibitory balance on resonance is shown for all *E*/*I* combinations, indicated as E_n/I_n (*n* is the number of synapses impinging on a given granule cell). Simulations were carried out as in Figure 7. **(A)** The effect of *E*/*I* combinations on RI for individual parameters (*sc, ssd, sd, amd*) are shown in the four panels. The columns I_0 correspond to absence of phasic inhibition. Note that peaks in the plots more often occur between 5 and 7 Hz. **(B)** The plots reports RA (defined in Materials and Methods) for individual parameters (*sc, ssd, sd, amd*) in the cases of coexistence of *E* and *I* (left), of phasic inhibition blocked (middle) or of both phasic and tonic inhibition blocked (right). For each point, RF is reported using a color code. Note that 5–7 Hz RF clusters are at $E/I \leq 1$ and correspond to the highest RA values, consistent with the enhancing effect of inhibition on resonance. Note also that, when both phasic and tonic inhibition are blocked, RF shifts toward higher values, as observed experimentally.

The behavior of the whole granule cell population was reconstructed by summating and averaging the compound RIs for a given statistical distribution of E/I combinations. The RI/frequency curve showed major peaks at 5–7 Hz, and the 7 Hz peak became dominant after blocking synaptic inhibition (**Figure 8B**). The reason of the enhanced effect of inhibition at 7 Hz compared to 5 Hz was analyzed by applying RI analysis to Golgi cells in the simulated network. In response to mossy fiber bursts, Golgi cells had a main resonance peakat around 6–7 Hz, thereby depressing the granule cell response more effectively at this specific frequency (**Figure 8B**).

MODEL PREDICTIONS OF THE CELLULAR MECHANISMS OF RESONANCE

Intrinsic granule cell resonance can be elicited by sinusoidal current injection depending on an *M*-like current (K_{slow}) and and A-current (KA) acting as "resonators" and a persistent Na current acting as "amplifier" (Hutcheon and Yarom, 2000; D'Angelo et al., 2001). In the present simulations, during repetitive burst transmission, K_{slow} was higher at high-frequency while KA was higher at low-frequency, so that the two current-frequency curves intersected and generated a minimum $K_{slow} + KA$ current at 5–7 Hz. At the same frequency, the persistent Na currents (Nap) and the NMDA current showed enhanced activation. The combined effect was that of generating a surplus of 2 pA in the 5–7 Hz range (**Figure 9A**). It should be noted that, over the high input resistance of granule cells (in the Giga-ohm range), a 2 pA current is indeed capable of causing a substantial enhancement in membrane depolarization and spike generation, as shown in previous studies (D'Angelo et al., 2001).

The time-course of K_{slow} and KA currents is shown in **Figure 9B**. While K_{slow} accumulated as the frequency of stimulation increased toward 10 Hz, KA decreased toward 10 Hz. The summed current was maximal at 5–7 Hz, just at the time of granule cell spike burst generation. The mechanism of frequency-dependence of K_{slow} and KA is analyzed in **Figure 9B**. K_{slow} activated slowly with time constants in the 100 ms range and therefore benefited of short inter-burst intervals. Conversely, KA inactivated rapidly with time constants in the 10 ms range and then

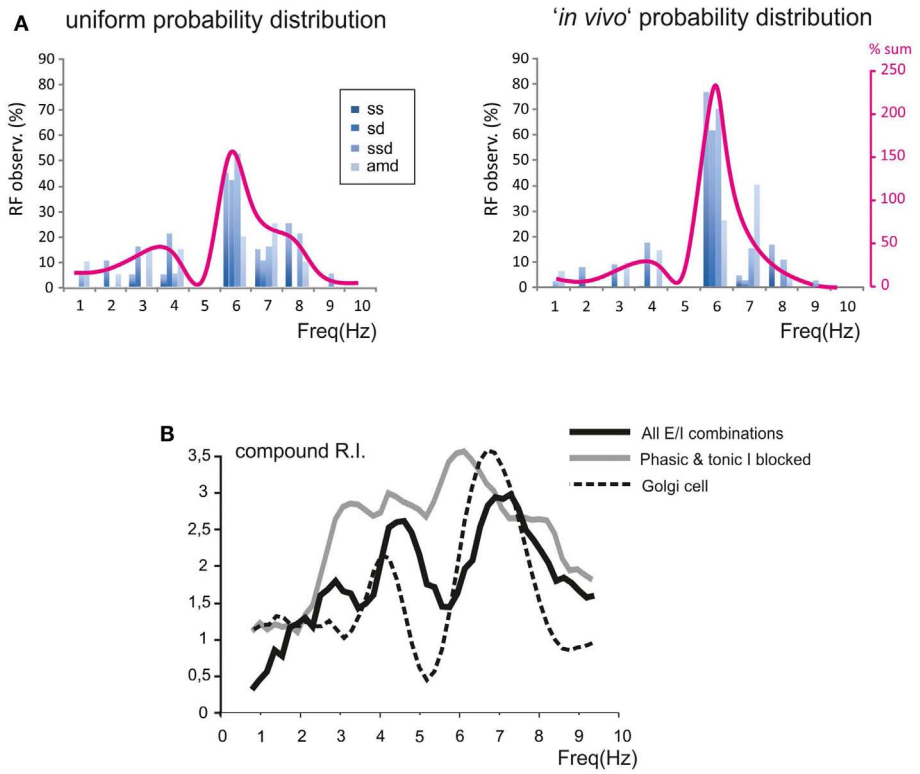

FIGURE 8 | Modeling the global effect of resonance on spike emission in the granular layer (GRL) network. The global effect of resonance on spike emission in the GRL network has been modeled using different proportional contributions of granule cells with respect to their *E*/*I* balance. **(A)** The histograms show, for each frequency, the probability of observing a certain RF for individual parameters (*sc, ssd, sd, amd*). The superimposed plots show, at each frequency, the sum of observations in individual parameters. Note peaks at 5–7 Hz as in experimental recordings. In the histogram on the left we assumed a uniform probability distribution of *E*/*I* combinations. In the plot on the right we assumed the probability *E*/*I* distribution derived from Diwakar et al. (2011) *in vivo*. **(B)** The plot shows the compound RI calculated from model simulations using the *E*/*I* distribution derived from Diwakar et al. (2011) either including all E/I combinations (black trace) or with phasic and tonic inhibition blocked (gray trace; gabazine effect). Note the similarity of RI plots to those observed experimentally. The compound RI of a Golgi cell in the network (dashed trace) shows a major peak at 6–7 Hz, explaining why inhibition block enhances RI at the same frequencies.

took time to de-inactivate, so that KA benefited of long inter-burst intervals. The gating properties of K_{slow} and KA were therefore mechanistically correlated with generation of resonance in granule cells during mossy fiber burst transmission.

DISCUSSION

Following recognition of the role of oscillations and resonance as fundamental aspects of neuronal communication in the brain (Llinas, 1988; Buzsaki, 2006), their phenomenological properties and mechanisms have remained unclear in several circuits. This paper demonstrates that the cerebellum GRL, once activated with periodic inputs, shows resonance at 5–7 Hz. Resonance was manifest both *in vivo* following sensory stimulation with air puffs delivered to the whisker pad and in acute cerebellar slices following electrical stimulation with short bursts delivered to the mossy fiber bundle. Resonance was modified but persisted after blocking inhibitory synaptic transmission. Thus, theta-frequency resonance largely depended on intrinsic properties of the neurons involved (Hutcheon and Yarom, 2000). Interestingly, resonance was expressed by a change in the composition of spike bursts emitted by granule cells with a modulation of spike timing on the millisecond time-scale. Therefore, GRL resonance could recode with millisecond precision the theta-bursts at the input into new bursts at the output.

GENERAL PROPERTIES OF GRANULAR LAYER RESONANCE: THE RELATIONSHIP WITH CIRCUIT INHIBITION

A striking property of GRL resonance evoked by theta-frequency patterns is that it has almost identical RF and gabazine sensitivity *in vivo* and *in vitro*. Resonance *in vivo* and *in vitro* are mechanistically correlated since each sensory stimulus generates a short high-frequency burst in mossy fibers (Chadderton et al., 2004; Rancz et al., 2007), so that the theta-frequency sensory volley is mimicked by theta-frequency stimulation of the mossy fiber bursts (Roggeri et al., 2008). This suggests that resonance observed *in vivo* is almost entirely generated in the GRL circuit rather than in the up-stream sensory pathway passing through the trigeminal nucleus (De Zeeuw et al., 1996). Also cerebro-cortical components were excluded, since the present analysis concerned only the trigeminal T wave of the cerebellar LFP (Morissette and Bower, 1996).

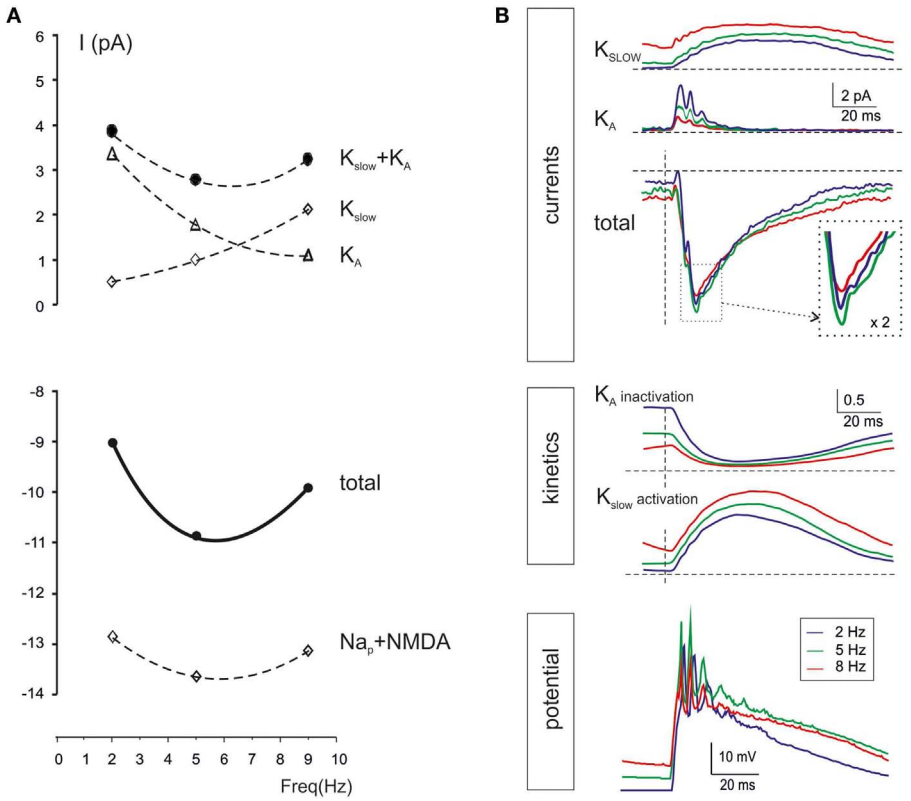

FIGURE 9 | Ionic mechanisms controlling single-neuron resonance. The ionic mechanisms controlling single granule cell resonance in response to patterned synaptic activity were analyzed in simulations on the E_2/I_1 combination. **(A)** The values of currents generated by K_{slow}, KA, Nap, and NMDA channels in response to simulated granule cells bursts were measured 20 ms after burst activation at three selected frequencies (2, 5, and 9 Hz). While i_{KA} decreases, $i\,K_{slow}$ increases with frequency, so that $i_{KA} + i_K slow$ has a minimum at around 5 Hz. The i_{Na} and i_{NMDA} increase at 5 Hz, so that a net inward current of about 2 pA is generated at 5 Hz. **(B)** The plot on *top* shows i_{KA} and $i_K slow$ during simulated granule cells bursts delivered at frequencies of 2, 5, and 9 Hz. Note the enhancement of the total current at 5 Hz. The plots in the *middle* show the kinetics of K_{slow} activation and KA inactivation. Note that K_{slow} accumulated activation with frequency, whereas KA accumulates inactivation with frequency, explain the global resonant effect of their combination. The *bottom* tracings show membrane potential at the three different frequencies. All traces are taken from the simulations with two active excitatory and inhibitory synapses (average of 25 of 30 consecutive traces, the first 5 excluded).

Both in LFPs *in vivo* and in VSD and whole-cell recordings in slices, the application of gabazine, a GABA-A receptor antagonist, to block inhibitory transmission between Golgi cells and granule cells did not suppress resonance but rather enhanced its component at 7 Hz. In general, GRL resonance was appropriately described by two components peaking at 5 and 7 Hz, and the 7 Hz peak prevailed when inhibitory transmission was blocked. In simulations, the Golgi cell showed maximum activity at 6–7 Hz, suggesting that the inhibitory circuit was indeed more effective at this particular frequency. It is thus possible that areas with 7 Hz resonance correspond to circuit regions that are less strongly inhibited than those with 5 Hz resonance. Double resonance peaks have been reported in the inferior olive, where the relative weight of the higher frequency peak is also depressed by synaptic inhibition (Llinas and Yarom, 1986). It could therefore be that in these circuits the inhibitory circuit has a modulatory role on resonance occurring along the main transmission pathway. Double resonance was also observed in cortical neurons, but in that case one peak was in the theta and one in the gamma band (Cobb et al., 1995). The inhibitory circuit passing through the cerebellar glomerulus also involves GABA-B receptors. Although a potential role of GABA-B receptors in GRL resonance remains unknown, it should be noted that GABA-B receptors down-regulate GABA-A receptor-mediated transmission at the Golgi cell – granule cell synapse [both by reducing GABA release (Mapelli et al., 2009) and postsynaptic receptor activation (Brandalise et al., 2012)] and enhance granule cell intrinsic excitability [by reducing an inward rectifier current (Rossi et al., 2006)]. At present, a major contribution of GABA-B receptors to resonance is therefore improbable.

GRANULAR LAYER RESONANCE EMERGES FROM MILLISECOND CONTROL OF SPIKE TIMING

Single cell analysis revealed that resonance in LFP and VSD recordings reflects the microscopic nature of spike generation in granule cells. At the RF, the granule cells showed higher probability of emitting spikes, which occurred with higher precision and shorter delay, resulting in a larger average depolarization. Since the LFP in the GRL is mostly due to extracellular spike currents (Diwakar et al., 2011), a higher probability of generating

spikes and a higher synchrony of the spikes could well explain LFP resonance. As far as the VSD signal is concerned, since this technique is currently unable to precisely measure individual spikes, VSD resonance was more probably correlated with average cell depolarization.

PREDICTION OF RESONANCE MECHANISMS USING REALISTIC COMPUTATIONAL MODELING

The mechanisms of granule cell resonance during synaptic transmission were explored using a realistic computational models of the GRL circuit. The model, faithfully reproduced all macroscopic properties of resonance, including RF at 5–7 Hz and the shift toward 7 Hz caused by inhibition blockage. At the microscopic level, the model showed that resonance properties depended from the combination of single cell components in a statistically distribute manner and that the specific combination of excitatory and inhibitory synapses activating granule cells *in vivo* was especially effective in generating resonance in ensemble network activities. In the model, intrinsic granule cell resonance emerged from the interplay of K_{slow} and KA causing a minimum repolarizing current at 5–7 Hz. However, opposite to the case of sinusoidal current injection (D'Angelo et al., 2001), K_{slow} prevailed at higher frequencies while KA prevailed at lower frequencies. This happened because, different from sinusoidal currents, the bursts have fixed duration and what determines the frequency-dependence of channel activation and inactivation is the inter-burst interval. Thus, in subsequent bursts, K_{slow} (Hu et al., 2002) accumulated activation while KA accumulated inactivation. Granule cell resonance was amplified by the persistent Na current (Hu et al., 2002) and by voltage-dependent unblock of the NMDA current in the just-subthreshold region, which enhanced EPSP-spike coupling (D'Angelo et al., 1995; Mapelli and D'Angelo, 2007). As already pointed out (D'Angelo et al., 2001) It should be noted that, due to the high input resistance of granule cells, currents of just a few picoamperes in the threshold region resulted in significant effects on membrane depolarization and spike generation.

RESONANCE AND OSCILLATIONS IN THE GRANULAR LAYER

Resonance is a condition occurring when a physical system undergoes a periodic activation with a frequency equal or close to the intrinsic oscillation frequency of the system itself, so that such a system tends to oscillate at its maximum amplitude. The nature of oscillations and resonance depends on the physical details of the system involved. So, what is the relationship between resonance and oscillations in the GRL? Theta-frequency oscillations are observed in the GRL during resting activity in the awake rat and monkey (Pellerin and Lamarre, 1997; Hartmann and Bower, 1998; Courtemanche et al., 2009). Computational analysis indicates that these oscillations require an intact feed-back inhibitory loop (Maex and De Schutter, 1998; Solinas et al., 2010). Conversely, as we report here, GRL resonance reflects intrinsic properties of granule cells. Finally, resonance and oscillations in the inhibitory interneuron network require gap-junctions between Golgi cells and other network components (Forti et al., 2006; Dugue et al., 2009) and possibly also intrinsic pacemaking in Golgi cells and other network components (Forti et al., 2006; Galliano et al., 2013). Thus, the circuit appears to be composed of two sub-systems, a resonator (the mossy fiber – granule cell synapse) coupled to a resonant oscillator (the Golgi cell inhibitory network). This latter also provides synchronicity through lateral inhibition and can enhance resonance in the granule cell population. In aggregate, resonance can amplify the granule cell output when the mossy fiber input is conveyed at 5–7 Hz. At this frequency the inhibitory circuit can spontaneously oscillate, thereby creating a condition at which the system can optimize phase locking and information transmission.

As pointed out above, by demonstrating similar resonance properties *in vivo* and *in vitro*, our results suggest that the major resonance mechanisms revealed by whisker pad stimulation reside in the GRL network. Indeed, the mossy fiber bursts evoked by eye-movements (Kase et al., 1980) correlate strictly with the sensory stimulus without any dependence on the phase or duration of the stimulus pattern. Nonetheless, the neuronal networks providing inputs to the GRL and even the whiskers might also present forms of resonance. For example, the thalamo-cortical circuit operates on a low-frequency bandwidth during whisking (Ahissar et al., 2000; Szwed et al., 2003; Kleinfeld et al., 2006) and both vibrissal motoneurons (Harish and Golomb, 2010) and trigeminal neurons (Wu et al., 2001) show forms of low-frequency oscillations and resonance. Therefore, low-frequency resonance in the cerebellar circuit is probably part of a resonant system distributed over the different nodes of the sensorimotor network controlling whisking. It should also be noted that mechanical resonance of vibrissae occurs at high-frequency and is probably relevant for detecting sharp changes in objects surface like edges or irregularities (Hartmann et al., 2003).

CONCLUSIONS AND FUNCTIONAL IMPLICATIONS

Granular layer network resonance, by reflecting millisecond regulation in spike emission, could fully exploit the outstanding timing capabilities of granule cells (Cathala et al., 2003; D'Angelo and De Zeeuw, 2009; Diwakar et al., 2009, 2011) and fine-tune information transfer (Arleo et al., 2010). One potential implication of GRL resonance is that, by occurring on the same band of Purkinje cell and inferior olive oscillations (Llinas and Yarom, 1986; Welsh et al., 1995; Lang et al., 2006; Abrams et al., 2012), could help maintaining a high level of coherence in the activity of the whole olivo-cerebellar system. On a larger scale, the cerebellum could be optimally designed to detect information carried by cerebro-cortical theta cycles implementing a well-tuned transmitter – receiver system (D'Angelo et al., 2009). For example, motor commands for whisking are emitted at theta-rhythm entraining the thalamo-cortical circuit (Szwed et al., 2003) and the cerebellum (O'Connor et al., 2002; Lang et al., 2006) providing the basis for complex resonant loops. Since oscillations in the GRL and in the Purinje cell – inferior olive circuits are tunable between 5 and 20 Hz (i.e., beyond the theta-band), the 5–7 Hz resonance reported here may be restricted to specific aspects of behavior. A hint comes from the specific sensitivity of the GRL to theta-bursts conveyed through sensory and cortical inputs, which can induce long-term synaptic plasticity in the cerebellum (Roggeri et al., 2008; Diwakar

et al., 2011) as well as in the cortex and hippocampus (Larson and Lynch, 1988; Huerta and Lisman, 1995). An intriguing hypothesis is that resonance may improve learning of salient patterns in relation to voluntary movement (Gross et al., 2005; Schnitzler et al., 2006), attention and sleep, in which theta activity prevails.

AUTHOR CONTRIBUTIONS

D. Gandolfi and J. Mapelli performed the imaging recordings and data analysis, P. Lombardo performed electrophysiological recordings and data analysis, S. Solinas performed computational simulations, J. Mapelli and S. Solinas contributed to write the work, E. D'Angelo coordinated the work and wrote the final version of the manuscript.

ACKNOWLEDGMENTS

This work was supported by the European Union (CEREBNET FP7-ITN238686, REALNET FP7-ICT270434), by grants of the Italian Ministry of Health to E. D'Angelo (RF-2008-1143418 and RF-2009- 1475845) and S. Solinas (GR-2009-1493804) and by a CASPUR grant for high performance computing to S. Solinas (std12-046). We thank G. Ferrari and M. Rossin for technical support.

REFERENCES

Abrams, Z. R., Warrier, A., Wang, Y., Trauner, D., and Zhang, X. (2012). Tunable oscillations in the Purkinje neuron. *Phys. Rev. E Stat. Nonlin. Soft. Matter. Phys.* 85, 041905.

Ahissar, E., Sosnik, R., and Haidarliu, S. (2000). Transformation from temporal to rate coding in a somatosensory thalamocortical pathway. *Nature* 406, 302–306.

Arleo, A., Nieus, T., Bezzi, M., D'Errico, A., D'Angelo, E., and Coenen, O. J. (2010). How synaptic release probability shapes neuronal transmission: information-theoretic analysis in a cerebellar granule cell. *Neural Comput.* 22, 2031–2058.

Bower, J. M., and Woolston, D. C. (1983). Congruence of spatial organization of tactile projections to granule cell and Purkinje cell layers of cerebellar hemispheres of the albino rat: vertical organization of cerebellar cortex. *J. Neurophysiol.* 49, 745–766.

Brandalise, F., Mapelli, L., Gerber, U., and Rossi, P. (2012). Golgi cell-mediated activation of postsynaptic GABA_B receptors induces disinhibition of the Golgi cell-granule cell synapse in rat cerebellum. *PLoS ONE* 7:e43417. doi:10.1371/journal.pone.0043417

Buzsaki, G. (2006). *Rhythms of The Brain.* New York: Oxford University Press.

Cathala, L., Brickley, S., Cull-Candy, S., and Farrant, M. (2003). Maturation of EPSCs and intrinsic membrane properties enhances precision at a cerebellar synapse. *J. Neurosci.* 23, 6074–6085.

Chadderton, P., Margrie, T. W., and Hausser, M. (2004). Integration of quanta in cerebellar granule cells during sensory processing. *Nature* 428, 856–860.

Cobb, S. R., Buhl, E. H., Halasy, K., Paulsen, O., and Somogy, P. (1995). Synchronization of neuronal activity in hippocampus by individual GABAergic interneurons. *Nature* 378, 75–78.

Courtemanche, R., Chabaud, P., and Lamarre, Y. (2009). Synchronization in primate cerebellar granule cell layer local field potentials: basic anisotropy and dynamic changes during active expectancy. *Front. Cell. Neurosci.* 3:6. doi:10.3389/neuro.03.006.2009

D'Angelo, E., De Filippi, G., Rossi, P., and Taglietti, V. (1995). Synaptic excitation of individual rat cerebellar granule cells in situ: evidence for the role of NMDA receptors. *J. Physiol. (Lond.)* 484(Pt 2), 397–413.

D'Angelo, E., and De Zeeuw, C. I. (2009). Timing and plasticity in the cerebellum: focus on the granular layer. *Trends Neurosci.* 32, 30–40.

D'Angelo, E., Koekkoek, S. K., Lombardo, P., Solinas, S., Ros, E., Garrido, J., et al. (2009). Timing in the cerebellum: oscillations and resonance in the granular layer. *Neuroscience* 162, 805–815.

D'Angelo, E., Nieus, T., Maffei, A., Armano, S., Rossi, P., Taglietti, V., et al. (2001). Theta-frequency bursting and resonance in cerebellar granule cells: experimental evidence and modeling of a slow K^+-dependent mechanism. *J. Neurosci.* 21, 759–770.

D'Angelo, E., Rossi, P., and Taglietti, V. (1993). Different proportions of N-methyl-D-aspartate and non-*N*-methyl-D-aspartate receptor currents at the mossy fibre-granule cell synapse of developing rat cerebellum. *Neuroscience* 53, 121–130.

De Zeeuw, C. I., Lang, E. J., Sugihara, I., Ruigrok, T. J., Eisenman, L. M., Mugnaini, E., et al. (1996). Morphological correlates of bilateral synchrony in the rat cerebellar cortex. *J. Neurosci.* 16, 3412–3426.

D'Errico, A., Prestori, F., and D'Angelo, E. (2009). Differential induction of bidirectional long-term changes in neurotransmitter release by frequency-coded patterns at the cerebellar input. *J. Physiol. (Lond.)* 587, 5843–5857.

Diwakar, S., Lombardo, P., Solinas, S., Naldi, G., and D'Angelo, E. (2011). Local field potential modeling predicts dense activation in cerebellar granule cells clusters under LTP and LTD control. *PLoS ONE* 6:e21928. doi:10.1371/journal.pone.0021928

Diwakar, S., Magistretti, J., Goldfarb, M., Naldi, G., and D'Angelo, E. (2009). Axonal Na^+ channels ensure fast spike activation and back-propagation in cerebellar granule cells. *J. Neurophysiol.* 101, 519–532.

Dugue, G. P., Brunel, N., Hakim, V., Schwartz, E., Chat, M., Levesque, M., et al. (2009). Electrical coupling mediates tunable low-frequency oscillations and resonance in the cerebellar Golgi cell network. *Neuron* 61, 126–139.

Forti, L., Cesana, E., Mapelli, J., and D'Angelo, E. (2006). Ionic mechanisms of autorhythmic firing in rat cerebellar Golgi cells. *J. Physiol. (Lond.)* 574, 711–729.

Galliano, E., Baratella, M., Sgritta, M., Ruigrok, T. J. H., Haasdijk, E. D., Hoebeek, F. E., et al. (2013). Anatomical investigation of potential contacts between climbing fibers and cerebellar Golgi cells in the mouse. *Front. Neural Circuits* (in press).

Gross, J., Pollok, B., Dirks, M., Timmermann, L., Butz, M., and Schnitzler, A. (2005). Task-dependent oscillations during unimanual and bimanual movements in the human primary motor cortex and SMA studied with magnetoencephalography. *Neuroimage* 26, 91–98.

Harish, O., and Golomb, D. (2010). Control of the firing patterns of vibrissa motoneurons by modulatory and phasic synaptic inputs: a modeling study. *J. Neurophysiol.* 103, 2684–2699.

Hartmann, M. J., and Bower, J. M. (1998). Oscillatory activity in the cerebellar hemispheres of unrestrained rats. *J. Neurophysiol.* 80, 1598–1604.

Hartmann, M. J., Johnson, N. J., Towal, R. B., and Assad, C. (2003). Mechanical characteristics of rat vibrissae: resonant frequencies and damping in isolated whiskers and in the awake behaving animal. *J. Neurosci.* 23, 6510–6519.

Hu, H., Vervaeke, K., and Storm, J. F. (2002). Two forms of electrical resonance at theta frequencies, generated by M-current, h-current and persistent Na^+ current in rat hippocampal pyramidal cells. *J. Physiol. (Lond.)* 545, 783–805.

Huerta, P. T., and Lisman, J. E. (1995). Bidirectional synaptic plasticity induced by a single burst during cholinergic theta oscillation in CA1 in vitro. *Neuron* 15, 1053–1063.

Hutcheon, B., and Yarom, Y. (2000). Resonance, oscillation and the intrinsic frequency preferences of neurons. *Trends Neurosci.* 23, 216–222.

Kase, M., Miller, D. C., and Noda, H. (1980). Discharges of Purkinje cells and mossy fibres in the cerebellar vermis of the monkey during saccadic eye movements and fixation. *J. Physiol. (Lond.)* 300, 539–555.

Kleinfeld, D., Ahissar, E., and Diamond, M. E. (2006). Active sensation: insights from the rodent vibrissa sensorimotor system. *Curr. Opin. Neurobiol.* 16, 435–444.

Lang, E. J., Sugihara, I., and Llinas, R. (2006). Olivocerebellar modulation of motor cortex ability to generate vibrissal movements in rat. *J. Physiol. (Lond.)* 571, 101–120.

Larson, J., and Lynch, G. (1988). Role of *N*-methyl-D-aspartate receptors in the induction of synaptic potentiation by burst stimulation patterned after the hippocampal theta-rhythm. *Brain Res.* 441, 111–118.

Llinas, R., and Yarom, Y. (1986). Oscillatory properties of guinea-pig inferior olivary neurones and their pharmacological modulation: an in-vitro study. *J. Physiol. (Lond.)* 376, 163–182.

Llinas, R. R. (1988). The intrinsic electrophysiological properties of mammalian neurons: insights into central nervous system function. *Science* 242, 1654–1664.

Lu, H., Hartmann, M. J., and Bower, J. M. (2005). Correlations between purkinje cell single-unit activity and simultaneously recorded field potentials in the immediately underlying granule cell layer. *J. Neurophysiol.* 94, 1849–1860.

Maex, R., and De Schutter, E. (1998). Synchronization of Golgi and granule cell firing in a detailed network model of the cerebellar granule cell layer. *J. Neurophysiol.* 80, 2521–2537.

Mapelli, J., and D'Angelo, E. (2007). The spatial organization of long-term synaptic plasticity at the input stage of cerebellum. *J. Neurosci.* 27, 1285–1296.

Mapelli, J., Gandolfi, D., and D'Angelo, E. (2010a). High-pass filtering and dynamic gain regulation enhance vertical bursts transmission along the mossy fiber pathway of cerebellum. *Front. Cell. Neurosci.* 4:14. doi:10.3389/fncel.2010.00014

Mapelli, J., Gandolfi, D., and D'Angelo, E. (2010b). Combinatorial responses controlled by synaptic inhibition in the cerebellum granular layer. *J. Neurophysiol.* 103, 250–261.

Mapelli, L., Rossi, P., Nieus, T., and D'Angelo, E. (2009). Tonic activation of GABA(B) receptors reduces release probability at inhibitory connections in the cerebellar glomerulus. *J. Neurophysiol.* 101, 3089–3099.

Marshall, S. P., and Lang, E. J. (2004). Inferior olive oscillations gate transmission of motor cortical activity to the cerebellum. *J. Neurosci.* 24, 11356–11367.

Mathy, A., Ho, S. S., Davie, J. T., Duguid, I. C., Clark, B. A., and Hausser, M. (2009). Encoding of oscillations by axonal bursts in inferior olive neurons. *Neuron* 62, 388–399.

Morissette, J., and Bower, J. M. (1996). Contribution of somatosensory cortex to responses in the rat cerebellar granule cell layer following peripheral tactile stimulation. *Exp. Brain Res.* 109, 240–250.

Nieus, T., Sola, E., Mapelli, J., Saftenku, E., Rossi, P., and D'Angelo, E. (2006). LTP regulates burst initiation and frequency at mossy fiber-granule cell synapses of rat cerebellum: experimental observations and theoretical predictions. *J. Neurophysiol.* 95, 686–699.

O'Connor, S. M., Berg, R. W., and Kleinfeld, D. (2002). Coherent electrical activity between vibrissa sensory areas of cerebellum and neocortex is enhanced during free whisking. *J. Neurophysiol.* 87, 2137–2148.

Pellerin, J. P., and Lamarre, Y. (1997). Local field potential oscillations in primate cerebellar cortex during voluntary movement. *J. Neurophysiol.* 78, 3502–3507.

Rancz, E. A., and Hausser, M. (2006). Dendritic calcium spikes are tunable triggers of cannabinoid release and short-term synaptic plasticity in cerebellar Purkinje neurons. *J. Neurosci.* 26, 5428–5437.

Rancz, E. A., Ishikawa, T., Duguid, I., Chadderton, P., Mahon, S., and Hausser, M. (2007). High-fidelity transmission of sensory information by single cerebellar mossy fibre boutons. *Nature* 450, 1245–1248.

Roggeri, L., Rivieccio, B., Rossi, P., and D'Angelo, E. (2008). Tactile stimulation evokes long-term synaptic plasticity in the granular layer of cerebellum. *J. Neurosci.* 28, 6354–6359.

Ros, H., Sachdev, R. N., Yu, Y., Sestan, N., and McCormick, D. A. (2009). Neocortical networks entrain neuronal circuits in cerebellar cortex. *J. Neurosci.* 29, 10309–10320.

Rossi, P., Mapelli, L., Roggeri, L., Gall, D., de Kerchove d'Exaerde, A., Schiffmann, S. N. et al. (2006). Inhibition of constitutive inward rectifier currents in cerebellar granule cells by pharmacological and synaptic activation of GABA receptors. *Eur. J. Neurosci.* 24, 419–432.

Sargent, P. B., Saviane, C., Nielsen, T. A., DiGregorio, D. A., and Silver, R. A. (2005). Rapid vesicular release, quantal variability, and spillover contribute to the precision and reliability of transmission at a glomerular synapse. *J. Neurosci.* 25, 8173–8187.

Schnitzler, A., Munks, C., Butz, M., Timmermann, L., and Gross, J. (2009). Synchronized brain network associated with essential tremor as revealed by magnetoencephalography. *Mov. Disord.* 24, 1629–1635.

Schnitzler, A., Timmermann, L., and Gross, J. (2006). Physiological and pathological oscillatory networks in the human motor system. *J. Physiol. Paris* 99, 3–7.

Siebert, W. M. (1986). *Circuits, Signals and Systems*. Cambridge: MIT press.

Silver, R. A., Cull-Candy, S. G., and Takahashi, T. (1996). Non-NMDA glutamate receptor occupancy and open probability at a rat cerebellar synapse with single and multiple release sites. *J. Physiol. (Lond.)* 494(Pt 1), 231–250.

Sola, E., Prestori, F., Rossi, P., Taglietti, V., and D'Angelo, E. (2004). Increased neurotransmitter release during long-term potentiation at mossy fibre-granule cell synapses in rat cerebellum. *J. Physiol. (Lond.)* 557, 843–861.

Solinas, S., Forti, L., Cesana, E., Mapelli, J., De Schutter, E., and D'Angelo, E. (2007a). Computational reconstruction of pacemaking and intrinsic electroresponsiveness in cerebellar Golgi cells. *Front. Cell. Neurosci.* 4:12. doi:10.3389/fncel.2010.00012

Solinas, S., Forti, L., Cesana, E., Mapelli, J., De Schutter, E., and D'Angelo, E. (2007b). Fast-reset of pacemaking and theta-frequency resonance patterns in cerebellar Golgi cells: simulations of their impact in vivo. *Front. Cell. Neurosci.* 1:4. doi:10.3389/neuro.03.004.2007

Solinas, S., Nieus, T., and D'Angelo, E. (2010). A realistic large-scale model of the cerebellum granular layer predicts circuit spatio-temporal filtering properties. *Front. Cell. Neurosci.* 4:12. doi:10.3389/fncel.2010.00012

Szwed, M., Bagdasarian, K., and Ahissar, E. (2003). Encoding of vibrissal active touch. *Neuron* 40, 621–630.

Tominaga, T., Tominaga, Y., Yamada, H., Matsumoto, G., and Ichikawa, M. (2000). Quantification of optical signals with electrophysiological signals in neural activities of Di-4-ANEPPS stained rat hippocampal slices. *J. Neurosci. Methods* 102, 11–23.

Van Der Giessen, R. S., Koekkoek, S. K., van Dorp, S., De Gruijl, J. R., Cupido, A., Khosrovani, S., et al. (2008). Role of olivary electrical coupling in cerebellar motor learning. *Neuron* 58, 599–612.

Welsh, J. P., Lang, E. J., Suglhara, I., and Llinas, R. (1995). Dynamic organization of motor control within the olivocerebellar system. *Nature* 374, 453–457.

Wu, N., Hsiao, C. F., and Chandler, S. H. (2001). Membrane resonance and subthreshold membrane oscillations in mesencephalic V neurons: participants in burst generation. *J. Neurosci.* 21, 3729–3739.

Zuo, Y., Perkon, I., and Diamond, M. E. (2011). Whisking and whisker kinematics during a texture classification task. *Philos. Trans. R. Soc. Lond., B, Biol. Sci.* 366, 3058–3069.

Conflict of Interest Statement: The authors declare that the research was conducted in the absence of any commercial or financial relationships that could be construed as a potential conflict of interest.

Received: 15 January 2013; accepted: 20 March 2013; published online: 10 April 2013.

Citation: Gandolfi D, Lombardo P, Mapelli J, Solinas S and D'Angelo E (2013) Theta-frequency resonance at the cerebellum input stage improves spike timing on the millisecond timescale. Front. Neural Circuits ***7****:64. doi: 10.3389/fncir.2013.00064*

frontiers in
NEURAL CIRCUITS

REVIEW ARTICLE
published: 17 May 2013
doi: 10.3389/fncir.2013.00093

The cerebellar Golgi cell and spatiotemporal organization of granular layer activity

Egidio D'Angelo[1,2]*, Sergio Solinas[2], Jonathan Mapelli[2,3], Daniela Gandolfi[2,3], Lisa Mapelli[1] and Francesca Prestori[1]

[1] *Department of Neuroscience, University of Pavia, Pavia, Italy*
[2] *Brain Connectivity Center, IRCCS C. Mondino, Pavia, Italy*
[3] *Department of Biomedical, Metabolic and Neural Sciences, University of Modena and Reggio Emilia, Modena, Italy*

Edited by:
Chris I. De Zeeuw, Erasmus Medical Center, Netherlands

Reviewed by:
Eric J. Lang, New York University, USA
Abigail L. Person, University of Colorado School of Medicine, USA

***Correspondence:**
Egidio D'Angelo, Laboratory of Neurophysiology, Via Forlanini 6, 27100 Pavia, Italy.
e-mail: dangelo@unipv.it

The cerebellar granular layer has been suggested to perform a complex spatiotemporal reconfiguration of incoming mossy fiber signals. Central to this role is the inhibitory action exerted by Golgi cells over granule cells: Golgi cells inhibit granule cells through both feedforward and feedback inhibitory loops and generate a broad lateral inhibition that extends beyond the afferent synaptic field. This characteristic connectivity has recently been investigated in great detail and been correlated with specific functional properties of these neurons. These include theta-frequency pacemaking, network entrainment into coherent oscillations and phase resetting. Important advances have also been made in terms of determining the membrane and synaptic properties of the neuron, and clarifying the mechanisms of activation by input bursts. Moreover, voltage sensitive dye imaging and multi-electrode array (MEA) recordings, combined with mathematical simulations based on realistic computational models, have improved our understanding of the impact of Golgi cell activity on granular layer circuit computations. These investigations have highlighted the critical role of Golgi cells in: generating dense clusters of granule cell activity organized in center-surround structures, implementing combinatorial operations on multiple mossy fiber inputs, regulating transmission gain, and cut-off frequency, controlling spike timing and burst transmission, and determining the sign, intensity and duration of long-term synaptic plasticity at the mossy fiber-granule cell relay. This review considers recent advances in the field, highlighting the functional implications of Golgi cells for granular layer network computation and indicating new challenges for cerebellar research.

Keywords: cerebellum, granular layer, Golgi cell

INTRODUCTION

The cerebellar Golgi cell was first identified through the pioneering investigations of C. Golgi (Golgi, 1874) and S. R. y Cajal (Ramón y Cajal, 1911), who predicted its function as a local interneuron. It was immediately clear from their studies that the Golgi cell was receiving a double excitatory input: from mossy fibers on the basal dendrites and from parallel fibers on the apical dendrites. Several decades later, other investigators demonstrated the inhibitory nature of Golgi cells (Eccles et al., 1964; Palay and Chan-Palay, 1974) and showed granular layer circuit organization to be based on characteristic double feedforward and feedback inhibitory loops directed toward granule cell dendrites in the cerebellar glomeruli (Eccles et al., 1966; Ito, 1984). The anatomical organization of these neurons also implied that Golgi cells generate a broad lateral inhibition extending beyond the afferent synaptic field. These discoveries suggested that the Golgi cell plays a central role in regulating granular layer activity (for an historical review of Golgi cell discovery, see Galliano et al., 2010) and, together with quantitative evaluation of cell numbers and convergence-divergence ratios in the cerebellar cortex, they became the basis of the classical models of cerebellar functioning (Marr, 1969; Albus, 1971; Ito, 1984).

In recent years, advanced electrophysiological investigations have revealed important aspects of the molecular and cellular functions of these neurons. Most remarkably, Golgi cells have been shown to beat as theta-frequency pacemakers, to be entrained into coherent network oscillations, and to be efficiently activated by localized input bursts, which can phase-reset their activity. These properties were shown to exploit membrane mechanisms including specific ionic channels, excitatory, and inhibitory chemical synapses and dendritic gap junctions. Moreover, clarification of the function of the Golgi cell within the granular layer circuit demanded an extensive analysis at network level, which was carried out using voltage sensitive dye (VSD) imaging and multi-electrode array (MEA) recordings combined with mathematical simulations based on realistic computational models. These investigations highlighted the critical role of Golgi cells in: generating dense clusters of granule cell activity organized in center-surround structures, implementing combinatorial operations on multiple mossy fiber inputs, regulating transmission gain and cut-off frequency, controlling spike timing and burst transmission, and determining the sign, intensity and extension of long-term synaptic plasticity at the mossy fiber-granule cell relay. But unanswered questions remain. What is the exact nature of the

relationship between these several and diverse activities and what is the exact role of Golgi cells in cerebellar computation?

FUNDAMENTAL PROPERTIES OF GOLGI CELLS

Ever since their discovery (Golgi, 1874), Golgi cells have been the focus of considerable interest for both experimental and modeling studies (for previous updates see: Maex and De Schutter, 1998; De Schutter, 2000; Geurts et al., 2001; Maex and De Schutter, 2005; D'Angelo, 2008; Galliano et al., 2010). In recent years, new clues as to the functional properties of Golgi cells and their crucial role in the granular layer circuit have come from the field of cellular and synaptic physiology (Dieudonne, 1998; Forti et al., 2006; Solinas et al., 2007a,b, 2010; Vervaeke et al., 2010; Hull and Regehr, 2012). Golgi cells show a rich electrophysiological pattern and receive input, directly, and indirectly, from all kinds of fibers afferent to the cerebellar cortex and the circuits therein. We here revisit these findings and their implications.

FUNDAMENTAL PROPERTIES OF GOLGI CELLS

The fundamental anatomical properties of Golgi cells (**Figure 1A**) were first described in the histological studies of Golgi and Cajal (reviewed by Galliano et al., 2010). Golgi cells are the largest and most numerous interneurons of the granular layer (Golgi, 1874; Ramón y Cajal, 1888, 1995), which contains one Golgi cell to every several hundred or thousand granule cells (∼6000 in cats Palkovits et al., 1971; ∼1200 in humans: Andersen et al., 1992; ∼400 in rats: Korbo et al., 1993). Typically, Golgi cells have an irregular soma (10–30 μm major diameter Dieudonne, 1998) giving off a series of basal dendrites, two or three apical dendrites and a widely ramified axon (**Figure 1A** Barmack and Yakhnitsa, 2008). Basal dendrites remain in the granular layer, while apical dendrites ascend into the molecular layer traversing the parallel fiber bundle. Golgi cells, although more abundant just below the Purkinje cell layer, can reside at different depths in the granular layer (**Figure 1B**). Attempts to identify Golgi cell subtypes by their biochemical fingerprints have revealed differential expression of certain biochemical markers (rat-303, calretinin, mGluR2, somatostatin, neurogranin) and of their coexpression with glycine, which can be co-released with GABA in certain Golgi cell subpopulations (Geurts et al., 2001, 2003; Simat et al., 2007). However, the absence of systematic differences in an extensive sample of electrophysiological recordings

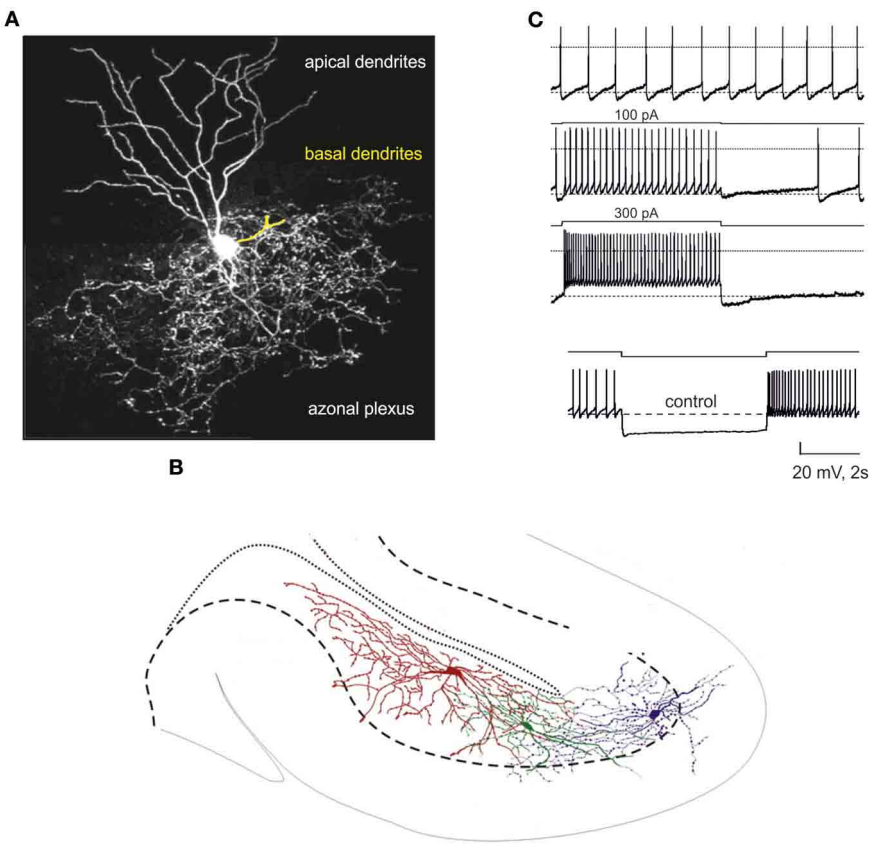

FIGURE 1 | The Golgi cell. (A) Confocal microscopy reconstruction of a Golgi cell (adapted from http://www.regehr.med.harvard.edu). The Golgi cell has a large axonal plexus extending beyond the area covered by the dendrites. One of the basal dendrites has been colored in yellow. **(B)** Three main features of Golgi cell spatial organization: (i) the axons extend in the granular layer (delimited by a dashed line), (ii) the axons spread over the sagittal plane, (iii) the axonal fields of adjacent Golgi cells overlap (adapted from Barmack and Yakhnitsa, 2008). **(C)** Electroresponsiveness of a Golgi cell (adapted from Forti et al., 2006). The neuron shows low-frequency pacemaking and, upon depolarizing current injection, high-frequency spike discharge. Spike discharges are followed by an after-hyperpolarization and a silent pause. Upon hyperpolarizing current injection, the Golgi cell shows sagging inward rectification followed by a post-inhibitory rebound.

(Forti et al., 2006; Solinas et al., 2007a,b; Vervaeke et al., 2010; Hull and Regehr, 2012) (**Figure 1C**) suggests that biochemical differences between Golgi cells may not have an immediate impact on intrinsic electro responsiveness, but could regulate more subtle modalities of their activity.

GOLGI CELL ACTIVATION *In vivo*

Available information on the activity of Golgi cells *in vivo* is limited, but important (**Figure 2**). *In vivo*, Golgi cell firing is modulated by sensory inputs (Vos et al., 1999a; Holtzman et al., 2006; Barmack and Yakhnitsa, 2008; Xu and Edgley, 2008), sensorimotor activity (Edgley and Lidierth, 1987; van Kan et al., 1993; Prsa et al., 2009; Heine et al., 2010) and cortical UP/DOWN states (Ros et al., 2009). Punctate peripheral stimulation generates a short-latency excitation (Vos et al., 1999a; Holtzman et al., 2006; Xu and Edgley, 2008) comprising an early component attributed to direct inputs from mossy fibers and granule cells and a late component attributed to delayed inputs of cerebrocortical origin (Vos et al., 1999a). Convergence of parallel fiber excitation from multiple modules could explain the broad receptive fields of Golgi cells (Vos et al., 1999a; Holtzman et al., 2006; Xu and Edgley, 2008; Prsa et al., 2009; Heine et al., 2010; Holtzman and Jörntell, 2011), as well as Golgi cell firing synchronization along the parallel fiber bundle (Vos et al., 1999b). Thus, both feedback circuits and associative circuits may connect granule cells and Golgi cells in the cerebellar cortex. Interestingly, single Golgi cells can be entrained into oscillatory phases of cerebrocerebellar activity reflecting the UP/DOWN states of the cerebral cortex (Ros et al., 2009). It should also be noted that *in vivo* recordings have revealed effects that could be mediated by the climbing fibers, although the nature of the corresponding pathway remains uncertain (see below). These fundamental observations have also been explained on a cellular and connectivity basis.

CELLULAR AND SYNAPTIC PROPERTIES OF THE GOLGI CELL REVISITED

Golgi cell activity and communication in the cerebellar network depend on the specific properties of the ionic and synaptic mechanisms involved.

MEMBRANE PROPERTIES AND INTRINSIC EXCITABILITY

The electroresponsive properties of the Golgi cell remained unknown until recently, when intrinsic excitability was investigated in cerebellar slice preparations and subsequently modeled (**Figure 1B** Dieudonne, 1998; Forti et al., 2006; Solinas et al., 2007a,b). Golgi cells have a rich repertoire of electroresponsive properties, including pacemaking, resonance, phase-resetting and response patterns characterized by rebounds and response adaptations to depolarizing and hyperpolarizing inputs. Golgi cells in slices have been shown to beat regularly at around 6 Hz (**Figure 1B** Dieudonne, 1998; Forti et al., 2006; Solinas et al., 2007a,b) and to show increased spike frequency and precision when repetitively depolarized at this same frequency (**Figure 1B** Dieudonne, 1998; Forti et al., 2006; Solinas et al., 2007a,b). When hyperpolarized, they generate sagging inward-rectifying responses followed by a rebound bursts upon return toward the basal membrane potential level. When depolarized, they generate repetitive discharge characterized by spike-frequency adaptation and followed by a post-burst hyperpolarizing rebound upon return toward the basal membrane potential level. Interestingly, following a burst, Golgi cells phase-reset their own discharge, restarting pacing after a pause corresponding exactly to the oscillatory period. It should be noted that a recent paper did not report Golgi cell pacemaking *in vitro* (Dugue et al., 2009); the same paper reported weak adaptation during depolarizing steps, weak after-hyperpolarization (AHP) at the end of prolonged firing, and weak rebound after hyperpolarizing steps. These weak dynamic properties could reflect a specific functional state determined by strong electrical coupling with adjacent Golgi cells, which decreases the cell input resistance (see below). However, given the multiple effects of drugs used to test the effect of gap junctions [carbenoxolone interferes with voltage-dependent calcium channels, (Vessey et al., 2004), NMDA receptors (Tovar et al., 2009) and GABA receptors (Beaumont and Maccaferri, 2011)], doubts remain over the physiological implications of these findings. Using two-photon glutamate uncaging and dendritic patch-clamp recordings, it was recently shown that Golgi cells act as passive cables. They confer distance-dependent sublinear synaptic integration and weaken distal excitatory inputs. Gap junctions are present at a higher density on distal dendrites and contribute substantially to membrane conductance.

The intrinsic electroresponsive properties of Golgi cells have been explained experimentally and subsequently modeled using a set of ionic channels (**Figure 1B** Dieudonne, 1998; Forti et al., 2006; Solinas et al., 2007a,b; see also Afshari et al., 2004) (**Figure 3** Forti et al., 2006; Solinas et al., 2010). These are schematically reported below[1]:

(1) Pacemaking depends on the action of four ionic currents, I_h, I_{Na-p}, I_{K-AHP}, and I_{K-slow}: I_h brings the membrane potential into the pacemaker region where the $I_{Na-p}/I_{K-AHP}/I_{K-slow}$ interaction generates pacemaking.
(2) Resonance is generated by I_{K-slow} and amplified by I_{Na-p}.
(3) Phase resetting is closely linked to calcium-dependent regulation of K currents. By being coupled to I_{K-BK}, I_{Ca-HVA} enhances the fast phase of spike AHP, thereby resetting the spiking mechanism and sustaining high-frequency discharge.
(4) Firing frequency regulation is based on the I_{Na-f}/I_{KV} system and modulated by the I_{K-BK}/I_{Ca-HVA} system.
(5) Burst response following depolarization is enhanced by I_{Na-r} and delayed by I_{K-A}; it is followed by spike frequency adaptation generated by the I_{Ca-HVA}/I_{K-AHP} system and by I_{K-slow}. Rebound excitation following hyperpolarization is generated by I_h and I_{Ca-LVA}.
(6) Dendritic integration and interneuronal network communication are enhanced by dendritic gap junctions.

[1]Transient Na current (I_{Na-t}); persistent Na current (I_{Na-p}); resurgent Na current (I_{Na-r}); high-voltage-activated Ca current (I_{Ca-HVA}); Ca-dependent K current of the BK-type (I_{K-BK}); Ca-dependent K current of the SK-type (I_{K-AHP}); delayed-rectifier K current (I_{KV}); slow K current of the M-type (I_{K-slow}); fast-inactivating K current of the A-type (I_{K-A}); slow inward-rectifier H-current (I_h).

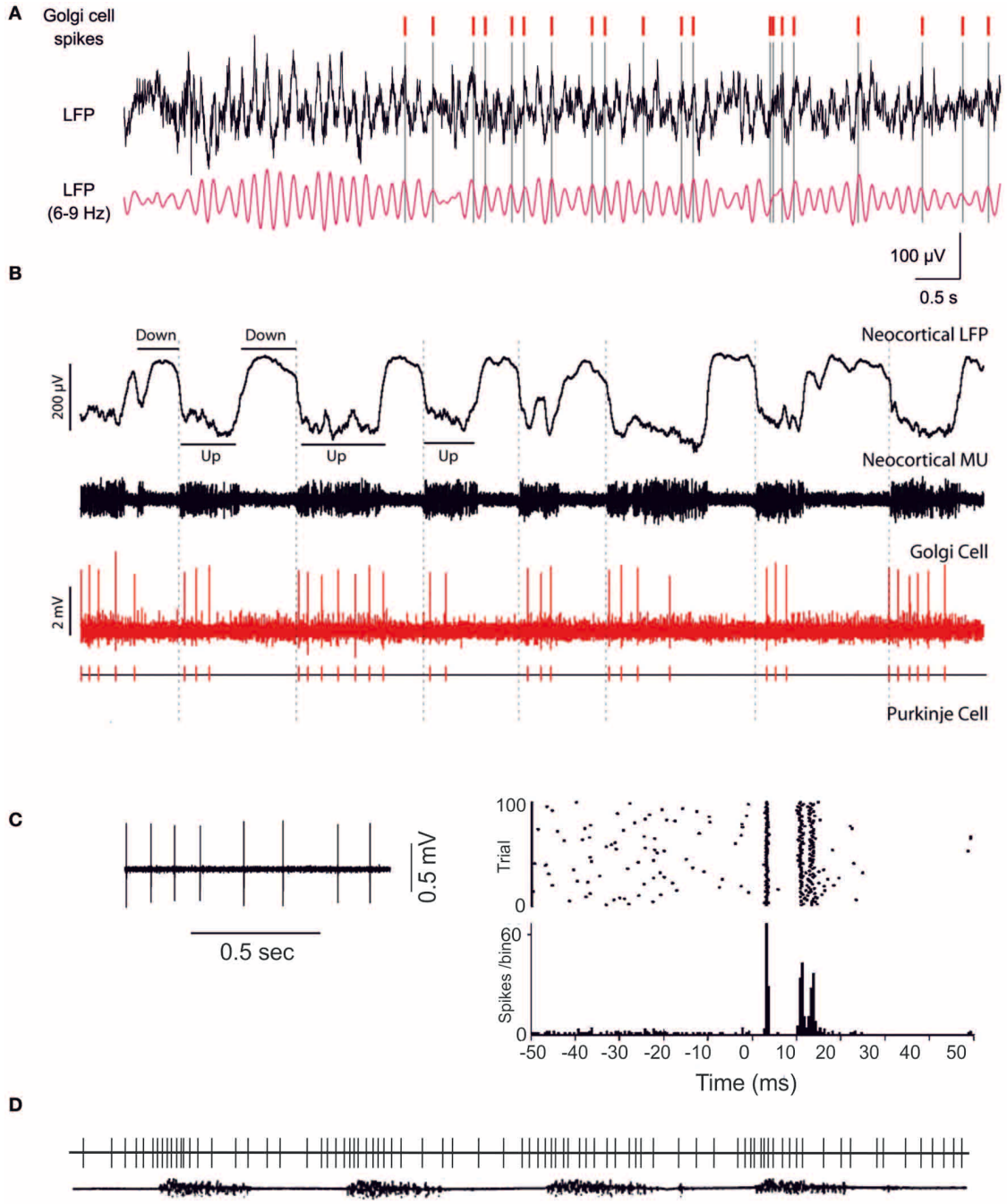

FIGURE 2 | Golgi cell activity *in vivo*. (A) The Golgi cell spikes are in phase with oscillations in the local field potential of the granular layer (Dugue et al., 2009). **(B)** Golgi cells can show rhythmic entrainment with the UP-DOWN states characterizing neocortical activity (Ros et al., 2009). The different behavior in **(A)** and **(B)** may reflect different functional states or simply the fact that the trace in **(A)** may be part of an UP state as shown in **(B)**. **(C)** The Golgi cell shows background activity, over which punctate sensory stimulation elicits bursts of activity (from Holtzman et al., 2006). Each burst is usually composed of 2–3 spikes and is followed by a long-lasting inhibitory period (or silent pause in Vos et al., 1999a). **(D)** During locomotion, the Golgi cell is entrained into repetitive activity cycles, which modulate its discharge frequency (partially redrawn from Edgley and Lidierth, 1987). The lower trace shows the EMG of a limb muscle during walking.

Analysis of this pattern shows that different functionalities correspond directly to specific subsets of ionic channels. In particular, pacemaking and resonance both involve the I_{Na-p}/I_{K-slow} system, and the pacemaker frequency is tuned by I_{K-AHP}. Pacemaking requires I_h, while phase resetting is based on the I_{K-BK}/I_{Ca-HVA} system. A special role is played by the $I_{Na-f}/I_{Na-p}/I_{Na-r}$ system, which controls various aspects of burst generation and resonance. Thus, although much remains

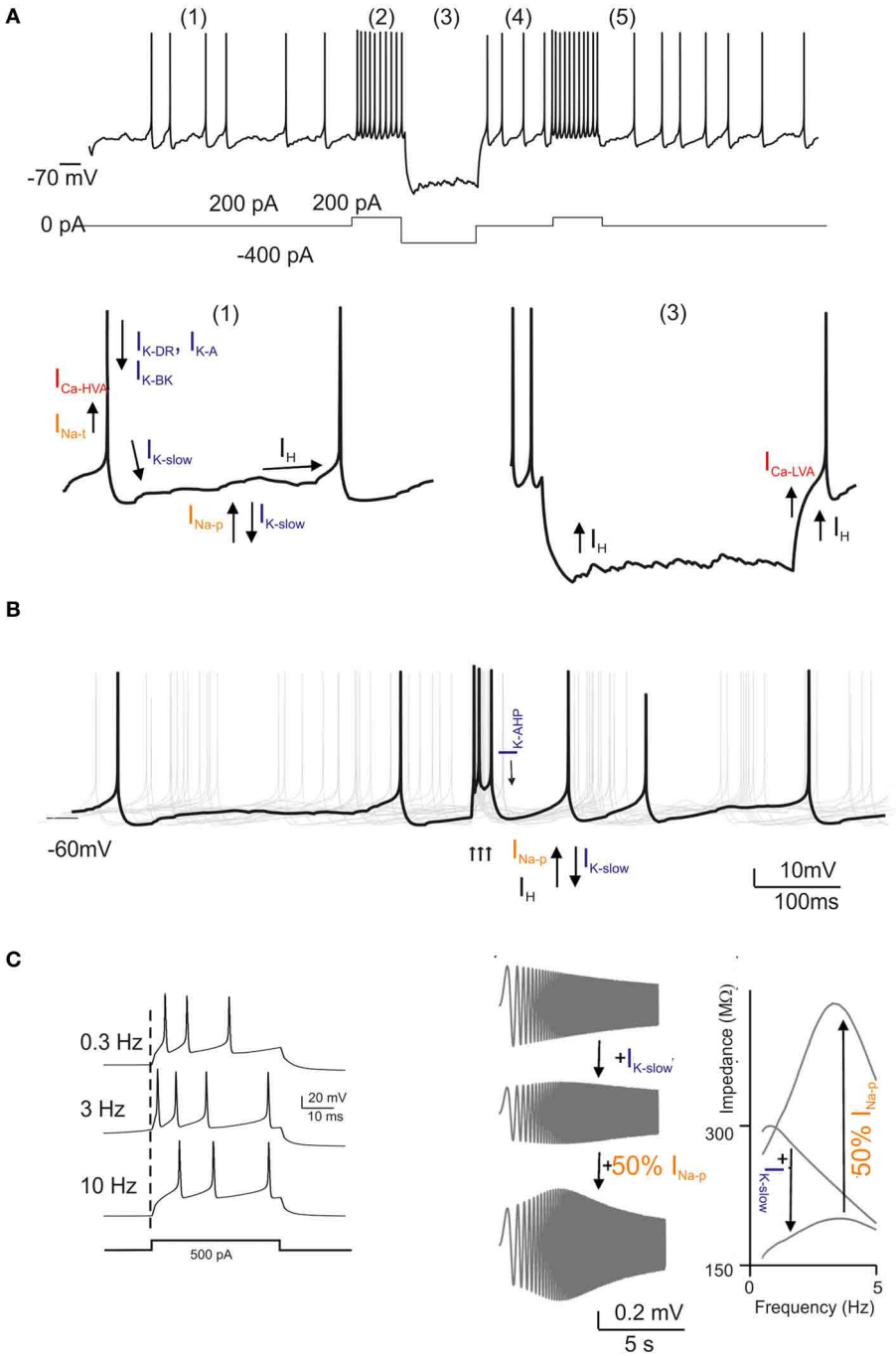

FIGURE 3 | Golgi cell ionic mechanisms. This is a reconstruction of the ionic mechanisms of the Golgi cell membrane obtained using computational models (Solinas et al., 2007a,b) based on previous electrophysiological analysis (Forti et al., 2006) and incorporated into a large-scale granular layer model network (Solinas et al., 2010). Transient Na current (I_{Na-t}); persistent Na current (I_{Na-p}); resurgent Na current (I_{Na-r}); high-voltage-activated Ca current (I_{Ca-HVA}); Ca-dependent K current of the BK-type (I_{K-BK}); Ca-dependent K current of the SK-type (I_{K-AHP}); delayed-rectifier K current (I_{KV}); slow K current of the M-type (I_{K-slow}); fast-inactivating K current of the A-type (I_{K-A}); slow inward-rectifier H-current (I_h). In the different panels, the ionic channels involved are shown with arrows indicating their depolarizing or hyperpolarizing action. **(A)** Golgi cell responses like those reported in **Figure 1A** can be elicited by the model: (1) low-frequency pacemaking, (2) high-frequency spike discharge upon current injection, (3) sagging inward rectification, (4) post-inhibitory rebound, (5) phase resetting. **(B)** Golgi cell responses to bursts in the mossy fibers (arrows). After a burst, all responses are phase reset, generating an apparent "silent pause". **(C)** Golgi cell responses to bursts in the mossy fibers repeated at different frequencies. Note that maximum responses are obtained around 6 Hz. The panels on the right show a "ZAP" protocol for investigating resonance. Resonance is determined by I_{K-slow} and is amplified by I_{Na-p}.

to be done in terms of molecular characterization of the ionic channels involved, the available data are sufficient to allow precise modeling of the Golgi cell.

REALISTIC MODELING OF GOLGI CELL ACTIVITY

The realistic model of the Golgi cell (Solinas et al., 2007a,b) incorporates the mechanisms indicated above in the somatic compartment and maintains passive dendrites. This model, in turn incorporated into a detailed granular layer network model (**Figure 3** Solinas et al., 2010), offers the following explanations for the main behaviors of the Golgi cell reported *in vivo*: pacemaking may underlie the rhythmic Golgi cell discharge *in vivo*, which, as a result of synaptic inputs, would then become irregular and spread over a broader frequency range (2–25 Hz); resonance could enhance Golgi cell entraining into coherent theta-frequency oscillations driven by cortical activity (see below), for example during sensorimotor behaviors like active whisking (Pellerin and Lamarre, 1997; Hartmann and Bower, 1998, 2001; Kleinfeld et al., 2006); the phase resetting of the pacemaker mechanism could provide the substrate of the "silent pause" observed after Golgi cell burst discharge (Vos et al., 1999a; Tahon et al., 2011); mechanisms enhancing spike bursting could determine the fast and precise Golgi cell responses to impulsive tactile stimuli (see also Morissette and Bower, 1996; Vos et al., 1999a, 2000; Volny-Luraghi et al., 2002; Tovar et al., 2009); firing frequency adaptation could help to limit Golgi cell spiking responses during prolonged stimulation (Tahon et al., 2011), and finally, the generation of rebounds in both the depolarizing and the hyperpolarizing directions could allow the Golgi cell to precisely follow the temporal evolution of afferent discharges observed during ongoing movement (Miles et al., 1980). Interestingly, by implementing the available realistic Golgi cell model (Solinas et al., 2007a,b) with dendritic gap junctions (Dugue et al., 2009; Vervaeke et al., 2010), it was shown that depolarization of one Golgi cell increased firing in its neighbors and enabled distal excitatory synapses to drive network activity more effectively. These mechanisms are tightly integrated with those governing chemical synaptic transmission, as explained below.

SYNAPTIC PROPERTIES AND CIRCUIT COMMUNICATION

The Golgi cell is extensively interconnected within the cerebellar network. In their classical analysis, which remains the fundamental reference for cerebellar circuit connectivity, Palay and Chan-Palay (1974) showed that Golgi cells receive a major excitatory input from mossy fibers, which form synapses on the basal dendrites, presumably in the glomeruli. Granule cells were reported to form their connections with Golgi cells through parallel fibers and also possibly through synapses *en passant* along the ascending axon. The climbing fibers have been suggested to form connections with Golgi cells, apparently by giving rise to thin collateral branches (called Scheibel's collaterals) just below the Purkinje cells which then reenter the upper part of the granular layer (Shinoda et al., 2000). Golgi cells have also been reported to receive inhibitory innervations from stellate/basket cells and Lugaro cells (Sotelo and Llinas, 1972). These original anatomical observations were corroborated by *in vivo* electrophysiological experiments, which showed that afferent activity, involving both the mossy fiber and the parallel fiber inputs, readily activated Golgi cells and that molecular layer interneurons could actually inhibit Golgi cells (Eccles et al., 1967).

In the last decade, the concepts of synaptic connectivity have been refined through a combination of electrophysiological and morphological investigations, which have unveiled a complex organization of neurotransmitters and receptors. Moreover, forms of short-term and long-term synaptic plasticity (long-term depression, LTD, and long-term potentiation, LTP) and several modulatory effects have been reported, with the suggestion that these could provide the basis for regulating circuit dynamics, homeostasis and learning (for previous reviews see Geurts et al., 2003; Farrant and Nusser, 2005; D'Angelo, 2008). Recent advances have increased our understanding of this complex system and allowed us to re-design the picture of the loops involved (**Figure 4**), although some controversies remain.

EXCITATORY SYNAPSES WITH GOLGI CELLS

The main excitatory inputs to Golgi cells are glutamatergic. Recent studies report the involvement of AMPA (Kanichay and Silver, 2008) and NMDA receptors (Cesana et al., 2010) at mossy fiber-Golgi cell relays. These synapses show moderate short-term depression; this makes the Golgi cells highly sensitive to mossy fiber afferent bursts, so that the Golgi cells then elicit new bursts in response to the input. Instead, activation of AMPA, NMDA and kainate receptors has been reported at parallel fiber-Golgi cell relays (Dieudonne, 1998; Bureau et al., 2000; Misra et al., 2000). While AMPA receptor-mediated currents undergo a marked short-term depression, kainate receptor responses are summed, enhancing temporal summation during repetitive parallel fiber activity. Thus, this synapse may be able to transmit both temporally precise single granule cell spikes and granule cell bursts (Chadderton et al., 2004; Rancz et al., 2007). Recently, a form of LTD was reported following intense high frequency stimulation of parallel fibers (Robberechts et al., 2010), although it remains to be established whether or not this LTD exists in the presence of natural patterns of stimulation. Metabotropic glutamate receptors also appear to regulate Golgi cell circuit functions. The mGluR2 receptors are expressed in Golgi cells (Geurts et al., 2001) and their activation enhances an inward rectifier K current which helps to silence the Golgi cell following intense granule cell-Golgi cell transmission (Watanabe and Nakanishi, 2003). This mGluR2-dependent mechanism may facilitate the transmission of protracted bursts along the mossy fiber-granule cell pathway (Arenz et al., 2008).

INHIBITORY SYNAPSES WITH GOLGI CELLS

The inhibitory inputs to Golgi cells are GABAergic or glycinergic. Pure GABAergic inputs have been suggested to come from stellate and basket cells, and mixed GABAergic glycinergic inputs from Lugaro cells (Dumoulin et al., 2001). The glycinergic inhibitory postsynaptic current (IPSC) component, being expressed in variable amounts and having the capacity to slow down IPSC kinetics, can fine tune the duration of Golgi cell inhibition (Dumoulin et al., 2001). Evidence was recently provided indicating that GABAergic Golgi cells are inhibited by other Golgi cells rather

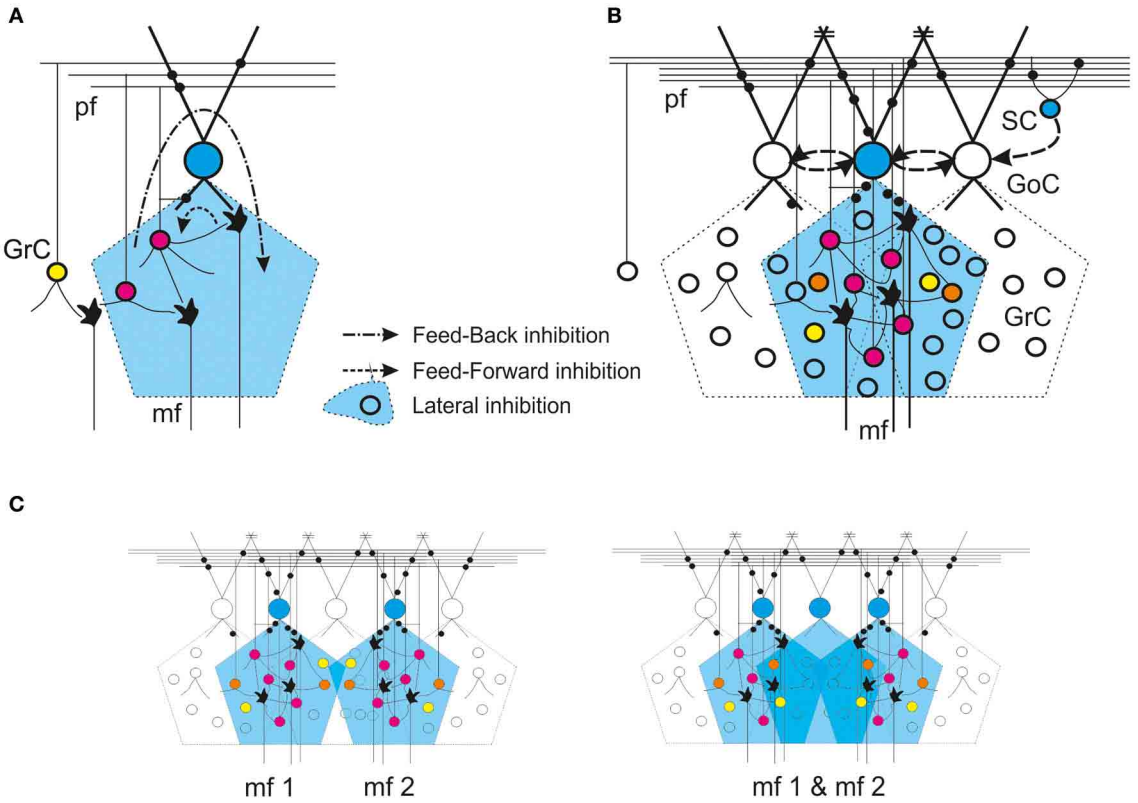

FIGURE 4 | Golgi cell connectivity. Schematic representation of different modalities of Golgi cell connectivity. In all panels, the active Golgi cells are depicted in blue and the intensity of granule cell activity is scaled from blue (no activity) through yellow and orange to red (increasing activity). Synapses are in black. *GoC* Golgi cell, *GrC* granule cell, *SC* stellate cell, *mf* mossy fiber, *pf* parallel fiber. Inhibitory connections between Golgi cells and from stellate to Golgi cells are indicated with dashed arrow-lines. The gap junctions are indicated by =. **(A)** Feedforward and feedback loops. **(B)** Lateral inhibition. **(C)** Overlapping of axonal fields. Note that, in the area in common to two neighboring mossy fiber bundles, the circuit can generate *combined excitation* of the granule cells, but activation of an extra Golgi cell can generate a *combined inhibition*.

than by molecular layer interneurons (Hull and Regehr, 2012). This report is somewhat controversial, however, in that *in vivo* electrophysiological recordings have clearly shown Golgi cell inhibition to be the consequence of a disynaptic pathway passing through granule cells and molecular layer interneurons (Eccles et al., 1967). The reason for this discrepancy remains to be determined.

To our knowledge, molecular layer interneurons remain the best candidates to mediate feedback inhibition deriving from activity in parallel fibers (and climbing fibers, see below) toward Golgi cells. Golgi cell inhibition by molecular layer interneurons could enhance post-inhibitory rebounds in granule cell activity and could also explain the long-lasting depressions of firing induced by strong electrical stimuli (Holtzman et al., 2006). Golgi cell inhibition indirectly caused by climbing fibers and molecular layer interneurons could also have the important effect of synchronizing the granular layer with the inferior olive, the molecular layer and the deep cerebellar nuclear circuits. Conversely, Golgi cell-Golgi cell synapses could serve to dampen and equalize Golgi cell responses within the granular layer circuit. While it is possible that the two mechanisms coexist, their relative importance in different functional conditions remains to be determined.

Finally, inhibition coming from Lugaro cells has been reported to depend on serotonergic activation of these neurons (Dieudonne and Dumoulin, 2000). This would allow Lugaro cells to correlate Golgi cell activity with general functional states of the brain.

INDIRECT INHIBITORY EFFECT OF CLIMBING FIBERS ON GOLGI CELLS

Although climbing fibers are glutamatergic, there exists electrophysiological evidence that they have an inhibitory effect on Golgi cells. *In vivo* recordings, synchronous stimulation of climbing fibers and peripheral afferents elicited a long-lasting depression of the Golgi cell inhibitory input to granule cells (Xu and Edgley, 2008), although the underlying mechanism remains unclear. Indeed, despite evidence of climbing fiber ramifications in the proximity of Golgi cells, i.e., the aforementioned Scheibel's collaterals (Shinoda et al., 2000), the presence of effective synaptic connections between climbing fibers and Golgi cells remains uncertain. A recent study that used advanced immunohistochemical techniques and 3D reconstruction, while supporting the prominent apposition of climbing fibers to Purkinje cells and molecular layer interneurons, did not provide comparable evidence for Golgi cells, thus arguing against

a functional significance of direct synaptic contacts between climbing fibers and Golgi cells (Galliano et al., 2013). This negative result does not exclude the possibility that spillover of glutamate from climbing fibers in the proximity of Golgi cell dendrites could activate mGluR2 receptors, thereby causing a long-lasting modulation of the Golgi cell response. Another possibility is that glutamate spillover from climbing fibers causes plastic changes at parallel fiber-molecular layer interneuron synapses (Mathews et al., 2012). These mechanisms remain to be investigated.

GOLGI CELL-GOLGI CELL COMMUNICATION THROUGH DENDRITIC GAP JUNCTIONS

Reported in early studies, the finding of gap junctions in Golgi cell dendrites suggested that these neurons could be electrically coupled with each other and with molecular layer interneurons (Sotelo and Llinas, 1972). Recently, functional evidence for gap junctions connecting Golgi cell apical dendrites was reported (Dugue et al., 2009; Vervaeke et al., 2010). This interconnection endows Golgi cells with a further level of complexity. Golgi cells are known to loosely synchronize their activity (Vos et al., 1999b) and this effect could be explained by their shared parallel fiber input (Maex and De Schutter, 1998). The gap junctions provide a further electrical link between Golgi cells which is capable of accelerating the rise and enhancing the stabilization of synchronous oscillations. Moreover, counter-intuitively, the heterogeneity of the conductance of the electrical connections gives rise to a transient desynchronization of adjacent Golgi cells driven by external stimuli (Vervaeke et al., 2010). The real relevance of gap junctions and their relative contribution to overall activity states of the cerebellar cortex *in vivo* remains largely to be determined.

INHIBITION OF GRANULE CELLS BY GOLGI CELLS

The synaptic output of Golgi cells is GABAergic and it inhibits the granule cells in the cerebellar glomeruli. The IPSCs consist of a fast and a slow component (Rossi et al., 2003) determined by differential receptor subtypes (Farrant and Nusser, 2005). The α1 subunit-containing receptors are localized in the synaptic cleft and are mainly involved in bringing about the IPSC peak. The α6 subunit-containing receptors, which have a high affinity for GABA, a low desensitization rate and are distributed from the synaptic junction to destinations several hundreds of nanometers apart, help to enhance the IPSC tail through a spillover-dependent mechanism (Tia et al., 1996; Nusser et al., 1998; Rossi and Hamann, 1998; Brickley et al., 1999; Hadley and Amin, 2007). This double receptor system is probably important for ensuring extremely precise timing of inhibition onset and, at the same time, efficient temporal summation during trains of Golgi cell spikes. As well as causing phasic inhibition, Golgi cells can contribute to the regulation of basal granule cell input conductance by helping to maintain a tonic GABA concentration level inside the glomerulus (Brickley et al., 1996; Chadderton et al., 2004; Duguid et al., 2012). This tonic level of GABA is thought to activate high-affinity receptors (Tia et al., 1996) primarily, but also to control the gain of the mossy fiber-granule cell relay (Mitchell and Silver, 2003) (see below).

In contrast to the inhibitory action exerted by fast GABAergic synaptic transmission and tonic inhibition, some other mechanisms limit the impact of Golgi cell inhibition in a homeostatic manner. A transient feedback depression of neurotransmitter release probability is determined by ambient GABA through presynaptic GABA-B autoreceptors and limits the first response in a burst (Mapelli et al., 2009). Two forms of medium-term adaptation of granule cell responses have been reported to occur through activation of postsynaptic GABA-B receptors. Both application of the GABA-B receptor agonist, baclofen, and spike bursts in Golgi cell axons can induce depression of the inward rectifier K current in granule cells causing membrane depolarization and (Rossi et al., 2006) depression of the GABA-A receptor-mediated current in granule cells reducing the inhibitory effect (Brandalise et al., 2012). These mechanisms, as well as glomerular crosstalk (Mitchell and Silver, 2000b, see below), could have an homeostatic effects and be responsible for the protracted granule cell responses to mossy fiber bursts observed in VSD recordings (Mapelli et al., 2010a).

GLOMERULAR FUNCTIONS: SPILLOVER, CROSSTALK AND TONIC INHIBITION

The control of granule cell activity by Golgi cells occurs almost exclusively in the glomerulus, which is a specialized structure in which the ambient concentration of neurotransmitters can be effectively regulated. The glomerular compartment, enwrapped in a glial sheet, is thought to act as a diffusion barrier entrapping neurotransmitter molecules, enhancing the effects of spillover, and giving rise to tonic inhibition (Barbour and Häusser, 1997; Rossi and Hamann, 1998; Hamann et al., 2002). Moreover, the close apposition of presynaptic and postsynaptic elements of both excitatory and inhibitory fibers enhances processes of synaptic crosstalk.

In the glomerulus, a tonic GABA level is established and regulated by the rate of vesicular release from Golgi terminals and the rate of non-vesicular release and re-uptake in glial cells (Rossi et al., 2003). Recently, the tonic component of granule cell inhibition was shown to depend largely on the GABA released by glial cells through bestrophin-1 anion channels (Lee et al., 2010). The contribution of non-vesicular GABA release from Golgi cells may be increased by acetylcholine (Rossi et al., 2003, see below).

There exists functional evidence of crosstalk between mossy fiber and Golgi cell terminals due to neurotransmitter spillover in the glomerulus, which results in heterosynaptic activation of presynaptic GABA and glutamate autoreceptors. Glutamate spillover from mossy fiber terminals on granule cells activates presynaptic mGluR2 receptors on Golgi cell terminals and inhibits GABA release (Mitchell and Silver, 2000a), while GABA spillover from Golgi cell-to-granule cell synapses activates presynaptic GABA-B receptors on mossy fiber terminals and inhibits glutamate release in a frequency-dependent manner (Mitchell and Silver, 2000b). These reciprocal actions may reinforce the switch from excitation to inhibition of granule cells, in such a way that once excitation prevails it becomes even more dominant over inhibition (and vice versa when inhibition prevails).

The combination of crosstalk and tonic inhibition orchestrates a complex control of the granule cell input/output relationship.

Tonic inhibition leads to a reduction of granule cell excitability, so that the slope of the input/output curve does not change and the frequency of the emitted spikes is similarly reduced at all input intensities (Brickley et al., 1996; Chadderton et al., 2004; Duguid et al., 2012). Conversely, crosstalk changes the slope of the firing input/output curve in a more complex manner, dampening responses during high-frequency mossy fiber-granule cell transmission and thus altering granule cell sensitivity to changes in input frequency (Mitchell and Silver, 2003). Finally, a crosstalk effect could also be mediated by glycine, which is co-released with GABA by Golgi cells (Dugué et al., 2005). Granule cells do not express glycine receptors, but it is tempting to speculate that glycine plays a role in regulating activation of granule cell NMDA receptors on their glycine binding site (D'Angelo et al., 1990). Conversely, both GABA and glycine receptors are expressed in unipolar brush cells (UBCs), in which Golgi cell activity generates mixed GABAergic/glycinergic responses (Dugué et al., 2005).

FUNCTIONAL CONNECTIVITY: EXPANDING THE VIEW

Golgi cell connectivity is closely bound up with the organization of the entire granular layer circuit (Eccles et al., 1967; Palay and Chan-Palay, 1974). At microscopic level, statistical rules govern the way granule cells, Golgi cells and mossy fibers are wired together to form local networks. On an intermediate scale, two network-organizing principles are especially relevant: the formation of "granule cell clusters" and of "center-surround" structures. The clusters, revealed by measuring or imaging the area activated by sensory punctate stimuli, are formed by 200–600 adjacent granule cells (Roggeri et al., 2008; Diwakar et al., 2011). In these clusters, the excitatory-inhibitory (E/I) balance is higher in the core, thus leading to the formation of a center-surround structure (Mapelli and D'Angelo, 2007). It is also important to consider how Golgi cell connectivity is related to the modular organization of the cerebellar cortex [(Voogd et al., 2003; Apps and Hawkes, 2009; Oberdick and Sillitoe, 2011); for a recent review see (D'Angelo and Casali, 2012)][2]. At this level, the granular layer performs complex operations of spatiotemporal recoding of the mossy fiber input, which can be recognized by analyzing intermodular connectivity and signal transmission along the vertical and transverse axis of the cerebellar cortex (Bower and Woolston, 1983; Mapelli et al., 2010a,b).

SYNAPTIC ORGANIZATION IN THE GRANULAR LAYER

Ultrastructural measurements have revealed that each granule cell receives, on average, three Golgi cell inhibitory synapses on as many different dendrites (Hamori and Somogyi, 1983; Jakab and Hamori, 1988). Golgi cell-granule cell synapses consist of small boutons located proximally to granule cell dendritic endings, which, in turn, receive excitatory mossy fiber terminals. Both mossy fiber and Golgi cell terminals, together with several tens of granule cell dendrites (Palkovits et al., 1971; Hamori and Somogyi, 1983) and Golgi cell basal dendrites are included in the cerebellar glomerulus. These investigations have opened up several physiological issues.

For example, there is the question of whether Golgi cell synapses impinging on a granule cell originate from the same or from different Golgi cells. Typically, multiple IPSCs in a granule cell can be recruited by increasing the stimulation intensity (Mapelli et al., 2009), which is consistent with 3–5 independent Golgi cells connected. Indeed, the frequency of spontaneous IPSCs, which are synaptic events determined by intrinsic activity in Golgi cells, exceeds the pacemaker frequency shown by single Golgi cells, further supporting the convergence of multiple Golgi cells onto the same granule cells.

Given that glomeruli receive an average of 53 dendrites (an estimate obtained from rat cerebellum: Jakab and Hamori, 1988) from as many different granule cells, another issue is whether a Golgi cell innervates all the granule cells impinging on the same glomerulus. Even a minimal stimulation (i.e., that activates a single synaptic contact) can elicit a direct and an indirect spillover-mediated component in granule cell IPSCs (Mapelli et al., 2009). Since spillover is a sign of release on neighboring synapses in the glomerulus (Rossi and Hamann, 1998), this indicates that a Golgi cell axon forms more than one synapse inside a glomerulus and inhibits numerous (if not all) granule cell dendrites in that glomerulus.

Therefore, in theory, a single Golgi cell should not innervate a granule cell more than once (and therefore should not innervate other glomeruli within reach of the dendrites of proximal granule cells) and each glomerulus should be innervated by a single Golgi cell. This configuration favors the expansion of the Golgi cell axonal field and the integration of multiple Golgi cell axons within the same volume of the granular layer (Solinas et al., 2010). Finally, it has been shown that, in the vestibulo-cerebellum, in addition to granule cells, Golgi cells also inhibit UBCs (Dugué et al., 2005).

QUANTITATIVE GOLGI CELL CONNECTION SCHEME

On the basis of current knowledge it is possible to generate a quantitative connection scheme for the Golgi cell, which is unique both for its high level of precision and for the quantity of available experimental data. Using morphological measurements, it can be calculated that the rat cerebellar granular layer has a cell density of $4 \times 10^6/\text{mm}^3$ for granule cells and $9300/\text{mm}^3$ for Golgi cells, with a Golgi cell:granule cell ratio of 1:430 (Korbo et al., 1993). Moreover, the density of the glomeruli is $3 \times 10^5/\text{mm}^3$, and each glomerulus is composed of one mossy fiber terminal, about 53 dendrites from separate granule cells (Jakab and Hamori, 1988), and one or more dendrites from Golgi cells. Network connections can be reconstructed by applying simple rules, most of which can be directly extracted from original works on cerebellar architecture (e.g., see Eccles et al., 1967).

[2]The cerebellum is composed of several hundred or thousand microzones or microcompartments, which are thought to represent effective cerebellar functional units [for a recent review see D'Angelo and Casali (2012)]. These have a complex relationships with stripes, zones and multizonal microcomplexes, which are also though to represent effective functional modules (Apps and Hawkes, 2009). A module is a conglomerate of several, non-adjacent parasagittal bands of Purkinje cells projecting to specific areas of deep cerebellar nuclei and gating segregated projections from the inferior olive (Oberdick and Sillitoe, 2011). Likewise, the mossy fibers projecting to a certain group of Purkinje cells through the granular layer also project to the deep cerebellar nucleus neuron receiving input from those Purkinje cells (Voogd et al., 2003).

Granule cell connection rules are quite simple and can be summarized as follows: granule cell dendrites cannot reach glomeruli located more than 40 μm away (mean dendritic length: 13.6 μm) and a single granule cell cannot send more than one dendrite into the same glomerulus. Conversely, Golgi cell connection rules are more complex. It can be assumed that only one Golgi cell axon enters a glomerulus, forming inhibitory synapses on all the afferent granule cell dendrites, and that a Golgi cell axon entering a glomerulus cannot access the neighboring glomeruli if they share granule cells with the first one. This should prevent a granule cell from being inhibited twice by the same Golgi cell (see above and Solinas et al., 2010). Each Golgi cell can inhibit as many as 40 different glomeruli and a total of about 2000 granule cells, accounting for the 1:430 Golgi cell:granule cell ratio and the aforementioned convergence and divergence ratios (see above). Recent calculations seem to indicate a specific organization of excitatory connectivity. Golgi cells were suggested to receive excitatory inputs from about 40 mossy fibers on basal dendrites (Kanichay and Silver, 2008). Moreover, a specific organization is emerging for granule cell inputs through the ascending axons and parallel fibers (Cesana et al., 2010). Golgi cells could receive about 400 connections from the ascending axons of local granule cells on the basal dendrites and another 400 connections through the parallel fibers of local granule cells, which would provide the basis for a powerful feedback circuit. In addition, Golgi cells receive about 1200 parallel fiber contacts on the apical dendrites from transversely organized granular layer fields. It has been calculated that the effectiveness of local granule cells is about 10 times greater than that of an equivalent population located outside the direct afferent field and forming only parallel fiber contacts toward the Golgi cell.

Much less is known about inhibitory connections. Each Golgi cell receives inhibitory input from several dozen molecular layer inhibitory interneurons (stellate cells and Basket cells) (Dumoulin et al., 2001) and from other Golgi cells (Hull and Regehr, 2012). Moreover Golgi cell dendrites are coupled through gap junctions (Vervaeke et al., 2010) and may also be connected with molecular layer interneurons in the same way (Sotelo and Llinas, 1972).

MODULAR AND INTERMODULAR CONNECTIVITY OF GOLGI CELLS

There are several other anatomical aspects that help to shed light on Golgi cell wiring and account for the most important aspects of Golgi cell functions in the cerebellar cortex. First, the Golgi cell axonal plexus extends exclusively in the granular layer and, through thin branches, can form secondary plexuses in the same or even in neighboring laminae (**Figure 1A**, see Eccles et al., 1967; Barmack and Yakhnitsa, 2008). The broader extension of the axonal plexus compared to the basal dendrites provides the basis for lateral inhibition and for intermodular connectivity. Second, axonal plexuses coming from different Golgi cells overlap (**Figure 1A**, see Barmack and Yakhnitsa, 2008). This property, by causing the convergence on one granule cell of inhibition from more than one Golgi cell, is necessary to allow the combinatorial inhibition of granule cells. Third, as revealed by immunostaining for zebrin-2, aldolase C and other markers (Sillitoe et al., 2008), Golgi cells emit their apical dendrites within Purkinje cell compartments. Fourth, the Golgi cell axonal field extends along the sagittal plane (**Figure 1A** Barmack and Yakhnitsa, 2008), as do mossy fiber (Wu et al., 1999; Sultan and Heck, 2003) and climbing fiber branching (Shinoda et al., 2000). Therefore, Golgi cell wiring appears rather complex: through mossy fiber inputs to their dendrites, Golgi cells are preferentially wired within microcircuits involving anatomically organized olivo-cerebellar and mossy fiber compartments (Brown and Bower, 2001, 2002; Voogd et al., 2003; Pijpers et al., 2006); meanwhile, through their apical and basal dendrites and axonal plexus (mean mediolateral extent is 180 ± 40 μm equivalent to 10–15 PC dendrites Barmack and Yakhnitsa, 2008), they are interconnected with multiple such compartments. Fourth, unlike Purkinje cell dendrites, Golgi cell dendrites are not rigorously organized on a plane but rather in a three-dimensional structure. Thus, Golgi cells may not be equipped to detect ordered temporal sequences transmitted through parallel fibers (Braitenberg, 1967; Braitenberg et al., 1997). This topographical organization is further complicated by the fact that parallel fibers cross several Golgi cell dendritic arbors along the transverse axis, while mossy fibers ramify along the sagittal axis (Wu et al., 1999; Sultan and Heck, 2003). Therefore, Golgi cell inhibition can be redistributed to mossy fiber clusters in the parasagittal plane.

Interestingly, granule cells have recently been reported to show a high rate of connectivity with local Golgi cells, and thus to implement a powerful feedback in the local microcircuit (Cesana et al., 2010). This, together with lateral inhibition, is probably one of the factors underlying the granule cell cluster organization shown on *in vivo* recordings (Diwakar et al., 2011) and the center-surround organization revealed in network imaging experiments (Mapelli and D'Angelo, 2007; Mapelli et al., 2010a,b). These observations, combined with electrophysiological and modeling data, support the view that Golgi cells can respond precisely to topographically organized inputs, but also perform widespread spatiotemporal integration of parallel fiber information (Vos et al., 1999a,b, see also below; De Schutter and Bjaalie, 2001).

MODELING GOLGI CELL INTERACTIONS IN THE GRANULAR LAYER

The cerebellar cortical network, characterized by a beautiful and regular connection matrix with rectangular symmetry (Braitenberg, 1967), stimulated the development of a series of network models (Pellionisz and Szentagothai, 1973; Pellionisz and Llinás, 1979; Buonomano and Mauk, 1994; Maex and De Schutter, 1998, 2005; Medina and Mauk, 2000; Santamaria et al., 2007). However, the recent advances in understanding of Golgi cell connectivity could significantly change our view on the role these neurons play in shaping the dynamics of the granular layer. A first attempt at reconstructing the complex connectivity, the intrinsic excitability and the short-term synaptic dynamics of the granular layer cell was made by Solinas et al. (2010), and further developed Solinas and D'Angelo (2012), who considered a homogeneous portion of the granular layer including about 4000 granule cells and a proportionate number of Golgi cells and glomeruli and accounted for the topological constraints relevant on this relatively limited scale. Relaxing these topological constraints and

transforming the connections from an organized into a random mesh (thus respecting only the numerical proportions of the elements) reduced the spatial discrimination and temporal precision of the responses to incoming mossy fiber inputs. Thus, the specific topology could indeed have a relevant functional significance in terms of spatial pattern separation and elaboration of internal temporal circuit dynamics. An explicit representation of the glomerulus with internal diffusion allowing for independent generation of direct and indirect IPSCs may further improve this description. Further modeling and simulations are needed to clarify the impact of the connectivity properties of Golgi cells on a larger scale and thus to account for their intermodular organization and for the 3D organization of the connections. In particular, it seems important to incorporate the effect of inhibition among Golgi cells, the effect of gap junctions between Golgi cells, the local connectivity rules determining appropriate proportions of excitatory synapses made by local granule cell patches along the ascending axon and parallel fibers, and the clustering of mossy fiber rosettes in the parasagittal plane. This could provide further insight into the importance of the topological organization of Golgi cells.

The resetting of Golgi cell activity was also studied using this Golgi cell model in a recent simulation study that showed the impact of dendritic gap junctions on the activity of sets of Golgi cells and their desynchronization driven by external stimuli (Vervaeke et al., 2010, all these models are available at http://senselab.med.yale.edu/ModelDB).

COHERENCE AND INDIVIDUALITY OF GOLGI CELL ACTIVITY

A fundamental functional property of neuronal networks is that of sustaining *coherent oscillations*: this occurs in such a way that neurons helping to generate the oscillations are, at the same time, themselves entrained into the oscillation. Akin with this, *resonance is* a condition occurring when a physical system undergoes a periodic activation with a frequency equal or similar to the intrinsic oscillation frequency of the system itself, so that such a system tends to oscillate at its maximum amplitude (French, 1971) (**Figures 2**, **3**). The counterpart of neuronal coherence is neuronal individuality. After all, neuronal networks would not be of much use if they had to beat with all their elements always fully synchronized. The mechanism that allows neurons to temporarily escape the coherent circuit pulsation is *phase resetting* (Llinas, 1988; Buzsaki, 2006) (**Figures 2**, **3**). Interestingly, the Golgi cell expresses specific ionic channels and mechanisms that allow an independent control over oscillation, resonance and phase resetting (Solinas et al., 2010, see above).

COHERENT OSCILLATIONS AND RESONANCE

The Golgi cell has been suggested to play a critical role in generating granular layer circuit oscillations and resonance. An important observation in this respect is that the theta band has specific relevance for brain functioning and important implications for the cerebellum (D'Angelo et al., 2009). Theta-frequency oscillations are observed in the granular layer during resting activity in the awake rat and monkey (Pellerin and Lamarre, 1997; Hartmann and Bower, 1998; Courtemanche et al., 2009) and theta rhythms are observed using magneteoencephalography in awake humans (Kujala et al., 2007). Computational analysis indicates that these oscillations require an intact feedback inhibitory loop and generate a loose synchrony of the neurons involved (Maex and De Schutter, 1998; Solinas et al., 2010). Interestingly, granular layer theta-frequency oscillations are correlated with cerebrocortical activity (O'Connor et al., 2002; Gross et al., 2005; Ros et al., 2009). Golgi cells, being theta-band pacemakers, could contribute to the maintenance of cerebrocerebellar coherence, and being integrated into a syncytium, could also help to maintain granular layer coherence. An evolution of this concept is the finding that the rhythmic activity of Golgi cells can be tuned, depending on the strength of gap junction connectivity, within a few and 20 Hz (Dugue et al., 2009). Therefore, the Golgi cell interneuron network may retune itself and regulate the sensitivity toward cerebrocortical activity over a broad frequency band. Factors controlling the strength of Golgi cell electrical coupling remain to be identified.

As the concept of oscillation is akin to that of resonance, what is the relationship between resonance and oscillations in the granular layer? The nature of both phenomena depends on the physical particularities of the system involved. We recently observed that granular layer resonance reflects intrinsic properties of granule cells (D'Angelo et al., 2001; Gandolfi et al., 2013), while resonance and oscillations in the inhibitory interneuron network require gap junctions between Golgi cells (Dugue et al., 2009) and possibly also intrinsic pacemaking in Golgi cells (Forti et al., 2006). Thus, the granular layer circuit appears to be composed of multiple resonators (the mossy fiber-granule cell synapse and the Golgi cell inhibitory network) coupled one to the other and tuned within the same frequency range. The Golgi cells also provide synchronicity through lateral inhibition and can enhance resonance in the granule cell population (Gandolfi et al., 2013). In aggregate, resonance can amplify the granule cell output when the mossy fiber input is conveyed at theta frequency. At this frequency the inhibitory circuit can spontaneously oscillate, thereby creating a condition in which the system is able to optimize phase locking, information transmission and, potentially, the induction of long-term synaptic plasticity.

CELL INDIVIDUALITY AND PHASE RESETTING

Golgi cells show a high sensitivity to sensory inputs, responding in about 10 ms to punctate sensory stimulation (Vos et al., 1999a; Kanichay and Silver, 2008; Xu and Edgley, 2008; Tahon et al., 2011). This response mechanism, based on specific ionic channels distinct from those causing oscillations and resonance (see above), allows Golgi neurons to be phase reset. Thus, after a local stimulus, specific Golgi cells could escape the coherent theta cycle entraining the inhibitory network and generate a specific regulation of spike transmission through those granule cells that are under their inhibitory control. Indeed, a loose rather than a tight coherence among Golgi neurons has been reported, possibly indicating that although these neurons tend to be paced with each other, at the same time a few of them can escape the coherent oscillation to generate a specific signal in a meaningful phase relationship with the diffuse theta oscillation (Vos et al., 1999b; Volny-Luraghi et al., 2002). Extensive phase resetting

may contribute to the desynchronization of granular layer local field potential oscillations when the rat is passing from resting attentiveness to active motor behavior (Hartmann and Bower, 1998).

Just as feedback inhibition is critical in bringing about oscillations in the Golgi interneuron network, feedforward inhibition is critical in bringing about phase resetting. Network simulations have shown that the balance of the two mechanisms is also critical, oscillations being prevented when the feedforward loop is strong compared with the feedback loop (Maex and De Schutter, 1998; Solinas et al., 2010). The balance of the two loops *in vivo* remains an open issue. It is tempting to speculate that diffuse activity in the parallel fibers might sustain coherent oscillations in large Golgi cell populations, while a sufficiently strong input in a mossy fiber subset could phase reset Golgi cells, thus allowing local control of transmission through dedicated granular layer channels.

CONTROL OF SIGNAL TRANSMISSION AND PLASTICITY AT THE MOSSY FIBER-GRANULE CELL RELAY

Golgi cell inhibition, in addition to regulating the entrainment of granule cells into coherent oscillations, has multiple and complex effects on the way granule cells retransmit signals conveyed by mossy fibers. Mossy fibers usually transmit bursts or long sequences of spikes and granule cells can also emit spike bursts. Thus, once a portion of the granular layer (ideally a "microzone," see Harvey and Napper, 1991; Mapelli et al., 2010a,b)[1] is activated by a specific input, both Golgi cells and granule cells are driven by spike bursts. This makes the process of Golgi cell inhibition of granule cells particularly complex, since several non-linear (voltage-dependent, time-dependent and frequency-dependent) effects are called into play. These include the voltage-dependent electroresponsiveness of the Golgi cell, the frequency dependence of synapses impinging on the Golgi cell, and all the specific properties of Golgi cell to granule cell transmission determined by the glomerular organization of the synapses involved (see above). As a whole, burst transmission mechanisms can control the following main operations: the time-window effect (D'Angelo and De Zeeuw, 2009) (**Figure 5**), the center-surround organization of cut-off and gain of signal transmission (**Figure 6**) (Mapelli et al., 2010b), the combinatorial rearrangement of granular layer activity (**Figure 7**), and the sign intensity and extension of long-term synaptic plasticity at the mossy fiber-granule cell relay (**Figure 8**).

SPIKE TIMING AND BURST TRANSMISSION: THE TIME-WINDOW EFFECT

Once a burst is conveyed through the mossy fibers, it simultaneously activates the granule cells and the Golgi cells, thus engaging the feedforward inhibitory loop. The effect is to inhibit granule cell firing after an interval corresponding to the sum of transmission and excitation delays along the mossy fiber-Golgi cell-granule cell pathway. The permissive "time window" lasts about 4–5 ms, so that granule cells have time to fire just 1–3 spikes (D'Angelo and De Zeeuw, 2009) (**Figure 5**). In particular, since mossy fiber-granule cell LTP tends to anticipate granule cell firing and to increase its frequency, while LTD does the opposite (Nieus et al., 2006), long-term synaptic plasticity cooperates with the time-window mechanism in determining the number of spikes emitted by granule cells. This mechanism is likely to have a profound impact on the way bursts are channeled toward the molecular layer and on the way parallel fibers activate Purkinje cells and molecular layer interneurons.

A different regime of inhibition could be set up during prolonged mossy fiber discharges, like those conveyed by tonic units

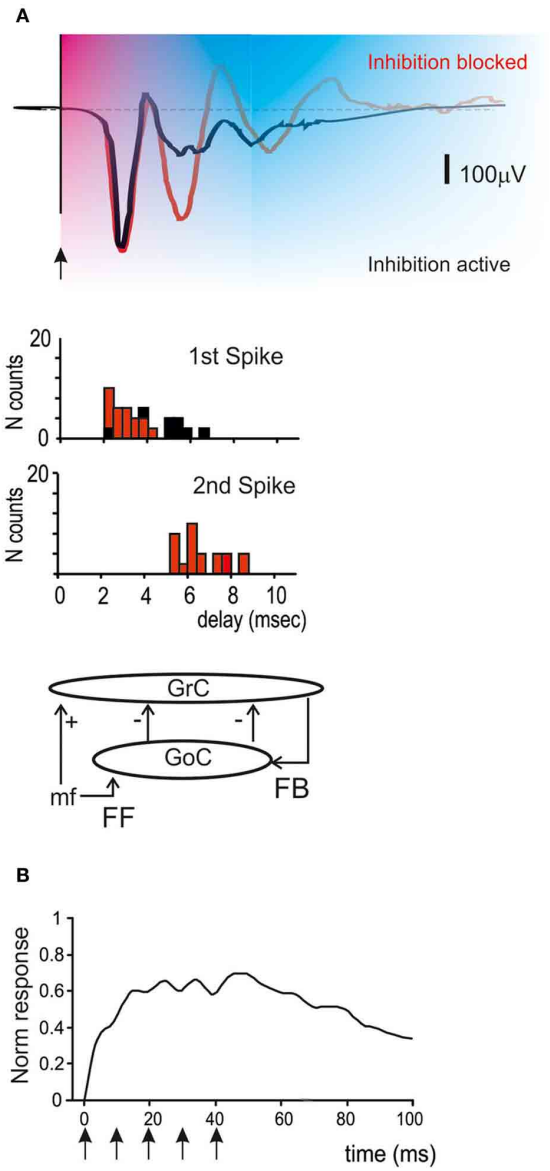

FIGURE 5 | Golgi cells and the time-window effect. (A) The time-window effect is generated due to activation of the feedforward and feedback inhibitory loops. After excitation, granule cells are inhibited by the feedforward and feedback loops in sequence leaving a permissive time window of just 4–5 ms. Then inhibition prevails, reducing or blocking the granule cell response. The histograms show spike generation in granule cells in the presence or absence of synaptic inhibition (Mapelli and D'Angelo, 2007; D'Angelo and De Zeeuw, 2009). **(B)** The time-window effect is observed in response to single pulses or short bursts but is suppressed during high-frequency repetitive stimulation of mossy fibers (see text). Stimuli are indicated by arrows [meta-analysis data from Mapelli et al. (2010a)].

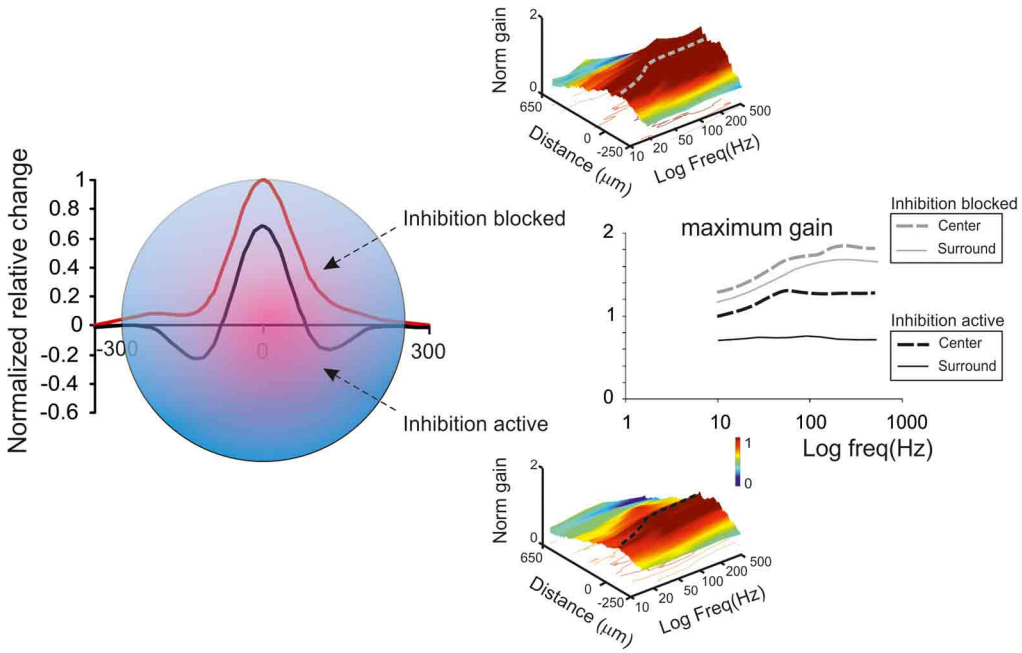

FIGURE 6 | Golgi cells and center-surround organization. The center-surround effect is generated by lateral inhibition. After excitation, granule cells in the core are excited much more strongly that those in the surrounding area. This results in the formation of a center-surround structure of about 300 μm diameter. Golgi cells modulate the gain in the center and generate net inhibition in the surround. Golgi cell inhibition tends to decrease the gain and increase the cut-off frequency of signal transmission [meta-analysis data from Mapelli et al. (2010b)].

in the proprioceptive (Kase et al., 1980) and vestibular system (Arenz et al., 2008). In this case, the inhibitory action exerted by Golgi cells over granule cells seems to be temporarily suppressed, possibly due to a series of candidate mechanisms including (i) presynaptic reduction of GABA release through tonic activation of GABA-B autoreceptors on Golgi cell synaptic terminals (Mapelli et al., 2009), (ii) presynaptic reduction of GABA release through glomerular crosstalk and activation of mGluRs on Golgi cell synaptic terminals (Mitchell and Silver, 2000a), (iii) post-synaptic reduction of granule cell inhibition through GABA-B receptor-mediated down-regulation of GABA-A IPSCs (Brandalise et al., 2012), (iv) post-synaptic enhancement of granule cell responsiveness by GABA-B receptors reducing an inward rectifier K current in granule cells (Rossi et al., 2006), (v) dendritic activation of Golgi cell mGluR2 enhancing an inward rectifier K current and helping to reduce Golgi cell firing (Watanabe and Nakanishi, 2003). It would be extremely useful to clarify the relevance of these mechanisms during natural circuit activation *in vivo*.

REGULATIONS OF TRANSMISSION GAIN AND CUT-OFF FREQUENCY

In the granular layer, signal transmission along the mossy fiber-granule cell pathway is strongly frequency-dependent (**Figure 6**), with a high-pass cut off around 50 Hz and a gain which is about two times larger at high compared to low frequencies (Mapelli et al., 2010b). This frequency dependence of gain is regulated by NMDA receptors, which, by exploiting their slow voltage-dependent kinetics and their regenerative voltage-dependent unblock, boost EPSP temporal summation (cf D'Angelo et al., 1995) in the 10–100 Hz range. AMPA receptors, which have kinetic time constants in the millisecond range, allow temporal summation at very high frequencies (200–500 Hz). Thus, the combination of the two receptor-dependent mechanisms allows transmission to be amplified over a broad frequency band covering the natural range of mossy fiber discharge (Chadderton et al., 2004; Jörntell and Ekerot, 2006).

GABA-A receptor activation through the Golgi cell loops, by reducing EPSP temporal summation in granule cells (Armano et al., 2000; for review see D'Angelo, 2008; Kanichay and Silver, 2008; D'Angelo and De Zeeuw, 2009), causes a global transmission decrease over the whole frequency range, which becomes particularly marked at low frequency (Mapelli et al., 2010b). Tonic inhibition could indeed intensify gain reduction at low frequencies (Mitchell and Silver, 2003). Therefore, the granular layer enhances transmission of high-frequency spike bursts through an alternating control of the E/I balance: at high frequencies (>50 Hz) NMDA receptor-dependent depolarization prevails over GABA-A receptor-dependent inhibition, while at low frequencies the opposite occurs. The weakening of the inhibitory loop at high frequencies could also reflect a number of mechanisms mediated by mGluR2 and GABA-B receptors (see above).

CONTROL OF THE INDUCTION OF LONG-TERM SYNAPTIC PLASTICITY

Long-term synaptic plasticity, in the form of LTP and LTD, is generated by mossy fiber bursts and requires activation of NMDA receptors and calcium influx (D'Angelo et al., 1999; Armano

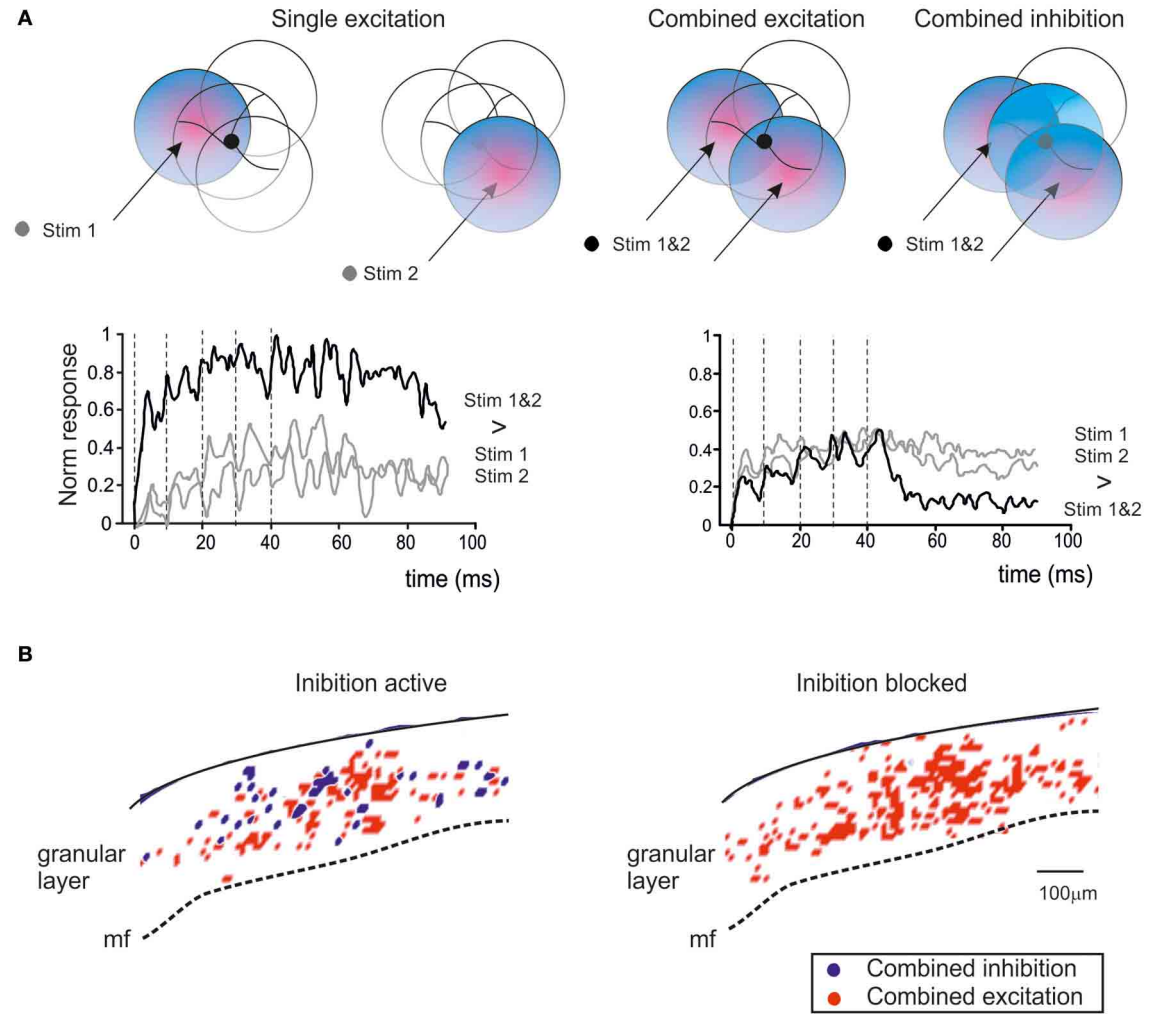

FIGURE 7 | Golgi cells and combinatorial operations. (A) When the granular layer is stimulated through multiple mossy fiber bundles (called Stim1 and Stim2), the variable arrangement of synaptic contacts can generate combined excitation of granule cells or combined excitation of Golgi cells. Combined excitation of granule cells determines responses which are stronger than those caused by each individual bundle, while combined excitation of Golgi cells results in granule cell responses smaller than those generated by each individual bundle. The plots show the intensity of granular layer responses (recorded as VSD traces) to a short mossy fiber burst (indicated by broken lines) in areas in which there is either an increase (left: *combined excitation*) or decrease (right: *combined inhibition*) of the response with combined Stim1&2 compared to Stim1 or Stim2 alone (Mapelli et al., 2010a). The effect of combined inhibition becomes evident after stimulation is terminated, probably indicating that during repeated stimulation the inhibitory effect is partially suppressed (see **Figure 5**). **(B)** Spatial distribution of areas of combined excitation and combined inhibition in the granular layer of a cerebellar slice (data elaborated from VSD recordings). Combined inhibition disappears when Golgi cell transmission is blocked with the GABA-A receptor antagonist gabazine (Mapelli et al., 2010a).

et al., 2000). LTP and LTD induction is bidirectional and follows the Bienenstock-Cooper-Munro theory (Bienenstock et al., 1982), so that the level of calcium discriminates whether LTP or LTD will occur (Gall et al., 2005; Prestori et al., 2013; D'Errico et al., 2009). Since the NMDA receptor-mediated conductance is voltage-dependent, the amount of calcium influx depends critically on the depolarization attained during the induction bursts. Interestingly, the level of granule cell depolarization attained during bursts strictly depends on synaptic inhibition provided by Golgi cells (Armano et al., 2000) and blocking inhibition turns the balance in favor of LTP both *in vitro* (Mapelli and D'Angelo, 2007) and *in vivo* (Roggeri et al., 2008). Considering the E/I balance, high E/I will determine LTP, intermediate E/I will determine LTD, and very low E/I will prevent any plasticity from occurring. Therefore, Golgi cell inhibition is a primary factor in controlling long-term synaptic plasticity in the granular layer circuit (D'Angelo and De Zeeuw, 2009).

CONTROL OF THE SPATIAL ORGANIZATION OF GRANULAR LAYER ACTIVITY

A critical aspect of circuit functioning is its topological organization during activity. The granular layer was long thought to effect a *spatiotemporal reconfiguration* of incoming inputs but the physiological basis of this process remained unclear.

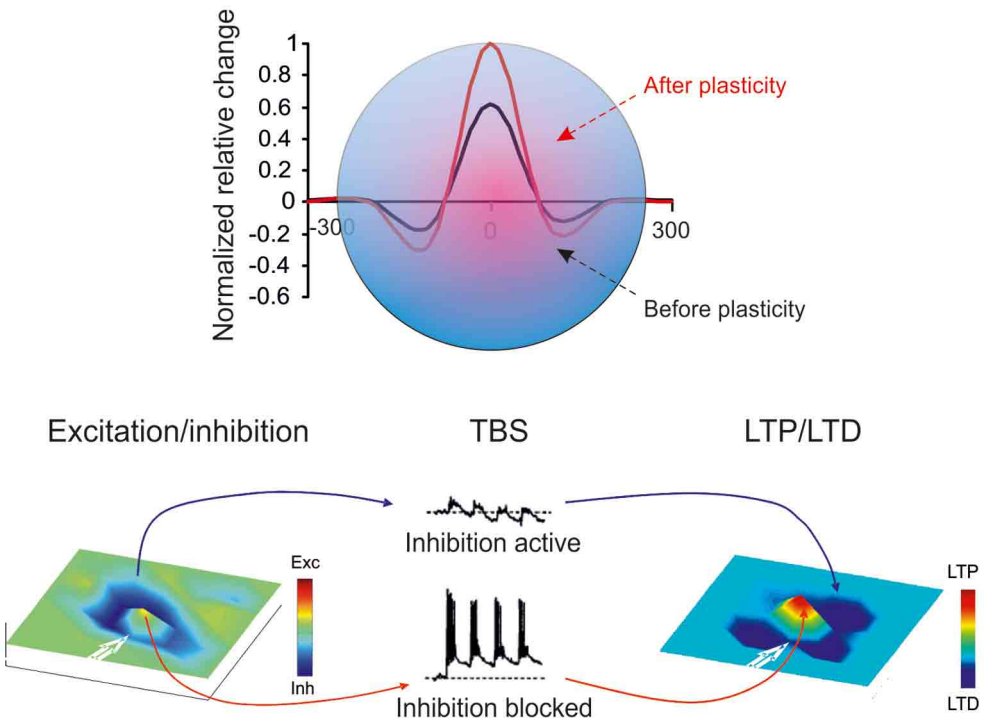

FIGURE 8 | Golgi cells and long-term synaptic plasticity. Long-term synaptic plasticity is controlled by Golgi cell synaptic inhibition through regulation of granule cell membrane potential, NMDA channel unblock at the mossy fiber-granule cell synapse, and the subsequent Ca influx in granule cell dendrites (for review see D'Angelo and De Zeeuw, 2009). The result is a marked LTP in the center and LTD in the surround, so that LTP and LTD assume a center-surround organization (Mapelli and D'Angelo, 2007).

The classical theoretical models of cerebellar function (Marr, 1969; Albus, 1971) and also subsequent cellular-based computational models (Maex and De Schutter, 1998; Medina and Mauk, 2000) used isotropic connectivity based on cell convergence/divergence ratio statistics, and left the topological problem unaddressed. Nonetheless, recent investigations using VSD imaging and MEA recordings (Mapelli and D'Angelo, 2007; Mapelli et al., 2010a,b) combined with mathematical simulations using realistic computational models (Solinas et al., 2010) have revealed that granular layer activity is topologically organized and that Golgi cells play a central role in determining this organization.

CENTER-SURROUND ORGANIZATION

As noted above, a fundamental concept of cerebellar physiology is that a punctate stimulation *in vivo* causes dense activation in granule cell clusters under LTP and LTD control (Roggeri et al., 2008; Diwakar et al., 2009; Ozden et al., 2012). High-resolution analysis *in vitro* showed that areas of dense spiking activity are surrounded by an inhibitory well (Mapelli and D'Angelo, 2007). This center-surround pattern (**Figure 6**) arises as follows: once a compact bundle of mossy fibers discharges in bursts, a group of granule cells is activated along with local Golgi cells. Since the inhibitory territory of Golgi cells is broader than their excitatory field, and since granule cell excitation diminishes radially from the excitation core, the E/I balance inverts sharply, so that excitation prevails in the core while inhibition prevails in the surrounding area (Mapelli and D'Angelo, 2007). The excited core has a radius of about 30 mm *in vivo* and contains about 260 granule cells with an up to 35% probability of firing; conversely, the firing probability in the surrounding area tends toward zero. This dense-core spiking activity can rise to 50% when Golgi cell inhibition is turned off (Diwakar et al., 2009). Thus, the Golgi cells, by virtue of lateral inhibition, play a critical role in generating center-surround responses, which have three main functional effects: (i) channeling of information through vertical transmission lines, (ii) generation of combinatorial operations among multiple inputs, and (iii) reconfiguration of network topology through control over the induction of long-term synaptic plasticity.

SIGNAL TRANSMISSION ALONG VERTICAL CHANNELS

A first consequence of granule cell cluster activation is generation of coherent activity in bundles of granule cell ascending axons running vertically toward the molecular layer followed by activation of a group of overlying Purkinje cells (Mapelli et al., 2010b). Along with this, the high E/I balance in the excitation core enhances high-frequency burst transmission, while the prevalence of inhibition in the surround selectively prevents low-frequency transmission (see above) and therefore noise diffusion throughout the network. Therefore, Golgi cells can delimit, focus and sharpen signal transmission through the molecular layer generating vertical transmission channels, as predicted by Bower's investigations (Bower and Woolston, 1983). Enhanced

activity-tracking techniques making use of 2PM and VSD imaging could be used to precisely define these signal pathways.

GENERATION OF COMBINATORIAL OPERATIONS

A second consequence of granule cell cluster activation is that it provides the basis for combining responses generated in neighboring center-surround structures (Mapelli et al., 2010a) (**Figure 7**). Simultaneous activation of two partially overlapping mossy fiber bundles gives rise to areas of combined excitation and combined inhibition, which are compatible with the concepts of *coincidence detection* and *spatial pattern separation* predicted by theory (Marr, 1969; Albus, 1971; Ito, 1984). Combined excitation appears as an area in which the combination of two inputs is greater than the arithmetic sum of the individual inputs and it is enhanced by GABA-A receptor blockers. Combined inhibition manifests itself as an area where the combination of two inputs results in a reduction of the activity evoked by either one of the two inputs alone and it is prevented by GABA-A receptor blockers. Combinatorial responses occupy small granular layer regions compatible with cluster size and they last for tens of milliseconds. Finally, it should be noted that combined inhibition occurs after bursts are terminated, in keeping with the observation that inhibition is temporarily suppressed during protracted bursts (see above).

The occurrence of combinatorial operations in multiple scattered areas points to specific local circuit topologies. In areas showing combined excitation, mossy fiber convergence onto granule cells needs to prevail (D'Angelo et al., 1995; Jörntell and Ekerot, 2006) over convergence onto Golgi cells, so that Golgi cells can only proportionately reduce granule cell activation. Conversely, in areas showing combined inhibition, the convergence of mossy fibers onto Golgi cells needs to prevail over the convergence onto granule cells, so that Golgi cells can generate effective and strong inhibition during double-bundle stimulation. It is likely that these effects require lateral inhibition (for a general discussion see Buzsaki, 2006), which has indeed been reported in the cerebellum granular layer (Mapelli and D'Angelo, 2007). These combinatorial operations, if engaged by natural input patterns *in vivo*, may be important in order to configure topologically organized spatiotemporal spike sequences to be relayed to Purkinje cells.

As shown in **Figure 7**, the generation of complex operation is expected to occur at the intersection of *center-surround* structures, so that combined inhibition occurs when most granule cell dendrites are activated in *surround* areas, while combined excitation occurs when most granule cell dendrites are activated in *center* areas. This hypothetical organization, which resembles the overlapping field hypothesis of J.C. Eccles for PCs in the molecular layer (Eccles et al., 1967), awaits for an experimental clarification.

RECONFIGURATION OF NETWORK TOPOLOGY THROUGH LONG-TERM SYNAPTIC PLASTICITY

A third consequence of the center-surround organization of activity derives from the ability of Golgi cell inhibition to control the induction of long-term synaptic plasticity (**Figure 8**; see also above). The strong excitation in the core favors LTP, while the weak excitation in the surround favors LTD. Thus, the center-surround organization of excitation and inhibition gives rise, after appropriate burst transmission, to a center-surround organization of LTP and LTD. With LTP in the center and LTD in the surround, the topological organization of transmission properties is rendered sharper.

According to Marr (1969), if input trains were to saturate granular layer plasticity, this would interfere with the efficient control of information processing. Experimental evidence (Mapelli and D'Angelo, 2007) supports the tenet that granular layer plasticity is not saturated but, instead, redistributes LTP and LTD in neighboring areas. The circuit therefore maintains a spatially organized homeostatic balance, in which activity is enhanced in certain areas while being reduced in others. Once established, LTP and LTD may be instrumental in regulating the contrast between granular layer fields, extending the original concept of spatial pattern separation (Marr, 1969), in which the excitatory/inhibitory balance of granule cells was predetermined and unchangeable. The LTP and LTD areas may represent channels for differential processing of mossy fiber inputs. In the LTP channel, the delay is reduced and the average frequency of granule cell discharge is enhanced, whereas the opposite is true in the LTD channel (Nieus et al., 2006). Moreover, on the basis of previous data (Mapelli et al., 2010b) and simulations (Solinas et al., 2010) it is expected that LTP channels show an enhanced high frequency transmission gain compared with LTD channels. This prediction awaits experimental confirmation.

CONCLUSIONS

EVOLUTION OF THE CONCEPTS OF GRANULAR LAYER FUNCTIONING

The original idea of a combinatorial arrangement of connections based on statistics rather than geometry led to the concept that the granular layer activates "sparsely" (i.e., with a very low probability of granule cell firing) and in an isotropic manner. Likewise, the predicted separation of incoming inputs into spatial patterns had no specified topology. Yet, Golgi cells were predicted to play a critical role in these processes (Marr, 1969; Albus, 1971). The granule cell-Golgi cell feedback circuit was then thought to generate temporal dynamics in the system during continuous signal processing (Fujita, 1982). However, no role was envisaged for Golgi cells in controlling long-term synaptic plasticity, simply because the latter was not thought to occur in the granular layer. This view, together with the role attributed to Golgi cells, is now radically changing, as is understanding of granular layer mechanisms as a whole. While basal activity in granule cells is sparse, activity following a localized input becomes concentrated in dense spiking clusters organized in center-surround structures (Diwakar et al., 2011; Ozden et al., 2012). Moreover, LTP and LTD do indeed exist in the granular layer (D'Angelo and De Zeeuw, 2009). Finally, granule and Golgi cells, as well as the synapses in between, show complex temporal dynamic properties (Solinas et al., 2007a,b), which impact on the behavior of the circuit.

AN INTEGRATED VIEW OF THE IMPACT OF GOLGI CELLS ON THE SPATIOTEMPORAL REGULATION OF GRANULAR LAYER ACTIVITY

At present, the main functions of the Golgi cell can be summarized as follows (**Figures 9**, **10**). Golgi cells control the timing

and rate of firing inside center-surround activity clusters and sharpen their limits through lateral inhibition. By integrating the activity of multiple center-surround structures, Golgi cells generate different kinds of associative operations. Moreover, Golgi cells regulate the balance between LTP and LTD, concentrating LTP in the more excited and LTD in the less excited areas. By so doing, Golgi cells help to generate selective transmission channels running toward the molecular layer. Interestingly, analysis of granular layer-molecular layer communication suggests that the transmission channels organized by Golgi cells strongly contribute to implementing a vertical organization of the cerebellar cortical function. This might then exploit preferential activation of local Purkinje cells and molecular layer interneurons by the granule cell ascending axon (Bower and Woolston, 1983; Mapelli et al., 2010a,b).

In addition to their effect on the topological organization and plastic rearrangement of activity, Golgi cells make an important contribution to the control of granular layer temporal dynamics. By sustaining low-frequency oscillations generated by randomly distributed inputs through their feedback loop, Golgi cells allow temporal binding of granule cell activity. By exploiting phase-resetting mechanisms through the feedforward loop, Golgi cells can convey specific mossy fiber signals through the network. In this operating mode, Golgi cells can control the number of spikes and the duration of granular layer activity following an impulse, implementing a "time-window" control mechanism, which operates differentially in the center and in the surround and is modulated by LTP and LTD.

All in all, Golgi cells seem to be the fundamental elements coordinating the spatiotemporal transformation of spike patterns occurring at the cerebellum input stage. This activity is deeply interrelated with that occurring in the cerebral cortex (Ros et al., 2009), which means that it would probably be very useful to understand how Golgi cells are activated in relation to the coordinated activity taking place in cerebrocortical loops during specific sensorimotor or cognitive operations.

Contrast enhancement in the granular layer and Purkinje cell selection could contribute to the spatiotemporal recoding of mossy fiber information predicted by theoretical network analysis (Eccles, 1973; Pellionisz and Llinás, 1979; Pellionisz and Llinas, 1980, 1982; Medina and Mauk, 2000; De Schutter and Bjaalie, 2001; Llinas and Roy, 2009) and could play a role in

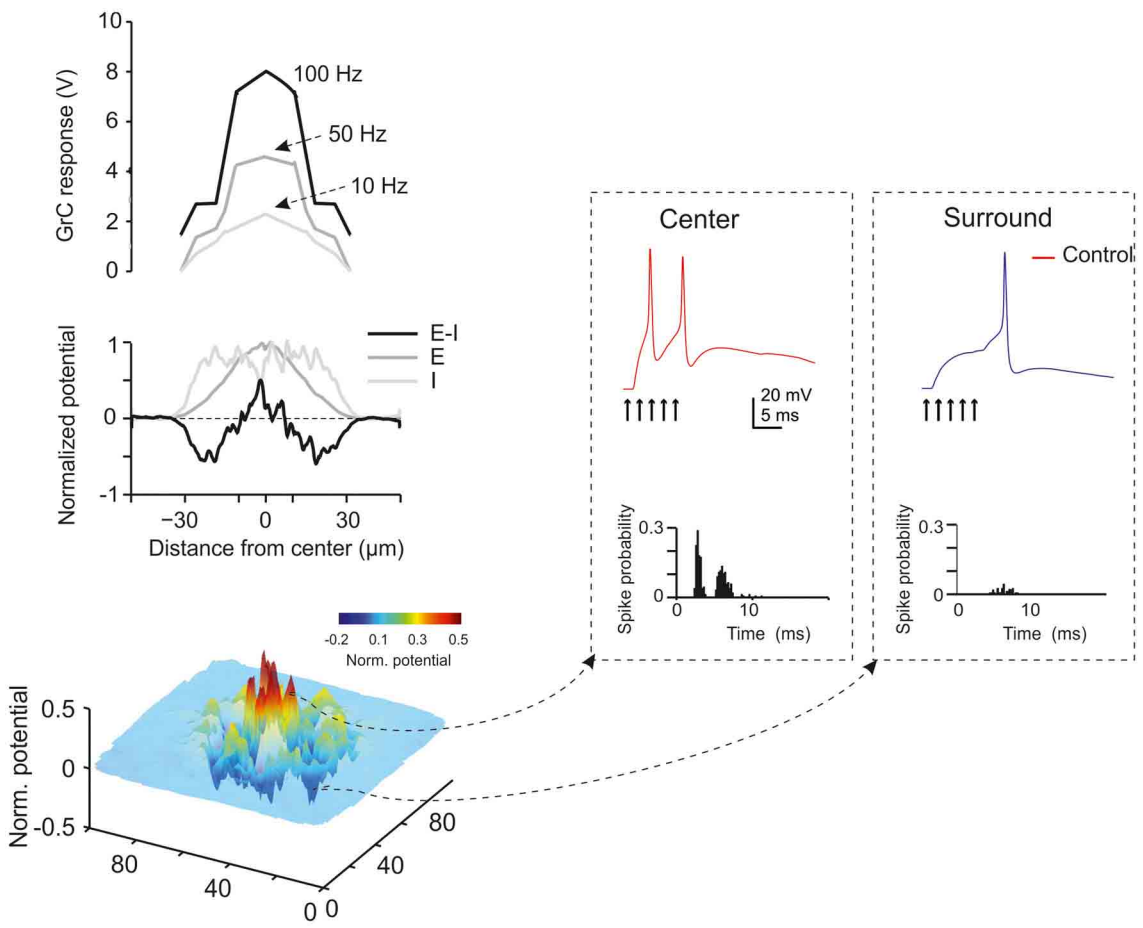

FIGURE 9 | Golgi cells and granule cell spike coding: modeling predictions. A large-scale realistic model of the granular layer predicts the impact of Golgi cell synaptic inhibition on granular layer functions including (i) center-surround organization, (ii) time windowing, (iii) gain and cut-off frequency regulation in the center-surround structure (Solinas et al., 2010).

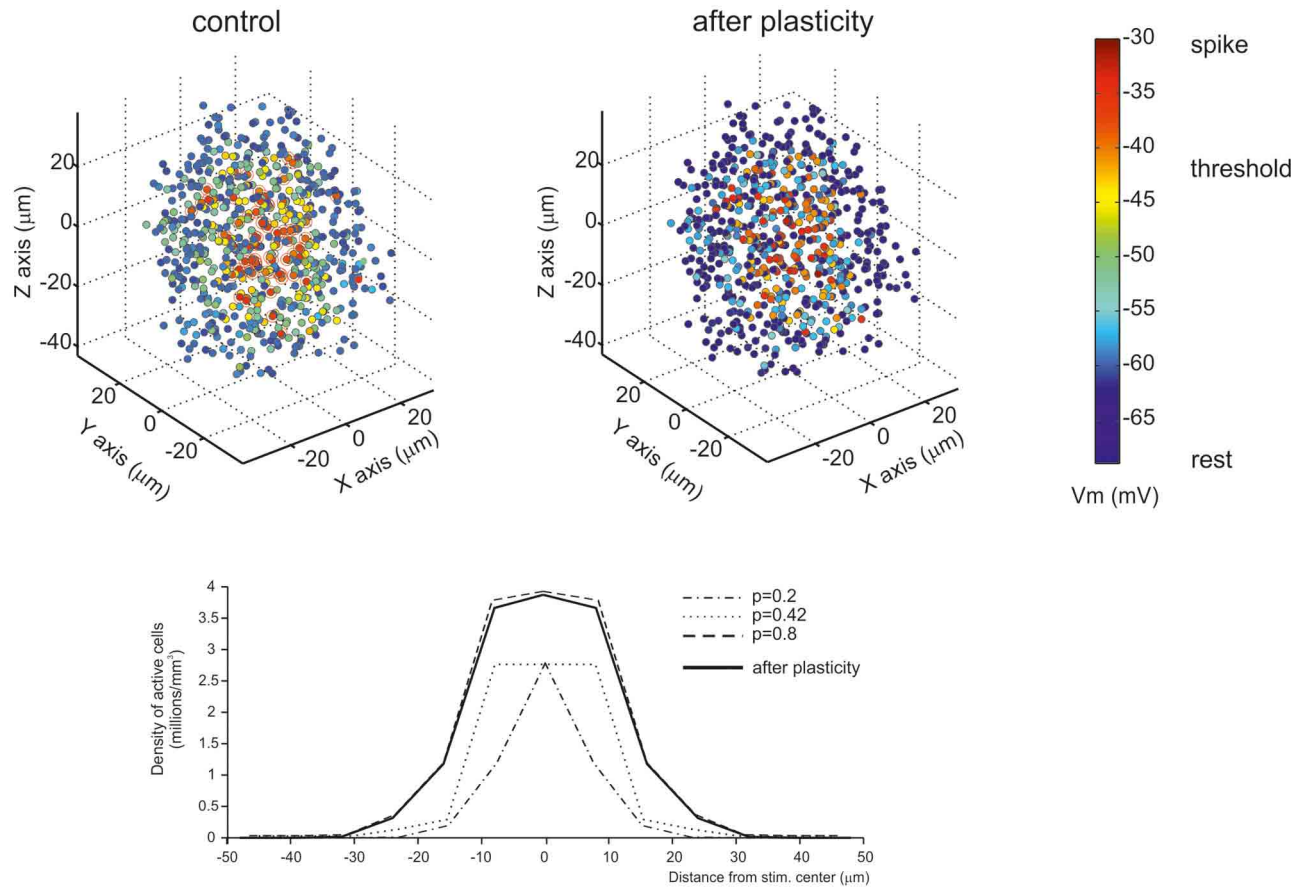

FIGURE 10 | Golgi cells and granule cell plasticity: modeling predictions. A large-scale realistic model of the granular layer predicts the impact of LTP and LTD on signal transmission in the center-surround structure. By changing neurotransmitter release probability at the mossy fiber-granule cell synapse (which is itself a function of Golgi cell synaptic inhibition, see **Figure 7**), the percentage of discharging granule cell increases in the center and decreases in the surround (from D'Angelo and Solinas, 2011).

cerebellar receptive field reshaping after sensory stimulation (Jörntell and Ekerot, 2006). Artificial network models indicate that combining lateral inhibition with Hebbian learning regulates competition between neighboring areas causing the emergence of self-organized topology, feature abstraction, and generalization (Kohonen, 1984; Rieke et al., 1997). It is important to note in this respect that, by implementing operations of the AND and XOR category, Golgi cells may constitute a *hidden layer* within the granular layer circuit, thus reinforcing the ability of the cerebellar input stage to perform extensive pattern recognition, categorization and generalization of mossy fiber inputs (Spitzer, 1998). New imaging and MEA techniques as well as appropriate large-scale network simulations may help to shed light on the potential occurrence of these properties in the granular layer of the cerebellum.

ACKNOWLEDGMENTS

This work was supported by grants from European Union to Egidio D'Angelo (CEREBNET FP7-ITN238686, REALNET FP7-ICT270434) and by grants from the Italian Ministry of Health to Egidio D'Angelo (RF-2009-1475845) and to Sergio Solinas (GR-2009-1493804).

REFERENCES

Afshari, F. S., Ptak, K., Khaliq, Z. M., Grieco, T. M., Slater, N. T., McCrimmon, D. R., et al. (2004). Resurgent Na currents in four classes of neurons of the cerebellum. *J. Neurophysiol.* 92, 2831–2843.

Albus, J. (1971). The theory of cerebellar function. *Math. Biosci.* 10, 25–61.

Andersen, B. B., Korbo, L., and Pakkenberg, B. (1992). A quantitative study of the human cerebellum with unbiased stereological techniques. *J. Comp. Neurol.* 326, 549–560.

Apps, R., and Hawkes, R. (2009). Cerebellar cortical organization: a one-map hypothesis. *Nat. Rev. Neurosci.* 10, 670–681.

Arenz, A., Silver, R. A., Schaefer, A. T., and Margrie, T. W. (2008). The contribution of single synapses to sensory representation *in vivo*. *Science* 321, 977–980.

Armano, S., Rossi, P., Taglietti, V., and D'Angelo, E. (2000). Long-term potentiation of intrinsic excitability at the mossy fiber-granule cell synapse of rat cerebellum. *J. Neurosci.* 20, 5208–5216.

Barbour, B., and Häusser, M. (1997). Intersynaptic diffusion of neurotransmitter. *Trends Neurosci.* 20, 377–384.

Barmack, N. H., and Yakhnitsa, V. (2008). Functions of interneurons in mouse cerebellum. *J. Neurosci.* 28, 1140–1152.

Beaumont, M., and Maccaferri, G. (2011). Is connexin36 critical for GABAergic hypersynchronization in the hippocampus? *J. Physiol.* 589, 1663–1680.

Bienenstock, E. L., Cooper, L. N., and Munro, P. W. (1982). Theory for the development of neuron selectivity: orientation specificity and binocular interaction in visual cortex. *J. Neurosci.* 2, 32–48.

Bower, J. M., and Woolston, D. C. (1983). Congruence of spatial organization of tactile projections to granule cell and Purkinje cell layers of cerebellar hemispheres of the albino rat: vertical organization of cerebellar cortex. *J. Neurophysiol.* 49, 745–766.

Braitenberg, V. (1967). Is the cerebellar cortex a biological clock in the millisecond range? *Prog. Brain Res.* 25, 334–346.

Braitenberg, V., Heck, D., and Sultan, F. (1997). The detection and generation of sequences as a key to cerebellar function: experiments and theory. *Behav. Brain Sci.* 20, 229–245; discussion 245–277.

Brandalise, F., Mapelli, L., Gerber, U., and Rossi, P. (2012). Golgi cell-mediated activation of postsynaptic $GABA_B$ receptors induces disinhibition of the Golgi cell-granule cell synapse in rat cerebellum. *PLoS ONE* 7:e43417. doi: 10.1371/journal.pone.0043417

Brickley, S. G., Cull-Candy, S. G., and Farrant, M. (1996). Development of a tonic form of synaptic inhibition in rat cerebellar granule cells resulting from persistent activation of GABAA receptors. *J. Physiol.* 497 (Pt 3), 753–759.

Brickley, S. G., Cull-Candy, S. G., and Farrant, M. (1999). Single-channel properties of synaptic and extrasynaptic GABAA receptors suggest differential targeting of receptor subtypes. *J. Neurosci.* 19, 2960–2973.

Brown, I. E., and Bower, J. M. (2001). Congruence of mossy fiber and climbing fiber tactile projections in the lateral hemispheres of the rat cerebellum. *J. Comp. Neurol.* 429, 59–70.

Brown, I. E., and Bower, J. M. (2002). The influence of somatosensory cortex on climbing fiber responses in the lateral hemispheres of the rat cerebellum after peripheral tactile stimulation. *J. Neurosci.* 22, 6819–6829.

Buonomano, D. V., and Mauk, M. D. (1994). Neural network model of the cerebellum: temporal discrimination and the timing of motor responses. *Neural Comput.* 6, 38–55.

Bureau, I., Dieudonné, S., Coussen, F., and Mulle, C. (2000). Kainate receptor-mediated synaptic currents in cerebellar Golgi cells are not shaped by diffusion of glutamate. *Proc. Natl. Acad. Sci. U.S.A.* 97, 6838–6843.

Buzsaki, G. (2006). *Rhythms of the Brain*. New York, NY: Oxford University Press.

Cesana, E., Dieudonné, S., Isope, P., Bidoret, C., D'Angelo, E., and Forti, L. (2010). Novel granule cell-Golgi cell excitatory input in the cerebellar granular layer. *FENS Abstr.* 5, 052.7.

Chadderton, P., Margrie, T. W., and Hausser, M. (2004). Integration of quanta in cerebellar granule cells during sensory processing. *Nature* 428, 856–860.

Courtemanche, R., Chabaud, P., and Lamarre, Y. (2009). Synchronization in primate cerebellar granule cell layer local field potentials: basic anisotropy and dynamic changes during active expectancy. *Front. Cell. Neurosci.* 3:6. doi: 10.3389/neuro.03.006.2009

D'Angelo, E. (2008). The critical role of Golgi cells in regulating spatio-temporal integration and plasticity at the cerebellum input stage. *Front. Neurosci.* 2, 35–46. doi: 10.3389/neuro.01.008.2008

D'Angelo, E., and De Zeeuw, C. I. (2009). Timing and plasticity in the cerebellum: focus on the granular layer. *Trends Neurosci.* 32, 30–40.

D'Angelo, E., Rossi, P., and Garthwaite, J. (1990). Dual-component NMDA receptor currents at a single central synapse. *Nature* 346, 467–470.

D'Angelo, E., De Filippi, G., Rossi, P., and Taglietti, V. (1995). Synaptic excitation of individual rat cerebellar granule cells *in situ*: evidence for the role of NMDA receptors. *J. Physiol.* 484 (Pt 2), 397–413.

D'Angelo, E., Rossi, P., Armano, S., and Taglietti, V. (1999). Evidence for NMDA and mGlu receptor-dependent long-term potentiation of mossy fiber-granule cell transmission in rat cerebellum. *J. Neurophysiol.* 81, 277–287.

D'Angelo, E., Nieus, T., Maffei, A., Armano, S., Rossi, P., Taglietti, V., et al. (2001). Theta-frequency bursting and resonance in cerebellar granule: experimental evidence and modeling of a slow K+-dependent mechanism. *J. Neurosci.* 21, 759–770.

D'Angelo, E., Koekkoek, S. K., Lombardo, P., Solinas, S., Ros, E., Garrido, J., et al. (2009). Timing in the cerebellum: oscillations and resonance in the granular layer. *Neuroscience* 162, 805–815.

D'Angelo, E., and Casali, S. (2012). Seeking a unified framework for cerebellar function and dysfunction: from circuit operations to cognition. *Front. Neural. Circuits* 6:116. doi: 10.3389/fncir.2012.00116

D'Errico, A., Prestori, F., and D'Angelo, E. (2009). Differential induction of bidirectional long-term changes in neurotransmitter release by frequency-coded patterns at the cerebellar input. *J. Physiol.* 587, 5843–5857.

De Schutter, E. (2000). *Computational Neuroscience: Realistic Modeling for Experimentalists*. Boca Raton, FL: CRC Press.

De Schutter, E., and Bjaalie, J. G. (2001). "Coding in the granular layer of the cerebellum, Chapter 18," in *Progress in Brain Research,* ed M. A. L. Nicolelis (Amsterdam: Elsevier), 279–296.

Dieudonne, S. (1998). Submillisecond kinetics and low efficacy of parallel fibre-Golgi cell synaptic currents in the rat cerebellum. *J. Physiol.* 510 (Pt 3), 845–866.

Dieudonne, S., and Dumoulin, A. (2000). Serotonin-driven long-range inhibitory connections in the cerebellar cortex. *J. Neurosci.* 20, 1837–1848.

Diwakar, S., Magistretti, J., Goldfarb, M., Naldi, G., and D'Angelo, E. (2009). Axonal Na+ channels ensure fast spike activation and back-propagation in cerebellar granule cells. *J. Neurophysiol.* 101, 519–532.

Diwakar, S., Lombardo, P., Solinas, S., Naldi, G., and D'Angelo, E. (2011). Local field potential modeling predicts dense activation in cerebellar granule cells clusters under LTP and LTD control. *PLoS ONE* 6:e21928. doi: 10.1371/journal.pone.0021928

Dugue, G. P., Brunel, N., Hakim, V., Schwartz, E., Chat, M., Levesque, M., et al. (2009). Electrical coupling mediates tunable low-frequency oscillations and resonance in the cerebellar Golgi cell network. *Neuron* 61, 126–139.

Duguid, I., Branco, T., London, M., Chadderton, P., and Häusser, M. (2012). Tonic inhibition enhances fidelity of sensory information transmission in the cerebellar cortex. *J. Neurosci.* 32, 11132–11143.

Dugué, G. P., Dumoulin, A., Triller, A., and Dieudonné, S. (2005). Target-dependent use of co-released inhibitory transmitters at central synapses. *J. Neurosci.* 25, 6490–6498.

Dumoulin, A., Triller, A., and Dieudonne, S. (2001). IPSC kinetics at identified GABAergic and mixed GABAergic and glycinergic synapses onto cerebellar Golgi cells. *J. Neurosci.* 21, 6045–6057.

D'Angelo, E., and Solinas, S. (2011). "Realistic modeling of large-scale networks: spatio-temporal dynamics and long-term synaptic plasticity in the cerebellum," in *Advances in Computational Intelligence*, eds J. Cabestany, I. Rojas, and G. Joya (Berlin, Heidelberg: Springer), 547–553.

Eccles, J., Llinàs, R., and Sasaki, K. (1964). Golgi cell inhibition in the cerebellar cortex. *Nature* 204, 1265–1266.

Eccles, J. C. (1973). The cerebellum as a computer: patterns in space and time. *J. Physiol.* 229, 1–32.

Eccles, J. C., Llinas, R., and Sasaki, K. (1966). The mossy fibre-granule cell relay of the cerebellum and its inhibitory control by Golgi cells. *Exp. Brain Res.* 1, 82–101.

Eccles, J. C., Ito, M., and Szentagothai, J. (1967). *The Cerebellum as a Neural Machine*. Berlin, Heidelberg; New York: Springer-Verlag.

Edgley, S. A., and Lidierth, M. (1987). The discharges of cerebellar Golgi cells during locomotion in the cat. *J. Physiol.* 392, 315–332.

Farrant, M., and Nusser, Z. (2005). Variations on an inhibitory theme: phasic and tonic activation of GABA(A) receptors. *Nat. Rev. Neurosci.* 6, 215–229.

Forti, L., Cesana, E., Mapelli, J., and D'Angelo, E. (2006). Ionic mechanisms of autorhythmic firing in rat cerebellar Golgi cells. *J. Physiol.* 574, 711–729.

French, A. (1971). Vibrations and waves. Boca Raton, FL: CRC press.

Fujita, M. (1982). Adaptive filter model of the cerebellum. *Biol. Cybern.* 45, 195–206.

Gall, D., Prestori, F., Sola, E., D'Errico, A., Roussel, C., Forti, L., et al. (2005). Intracellular calcium regulation by burst discharge determines bidirectional long-term synaptic plasticity at the cerebellum input stage. *J. Neurosci.* 25, 4813–4822.

Galliano, E., Mazzarello, P., and D'Angelo, E. (2010). Discovery and rediscoveries of Golgi cells. *J. Physiol.* 588, 3639–3655.

Galliano, E., Baratella, M., Sgritta, M., Ruigrok, T. J., Haasdijk, E. D., Hoebeek, F. E., et al. (2013). Anatomical investigation of potential contacts between climbing fibers and cerebellar Golgi cells in the mouse. *Front. Neural Circuits* 7:59. doi: 10.3389/fncir.2013.00059

Gandolfi, D., Lombardo, P., Mapelli, J., Solinas, S., and D'Angelo, E. (2013). Theta-frequency resonance at the cerebellum input stage improves spike-timing on the millisecond

time-scale. *Front. Neural Circuits* 7:64. doi: 10.3389/fncir.2013.00064

Geurts, F., Schutter, E., and Dieudonné, S. (2003). Unraveling the cerebellar cortex: cytology and cellular physiology of large-sized interneurons in the granular layer. *Cerebellum* 2, 290–299.

Geurts, F. J., Timmermans, J., Shigemoto, R., and De Schutter, E. (2001). Morphological and neurochemical differentiation of large granular layer interneurons in the adult rat cerebellum. *Neuroscience* 104, 499–512.

Golgi, C. (1874). Sulla fine anatomia del cervelletto umano. *Archivio Italiano per le Malattie Nervose* 2, 90–107.

Gross, J., Pollok, B., Dirks, M., Timmermann, L., Butz, M., and Schnitzler, A. (2005). Task-dependent oscillations during unimanual and bimanual movements in the human primary motor cortex and SMA studied with magnetoencephalography. *Neuroimage* 26, 91–98.

Hadley, S. H., and Amin, J. (2007). Rat α6β2δ GABAA receptors exhibit two distinct and separable agonist affinities. *J. Physiol.* 581, 1001–1018.

Hamann, M., Rossi, D. J., and Attwell, D. (2002). Tonic and spillover inhibition of granule cells control information flow through cerebellar cortex. *Neuron* 33, 625–633.

Hamori, J., and Somogyi, J. (1983). Differentiation of cerebellar mossy fiber synapses in the rat: a quantitative electron microscope study. *J. Comp. Neurol.* 220, 365–377.

Hartmann, M. J., and Bower, J. M. (1998). Oscillatory activity in the cerebellar hemispheres of unrestrained rats. *J. Neurophysiol.* 80, 1598–1604.

Hartmann, M. J., and Bower, J. M. (2001). Tactile responses in the granule cell layer of cerebellar folium crus IIa of freely behaving rats. *J. Neurosci.* 21, 3549–3563.

Harvey, R. J., and Napper, R. M. (1991). Quantitative studies on the mammalian cerebellum. *Prog. Neurobiol.* 36, 437–463.

Heine, S. A., Highstein, S. M., and Blazquez, P. M. (2010). Golgi cells operate as state-specific temporal filters at the input stage of the cerebellar cortex. *J. Neurosci.* 30, 17004–17014.

Holtzman, T., and Jörntell, H. (2011). Sensory coding by cerebellar mossy fibres through inhibition-driven phase resetting and synchronisation. *PLoS ONE* 6:e26503. doi: 10.1371/journal.pone.0026503

Holtzman, T., Rajapaksa, T., Mostofi, A., and Edgley, S. A. (2006). Different responses of rat cerebellar Purkinje cells and Golgi cells evoked by widespread convergent sensory inputs. *J. Physiol.* 574, 491–507.

Hull, C., and Regehr, W. G. (2012). Identification of an inhibitory circuit that regulates cerebellar Golgi cell activity. *Neuron* 73, 149–158.

Ito, M. (1984). *The Cerebellum and Neural Control*. New York, NY: Raven Press.

Jakab, R. L., and Hamori, J. (1988). Quantitative morphology and synaptology of cerebellar glomeruli in the rat. *Anat. Embryol. (Berl.)* 179, 81–88.

Jörntell, H., and Ekerot, C.-F. (2006). Properties of somatosensory synaptic integration in cerebellar granule cells *in vivo*. *J. Neurosci.* 26, 11786–11797.

Kanichay, R., and Silver, R. (2008). Synaptic and cellular properties of the feedforward inhibitory circuit within the input layer of the cerebellar cortex. *J. Neurosci.* 28, 8955–8967.

Kase, M., Miller, D. C., and Noda, H. (1980). Discharges of Purkinje cells and mossy fibres in the cerebellar vermis of the monkey during saccadic eye movements and fixation. *J. Physiol.* 300, 539–555.

Kleinfeld, D., Ahissar, E., and Diamond, M. E. (2006). Active sensation: insights from the rodent vibrissa sensorimotor system. *Curr. Opin. Neurobiol.* 16, 435–444.

Kohonen, T. (1984). *Self-Organization and Associative Memory*. Berlin: Springer-Verlag.

Korbo, L., Andersen, B. B., Ladefoged, O., and Møller, A. (1993). Total numbers of various cell types in rat cerebellar cortex estimated using an unbiased stereological method. *Brain Res.* 609, 262–268.

Kujala, J., Pammer, K., Cornelissen, P., Roebroeck, A., Formisano, E., and Salmelin, R. (2007). Phase coupling in a cerebro-cerebellar network at 8–13 Hz during reading. *Cereb. Cortex* 17, 1476–1485.

Lee, S., Yoon, B.-E., Berglund, K., Oh, S.-J., Park, H., Shin, H.-S., et al. (2010). Channel-mediated tonic GABA release from Glia. *Science* 330, 790–796.

Llinas, R. R. (1988). The intrinsic electrophysiological properties of mammalian neurons: insights into central nervous system function. *Science* 242, 1654–1664.

Llinas, R. R., and Roy, S. (2009). The prediction imperative' as the basis for self-awareness. *Philos. Trans. R Soc. Lond. B Biol. Sci.* 364, 1301–1307.

Maex, R., and De Schutter, E. (1998). Synchronization of golgi and granule cell firing in a detailed network model of the cerebellar granule cell layer. *J. Neurophysiol.* 80, 2521–2537.

Maex, R., and De Schutter, E. (2005). Oscillations in the cerebellar cortex: a prediction of their frequency bands. *Prog. Brain Res.* 148, 181–188.

Mapelli, J., and D'Angelo, E. (2007). The spatial organization of long-term synaptic plasticity at the input stage of cerebellum. *J. Neurosci.* 27, 1285–1296.

Mapelli, J., Gandolfi, D., and D'Angelo, E. (2010a). Combinatorial responses controlled by synaptic inhibition in the cerebellum granular layer. *J. Neurophysiol.* 103, 250–261.

Mapelli, J., Gandolfi, D., and D'Angelo, E. (2010b). High-pass filtering and dynamic gain regulation enhance vertical bursts transmission along the mossy fiber pathway of cerebellum. *Front. Cell. Neurosci.* 4:14. doi: 10.3389/fncel.2010.00014

Mapelli, L., Rossi, P., Nieus, T., and D'Angelo, E. (2009). Tonic activation of GABAB receptors reduces release probability at inhibitory connections in the cerebellar glomerulus. *J. Neurophysiol.* 101, 3089–3099.

Marr, D. (1969). A theory of cerebellar cortex. *J. Physiol.* 202, 437–470.

Mathews, P. J., Lee, K. H., Peng, Z., Houser, C. R., and Otis, T. S. (2012). Effects of climbing fiber driven inhibition on purkinje neuron spiking. *J. Neurosci.* 32, 17988–17997.

Medina, J. F., and Mauk, M. D. (2000). Computer simulation of cerebellar information processing. *Nat. Neurosci.* 3(Suppl) 1205–1211.

Miles, F. A., Fuller, J. H., Braitman, D. J., and Dow, B. M. (1980). Long-term adaptive changes in primate vestibuloocular reflex. III. Electrophysiological observations in flocculus of normal monkeys. *J. Neurophysiol.* 43, 1437–1476.

Misra, C., Brickley, S. G., Farrant, M., and Cull-Candy, S. G. (2000). Identification of subunits contributing to synaptic and extrasynaptic NMDA receptors in Golgi cells of the rat cerebellum. *J. Physiol.* 524, 147–162.

Mitchell, S. J., and Silver, R. A. (2000a). Glutamate spillover suppresses inhibition by activating presynaptic mGluRs. *Nature* 404, 498–502.

Mitchell, S. J., and Silver, R. A. (2000b). GABA spillover from single inhibitory axons suppresses low-frequency excitatory transmission at the cerebellar glomerulus. *J. Neurosci.* 20, 8651–8658.

Mitchell, S. J., and Silver, R. A. (2003). Shunting inhibition modulates neuronal gain during synaptic excitation. *Neuron* 38, 433–445.

Morissette, J., and Bower, J. M. (1996). Contribution of somatosensory cortex to responses in the rat cerebellar granule cell layer following peripheral tactile stimulation. *Exp. Brain Res.* 109, 240–250.

Nieus, T., Sola, E., Mapelli, J., Saftenku, E., Rossi, P., and D'Angelo, E. (2006). LTP regulates burst initiation and frequency at mossy fiber-granule cell synapses of rat cerebellum: experimental observations and theoretical predictions. *J. Neurophysiol.* 95, 686–699.

Nusser, Z., Sieghart, W., and Somogyi, P. (1998). Segregation of Different GABAA Receptors to Synaptic and Extrasynaptic Membranes of Cerebellar Granule Cells. *J. Neurosci.* 18, 1693–1703.

O'Connor, S. M., Berg, R. W., and Kleinfeld, D. (2002). Coherent electrical activity between vibrissa sensory areas of cerebellum and neocortex is enhanced during free whisking. *J. Neurophysiol.* 87, 2137–2148.

Oberdick, J., and Sillitoe, R. V. (2011). Cerebellar zones: history, development, and function. *Cerebellum* 10, 301–306.

Ozden, I., Dombeck, D. A., Hoogland, T. M., Tank, D. W., and Wang, S. S. H. (2012). Widespread state-dependent shifts in cerebellar activity in locomoting mice. *PLoS ONE* 7:e42650. doi: 10.1371/journal.pone.0042650

Palay, S. L., and Chan-Palay, V. (1974). *Cerebellar Cortex: Cytology and Organization*. New York, NY: Springer-Verlag.

Palkovits, M., Magyar, P., and Szentágothai, J. (1971). Quantitative histological analysis of the cerebellar cortex in the cat: II. Cell numbers and densities in the granular layer. *Brain Res.* 32, 15–30.

Pellerin, J. P., and Lamarre, Y. (1997). Local field potential oscillations in primate cerebellar cortex during voluntary movement. *J. Neurophysiol.* 78, 3502–3507.

Pellionisz, A., and Szentagothai, J. (1973). Dynamic single unit simulation of a realistic cerebellar network model. *Brain Res.* 49, 83–99.

Pellionisz, A., and Llinás, R. (1979). Brain modeling by tensor network theory and computer simulation.

The cerebellum: distributed processor for predictive coordination. *Neuroscience* 4, 323–348.

Pellionisz, A., and Llinas, R. (1980). Tensorial approach to the geometry of brain function: cerebellar coordination via a metric tensor. *Neuroscience* 5, 1125–1138.

Pellionisz, A., and Llinas, R. (1982). Space-time representation in the brain. the cerebellum as a predictive space-time metric tensor. *Neuroscience* 7, 2949–2970.

Pijpers, A., Apps, R., Pardoe, J., Voogd, J., and Ruigrok, T. J. (2006). Precise spatial relationships between mossy fibers and climbing fibers in rat cerebellar cortical zones. *J. Neurosci.* 26, 12067–12080.

Prestori, F., Bonardi, C., Mapelli, L., Lombardo, P., Goselink, R., De Stefano, M. E., et al. (2013). Gating of long-term potentiation by nicotinic acetylcholine receptors at the cerebellum input stage. *PLoS ONE* (in press).

Prsa, M., Dash, S., Catz, N., Dicke, P. W., and Thier, P. (2009). Characteristics of responses of Golgi cells and mossy fibers to eye saccades and saccadic adaptation recorded from the posterior vermis of the cerebellum. *J. Neurosci.* 29, 250–262.

Ramón y Cajal, S. (1888). Sobre las fibras nerviosas de la capa molecular del cerebelo. *Rev. Trim. Histol. Norm. Patol.* 1, 65–78.

Ramón y Cajal, S. (1911). *Histologie du Sistéme Nerveux de L'homme et des Vertebras* (Transl, L. Azoulay). Paris: Maloine.

Ramón y Cajal, S. (1995). *Histology of the Nervous system of Man and Vertebrates* (Transl. N. Swanson and L. Swanson). New York, NY: Oxford University Press.

Rancz, E. A., Ishikawa, T., Duguid, I., Chadderton, P., Mahon, S., and Hausser, M. (2007). High-fidelity transmission of sensory information by single cerebellar mossy fibre boutons. *Nature* 450, 1245–1248.

Rieke, F., Warland, D., de Ruyter van Steveninck, R., and Bialek, W. (1997). *Spikes: Exploring the Neural Code*. Cambridge, MA: MIT Press.

Robberechts, Q., Wijnants, M., Giugliano, M., and De Schutter, E. (2010). Long-term depression at parallel fiber to Golgi cell synapses. *J. Neurophysiol.* 104, 3413–3423.

Roggeri, L., Rivieccio, B., Rossi, P., and D'Angelo, E. (2008). Tactile stimulation evokes long-term synaptic plasticity in the granular layer of cerebellum. *J. Neurosci.* 28, 6354–6359.

Ros, H., Sachdev, R. N. S., Yu, Y., Sestan, N., and McCormick, D. A. (2009). Neocortical networks entrain neuronal circuits in cerebellar cortex. *J. Neurosci.* 29, 10309–10320.

Rossi, D. J., and Hamann, M. (1998). Spillover-mediated transmission at inhibitory synapses promoted by high affinity alpha6 subunit GABA(A) receptors and glomerular geometry. *Neuron* 20, 783–795.

Rossi, D. J., Hamann, M., and Attwell, D. (2003). Multiple modes of GABAergic inhibition of rat cerebellar granule cells. *J. Physiol.* 548, 97–110.

Rossi, P., Mapelli, L., Roggeri, L., Gall, D., de Kerchove d'Exaerde, A., Schiffmann, S. N., et al. (2006). Inhibition of constitutive inward rectifier currents in cerebellar granule cells by pharmacological and synaptic activation of GABA receptors. *Eur. J. Neurosci.* 24, 419–432.

Santamaria, F., Tripp, P. G., and Bower, J. M. (2007). Feedforward inhibition controls the spread of granule cell-induced Purkinje cell activity in the cerebellar cortex. *J. Neurophysiol.* 97, 248–263.

Shinoda, Y., Sugihara, I., Wu, H. S., and Sugiuchi, Y. (2000). The entire trajectory of single climbing and mossy fibers in the cerebellar nuclei and cortex. *Prog. Brain Res.* 124, 173–186.

Sillitoe, R. V., Chung, S. H., Fritschy, J. M., Hoy, M., and Hawkes, R. (2008). Golgi cell dendrites are restricted by Purkinje cell stripe boundaries in the adult mouse cerebellar cortex. *J. Neurosci.* 28, 2820–2826.

Simat, M., Parpan, F., and Fritschy, J. M. (2007). Heterogeneity of glycinergic and gabaergic interneurons in the granule cell layer of mouse cerebellum. *J. Comp. Neurol.* 500, 71–83.

Solinas, S., and D'Angelo, E. (2012). Realistic computational modelling of the cerebellar cortex. *FENS Abstr.* 6, 153.22.

Solinas, S., Nieus, T., and D'Angelo, E. (2010). A realistic large-scale model of the cerebellum granular layer predicts circuit spatio-temporal filtering properties. *Front. Cell. Neurosci.* 4:12. doi: 10.3389/fncel.2010.00012

Solinas, S., Forti, L., Cesana, E., Mapelli, J., De Schutter, E., and D'Angelo, E. (2007a). Computational reconstruction of pacemaking and intrinsic electroresponsiveness in cerebellar Golgi cells. *Front. Cell. Neurosci.* 1:2. doi: 10.3389/neuro.03.002.2007

Solinas, S., Forti, L., Cesana, E., Mapelli, J., De Schutter, E., and D'Angelo, E. (2007b). Fast-reset of pacemaking and theta-frequency resonance patterns in cerebellar golgi cells: simulations of their impact *in vivo*. *Front. Cell. Neurosci.* 1:4. doi: 10.3389/neuro.03.004.2007

Sotelo, C., and Llinas, R. (1972). Specialized membrane junctions between neurons in the vertebrate cerebellar cortex. *J. Cell Biol.* 53, 271–289.

Spitzer, M. (ed.). (1998). *The Mind Within the Net*. Cambridge, MA: MIT Press.

Sultan, F., and Heck, D. (2003). Detection of sequences in the cerebellar cortex: numerical estimate of the possible number of tidal-wave inducing sequences represented. *J. Physiol. (Paris)* 97, 591–600.

Tahon, K., Wijnants, M., De Schutter, E., and Maex, R. (2011). Current source density correlates of cerebellar Golgi and Purkinje cell responses to tactile input. *J. Neurophysiol.* 105, 1327–1341.

Tia, S., Wang, J. F., Kotchabhakdi, N., and Vicini, S. (1996). Developmental changes of inhibitory synaptic currents in cerebellar granule neurons: role of GABAA receptor α6 subunit. *J. Neurosci.* 16, 3630–3640.

Tovar, K. R., Maher, B. J., and Westbrook, G. L. (2009). Direct actions of carbenoxolone on synaptic transmission and neuronal membrane properties. *J. Neurophysiol.* 102, 974–978.

van Kan, P. L., Gibson, A. R., and Houk, J. C. (1993). Movement-related inputs to intermediate cerebellum of the monkey. *J. Neurophysiol.* 69, 74–94.

Vervaeke, K., Lorincz, A., Gleeson, P., Farinella, M., Nusser, Z., and Silver, R. A. (2010). Rapid desynchronization of an electrically coupled interneuron network with sparse excitatory synaptic input. *Neuron* 67, 435–451.

Vessey, J. P., Lalonde, M. R., Mizan, H. A., Welch, N. C., Kelly, M. E. M., and Barnes, S. (2004). Carbenoxolone inhibition of voltage-gated Ca channels and synaptic transmission in the retina. *J. Neurophysiol.* 92, 1252–1256.

Volny-Luraghi, A., Maex, R., Vosdagger, B., and De Schutter, E. (2002). Peripheral stimuli excite coronal beams of Golgi cells in rat cerebellar cortex. *Neuroscience* 113, 363–373.

Voogd, J., Pardoe, J., Ruigrok, T. J., and Apps, R. (2003). The distribution of climbing and mossy fiber collateral branches from the copula pyramidis and the paramedian lobule: congruence of climbing fiber cortical zones and the pattern of zebrin banding within the rat cerebellum. *J. Neurosci.* 23, 4645–4656.

Vos, B. P., Volny-Luraghi, A., and De Schutter, E. (1999a). Cerebellar Golgi cells in the rat: receptive fields and timing of responses to facial stimulation. *Eur. J. Neurosci.* 11, 2621–2634.

Vos, B. P., Maex, R., Volny-Luraghi, A., and De Schutter, E. (1999b). Parallel fibers synchronize spontaneous activity in cerebellar Golgi cells. *J. Neurosci.* 19, RC6.

Vos, B. P., Volny-Luraghi, A., Maex, R., and Schutter, E. D. (2000). Precise spike timing of tactile-evoked cerebellar Golgi cell responses: a reflection of combined mossy fiber and parallel fiber activation? *Prog. Brain Res.* 124, 95–106.

Watanabe, D., and Nakanishi, S. (2003). mGluR2 postsynaptically senses granule cell inputs at Golgi cell synapses. *Neuron* 39, 821–829.

Wu, H. S., Sugihara, I., and Shinoda, Y. (1999). Projection patterns of single mossy fibers originating from the lateral reticular nucleus in the rat cerebellar cortex and nuclei. *J. Comp. Neurol.* 411, 97–118.

Xu, W., and Edgley, S. A. (2008). Climbing fibre-dependent changes in Golgi cell responses to peripheral stimulation. *J. Physiol.* 586, 4951–4959.

Conflict of Interest Statement: The authors declare that the research was conducted in the absence of any commercial or financial relationships that could be construed as a potential conflict of interest.

Received: 21 February 2013; accepted: 27 April 2013; published online: 17 May 2013.

Citation: D'Angelo E, Solinas S, Mapelli J, Gandolfi D, Mapelli L and Prestori F (2013) The cerebellar Golgi cell and spatiotemporal organization of granular layer activity. Front. Neural Circuits 7:93. doi: 10.3389/fncir.2013.00093

frontiers in
NEURAL CIRCUITS

ORIGINAL RESEARCH ARTICLE
published: 21 May 2013
doi: 10.3389/fncir.2013.00095

High frequency burst firing of granule cells ensures transmission at the parallel fiber to Purkinje cell synapse at the cost of temporal coding

Boeke J. van Beugen[1], Zhenyu Gao[1], Henk-Jan Boele[1], Freek Hoebeek[1] and Chris I. De Zeeuw[1,2]*

[1] Department of Neuroscience, Erasmus MC Rotterdam, Netherlands
[2] Netherlands Institute for Neuroscience, Royal Dutch Academy of Arts and Sciences, Amsterdam, Netherlands

Edited by:
Egidio D'Angelo, University of Pavia, Italy

Reviewed by:
Egidio D'Angelo, University of Pavia, Italy
David Parker, Cambridge University, UK

***Correspondence:**
Chris I. De Zeeuw, Department of Neuroscience, Erasmus MC, 3000 DR Rotterdam, Netherlands.
e-mail: c.dezeeuw@erasmusmc.nl

Cerebellar granule cells (GrCs) convey information from mossy fibers (MFs) to Purkinje cells (PCs) via their parallel fibers (PFs). MF to GrC signaling allows transmission of frequencies up to 1 kHz and GrCs themselves can also fire bursts of action potentials with instantaneous frequencies up to 1 kHz. So far, in the scientific literature no evidence has been shown that these high-frequency bursts also exist in awake, behaving animals. More so, it remains to be shown whether such high-frequency bursts can transmit temporally coded information from MFs to PCs and/or whether these patterns of activity contribute to the spatiotemporal filtering properties of the GrC layer. Here, we show that, upon sensory stimulation in both un-anesthetized rabbits and mice, GrCs can show bursts that consist of tens of spikes at instantaneous frequencies over 800 Hz. *In vitro* recordings from individual GrC-PC pairs following high-frequency stimulation revealed an overall low initial release probability of ∼0.17. Nevertheless, high-frequency burst activity induced a short-lived facilitation to ensure signaling within the first few spikes, which was rapidly followed by a reduction in transmitter release. The facilitation rate among individual GrC-PC pairs was heterogeneously distributed and could be classified as either "reluctant" or "responsive" according to their release characteristics. Despite the variety of efficacy at individual connections, grouped activity in GrCs resulted in a linear relationship between PC response and PF burst duration at frequencies up to 300 Hz allowing rate coding to persist at the network level. Together, these findings support the hypothesis that the cerebellar granular layer acts as a spatiotemporal filter between MF input and PC output (D'Angelo and De Zeeuw, 2009).

Keywords: cerebellum, synaptic transmission, parallel fiber, Purkinje cell, bursting activity, granule cell

INTRODUCTION

Understanding synaptic efficacy is a critical step toward unraveling the computational properties of a neuronal network. In the cerebellum, the cortical network is fed by two distinct inputs including mossy fibers (MFs) and climbing fibers (CFs), both known to fire action potentials at high frequencies paired with a high probability of vesicular release (Saviane and Silver, 2006; De Zeeuw et al., 2011). Even though both projections share these characteristics, each has a very distinct way of transmitting information to their postsynaptic targets; whereas CF-terminals display rapid vesicular depletion and lose synaptic power with consecutive action potentials (Schmolesky et al., 2005), MF-terminals are remarkably well equipped to facilitate reliable signaling at a high-frequency up to 1 kHz (Sargent et al., 2005; Saviane and Silver, 2006; Hallermann et al., 2010). Thus, while CFs and MFs both display high-frequency activity, in terms of functional implications they represent both ends of the high-frequency bursting spectrum, namely highly reliable non-graded signaling versus frequency dependent signaling, respectively.

Mossy fibers convey their information to the Purkinje cells via granule cells (GrCs), each of which provides a single ascending axon that bifurcates into a parallel fiber (PF). Like MF to GrC signaling, GrCs themselves can also fire bursts of action potentials (Eccles et al., 1966; Chadderton et al., 2004; Hensbroek et al., 2005; Jörntell and Ekerot, 2006). At rest they are rather silent, but following sensory activation GrCs display bursts of tens of action potentials with instantaneous frequencies up to 1 kHz (Isope and Barbour, 2002; Chadderton et al., 2004). As such GrCs may serve as a high-pass spatiotemporal filter, in which frequency dependent activity from MFs creates a time-window in which information can be relayed from MFs to PCs (D'Angelo and De Zeeuw, 2009; Mapelli et al., 2010; Solinas et al., 2010). This filter function probably results partly from Golgi cell inhibition (Brickley et al., 1996), but in principle additional filtering might occur at the PF-PC synapse. Indeed, the burst-like activity of GrCs may have two potential implications: (1) when paired with a high synaptic efficacy at the PF to PC input, it would allow GrCs to act as a relay, preserving frequency-coded information from MFs; and/or (2) when paired with a low synaptic efficacy, it could allow GrCs to filter individual inputs and signal only when strongly activated, albeit at the expense of temporal precision. When addressing the synaptic efficacy at the PF to PC input, the release probability (RP)

is one of the main factors that should be taken into account. Yet, most variables that make up the RP, such as presynaptic calcium influx and the number of vesicles readily available for release, are influenced by preceding activity, and as a consequence, the RP becomes a dynamic variable within a high-frequency burst. Thus, the functional implications of PF bursts cannot be deduced from the initial RP alone and ongoing processes such as facilitation, depression and depletion should also be considered.

The burst-like activity in GrCs has been demonstrated in various anesthetized or decerebrated mammals (Eccles et al., 1966; Chadderton et al., 2004; Jörntell and Ekerot, 2006). However, it remains to be shown whether high-frequency GrC bursts can also be demonstrated in awake behaving animals (but see Hensbroek et al., 2005, 2006), and if so, to what extent high-frequency information can be conveyed onto PCs. This latter question is of importance because different results have been found for different strains of rats in this respect. For example, estimates of RP at the PF-PC synapse gathered in different rat strains using different experimental protocols range from 0.05 to 0.9 (Dittman et al., 2000; Isope and Barbour, 2002; Valera et al., 2012). Thus, in order to elucidate the potential role of high-frequency bursts in GrCs in spatiotemporal filtering of the cerebellar cortical network, we set out a series of experiments. We investigated the occurrence of bursting activity of GrCs by performing extracellular recordings in awake, behaving animals; we studied the impact of bursting activity in groups of PFs on excitatory postsynaptic currents (EPSCs) in PCs using whole cell recordings *in vitro*; and we examined the impact of a burst within a single PF on a PC using paired GrC – PC recordings.

MATERIALS AND METHODS

IN VIVO GrC RECORDING IN RABBIT

To give an example of GrC bursting activity in larger mammals as highlighted in the introduction, we present a recording of high-frequency activity in Dutch-belted rabbits, which have been investigated as partially discussed by Hensbroek et al. (2006). In short, extracellular recordings of cerebellar GrCs located in the flocculus were acquired from awake, behaving rabbits (3–6 months of age) using fine-tipped glass micro-electrodes (∼1 μm tip diameter). Given the predominant silent behavior of GrCs at rest, cells were located while the animal was stimulated by rotation around the vertical axis. While characteristic spiking behavior was often suggestive of the cells subtype, further identification was confirmed by comparison of spontaneous spiking behavior to the algorithm as described (Ruigrok et al., 2011). Recordings were filtered below 100 Hz and above 3 kHz and sampled at 20 kHz (CED power 1401, Cambridge Electronic Design, UK).

IN VIVO GrC RECORDINGS IN MICE

Extracellular recordings of cerebellar GrCs located in crus I were acquired from awake behaving C57Bl/6 wild-type mice (12–20 weeks of age) using glass microelectrodes (∼0.5 μm tip diameter). Head-fixed mice were placed on top of a cylindrical treadmill that enabled the animal to walk freely during the experiment. Responsive GrCs were located while the animal was stimulated by a mild air puff to the whiskers (duration 10 ± 2 ms) every 10 s ipsilateral to the recording side. Identification was confirmed by comparison of spontaneous spiking behavior to the algorithm as described (Ruigrok et al., 2011). Recordings were filtered below 300 Hz and above 3 kHz and sampled at 25 kHz (RZ5 Tucker-Davis Technologies, Alachua, FL, USA).

IN VITRO PATCH CLAMP RECORDINGS FROM PCs FOLLOWING GROUPED PF STIMULATION IN MICE

Sagittal slices (200–250 μm thickness) of the cerebellar vermis of adult male C57Bl/6 wild-type mice (8–30 weeks) were prepared in ice-cold artificial cerebrospinal fluid (aCSF) and stored at room temperature in carbogen-bubbled (95% O_2 and 5% CO_2) aCSF containing (in mM): 124 NaCl, 5 KCl, 1.25 Na_2HPO_4, 2 $MgSO_4$, 2 $CaCl_2$, 26 $NaHCO_3$, and 10 D-glucose. Whole-cell patch clamp recordings were acquired 1–6 h after slice preparation from PCs using a HEKA EPC-10 amplifier (HEKA Electronics, Germany) at near physiological temperature (34 ± 1°C). Recording electrodes (2.5–4.0 MΩ) were filled with a solution containing (in mM): 9 KCl, 10 KOH, 3.48 $MgCl_2$, 4 NaCl, 120 K-gluconate, 10 HEPES, 4 Na_2ATP, 0.4 Na_3GTP, and 28.5 sucrose (pH-adjusted to 7.25 ± 0.05). For experiments conducted in current clamp, the membrane-impermeable voltage gated sodium channel blocker QX314 was added to prevent generation of action potentials. Throughout recordings, slices were perfused with carbogen-bubbled aCSF to which picrotoxin (100 μM) was supplemented in order to isolate excitatory inputs. All drugs were acquired from Sigma-Aldrich, except γ-D-glutamylglycine (γDGG; Tocris). Recorded currents were filtered (low-pass Bessel, 3 kHz) and sampled at 20 kHz using Pulse-software (HEKA Electronics, Germany). PFs were activated by current injection (100 μs, 0.5–2.0 mA; ISO-flex current generator, A.M.P.I., Israel) using a bipolar glass microelectrode positioned in the molecular layer. Input and series resistance were monitored in each experiment and cells were rejected if a change of >10% occurred. In general, the stimulus protocol consisted of a sequence of high-frequency bursts of 2, 3, 4, 5, 10, 15, and 20 pulses. This sequence was tested with burst-frequencies varying between 100, 300, 500, and 700 Hz (with a 10, 3.33, 2, and 1.47 ms interstimulus interval, respectively) and repeated three times. Consecutive bursts were given at 0.05 Hz to minimize residual effects. For some experiments responses were also tested with bursts at 200 Hz (5 ms stimulus interval). To minimize the possibility of recruiting additional PFs with consecutive pulses in a burst and to promote reproducibility between recordings we applied several strategies: (1) a low-resistance bipolar stimulus electrode was used to reduce stimulus width and minimize current build-up within a burst keeping the stimulus region restricted; (2) the stimulus electrode was positioned close to the pial surface of the molecular layer where PF density is lowest; and (3) stimulus strength was adjusted to elicit a response of ∼100 pA to a single stimulus. It is important to note that a limitation to signaling (see results) could only be demonstrated when careful attention was given to minimizing recruitment. However, residual recruitment cannot be ruled out completely and, in fact, is likely to have occurred to some degree.

IN VITRO DOUBLE PATCH CLAMP RECORDINGS FROM GrC-PC PAIRS IN MICE

A double patch clamp configuration was favored over the "loose-cell-attached"-configuration (Isope and Barbour, 2002;

Valera et al., 2012) to exclude the possibility of exciting more than a single GrC. Slices and electrodes were prepared under similar conditions as mentioned above. GrC patch pipettes had a resistance of 8–15 MΩ and contained: 126 K-Gluconate, 1 $MgSO_4$, 4 NaCl, 5 HEPES, 0.05 $CaCl_2$, 0.1 BAPTA, 15 D-Glucose, 3 MgATP, 0.1, and Na_3GTP (pH 7.25–7.35). Experiments were performed at 34 ± 1°C. After the double patch clamp configuration was established, spike trains were elicited by somatic current injections for 50 ms in the GrC. The amplitude was adjusted such that spiking occurred at ∼200 Hz. During the experiment connectivity was confirmed by eye when an EPSC was detected in the PC after averaging a minimum of 10 trains.

ANALYSES

In vivo recordings

Extracellular recordings from the rabbit were acquired using Spike 2 (Cambridge Electronic Design). Extracellular recordings from the mouse were acquired using open exe software by Tucker-Davis Technologies (Alachua, FL, USA). Data was analyzed using custom written routines in MATLAB (Mathworks). Spikes were separated upon waveform templates and values were exported to Excel (Microsoft) for further analysis.

PF group stimulation and in vitro recordings

Measurements of peak amplitude and charge were averaged over three recordings to minimize variance and then normalized to the response elicited by two pulses at 300 Hz. This particular response was chosen as a reference, because, generally, it would elicit the most consistent response and, therefore, allowed for better comparison between cells. For those experiments in which individual EPSC amplitudes were measured, the first derivative of the stimulus artifact was used to define intervals. Amplitudes were calculated as the difference between the local minimum and the current directly preceding the stimulus artifact. When stimuli took place within the rising phase of the preceding EPSC (which was especially prominent at the higher frequencies) and the response to the first pulse in the burst was more than 10% smaller than the response measured for a single stimulus, the recordings were excluded from analysis. During prolonged activation (burst length >100 ms) a plateau current could be observed. The level of this current was determined by averaging all values that preceded each individual stimulus artifact over a 50 ms time window.

Double patch granule cell – Purkinje cell recordings

After connectivity was confirmed, high-frequency noise was eliminated offline from individual recordings using a running average (1 ms width). The recording was further processed by averaging the measured current over 800 μs creating virtual bins. Whenever the derivative of these values was negative over two or more consecutive bins, events were considered for analysis and both amplitude and derivative of the rising phase were measured. Baseline values of these parameters were determined over a 50 ms period preceding the current injection. Detected events were considered evoked responses when both amplitude and derivative exceeded 1 × SD over baseline levels and the detected amplitude rose 2 × SD above background noise levels. This method proved very effective to detect wider EPSCs while simultaneously rejecting high-frequency background noise. As an indicator of sensitivity, detected EPSC amplitudes were 5.2 ± 0.2 × SD larger than baseline events. Detection thresholds were −5.76 ± 0.32 pA and −5.9 ± 1.4 pA for 'reluctant' and 'responsive' pairs, respectively (see text); these values did not differ significantly ($p > 0.05$). For a given cell, failure rate (FR) was calculated for each individual stimulus number as the number of recordings in which no evoked response could be detected divided by the total number of recordings. RP was calculated as 1-FR. Note that RP indicates the chance that an action potential results in a detectable postsynaptic response (irrespective of its size) and does not reflect the probability of release for an individual vesicle (in the literature commonly described as "p"). Significance was tested using (un-)paired Student's *t*-test or ANOVA where applicable. All values are expressed as average ± SEM unless otherwise noted.

RESULTS

BURSTING ACTIVITY *IN VIVO*

Several observations have shown that GrCs can fire bursts of action potentials at surprisingly high frequencies of several 100 Hz with instantaneous frequencies up to 1 kHz (Chadderton et al., 2004; Hensbroek et al., 2005; Jörntell and Ekerot, 2006; for earlier observations in anesthetized cats see Eccles et al., 1966). Hensbroek et al. (2005) have been able to demonstrate that in the awake, behaving rabbit, GrCs remain predominantly silent at rest, but can generate bursts of action potentials of tens of spikes with average frequencies as high as 700 Hz during vestibular stimulation. Because, to the best of our knowledge, no recording of GrC activity in a behaving, un-anesthetized animal has been published in the scientific literature so far, we have included an example trace taken from the rabbit to illustrate these physiologically relevant bursting patterns (**Figures 1A–C**). This particular GrC did not show any activity when the animal was at rest, whereas vestibular stimulation via sigmoidal rotation around the vertical axis caused it to fire bursts of action potentials both during movement in the contralateral direction and while the animal was stationary in the contralateral position. A total of 31 bursts were fired over six cycles. Bursts had an average firing frequency of 529.8 ± 45.7 Hz, contained 11.6 ± 6.6 spikes and were 23.66 ± 15.86 ms in length (all values AVG ± SD). Surprisingly, for this cell, timing of burst onset was variable [1.85 ± 1.08 ms from start of movement (AVG ± SD), $n = 6$] and multiple bursts could occur within a single movement (5.17 ± 3.49 bursts per cycle; AVG ± SD). Due to this inconsistent behavior, bursting did not directly relate to either velocity, acceleration, position of the table or position of the eye, but rather seemed to signal movement in the contralateral direction indistinctively.

To confirm that similar activity patterns exist in awake, behaving mice, we performed extracellular recordings in crus I, while sensory stimulation was provided by applying a brief air puff to the whiskers (**Figures 1D–F**). In homology with the rabbit, the GrC shown here displayed very little activity at rest, whereas mild whisker stimulation with an air puff caused it to fire bursts of action potentials (**Figures 1D,E**). A single air puff to the whiskers could elicit multiple bursts, resulting in a total of 26 bursts identified over 15 trials. Bursts had an average firing frequency of 358.3 ± 82.9 Hz, but could reach instantaneous frequencies up to 815.9 Hz. They contained 10.8 ± 13.5 spikes and were

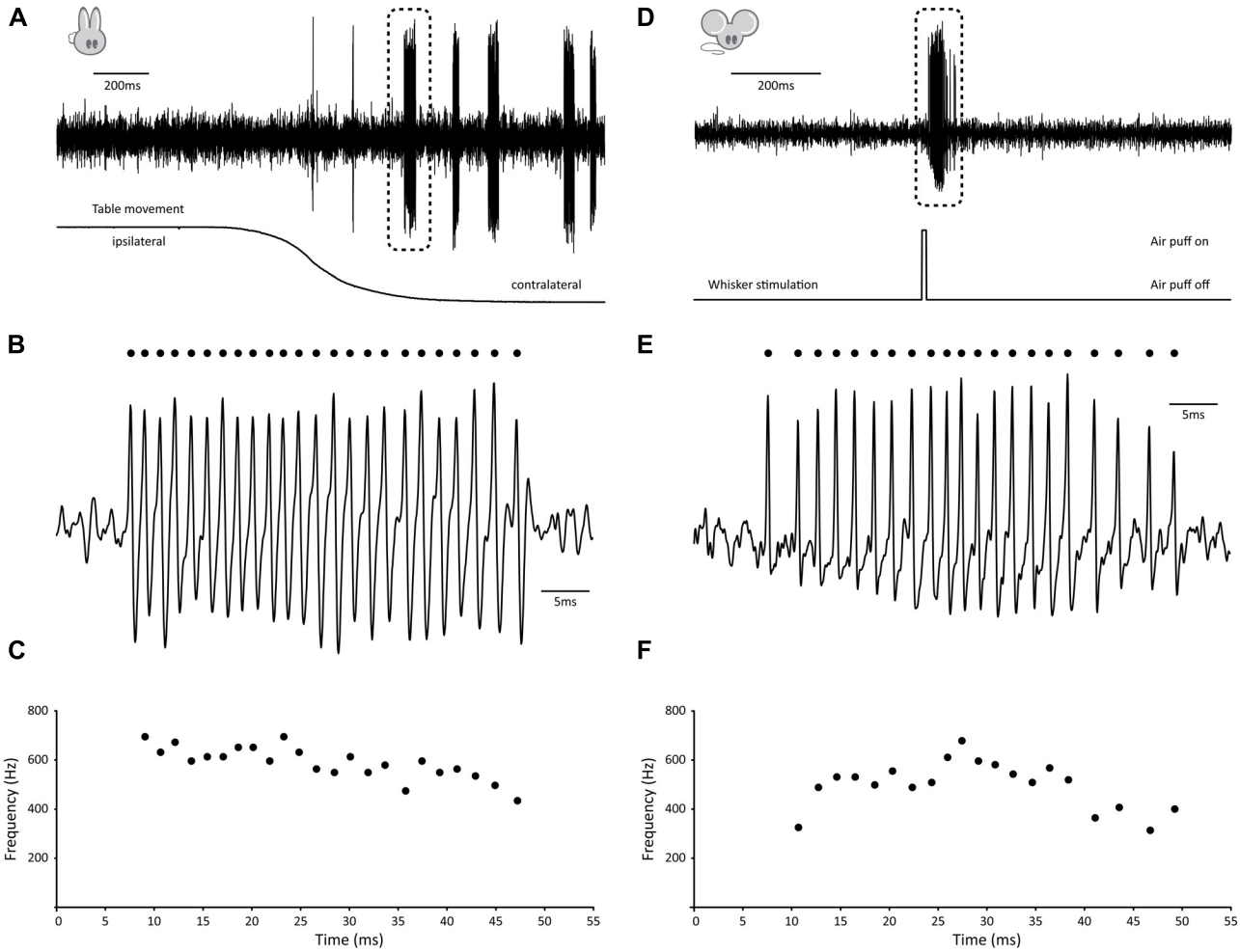

FIGURE 1 | Examples of burst firing in cerebellar granule cells. (A–C) Example of high-frequency GrC burst in the awake behaving rabbit. **(A)** (top) Extracellular recording of granule cell in the flocculus of a Dutch-belted rabbit during vestibular stimulation around the vertical axis. Note absence of activity prior to movement onset, whereas several distinct, high-frequency bursts occur during rotation (table position is displayed at bottom). **(B)** Burst demarked in A shown at larger scale. Identified spikes are indicated by dots. **(C)** Instantaneous frequency plot of burst shown in B. This particular burst consisted of 24 consecutive spikes with instantaneous frequencies as high as 694 Hz and had an average firing frequency of 589 Hz. **(D–F)** Example of high-frequency GrC burst in the awake behaving mouse. **(D)** (top) Extracellular recording of granule cell in crus I of an awake mouse following whisker stimulation. Note absence of activity prior to movement onset, whereas a distinct, high-frequency burst occurs during stimulation. **(E)** Burst demarked in D shown at larger scale. Identified spikes are indicated by dots. **(F)** Instantaneous frequency plot of burst shown in E. This particular burst consisted of 21 consecutive spikes with instantaneous frequencies as high as 678 Hz and had an average firing frequency of 501 Hz.

24.1 ± 26.5 ms in length (all values AVG ± SD). In addition, timing of burst onset was variable (28.08 ± 24.46 ms) from the start of whisker stimulation.

IMPACT OF BURSTING ACTIVITY IN GROUPS OF PFs *IN VITRO* IN MICE

Having confirmed that also in the mouse physiologically relevant activity patterns in GrCs consist of high-frequency bursts, we performed experiments to characterize postsynaptic responses evoked by stimulation of a bundle of PFs. We performed whole cell somatic patch-clamp recordings from PCs to measure EPSCs evoked by extracellular stimulation of groups of PFs. Bursts of 2, 3, 4, 5, 10, 15, and 20 pulses were given at frequencies of 100, 200, 300, 500, and 700 Hz (**Figure 2**; data obtained at 200 and 700 Hz are only shown in part of the panels). The peak amplitude of the EPSCs showed a significant increase with each additional stimulus ($p < 0.05$ for all frequencies; $n = 11$) until a maximum level was reached (**Figure 2A**); from 10 pulses on additional pulses did not contribute to a significant increase in peak amplitudes ($p > 0.05$ for all frequencies; $n = 11$; **Figure 2B**). Comparing bursts of equal numbers of stimuli over different frequencies, a significant increase in the relative peak amplitude of the EPSCs was seen (i.e., normalized to the response elicited by two pulses at 300 Hz) for each condition between 100 and 300 Hz ($p < 0.05$ for all numbers of stimulus pulses; $n = 11$; **Figure 2B**). No further effect on EPSC amplitudes could be observed for frequencies higher than 300 Hz ($p > 0.05$ for all numbers of stimulus pulses; $n = 11$) and in fact, the EPSCs following bursts of 2, 3, and 4 stimuli at 700 Hz were significantly smaller than those at 300 and

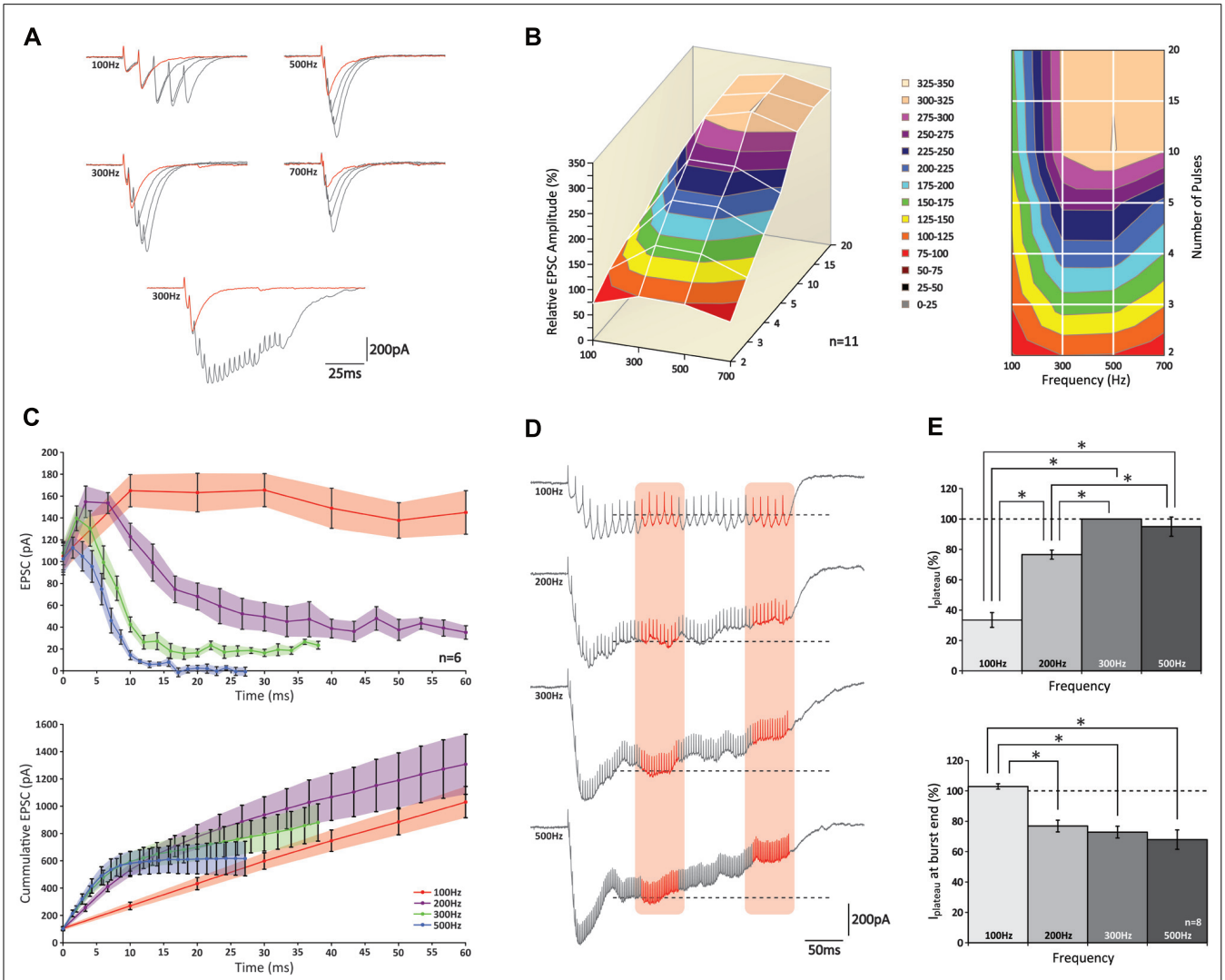

FIGURE 2 | PCs can increase the peak amplitude of their EPSCs following high-frequency stimulation of groups of PFs up to 300 Hz. **(A)** (top) Traces of PC EPSCs following stimulus bursts of 2, 3, 4, or 5 stimuli at 100, 300, 500, or 700 Hz. Response to two stimuli is shown in red for reference. Note the effect of temporal summation on peak amplitude at higher frequencies. (bottom) Recordings of 2 and 20 stimuli at 300 Hz. Note how in the last half of the long burst no robust responses can be distinguished. **(B)** 3D representation (left) and top-down view (right) relative peak amplitudes of EPSCs with respect to different stimulus conditions. No increase in EPSC amplitude was observed for bursts of more than 10 stimuli at any of the stimulus frequencies ($p > 0.05$). **(C)** Relative EPSC increases per stimulus (top) and cumulative EPSC (bottom) over time. **(D)** Example traces of EPSCs following prolonged stimulation for 300 ms at 100, 200, 300, and 500 Hz. A plateau was established after ~100 ms for all frequencies. Average current levels were measured early (left orange column) and late (right orange column) during the plateau over a 50 ms time period. Levels measured during first period are indicated by dashed lines for reference. **(E)** (top) Bar graph of early plateau current levels; no significant increase was observed between 300 and 500 Hz ($p < 0.05$; $n = 8$). (bottom) Relative attenuation of plateau current levels at end of burst; no reduction was observed only at 100 Hz ($p > 0.05$).

500 Hz ($p < 0.05$ for all comparisons; $n = 11$) possibly reflecting insufficient presynaptic calcium entry, which may occur at higher frequencies (Brenowitz and Regehr, 2007).

Temporal summation of consecutive EPSCs grossly affected the compound EPSC amplitude, in particular at higher frequencies. For example, at 100 Hz the second stimulus always occurred late in the decay phase of the preceding response, whereas at 500 Hz the second stimulus usually occurred around its peak (**Figure 2A**). To eliminate the effect of temporal summation and better reveal underlying processes of short-term plasticity, we looked at the response elicited by each individual stimulus within a burst. However, because stimuli could take place within the rise phase of the preceding EPSC (and thus underestimate the amplitude of the first response) many recordings had to be rejected from analysis (see methods). Of all the recordings that were included in the analyses none of the first EPSCs showed a significant attenuation ($p > 0.05$ for all frequencies; $n = 6$; **Figures 2A–C**).

Remarkably, while facilitation was observed during onset of the burst at all frequencies, such augmented responses could only be maintained at 100 Hz (**Figure 2C**, top graph); at higher frequencies

a rapid decline was observed. Later in the burst (up to 20 stimuli), currents eventually reached a stable amplitude, but these levels reduced progressively at higher frequencies and at 700 Hz virtually no current could be detected. These levels all differed significantly from one another ($p < 0.05$ at 20 pulses for all comparisons; $n = 6$). When expressed as cumulative responses over burst duration (**Figure 2C**, bottom graph), the slope fitted to the first 10 ms grew significantly up to 300 Hz ($p < 0.05$ between frequencies of 100, 200, and 300 Hz; $n = 6$), while no additional rise was seen above 300 Hz ($p > 0.05$; $n = 6$).

Also when PFs were stimulated for a prolonged period of 300 ms, compound responses showed a distinct rising and decaying phase until a plateau was reached after approximately 100 ms (**Figure 2D**). Because a plateau establishes when both driving and restricting forces are at equilibrium, its level indicates the relative contribution of each force (Saviane and Silver, 2006). The amplitude of the steady-state level, which was measured as the average current recorded prior to each stimulus over a 50 ms period (period indicated by left red column in **Figure 2D**), was lowest for 100 Hz and significantly increased for bursts at 200–300 Hz ($p < 0.05$; $n = 8$; **Figure 2E**, top graph). No further increase was observed between 300 and 500 Hz ($p > 0.05$; $n = 8$), indicating that the driving force showed no further increase above 300 Hz. As stimulation continued beyond 150 ms, the plateau could be maintained up to 300 ms for bursts at 100 Hz, whereas at the higher frequency levels it showed a significant reduction toward the end of the burst ($p < 0.05$; $n = 8$; **Figure 2E**). Remarkably, whereas at 200 Hz the steady-state had not reached its maximum yet, we saw a reduction of the plateau toward the end of the stimulus, pointing toward a presynaptic origin of this insufficiency. While these results show that release is optimized around 300 Hz, it is important to note that frequency-dependent limitation of release and presynaptic insufficiency probably occur at frequencies lower than reported here, because the results above apply to PF-activity *as a bundle*; in this experimental configuration inactivity of a particular fiber can be compensated for by activity from others, and unless all fibers are continuously active, equilibrium can be established at a higher level than would be possible for fibers independently. Indeed, this tenet is supported by our double-patch recordings (see below) indicating that individual PFs cannot maintain sustained release.

While the analysis of peak amplitudes can describe the physiologically relevant effect of temporal summation within a compound response to high-frequency activity, this approach cannot fully describe the properties of synaptic release, because other processes, such as postsynaptic receptor saturation and voltage-sensitive repolarizing currents, can potentially mask any ongoing release. Therefore, to get a better understanding of the total amount of neurotransmitter released throughout a burst, we looked at the total charge (i.e., "area-under-the-curve" of an EPSC). Correlating the total charge to burst duration revealed a remarkable nearly perfect linear fit for all frequencies (R^2-values 0.990 ± 0.002; $n = 6$; **Figure 3A**). The slope increased significantly with a rise in frequency for 100 and 300 Hz ($p < 0.05$ for all combinations; $n = 6$), which indicates that the stimulated PF bundle sustains the release at these frequencies. However, in accordance with our observations described above, no further rise in the slope was found for frequencies above 300 Hz ($p < 0.05$ for all frequencies; $n = 6$). This finding indicates that, within a given time period, stimuli at frequencies higher than 300 Hz are ineffective in eliciting any additional release. These "false" stimuli occur at a rate faster than a bundle of PFs can compensate for. Considering the compensatory mechanism of alternate activity that occurs within a group of fibers, the maximum frequency at which individual fibers can signal is likely lower. These results are a first indication that GrC burst firing at frequencies higher than 300 Hz cannot relay temporally coded information from MFs to PCs. To exclude the possibility that these findings resulted from our whole-cell voltage-clamp recording conditions, we repeated the experiment in current-clamp mode so as not to restrict the flow of electrical currents in PCs. Again, no differences were found at higher frequencies ($p < 0.05$ for 100 Hz against 300, 500, and 700 Hz, $p > 0.05$ between 300, 500, and 700 Hz; $n = 6$; **Figure 3B**). To confirm that a transitional trajectory existed before the observed limit of 300 Hz was reached, we also included bursts of 200 Hz (**Figure 3C**). The slope measured for 200 Hz was indeed larger than 100 Hz ($p < 0.05$; $n = 8$), yet smaller than 300–500 Hz ($p < 0.05$; $n = 8$).

To detect any involvement of postsynaptic receptor desensitization on signaling, we applied CX546, which acts as an allosteric modulator that prevents α-amino-3-hydroxy-5-methyl-4-isoxazolepropionic acid receptors (AMPARs) to reside in the desensitized state (Lynch and Gall, 2006). With CX546 present (200 μM) the data did not fall along a linear fit as perfectly as without (R^2-values 0.974 ± 0.004; $n = 6$), due to a small facilitation in responses to bursts shorter than 20 ms in duration (**Figure 3D**). While hypothetically this finding could also be explained by depression of longer bursts, our results from both the γDGG experiments and the double-patch GrC-PC recordings (see below) confirm that initial facilitation followed by rapid depletion underlie these findings. Still, over the first 20 ms the slope with CX546 displayed a linear relation (R^2-values 0.989 ± 0.002; $n = 6$) and differed only significantly at 100 Hz ($p < 0.05$; $n = 6$). No differences were found for the remaining frequencies ($p > 0.05$; $n = 6$). While these results suggest some role of AMPAR desensitization in PF-PC signaling, it cannot explain the restrictions in signaling found for stimulus frequencies over 300 Hz.

Next, to exclude any major involvement of postsynaptic receptor saturation we investigated the impact of γDGG, which is a competitive antagonist of AMPARs that effectively suppresses EPSCs by occupying a portion of the available AMPARs. Because of its competitive behavior and fast unbinding rate, the relative suppression by γDGG is a perfect reporter of glutamate transients; in the case of postsynaptic receptor saturation, excessive glutamate will compete with γDGG to overcome its suppressive effect and EPSCs will be unaffected by its presence. At 1 mM, γDGG effectively suppressed all responses by more than 35% of their original size. However, no effect was observed on the linear behavior of responses (R^2-values 0.993 ± 0.001; $n = 5$). In addition, in accordance with our earlier results, slopes were significantly lower at 100 and 200 Hz compared with other frequencies ($p < 0.05$; $n = 5$), yet those at 300, 500, and 700 Hz were indistinguishable from each other ($p > 0.05$; $n = 5$; **Figure 3E**). Interestingly, the relative reduction was strongest for short bursts,

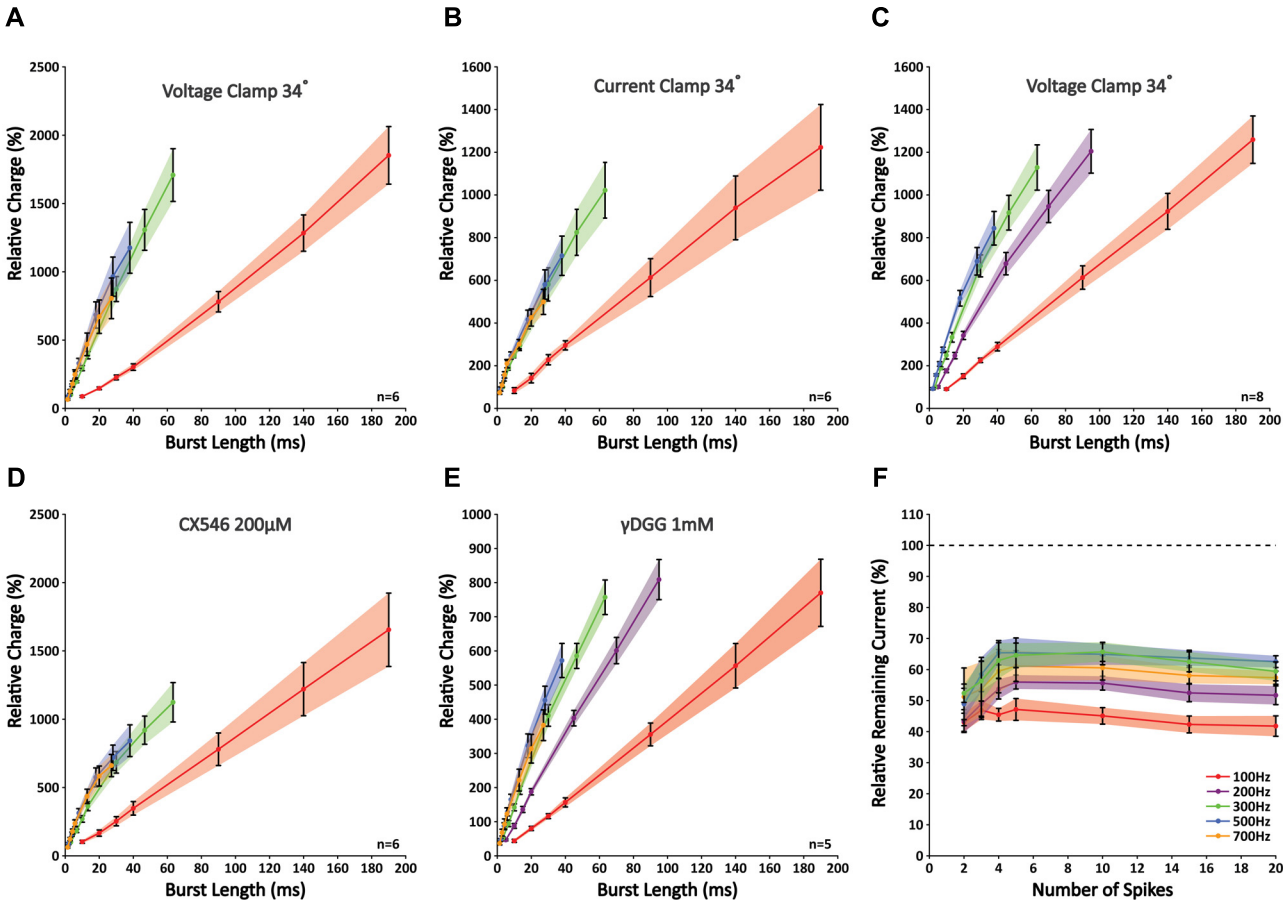

FIGURE 3 | Slopes of nearly perfect linear correlations between charge and burst length reveal limited signaling for frequencies higher than 300 Hz as a result of insufficient glutamate release. (A) Correlations between relative charge and burst length at 100, 300, 500, and 700 Hz; no differences were seen in the slopes between 300, 500, and 700 Hz ($p > 0.05$; $n = 6$). **(B)** Similar experiment as shown in A repeated in current clamp. Recording conditions had no effect on the outcome ($n = 6$). **(C)** Similar experiment as shown in A, now including 200 Hz. Note that the slope measured for 200 Hz differed significantly from that at 100, 300, and 500 Hz ($p < 0.05$; $n = 8$). **(D)** When CX546 was applied, correlations were less linear as a result of small facilitations for bursts smaller than 20 ms (see text). However, bursts that were shorter than 20 ms in duration still displayed a linear relationship and the slopes at 300, 500, and 700 Hz did not differ significantly from each other ($p > 0.05$; $n = 6$). **(E)** Application of γDGG (1 mM) did not affect the observed limitation of signaling at frequencies higher than 300 Hz ($n = 5$). **(F)** γDGG (1 mM) effectively suppressed all responses by more than 35%. Relative suppression was significantly smaller after five stimuli at 200, 300, and 500 Hz, although no further decrease was observed for longer stimulus trains. This indicates that release might be facilitated within the first few stimuli, but quickly reaches its optimum ($n = 5$).

but showed a gradual decrease toward bursts of five pulses at 200, 300, and 500 Hz ($p < 0.05$ for responses of two versus five pulses at all three frequencies; $n = 5$; **Figure 3F**), indicative of additional glutamate release with consecutive pulses. However, no further decrease was observed for longer bursts ($p < 0.05$ for responses of five versus 20 pulses; $n = 5$), meaning that release had reached its optimum within five pulses. Together, these results indicate that signaling at high-frequency between PF-PC is restricted to the presynaptic site by insufficient release. While some additional release might occur within the first few pulses of a burst, prolonged activation cannot be maintained. Also, despite the facilitation we found for individual EPSCs at 100 Hz (**Figure 2C**), this was not accompanied by a shift in the relative glutamate content per synapse (**Figure 3F**). Therefore, the reported facilitation mostly reflects recruitment of more synapses and not additional transmitter release at individual synapses, highlighting that results obtained through stimulation of a bundle of PFs cannot be extrapolated directly to the level of individual synapses. More so, our data show that overall synaptic release is not facilitated at 100 Hz.

PAIRED RECORDINGS OF GrCs AND PCs *IN VITRO*

The results described above showed the implications of grouped activity from synchronously activated GrCs, but they failed to accurately describe the behavior of individual connections. We therefore performed paired whole-cell patch clamp recordings from 13 connected GrC – PC pairs in mice. Because this configuration turned out to be relatively short-lived, we could not test responses for the same wide range of stimuli as with extracellular stimulation. We chose to elicit bursts of action potentials at 200 Hz, because at this frequency, on the one hand, we found some limitations such as depletion with prolonged activity, while on the

other hand we observed potential room for additional signaling at higher frequencies (up to 300 Hz; see above).

Recordings from individual GrC-PC pairs confirmed a low initial RP, yet substantial differences were observed between these pairs (**Figures 4A–D**). Overall, we found an initial failure rate (FR) of 0.83 ± 0.01 (**Figure 4D**). The FR was significantly reduced to a minimum of 0.66 ± 0.02 at the third action potential ($p < 0.05$; $n = 13$). However, from the third action potential on, the FR began to show a gradual increase again and returned to baseline levels at the sixth action potential ($p > 0.05$ 1st versus 6th action potential, $p < 0.05$ 3rd versus 6th action potential; $n = 13$). On the basis of the cumulative RP calculated over the first 3 action potentials [$RP_{cumulative\ 1-3} = 1\text{-}(FR_1{*}FR_2{*}FR_3)$], pairs could be separated into a "reluctant"-group ($RP_{cumulative\ 1-3} < 0.55$, average $RP_{cumulative\ 1-3} = 0.41 \pm 0.05$; $n = 8$) and a "responsive"-group ($RP_{cumulative\ 1-3} > 0.8$, average $RP_{cumulative\ 1-3} = 0.86 \pm 0.02$; $n = 4$; **Figure 4A**). Even though the initial FR was similar between the two groups ($p > 0.05$; $n = 8$ and $n = 4$), a dramatic difference was observed between the FR of the 2nd and 3rd spike ($p > 0.05$, 0.86 ± 0.01 and 0.78 ± 0.01 for reluctant connections; 0.48 ± 0.03 and 0.43 ± 0.05 for responsive connections, respectively; $n = 8$ and $n = 4$, respectively; **Figure 4D**). No difference in FR was observed after the 3rd spike ($p > 0.05$; $n = 8$ and $n = 4$). Accordingly, the cumulative RP ($RP_{cumulative\ 1-n} = 1\text{-}(FR_1{*}FR_2{*}FR_n)$, unveiled a striking difference between the two groups (**Figure 4E**); whereas the chance of release for at least one of the action potentials reached >90% for the responsive connections at the fourth action potential this chance grew to ∼50% for reluctant connections and had only reached ∼75% at the 7th action potential.

The EPSC amplitude of the response to the first action potential was 8.54 pA ± 0.22 ($n = 8$) for reluctant connections (**Figure 4C**). No further change in amplitude occurred throughout the burst. Amplitudes for responsive connections were significantly larger for the 2nd, 3rd, and 6th action potential ($p < 0.05$; $n = 4$) and also responses to the 4th and 5th spike followed this trend. Thus, although the initial RP is low at PF-PC synapses, we conclude that high-frequency burst activity may facilitate release within the first few spikes (both in reluctant and responsive connections) and result in a high cumulative RP (in particular in responsive connections) to ensure signaling and overcome a low initial RP.

DISCUSSION

For a long time, it was believed that cerebellar GrCs operate at low firing frequencies (but see Eccles et al., 1966). It is only due to recent technical advances that GrCs have been shown to fire bursts of action potentials at surprisingly high frequencies of several 100 Hz with instantaneous frequencies up to 1 kHz (Chadderton et al., 2004; Hensbroek et al., 2006; Jörntell and Ekerot, 2006; Valera et al., 2012) and that individual action potentials in high-frequency bursts of GrCs are reliably translated into consistent calcium transients at presynaptic PF varicosities, showing only minor attenuation for intervals starting at approximately 500 Hz (Brenowitz and Regehr, 2007). Here, we demonstrate that mice can also show bursts of GrC activity at high-frequency, but that the capability of their PFs to relay frequency coded information to PCs is limited to ∼300 Hz for grouped activity. Moreover, at the level of individual PFs, release is too unreliable to convey temporally coded information. In line with previous studies in rat (Brenowitz and Regehr, 2007; for review see Le Guen and De Zeeuw, 2010), murine PF inputs constitute a heterogenic group of terminals with various levels of RP allowing differential filtering. Our data suggest that high-frequency PF activity may facilitate transmitter release during initial spiking to ensure signaling onto PCs, but that variability is too high to allow temporally coded signaling at individual synapses.

LIMITATIONS OF TRANSMITTER RELEASE AT THE MURINE PF-PC SYNAPSE

Our main finding demonstrates that release from PF terminals onto PC dendrites is limited during physiologically relevant high-frequency bursts. Although the current observations in awake behaving mice and those of others in rabbits and anesthetized rats indicate that cerebellar GrCs can fire bursts of action potentials with instantaneous frequencies up to ∼1 kHz (Chadderton et al., 2004; Hensbroek et al., 2005; Ruigrok et al., 2011), our *in vitro* results following stimulation of bundles of PFs show that signaling at the murine PF-PC synapse is confined to ∼300 Hz at best. This maximal limit is likely to be an overestimation, because the stimulus conditions under which these results were obtained allow for different PFs to be active at different time points within a burst. In this manner, a group of PFs can maintain a highly effective activity pattern, while the effective activity of each individual terminal is in fact substantially lower (see also below). Indeed, our double patch-clamp recordings of connected GrC-PC pairs in mice confirmed that overall PF terminals exhibit a low RP. These recordings showed a low average initial RP of ∼0.17, which is in line with previous observations obtained in rats by Dittman et al. (2000), but not by those of Valera et al. (2012), who reported an initial RP of 0.44. The differences with the latter study may be partially due to the specific strains of rodents used, differences in extracellular calcium concentration in the bath, and/or the approach used to calculate the RP. Valera et al. (2012) calculated RP with the multi-probability-fluctuation-analysis (MPFA), a method that relies on a presumed distribution of Pr_{site} (i.e., the probability for a single vesicle to be released at a particular site) to calculate RP from the quantal distribution. However, this approach does not take into account heterogeneity among synapses that arises from differential factors such as presynaptic calcium transients and/or build-up of residual calcium (Brenowitz and Regehr, 2007). Moreover, whereas Valera et al. (2012) used a noise-based signal-to-noise ratio to discriminate events in paired recordings, we applied a noise-based multi-variable threshold detection method; both methods have the potential to misrepresent RP either by missing small events or detecting noise, resulting in an underestimation or overestimation, respectively.

PF TERMINALS IN MICE ARE HETEROGENIC

We noticed a clear heterogeneous distribution between release properties of individual connected GrC-PC pairs. Given that larger EPSC amplitudes coincided with a higher RP, this difference might reflect diversity between potentiated and depressed synapses (Bender et al., 2009). However, we cannot exclude the possibility that this heterogeneity also results partly from differences between terminals from the ascending versus the horizontal segment of

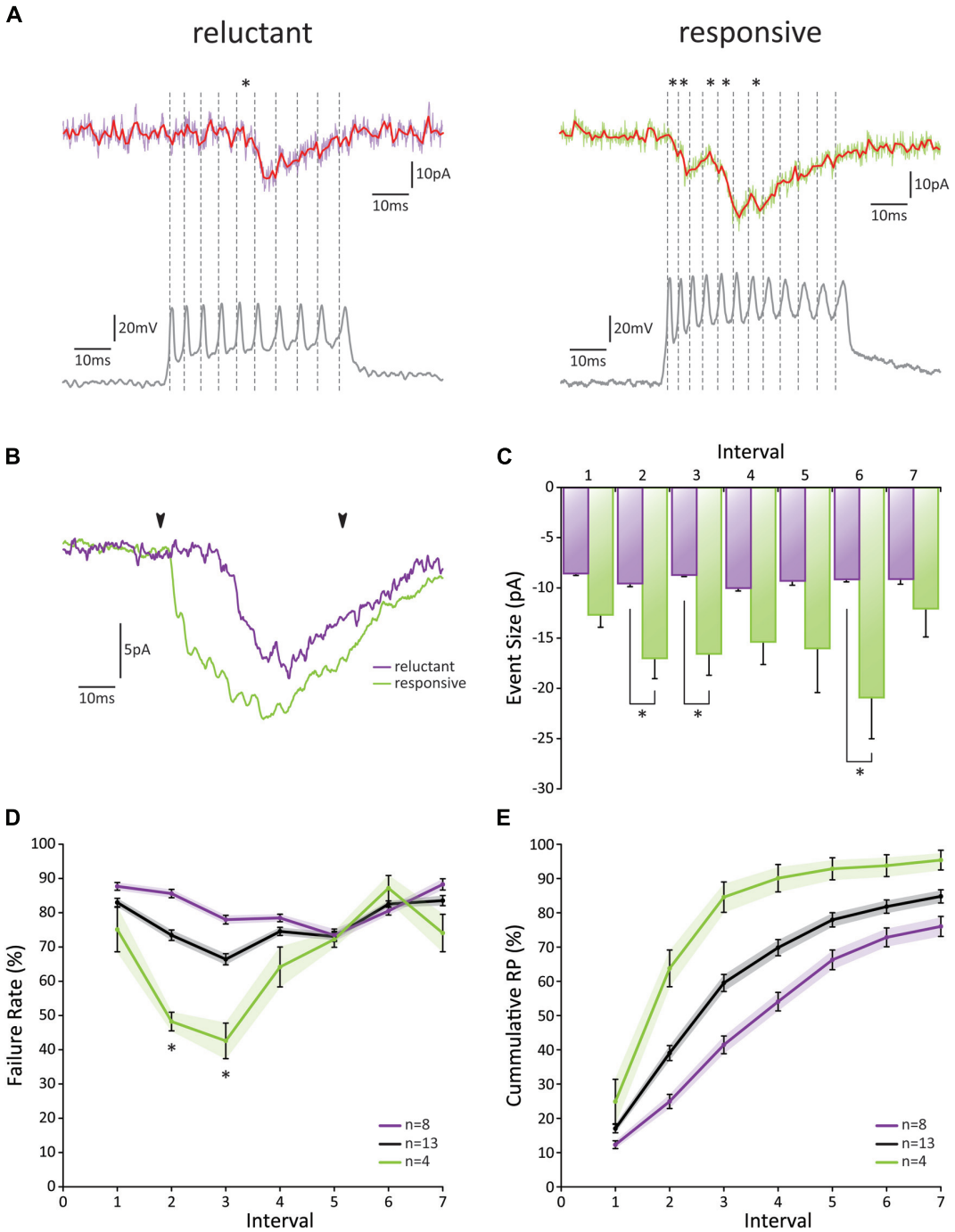

FIGURE 4 | Paired GrC-PC recordings reveal heterogeneity in PF release probability. (A) Examples of paired recordings. Based on the cumulative release probability over the first three spikes, pairs could be subdivided into a "reluctant" group (left) and "responsive" group (right). (top traces) Original voltage clamp recordings from PCs (purple and green for "reluctant" and "responsive" connections, respectively) and their processed signals used for analysis (red); asterisks indicate detected events. (bottom traces) Current clamp recordings from GrCs. Spiking is induced via current injection. Dashed lines indicate detected spikes. **(B)** Averaged responses over all recordings from cells shown in A. Beginning and end of current injections are indicated by arrowheads. Note a faster overall response in the responsive connection (green). **(C)** EPSC amplitudes did not change in size during the burst for reluctant connections (purple, $p > 0.05$ for all comparisons). However, for responsive connections (green) EPSCs elicited by the 2nd, 3rd, and 6th spike were significantly larger than that by the 1st spike. No significant difference was observed between reluctant and responsive connections for EPSCs following the first spike. **(D)** Failure rate for all recorded pairs (gray), reluctant (purple), and responsive (green) connections. Responsive connections showed a short-lived facilitation for the 2nd and 3rd spike, resulting in a significantly smaller failure rate compared to reluctant connections ($p < 0.05$; $n = 8$ and $n = 4$, respectively; one cell out of the 13 was ambiguous and not included in one of the two main categories). **(E)** Cumulative probability of release for all recorded pairs (gray), reluctant (purple), and responsive (green) connections.

PFs (Sims and Hartell, 2005, 2006). In addition, the heterogeneity may be related to the great diversity found in presynaptic calcium transients of PF terminals, which can differ more than 10-fold (Brenowitz and Regehr, 2007). It is not unlikely that this heterogeneity has resulted from experience-driven long-term plasticity, either facilitating or repressing the responsiveness of connections by adjusting presynaptic calcium transients.

Despite a heterogeneous distribution, we found a low initial RP for all PF-PC synapses; whereas the PF to Golgi cell synapse is considered to be weak (Dieudonné, 1998; Robberechts et al., 2010), the PF to molecular layer interneuron synapse has been shown to be more reliable (Crowley et al., 2007; Satake et al., 2012). These observations are remarkable, because all types of PF connections mentioned above probably persist along a single PF (Palay and Chan-Palay, 1974; Napper and Harvey, 1988), which inherently suggests differential filtering. Therefore, it will be intriguing to see how heterogeneity will affect the ability of PFs to signal at high frequencies, not only at their input to PCs, but also to Golgi cells and molecular layer interneurons. Moreover, it will be interesting to find out how the plasticity rules that control the efficacy at PF-PC synapses compare to those controlling PF-interneuron synapses (Gao et al., 2012).

TECHNICAL LIMITATIONS AND CAVEATS

We took three different approaches in the current study to investigate GrC–PC interactions; these included extracellular recordings of GrCs *in vivo*, recordings of intracellular PC responses *in vitro* following extracellular stimulation of bundles of PFs, and intracellular recordings of individual GrC-PC pairs *in vitro*. The *in vitro* approaches presented particular technical limitations and caveats. Recording EPSCs from PCs following PF activity is made notoriously complicated by several factors (Roth and Häusser, 2001): the large dimension of a PC prevents the desired control over electrical properties in patch-clamp experiments; the extensive dendritic arborization filters postsynaptic currents; the small size and condense packing of PFs make isolated activation difficult; and spontaneously active inputs obscure individually evoked events. These complications probably had some effect on the measurements following PF bundle stimulations as well as those during the paired recordings. When stimulating a bundle of PFs, the elicited response will be the multiplication of dynamic stochastic variables and, given a relatively low RP, will only reflect activity from a subset of all the stimulated PFs. Considering the heterogenic behavior, when some fibers might show activity to a substantial portion of the stimuli in a burst, while others might respond only periodically, the composed response will not reflect activity from a constant number of terminals. Because the total number of stimulated fibers is unknown, it is unclear what proportion is unresponsive. When, for example, a burst of 10 stimuli is given, the response to the 4th and 5th stimulus can be made up by a completely different subset of PFs. As a result, heterogeneity greatly limits the possibilities for analysis of those responses elicited by grouped activity and, in fact, limits applicability of methods proven effective at other release sites (Saviane and Silver, 2007; Valera et al., 2012). Yet, an equilibrium between driving and suppressing forces will establish as heterogenic differences and asynchronous activation of fibers will be averaged out at least partly by sustained activity. Thus, the measurements following extracellular bundle stimulation may to some degree be subject to misrepresentation, but the steady-state current can probably serve as an indirect indicator of overall synaptic efficacy (Saviane and Silver, 2006; Valera et al., 2012). Finally, finding connected pairs of GrCs and PCs was indeed difficult and holding on to both cells for long periods of time proved even more challenging. These technical difficulties forced us to restrict ourselves to investigate only the most physiologically relevant stimulus parameters and limited the power of our statistical analyses.

FUNCTIONAL IMPLICATIONS

The notion that frequency coding is partially lost in individual GrC firing patterns has interesting implications for the cerebellar network as a whole and challenges the idea that GrCs merely act as interposed relay-neurons. What is the purpose for a GrC to fire a high-frequency burst when actual release falls behind? The main benefit of a relatively low RP is that few spontaneous events occur, creating a relatively noise-free environment. However, this comes at the expense of reliability and consistency; such a system is not well-designed to employ rate coding over its entire frequency range in a linear fashion. Nevertheless, as depicted in **Figure 4**, the cumulative probability of release at the murine PF-PC synapse reached nearly 1 within a few spikes for the "High RP"-group. This means that a brief PF burst could overcome the initial low RP to ensure release within the time window of the burst. Moreover, as the presynaptic insufficiency caused a rapid fall in RP, restricted release prevents immediate saturation of the postsynaptic site, thus leaving room for temporal summation at a lower rate. Ultimately, these characteristics point toward a non-linear mode of synaptic transmission, in which the actual occurrence of a synaptic event bears significance as well as its timing within a burst.

Granule cell activity is tightly controlled by tonic inhibition from Golgi cells, resulting in few action potentials at rest (Hensbroek et al., 2006; Mapelli and D'Angelo, 2007); GrCs can be relieved from this inhibition when Golgi cell activity is diminished or when excitatory MF input exceeds the inhibiting force. Moreover, glutamate released by MFs can directly act on Golgi cell terminals and suppress GABA release, forming an activity-dependent feed-forward loop (Gao et al., 2012). When the balance is shifted from inhibition to excitation, a time window is created in which a GrC can fire a burst of action potentials (D'Angelo and De Zeeuw, 2009; Mapelli et al., 2010; Solinas et al., 2010). As such, the granular layer can be regarded as a "gate-keeper" that can selectively allow information to pass from MFs to PCs. Because MF terminals are tailored to maintain reliable signaling at very high frequencies (Sargent et al., 2005; Hallermann et al., 2010), it is remarkable that, to some extent, rate coding is lost further down the network. This implies that the information encoded by high-frequency firing of MFs may have limited value for PCs, but rather shapes the time window in which GrCs can produce a burst of activity. Thus, combining strong inhibition together with a relatively low RP results in a system in which synaptic events are restricted and a high signal-to-noise ratio is effectuated.

Our finding that bundles of PFs can display a nearly linear, frequency-sensitive relationship between burst duration and total synaptic charge has some physiological relevance, because there is evidence that PFs are activated in bundles (Ebner et al., 2005). Moreover, GrCs are also prone to fire together in groups, because of the impact of Golgi cell inhibition, which can produce a center-surround pattern of activity in the granular layer further enhancing the filter function of the granular layer (Mapelli and D'Angelo, 2007). This leads to the interesting possibility that, while output from individual PFs can be relatively insignificant and poorly timed, a group of selectively activated PFs can reliably convey and maintain frequency coded MF activity, while background noise from spontaneous release can be minimized.

In conclusion, our findings indicate that at the PF-PC synapse the firing mode of GrCs in high-frequency bursts overcomes the unreliability and inconsistency this synapse exhibits so as to ensure signaling at the partial cost of rate coding. Together with strong Golgi cell inhibition and center-surround activation of PF groups, this creates an environment in which the granular layer forms a strong spatiotemporal filter and, while a single GrC action potential becomes insignificant, controlled bursting can reliably convey selective information from MF input to PC output.

ACKNOWLEDGMENTS

We kindly thank the Dutch Organization for Medical Sciences (ZonMw; FEH, CIDZ), Life Sciences (ALW; BvB, ZG, FEH, CIDZ), Erasmus university fellowship (FEH), Senter (NeuroBasic; CIDZ), and the ERC-advanced, CEREBNET and C7 programs of the European Community (CIDZ) for their financial support. The extracellular data recorded in the rabbit were acquired with the help of R. Hensbroek and J.I. Simpson and are included with their consent. We thank C. Hansel, J.I. Simpson as well as E. Galliano and other members of the De Zeeuw-lab for helpful discussions and critically reviewing the paper. The authors declare no competing financial interest.

REFERENCES

Bender, V. A., Pugh, J. R., and Jahr, C. E. (2009). Presynaptically expressed long-term potentiation increases multivesicular release at parallel fiber synapses. *J. Neurosci.* 29, 10974–10978.

Brenowitz, S. D., and Regehr, W. G. (2007). Reliability and heterogeneity of calcium signaling at single presynaptic boutons of cerebellar granule cells. *J. Neurosci.* 27, 7888–7898.

Brickley, S. G., Cull-Candy, S. G., and Farrant, M. (1996). Development of a tonic form of synaptic inhibition in rat cerebellar granule cells resulting from persistent activation of GABAA receptors. *J. Physiol.* 497(Pt 3), 753–759.

Chadderton, P., Margrie, T. W., and Hausser, M. (2004). Integration of quanta in cerebellar granule cells during sensory processing. *Nature* 428, 856–860.

Crowley, J. J., Carter, A. G., and Regehr, W. G. (2007). Fast vesicle replenishment and rapid recovery from desensitization at a single synaptic release site. *J. Neurosci.* 27, 5448–5460.

D'Angelo, E., and De Zeeuw, C. I. (2009). Timing and plasticity in the cerebellum: focus on the granular layer. *Trends Neurosci.* 32, 30–40.

De Zeeuw, C. I., Hoebeek, F. E., Bosman, L. W., Schonewille, M., Witter, L., and Koekkoek, S. K. (2011). Spatiotemporal firing patterns in the cerebellum. *Nat. Rev. Neurosci.* 12, 327–344.

Dieudonné, S. (1998). Submillisecond kinetics and low efficacy of parallel fibre-Golgi cell synaptic currents in the rat cerebellum. *J. Physiol.* 510(Pt 3), 845–866.

Dittman, J. S., Kreitzer, A. C., and Regehr, W. G. (2000). Interplay between facilitation, depression, and residual calcium at three presynaptic terminals. *J. Neurosci.* 20, 1374–1385.

Ebner, T. J., Chen, G., Gao, W., and Reinert, K. (2005). Optical imaging of cerebellar functional architectures: parallel fiber beams, parasagittal bands and spreading acidification. *Prog. Brain Res.* 148, 125–138.

Eccles, J. C., Llinás, R., and Sasaki, K. (1966). The mossy fibre-granule cell relay of the cerebellum and its inhibitory control by Golgi cells. *Exp. Brain Res.* 1, 82–101.

Gao, Z., van Beugen, B. J., and De Zeeuw, C. I. (2012). Distributed synergistic plasticity and cerebellar learning. *Nat. Rev. Neurosci.* 13, 619–635.

Hallermann, S., Fejtova, A., Schmidt, H., Weyhersmüller, A., Silver, R. A., Gundelfinger, E. D., et al. (2010). Bassoon speeds vesicle reloading at a central excitatory synapse. *Neuron* 68, 710–723.

Hensbroek, R. A., Ruigrok, T. J. H., van Beugen, B. J., and Simpson, J. I. (2005). Burst modulation of cerebellar granule cells during vestibular stimulation. *Soc. Neurosci. Abstr.* 297.4.

Hensbroek, R. A., van Beugen, B. J., Ruigrok, T. J. H., and Simpson, J. I. (2006). Spike modulation of unipolar brush cells and granule cells in the awake rabbit. *Soc. Neurosci. Abstr.* 740.2.

Isope, P., and Barbour, B. (2002). Properties of unitary granule cell–>Purkinje cell synapses in adult rat cerebellar slices. *J. Neurosci.* 22, 9668–9678.

Jörntell, H., and Ekerot, C. F. (2006). Properties of somatosensory synaptic integration in cerebellar granule cells in vivo. *J. Neurosci.* 26, 11786–11797.

Le Guen, M. C., and De Zeeuw, C. I. (2010). Presynaptic plasticity at cerebellar parallel fiber terminals. *Funct. Neurol.* 25, 141–151.

Lynch, G., and Gall, C. M. (2006). Ampakines and the threefold path to cognitive enhancement. *Trends Neurosci.* 29, 554–562.

Mapelli, J., and D'Angelo, E. (2007). The spatial organization of long-term synaptic plasticity at the input stage of cerebellum. *J. Neurosci.* 27, 1285–1296.

Mapelli, J., Gandolfi, D., and D'Angelo, E. (2010). High-pass filtering and dynamic gain regulation enhance vertical bursts transmission along the mossy fiber pathway of cerebellum. *Front. Cell. Neurosci.* 4:14. doi: 10.3389/fncel.2010.00014

Napper, R. M., and Harvey, R. J. (1988). Number of parallel fiber synapses on an individual Purkinje cell in the cerebellum of the rat. *J. Comp. Neurol.* 274, 168–177.

Palay, S. L., and Chan-Palay, V. (1974). *Cerebellar Cortex: Cytology and Organization.* Berlin: Springer.

Robberechts, Q., Wijnants, M., Guigliano, M., and De Schutter, E. (2010). Long-term depression at parallel fiber to Golgi cell synapses. *J. Neurophysiol.* 104, 3413–3423.

Roth, A., and Häusser, M. (2001). Compartmental models of rat cerebellar Purkinje cells based on simultaneous somatic and dendritic patch-clamp recordings. *J. Physiol.* 535(Pt 2), 445–472.

Ruigrok, T. J., Hensbroek, R. A., and Simpson, J. I. (2011). Spontaneous activity signatures of morphologically identified interneurons in the vestibulocerebellum. *J. Neurosci.* 31, 712–724.

Sargent, P. B., Saviane, C., Nielsen, T. A., DiGregorio, D. A., and Silver, R. A. (2005). Rapid vesicular release, quantal variability, and spillover contribute to the precision and reliability of transmission at a glomerular synapse. *J. Neurosci.* 25, 8173–8187.

Satake, S., Inoue, T., and Imoto, K. (2012). Paired-pulse facilitation of multivesicular release and intersynaptic spillover of glutamate at rat cerebellar granule cell-interneurone synapses. *J. Physiol.* 590(Pt 22), 5653–5675.

Saviane, C., and Silver, R. A. (2006). Fast vesicle reloading and a large pool sustain high bandwidth transmission at a central synapse. *Nature* 439, 983–987.

Saviane, C., and Silver, R. A. (2007). Estimation of quantal parameters with multiple-probability fluctuation analysis. *Methods Mol. Biol.* 403, 303–317.

Schmolesky, M. T., De Zeeuw, C. I., and Hansel, C. (2005). Climbing fiber synaptic plasticity and modifications in Purkinje cell excitability. *Prog. Brain Res.* 148, 81–94.

Sims, R. E., and Hartell, N. A. (2005). Differences in transmission properties and susceptibility to long-term depression reveal functional specialization of ascending axon and parallel fiber synapses to Purkinje cells. *J. Neurosci.* 25, 3246–3257.

Sims, R. E., and Hartell, N. A. (2006). Differential susceptibility to synaptic plasticity reveals a functional specialization of ascending axon and parallel fiber synapses to cerebellar Purkinje cells. *J. Neurosci.* 26, 5153–5159.

Solinas, S., Nieus, T., and D'Angelo, E. (2010). A realistic large-scale model

of the cerebellum granular layer predicts cicuit spatio-temporal filtering properties. *Front. Cell. Neurosci.* 4:12. doi: 10.3389/fncel.2010.00012

Valera, A. M., Doussau, F., Poulain, B., Barbour, B., and Isope, P. (2012). Adaptation of granule cell to Purkinje cell synapses to high-frequency transmission. *J. Neurosci.* 32, 3267–3280.

Conflict of Interest Statement: The authors declare that the research was conducted in the absence of any commercial or financial relationships that could be construed as a potential conflict of interest.

Received: 27 November 2012; paper pending published: 17 February 2013; accepted: 30 April 2013; published online: 21 May 2013.

Citation: van Beugen BJ, Gao Z, Boele H-J, Hoebeek F and De Zeeuw CI (2013) High frequency burst firing of granule cells ensures transmission at the parallel fiber to Purkinje cell synapse at the cost of temporal coding. Front. Neural Circuits **7**:*95. doi: 10.3389/fncir.2013.00095*

frontiers in
NEURAL CIRCUITS

REVIEW ARTICLE
published: 11 January 2013
doi: 10.3389/fncir.2012.00124

Non-Hebbian spike-timing-dependent plasticity in cerebellar circuits

Claire Piochon, Peter Kruskal, Jason MacLean and Christian Hansel*

Department of Neurobiology, University of Chicago, Chicago, IL, USA

Edited by:
Egidio D'Angelo, University of Pavia, Italy

Reviewed by:
Arnaud J. Ruiz, UCL School of Pharmacy, UK
Andreas Frick, INSERM, France

***Correspondence:**
Christian Hansel, Department of Neurobiology, University of Chicago, 947 E. 58th Street/J243, Chicago, IL 60637, USA.
e-mail: chansel@bsd.uchicago.edu

Spike-timing-dependent plasticity (STDP) provides a cellular implementation of the Hebb postulate, which states that synapses, whose activity repeatedly drives action potential firing in target cells, are potentiated. At glutamatergic synapses onto hippocampal and neocortical pyramidal cells, synaptic activation followed by spike firing in the target cell causes long-term potentiation (LTP)—as predicted by Hebb—whereas excitatory postsynaptic potentials (EPSPs) evoked after a spike elicit long-term depression (LTD)—a phenomenon that was not specifically addressed by Hebb. In both instances the action potential in the postsynaptic target neuron is an instructive signal that is capable of supporting synaptic plasticity. STDP generally relies on the propagation of Na^+ action potentials that are initiated in the axon hillhock back into the dendrite, where they cause depolarization and boost local calcium influx. However, recent studies in CA1 hippocampal pyramidal neurons have suggested that local calcium spikes might provide a more efficient trigger for LTP induction than backpropagating action potentials. Dendritic calcium spikes also play a role in an entirely different type of STDP that can be observed in cerebellar Purkinje cells. These neurons lack backpropagating Na^+ spikes. Instead, plasticity at parallel fiber (PF) to Purkinje cell synapses depends on the relative timing of PF-EPSPs and activation of the glutamatergic climbing fiber (CF) input that causes dendritic calcium spikes. Thus, the instructive signal in this system is externalized. Importantly when EPSPs are elicited before CF activity, PF-LTD is induced rather than LTP. Thus, STDP in the cerebellum follows a timing rule that is opposite to its hippocampal/neocortical counterparts. Regardless, a common motif in plasticity is that LTD/LTP induction depends on the relative timing of synaptic activity and regenerative dendritic spikes which are driven by the instructive signal.

Keywords: calcium, climbing fiber, dendrite, long-term depression, long-term potentiation, parallel fiber, Purkinje cell, pyramidal cell

INTRODUCTION

Hebb's postulate on synaptic modifications, which was formulated in 1949 in his book "*The Organization of Behavior,*" has laid the foundation for subsequent experimental work on memory storage by neuronal assemblies (Hebb, 1949):

> "*When an axon of cell A is near enough to excite a cell B and repeatedly or persistently takes part in firing it, some growth process or metabolic change takes place in one or both cells such that A's efficiency, as one of the cells firing B, is increased.*"

A more popular version of this rule—assigned to neurobiologist Carla Shatz—says "neurons that fire together wire together." The discovery of long-term potentiation (LTP) in 1973 demonstrated that synaptic connections can indeed be strengthened in a use-dependent way, thus reflecting a key prediction of the Hebb postulate (Bliss and Lømo, 1973). LTP is now widely regarded as a potentiation mechanism involved in circuit development and adult learning. However, for more than 20 years, researchers did not dissociate the relative roles of synaptic input and action potential generation in the postsynaptic neuron in the induction of LTP (see Linden, 1999). The implication inherent to Hebb's postulate is that excitatory synapses that contribute to the initiation of action potentials in the target cell will be strengthened. This component of the Hebb rule was demonstrated by spike-timing-dependent plasticity (STDP) studies, in which the relative timing of presynaptic activity and postsynaptic spike firing determines the direction and amplitude of synaptic weight change. Excitatory postsynaptic potentials (EPSPs) preceding postsynaptic action potentials within a time window of up to tens of milliseconds cause LTP, while activation in the reverse order induces long-term depression (LTD) (Markram et al., 1997; Bi and Poo, 1998; Debanne et al., 1998). While Hebb did not explicitly discuss the weakening of synapses in his hypothesis, LTD was suggested in a complementary statement by Stent (Stent, 1973) based on studies by Hubel and Wiesel examining plasticity during the critical period in visual cortex (Hubel and Wiesel, 1965; Wiesel and Hubel, 1965). STDP has generated immense interest as a plasticity mechanism that not only obeys Hebb's rule, but also reconciled LTP

studies with a renewed interest in temporal coding (König et al., 1996).

We will begin this review with a description of key features of STDP as observed in hippocampal and neocortical pyramidal cells. Then, we will present recent observations that in CA1 hippocampal pyramidal cells LTP is more sensitive to local dendritic spikes than to backpropagating action potentials that originate in the axon hillhock (Golding et al., 2002). We will discuss these findings in an attempt to reach a general assessment of the role of dendritic spikes in forms of plasticity that depend on the detection of temporal order. There are more variations on the STDP theme: in cerebellum-like structures, such as the dorsal cochlear nucleus (DCN) or the electrosensory lobe (ELL) of mormyrid electric fish, anti-Hebbian STDP has been described, in which EPSPs followed by spikes induce LTD, and activation in the reverse order leads to LTP (Bell et al., 1997; Tzounopoulos et al., 2004). In the cerebellum itself, the available data also point toward an STDP rule with anti-Hebbian timing requirements (Wang et al., 2000). However, there are no regenerative Na^+ spikes in Purkinje cell dendrites (Stuart and Häusser, 1994; Ohtsuki et al., 2012), and the direction of synaptic gain change at parallel fiber (PF) to Purkinje cell synapses depends on the co-activation of the climbing fiber (CF) input instead (Coesmans et al., 2004). CF activation causes two types of spikes that remain locally restricted: complex spikes in the soma and calcium spikes in the dendrite (Schmolesky et al., 2002; Davie et al., 2008). We will suggest that backpropagating action potentials provide an instructive plasticity signal in the neocortex and hippocampus, and that a similar function is served by the temporal correlation between local dendritic calcium spikes and synaptic activity in Purkinje cells. Thus, cerebellar plasticity is timing-dependent, but does not depend on somatic spike output and is thus non-Hebbian in nature.

STDP AND THE BACKPROPAGATION OF SOMATIC ACTION POTENTIALS INTO DENDRITES

Hebbian plasticity requires that activity at impinging synaptic inputs is paired with an instructive signal in the postsynaptic target neuron. This role can be served by the occurrence of an appropriately timed action potential, which propagates from the initial segment "back" into the dendrites. The discovery of action potential backpropagation into the dendrites was thus a prerequisite for an initial mechanistic description of Hebbian-style STDP. To demonstrate that action potentials are initiated close to the soma and actively invade the dendrites, Stuart, and Sakmann performed somato-dendritic double-patch recordings from layer V pyramidal neurons. They observed that (a) action potentials can be recorded in the dendrites after injection of depolarizing current pulses or synaptic stimulation, and (b) that action potentials are initiated in the axon hillock regardless of whether these action potentials were evoked by somatic or dendritic current injection, or by synaptic stimulation (Stuart and Sakmann, 1994). In summary, these results indicate that action potentials in these neurons are initiated close to the soma, and subsequently backpropagate into the dendrites. Similar observations were made in CA1 hippocampal pyramidal neurons (Spruston et al., 1995).

A role for backpropagating action potentials in plasticity was demonstrated a few years later. It was shown that in CA1 hippocampal pyramidal neurons pairing of subthreshold EPSPs with backpropagating action potentials causes LTP, and that the potentiation did not occur when these two stimuli were applied in isolation, or when spike backpropagation was blocked with local application of tetrodotoxin (TTX; Magee and Johnston, 1997). In a back-to-back paper in the same issue of *Science*, it was demonstrated using dual patch-clamp recordings that pairing of EPSPs with postsynaptic action potentials promotes LTP at synapses between connected layer 5 pyramidal neurons (Markram et al., 1997). This study also looked at the timing of pre- and postsynaptic activity in more detail, and found that LTP is induced when EPSPs precede the action potentials by 10 ms, but that application of these stimuli in reverse order results in LTD. Longer intervals (100 ms) neither elicit LTP nor LTD (Markram et al., 1997). Similarly narrow timing windows ($\leq$20 ms) were found in STDP studied in hippocampal cultures/slice cultures (Bi and Poo, 1998; Debanne et al., 1998). **Figure 1A** shows original data from the study by Bi and Poo (1998), and illustrate that LTP results either from coincident occurrence of EPSPs and action potentials (0 ms latency), or from EPSPs followed by an action potential (positive latency), whereas LTD is observed when the spike precedes the EPSP (negative latency, see **Figure 1B** for a model scheme). Backpropagating action potentials evoke calcium transients in the dendrites that result from the activation of voltage-dependent calcium channels (Markram et al., 1995). The amplitude of spine calcium transients evoked by paired activation of EPSPs and action potentials depends on the temporal order. Calcium signals are larger when EPSPs precede action potentials by latencies of less than 50 ms and that calcium influx is less when the sequence is reversed (Koester and Sakmann, 1998; see also Graupner and Brunel, 2007). These findings are in line with the idea that LTP induction has a higher calcium threshold than LTD induction (Bienenstock et al., 1982; Bear et al., 1987; Hansel et al., 1997). This timing between pairings is not sufficient by itself. Packets of multiple pairings with this temporal structure are needed to provide sufficient depolarization, but lower frequency STDP pairings can also be effective given additional somatic depolarization (Sjöström et al., 2001). Further, given a burst of postsynaptic action potential firing paired with a single presynaptic action potential, the direction and extent of plasticity depends on the timing of dendritic calcium transients with the presynaptic spike (Zilberter et al., 2009). It should be noted, however, that the calcium transient amplitude is likely not the only factor involved. For example, it has been shown that the potentiation in STDP-style protocols is NMDA receptor-dependent, while LTD requires the activation of metabotropic glutamate (mGluR) receptors, suggesting that two different calcium sensors downstream of these receptors might regulate LTP and LTD induction (Nevian and Sakmann, 2006). Thus, the localization and specific activation/inactivation conditions of these calcium sensors are likely to influence the calcium signaling requirements as well. Regardless of the underlying details, it seems fair to say that local depolarization events and calcium transients serve key functions in controlling the LTP/LTD balance. But which dendritic activity patterns evoke the

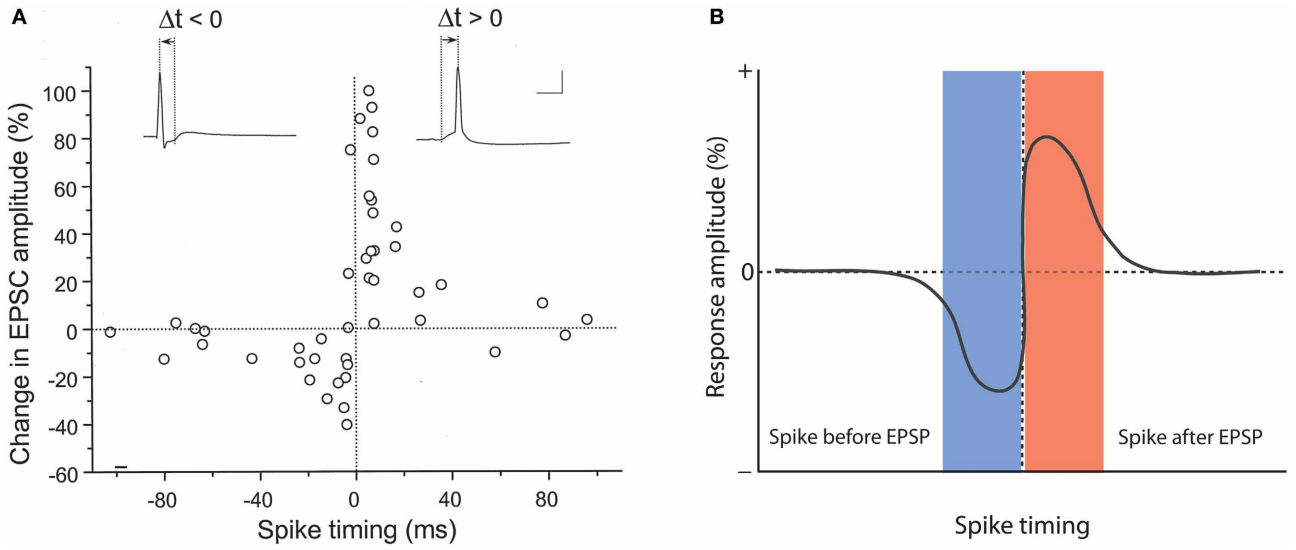

FIGURE 1 | Hebbian-style STDP in hippocampal neurons. (A) Temporal order for the induction of LTP and LTD at glutamatergic synapses onto cultured rat hippocampal neurons. The change in EPSC amplitudes measured at 20–30 min after tetanization (60 stimuli at 1 Hz) is plotted against spike timing. Spike timing is defined by the time interval (Δt) between the onset of the EPSP and the spike peak (see traces on top). Scale bars: 50 mV and 10 ms. **(B)** Model scheme for Hebbian STDP. LTD results when the spikes precede the EPSPs, whereas LTP is induced when the EPSPs are evoked before spike onset. **(A)** is taken from Bi and Poo (1998). Copyright 1998 by the Society for Neuroscience.

appropriate calcium transients under physiological conditions? It has been argued that local dendritic spikes, rather than back-propagating Na^+ spikes may be instrumental for plasticity control (see Lisman and Spruston, 2010). This challenge to the classic STDP model is based on the observation that (a) backpropagating action potentials typically do not invade distal dendrites, and thus STDP may not be a general plasticity mechanism, (b) LTP can be induced in the absence of Na^+ spikes, and (c) local depolarization can be more efficient in triggering LTP than back-propagating action potentials (Golding et al., 2002; Hardie and Spruston, 2009). This latter effect might result from the fact that local dendritic events, such as calcium spikes or AMPA/NMDA receptor-mediated responses provide a more prolonged depolarization than fast Na^+ spikes (Lisman and Spruston, 2010). It is, however, conceivable that Na^+ spikes, under conditions where they contribute to plasticity, facilitate the initiation of local calcium spikes, and that thus STDP is a physiologically relevant model for plasticity, but acts locally through dendritic calcium spikes. From a mechanistic point of view, these local calcium spikes can present an instructive signal whether or not their occurrence is facilitated by Na^+ spike backpropagation (Hardie and Spruston, 2009).

VARIATIONS OF SPIKE-TIMING-DEPENDENT PLASTICITY: ANTI-HEBBIAN STDP

One of the very first reports of STDP did not result from recordings from hippocampal or neocortical pyramidal neurons, but from medium ganglion (MG) cells of the ELL of the mormyrid electric fish *Gnathonemus petersii* (Bell et al., 1997). The ELL is a cerebellum-like structure, and MG cells are GABAergic neurons that are described as Purkinje-like cells—they receive glutamatergic PF synapses, but lack the CF input that is characteristic for cerebellar Purkinje cells. In these Purkinje-like neurons, pairing of a PF-EPSP with a postsynaptic spike results in LTD if the spike follows the EPSP onset within 60 ms. In contrast, LTP is induced when the spikes are delivered outside this time window, or PF-EPSPs are evoked at 1 Hz in the absence of spikes (Bell et al., 1997; Han et al., 2000). Thus, STDP in this cerebellum-like structure follows an anti-Hebbian temporal order (**Figure 2**). The available data support the notion that this type of STDP is under control of the spike output of the postsynaptic target cell. The spikes that were evoked in these experiments by somatic current injection are so-called "broad spikes" that are TTX-sensitive (Bell et al., 1997), and are initiated in the soma/proximal dendrite, from where they propagate into the apical dendrite (Gomez et al., 2005; Engelmann et al., 2008). Broad spikes certainly differ from fast action potentials that are capable of producing cortical STDP—broad spikes are 8–15 ms wide and only reach amplitudes in the range of 40–60 mV (Bell et al., 1997). Still, these spikes are at least partially mediated by voltage-gated Na^+ influx and are initiated in or near the soma, providing a signal that reflects the electrical output of MG cells. Thus, it seems fair to state that STDP in the ELL is anti-Hebbian with regard to the temporal order controlling LTP and LTD induction, but nevertheless falls into the category of Hebbian-style learning rules, because of the critical involvement of spike backpropagation into the dendrites. This type of anti-Hebbian STDP is not restricted to non-mammalian vertebrates, but has also been described in a mammalian cerebellum-like structure, the DCN, which is a brainstem region that is part of the auditory system. In cartwheel cells, which are inhibitory interneurons that resemble MG cells in the fish ELL, activation of EPSPs by PF stimulation leads to LTD if the

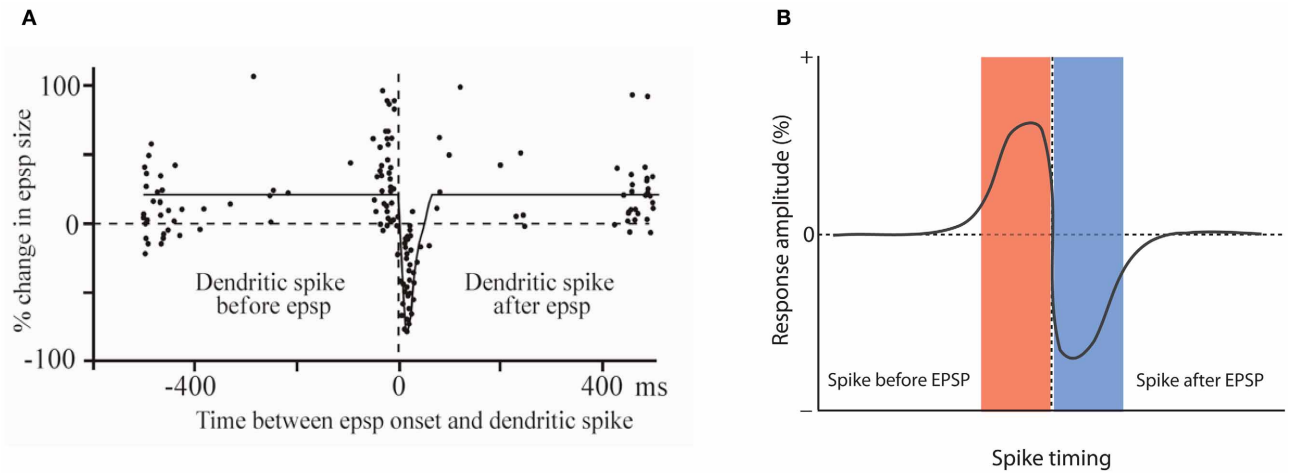

FIGURE 2 | Anti-Hebbian STDP in a cerebellum-like structure. **(A)** Temporal order for the induction of LTP and LTD at parallel fiber synapses onto Purkinje-like cells in the electrosensory lobe of the mormyrid fish *Gnathonemus petersii*. Changes in EPSP amplitudes are plotted against the delay between EPSP onset and the broad spike peak during the pairing period (360 stimuli at 1 Hz). **(B)** Model scheme for anti-Hebbian STDP. LTP is induced when the spike is initiated before an EPSP is evoked. Stimulation in the reverse order (EPSP-spike) results in LTD. Note that this figure panel shows an idealized model of anti-Hebbian STDP and differs from the experimentally obtained data presented in **(A)**, in which potentiation is also seen with intervals >400 ms. **(A)** is modified from Bell et al. (1997) with permission from Macmillan Publishers Ltd: Nature, copyright 1997.

EPSPs are followed after 5 ms by spike activity. No synaptic change results from activation in the reverse order (Tzounopoulos et al., 2004). In cartwheel cells, somatic depolarization leads to simple spike and/or complex spike firing, and is believed to trigger dendritic calcium spikes. The depression resulting from EPSP-spike sequences is presynaptically expressed and requires retrograde cannabinoid signaling (Tzounopoulos et al., 2007). Similarly, LTD induced by spike-EPSP sequences in layer 5 pyramidal neurons has been shown to require the activation of presynaptic CB1 receptors (Sjöström et al., 2003). Thus, this signaling mechanism is not restricted to anti-Hebbian STDP. We will discuss below that while anti-Hebbian STDP has been described in most detail in cerebellum-like structures, a form of STDP with anti-Hebbian (and non-Hebbian) components also plays a role in the cerebellum itself. Moreover, modeling studies have suggested that in CA1 hippocampal pyramidal neurons, anti-Hebbian STDP could function to equalize synaptic weights along the axis of the apical dendrite (Rumsey and Abbott, 2006). Due to the scope of this review, however, we will not discuss these modeling studies in detail.

NON-HEBBIAN STDP IN THE CEREBELLUM

Surprisingly, STDP has not been studied in as much detail in the cerebellum proper. This might be due to the fact that in the cerebellum, LTP has been discovered later than in most other brain areas. While a presynaptic form of LTP has been described in 1996 (Salin et al., 1996), postsynaptic LTP—a potential reversal mechanism for the postsynaptically expressed LTD—has only been documented in 2002 (Lev-Ram et al., 2002). Nevertheless, sufficient data are available to draw some conclusions. LTD at PF synapses onto Purkinje cells results from co-activity of the PF and the CF input (Ito et al., 1982), during which the CF triggers complex spikes that can be recorded in the soma (for review, see Schmolesky et al., 2002). The first study that looked at timing requirements reported that LTD was induced best when CF stimulation (and complex spike activity) preceded PF activation with an interval of less than 250 ms (Ekerot and Kano, 1989). However, this report was inconclusive as (a) LTD was monitored with extracellular recordings of simple spikes—a measure that does not directly reflect synaptic plasticity, and (b) LTD was also observed when PF activity preceded CF activity by 5–20 ms. Subsequent studies found that LTD is most efficiently induced when PF stimulation precedes complex spike activity by 50–250 ms (Chen and Thompson, 1995; Wang et al., 2000; Safo and Regehr, 2008). Chen and Thompson showed that 600 pairings of PF and CF activity caused LTD independent of the timing interval. However, when using only 100 pairings, LTD is more sensitive to timing requirements: LTD was induced best when PF stimulation preceded CF activity by 250 ms, a depression that did not reach statistical significance resulted from PF+CF co-activation with 125 ms or 0 ms intervals, and no change was observed when CF stimulation preceded PF activity by 250 ms (Chen and Thompson, 1995). Similarly, Wang et al. showed that LTD is induced when PF stimulation precedes complex spike activity by 150 ms or when the two inputs are simultaneously activated, but LTD does not result from co-activation using a 500 ms interval, or a reversed activation sequence (150/500 ms interval). Interestingly, although not discussed by the authors, CF-PF stimulation with an interval of 150 ms results in a weak potentiation that lasts about 20 min (Wang et al., 2000). Safo and Regehr obtained similar results, but also noted a depression when CF activity preceded PF activity by 50 ms (Safo and Regehr, 2008). However, since more pronounced LTD was induced by PF stimulation first (50 and 150 ms), these data generally seem to confirm the observations made by the other two groups. These studies point toward an anti-Hebbian STDP mechanism in the cerebellum, similar to the anti-Hebbian

STDP described in cerebellum-like structures (but note that in cerebellum-like structures the timing intervals seem to be shorter). In the light of the discrepancies in the literature, we would like to point out that in our hands 100 Hz PF burst stimulation followed after 120 ms by CF activity causes LTD (Piochon et al., 2010), which is in line with the observations by Chen and Thompson (1995) and Wang et al. (2000). At the single spine level, evoked calcium transients are largest when the PF input is activated before CF stimulation (Wang et al., 2000). This observation might explain why this temporal sequence is optimal for LTD induction, since at these cerebellar synapses LTD has a higher calcium threshold for induction than LTP (Coesmans et al., 2004).

Remarkably, such a requirement for specific temporal order and similar activation sequences can also be observed in behavioral learning. One example is the need for temporal specificity in associative eyeblink conditioning—a form of motor learning that involves the cerebellum: the optimal interval between application of a tone (conditioned stimulus; conveyed by the PF input) and an air puff application to the eye (unconditioned stimulus; conveyed by the CF input) is between 200–400 ms, thus offering a rare opportunity to relate timing intervals that were observed in *in vitro* and *in vivo* learning studies, respectively (Thompson and Krupa, 1994). In line with these results, in gain adaptation of the vestibulo-ocular reflex (VOR), another type of learning mediated by the cerebellum, CF activity needs to follow PF activity by 100 ms (Raymond and Lisberger, 1998). These examples illustrate that both LTD induction and forms of behavioral learning require PF activity prior to CF activation for the adaptive change to occur.

Cerebellar plasticity depends on the relative timing between the activation of PF synapses and the occurrence of CF-evoked complex spikes. As a result it appears that in STDP an instructive signal for the strengthening or weakening of a synapse can arise from a number of sources: a backpropagating action potential or a synaptically evoked calcium spike depending on the structure or system. However, cerebellar STDP differs from STDP at hippocampal/neocortical synapses, and also from STDP in cerebellum-like structures, in that it does not depend on the axonal spike output. In cerebellar Purkinje cells—in contrast to pyramidal cells and Purkinje-like cells—Na^+ action potentials that are elicited in the axon hillhock do not actively backpropagate, but rather spread passively into the dendrites (Stuart and Häusser, 1994; Ohtsuki et al., 2012). Thus, the dendrite does not receive feedback information on whether action potentials were fired or not, which is a key component of Hebbian plasticity (but note that dendritic calcium transients can vary in amplitude depending on whether the cell is in an up or down state; Kitamura and Häusser, 2011). Rather, bidirectional PF plasticity depends on the relative timing with activity of the heterosynaptic CF input, which provides an externalized instructive signal. Interestingly, the somatically recorded complex spike does not seem to play a role in cerebellar STDP: double-patch recordings from the soma and dendrite of Purkinje cells have shown that the classic complex spike waveform only occurs in the soma, and that CF activation results in all-or-none EPSPs in the dendrites instead, which can be associated with local spike activity (Davie et al., 2008; Ohtsuki et al., 2009, 2012). As these dendritic spikes typically do not cause additional spikes near the soma, it seems that CF activity evokes two types of spikes in the soma and dendrites that occur independently from each other. Thus, STDP at cerebellar PF to Purkinje cell synapses is anti-Hebbian with regard to the optimal temporal order of synaptic activation and the occurrence of local dendritic spikes, but is non-Hebbian with regard to the lack of action potential backpropagation and thus information on the neuron's spike firing output.

As outlined above, PF plasticity in both the cerebellum proper and in cerebellum-like structures follows an anti-Hebbian STDP rule, but in contrast to Purkinje cells in the mammalian cerebellum, Purkinje-like cells in cerebellum-like structures such as the mormyrid ELL show action potential backpropagation, which may be involved in STDP. To reconcile these observations we review plasticity mechanisms in the mormyrid cerebellum proper. Neither STDP nor action potential backpropagation have been systematically studied in cerebellar Purkinje cells of mormyrid fish. However, it has been shown that PF-LTD results from PF activation followed after 20–50 ms by CF stimulation, pointing toward an anti-Hebbian STDP mechanism (Han et al., 2007). The role of the axonal spike output remains unclear. CF activation does not result in complex spikes, but in all-or-none EPSPs. Moreover, Na^+ action potentials recorded from the somata of mormyrid Purkinje cells have unusually small amplitudes, typically not exceeding 30 mV (de Ruiter et al., 2006). It seems unlikely that these reduced Na^+ spikes backpropagate, although mormyrid Purkinje cells express the Na^+ channel α subunits $Na_v1.1$, $Na_v1.2$, and $Na_v1.6$ in their dendrites (de Ruiter et al., 2006). On the other hand, somatic depolarization or CF stimulation can evoke broad spikes that can be recorded in the somata of mormyrid Purkinje cells and are associated with dendritic calcium transients that are at least partially mediated by P/Q-type voltage-gated calcium channels (Han et al., 2007). In contrast to their mammalian counterparts, mormyrid CFs only contact very proximal parts of the dendrite ("horizontal dendrite") and do not invade the molecular layer. Thus, activation in or close to the soma can evoke calcium spikes (broad spikes) in the dendrites. The relevance of these broad spikes for plasticity is currently not understood: pairing PF activation with broad spikes evoked by CF stimulation causes LTD, but when the broad spikes are triggered by somatic injection of depolarizing currents LTP is induced instead (Han et al., 2007). Further studies are needed to determine under which conditions broad spike activity promotes LTD and LTP, respectively, and to assess the role of the axonal spike output in STDP in cerebellar Purkinje cells of mormyrid fish.

In summary, it can be concluded that a form of STDP does exist in cerebellar Purkinje cells, but that there are two important differences to STDP in pyramidal cells: (a) the optimal temporal order of synaptic activation and spike firing is reversed, so that synaptic activity followed by spike activity results in LTD rather than LTP induction, and (b) in mammalian Purkinje cells (and possibly mormyrid Purkinje cells), the instructive signal is externalized, and locally elicited calcium spikes play a key role instead. This latter difference has important functional consequences: in contrast to Hebbian plasticity, what matters is not the timing relative to the axonal spike output, but rather the timing relative to the

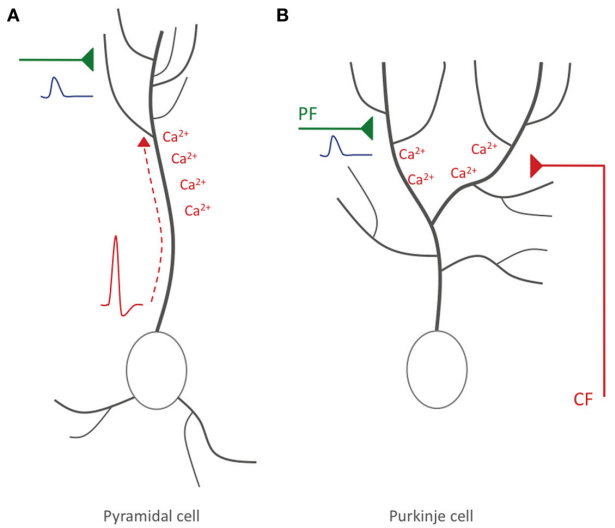

FIGURE 3 | Hebbian-style and non-Hebbian STDP. (A) Hebbian STDP in hippocampal and neocortical pyramidal cells. Action potentials are elicited near the soma and backpropagate into the dendrite, where the accompanying depolarization leads to calcium influx (red). The timing relative to incoming EPSPs (blue) evoked at glutamatergic synaptic inputs (green) determines whether LTP or LTD is induced. **(B)** Non-Hebbian STDP in cerebellar Purkinje cells. Here, somatic/axonal action potentials do not actively invade the dendrite. Rather, CF activation causes local dendritic calcium spikes. LTD results if PF-EPSPs precede CF activity. In hippocampal/neocortical circuits this activation sequence (synaptic activity—spike) promotes LTP instead.

activity of the CF input, a qualitatively different, heterosynaptic input (**Figure 3**).

WAS DONALD HEBB WRONG?

To answer this question, it needs to be acknowledged first that the famous Hebb postulate—as cited in the introduction—is only a small component within a larger conceptual framework that Hebb presented in his book "The Organization of Behavior." When using the terms "Hebbian" and "non-Hebbian," we thus specifically refer to the spike timing mechanism described in the Hebb postulate. Within this framework, the Hebb postulate describes a learning rule for types of neurons, in which action potential backpropagation takes place. By extension, cerebellar STDP can be described as "non-Hebbian" as Purkinje cells lack regenerative backpropagating Na^+ spikes (Stuart and Häusser, 1994; Ohtsuki et al., 2012).

STDP does exist in the cerebellum, but depends on dendritic calcium spikes instead. Moreover, the temporal order of STDP found in the cerebellum and in cerebellum-like structures is opposite to that expected from an STDP mechanism that follows the Hebb rule (e.g., Bell et al., 1997; Wang et al., 2000). We argue that the Hebb rule remains a widely applicable plasticity concept, but that there are important exceptions and limitations that need to be acknowledged when generalizing.

To understand STDP rules, it is useful to take mechanistic aspects of LTP and LTD induction into consideration. Both forms of plasticity are initiated by local dendritic calcium transients, whose specific features, such as amplitude, localization, and kinetics ultimately determine the polarity of synaptic weight change (for discussion, see Bear et al., 1987; Hansel et al., 1997; Wang et al., 2000; Coesmans et al., 2004; Nevian and Sakmann, 2006). This strict dependence on calcium signaling explains why, for example, LTP in pyramidal cells can be triggered either by local spikes in the dendrites, or by action potential backpropagation: both types of spike activity are associated with local calcium influx (Markram et al., 1995; Golding et al., 2002). At more distal synaptic input locations local calcium spikes may be the most effective means to trigger LTP (Golding et al., 2002; Hardie and Spruston, 2009). However, this observation does not generally exclude a role for Hebbian STDP in plasticity, particularly at more proximal synapses. It remains to be determined which type of spike activity is most relevant under physiological conditions (see also Lisman and Spruston, 2010).

Does the existence of a very different type of STDP (non-Hebbian/reverse temporal order) in the cerebellum challenge the general importance of Hebbian-style plasticity mechanisms? Not necessarily, because cerebellar Purkinje cells have unique features that set them apart from other types of neurons. Of these features, two are particularly relevant for our discussion, because they mark significant differences to hippocampal and neocortical pyramidal cells: first, there is no action potential backpropagation into Purkinje cell dendrites (Stuart and Häusser, 1994; Ohtsuki et al., 2012). As a consequence, the dendrites receive no information on the axonal spike output. However, we suggest that the role of the backpropagating action potential is served by the instructive signal from the CF. Second, Purkinje cells spontaneously fire action potentials (simple spikes) at discharge rates in the range of ~20–80 Hz (Häusser and Clark, 1997), whereas pyramidal cells are almost silent at rest (Margrie et al., 2002). This latter difference is important, because low firing rates allow pyramidal neurons to act as coincidence detectors (König et al., 1996). In contrast, the high firing rates found in Purkinje cells prevent these neurons from using relative spike timing as a relevant measure for processes such as STDP, because the short interval between spikes makes it difficult to distinguish between post- and pre-spike events. This notion holds for simple spikes—that are intrinsically triggered and can result from PF activity—but not for spikes evoked by CF discharges that occur at 1–2 Hz at rest (Simpson et al., 1996). Thus, it does not come as a surprise that STDP at PF synapses onto Purkinje cells is based on timing relative to CF-evoked spike activity (Chen and Thompson, 1995; Wang et al., 2000). A remarkable consequence is that STDP at these cerebellar synapses depends on the relative timing of activity at two qualitatively different, independent synaptic inputs. The externalization of the instructive signal in the cerebellum is very different from the prevalent theme of Hebbian plasticity in neocortex and hippocampus of timing relative to somatic/axonal action potential firing (**Figure 3**). In the cerebellum, this non-Hebbian form of STDP allows the CF input to assume the role of a teacher and instructor in cerebellar motor learning (Simpson et al., 1996). Cerebellar STDP seems unique in that it depends on specific features of Purkinje cell physiology and of the cerebellar microcircuit. Thus, a more general reading of Hebb's postulate

is necessary for it to be applied throughout the central nervous system.

ACKNOWLEDGMENTS

We would like to thank Curtis C. Bell and Nicolas Brunel for invaluable comments on the manuscript and members of the MacLean and Hansel laboratories for helpful discussions. The authors were supported by the DANA Foundation (Jason MacLean), a National Science Foundation CAREER Award (0952686 to Jason MacLean), and a grant from the National Institute of Neurological Disorders and Stroke (NS-062771 to Christian Hansel).

REFERENCES

Bear, M. F., Cooper, L. N., and Ebner, F. F. (1987). A physiological basis for a theory of synapse modification. *Science* 237, 42–48.

Bell, C. C., Han, V. Z., Sugawara, Y., and Grant, K. (1997). Synaptic plasticity in a cerebellum-like structure depends on temporal order. *Nature* 387, 278–281.

Bi, G. Q., and Poo, M. M. (1998). Synaptic modifications in cultured hippocampal neurons: dependence on spike timing, synaptic strength, and postsynaptic cell type. *J. Neurosci.* 18, 10464–10472.

Bienenstock, E. L., Cooper, L. N., and Munro, P. W. (1982). Theory for the development of neuron selectivity: orientation specificity and binocular interaction in visual cortex. *J. Neurosci.* 2, 32–48.

Bliss, T. V. P., and Lømo, T. (1973). Long-lasting potentiation of synaptic transmission in the dentate area of the anesthetized rabbit following stimulation of the perforant path. *J. Physiol.* 232, 331–356.

Chen, C., and Thompson, R. F. (1995). Temporal specificity of long-term depression in parallel fiber-Purkinje synapses in rat cerebellar slice. *Learn. Mem.* 2, 185–198.

Coesmans, M., Weber, J. T., De Zeeuw, C. I., and Hansel, C. (2004). Bidirectional parallel fiber plasticity in the cerebellum under climbing fiber control. *Neuron* 44, 691–700.

Davie, J. T., Clark, B. A., and Häusser, M. (2008). The origin of the complex spike in cerebellar Purkinje cells. *J. Neurosci.* 28, 7599–7609.

de Ruiter, M. M., De Zeeuw, C. I., and Hansel, C. (2006). Voltage-gated sodium channels in cerebellar Purkinje cells of mormyrid fish. *J. Neurophysiol.* 96, 378–390.

Debanne, D., Gähwiler, B. H., and Thompson, S. M. (1998). Long-term synaptic plasticity between pairs of individual CA3 pyramidal cells in rat hippocampal slice cultures. *J. Physiol.* 507(Pt 1), 237–247.

Ekerot, C. F., and Kano, M. (1989). Stimulation parameters influencing climbing fibre induced long-term depression of parallel fibre synapses. *Neurosci. Res.* 6, 264–268.

Engelmann, J., van den Burg, E., Bacelo, J., de Ruiter, M., Kuwana, S., Sugawara, Y., et al. (2008). Dendritic backpropagation and synaptic plasticity in the mormyrid electrosensory lobe. *J. Physiol. (Paris)* 102, 233–245.

Golding, N. L., Staff, N. P., and Spruston, N. (2002). Dendritic spikes as a mechanism for cooperative long-term potentiation. *Nature* 418, 326–331.

Gomez, L., Kanneworff, M., Budelli, R., and Grant, K. (2005). Dendritic spike back propagation in the electrosensory lobe of *Gnathonemus petersii*. *J. Exp. Biol.* 208, 141–155.

Graupner, M., and Brunel, N. (2007). STDP in a bistable synapse model based on CaMKII and associated signaling pathways. *PLoS Comp. Biol.* 3:e221. doi: 10.1371/journal.pcbi.0030221

Han, V. Z., Grant, K., and Bell, C. C. (2000). Reversible associative depression and nonassociative potentiation at a parallel fiber synapse. *Neuron* 27, 611–622.

Han, V. Z., Zhang, Y., Bell, C. C., and Hansel, C. (2007). Synaptic plasticity and calcium signaling in Purkinje cells of the central cerebellar lobes of mormyrid fish. *J. Neurosci.* 27, 13499–13512.

Hansel, C., Artola, A., and Singer, W. (1997). Relation between dendritic Ca2+ levels and the polarity of synaptic long-term modifications in rat visual cortex neurons. *Eur. J. Neurosci.* 9, 2309–2322.

Hardie, J., and Spruston, N. (2009). Synaptic depolarization is more effective than back-propagating action potentials during induction of associative long-term potentiation in hippocampal pyramidal neurons. *J. Neurosci.* 29, 3233–3241.

Häusser, M., and Clark, B. A. (1997). Tonic synaptic inhibition modulates neuronal output pattern and spatiotemporal synaptic integration. *Neuron* 19, 665–678.

Hebb, D. O. (1949). *The Organization of Behavior.* New York, NY: Wiley.

Hubel, D. H., and Wiesel, T. N. (1965). Binocular interaction in striate cortex of kittens reared with artificial squint. *J. Neurophysiol.* 28, 1041–1059.

Ito, M., Sakurai, M., and Tongroach, P. (1982). Climbing fibre induced depression of both mossy fibre responsiveness and glutamate sensitivity of cerebellar Purkinje cells. *J. Physiol.* 324, 113–134.

Kitamura, K., and Häusser, M. (2011). Dendritic calcium signaling triggered by spontaneous and sensory-evoked climbing fiber input to cerebellar Purkinje cells *in vivo*. *J. Neurosci.* 31, 10847–10858.

Koester, H. J., and Sakmann, B. (1998). Calcium dynamics in single spines during coincident pre- and postsynaptic activity depend on relative timing of back-propagating action potentials and subthreshold excitatory postsynaptic potentials. *Proc. Natl. Acad. Sci. U.S.A.* 95, 9596–9601.

König, P., Engel, A. K., and Singer, W. (1996). Integrator or coincidence detector? The role of the cortical neuron revisited. *Trends Neurosci.* 19, 130–137.

Lev-Ram, V., Wong, S. T., Storm, D. R., and Tsien, R. Y. (2002). A new form of cerebellar long-term potentiation is postsynaptic and depends on nitric oxide but not cAMP. *Proc. Natl. Acad. Sci. U.S.A.* 99, 8389–8393.

Linden, D. J. (1999). The return of the spike: postsynaptic action potentials and the induction of LTP and LTD. *Neuron* 22, 661–666.

Lisman, J., and Spruston, N. (2010). Questions about STDP as a general model of synaptic plasticity. *Front. Syn. Neurosci.* 2:140. doi: 10.3389/fnsyn.2010.00140

Magee, J. C., Johnston, D. (1997). A synaptically controlled, associative signal for Hebbian plasticity in hippocampal neurons. *Science* 275, 209–213.

Margrie, T. W., Brecht, M., and Sakmann, B. (2002). *In vivo*, low resistance, whole-cell recordings from neurons in the anaesthetized and awake mammalian brain. *Pflugers Arch.* 444, 491–498.

Markram, H., Helm, P. J., and Sakmann, B. (1995). Dendritic calcium transients evoked by single back-propagating action potentials in rat neocortical pyramidal neurons. *J. Physiol.* 485.1, 1–20.

Markram, H., Lübke, J., Frotscher, M., and Sakmann, B. (1997). Regulation of synaptic efficacy by coincidence of postsynaptic APs and EPSPs. *Science* 275, 213–215.

Nevian, T., and Sakmann, B. (2006). Spine Ca2+ signaling in spike-timing-dependent plasticity. *J. Neurosci.* 26, 11001–11013.

Ohtsuki, G., Piochon, C., Adelman, J. P., and Hansel, C. (2012). SK2 channel modulation contributes to compartment-specific dendritic plasticity in cerebellar Purkinje cells. *Neuron* 75, 108–120.

Ohtsuki, G., Piochon, C., and Hansel, C. (2009). Climbing fiber signaling and cerebellar gain control. *Front. Cell. Neurosci.* 3:4. doi:10.3389/neuro.03.004.2009

Piochon, C., Levenes, C., Ohtsuki, G., and Hansel, C. (2010). Purkinje cell NMDA receptors assume a key role in synaptic gain control in the mature cerebellum. *J. Neurosci.* 30, 15330–15335.

Raymond, J. L., and Lisberger, S. G. (1998). Neural learning rules for the vestibulo-ocular reflex. *J. Neurosci.* 18, 9112–9129.

Rumsey, C. C., and Abbott, L. F. (2006). Synaptic democracy in active dendrites. *J. Neurophysiol.* 96, 2307–2318.

Safo, P., and Regehr, W. G. (2008). Timing dependence of the induction of cerebellar LTD. *Neuropharmacology* 54, 213–218.

Salin, P. A., Malenka, R. C., and Nicoll, R. A. (1996). Cyclic AMP mediates a presynaptic form of LTP at cerebellar parallel fiber synapses. *Neuron* 16, 797–803.

Schmolesky, M. T., Weber, J. T., De Zeeuw, C. I., and Hansel, C. (2002). The making of a complex spike: ionic composition and plasticity. *Ann. N.Y. Acad. Sci.* 978, 359–390.

Simpson, J. I., Wylie, D. R., and De Zeeuw, C. I. (1996). On climbing fiber signals and their consequence(s). *Behav. Brain Sci.* 19, 384–398.

Sjöström, P. J., Turrigiano, G. G., and Nelson, S. B. (2001). Rate, timing, and cooperativity jointly determine cortical synaptic plasticity. *Neuron* 32, 1149–1164.

Sjöström, P. J., Turrigiano, G. G., and Nelson, S. B. (2003). Neocortical

LTD via coincident activation of presynaptic NMDA and cannabinoid receptors. *Neuron* 39, 641–654.

Spruston, N., Schiller, Y., Stuart, G., and Sakmann, B. (1995). Activity-dependent action potential invasion and calcium influx into hippocampal CA1 dendrites. *Science* 268, 297–300.

Stent, G. S. (1973). A physiological mechanism for Hebb's postulate of learning. *Proc. Nat. Acad. Sci. U.S.A.* 70, 997–1001.

Stuart, G., and Häusser, M. (1994). Initiation and spread of sodium action potentials in cerebellar Purkinje cells. *Neuron* 13, 703–712.

Stuart, G., and Sakmann, B. (1994). Active propagation of somatic action potentials into neocortical pyramidal cell dendrites. *Nature* 367, 69–72.

Thompson, R. F., and Krupa, D. J. (1994). Organization of memory traces in the mammalian brain. *Annu. Rev. Neurosci.* 17, 519–549.

Tzounopoulos, T., Kim, Y., Oertel, D., and Trussell, L. O. (2004). Cell-specific, spike timing-dependent plasticities in the dorsal cochlear nucleus. *Nat. Neurosci.* 7, 719–725.

Tzounopoulos, T., Rubio, M. E., Keen, J. E., and Trussell, L. O. (2007). Coactivation of pre- and postsynaptic signaling mechanisms determines cell-specific spike-timing-dependent plasticity. *Neuron* 54, 291–301.

Wang, S. S. H., Denk, W., and Häusser, M. (2000). Coincidence detection in single dendritic spines mediated by calcium release. *Nat. Neurosci.* 3, 1266–1273.

Wiesel, T. N., and Hubel, D. H. (1965). Comparison of the effects of unilateral and bilateral eye closure on cortical unit responses in kittens. *J. Neurophysiol.* 28, 1029–1040.

Zilberter, M., Holmgren, C., Shemer, I., Silberberg, G., Grillner, S., Harkany, T., et al. (2009). Input specificity and dependence of spike timing-dependent plasticity on preceding postsynaptic activity at unitary connections between neocortical layer 2/3 pyramidal cells. *Cereb. Cortex* 19, 2308–2320.

Conflict of Interest Statement: The authors declare that the research was conducted in the absence of any commercial or financial relationships that could be construed as a potential conflict of interest.

Received: 12 September 2012; accepted: 26 December 2012; published online: 11 January 2013.

Citation: Piochon C, Kruskal P, MacLean J and Hansel C (2013) Non-Hebbian spike-timing-dependent plasticity in cerebellar circuits. Front. Neural Circuits ***6****:124. doi: 10.3389/fncir.2012.00124*

frontiers in
NEURAL CIRCUITS

ORIGINAL RESEARCH ARTICLE
published: 22 November 2012
doi: 10.3389/fncir.2012.00091

Olivary subthreshold oscillations and burst activity revisited

Paolo Bazzigaluppi[1†], Jornt R. De Gruijl[2†], Ruben S. van der Giessen[1], Sara Khosrovani[1], Chris I. De Zeeuw[1,2] and Marcel T. G. de Jeu[1]*

[1] *Department of Neuroscience, Erasmus Medical Center, Rotterdam, Netherlands*
[2] *Netherlands Institute for Neuroscience, Royal Netherlands Academy of Arts and Sciences, Amsterdam, Netherlands*

Edited by:
Egidio D'Angelo, University of Pavia, Italy

Reviewed by:
Leonard Maler, University of Ottawa, Canada
Scott Hooper, Ohio University, USA

***Correspondence:**
Marcel T. G. de Jeu, Department of Neuroscience, Erasmus Medical Center, P.O. Box 2040, 3000 CA Rotterdam, Netherlands.
e-mail: m.dejeu@erasmusmc.nl

† These authors have equally contributed to this work.

The inferior olive (IO) forms one of the major gateways for information that travels to the cerebellar cortex. Olivary neurons process sensory and motor signals that are subsequently relayed to Purkinje cells. The intrinsic subthreshold membrane potential oscillations of the olivary neurons are thought to be important for gating this flow of information. *In vitro* studies have revealed that the phase of the subthreshold oscillation determines the size of the olivary burst and may gate the information flow or encode the temporal state of the olivary network. Here, we investigated whether the same phenomenon occurred in murine olivary cells in an intact olivocerebellar system using the *in vivo* whole-cell recording technique. Our *in vivo* findings revealed that the number of wavelets within the olivary burst did not encode the timing of the spike relative to the phase of the oscillation but was related to the amplitude of the oscillation. Manipulating the oscillation amplitude by applying Harmaline confirmed the inverse relationship between the amplitude of oscillation and the number of wavelets within the olivary burst. Furthermore, we demonstrated that electrotonic coupling between olivary neurons affect this modulation of the olivary burst size. Based on these results, we suggest that the olivary burst size might reflect the "expectancy" of a spike to occur rather than the spike timing, and that this process requires the presence of gap junction coupling.

Keywords: inferior olive, subthreshold oscillations, wavelets, climbing fiber, cerebellum, gap junctions

INTRODUCTION

The inferior olive (IO) forms the sole source of climbing fiber inputs to Purkinje cells in the cerebellar cortex (Szentágothai and Rajkovits, 1959; Desclin, 1974). Climbing fibers excite Purkinje cells in the cerebellar cortex, resulting in a powerful, all-or-none depolarization called a complex spike (Eccles et al., 1966; Thach, 1967; Ito and Simpson, 1971). Climbing fibers may fire in bursts (Crill and Kennedy, 1967; Crill, 1970; Maruta et al., 2007; Mathy et al., 2009) and thereby they can modify the complex spike (Mathy et al., 2009). These climbing fiber bursts are generated at the axon hillock of olivary cells and they backpropagate to the soma where they give rise to small wavelets (Mathy et al., 2009).

IO neurons have two intrinsic properties that play an important role in their firing behavior: IO neurons generate subthreshold oscillations (Llinás and Yarom, 1986; Khosrovani et al., 2007) and they are coupled to one another via dendrodendritic gap junctions (Llinás et al., 1974; Sotelo et al., 1974; Khosrovani et al., 2007; Van Der Giessen et al., 2008). The subthreshold oscillations may serve as a timekeeping device, whereas the gap junctions (i.e., connexin 36) may be necessary to form functional ensembles of olivary cells (Llinás et al., 1974; Lang et al., 1996; De Zeeuw et al., 1998).

Recently, Mathy et al. (2009) have demonstrated that the burst activity of climbing fibers conveys information about the timing of the spike relative to the phase of the olivary subthreshold oscillations. The timing of the olivary activity was encoded by the number of spikes in the olivary axonal burst (i.e., climbing fiber burst). Furthermore, they showed that this climbing fiber burst (timing information) affected downstream Purkinje cells by altering the strength of the synaptic transmission between parallel fibers and Purkinje cells. Their results challenge current views concerning the role of climbing fibers in motor control, and they might reconcile the opposing theories established for motor timing and motor learning (Simpson et al., 1996; Mauk et al., 2000). However, an important part of their dataset was collected using whole-cell patch-clamp recordings from *ex vivo* slice preparations of the IO. Their *ex vivo* slice preparation had two major disadvantages; the olivary cells were isolated from their olivocerebellar module [which alters their electrophysiological behavior (Chorev et al., 2007; Khosrovani et al., 2007)] and the oscillations were artificially imposed to the neurons by injecting a fixed-amplitude sinusoidal current. Consequently, the finding that the climbing fiber signal encodes the temporal state of the olivary network could be due to the altered physiological condition of the IO neurons.

Abbreviations: IO, inferior olive; Cx36, connexin 36; C57BL/6 mice, C57 black 6 mice; WT, wild type; KX, ketamine and xylazine; MMF, medetomidine, midazolam, and fentanyl; SSTO, sinusoidal subthreshold oscillation; LTO, low-threshold calcium (Ca^{2+}) oscillation; ADP, afterdepolarization; SEM, standard error of the mean.

In the present study, we investigated whether this timing code was also generated in olivary cells present in an intact olivocerebellar system using the *in vivo* whole-cell recording technique. *In vivo* recordings were obtained under two different anaesthetic conditions to exclude drug-specific effects. Comparisons between spontaneous and somatosensory-evoked action potentials were made to elucidate origin-related differences. And we studied the consequences of genetically (connexin 36 knock-out mice: $Cx36^{-/-}$) as well as pharmacologically manipulated (Harmaline) subthreshold oscillations on these olivary bursts.

MATERIALS AND METHODS

In vivo WHOLE-CELL RECORDINGS

C57 black 6 mice (C57BL/6 mice) were anesthetized by an intraperitoneal injection of a mixture of ketamine and xylazine (KX; 65 and 10 mg/kg; $n = 40$), or a mixture of medetomidine, midazolam, and fentanyl (MMF; 0.5 mg/kg, 5 mg/kg, and 0.05 mg/kg; $n = 6$). All $Cx36^{-/-}$ mutants ($n = 9$) were anesthetized with KX. *In vivo* whole-cell recordings were performed as described by Khosrovani et al. (2007). In a subset of KX anesthetized animals ($n = 4$), peripheral stimulations were provided by electrical stimulation of the whisker pad to generate somatosensory evoked action potentials in the recorded olivary neuron. The stimulation protocol consisted of short bipolar stimulations (2 ms, 0.5 mA) that were randomly administered. In a second subset of KX anesthetized animals ($n = 6$), harmaline (50 mg/kg) was injected intraperitoneally after all baseline recordings were established. In each neuron, the following membrane properties were determined: input resistance, membrane capacitance (C_m), resting membrane potential, and firing rate. The access resistance (R_a), membrane resistance (R_m), and C_m were calculated using the following formulas: $R_a = V_\Delta / I_i$; $R_m = (V_\Delta - R_a I_{ss}) / I_{ss}$ and $C_m = \tau\,(1/R_a + 1/R_m)$. Tau ($\tau$), instantaneous ($I_i$), and steady state currents (I_{ss}) were determined from current responses evoked by −10 mV steps. The resting membrane potential (V_m) was determined from the readout of the baseline potential. All animal procedures were in accordance with the guidelines of the ethics committee of the Erasmus Medical Center.

DATA ANALYSIS

Data analyses were performed for neurons with resting membrane potentials lower than −45 mV, typical olivary spike waveforms (i.e., expressing spike afterdepolarizations with at least one wavelet), and spike amplitudes >60 mV (number of neurons: $n_{KX} = 37$, $n_{MMF} = 8$, $n_{Cx36^{-/-}} = 10$). Subthreshold oscillations in the spontaneous membrane potential were quantified by measuring the frequency and amplitude of the oscillations. In neurons that expressed sinusoidal subthreshold oscillations (SSTOs), the phase spiking preference was determined by fitting the SSTO prior to the spontaneous action potential to a sine wave function. The fitted curve was extrapolated following the action potential, and spike occurrence was determined within phase bins of 45° (**Figure 1**). In neurons that expressed low-threshold calcium (Ca^{2+}) oscillations (LTOs), the spike position was determined as either on top of the low-threshold Ca^{2+} spike or between them (**Figure 8A**). The number of wavelets on a typical olivary spike afterdepolarization (ADP) was counted for each spike.

STATISTICAL ANALYSIS

Statistical analysis of basic membrane properties was performed using Mann–Whitney *U*-test. The spiking preference in relation to the phase of the SSTO oscillation was examined using the Rayleigh test, and the shifts in the phase–frequency distributions under different conditions were compared using the Student's *t*-test. Modulations of the number of wavelets were tested by comparing the number of wavelets in each phase bin with the overall average number of wavelets using the one-sample Student's *t*-test. For bimodal analysis of the spiking preference in neurons expressing LTOs, the χ^2 test was used. Modulations of the number of wavelets in these LTO neurons were analyzed statistically using the Student's *t*-test. Student's *t*-tests were also employed to test the significance of the correlation coefficients. For statistical comparisons of the linear regression lines, we used the analysis of covariance (ANCOVA) followed by a *post hoc* Tukey's HSD analysis (Matlab, The Mathworks, Natick, MA). All of the numerical values presented in the text represent the mean ± SEM.

RESULTS

THE GENERATION OF OLIVARY WAVELETS *In vivo* DOES NOT DEPEND ON THE PHASE OF SINUSOIDAL SUBTHRESHOLD OSCILLATIONS

In vivo whole-cell patch-clamp recordings were obtained from neurons of the mouse IO. These recordings were collected under two different anaesthetic conditions induced by either KX or MMF to exclude anaesthesia-specific effects. Olivary neurons that were recorded under KX and MMF conditions revealed similar basic membrane properties (**Table 1**), and these properties were comparable to those obtained in previous *ex vivo* measurements (Llinás and Yarom, 1981; Long et al., 2002; De Zeeuw et al., 2003; Leznik and Llinas, 2005). However, the input resistance was slightly, but not significantly, higher under MMF conditions.

We have previously shown that *in vivo* olivary neurons can exhibit two different types of subthreshold oscillations: typical rhythmic 3–9 Hz SSTOs, or rhythmic 1–3 Hz LTOs (Khosrovani et al., 2007). Spontaneous action potentials in olivary cells that exhibited SSTOs depend on the peak phase of the oscillation under both anaesthetic conditions (both $r = 0.71$, both $p < 0.05$), but the phase-frequency distribution of spikes under MMF was slightly shifted compared to that under the KX condition (**Figures 2A** and **3A**; KX: 98 ± 5°, MMF: 119 ± 7°; $p < 0.05$). To find out whether the phase of the subthreshold oscillations determines the number of wavelets in an olivary spike *in vivo*, we counted the number of wavelets that were superimposed on the spike ADP (**Figure 1B**; see arrows) and examined their dependency on the phase and amplitude of the subthreshold oscillation. On average, olivary spikes expressed 2.2 ± 0.1 wavelets ($n = 155$ spikes) under KX anaesthesia and 2.5 ± 0.2 wavelets ($n = 73$ spikes) under MMF anaesthesia. These values were not significantly different ($p = 0.08$) and were comparable to those measured *ex vivo* (Mathy et al., 2009). The timing of the spike in relation to the phase of the SSTO did not

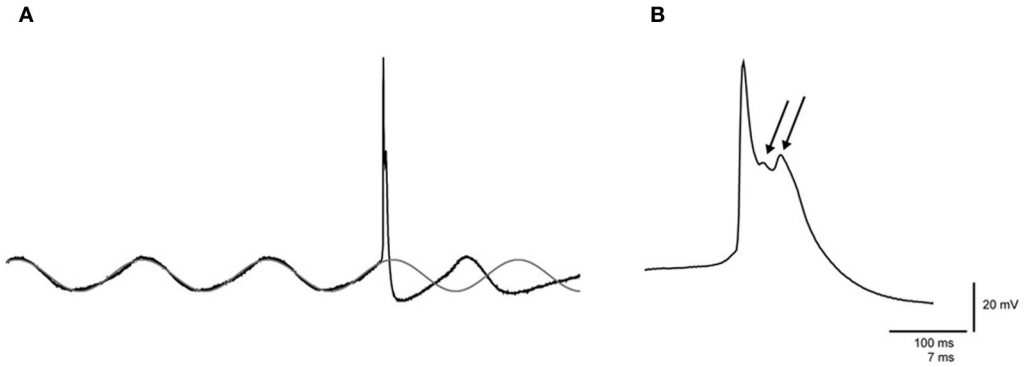

FIGURE 1 | Spontaneous sinusoidal subthreshold oscillations and wavelets of an olivary neuron. (A) Left panel: trace of a spontaneous sinusoidal subthreshold oscillation (SSTO) from an olivary neuron *in vivo*. The gray trace indicates the sinusoidal fit of the SSTO prior to the occurrence of the action potential, followed by an extrapolation after the occurrence of the action potential. **(B)** Right panel: enlargement of the olivary action potential shown in the left panel. The arrows indicate the olivary wavelets on top of the afterdepolarization (ADP).

Table 1 | Membrane properties of *in vivo* olivary neurons under different anaesthetic and genetic conditions.

Membrane properties	KX anaesthesia ($n = 37$)	MMF anaesthesia ($n = 8$)	$Cx36^{-/-}$ mutants* ($n = 10$)	*p* value
Rm (MΩ)	28.8 (22.3–38.2)	39.1 (31.7–41.8)	41.2 (39.8–49.7)	$p_{(KX-Cx36)} < 0.05$
Cm (pF)	207.5 (142.4–277.1)	203.5 (198.3–222.1)	130.9 (113.1–152.6)	$p_{(KX-Cx36)} < 0.05$
				$p_{(MMF-Cx36)} < 0.05$
Vm (mV)	−54.0 (−56.8 to −51.0)	−55.0 (−48.0 to −56.0)	−52.8 (−49.9 to −54.4)	ns
f (Hz)	0.44 (0.20–0.58)	0.24 (0.12–0.44)	0.47 (0.39–0.59)	ns

Statistical analyses of basic membrane properties were performed using the Mann–Whitney U-test.

**$Cx36^{-/-}$ mutant mice were anaesthetized using the KX mixture.*

Rm, membrane resistance; Cm, membrane capacitance; Vm, membrane potential; f, firing frequency. All numerical values indicate the median (25–75th percentile).

determine the number of olivary wavelets in either of the two conditions (**Figures 2B** and **3B**; all $p > 0.05$). Inspection of the data of each neuron separately also did not reveal any correlation between the timing of the spike and the number of olivary wavelets. Thus, across the phase bins in which spikes occurred, there was no clear dependence of wavelet number on oscillation phase in our *in vivo* preparation. Alternatively, the amplitude of oscillation might be able to impose a modulatory effect on the number of wavelets. Therefore, we correlated the number of wavelets with the amplitude of the oscillation. This analysis was performed using data collected under both types of anaesthesia (**Figures 2C** and **3C**). Significant correlations between the amplitude of the SSTO and the number of wavelets were detected for both anaesthetic conditions (**Figures 2C** and **3C**, all phase-bins together, $r_{KX} = -0.36$, $r_{MMF} = -0.58$, both $p < 0.01$). The overall correlations revealed a negative relationship between the amplitude of the oscillation and the number of wavelets. Furthermore, the phase subset plots of **Figures 2C** and **3C** show that there is no number of wavelet preferences between the different phase-bins.

SPONTANEOUS vs. SOMATOSENSORY-EVOKED ACTION POTENTIALS

Up to now, all the analyses were performed on spontaneous action potentials. Spike triggering inputs of olivary neurons can activate a subset of cellular responses that might alter the relationship between SSTO, spikes and wavelets. Therefore, we also investigated the relationship between SSTO and wavelets in somatosensory-evoked action potentials. Although strong stimuli were applied randomly to the mouse whisker pad, somatosensory-evoked action potentials in olivary cells that exhibited SSTOs were more easily generated at the peak of the oscillation, indicating also under this condition a clear spiking preference (**Figure 4A**, $r = 0.57$, $p < 0.05$, $n = 78$). The phase-frequency distribution of somatosensory-evoked spikes was slightly shifted compared to the spontaneous spikes under the KX condition (**Figures 2A** and **4A**; spontaneous: $98 \pm 5°$ and evoked: $119 \pm 8°$; $p < 0.05$). On average, the evoked olivary spikes expressed 1.4 ± 0.1 wavelets ($n = 78$ spikes), which is significantly smaller than the amount expressed on spontaneous spikes (2.2 ± 0.1 wavelets; $p < 0.05$). However, it is important to note that our somatosensory-evoked action potential group contain more recordings of cells with bigger SSTO amplitudes (see below). The timing of the evoked spike in relation to the phase of the SSTO did not determine the number of olivary wavelets (**Figure 4B**; all $p > 0.05$); indicating that the phase of the oscillation did not modulate the number of olivary wavelets on these spikes either. The amplitude of the oscillation and number of wavelets of these evoked spikes were significantly correlated to each other (**Figure 4C**, all phase-bins together, $r_{SSS} = -0.49$, $p < 0.01$), indicating also an inverse relationship

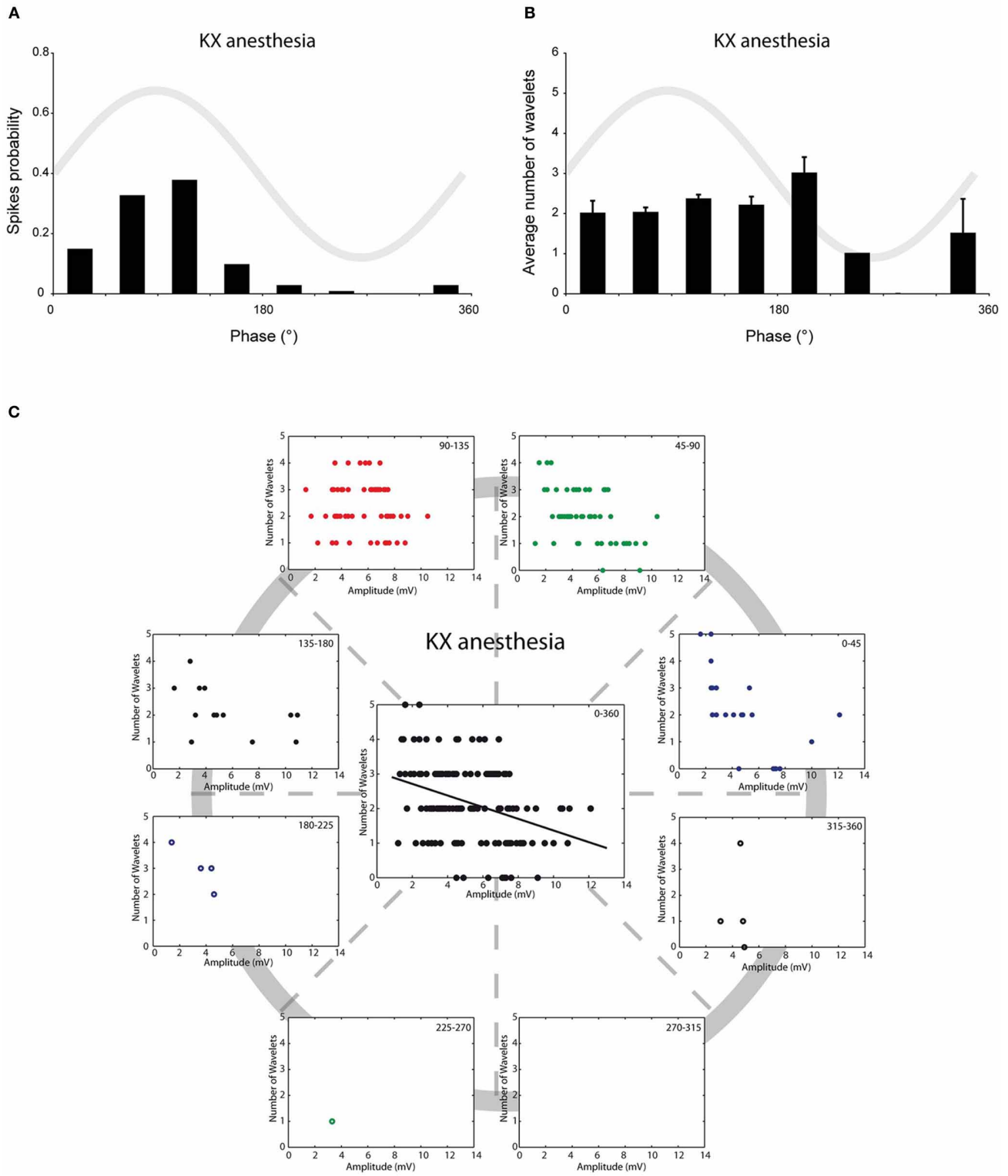

FIGURE 2 | Burst size of olivary wavelets and SSTOs under KX anaesthesia. (A) The occurrence of spontaneous spikes (spike probability) in relation to the phase of the SSTO obtained from olivary neurons recorded under KX anaesthesia ($n = 155$). **(B)** Average number of wavelets on the ADP of spontaneous spikes in relation to the phase of the SSTO obtained from olivary neurons recorded under KX anaesthesia ($n = 155$). **(C)** Relationship between number of wavelets and amplitude of SSTO were plotted for each phase-bin. The center graph shows the correlation between the amplitude of the SSTOs and the number of wavelets of all data (all phase-bins together) measured under KX anaesthesia. Least squares linear regression lines and correlation coefficients were computed [$r_{KX} = -0.36$, $n = 155$, and $p < 0.01$ (t-test)].

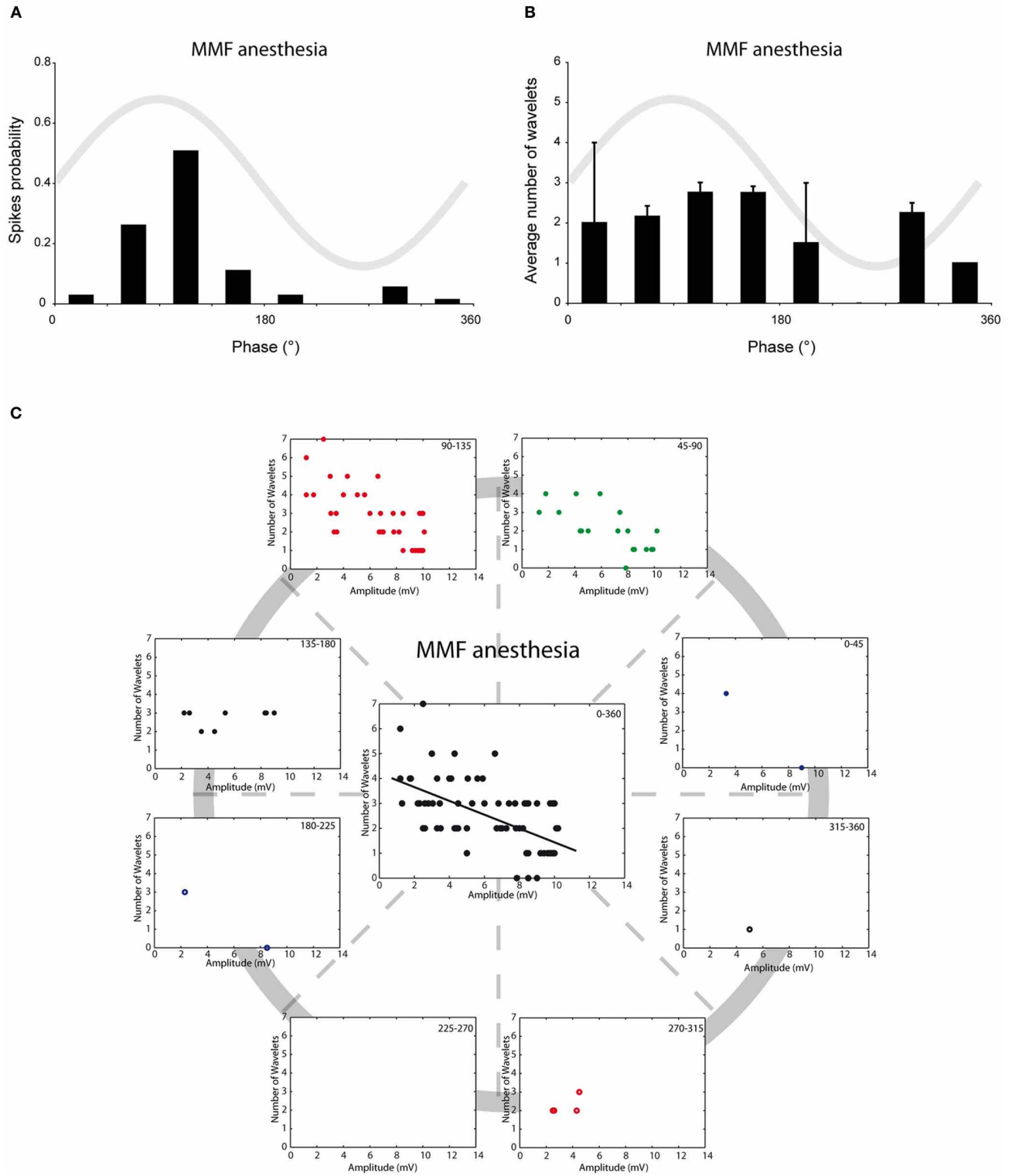

FIGURE 3 | Burst size of olivary wavelets and SSTOs under MMF anaesthesia. (A) The occurrence of spontaneous spikes (spike probability) in relation to the phase of the SSTO obtained from olivary neurons recorded under MMF anaesthesia ($n = 73$). **(B)** Average number of wavelets on the ADP of spontaneous spikes in relation to the phase of the SSTO obtained from olivary neurons recorded under MMF anaesthesia ($n = 73$). **(C)** Relationship between number of wavelets and amplitude of SSTO were plotted for each phase-bin. The center graph shows the correlation between the amplitude of the SSTOs and the number of wavelets of all data (all phase-bins together) measured under MMF anaesthesia. Least squares linear regression lines and correlation coefficients were computed [$r_{MMF} = -0.58$, $n = 73$, and $p < 0.01$ (t-test)].

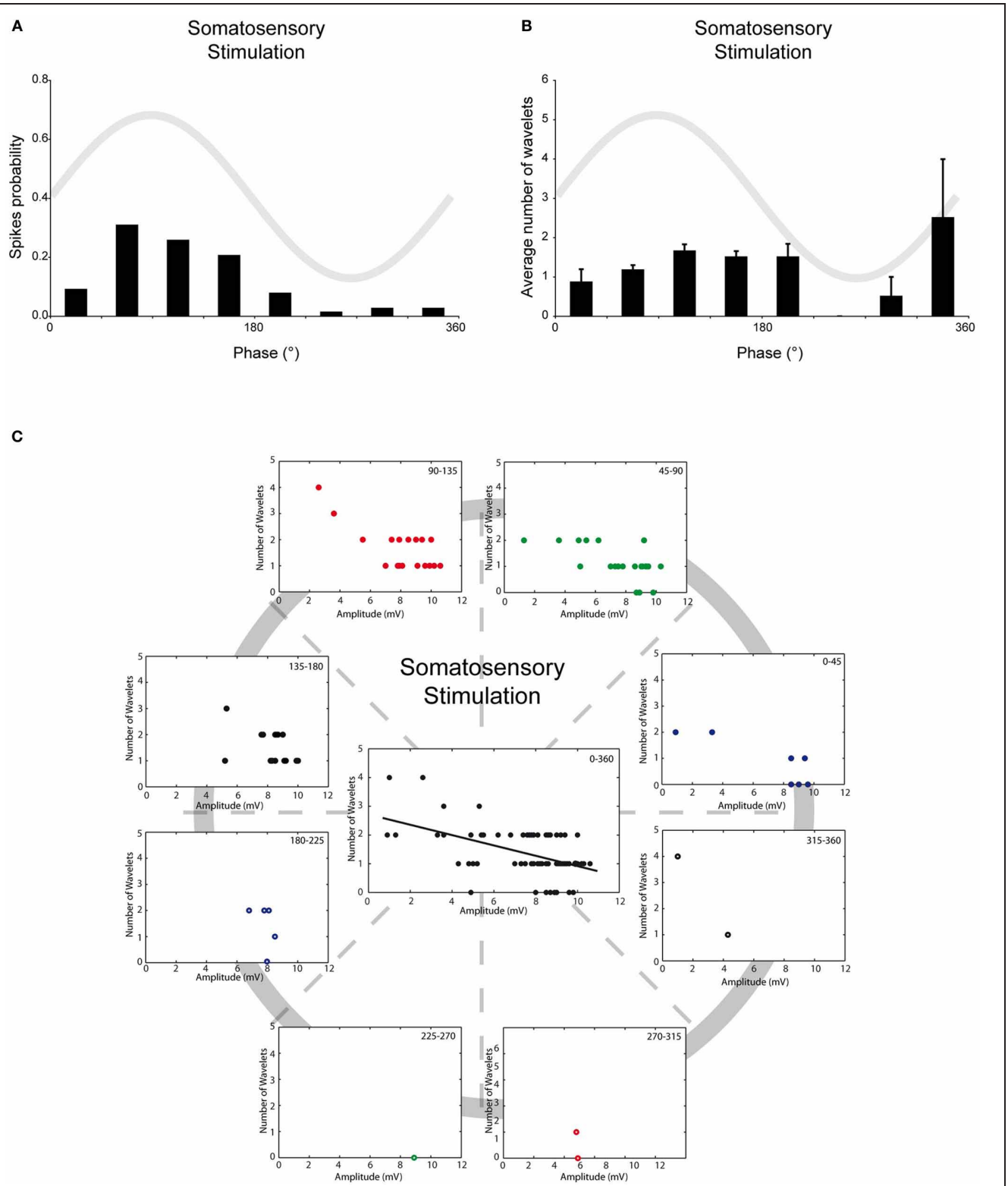

FIGURE 4 | Burst size of olivary wavelets and SSTOs of somatosensory-evoked spikes. (A) The occurrence of stimulus evoked spikes (spike probability) in relation to the phase of the SSTO obtained from olivary neurons recorded under KX anaesthesia ($n = 78$). **(B)** Average number of wavelets on the ADP of stimulus evoked spikes in relation to the phase of the SSTO obtained from olivary neurons recorded under KX anaesthesia ($n = 78$). **(C)** Relationship between number of wavelets and amplitude of SSTO were plotted for each phase-bin. The center graph shows the correlation between the amplitude of the SSTOs and the number of wavelets of all data (all phase-bins together) measured on somatosensory evoked spikes. Least squares linear regression lines and correlation coefficients were computed [$r_{SSS} = -0.49$, $n = 78$, and $p < 0.01$ (t-test)].

between the amplitude of the oscillation and the number of wavelets on somatosensory-evoked spikes. Overall, we conclude that under *in vivo* conditions, the phase of the SSTO does not regulate the number of wavelets (i.e., output) on olivary spikes, but that the number of wavelets depends on the amplitude of the SSTO. This phenomenon can be observed on both spontaneous as well as somatosensory-evoked action potentials, despite their different origin and the activation of different cellular responses.

ELECTRICAL SYNAPSES

Olivary neurons are interconnected via gap junctions formed by connexin 36 (Cx36). The lack of Cx36 leads to an absence of electrotonic coupling, to a more voltage-dependent SSTO, to an increased excitability at hyperpolarizing states and to an altered interaction between SSTO and the generation of an action potential (Long et al., 2002; De Zeeuw et al., 2003; Van Der Giessen et al., 2008). Therefore, $Cx36^{-/-}$ mutant mice provide a condition in which the relationship between the generation of action potentials and the phase of the oscillation is weakened, which might give the opportunity to unmask possible phase-related modulatory effects on olivary burst firing. *In vivo* whole-cell recordings from the SSTO neurons of $Cx36^{-/-}$ mutants anesthetized with KX revealed a reduction in the spiking preference in relation to the phase of the oscillation (**Figure 5A**, $r = 0.56$, $p < 0.05$). Also the phase-frequency distribution of spikes from olivary neurons in the $Cx36^{-/-}$ mutants was shifted compared to spikes recorded from olivary neurons in wild type (WT) mice under KX anaesthetic conditions (**Figures 2A** and **5A**; WT: $98 \pm 5°$, $Cx36^{-/-}$: $123 \pm 8°$; $p < 0.05$). On average, the olivary spikes of $Cx36^{-/-}$ mutants expressed 2.3 ± 0.1 wavelets ($n = 83$ spikes) under KX anaesthesia. This value was not significantly different compared to the value obtained from the olivary neurons of WT mice under either KX or MMF anaesthesia ($p = 0.38$ and $p = 0.30$, respectively). In the recordings from mutant mice, we did not detect a significant modulation of the number of wavelets in relation to the phase of the oscillation (**Figure 5B**, all $p > 0.05$). Thus, the phase of the SSTO did also not modulate the number of olivary wavelets in our *in vivo* $Cx36^{-/-}$ preparations exhibiting a weakened relationship between the oscillation phase and the spiking preference. However, different from all our previous results, the amplitude of the oscillation and number of olivary spike wavelets were not significantly correlated in $Cx36^{-/-}$ mutants (**Figure 5C**, $r_{CX36} = -0.20$, $p > 0.05$). Therefore, we conclude that under *in vivo* conditions, gap junction coupling via Cx36 may be involved in the modulatory effect of the amplitude of oscillation.

In all four conditions (KX anesthesia, MMF anesthesia, somatosensory-evoked action potentials and $Cx36^{-/-}$), the majority of the action potentials occur during the peak of the oscillation (∼45–135°). In order to analyze the impact of the oscillation amplitude on the number of wavelets, we selected and pooled the action potentials of the 45–90° and 90–135° phase subsets for further analysis and cross-conditional comparisons. Consequently, we removed any putative confounding factors of other phase-subsets. Also under these new constraints, the amplitude of oscillation and number of wavelets were significantly correlated to each other in three out of four conditions (**Figure 6**; $r_{KX} = -0.27$, $r_{MMF} = -0.67$, $r_{SSS} = -0.55$, all $p < 0.01$; $r_{CX36} = -0.21$, $p > 0.05$), confirming the amplitude dependency under all circumstances except in animals lacking electrical coupling. Cross-conditional comparisons of the regression lines revealed a significant difference in amplitude dependency between these groups ($p < 0.01$, ANCOVA). Further analyses revealed that the linear regression line made from the MMF data (the slope as well as the intercept) was significantly different from the linear regression lines of the other conditions (all $p < 0.05$, Tukey's HSD test).

HARMALINE

So far, this correlation was obtained by combining the results from many cells. This was necessary because under our *in vivo* conditions, the variability of the oscillation amplitude within a single cell is limited. In order to investigate the causality of this relationship further, we manipulated the amplitude of the oscillations by injecting mice with harmaline (50 mg/kg) during the recordings and correlated the number of wavelets with the manipulated amplitude of the oscillation of a single cell. In all recorded cells ($n = 6$), harmaline increased the amplitude of the oscillation but did not affect the firing rate (**Figure 7A**). Single cell analysis of data collected from harmaline-injected WT animals ($n = 3$) revealed also significant correlations between the amplitude of the SSTO and the number of wavelets (**Figure 7B**, all three WTs $p < 0.01$), confirming the inverse relationship between the amplitude of the oscillation and the number of wavelets but now demonstrated within single cells. The three cells that were collected from $Cx36^{-/-}$ mutants did not show any significant correlations (**Figure 7B**, all three $Cx36^{-/-}$ $p > 0.05$), which also agrees with our results mentioned previously. Thus, manipulating the amplitude of the oscillation from small to large reduced the probability of expressing wavelets (i.e., a smaller burst in olivary axons/climbing fibers), and this causal relationship was not observed in olivary neurons lacking Cx36 gap junctions.

LOW-THRESHOLD Ca^{2+} DEPOLARIZATIONS AFFECT THE GENERATION OF OLIVARY WAVELETS

In addition to neurons that exhibit SSTO, the IO also contains neurons that express rhythmic 1–3 Hz LTOs. Because this type of oscillation was never observed in mice that were anesthetized with MMF, the following analyses were only conducted for olivary neurons recorded from mice that were anesthetized by KX. Spontaneous action potentials in olivary neurons that exhibited LTOs revealed a significant preference for spiking on top of the low-threshold Ca^{2+} depolarizations (**Figures 8A,B**, $p < 0.05$). Because the waveform of the LTO cannot be fitted correctly to a sine wave, it is impossible to determine the oscillation phase and subsequently the phase-spiking relationship. Therefore, wavelet analysis was performed using a simpler bimodal approach. The number of wavelets was counted on the ADP of spontaneous olivary spikes and grouped for the spikes that were on top of and in between the low-threshold Ca^{2+} depolarizations. On average,

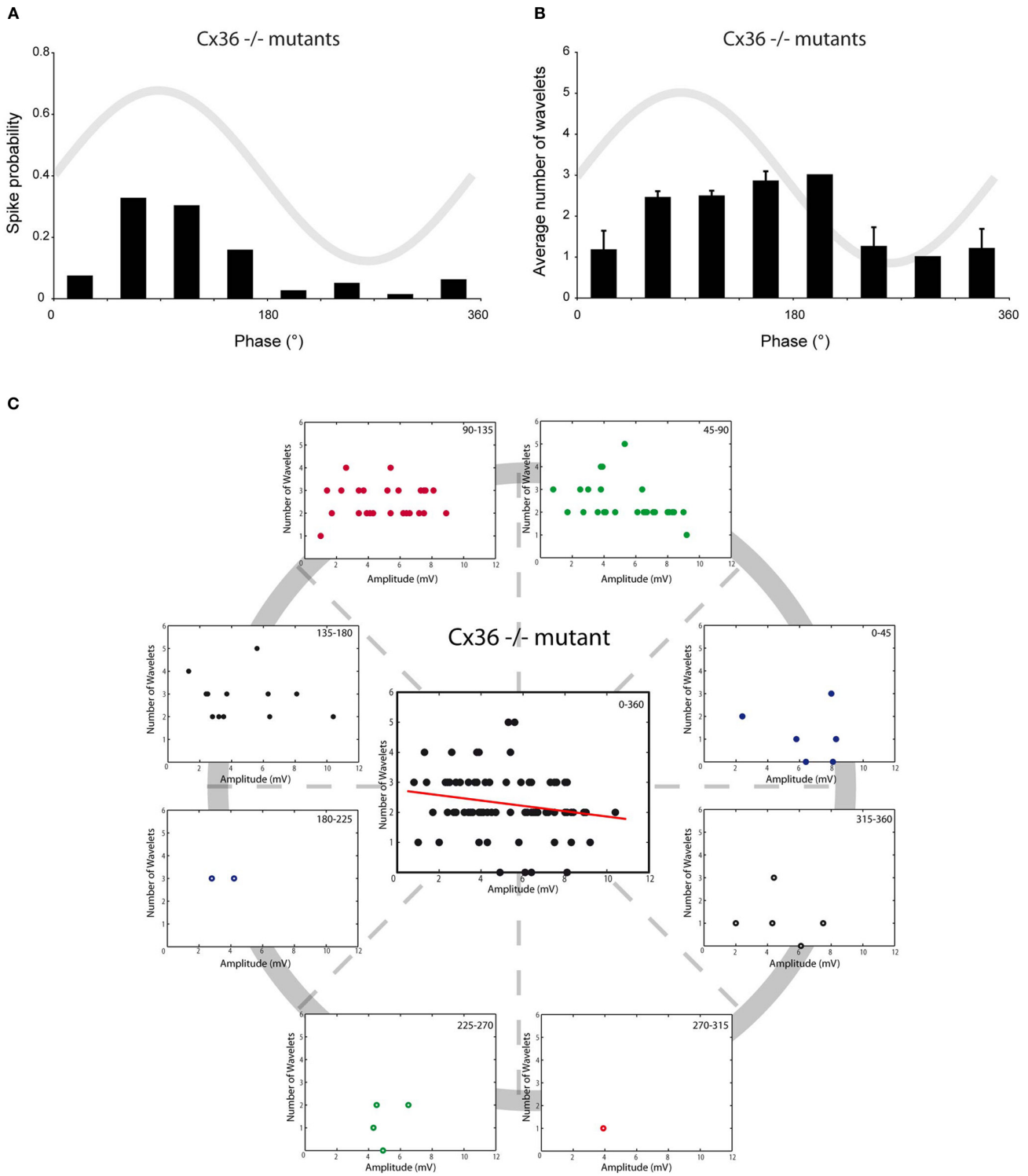

FIGURE 5 | Burst size of olivary wavelets and SSTOs in Cx36$^{-/-}$ mutants. (A) The occurrence of spontaneous spikes (spike probability) in relation to the phase of the SSTO obtained from olivary neurons recorded in Cx36$^{-/-}$ mutants ($n = 83$). **(B)** Average number of wavelets on the ADP of spontaneous spikes in relation to the phase of the SSTO obtained from olivary neurons recorded in Cx36$^{-/-}$ mutants ($n = 83$). **(C)** Relationship between number of wavelets and amplitude of SSTO were plotted for each phase-bin. The center graph shows the correlation between the amplitude of the SSTOs and the number of wavelets of all data (all phase-bins together) measured in Cx36$^{-/-}$ mutant mice. Least squares linear regression lines and correlation coefficients were computed [$r_{CX36} = -0.20$, $n = 83$, and $p > 0.05$ (t-test)].

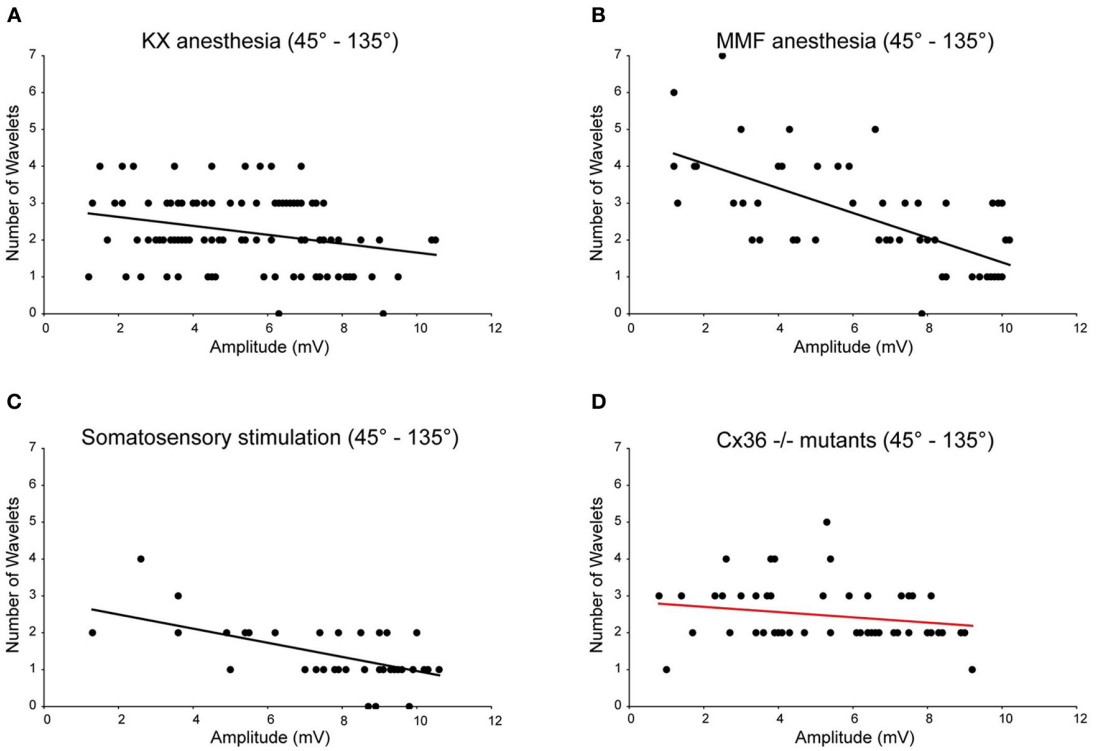

FIGURE 6 | Burst size of olivary wavelets during the peak phase (45–135°) of the SSTOs. Relationships between number of wavelets and amplitude of SSTO were plotted of spikes that occur during the peak phase (45–135°) of the SSTOs. Least squares linear regression lines and correlation coefficients were computed for all four conditions (KX anesthesia, MMF anesthesia, somatosensory-evoked action potentials and Cx36$^{-/-}$). Amplitude of the oscillation and number of olivary spike wavelets are significantly correlated under KX conditions [**A**; $r_{KX} = -0.27$, $n = 110$ (71%), $p < 0.01$ (*t*-test)] and under MMF conditions [**B**; $r_{MMF} = -0.67$, $n = 56$ (77%), $p < 0.01$ (*t*-test)]. Amplitude of the oscillation and number of olivary spike wavelets are significantly correlated when measured on somatosensory evoked spikes [**C**; $r_{SSS} = -0.55$, $n = 44$ (56%), $p < 0.01$ (*t*-test)] and are not significantly correlated when measured in Cx36$^{-/-}$ mutant mice [**D**; $r_{CX36} = -0.21$, $n = 53$ (64%), $p > 0.05$ (*t*-test)].

these olivary spikes also expressed 2.2 ± 0.1 wavelets ($n = 165$ spikes) under KX anaesthesia, but the number of wavelets was significantly higher in olivary spikes that were not elicited by a low-threshold Ca^{2+} depolarization (**Figure 8C**, $p < 0.01$).

Olivary neurons that were not interconnected to one another via Cx36 gap junctions showed a preference for spiking on top of the low-threshold Ca^{2+} depolarizations (**Figure 8B**, $p < 0.05$), similar to olivary neurons that expressed Cx36. However, the olivary neurons recorded from Cx36$^{-/-}$ mutants did not modulate the number of wavelets in a manner dependent on the spike timing in relation to the LTO (**Figure 8C**, $p = 0.9$).

The bimodal analysis of the relationship between spike timing and the number of olivary wavelets was relatively crude. Therefore, we correlated the number of wavelets with the size of the low-threshold Ca^{2+} depolarization. A significant correlation between the size of the low-threshold Ca^{2+} depolarization and the number of wavelets was found (**Figure 8D**, $p < 0.01$). These correlations revealed a negative relationship between the size of the low-threshold Ca^{2+} depolarization and the number of wavelets. In the Cx36$^{-/-}$ mutants, no correlation was detected (**Figure 8E**, both $p > 0.05$). However, the size and number of the low-threshold Ca^{2+} depolarizations were limited in this Cx36$^{-/-}$ mutant study (**Figure 8E**).

Overall, the size of the olivary axonal burst can be regulated, but it depends on the amplitude of subthreshold oscillation or size of the low-threshold Ca^{2+} depolarization that is expressed by the olivary neuron. Furthermore, gap junction coupling via Cx36 may be involved in this process.

DISCUSSION

We demonstrated that the phase of the olivary SSTO did not regulate the number of wavelets in olivary bursts under *in vivo* conditions. Instead, we found that the number of wavelets in olivary bursts correlated with the amplitude of the olivary subthreshold oscillation. In addition, this property was not observed in olivary neurons that lacked Cx36 gap junctions. These findings change the current view regarding the nature of the information that is transmitted from the IO to Purkinje cells.

NUMBER OF WAVELETS: MODULATION BY PHASE OR AMPLITUDE?

Our electrophysiological recordings confirm that olivary neurons can generate wavelets under *in vivo* conditions, which was first reported by Crill (1970). The average number of olivary wavelets observed in the present study is similar to previously reported results obtained both *in vivo* and *ex vivo*

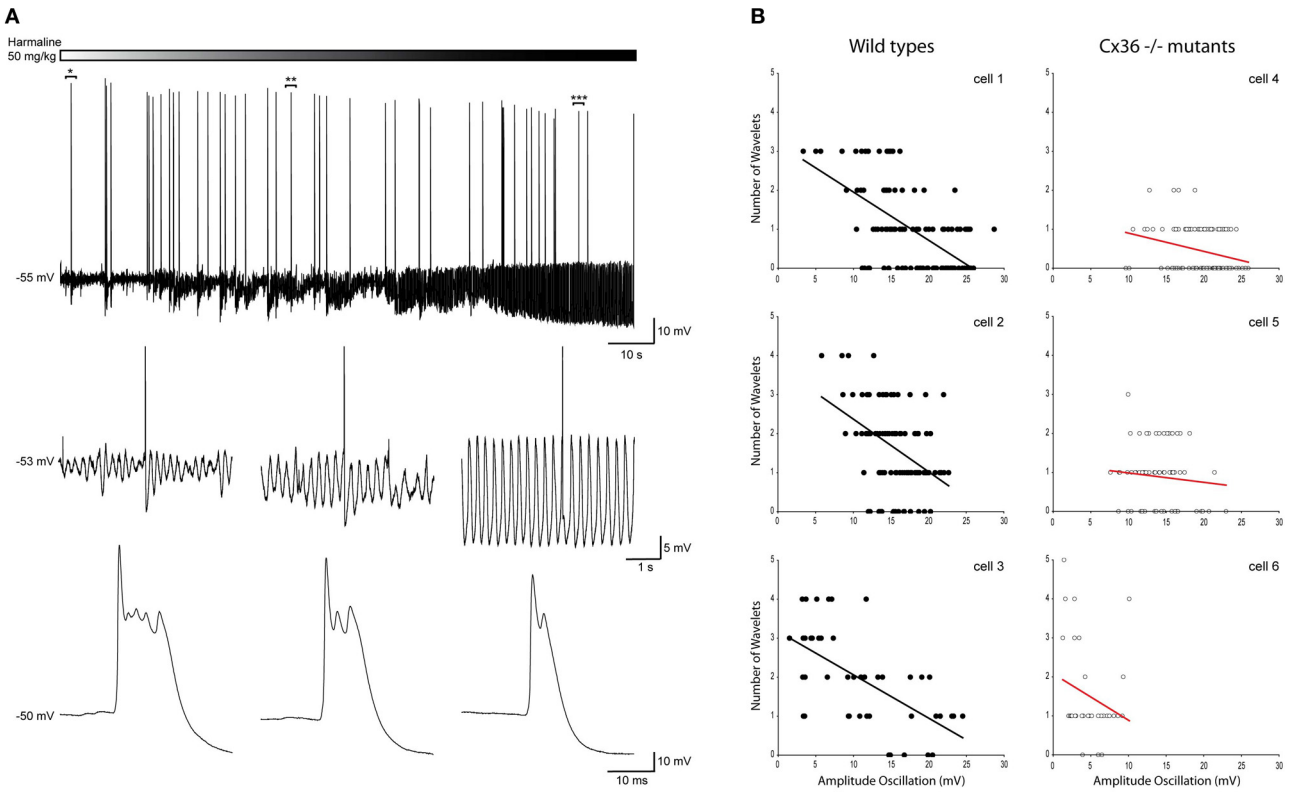

FIGURE 7 | Harmaline induced alteration of the oscillation amplitude confirms the negative relationship between the amplitude of the SSTOs and the number of wavelets on the ADP of olivary spikes within a single cell. (A) Top panel: trace of a spontaneous sinusoidal subthreshold oscillating olivary neuron (*in vivo*) during the application of harmaline. Middle panel: three magnifications obtained from the trace above. Magnifications were taken from the marked time windows (*, **, and ***) and show the effect of harmaline on the subhreshold oscillation. Lower panel: enlargement of the olivary action potential shown in the panel above. The number of the olivary wavelets on top of the afterdepolarization declines, while the amplitude of the oscillation increases. **(B)** Correlation between the amplitude of the SSTOs and the number of wavelets on the ADP of olivary spikes measured in cells from wild type (left panel) and from $Cx36^{-/-}$ mutant mice (right panel). Least squares linear regression lines and correlation coefficients were computed from each cell. Wild types (left panel) cell 1: $r = -0.59$, $n = 116$, and $p < 0.01$ (*t*-test); cell 2: $r = -0.55$, $n = 143$, and $p < 0.01$ (*t*-test); cell 3: $r = -0.63$, $n = 46$, and $p < 0.01$ (*t*-test). $Cx36^{-/-}$ mutants (right panel) cell 4: $r = -0.04$, $n = 223$, and $p > 0.05$ (*t*-test); cell 5: $r = -0.14$, $n = 74$, and $p > 0.05$ (*t*-test); cell 6: $r = -0.23$, $n = 35$, and $p > 0.05$ (*t*-test).

(Crill, 1970; Mathy et al., 2009). We found that the timing of the spike in relation to the phase of these spontaneous subthreshold oscillations did not determine the number of olivary wavelets in our *in vivo* preparation. It is, though, important to note that in the trough of the oscillation phase bins are present in which no spikes occurred and therefore no wavelets were generated. This scenario is substantially different from a spike that generates no wavelets, because in the first case there is an absence of signal whereas in the latter case the number of wavelets is completely down modulated. This result is inconsistent with the *ex vivo* findings of Mathy et al. (2009). This opposite result might be due to differences in the experimental design. First, Mathy et al. (2009) injected an artificial fixed-amplitude sinusoidal current into the soma to compensate for the lack of spontaneous subthreshold oscillations in their *ex vivo* preparation. Such an induced subthreshold oscillation does not mimic the spontaneous subthreshold oscillation generated by a rhythmic ensemble of dendritic high-threshold and somatic low-threshold Ca^{2+} conductances together with a Ca^{2+}-dependent potassium conductance and an H-conductance (Llinás and Yarom, 1986). Second, the IO is isolated in the slice preparation. Removal of the IO from the olivocerebellar loop changes the physiology of olivary cells (Chorev et al., 2007; Khosrovani et al., 2007; Bracha et al., 2009). The observed phase modulation in olivary cells could be due to one or both of these altered physiological conditions. The potential drawback of the *in vivo* preparation is the use and influence of anaesthetics. To address this issue, we used two different kinds of anaesthetics: KX and MMF. Neither condition revealed a phase modulation of the number of wavelets across the phase bins in which spikes occurred. Despite their different influences on a variety of membrane properties, the effects on the phase modulation of the number of wavelets were unambiguous. This result indicates that the type of anaesthetic used does not affect this process. Furthermore, similar results were obtained by analyzing somatosensory-evoked action potentials, suggesting no additional effects by cellular responses related to input processing.

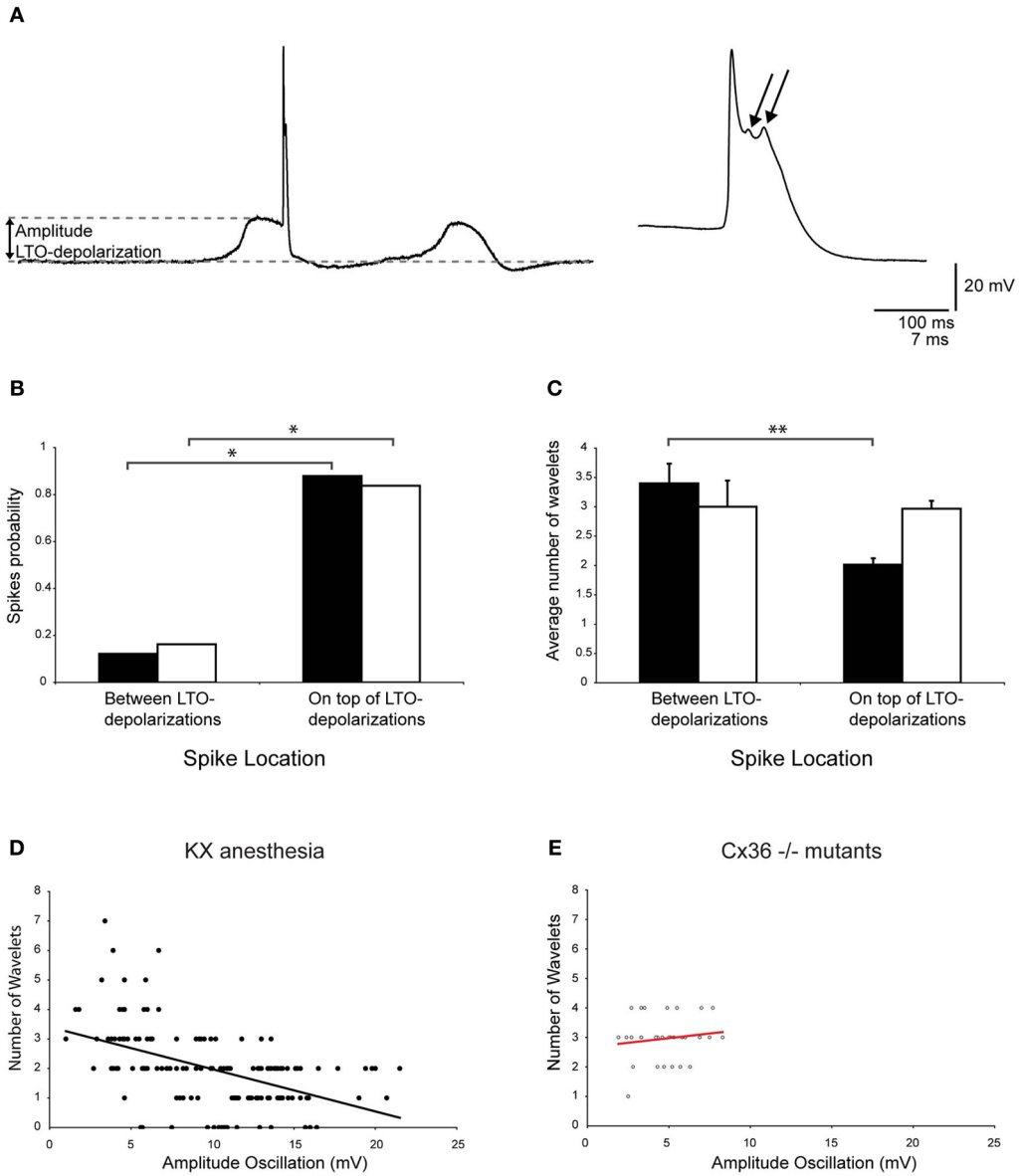

FIGURE 8 | Modulation of olivary wavelets by low-threshold Ca^{2+} depolarizations. (A) Left panel: trace of a spontaneous low-threshold Ca^{2+} depolarizations from an *in vivo* olivary neuron. The gray dashed lines indicate the amplitude of the low-threshold Ca^{2+} depolarization. Right panel: enlargement of the olivary action potential shown in the left panel. The arrows indicate the olivary wavelets on top of the afterdepolarization. **(B)** The occurrence of spikes (spike probability) in relation to spike position relative to the low-threshold Ca^{2+} oscillations obtained from recordings measured from either wild type (black bars, $n = 165$) or $Cx36^{-/-}$ mutant mice (open bars, $n = 37$). $^{*}p < 0.05$ (χ^2-test). **(C)** Average number of wavelets on the ADP of olivary spikes in relation to spike position relative to the low-threshold Ca^{2+} oscillations obtained from recordings measured from either wild type (black bars, $n = 165$) or $Cx36^{-/-}$ mutant mice (open bars, $n = 37$). $^{**}p < 0.01$ (*t*-test). **(D**,**E)** Correlation between the amplitude of the LTOs and the number of wavelets on the ADP of olivary spikes measured under KX anaesthesia **(D)** in wild type and $Cx36^{-/-}$ mutant mice **(E)**. Least squares linear regression lines and correlation coefficients were computed from each data set. KX anaesthesia: $r = -0.51$, $n = 145$, and $p < 0.01$ (*t*-test); $Cx36^{-/-}$ mutants: $r = 0.14$, $n = 31$, and $p > 0.05$ (*t*-test).

In the present study, however, we provide direct evidence that the number of olivary wavelets is related to the oscillation amplitude. Interestingly, oscillations with small amplitudes showed larger numbers of olivary wavelets compared to oscillations with large amplitudes. To our knowledge, this is the first study to report that the amplitude of the subthreshold oscillation can modulate wavelet number in olivary cells. Both anaesthetics (KX and MMF) revealed an amplitude dependency of the number of wavelets, but the dependency on amplitude was also significantly stronger under MMF than under KX conditions, indicating a possible role for NMDA and/or GABA receptors in this process. The existence of this relationship was

confirmed by using Harmaline to manipulate the amplitude of the subthreshold oscillations. The drug is known to cause an 8–14 Hz tremor in mice (Wang and Fowler, 2001) and it is assumed to act by modulating the rhythm-generating ionic currents of IO cells (Llinás and Yarom, 1986; Choi et al., 2010; Park et al., 2010). In our experimental set-up Harmaline caused a prominent increase in the amplitude of the oscillations, without affecting the frequency of the oscillations and the firing frequency. The data collected in these experiments demonstrate the causality of the inverse relationship between oscillations amplitude and number of wavelets, and agrees with the results obtained during physiological oscillations. We also demonstrated that this inverse relationship was not present in olivary neurons that lacked Cx36 gap junction coupling to other olivary neurons. Although gap junction coupling is not necessary for the generation and maintenance of olivary oscillations, it can clearly affect the oscillatory properties of IO cells (Long et al., 2002; De Zeeuw et al., 2003; Leznik and Llinas, 2005). However, it is not yet clear how (mechanistically) the gap junctions are involved in the amplitude-dependent modulation of the wavelets.

FUNCTIONAL RELEVANCE OF CLIMBING FIBER BURST MODULATION

We have demonstrated that the amplitude, but not the phase, of olivary oscillations modulates the climbing fiber bursts. This mechanism allows olivary axons to convey information about the amplitude of the olivary subthreshold oscillation to Purkinje cells. In the present results, the olivary axonal bursts are smaller when the spike is evoked on a subthreshold oscillation with large amplitude than when it is evoked on a subthreshold oscillation with small amplitude. Studies of Gellman et al. (1985) and Andersson and Armstrong (1987) revealed that the IO can function as an "unexpected" event detector; complex spikes were induced in animals that received an "unexpected" perturbation during their movement. We hypothesize that from the movement command an expected sensory profile is generated. The IO compares this expected sensory profile with the achieved sensory profile that is generated during the movement. An unexpected perturbation induces a mismatch between these two profiles and consequently the IO cells generate a burst of action potentials. We suggest that this expected sensory profile is encoded in the amplitude of the subthreshold oscillations in that a high level of "expectation" is reflected in high amplitude of the oscillation. Or in other words, low-amplitude oscillations make the olivary neurons more likely to respond strongly to signals with a high teaching level. Subsequently, olivary bursts are relayed to Purkinje cells, where they can modify the synaptic transmission between parallel fibers and Purkinje cells (Mathy et al., 2009) and adjust motor performance. According to this theory, the inability of olivary neurons without Cx36 to modulate the axonal bursts should, in Cx36 mutant mice, result in impairment in discriminating between the occurrences of expected and unexpected events during movements. Both locomotion and eye-blink conditioning experiments in $Cx36^{-/-}$ mutant mice revealed that these mice were indeed not able to correctly convert the associated conditional tone into an expected sensory event (Van Der Giessen et al., 2008), which is in line with our hypothesis.

Thus, the amplitudes of olivary subthreshold oscillations might provide a mechanism to grade the expectancy of an event. This information is conveyed by olivary axons to Purkinje cells and is encoded by the size of the burst. Because amplitude modulation of the olivary oscillations in $Cx36^{-/-}$ neurons cannot regulate the burst size, we conclude that the Cx36 gap junction coupling of olive cells is necessary for this mechanism.

AUTHOR CONTRIBUTIONS

All experiments were performed at the Erasmus MC. Paolo Bazzigaluppi, Jornt R. De Gruijl, and Marcel T. G. de Jeu designed the experiments, Ruben S. van der Giessen, Sara Khosrovani, and Paolo Bazzigaluppi performed the experiments. Paolo Bazzigaluppi, Jornt R. De Gruijl, and Marcel T. G. de Jeu analysed the experiments, Paolo Bazzigaluppi, Jornt R. De Gruijl, Chris I. De Zeeuw, and Marcel T. G. de Jeu wrote the manuscript. All authors approved the final version.

ACKNOWLEDGMENTS

We thank Dr. T. Ruigrok for carefully reading the manuscript and for providing helpful suggestions. This work was supported by The Netherlands Organization for Scientific research—ZonMw; grant 917.96.347 (Marcel T. G. de Jeu).

REFERENCES

Andersson, G., and Armstrong, D. M. (1987). Complex spikes in Purkinje cells in the lateral vermis (b zone) of the cat cerebellum during locomotion. *J. Physiol.* 385, 107–134.

Bracha, V., Zbarska, S., Parker, K., Carrel, A., Zenitsky, G., and Bloedel, J. R. (2009). The cerebellum and eye-blink conditioning: learning versus network performance hypotheses. *Neuroscience* 162, 787–796.

Choi, S., Yu, E., Kim, D., Urbano, F. J., Makarenko, V., Shin, H. S., et al. (2010). Subthreshold membrane potential oscillations in inferior olive neurons are dynamically regulated by P/Q- and T-type calcium channels: a study in mutant mice. *J. Physiol.* 588, 3031–3043.

Chorev, E., Yarom, Y., and Lampl, I. (2007). Rhythmic episodes of subthreshold membrane potential oscillations in the rat inferior olive nuclei *in vivo*. *J. Neurosci.* 27, 5043–5052.

Crill, W. E. (1970). Unitary multiple-spiked responses in cat inferior olive nucleus. *J. Neurophysiol.* 33, 199–209.

Crill, W. E., and Kennedy, T. T. (1967). Inferior olive of the cat: intracellular recording. *Science* 157, 716–718.

De Zeeuw, C. I., Chorev, E., Devor, A., Manor, Y., Van Der Giessen, R. S., De Jeu, M. T., et al. (2003). Deformation of network connectivity in the inferior olive of connexin 36-deficient mice is compensated by morphological and electrophysiological changes at the single neuron level. *J. Neurosci.* 23, 4700–4711.

De Zeeuw, C. I., Simpson, J. I., Hoogenraad, C. C., Galjart, N., Koekkoek, S. K., and Ruigrok, T. J. (1998). Microcircuitry and function of the inferior olive. *Trends Neurosci.* 21, 391–400.

Desclin, J. C. (1974). Histological evidence supporting the inferior olive as the major source of cerebellar climbing fibers in the rat. *Brain Res.* 77, 365–384.

Eccles, J. C., Llinas, R., and Sasaki, K. (1966). The excitatory synaptic action of climbing fibres on the purinje cells of the cerebellum. *J. Physiol.* 182, 268–296.

Gellman, R., Gibson, A. R., and Houk, J. C. (1985). Inferior olivary neurons in the awake cat: detection of contact and passive body displacement. *J. Neurophysiol.* 54, 40–60.

Ito, M., and Simpson, J. I. (1971). Discharges in Purkinje cell axons during climbing fiber activation. *Brain Res.* 31, 215–219.

Khosrovani, S., Van Der Giessen, R. S., De Zeeuw, C. I., and De Jeu, M. T. (2007). *In vivo* mouse inferior olive neurons exhibit heterogeneous subthreshold oscillations and spiking patterns. *Proc. Natl. Acad. Sci. U.S.A.* 104, 15911–15916.

Lang, E. J., Sugihara, I., and Llinas, R. (1996). GABAergic modulation of complex spike activity by the cerebellar nucleoolivary pathway in rat. *J. Neurophysiol.* 76, 225–275.

Leznik, E., and Llinas, R. (2005). Role of gap junctions in synchronized neuronal oscillations in the inferior olive. *J. Neurophysiol.* 94, 2447–2456.

Llinás, R., Baker, R., and Sotelo, C. (1974). Electrotonic coupling between neurons in cat inferior olive. *J. Neurophysiol.* 37, 560–571.

Llinás, R., and Yarom, Y. (1981). Properties and distribution of ionic conductances generating electroresponsiveness of mammalian inferior olivary neurones *in vitro*. *J. Physiol.* 315, 569–584.

Llinás, R., and Yarom, Y. (1986). Oscillatory properties of guinea-pig inferior olivary neurones and their pharmacological modulation: an *in vitro* study. *J. Physiol.* 376, 163–182.

Long, M. A., Deans, M. R., Paul, D. L., and Connors, B. W. (2002). Rhythmicity without synchrony in the electrically uncoupled inferior olive. *J. Neurosci.* 22, 10898–10905.

Maruta, J., Hensbroek, R. A., and Simpson, J. I. (2007). Intraburst and interburst signaling by climbing fibers. *J. Neurosci.* 27, 11263–11270.

Mathy, A., Ho, S. S., Davie, J. T., Duguid, I. C., Clark, B. A., and Hausser, M. (2009). Encoding of oscillations by axonal bursts in inferior olive neurons. *Neuron* 62, 388–399.

Mauk, M. D., Medina, J. F., Nores, W. L., and Ohyama, T. (2000). Cerebellar function: coordination, learning or timing? *Curr. Biol.* 10, R522–R525.

Park, Y. G., Park, H. Y., Lee, C. J., Choi, S., Jo, S., Choi, H., et al. (2010). Ca(V)3.1 is a tremor rhythm pacemaker in the inferior olive. *Proc. Natl. Acad. Sci. U.S.A.* 107, 10731–10736.

Simpson, J. I., Wylie, D. R., and De Zeeuw, C. I. (1996). On climbing fiber signals and their consequence(s). *Behav. Brain Sci.* 19, 380–394.

Sotelo, C., Llinas, R., and Baker, R. (1974). Structural study of inferior olivary nucleus of the cat: morphological correlates of electrotonic coupling. *J. Neurophysiol.* 37, 541–559.

Szentágothai, J., and Rajkovits, K. (1959). The origin of the climbing fibers of the cerebellum. *Z. Anat. Entw. Gesch.* 121, 130–141.

Thach, W. T. Jr. (1967). Somatosensory receptive fields of single units in cat cerebellar cortex. *J. Neurophysiol.* 30, 675–696.

Van Der Giessen, R. S., Koekkoek, S. K., Van Dorp, S., De Gruijl, J. R., Cupido, A., Khosrovani, S., et al. (2008). Role of olivary electrical coupling in cerebellar motor learning. *Neuron* 58, 599–612.

Wang, G., and Fowler, S. C. (2001). Concurrent quantification of tremor and depression of locomotor activity induced in rats by harmaline and physostigmine. *Psychopharmacology (Berl.)* 158, 273–280.

Conflict of Interest Statement: The authors declare that the research was conducted in the absence of any commercial or financial relationships that could be construed as a potential conflict of interest.

Received: 31 August 2012; accepted: 02 November 2012; published online: 22 November 2012.

Citation: Bazzigaluppi P, De Gruijl JR, van der Giessen RS, Khosrovani S, De Zeeuw CI and de Jeu MTG (2012) Olivary subthreshold oscillations and burst activity revisited. Front. Neural Circuits ***6****:91. doi: 10.3389/fncir.2012.00091*

frontiers in
NEURAL CIRCUITS

ORIGINAL RESEARCH ARTICLE
published: 21 August 2013
doi: 10.3389/fncir.2013.00133

Strength and timing of motor responses mediated by rebound firing in the cerebellar nuclei after Purkinje cell activation

Laurens Witter*[1†], *Cathrin B. Canto*[1†], *Tycho M. Hoogland*[1], *Jornt R. de Gruijl*[1] and *Chris I. De Zeeuw*[1,2]

[1] Netherlands Institute for Neuroscience, Royal Netherlands Academy of Arts and Sciences, Amsterdam, Netherlands
[2] Department of Neuroscience, Erasmus Medical Center, Rotterdam, Netherlands

Edited by:
Egidio D'Angelo, University of Pavia, Italy

Reviewed by:
Deborah Baro, Georgia State University, USA
Sergio Solinas, University of Pavia, Italy

****Correspondence:***
Chris I. De Zeeuw, Cerebellar Coordination and Cognition Group, Netherlands Institute for Neuroscience, Royal Netherlands Academy of Arts and Sciences, Meibergdreef 47, NL-1105 BA Amsterdam, Netherlands
e-mail: c.de.zeeuw@nin.knaw.nl
[†] *These authors have contributed equally to this work.*

The cerebellum refines the accuracy and timing of motor performance. How it encodes information to perform these functions is a major topic of interest. We performed whole cell and extracellular recordings of Purkinje cells (PCs) and cerebellar nuclei neurons (CNs) *in vivo*, while activating PCs with light in transgenic mice. We show for the first time that graded activation of PCs translates into proportional CN inhibition and induces rebound activity in CNs, which is followed by graded motor contractions timed to the cessation of the stimulus. Moreover, activation of PC ensembles led to disinhibition of climbing fiber activity, which coincided with rebound activity in CNs. Our data indicate that cessation of concerted activity in ensembles of PCs can regulate both timing and strength of movements via control of rebound activity in CNs.

Keywords: olivo-cerebellar network, Purkinje cells, rebound, cerebellar nuclei, motor control

INTRODUCTION

The cerebellum integrates sensory and motor information to learn and refine the timing of motor performance. Sensory and motor information enters the cerebellar cortex via climbing fibers that originate in the inferior olive (IO) and via mossy fibers that originate in a variety of precerebellar sources (Ito, 1984). Climbing fibers synapse onto Purkinje cells (PCs) in rostrocaudally oriented cerebellar cortical zones (Ozden et al., 2009) and generate complex spikes (CSs) (Eccles et al., 1964). There is a one-to-one relation between IO neuron firing and the occurrence of a CS in the target PC (Eccles et al., 1966). Apart from CSs, which occur at a relatively low rate of about 1 Hz at rest and up to 5–8 Hz during optimal stimulation (Llinas and Volkind, 1973; Llinas and Yarom, 1986; Llinas and Sasaki, 1989; Sasaki et al., 1989; Lang et al., 1999), PCs fire simple spikes (SSs) at 50–100 Hz (Latham and Paul, 1971). SSs are intrinsically driven in PC cell bodies by resurgent sodium currents (Raman and Bean, 1997; Afshari et al., 2004; Aman and Raman, 2007) and are modulated by excitatory and inhibitory inputs from the mossy fiber—parallel fiber pathway and molecular layer interneurons (MLIs), respectively (Jacobson et al., 2008; Oldfield et al., 2010). The activity of MLIs, the axons of which target PCs within an individual sagittal zone, can be influenced by both parallel fibers and climbing fibers (Ekerot and Jorntell, 2001; Jorntell and Ekerot, 2002, 2003; Szapiro and Barbour, 2007; Bosman et al., 2010; Mathews et al., 2012; Badura et al., 2013). Ultimately, information from the zones of PCs is processed by cerebellar nuclei neurons (CNs) (Palay and Chan-Palay, 1974; Palkovits et al., 1977), which can inhibit the IO (De Zeeuw et al., 1988; Angaut and Sotelo, 1989; Ruigrok and Voogd, 1990; Fredette and Mugnaini, 1991) or provide an excitatory projection to a variety of premotor targets in the brainstem or thalamus (Bentivoglio and Kuypers, 1982; Voogd and Ruigrok, 1997; Garwicz, 2000).

Given the central hub position of the PC—CN projection, it is key to understand how PCs and CNs encode their information and how their activities integrate to control motor behavior (Aizenman and Linden, 1999; Alvina et al., 2008; Hoebeek et al., 2010; Bengtsson et al., 2011; De Zeeuw et al., 2011; Witter et al., 2011a; Person and Raman, 2012a,b). One of the main questions is to what extent behaviorally relevant information is transferred by individual PCs through rate coding or by synchronously timed activity and silent periods in ensembles of PCs (Bell and Grimm, 1969; Sjolund et al., 1977; Sasaki et al., 1989; Welsh et al., 1995; Levin et al., 2006; Walter et al., 2006; Heck et al., 2007; Catz et al., 2008; de Solages et al., 2008; Ozden et al., 2009; Schultz et al., 2009; Wise et al., 2010; Person and Raman, 2012a,b). Since PC axons are, like climbing fibers, organized in sagittal zones enabling ensembles of PCs to innervate a specific set of CNs, it is conceivable that PCs employ this modular organization to direct CN activity. A potential mechanistic target for such modulation is rebound activity in CN neurons, which is characterized by an elevated firing frequency following release from PC inhibition and which may rely on concerted activation and/or silencing of PCs (Llinas and Muhlethaler, 1988; Aizenman and Linden, 1999; Molineux et al., 2006, 2008; Tadayonnejad et al., 2010; Engbers et al., 2011). Rebound activity could impact postsynaptic

structures such as the thalamus, red nucleus, IO and lateral reticular formation (Teune et al., 2000), and eventually motor behavior (De Zeeuw et al., 2011). However, whether CN rebound firing can be proportionally induced by graded and timed modulation of activity in specific ensembles of PCs *in vivo* and whether such a titrating process can shape motor output accordingly has not been resolved. Investigating these questions has been hampered by the difficulty of classical electrophysiological tools to stimulate specific cell types selectively, let alone to stimulate these cells in small ensembles, and to record from CNs in the whole cell mode *in vivo*. Here we used a genetic approach to express the H134R variant of channelrhodopsin-2 (ChR2) specifically in PCs by crossing L7-cre (Oberdick et al., 1990) with ChR2(H134R) (Ai32line) mice (Madisen et al., 2012). We performed whole cell and extracellular recordings of PCs and CNs as well as video recordings of tail and limb movements, while stimulating ensembles of PCs with different intensities of light during precisely determined, yet variable time periods. We found that graded activation and subsequent cessation of sagittal PC ensembles *in vivo* translated into corresponding CN inhibitions and rebounds, which in turn evoked proportional muscle contractions and movements, indicating that rebound firing may orchestrate activity in premotor brain areas and thereby control muscle activity.

RESULTS

To assess network connectivity between PC ensembles and CNs at the physiological level we performed whole cell and extracellular *in vivo* recordings of PCs and CNs in genetically modified mice that expressed ChR2(H134R)-eYFP under the L7 promotor (Oberdick et al., 1990; Madisen et al., 2012). Expression of the channelrhodopsin-2/eYFP fusion protein was restricted exclusively to PCs in these mice (**Figures 1A–C**). In the cerebellar nuclei, the fusion protein was present in axons and PC terminals surrounding CNs. There was no expression in other neuronal cell types in the cerebellum or the rest of the brain.

LIGHT-DRIVEN PURKINJE CELL MODULATION

We first made whole cell current clamp and extracellular recordings from PCs *in vivo* in response to light stimulation by three blue LED lights positioned around the cerebellum of anesthetized mice ($N = 7$) (**Figure 2A**). The LEDs were controlled by a custom-made linear LED driver (**Figure 2B**), which allowed us to adjust the strength of the light in a linear fashion (see **Figure 2C** for power curve). PCs were identified by CS and SS activity and the characteristic climbing fiber pause (De Zeeuw et al., 2011). Baseline SS activity (i.e., without light stimulus) was 72 ± 19 Hz (**Figure 3A**). Enhancing the light from 10 to 100% significantly increased the SS firing frequency of PCs from 80 ± 25 Hz to 124 ± 11 Hz [cell-wise comparison: $t_{(5)} = -4.742$, $p = 0.005$], while it reduced the latency of the first SS from 9.1 ± 5.8 ms to 6.0 ± 4.7 ms [all latencies: $t_{(148)} = 5.181$, $p < 0.001$] (**Figures 3A–C**). Interestingly, light stimulation was also effective in increasing SS activity when the PC was in the downstate (compare **Figures 3B,C**) (Loewenstein et al., 2005; Schonewille et al., 2006; Jacobson et al., 2008). We were unable to find a direct response within the first 50 ms of light stimulation in any other cell type in the cerebellar cortex. These data demonstrate that with our stimulus device and protocol we were able to selectively activate PCs in L7-ChR2 (H134R) mice in a reliable and graded manner.

GRADED PURKINJE CELL ACTIVATION TRANSLATES INTO PROPORTIONAL CEREBELLAR NUCLEI INHIBITION

We assessed the effect of graded, transient light-driven activation of PCs on CN spiking using different stimulus intensities and frequencies in anesthetized mice. CNs were identified based on their depth measured from the pial surface (1500–2400 μm), their direct response to PC stimulation and their basic electrophysiological properties (Uusisaari et al., 2007; Bengtsson et al., 2011; Witter et al., 2011b). Recordings of CNs were targeted at the interposed nucleus of the cerebellum. CN membrane resistance, capacitance, and firing frequency varied from 11.7–779.1 MΩ, 60.1–772.6 pF, and 0–138.4 Hz, respectively ($N = 21$). Despite the large differences in cell physiological parameters, we were not able to distinguish separate clusters of cells indicative of neuronal subtypes. Also, depth of the recording was not associated with any cell physiological parameter or with the occurrence of rebound firing in these CNs. In current clamp, short light activations (1–3 ms) evoked single inhibitory postsynaptic potentials (IPSPs) in CNs ($N = 8$) (**Figure 4A**). As expected due to differences in

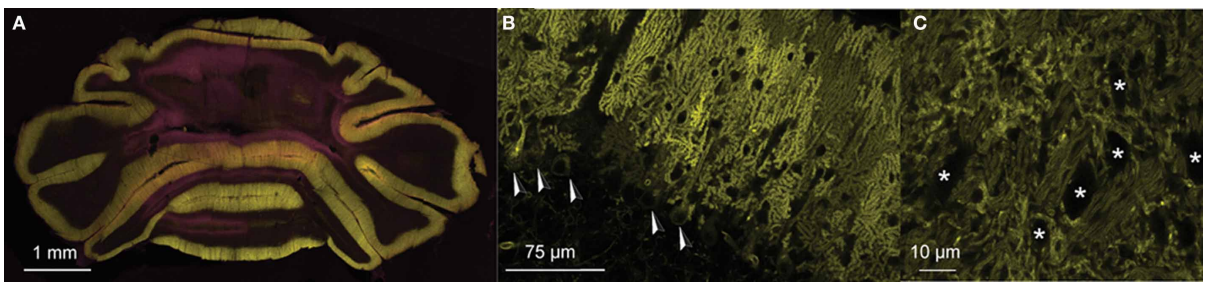

FIGURE 1 | PC-specific expression of ChR2(H134R)-eYFP under control of L7-pcp2. (A) Coronal section of the cerebellum of an L7-ChR2(H134R)-eYFP mice. PC and molecular layers show dense expression of the ChR2-eYFP fusion protein (eYFP: yellow). **(B)** Detail of a sagittal section of an L7-ChR2(H134R)-eYFP mouse. ChR2-eYFP protein expression was restricted to PC membranes. PC somata are indicated with arrowheads. Note that MLIs are visible as small dark exclusions in the PC arborizations of the molecular layer. The neuronal expression of ChR2-eYFP fusion protein was found only in PCs of the cerebellum, but not in other neuronal structures in the rest of the brain. **(C)** Detail of PC axons innervating the cerebellar nuclei. CNs are marked with '∗'. Counterstain in **(A)** with DAPI (pink).

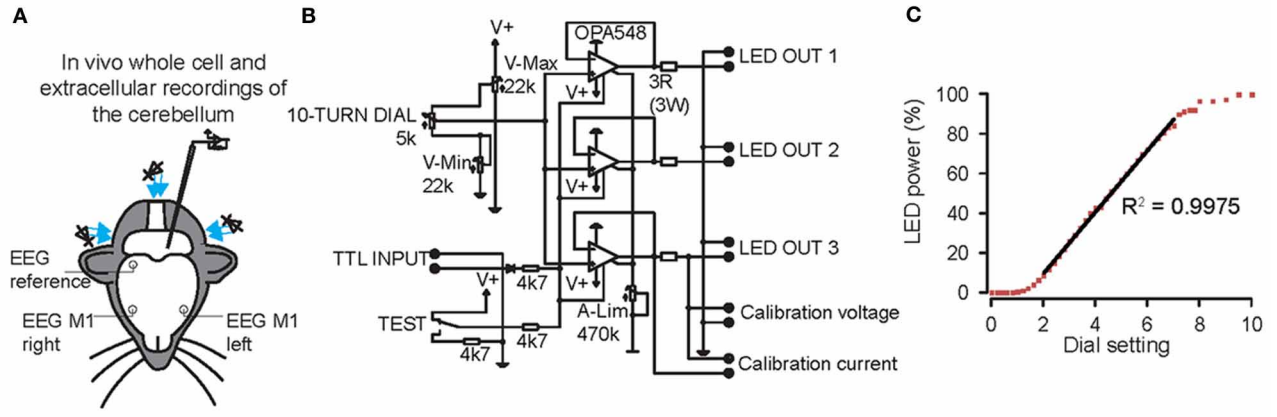

FIGURE 2 | Graded whole field light stimulation by three blue light emitting diodes (LEDs) positioned around the cerebellum of mice controlled by a custom-built linear LED driver. (A) Overview of the experimental set-up. Whole cell and extracellular recordings were made from Purkinje cells (PCs), cerebellar nuclei neurons (CNs), molecular layer interneurons (MLIs) and granule cells. At the same time, bilateral electroencephalogram (EEG) was recorded from motor cortex, referenced on the right parietal cortex. **(B)** Circuit diagram of one channel of the LED driver. A 10-turn dial permitted setting of light-intensity during experiments. A TTL input can be used to trigger the light from an external source. V-Max, V-Min, and A-Lim (measuring from calibration voltage or current) are used to limit the voltage and current through the LED and to calibrate the 10-turn dial. Up to three LEDs can be connected in parallel on a single channel. **(C)** LED power is a linear function of the dial setting in the range between 20 and 75%.

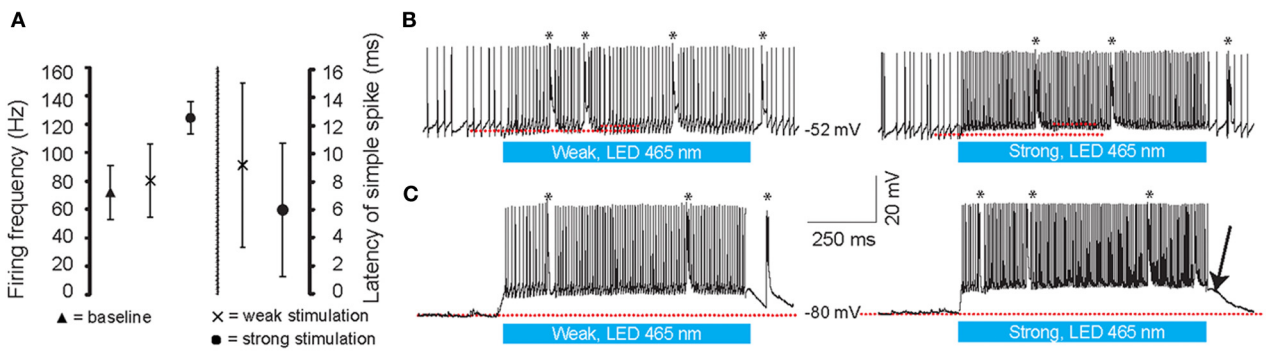

FIGURE 3 | Whole cell *in vivo* recordings of PCs during optogenetic stimulation. (A) Latency to the first simple spike (SS) and the increase in firing frequency during the light stimuli at different intensities. **(B,C)** Light stimulation (465 nm, 1000 ms, denoted by the blue bars below the traces) of the cerebellum at weak (left panels) and strong (right panels) light intensities. Both in the upstate **(B)** and downstate **(C)** PCs show graded increases of SSs and CSs during stimulation. Note, ChR2 (H134R) has slow kinetics; at light-offset, the cell remains depolarized for a few milliseconds before it settles back down to a baseline state (arrow). Red lines indicate the subthreshold membrane potentials before and during the light stimulation. Asterisks indicate CSs.

connectivity with PCs and differences in stimulation intensities, these IPSPs varied in amplitude among cells (-3.84 ± 2.13 mV) and onset latency (4.21 ± 1.44 ms). Nevertheless, weaker light activation consistently induced smaller IPSP amplitudes compared to those following strong stimulations in all CNs tested. Next, in voltage clamp we held cells at potentials between -30 and -100 mV while stimulating PCs to calculate the current-voltage relationship (IV curve) of PC input. When stimulating PCs for several tens of ms, summations of postsynaptic currents were indicative of synchronized inputs to CNs (**Figure 4B**). In most traces we were able to identify two or three summated postsynaptic currents before the inputs became less synchronized. The onset of the evoked currents occurred at 4.04 ± 1.34 ms following the stimulus, while the timing of the first and that of the second peak synaptic current after the onset of the stimulus were 7.08 ± 1.80 ms and 11.93 ± 3.38 ms, respectively (**Figure 4B**). We determined the reversal potential for the synaptic current from the peaks of both the first and second peak-current. An inward current was observed at strongly hyperpolarized potentials, while outward currents were observed at more depolarized potentials ($E_{rev} = -76.42 \pm 8.66$ mV, slope: 4.37 ± 2.06 pA/mV; $N = 3$) (**Figure 4C**), which is in line with previously reported characteristics of the PC to CN synapse (Llinas and Muhlethaler, 1988; Zheng and Raman, 2009; Hoebeek et al., 2010). In current clamp mode recordings, we were able to inhibit CNs in a graded fashion using different intensities of light showing that a gradually changing rate of PC firing can lead to a proportional change in CN firing (**Figures 4D,F,G**). At cessation of the light stimulus, neurons remained inhibited for a variable period depending on the strength of the light stimulus. Following a weak stimulation

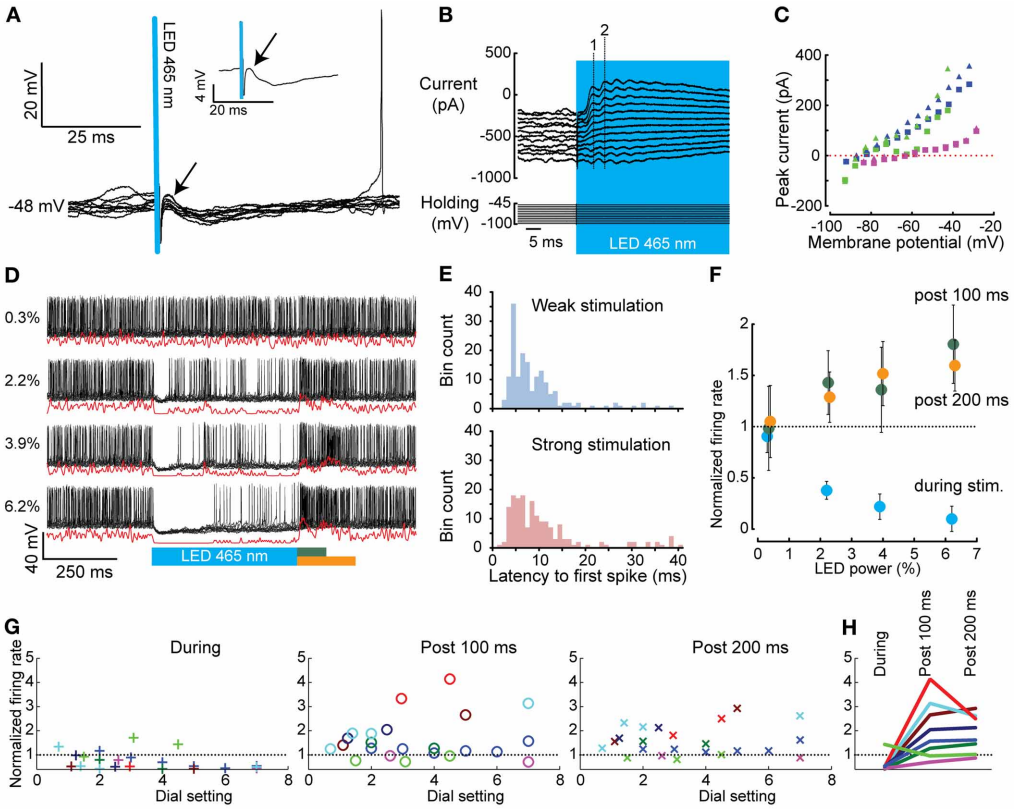

FIGURE 4 | Whole cell and extracellular *in vivo* recordings of CNs before, during, and after optogenetic activation of PCs. (A) Brief 1 ms activation of PCs (blue bar) was sufficient to evoke IPSPs in CNs (onset is indicated with an arrow). The inset shows the average trace. **(B)** CN responses (top panel) at various holding potentials (lower panel) used to determine the reversal potential of the evoked events in CNs (stimulus in blue). The dashed numbered lines indicate the peaks of the first (1) and second (2) induced postsynaptic event, respectively. **(C)** IV curves of all CN neurons tested (individual CN neurons are indicated with different colors, squares indicate responses to the first peak, triangles to the second). The reversal potential ($E_{rev} = -76.42 \pm 8.66$ mV) is in agreement with a $GABA_A$-mediated current. **(D)** Graded PC stimulation (blue bar) [ranging from 0.3 to 6.2 dial setting (**Figure 2C**)] evoked a graded response in CNs. Black lines indicate raw data, red lines Gaussian convolved traces. **(E)** Histograms of the latency of the first spike in CNs after light-driven PC mediated inhibition. The distribution shows a long tail for both weak and strong stimulation intensities. **(F)** The normalized firing rate (firing rate during stimulation or rebound divided by the prestimulus firing rate) of the CN shown in **(D)** during light stimulus (blue), 100 ms post light stimulus (green dots), or 200 ms post light stimulus (orange dots). **(G)** Summary as in **(F)**, but for all cells. Different neurons are color coded over the three panels. **(H)** The maximal stimulation intensities from the panels in **(F)** are plotted to show that inhibition during the stimulation is necessary for rebound to occur.

of 1000 ms the latency to the first spike (time from stimulation offset to first spike) ranged from 1.62 to 448 ms with an average of 41.45 ± 80.85 ms, whereas following a strong stimulation of the same duration it varied from 0.52 to 91.47 ms with an average of 19.37 ± 20.70 ms ($N = 10$, **Figure 4E**). Thus, the time to onset is shorter [$t_{(243.287)} = 3.621$, $p < 0.001$] with a smaller variance [Levene's test: $F_{(61.36)}$, $p < 0.001$] for strong stimulation indicating that release from strong synchronous PC inhibition leads to more precisely timed CN firing compared to weak PC-mediated inhibition.

REBOUND FIRING IN CEREBELLAR NUCLEI NEURONS FOLLOWS TIMED OFFSET OF PURKINJE CELLS

In most CNs (10 out of 13) optogenetically-induced inhibition was followed by a rebound wave of excitation, which lasted up to tens of milliseconds. We did not observe a relation with the occurrence or the strength of rebound firing and cell physiological parameters such as membrane resistance, nor with the recording location. Rebound excitation was often biphasic with an initial excitation followed by inhibition and a second excitation (**Figure 4D**). The timing of the peak excitation as well as the first inhibition and second excitation [as determined by convolving the spike train with a Gaussian of width $\sigma = 1$ ms, see Materials and methods, (Hoebeek et al., 2010)] after either 500 or 1000 ms of PC stimulation were not significantly different [500 vs. 1000 ms; first peak: 32.2 ± 17.0 vs. 45.7 ± 30.8, $t_{(15)} = 0.95$, $p = 0.36$; inhibition: 50.4 ± 11.9 vs. 62.6 ± 20.9, $t_{(12)} = 1.13$, $p = 0.28$; second peak: 85.8 ± 28.6 vs. 91.8 ± 20.4, $t_{(10)} = 0.38$, $p = 0.71$]. The average firing rate over the period after the stimulus (100 and 200 ms, for both 500 and 1000 ms) was significantly higher than the pre-stimulus firing rate in all comparisons [$F_{(1, 35)} = 14.69$, $p < 0.001$, and $F_{(2, 41)} = 13.82$, $p < 0.001$ for 500 and 1000 ms stimulation, respectively; *post-hoc* all $p < 0.001$] (**Figures 4F–H**). Comparing different stimulus

strengths revealed that five out of eight cells showed a significantly stronger inhibitory response during the stimulus when the stimulus strength was increased (power from 8.59 ± 8.55% to 58.89 ± 25.07%; ANOVA; $p < 0.001$, **Figures 4F,G**). Similarly, five out of eight cells showed a significantly stronger rebound after stronger light stimulation (ANOVA; $p < 0.001$) (**Figure 4G**). Thus, the strength of this rebound was also related to the strength and duration of the light stimulus. In general it was the case that cells showing strong inhibition also showed rebound firing (**Figure 4H**).

EVOKED MOVEMENTS FOLLOW TERMINATION OF SYNCHRONOUSLY ACTIVATED PURKINJE CELLS IN AWAKE MICE

To directly investigate the impact of light stimulation of PCs on movements, we optogenetically stimulated PCs over lobules V and VI in awake mice (**Figure 5A**) (Stark et al., 2012). These cerebellar lobules have been reported to show zonal proximal limb and tail representations in cats and rodents (Provini et al., 1968; Robertson, 1984; Buisseret-Delmas and Angaut, 1993; Jorntell et al., 2000; Ekerot and Jorntell, 2001). Mice were placed in a dark environment on a freely rotating transparent disc to allow recording of behavior from underneath with an infrared camera (**Figure 5A**), while we stimulated an estimated 400 PCs (see Materials and Methods) with flashes of blue light. Stimulations in resting mice resulted in stereotypical twitches of tail and proximal limbs (**Figures 5B–F**). Robust behavioral responses could be elicited by stimuli ranging from 25 to 500 ms (**Figure 5F**). In line with PC and CN responses, the behavioral response was graded and linearly related to the power density of the light stimulus ($R^2 = 1.00$) (**Figure 5D**), while the onsets of the muscle contractions were strongly related to the offset of the stimulus ($R^2 = 1.00$) (**Figures 5E–H**). The behavioral response was delayed with respect to the end of the stimulus by an average of 81.5 ± 27.9 ms (129 trials, $N = 3$ mice; 68.7 ± 36.0 ms, 85.1 ± 24.8 ms, 86.3 ± 22.2 ms for individual mice) (**Figure 5E**). The strength of the response did not diminish or enhance with repeated activation for the intervals used ($r = -0.07$, $p = 0.49$; mean response: 104.9 ± 36.5% of first response at 2.9 ± 1.4 s) (**Figure 5E**).

MUSCLE CONTRACTIONS RESULTING FROM SYNCHRONOUSLY ACTIVATED PURKINJE CELLS ARE NOT MEDIATED BY CEREBRAL CORTEX

To examine whether the cerebral cortex was required to initiate movements following optogenetic stimulation of the cerebellar cortex we recorded electroencephalograms (EEGs) from primary motor cortex and electromyograms (EMGs) from the musculus biceps femoris of the hind limb in anesthetized mice, while stimulating PCs and recording CN activity in the medial cerebellar nucleus ($N = 14$) (**Figures 2A**, **5I,J**). Stimulation-offset triggered averages of the cortical EEG showed a stereotypic EEG waveform consisting of a sequence of peaks and troughs (P1, N1, P2, N2, and P3 subsequently, $N = 14$) (**Figures 5I,J**). The timing between the left and right EEG for these components was identical for 500 and 1000 ms light stimulations (**Table 1**). Apart from yielding a robust response in the cortical EEG, stimulations of 500 to 1000 ms duration resulted in stereotypical twitch responses in the tail and proximal limbs of anesthetized mice. The onset of muscle twitches was related to the termination of the light stimulus, with the maximal rectified EMG response at 48.0 ± 10.3 ms after stimulus offset [41.2 ± 2.2 ms and 52.0 ± 11.2 ms after 500 and 1000 ms stimulation, respectively, $t_{(18)} = 3.07$, $p = 0.007$; $N = 7$, and $N = 12$] (**Figures 5I,J**). Instead, the onset of the EMG response occurred earlier at 36.18 ± 11.05 ms [30.52 ± 7.21 ms and 39.48 ± 11.79 ms after 500 and 1000 ms stimulation, respectively $t_{(18)} = 2.04$, $p = 0.055$; $N = 7$, and $N = 12$], which places it at similar times as the first input to the cerebral cortex (Meeren et al., 1998). Thus, the movements evoked by optogenetic stimulation of the cerebellum were likely initiated via a direct pathway (e.g., red nucleus and/or lateral reticular formation) and not through projections to the cerebral cortex.

MODULATION OF THE OLIVO-CEREBELLAR FEEDBACK LOOP BY PURKINJE CELLS

Optogenetic stimulation of PCs elicited robust SS activity (**Figure 3**). This, in theory should lead to inhibition of GABAergic CNs that project to the IO and a resulting disinhibition of olivary neurons to cause an increase of CS activity. This prediction indeed holds. During light activation for 1000 ms the average CS rate ($N = 7$) increased significantly from a baseline of 0.73 ± 0.38 Hz to 1.54 ± 0.89 Hz and 1.84 ± 0.45 with a low and high stimulus strength, respectively [baseline vs. weak $t_{(12)} = -2.194$, $p = 0.049$; weak vs. strong $t_{(6.002)} = -2.811$, $p = 0.031$; baseline vs. strong $t_{(6)} = -2.841$, $p = 0.030$]. The observed increase in CS activity, which occurs consistently throughout trials, might in principle result from single cell connections in the olivocerebellar loop, but it may be facilitated through more extensive network properties in that multiple PCs of the same sagittal zone converge onto individual CNs (De Zeeuw et al., 2011). When the membrane depolarization of a single PC during light stimulation *in vivo* was prevented by hyperpolarizing current injections, the SS frequency of that particular cell did not increase, whereas its CS rate increased persistently during and directly after the light stimulus that was applied to multiple PCs within a zone (**Figure 6A**). This indicates that the network properties of an ensemble of PCs are sufficient to induce an increase in CS activity, even when the SS activity of the recorded PC is suppressed. If the CS activity of a particular zone is enhanced following optogenetic stimulation of PCs through the network properties of the olivocerebellar loop, one expects that the activity of MLIs, which receive climbing fiber input through spillover (Jorntell and Ekerot, 2003; Szapiro and Barbour, 2007), will also be increased once the CS increase occurs, but not earlier than that. Indeed, MLIs responded to a 1000 ms light stimulation with a significant increase in firing frequency from 11.61 ± 2.43 Hz to 28.89 ± 4.32 Hz [$t_{(4)} = -3.476$, $p = 0.025$; $N = 3$], but this increase was delayed for more than 50 ms relative to the onset of the light stimulus reflecting elapsed time prior to disinhibition of the IO by the light stimulus (**Figure 6B**). We observed several large postsynaptic events in voltage clamp recordings of CNs both during and after light stimulation, which probably reflect climbing fiber collateral input (**Figure 7**). In addition, activity in the climbing fibers probably also facilitated late CN rebound via their collaterals (**Figures 6C,D**, **7**), because during voltage clamp recordings of CNs we observed putative climbing

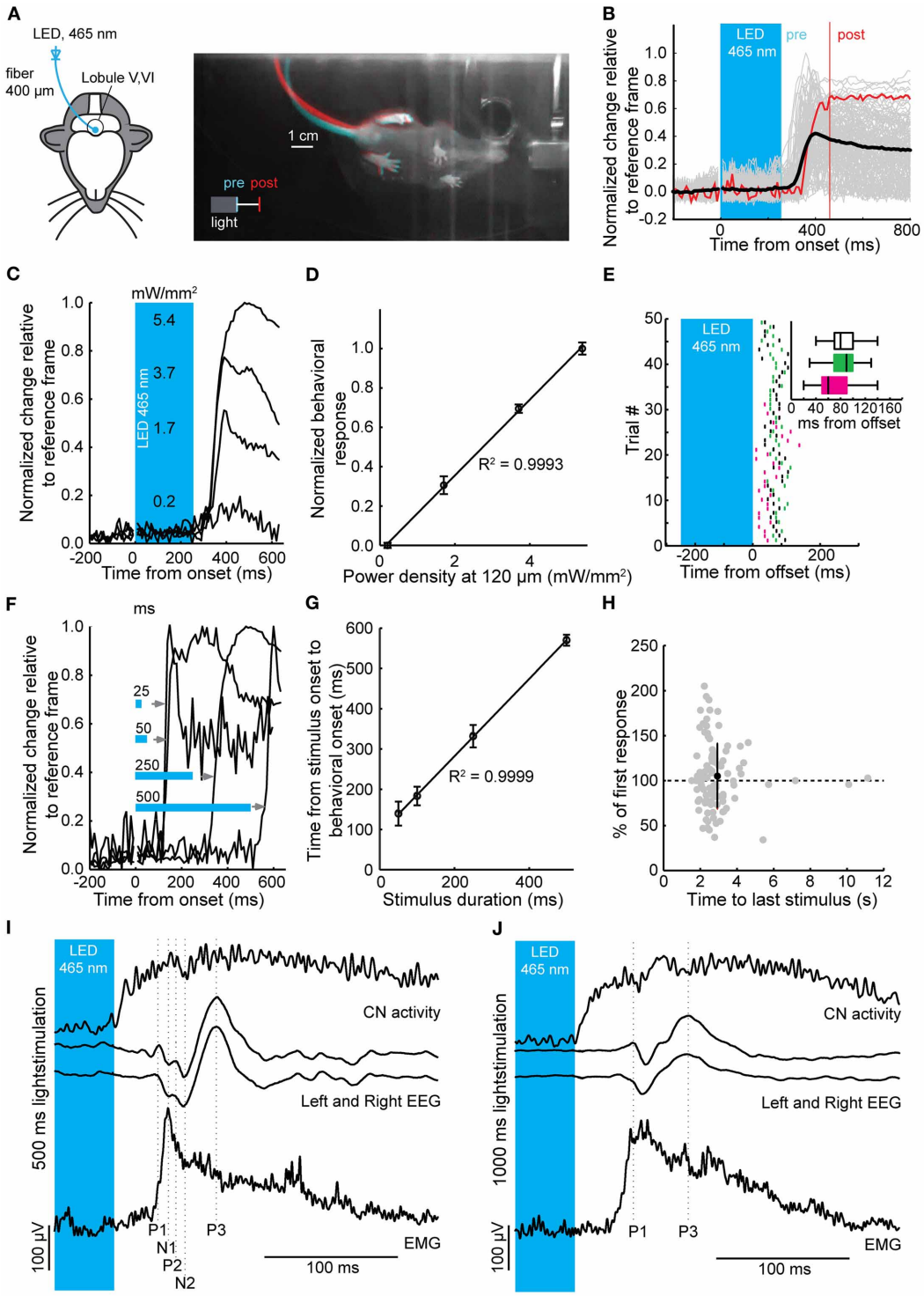

FIGURE 5 | Timed motor responses in awake mice during optogenetic activation of PCs. (A) For the behavioral assay head-fixed mice were placed on a transparent disc that could freely rotate. The optic fiber was placed on the brain surface of lobules V and VI (left) for optogenetic stimulation. Light was delivered to the brain via a LED coupled to the optic fiber. Right: Bottom view of a mouse responding to optogenetic activation of PCs (250 ms, ~5 mW/mm^2) with a twitch of its tail and hind legs after stimulus offset. Camera frames were acquired at 100 Hz. Differences between two frames at the stimulus offset ("pre," cyan) and 200 ms post-offset ("post," red) show relative position change between the two time points. **(B)** Individual behavioral responses (gray traces), response corresponding to twitch shown in **(A)** [red trace, one frame chosen at offset (pre), and one 200 ms post-offset (post)] and mean behavioral response (black trace) following a 250 ms light stimulus. **(C)** Behavioral responses were graded with increases in light intensity. Estimated power densities are shown at a depth of the PC monolayer (~120 µm). **(D)** Normalized behavioral response plotted vs. power density showing a linear correlation ($R^2 = 0.9993$, slope = 0.19).

(Continued)

FIGURE 5 | Continued
(E) Raster plot showing individual behavioral onsets relative to the stimulus offset (time = 0). Inset: box plots (three mice indicated by different colors) of behavioral onsets relative to the stimulus offset (whiskers indicate distance from 25 to 75% interquartile ranges to furthest observations, center mark represents the median). **(F)** The onset of behavior shifted with an increase in stimulus duration, such that the relative delay to a behavioral response onset relative to stimulus offset was maintained. Note that behavioral responses can be elicited by stimuli with durations of 25 ms. **(G)** Time from stimulus onset to behavioral onset plotted against stimulus duration followed a linear relationship ($R^2 = 0.9999$ and slope = 0.96) demonstrating that the onset of behavioral responses shifts relative to the stimulus duration. **(H)** The interstimulus interval did not have an effect on strength of the behavioral response ($r = -0.071$, $p = 0.49$). **(I)** and **(J)** Simultaneous recordings of CNs, bihemispheric EEG, and EMG to 500 ms **(I)** and 1000 ms **(J)** light stimulation of PCs in anesthetized mice. For clarity, the stimulation period has been truncated and only the last 45 ms of the stimulus is shown in the blue box. Vertical scale bars apply to both EEG traces and EMG traces in **(I)** and **(J)**. Top panels, average Gaussian-convoluted spike train of all CNs. Middle panels, left and right EEG. Bottom panels, rectified, differentiated and again rectified EMG responses. The vertical dotted lines indicate the location of the positive (P1 to P3) and negative (N1 to N2) deflections in the EEG signals. Note that the onset of the EMG response occurs before the first response peak in the EEG, while the EMG signal itself is preceded by CN activity.

Table 1 | Timing of EEG and EMG components.

	P1	N1	P2	N2	P3
500 ms left EEG	32.2 ± 2.1 ms $N = 3$	48.3 ± 12.7 ms $N = 4$	55.3 ± 14.3 ms $N = 3$	58.5 ± 13.3 ms $N = 4$	72.7 ± 9.1 ms $N = 9$
500 ms right EEG	28.6 ± 5.2 ms $N = 6$	39.4 ± 1.5 ms $N = 6$	47.1 ± 3.4 ms $N = 3$	52.0 ± 3.2 ms $N = 7$	71.0 ± 5.6 ms $N = 11$
Left vs. Right	$t_{(8)} = 1.09$ $p = 0.31$	$t_{(9)} = 1.74$ $p = 0.12$	$t_{(5)} = 0.94$ $p = 0.39$	$t_{(10)} = 1.28$ $p = 0.23$	$t_{(19)} = 0.50$ $p = 0.63$
1000 ms left EEG	33.9 ± 1.1 ms $N = 4$	48.5 ± 6.8 ms $N = 5$	53.7 ± 4.5 ms $N = 2$	59.7 ± 2.2 ms $N = 2$	71.1 ± 8.0 ms $N = 10$
1000 ms right EEG	33.2 ± 1.7 ms $N = 6$	42.9 ± 5.4 ms $N = 3$	52.7 ± 1.7 ms $N = 3$	62.4 ± 10.9 ms $N = 4$	77.0 ± 12.7 $N = 7$
Left vs. Right	$t_{(9)} = 0.80$ $p = 0.45$	$t_{(7)} = 1.25$ $p = 0.25$	$t_{(4)} = 0.25$ $p = 0.81$	$t_{(5)} = 0.46$ $p = 0.67$	$t_{(16)} = 1.06$ $p = 0.31$
500 vs. 1000 ms	$t_{(17)} = 0.62$ $p = 0.54$	$t_{(17)} = 0.40$ $p = 0.69$	$t_{(10)} = 0.02$ $p = 0.98$	$t_{(16)} = 0.49$ $p = 0.63$	$t_{(36)} = 0.27$ $p = 0.79$
Grand average EEG	32.5 ± 1.9 $N = 18$	44.5 ± 7.8 $N = 18$	52.0 ± 7.6 $N = 11$	56.9 ± 8.9 $N = 17$	72.6 ± 8.7 $N = 37$
EEG vs. EMG onset	$t_{(28)} = -0.52$ $p = 0.30$	$t_{(26)} = -2.91$ $p = 0.004$	$t_{(23)} = -5.97$ $p < 0.001$	$t_{(24)} = -4.56$ $p < 0.001$	$t_{(35)} = -10.37$ $p < 0.001$

Timing of motor cortex EEG relative to optogenetic activation of PCs. Each column lists the average delay from stimulus offset to the indicated response. Each row lists a different condition or statistical test. N lists number of sets of ten traces analyzed.

fiber-mediated excitatory postsynaptic currents (EPSCs) within 50 to 100 ms after termination of the light stimulation coinciding with the moments when CSs occur in PCs (see also **Figure 7**). Indeed in PCs, a robust but loosely timed CS was observed after stimulus offset. For 1000 ms excitation of PCs this CS had an average latency of 73.11 ± 32.73 ms ($N = 6$), whereas for 500 ms excitation this latency (82.13 ± 49.43 ms) was slightly, but not significantly longer [$t_{(275.53)} = -1.904$, $p = 0.058$]. Taken together, these observations indicate that light-driven activation of PCs is effective in disinhibiting the IO and that the timing of the CS activity of PCs and that of the activity in the presumptive climbing fiber collaterals after offset of the light stimulus both correlate well with the temporal characteristics of the rebound in CNs.

DISCUSSION

Over the past years various studies have shown that synchronous activation of PC ensembles is essential for the transfer of behaviorally relevant information from the cerebellar cortex to the cerebellar nuclei (Bell and Grimm, 1969; Sjolund et al., 1977; Sasaki et al., 1989; De Zeeuw et al., 1993, 1997a, 2011; Welsh et al., 1995; Levin et al., 2006; Walter et al., 2006; Heck et al., 2007; Catz et al., 2008; de Solages et al., 2008; Van Der Giessen et al., 2008; Ozden et al., 2009; Schultz et al., 2009; Wise et al., 2010; Person and Raman, 2012a,b). Yet, technical limitations have hampered intracellular *in vivo* whole cell recordings of CNs and selective PC stimulation. In the present study, we used the Ai32 (ChR2(H134R)-eYFP) transgenic mouse and a L7-Cre driver line to allow for selective and temporally well controlled activation

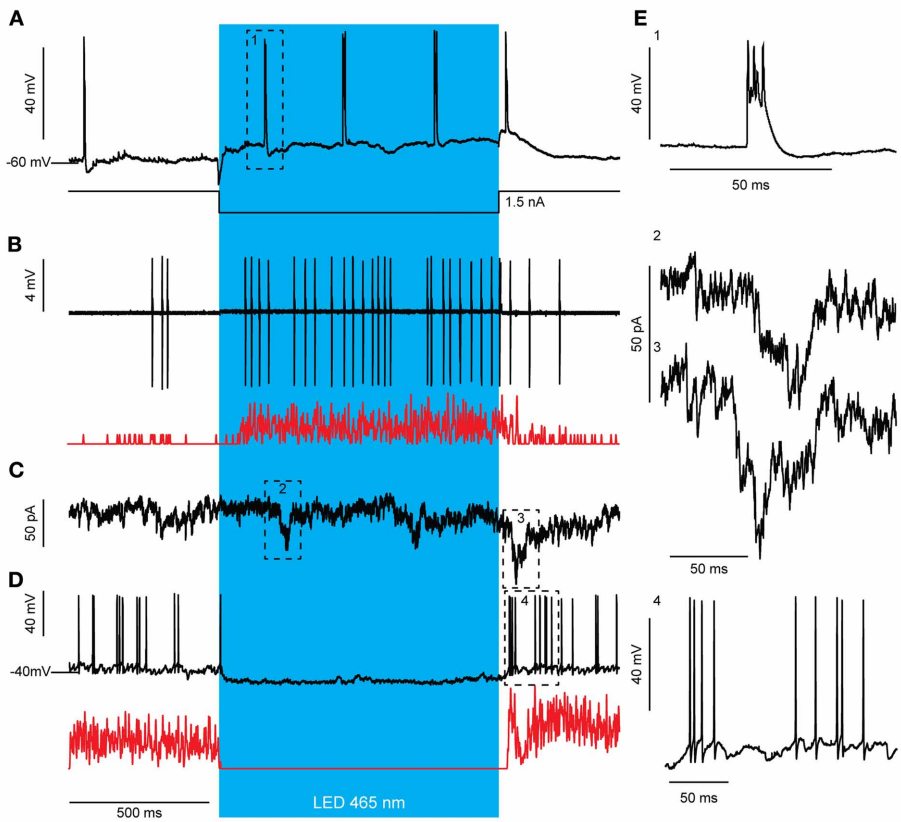

FIGURE 6 | Optogenetic stimulation of PCs elicits an increase in CS activity, which is most likely a network effect. (A) Light stimulation (blue bar) evokes an increase in CS activity even when the SS increase is prevented by intracellular current injection via the patch electrode. Additionally, a CS was observed after stimulus offset. Notice the depolarized membrane potentials after stimulus offset indicating slow inactivation of the ChR2 (H134R) channel (arrows). **(B)** MLI activity is not directly increased in response to PC stimulation but after >50 ms delay. This activation is likely due to the recorded CS increase **(A)** that leads to MLI activation through glutamate spillover. The increase in MLI firing frequency outlasted the light stimulus [see also Gaussian-convoluted trace in red; Putative MLIs, $N = 3$; baseline firing rate 50 ms before light stimulation: 1.69 ± 9.54, firing rate <50 ms after strong light stimulation: 1.93 ± 8.97, $t_{(123)} = -0.421$, $p = 0.675$] similar to what we see for CS activity **(A)**. **(C)** A voltage and subsequent current clamp recording **(D)** of a single representative CN during light stimulation of PCs. **(C)** Voltage clamp recordings of CNs reveal several large, summating EPSCs present during and directly after the light stimulus (arrows), which may be evoked by the increased climbing fiber activity **(A)**. **(D)** In current clamp, the inhibition from firing during PC stimulation (blue bar) and the biphasic rebound activity after the inhibition is visible. Note, the timing of the CS activity **(A, C)** of PCs after offset of the light stimulus precedes the break in the CN rebound (**D**, see also Gaussian-convoluted trace in red). **(E)** Example complex spike from the trace in **(A)** (1), example EPSCs from the trace in **(C)** (2 and 3), and magnification of rebound firing in **(D)** (4).

of PCs and combined this with *in vivo* whole cell recordings to examine the effect of well-timed PC activation on CNs and the olivo-cerebellar network. Using whole cell *in vivo* recordings of PCs and CNs we have shown that timed light onset evokes synchronized activation of PCs. This is supported by the findings that evoked inhibitory events in CNs were visible in response to light stimulation and that these inhibitory potentials summated well, demonstrating that a CN receives multiple synchronized events. With increased light intensity, shorter latency responses with a reduced variation in the onset time of PCs were observed, suggesting that with a reduction in variability more synchronization occurs. To the best of our knowledge, this is the first study showing how the olivo-cerebellar network responds to synchronized activation and subsequent deactivation of PCs and how such synchronization may generate timed motor responses.

REBOUND FIRING EVOKED BY SYNCHRONOUS PC DISINHIBITION

As suggested earlier, we find that timed release from PC inhibition leads to a signature rebound response in CNs (Aizenman and Linden, 1999; Nelson et al., 2003; Hoebeek et al., 2010; De Zeeuw et al., 2011). We also show that by increasing the strength of the preceding PC light-stimulation, the onset of rebound activity becomes more precisely timed. This matches our previous findings in which olivary stimulation was more effective in evoking rebound in CNs than focal electrical, cortical stimulation (Hoebeek et al., 2010). Complementing and extending previous studies (Jahnsen, 1986; Aizenman and Linden, 1999; Molineux et al., 2006, 2008; Pugh and Raman, 2006; Alvina et al., 2008; Steuber et al., 2011) we demonstrate that rebounds can be observed even when completely silenced prior to the rebound. This can be explained by a massive distributed input from the orchestrated activation of PCs by our light stimulus compared

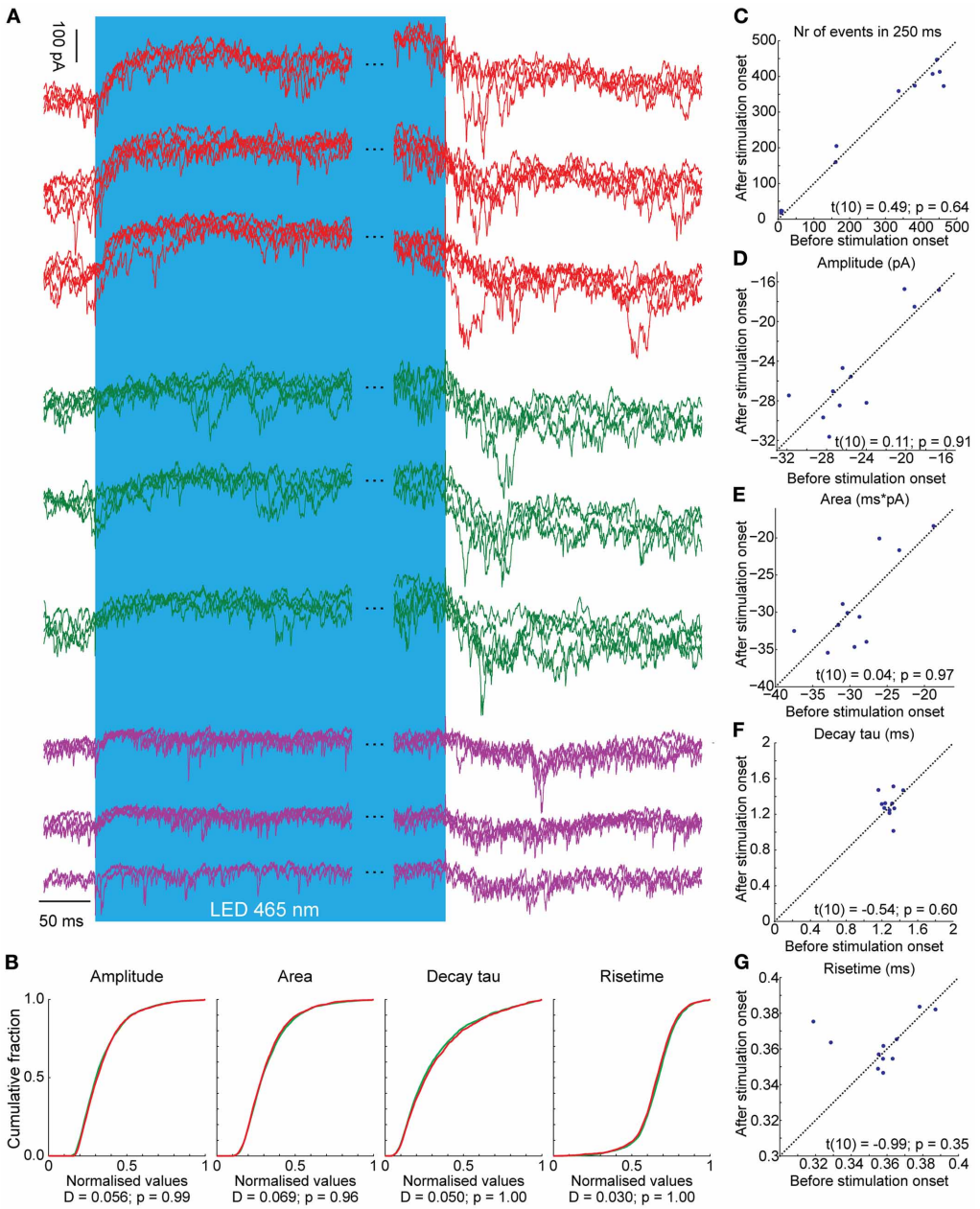

FIGURE 7 | Voltage clamp recordings of three CNs during light stimulation of PCs (blue bar, the time during the stimulus is not completely shown; notice the break between the blue bars). Three representative CNs are shown. Per neuron we show three overlays of each four traces (so, a total of 12 traces per cell). **(A)** CNs react with an outward current in response to the light stimulus. In addition, there are several large, summating EPSCs present during and directly after the light stimulus, probably induced by climbing fiber activity. **(B)** There were no differences in the distributions of various EPSC kinetics before (green) and after (red) stimulation onset. Also, the **(C)** number of events, **(D)** amplitude of the excitatory postsynaptic potentials, **(E)** the area, **(F)** the decay and **(G)** rise time do not differ before and after stimulation onset, suggesting that the mossy and climbing fiber inputs share similar kinetics. The significance of pairwise comparisons is listed for each panel separately.

to a point-source current injection at the soma (Gauck et al., 2001). Therefore, subtle changes in the timing of PC activity could already lead to pivotal CN firing adjustments that could influence not only behavior but also CN plasticity by timed coding (Pugh and Raman, 2006). Indeed, we show that even weak activation of an ensemble of PCs is sufficient to evoke rebounds *in vivo*.

TIMED PURKINJE CELL INACTIVATION EVOKES MUSCLE CONTRACTIONS

The cerebellum may modulate ongoing movement and specific reflexes in part through synchrony of PC CS firing, likely causing larger and more sudden changes in motor output the more synchronized CSs are involved (De Zeeuw et al., 2011). Key to this hypothesis is the synchrony and magnitude with which changes

in a PC population's ongoing SS activity occur, as a CS occurrence has a profound effect on SS activity and the SS coding is assumed to shape the continuous output from the cerebellum that is required for ongoing motor control. We were able to show that light-driven SS modulation in PC ensembles is able to control rebound activity in CNs and subsequently regulate the onset of motor behavior via cessation of PC stimulation. To determine how synchronous activation of the cerebellum could possibly influence timed motor responses, we recorded simultaneously the EEG of the motor cortex and the EMG of the biceps femoris of anesthetized mice. In an extra set of experiments we monitored evoked movements in awake mice. We found that EEG responses and muscle twitches are timed to the offset of the light stimulus rather than the onset. Furthermore, our data show that the CN rebound rather than PC activity is related to the onset of synchronous activity in the motor cortex (Fujikado and Noda, 1987; Noda and Fujikado, 1987; Godschalk et al., 1994). Despite the relatively fast first response in neocortical EEG, it is not possible that all behavioral output generated in our experiments is mediated and initiated via the motor cortex, since the onset of the EMG response occurred at similar times as the first response in the EEG, which reflects thalamic input to the neocortex (Meeren et al., 1998). Therefore, we propose that at least the initial part of the behavioral output, as measured with EMG and in our awake behavioral assay, is mediated via other routes than projections through thalamus and motor cortex. A more direct route probably relies on brainstem nuclei such as the red nucleus and/or lateral reticular formation (Teune et al., 2000). Altogether, we demonstrate that light-driven activation of PC ensembles is able to regulate the onset of motor behavior via graded control of rebound activity in CNs.

ACTIVATION OF PC ENSEMBLES MODULATES THE OLIVO-CEREBELLAR FEEDBACK LOOP

PCs responded to graded light activation with a graded increase in the firing rate of SS and CS. We show here that the increase of CS rate was not a direct effect of the channelrhodopsin stimulation upon the cell, but rather a result of the activation of the olivo-cerebellar feedback loop. An increase in SS rate depresses the CN, including the inhibitory projections to the IO (De Zeeuw et al., 1988; Angaut and Sotelo, 1989; Ruigrok and Voogd, 1990; Fredette and Mugnaini, 1991). Such disinhibition of the IO may increase the activity and rhythmicity of the climbing fibers (Stratton and Lorden, 1991; Lang et al., 1996; Bengtsson et al., 2004). CS rate increased independent of membrane voltage as shown by experiments in which single PCs were hyperpolarized with current injections, supporting the idea that the persisting increase of CSs was caused by reverberation in the olivo-cerebellar loop. The fact that rebound firing was biphasic due to synchronous CS firing in PCs further underscores the idea that PCs-CNs-IO neurons form a closed feedback loop (Lang et al., 1996; Marshall and Born, 2007). Thus, by modulating their own firing, PCs may be able to influence climbing fiber dependent plasticity and conditioning (Rasmussen et al., 2008).

The olivo-cerebellar loop and its impact on the cerebellar cortical network may also explain in part why PC-mediated inhibition could evoke first a deep hyperpolarization in CNs and subsequently, after a short few millivolt recovery, some spike activity although the light stimulus was maintained (**Figure 4D**). Possibly, IO disinhibition by CN inactivation could provide enough excitatory input from climbing fiber collaterals to CNs to drive spike firing during PC-mediated inhibition (Van der Want et al., 1989; De Zeeuw et al., 1997b; Ruigrok and Voogd, 2000). Indeed, in voltage clamp we often observed EPSCs in CNs after several ms of PC inhibition (**Figures 6**, **7**). An additional explanation may be found in the fact that PC to CN synapses show profound short-term depression (Telgkamp and Raman, 2002; Pedroarena and Schwarz, 2003; Luthman et al., 2011), which can limit the synaptic current during strong PC activation. Such short-term depression was also observed during activation of PCs while voltage-clamping CNs (**Figures 4**, **6**, **7**). Finally, hyperpolarization-activated depolarizing currents, which were observed before in CNs (Aizenman and Linden, 1999; Molineux et al., 2006; Engbers et al., 2011), can limit the extent of the hyperpolarization induced by synaptic inputs.

Although we did see an apparent increase in the occurrence of high amplitude EPSCs during and directly after the light stimulation, overall the distributions and averages of all postsynaptic excitatory events did not change before and after stimulus onset. This indicates that climbing fiber collateral-mediated EPSCs do not have different kinetics from mossy fiber collateral-mediated EPSCs, which are expected to make up the majority of excitatory inputs to CNs. Even though our data seems to indicate a functional equivalence of mossy and climbing fiber collaterals, more experiments are needed to directly address this issue.

We conclude that temporally appropriately configured activity and silencing of ensembles of PCs will allow graded control of rebound activity in CNs and thereby motor activity, and that this control may be supported by reverberating activity in the modular olivo-cerebellar loops.

MATERIALS AND METHODS

All procedures adhered to the European guidelines for the care and use of laboratory animals (Council Directive 86/6009/EEC). Protocols were also approved by the animal committee of the Royal Netherlands Academy of Arts and Sciences (DEC-KNAW). L7-cre mice were crossed with ChR2(H134R)-eYFP mice to obtain L7-ChR2(H134R)-eYFP animals which express the channelrhodopsin-2 H134R variant (Berndt et al., 2011; Madisen et al., 2012) under control of the L7 promoter (Oberdick et al., 1990). Mice ($N = 17$) were prepared for the experiment by placing three EEG connectors and a pedestal on the skull under isoflurane anesthesia (1.5% in 0.5 l/min O2 and 0.2 l/min air). The skin on top of the head was shaved and cut sagittaly to expose the bone. The bone was then quickly etched with phosphoric acid gel (37.5%) and washed with saline. Three <2 mm diameter holes for the EEG electrodes were drilled over the motor cortices (1.5 mm frontal and 2.0 mm lateral from bregma) and over the parietal cortex. EEG electrodes were made from silver wires soldered to IC connectors. The silver wires were bent at the end as to protect the dura from puncturing and carefully inserted into the holes. Primer and adhesive were applied according to manufacturer's specification (Kerr, Orange, California). A pedestal, consisting of two M1.4 nuts soldered together, was attached to

the skull with dental acrylic (flowline; Heraeus Kulzer, Hanau, Germany). Care was taken to incorporate the EEG electrodes in the pedestal and to come to a solid block on top of the mouse's skull. The skin was then sutured to obtain a nice connection to the pedestal. Animals received analgesia in the form of Metacam (AUV, 2 mg/kg) and were allowed to recover for at least 1 day.

IN VIVO PATCH CLAMP AND EXTRACELLULAR RECORDINGS

On the day of the experiment animals received an initial i.p. injection of ketamine/ xylazine (75 and 12 mg/kg) and supplemented when needed. Animals were kept at 37°C body temperature via a feedback controlled heating pad. The mouse was fixed in the setup via the pedestal, the cerebellar cortex was revealed by drilling a large hole covering most of the occipital bone and the dura mater was removed. EMG electrodes consisted of a syringe needle (25G) connected to the amplifier. EMG electrodes were inserted in the biceps femoris of the hind leg. EEG leads were connected to the IC connectors on the skull of the mouse on one end and to a simple amplifier, together with the EMG electrode lead (adapted MEA60, Multichannel systems, Reutlingen, Germany). Whole-cell recordings of CNs were made using borosilicate glass electrodes (Harvard Apparatus, Holliston, Massachusetts) with 1- to 2-μm tips and 8 to 12 MΩ, filled with internal solution (in mM: 10 KOH, 3.48 MgCl2, 4 NaCl, 129 K-Gluconate, 10 hepes, 17.5 glucose 4 Na2ATP, and 0.4 Na3GTP), amplified with a Multiclamp 700B amplifier (Axon Instruments, Molecular Devices, Sunnyvale, California), and digitized at 50 KHz with a Digidata 1440 (Axon Instruments, Molecular Devices, Sunnyvale, California, United States).

IN VIVO VOLTAGE CLAMP RECORDINGS OF CNS

CNs were patched as described above. Voltage clamp recordings were obtained in a subset of cells with sufficiently low access resistance (<50 MΩ). Neurons were clamped at voltages between −60 and −75 mV, which was sufficient in all cases to prevent voltage escape inducing spikes. After voltage clamp recordings were completed, the cell was recorded in current clamp following the exact same stimulation parameters. From one cell we normally could obtain recordings from both 500 and 1000 ms stimulation durations.

LIGHT STIMULATION FOR IN VIVO PATCH CLAMP AND EXTRACELLULAR RECORDINGS

For strong, timed stimulation of channelrhodopsins, we developed a LED driver capable of driving three LEDs at a maximum of 5 watts of power per LED. Light intensity was set for the latter with a ten-turn dial for LED-light stimulation. Three LED lights (465 nm, 60 lm, LZ1-B200, LED Engin, San Jose, California), positioned around the cerebellum of the mouse, were used to illuminate the whole cerebellum (**Figure 2A**). This stimulus was powerful enough to activate PCs on every trial (**Figures 3**, **4**).

DATA ANALYSIS OF IN VIVO PATCH CLAMP AND EXTRACELLULAR RECORDINGS

Latencies to first spike for PCs were calculated as the time difference between the first spike and the onset of the stimulus, while for CNs the offset of the stimulus was used.

Firing rate increases and decreases were calculated of the period of 999 or 499 ms during the stimulus (for 1000 and 500 ms stimulation lengths resp.) and an equal time before the stimulus. Gaussian convolution of spike trains was done as described previously (Hoebeek et al., 2010). In short, each spike time was convolved with a Gaussian distribution (kernel) with peak 1 and width (σ) of 1–20 ms. Patch clamp data was analyzed in Clampfit (Axon Instruments, Molecular Devices, Sunnyvale, California, United States) to detect spikes and to measure membrane potential and membrane currents. EEG, EMG, and Gaussian-convolved traces were analyzed in Matlab (R2010b, Mathworks, Natick, Massachusetts, United States). Raw EMG recordings were low-pass filtered up to 500 Hz, then rectified, differentiated and again rectified. This resulted in a clear signal at the time at which motor endplate activity could be discerned as high frequency activity in the raw signal.

BEHAVIORAL ASSAY OF PURKINJE CELL ACTIVATION

Mice were head-fixed and placed on a freely rotating transparent disc before light stimulation experiments commenced. The disc was secured on a ball bearing, to ensure that forces exerted by the animal would not compromise head fixation and mice could move at will. A blue LED (465 nm, see above) was coupled into a 400 μm multimode optical fiber (Thorlabs, Newton, New Jersey), which was placed at the border of the anterior vermis regions lobule V and VI through a small (0.5–1 mm) drilled hole. The hole was covered with Kwik-Sil (World Precision Instruments, Sarasota, Florida) and the fiber was secured with dental cement. (Super-Bond, Generinter, France). Our custom-made LED driver was used to apply linearly increasing amounts of light intensity. We estimated the number of activated PCs by first calculating surface area at the bottom of the cone of light emitted from the fiber:

$$A = \left\{ \left(\frac{r_{\text{fiber}}}{\tan\left(\sin^{-1}\frac{NA_{\text{fiber}}}{NA_{\text{brain}}}\right)} + d \right) * \tan\left(\sin^{-1}\frac{NA_{\text{fiber}}}{NA_{\text{brain}}}\right) \right\}^2 * \pi$$

Where r_{fiber} is the radius of the fiber, NA_{fiber}, and NA_{brain} are the numerical apertures of the fiber and brain tissue (0.37 and 1.35 resp.) and d is the depth in μm; A is defined in μm^2. For the current experiments this means a radius of 234.2 μm (120 μm depth, 0.172 mm^2). Light is spread over this area and is attenuated by scattering and absorption by brain tissue following the rule (Yizhar et al., 2011):

$$P = 100\% * e\frac{-2.556 * d}{1000}$$

Where P is the resulting power at depth d in percent of the original power from the fiber tip. For the current set of experiments we obtained 73.6% power of the original 1.325 mW. This was spread over a surface of 0.17 mm^2, resulting in 5.66 mW/mm^2, which should be sufficient for reliable channelrhodopsin activation (Berndt et al., 2011). Harvey and Napper (1991) estimate the density of PCs in the rat cerebellum to be 936 PCs/mm^2, which would correspond to 161 PCs in the illuminated area.

A theoretical maximum is given by the optimal hexagonal packing of circles within the illuminated area:

$$\eta = \frac{1}{6} * \pi * \sqrt{3} \approx 0.9069$$

With η representing the packing density. Assuming a PC soma diameter of 22 μm, this gives a theoretical maximum of 411.09 stimulated PCs. Therefore, we estimate that with the current light fiber we stimulate 150–400 PCs.

Behavior was recorded at 100 Hz with an infrared camera. In order to detect movements caused by light-driven activation of PC ensembles, a custom-written twitch detection algorithm was used to extract twitch responses from a sequence of camera frames. First, the frame coinciding with the onset of the TTL pulse to the LED stimulation box was selected as a reference frame. This frame was de-noised using a median filter of 5-by-5 pixels. Then, 20 frames before and 80 frames after were analyzed by the algorithm (thus spanning a total length of 1010 ms, including the reference frame). The reference frame was subtracted from all frames in the analyzed sequence:

$$y_n = \left\| x_n - x_{ref} \right\|$$

where y_n is the resultant image at the n^{th} position of the processed image sequence, x_n the original image and x_{ref} the reference image. The resultant frames were then flattened to two separate 1-dimensional vectors representing both the vertically and horizontally summed difference values:

$$\hat{v}_n(q)_{vt} = \sum_{k=1}^{m} y_n(q,k)$$

$$\hat{v}_n(q)_{hz} = \sum_{k=1}^{p} y_n(q,k)$$

where v_{vt} and v_{hz} are the summed difference values taken vertically and horizontally, respectively; m and p are the width and height of the image (in pixels), respectively; and q is the position of the value in vector v, corresponding with either an image line or column. For the first 20 vectors in both dimensions, the standard deviation in values per position was determined. Based on these values, a weighting vector was constructed for both the vertical and horizontal dimension vectors:

$$\hat{w}_{\text{dim}} = \hat{\sigma}_{\text{dim}}^{-1}$$

where w is the weighting vector, *dim* denotes the dimension (vertical or horizontal) and σ is the vector containing standard deviations. The inner product of the weighting vectors and the summed difference value vectors were then used to get one mean change trace:

$$t_n = \frac{(\hat{w}_{vt} \cdot \hat{v}_{n,vt}) + (\hat{w}_{hz} \cdot \hat{v}_{n,hz})}{2}$$

where t_n is the trace value at index n. The mean and variance for the first 20 values of t were then determined. A deviation of more than four standard deviations from the mean as based on the first 20 values of t was counted as a twitch.

ACKNOWLEDGMENTS

The authors wish to thank J. Plugge for her expert technical assistance, F. Hoebeek for comments on previous versions of the manuscript and R. Nooij and D. Van der Werf for their excellent work in helping developing and producing the LED driver. This work was supported by the Dutch Organization for Medical Sciences (ZonMw; Chris I. De Zeeuw), Life Sciences (ALW; Chris I. De Zeeuw), Senter (Neuro-Basic), and ERC-adv, CEREBNET, and C7 programs of the EU (Chris I. De Zeeuw).

REFERENCES

Afshari, F. S., Ptak, K., Khaliq, Z. M., Grieco, T. M., Slater, N. T., McCrimmon, D. R., et al. (2004). Resurgent Na currents in four classes of neurons of the cerebellum. *J. Neurophysiol.* 92, 2831–2843. doi: 10.1152/jn.00261.2004

Aizenman, C. D., and Linden, D. J. (1999). Regulation of the rebound depolarization and spontaneous firing patterns of deep nuclear neurons in slices of rat cerebellum. *J. Neurophysiol.* 82, 1697–1709.

Alvina, K., Walter, J. T., Kohn, A., Ellis-Davies, G., and Khodakhah, K. (2008). Questioning the role of rebound firing in the cerebellum. *Nat. Neurosci.* 11, 1256–1258. doi: 10.1038/nn.2195

Aman, T. K., and Raman, I. M. (2007). Subunit dependence of Na channel slow inactivation and open channel block in cerebellar neurons. *Biophys. J.* 92, 1938–1951. doi: 10.1529/biophysj.106.093500

Angaut, P., and Sotelo, C. (1989). Synaptology of the cerebello-olivary pathway. Double labelling with anterograde axonal tracing and GABA immunocytochemistry in the rat. *Brain Res.* 479, 361–365. doi: 10.1016/0006-8993(89)91641-7

Badura, A., Schonewille, M., Voges, K., Galliano, E., Renier, N., Gao, Z., et al. (2013). Climbing fiber input shapes reciprocity of Purkinje cell firing. *Neuron.* 22, 700–713. doi: 10.1016/j.neuron.2013.03.018

Bell, C. C., and Grimm, R. J. (1969). Discharge properties of Purkinje cells recorded on single and double microelectrodes. *J. Neurophysiol.* 32, 1044–1055.

Bengtsson, F., Ekerot, C. F., and Jorntell, H. (2011). *In vivo* analysis of inhibitory synaptic inputs and rebounds in deep cerebellar nuclear neurons. *PLoS ONE* 6:e18822. doi: 10.1371/journal.pone.0018822

Bengtsson, F., Svensson, P., and Hesslow, G. (2004). Feedback control of Purkinje cell activity by the cerebello-olivary pathway. *Eur. J. Neurosci.* 20, 2999–3005. doi: 10.1111/j.1460-9568.2004.03789.x

Bentivoglio, M., and Kuypers, H. G. (1982). Divergent axon collaterals from rat cerebellar nuclei to diencephalon, mesencephalon, medulla oblongata and cervical cord. A fluorescent double retrograde labeling study. *Exp. Brain Res.* 46, 339–356.

Berndt, A., Schoenenberger, P., Mattis, J., Tye, K. M., Deisseroth, K., Hegemann, P., et al. (2011). High-efficiency channelrhodopsins for fast neuronal stimulation at low light levels. *Proc. Natl. Acad. Sci. U.S.A.* 108, 7595–7600. doi: 10.1073/pnas.1017210108

Bosman, L. W., Koekkoek, S. K., Shapiro, J., Rijken, B. F., Zandstra, F., van der Ende, B., et al. (2010). Encoding of whisker input by cerebellar Purkinje cells. *J. Physiol.* 588(Pt 19), 3757–3783. doi: 10.1113/jphysiol.2010.195180

Buisseret-Delmas, C., and Angaut, P. (1993). The cerebellar olivo-corticonuclear connections in the rat. *Prog. Neurobiol.* 40, 63–87. doi: 10.1016/0301-0082(93)90048-W

Catz, N., Dicke, P. W., and Thier, P. (2008). Cerebellar-dependent motor learning is based on pruning a Purkinje cell population response. *Proc. Natl. Acad. Sci. U.S.A.* 105, 7309–7314. doi: 10.1073/pnas.0706032105

de Solages, C., Szapiro, G., Brunel, N., Hakim, V., Isope, P., Buisseret, P., et al. (2008). High-frequency organization and synchrony of activity in the purkinje cell layer of

the cerebellum. *Neuron* 58, 775–788. doi: 10.1016/j.neuron.2008.05.008

De Zeeuw, C. I., Hoebeek, F. E., Bosman, L. W., Schonewille, M., Witter, L., and Koekkoek, S. K. (2011). Spatiotemporal firing patterns in the cerebellum. *Nat. Rev. Neurosci*. 12, 327–344. doi: 10.1038/nrn3011

De Zeeuw, C. I., Holstege, J. C., Calkoen, F., Ruigrok, T. J., and Voogd, J. (1988). A new combination of WGA-HRP anterograde tracing and GABA immunocytochemistry applied to afferents of the cat inferior olive at the ultrastructural level. *Brain Res*. 447, 369–375. doi: 10.1016/0006-8993(88)91142-0

De Zeeuw, C. I., Koekkoek, S. K., Wylie, D. R., and Simpson, J. I. (1997a). Association between dendritic lamellar bodies and complex spike synchrony in the olivocerebellar system. *J. Neurophysiol*. 77, 1747–1758.

De Zeeuw, C. I., van Alphen, A. M., Hawkins, R. K., and Ruigrok, T. J. (1997b). Climbing fibre collaterals contact neurons in the cerebellar nuclei that provide a GABAergic feedback to the inferior olive. *Neuroscience* 80, 981–986. doi: 10.1016/S0306-4522(97)00249-2

De Zeeuw, C. I., Wentzel, P., and Mugnaini, E. (1993). Fine structure of the dorsal cap of the inferior olive and its GABAergic and non-GABAergic input from the nucleus prepositus hypoglossi in rat and rabbit. *J. Comp. Neurol*. 327, 63–82. doi: 10.1002/cne.903270106

Eccles, J. C., Llinas, R., and Sasaki, K. (1964). Excitation of cerebellar Purkinje cells by the climbing fibers. *Nature* 203, 245–246.

Eccles, J. C., Llinas, R., and Sasaki, K. (1966). The excitatory synaptic action of climbing fibres on the purinje cells of the cerebellum. *J. Physiol*. 182, 268–296.

Ekerot, C. F., and Jorntell, H. (2001). Parallel fibre receptive fields of Purkinje cells and interneurons are climbing fibre-specific. *Eur. J. Neurosci*. 13, 1303–1310. doi: 10.1046/j.0953-816x.2001.01499.x

Engbers, J. D., Anderson, D., Tadayonnejad, R., Mehaffey, W. H., Molineux, M. L., and Turner, R. W. (2011). Distinct roles for I(T) and I(H) in controlling the frequency and timing of rebound spike responses. *J. Physiol.* 589(Pt 22), 5391–5413. doi: 10.1113/jphysiol.2011.215632

Fredette, B. J., and Mugnaini, E. (1991). The GABAergic cerebello-olivary projection in the rat. *Anat. Embryol. (Berl.)* 184, 225–243.

Fujikado, T., and Noda, H. (1987). Saccadic eye movements evoked by microstimulation of lobule VII of the cerebellar vermis of macaque monkeys. *J. Physiol*. 394, 573–594.

Garwicz, M. (2000). Micro-organisation of cerebellar modules controlling forelimb movements. *Prog. Brain Res*. 124, 187–199. doi: 10.1016/S0079-6123(00)24016-8

Gauck, V., Thomann, M., Jaeger, D., and Borst, A. (2001). Spatial distribution of low- and high-voltage-activated calcium currents in neurons of the deep cerebellar nuclei. *J. Neurosci*. 21, RC158.

Godschalk, M., Van der Burg, J., Van, D. B., and De Zeeuw, C. I. (1994). Topography of saccadic eye movements evoked by microstimulation in rabbit cerebellar vermis. *J. Physiol*. 480(Pt 1), 147–153.

Harvey, R. J., and Napper, R. M. (1991). Quantitative studies on the mammalian cerebellum. *Prog. Neurobiol.* 36, 437–463. doi: 10.1016/0301-0082(91)90012-P

Heck, D. H., Thach, W. T., and Keating, J. G. (2007). On-beam synchrony in the cerebellum as the mechanism for the timing and coordination of movement. *Proc. Natl. Acad. Sci. U.S.A*. 104, 7658–7663. doi: 10.1073/pnas.0609966104

Hoebeek, F. E., Witter, L., Ruigrok, T. J., and De Zeeuw, C. I. (2010). Differential olivo-cerebellar cortical control of rebound activity in the cerebellar nuclei. *Proc. Natl. Acad. Sci. U.S.A*. 107, 8410–8415. doi: 10.1073/pnas.0907118107

Ito, M. (1984). *The Cerebellum and Neural Control*. New York, NY: Raven Press.

Jacobson, G. A., Rokni, D., and Yarom, Y. (2008). A model of the olivo-cerebellar system as a temporal pattern generator. *Trends Neurosci*. 31, 617–625. doi: 10.1016/j.tins.2008.09.005

Jahnsen, H. (1986). Electrophysiological characteristics of neurones in the guinea-pig deep cerebellar nuclei *in vitro*. *J. Physiol*. 372, 129–147.

Jorntell, H., Ekerot, C., Garwicz, M., and Luo, X. L. (2000). Functional organization of climbing fibre projection to the cerebellar anterior lobe of the rat. *J. Physiol*. 522(Pt 2), 297–309. doi: 10.1111/j.1469-7793.2000.00297.x

Jorntell, H., and Ekerot, C. F. (2002). Reciprocal bidirectional plasticity of parallel fiber receptive fields in cerebellar Purkinje cells and their afferent interneurons. *Neuron* 34, 797–806.

Jorntell, H., and Ekerot, C. F. (2003). Receptive field plasticity profoundly alters the cutaneous parallel fiber synaptic input to cerebellar interneurons *in vivo*. *J. Neurosci*. 23, 9620–9631.

Lang, E. J., Sugihara, I., and Llinas, R. (1996). GABAergic modulation of complex spike activity by the cerebellar nucleoolivary pathway in rat. *J. Neurophysiol*. 76, 255–275.

Lang, E. J., Sugihara, I., Welsh, J. P., and Llinas, R. (1999). Patterns of spontaneous purkinje cell complex spike activity in the awake rat. *J. Neurosci*. 19, 2728–2739.

Latham, A., and Paul, D. H. (1971). Spontaneous activity of cerebellar Purkinje cells and their responses to impulses in climbing fibres. *J. Physiol*. 213, 135–156.

Levin, S. I., Khaliq, Z. M., Aman, T. K., Grieco, T. M., Kearney, J. A., Raman, I. M., et al. (2006). Impaired motor function in mice with cell-specific knockout of sodium channel Scn8a (NaV1.6) in cerebellar purkinje neurons and granule cells. *J. Neurophysiol*. 96, 785–793 doi: 10.1152/jn.01193.2005

Llinas, R., and Muhlethaler, M. (1988). Electrophysiology of guinea-pig cerebellar nuclear cells in the *in vitro* brain stem-cerebellar preparation. *J. Physiol*. 404, 241–258.

Llinas, R., and Sasaki, K. (1989). The functional organization of the olivo-cerebellar system as examined by multiple purkinje cell recordings. *Eur. J. Neurosci*. 1, 587–602.

Llinas, R., and Volkind, R. A. (1973). The olivo-cerebellar system: functional properties as revealed by harmaline-induced tremor. *Exp. Brain Res*. 18, 69–87.

Llinas, R., and Yarom, Y. (1986). Oscillatory properties of guinea-pig inferior olivary neurones and their pharmacological modulation: an *in vitro* study. *J. Physiol*. 376, 163–182.

Loewenstein, Y., Mahon, S., Chadderton, P., Kitamura, K., Sompolinsky, H., Yarom, Y., et al. (2005). Bistability of cerebellar Purkinje cells modulated by sensory stimulation. *Nat. Neurosci*. 8, 202–211. doi: 10.1038/nn1393

Luthman, J., Hoebeek, F. E., Maex, R., Davey, N., Adams, R., De Zeeuw, C. I., et al. (2011). STD-dependent and independent encoding of input irregularity as spike rate in a computational model of a cerebellar nucleus neuron. *Cerebellum* 10, 667–682. doi: 10.1007/s12311-011-0295-9

Madisen, L., Mao, T., Koch, H., Zhuo, J. M., Berenyi, A., Fujisawa, S., et al. (2012). A toolbox of Cre-dependent optogenetic transgenic mice for light-induced activation and silencing. *Nat. Neurosci*. 15, 793–802. doi: 10.1038/nn.3078

Marshall, L., and Born, J. (2007). The contribution of sleep to hippocampus-dependent memory consolidation. *Trends Cogn. Sci*. 11, 442–450. doi: 10.1016/j.tics.2007.09.001

Mathews, P. J., Lee, K. H., Peng, Z., Houser, C. R., and Otis, T. S. (2012). Effects of climbing fiber driven inhibition on Purkinje neuron spiking. *J. Neurosci*. 32, 17988–17997. doi: 10.1523/JNEUROSCI.3916-12.2012

Meeren, H. K., Van Luijtelaar, E. L., and Coenen, A. M. (1998). Cortical and thalamic visual evoked potentials during sleep-wake states and spike-wave discharges in the rat. *Electroencephalogr. Clin. Neurophysiol*. 108, 306–319.

Molineux, M. L., McRory, J. E., McKay, B. E., Hamid, J., Mehaffey, W. H., Rehak, R., et al. (2006). Specific T-type calcium channel isoforms are associated with distinct burst phenotypes in deep cerebellar nuclear neurons. *Proc. Natl. Acad. Sci. U.S.A*. 103, 5555–5560. doi: 10.1073/pnas.0601261103

Molineux, M. L., Mehaffey, W. H., Tadayonnejad, R., Anderson, D., Tennent, A. F., and Turner, R. W. (2008). Ionic factors governing rebound burst phenotype in rat deep cerebellar neurons. *J. Neurophysiol*. 100, 2684–2701. doi: 10.1152/jn.90427.2008

Nelson, A. B., Krispel, C. M., Sekirnjak, C., and du Lac, S. (2003). Long-lasting increases in intrinsic excitability triggered by inhibition. *Neuron* 40, 609–620.

Noda, H., and Fujikado, T. (1987). Involvement of Purkinje cells in evoking saccadic eye movements by microstimulation of the posterior cerebellar vermis of monkeys. *J. Neurophysiol*. 57, 1247–1261.

Oberdick, J., Smeyne, R. J., Mann, J. R., Zackson, S., Morgan, J. I. (1990). A promoter that drives transgene expression in cerebellar Purkinje and retinal bipolar neurons. *Science* 248, 223–226. doi: 10.1126/science.2109351

Oldfield, C. S., Marty, A., and Stell, B. M. (2010). Interneurons of the cerebellar cortex toggle Purkinje cells between up and down states. *Proc. Natl. Acad. Sci.*

U.S.A. 107, 13153–13158. doi: 10.1073/pnas.1002082107

Ozden, I., Sullivan, M. R., Lee, H. M., and Wang, S. S. (2009). Reliable coding emerges from coactivation of climbing fibers in microbands of cerebellar Purkinje neurons. *J. Neurosci*. 29, 10463–10473. doi: 10.1523/JNEUROSCI.0967-09.2009

Palay, S. L., and Chan-Palay, V. (1974). *Cerebellar Cortex: Cytology and Organization*. Berlin: Springer.

Palkovits, M., Mezey, E., Hamori, J., and Szentagothai, J. (1977). Quantitative histological analysis of the cerebellar nuclei in the cat. I. Numerical data on cells and on synapses. *Exp. Brain Res*. 28, 189–209.

Pedroarena, C. M., and Schwarz, C. (2003). Efficacy and short-term plasticity at GABAergic synapses between Purkinje and cerebellar nuclei neurons. *J. Neurophysiol*. 89, 704–715. doi: 10.1152/jn.00558.2002

Person, A. L., and Raman, I. M. (2012a). Purkinje neuron synchrony elicits time-locked spiking in the cerebellar nuclei. *Nature* 481, 502–505. doi: 10.1038/nature10732

Person, A. L., and Raman, I. M. (2012b). Synchrony and neural coding in cerebellar circuits. *Front. Neural Circuits* 6:97 doi: 10.3389/fncir.2012.00097

Provini, L., Redman, S., and Strata, P. (1968). Mossy and climbing fibre organization on the anterior lobe of the cerebellum activated by forelimb and hindlimb areas of the sensorimotor cortex. *Exp. Brain Res*. 6, 216–233.

Pugh, J. R., and Raman, I. M. (2006). Potentiation of mossy fiber EPSCs in the cerebellar nuclei by NMDA receptor activation followed by postinhibitory rebound current. *Neuron* 51, 113–123. doi: 10.1016/j.neuron.2006.05.021

Raman, I. M., and Bean, B. P. (1997). Resurgent sodium current and action potential formation in dissociated cerebellar Purkinje neurons. *J. Neurosci*. 17, 4517–4526.

Rasmussen, A., Jirenhed, D. A., and Hesslow, G. (2008). Simple and complex spike firing patterns in Purkinje cells during classical conditioning. *Cerebellum* 7, 563–566. doi: 10.1007/s12311-008-0068-2

Robertson, L. T. (1984). Topographic features of climbing fiber input in the rostral vermal cortex of the cat cerebellum. *Exp. Brain Res*. 55, 445–454.

Ruigrok, T. J., and Voogd, J. (1990). Cerebellar nucleo-olivary projections in the rat: an anterograde tracing study with *Phaseolus vulgaris*-leucoagglutinin (PHA-L). *J. Comp. Neurol*. 298, 315–333. doi: 10.1002/cne.902980305

Ruigrok, T. J., and Voogd, J. (2000). Organization of projections from the inferior olive to the cerebellar nuclei in the rat. *J. Comp. Neurol*. 426, 209–228. doi: 10.1002/1096-9861(20001016)426:2<209::AID-CNE4>3.0.CO;2-0

Sasaki, K., Bower, J. M., and Llinas, R. (1989). Multiple Purkinje cell recording in rodent cerebellar cortex. *Eur. J. Neurosci*. 1, 572–586.

Schonewille, M., Khosrovani, S., Winkelman, B. H., Hoebeek, F. E., De Jeu, M. T., Larsen, I. M., et al. (2006). Purkinje cells in awake behaving animals operate at the upstate membrane potential. *Nat. Neurosci*. 9, 459–461. doi: 10.1038/nn0406-459

Schultz, S. R., Kitamura, K., Post-Uiterweer, A., Krupic, J., and Hausser, M. (2009). Spatial pattern coding of sensory information by climbing fiber-evoked calcium signals in networks of neighboring cerebellar Purkinje cells. *J. Neurosci*. 29, 8005–8015. doi: 10.1523/JNEUROSCI.4919-08.2009

Sjolund, B., Bjorklund, A., and Wiklund, L. (1977). The indolaminergic innervation of the inferior olive. 2. Relation to harmaline induced tremor. *Brain Res*. 131, 23–37. doi: 10.1016/0006-8993(77)90026-9

Stark, E., Koos, T., and Buzsaki, G. (2012). Diode probes for spatiotemporal optical control of multiple neurons in freely moving animals. *J. Neurophysiol*. 108, 349–363. doi: 10.1152/jn.00153.2012

Steuber, V., Schultheiss, N. W., Silver, R. A., De, S. E., and Jaeger, D. (2011). Determinants of synaptic integration and heterogeneity in rebound firing explored with data-driven models of deep cerebellar nucleus cells. *J. Comput. Neurosci*. 30, 633–658. doi: 10.1007/s10827-010-0282-z

Stratton, S. E., and Lorden, J. F. (1991). Effect of harmaline on cells of the inferior olive in the absence of tremor: differential response of genetically dystonic and harmaline-tolerant rats. *Neuroscience* 41, 543–549. doi: 10.1016/0306-4522(91)90347-Q

Szapiro, G., and Barbour, B. (2007). Multiple climbing fibers signal to molecular layer interneurons exclusively via glutamate spillover. *Nat. Neurosci*. 10, 735–742. doi: 10.1038/nn1907

Tadayonnejad, R., Anderson, D., Molineux, M. L., Mehaffey, W. H., Jayasuriya, K., and Turner, R. W. (2010). Rebound discharge in deep cerebellar nuclear neurons *in vitro*. *Cerebellum*. 9, 352–374. doi: 10.1007/s12311-010-0168-7

Telgkamp, P., and Raman, I. M. (2002). Depression of inhibitory synaptic transmission between Purkinje cells and neurons of the cerebellar nuclei. *J. Neurosci*. 22, 8447–8457.

Teune, T. M., Van der Burg, J., van der Moer, J., Voogd, J., and Ruigrok, T. J. (2000). Topography of cerebellar nuclear projections to the brain stem in the rat. *Prog. Brain Res*. 124, 141–172. doi: 10.1016/S0079-6123(00)24014-4

Uusisaari, M., Obata, K., and Knopfel, T. (2007). Morphological and electrophysiological properties of GABAergic and non-GABAergic cells in the deep cerebellar nuclei. *J. Neurophysiol*. 97, 901–911. doi: 10.1152/jn.00974.2006

Van Der Giessen, R. S., Koekkoek, S. K., van Dorp, S., de Gruijl, J. R., Cupido, A., Khosrovani, S., et al. (2008). Role of olivary electrical coupling in cerebellar motor learning. *Neuron* 58, 599–612. doi: 10.1016/j.neuron.2008.03.016

Van der Want, J. J., Wiklund, L., Guegan, M., Ruigrok, T., and Voogd, J. (1989). Anterograde tracing of the rat olivocerebellar system with *Phaseolus vulgaris* leucoagglutinin (PHA-L). Demonstration of climbing fiber collateral innervation of the cerebellar nuclei. *J. Comp. Neurol*. 288, 1–18. doi: 10.1002/cne.902880102

Voogd, J., and Ruigrok, T. J. (1997). Transverse and longitudinal patterns in the mammalian cerebellum. *Prog. Brain Res*. 114, 21–37.

Walter, J. T., Alvina, K., Womack, M. D., Chevez, C., and Khodakhah, K. (2006). Decreases in the precision of Purkinje cell pacemaking cause cerebellar dysfunction and ataxia. *Nat. Neurosci*. 9, 389–397. doi: 10.1038/nn1648

Welsh, J. P., Lang, E. J., Suglhara, I., and Llinas, R. (1995). Dynamic organization of motor control within the olivocerebellar system. *Nature* 374, 453–457. doi: 10.1038/374453a0

Wise, A. K., Cerminara, N. L., Marple-Horvat, D. E., and Apps, R. (2010). Mechanisms of synchronous activity in cerebellar Purkinje cells. *J. Physiol*. 588(Pt 13), 2373–2390. doi: 10.1113/jphysiol.2010.189704

Witter, L., De Zeeuw, C. I., Ruigrok, T. J., and Hoebeek, F. E. (2011a). The cerebellar nuclei take center stage. *Cerebellum* 10, 633–636. doi: 10.1007/s12311-010-0245-y

Witter, L., Ozcelik, S., and De Zeeuw, C. I. (2011b). "Clustering of neuronal subtypes in the cerebellar nuclei," in *Poster Presented at the Society for Neuroscience 2011* (Washington, DC).

Yizhar, O., Fenno, L. E., Davidson, T. J., Mogri, M., and Deisseroth, K. (2011). Optogenetics in neural systems. *Neuron* 71, 9–34. doi: 10.1016/j.neuron.2011.06.004

Zheng, N., and Raman, I. M. (2009). Ca currents activated by spontaneous firing and synaptic disinhibition in neurons of the cerebellar nuclei. *J. Neurosci*. 29, 9826–9838. doi: 10.1523/JNEUROSCI.2069-09.2009

Conflict of Interest Statement: The authors declare that the research was conducted in the absence of any commercial or financial relationships that could be construed as a potential conflict of interest.

Received: 13 June 2013; accepted: 26 July 2013; published online: 21 August 2013.
Citation: Witter L, Canto CB, Hoogland TM, de Gruijl JR and De Zeeuw CI (2013) Strength and timing of motor responses mediated by rebound firing in the cerebellar nuclei after Purkinje cell activation. Front. Neural Circuits 7:133. doi: 10.3389/fncir.2013.00133
This article was submitted to the journal Frontiers in Neural Circuits.

frontiers in
NEURAL CIRCUITS

REVIEW ARTICLE
published: 28 January 2014
doi: 10.3389/fncir.2013.00096

The olivo-cerebellar system: a key to understanding the functional significance of intrinsic oscillatory brain properties

Rodolfo R. Llinás*

Department of Physiology and Neuroscience, New York University School of Medicine, New York, NY, USA

Edited by:
Egidio D'Angelo, University of Pavia, Italy

Reviewed by:
Egidio D'Angelo, University of Pavia, Italy
Chris I. De Zeeuw, Erasmus MC Rotterdam and Royal Dutch Academy of Arts and Sciences, Netherlands

****Correspondence:***
Rodolfo R. Llinás, Department of Physiology and Neuroscience, New York University School of Medicine, 550 1st Ave., New York, NY 10016, USA
e-mail: rodolfo.llinás@med.nyu.edu

The reflexological view of brain function (Sherrington, 1906) has played a crucial role in defining both the nature of connectivity and the role of the synaptic interactions among neuronal circuits. One implicit assumption of this view, however, has been that CNS function is fundamentally driven by sensory input. This view was questioned as early as the beginning of the last century when a possible role for intrinsic activity in CNS function was proposed by Thomas Graham Brow (Brown, 1911, 1914). However, little progress was made in addressing intrinsic neuronal properties in vertebrates until the discovery of calcium conductances in vertebrate central neurons leading dendritic electroresponsiveness (Llinás and Hess, 1976; Llinás and Sugimori, 1980a,b) and subthreshold neuronal oscillation in mammalian inferior olive (IO) neurons (Llinás and Yarom, 1981a,b). This happened in parallel with a similar set of findings concerning invertebrate neuronal system (Marder and Bucher, 2001). The generalization into a more global view of intrinsic rhythmicity, at forebrain level, occurred initially with the demonstration that the thalamus has similar oscillatory properties (Llinás and Jahnsen, 1982) and the ionic properties responsible for some oscillatory activity were, in fact, similar to those in the IO (Jahnsen and Llinás, 1984; Llinás, 1988). Thus, lending support to the view that not only motricity, but cognitive properties, are organized as coherent oscillatory states (Pare et al., 1992; Singer, 1993; Hardcastle, 1997; Llinás et al., 1998; Varela et al., 2001).

Keywords: intrinsic oscillatory, olivo-cerebellar, electrophysiology, IO neurons, PO neuron oscillation

INTRODUCTION

The reflexological view of brain function (Sherrington, 1906) has played a crucial role in defining both the nature of connectivity and the role of the synaptic interactions among neuronal circuits. One implicit assumption of this view, however, has been that CNS function is fundamentally driven by sensory input.

This view was questioned as early as the beginning of the last century when Thomas Graham Brown proposed a possible role for intrinsic activity in CNS function (Brown, 1911, 1914). However, little progress was made in addressing intrinsic neuronal properties in vertebrates until the discovery of calcium conductances in vertebrate central neurons leading dendritic electroresponsiveness (Llinás and Hess, 1976; Llinás and Sugimori, 1980a,b) and subthreshold neuronal oscillation in mammalian inferior olive (IO) neurons (Llinás and Yarom, 1981a,b). This happened in parallel with a similar set of findings concerning invertebrate neuronal system (Marder and Bucher, 2001). The generalization into a more global view of intrinsic rhythmicity at forebrain level occurred initially with the demonstration that the thalamus has similar oscillatory properties (Llinás and Jahnsen, 1982) and the ionic properties responsible for some oscillatory activity were, in fact, similar to those in the IO (Jahnsen and Llinás, 1984; Llinás, 1988). Thus, lending support to the view that not only motricity, but also cognitive properties, are organized as coherent oscillatory states (Pare et al., 1992; Singer, 1993; Hardcastle, 1997; Llinás et al., 1998; Varela et al., 2001).

Concerning the functional significance of IO intrinsic properties two main issues should be addressed; (1) the predictive aspects movement intentionality and its translation into motor strategy and tactics and (2) the timing of motor execution. In reviewing the global properties of IO function I will briefly address general anatomy and electrophysiology of IO nucleus and it neurons.

GENERAL IO ANATOMY

The olivocerebellar system is one of the most conserved in the vertebrate brain, being present in all such forms studied (Ariens-Kappers et al., 1936). It comprises a set of bilaterally symmetrical inferior olivary nuclei (IO) and the overlaying cerebellum. These two structures are mutually linked through axonal pathways within the cerebellar peduncles. Some IO neurons have spherical dendritic trees (**Figure 1C**). Their axons traverse the midline at the bulbar region (**Figure 1A**, orange), course up the contralateral cerebellar peduncle, and enter the cerebellar white matter. From there branches establish excitatory synaptic contacts with the cerebellar nuclear neurons (**Figure 1A** green and purple) while the axons proceed into the cerebellar cortex to establish the most powerful synaptic contact in the brain the so called climbing fiber

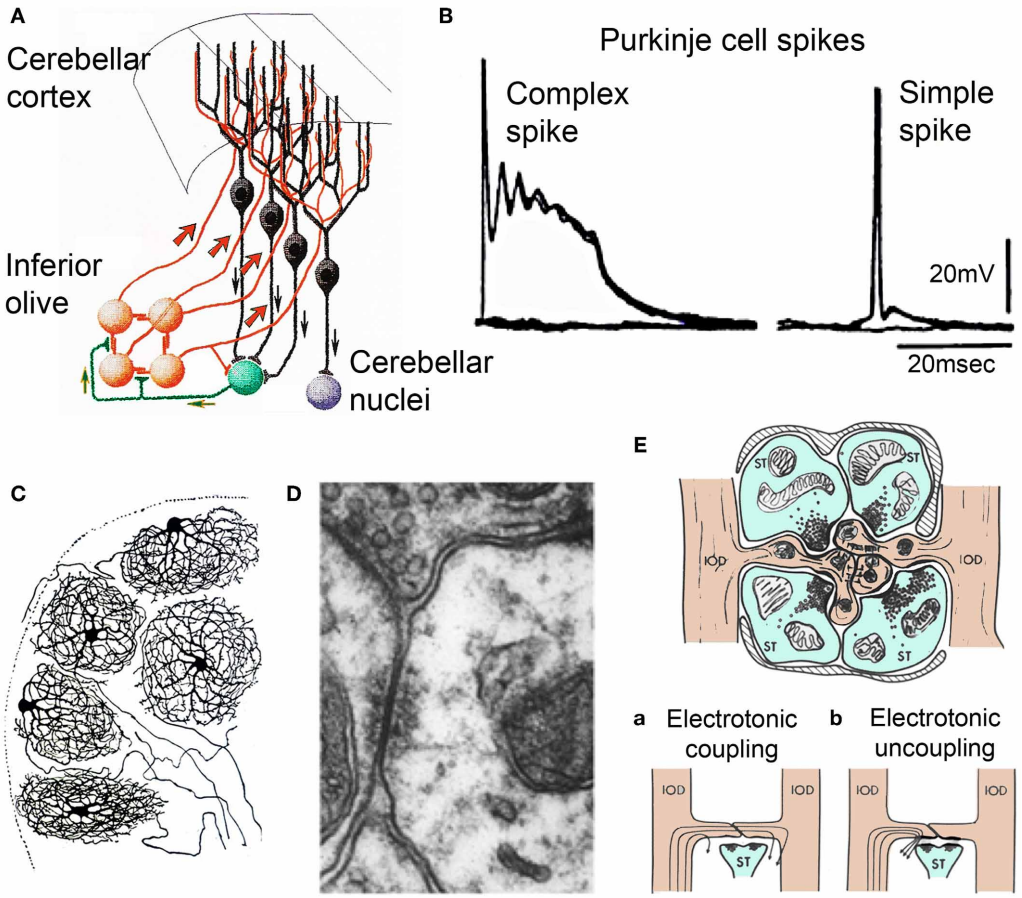

FIGURE 1 | Olivocerebellar circuit. (A) Cerebellar cortex. Inferior olive axons (IO, orange) activate Purkinje cells (black) through the climbing fibers and send collaterals to cerebellar nuclear cells (green) that feed back to IO and projection cerebellar nuclear cells (purple) (After Ramon y Cajal, 1911). **(B)** Intracellular recordings of an-all or-none complex spike elicited by climbing fiber stimulation and a simple spike elicited by mossy fiber activation. **(C)** Inferior olivary neurons (Ramon y Cajal, 1911). Note the spherical dendritic trees. **(D)** Electronmicrograph showing gap junction between spines of IO dendrites within IO glomerulus. Modified from Llinás et al. (1974). **(E)** Diagram of IO glomerulus. The center shows spines from IO dendrites (IODs) coupled by gap junctions. (a) coupling current path between IO dendrites, (b) current flow shunted when gabaergic synapses are active at the gap junction. (Modified from Llinás, 1974).

Purkinje cell synapse (Ramon y Cajal, 1911) (**Figure 1A**, black). This synapse is a one-to-one chemical junction and is all of IO origin, exclusively (Szentagothai and Rajkovits, 1959). This input establishing hundreds of junctions with the large spines in the main branches of the Purkinje cell dendritic tree. Activation of a climbing fiber elicits an all-or-none excitatory response in the Purkinje cells (Eccles et al., 1965, 1966a,b,c) (**Figure 1B**, left trace) later named a "complex spike," (Thach, 1968) as opposed to the simple spike produced by parallel fiber activation (**Figure 1B**, right trace). There are about ten times more PCs than IO neurons and so each IO neuron generates an average of ten climbing fibers (Armstrong and Schild, 1970). The PC axons, the only output of the cerebellar cortex, terminate in the cerebellar and related vestibular nuclei where they form inhibitory synapses (Ito and Yoshida, 1966) (**Figure 1A**). Cerebellar nuclei neurons are the only output of the cerebellum.

Concerning the cerebellar nucleus neurons they exist in two varieties with about half being excitatory and the other half inhibitory. The excitatory variety innervates brain stem, thalamus, and spinal cord via direct and indirect pathways. The inhibitory neurons return, in their entirety, to the centro-lateral IO where they form synapses in structures called "glomeruli" (**Figure 1E**) as well as with the dendritic tree directly (Sotelo et al., 1986; de Zeeuw et al., 1990a; Fredette and Mugnaini, 1991; Medina et al., 2002). Each IO glomerulus contains five to eight spines from dendrites of different IO neurons and support IO electrotonic coupling via gap junctions (Llinás, 1974; Llinás et al., 1974; Sotelo et al., 1974; de Zeeuw et al., 1990b) (**Figure 1D**). The degree of coupling is, thus, dynamically modulated by the inhibitory synaptic shunting (**Figure 1E**) (Llinás, 1974; Lang et al., 1996) as a feed back from the cerebellar nuclear output (de Zeeuw et al., 1990a, 1996).

TIMING P ROPE R TIES OF THE OLIVOCEREBELLAR SYSTEM

MOTOR COORDINATION AND TIMING

Concerning motor coordination and timing three general issues are evident in the electrophysiology of the olivocerebellar system. (1) The system generates a timing signal that is inscribed in the

intrinsic electrical properties of single IO (**Figures 2–4**) and cerebellar nuclear (**Figure 5**) neurons, (2) the organization of the nucleus via electrical coupling allows for synchronous multicellular temporal coherence that generates a close to simultaneous neuronal cluster activation (**Figures 6**, **7**), and (3) due to the remarkable property of conduction isochronicity (**Figure 8**) the timing signal does not disperse against distance as it is conducted along the pathways carrying it to the final integration sites at cerebellar nuclear level. Each of these issues will be considered in turn.

SINGLE CELL ELECTROPHYSIOLOGY

With the exception described below, concerning two types of IO neurons, most of the olivocerebellar has been known to generate synchronous rhythmic activity attributed to the intrinsic oscillatory properties of the IO neurons (Llinás and Yarom, 1981a,b; Benardo and Foster, 1986; Bal and McCormick, 1997) and their multicellular synchrony supported by their electrotonic coupling (Llinás, 1974; Sotelo et al., 1974; Llinás and Yarom, 1981a,b; Lampl and Yarom, 1997; Makarenko and Llinás, 1998; Yarom and Cohen, 2002). Recently, asynchronous release of GABA has been reported to determine an inhibitory regulation of electrical coupling of neurons in the IO (Best and Regehr, 2009).

Such intrinsic oscillatory properties are supported by a set of voltage-dependent calcium and potassium conductances (in addition to those involved in action potential generation) enabling IO cells to oscillate and fire rhythmically at 1–10 Hz. These conductances include a high-threshold Ca2+ conductance, a low-threshold Ca2+ conductance, a Ca2+-activated K+ conductance, and a hyperpolarization-activated cationic conductance (Llinás and Yarom, 1981a,b, 1986; Bal and McCormick, 1997). There is as mentioned above, a separate group of IO neurons with quite different electrical properties.

Two basic IO neuron types

An important, but often forgotten, aspect of IO function is the fundamental differences between two parts of the olive, what may be called the principal olive (PO) represented by the three main nuclei (lateral medial and central) and the Dorsal Cap of Kooy (DCK). Morphologically PO neurons are characterized by a spherical dendritic tree (**Figure 1C**) while the dendrites of DCK neurons have a bipolar-like arrangement that extended farther away from the soma (Urbano et al., 2006). The two different morphological type neurons present in the IO are also electrophysiologically distinct.

The PO comprises most of the IO neurons, are concerned with limb and digit movements and to the so-called "physiological tremor" i.e., the non-continuous nature of motor organization (Llinás, 1991; Welsh and Llinás, 1997). This tremor supports the timing of motor execution in all systems other than the oculomotor. The functional character of PO neurons can be easily observed by measuring, for instance, the velocity of voluntary human finger movements (Vallbo and Wessberg, 1993) that occur at a close to constant of 8–10 Hz steps independently of movement speed. Synchronous IO oscillations have been shown to modulate periodic vibrissal movements (Lang et al., 2006) in the same frequency range. Electrophysiologically, such IO neurons are characterized by their ability to generate high-threshold **Figure 2A** and "low-threshold" calcium spike as recorded *in vitro* **Figure 2B** (Llinás and Yarom, 1981a,b). The latter is generated by the activation of both T-type calcium channels (Cav3.1) and Ih potassium currents (Llinás and Yarom, 1981a,b, 1986; Bal and McCormick, 1997; Lampl and Yarom, 1997), which limits their frequency to 8–10 Hz. PO neurons are characterized by subthreshold oscillations at 8–10 Hz that are very stable (**Figure 2C**). *In vivo* intracellular recordings from IO neurons have shown transient subthreshold oscillations at 6–12 Hz with spikes generated on the depolarization phase of the oscillations (Chorev et al., 2007). A single action potential in the IO triggers a burst of axonic spikes. The properties of the spike burst are modulated by the phase (Mathy et al., 2009) and or amplitude (Bazzigaluppi et al., 2012) of the subthreshold oscillations.

The DCK is a smaller nucleus that is involved with the organization of eye movements. These neurons lack both T-type calcium

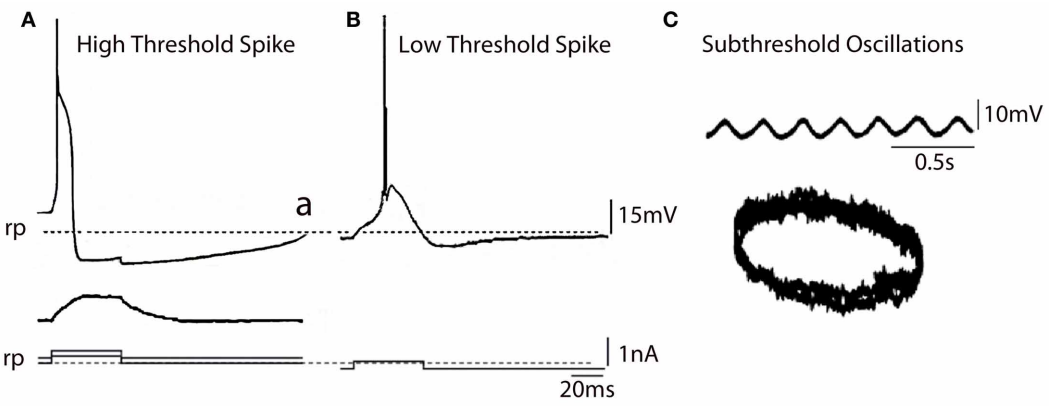

FIGURE 2 | IO Electrophysiology. (A) *In vitro* intracellular recordings from IO neuron showing high threshold spike (a) activated by an outward pulse from a depolarized potential with respect to rest (broken line) the same outward pulse delivered from the rest potential (broken line) did not elicit a spike (b). **(B)** Same pulse as in **(A)** delivered from a hyperpolarized membrane potential level generated a low voltage activate spike (Modified from Llinás and Yarom, 1981a,b). **(C)** Subthreshold membrane oscillation recorded intracellularly from an IO neuron and associated *Lissajeux* image demonstrating oscillatory stability. (Modified from Llinás and Yarom, 1986). rp, resting potential.

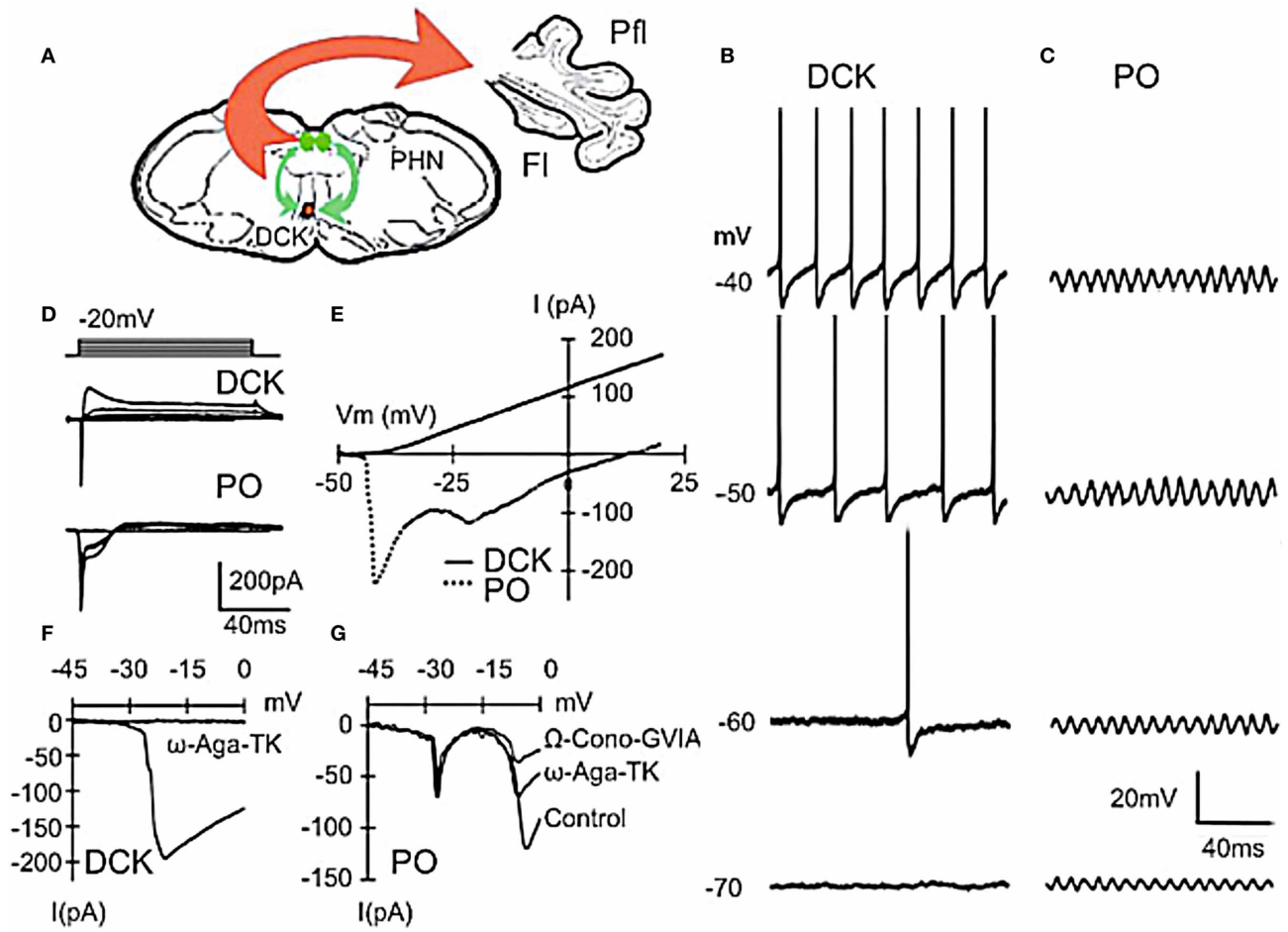

FIGURE 3 | Differences between principal olive (PO) and Dorsal cap of Kooy (DCK) neurons. (A) Drawing If brain slice showing climbing fiber projection (red) of DCK neurons to the contralateral cerebellar flocculus, and afferent GABAergic input (green) to the DCK from the bilateral prepositus hypoglossi nuclei. **(B–D)** Effect of membrane potential on DCK and PO firing (in same slice). **(B)** Recordings from DCK neuron showing increased firing frequency with membrane potential. Each action potential is followed by a large, long-lasting afterhyperpolarization. (Action potentials were truncated and recorded with a high-potassium intracellular solution) **(C)** Patch recordings from a PO neuron showing subthreshold oscillations at the same membrane potentials as in **(A)** Amplitude increased, but frequency was unchanged. **(D)** Representative currents in DCK and PO neurons (in response to 100-ms depolarizing square pulses recorded by using a high-potassium electrode solution). Inward currents were followed by a small outward current in PO neurons while the same depolarizing square pulses activated a strong outward current in DCK neurons. **(E)** I–V curve for cells in panel **(D)**. **(F)** DCK neurons had a single current peak near a membrane potential of −20 mV that was blocked by ω-Agatoxin-TK (a specific P/Q calcium channel blocker). **(G)** In the PO cells, two inward components, peaking near −20 and −10 mV were seen. The second component was reduced by application of ω-Agatoxin-TK and further reduced by application of ω-Conotoxin-GVIA (a specific N-type calcium channel blocker). Thus, the inward calcium currents of DCK neurons were mediated only by P/Q-type channels, while both P/Q-type and N-type channels are present in PO neurons. Fl, flocc; Pfl, paraflocculus; PHN, prepositus hypoglossi nuclei. (Modified from Urbano et al., 2006).

channels and the Ih potassium current (Urbano et al., 2006) underlying the intrinsic subthreshold oscillation characteristics of PO neurons and so do not display subthreshold oscillatory behavior. They are, however, electrotonically coupled, but only to each other, shunning contacts with their oscillatory counterpart (Urbano et al., 2006). These fundamental differences go a long way toward addressing the apparent functional inconsistencies that have plagued the field of cerebellar motor control and, more importantly, give further support to the findings concerning the time binding proposal for non-ocular motricity (Carpenter, 1977; Farmer, 1998; Llinás, 2009).

Because DKC Neurons do not oscillate one of the arguments often voiced against the timing hypothesis of IO function has related to the absence of the physiological tremor in the oculomotor system (Carpenter, 1977). Thus, as stated above, while physiological tremor is observed in somatomotor systems (Llinás, 1991; Vallbo and Wessberg, 1993; Lang et al., 2006), where it has been shown to play an important role in motor binding by providing coherent activation of the motoneuronal pools responsible for motor execution, such physiological tremor is conspicuously absent in ocular motricity. Indeed, it has been known for many years now (Carpenter, 1977) that the oculomotor system

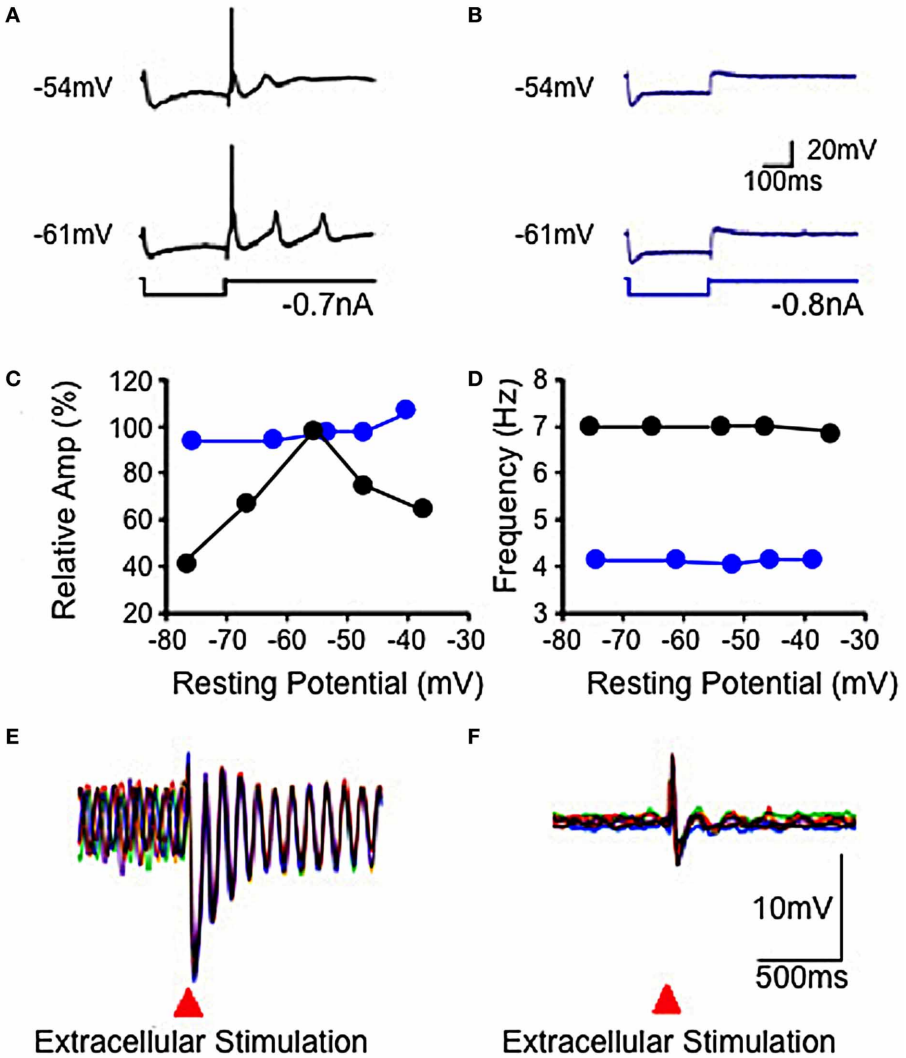

FIGURE 4 | Electrophysiological properties of IO in wild-type and mutant mice. (A,B) Hyperpolarizing current injection elicited a low threshold spike from IO cell in slice from wild-type mouse **(A)**, but not from mutant mouse **(B)** at resting potentials of −54 and −61 mV. Subthreshold rebound mediated by Ih was present in the mutant mouse. **(C)** Plot showing modulation of subthreshold sinusoidal oscillation (SSTO) amplitude by membrane potential in wild-type (black) but not in mutant (blue) mice. **(D)** Frequency of SSTO was lower in mutant than in wild-type mice but neither was modulated by membrane potential. **(E,F)** Superposition of six traces showing SSTO recorded from single IO neuron in wild-type **(E)** or mutant **(F)** mouse. Extracellular stimulation lead to phase reset of SSTO in IO cell in slice from the wild-type mouse. Such stimulation had a minor, if any, effect in the mutant mouse **(F)**. (Modified from Choi et al., 2010).

is capable of both smooth pursuit (an object is followed on a moving trajectory) and saccadic eye movements (the eye position is quickly reset having reached maximal displacement from its central orbital position).

The findings of a recent study comparing the electrophysiological properties of PO and DCK neurons helps explain the discrepancies observed between somato-motor and oculomotor cerebellar control (**Figure 3**). DCK neurons, identified using Biocytin during patch recordings (Urbano et al., 2006), responded differently to current injection than do PO cells. They did not present an h-current- dependent "depolarizing sag" during hyperpolarization and the T-current-dependent rebound of membrane potential was absent. When depolarized, DCK fired at a much higher frequency than PO neurons. The average frequency of DCK firing could reach gamma-band frequencies (>30 Hz) while PO neurons only reached theta-band range (4–8 Hz). The same frequency range of membrane potential events was observed using voltage sensitive dye imaging. We stained transversal slices using the voltage-sensitive dye di-4ANEPPS and used a bipolar electrode to deliver a pair of stimuli (50 Hz, 2 shocks of 200 μs of duration) at the edge of the DCK nucleus. After such stimulation the entire DCK nucleus depolarized rhythmically with peaks of activity every 1.5 s.

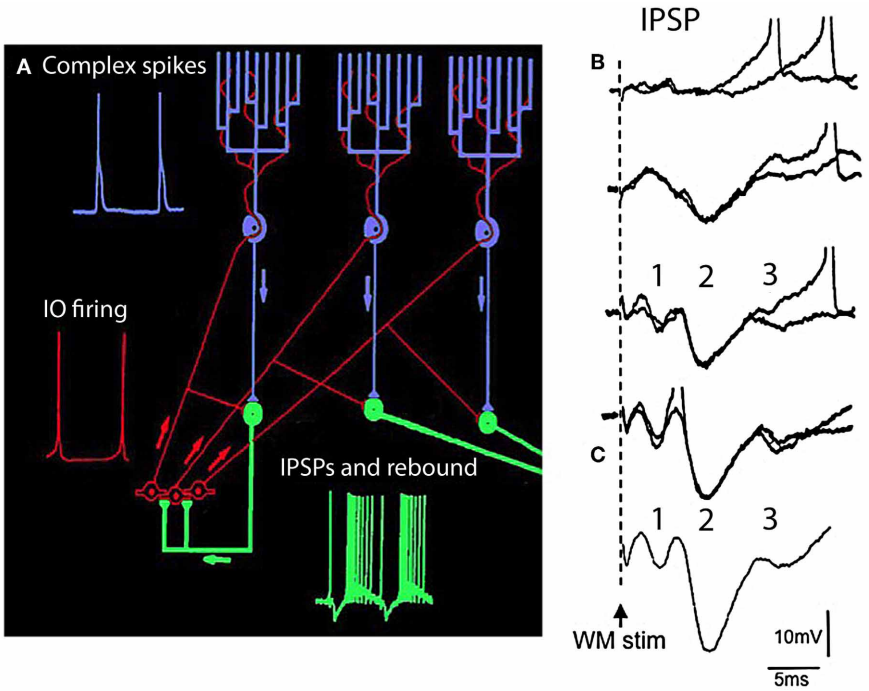

FIGURE 5 | The olivocerebellar loop circuit. (A) Diagram of olivocerebellar circuit. Action potentials in IO neurons (red) are generated at the crest of the subthreshold oscillations; example of subthreshold oscillations is shown in **Figure 2C**. These elicit complex spikes in Purkinje cells (green) and activate cerebellar nuclear cells (purple and yellow). Purkinje cell output is inhibitory to cerebellar nuclear cells where the IPSPs trigger rebound firing in cerebellar nuclear cells. Arrows indicate direction of action potential conduction. **(B,C)** Synaptic potentials and firing of cerebellar nuclear cells. White matter stimulation (WM stim) at increasing stimulus strength elicits graded EPSP-IPSP sequences. The first sequence (1) is due to direct stimulation of mossy fiber collaterals (EPSP) and Purkinje cell axons (IPSP). The second sequence is due to activation of the climbing fiber system (2) the Purkinje cell IPSP was strong enough to activate the rebound response (3 and spikes). **(C)** Average of 10 responses showing the timing of the EPSP-IPSP sequences. (Modified from Llinás and Muhlethaler, 1988).

PO Neuron Oscillation are Dynamically Regulated by P/Q-Type and T-Type Calcium Channels

Concerning mechanisms responsible for membrane potential oscillation in PO neurons, one of the remarkable properties is the set of ionic conductances that generate such electrical activity. Thus, the electrophysiological properties of IO neurons have recently been investigated using knock out (KO) mice that lacked the gene for the pore-forming α1G subunit of the T-type calcium channel ($CaV3.1^{-/-}$) and their littermate wild type (WT) mice (Choi et al., 2010). The low-threshold calcium spike and the sustained endogenous oscillation following rebound potentials were absent in IO neurons from $CaV3.1^{-/-}$ mice.

In addition to spikes, PO neurons support spontaneous subthreshold membrane potential oscillations near 10 Hz (see **Figure 2C**) (Benardo and Foster, 1986; Llinás and Yarom, 1986). It has been proposed that calcium current and calcium-activated potassium current may be account for the oscillatory behaviors of IO neurons (Llinás and Yarom, 1981a,b, 1986). The other group of mice lacked the gene for the pore-forming α1G subunit of the T-type calcium channel ($CaV3.1^{-/-}$). In these mice the LTS, activated as a rebound from a hyperpolarizing square current pulse, was absent (compare **Figures 4A,B**) but the HTS was not affected. Although the rebound activity mediated by the hyperpolarization-activated cation current (Ih) was still present in IO neurons from $CaV3.1^{-/-}$ mice, it was not strong enough to evoke sodium spikes (**Figure 4B**). IO neurons from these mice also showed altered patterns of subthreshold oscillations and the probability of their occurring was only 15%, significantly lower than the one found in wild-type animals (78%). In addition, the low-threshold calcium spike and the sustained endogenous oscillation of rebound potentials were absent in IO neurons from these mice. The results from studies of these KO mice suggest that both α1A P/Q- and α1G T-type calcium channels are required for the dynamic control of IO oscillations.

No significant changes in the input resistance, time constant, and capacitance of membrane were observed between IO neurons recorded in either mutants or WT mice (Choi et al., 2010). These findings indicate that the α1A P/Q-type calcium channels are involved in the generation of HTS and calcium conductance by α1G T-type calcium channels also play a crucial role in the generation of LTS.

In WT mice IO cell oscillation modulate spike initiation, and so action potentials are normally generated at the crest of such oscillations and fire at 1–10 Hz. This intrinsic rhythm is thus entrained with the speed of movement execution as mentioned above. Moreover, the phase of subthreshold oscillations may be

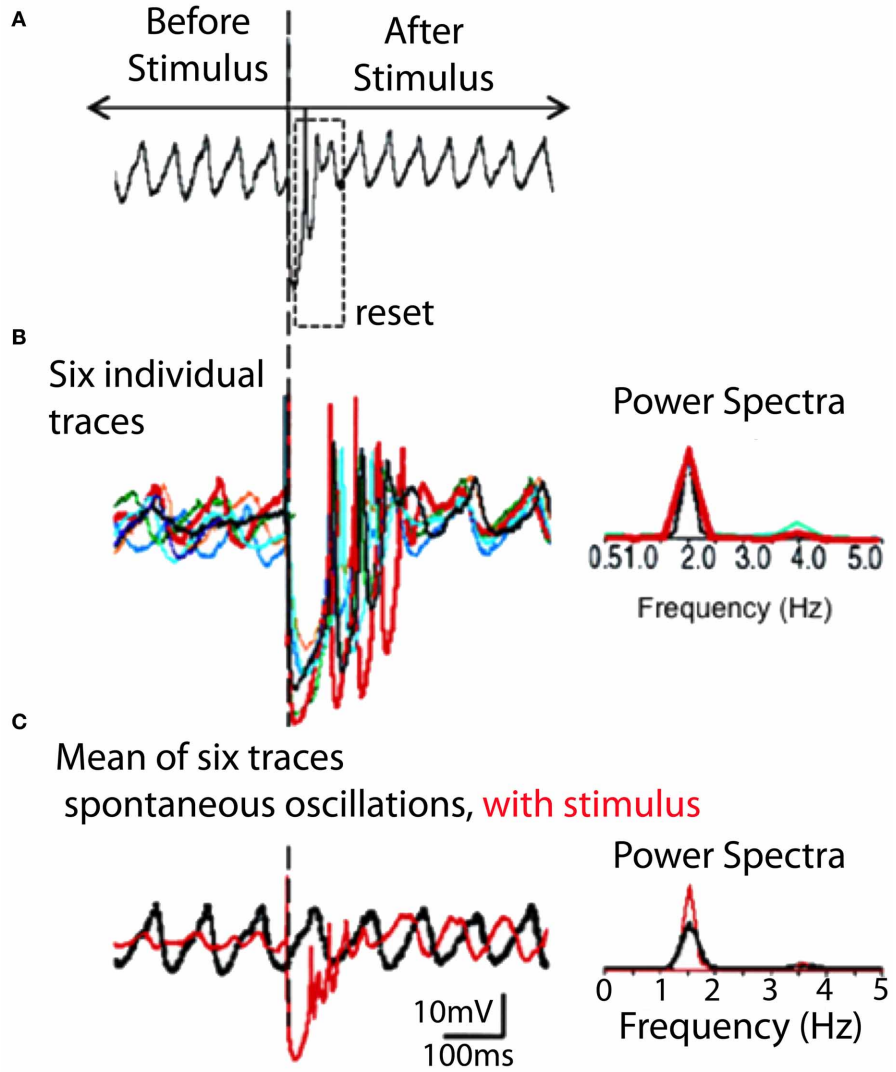

FIGURE 6 | IO spontaneous and stimulus-evoked oscillations. (A) Intracellular recording of spontaneous oscillations at 2 Hz interrupted by an extracellular stimulus. After extracellular stimulation the oscillations disappeared for 750 ms (boxed area) and then resumed. **(B)** Left. Superimposition of six individual intracellular traces (each a different color) of stimulus-evoked oscillations recorded from the same cell. Right. Power spectra. The frequency of stimulation-evoked oscillation was the same (2.0 Hz). Oscillations are clear after the stimulus-induced reset but can be barely detected before the stimulation. **(C)** Superposition of average of six traces of stimulus-evoked oscillations (red) and spontaneous oscillations (black). The stimulus-evoked and spontaneous oscillations have the same frequency. Calibration, 1 mV; **(A)** 1 s; **(B)** 415 ms; **(C)** 500 ms. (Modified from Leznik et al., 2002).

influenced by subthreshold activity, as shown in **Figures 4E,F**). Indeed, extracellular local electrical stimuli, or strong excitatory synaptic input will reset the phase, but not the amplitude or frequency, of subthreshold oscillations (Leznik et al., 2002).

ELECTROTONIC COUPLING

Concerning the electrical coupling, as in other CNS structures (Bennett, 2000), gap junctions constitute the main communication pathway between the IO neurons (Sotelo et al., 1974; de Zeeuw et al., 1996; Devor and Yarom, 2002). Such electrotonic coupling has been assumed to play a crucial role in synchronizing IO oscillations and in generating groups of concurrently oscillating neurons (Llinás and Yarom, 1986). This coupling was also assumed to be controlled by return glomerular inhibition (Llinás, 1975). IO afferents were, in fact, found to modulate the efficiency of electrotonic coupling via inhibition at the glomerulus. The pathway function is actually supported, as stated above, by the cerebellar nuclear GABAergic neurons (Sotelo et al., 1986; Fredette and Mugnaini, 1991; de Zeeuw et al., 1996; Medina et al., 2002). These neurons represent 50% of the total neuronal population in such nuclei giving some measure of the importance of this feedback inhibitory pathway. Accordingly, it was determined that such input can control the degree and distribution of synchronous oscillatory activity in the IO nucleus (Leznik and

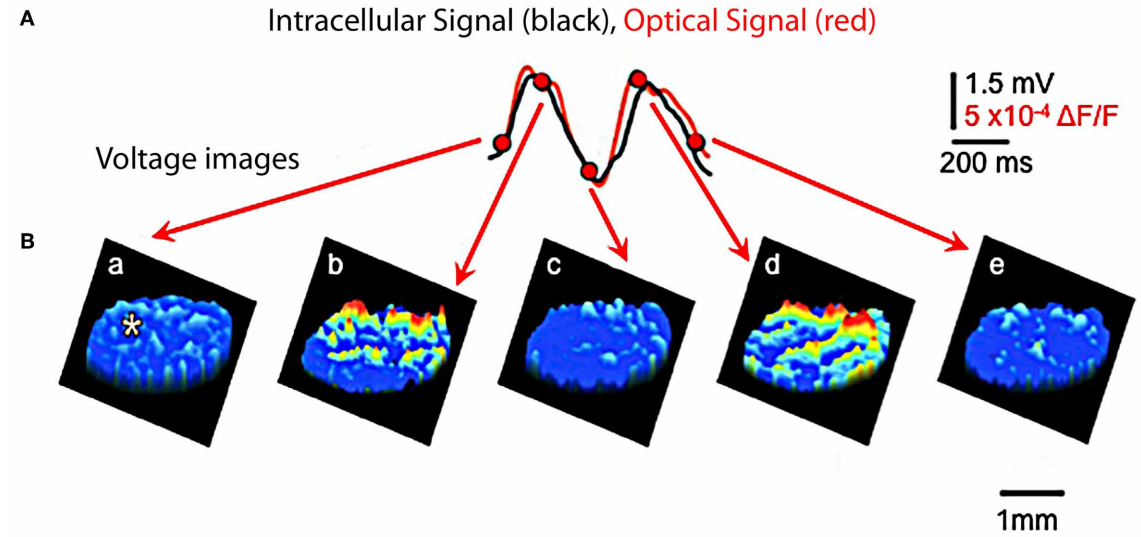

FIGURE 7 | Optical and intracellular recordings in brainstem slice. (A) Recordings of IO subthreshold oscillations are quite similar using optical (red) and using intracellular voltage (black) methods. (Recording site indicated by asterisk in first image panel in **B**). **(B)** Spatial profiles of optically recorded oscillations at five times during the oscillation shown in panel **(A)**. (Modified from Leznik and Llinás, 2005).

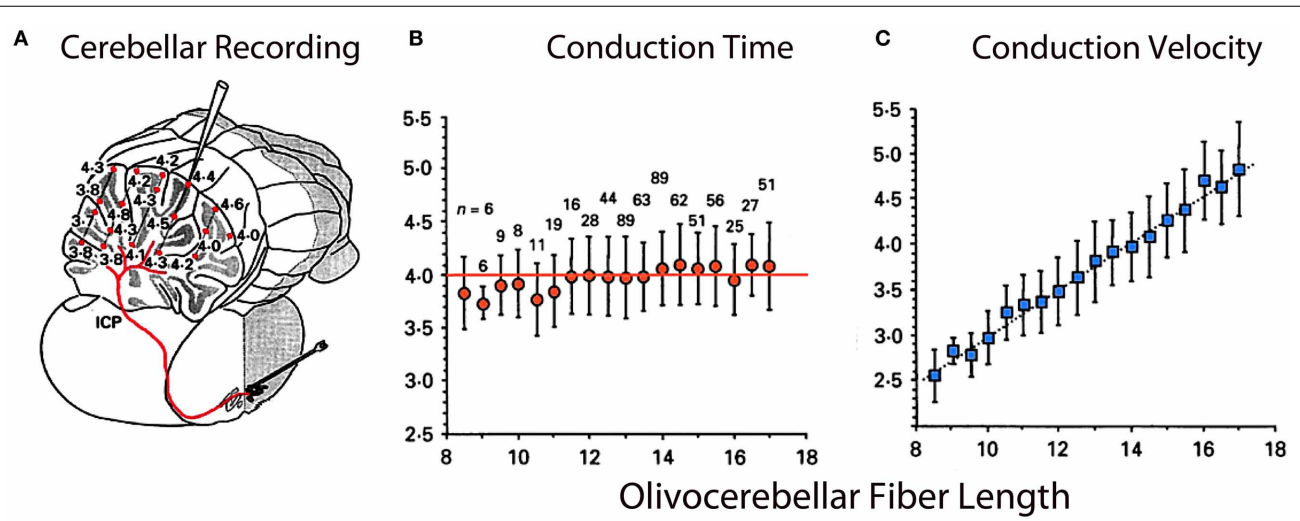

FIGURE 8 | Olivocerebellar conduction times. (A) Drawing of cerebellum showing conduction times for evoked complex spikes (parasagittal plane 4 mm from midline) in an *in vivo* preparation. **(B)** Plot of mean conduction time (±sem) as a function of olivocerebellar fiber length (0.5 mm bins) showing that conduction time was independent of distance between IO and individual Purkinje cell. **(C)** Plot showing close to linear relationship between mean conduction velocity (±sem) and fiber length. (Modified from Sugihara et al., 1993).

Llinás, 2005) and the cerebellar cortex (Lang et al., 1996; Lang, 2001, 2002). Moreover, dynamic groups of IO neurons oscillating in-phase can synchronously activate a population of PCs and thereby control patterns of synchronous activity in the cerebellum during motor coordination (Welsh et al., 1995). Models of IO cells that includes conductances as well as gap junctions explores the interaction of coupling strength, membrane potential level, and conductance modulation in IO synchronization at the network level (Manor et al., 1997; Schweighofer et al., 1999, 2004a,b; Manor et al., 2000; Jacobson et al., 2008; Torben-Nielsen et al., 2012) and effect on the climbing fiber burst (De Gruijl et al., 2012).

As in other brain regions the gap junctions are formed by connexin 36 (Cx36) (Condorelli et al, 1998; Belluardo et al., 2000; Rash et al., 2001). Yet, in Cx36 knock-out mutant mice subthreshold oscillations are present (Long et al., 2002). This has been shown to be due to morphological and electrophysiological compensations in the mutant IO neurons making them more excitable (De Zeeuw et al., 2003). A recent study utilizing tracers and paired electrophysiological recordings has shown

that the coupling between IO neurons is highly variable (Hoge et al., 2011). This introduces another important parameter in considering IO function in motricity.

Visualization of IO cluster activity

Although synchronized IO oscillations are a neuronal ensemble event, they have been studied primarily on a single-cell level and no information has been available about their spatial profiles. Thus, an attempt was made to address this issue by utilizing voltage-sensitive dye optical imaging (Leznik and Llinás, 2005; Leznik et al., 2002). This technique is presently the methodology of choice in studying the geometrical distribution of activity in a large neuronal ensemble (see, for instance, Ebner and Chen, 1995). We have shown that ensemble oscillations in the IO originate in synchronized activity clusters, where each cluster is a localized functional event composed of hundreds of cells. Given the distribution of complex spike activity in the cerebellum cortex, we have proposed that these clusters are very likely to be responsible for the synchronized activation of the PCs observed in previous *in vivo* multielectrode experiments (Lang et al., 1996). Furthermore, when comparing our experimental results with those obtained by computational modeling of IO neuronal ensembles endowed with oscillatory electrical properties and electrotonic coupling (Makarenko and Llinás, 1998; Velarde et al., 2002), we could show that neuronal oscillatory clustering is a direct consequence of the combined electrotonic/intrinsic properties of coupled IO neurons (Leznik et al., 2002).

While electrical recording of IO neurons *in vitro* had indicated the possibility that electrically coupled IO cells could actually cluster into synchronized ensemble neuronal groupings, there was no direct demonstration of such dissipative structures. In searching for such dissipative structures, voltage-sensitive dye imaging of oscillatory activity was attempted and successfully implemented in rodent IO slices (Leznik et al., 2002). Thus, spatio-temporal profiles of ensemble IO oscillations were unambiguously observed following IO electrical stimuli. The stimulation serves to both reset the phase of subthreshold oscillation and to entrain a large proportion of neurons to in-phase oscillations. Indeed, synchronization of oscillatory activity over the IO network increased the amplitude of the optical signal to a level that could be detected easily with our imaging set up. Such oscillatory reset was also observed with intracellular recordings from IO neurons (**Figures 4**, **6**). The optically recorded oscillatory clusters have a dynamic spatial organization, and their amplitude depends on the oscillation phase such that they embraced the largest area during the upward phase of the oscillations. Each cluster consisted of a core region and the adjoining area. The core region demonstrated a close to constant size, but the extent of the adjoining area was found to be phase-dependent.

Direct calculation of core and maximum area (i.e., the core region plus the adjoining area at its utmost extent) for several representative clusters gave a mean core area and a mean maximum of several hundred $\mu 2$. Because IO clusters are three-dimensional structures, observed in this case as a planar structure indicate that in depth they comprise hundreds of cells. Thus, our optical data indicate that at the network level, the IO nucleus is organized in functionally coupled tridimensional activity clusters. Each cluster is comprised of several hundred cells, which may act in unison to activate groups of thousands of cerebellar PCs simultaneously in agreement with the multiple electrode recordings observed previously.

In conclusion, the dimensions of clusters are probably determined by the IO electrical coupling coefficient, and thus by the magnitude and distribution of the return inhibition from the cerebellar nuclear feedback, which has been demonstrated in previous *in vivo* experiments (Ruigrok and Voogd, 1995; Lang et al., 1996) and supported with mathematical modeling (Leznik et al., 2002; Velarde et al., 2002).

THE CLIMBING FIBER CONDUCTION ISOCHRONICITY

From another perspective, while the temporal distribution of activity is well-demonstrated at the olivary level, one may wonder about the time dispersion produced by the olivocerebellar pathway given the different distances between the IO axons and their target PCs. However, if isochronicity is present, then the conduction time between an IO neuron and its PC should be close to uniform and independent of the distance such a signal had to travel. This issue is particularly significant given that the folded nature of such a cortex can increase the path length to the PCs by more than 50%. Furthermore, the correction of the conduction velocity needed to insure synchronicity should be related linearly to distance. This was, in fact, shown to be the case. The time dispersion for a nearly 4 ms conduction time was plus or minus 500 μs to any regions of the cerebellar mantle, regardless of the distance between the IO and the cerebellar cortex at the bottom or top of the of the deep cerebellar folia or at any point in between (Sugihara et al., 1993). The results were based on complex spike latency from 660 different PCs from 12 rats (**Figure 8**).

Since our original demonstration, this isosynchronicity has been confirmed in further experiments with other cerebellar systems (Ariel, 2005; Brown and Ariel, 2009). A similar finding concerning conduction isochronicity has also been observed in the thalamocortical system and has been interpreted, as in the case of the olivo-cerebellar system, as a mechanism for temporal coherence. In this case, such timing has been related to the temporal coherence associated with cognitive binding (Engel et al., 1997; Salami et al., 2003; Chomiak and PetersHu, 2008; Vicente et al., 2008).

Therefore, the results indicated that the cerebellar cortex, while being deeply folded anatomically behaves, functionally, as an isochronous sphere as far as the olivocerebellar system is concerned. Further, such isochronicity is actually related to the onset time and duration required for proper motor execution (Welsh et al., 1995).

THE OLIVOCEREBELLAR SYSTEM AND ERROR SENSING

Finally, the issue of error sensing, which was previously of great interest to cerebellar physiologists, has been treated in detail in excellent reviews concerning IO function (Simpson et al., 1996; De Zeeuw et al., 1998). My personal view is that the error-sensing signal that is often observed in climbing fiber responses—while being a very important functional phenotype—may not be "the central cerebellar function" as some authors claim. From my perspective, the high probability of complex spike activation in

relation to unexpected error signals correlates well with such events simply because it is easy to detect. This is the case because climbing fiber activation is massive both when a large reset of the oscillatory phase occurs (Makarenko and Llinás, 1998; Leznik et al., 2002; Chorev et al., 2007; Khosrovani et al., 2007; see also Van Der Giessen et al., 2008 for the connexin 36 role in this large reset), and when a massive temporal reorganization of motor pattern activity is required.

Experimental findings

This question was addressed in studies rodent brainstem slices. In agreement with previous intracellular results (Llinás and Yarom, 1986), an extracellular stimulation given at the dorsal border of the IO nucleus generates a full action potential demonstrate that if the cell was oscillating at the time of the stimulus, its oscillations are stopped momentarily, but resumed with a different phase shortly after the stimulation (Llinás et al., 2002). Moreover, in later experiments, it was also determined that such extracellular stimulation may reset the phase without affecting the amplitude or frequency of the subthreshold oscillation (Leznik and Llinás, 2005), and that for most cells recorded, this phase reset could be observed repeatedly with subsequent stimuli (**Figure 3**). However, the most surprising property discovered was the fact that the oscillation phase shift was remarkably constant and independent of the original phase moment at which the stimulus was delivered.

This constant phase shift is of central importance in defining IO function, as it gives a clear time constraint to the functional states generated by the neuronal ensemble. The reset property of the IO circuit can thus be considered as the main component in the large correction that must be generated when a movement error occurs. This is best illustrated by the fast recovery that we all experience when tripping during locomotion and the fact that we do not fall, while robots do, under similar circumstances.

The issue of error correction has been studied elegantly under conditions where random stimuli require temporal resting under circumstances of robust activation of the cerebellar system (Schweighofer et al., 2004a,b); however, this issue must be addressed further as other views are also clearly present (Gilbert and Thach, 1977; Horn et al., 2004; Catz et al., 2005; Kojima et al., 2010; Popa et al., 2012, 2013). The image one has is of the activation of a very large population of Purkinje cells that mediate a rapid inhibition of the inhibitory cells of the nucleo-olivary pathway, resulting in increased coupling at the olivary level. This event will produce a large and coherent activation of IO neurons; thus, an increased probability of PC complex spike activation ensues. In short, then, error correction is one mode, but not the main mode of IO function.

THOUGHTS ON THE FUNCTIONAL SIGNIFICANCE OF TWO DISTINCT OLIVOCEREBELLAR SYSTEMS

The rather remarkable differences observed in both the electrophysiology and morphology of these two types of IO neurons clearly implies that the IO nucleus must operate in at least two different modes. While with hindsight we now better understand the problems presented by the lack of oscillatory behavior in the oculomotor system and the presence of physiological tremor in the somato-motor system the findings reported here requires a hypothesis that addresses the necessity of two types of IO neurons in the organization of coordinated motricity.

While the importance of a timing signal has been theoretically assign to the requirements of motor temporal binding (Welsh and Llinás, 1997) by allowing time coherence of motoneuron activation to provide a basic element for motor coordination, a similar case may be made for the oculomotor system. So what would be the difference between somatic and ocular motricity that would require such dramatic functional differentiation? One possible hypothesis relates to the multiple joint organization of the somato-motor system as opposed to the single joint organization of the oculomotor system. In the former case multiple parameters corresponding to different coordinate systems must operate in unison to attain coordination. To this parameter is added muscle feed back that operates in all myotatic reflexes where muscle spindles are simultaneously informing the CNS about the position and rate of movement of each segment of any of our multi-jointed limbs. Because of the tremendous complexity afforded by such massive co-activation of motoneuron pools the temporal requirements become astronomically complicated and a welcome control approach might be to restrict movement to the ballistic properties that we know characterize somato-motor movements (Welsh and Llinás, 1997). By contrast, oculomotor activity does not require the ballistic approach to motor generation since all the parameters are regulated to only one vector in tridimensional space. To this parameter is added the fact that eye movements require a degree of precision not usually demanded of the somato-motor system. Indeed eye movement fixation is only modulated by the microsacadic system that operates at 0.2° in amplitude in an open loop mode. The somatomotor system is far less precise and must operate under conditions where the movement load and momentum vary continuously. For example, as we reach, hold, and lift objects, masticate hard or soft materials, throw a projectile, or return a fast serve with a tennis racket.

In short, we may consider the enormous difference in motor organization as the evolutionary pressure that ultimately determined the motor organization of these two different motor strategies as the root for the very crisp differences in the electrophysiological properties of these two different types of IO neuron.

CONCLUSIONS AND IMPLICATIONS

Four main issues have been addressed in this short paper concerning the functional organization of the olivo-cerebellar system. (1) The olivocerebellar system seems to be related centrally to the control of motor timing. It's exceptional neuronal characteristics and the network properties that it supports make the olivo-cerbellar system a unique control system, where timing seems to be a central theme. (2) The combination of strong and rather stereotyped intrinsic electrical properties with electrical coupling among the neuronal elements allows the synchronous activation of clusters of neurons. Further, feedback inhibition provides the dynamic variance of the membership of such coupled clusters. (3) The very fundamental property of the resetting of the phase of groups of neurons by a stimulus, such that the new phase is coherent and independent from the original phase, makes this event truly spectacular. (4) When movements require

truly continuous control and the issues if multi-joint dynamics are not considered, the IO generates non-oscillatory behavior, as is the case in eye movement kinetics. These four elements give the IO a very powerful set of network properties allowing not only the temporal control of many variables simultaneously, as occurs during motor control, and the possibility of rapid correction in the presence of unexpected events that require rapid global motor correction, but also the possibility of the smooth control that allow eye movement pursue of object displacement in the visual field.

Finally, nature has evolved a mechanism by which this very elaborate cluster dynamic generating system can transmit the timing sequences into a folded cortical geometry, without differential conduction time aberrations, and terminate its path by generating the most powerful synapse in the CNS. If this were not sufficient, the neurons it activates are the largest in the brain, receive just one such climbing fiber afferent, and its output is inhibitory (Ito and Yoshida, 1966). And so, nature has devised one of its most conserved neuronal systems to control motricity by inhibition, a very fitting attribute because it is by selection, via inhibition that the most elaborate neuronal patterns are generated in the CNS.

REFERENCES

Ariel, M. (2005). Latencies of climbing fiber inputs to turtle cerebellar cortex. *J. Neurophysiol.* 93, 1042–1054. doi: 10.1152/jn.00132.2004

Ariens-Kappers, C. U., Huber, G. C., and Crosby, E. C. (1936). *The Comparative Anatomy of the Nervous System of Vertebrates Including Man.* New York, NY: Macmillan.

Armstrong, D. M., and Schild, R. F. (1970). A quantitative study of the Purkinje cells in the cerebellum of the albino rat. *J. Comp. Neurol.* 139, 449–456. doi: 10.1002/cne.901390405

Bal, T., and McCormick, D. A. (1997). Synchronized oscillations in the inferior olive are controlled by the hyperpolarization-activated cation current I(h). *J. Neurophysiol.* 77, 3145–3156.

Bazzigaluppi, P., De Gruijl, J. R., van der Giessen, R. S., Khosrovani, S., De Zeeuw, C. I., and de Jeu, M. T. (2012). Olivary subthreshold oscillations and burst activity revisited. *Front. Neural Circuits* 6:91. doi: 10.3389/fncir.2012.00091

Belluardo, N., Mudo, G., Trovato-Salinaro, A., Le Gurun, S., Charollais, A., Serre-Beinier, V., et al. (2000). Expression of Connexin 36 in the adult and developing rat brain. *Brain Res.* 865, 121–138.

Benardo, L. S., and Foster, R. E. (1986). Oscillatory behavior in inferior olive neurons: mechanism, modulation, cell aggregates. *Brain Res. Bull.* 17, 773–784. doi: 10.1016/0361-9230(86)90089-4

Bennett, M. (2000). Electrical synapses, a personal perspective (or history). *Brain Res. Brain Res. Rev*. 32, 16–28. doi: 10.1016/S0165-0173(99)00065-X

Best, A. R., and Regehr, W. G. (2009). Inhibitory regulation of electrically coupled neurons in the inferior olive is mediated by asynchronous release of GABA. *Neuron* 62, 555–565. doi: 10.1016/j.neuron.2009.04.018

Brown, M., and Ariel, M. (2009). Topography and response timing of intact cerebellum stained with absorbance voltage-sensitive dye. *J. Neurophysiol.* 101, 474–490. doi: 10.1152/jn.90766.2008

Brown, T. (1911). The intrinsic factors in the act of progression in the mammal. *Proc Roy. Soc. Lond. B Biol Sci*. 84, 308–319. doi: 10.1098/rspb.1911.0077

Brown, T. (1914). On the nature of the fundamental activity of the nervous centres; together with an analysis of the conditioning of rhythmic activity in progression, and a theory of the evolution of function in the nervous system. *J. Physiol.* 28, 18–46.

Carpenter, R. (1977). *Movements of the Eyes*. London: Pion.

Catz, N., Dicke, P. W., and Their, P. (2005) Cerebellar complex spike firing is suitable to induce as well as to stabilize motor learning. *Curr. Biol.* 15, 2179–2189. doi: 10.1016/j.cub.2005.11.037

Choi, S., Yu, E., Kim, D., Urbano, F. J., Makarenko, V., Shin, H. S., and Llinás, R. R. (2010) Subthreshold membrane potential oscillations in inferior olive neurons are dynamically regulated by P/Q- and T-type calcium channels: a study in mutant mice. *J. Physiol.* 588(Pt 16), 3031–3043. doi: 10.1113/jphysiol.2009.184705

Chomiak, T., S. Peters, and Hu, B. (2008). Functional architecture and spike timing properties of corticofugal projections from rat ventral temporal cortex. *J. Neurophysiol.* 100, 327–335. doi: 10.1152/jn.90392.2008

Chorev, E., Yarom, Y., and Lampl, I. (2007). Rhythmic episodes of subthreshold membrane potential oscillations in the rat inferior olive nuclei *in vivo*. *J. Neurosci.* 27, 5043–5052. doi: 10.1523/JNEUROSCI.5187-06.2007

Condorelli, D. F., Parenti, R., Spinella, F., Trovato Salinaro, A., Belluardo, N., Cardile, V., et al. (1998). Cloning of a new gap junction gene (Cx36) highly expressed in mammalian brain neurons. *Eur. J. Neurosci.* 10, 1202–1208. doi: 10.1046/j.1460-9568.1998.00163.x

De Gruijl, J. R., Bazzigaluppi, P., de Jeu, M. T., and De Zeeuw, C. I. (2012). Climbing fiber burst size and olivary sub-threshold oscillations in a network setting. *PLoS Comput. Biol.* 8:e1002814. doi: 10.1371/journal.pcbi.1002814

De Zeeuw, C. I., Chorev, E., Devor, A., Manor, Y., Van Der Giessen, R. S., De Jeu, M. T., et al. (2003). Deformation of network connectivity in the inferior olive of connexin 36-deficient mice is compensated by morphological and electrophysiological changes at the single neuron level. *J. Neurosci.* 23, 4700–4711.

de Zeeuw, C. I., Holstege, J. C., Ruigrok, T. J., and Voogd, J. (1990a). Mesodiencephalic and cerebellar terminals terminate upon the same dendritic spines in the glomeruli of the cat and rat inferior olive: an ultrastructural study using a combination of [3H]leucine and wheat germ agglutinin coupled horseradish peroxidase anterograde tracing. *Neuroscience* 34, 645–655. doi: 10.1016/03064522(90)90171-y

de Zeeuw, C. I., Ruigrok, T. J., Holstege, J. C., Jansen, H. G., and Voogd, J. (1990b). Intracellular labeling of neurons in the medial accessory olive of the cat: II. Ultrastructure of dendritic spines and their GABAergic innervation. *J. Comp. Neurol.* 300, 478–494. doi: 10.1002/cne.903000404

de Zeeuw, C. I., Lang, E. J., Sugihara, I., Ruigrok, T. J., Eisenman, L. M., Mugnaini, E., et al. (1996). Morphological correlates of bilateral synchrony in the rat cerebellar cortex. *J. Neurosci.* 16, 3412–3426.

De Zeeuw, C., Simpson, J., Hoogenraad, C., Galjart, N., Koekkoek, S., and Ruigrok, T. (1998). Microcircuitry and function of the inferior olive. *Trends Neurosci.* 21, 391–400. doi: 10.1016/S0166-2236(98)01310-1

Devor, A., and Yarom, Y. (2002) Electrotonic coupling in the inferior olivary nucleus revealed by simultaneous double patch recordings. *J. Neurophysiol.* 87, 3048–3058.

Ebner, T. J., and Chen, G. (1995). Use of voltage-sensitive dyes and optical recordings in the central nervous system. *Prog. Neurobiol.* 46, 463–506. doi: 10.1016/0301-0082(95)00010-S

Eccles, J. C., Llinás, R., and Sasaki, K. (1965). Inhibitory systems in the cerebellar cortex. *Proc. Aust. Assoc. Neurol.* 3, 7–14.

Eccles, J. C., Llinás, R., and Sasaki, K. (1966a). The action of antidromic impulses on the cerebellar Purkinje cells. *J. Physiol. (Lond.)* 182, 316–345.

Eccles, J. C., Llinás, R., and Sasaki, K. (1966b). The excitatory synaptic action of climbing fibres on the purinje cells of the cerebellum. *J. Physiol.* 182, 268–296.

Eccles, J. C., Llinás, R., and Sasaki, K. (1966c). Intracellularly recorded responses of the cerebellar Purkinje cells. *Exp. Brain Res. Exp. Hirnforsch. Exp. Cereb.* 1, 161–183. doi: 10.1007/BF00236869

Engel, A. K., Roelfsema, P. R., Fries, P., Brecht, M., and Singer, W. (1997). Role of the temporal domain for response selection and perceptual binding. *Cereb. Cortex* 7, 571–582. doi: 10.1093/cercor/7.6.571

Farmer, S. F. (1998). Rhythmicity, synchronization and binding in human and primate motor systems. *J. Physiol.* 509 (Pt 1), 3–14. doi: 10.1111/j.1469-7793.1998.003bo.x

Fredette, B. J., and Mugnaini, E. (1991). The GABAergic cerebello-olivary projection in the rat. *Anat. Embryol.* 184, 225–243. doi: 10.1007/BF01673258

Gilbert, P. F., and Thach, W. T. (1977). Purkinje cell activity during motor learning. *Brain Res.* 128, 309–328. doi: 10.1016/0006-8993(77)90997-0

Hardcastle, V. G. (1997). Consciousness and the neurobiology of perceptual binding. *Semin. Neurol.* 17, 163–170. doi: 10.1055/s-2008-1040926

Hoge, G. J., Davidson, K. G., Yasumura, T., Castillo, P. E., Rash, J. E., and Pereda, A. E. (2011) The extent and strength of electrical coupling between inferior olivary neurons is heterogeneous. *J. Neurophysiol.* 105, 1089–1101. doi: 10.1152/jn.00789.2010

Horn, K. M., Pong, M., and Gibson, A. R. (2004). Discharge of inferior olive cells during reaching errors and perturbations.[erratum appears in

Brain Res. 2004 May 15;1008(1):137-138]. *Brain Res.* 996, 148–158. doi: 10.1016/j.brainres.2003.10.021

Ito, M., and Yoshida, M. (1966). The origin of cerebral-induced inhibition of Deiters neurones. I. Monosynaptic initiation of the inhibitory postsynaptic potentials. *Exp. Brain Res. Exp. Hirnforsch. Exp. Cereb.* 2, 330–349.

Jacobson, G. A., Rokni, D., and Yarom, Y. (2008). A model of the olivo-cerebellar system as a temporal pattern generator. *Trends Neurosci.* 31, 617–625. doi: 10.1016/j.tins.2008.09.005

Jahnsen, H., and Llinás, R. (1984). Ionic basis for the electro-responsiveness and oscillatory properties of guinea-pig thalamic neurones *in vitro*. *J. Physiol. (Lond.)* 349, 227–247.

Khosrovani, S., Van Der Giessen, R. S., de Zeeuw, C. I., de Jeu, M. T. (2007). *In vivo* mouse inferior olive neurons exhibit heterogeneous subthreshold oscillations and spiking patterns. *Proc. Natl. Acad. Sci. U.S.A.* 104, 15911–15916. doi: 10.1073/pnas.0702727104

Kojima, Y., Soetedjo, R., and Fuchs, A. F. (2010). Changes in simple spike activity of some Purkinje cells in the oculomotor vermis during saccade adaptation are appropriate to participate in motor learning. *J. Neurosci.* 30, 3715–3727. doi: 10.1523/JNEUROSCI.4953-09.2010

Lampl, I., and Yarom, Y. (1997). Subthreshold oscillations and resonant behavior: two manifestations of the same mechanism. *Neuroscience* 78, 325–341. doi: 10.1016/S0306-4522(96)00588-X

Lang, E. J. (2001). Organization of olivocerebellar activity in the absence of excitatory glutamatergic input. *J. Neurosci.* 21, 1663–1675.

Lang, E. J. (2002). GABAergic and glutamatergic modulation of spontaneous and motor-cortex-evoked complex spike activity. *J. Neurophysiol.* 87, 1993–2008. doi: 10.1152/jn.00477.2001

Lang, E. J., Sugihara, I., and Llinás, R. (1996). GABAergic modulation of complex spike activity by the cerebellar nucleoolivary pathway in rat. *J. Neurophysiol.* 76, 255–275.

Lang, E. J., Sugihara, I., and Llinás, R. (2006). Olivocerebellar modulation of motor cortex ability to generate vibrissal movements in rat. *J. Physiol.* 571(Pt 1), 101–120. doi: 10.1113/jphysiol.2005.102764

Leznik, E., and Llinás, R. (2005). Role of gap junctions in synchronized neuronal oscillations in the inferior olive. *J. Neurophys.* 94, 2447–2456. doi: 10.1152/jn.00353.2005

Leznik, E., Makarenko, V., and Llinás, R. (2002). Electrotonically mediated oscillatory patterns in neuronal ensembles: an *in vitro* voltage-dependent dye-imaging study in the inferior olive. *J. Neurosci.* 22, 2804–2815.

Llinás, R. (1974). Eighteenth bowditch lecture: motor aspects of cerebellar control. *Physiologist* 17, 19–46.

Llinás, R. (1975). Structure and function of the cerebellar cortex. *Sci. Am.* 232, 56–71.

Llinás, R. (1988). The intrinsic electrophysiological properties of mammalian neurons: a new insight into CNS function. *Science* 242, 1654–1664.

Llinás, R. (1991). "The noncontinuous nature of movement execution," in *Motor Control: Concepts and Issues*, eds D. Humphrey and H. Freund (New York, NY: Wiley), 223–242.

Llinás, R. R. (2009). Inferior olive oscillation as the temporal basis for motricity and oscillatory reset as the basis for motor error correction. *Neuroscience* 162, 797–804. doi: 10.1016/j.neuroscience.2009.04.045

Llinás, R., Baker, R., and Sotelo, C. (1974). Electrotonic coupling between neurons in cat inferior olive. *J. Neurophysiol.* 37, 560–571.

Llinás, R., and Hess, R. (1976). Tetrodotoxin-resistant dendritic spikes in avian Purkinje cells. *Proc. Natl. Acad. Sci. U.S.A.* 73, 2520–2523. doi: 10.1073/pnas.73.7.2520

Llinás, R., and Jahnsen, H. (1982). Electrophysiology of mammalian thalamic neurones *in vitro*. *Nature* 297, 406–408. doi: 10.1038/297406a0

Llinás, R., Leznik, E., and Makarenko, V. I. (2002). On the amazing olivocerebellar system. *Ann. N. Y. Acad. Sci.* 978, 258–272. doi: 10.1111/j.1749-6632.2002.tb07573.x

Llinás, R., and Muhlethaler, M. (1988). Electrophysiology of guinea-pig cerebellar nuclear cells in the *in vitro* brain stem-cerebellar preparation. *J. Physiol.* 404, 241–258.

Llinás, R., and Sugimori, M. (1980a). Electrophysiological properties of *in vitro* Purkinje cell somata in mammalian cerebellar slices. *J. Physiol.* 305, 171–195.

Llinás, R., and Sugimori, M. (1980b). Electrophysiological properties of *in vitro* Purkinje cell dendrites in mammalian cerebellar slices. *J. Physiol.* 305, 197–213.

Llinás, R., and Yarom, Y. (1981a). Electrophysiology of mammalian inferior olivary neurones *in vitro*. Different types of voltage-dependent ionic conductances. *J. Physiol.* 315, 549–567.

Llinás, R., and Yarom, Y. (1981b). Properties and distribution of ionic conductances generating electroresponsiveness of mammalian inferior olivary neurones *in vitro*. *J. Physiol.* 315, 569–584.

Llinás, R., and Yarom, Y. (1986). Oscillatory properties of guinea-pig inferior olivary neurones and their pharmacological modulation: an *in vitro* study. *J. Physiol.* 376, 163–182.

Llinás, R., Ribary, U., Contreras, D., and Pedroarena, C. (1998). The neuronal basis for consciousness. *Philos. Trans. R. Soc. Lond. B Biol. Sci.* 353, 1841–1849. doi: 10.1098/rstb.1998.0336

Long, M. A., Deans, M. R., Paul, D. L., and Connors, B. W. (2002). Rhythmicity without synchrony in the electrically uncoupled inferior olive. *J. Neurosci.* 22, 10898–10905.

Makarenko, V., and Llinás, R. (1998). Experimentally determined chaotic phase synchronization in a neuronal system. *Proc. Natl. Acad. Sci. U.S.A.* 95, 15747–15752. doi: 10.1073/pnas.95.26.15747

Manor, Y., Rinzel, J., Segev, I., and Yarom, Y. (1997). Low-amplitude oscillations in the inferior olive: a model based on electrical coupling of neurons with heterogeneous channel densities. *J. Neurophysiol.* 77, 2736–2752.

Manor, Y., Yarom, Y., Chorev, E., and Devor, A. (2000). To beat or not to beat: a decision taken at the network level. *J. Physiol. Paris* 94, 375–390. doi: 10.1016/S0928-4257(00)01085-8

Marder, E., and Bucher, D. (2001). Central pattern generators and the control of rhythmic movements. *Curr. Biol.* 11, R986–R996. doi: 10.1016/S0960-9822(01)00581-4

Mathy, A., Ho, S. S., Davie, J. T., Duguid, I. C., Clark, B. A., and Hausser, M. (2009) Encoding of oscillations by axonal bursts in inferior olive neurons. *Neuron* 62, 388–399. doi: 10.1016/j.neuron.2009.03.023

Medina, J. F., Nores, W. L., and Mauk, M. D. (2002). Inhibition of climbing fibres is a signal for the extinction of conditioned eyelid responses. *Nature* 416, 330–333. doi: 10.1038/416330a

Pare, D., deCurtis, M., and Llinás, R. (1992). Role of the hippocampal-entorhinal loop in temporal lobe epilepsy: extra- and intracellular study in the isolated guinea pig brain *in vitro*. *J. Neurosci.* 12, 1867–1881.

Popa, L. S., Hewitt, A. L., and Ebner, T. J. (2012). Predictive and feedback performance errors are signaled in the simple spike discharge of individual Purkinje cells. *J. Neurosci.* 32, 15345–15358. doi: 10.1523/JNEUROSCI.2151-12.2012

Popa, L. S., Hewitt, A. L., and Ebner, T. J. (2013). Purkinje cell simple spike discharge encodes error signals consistent with a forward internal model. *Cerebellum* 12, 331–333. doi: 10.1007/s12311-013-0452-4

Ramon y Cajal, S. (1911). *Histologie du Systeme Nerveux de l'homme et des Vertebres*, Vol. II. Paris: Maloine.

Rash, J. E., Yasumura, T., Dudek, F. E., and Nagy, J. I. (2001). Cell specific expression of connexins and evidence of restricted gap junctional coupling between glial cells and between neurons. *J. Neurosci.* 21, 1983–2000.

Ruigrok, T. J., and Voogd, J. (1995). Cerebellar influence on olivary excitability in the cat. *Eur. J. Neurosci.* 7, 679–693. doi: 10.1111/j.1460-9568.1995.tb00672.x

Salami, M., Itami, C., Tsumoto, T., and Kimura, F. (2003). Change of conduction velocity by regional myelination yields constant latency irrespective of distance between thalamus and cortex. *Proc. Natl. Acad. Sci. U.S.A.* 100, 6174–6179. doi: 10.1073/pnas.0937380100

Schweighofer, N., Doya, K., and Kawato, M. (1999). Electrophysiological properties of inferior olive neurons: a compartmental model. *J. Neurophysiol.* 82, 804–817.

Schweighofer, N., Doya, K., Fukai, H., Chiron, J. V., Furukawa, T., and Kawato, M. (2004a). Chaos may enhance information transmission in the inferior olive. *Proc. Natl. Acad. Sci. U.S.A.* 101, 4655–4660. doi: 10.1073/pnas.0305966101

Schweighofer, N., Doya, K., and Kuroda, S. (2004b). Cerebellar aminergic neuromodulation: towards a functional understanding. *Brain Res. Brain Res. Rev.* 44, 103–116. doi: 10.1016/j.brainresrev.2003.10.004

Sherrington, C. (1906). *The Integrative Actions of the Nervous System*. New Haven, CT: Yale University Press.

Simpson, J. I., Wylie, D. R., and De Zeeuw, C. I. (1996). More on climbing fiber signals and their consequence(s). *Behav. Brain Sci.* 384–398. doi: 10.1017/S0140525X00081991

Singer, W. (1993). Synchronization of cortical activity and its putative role in information processing and learning. *Annu. Rev. Physiol.* 55, 349–374. doi: 10.1146/annurev.ph.55.030193.002025

Sotelo, C., Gotow, T., and Wassef, M. (1986). Localization of glutamic-acid-decarboxylase-immunoreactive axon terminals in the inferior olive of the rat, with special emphasis on anatomical relations between GABAergic synapses and dendrodendritic gap junctions. *J. Comp. Neurol.* 252, 32–50. doi: 10.1002/cne.902520103

Sotelo, C., Llinás, R., and Baker, R. (1974). Structural study of inferior olivary nucleus of the cat: morphological correlates of electrotonic coupling. *J. Neurophysiol.* 37, 541–559.

Sugihara, I., Lang, E. J., and Llinás, R. (1993). Uniform olivocerebellar conduction time underlies Purkinje cell complex spike synchronicity in the rat cerebellum. *J. Physiol.* 470, 243–271. doi: 10.1016/S0921-8696(05)81125-9

Szentagothai, J., and Rajkovits, K. (1959). Ueber den Ursprung der Kletterfasern des kleinhirns. *Z. Anat. Entwicklungsgeschicht*. 121, 130–141. doi: 10.1007/BF00525203

Thach, W. (1968). Discharge of Purkinje and cerebellar nuclear neurons during rapidly alternating arm movements in the monkey. *J. Neurophysiol.* 31, 785–797.

Torben-Nielsen, B., Segev, I., and Yarom, Y. (2012) The generation of phase differences and frequency changes in a network model of inferior olive subthreshold oscillations. *PLoS Comput. Biol.* 8:e1002580. doi: 10.1371/journal.pcbi.1002580

Urbano, F. J., Simpson, J. I., and Llinás, R. R. (2006). Somatomotor and oculomotor inferior olivary neurons have distinct electrophysiological phenotypes. *Proc. Natl. Acad. Sci. U.S.A.* 103, 16550–16555. doi: 10.1073/pnas.0607888103

Vallbo, A. B., and Wessberg, J. (1993). Organization of motor output in slow finger movements in man. *J. Physiol.* 469, 673–691.

Van Der Giessen, R. S., Koekkoek, S. K., van Dorp, S., De Gruijl, J. R., Cupido, A., Khosrovani, S., et al. (2008). Role of olivary electrical coupling in cerebellar motor learning. *Neuron* 58, 599–612. doi: 10.1016/j.neuron.2008.03.016

Varela, F., Lachaux, J. P., Rodriguez, E., and Martinerie, J. (2001). The brainweb: phase synchronization and large-scale integration. *Nat. Rev. Neurosci.* 2, 229–239. doi: 10.1038/35067550

Velarde, M. G., Nekorkin, V. I., Kazantsev, V. B., Makarenko, V. I., and Llinás, R. (2002). Modeling inferior olive neuron dynamics. *Neural Net.* 15, 5–10. doi: 10.1016/S0893-6080(01)00130-7

Vicente, R., Gollo, L. L., Mirasso, C. R., Fischer, I., and Pipa, G. (2008). Dynamical relaying can yield zero time lag neuronal synchrony despite long conduction delays. *Proc. Natl. Acad. Sci. U.S.A.* 105, 17157–17162. doi: 10.1073/pnas.0809353105

Welsh, J. P., and Llinás, R. (1997). Some organizing principles for the control of movement based on olivocerebellar physiology. *Prog. Brain Res.* 114, 449–461. doi: 10.1016/S0079-6123(08)63380-4

Welsh, J. P., Lang, E. J., Sugihara, I., and Llinás, R. (1995). Dynamic organization of motor control within the olivocerebellar system. *Nature* 374, 453–457. doi: 10.1038/374453a0

Yarom, Y., and Cohen, D. (2002). The olivocerebellar system as a generator of temporal patterns. *Ann. N.Y. Acad. Sci.* 978, 122–134. doi: 10.1111/j.1749-6632.2002.tb07561.x

Conflict of Interest Statement: The author declares that the research was conducted in the absence of any commercial or financial relationships that could be construed as a potential conflict of interest.

Received: 10 January 2013; accepted: 25 October 2013; published online: 28 January 2014.

Citation: Llinás RR (2014) The olivo-cerebellar system: a key to understanding the functional significance of intrinsic oscillatory brain properties. Front. Neural Circuits ***7****:96. doi: 10.3389/fncir.2013.00096*

This article was submitted to the journal Frontiers in Neural Circuits.

frontiers in
NEURAL CIRCUITS

ORIGINAL RESEARCH ARTICLE
published: 08 October 2013
doi: 10.3389/fncir.2013.00157

Cerebellar cortical neuron responses evoked from the spinal border cell tract

Pontus Geborek, Anton Spanne, Fredrik Bengtsson and Henrik Jörntell*

Neural Basis of Sensorimotor Control, Department of Experimental Medical Science, Lund University, Lund, Sweden

Edited by:
Egidio D'Angelo, University of Pavia, Italy

Reviewed by:
Egidio D'Angelo, University of Pavia, Italy
Pablo M. Blazquez, Washington University School of Medicine, USA

****Correspondence:***
Henrik Jörntell, Neural Basis of Sensorimotor Control, Department of Experimental Medical Science, Lund University, BMC F10, Tornavägen 10, SE-221 84, Lund, Sweden
e-mail: henrik.jorntell@med.lu.se

Spinocerebellar systems are likely to be crucial for cerebellar hallmark functions such as coordination. However, in terms of cerebellar functional analyses, these are perhaps among the least explored systems. The aim of the present study is to achieve activation of a single component of the spinocerebellar systems and to explore to what extent it can influence the spike output of granule cells, Golgi cells, molecular layer (ML) interneurons (stellate and basket cells) and Purkinje cells (PCs). For this purpose, we took advantage of a unique arrangement discovered in neuroanatomical studies, in which the spinal border cell (SBC) component of the ventral spinocerebellar system was found to be the only spinocerebellar tract which ascends in the contralateral lateral funiculus (coLF) and have terminations in sublobulus C1 of the paramedian lobule in the posterior cerebellum. Using electrical stimulation of this tract, we find a subset of the cerebellar cortical neurons in this region to be moderately or powerfully activated. For example, some of our granule cells displayed high intensity responses whereas the majority of the granule cells displayed no response at all. The finding that more than half of the PCs were activated by stimulation of the SBC tract indicated that this system is capable of directly influencing cerebellar cortical output. The implications of these findings for the view of the integrative functions of the cerebellar cortex are discussed.

Keywords: spinocerebellar tracts, granule cells, mossy fibers, Purkinje cells, golgi cells, interneurons, spinal cord, cerebellar cortex

INTRODUCTION

The spinocerebellar tracts constitute a major part of the total mossy fiber input to the cerebellum (Oscarsson, 1973) and are likely to be crucial components in the cerebellar function of coordination (Spanne and Jorntell, 2013). However, there is a multitude of different spinocerebellar pathways (Oscarsson, 1973; Matsushita et al., 1979; Matsushita and Ikeda, 1980) and there is today limited knowledge of the potency with which individual pathways can affect the different neurons of the cerebellar circuitry.

The purpose of the present study is to characterize the responses of cerebellar cortical neurons to mossy fiber input from the spinal border cell (SBC) tract. The SBC tract is one of the spinocerebellar tracts, specifically one of the subcomponents of the ventral spinocerebellar tract (Matsushita et al., 1979; Matsushita and Ikeda, 1980). In the posterior lobe of the cerebellum, SBC terminations are believed to be concentrated to, or even limited to, the sublobulus C1 of the paramedian lobule (Matsushita and Ikeda, 1980; Matsushita and Yaginuma, 1989). Since this region does not appear to receive input from other components of the ventral spinocerebellar tract (Matsushita and Ikeda, 1980), the SBC tract should be the only spinocerebellar tract which ascends in the contralateral lateral funiculus (coLF) and have terminations in sublobulus C1. Hence, stimulation of the coLF and recording cerebellar neuron responses would pose a unique opportunity to record the effects of one spinocerebellar tract in isolation. This can substantially facilitate the interpretation of how the responses are generated, as opposed to most *in vivo* studies of cerebellar cortex where multiple parallel pathways with widely different conduction times and synaptic linkages are activated.

In the present study, we use mid-thoracic electrical stimulation of the coLF, verified to antidromically activate SBCs, and record the responses of the cerebellar cortical neurons in sublobulus C1. We find only a small fraction of the granule cells to be activated by coLF stimulation, but many of these granule cells have strong spike responses. Among Golgi cells, molecular layer (ML) interneurons and Purkinje cells (PCs), somewhat less than half of the neurons display weak to moderate spike responses. We conclude that a single spinocerebellar tract appears to be capable of driving cerebellar cortex activity and hence influence the cortical output to the deep cerebellar nucleus.

MATERIALS AND METHODS

All experiments ($N = 20$) were made in the acute decerebrated preparation of the cat. The cats were prepared as previously described (Ekerot and Jorntell, 2001; Jorntell and Ekerot, 2002, 2003). Briefly, following an initial anesthesia with propofol (Diprivan® Zeneca Ltd, Macclesfield Cheshire, UK), the animals were decerebrated at the intercollicular level and the anesthesia

was discontinued. The animals were artificially ventilated and the end-expiratory CO_2, blood pressure and rectal temperature were continuously monitored and maintained within physiological limits. Mounting in a stereotaxic frame, drainage of cerebrospinal fluid, pneumothorax and clamping the spinal processes of a few cervical and lumbar vertebral bodies served to increase the mechanical stability of the preparation. To verify that the animal was decerebrated, we made EEG recordings using a silver ball electrode placed on the surface of the superior parietal cortex. Our EEG recordings were characterized by a background of periodic 1–4 Hz oscillatory activity, periodically interrupted by large-amplitude 7–14 Hz spindle oscillations lasting for 0.5 sec or more. These forms of EEG activities are normally associated with deep stages of sleep (Niedermayer and Lopes da Silva, 1993). The pattern of EEG activity and the blood pressure remained stable, also on noxious stimulation, throughout experiments (see also, Jorntell and Ekerot, 2006).

RECORDINGS AND STIMULATION

Before recordings, the bone and dura covering the posterior part of the left cerebellar paramedian lobule was removed. Laminectomies were made at the level of spinal segments T7–T9 and at the level of the spinal segments L3–L5. We aimed to make *in vivo* patch clamp recordings from neurons of the cerebellar cortex, in the sublobulus C1. This was done with patch clamp pipettes pulled to 6–19 MOhm potassium-gluconate based internal solution. Obtaining whole cell recordings from granule cells in the sublobule C1, however, proved more difficult than in the more accessible anterior lobe (Jorntell and Ekerot, 2006). Therefore the present paper includes only loose cell-attached recordings. The general procedures for patch pipette recordings in the granule layer in this preparation have been described previously (Jorntell and Ekerot, 2006). The seal resistances of the recordings of the present material were between 200–2000 MOhm. A HEKA EPC 800 patch clamp amplifier, set to current clamp, was used to amplify the responses from the micropipettes. The signal was converted to a digital signal using the analog-to-digital converter Power 1401 mkII from Cambridge Electronic Design (CED, Cambridge, UK). Extracellular metal electrode recordings (tungsten-in-glass microelectrodes with conical metal tips of 10–30 μm exposed length, with a tip diameter of well below 1 μm) were made from the granule cell layer (GCL) in the sublobulus C1 and SBCs at the L4 segment of the spinal cord, respectively. In order to be able to analyze the activity with a computer the analog-to-digital converter (Power 1401 mkII) from CED was used. The neural responses were sampled at 100 KHz and recorded continuously with the software Spike 2 from CED. The signal from the amplifiers was split between the Power 1401 mkII, and a NAD 302 stereo amplifier. The NAD 302 was used to listen to the analogue signal for monitoring activity during the experiment. The lateral funiculus, the cerebellar cortex and the SBC region were stimulated with tungsten microelectrodes with exposed tips of 30–120 μm. The Digitimer DS3 (Isolated constant current stimulator/stimulus isolator, Digitimer Ltd, Letchworth Garden City, UK) were used in order to deliver reproducible square stimulus pulses with a constant current. The Power 1401 mkII was used as an event timer for the Digitimer stimulators.

DATA PROCESSING

All neural data was converted from analogue to digital form using the Power 1401 mkII from CED. The software Spike 2 from CED was used to record the digital data. Spike 2 was also used to sort spike activity from noise. Spike shapes were required to have a characteristic spike shape as well as a signal to noise ratio of at least 1:3 in order to verify that it was a neural response rather than ambient noise being analyzed. Peristimulus histograms were made using Matlab. The local field potential analysis was done using a kernel estimation method to interpolate between the recording points in the cerebellum sublobulus C1.

CORTICAL CELL RECORDINGS WITHIN THE MEDIAL PART OF SUBLOBULUS C1

We made loose cell-attached extracellular recordings from granule cells and Golgi cells within the GCL of the medial sublobulus C1, and from PCs and ML interneurons in the overlying Purkinje cell layer (PCL) and ML. The definition of a unit as a granule cell was primarily done using the characteristic spike signature of granule cells, in particular the presence of interspike intervals of < 2.0 ms (Van Dijck et al., 2013), and by verifying that they were located in the granule layer based on field potential recordings (Bengtsson and Jorntell, 2007) and by keeping track of the depths at which PCs were encountered in each experiment for each plane of penetration (this could be done since each experiment involved a high number of electrode tracks). In some experiments, recorded granule cells were recovered morphologically and verified to have the characteristic morphology of granule cells ($N = 4$). In these experiments, the recording solution of the patch pipettes contained neurobiotin (1.8%) to obtain juxtacellular labeling (Pinault, 1996) of the granule cells we recorded from. In order to increase probability of staining electroporation was done at the end of recording, after all other electrophysiological tests were done. Electroporation was made with 0.1–0.4 nA square pulses with a 300 ms duty, and a 200 ms rest phase, repeated for at least 1 min. At the end of these experiments, the animals were sacrificed by injecting a lethal dose of 3 ml barbiturate and subsequently perfused with paraformaldehyde (4%). The posterior lobe of the cerebellum was excised and stored in paraformaldehyde for up to a week, before the cerebella was sectioned into 60 μm sagittal slices. The slices were incubated with streptavidin conjugated with Alexa 488 Fluor (Molecular Probes, Invitrogen Inc.) and mounted for visualization under the confocal microscope (Zeiss 310 LSM and Zeiss 510 LSM).

QUANTIFICATION OF THE RESPONSES IN CEREBELLAR CORTICAL NEURONS

In order to quantify the responses evoked by coLF stimulation we made peristimulus histograms of the evoked spike responses with 1 ms bin widths. For each histogram, an increase of the response by more than 1 S.D. from the 100 ms prestimulus baseline activity for at least three out of five consecutive bins was taken as an evoked response. Assuming that the frequencies of the Peristimulus time histogram (PSTH) bins are normally distributed, the likelihood of reaching above one standard deviation in a single bin would be approximately 15.9%. By choosing three out of the five PSTH bins as the limit for detection, the risk of a false positive

can be calculated to be 3.07%. This is the combined probability for all permutations where at least three out of five bins have values higher than one standard deviation above the mean value. This test was a good way to measure both slow broad based responses as well as rapid sharp responses. Only responses at 10 ms or shorter response latency time from effective stimulation were considered, since responses evoked at longer latency times were considered unlikely to be due to activation of the SBC tract. In order to calculate the mean net change in firing frequency, spontaneous activity, if it existed, was subtracted from the evoked response and the mean change in spike firing frequency over five consecutive bins was calculated. For the systematic data quantification, we included only the responses evoked by the three pulse stimulations (3 pulses at 3 ms interval) of the coLF.

The experimental procedures were approved in advance by the local Swedish Animal Research Ethics Committee.

RESULTS

We aimed to make loose-patch recordings from the cerebellar cortical neurons of sublobule C1 (**Figure 1A**), since patch clamp recordings are essentially required to obtain granule cell recordings *in vivo* (Jorntell and Ekerot, 2006). However, before recording sessions commenced, we delineated the functional organization of the climbing fiber inputs of the paramedian lobule, within which the sublobule C1 is located. We found that the more rostral parts of the C1 zone (not to be confused with the sublobule C1) in the paramedian lobule received climbing fiber input from the ipsilateral distal forelimb, as previously described (Armstrong et al., 1971a,b; Trott and Apps, 1993), and the caudal termination of this representation was found to be a reliable indicator of where the anatomically defined sublobule C1 and the representation of the coLF input began (**Figure 1B**). This part of the cerebellum was sometimes also found to receive a weak climbing fiber input from the distal ipsilateral hindlimb.

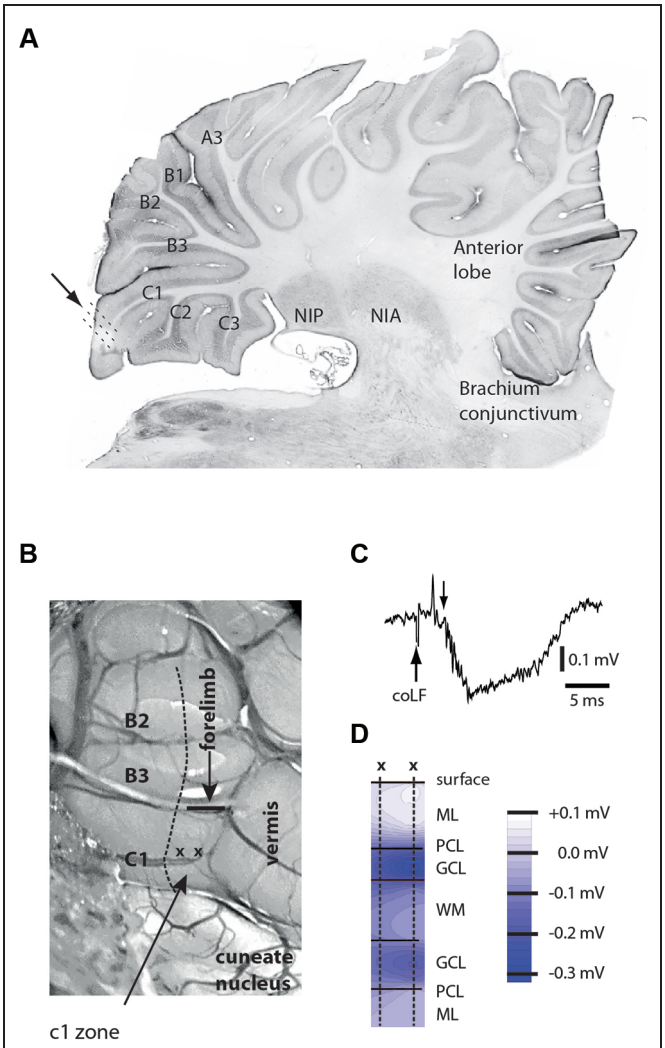

FIGURE 1 | Anatomical and physiological identification of the recording region. (A) Microelectrode and patch clamp recording electrodes were inserted at an angle of 30–45° relative to the surface of sublobulus C1 (arrow and dotted lines). Letters and numerals refer to the nomenclature of the sublobules in the paramedian lobule (Matsushita and Ikeda, 1980). NIP, nucleus interpositus posterior; NIA, nucleus interpositus anterior. **(B)** Surface view of the posterior part of the paramedian lobule, viewed at an angle of approximately 30°. Sublobules are indicated to the left. The arrow points to the C1 zone (not to be confused with the sublobule C1), within which all unit recordings were made. Also indicated are the location of the vermis and the caudal termination (horizontal bar) of the forelimb representation of the C1 zone. The horizontal bar is also a calibration for a 1 mm distance. **(C)** Sample field potential response, evoked in the GCL by coLF stimulation at 300 μA. Downward arrow indicates the onset of the evoked field potential. The preceding volley reflects evoked ascending activity from the brain stem. **(D)** Depth profiles of responses evoked in medial sublobulus C1 by single pulse stimulation of coLF at 0.5 mA. ML, PCL, GCL, WM.

FIELD POTENTIAL RECORDINGS OF coLF RESPONSES IN SUBLOBULUS C1

In order to further maximize our chances of finding cortical neurons activated by putative SBC input, we first conducted a field potential study of responses evoked by stimulation of the coFL. Focussing on sublobule C1, we recorded the distribution of evoked field potentials (**Figures 1C,D**). The distribution of maximal mossy fiber field potentials was investigated in eight experiments. In all cases, we found that maximal field potentials evoked by coLF stimulation were located in the most medial part of the sublobule C1. The response latency times of the onset of these potentials were 4.3 +/−0.1 ms (mean +/− standard deviation) for field potentials evoked from Th8–Th9 ($N = 8$).

ANTIDROMIC ACTIVATION OF SBCs FROM THE CEREBELLAR CORTEX AND THE coLF

In order to verify that our coLF stimulation was effective in activating the SBCs, we made direct tungsten electrode recordings from SBCs ($N = 25$) in the L4 segment of the spinal cord and tested whether they were antidromically activated. To obtain SBC recordings, we used two alternate types of tracks (**Figure 2A**). In one of the approaches, the electrode had 0° angle in the mediolateral plane and entered the spinal cord at the same mediolateral level as the dorsal root entrance. In the second approach, the electrode was tilted 10° in the mediolateral plane and entered the spinal cord a few 100 μms lateral to the dorsal root entrance. With both approaches, the electrode travelled through white matter

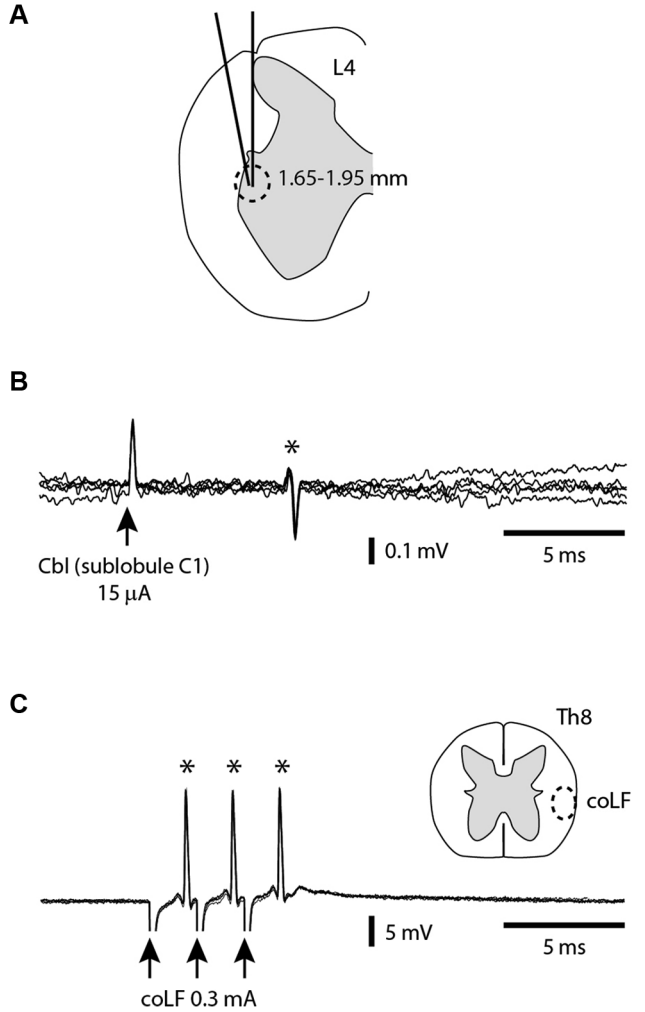

FIGURE 2 | Antidromic activation of SBCs from the sublobule C1 and the coLF. (A) A cross-section of the L4 segment (from Shrestha et al., 2012a) indicating the two alternative orientation of the electrode tracks and the depths at which the SBCs were found. **(B)** Example of SBC extracellular unit (*) antidromically activated from sublobule C1 in the cerebellum. **(C)** Example of SBC unit (*) antidromically activated from the coLF. Also indicated is the targeted location in the Th8 segment of the coLF stimulation electrode, based on Matsushita et al. (1979); Matsushita and Ikeda (1980).

(WM), where we monitored the ambient noise level by sound, the impalement of axons by the sharp tip of the electrode, and the lack of somatic neuronal unit recordings, all the way down to a depth of 1.5–1.7 mm, where noise indicative of neuronal units started to appear. Since our recordings were obtained from the first neurons encountered as we entered grey matter substance in the dorsal part of the ventral horn, they would by definition correspond to SBCs (Matsushita and Ikeda, 1980; Shrestha et al., 2012b). All SBC units encountered were located at a depth of 1.65–1.95 mm. Their antidromic activation was verified by recording a constant response latency time of the SBC spike at both single and triple pulse stimulation (three pulses at 3 ms interpulse interval) using interstimulus intervals of 300 ms (**Figures 2A,B**). Without antidromic stimulation, they were all ($N = 25$) completely silent.

For a subset of the recorded SBCs ($N = 9$), we investigated the points of minimal threshold for antidromic activation from the sublobuli B2, B3 and C1 (see **Figure 1A**) of the cerebellar cortex. This was done by using a tungsten stimulation electrode. As we tracked for low threshold points, the stimulation electrode was switched to recording mode so that the type of cerebellar layer the electrode was located in could be monitored. For each SBC, we managed to find points of minimal thresholds for antidromic activation within the cerebellar cortex (**Figure 2B**) with minimal effective intensities below 30 μA, in a few cases below 10 μA. These low threshold points were always located within the GCL of the medial part of sublobulus C1, confirming the findings that we previously made with field potential recordings that the SBC tract terminated primarily medially within the sublobule C1 (**Figure 1**). The response latency times for antidromic activation of SBCs from the cerebellar cortex was 6.0 +/−1.9 ms, with a range of 4.2–9.8 ms ($N = 9$).

The next step was to verify that the SBCs were also antidromically activated by the coLF stimulation (**Figure 2C**) that we used for evoking activity in the cerebellar cortical neurons. A separate tungsten stimulation electrode was lowered about 1.8–2.0 mm into the ventrolateral quadrant of the spinal cord at the thoracic level 8. The stimulation intensity was adjusted to find the threshold for antidromic activation, which could be as low as 30 μA. A fixed response latency time (with a standard deviation of 0.0 ms in all cases, $N = 25$) already at threshold stimulation was taken as an indication that these neurons were antidromically rather than synaptically activated. To increase the likelihood that these neurons were not synaptically activated by the stimulation, we compared the highest possible subthreshold stimulation intensity (with no response) with the threshold intensities. The differences were less than 5% in all cases. However, collision tests, where a spontaneous spike blocks the arrival of the antidromically activated spike, were not possible to perform since the SBC neurons in our preparation were completely silent and exhibited no spontaneous spiking. Nevertheless, we believe that the other measures we did obtain are sufficient to make it highly likely that the SBC neurons were indeed antidromically activated by the coLF stimulation, as previously shown (Jankowska et al., 2011a,b; Shrestha et al., 2012a,b). The highest thresholds for antidromic activation of SBCs using coLF stimulation was 0.3–0.5 mA, and this was also the intensity chosen for activation of cerebellar cortical neurons in the subsequent parts of the paper. For coLF stimulation, the response latency times for antidromic activation of SBCs was 1.9 +/−0.8 ms, with a range of 1.2–2.8 ms ($N = 25$).

RESPONSES OF GRANULE CELLS TO coLF STIMULATION

Granule cells (**Figure 3A**) and the other neurons were recorded in the cell-attached mode. The identification of neurons as single units was made on basis of single spike shape (using templates in software) and a consistent spike amplitude. During the experiments we continuously monitored the spike signals on loudspeakers and computer screens to make sure that the isolated unit was a single unit. Against the background that the cell-

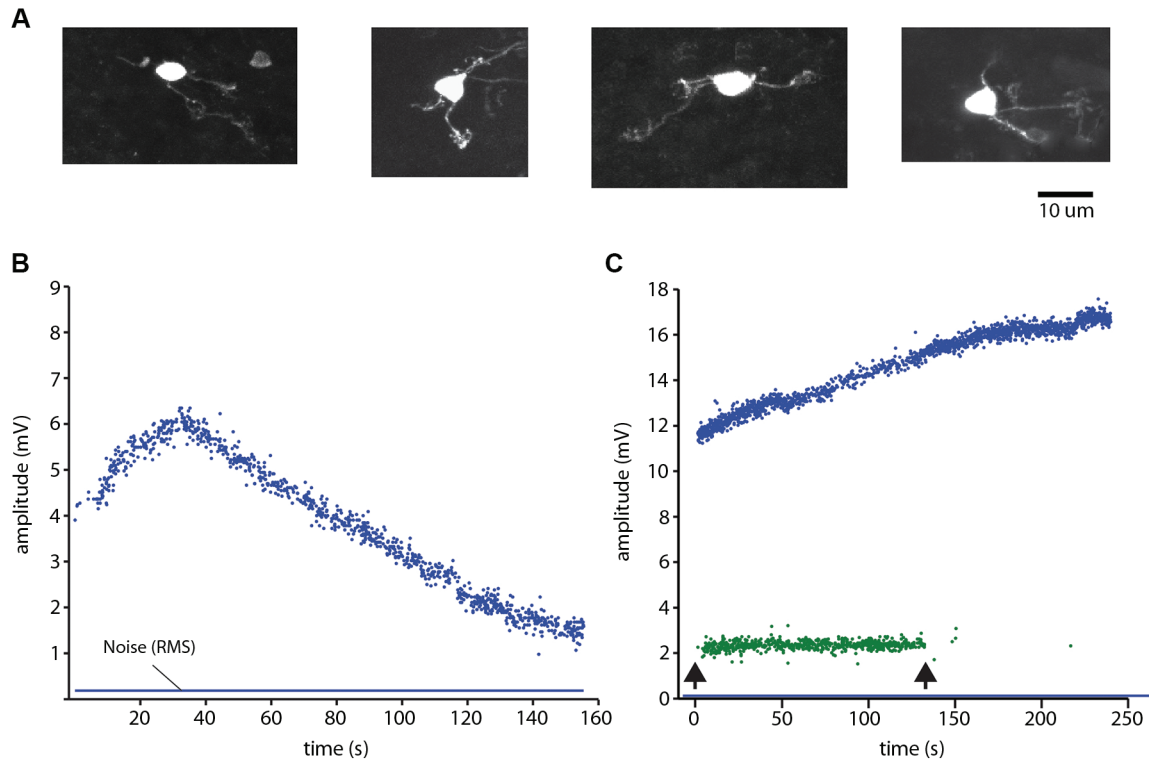

FIGURE 3 | Granule cell identification. (A) Examples of morphologically identified granule cells recovered from the sublobule C1. **(B)** Plot of the peak to peak amplitude of a spike recording of a granule cell in cell-attached mode. Note the variation over time of the spike amplitude. Blue line indicates the root mean square of the noise level of the recordings. Spike activity was evoked by ongoing coLF stimulation. **(C)** Single electrode-parallel recording of a Golgi cell (blue) and a granule cell (green) (Bengtsson and Jorntell, 2009a; Bengtsson et al., 2013). Arrows indicate onset and offset, respectively, of the coLF stimulation.

attached mode has been reported to in rare cases generate dual cell recordings (Bengtsson and Jorntell, 2009a; Bengtsson et al., 2013), we here illustrate how we can be sure that we recorded from single granule cells. **Figure 3B** illustrates the amplitude of a granule cell spike, which could vary over time. **Figure 3C** illustrates a rare example of a dual cell recording in the GCL, from a Golgi cell and a granule cell. Here, too, the spike amplitude varied over time, but the variation was different for the two neurons, which was an additional means to verify that the two neurons were distinct units and that single neuron recordings were derived from a single neuron. Note that this measurement started already as we approached the neuron, before the seal was established but when we could detect spike activity, which was monitored throughout all electrode tracks. Hence, the possibility that any neural recording labeled as unitary was rather a dual recording must be minimal or negligible.

A subset of the granule cells recorded ($N = 164$) responded to coLF stimulation with one or two spikes at a regular response latency time of 5–7 ms (**Figure 4A**). Such responses resulted in very sharp peaks in the peri-stimulus histograms (**Figure 4B**). In other granule cells, the spike responses were also powerful but consisted of more variable spike response times, which created more broad-based responses in the peristimulus histograms (**Figure 4C**, black bars). In such cases, the apparent response latency time was typically longer. However, we routinely checked the granule cell responses also to triple pulse stimulation (3 ms interpulse interval). For longer latency responses, the triple pulse stimulation typically provided additional responses at the same time or even before the response evoked by the single pulse stimulation, despite that the stimulations both started at time zero. Since the second pulse added to the response evoked by the single pulse (compare grey and black bars in **Figure 4C**), the response latency time from the second pulse was taken as the *effective response latency* in these cases. Based on the antidromic response latency times of the SBCs, which fell in the range of 4–10 ms (**Figure 2**), only granule cell responses that had an effective response latency time of less than 11 ms were considered to be due to activation of SBCs. In this group of granule cells, the effective response latency time was 6.5 +/−1.2 ms (range 4.5–9.0 ms, $N = 29$). The magnitude of the responses was measured from the first 5 ms of the response evoked by the 3 pulse stimulation. Based on the response magnitudes, we could segregate the granule cells into two groups ($p < 0.05$, t-test); those responding with an average spike intensity of 90 Hz or more and those responding at less than 60 Hz. For the high-intensity group, the average firing frequency of the evoked response was 257 +/−98 Hz ($N = 16$). For the low-intensity group, the firing frequency of the evoked response was 46 +/−21 Hz ($N = 13$).

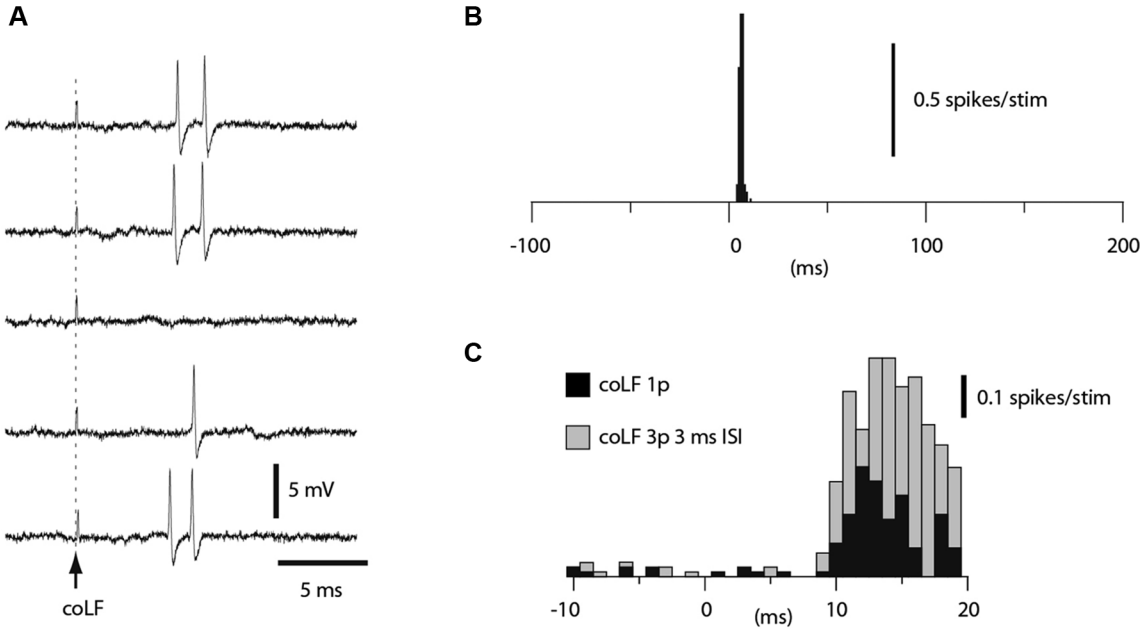

FIGURE 4 | Granule cell responses evoked by coLF stimulation. (A) Loose cell-attached extracellular recording of a granule cell responding to coLF stimulation at 0.5 mA. **(B)** Peristimulus histogram for the granule cell in A. **(C)** Peristimulus histogram of the responses of another granule cell to coLF stimulation using single (black bars) and three pulse stimulation (3 ms interpulse interval) (grey bars), respectively. The bin width in the histograms was 1 ms.

RESPONSES OF GOLGI CELLS, PURKINJE CELLS AND MOLECULAR LAYER INTERNEURONS TO coLF STIMULATION

We also recorded the evoked spike responses in Golgi cells (N = 27), PCs (N = 16) and ML interneurons (N = 11) in the medial part of sublobule C1. Golgi cells were identified by their location in the granule layer (see description for granule cells in Section Materials and Methods; briefly, the definition relies on the characteristic polarity changes of evoked mossy fiber field potential responses and the location of the PCL where the characteristic complex spikes can be recorded (Eccles et al., 1967; Bengtsson and Jorntell, 2007)) and their long tuning distances as well as their firing characteristics (Van Dijck et al., 2013), PCs were identified by the presence of complex spikes whereas interneurons were identified by their location in the ML interneurons and the absence of complex spikes (Jorntell and Ekerot, 2011). Complex spikes were separated from simple spikes by their distinct secondary depolarization and secondary spikelets within 1–5 ms after the initial spike (cf. **Figure 5B**).

Among Golgi cells, direct responses to coLF stimulation (**Figure 5A**) were more common (11/27) than among granule cells, possibly reflecting the large dendritic trees and more widespread input sampling of these cells. Similar to granule cells, the intensity of the response could vary substantially between Golgi cells (**Figure 5A**). The effective response latency times were 6.5 +/−1.6 ms (N = 11), also this value was similar to that of granule cells. The net evoked responses were 62 +/−27 Hz (N = 11), with a considerable range (4–82 Hz). Also some PCs in this region responded quite powerfully to coLF stimulation (**Figure 5B**), whereas other PCs had weaker input. Only 6 out of the 16 PCs recorded lacked detectable responses to coLF stimulation. The effective response latency time was 8.7 +/−1.6 ms and the net evoked responses were 40 +/−32 Hz (range 10–103 Hz). For ML interneurons (**Figure 5C**), 5 of the 11 recorded neurons had responses with an effective response latency time of 8.8 +/−1.6 ms and a net response of 42 +/−26 Hz (range 8–93 Hz).

DISCUSSION

The present paper is the first investigation of the responses evoked in all the major types of cerebellar cortical neurons from a putative single component of the spinocerebellar systems. The approach of directly activating mossy fibers greatly facilitates the interpretation of how the responses are generated as compared to other studies where more complex inputs (i.e., peripheral activation of multiple parallel pathways) or behaviorally generated spike discharges have been analyzed. The analysis of the responses of cerebellar cortical neurons to the direct activation of the SBC mossy fiber pathway indicated that these responses are relatively straight forward reflections of the input, although the synaptic weights of the input may vary across the population. Some of the neurons responded with very powerful responses and the responses evoked in the PCs suggest that the information conveyed by a single component of the spinocerebellar pathways can readily make its way to the cerebellar cortical output. The implications of our findings in relation to our understanding of cerebellar function in general, and the Marr-Albus family of ideas of cerebellar granule layer function in particular, are discussed.

TRANSMISSION OF THE SPINOCEREBELLAR MOSSY FIBER INFORMATION THROUGH THE CEREBELLAR CORTEX

Different neurons had different effective response latency times, which is compatible with our observations that the antidromic

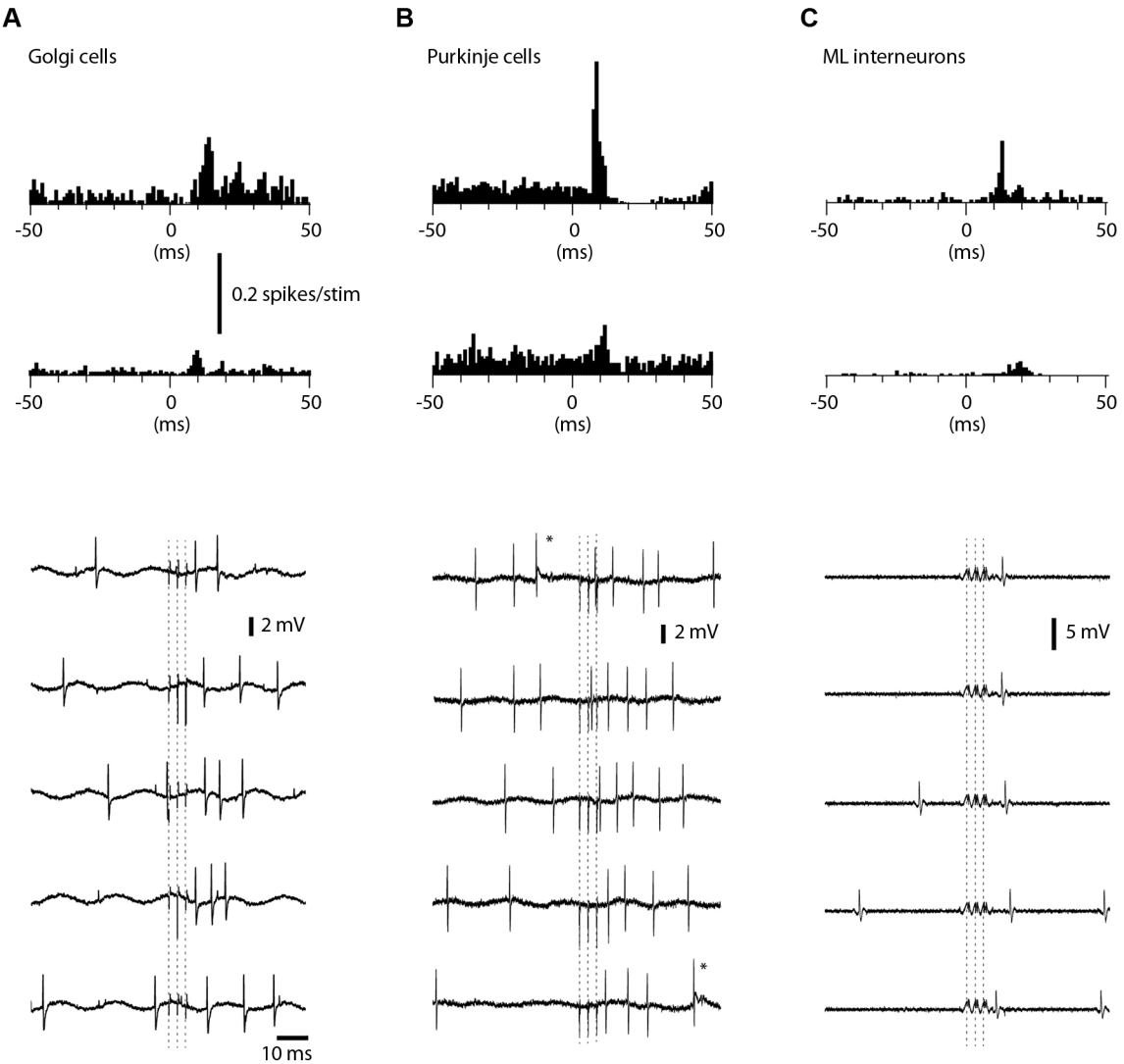

FIGURE 5 | Responses of Golgi cells, PCs and ML interneurons to coLF stimulation. coLF triple pulse stimulation at 0.5 mA was used in all panels. At the top are peristimulus histograms with a bin width of 1 ms of the responses, at the bottom sample raw traces. **(A)** Peristimulus histograms for two examples of Golgi cells, one with a strong response and a second with a weaker response. Sample raw traces below are from the Golgi cell with strong responses. Dashed lines indicate time of stimulation (three pulses). **(B)** Peristimulus histograms for two examples of PCs (only simple spike activity was analyzed). Sample raw traces are from the PC with moderate response. Asterisks indicate complex spikes. **(C)** Peristimulus histograms for two examples of ML interneurons. Sample raw traces are from the ML with a strong response. Due to the very large artefacts from the coLF stimulation (due to the high seal in this recording) software filtering was applied in this case only.

response latency times of the SBCs varied considerably, similar to the antidromic response latency times for other components of the ventral spinocerebellar tract (Geborek et al., 2013). Quite possibly, some granule cells received SBC inputs from units with similar conduction velocity, which would be expected to result in very sharp response profiles in the histograms as in **Figure 4B**, whereas others received inputs from less well synchronized SBC inputs whereby the response profiles in the histograms would become broader (**Figure 4C**). Since granule cells typically have a relatively wide gap between the resting membrane potential and firing threshold and requires the summation of three or four mossy fiber synapses to fire (Chadderton et al., 2004; Jorntell and Ekerot, 2006; Duguid et al., 2012), even a low-amplitude broad based response could be considered a strong response. Notably, since we used direct electrical stimulation of a population of mossy fibers, the input generated is artificially synchronous and does of course not reflect the spatiotemporal patterns of activity that these mossy fibers would display during behavior. Nevertheless, it does provide a measure of how effective the synaptic input is and whether it can be transmitted to downstream neurons. The range of different intensities in the responses suggests that we recorded from Golgi cells, PCs and ML interneurons with different locations relative to the clusters of granule cells receiving strong activation from the coLF stimulation. The fact that the

granule cell responses were transmitted, suggests that this population of granule cells (i.e., those activated by the SBC tract) provide relatively effective synapses to the other cortical neuron types.

IMPLICATIONS FOR MODELS OF CEREBELLAR CORTICAL FUNCTION

For granule cells, the average response frequency of 260 Hz (in the group of granule cells labeled high-intensity responders) is a very strong response, although higher intensity responses have been reported using more natural types of activation of the mossy fiber input (Jorntell and Ekerot, 2006). Nevertheless, for a stimulation that would be expected to set up only 3 spikes at 333 Hz in each of the activated mossy fibers, such response intensities in granule cells is compatible with that most or all of the mossy fiber inputs to these granule cells were activated from the stimulated tract, in agreement with our previous analysis of granule cells in the cerebellar C3 zone of the anterior lobe (Jorntell and Ekerot, 2006; Bengtsson and Jorntell, 2009b). The present study could however not provide any direct evidence for this since we failed to obtain any intracellular recordings from the high-intensity responders. At any rate, the demonstration that the information is transmitted so powerfully through some of the granule cells, verified by the fact that we also recorded responses in the PCs and ML interneurons (**Figure 4**) has some important implications for the original Marr-Albus ideas of cerebellar granule layer processing (Marr, 1969; Albus, 1971). In Marr's important theoretical paper, it was assumed that each of the four mossy fiber synapses that the granule cell received were needed to be activated in conjunction in order to trigger the output of the granule cells, which is also in agreement with findings from *in vitro* and *in vivo* studies (D'Angelo et al., 1995; Jorntell and Ekerot, 2006; Bengtsson and Jorntell, 2009b). However, Marr postulated that each of these mossy fibers carried unique information and it was only when input from these separate sources of information were driven coincidentally that the granule cell could be made to fire. Granule cell firing was hence believed to be a rare event and the idea of sparse coding in the GCL, which is a widespread notion in cerebellar theories, was a natural consequence of this line of reasoning. This part of the original Marr-Albus ideas would hence predict that a single mossy fiber pathway should not be capable of activating a granule cell. However, the present study tested this prediction and the result was that a single pathway is capable of activating a substantial part of the granule cells in the region. Some of them were in fact quite powerfully activated, and the output from these granule cells was also sufficient to activate many downstream neurons including nearly half of the PCs, which mediate the output of the cerebellar cortex. Similar conclusions have previously been drawn for a completely different system of the cerebellar cortex, i.e., the responses generated by the cuneate nucleus in the granule cells and the cortical neurons of the the C3 zone of the cerebellar anterior lobe (Dean et al., 2010). In the C3 zone, activation from single, small receptive fields from a single submodality evokes very intense granule cell responses, and the cells are easily sustaining firing frequencies of 100's of Hz for many seconds if the peripheral input is delivered appropriately (Jorntell and Ekerot, 2006; Bengtsson and Jorntell, 2009b). The PCs of the C3 zone are powerfully driven by this input (Jorntell and Ekerot, 2002, 2011).

Nevertheless, in the present study, we also found a group of granule cells with weaker responses to SBC tract stimulation. For this group of cells, it cannot be excluded that some of the mossy fiber synapses that converged onto them were not activated by the SBC tract but derived from another, unidentified, input source. This would imply that the principle of similar coding convergence between mossy fibers and granule cells (Bengtsson and Jorntell, 2009b) does not always apply for 100% of the mossy fiber inputs to all granule cells but that there could be examples of granule cells that sample inputs from pathways that are not functionally identical. This principle has recently been demonstrated using cell-type specific projection mapping of external cuneate nucleus (ECN) and basilar pontine nucleus (BPN) mossy fibers to the cerebellar cortex of the mouse (Huang et al., 2013). ECN and BPN target mostly non-overlapping areas of the cerebellar cortex, but there are fringe zones in their terminations in which they overlap. In these fringe zones, Huang et al. demonstrated the existence of granule cells, which receive input from both BPN and ECN. An uncertainty in that paper is whether all the projections labeled were derived solely from ECN or BPN, since at least the termination of ECN mossy fibers were wider and less focused than those obtained with axon labeling of single, verified ECN cells (Quy et al., 2011). But the essence of their conclusion, that there exist granule cells which sample mossy fiber input from non-identical sources, seems undisputable. This would hence be compatible with our findings for the smaller group of granule cells that were low-intensity responders. It is important to recall that the existence of such granule cells does not change the conclusions with respect to the original Marr-Albus idea and cerebellar function discussed above—the fact that SBC tract stimulation alone can powerfully drive cerebellar output is sufficient to say that these original ideas cannot be correct in this respect.

ALTERNATIVE SOURCES OF MOSSY FIBER INPUTS TO SUBLOBULE C1

The region we recorded from could be defined as the physiological C1 zone of the paramedian lobule based on the climbing fiber responses that we recorded. The physiological C1 zone has a second representation in the cerebellar anterior lobe (Apps and Garwicz, 2005). Since the mossy fiber input to different parts of a single climbing fiber zone is at least partly branches from the same systems (Pijpers et al., 2006), the C1 zone of the sublobule C1 may be expected to receive mossy fiber inputs from similar systems as in the C1 zone of the anterior lobe. These systems are the bilateral ventral flexor reflex tract (bVFRT)-component of the lateral reticular nucleus (LRN; Clendenin et al., 1974; Ekerot, 1990), cortico-pontine input and dorsal column nucleus input from the trunk or hindlimb (Cooke et al., 1971; Gerrits et al., 1985). In addition, the neurons of the Clarke's column of the thoracic segments, i.e., the thoracic component of the dorsal spinocerebellar tract (DSCT), has been shown to terminate in the sublobule C1 (Matsushita and Ikeda, 1980). None of these systems would be directly excited by coLF stimulation, as their fibers are all located on the ipsilateral side of the spinal cord: DSCT ascends ipsilaterally, the dorsal funiculus input ascends ipsilaterally, the bVFRT-input to the LRN ascends ipsilaterally, and the corticospinal fibers that activate the pontine nuclei is located in the ipsilateral dorsolateral funiculus,

although a contribution from the uncrossed corticospinal fibers cannot be excluded. In the latter case, however, the fibers are few, are located ventrally in the spinal cord (Armand and Kuypers, 1980), and the input would involve an extra synaptic relay in the pons, which would imply later responses than the ones we observed. Taken together, this is an unlikely alternative. Activation of other descending motor command systems, such as the tecto- and vestibulospinal tracts, which could be located in the vicinity of the coLF, have bilateral terminations and therefore could activate one of the spinocerebellar systems targeting the sublobule C1, remains a likely alternative. However, this would involve extra synaptic delays and their responses would therefore be expected to occur later than inputs from the SBCs—in fact, in quite a few cases we saw substantial activations well beyond the 12 ms response latency limit we applied, which could correspond to this alternative route of cerebellar activation. For the granule cell spike responses we recorded, with an average effective latency time of 6 ms, direct activation of the ascending SBC axons remains the most probable route.

INFORMATION CONVEYED BY SPINOCEREBELLAR TRACTS

Spinocerebellar neurons integrate information from descending motor command systems with sensory feedback information mediated by spinal premotor interneurons (summarized in Oscarsson, 1973; Jankowska et al., 2010; Hammar et al., 2011; Jankowska et al., 2011a,b; Krutki et al., 2011; Shrestha et al., 2012a,b; Spanne and Jorntell, 2013). Specifically, SBCs receive monosynaptic excitatory inputs from the reticulospinal tract, indirect information from rubro- and corticospinal tracts and primarily inhibitory inputs from interneurons activated by group I and group II muscle afferents (Hammar et al., 2011; Jankowska et al., 2011a; Shrestha et al., 2012a,b). The information conveyed seems to be sensory events and motor command components that applies to multiple limb segments and is therefore likely to be important for the function of coordination (Spanne and Jorntell, 2013). A possible explanation for the relatively powerful activation of the downstream cortical neurons from the SBC tract, despite that only a relatively small part of the granule cell population was activated by this input, is that this type of crucial signals for coordination are given high synaptic weights in a larger population of cortical neurons. In addition, the integration of sensory feedback with internal motor command signals makes these systems ideal substrates for the formation of internal models. The observation that PCs can signal in a fashion compatible with an internal model representation (Pasalar et al., 2006; Popa et al., 2012, 2013) could be due to the information conveyed by the spinocerebellar systems.

ACKNOWLEDGMENTS

This study was supported by grants from NINDS/NIH (R01 NS040863), The Hand Embodied (THE) (an Integrated Project funded by the EU under FP7, project no. 248587) and the Swedish Research Council (VR Medicine).

REFERENCES

Albus, J. S. (1971). A theory of cerebellar function. *Math. Biosci.* 10, 25–61.

Apps, R., and Garwicz, M. (2005). Anatomical and physiological foundations of cerebellar information processing. *Nat. Rev. Neurosci.* 6, 297–311. doi: 10.1038/nrn1646

Armand, J., and Kuypers, H. G. (1980). Cells of origin of crossed and uncrossed corticospinal fibers in the cat: a quantitative horseradish peroxidase study. *Exp. Brain Res.* 40, 23–34.

Armstrong, D. M., Harvey, R. J., and Schild, R. F. (1971a). Climbing fibre pathways from the forelimbs to the paramedian lobule of the cerebellum. *Brain Res.* 25, 199–202. doi: 10.1016/0006-8993(71)90582-8

Armstrong, D. M., Harvey, R. J., and Schild, R. F. (1971b). Distribution in the anterior lobe of the cerebellum of branches from climbing fibres to the paramedian lobule. *Brain Res.* 25, 203–206. doi: 10.1016/0006-8993(71)90583-x

Bengtsson, F., and Jorntell, H. (2007). Ketamine and xylazine depress sensory-evoked parallel fiber and climbing fiber responses. *J. Neurophysiol.* 98, 1697–1705. doi: 10.1152/jn.00057.2007

Bengtsson, F., and Jorntell, H. (2009a). Climbing fiber coupling between adjacent purkinje cell dendrites in vivo. *Front. Cell. Neurosci.* 3:7. doi: 10.3389/neuro.03.007.2009

Bengtsson, F., and Jorntell, H. (2009b). Sensory transmission in cerebellar granule cells relies on similarly coded mossy fiber inputs. *Proc. Natl. Acad. Sci. U S A* 106, 2389–2394. doi: 10.1073/pnas.0808428106

Bengtsson, F., Geborek, P., and Jorntell, H. (2013). Cross-correlations between pairs of neurons in cerebellar cortex in vivo. *Neural Netw.* 47, 88–94. doi: 10.1016/j.neunet.2012.11.016

Chadderton, P., Margrie, T. W., and Hausser, M. (2004). Integration of quanta in cerebellar granule cells during sensory processing. *Nature* 428, 856–860. doi: 10.1038/nature02442

Clendenin, M., Ekerot, C. F., Oscarsson, O., and Rosen, I. (1974). The lateral reticular nucleus in the cat. I. Mossy fibre distribution in cerebellar cortex. *Exp. Brain Res.* 21, 473–486. doi: 10.1007/bf00237166

Cooke, J. D., Larson, B., Oscarsson, O., and Sjolund, B. (1971). Origin and termination of cuneocerebellar tract. *Exp. Brain Res.* 13, 339–358. doi: 10.1007/bf00234336

D'Angelo, E., De, F. G., Rossi, P., and Taglietti, V. (1995). Synaptic excitation of individual rat cerebellar granule cells in situ: evidence for the role of NMDA receptors. *J. Physiol.* 484, 397–413.

Dean, P., Porrill, J., Ekerot, C. F., and Jorntell, H. (2010). The cerebellar microcircuit as an adaptive filter: experimental and computational evidence. *Nat. Rev. Neurosci.* 11, 30–43. doi: 10.1038/nrn2756

Duguid, I., Branco, T., London, M., Chadderton, P., and Hausser, M. (2012). Tonic inhibition enhances fidelity of sensory information transmission in the cerebellar cortex. *J. Neurosci.* 32, 11132–11143. doi: 10.1523/jneurosci.0460-12.2012

Eccles, J. C., Ito, M., and Szentágothai, J. (1967). *The Cerebellum as a Neuronal Machine.* Berlin: Springer-Verlag.

Ekerot, C. F. (1990). The lateral reticular nucleus in the cat. VIII. Excitatory and inhibitory projection from the bilateral ventral flexor reflex tract (bVFRT). *Exp. Brain Res.* 79, 129–137. doi: 10.1007/bf00228881

Ekerot, C. F., and Jorntell, H. (2001). Parallel fibre receptive fields of Purkinje cells and interneurons are climbing fibre-specific. *Eur. J. Neurosci.* 13, 1303–1310. doi: 10.1046/j.0953-816x.2001.01499.x

Geborek, P., Nilsson, E., Bolzoni, F., and Jankowska, E. (2013). A survey of spinal collateral actions of feline ventral spinocerebellar tract neurons. *Eur. J. Neurosci.* 37, 380–392. doi: 10.1111/ejn.12060

Gerrits, N. M., Voogd, J., and Nas, W. S. (1985). Cerebellar and olivary projections of the external and rostral internal cuneate nuclei in the cat. *Exp. Brain Res.* 57, 239–255. doi: 10.1007/bf00236529

Hammar, I., Krutki, P., Drzymala-Celichowska, H., Nilsson, E., and Jankowska, E. (2011). A trans-spinal loop between neurones in the reticular formation and in the cerebellum. *J. Physiol.* 589, 653–665. doi: 10.1113/jphysiol.2010.201178

Huang, C. C., Sugino, K., Shima, Y., Guo, C., Bai, S., Mensh, B. D., et al. (2013). Convergence of pontine and proprioceptive streams onto multimodal cerebellar granule cells. *Elife* 2:e00400. doi: 10.7554/elife.00400

Jankowska, E., Krutki, P., and Hammar, I. (2010). Collateral actions of premotor interneurons on ventral spinocerebellar tract neurons in the cat. *J. Neurophysiol.* 104, 1872–1883. doi: 10.1152/jn.00408.2010

Jankowska, E., Nilsson, E., and Hammar, I. (2011a). Do spinocerebellar neurones forward information on spinal actions of neurones in the feline red nucleus? *J. Physiol.* 589, 5727–5739. doi: 10.1113/jphysiol.2011.213694

Jankowska, E., Nilsson, E., and Hammar, I. (2011b). Processing information related to centrally initiated locomotor and voluntary movements by feline spinocerebellar neurones. *J. Physiol.* 589, 5709–5725. doi: 10.1113/jphysiol.2011.213678

Jorntell, H., and Ekerot, C. F. (2002). Reciprocal bidirectional plasticity of parallel fiber receptive fields in cerebellar Purkinje cells and their afferent interneurons. *Neuron* 34, 797–806. doi: 10.1016/s0896-6273(02)00713-4

Jorntell, H., and Ekerot, C. F. (2003). Receptive field plasticity profoundly alters the cutaneous parallel fiber synaptic input to cerebellar interneurons in vivo. *J. Neurosci.* 23, 9620–9631.

Jorntell, H., and Ekerot, C. F. (2006). Properties of somatosensory synaptic integration in cerebellar granule cells in vivo. *J. Neurosci.* 26, 11786–11797. doi: 10.1523/jneurosci.2939-06.2006

Jorntell, H., and Ekerot, C. F. (2011). Receptive field remodeling induced by skin stimulation in cerebellar neurons in vivo. *Front. Neural Circuits* 5:3. doi: 10.3389/fncir.2011.00003

Krutki, P., Jelen, S., and Jankowska, E. (2011). Do premotor interneurons act in parallel on spinal motoneurons and on dorsal horn spinocerebellar and spinocervical tract neurons in the cat? *J. Neurophysiol.* 105, 1581–1593. doi: 10.1152/jn.00712.2010

Marr, D. (1969). A theory of cerebellar cortex. *J. Physiol.* 202, 437–470.

Matsushita, M., Hosoya, Y., and Ikeda, M. (1979). Anatomical organization of the spinocerebellar system in the cat, as studied by retrograde transport of horseradish peroxidase. *J. Comp. Neurol.* 184, 81–106. doi: 10.1002/cne.901840106

Matsushita, M., and Ikeda, M. (1980). Spinocerebellar projections to the vermis of the posterior lobe and the paramedian lobule in the cat, as studied by retrograde transport of horseradish peroxidase. *J. Comp. Neurol.* 192, 143–162. doi: 10.1002/cne.901920110

Matsushita, M., and Yaginuma, H. (1989). Spinocerebellar projections from spinal border cells in the cat as studied by anterograde transport of wheat germ agglutinin-horseradish peroxidase. *J. Comp. Neurol.* 288, 19–38. doi: 10.1002/cne.902880103

Niedermayer, E., and Lopes da Silva, F. (1993). *Electroencephalography: Basic Principles, Clinical Applications, and Related Fields.* Baltimore: Williams and Wilkins.

Oscarsson, O. (1973). "Functional organization of spinocerebellar paths," in *Handbook of Sensory Physiology*, ed A. Iggo (New York: Springer-Verlag), 339–380.

Pasalar, S., Roitman, A. V., Durfee, W. K., and Ebner, T. J. (2006). Force field effects on cerebellar Purkinje cell discharge with implications for internal models. *Nat. Neurosci.* 9, 1404–1411. doi: 10.1038/nn1783

Pijpers, A., Apps, R., Pardoe, J., Voogd, J., and Ruigrok, T. J. (2006). Precise spatial relationships between mossy fibers and climbing fibers in rat cerebellar cortical zones. *J. Neurosci.* 26, 12067–12080. doi: 10.1523/jneurosci.2905-06.2006

Pinault, D. (1996). A novel single-cell staining procedure performed in vivo under electrophysiological control: morpho-functional features of juxtacellularly labeled thalamic cells and other central neurons with biocytin or Neurobiotin. *J. Neurosci. Methods* 65, 113–136. doi: 10.1016/0165-0270(95)00144-1

Popa, L. S., Hewitt, A. L., and Ebner, T. J. (2012). Predictive and feedback performance errors are signaled in the simple spike discharge of individual Purkinje cells. *J. Neurosci.* 32, 15345–15358. doi: 10.1523/jneurosci.2151-12.2012

Popa, L. S., Hewitt, A. L., and Ebner, T. J. (2013). Purkinje cell simple spike discharge encodes error signals consistent with a forward internal model. *Cerebellum* 12, 331–333.

Quy, P. N., Fujita, H., Sakamoto, Y., Na, J., and Sugihara, I. (2011). Projection patterns of single mossy fiber axons originating from the dorsal column nuclei mapped on the aldolase C compartments in the rat cerebellar cortex. *J. Comp. Neurol.* 519, 874–899. doi: 10.1002/cne.22555

Shrestha, S., Bannatyne, B. A., Jankowska, E., Hammar, I., Nilsson, E., and Maxwell, D. J. (2012a). Inhibitory inputs to four types of spinocerebellar tract neurons in the cat spinal cord. *Neuroscience* 226, 253–269. doi: 10.1016/j.neuroscience.2012.09.015

Shrestha, S. S., Bannatyne, B. A., Jankowska, E., Hammar, I., Nilsson, E., and Maxwell, D. J. (2012b). Excitatory inputs to four types of spinocerebellar tract neurons in the cat and the rat thoracolumbar spinal cord. *J. Physiol.* 590, 1737–1755. doi: 10.1113/jphysiol.2011.226852

Spanne, A., and Jorntell, H. (2013). Processing of multi-dimensional sensorimotor information in the spinal and cerebellar neuronal circuitry: a new hypothesis. *PLoS Comput. Biol.* 9:e1002979. doi: 10.1371/journal.pcbi.1002979

Trott, J. R., and Apps, R. (1993). Zonal organization within the projection from the inferior olive to the rostral paramedian lobule of the cat cerebellum. *Eur. J. Neurosci.* 5, 162–173. doi: 10.1111/j.1460-9568.1993.tb00482.x

Van Dijck, G., Van Hulle, M. M., Heiney, S. A., Blazquez, P. M., Meng, H., Angelaki, D. E., et al. (2013). Probabilistic identification of cerebellar cortical neurones across species. *PloS One* 8:e57669. doi: 10.1371/journal.pone.0057669

Conflict of Interest Statement: The authors declare that the research was conducted in the absence of any commercial or financial relationships that could be construed as a potential conflict of interest.

Received: 01 May 2013; accepted: 17 September 2013; published online: 08 October 2013.

Citation: Geborek P, Spanne A, Bengtsson F and Jörntell H (2013) Cerebellar cortical neuron responses evoked from the spinal border cell tract. Front. Neural Circuits 7:157. doi: 10.3389/fncir.2013.00157

This article was submitted to the journal Frontiers in Neural Circuits.

frontiers in
NEURAL CIRCUITS

ORIGINAL RESEARCH ARTICLE
published: 17 January 2013
doi: 10.3389/fncir.2012.00120

Stimulation within the cuneate nucleus suppresses synaptic activation of climbing fibers

Pontus Geborek, Henrik Jörntell and Fredrik Bengtsson*

Department of Experimental Medical Science, Lund University, Lund, Sweden

Edited by:
Chris I. De Zeeuw, Erasmus Medical Center, Netherlands

Reviewed by:
Edward S. Ruthazer, Montreal Neurological Institute, Canada
Alan Gibson, St. Joseph's Hospital and Medical Center, USA

***Correspondence:**
Fredrik Bengtsson, Department of Experimental Medical Science, Lund University, BMC F10, 22184 Lund, Sweden.
e-mail: fredrik.bengtsson@med.lu.se

Several lines of research have shown that the excitability of the inferior olive is suppressed during different phases of movement. A number of different structures like the cerebral cortex, the red nucleus, and the cerebellum have been suggested as candidate structures for mediating this gating. The inhibition of the responses of the inferior olivary neurons from the red nucleus has been studied extensively and anatomical studies have found specific areas within the cuneate nucleus to be target areas for projections from the magnocellular red nucleus. In addition, GABA-ergic cells projecting from the cuneate nucleus to the inferior olive have been found. We therefore tested if direct stimulation of the cuneate nucleus had inhibitory effects on a climbing fiber field response, evoked by electrical stimulation of the pyramidal tract, recorded on the surface of the cerebellum. When the pyramidal tract stimulation was preceded by weak electrical stimulation (5–20 μA) within the cuneate nucleus, the amplitude of the climbing fiber field potential was strongly suppressed (approx. 90% reduction). The time course of this suppression was similar to that found after red nucleus stimulation, with a peak suppression occurring at 70 ms after the cuneate stimulation. Application of CNQX (6-cyano-7-nitroquinoxaline-2,3-dione, disodium salt) on the cuneate nucleus blocked the suppression almost completely. We conclude that a relay through the cuneate nucleus is a possible pathway for movement-related suppression of climbing fiber excitability.

Keywords: cuneate nucleus, inferior olive, inhibition, climbing fiber field response, pyramidal tract

INTRODUCTION

Essential to all theories of cerebellar function is the causes and conditions of climbing fiber activation. Several groups have shown that climbing fiber excitability is not constant but may change during different conditions in relation to movement. For example, the forelimb area of the C1-C3-Y zone system of the cerebellar cortex, which is innervated by the rostral subdivision of the dorsal accessory subdivision of the inferior olive (rDAO), is devoted to forelimb movement control via the motor cortex and the red nucleus. However, during different phases of movements, like reach-to-grasp (Gellman et al., 1985; Horn et al., 2004) and locomotion (Lidierth and Apps, 1990; Apps, 1999) climbing fiber excitability in the rDAO, is strongly modulated. Observations such as these have led to the idea of gating of synaptic transmission in the inferior olive (IO) during movement. An example of gating would be if an excitatory and an inhibitory synapse converged on the same cell, where the inhibitory synapse has the ability to prevent somatic depolarization from reaching firing threshold. An obvious candidate system for this gating would be the inhibitory nucleo-olivary pathway (Hesslow, 1986; Bengtsson and Hesslow, 2006). It has also been shown that stimulation of the magnocellular part of the red nucleus (RNm) inhibits responses evoked from the forelimb in rDAO neurons (Weiss et al., 1990; Horn et al., 1998; Gibson et al., 2002). This would represent a pathway by which the motor command itself can actively suppress climbing fiber discharge. This inhibition does not involve the cerebellum since the inhibition evoked from the red nucleus persisted after the cerebellum had been removed. Since the projection neurons of the RNm are not known to be inhibitory, RNm stimulation probably activates an additional pathway that has inhibitory effects in the IO.

Although numerous investigations were carried out to determine the location of this inhibitory pathway or the structure that mediates this effect, its location is still unknown. However, a possible candidate has been identified: descending fibers from the red nucleus and the cerebral cortex converge in a specific region of the cuneate nucleus in which the neurons have efferent projections to the rDAO (Kuypers and Tuerk, 1964; Holstege and Kuypers, 1982; McCurdy et al., 1992, 1998). The purpose of the present study is to investigate directly if this region of the cuneate nucleus has inhibitory effects on inferior olivary neurons. For this purpose, we use microelectrodes to stimulate within the caudal part of the cuneate nucleus and test the inhibitory effects on synaptic activation of climbing fiber field potentials in the C3 zone of the cerebellar cortex (see **Figure 1**).

MATERIALS AND METHODS

Seven adult cats were prepared as previously described (Ekerot and Jorntell, 2001; Jorntell and Ekerot, 2002, 2003). Briefly, the animals were initially anesthesia with propofol (Diprivan® Zeneca Ltd., Macclesfield Cheshire, UK), and mounted in a stereotaxic

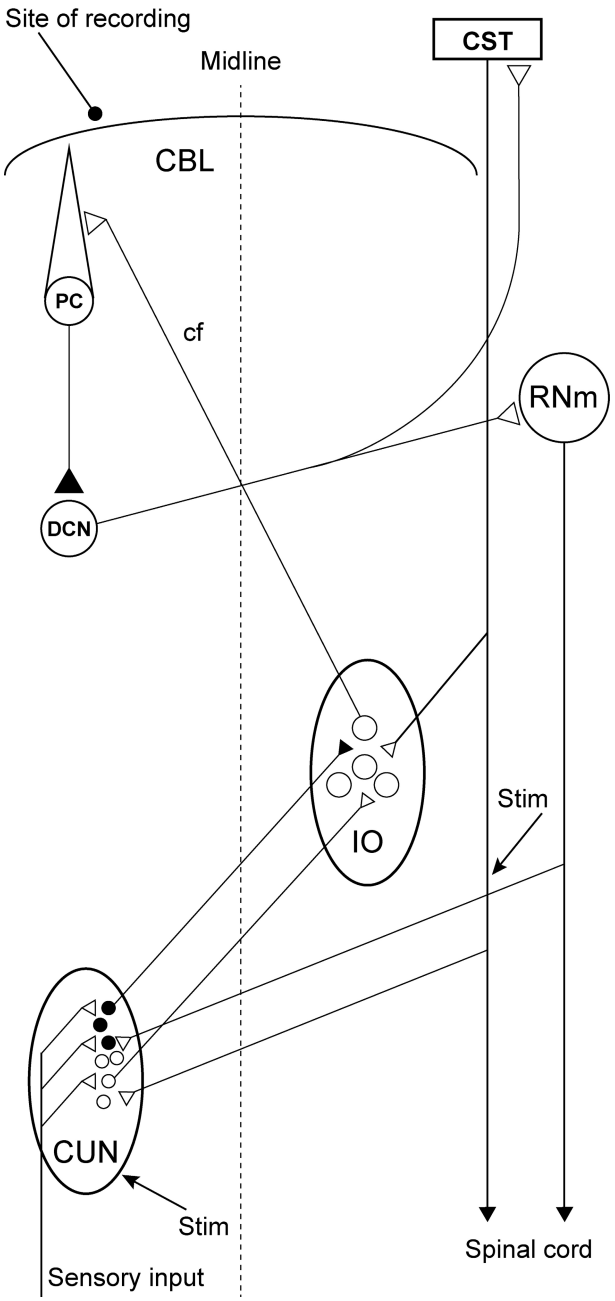

FIGURE 1 | Experimental set-up and schematic diagram outlining the anatomical connectivity of the structures studied. RNm, Magno cellular red nucleus; IO, inferior olive; CUN, main cuneate; CBL, the cerebellum; PC, Purkinje cell; DCN, deep cerebellar nucleus; CST, cortico spinal tract. Inhibitory neurons (filled circles).

frame and decerebrated at a high decerebration point (just rostral to the superior colliculus). Subsequent to this, the anesthesia was terminated and the animals were kept paralyzed with pancuronium (Pavulon â Organon Teknika B.V., Boxtel, Holland) throughout the experiment. The animals were artificially ventilated and the end-expiratory CO_2, blood pressure and rectal temperature were continuously monitored and maintained within physiological limits. Drainage of cerebrospinal fluid, pneumothorax and clamping the spinal processes of a few cervical and lumbar vertebral bodies served to increase the mechanical stability of the preparation. EEG recordings were characterized by a background of periodic 1–4 Hz oscillatory activity, periodically interrupted by large-amplitude 7–14 Hz spindle oscillations lasting for 0.5 s or more. These forms of EEG activities are normally associated with deep stages of sleep cf. (Niedermayer and Lopes Da Silva, 1993). The pattern of EEG activity and the blood pressure remained stable, also on noxious stimulation, throughout experiments.

RECORDINGS AND STIMULATION

The initial delineation of the forelimb area of the C3 zone in the cerebellar anterior lobe was performed as described previously (Jorntell and Ekerot, 2003). In order to access the cuneate nucleus the occipital bone surrounding the foramen magnum was cut 7 mm rostrally. In addition, the bone of the first cervical vertebra was cut to the rostral border of the second cervical vertebra. Subsequently, a tungsten-in-glass microelectrode, with an exposed metal tip of 10–30 μm, was placed stereotaxically in the pyramidal tract just caudal (2 mm) to the IO at a depth of 4 mm from the surface of the brainstem, 1 mm lateral to the midline. The effectiveness of the pyramidal tract stimulation was verified by recording pyramidal tract volleys in the contralateral dorsolateral funiculus and, in some cases, through recordings from alpha-motoneurons that were synaptically excited by the pyramidal tract stimulation. The pyramidal tract stimulation was confirmed to evoke synaptic (in contrast to directly excited climbing fiber axons, cf. Jorntell and Ekerot, 2003) climbing fiber responses by recording with a silver ball electrode ($Ø = 250$ μm) placed on the surface in the C3 zone of the cerebellar cortex.

A similar tungsten-in-glass microelectrode, exposed tip (10–30 μm), was used to locate the cuneate nucleus (**Figure 2A**, see below). The electrode was lowered into the brainstem 5–15 mm caudal to the obex, 3 mm lateral to the midline. To evoke a synaptic field and neuronal activity in the cuneate nucleus, the skin of the distal forelimb (**Figure 2B**) was stimulated electrically through a pair of percutaneous needle electrodes separated by approximately 5 mm (1.2 mA, with single shocks, 0.1 ms long, at 1 Hz). The recording electrode was lowered systematically at different medio-lateral and rostro-caudal positions while recording the spontaneous activity, evoked field potentials and unitary responses to the stimulation throughout the electrode track (**Figures 2C,D,E**). The electrode was then left in a position where the recorded cells showed characteristic responses of cuneate cells (see **Figure 2D**). Two loci in the cuneate nucleus, one rostro-ventral and one caudo-ventral, have been reported for the termination of the fibers originating in the red nucleus (McCurdy et al., 1992, 1998). Here we focused on stimulation of the caudo-ventral locus. The cuneate electrode was switched to stimulation mode and subsequently used to condition the pyramidal tract stimulation, by preceding the latter at fixed intervals of 5–300 ms. The stimulation in the cuneate nucleus consisted of 1 or 2 pulses, 0.1 ms wide, with an interstimulus interval (ISI) of 3 ms and a constant current of 5–20 μA. After formaldehyde

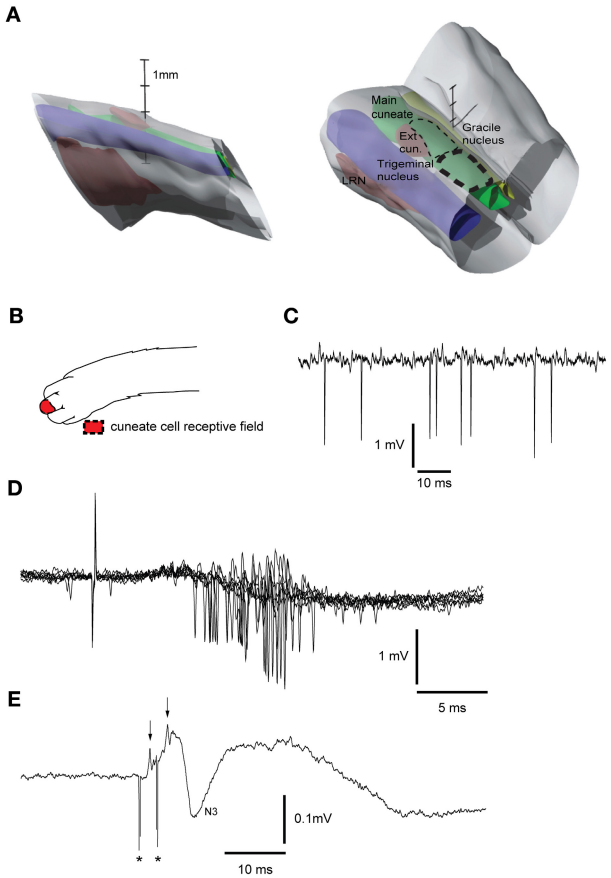

FIGURE 2 | Reconstruction of brainstem recording/stimulation site and sample recordings. (A) 3D reconstruction of the brainstem recording/stimulation sites. Thick dashed line represents the primary recording/stimulation area of the main cuneate nucleus. Thin dashed line shows the rostral extent of the recordings. LRN, Lateral reticular nucleus. Vertical scale bar tics: 1 mm. **(B)** Receptive field of cuneate cell recorded in **(C). (C)** Sample recording showing spontaneous cuneate cell activity. **(D)** Cuneate cell responses to electrical skin stimulation (1 pulse, 2 mA). **(E)** Response to electrical stimulation (2 pulses, 20 μA, 333 Hz) in the cuneate nucleus recorded on the surface of the cerebellar cortex. Asterisks indicate shock artifacts. Arrows indicate the afferent nerve volleys elicited by the stimulation. N3 field potential, [an indicator of activity in the parallel fiber synapses of the cerebellar cortex (Bengtsson and Jorntell, 2007)].

fixation of the tissue the brainstem was sectioned in 60 μm slices, stained with Cresyl Violet (Svensson et al., 2006) and scanned into an open source 3D-computer program (artofillusion.org) to render a 3D-reconstruction of the brainstem (**Figure 2A**).

Evoked synaptic climbing fiber activity was measured from the surface of the cerebellum while stimulating in the contralateral pyramidal tract. The pyramidal stimulation (1 pulse, 100–150 μA, 1 Hz) readily evoked large (300–600 μV) climbing fiber field potentials at a latency of 5–6 ms, sometimes preceded by a smaller mossy fiber field potential (see **Figure 3A**). Increasing the stimulation frequency beyond 2 Hz gradually reduced the amplitude of the evoked response which is a characteristic of synaptically evoked climbing fiber responses (Armstrong et al., 1968).

APPLICATION OF CNQX

In order to test if blocking the excitatory synaptic transmission within the cuneate nucleus affected the suppression of the pyramidal tract response evoked from the cuneate nucleus, we applied small volumes of the ampa-kainate receptor blocker CNQX (6-cyano-7-nitroquinoxaline-2,3-dione, disodium salt) (Disodium salt; Tocris Cookson, Bristol, UK) topically to the surface of the dorsal column nuclei. For this purpose a small piece of filter paper [corresponding to the size of the exposed surface area of the main cuneate nucleus (**Figure 2A**)] soaked in a solution containing CNQX [5 mM dissolved in phosphate-buffer (0.01 M, pH 7.4)] was placed on the surface of the main cuneate nucleus while we recorded the evoked climbing fiber field potential on surface of the cerebellum (as described above).

The experimental procedures were approved in advance by the local Swedish Animal Research Ethics Committee.

RESULTS

To test the gating of climbing fiber responses driven by motor command signals, we used the pyramidal tract as a test input. Pyramidal tract stimulation readily evokes climbing fiber responses in the cerebellum (Baker et al., 2001; Pardoe et al., 2004) (**Figure 3A**). Notably, electrical stimulation within the IO evoked a direct, non-synaptic climbing fiber field potential with a shorter response latency time than the climbing fiber response evoked from the pyramidal tract, consistent with a synaptic activation of inferior olivary neurons from the latter (**Figure 3A**) The site within the forelimb area of the C3 zone, at which the largest climbing fiber field potential was evoked from the pyramidal tract, was identified. The area of the forelimb from which electrical skin stimulation evoked the largest field potentials at this site was then identified. Subsequently, the cuneate nucleus was identified by stimulating the same forelimb skin site while recording cellular responses in the cuneate nucleus. After having localized a region in the caudal cuneate nucleus activated from this skin site, the electrode was left in position and switched to stimulation mode. We then proceeded by testing if conditioning stimulation in the cuneate nucleus had effects on the climbing fiber field response evoked by the pyramidal tract stimulation.

As is shown in **Figures 3A,B**, cuneate stimulation could in some cases almost completely block the climbing fiber field potential evoked by pyramidal tract stimulation. At an interval between the cuneate and pyramidal tract stimulations of 70 ms, the pyramidal tract response was substantially depressed (88% ± 4% SEM, $n = 35$, reduction of the evoked climbing fiber response amplitude).

LATENCY

By changing the interval between the cuneate and pyramidal tract stimulation, we characterized a time profile for the suppression of the climbing fiber field potential. The onset of the suppression was 30–35 ms (**Figure 4**). Maximal depression of the evoked climbing fiber response amplitude was found at an ISI of 70 ms (88% ± 4% SEM, $n = 35$, reduction of the evoked climbing fiber response amplitude). Interestingly, at intervals shorter than 10 ms, the paired stimulation occasionally

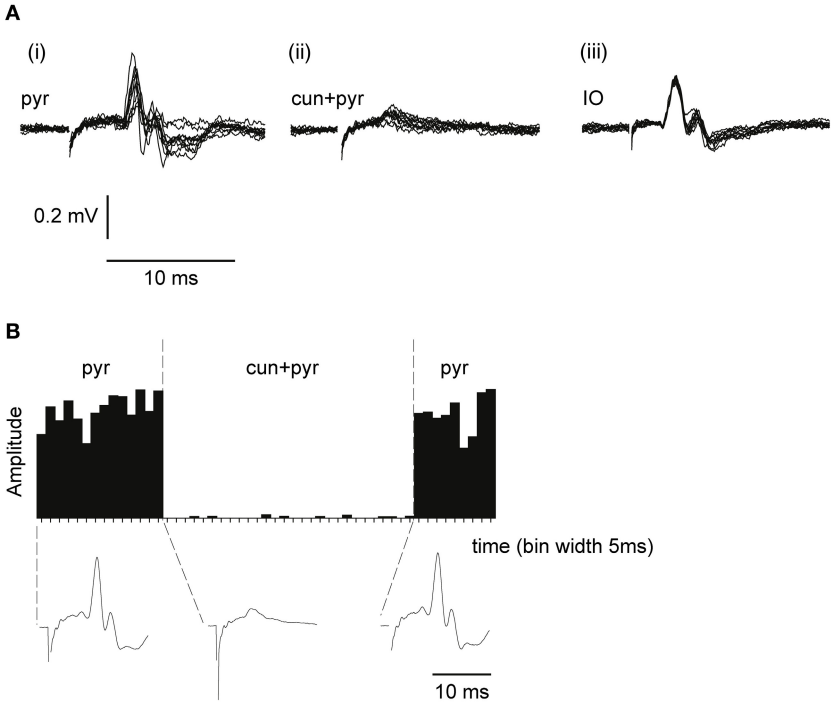

FIGURE 3 | Climbing fiber field potentials evoked from the pyramidal tract are depressed by a preceding cuneate stimulation. (A) From left to right, (i) climbing fiber field potential responses in the C3 zone evoked by electrical stimulation in the pyramidal tract (1 pulse, 300 μA, 1 Hz). (ii) Pyramidal tract stimulation preceded (70 ms interstimulus interval) by cuneate stimulation (2 pulses, 20 μA, 1 Hz). (iii) Climbing fiber field response evoked by electrical stimulation in the IO (1 pulse, 30 μA, 1 Hz). **(B)** Sample histogram showing the amplitude of climbing fiber field responses evoked by pyramidal tract stimulation before during and after a preceding (70 ms) cuneate stimulation (2 pulses, 20 μA, 1 Hz). Each bar represents the average of 5 consecutive responses (bin width, 5 s). Below the histogram, average response profiles for the evoked responses.

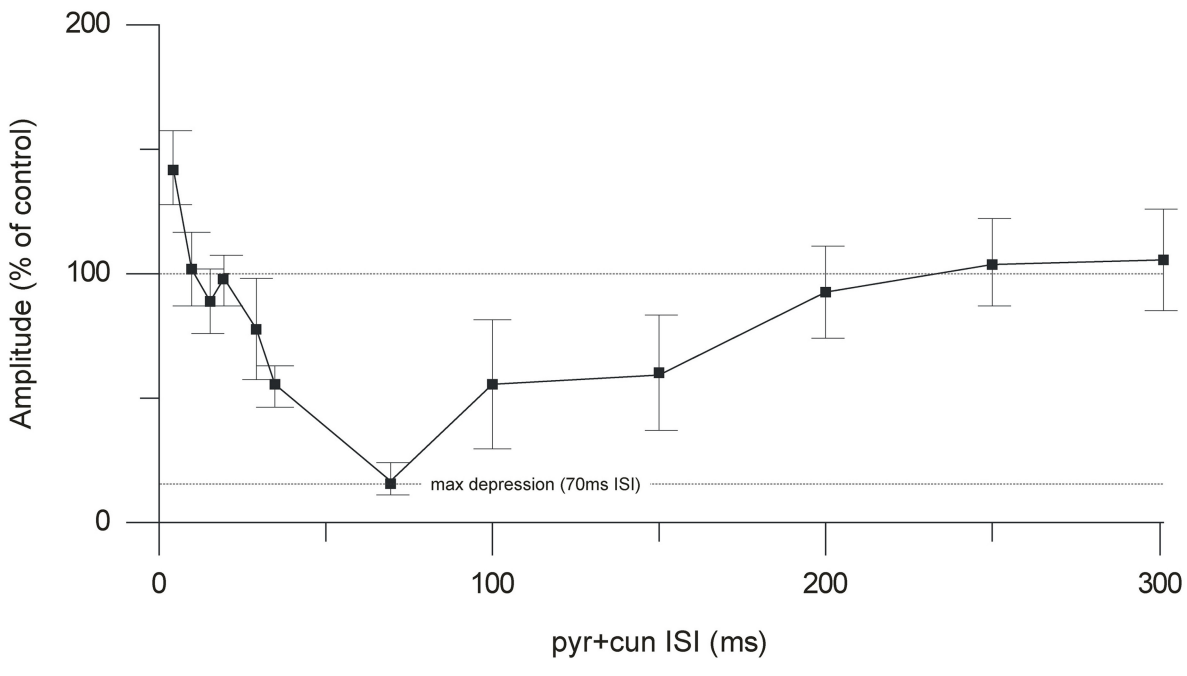

FIGURE 4 | Time course of the cuneate suppression of climbing fiber field responses evoked from the pyramidal tract. Average effect (% of control) (mean ± SEM, $n = 35$) of conditioning the evoked climbing fiber field response (70 ms) with cuneate stimulation (2 pulses, 20 μA, 1 Hz).

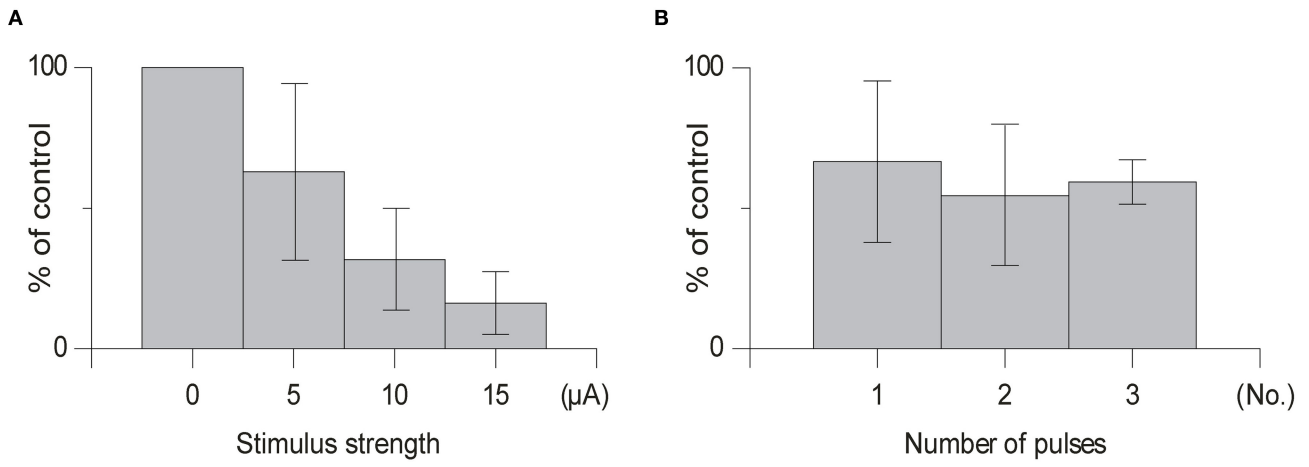

FIGURE 5 | Dorso-ventral and medio-lateral stimulation profiles. **(A)** Depth profile of the effect of the conditioning stimulus in the cuneate on the response amplitude of the climbing fiber field response evoked by stimulation in the pyramidal tract (1 pulse, 150 μA, 1 Hz). The cuneate stimulation preceded the pyramidal tract stimulation by 70 ms (2 pulses, 20 μA, 1 Hz) and was applied at different depths as indicated. **(B)** Depth profile of the conditioning effect in electrode track made 250 μm lateral to the cuneate nucleus. Same stimulation parameters as in **(A)**.

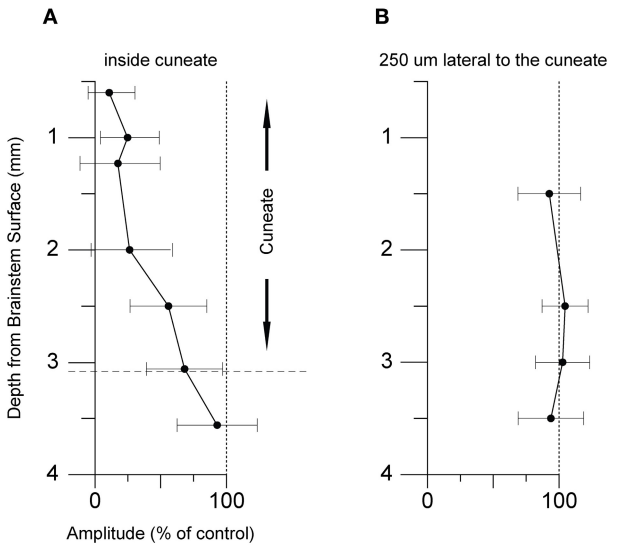

FIGURE 6 | Effect of varying the stimulation strength and number of stimulation pulses. **(A)** Average effect of cuneate stimulation strength on evoked climbing fiber field potential amplitude. Increasing stimulation strength from 5 μA to 15 μA (% of control, mean ± SD, $n = 5$). **(B)** Effect of the number of pulses in the cuneate stimulation train on the evoked climbing fiber field potential amplitude. Increasing number of pulses from 1 to 3 (% of control, mean ± SD, $n = 5$).

(observed in 5 out of 9 cases) resulted in a facilitation of the response evoked from the pyramidal tract (the response amplitude being 140% ± 8% SEM, $n = 5$, of its control value) rather than a suppression. In two animals we tested longer interstimulus intervals (80–300 ms). The results showed a gradual decline in the suppression from 100 to 200 ms interstimulus interval (**Figure 3**).

STIMULATION STRENGTH

In order to avoid activation of neighboring structures in the brainstem minimum stimulation strengths were used (range 5–20 μA). As can be seen in **Figure 5** in some cases the depressive effect occurred already at stimulation strengths as low as 5 μA. However, the effects clearly increased with increased stimulation intensity, when a larger number of cells and fibers in the cuneate nucleus would be expected to be activated.

NUMBER OF PULSES

We found that using one pulse was sufficient to suppress olivary transmission and that increasing the number of pulses in the same animal from 1 to 2 or 1 to 3 pulses had little effect (**Figure 5**) [1 pulse: mean suppression (79% ± 15% SD, $n = 5$); 2 pulses: (66% ± 16% SD, $n = 4$); 3 pulses (59% ± 9% SD, $n = 4$); $t > 0.14$] on the amplitude of the evoked climbing fiber field response. In all cases when testing the effect of the number of pulses the offset of the cuneate stimulation was kept constant.

POSITION

Next, we tested whether the inhibitory effects on the pyramidal tract-evoked climbing fiber field responses were confined to the region of the cuneate nucleus. For this purpose we made depth profiles, comparing suppression effects from a number of positions in the caudal cuneate. As the electrode was lowered in the tracks from a dorsal to a ventral position, the depression weakened (**Figure 6A**). Just ventral to the cuneate nucleus, at 3 mm or more of depth, the depression weakened and eventually ceased. We then proceeded to test the medio-lateral limits of the depression and found that positioning the electrode 250 μm lateral to the cuneate nucleus had no effect on the evoked response (**Figure 6B**). These findings were hence compatible with that the effect was due to stimulation of elements within the cuneate nucleus.

APPLICATION OF CNQX

In an attempt to further localize the origin of the suppression, in one experiment we applied the non-NMDA ionotropic glutamate receptor antagonist 6-cyano-7-nitroquinoxaline-2,3-dione (CNQX) (Sheardown, 1988), over the region overlying the cuneate nucleus. The effect on the climbing fiber field suppression obtained by paired cuneate and pyramidal tract stimulation was continuously monitored. As can be seen in **Figure 7** there was a marked reduction of the suppression. After 54 min the suppression had been reduced by 26% (26% ± 16% SD). After 152 min the effect had been reduced by 83% (83% ± 14% SD). The relatively long time that it took for the effects of CNQX application to develop fully, as well as the almost irreversible nature of the effect (which partly remained 4 h after the filter paper had been removed, 360 min after initial application) are compatible with similar observations made *in vitro* (Andreasen et al., 1989). We also monitored the transmission of synaptic input through the cuneate nucleus by recording the short-latency climbing fiber field response evoked by electrical skin stimulation (1 pulse, 2 mA), a response known to be mediated via the dorsal funiculus and the cuneate nucleus (Ekerot and Larson, 1980, 1982). Roughly in parallel to the developing reduction of the suppression of the pyramidal tract response over time, also the climbing fiber field response evoked from the skin was reduced

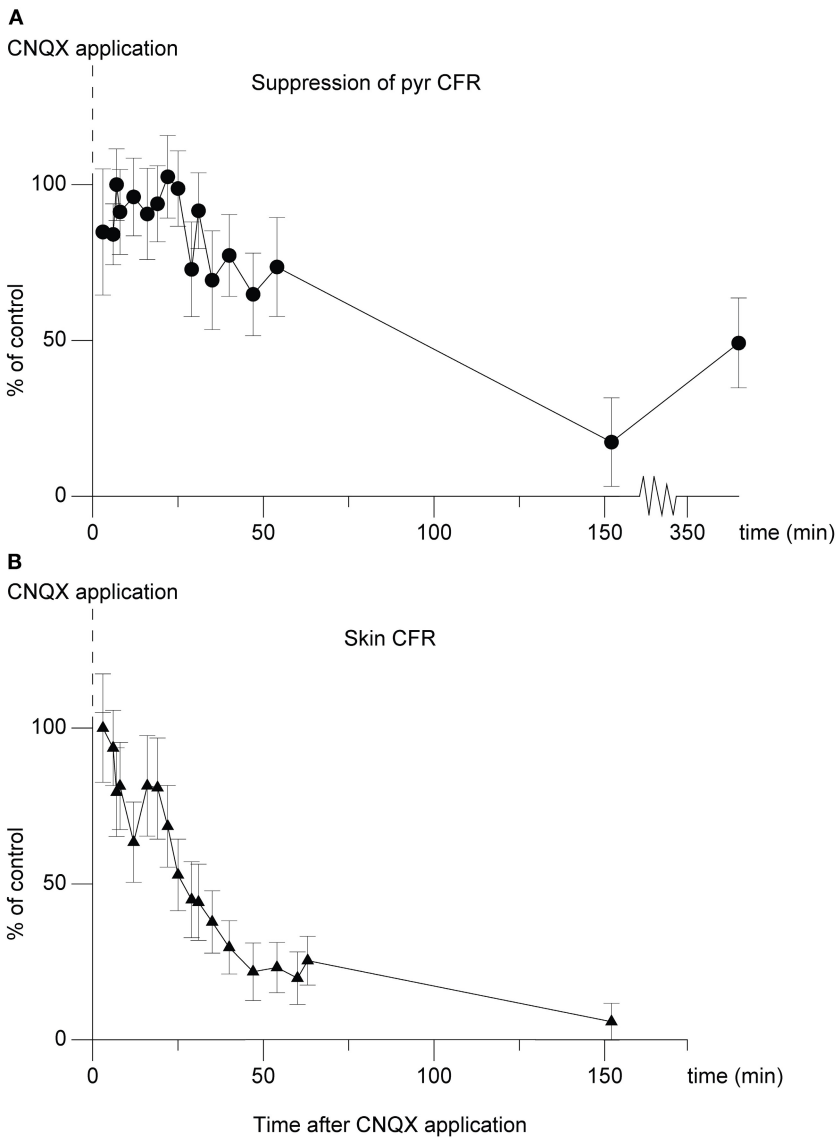

FIGURE 7 | Effect of CNQX application on the cuneo-olivary suppression and on climbing fiber field responses evoked from the forelimb skin. **(A)** Dots (●), shows the effect of CNQX application (5 mM) on the cuneate suppression of pyramidal climbing fiber field responses. Note that in this graph, 100% equals maximal suppressive effect, or control suppression level. The graph displays mean ± SD values for 20 stimulations at each time point displayed. The cuneate stimulation (2 pulses, 20 μA, 1 Hz) preceded the pyramidal climbing fiber field response by 70 ms. **(B)** Triangles (▲), parallel development of the climbing fiber field response evoked by electrical stimulation of the forelimb skin.

(peak reduction 94% ± 6% SD at 152 min) (**Figure 7**). This is in concert with that there are both excitatory and inhibitory connections from the cuneate to the IO (McCurdy et al., 1992, 1998). In contrast, the direct response evoked by the pyramidal tract was unaffected. After 54 min the amplitude of the latter was 109% (109% ± 19% SD) (% of control). After 152 min the amplitude was 115% (115% ± 19% SD) (% of control).

NUCLEO-OLIVARY INHIBITION

As it is known that output from the deep cerebellar nuclei inhibits olivary transmission (Hesslow, 1986; Bengtsson and Hesslow, 2006; Svensson et al., 2006; Bazzigaluppi et al., 2012) we made two experiments in which we lowered the level of decerebration to a mid-inferior collicular level so that the nucleo-olivary fibers known to run just ventral to the brachium conjunctivum (Legendre and Courville, 1987) were severed. The inhibitory effect observed in the high and low decerebrate preparations could not be separated ($p = 0.65$, student's t-test). These findings would suggest that the suppression of the pyramidal tract response was not mediated via the cerebellum.

DISCUSSION

Here we showed that electrical stimulation within the cuneate nucleus induced a remarkably potent suppression of synaptically evoked climbing fiber field responses. The effect was not obtained lateral or ventral to the cuneate. Blocking excitatory synaptic responses by CNQX applied over the cuneate nucleus essentially eliminated the suppressing effect. This reduction of the suppressing effect occurred in parallel with the development of a reduction of short-latency, skin-evoked climbing fiber field responses known to be transmitted through the cuneate nucleus. All these findings are compatible with the existence of a pathway through the cuneate nucleus being involved in the suppression of climbing fiber excitability. This pathway could be responsible for the inhibition of inferior olivary neuron firing that follows red nucleus stimulation (Weiss et al., 1990; Horn et al., 1998), compatible with the findings that fibers of the RNm terminate within specific regions of the cuneate nucleus and that these parts of the cuneate nucleus projects to the IO. Also pyramidal tract fibers terminate in this part of the cuneate (McCurdy et al., 1992, 1998), meaning that the depression of climbing fiber excitability observed during the initial phase of reaching movements (Horn et al., 1996; Gibson et al., 2002) could potentially involve this pathway. Leicht et al. (1973) found that stimulation of the pericruciate area of the cerebral cortex evoked inhibition of peripherally evoked climbing fiber responses at low thresholds and that the same stimulation evoked excitation of the IO at higher thresholds. An inhibitory pathway through the cuneate which is more easily excited than the pathway of the pyramidal tract to the inferior olivary neuron excitatory synaptic junction is compatible with may explain these findings.

Even single pulse stimulation at very low intensity (5 μA) elicited a strong suppression of the synaptically evoked climbing fiber field responses. McCurdy et al. (1992, 1998) found two ventral termination sites within the cuneate, one rostral, and one caudal, for the rubral fibers. Interestingly, in our case the suppression was most effective from sites located in the dorsal parts of the cuneate. Presumably this is due to the fact that the primary sensory afferent fibers that provide excitation to the cuneate neurons, which run from caudal to rostral just dorsal to the nucleus, branch widely in the rostrocaudal plane (Weinberg et al., 1990) and might hence serve to distribute the effects of the stimulation to a larger population of cuneate neurons. That the main effect of the cuneate nucleus stimulation was due to synaptic excitation of these neurons (the results of the CNQX experiment) is compatible with this interpretation.

The maximum suppression of the pyramidal tract climbing fiber field potential occurred when it was preceded by the cuneate stimulation by 70 ms. This is slightly longer than the response latency times of peak inhibition of inferior olivary neuron responses following red nucleus stimulation (50 ms) (Weiss et al., 1990), although the latency time in this case was calculated from the last pulse in a long train of pulses. Interestingly, these findings roughly match the timing of the inhibition elicited through the nucleo-olivary pathway in the cat (70 ms) and in the ferret (50 ms) (Hesslow, 1986; Svensson et al., 2006). Such long latency times are difficult to explain if one assumes a monosynaptic inhibitory connection. However, a possible explanation proposed is that the GABAergic transmission between the deep cerebellar nuclei and the IO could depend on asynchronous release of GABA, limiting the speed of the synapse (Best and Regehr, 2009).

POTENTIAL MECHANISMS OF THE SUPPRESSION

There are a few not mutually exclusive explanations for the recorded suppression. The first is that there are inhibitory cells projecting to the IO from the cuneate nucleus that are activated by the intra cuneate stimulation. The second is that the suppression occurs as a result of the refractory properties of the IO and as an effect of subthreshold olivary activation. The third is that other pre-olivary regions that have suppressing effects on transmission in the IO were activated.

For the first scenario, the existence of inhibitory (GABAergic) neurons in the cuneate nucleus projecting to the IO have been reported (Isomura and Hamori, 1988; Nelson et al., 1989a,b; Fredette et al., 1992). The cuneate stimulation could naturally result in synaptic excitation of these cells, which would be a straight-forward explanation for our results. Bazzigaluppi et al. (2012) recently showed that there, indeed, is a strong inhibitory effect in the IO cells when the deep cerebellar nuclei are activated and that this effect is dependent on activation of $GABA_A$ receptors. Given the similarity of the time course of the effect to our results, the same type of inhibitory mechanisms may also form the substrate for the inhibitory effects of cuneate activation.

For the second scenario, it cannot be excluded that the suppression occurs as an effect of intrinsic refractory properties of the IO. In fact, the facilitation of the pyramidal tract response when the conditioning stimulus occurred at less than 25 ms in advance is compatible with this interpretation. The mechanism would then be that the cuneate stimulation activates excitatory afferents to the rDAO that could cause a subthreshold excitatory response, possibly triggering Ca^{2+} influx in these cells.

A Ca^{2+}-dependent K^+ conductance is a prominent feature determining the physiology of the olivary cells (Llinas and Yarom, 1981a,b). The subthreshold Ca^{2+} influx could trigger this conductance, which would result in strong hyperpolarization with a time course that fits our observations. Consecutive synaptic excitations of inferior olivary cells are known to result in a strong suppression of the second response, essentially blocking transmission for intervals shorter than 100–150 ms (Armstrong and Harvey, 1968; Armstrong et al., 1968).

Thirdly, the suppression could have occurred through other brainstem pathways rather than the cuneate nucleus itself. A possible candidate is the relay in the cerebro-olivary pathway across the matrix region (Ackerley et al., 2006), which is located medially and ventrally to the caudal cuneate nucleus. However, this candidate is made less likely since the stimulating current required to evoke the suppression from the dorsal part of the cuneate was extremely low, the primary afferent fibers in this region run rostro-caudally rather than medio-laterally and are not known to make synapses with neurons in the matrix region. By lowering the decerebration level to a mid-collicular position we could exclude that the suppression originated in the deep cerebellar nuclei. This would for example, rule out that the effects of the stimulation resulted from synaptic excitation of cells in the lateral reticular nucleus, which would synaptically excite the deep cerebellar nuclear cells (Wu et al., 1999; Shinoda et al., 2000) and inhibit the IO via the nucleo-olivary cells (Bengtsson and Hesslow, 2006).

The present study illustrates that weak electrical stimulation within the cuneate nucleus, in particular its dorsal part, elicits a powerful suppression of synaptically evoked climbing fiber field responses. Combined with the results from numerous anatomical studies, we conclude that the cuneate nucleus is a possible candidate pathway involved in the suppression of inferior olivary excitability observed from the onset of reaching movements (Horn et al., 1996; Gibson et al., 2002).

In summary, inhibition of the IO seems to be an important feature, this especially so during active movement (Horn et al., 1996; Apps, 1999; Apps and Lee, 1999; Gibson et al., 2002). So far, at least two separate but parallel inhibitory pathways that are active during movement have been identified. The first, the nucleo-olivary pathway known to exert a powerful inhibition of the IO (Hesslow, 1986; Svensson et al., 2006; Bazzigaluppi et al., 2012) and to be active during the expression of conditioned reflex movements (Hesslow and Ivarsson, 1996). The second, the cuneo-olivary pathway, which most likely is activated by a number of different sources acting on the cuneate, like the red nucleus (McCurdy et al., 1992, 1998) and the cerebral cortex (Leicht et al., 1973), during movement. The common feature of these pathways is that they are all activate during movement and thus probably at least partly responsible for the lack of relationship between olivary discharge and movement. However, further studies are needed to explore if there are yet other pathways that can inhibit olivary transmission during active movement.

REFERENCES

Ackerley, R., Pardoe, J., and Apps, R. (2006). A novel site of synaptic relay for climbing fibre pathways relaying signals from the motor cortex to the cerebellar cortical C1 zone. *J. Physiol.* 576, 503–518.

Andreasen, M., Lambert, J. D., and Jensen, M. S. (1989). Effects of new non-N-methyl-D-aspartate antagonists on synaptic transmission in the *in vitro* rat hippocampus. *J. Physiol.* 414, 317–336.

Apps, R. (1999). Movement-related gating of climbing fibre input to cerebellar cortical zones. *Prog. Neurobiol.* 57, 537–562.

Apps, R., and Lee, S. (1999). Gating of transmission in climbing fibre paths to cerebellar cortical C1 and C3 zones in the rostral paramedian lobule during locomotion in the cat [see comments]. *J. Physiol. (Lond.)* 516(Pt 3), 875–883.

Armstrong, D. M., Eccles, J. C., Harvey, R. J., and Matthews, P. B. (1968). Responses in the dorsal accessory olive of the cat to stimulation of hind limb afferents. *J. Physiol.* 194, 125–145.

Armstrong, D. M., and Harvey, R. J. (1968). Responses to a spino-olivo-cerebellar pathway in the cat. *J. Physiol. (Lond.)* 194, 147–168.

Baker, M. R., Javid, M., and Edgley, S. A. (2001). Activation of cerebellar climbing fibres to rat cerebellar posterior lobe from motor cortical output pathways. *J. Physiol.* 536, 825–839.

Bazzigaluppi, P., Ruigrok, T., Saisan, P., De Zeeuw, C. I., and De Jeu, M. (2012). Properties of the nucleo-olivary pathway: an *in vivo* whole-cell patch clamp study. *PLoS ONE* 7:e46360. doi: 10.1371/journal.pone.0046360

Bengtsson, F., and Hesslow, G. (2006). Cerebellar control of the inferior olive. *Cerebellum* 5, 7–14.

Bengtsson, F., and Jorntell, H. (2007). Ketamine and xylazine depress sensory-evoked parallel fiber and climbing fiber responses. *J. Neurophysiol.* 98, 1697–1705.

Best, A. R., and Regehr, W. G. (2009). Inhibitory regulation of electrically coupled neurons in the inferior olive is mediated by asynchronous release of GABA. *Neuron* 62, 555–565.

Ekerot, C. F., and Jorntell, H. (2001). Parallel fibre receptive fields of Purkinje cells and interneurons are climbing fibre-specific. *Eur. J. Neurosci.* 13, 1303–1310.

Ekerot, C. F., and Larson, B. (1980). Termination in overlapping sagittal zones in cerebellar anterior lobe of mossy and climbing fiber paths activated from dorsal funiculus. *Exp. Brain Res.* 38, 163–172.

Ekerot, C. F., and Larson, B. (1982). Branching of olivary axons to innervate pairs of sagittal zones in the cerebellar anterior lobe of the cat. *Exp. Brain Res.* 48, 185–198.

Fredette, B. J., Adams, J. C., and Mugnaini, E. (1992). GABAergic neurons in the mammalian inferior olive and ventral medulla detected by glutamate decarboxylase immunocytochemistry. *J. Comp. Neurol.* 321, 501–514.

Gellman, R., Gibson, A. R., and Houk, J. C. (1985). Inferior olivary neurons in the awake cat: detection of contact and passive body displacement. *J. Neurophysiol.* 54, 40–60.

Gibson, A. R., Horn, K. M., and Pong, M. (2002). Inhibitory control of olivary discharge. *Ann. N.Y. Acad. Sci.* 978, 219–231.

Hesslow, G. (1986). Inhibition of inferior olivary transmission by mesencephalic stimulation in the cat. *Neurosci. Lett.* 63, 76–80.

Hesslow, G., and Ivarsson, M. (1996). Inhibition of the inferior olive during conditioned responses in the decerebrate ferret. *Exp. Brain Res.* 110, 36–46.

Holstege, G., and Kuypers, H. G. (1982). The anatomy of brain stem pathways to the spinal cord in cat. A labeled amino acid tracing study. *Prog. Brain Res.* 57, 145–175.

Horn, K. M., Hamm, T. M., and Gibson, A. R. (1998). Red nucleus stimulation inhibits within the inferior olive. *J. Neurophysiol.* 80, 3127–3136.

Horn, K. M., Pong, M., and Gibson, A. R. (2004). Discharge of inferior olive cells during reaching errors and perturbations. *Brain Res.* 996, 148–158.

Horn, K. M., Van Kan, P. L., and Gibson, A. R. (1996). Reduction of rostral dorsal accessory olive responses during reaching. *J. Neurophysiol.* 76, 4140–4151.

Isomura, G., and Hamori, J. (1988). Three types of neurons in the medial cuneate nucleus of the cat. *Neurosci. Res.* 5, 395–408.

Jorntell, H., and Ekerot, C. F. (2002). Reciprocal bidirectional plasticity of parallel fiber receptive fields in cerebellar Purkinje cells and their afferent interneurons. *Neuron* 34, 797–806.

Jorntell, H., and Ekerot, C. F. (2003). Receptive field plasticity profoundly alters the cutaneous parallel fiber synaptic input to cerebellar

interneurons *in vivo*. *J. Neurosci.* 23, 9620–9631.

Kuypers, H. G., and Tuerk, J. D. (1964). The distribution of the cortical fibres within the nuclei cuneatus and gracilis in the cat. *J. Anat.* 98, 143–162.

Legendre, A., and Courville, J. (1987). Origin and trajectory of the cerebello-olivary projection: an experimental study with radioactive and fluorescent tracers in the cat. *Neuroscience* 21, 877–891.

Leicht, R., Rowe, M. J., and Schmidt, R. F. (1973). Cortical and peripheral modification of cerebellar climbing fibre activity arising from cutaneous mechanoreceptors. *J. Physiol.* 228, 619–635.

Lidierth, M., and Apps, R. (1990). Gating in the spino-olivocerebellar pathways to the c1 zone of the cerebellar cortex during locomotion in the cat. *J. Physiol. (Lond.)* 430, 453–469.

Llinas, R., and Yarom, Y. (1981a). Electrophysiology of mammalian inferior olivary neurones *in vitro*. Different types of voltage-dependent ionic conductances. *J. Physiol. (Lond.)* 315, 549–567.

Llinas, R., and Yarom, Y. (1981b). Properties and distribution of ionic conductances generating electroresponsiveness of mammalian inferior olivary neurones *in vitro*. *J. Physiol. (Lond.)* 315, 569–584.

McCurdy, M. L., Gibson, A. R., and Houk, J. C. (1992). Spatial overlap of rubrospinal and corticospinal terminals with input to the inferior olive. *Neuroimage* 1, 23–41.

McCurdy, M. L., Houk, J. C., and Gibson, A. R. (1998). Organization of ascending pathways to the forelimb area of the dorsal accessory olive in the cat. *J. Comp. Neurol.* 392, 115–133.

Nelson, B., Mugnaini, E., and Strata, P. (1989a). "Origins of GABA-ergic inputs to the inferior olive," in *The Olivocerebellar System in Motor Control*, ed P. Strata (Berlin; Heidelberg; New York; London; Paris; Tokyo: Springer-Verlag), 86–107.

Nelson, B. J., Adams, J. C., Barmack, N. H., and Mugnaini, E. (1989b). Comparative study of glutamate decarboxylase immunoreactive boutons in the mammalian inferior olive. *J. Comp. Neurol.* 286, 514–539.

Niedermayer, E., and Lopes Da Silva, F. (1993). *Electroencephalography: Basic Principles, Clinical Applications, and Related Fields*. Baltimore, MD: Williams and Wilkins.

Pardoe, J., Edgley, S. A., Drew, T., and Apps, R. (2004). Changes in excitability of ascending and descending inputs to cerebellar climbing fibres during locomotion. *J. Neurosci.* 24, 2656–2666.

Sheardown, M. J. (1988). A new and specific non-NMDA receptor antagonist, FG 9065, blocks L-AP4-evoked depolarization in rat cerebral cortex. *Eur. J. Pharmacol.* 148, 471–474.

Shinoda, Y., Sugihara, I., Wu, H. S., and Sugiuchi, Y. (2000). The entire trajectory of single climbing and mossy fibers in the cerebellar nuclei and cortex. *Prog. Brain Res.* 124, 173–186.

Svensson, P., Bengtsson, F., and Hesslow, G. (2006). Cerebellar inhibition of inferior olivary transmission in the decerebrate ferret. *Exp. Brain Res.* 168, 241–253.

Weinberg, R. J., Pierce, J. P., and Rustioni, A. (1990). Single fiber studies of ascending input to the cuneate nucleus of cats: I. Morphometry of primary afferent fibers. *J. Comp. Neurol.* 300, 113–133.

Weiss, C., Houk, J. C., and Gibson, A. R. (1990). Inhibition of sensory responses of cat inferior olive neurons produced by stimulation of red nucleus. *J. Neurophysiol.* 64, 1170–1185.

Wu, H. S., Sugihara, I., and Shinoda, Y. (1999). Projection patterns of single mossy fibers originating from the lateral reticular nucleus in the rat cerebellar cortex and nuclei. *J. Comp. Neurol.* 411, 97–118.

Conflict of Interest Statement: The authors declare that the research was conducted in the absence of any commercial or financial relationships that could be construed as a potential conflict of interest.

Received: 17 September 2012; accepted: 21 December 2012; published online: 17 January 2013.

*Citation: Geborek P, Jörntell H and Bengtsson F (2013) Stimulation within the cuneate nucleus suppresses synaptic activation of climbing fibers. Front. Neural Circuits **6**:120. doi: 10.3389/fncir.2012.00120*

frontiers in
NEURAL CIRCUITS

REVIEW ARTICLE
published: 19 April 2013
doi: 10.3389/fncir.2013.00073

In and out of the loop: external and internal modulation of the olivo-cerebellar loop

***Avraham M. Libster*[1,2]* *and Yosef Yarom*[1,2]**

[1] *Department of Neurobiology, Life Science Institute, Hebrew University, Jerusalem, Israel*
[2] *Edmund and Lily Safra Center for Brain Sciences, Hebrew University, Jerusalem, Israel*

Edited by:
Egidio D'Angelo, University of Pavia, Italy

Reviewed by:
Gilad Silberberg, Karolinska Institute, Sweden
Deborah Baro, Georgia State University, USA

****Correspondence:***
Avraham M. Libster, Department of Neurobiology, Life Science Institute, Hebrew University, Silberman Building, Jerusalem 91904, Israel.
e-mail: avi.libster@mail.huji.ac.il

Cerebellar anatomy is known for its crystal like structure, where neurons and connections are precisely and repeatedly organized with minor variations across the Cerebellar Cortex. The olivo-cerebellar loop, denoting the connections between the Cerebellar cortex, Inferior Olive and Cerebellar Nuclei (CN), is also modularly organized to form what is known as the cerebellar module. In contrast to the relatively organized and static anatomy, the cerebellum is innervated by a wide variety of neuromodulator carrying axons that are heterogeneously distributed along the olivo-cerebellar loop, providing heterogeneity to the static structure. In this manuscript we review modulatory processes in the olivo-cerebellar loop. We start by discussing the relationship between neuromodulators and the animal behavioral states. This is followed with an overview of the cerebellar neuromodulatory signals and a short discussion of why and when the cerebellar activity should be modulated. We then devote a section for three types of neurons where we briefly review its properties and propose possible neuromodulation scenarios.

Keywords: cerebellum, neuromodulation, olivo-cerebellar loop, aminergic modulation, inferior olive, cerebellar nuclei, cerebellar cortex

INTRODUCTION

The close relationships between the psychiatric state and the motor system is beautifully demonstrated in a clinical report describing a post-traumatic disorder case where exposure to loud sound lead to tremors lasting from several minutes to several days (Walters and Hening, 1992). The observed reaction to loud sound is a classic symptom of Psychogenic Tremor (PT), a movement disorder classified as Psychogenic Motor Disorder (PMD) (Jankovic et al., 2006). PMD, as its name suggests, is a movement disorder having a psychological origin (Association, 2000) and it clearly demonstrate that the properties of the motor control system can be altered on a transition to a different behavioral state.

The shifts between different behavioral states are commonly observed in animal behavior (Irwin, 1968). The shifts, which can be triggered by either internal or external stimuli, can be accompanied by changes in motor activity. Switching between the different states allows the animal to cope with changes that happened or about to happen in the external world. It is of no surprise that each behavioral state is accompanied by a distinct global brain activity manifested over different brain areas. A variety of physiological measurements, EEG (Lindsley, 1952), LFP (Gervasoni et al., 2004), and single unit activity (Abeles et al., 1995; Fanselow et al., 2001; Steriade et al., 2001), were used to characterize a state related brain activity [reviewed in Lee and Dan (2012)].

Changing global brain activity doesn't seem to be a cascading event but rather a simultaneous modification in activity of many parts of the CNS. The coordinated modification is regulated by a set of subcortical structures, each composed of neurons containing aminergic substances (Graeff et al., 1996; Everitt and Robbins, 1997; Taheri et al., 2002; Berridge and Waterhouse, 2003; Burgess, 2010). These aminergic substances, operates as neuromodulators, binding to specific, usually metabotropic membrane receptors. Upon binding they affect both, the cells intrinsic properties and the properties of the synaptic inputs. Neuromodulators can be co-released with neurotransmitters, such as glutamate (Trudeau, 2004), either at or in the vicinity of the synaptic site. Alternatively neuromodulators can have a global effect via what is known as volume transmission. A neuromodulator is said to be volume transmitted when it release sites and the matching receptors, in the target area, are relatively far from each other (Agnati et al., 2006).

Measuring the activity of neurons in these subcortical areas shows correlation between their activity and the animal behavioral state, i.e., both serotonergic neurons in the Dorsal Reticular Nucleus (DRN) and noradrenergic neurons in the Locus Coeruleus (LC) increase their rate of activation as the animal shifts from REM sleep through quite wakefulness to attentive behavior (Hobson et al., 1975; Trulson and Jacobs, 1979; Veasey et al., 1997; Jacobs et al., 2002). The role of aminergic neurons has been recently supported by experiments using optogenetic tools, showing that specific alteration of the activity in these

Abbreviations: bPN, Big Projection Neuron; CF, Climbing Fibers; CN, Cerebellar Nuclei; DAO, Dorsal Accessory Olivary Nucleus; DN, Dentate Nucleous; DRN, Dorsal Reticular Nucleus; GiC, Nucleus Reticularis Gigantocellularis/Paragigantocellularis Complex; IN, Interposed Cerebellar Nucleus; IO, Inferior Olive; LC, Locus Coeruleus; MAO, Medial Accessory Olivary Nucleus; MdR, Medullary Reticular Formation; MF, Mossy Fibers; PC, Purkinje Cell; PeFLH, Perifornical Part of Lateral Hypothalamus; PnO, Oral Pontine Reticularis nucleus; PnR, Pontine Reticular Formation; PTn, Pedunculopontine Tegmental Nucleus; ROb, Raphe Obscurus Nucleus; RPa, Raphe Pallidus Nucleus; TMN, Tuberomammillary Nucleus; VTA, Ventral Tegmental Area.

areas affected the animal sleep-awake cycle and motor behavior (Carter et al., 2010; McGregor and Siegel, 2010), social behavior (Chaudhury et al., 2013) and attention (Narayanan et al., 2012).

Within a behavioral state the neuromodulatory system operates in two release modes: tonic and phasic. While tonic release, which lasts throughout the behavioral state, regulates non-specific aspects, the phasic release is activated by specific stimuli or during specific task. For example dopaminergic neurons encode the predicted reward of stimuli (Schultz et al., 1997; Hollerman and Schultz, 1998), neurons in the LC have different responses to target or distractor stimuli in visual discrimination tasks (Aston-Jones et al., 1999) and serotonergic neurons in the DRN exhibit stimulus related (Ranade and Mainen, 2009) and specific motor activity (Veasey et al., 1995; Jacobs and Fornal, 1997) related firing.

EXTRINSIC AND INTRINSIC MODULATION

Neuromodulation in the CNS can be divided to extrinsic and intrinsic systems. The subcortical structures described in the previous section are extrinsic, as they are located outside the modulated target structure and operate almost independently of the target structure's activity. In intrinsic system the source of the modulating substance is within the structure and its release is almost entirely dependent on the activity of the local neural circuit. Another distinction between the systems is the possibility of activation of only subset of the secretory cells thus providing the intrinsic neuromodulatory system with a better spatial resolution.

In the case of the cerebellum, some of the extrinsic neuromodulators are: 5-HT, Dopamine, Ach, NE, Orexin and Histamine. The release pattern of these neuromodulators is relatively independent of the activity of the olivo-cerebellar loop [i.e., dopamine, (Rogers et al., 2011)]. Intrinsic neuromodulators, such as CRF [reviewed by Ito (2009)], Endocannabinoids (Safo et al., 2006), NO (Shibuki and Okada, 1991; Saxon and Beitz, 1996) and glutamate (Kano et al., 2008), are mostly produced and released within, and under the control of the olivo-cerebellar loop.

THE CEREBELLUM IN DIFFERENT BEHAVIORAL STATES

The neuromodulators of the cerebellum are well documented. Numerous subcortical areas such as the hypothalamus (Dietrichs and Haines, 1989), Ventral Tegmental Area (VTA) (Ikai et al., 1992, 1994), DRN (Pierce et al., 1977; Mendlin et al., 1996) and LC (Somana and Walberg, 1979) provide various modulatory agents (**Figure 1**) and their effects on different parts of the olivo-cerebellar loop, both *in vivo* and *in vitro* were documented (Schweighofer et al., 2004). Yet, the role of the cerebellum in different behavioral states was largely ignored.

One of the few studies on cerebellar function and its relation to behavioral state, recently published by Wu et al., demonstrated that the timing activity in the cerebellum is awareness independent. It concludes that coding of the sensory stimuli timing is largely independent of "…attentional, top-down or cognitive control mechanisms" (Wu et al., 2011). Although it might imply that cerebellar function is independent of the behavioral state, we argue that in order to preserve the cerebellar "timing function," and given that the cerebellar circuitry is modified upon the shift in the behavioral state, one have to change the "coding of time." In generalizing this idea, we argue that given a global change of brain activity, the input to the cerebellum and the response to cerebellar output are bound to change. Therefore, cerebellar activity most be modified in order to either ensure that the response is independent of the behavioral state or to provide a response that fit the behavioral requirements of the new state (**Figure 2**).

In the following sections we will review the effects of neuromodulators on one cell type from each of the constituents of the olivo-cerebellar loop: the Cerebellar Nuclei (CN) neuron, the Purkinje Cell (PC) and olivary neurons. For each cell type, we will describe one of its many observed electrophysiological phenomena and speculate on possible modulation scenarios.

THE CN NEURONS

THE BIOPHYSICAL PROPERTIES OF CN NEURONS

One of the ongoing debates in the field of cerebellar research is whether the output of the cerebellar cortex is conveyed via the rebound burst occurring in the CN neurons (Alviña et al., 2008; Boehme et al., 2011). Rebound burst (see **Figure 3A**) is a high frequency spikes burst triggered by a prolonged period of hyperpolarization (Tadayonnejad et al., 2010). The rebound response in CN neurons is mediated by the activation of T-type calcium channels (Cav3.x) and HCN channels (Molineux et al., 2006, 2008; Alviña et al., 2009; Engbers et al., 2011). The expression of either Cav3.1, or Cav 3.3, governs the number of spikes in the rebound burst and their inter-spike-intervals (see **Figure 3B**). The activation of these channels, expressed in the soma and non-uniformly distributed along the dendrites (Gauck et al., 2001; McKay et al., 2006), trigger either "strong" or "weak" bursts reported *in vitro* (Molineux et al., 2006). The HCN channels generate a non-specific, slowly inactivated cationic current (h-current). This current, which is activated by membrane hyperpolarization (Wahl-Schott and Biel, 2009), contributes to the rebound response by increasing the depolarization at the end of a hyperpolarizing period. The depolarization will act to increase the intra-burst firing rate and decrease the variance of the latency to the first spike (Engbers et al., 2011) (**Figure 3C**). The three types of HCN channels found in the CN neurons are HCN1, HCN2 and HCN 4. The HCN variants are spatially segregated: HCN2 is located proximally whereas HCN4 is found mainly at the distal dendrites (Santoro et al., 2000; Notomi and Shigemoto, 2004). Out of the three HCN isoforms, HCN2, and HCN4 are more susceptible to regulation by cAMP levels. An increase in intracellular cAMP concentration causes a rightward shift of the HCN activation curve and induces faster opening kinetics (Wahl-Schott and Biel, 2009).

NEUROMODULATION OF CN NEURONS

Table 1 summarizes some of the current knowledge on the neuromodulators operating within the CN. Here we describe presumable modulation strategies that can change the output of the CN by altering either the "rebound response" or modulating the CN inputs.

The most straightforward modulation of rebound response is to change the kinetic of either the calcium current, the h-current or both. Modulation of the t-type or HCN channel kinetics can either change the frequency of spikes in the burst or the latency

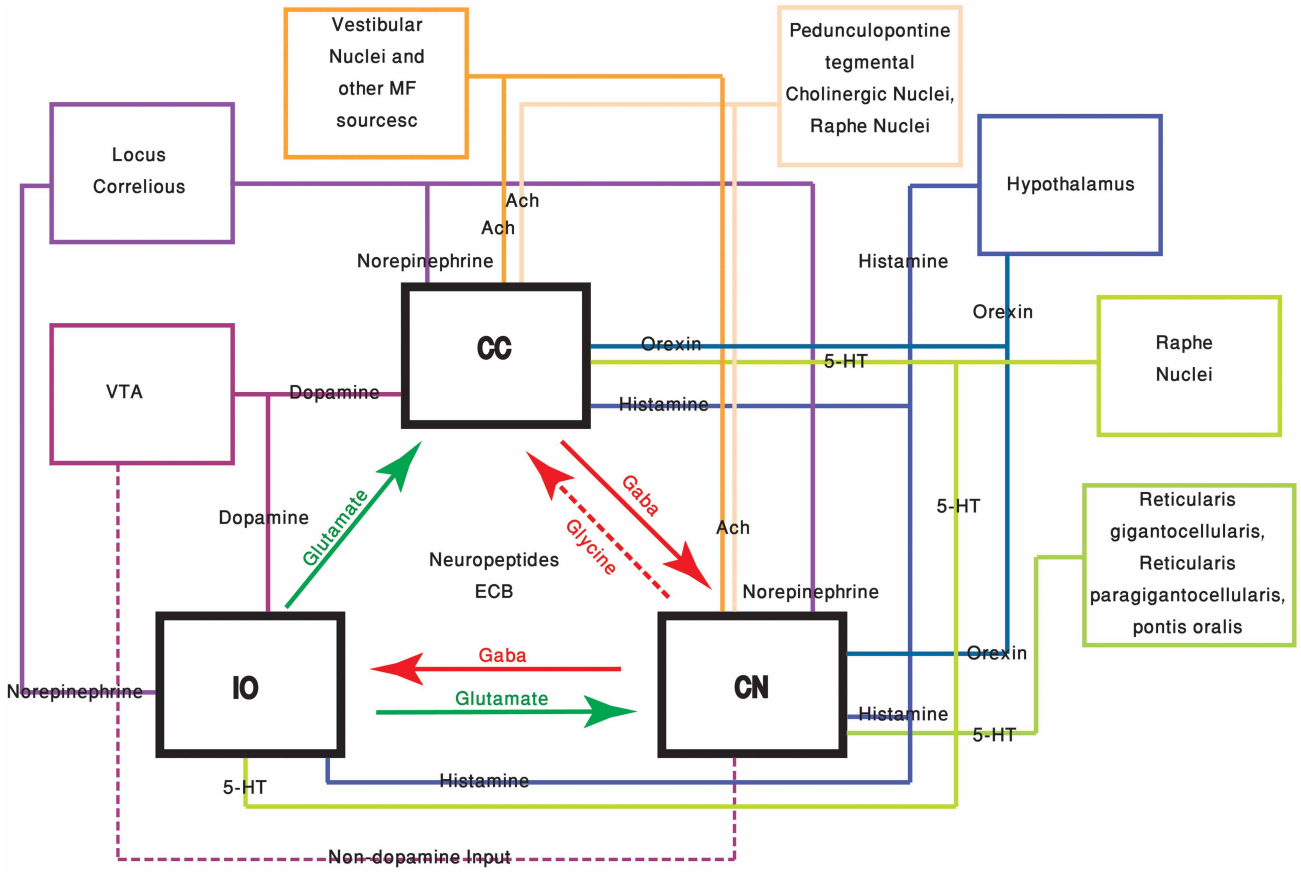

FIGURE 1 | The olivo-cerebellar and neuromodulation sources. The different parts of the olivo-cerebellar loop, Cerebellar Cortex (CC), Inferior Olive (IO), and Cerebellar Nuclei (CN) are schematically drawn. Excitatory and inhibitory connections between them are marked in green and red arrows respectively. Each box represents an external source of neuromodulation to the loop. The represented neuromodulators are: 5-HT—marked in light green. Notice the diagram doesn't include the contribution of 5-HT from serotonerigic neurons located in the precerebellar areas. Orexin and histamine—marked, respectively, in light and dark blue. Both are secreted from cells located in different areas in the hypothalamus. Ach—marked in light and dark orange. The two main sources are precerebellar regions and nuclei in the reticular formation. Note that cholinergic input to the IO is not represented in the diagram. Norepinephrine—marked in dark purple. Dopamine—marked in light purple. Dashed line represents input from the VTA to the CN which is not dopaminergic. Autocrine signaling of dopamine in PCs (Kim et al., 2009) is not represented in the scheme.

to the first spike (**Figure 3A** inset) (Engbers et al., 2011). While changing the time of the first spike is bound to change the "time representation," changing the frequency of the burst will alter the intensity of the CN output. The later may reflect the need to adapt to the new behavioral state.

HCN channels, as mentioned above, are regulated by the intracellular levels of cAMP and cGMP. Since many neuromodulatory pathways use cAMP and cGMP as second messengers, the modulation of HCN channels during a shift in behavioral state is likely to occur. Therefore, we will consider possible interesting scenarios of HCN modulation.

One of the intriguing neuromodulation scenarios is the differential effect on specific input. Neurons assign "value" to the different inputs carried by afferents from diverse pathways. This "value" is determined by either the location of the input or its relative strength. Differential neuromodulation can occur if the neuromodulators receptors are non-homogeneously distributed [This scenario, among many others, is discussed in (Dayan, 2012)].

The big Projection Neurons (bPNs) of the CN are suited for differential neuromodulation. A typical bPN receives excitatory input from the Mossy Fibers (MF) and Climbing Fibers (CF) collaterals and inhibitory input from PCs and local interneurons. Studies have shown that, at least in the Dentate Nucleus (DN), PCs synapses are located at the soma with a decreasing gradient along the dendrites. The MF excitatory input, on the other hand, is mostly located on the distal parts of the dendritic tree, as oppose to the CF input that is found on proximal dendrites (Chan-Palay, 1977; Uusisaari and Knöpfel, 2011). Furthermore, a non-homogeneous distribution of HCN channel has been reported (Santoro et al., 2000; Notomi and Shigemoto, 2004; Wilson and Garthwaite, 2010) as well as location specific innervations of neuromodulators [i.e., the cholinergic system has synaptic junctions close to the dendrites (Jaarsma et al., 1997)]. As a result of this high degree of non-uniformity, neuromodulation can be highly specific. For example, modulation of HCN channels located at the distal part of the dendrites will affect the input from the MF while modulation of the more proximal parts

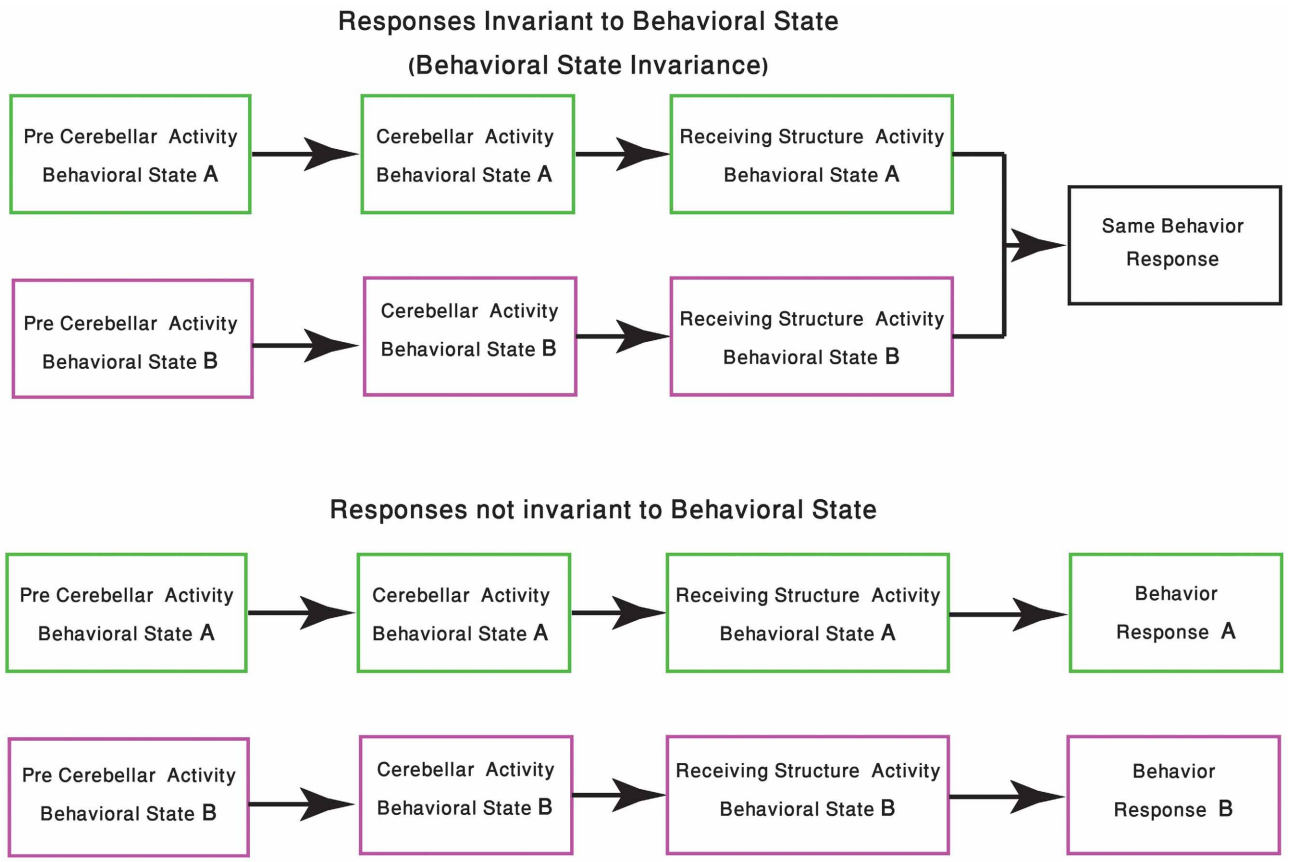

FIGURE 2 | Change in response due the behavioral state shift. The schematic diagram represents the two possible outcomes of cerebellar processing which is dependent on the animal behavioral state. In the upper panel the same sensory-motor information is presented to the cerebellar system, tough due to changes in precerebellar regions, the representation of this sensory-motor information might differ. In both behavioral states the cerebellum produces an output, received by other structures in the CNS, resulting in the animal having the same behavioral response. The lower panel describes a scenario in which the behavioral response should be different. Neuromodulation processes, occurring in different states, should be able to select the behavioral responses which are kept invariant.

of the dendrite can affect the CF input. This modulation strategy enables the bPN to selectively augment or attenuate EPSPs of different input sources. This "input" targeted modulation, can be viewed as a way of differentially changing the "sensitivity" of a bPN to inputs from the olivo-cerebellar loop or external input from precerebellar regions. Interestingly, this effect might also be achieved by modulating T-type calcium channels. The T-type channels are expressed in distal parts of the dendrite (Gauck et al., 2001) and might play a role in amplifying the excitatory input as seen in other parts of the CNS (i.e., Urban et al., 1998).

What are the advantages of having a differential modulation of rebound burst and excitatory input? We may answer it by assuming a different "expected" bPN output during different input regimes. When most of the inputs are inhibitory, prolonged hyperpolarization of the bPN membrane potential will enable the rebound burst mechanism. The rebound burst can then be considered as the "expected" output. In this case modulation of the rebound burst properties would have it largest effect on the information, conveyed by the bPN to the rest of CNS. On the other hand when the bPN receives prolonged excitatory drive, inhibition will modulate the timing and intensity of bPN response (Holdefer et al., 2005). In the "excitatory" input regime, modulation of EPSPs and spiking probability will have a larger effect on the information, conveyed by the bPN to the rest of CNS, then changing the properties of the rebound burst.

THE PURKINJE CELLS

THE BIOPHYSICAL PROPERTIES OF PURKINE CELLS

The properties of cerebellar PC have been extensively studied both *in vitro* and *in vivo* in anaesthetized and awake animals. It is commonly accepted that these unique neurons are endowed with a variety of ionic channels that provide a large repertoire of electrical activity (Llinas and Sugimori, 1980a,b; Williams et al., 2002). It is beyond the scope of this manuscript to review the vast literature describing the electrophysiological properties of PC and therefore we will limit our description to few of these properties. The three main ionic currents that control the firing of PC are Na, Ca and h-current. To this short list one should add a variety of potassium currents that are either voltage dependent,

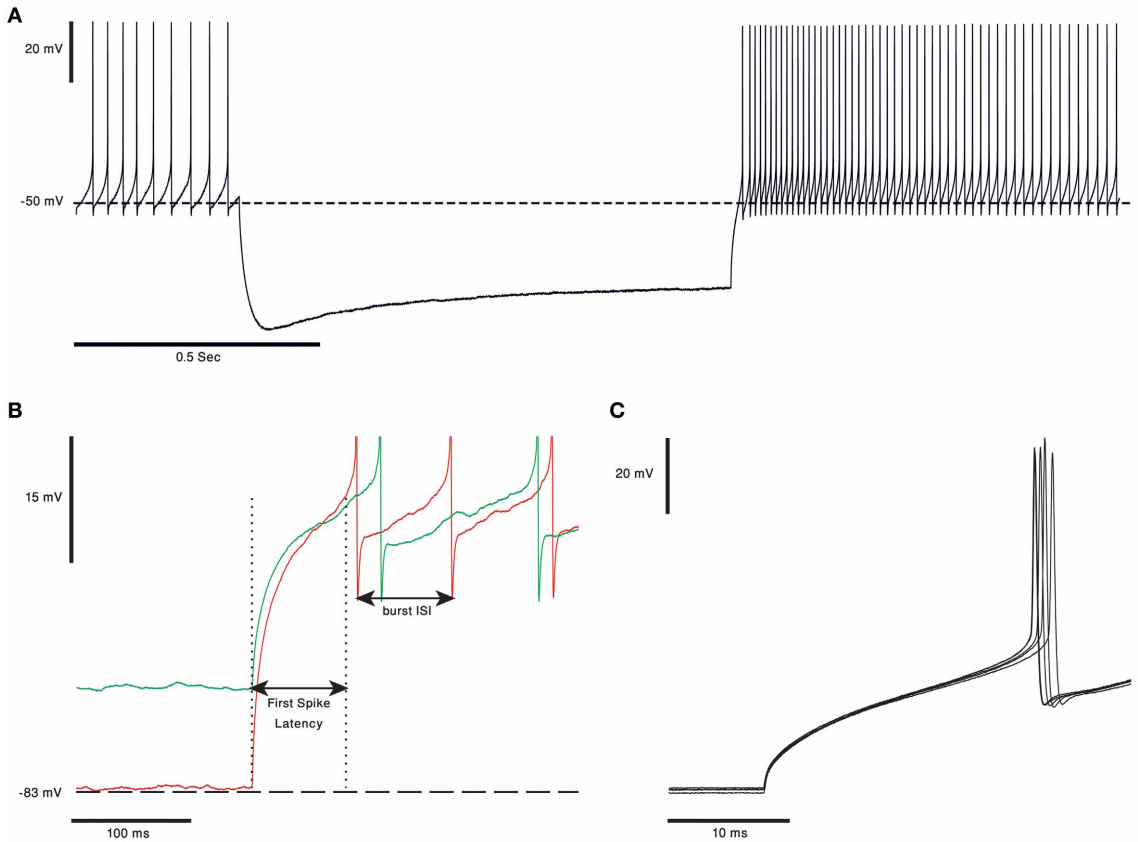

FIGURE 3 | Rebound burst in CN neurons. (A) Voltage trace from *in vitro* recording of a bPN. In response to 1 s of hyperpolarization the cell responds with a long rebound burst response, as evident in the increase in firing rate. Notice the voltage "sag" clearly visible during the hyperpolarization of the membrane voltage, probably due to activation of HCN channels (the voltage traces are courtesy of Dr. Uusisaari). **(B)** Rebound burst in response to different hyperpolarization levels. The first spike latency was shorter and burst frequency was higher when the membrane voltage was more hyperpolarized (red). Spikes were cut for better visualization. **(C)** The first spikes in the rebound burst from five repeats of the protocol, from panel **(A)**, done on the same cell. The latency to the first spike has a clear and noticeable small jitter.

calcium dependent or both. While the first three currents control the excitability of the neurons, the potassium currents have a prominent role in shaping the frequency and pattern of activity (Womack and Khodakhah, 2002, 2004). The kinetics of most, if not all, of these ionic currents can be modified by neuromodulators, resulting in a profound change in the electrical behavior.

One of the most characteristic features of PCs is their high firing rate, which can go up to 200 Hz and last for prolonged periods of time (Loewenstein et al., 2005; Shin et al., 2007). It has been proposed that this high firing frequency reflects intrinsic properties rather than the rate of synaptic inputs. Indeed, PC firing, *in vivo* and *in vitro*, persists in the presence of various synaptic blockers. It follows that the intrinsic properties determine the level of firing, upon which the synaptic inputs provides fine modulation. More recently, it was demonstrated that under *in vitro* conditions, as well as under anesthesia, the firing pattern is characterized by abrupt transitions between tonic firing and quiescence (**Figure 4A**). The terms "up" and "down" states were assigned to denote the firing and the quiescent periods and a corresponding bistable membrane potential has been demonstrated [for a review see (Engbers et al., 2012)]. Whether these transitions occur in awake behaving animals is still debated [see (Yartsev et al., 2009) but (Schonewille et al., 2006)]. Regardless of its outcome, this debate shows the importance of the underlying fact that the firing properties of PCs are robustly modulated between different behavioral states.

NEUROMODULATION OF PURKINJE CELLS

Table 2 summarizes some of the current knowledge on the neuromodulators operating in the cerebellar cortex particularly on PCs. We then use this case to discuss and compare the possibilities of phasic and tonic effects of neuromodulation.

Receptors for the same modulator having different affinity might play a key role in the ability of cerebellar system to respond to tonic and phasic neuromodulatory signals, providing the system with the ability to modulate its processing over different time scales while preserving its ability to response to transient signals. In the tonic release state, where a low level of the modulator is present, the high affinity receptor will be activated (**Figure 4C**). Thus, it is likely that this receptor will monitor the different basal level of the neuromodulator,

Table 1 | Neuromodulators of CN.

Neuromodulator	Source	Receptors	Known effects
5-HT	GiC, PnO (Bishop and Ho, 1985).	5-HT1B (might be expressed by PCs axons) 5-HT1C,5-HT2A, 5-HT2B (Might be expressed only in IN) 5-HT3 (low levels), 5-HT5A (Choi and Maroteaux, 1996; Kia et al., 1996; Sari et al., 1999; Geurts et al., 2002).	*In vitro* Attenuates the HCN current and decreases the amplitude of IPSCs by a presynaptic mechanism (Saitow et al., 2009). Increases the firing rate and reduces the response to glutamate via a postsynaptic mechanism (Gardette et al., 1987). *In vivo* 5-HT1A and 5-HT2 agonists induce a decrease in firing rate and 5-HT5A agonist increase firing rate (Di Mauro et al., 2003). In other studies only decreases in firing rate and response to glutamate, were documented (Kitzman and Bishop, 1997). Neurons excited by 5-HT were located at cerebellar nuclei projecting to the thalamus and cortex, whereas the nuclei projecting to peripheral motor centers reduced their firing rate when levels of 5-HT increased (Di Mauro et al., 2003).
NE	LC (Hokfelt and Fuxe, 1969; Somana and Walberg, 1978).		*In vivo* Direct application of NE decreases the firing rate of neurons in all nuclei (Di Mauro et al., 2003). Decreases response to application of GABA in the FN and Posterior IN while increasing it in the anterior IN. The LN has mixed responses (Di Mauro et al., 2012).
Ach	Vestibular nuclei (non-beaded fibers) PTg, GiC and Raphe nuclei (beaded fibers creating a dense network) (Jaarsma et al., 1997).		
Dopamine	But source of dopamine is unknown as nuclei is innervated by non-dopaminergic neurons from the VTA (Ikai et al., 1992).	DAT presence is demonstrated (Delis et al., 2004, 2008).	
Histamine	TMN (Haas and Panula, 2003).	H1, H2 (Qin et al., 2011) and H3 (mRNA in FN and IN) (Pillot et al., 2002).	*In vitro* Increases firing rate of neurons in all of the CN, probably through H2 activation (Shen et al., 2002; Tang et al., 2008; Qin et al., 2011).
Orexin	PeFLH (Peyron et al., 1998).	OX1R, OX2R (Hervieu et al., 2001; Cluderay et al., 2002).	*In vitro* Increases firing rate of neurons in the IN probably through OX2R activation (Yu et al., 2010).

providing long time scale modulation. When a sudden increase in neuromodulator occurs, the second receptor will be activated, enabling the system to respond to transient signals. As mentioned above, tonic and phasic release is a common strategy in neuromodulatory systems [reviewed in depth in Dayan (2012)].

The CRF system in the cerebellum is an example of a tonic and phasic modulation system. CRF, a neuropeptide, is released from both the MFs and the CFs (Cummings et al., 1989; Errico and Barmack, 1993). In the cerebellar cortex, the two CRF receptors CRF-R1 and CRF-R2 are expressed in all of the PCs. The two receptor types have a compartment specific distribution pattern (illustrated in **Figure 4B**) (King and Bishop, 2002; Lee et al., 2004). The properties of the olivo-cerebellar CRF system that support phasic and tonic modulation by the same modulator are: (1) Two receptor types with different affinity to CRF (Lovenberg et al., 1995) (2) A tonic and phasic components [although this hasn't been thoroughly examined, there are some supporting evidence; (Barmack and Young, 1990; Tian and Bishop, 2003; Beitz and Saxon, 2004)] (3) Two distinct sources of CRF, the CF, and

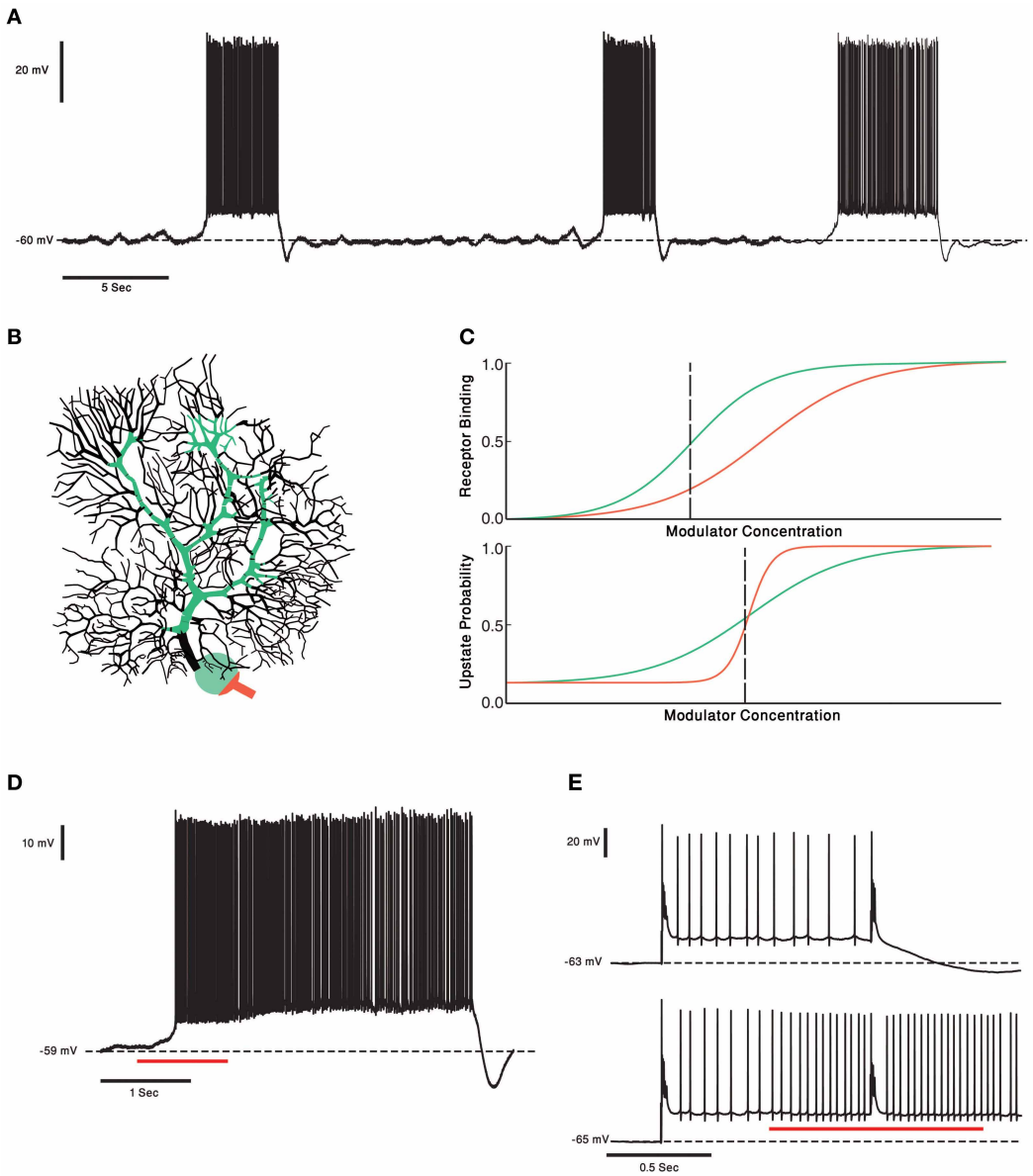

FIGURE 4 | PCs and two Receptors modulation. (A) Voltage trace from *in vitro* recording of a PC. The PC two states of membrane voltage, the "up" and "down" state are visible. **(B)** Schematic representation of the two receptor model. In this case the receptor with high affinity (green) is localized to soma and proximal dendrite and the Low affinity receptor (orange) is localized to the axon hillock and initial segment. This compartmental distribution resembles the distribution of CRF receptors in PCs. **(C)** Schematic plot of the two receptor's affinities (upper panel). Activation of the receptors changes the PCs probability to be in an "up" state. The relationship between the neuromodulator concentration and the probability of the cell to be in an "up" state is depicted in the lower panel. Left of the black dashed line the PC has a probability to be in a "down" state. If the neuromodulators levels are to the right of the black dashed line the PC will be in an "up" state. **(D)** One second puff of 1 μM of CRF (red underline) shifts the Cell to an "up" state. In our toy model it means the concentration of CRF was to the right of the dashed black line. **(E)** Complex spike shifts the PC between the membrane voltage states (upper panel). In the presence of CRF (red underline) the complex spike was unable to shift the cell to a "down" state. The PC became less "sensitive" to input from the olivo- cerebellar loop, due to modulation by CRF.

MF systems. The first two properties allow the CRF system to be sensitive to tonic and phasic signals and the third provides the possibility of a different functional role to each pathway.

The diverse effects CRF have on PCs are well documented. One study showed that by itself CRF doesn't induce a change in the simple spike firing rate but attenuates the increase in the simple spike firing rate in response to excitatory neurotransmitters (Bishop, 1990). In our ongoing research we demonstrate that in an *in vitro* preparation, application of CRF tends to shift PCs into their firing mode (Libster et al., 2010) (**Figure 4D**). Other studies demonstrated an increase in the PCs firing rate in response to CRF (Bishop and King, 1992; Bishop, 2002). CFs

Table 2 | Neuromodulators of Purkinje cells.

Neuromodulator	Source	Receptors	Known effects
5-HT	MdR, PnR And Serotonergic neurons in precerebellar regions (Bishop and Ho, 1985).	5-HT1A (Expression decreases in adults), 5-HT2A,B, 5-HT5A, 5-HT7 (Pazos and Palacios, 1985; Pazos et al., 1985; Kinsey et al., 2001; Geurts et al., 2002).	*In vitro* Augmenting the HCN current (Li et al., 1993). Altering the bi-stability of PCs (Williams et al., 2002). Increases PC excitability by decreasing the IA current (Wang et al., 1992). Decreases PC firing rate through activation of 5-HT1A, Applying 5-HT while blocking 5-HT1A causes an increase in firing rate (Darrow et al., 1990). *In vivo* Opposes changes in PC firing rate: increasing the rate when it becomes smaller and decreasing it when it becomes higher (Strahlendorf et al., 1984) effect can be species (Kerr and Bishop, 1992) and anesthesia (Strahlendorf et al., 1988) dependent. Reduces inward current caused by excitatory input (Hicks et al., 1989).
NE	LC (Watson and McElligott, 1984; Loughlin et al., 1986a,b).	Alpha adrenoreceptors 1A,B (low levels), D(very low levels) (Day et al., 1997), alpha adrenoreceptors2 (Nicholas et al., 1993) and beta adrenoreceptors2 (Wanaka et al., 1989).	*In vitro* Increases IPSCs amplitude. Mechanism is both post-synaptic (Woodward et al., 1991) and pre-synaptic (Saitow et al., 2000). *In vivo* Decreases the firing rate of PCs (Woodward et al., 1991).
Ach	Vestibular nuclei (non-beaded fibers) PTg, GiC and Raphe nuclei (beaded fibers) (Jaarsma et al., 1997).	Musacrenic receptors expression, mainly m2, is seen in the PCs layer in a species dependent fashion (Jaarsma et al., 1995) and Nicotinic receptors (Wada et al., 1989; Graham et al., 2002).	*In vivo* Decreases the firing rate of PCs by activation of nicotinic receptors (De La Garza et al., 1987).
Dopamine	VTA (Ikai et al., 1992).	DAT presence is demonstrated (Delis et al., 2004, 2008) and D2,D3,D4,D5 receptors (Khan et al., 1998, 2000; Kim et al., 2009).	*In vitro* Autocrine release from PCs. causes a slow inward cation current. (Kim et al., 2009).
Histamine	TMN (Haas and Panula, 2003).	H1, H2, and H3 (Drutel et al., 2001; Takemura et al., 2003).	*In vitro* Causes release of calcium from intracellular storages (Kirischuk et al., 1996). Increases PC firing rate through activation of H2 (Tian et al., 2000).
Various neuropeptides			Summarized in a review by Ito (2009).

have a basal firing rate, so we can view the CFs as setting the tonic levels of CRF, and by activation the CRF-R1 (**Figure 4B** green), increasing the PCs excitability without increasing PCs firing rate. A phasic increase in CRF, either due to increase in the CF activity or released from MFs, will activate the low affinity CRF-R2 receptor which is located mainly on the PCs axon initial segment (**Figure 4B** orange) (Bishop et al., 2000). We propose, therefore, that cerebellar CRF system is organized in a way that low tonic level, CRF serves to modulate the sensitivity of PCs to excitatory input and in higher level it directly increase PC's firing rate (**Figure 4E**). Increasing the firing rate lowers the probability of PCs transitions to a down state and reduces the sensitivity to external inputs (**Figure 4E**). This possible model mechanism is realized in **Figure 4C**. The sensitivity of the two receptors is depicted as dose response curves in **Figure 4C** and can be translated into the probability to shift to an up state (**Figure 4C**). In our hypothetical model the steeper probability curve of the low affinity receptor denotes a threshold

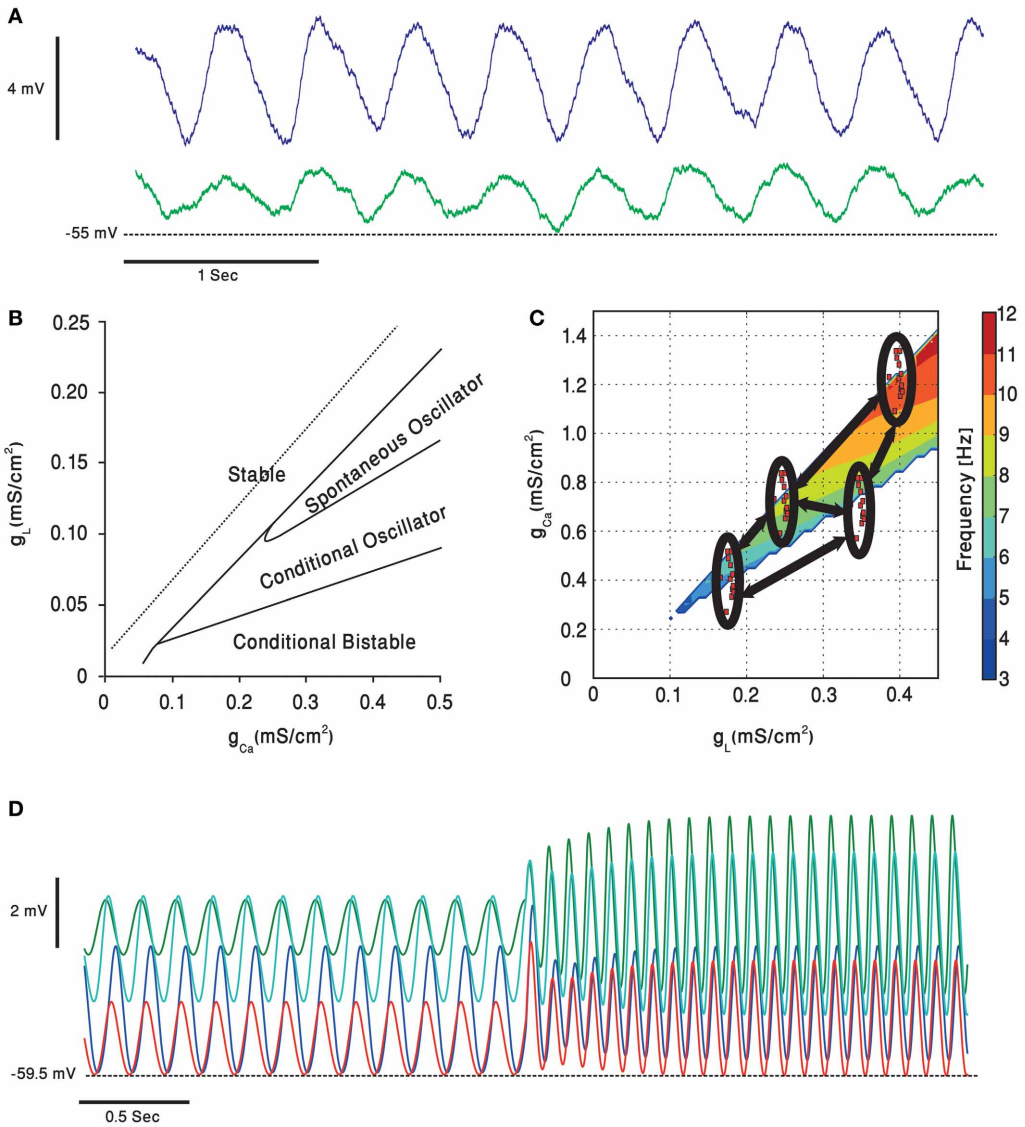

FIGURE 5 | Subthreshold oscillations of the olivary neurons membrane potential. (A) Whole cell recording, in an *in vitro* preparation, of two coupled olivary neurons oscillating together. **(B)** A simulated olivary neuron behavior on dependence on the calcium and potassium leak conductance [adapted from Manor et al. (1997)]. Oscillations spontaneously occur in a restricted part of the plane. **(C)** Dependence of the olivary neurons subthreshold oscillations frequency, in the clustered olive model, on potassium leak and calcium conductance [adapted from Torben-Nielsen et al. (2012)]. Each of the clusters (red dots inside black ellipses) contains cells having, roughly, the same value of conductance. The cells inside the clusters have higher coupling coefficients relative to each other and lower coupling strength (marked in black arrows) to cells from other clusters. **(D)** The clustered olive model provides the olivary cells with phase invariance relative to the frequency. Each of the voltage traces is taken from a cell in a different cluster. The cells oscillate in a phase, relative to each other, which is preserved when the oscillation frequency is suddenly increased [adapted from Torben-Nielsen et al. (2012)].

like response to CRF level. Activating the high affinity receptors increases the probability to shift to firing mode (**Figure 4D**). Activating the low affinity receptors directly activates the PCs (orange line, **Figure 4C**). The entire range of electrical activity is grossly divided into two types of behavior (dashed vertical line). At low concentration of CRF, PC will shift to its firing mode upon synaptic input. At high concentration of CRF PCs shift to their firing mode, where the rate of firing increases with CRF levels. A transient increase in CRF level may, therefore, shift the PC to a continuous firing rendering it more input insensitive.

THE OLIVARY NEURONS

THE BIOPHYSICAL PROPERTIES OF OLIVARY NEURONS AND NETWORK

The role of the inferior olive, at least by some researchers, is to endow the cerebellar system with timing capabilities (Xu et al., 2006; Jacobson et al., 2008; Liu et al., 2008; Llinas, 2009). The electrophysiological manifestation of the timing capability

Table 2 | Neuromodulators of Purkinje cells.

Neuromodulator	Source	Receptors	Known effects
5-HT	MdR, PnR And Serotonergic neurons in precerebellar regions (Bishop and Ho, 1985).	5-HT1A (Expression decreases in adults), 5-HT2A,B, 5-HT5A, 5-HT7 (Pazos and Palacios, 1985; Pazos et al., 1985; Kinsey et al., 2001; Geurts et al., 2002).	*In vitro* Augmenting the HCN current (Li et al., 1993). Altering the bi-stability of PCs (Williams et al., 2002). Increases PC excitability by decreasing the IA current (Wang et al., 1992). Decreases PC firing rate through activation of 5-HT1A, Applying 5-HT while blocking 5-HT1A causes an increase in firing rate (Darrow et al., 1990). *In vivo* Opposes changes in PC firing rate: increasing the rate when it becomes smaller and decreasing it when it becomes higher (Strahlendorf et al., 1984) effect can be species (Kerr and Bishop, 1992) and anesthesia (Strahlendorf et al., 1988) dependent. Reduces inward current caused by excitatory input (Hicks et al., 1989).
NE	LC (Watson and McElligott, 1984; Loughlin et al., 1986a,b).	Alpha adrenoreceptors 1A,B (low levels), D(very low levels) (Day et al., 1997), alpha adrenoreceptors2 (Nicholas et al., 1993) and beta adrenoreceptors2 (Wanaka et al., 1989).	*In vitro* Increases IPSCs amplitude. Mechanism is both post-synaptic (Woodward et al., 1991) and pre-synaptic (Saitow et al., 2000). *In vivo* Decreases the firing rate of PCs (Woodward et al., 1991).
Ach	Vestibular nuclei (non-beaded fibers) PTg, GiC and Raphe nuclei (beaded fibers) (Jaarsma et al., 1997).	Musacrenic receptors expression, mainly m2, is seen in the PCs layer in a species dependent fashion (Jaarsma et al., 1995) and Nicotinic receptors (Wada et al., 1989; Graham et al., 2002).	*In vivo* Decreases the firing rate of PCs by activation of nicotinic receptors (De La Garza et al., 1987).
Dopamine	VTA (Ikai et al., 1992).	DAT presence is demonstrated (Delis et al., 2004, 2008) and D2,D3,D4,D5 receptors (Khan et al., 1998, 2000; Kim et al., 2009).	*In vitro* Autocrine release from PCs. causes a slow inward cation current. (Kim et al., 2009).
Histamine	TMN (Haas and Panula, 2003).	H1, H2, and H3 (Drutel et al., 2001; Takemura et al., 2003).	*In vitro* Causes release of calcium from intracellular storages (Kirischuk et al., 1996). Increases PC firing rate through activation of H2 (Tian et al., 2000).
Various neuropeptides			Summarized in a review by Ito (2009).

have a basal firing rate, so we can view the CFs as setting the tonic levels of CRF, and by activation the CRF-R1 (**Figure 4B** green), increasing the PCs excitability without increasing PCs firing rate. A phasic increase in CRF, either due to increase in the CF activity or released from MFs, will activate the low affinity CRF-R2 receptor which is located mainly on the PCs axon initial segment (**Figure 4B** orange) (Bishop et al., 2000). We propose, therefore, that cerebellar CRF system is organized in a way that low tonic level, CRF serves to modulate the sensitivity of PCs to excitatory input and in higher level it directly increase PC's firing rate (**Figure 4E**). Increasing the firing rate lowers the probability of PCs transitions to a down state and reduces the sensitivity to external inputs (**Figure 4E**). This possible model mechanism is realized in **Figure 4C**. The sensitivity of the two receptors is depicted as dose response curves in **Figure 4C** and can be translated into the probability to shift to an up state (**Figure 4C**). In our hypothetical model the steeper probability curve of the low affinity receptor denotes a threshold

predict motor outcomes, whereas in motor processing it provides temporal patterns to accurately execute motor commands. Second, we assume that the subthreshold oscillations are generated from complex interactions between intrinsic membrane properties and electrotonic connections that are best described by our heterogeneity model (see above).

With these assumptions one should wonder: should representation of time be modulated? Do we need a different representation of time in different behavioral sates? It is rather difficult, if not impossible, to answer these questions. It seems inevitable to conclude that time representation should be accurately preserved irrespective of the behavioral state. After all keeping accurate time is crucial for survival. Keeping accurate time for predicting motor outcome is definitely essential, but execution of motor commands is, and should be, modified upon a shift in the behavioral state. Motor performance is affected by the current level of alertness and motivation. Increase alertness is associated with faster movement time (Gray, 2011; Shiner et al., 2012). Therefore, an increase in movement velocity that maintains the temporal structure of the movement entails a change in the temporal pattern generated by the cerebellar system. We propose that these contradictory needs, preserving time representation for sensory function and altering timing of motor execution, are manifested in the non-homogeneous innervations of the olivary complex by neuromodulators. In the case of serotonergic innervations, some parts are heavily innervated while others are almost or completely devoid of such innervations (Wiklund et al., 1977; Leger et al., 2001). Thus, if behavioral state defines the serotonin level, the function will be modified in some olivary subnuclei while preserved in others.

To understand how temporal patterns can be modified in a way that will support faster movements one should consider the heterogeneity model. The gl-gCa plane shown in **Figure 5C** demonstrates that the higher the leak and the calcium conductance, the higher is the frequency of oscillation. Serotonin decreases both conductance and therefore a lower frequency is expected and indeed was experimentally observed (Sugihara et al., 1995; Placantonakis et al., 2000). We previously demonstrated that under harmaline intoxication sudden shifts in frequency of cortical complex spikes activity was frequently observed (Jacobson et al., 2009; Choi et al., 2010). Interestingly during this frequency shift, the phase difference between neurons was maintained. Similar phenomenon is also predicted by our heterogeneity model (**Figure 5D**). It is tempting to suggest that neuromodulators can change the frequency of the temporal pattern while maintaining the temporal order within the pattern, thus producing faster movement while maintaining coordination.

CONCLUDING REMARKS

This short review is focused on the effects of modulatory agents that operate within the olivo-cerebellar system. Beyond references to published studies, we presented various hypothetical possibilities by which neuromodulators can exert differential effects that are both spatial and temporal specific. We speculate that such mechanisms endowed the system with the capabilities to adjust cerebellar processing to a given behavioral state.

ACKNOWLEDGMENTS

Supported by PITN-GA-2009-238686 (CEREBNET), FP7-ICT (REALNET) and ISF (Yosef Yarom).

REFERENCES

Abeles, M., Bergman, H., Gat, I., Meilijson, I., Seidemann, E., Tishby, N., et al. (1995). Cortical activity flips among quasi-stationary states. *Proc. Natl. Acad. Sci. U.S.A.* 92, 8616–8620.

Agnati, L. F., Leo, G., Zanardi, A., Genedani, S., Rivera, A., Fuxe, K., et al. (2006). Volume transmission and wiring transmission from cellular to molecular networks: history and perspectives. *Acta Physiol.* 187, 329–344.

Alviña, K., Ellis-Davies, G., and Khodakhah, K. (2009). T-type calcium channels mediate rebound firing in intact deep cerebellar neurons. *Neuroscience* 158, 635–641.

Alviña, K., Walter, J. T., Kohn, A., Ellis-Davies, G., and Khodakhah, K. (2008). Questioning the role of rebound firing in the cerebellum. *Nat. Neurosci.* 11, 1256–1258.

Association A. P. (2000). *Diagnostic and Statistical Manual of Mental Disorders DSM-IV-TR, 4th Edn.* Washington: Amer Psychiatric Pub.

Aston-Jones, G., Rajkowski, J., and Cohen, J. (1999). Role of locus coeruleus in attention and behavioral flexibility. *Biol. Psychiatry* 46, 1309–1320.

Barmack, N. H., and Young, W. S. 3rd. (1990). Optokinetic stimulation increases corticotropin-releasing factor mRNA in inferior olivary neurons of rabbits. *J. Neurosci.* 10, 631–640.

Bazzigaluppi, P., Ruigrok, T., Saisan, P., De Zeeuw, C. I., and De Jeu, M. (2012). Properties of the nucleo-olivary pathway: an *in vivo* whole-cell patch clamp study. *PLoS ONE* 7:e46360. doi: 10.1371/journal.pone.0046360

Beitz, A. J., and Saxon, D. (2004). Harmaline-induced climbing fiber activation causes amino acid and peptide release in the rodent cerebellar cortex and a unique temporal pattern of Fos expression in the olivo-cerebellar pathway. *J. Neurocytol.* 33, 49–74.

Berridge, C. W., and Waterhouse, B. D. (2003). The locus coeruleus-noradrenergic system: modulation of behavioral state and state-dependent cognitive processes. *Brain Res. Brain Res. Rev.* 42, 33–84.

Bishop, G. A. (1990). Neuromodulatory effects of corticotropin releasing factor on cerebellar Purkinje cells: an *in vivo* study in the cat. *Neuroscience* 39, 251–257.

Bishop, G. A. (2002). Development of a corticotropin-releasing factor-mediated effect on the firing rate of Purkinje cells in the postnatal mouse cerebellum. *Exp. Neurol.* 178, 165–174.

Bishop, G. A., and Ho, R. H. (1985). The distribution and origin of serotonin immunoreactivity in the rat cerebellum. *Brain Res.* 331, 195–207.

Bishop, G. A., and Ho, R. H. (1986). Cell bodies of origin of serotonin-immunoreactive afferents to the inferior olivary complex of the rat. *Brain Res.* 399, 369–373.

Bishop, G. A., and King, J. S. (1992). Differential modulation of Purkinje cell activity by enkephalin and corticotropin releasing factor. *Neuropeptides* 22, 167–174.

Bishop, G. A., Seelandt, C. M., and King, J. S. (2000). Cellular localization of corticotropin releasing factor receptors in the adult mouse cerebellum. *Neuroscience* 101, 1083–1092.

Boehme, R., Uebele, V. N., Renger, J. J., and Pedroarena, C. (2011). Rebound excitation triggered by synaptic inhibition in cerebellar nuclear neurons is suppressed by selective T-type calcium channel block. *J. Neurophysiol.* 106, 2653–2661.

Bouthenet, M. L., Martres, M. P., Sales, N., and Schwartz, J. C. (1987). A detailed mapping of dopamine D-2 receptors in rat central nervous system by autoradiography with [125I]iodosulpride. *Neuroscience* 20, 117–155.

Bouthenet, M. L., Souil, E., Martres, M. P., Sokoloff, P., Giros, B., and Schwartz, J. C. (1991). Localization of dopamine D3 receptor mRNA in the rat brain using *in situ* hybridization histochemistry: comparison with dopamine D2 receptor mRNA. *Brain Res.* 564, 203–219.

Burgess, C. R. (2010). Histamine and orexin in the control of arousal, locomotion, and motivation. *J. Neurosci.* 30, 2810–2811.

Carter, M. E., Yizhar, O., Chikahisa, S., Nguyen, H., Adamantidis, A., Nishino, S., et al. (2010). Tuning arousal with optogenetic modulation of locus coeruleus neurons. *Nat. Neurosci.* 13, 1526–1533.

Chan-Palay, V. (1977). *Cerebellar Dentate Nucleus: Organization, Cytology and Transmitters*. Berlin; Heidelberg; New York: Springer-Verlag.

Chaudhury, D., Walsh, J. J., Friedman, A. K., Juarez, B., Ku, S. M., Koo, J. W., et al. (2013). Rapid regulation of depression-related behaviours by control of midbrain dopamine neurons. *Nature* 493, 532–536.

Choi, D. S., and Maroteaux, L. (1996). Immunohistochemical localisation of the serotonin 5-HT2B receptor in mouse gut, cardiovascular system, and brain. *FEBS Lett.* 391, 45–51.

Choi, S., Yu, E., Kim, D., Urbano, F. J., Makarenko, V., Shin, H.-S., et al. (2010). Subthreshold membrane potential oscillations in inferior olive neurons are dynamically regulated by P/Q- and T-type calcium channels: a study in mutant mice. *J. Physiol.* 588, 3031–3043.

Cluderay, J. E., Harrison, D. C., and Hervieu, G. J. (2002). Protein distribution of the orexin-2 receptor in the rat central nervous system. *Regul. Pept.* 104, 131–144.

Cummings, S. L., Young, W. S. 3rd., Bishop, G. A., De Souza, E. B., and King, J. S. (1989). Distribution of corticotropin-releasing factor in the cerebellum and precerebellar nuclei of the opossum: a study utilizing immunohistochemistry, *in situ* hybridization histochemistry, and receptor autoradiography. *J. Comp. Neurol.* 280, 501–521.

Darrow, E. J., Strahlendorf, H. K., and Strahlendorf, J. C. (1990). Response of cerebellar Purkinje cells to serotonin and the 5-HT1A agonists 8-OH-DPAT and ipsapirone *in vitro*. *Eur. J. Pharmacol.* 175, 145–153.

Day, H. E., Campeau, S., Watson, S. J. Jr., and Akil, H. (1997). Distribution of alpha 1a-, alpha 1b- and alpha 1d-adrenergic receptor mRNA in the rat brain and spinal cord. *J. Chem. Neuroanat.* 13, 115–139.

Dayan, P. (2012). Twenty-five lessons from computational neuromodulation. *Neuron* 76, 240–256.

De La Garza, R., McGuire, T. J., Freedman, R., and Hoffer, B. J. (1987). The electrophysiological effects of nicotine in the rat cerebellum: evidence for direct postsynaptic actions. *Neurosci. Lett.* 80, 303–308.

De Zeeuw, C. I., Simpson, J. I., Hoogenraad, C. C., Galjart, N., Koekkoek, S. K., and Ruigrok, T. J. (1998). Microcircuitry and function of the inferior olive. *Trends Neurosci.* 21, 391–400.

Delis, F., Mitsacos, A., and Giompres, P. (2004). Dopamine receptor and transporter levels are altered in the brain of Purkinje Cell Degeneration mutant mice. *Neuroscience* 125, 255–268.

Delis, F., Mitsacos, A., and Giompres, P. (2008). Pharmacological characterization and anatomical distribution of the dopamine transporter in the mouse cerebellum. *Cerebellum* 7, 242–251.

Devor, A., Fritschy, J. M., and Yarom, Y. (2001). Spatial distribution and subunit composition of GABA(A) receptors in the inferior olivary nucleus. *J. Neurophysiol.* 85, 1686–1696.

Devor, A., and Yarom, Y. (2002). Electrotonic coupling in the inferior olivary nucleus revealed by simultaneous double patch recordings. *J. Neurophysiol.* 87, 3048–3058.

Di Mauro, M., Fretto, G., Caldera, M., Li Volsi, G., Licata, F., Ciranna, L., et al. (2003). Noradrenaline and 5-hydroxytryptamine in cerebellar nuclei of the rat: functional effects on neuronal firing. *Neurosci. Lett.* 347, 101–105.

Di Mauro, M., Li Volsi, G., and Licata, F. (2012). Noradrenergic control of neuronal firing in cerebellar nuclei: modulation of GABA responses. *Cerebellum*. doi: 10.1007/s12311-012-0422-2. [Epub ahead of print].

Dietrichs, E., and Haines, D. E. (1989). Interconnections between hypothalamus and cerebellum. *Anat. Embryol.* 179, 207–220.

Drutel, G., Peitsaro, N., Karlstedt, K., Wieland, K., Smit, M. J., Timmerman, H., et al. (2001). Identification of rat H3 receptor isoforms with different brain expression and signaling properties. *Mol. Pharmacol.* 59, 1–8.

Engbers, J. D., Anderson, D., Tadayonnejad, R., Mehaffey, W. H., Molineux, M. L., and Turner, R. W. (2011). Distinct roles for I(T) and I(H) in controlling the frequency and timing of rebound spike responses. *J. Physiol.* 589, 5391–5413.

Engbers, J. D., Fernandez, F. R., and Turner, R. W. (2012). Bistability in Purkinje neurons: Ups and downs in cerebellar research. *Neural Netw.* doi: 10.1016/j.neunet.2012.09.006. [Epub ahead of print].

Errico, P., and Barmack, N. H. (1993). Origins of cerebellar mossy and climbing fibers immunoreactive for corticotropin-releasing factor in the rabbit. *J. Comp. Neurol.* 336, 307–320.

Everitt, B. J., and Robbins, T. W. (1997). Central cholinergic systems and cognition. *Annu. Rev. Psychol.* 48, 649–684.

Fanselow, E. E., Sameshima, K., Baccala, L. A., and Nicolelis, M. A. L. (2001). Thalamic bursting in rats during different awake behavioral states. *Proc. Natl. Acad. Sci. U.S.A.* 98, 15330–15335.

Gardette, R., Krupa, M., and Crepel, F. (1987). Differential effects of serotonin on the spontaneous discharge and on the excitatory amino acid-induced responses of deep cerebellar nuclei neurons in rat cerebellar slices. *Neuroscience* 23, 491–500.

Gauck, V., Thomann, M., Jaeger, D., and Borst, A. (2001). Spatial distribution of low- and high-voltage-activated calcium currents in neurons of the deep cerebellar nuclei. *J. Neurosci.* 21, RC158.

Gervasoni, D., Lin, S.-C., Ribeiro, S., Soares, E. S., Pantoja, J., and Nicolelis, M.aL. (2004). Global forebrain dynamics predict rat behavioral states and their transitions. *J. Neurosci.* 24, 11137–11147.

Geurts, F. J., De Schutter, E., and Timmermans, J.-P. (2002). Localization of 5-HT2A, 5-HT3, 5-HT5A and 5-HT7 receptor-like immunoreactivity in the rat cerebellum. *J. Chem. Neuroanat.* 24, 65–74.

Graeff, F. G., Guimarães, F. S., De Andrade, T. G. C. S., and Deakin, J. F. W. (1996). Role of 5-HT in stress, anxiety, and depression. *Pharmacol. Biochem. Behav.* 54, 129–141.

Graham, A., Court, J. A., Martin-Ruiz, C. M., Jaros, E., Perry, R., Volsen, S. G., et al. (2002). Immunohistochemical localisation of nicotinic acetylcholine receptor subunits in human cerebellum. *Neuroscience* 113, 493–507.

Gray, R. (2011). Links between attention, performance pressure, and movement in skilled motor action. *Curr. Dir. Psychol. Sci.* 20, 301–306.

Haas, H., and Panula, P. (2003). The role of histamine and the tuberomamillary nucleus in the nervous system. *Nat. Rev. Neurosci.* 4, 121–130.

Hervieu, G. J., Cluderay, J. E., Harrison, D. C., Roberts, J. C., and Leslie, R. A. (2001). Gene expression and protein distribution of the orexin-1 receptor in the rat brain and spinal cord. *Neuroscience* 103, 777–797.

Hicks, T. P., Krupa, M., and Crepel, F. (1989). Selective effects of serotonin upon excitatory amino acid-induced depolarizations of Purkinje cells in cerebellar slices from young rats. *Brain Res.* 492, 371–376.

Hobson, J. A., McCarley, R. W., and Wyzinski, P. W. (1975). Sleep cycle oscillation: reciprocal discharge by two brainstem neuronal groups. *Science* 189, 55–58.

Hokfelt, T., and Fuxe, K. (1969). Cerebellar monoamine nerve terminals, a new type of afferent fibers to the cortex cerebelli. *Exp. Brain Res.* 9, 63–72.

Holdefer, R. N., Houk, J. C., and Miller, L. E. (2005). Movement-related discharge in the cerebellar nuclei persists after local injections of GABA(A) antagonists. *J. Neurophysiol.* 93, 35–43.

Hollerman, J. R., and Schultz, W. (1998). Dopamine neurons report an error in the temporal prediction of reward during learning. *Nat. Neurosci.* 1, 304–309.

Ikai, Y., Takada, M., and Mizuno, N. (1994). Single neurons in the ventral tegmental area that project to both the cerebral and cerebellar cortical areas by way of axon collaterals. *Neuroscience* 61, 925–934.

Ikai, Y., Takada, M., Shinonaga, Y., and Mizuno, N. (1992). Dopaminergic and non-dopaminergic neurons in the ventral tegmental area of the rat project, respectively, to the cerebellar cortex and deep cerebellar nuclei. *Neuroscience* 51, 719–728.

Inagaki, N., Yamatodani, A., Ando-Yamamoto, M., Tohyama, M., Watanabe, T., and Wada, H. (1988). Organization of histaminergic fibers in the rat brain. *J. Comp. Neurol.* 273, 283–300.

Irwin, S. (1968). Comprehensive observational assessment: Ia. A systematic, quantitative procedure for assessing the behavioral and physiologic state of the mouse. *Psychopharmacologia* 13, 222–257.

Ito, M. (2009). Functional roles of neuropeptides in cerebellar circuits. *Neuroscience* 162, 666–672.

Jaarsma, D., Levey, A. I., Frostholm, A., Rotter, A., and Voogd, J. (1995). Light-microscopic distribution and parasagittal organisation of muscarinic receptors in rabbit cerebellar cortex. *J. Chem. Neuroanat.* 9, 241–259.

Jaarsma, D., Ruigrok, T. J., Caffe, R., Cozzari, C., Levey, A. I., Mugnaini, E., et al. (1997). Cholinergic innervation and receptors in the cerebellum. *Prog. Brain Res.* 114, 67–96.

Jacobs, B. L., and Fornal, C. A. (1997). Serotonin and motor activity. *Curr. Opin. Neurobiol.* 7, 820–825.

Jacobs, B. L., Martin-Cora, F. J., and Fornal, C. A. (2002). Activity of medullary serotonergic neurons in freely moving animals. *Brain Res. Brain Res. Rev.* 40, 45–52.

Jacobson, G. A., Lev, I., Yarom, Y., and Cohen, D. (2009). Invariant phase structure of olivo-cerebellar oscillations and its putative role in temporal pattern generation. *Proc. Natl. Acad. Sci. U.S.A.* 106, 3579–3584.

Jacobson, G. A., Rokni, D., and Yarom, Y. (2008). A model of the olivo-cerebellar system as a temporal pattern generator. *Trends Neurosci.* 31, 617–625.

Jankovic, J., Vuong, K. D., and Thomas, M. (2006). Psychogenic tremor: long-term outcome. *CNS Spectr.* 11, 501–508.

Kano, M., Hashimoto, K., and Tabata, T. (2008). Type-1 metabotropic glutamate receptor in cerebellar Purkinje cells: a key molecule responsible for long-term depression, endocannabinoid signalling and synapse elimination. *Philos. Trans. R. Soc. Lond. B Biol. Sci.* 363, 2173–2186.

Kerr, C. W., and Bishop, G. A. (1992). The physiological effects of serotonin are mediated by the 5HT1A receptor in the cat's cerebellar cortex. *Brain Res.* 591, 253–260.

Khan, Z. U., Gutierrez, A., Martin, R., Penafiel, A., Rivera, A., and De La Calle, A. (1998). Differential regional and cellular distribution of dopamine D2-like receptors: an immunocytochemical study of subtype-specific antibodies in rat and human brain. *J. Comp. Neurol.* 402, 353–371.

Khan, Z. U., Gutierrez, A., Martin, R., Penafiel, A., Rivera, A., and De La Calle, A. (2000). Dopamine D5 receptors of rat and human brain. *Neuroscience* 100, 689–699.

Kia, H. K., Miquel, M. C., Brisorgueil, M. J., Daval, G., Riad, M., El Mestikawy, S., et al. (1996). Immunocytochemical localization of serotonin1A receptors in the rat central nervous system. *J. Comp. Neurol.* 365, 289–305.

Kim, Y. S., Shin, J. H., Hall, F. S., and Linden, D. J. (2009). Dopamine signaling is required for depolarization-induced slow current in cerebellar Purkinje cells. *J. Neurosci.* 29, 8530–8538.

Kimura, H., McGeer, P. L., Peng, J. H., and McGeer, E. G. (1981). The central cholinergic system studied by choline acetyltransferase immunohistochemistry in the cat. *J. Comp. Neurol.* 200, 151–201.

King, J. S. (1976). The synaptic cluster (glomerulus) in the inferior olivary nucleus. *J. Comp. Neurol.* 165, 387–400.

King, J. S., and Bishop, G. A. (2002). The distribution and cellular localization of CRF-R1 in the vermis of the postnatal mouse cerebellum. *Exp. Neurol.* 178, 175–185.

Kinsey, A. M., Wainwright, A., Heavens, R., Sirinathsinghji, D. J., and Oliver, K. R. (2001). Distribution of 5-ht(5A), 5-ht(5B), 5-ht(6) and 5-HT(7) receptor mRNAs in the rat brain. *Brain Res. Mol. Brain Res.* 88, 194–198.

Kirischuk, S., Matiash, V., Kulik, A., Voitenko, N., Kostyuk, P., and Verkhratsky, A. (1996). Activation of P2-purino-, alpha 1-adreno and H1-histamine receptors triggers cytoplasmic calcium signalling in cerebellar Purkinje neurons. *Neuroscience* 73, 643–647.

Kitzman, P. H., and Bishop, G. A. (1997). The physiological effects of serotonin on spontaneous and amino acid-induced activation of cerebellar nuclear cells: an *in vivo* study in the cat. *Prog. Brain Res.* 114, 209–223.

Kobayashi, R. M., Palkovits, M., Kopin, I. J., and Jacobowitz, D. M. (1974). Biochemical mapping of noradrenergic nerves arising from the rat locus coeruleus. *Brain Res.* 77, 269–279.

Lee, K. H., Bishop, G. A., Tian, J. B., and King, J. S. (2004). Evidence for an axonal localization of the type 2 corticotropin-releasing factor receptor during postnatal development of the mouse cerebellum. *Exp. Neurol.* 187, 11–22.

Lee, S. H., and Dan, Y. (2012). Neuromodulation of brain states. *Neuron* 76, 209–222.

Leger, L., Charnay, Y., Hof, P. R., Bouras, C., and Cespuglio, R. (2001). Anatomical distribution of serotonin-containing neurons and axons in the central nervous system of the cat. *J. Comp. Neurol.* 433, 157–182.

Leznik, E., and Llinas, R. (2005). Role of gap junctions in synchronized neuronal oscillations in the inferior olive. *J. Neurophysiol.* 94, 2447–2456.

Li, S. J., Wang, Y., Strahlendorf, H. K., and Strahlendorf, J. C. (1993). Serotonin alters an inwardly rectifying current (Ih) in rat cerebellar Purkinje cells under voltage clamp. *Brain Res.* 617, 87–95.

Libster, A. M., Lefler, Y., Yaron-Jakoubovitch, A., and Yarom, Y. (2010). Ataxia and the olivo-cerebellar module. *Funct. Neurol.* 25, 129–133.

Lindsley, D. B. (1952). Psychological phenomena and the electroencephalogram. *Electroencephalogr. Clin. Neurophysiol.* 4, 443–456.

Liu, T., Xu, D., Ashe, J., and Bushara, K. (2008). Specificity of inferior olive response to stimulus timing. *J. Neurophysiol.* 100, 1557–1561.

Llinas, R., Baker, R., and Sotelo, C. (1974). Electrotonic coupling between neurons in cat inferior olive. *J. Neurophysiol.* 37, 560–571.

Llinas, R., and Sugimori, M. (1980a). Electrophysiological properties of *in vitro* Purkinje cell dendrites in mammalian cerebellar slices. *J. Physiol.* 305, 197–213.

Llinas, R., and Sugimori, M. (1980b). Electrophysiological properties of *in vitro* Purkinje cell somata in mammalian cerebellar slices. *J. Physiol.* 305, 171–195.

Llinas, R. R. (2009). Inferior olive oscillation as the temporal basis for motricity and oscillatory reset as the basis for motor error correction. *Neuroscience* 162, 797–804.

Loewenstein, Y., Mahon, S., Chadderton, P., Kitamura, K., Sompolinsky, H., Yarom, Y., et al. (2005). Bistability of cerebellar Purkinje cells modulated by sensory stimulation. *Nat. Neurosci.* 8, 202–211.

Loughlin, S. E., Foote, S. L., and Bloom, F. E. (1986a). Efferent projections of nucleus locus coeruleus: topographic organization of cells of origin demonstrated by three-dimensional reconstruction. *Neuroscience* 18, 291–306.

Loughlin, S. E., Foote, S. L., and Grzanna, R. (1986b). Efferent projections of nucleus locus coeruleus: morphologic subpopulations have different efferent targets. *Neuroscience* 18, 307–319.

Lovenberg, T. W., Liaw, C. W., Grigoriadis, D. E., Clevenger, W., Chalmers, D. T., De Souza, E. B., et al. (1995). Cloning and characterization of a functionally distinct corticotropin-releasing factor receptor subtype from rat brain. *Proc. Natl. Acad. Sci. U.S.A.* 92, 836–840.

Manor, Y., Rinzel, J., Segev, I., and Yarom, Y. (1997). Low-amplitude oscillations in the inferior olive: a model based on electrical coupling of neurons with heterogeneous channel densities. *J. Neurophysiol.* 77, 2736–2752.

McGregor, R., and Siegel, J. M. (2010). Illuminating the locus coeruleus: control of posture and arousal. *Nat. Neurosci.* 13, 1448–1449.

McKay, B. E., McRory, J. E., Molineux, M. L., Hamid, J., Snutch, T. P., Zamponi, G. W., et al. (2006). Ca(V)3 T-type calcium channel isoforms differentially distribute to somatic and dendritic compartments in rat central neurons. *Eur. J. Neurosci.* 24, 2581–2594.

Mendlin, A., Martin, F. J., Rueter, L. E., and Jacobs, B. L. (1996). Neuronal release of serotonin in the cerebellum of behaving rats: an *in vivo* microdialysis study. *J. Neurochem.* 67, 617–622.

Molineux, M. L., McRory, J. E., McKay, B. E., Hamid, J., Mehaffey, W. H., Rehak, R., et al. (2006). Specific T-type calcium channel isoforms are associated with distinct burst phenotypes in deep cerebellar nuclear neurons. *Proc. Natl. Acad. Sci. U.S.A.* 103, 5555–5560.

Molineux, M. L., Mehaffey, W. H., Tadayonnejad, R., Anderson, D., Tennent, A. F., and Turner, R. W. (2008). Ionic factors governing rebound burst phenotype in rat deep cerebellar neurons. *J. Neurophysiol.* 100, 2684–2701.

Narayanan, N. S., Land, B. B., Solder, J. E., Deisseroth, K., and Dileone, R. J. (2012). Prefrontal D1 dopamine signaling is required for temporal control. *Proc. Natl. Acad. Sci. U.S.A.* 109, 20726–20731.

Nicholas, A. P., Pieribone, V., and Hokfelt, T. (1993). Distributions of mRNAs for alpha-2 adrenergic receptor subtypes in rat brain: an *in situ* hybridization study. *J. Comp. Neurol.* 328, 575–594.

Notomi, T., and Shigemoto, R. (2004). Immunohistochemical localization of Ih channel subunits, HCN1–4, in the rat brain. *J. Comp. Neurol.* 471, 241–276.

Pazos, A., Cortes, R., and Palacios, J. M. (1985). Quantitative autoradiographic mapping of serotonin receptors in the rat brain. II. Serotonin-2 receptors. *Brain Res.* 346, 231–249.

Pazos, A., and Palacios, J. M. (1985). Quantitative autoradiographic mapping of serotonin receptors in the rat brain. I. Serotonin-1 receptors. *Brain Res.* 346, 205–230.

Peyron, C., Tighe, D. K., Van Den Pol, A. N., De Lecea, L., Heller, H. C., Sutcliffe, J. G., et al. (1998). Neurons containing hypocretin

(orexin) project to multiple neuronal systems. *J. Neurosci.* 18, 9996–10015.

Pierce, E. T., Hoddevik, G. H., and Walberg, F. (1977). The cerebellar projection from the raphe nuclei in the cat as studied with the method of retrograde transport of horseradish peroxidase. *Anat. Embryol.* 152, 73–87.

Pillot, C., Heron, A., Cochois, V., Tardivel-Lacombe, J., Ligneau, X., Schwartz, J. C., et al. (2002). A detailed mapping of the histamine H(3) receptor and its gene transcripts in rat brain. *Neuroscience* 114, 173–193.

Placantonakis, D. G., Schwarz, C., and Welsh, J. P. (2000). Serotonin suppresses subthreshold and suprathreshold oscillatory activity of rat inferior olivary neurones *in vitro*. *J. Physiol.* 524(Pt 3), 833–851.

Probst, A., Cortes, R., and Palacios, J. M. (1984). Distribution of alpha 2-adrenergic receptors in the human brainstem: an autoradiographic study using [3H]p-aminoclonidine. *Eur. J. Pharmacol.* 106, 477–488.

Qin, Y. T., Ma, S. H., Zhuang, Q. X., Qiu, Y. H., Li, B., Peng, Y. P., et al. (2011). Histamine evokes excitatory response of neurons in the cerebellar dentate nucleus via H2 receptors. *Neurosci. Lett.* 502, 133–137.

Ranade, S. P., and Mainen, Z. F. (2009). Transient firing of dorsal raphe neurons encodes diverse and specific sensory, motor, and reward events. *J. Neurophysiol.* 102, 3026–3037.

Rogers, T. D., Dickson, P. E., Heck, D. H., Goldowitz, D., Mittleman, G., and Blaha, C. D. (2011). Connecting the dots of the cerebro-cerebellar role in cognitive function: neuronal pathways for cerebellar modulation of dopamine release in the prefrontal cortex. *Synapse* 65, 1204–1212.

Safo, P. K., Cravatt, B. F., and Regehr, W. G. (2006). Retrograde endocannabinoid signaling in the cerebellar cortex. *Cerebellum* 5, 134–145.

Saitow, F., Murano, M., and Suzuki, H. (2009). Modulatory effects of serotonin on GABAergic synaptic transmission and membrane properties in the deep cerebellar nuclei. *J. Neurophysiol.* 101, 1361–1374.

Saitow, F., Satake, S., Yamada, J., and Konishi, S. (2000). beta-adrenergic receptor-mediated presynaptic facilitation of inhibitory GABAergic transmission at cerebellar interneuron-Purkinje cell synapses. *J. Neurophysiol.* 84, 2016–2025.

Santoro, B., Chen, S., Luthi, A., Pavlidis, P., Shumyatsky, G. P., Tibbs, G. R., et al. (2000). Molecular and functional heterogeneity of hyperpolarization-activated pacemaker channels in the mouse CNS. *J. Neurosci.* 20, 5264–5275.

Sari, Y., Miquel, M. C., Brisorgueil, M. J., Ruiz, G., Doucet, E., Hamon, M., et al. (1999). Cellular and subcellular localization of 5-hydroxytryptamine1B receptors in the rat central nervous system: immunocytochemical, autoradiographic and lesion studies. *Neuroscience* 88, 899–915.

Saxon, D. W., and Beitz, A. J. (1996). An experimental model for the non-invasive trans-synaptic induction of nitric oxide synthase in Purkinje cells of the rat cerebellum. *Neuroscience* 72, 157–165.

Schonewille, M., Khosrovani, S., Winkelman, B. H., Hoebeek, F. E., De Jeu, M. T., Larsen, I. M., et al. (2006). Purkinje cells in awake behaving animals operate at the upstate membrane potential. *Nat. Neurosci.* 9, 459–461, author reply 461.

Schultz, W., Dayan, P., and Montague, P. R. (1997). A neural substrate of prediction and reward. *Science* 275, 1593–1599.

Schwartz, J. C., Arrang, J. M., Garbarg, M., Pollard, H., and Ruat, M. (1991). Histaminergic transmission in the mammalian brain. *Physiol. Rev.* 71, 1–51.

Schweighofer, N., Doya, K., and Kuroda, S. (2004). Cerebellar aminergic neuromodulation: towards a functional understanding. *Brain Res. Brain Res. Rev.* 44, 103–116.

Shen, B., Li, H.-Z., and Wang, J.-J. (2002). Excitatory effects of histamine on cerebellar interpositus nuclear cells of rats through H2 receptors *in vitro*. *Brain Res.* 948, 64–71.

Shibuki, K., and Okada, D. (1991). Endogenous nitric oxide release required for long-term synaptic depression in the cerebellum. *Nature* 349, 326–328.

Shin, S. L., Hoebeek, F. E., Schonewille, M., De Zeeuw, C. I., Aertsen, A., and De Schutter, E. (2007). Regular patterns in cerebellar Purkinje cell simple spike trains. *PLoS ONE* 2:e485. doi:10.1371/journal.pone.0000485

Shiner, T., Seymour, B., Symmonds, M., Dayan, P., Bhatia, K. P., and Dolan, R. J. (2012). The effect of motivation on movement: a study of bradykinesia in Parkinson's disease. *PLoS ONE* 7:e47138. doi: 10.1371/journal.pone.0047138

Somana, R., and Walberg, F. (1978). The cerebellar projection from locus coeruleus as studied with retrograde transport of horseradish peroxidase in the cat. *Anat. Embryol.* 155, 87–94.

Somana, R., and Walberg, F. (1979). The cerebellar projection from locus coeruleus as studied with retrograde transport of horseradish peroxidase in the cat. *Anat. Embryol.* 155, 87–94.

Sotelo, C., Llinas, R., and Baker, R. (1974). Structural study of inferior olivary nucleus of the cat: morphological correlates of electrotonic coupling. *J. Neurophysiol.* 37, 541–559.

Steriade, M., Timofeev, I., and Grenier, F. (2001). Natural waking and sleep states: a view from inside neocortical neurons. *J. Neurophysiol.* 85, 1969–1985.

Strahlendorf, J. C., Lee, M., Netzeband, J. G., and Strahlendorf, H. K. (1988). Pentobarbital augments serotonin-mediated inhibition of cerebellar Purkinje cells. *Neuroscience* 27, 107–115.

Strahlendorf, J. C., Lee, M., and Strahlendorf, H. K. (1984). Effects of serotonin on cerebellar Purkinje cells are dependent on the baseline firing rate. *Exp. Brain Res.* 56, 50–58.

Sugihara, I., Lang, E. J., and Llinas, R. (1995). Serotonin modulation of inferior olivary oscillations and synchronicity: a multiple-electrode study in the rat cerebellum. *Eur. J. Neurosci.* 7, 521–534.

Swanson, L. W., Simmons, D. M., Whiting, P. J., and Lindstrom, J. (1987). Immunohistochemical localization of neuronal nicotinic receptors in the rodent central nervous system. *J. Neurosci.* 7, 3334–3342.

Tadayonnejad, R., Anderson, D., Molineux, M. L., Mehaffey, W. H., Jayasuriya, K., and Turner, R. W. (2010). Rebound discharge in deep cerebellar nuclear neurons *in vitro*. *Cerebellum* 9, 352–374.

Taheri, S., Zeitzer, J. M., and Mignot, E. (2002). The role of hypocretins (orexins) in sleep regulation and narcolepsy. *Annu. Rev. Neurosci.* 25, 283–313.

Takemura, M., Kitanaka, N., and Kitanaka, J. (2003). Signal transduction by histamine in the cerebellum and its modulation by N-methyltransferase. *Cerebellum* 2, 39–43.

Tang, B., Zhang, J., Yu, L., Li, H. Z., Zhu, J. N., and Wang, J. J. (2008). Excitation of histamine on neuronal activity of cerebellar fastigial nucleus in rat. *Inflamm. Res.* 57(Suppl. 1), S41–S42.

Tian, J. B., and Bishop, G. A. (2003). Frequency-dependent expression of corticotropin releasing factor in the rat's cerebellum. *Neuroscience* 121, 363–377.

Tian, L., Wen, Y. Q., Li, H. Z., Zuo, C. C., and Wang, J. J. (2000). Histamine excites rat cerebellar Purkinje cells via H2 receptors *in vitro*. *Neurosci. Res.* 36, 61–66.

Toonen, M., Van Dijken, H., Holstege, J. C., Ruigrok, T. J., Koekkoek, S. K., Hawkins, R. K., et al. (1998). Light microscopic and ultrastructural investigation of the dopaminergic innervation of the ventrolateral outgrowth of the rat inferior olive. *Brain Res.* 802, 267–273.

Torben-Nielsen, B., Segev, I., and Yarom, Y. (2012). The generation of phase differences and frequency changes in a network model of inferior olive subthreshold oscillations. *PLoS Comput. Biol.* 8:e1002580. doi: 10.1371/journal.pcbi.1002580

Trudeau, L.-É. (2004). Glutamate cotransmission as an emerging concept in monoamine neuron function. *J. Psychiatry Neurosci.* 29, 296–310.

Trulson, M. E., and Jacobs, B. L. (1979). Raphe unit activity in freely moving cats: correlation with level of behavioral arousal. *Brain Res.* 163, 135–150.

Urban, N. N., Henze, D. A., and Barrionuevo, G. (1998). Amplification of perforant-path EPSPs in CA3 pyramidal cells by LVA calcium and sodium channels. *J. Neurophysiol.* 80, 1558–1561.

Uusisaari, M., and De Schutter, E. (2011). The mysterious microcircuitry of the cerebellar nuclei. *J. Physiol.* 589, 3441–3457.

Uusisaari, M., and Knöpfel, T. (2011). Functional classification of neurons in the mouse lateral cerebellar nuclei. *Cerebellum* 10, 637–646.

Veasey, S. C., Fornal, C. A., Metzler, C. W., and Jacobs, B. L. (1995). Response of serotonergic caudal raphe neurons in relation to specific motor activities in freely moving cats. *J. Neurosci.* 15, 5346–5359.

Veasey, S. C., Fornal, C. A., Metzler, C. W., and Jacobs, B. L. (1997). Single-unit responses of serotonergic dorsal raphe neurons to specific motor challenges in freely moving cats. *Neuroscience* 79, 161–169.

Wada, E., Wada, K., Boulter, J., Deneris, E., Heinemann, S., Patrick, J., et al. (1989). Distribution of alpha 2,

alpha 3, alpha 4, and beta 2 neuronal nicotinic receptor subunit mRNAs in the central nervous system: a hybridization histochemical study in the rat. *J. Comp. Neurol.* 284, 314–335.

Wahl-Schott, C., and Biel, M. (2009). HCN channels: structure, cellular regulation and physiological function. *Cell. Mol. Life Sci.* 66, 470–494.

Walters, A. S., and Hening, W. A. (1992). Noise-induced psychogenic tremor associated with post-traumatic stress disorder. *Mov. Disord.* 7, 333–338.

Wamsley, J. K., Lewis, M. S., Young, W. S. 3rd., and Kuhar, M. J. (1981). Autoradiographic localization of muscarinic cholinergic receptors in rat brainstem. *J. Neurosci.* 1, 176–191.

Wanaka, A., Kiyama, H., Murakami, T., Matsumoto, M., Kamada, T., Malbon, C. C., et al. (1989). Immunocytochemical localization of beta-adrenergic receptors in the rat brain. *Brain Res.* 485, 125–140.

Wang, Y., Strahlendorf, J. C., and Strahlendorf, H. K. (1992). Serotonin reduces a voltage-dependent transient outward potassium current and enhances excitability of cerebellar Purkinje cells. *Brain Res.* 571, 345–349.

Watson, M., and McElligott, J. G. (1984). Cerebellar norepinephrine depletion and impaired acquisition of specific locomotor tasks in rats. *Brain Res.* 296, 129–138.

Wiklund, L., Bjorklund, A., and Sjolund, B. (1977). The indolaminergic innervation of the inferior olive. 1. Convergence with the direct spinal afferents in the areas projecting to the cerebellar anterior lobe. *Brain Res.* 131, 1–21.

Wiklund, L., Descarries, L., and Mollgard, K. (1981a). Serotoninergic axon terminals in the rat dorsal accessory olive: normal ultrastructure and light microscopic demonstration of regeneration after 5, 6-dihydroxytryptamine lesioning. *J. Neurocytol.* 10, 1009–1027.

Wiklund, L., Sjolund, B., and Bjorklund, A. (1981b). Morphological and functional studies on the serotoninergic innervation of the inferior olive. *J. Physiol.* 77, 183–186.

Williams, S. R., Christensen, S. R., Stuart, G. J., and Hausser, M. (2002). Membrane potential bistability is controlled by the hyperpolarization-activated current I(H) in rat cerebellar Purkinje neurons *in vitro*. *J. Physiol.* 539, 469–483.

Wilson, G. W., and Garthwaite, J. (2010). Hyperpolarization-activated ion channels as targets for nitric oxide signalling in deep cerebellar nuclei. *Eur. J. Neurosci.* 31, 1935–1945.

Womack, M. D., and Khodakhah, K. (2002). Characterization of large conductance Ca2+-activated K+ channels in cerebellar Purkinje neurons. *Eur. J. Neurosci.* 16, 1214–1222.

Womack, M. D., and Khodakhah, K. (2004). Dendritic control of spontaneous bursting in cerebellar Purkinje cells. *J. Neurosci.* 24, 3511–3521.

Woodward, D. J., Moises, H. C., Waterhouse, B. D., Yeh, H. H., and Cheun, J. E. (1991). The cerebellar norepinephrine system: inhibition, modulation, and gating. *Prog. Brain Res.* 88, 331–341.

Wu, X., Ashe, J., and Bushara, K. O. (2011). Role of olivocerebellar system in timing without awareness. *Proc. Natl. Acad. Sci. U.S.A.* 108, 13818–13822.

Xu, D., Liu, T., Ashe, J., and Bushara, K. O. (2006). Role of the olivo-cerebellar system in timing. *J. Neurosci.* 26, 5990–5995.

Yartsev, M. M., Givon-Mayo, R., Maller, M., and Donchin, O. (2009). Pausing purkinje cells in the cerebellum of the awake cat. *Front. Syst. Neurosci.* 3:2. doi: 10.3389/neuro.06.002.2009

Yu, L., Zhang, X.-Y., Zhang, J., Zhu, J.-N., and Wang, J.-J. (2010). Orexins excite neurons of the rat cerebellar nucleus interpositus via orexin 2 receptors *in vitro*. *Cerebellum* 9, 88–95.

Conflict of Interest Statement: The authors declare that the research was conducted in the absence of any commercial or financial relationships that could be construed as a potential conflict of interest.

Received: 10 January 2013; accepted: 03 April 2013; published online: 19 April 2013.

Citation: Libster AM and Yarom Y (2013) In and out of the loop: external and internal modulation of the olivo-cerebellar loop. Front. Neural Circuits 7:73. doi: 10.3389/fncir.2013.00073

frontiers in
NEURAL CIRCUITS

REVIEW ARTICLE
published: 11 December 2012
doi: 10.3389/fncir.2012.00097

Synchrony and neural coding in cerebellar circuits

Abigail L. Person*[1] *and Indira M. Raman*[2]

[1] *Department of Physiology and Biophysics, University of Colorado School of Medicine, Aurora, CO, USA*
[2] *Department of Neurobiology, Northwestern University, Evanston, IL, USA*

Edited by:
Chris I. De Zeeuw, Erasmus Medical Center, Netherlands

Reviewed by:
Nathan Urban, Carnegie Mellon University, USA
Michael Nitabach, Yale University School of Medicine, USA

****Correspondence:***
Indira M. Raman, Department of Neurobiology, Northwestern University, 2205 Tech Drive, Evanston, IL 60208, USA.
e-mail: i-raman@northwestern.edu

The cerebellum regulates complex movements and is also implicated in cognitive tasks, and cerebellar dysfunction is consequently associated not only with movement disorders, but also with conditions like autism and dyslexia. How information is encoded by specific cerebellar firing patterns remains debated, however. A central question is how the cerebellar cortex transmits its integrated output to the cerebellar nuclei via GABAergic synapses from Purkinje neurons. Possible answers come from accumulating evidence that subsets of Purkinje cells synchronize their firing during behaviors that require the cerebellum. Consistent with models predicting that coherent activity of inhibitory networks has the capacity to dictate firing patterns of target neurons, recent experimental work supports the idea that inhibitory synchrony may regulate the response of cerebellar nuclear cells to Purkinje inputs, owing to the interplay between unusually fast inhibitory synaptic responses and high rates of intrinsic activity. Data from multiple laboratories lead to a working hypothesis that synchronous inhibitory input from Purkinje cells can set the timing and rate of action potentials produced by cerebellar nuclear cells, thereby relaying information out of the cerebellum. If so, then changing spatiotemporal patterns of Purkinje activity would allow different subsets of inhibitory neurons to control cerebellar output at different times. Here we explore the evidence for and against the idea that a synchrony code defines, at least in part, the input–output function between the cerebellar cortex and nuclei. We consider the literature on the existence of simple spike synchrony, convergence of Purkinje neurons onto nuclear neurons, and intrinsic properties of nuclear neurons that contribute to responses to inhibition. Finally, we discuss factors that may disrupt or modulate a synchrony code and describe the potential contributions of inhibitory synchrony to other motor circuits.

Keywords: Purkinje, cerebellar nuclei, interpositus, corticonuclear, action potential, inhibition, IPSC, spatiotemporal

Purkinje neurons are the principal neurons of the cerebellar cortex (**Figure 1A**). They receive processed sensory information via the mossy fiber to granule cell pathway as well as input from climbing fibers of the inferior olive, often considered an error or teaching signal (Marr, 1969; Albus, 1971; Gilbert and Thach, 1977; Medina et al., 2002). In addition to these excitatory synapses, Purkinje cells are subject to inhibition by basket and stellate cells. All these synaptic inputs modulate the high intrinsic firing rates of Purkinje cells (Thach, 1968; Latham and Paul, 1971). Non-vestibular Purkinje cell output is transmitted exclusively to the cerebellar nuclei, a heterogeneous set of neurons that project widely to premotor areas, as well as back to the inferior olive. The corticonuclear projection is inhibitory (Ito and Yoshida, 1966; Ito et al., 1970), and the target cells in the nuclei are also intrinsically active (Thach, 1968), setting up the specialized situation of spontaneously firing principal cells connected by inhibitory synapses.

REAL-TIME CODING BY CORTICONUCLEAR SYNAPSES

A primary question in cerebellar physiology, therefore, is how cerebellar nuclear cells transduce input from Purkinje cells to generate cerebellar output (**Figure 1B**). Because Purkinje neurons are GABAergic and outnumber neurons in the cerebellar nuclei—by 26:1 in the cat (Palkovits et al., 1977) and 11:1 in the mouse (Caddy and Biscoe, 1979; Harvey and Napper, 1991; Heckroth, 1994)—they are expected to exert a powerful inhibitory influence on their targets. Indeed, the fact that Purkinje cells regulate cerebellar nuclear cell output is unambiguous. Alterations of Purkinje cell firing are often associated with disease states: In motor disorders like ataxia and dystonia, changes in Purkinje action potential firing have been directly recorded in rodent models. Ataxia can result from degeneration of Purkinje cells or reductions in Purkinje spike rates (Mullen et al., 1976; Levin et al., 2006); this drastic loss of inhibitory input is expected to elevate nuclear cell firing rates. Irregular Purkinje cell firing, however, also correlates with ataxia (Walter et al., 2006). Likewise in dystonia, both Purkinje and nuclear cells fire irregular bursts of spikes (LeDoux et al., 1998). Remarkably, removing all cerebellar output by cerebellar ablation relieves dystonia, but this extreme manipulation also generates ataxia (LeDoux et al., 1993, 1998; Calderon et al., 2011). Thus, increases, decreases, and

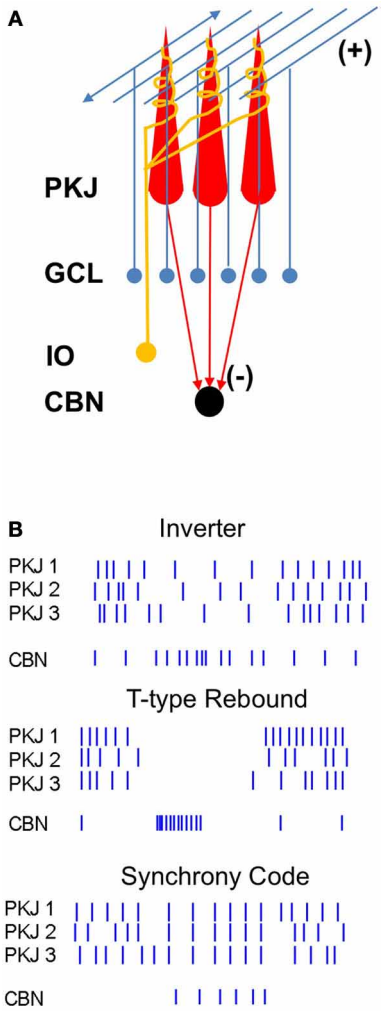

FIGURE 1 | Diagram of the corticonuclear circuit and mechanisms of corticonuclear signaling. (A) Cerebellar Purkinje cells (PKJ) receive glutamatergic inputs from the granule cell layer (GCL) whose axons form ascending inputs onto Purkinje cells and also ramify to form the parallel fibers, as well as from the inferior olive (IO), whose axons form the climbing fibers. Molecular layer inhibitory neurons are not shown. Purkinje cells form GABAergic synapses onto neurons of the cerebellar nuclei (CBN). **(B)** Schematized spike rasters showing the key features of three non-mutually-exclusive models of Purkinje cell regulation of nuclear cell firing. Nuclear cell spikes reflect responses to three afferent Purkinje cells. *Inverter,* nuclear cell firing rate varies inversely with Purkinje cell firing rate. *T-type Rebound,* nuclear cells are largely silenced by Purkinje cell activity, but fire bursts of action potentials driven by low-voltage-activated Ca currents when Purkinje cells stop firing. *Synchrony code,* nuclear cells are silenced by asynchronous inhibition but produce short-latency spikes after IPSPs from synchronous inputs.

irregularities in cerebellar output all induce motor dysfunctions, indicating that both the rate and timing of spiking by cerebellar nuclear neurons must be precisely regulated under normal conditions. This regulation must be accomplished at least in part by Purkinje cells.

The most straightforward prediction is that firing rates of nuclear cells should be the inverse of those in their Purkinje afferents (**Figure 1B**, *top*). Consistent with this idea, nuclear cells often respond to sensory inputs with reduced spike rates (Armstrong et al., 1975; Cody et al., 1981; Rowland and Jaeger, 2005), suggestive of a suppression of nuclear cell activity by stimuli expected to raise Purkinje cell spike rates. Studies of populations of Purkinje neurons and cerebellar nuclear neurons, however, often show correlated changes in addition to anti-correlated changes in firing rates, both in the basal state and during behaviors associated with modulation of Purkinje cell activity. For example, in rhesus monkeys, Purkinje neurons as well as nuclear neurons increase their firing rates during brief, cue-initiated movements (Thach, 1970a,b). Similarly, during locomotion in cats, the majority of both Purkinje and interpositus neurons increase their firing rates more during forelimb swing than during stances (**Figure 2**; Armstrong and Edgley, 1984a,b). The absence of clearly opposing firing rate changes in these studies might be accounted for if the specific Purkinje cells and nuclear cells whose activity was recorded were not synaptically linked, but similar results have been obtained from simultaneous recordings from putative connected pairs of Purkinje and nuclear neurons. In decerebrate cats, for example, spontaneous activity of such Purkinje-nuclear pairs is not correlated, and firing rate modulation in response to periodic sensory stimuli is not consistently reciprocal, leading to the conclusion that single Purkinje afferents are insufficient to regulate the spiking behavior of nuclear cell targets (McDevitt et al., 1987). The characterization of corticonuclear synapses exclusively as inverters, therefore, may be an oversimplification.

The alternative to nuclear cells' tracking the spike rate of individual Purkinje afferents is that it is the activity of populations of Purkinje cells that encodes meaningful signals. This idea has been supported by studies of the oculomotor system of rhesus monkeys. In a task involving visually guided saccades, bursts produced by individual Purkinje cells turn out to be imperfect predictors of saccade duration, but saccade onset and termination is precisely represented by the activity of a population of Purkinje cells considered together (Thier et al., 2000; Catz et al., 2008). The authors point out that the idea that neurons of the cerebellar nuclei respond to groups of Purkinje cells rather than to individual cells is virtually an obligate outcome of the anatomical convergence of Purkinje cells onto nuclear cells.

Nevertheless, when the question is further examined at the cellular level, paradoxes remain. Both Purkinje neurons and their target cells in the nuclei spontaneously fire tens of spikes per second in the absence of synaptic input (Llinás and Sugimori, 1980; Jahnsen, 1986a; Mouginot and Gähwiler, 1995; Häusser and Clark, 1997; Raman and Bean, 1997). The high basal firing rates of Purkinje cells (>50 spikes/s), extensive inhibitory innervation of nuclear cell somata and proximal dendrites (Chan-Palay, 1977; Palkovits et al., 1977; De Zeeuw et al., 1994; Sugihara et al., 2009), and minimal synaptic depression (Mouginot and Gähwiler, 1995; Telgkamp et al., 2004) predict a complete shunt of nuclear cells even in the basal state. Nuclear cells, however, show basal firing rates of >20 spikes/s in the brains of monkeys, cats, rats, and mice (Thach, 1968; Rowland and Jaeger, 2005; Bengtsson et al., 2011; Blenkinsop and Lang, 2011; Person

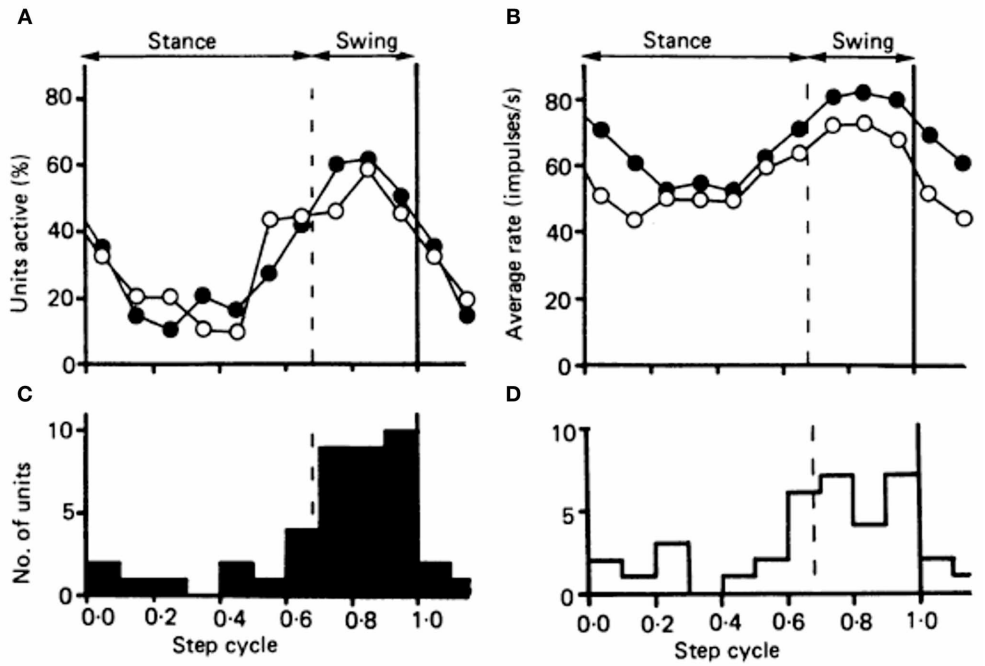

FIGURE 2 | Comparison of the timing of the activity in the population of 34 Purkinje cells in the cat identified as belonging to cl zone, with the timing of the activity in a population of forelimb-related neurons of nucleus interpositus. (A) Plots showing the proportion of neurons in each population "active" during each tenth of the step cycle. Open circles, cl Purkinje cell population; filled circles, the population of interpositus neurons. **(B)** The fluctuation in discharge rate amongst the two populations during the course of the step cycle. Open circles represent the Purkinje cells of the cl zone; and filled circles the interpositus neurons. **(C** and **D)** Histograms showing the number of neurons attaining their peak discharge rate during each tenth of the step cycle, for the interpositus neurons and the Purkinje cells of the cl zone respectively. Reprinted from Armstrong and Edgley (1984b), with permission.

and Raman, 2012), raising the question of what types of signals are required to suppress—or trigger—nuclear cell firing. One possibility is that nuclear cells are indeed fully silenced by Purkinje inhibition, so that their spiking relies entirely on excitation by mossy fibers, an idea that emerged from models based on early recordings of synaptic properties (Anchisi et al., 2001; Gauck and Jaeger, 2003). This idea, however, implies that the intrinsic activity of nuclear cells is necessarily suppressed by the intrinsic activity of Purkinje cells, a surprisingly energetically costly mode of re-establishing the common scenario of a silent principal cell that requires excitation to fire. Another possibility is that only when Purkinje cells cease firing for prolonged periods, on the order of a few hundred milliseconds, do nuclear cells fire post-inhibitory "rebound" spikes (Llinás and Mühlethaler, 1988; **Figure 1B**, *middle*). This idea is attractive, especially given the high densities of low-voltage activated "T-type" Ca currents in nuclear cells (Aizenman and Linden, 1999; Czubayko et al., 2001; Molineux et al., 2006). The notion that nuclear cells generate action potentials only when afferent Purkinje cells are collectively silenced for durations long enough to permit recovery of T-type Ca channels, however, implies that information encoded in spike rates of Purkinje cells may not be transmitted. Moreover, it predicts lags between Purkinje and nuclear cell activity, inconsistent with cerebellar response latencies of a few milliseconds (Mauk and Buonomano, 2004).

SYNCHRONOUS FIRING BY PURKINJE CELLS

A resolution to these paradoxes may emerge from the observation that populations of Purkinje cells can synchronize their spiking, especially during cerebellar behaviors. It has long been recognized that multiple Purkinje cells coincidently fire complex spikes (Sasaki et al., 1989), a synchrony that may result from innervation of several Purkinje cells by a common climbing fiber, but which is likely intensified by simultaneous firing by inferior olivary cells promoted by gap junctions (Lampl and Yarom, 1993; Devor and Yarom, 2002; Blenkinsop and Lang, 2006). In contrast to the inconsistent responses to Purkinje cell simple spike rate, inhibition of nuclear cells by complex spikes is more readily evident experimentally. Spontaneous complex spikes in Purkinje neurons of ketamine-xylazine anesthetized rats can elicit prolonged inhibitory responses in connected nuclear cells (Blenkinsop and Lang, 2011). Likewise, in decerebrate cats, inferior olivary stimulation elicits giant IPSPs in whole-cell recordings of cells in the cerebellar nuclei (Bengtsson et al., 2011).

Complex spikes may be particularly effective at inducing overt inhibition of nuclear cells because the multiple spikelets in each complex spike propagate as two or three high-frequency action potentials (Khaliq and Raman, 2005; Monsivais et al., 2005), likely eliciting a brief burst of postsynaptic IPSCs. An alternative, not mutually exclusive interpretation, however, is that a key

parameter is the synchrony with which Purkinje cells tend to fire complex spikes (Welsh et al., 1995; Mukamel et al., 2009; Ozden et al., 2009; Schultz et al., 2009). If some of these coincidently firing Purkinje cells converge, nuclear cells may be subject to inhibition from many Purkinje cells at once. By extension, the termination of the synchronous IPSP may provide a window in which spike probability is transiently increased owing to the relief of inhibition.

The temporal relationship of action potential firing by multiple convergent Purkinje cells may therefore be a central factor in determining nuclear cell responses to inhibitory signals (see also De Zeeuw et al., 2011). This idea is particularly interesting because Purkinje cells tend not only to generate complex spikes coincidently, but also to fire simple spikes synchronously during both movement and sensory stimulation. In one of the earliest demonstrations of simple spike synchrony, Bell and Grimm (1969) made double microelectrode recordings in pentobarbital-anesthetized cats and showed that Purkinje neurons located close together ($<70\,\mu m$) often fired nearly simultaneously. Cross correlograms, calculated with 1-ms resolution, consistently showed peaks at 0 delays. Similar observations were made in pentobarbital-anesthetized guinea pigs, in which Purkinje neurons located along parallel fiber beams showed large cross-correlation peaks at 1 ms (Bell and Kawasaki, 1972). Since these early studies, numerous groups have observed synchronous simple spikes, in several preparations, with several anesthetic regimens. A consistent finding is that Purkinje cells that synchronize with one another are also located near one another, such that submillisecond correlations at time 0 are evident only in Purkinje neurons that are fewer than 100 microns apart (MacKay and Murphy, 1976; Ebner and Bloedel, 1981; De Zeeuw et al., 1997; Shin and De Schutter, 2006; Heck et al., 2007; de Solages et al., 2008; Bosman et al., 2010; Wise et al., 2010).

Synchrony is subject to modulation by sensory input or motor behaviors associated with cerebellar activity. Several groups report that synchrony is enhanced by somatosensory or proprioceptive stimulation (MacKay and Murphy, 1976; Ebner and Bloedel, 1981; Wise et al., 2010). In a breakthrough series of experiments, Heck et al. (2007) demonstrated that bands of Purkinje neurons fired synchronously during a learned motor task in rats, and that the increase of synchrony was time-locked to movement (**Figure 3**). Not only was synchrony resolved with high temporal precision, in cross correlations with bins <1 ms wide, but it was also shown to be widespread, with synchrony being evident in most Purkinje pairs located within a few hundred microns of each other.

MECHANISMS OF SIMPLE SPIKE SYNCHRONY

Despite the repeated and robust observations of Purkinje cell simple spike synchrony, results vary regarding *which* Purkinje cells synchronize and *how* they do so. Some studies report simple spike synchrony in the parasagittal plane within microzones of Purkinje cells that fire synchronous complex spikes; in these studies, cells with synchronous complex spikes were

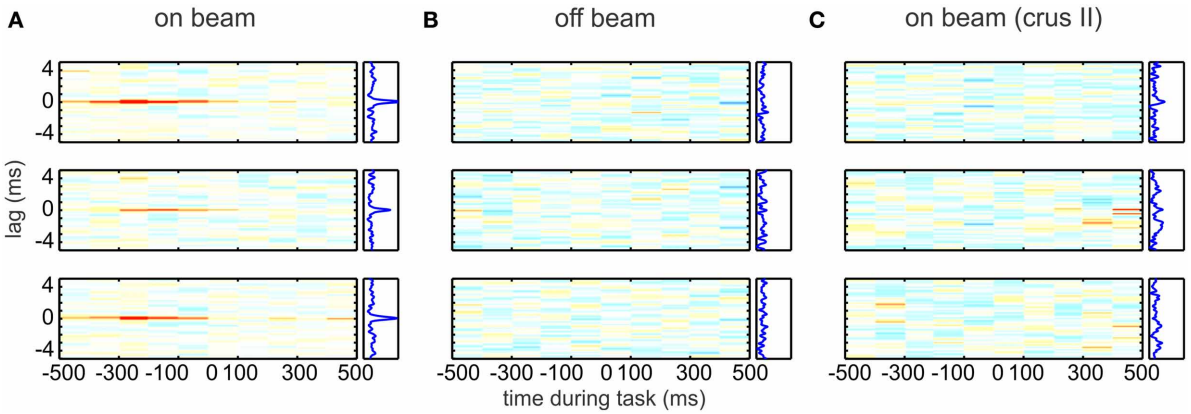

FIGURE 3 | Simple spike synchrony in Purkinje cells. On-beam Purkinje cells (Pcs) in the paramedian lobe fired precisely synchronized simple spikes (SSs) time-locked to behavior. Each plot represents the time-resolved cross-correlogram of Pc SS activity recorded at two different electrodes during reaching–grasping movements by awake rats. Average cross-correlations were calculated for epochs of 100-ms duration with a temporal resolution of spike delays of 40 μs. In each plot, the abscissa indicates time during the movement. At time 0, the rat has completed paw extension and touches the food pellet. The ordinate indicates the cross-spike train interval. All plots use the same color map (from red = 0.01 through white = 0 to blue = −0.01). Plots to the right side of the time-resolved cross-correlation matrix show the average excess correlation, i.e., the integral along the abscissa. The time-resolved cross-correlations shown here were generated from the data shown in Figure 1 of Heck et al. (2007). Data were analyzed by subdividing the experimental time into 100-ms bins and calculating the average excess correlation within each bin at 40-μs resolution. The resulting color-coded matrix was smoothed across delays by convolving with a 120-μs Gaussian. **(A)** Correlation analysis of spike activity recorded with the electrode array in on-beam orientation in the paramedian lobe. (Top to Bottom) Plotted cross-correlations of spike activity recorded on electrode 1 vs. 2, 2 vs. 3, and 1 vs. 3. Behavior-related occurrence of on-beam synchronous activity is visualized by the red lines at zero lag in the on-beam matrix. The occurrence of synchronous activity was not directly correlated with spike rate or change of rate. **(B)** (Top to Bottom) Arrangement of cross-correlation plots as in **(A)**. Here, the electrode array was in off-beam orientation. No synchronous activity was seen in paired off-beam recordings. **(C)** Correlation analysis of SS activity recorded during behavior in crus II, an area outside the arm representation, with the electrode array in on-beam orientation. No behavior-modulated SS activity or synchronous firing was observed. Reprinted from Heck et al. (2007), with permission.

more likely also to fire simple spikes synchronously, suggestive of a common mechanism underlying both types of action potentials (Bell and Kawasaki, 1972; Wise et al., 2010). In contrast, in several preparations, synchrony is evident in on-beam Purkinje cells, expected to be innervated by common parallel fibers, but different climbing fibers (MacKay and Murphy, 1976; Ebner and Bloedel, 1981; Heck et al., 2007; Bosman et al., 2010). Interestingly, some of this work reporting on-beam synchrony was initially directed toward documenting the functional correlate of delay lines predicted by parallel fiber anatomy (Braitenberg, 1967; Eccles et al., 1967), and sought to find sequential, not synchronous Purkinje cell firing. Even examining Purkinje responses separated by a range of distances (0.1–1.5 mm in anesthetized rats), however, reveals no such delay-line like behavior (Jaeger, 2003). These experiments add to the growing body of data demonstrating that, despite their striking anatomy, parallel fibers may not effectively deliver information to Purkinje cells in a precise temporal sequence (e.g., Bower and Woolston, 1983).

Granule cells may, nevertheless, play a significant role in synchronizing simple spikes. One proposal is that Purkinje simple spike synchrony arises from common input patterns from ascending granule cell axons that receive inputs from the same mossy fibers (Heck et al., 2007). In this case, small groups or "patches" of granule cells would synchronize simple spikes in Purkinje cells in a restricted transverse and parasagittal region. Consistent with this idea, in response to muscle stretch, the shortest response latencies among granule cells are of those that lie directly beneath the responsive region of Purkinje neurons (MacKay and Murphy, 1976; Murphy et al., 1976). In addition, direct mossy fiber stimulation only activates groups of Purkinje cells located directly above the mossy fiber termination zone (Eccles et al., 1972; Bower and Woolston, 1983; Cohen and Yarom, 1998; Bower, 2002; Dizon and Khodakhah, 2011).

Both anatomical and physiological studies have led to the proposal that ascending axons may have specializations that permit them to drive Purkinje spiking more effectively than do parallel fibers. Electron microscopic studies reveal larger synaptic volume and more vesicles in ascending than in parallel fibers (Gundappa-Sulur et al., 1999). Electrophysiological recordings in slices report that more ascending synapses than parallel fiber synapses are functional (Isope and Barbour, 2002) and that ascending branches have higher release probability and are relatively resistant to long-term depression (Sims and Hartell, 2005, 2006). These attributes, however, do not indicate that ascending axons necessarily evoke larger unitary responses in Purkinje cells than parallel fibers do, and, in fact, evidence that both ascending and parallel fiber inputs are functionally equivalent has also been presented (Isope and Barbour, 2002; Walter et al., 2009; Zhang and Linden, 2012).

Regardless of the relative strength of the two branches of granule cell input, Purkinje neurons may still be preferentially excited by granule neurons directly beneath them. In rat cerebellar slices, stimulating granule cells leads to excitation of the Purkinje cell located just superficially, while stimulating more lateral groups of granule cells (in the parasagittal plane) recruit inhibitory inputs to that Purkinje cell, by activating molecular layer interneurons (Dizon and Khodakhah, 2011). These data suggest that simple spike synchrony would require co-activation of several discrete groups of granule cells to overcome lateral inhibition by basket and/or stellate cells. In addition, the inhibition of Purkinje cells by basket and stellate cells (in coronal slices, along the parallel fibers) has been reported to provide a feedforward inhibition that narrows the duration of granule-cell mediated excitation to 1–2 ms (at 32–35°C), an effect that would be expected to increase the precision of Purkinje cell firing in response to excitation (Brunel et al., 2004; Mittmann et al., 2005; Kanichay and Silver, 2008; D'Angelo and De Zeeuw, 2009; Dizon and Khodakhah, 2011). Consistent with this idea, Shin and De Schutter (2006) found that simple spikes separated by longer intervals (>12 ms) were more likely to synchronize than those with shorter gaps, such that the onset or offset of longer pauses were likely to occur simultaneously. This synchrony of pauses was not attributable to complex spikes, and thus seems likely to involve local inhibition.

Other forms of inhibition may actively facilitate simple spike synchrony. For instance, in a clever series of pharmacological experiments, de Solages et al. (2008) demonstrated that blocking $GABA_A$ receptor-mediated inhibition disrupted synchrony; suppressing activity of inhibitory interneurons with cannabinoid (CB1) receptor agonists, however, left synchrony unaffected, leading to the conclusion that Purkinje–Purkinje inhibition, mediated by local collaterals, provided the GABAergic signals that were crucial to maintaining synchrony. This idea is consistent with computational work demonstrating that synchrony is an extremely common consequence of synaptically connected oscillatory inhibitory cells (Salinas and Sejnowski, 2001). Coupling by gap junctions between Purkinje neurons and molecular layer interneurons has also been proposed to support synchronization of Purkinje cells (Middleton et al., 2008).

An alternative mechanism for simple spike synchrony involves complex spikes organizing simple spikes. As mentioned above, complex spikes occur synchronously in Purkinje neurons across parasagittal bands of the cerebellar cortex. Since the cell bodies of climbing fibers, which drive complex spikes in Purkinje cells, are electrically coupled in the inferior olive (Llinás and Yarom, 1986; Lampl and Yarom, 1993; Devor and Yarom, 2002; Blenkinsop and Lang, 2006) and since single climbing fibers can contact multiple Purkinje neurons, coincident activity in multiple climbing fibers tends to drive a sizable population of Purkinje neurons to fire synchronous complex spikes (Welsh et al., 1995; Mukamel et al., 2009; Ozden et al., 2009; Schultz et al., 2009), leading to the measurable inhibition of nuclear neurons described above. Of possible significance for simple spike synchrony, complex spikes are often followed by a pause in firing. If several Purkinje cells with common basal firing rates were to experience pauses of equivalent durations, the synchronous complex spikes might lead to a phase resetting of simple spikes, such that simple spikes in a population of Purkinje neurons would be synchronized upon resumption of firing. Although this scenario presents an intriguing potential link between complex and simple spike synchrony, pauses following complex spikes tend to be highly variable, ranging from tens to hundreds of milliseconds even within cells (Bell and Grimm, 1969; Latham and Paul,

1971; Murphy and Sabah, 1971; McDevitt et al., 1982; Steuber et al., 2007), suggesting that additional factors may be necessary to achieve a precise phase resetting by complex spikes. The generation of simple spike synchrony may thus rely on several mechanisms working together—or different mechanisms active under different conditions. Nevertheless, the observation that synchrony increases during behaviors that involve the cerebellum suggests that synchronously firing Purkinje neurons may encode information that is specifically transmitted to the cerebellar nuclei.

PURKINJE-TO-NUCLEAR CONVERGENCE: 1000s, 100s, OR 10s?

Understanding the extent to which synchronous and asynchronous Purkinje inhibition differentially affect nuclear cells requires answering the apparently basic question of how many Purkinje cells converge onto a cerebellar nuclear neuron. This information will define the basal level of inhibition, which in turn will influence how many Purkinje cells must synchronize to be detected by the nuclear cell. The most widely cited estimate of the convergence of Purkinje neurons onto nuclear neurons comes from the heroic and careful quantitative electron microscopic study of the cat by Palkovits et al. (1977). Comparing the total number of "synaptic profiles," or boutons, of Purkinje cells to the total number of neurons in the cerebellar nuclei led to an estimate of 11,600 Purkinje boutons per nuclear cell, with each Purkinje cell calculated to have 474 boutons. The number of nuclear cells targeted by each Purkinje cell, i.e., the degree of divergence, was estimated to be roughly 35 from the number of nuclear cells that could fall within the axonal arbor of the Purkinje cell, a number that Palkovits et al. described as an "order of magnitude" measurement. Thus, each nuclear cell was calculated to receive 474/35 or 13.5 boutons from any given Purkinje cell. Dividing 11,600 by 13.5 gave the final value of convergence of 860 Purkinje neurons per nuclear cell.

As the authors acknowledged, the degree of divergence was only weakly constrained, making the number of boutons from each Purkinje neuron synapsing onto each nuclear cell also only loosely approximated. An updated measure of the number of boutons from a single Purkinje cell contacting an individual nuclear cell can be obtained from physiological measurements, however. In brain slices from mice, the ratio of the unitary IPSC to the miniature IPSC estimates the quantal content at 12–18 (Telgkamp and Raman, 2002; Pedroarena and Schwarz, 2003; Person and Raman, 2012) and the release probability per bouton is near 0.5 (Telgkamp et al., 2004). Multiplying these values gives an estimate of the number of boutons at a single Purkinje-nuclear contact at 24–36; this higher value is within the range (1–50) proposed by Palkovits et al. for the cat, and is therefore unlikely to reflect species differences. Incorporating this value into their calculation reduces the estimate of convergence to 322–483.

Perhaps more importantly, as the authors state explicitly, their "apparently excessive" numerical estimate for average convergence is based on the simplifying assumption that each Purkinje cell ramifies to the same extent on all nuclear cells. They point out, however, that Purkinje neurons consistently make non-uniform contacts onto nuclear cells, occasionally "erupting" into "numerous (∼50) boutons all in contact with the same cell body." Ramón y Cajal similarly observed that each Purkinje neuron axon formed six to eight "nests" onto as many cells (Chan-Palay, 1977). Such dense terminal perisomatic plexes are also mentioned in other descriptions of Purkinje axonal arbors (Chan-Palay, 1977; Bishop et al., 1979; De Zeeuw et al., 1994; Wylie et al., 1994; Teune et al., 1998; Sugihara et al., 2009), suggesting that they are a common specialization of Purkinje neuron terminals. Palkovits et al. (1977) propose that each Purkinje neuron may have 3–6 primary targets, while providing weak input to many more, and conversely that nuclear cells may only receive strong somatic input from "several"—that is, a relatively small number of— Purkinje cells (see also Sugihara et al., 2009).

The scenario of a few dozen dominant Purkinje cell inputs per nuclear cell is consistent with physiological measurements. From recordings either in Deiter's nucleus *in vivo* or in the cerebellar nuclei in an acute brain slice preparation, the ratio of the maximal and minimal responses evoked by Purkinje cell activation gives convergence estimates of 22–30 *in vivo* (Eccles et al., 1967) and 10–20 *in vitro;* the latter estimate provides only a lower bound, given that some inputs are likely lost during slicing (Person and Raman, 2012). Additional measurements, however, constrain the functional convergence in the mouse to be between 30 and 50. First, based on anatomical measurements of cell surface area, boutonal area, and extent of inhibitory innervation (Chan-Palay, 1977; Telgkamp et al., 2004; Uusisaari et al., 2007), it seems likely that a large nuclear neuron can likely maximally accommodate 1250 Purkinje boutons. A similar calculation has recently been made for the cat, estimating the number of inhibitory synapses at 600–1200 (Bengtsson et al., 2011). (Note that this value is an order of magnitude lower than the estimate of 11,600 of Palkovits et al. (1977). Person and Raman (2012) initially proposed that the high estimate might have resulted from counting synaptic densities and assuming one rather than ∼10 densities per bouton, but this does not seem to be the case). Dividing 1250 boutons on each nuclear cells by 24–36 boutons per Purkinje-nuclear contact (as described above) predicts 34–52 Purkinje cells/nuclear cell (Person and Raman, 2012). Corroborating this result, dividing the maximal $GABA_A$-evoked conductance in a nuclear cell by the unitary IPSC predicts that a maximum of 30 Purkinje cells, evoking currents of the mean unitary size, converge onto the nuclear cell (Person and Raman, 2012).

Interestingly, by analyzing single reconstructed Purkinje axons at the light microscope level, Sugihara et al. (2009) quantified the number of putative axonal boutons (axonal swellings) made by individual Purkinje axons in rats, reporting values between 120 and 150 (somewhat lower than the 474 originally estimated in the cat). If each Purkinje axon contributes ∼30 boutons per nuclear neuron, then divergence must be 4–5, values that align well with numerical ratios of Purkinje to nuclear neurons of 11:1 in the mouse and convergence of ∼50:1.

DO CONVERGENT PURKINJE CELLS SYNCHRONIZE?

For inhibitory synchrony to influence firing by nuclear neurons, synchronously firing Purkinje cells must converge on a common target neuron. Numerous studies have established that the olivocerebellar loops are highly topographically organized,

suggesting that neighboring Purkinje neurons target neighboring nuclear neurons (**Figures 4A,B**; Groenewegen and Voogd, 1977; Andersson and Oscarsson, 1978; Buisseret-Delmas and Angaut, 1993; Sugihara et al., 2009). Since synchrony of simple spikes appears restricted to neighboring Purkinje neurons, it seems likely that target nuclear neurons indeed receive synchronous inhibitory input. Unfortunately, it remains technically unfeasible to record simultaneously from a population of Purkinje neurons with known convergence and their target neurons. Advances in transneuronal labeling and imaging will be necessary before such experiments become possible. Nevertheless, restricted tract tracing of neighboring Purkinje neurons reveal intermingled terminal arbors in the nuclei (De Zeeuw et al., 1994; Sugihara et al., 2009). Furthermore, tantalizing data from transsynaptic viral tracing from muscle labels small patches of 3–10 directly adjacent Purkinje neurons (**Figure 4C**; Morcuende et al., 2002; Ruigrok et al., 2008; Sun, 2012). It seems likely that these patches not only form functional units related to a given muscle, but also may indeed converge on a common target neuron.

CORTICONUCLEAR SIGNALING: WHAT PURKINJE NEURONS CAN TELL NUCLEAR NEURONS

On the assumption that synchronously firing Purkinje cells indeed converge on target neurons, the question becomes how nuclear cells transduce this synchrony. While the idea of rebound bursts in response to the concerted offset of prolonged inhibition has been discussed for decades (Jahnsen, 1986b; Llinás and Mühlethaler, 1988), the idea that the relief of synchronous inhibition permits simple spiking by nuclear cells was initially proposed by Gauck and Jaeger (2000). Using dynamic clamp to simulate excitatory and inhibitory inputs to nuclear cells in rat cerebellar slices, they demonstrated that nuclear cell simple spike probability increased whenever simulated Purkinje cell inhibition was reduced. As the synchrony of Purkinje input increased, so did the reliability that a spike would occur after coincident IPSPs, raising the overall nuclear cell spike rate (**Figure 1B** *bottom*; see also Hoebeek et al., 2010, below). Later modeling studies further predicted that if the simulated convergence ratio of Purkinje cells onto nuclear cells were decreased, a modification comparable to an increase in synchrony, nuclear cells would tend to spike more in the synchronous gaps in inhibition (Luthman et al., 2011). The insight that the degree of inhibitory synchrony is a key determinant of cerebellar output may be central to resolving the paradoxes in Purkinje-to-nuclear cell signaling described above.

The quantitative components of the model by Gauck and Jaeger, however, were limited by the experimental data available at the time. The first recordings of Purkinje mediated IPSCs were obtained from young rats at room temperature (Anchisi et al., 2001), which estimated the decay time constant of IPSCs to be near 14 ms, and convergence was set at 860 based on the work of Palkovits et al. (1977). As a consequence, nuclear cells were shunted by ongoing inhibition. Related results came from cerebellar slices from ∼2 week old mice, in which IPSPs evoked by stimulating multiple Purkinje afferents at 50–100 Hz at 31°C led to standing or tonic inhibitory current that tended to shunt nuclear cell spiking. In contrast, IPSPs evoked at 10 Hz delayed the spikes of cerebellar nuclear cells spontaneously firing between 15 and 25 Hz, such that nuclear cells spikes entrained

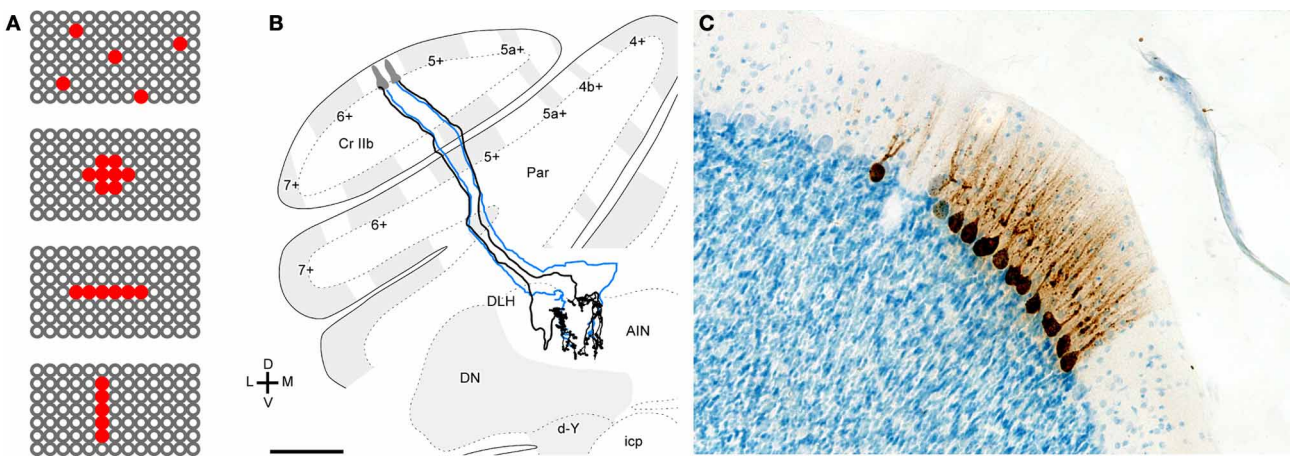

FIGURE 4 | Evidence for related functional roles of neighboring Purkinje cells. (A) Schematic illustrating a surface view of the cerebellar cortex with red indicating possible patterns of convergent Purkinje cells. Converging Purkinje cells can be (top to bottom) widespread, clustered, on-beam, or ordered parasagittally. **(B)** Projections of two rat Purkinje cells that were separated transversely but located in the same aldolase C compartment. Two small injections were made in medial and lateral 5- in the apex of crus IIa. Purkinje cell axons that originated from each of the injections were reconstructed. Blue axons indicate those that were partially reconstructed, except for the fine branches in the terminal arbor. The medial Purkinje cells projected to the lateral anterior interpositus nucleus (AIN) while the lateral Purkinje cells projected to the junction between the dorsolateral hump (DLH) of the anterior interpositus and lateral anterior interpositus nucleus. Scale bar = 500 μm. Panel **(B)** reprinted from Sugihara et al. (2009), with permission. **(C)** Labeling of Purkinje after injection of rabies virus into various limb muscles of the rat. Microphotographs showing labeling of a cluster of Purkinje cells in the lateral vermis. Purkinje cells within such a cluster display a uniform level of infection. Scale bar: 100 μm. Panel **(C)** reprinted from Ruigrok et al. (2008), with permission.

to the 10-Hz input (Telgkamp and Raman, 2002). While this observation provided an interesting example of how gaps in Purkinje mediated inhibition could permit nuclear cell spikes to escape, the observation was hard to relate to anything physiological, since such low frequency firing does not usually typify Purkinje cells.

Our recent work (Person and Raman, 2012), however, illustrates two additional features of cerebellar nuclear cells that are likely to exert a significant influence on the response to simple spike synchrony under physiological conditions. First, in cerebellar slices of weanling mice, recorded at near-physiological temperatures (36–37°C), the intrinsic firing rates of cerebellar nuclear cells are near 90 spikes/s, a value that is considerably higher than the 20 spikes/s recorded in younger (~2 weeks old) animals that have been the focus of most earlier studies (Aizenman and Linden, 1999; Czubayko et al., 2001; Telgkamp and Raman, 2002). Second, the IPSC kinetics decay with a time constant of about 2.5 ms, a time course that is much briefer than at the cooler temperatures at which the majority of previous recordings have been made (Anchisi et al., 2001; Telgkamp and Raman, 2002; Pedroarena and Schwarz, 2003; see also Uusisaari and Knöpfel, 2008). As a consequence of their very brief IPSCs and fast intrinsic firing, nuclear cells generate short-latency, well-timed action potentials immediately after synchronous IPSPs and can entrain to synchronous inhibition at much higher frequencies. Even when only a subset of afferents synchronizes—as few as 2 out of 40—the spike probability increases immediately after the synchronized IPSPs. As a result, when Purkinje cells are made to fire synchronously at a regular frequency, the interspike interval histograms of nuclear cell spikes show peaks at multiples of the interval between synchronous IPSPs (the interstimulus interval). Thus, elements of the spike timing of synchronously firing Purkinje cells can be encoded in nuclear cell output. This phenomenon is evident *in vitro*, with dynamically clamped IPSC inputs, as well as *in vivo* in ketamine-xylazine anesthetized mice, with electrical stimulation of the molecular layer applied to synchronize Purkinje cell firing (**Figure 5**; Person and Raman, 2012). If such a phenomenon persists in alert animals,

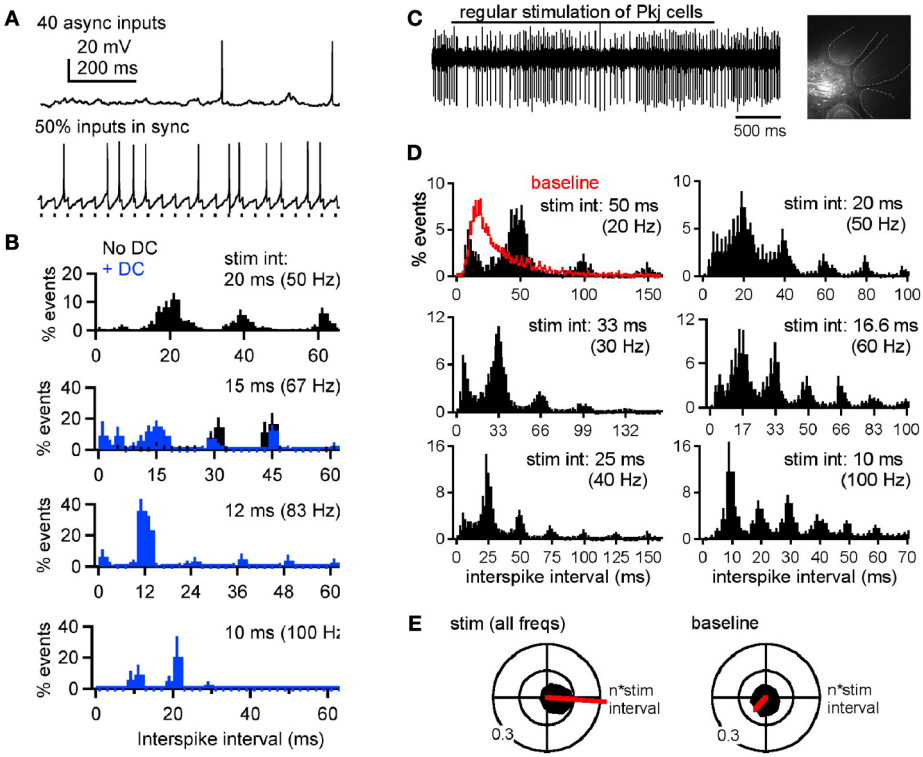

FIGURE 5 | Synchronous Purkinje inputs set spike timing of nuclear neurons, *in vitro* and *in vivo*. (A) Responses of a whole-cell current-clamped cerebellar nuclear neuron in a mouse cerebellar slice to dynamically clamped (dyn) IPSPs mimicking 40 asynchronous (top) or 20 asynchronous and 20 synchronous Purkinje inputs (bottom). **(B)** Normalized *interspike* interval distributions during partially synchronized (50%, i.e., 20 out of 40) dynIPSPs, where the rates of the synchronous input ranged from 50 to 100 Hz. Abscissa tick marks indicate multiples of the *interstimulus* intervals of the synchronous subpopulation. Bin width, 2 ms. Black: no current injection. Blue: with 200 pA steady current (DC) applied to increase spike probability during inhibition. **(C)** Responses of an extracellularly recorded cerebellar nuclear neuron in a ketamine-xylazine anesthetized mouse. Upper trace, response of a nuclear neuron to 40-Hz molecular layer stimulation (bar). Inset, recording site in the cerebellar nuclei recovered after focal Alexa 568 injection. Dashed lines demarcate cerebellar folia. Scale bar, 200 μm. **(D)** Mean normalized interspike interval distributions during molecular layer stimulation from 20 to 100 Hz. Abscissa tick marks indicate multiples of the interstimulus intervals. Red baseline histogram includes intervals before and after stimulation. Bin width, 2 ms. **(E)** Black: polar histograms of interspike intervals during stimulation across rates (left) or during baseline periods. Red: net vectors of polar histograms. Reprinted from Person and Raman (2012), with permission.

then synchronized inhibitory input may dictate the output of cerebellar nuclear cells. Indeed, in awake mice, single stimuli applied to the paravermal lobes, which likely evoke synchronous action potentials in multiple Purkinje cells, elicit "timed spiking" in their nuclear cell targets, i.e., an increased probability of action potential firing at a fixed short latency (∼10 ms) after the stimulus (Hoebeek et al., 2010). Assuming that this observation can be extended to a train of simple spikes, the spike timing of coincidently firing Purkinje cells may be relayed to downstream targets. As synchrony shifts from one group of Purkinje cells to another, different subsets of Purkinje cells may control cerebellar output at different times.

For nuclear cells to encode timing even of high-frequency Purkinje inputs, the kinetics of IPSCs must be highly constrained. In slice recordings made at subphysiological temperatures, IPSCs decay in 5–15 ms, and trains of IPSPs applied at frequencies at or above 50 Hz fully suppress nuclear cell firing (e.g., Aizenman and Linden, 1999; Telgkamp and Raman, 2002; Pedroarena and Schwarz, 2003). In contrast, at 36–37°C, similar stimuli do not silence nuclear neurons, instead permitting spikes to escape occasionally between IPSPs. That this persistence of firing depends on IPSC kinetics is evident from dynamic clamp studies prolonging the decay time to that measured at room temperature and 31°C (Person and Raman, 2012). Comparably fast kinetics have been reported only rarely (Bartos et al., 2001). Thus, the rapid gating of nuclear cell IPSCs emerges as a key specialization required for nuclear cells to follow high-frequency, synchronous Purkinje inputs.

It is worth emphasizing, however, that despite this control of spike timing, the net effect of Purkinje activity is not excitatory. In slices with dynamically clamped inhibitory inputs and fast synaptic excitation blocked pharmacologically, spike rate always dropped relative to the spontaneous spike rate. Importantly, however, firing rates of nuclear cells varied not only according to the spike rate of the synchronous inhibitory inputs, but also according to the number of afferents that synchronized. A greater percent synchrony favored higher firing rates, consistent with paired recordings demonstrating that the output rate of nuclear cells could not be predicted from the input rate of one afferent Purkinje cell (McDevitt et al., 1987). Likewise *in vivo*, with excitation unblocked but probably reduced owing to ketamine-xylazine anesthesia, the net firing rate of nuclear cells generally decreased with molecular layer stimulation (Person and Raman, 2012), consistent with studies showing reduced nuclear cell firing in response to sensory stimuli expected to raise the activity of Purkinje cells (Rowland and Jaeger, 2005). In fact, the proposed cellular mechanism (see below) predicts that ongoing inhibition cannot accelerate firing, but simply permits intrinsically driven action potentials to escape during transient gaps in inhibition induced by synchrony. Since these action potentials do not necessarily occur after every synchronous IPSP, the output rate of nuclear cells is likely to be lower than the input rate of coincidently firing Purkinje cells. Nevertheless, the spikes that do occur will be time-locked to the synchronous input.

It is also appropriate to stress that the idea that Purkinje simple spike synchrony is a key factor in determining nuclear cell output, does not make predictions about whether sensorimotor information transmitted out of the cerebellum is encoded either in spike rates or in spike times of nuclear cells. Instead, synchronization of Purkinje cell spiking will necessarily affect both the rate and timing of nuclear cell action potentials. Specifically, if nuclear cell action potentials follow synchronized IPSPs with highly consistent latencies, the relative timing of Purkinje spikes will be faithfully preserved. If these spikes occur with fixed probability, rate information will be encoded as well. If jitter arises, however, spike timing information from afferent Purkinje cells may be degraded, but the firing rate may be still be relayed. Indeed, a preliminary report suggests that nuclear cells integrate Purkinje firing rates over a 12.5 ms window (Cao et al., 2012); the brevity of this window (2 spikes for a Purkinje cell firing at 80 Hz) is consistent with a mild jitter on a putative response to synchronized IPSPs.

MECHANISMS OF POST-INHIBITORY ACTION POTENTIAL FIRING

What is the ionic basis of cerebellar nuclear cell action potentials that follow synchronized IPSPs? As mentioned above, nuclear neurons are known for their expression of low-voltage-activated or T-type Ca channels (Llinás and Mühlethaler, 1988; Muri and Knöpfel, 1994; Aizenman et al., 1998; Czubayko et al., 2001; Gauck et al., 2001; Molineux et al., 2006). Because these channels activate at relatively hyperpolarized voltages, inactivate within tens of milliseconds, and recover at strongly hyperpolarized potentials (Zheng and Raman, 2009), they are well suited to produce high-frequency bursts of action potentials after periods of strong hyperpolarization. It remains a question, however, what types of physiological stimuli maximally recruit and activate these currents. Purkinje-mediated inhibition alone is not an ideal candidate, as IPSPs cannot hyperpolarize neurons beyond E_{Cl}—near −75 mV in nuclear cells—a voltage at which recovery of T-type current is minimal (Jahnsen, 1986b; Zheng and Raman, 2009). Indeed, cerebellar slices from guinea pig, post-IPSP bursts are not evident (Jahnsen, 1986b), and in cerebellar slices from mouse, little T-type current is evoked in either the somatic or dendritic compartments even after 300-ms high-frequency trains of IPSPs that silence postsynaptic firing (Zheng and Raman, 2009). Furthermore, in anesthetized rats, high-frequency stimulation of Purkinje neurons only rarely elicited rebound-like bursts of action potentials in nuclear neurons (Alviña et al., 2008). Studies in rat cerebellar slices nevertheless suggest that the small fraction of T-type current that recovers during 300-ms IPSP trains is sufficient to increase burst probability (Engbers et al., 2011); such periods of spike suppression can also lead to prolonged post-inhibitory firing through additional ionic mechanisms (Sangrey and Jaeger, 2010; see also Zheng and Raman, 2011). It is unlikely, however, that T-type currents are engaged by single synchronous IPSPs, which hyperpolarize cells no further than about −70 mV for durations only on the order of ten milliseconds (Jahnsen, 1986b; Person and Raman, 2012). Instead, action potentials that occur after synchronous IPSPs are likely to be driven by nuclear cells' intrinsic propensity to fire regular trains of simple spikes. When bathed in tetrodotoxin to block voltage-gated Na channels and prevent firing, cerebellar nuclear cells rest at unusually depolarized potentials, near −40 mV, owing to an apparently

low density of leak K conductances relative to a leak-like tonic cation conductance (Raman et al., 2000), probably carried by NALCN1 (Lu et al., 2007). As a consequence, after a perturbation such as a brief hyperpolarization by an IPSP, cells seek a "resting" potential that is above threshold, and, barring further inhibitory input, inevitably produce a spike. This scenario, of Purkinje-activated $GABA_A$ receptors generating the primary currents that hold nuclear cells below threshold, presents another apparently ideal specialization for action potentials serving to signal the transient relief of inhibition.

SYNCHRONY THROUGHOUT MOTOR PATHWAYS

The proposal that synchronous Purkinje activity produces precise spike timing in the cerebellar nuclei raises the question of whether cerebellar inputs or targets also display coherent firing associated with movement. In fact, temporally precise spiking associated with synchronous neuronal firing appears to be a common theme in motor structures. For example, in the primary motor cortex (M1) of behaving monkeys, spike synchronization is observed during voluntary movement, even without significant changes in firing rates, giving rise to the notion that dynamically organized cell assemblies are involved in generating movement (Riehle et al., 1997; Baker et al., 2001). Further supporting this idea, M1 neurons in macaques have been shown to increase their synchrony upon initiation of movement, and analysis of the M1 spike trains reveals that synchronous activity encodes more information about a movement than the mean firing rate alone (Hatsopoulos et al., 1998). Additionally, synchrony increases with training in monkeys, leading to the proposal that synapses that are active during a successful task are reinforced, thereby recruiting increasing numbers of cortical neurons into a synchronous population (Schieber, 2002; Kilavik et al., 2009). Correlations between MEG and EMG signals in people performing motor tasks have been interpreted to indicate that synchronously active neurons in M1 may preferentially recruit motor neurons and muscle fibers in humans, as well (Schoffelen et al., 2005). Even in some sensory systems, although synchronous events can be sparse, sampling over populations of cortical neurons reveals a "synchrony code" that can encode information about somatosensory stimuli (Jadhav et al., 2009), although the significance of such coding strategies remains debated (Shadlen and Movshon, 1999).

A recurring theme in motor systems, however, is that precisely timed spiking occurs in phase with broader oscillatory neural activity. For instance, a recent report showed that M1 neurons that fire coherently with local field potential (LFP) beta frequency (10–15 Hz) oscillations selectively predict motor performance in a coordinated arm and eye movement task in monkeys, leading to the suggestion that LFP oscillations help coordinate activity in distant, distinct cortical areas that control arm reaching and saccadic eye movements (Dean et al., 2012). The source of cortical oscillations is not known, but one possibility is that the cerebellum may help produce or support them. Indeed, beta frequency oscillations are observed in the cerebellum (Courtemanche et al., 2002; D'Angelo et al., 2009), are coherent between the cerebellum and the cortex during sustained movements in monkeys (Soteropoulos and Baker, 2006), and may be causally related (Holdefer et al., 2000). In addition, it has been proposed that synchronous Purkinje activity is organized by ultrafast oscillations (~200 Hz) in the cerebellar cortex (de Solages et al., 2008). Interestingly, simultaneously recorded cerebellar nuclear neurons occasionally fire synchronously themselves, though this behavior has been seen only rarely (Soteropoulos and Baker, 2006). Moreover, both Purkinje neuron and nuclear neuron firing is phase-locked to beta band LFPs in the motor cortex during steady muscle contraction (Holdefer et al., 2000; Courtemanche et al., 2002; Courtemanche and Lamarre, 2005). It is possible that synchronous spiking by nuclear neurons is evoked by synchronized Purkinje neurons, and oscillatory activity is then relayed to M1 and to muscle groups. Consistent with the latter idea, nuclear neurons show some beta frequency oscillations that are coherent with EMG oscillations in shoulder and wrist muscles, and single pulse microstimulation in the cerebellar nuclei evokes several cycles of periodic muscle activity (Aumann and Fetz, 2004). The relationship between activity in the cerebellum and cerebral cortex is not necessarily unidirectional, however, and may include cortical oscillations driving cerebellar waves (Rowland and Jaeger, 2008; Roš et al., 2009; Rowland et al., 2010).

FACTORS AFFECTING THE LIKELIHOOD OF SYNCHRONY CODING AT CORTICONUCLEAR SYNAPSES

Two major aspects of the hypothesis that the degree of Purkinje cell synchrony affects nuclear cell output, which we refer to as "synchrony coding," are well supported by evidence: first, Purkinje cells indeed synchronize their simple spikes during behaviors, and second, the biophysical specializations of nuclear cells are well suited to permit entrainment to synchronized IPSPs. Nevertheless, to what extent, if at all, and under what conditions, if any, a time-locked response to synchronous IPSPs is a significant mechanism for encoding cerebellar output has yet to be demonstrated. At the level of the cerebellar cortex, specific remaining questions are how many Purkinje cells actually synchronize in response to specific stimuli, and how many of these cells converge onto common targets. At the level of the nuclei, major questions are whether the naturally occurring fractional synchrony is sufficient to engage time-locking, and how concomitant excitation or neuromodulatory input shapes the response to synchronized inhibition.

None of these questions need have unique answers. The likelihood of simple spike synchrony, for example, may depend on the mode of firing by Purkinje cells. Analyzing data from awake and anesthetized rodents, De Schutter and Steuber (2009) noted bouts of Purkinje cells firing with Poisson statistics and bouts of more regular firing. The periods of regular firing exhibited precise synchrony of inter-spike pauses and, by extension, action potentials, whereas periods of Poisson-like firing did not, leading the authors to propose that Purkinje cells have the capacity to alternate between a rate and a temporal code. Modeling studies suggest that drugs that increase the regularity of firing, which is therapeutic for some forms of ataxia (Walter et al., 2006; Alviña and Khodakhah, 2010), raise the probability of Purkinje cell synchrony (Glasauer et al., 2011). Glasauer et al. further predict, however, that high synchrony facilitates an entrainment of nuclear cell spikes to Purkinje cell spikes that may actually be maladaptive for computations requiring more linear integration,

such as gaze holding in the oculomotor system (c.f. Lisberger and Fuchs, 1978). Thus, it may be necessary to control synchrony either regionally or according to task.

Regarding regional variation, synchrony of Purkinje cell simple spikes indeed appears to differ across cerebellar cortical areas. In crus I and II, synchrony is more difficult to detect (Heck et al., 2007; Bosman et al., 2010; but see Shin and De Schutter, 2006), whereas it is particularly widespread in the paramedian lobule (Heck et al., 2007; Bosman et al., 2010; Wise et al., 2010). Such differences may be significant, given that patterns of convergence of neighboring Purkinje cells may vary by zone (Sugihara et al., 2009). In addition, synaptic excitation of cerebellar nuclear cells may modulate corticonuclear synchrony coding. Mossy fiber input is expected to precede Purkinje input by two synaptic delays, and, with continuous activation, trains of EPSPs and IPSPs may overlap. Excitation may either facilitate or disrupt the ability of nuclear cells to generate well-timed spikes following synchronous IPSCs. If glutamatergic EPSCs are smoothed, e.g., by prolonged NMDA receptor currents (Gauck and Jaeger, 2003; Pugh and Raman, 2006) or mGluR currents (Zhang and Linden, 2006; Zheng and Raman, 2011), the probability of generating precisely timed post-inhibitory spikes is likely to be increased (Person and Raman, 2012). Noisy or brief excitatory inputs, as predicted for AMPAR-mediated EPSCs, however, may reduce the temporal precision of any code depending on post-inhibitory action potentials.

Regarding alternative mechanisms to synchrony coding, recordings from rat cerebellar slices have presented arguments for linear processing in the cerebellar cortex, by illustrating the linearity of input-output relations of several cerebellar synapses, including parallel fiber synapses and inhibitory synapses onto Purkinje cells (Walter and Khodakhah, 2006). These observations, along with modeling studies of corticonuclear synapses, have led to the suggestion that a linear rate code would provide a particularly information-rich coding strategy (Walter and Khodakhah, 2009). Other computational models, however, predict synchrony coding at corticonuclear synapses as an obligate outcome of Purkinje cell intrinsic properties and convergence, with asynchronous IPSCs effectively suppressing spiking and synchronous input permitting or entraining nuclear firing (Kistler and De Zeeuw, 2003; Glasauer et al., 2011). Related studies include experimental data indicating that Golgi cells in the cerebellar cortex can fire in synchrony; when they do so, they are predicted to exert a relatively weak inhibition on their granule cell targets, while desynchronization of Golgi cell firing by mossy fiber excitation is expected to increase the efficacy of inhibition (Vervaeke et al., 2010). Both electrical and chemical synapses may contribute to this synchrony in Golgi cells (Hull and Regehr, 2012) and this interplay has been illustrated by modeling (c.f. Kopell and Ermentrout, 2004). Abstract models also demonstrate that inhibitory efficacy varies with synchrony (Akam and Kullmann, 2010). Furthermore, the influence of $GABA_A$ receptor kinetics on synchrony has been shown at other synapses. In the hippocampus, the kinetics of $GABA_A$ receptor mediated currents determine in part the rate at which the network can oscillate, such that rapid decay time constants support high frequency oscillations (Wang and Buzsáki, 1996; Bartos et al., 2002). Similarly, experimental and modeling studies reveal well-timed post-inhibitory spikes after brief IPSGs in the medial superior olive (Dodla et al., 2006).

A parallel example of spike timing shaped by inhibition is evident in the basal ganglia output to the thalamus, an anatomical and physiological sister circuit of the corticonuclear pathway. Spontaneously active, GABAergic internal pallidal neurons, like Purkinje neurons, often show overall increases in firing rate during target thalamic neuron activation (Anderson and Horak, 1985; DeLong et al., 1985; Anderson and Turner, 1991; Inase et al., 1996; Turner and Anderson, 1997; but see also Hikosaka and Wurtz, 1983; Deniau and Chevalier, 1985; Kravitz et al., 2010), leading to the hypothesis that concurrently active pallidal neurons mediate lateral inhibition onto thalamic neurons (Nambu et al., 2002). The paradoxical relationship in firing rates persists, however, in simultaneous recordings of synaptically connected pairs of pallidal and thalamic neurons during sensory relay or movement, which verify that coupled pallidal and thalamic neuron increase their overall firing rates in parallel but can show inverse relationships in instantaneous firing rates (Person and Perkel, 2007; Goldberg and Fee, 2012a,b). Interestingly, thalamic neuron activation is due to concurrent excitatory drive to the thalamus, which overcomes inhibition from the basal ganglia (Goldberg and Fee, 2012a,b). As a result, the effective role of the GABAergic output neurons of the basal ganglia becomes to control the spike timing of thalamic relay neurons.

Resolving whether and when synchrony coding is useful or necessary to cerebellar function will depend in part on understanding what nuclear cells communicate to down-stream targets. In the red nucleus, individual interpositus axons ramify parasagittally (Shinoda et al., 1988), with about 50 axons converging onto each target neuron. Electrophysiological studies of this pathway show that cerebellar nuclear-to-red nucleus axons produce EPSPs with little short-term plasticity (Toyama et al., 1970). These properties may, in principle, allow nuclear input to the red nucleus to drive spiking that follows the firing pattern of the synchronized Purkinje subpopulation. Similarly, large EPSPs have been measured in the cerebellar recipient areas of ventrolateral thalamus (Sawyer et al., 1994). Thus, well-timed post-inhibitory spikes in cerebellar nuclear neurons may be a mechanism whereby both the rate and timing of signals from varying groups of synchronized Purkinje cells are preferentially transmitted to premotor areas and other cerebellar targets. Given the wide variety of structures receiving cerebellar nuclear cell input—the red nucleus, thalamic nuclei, inferior olive, and cerebellar cortex, among others—the relevant aspects of cerebellar output signals may not be homogeneous. Instead, the idea that temporal and rate coding coexist in the cerebellum, either alternating or simultaneously, may be central to resolving the ways in which nuclear cells transduce and transform inputs from Purkinje cells.

ACKNOWLEDGMENTS

We thank Drs. S. A. Edgley, D. H. Heck, T. J. H. Ruigrok, and I. Sugihara for permission to reprint data from their articles and for kindly providing figure copies. Supported by NIH R01 NS39395 (Indira M. Raman).

REFERENCES

Aizenman, C. D., and Linden, D. J. (1999). Regulation of the rebound depolarization and spontaneous firing patterns of deep nuclear neurons in slices of rat cerebellum. *J. Neurophysiol.* 82, 1697–1709.

Aizenman, C. D., Manis, P. B., and Linden, D. J. (1998). Polarity of long-term synaptic gain change is related to postsynaptic spike firing at a cerebellar inhibitory synapse. *Neuron* 21, 827–835.

Akam, T., and Kullmann, D. M. (2010). Oscillations and filtering networks support flexible routing of information. *Neuron* 67, 308–320.

Albus, J. S. (1971). Theory of cerebellar function. *Math. Biosci.* 10, 25–61.

Alviña, K., and Khodakhah, K. (2010). The therapeutic mode of action of 4-aminopyridine in cerebellar ataxia. *J. Neurosci.* 30, 7258–7268.

Alviña, K., Walter, J. T., Kohn, A., Ellis-Davies, G., and Khodakhah, K. (2008). Questioning the role of rebound firing in the cerebellum. *Nat. Neurosci.* 11, 1256–1258.

Anchisi, D., Scelfo, B., and Tempia, F. (2001). Postsynaptic currents in deep cerebellar nuclei. *J. Neurophysiol.* 85, 323–331.

Andersson, G., and Oscarsson, O. (1978). Climbing fiber microzones in cerebellar vermis and their projection to different groups of cells in the lateral vestibular nucleus. *Exp. Brain Res.* 32, 565–579.

Anderson, M. E., and Horak, F. B. (1985). Influence of the globus pallidus on arm movements in monkeys. III. Timing of movement-related information. *J. Neurophysiol.* 54, 433–448.

Anderson, M. E., and Turner, R. S. (1991). Activity of neurons in cerebellar-receiving and pallidal receiving areas of the thalamus of the behaving monkey. *J. Neurophysiol.* 66, 879–893.

Armstrong, D. M., Cogdell, B., and Harvey, R. (1975). Effects of afferent volleys from the limbs on the discharge patterns of interpositus neurons in cats anaesthetized with alpha-chloralose. *J. Physiol.* 248, 489–517.

Armstrong, D. M., and Edgley, S. A. (1984a). Discharges of nucleus interpositus neurones during locomotion in the cat. *J. Physiol.* 351, 411–432.

Armstrong, D. M., and Edgley, S. A. (1984b). Discharges of Purkinje cells in the paravermal part of the cerebellar anterior lobe during locomotion in the cat. *J. Physiol.* 352, 403–424.

Aumann, T. D., and Fetz, E. E. (2004). Oscillatory activity in forelimb muscles of behaving monkeys evoked by microstimulation in the cerebellar nuclei. *Neurosci. Lett.* 361, 106–110.

Baker, S. N., Spinks, R., Jackson, A., and Lemon, R. N. (2001). Synchronization in monkey motor cortex during a precision grip task. I. Task-dependent modulation in single-unit synchrony. *J. Neurophysiol.* 85, 869–885.

Bartos, M., Vida, I., Frotscher, M., Geiger, J. R., and Jonas, P. (2001). Rapid signaling at inhibitory synapses in a dentate gyrus interneuron network. *J. Neurosci.* 21, 2687–2698.

Bartos, M., Vida, I., Frotscher, M., Meyer, A., Monyer, H., Geiger, J. R., et al. (2002). Fast synaptic inhibition promotes synchronized gamma oscillations in hippocampal interneuron networks. *Proc. Natl. Acad. Sci. U.S.A.* 99, 13222–13227.

Bell, C. C., and Grimm, R. J. (1969). Discharge properties of Purkinje cells recorded on single and double microelectrodes. *J. Neurophysiol.* 32, 1044–1055.

Bell, C. C., and Kawasaki, T. (1972). Relations among climbing fiber responses of nearby Purkinje Cells. *J. Neurophysiol.* 35, 155–169.

Bengtsson, F., Ekerot, C. F., and Jörntell, H. (2011). *In vivo* analysis of inhibitory synaptic inputs and rebounds in deep cerebellar nuclear neurons. *PLoS ONE* 6:e18822. doi: 10.1371/journal.pone.0018822

Bishop, G. A., McCrea, R. A., Lighthall, J. W., and Kitai, S. T. (1979). An HRP and autoradiographic study of the projection from the cerebellar cortex to the nucleus interpositus anterior and nucleus interpositus posterior of the cat. *J. Comp. Neurol.* 185, 735–756.

Blenkinsop, T. A., and Lang, E. J. (2006). Block of inferior olive gap junctional coupling decreases Purkinje cell complex spike synchrony and rhythmicity. *J. Neurosci.* 26, 1739–1748.

Blenkinsop, T. A., and Lang, E. J. (2011). Synaptic action of the olivocerebellar system on cerebellar nuclear spike activity. *J. Neurosci.* 31, 14707–14720.

Bosman, L. W., Koekkoek, S. K., Shapiro, J., Rijken, B. F., Zandstra, F., van der Ende, B., et al. (2010). Encoding of whisker input by cerebellar Purkinje cells. *J. Physiol.* 588, 3757–3783.

Bower, J. M. (2002). The organization of cerebellar cortical circuitry revisited: implications for function. *Ann. N.Y. Acad. Sci.* 978, 135–155.

Bower, J. M., and Woolston, D. C. (1983). Congruence of spatial organization of tactile projections to granule cell and Purkinje cell layers of cerebellar hemispheres of the albino rat: vertical organization of cerebellar cortex. *J. Neurophysiol.* 49, 745–766.

Braitenberg, V. (1967). Is the cerebellar cortex a biological clock in the millisecond rage? *Prog. Brain Res.* 25, 334–346.

Brunel, N., Hakim, V., Isope, P., Nadal, J. P., and Barbour, B. (2004). Optimal information storage and the distribution of synaptic weights: perceptron versus Purkinje cell. *Neuron* 43, 745–757.

Buisseret-Delmas, C., and Angaut, P. (1993). The cerebellar olivocorticonuclear connections in the rat. *Prog. Neurobiol.* 40, 63–87.

Caddy, K. W., and Biscoe, T. J. (1979). Structural and quantitative studies on the normal C3H and Lurcher mutant mouse. *Philos. Trans. R. Soc. Lond. B Biol. Sci.* 287, 167–201.

Calderon, D. P., Fremont, R., Kraenzlin, F., and Khodakhah, K. (2011). The neural substrates of rapid-onset Dystonia-Parkinsonism. *Nat. Neurosci.* 143, 357–365.

Cao, Y., Maran, S., Jaeger, D., and Heck, D. (2012). "Representation of behaviors in the cerebellum: spike rate modulation vs. spike timing," in *Program No. 477.07. Neuroscience Meeting Planner* (New Orleans, LA: Society for Neuroscience). [Online].

Catz, N., Dicke, P. W., and Thier, P. (2008). Cerebellar-dependent motor learning is based on pruning a Purkinje cell population response. *Proc. Natl. Acad. Sci. U.S.A.* 105, 7309–7314.

Chan-Palay, V. (1977). *Cerebellar Dentate Nucleus. Organization, Cytology, and Transmitters.* New York, NY: Springer.

Cody, F. W., Moore, R. B., and Richardson, H. C. (1981). Patterns of activity evoked in cerebellar interpositus nuclear neurons by natural somatosensory stimuli in awake cats. *J. Physiol.* 317, 1–20.

Cohen, D., and Yarom, Y. (1998). Patches of synchronized activity in the cerebellar cortex evoked by mossy-fiber stimulation: questioning the role of parallel fibers. *Proc. Natl. Acad. Sci. U.S.A.* 95, 15032–15036.

Courtemanche, R., and Lamarre, Y. (2005). Local field potential oscillations in primate cerebellar cortex: synchronization with cerebral cortex during active and passive expectancy. *J. Neurophysiol.* 93, 2039–2052.

Courtemanche, R., Pellerin, J. P., and Lamarre, Y. (2002). Local field potential oscillations in primate cerebellar cortex: modulation during active and passive expectancy. *J. Neurophysiol.* 88, 771–782.

Czubayko, U., Sultan, F., Thier, P., and Schwarz, C. (2001). Two types of neurons in the rat cerebellar nuclei as distinguished by membrane potentials and intracellular fillings. *J. Neurophysiol.* 85, 2017–2029.

D'Angelo, E., and De Zeeuw, C. I. (2009). Timing and plasticity in the cerebellum: focus on the granular layer. *Trends Neurosci.* 32, 30–40.

D'Angelo, E., Koekkoek, S. K., Lombardo, P., Solinas, S., Ros, E., Garrido, J., et al. (2009). Timing in the cerebellum: oscillations and resonance in the granular layer. *Neuroscience* 162, 805–815.

Dean, H. L., Hagan, M. A., and Pesaran, B. (2012). Only coherent spiking in posterior parietal cortex coordinates looking and reaching. *Neuron* 73, 829–841.

DeLong, M. R., Crutcher, M. D., and Georgopoulos, A. P. (1985). Primate globus pallidus and subthalamic nucleus: functional organization. *J. Neurophysiol.* 53, 530–543.

Deniau, J. M., and Chevalier, G. (1985). Disinhibition as a basic process in the expression of striatal functions. II. The striato-nigral influence on thalamocortical cells of the ventromedial thalamic nucleus. *Brain Res.* 334, 227–233.

De Schutter, E., and Steuber, V. (2009). Patterns and pauses in Purkinje cell simple spike trains: experiments, modeling and theory. *Neuroscience* 162, 816–826.

de Solages, C., Szapiro, G., Brunel, N., Hakim, V., Isope, P., Buisseret, P., et al. (2008). High-frequency organization and synchrony of activity in the Purkinje cell layer of the cerebellum. *Neuron* 58, 775–788.

Devor, A., and Yarom, Y. (2002). Electrotonic coupling in the inferior olivary nucleus revealed by simultaneous double patch recordings. *J. Neurophysiol.* 87, 3048–3058.

De Zeeuw, C. I., Hoebeek, F. E., Bosman, L. W., Schonewille, M., Witter, L., and Koekkoek, S. K. (2011). Spatiotemporal firing patterns in the cerebellum. *Nat. Rev. Neurosci.* 12, 327–344.

De Zeeuw, C. I., Koekkoek, S. K., Wylie, D. R., and Simpson, J. I. (1997). Association between dendritic lamellar bodies and complex spike synchrony in the olivocerebellar system. *J. Neurophysiol.* 77, 1747–1758.

De Zeeuw, C. I., Wylie, D. R., DiGiorgi, P. L., and Simpson, J. I. (1994). Projections of individual Purkinje cells of identified zones in the flocculus to the vestibular and cerebellar nuclei in the rabbit. *J. Comp. Neurol.* 15, 428–447.

Dizon, M. J., and Khodakhah, K. (2011). The role of interneurons in shaping Purkinje cell responses in the cerebellar cortex. *J. Neurosci.* 20, 10463–10473.

Dodla, R., Svirskis, G., and Rinzel, J. (2006). Well-timed, brief inhibition can promote spiking: postinhibitory facilitation. *J. Neurophysiol.* 95, 2664–2677.

Ebner, T. J., and Bloedel, J. R. (1981). Correlation between activity of Purkinje cells and its modification by natural peripheral stimuli. *J. Neurophysiol.* 45, 948–961.

Eccles, J. C., Ito, M., and Szentagothai, J. (1967). *The Cerebellum as a Neuronal Machine.* New York, NY: Springer-Verlag, Inc.

Eccles, J. C., Sabah, N. H., Schmidt, R. F., and Taborikova, H. (1972). Integration by Purkyne cells of mossy and climbing fibre inputs from cutaneous mecahnoreceptors. *Exp. Brain Res.* 15, 498–520.

Engbers, J. D., Anderson, D., Tadayonnejad, R., Mehaffey, W. H., Molineux, M. L., and Turner, R. W. (2011). Distinct roles for I(T) and I(H) in controlling the frequency and timing of rebound spike responses. *J. Physiol.* 589, 5391–5413.

Gauck, V., and Jaeger, D. (2000). The control of rate and timing of spikes in the deep cerebellar nuclei by inhibition. *J. Neurosci.* 20, 3006–3016.

Gauck, V., and Jaeger, D. (2003). The contribution of NMDA and AMPA conductances to the control of spiking in neurons of the deep cerebellar nuclei. *J. Neurosci.* 23, 8109–8118.

Gauck, V., Thomann, M., Jaeger, D., and Borst, A. (2001). Spatial distribution of low- and high-voltage-activated calcium currents in neurons of the deep cerebellar nuclei. *J. Neurosci.* 21, RC158.

Gilbert, P. F., and Thach, W. T. (1977). Purkinje cell activity during motor learning. *Brain Res.* 128, 309–328.

Glasauer, S., Rössert, C., and Strupp, M. (2011). The role of regularity and synchrony of cerebellar Purkinje cells for pathological nystagmus. *Ann. N.Y. Acad. Sci.* 1233, 162–167.

Goldberg, J. H., and Fee, M. S. (2012a). A cortical motor nucleus drives the basal ganglia-recipient thalamus in singing birds. *Nat. Neurosci.* 15, 620–627.

Goldberg, J. H., and Fee, M. S. (2012b). Integration of cortical and pallidal inputs in the basal ganglia-recipient thalamus of singing birds. *J. Neurophysiol.* 108, 1403–1429.

Groenewegen, H. J., and Voogd, J. (1977). The parasagittal zonation within the olivocerebellar projection. I. Climbing fiber distribution in the vermis of the cat cerebellum. *J. Comp. Neurol.* 174, 417–488.

Gundappa-Sulur, G., De Schutter, E., and Bower, J. M. (1999). Ascending granule cell axon: an important component of cerebellar cortical circuitry. *J. Comp. Neurol.* 408, 580–596.

Harvey, R. J., and Napper, R. M. (1991). Quantitative studies on the mammalian cerebellum. *Prog. Neurobiol.* 36, 437–463.

Hatsopoulos, N. G., Ojakangas, C. L., Paninski, L., and Donoghue, J. P. (1998). Information about movement direction obtained from synchronous activity of motor cortical neurons. *Proc. Natl. Acad. Sci. U.S.A.* 95, 15706–15711.

Häusser, M., and Clark, B. A. (1997). Tonic synaptic inhibition modulates neuronal output pattern and spatiotemporal synaptic integration. *Neuron* 19, 665–678.

Heck, D. H., Thach, W. T., and Keating, J. G. (2007). On-beam synchrony in the cerebellum as the mechanism for the timing and coordination of movement. *Proc. Natl. Acad. Sci. U.S.A.* 104, 7658–7663.

Heckroth, J. A. (1994). Quantitative morphological analysis of the cerebellar nuclei in normal and lurcher mutant mice. I. Morphology and cell number. *J. Comp. Neurol.* 343, 173–182.

Hikosaka, O., and Wurtz, R. H. (1983). Visual and oculomotor functions of monkey substantia nigra pars reticulata. IV. Relation of substantia nigra to superior colliculus. *J. Neurophysiol.* 49, 1285–1301.

Hoebeek, F. E., Witter, L., Ruigrok, T. J., and De Zeeuw, C. I. (2010). Differential olivo-cerebellar cortical control of rebound activity in the cerebellar nuclei. *Proc. Natl. Acad. Sci. U.S.A.* 107, 8410–8415.

Holdefer, R. N., Miller, L. E., Chen, L. L., and Houk, J. C. (2000). Functional connectivity between cerebellum and primary motor cortex in the awake monkey. *J. Neurophysiol.* 84, 585–590.

Hull, C., and Regehr, W. G. (2012). Identification of an inhibitory circuit that regulates cerebellar Golgi cell activity. *Neuron* 73, 149–158.

Inase, M., Buford, J. A., and Anderson, M. E. (1996). Changes in control of arm position, movement, and thalamic discharge during local inactivation in the globus pallidus of the monkey. *J. Neurophysiol.* 75, 1087–1104.

Isope, P., and Barbour, B. (2002). Properties of unitary granule cell–>Purkinje cell synapses in adult rat cerebellar slices. *J. Neurosci.* 22, 9668–9678.

Ito, M., and Yoshida, M. (1966). The origin of cerebral-induced inhibition of Deiters neurones. I. Monosynaptic initiation of the inhibitory postsynaptic potentials. *Exp. Brain Res.* 2, 330–349.

Ito, M., Yoshida, M., Obata, K., Kawai, N., and Udo, M. (1970). Inhibitory control of intracerebellar nuclei by the Purkinje cell axons. *Exp. Brain Res.* 10, 64–80.

Jadhav, S. P., Wolfe, J., and Feldman, D. E. (2009). Sparse temporal coding of elementary tactile features during active whisker sensation. *Nat. Neurosci.* 12, 792–800.

Jaeger, D. (2003). No parallel fiber volleys in the cerebellar cortex: evidence from cross-correlation analysis between Purkinje cells in a computer model and in recordings from anesthetized rats. *J. Comput. Neurosci.* 14, 311–327.

Jahnsen, H. (1986a). Electrophysiological characteristics of neurones in the guinea-pig deep cerebellar nuclei *in vitro*. *J. Physiol.* 372, 129–147.

Jahnsen, H. (1986b). Extracellular activation and membrane conductances of neurones in the guinea-pig deep cerebellar nuclei *in vitro*. *J. Physiol.* 372, 149–168.

Kanichay, R. T., and Silver, R. A. (2008). Synaptic and cellular properties of the feedforward inhibitory circuit within the input layer of the cerebellar cortex. *J. Neurosci.* 28, 8955–8967.

Khaliq, Z. M., and Raman, I. M. (2005). Axonal propagation of simple and complex spikes in cerebellar Purkinje neurons. *J. Neurosci.* 25, 454–463.

Kilavik, B. E., Roux, S., Ponce-Alvarez, A., Confais, J., Grün, S., and Riehle, A. (2009). Long-term modifications in motor cortical dynamics induced by intensive practice. *J. Neurosci.* 29, 12653–12663.

Kistler, W. M., and De Zeeuw, C. I. (2003). Time windows and reverberating loops: a reverse-engineering approach to cerebellar function. *Cerebellum* 2, 44–54.

Kopell, N., and Ermentrout, B. (2004). Chemical and electrical synapses perform complementary roles in the synchronization of interneuronal networks. *Proc. Natl. Acad. Sci. U.S.A.* 101, 15482–15487.

Kravitz, A. V., Freeze, B. S., Parker, P. R., Kay, K., Thwin, M. T., Deisseroth, K., et al. (2010). Regulation of Parkinsonian motor behaviours by optogenetic control of basal ganglia circuitry. *Nature* 466, 622–626.

Lampl, I., and Yarom, Y. (1993). Subthreshold oscillations of the membrane potential: a functional synchronizing and timing device. *J. Neurophysiol.* 70, 2181–2186.

Latham, A., and Paul, D. H. (1971). Spontaneous activity of cerebellar Purkinje cells and their responses to impulses in climbing fibres. *J. Physiol.* 213, 135–156.

LeDoux, M. S., Hurst, D. C., and Lorden, J. F. (1998). Single-unit activity of cerebellar nuclear cells in the awake genetically dystonic rat. *Neuroscience* 86, 533–545.

LeDoux, M. S., Lorden, J. F., and Ervin, J. M. (1993). Cerebellectomy eliminates the motor syndrome of the genetically dystonic rat. *Exp. Neurol.* 120, 302–310.

Levin, S. I., Khaliq, Z. M., Aman, T. K., Grieco, T. M., Kearney, J. A., Raman, I. M., et al. (2006). Impaired motor function in mice with cell-specific knockout of sodium channel Scn8a (NaV1.6) in cerebellar purkinje neurons and granule cells. *J. Neurophysiol.* 96, 785–793.

Lisberger, S. G., and Fuchs, A. F. (1978). Role of primate flocculus during rapid behavioral modification of vestibuloocular reflex. I. Purkinje cell activity during visually guided horizontal smooth-pursuit eye movements and passive head rotation. *J. Neurophysiol.* 41, 733–763.

Llinás, R., and Mühlethaler, M. (1988). Electrophysiology of guinea-pig cerebellar nuclear cells in the *in vitro* brain stem-cerebellar preparation. *J. Physiol.* 404, 241–258.

Llinás, R., and Sugimori, M. (1980). Electrophysiological properties of *in vitro* Purkinje cell somata in mammalian cerebellar slices. *J. Physiol.* 305, 171–195.

Llinás, R., and Yarom, Y. (1986). Oscillatory properties of guinea-pig inferior olivary neurones and their pharmacological modulation: an *in vitro* study. *J. Physiol.* 376, 163–182.

Lu, B., Su, Y., Das, S., Liu, J., Xia, J., and Ren, D. (2007). The neuronal channel NALCN contributes resting sodium permeability and is required for normal respiratory rhythm. *Cell* 129, 371–383.

Luthman, J., Hoebeek, F. E., Maex, R., Davey, N., Adams, R., De Zeeuw,

C. I., et al. (2011). STD-dependent and independent encoding of input irregularity as spike rate in a computational model of a cerebellar nucleus neuron. *Cerebellum* 10, 667–682.

MacKay, W. A., and Murphy, J. T. (1976). Integrative versus delay line characteristics of cerebellar cortex. *Can. J. Neurol. Sci.* 3, 85–97.

Marr, D. (1969). A theory of cerebellar cortex. *J. Physiol.* 202, 437–470.

Mauk, M. D., and Buonomano, D. V. (2004). The neural basis of temporal processing. *Ann. Rev. Neurosci.* 27, 307–340.

McDevitt, C. J., Ebner, T. J., and Bloedel, J. R. (1982). The changes in Purkinje cell simple spike activity following spontaneous climbing fiber inputs. *Brain Res.* 237, 484–491.

McDevitt, C. J., Ebner, T. J., and Bloedel, J. R. (1987). Relationships between simultaneously recorded Purkinje cells and nuclear neurons. *Brain Res.* 425, 1–13.

Medina, J. F., Nores, W. L., and Mauk, M. D. (2002). Inhibition of climbing fibers is a signal for the extinction of conditioned eyelid responses. *Nature* 416, 330–333.

Middleton, S. J., Racca, C., Cunningham, M. O., Traub, R. D., Monyer, H., Knöpfel, T., et al. (2008). High-frequency network oscillations in cerebellar cortex. *Neuron* 58, 763–774.

Mittmann, W., Koch, U., and Häusser, M. (2005). Feed-forward inhibition shapes the spike output of cerebellar Purkinje cells. *J. Physiol.* 563(Pt 2), 369–378.

Molineux, M. L., McRory, J. E., McKay, B. E., Hamid, J., Mehaffey, W. H., Rehak, R., et al. (2006). Specific T-type calcium channel isoforms are associated with distinct burst phenotypes in deep cerebellar nuclear neurons. *Proc. Natl. Acad. Sci. U.S.A.* 103, 5555–5560.

Monsivais, P., Clark, B. A., Roth, A., and Häusser, M. (2005). Determinants of action potential propagation in cerebellar Purkinje cell axons. *J. Neurosci.* 25, 464–472.

Morcuende, S., Delgado-Garcia, J. M., and Ugolini, G. (2002). Neuronal premotor networks involved in eyelid responses: retrograde transneuronal tracing with rabies virus from the orbicularis oculi muscle in the rat. *J. Neurosci.* 22, 8808–8818.

Mouginot, D., and Gähwiler, B. H. (1995). Characterization of synaptic connections between cortex and deep nuclei of the rat cerebellum *in vitro*. *Neuroscience* 64, 699–712.

Mukamel, E. A., Nimmerjahn, A., and Schnitzer, M. J. (2009). Automated analysis of cellular signals from large-scale calcium imaging data. *Neuron* 63, 747–760.

Mullen, R. J., Eicher, E. M., and Sidman, R. L. (1976). Purkinje cell degeneration, a new neurological mutation in the mouse. *Proc. Natl. Acad. Sci. U.S.A.* 73, 208–212.

Muri, R., and Knöpfel, T. (1994). Activity induced elevations of intracellular calcium concentration in neurons of the deep cerebellar nuclei. *J. Neurophysiol.* 71, 420–428.

Murphy, J. T., Johnson, F., Kwan, H. C., and Mackay, W. A. (1976). Activation of mossy fiber inputs to cerebellar cortex by natural stimulation. *Brain Res.* 43, 635–639.

Murphy, J. T., and Sabah, N. H. (1971). Cerebellar Purkinje cell responses of afferent inputs. I. Climbing fiber activation. *Brain Res.* 25, 449–467.

Nambu, A., Tokuno, H., and Takada, M. (2002). Functional significance of the cortico-subthalamo-pallidal "hyperdirect" pathway. *Neurosci. Res.* 43, 111–117.

Ozden, I., Sullivan, M. R., Lee, H. M., and Wang, S. S. (2009). Reliable coding emerges from coactivation of climbing fibers in microbands of cerebellar Purkinje neurons. *J. Neurosci.* 29, 10463–10473.

Palkovits, M., Mezey, E., Hamori, J., and Szentagothai, J. (1977). Quantitative histological analysis of the cerebellar nuclei in the cat. I. Numerical data on cells and on synapses. *Exp. Brain Res.* 28, 189–209.

Pedroarena, C. M., and Schwarz, C. (2003). Efficacy and short-term plasticity at GABAergic synapses between Purkinje and cerebellar nuclei neurons. *J. Neurophysiol.* 89, 704–715.

Person, A. L., and Perkel, D. J. (2007). Pallidal neuron activity increases during sensory relay through thalamus in a songbird circuit essential for learning. *J. Neurosci.* 8, 8687–8698.

Person, A. L., and Raman, I. M. (2012). Purkinje neuron synchrony elicits time-locked spiking in the cerebellar nuclei. *Nature* 481, 502–505.

Pugh, J. R., and Raman, I. M. (2006). Potentiation of mossy fiber EPSCs in the cerebellar nuclei by NMDA receptor activation followed by postinhibitory rebound current. *Neuron* 51, 113–123.

Raman, I. M., and Bean, B. P. (1997). Resurgent sodium current and action potential formation in dissociated cerebellar Purkinje neurons. *J. Neurosci.* 17, 4517–4526.

Raman, I. M., Gustafson, A. E., and Padgett, D. E. (2000). Ionic currents and spontaneous firing in neurons isolated from the cerebellar nuclei. *J. Neurosci.* 20, 9004–9016.

Riehle, A., Grün, S., Diesmann, M., and Aertsen, A. (1997). Spike synchronization and rate modulation differentially involved in motor cortical function. *Science* 278, 1950–1953.

Roš, H., Sachdev, R. N., Yu, Y., Sestan, N., and McCormick, D. A. (2009). Neocortical networks entrain neuronal circuits in cerebellar cortex. *J. Neurosci.* 29, 10309–10320.

Rowland, N. C., Goldberg, J. A., and Jaeger, D. (2010). Cortico-cerebellar coherence and causal connectivity during slow-wave activity. *Neuroscience* 166, 698–711.

Rowland, N. C., and Jaeger, D. (2005). Coding of tactile response properties in the rat deep cerebellar nuclei. *J. Neurophysiol.* 94, 1236–1251.

Rowland, N. C., and Jaeger, D. (2008). Responses to tactile stimulation in deep cerebellar nucleus neurons result from recurrent activation in multiple pathways. *J. Neurophysiol.* 99, 704–717.

Ruigrok, T. J. H., Pijpers, A., Goedknegt-Sabel, E., and Coulon, P. (2008). Multiple cerebellar zones are involved in the control of individual muscles: a retrograde transneuronal tracing study with rabies virus in the rat. *Eur. J. Neurosci.* 28, 181–200.

Salinas, E., and Sejnowski, T. J. (2001). Correlated neuronal activity and the flow of neural information. *Nat. Rev. Neurosci.* 2, 539–550.

Sangrey, T., and Jaeger, D. (2010). Analysis of distinct short and prolonged components in rebound spiking of deep cerebellar nucleus neurons. *Eur. J. Neurosci.* 32, 1646–1657.

Sasaki, K., Bower, J. M., and Llinás, R. (1989). Multiple Purkinje cell recording in rodent cerebellar cortex. *Eur. J. Neurosci.* 1, 572–586.

Sawyer, S. F., Young, S. J., Groves, P. M., and Tepper, J. M. (1994). Cerebellar-responsive neurons in the thalamic ventroanterior-ventrolateral complex of rats: *in vivo* electrophysiology. *Neuroscience* 63, 711–724.

Schieber, M. H. (2002). Training and synchrony in the motor system. *J. Neurosci.* 22, 5277–5281.

Schoffelen, J. M., Oostenveld, R., and Fries, P. (2005). Neuronal coherence as a mechanism of effective corticospinal interaction. *Science* 308, 111–113.

Schultz, S. R., Kitamura, K., Post-Uiterweer, A., Krupic, J., and Häusser, M. (2009). Spatial pattern coding of sensory information by climbing fiber-evoked calcium signals in networks of neighboring cerebellar Purkinje neurons. *J. Neurosci.* 29, 8005–8015.

Shadlen, M. N., and Movshon, J. A. (1999). Synchrony unbound: a critical evaluation of the temporal binding hypothesis. *Neuron* 24, 67–77.

Shin, S. L., and De Schutter, E. (2006). Dynamic synchronization of Purkinje cell simple spikes. *J. Neurophysiol.* 96, 3485–3491.

Shinoda, Y., Futami, T., Mitoma, H., and Yokota, J. (1988). Morphology of single neurons in the cerebello-rubrospinal system. *Behav. Brain Res.* 28, 59–64.

Sims, R. E., and Hartell, N. A. (2005). Differences in transmission properties and susceptibility to long-term depression reveal functional specialization of ascending axon and parallel fiber synapses to Purkinje cells. *J. Neurosci.* 25, 3246–3257.

Sims, R. E., and Hartell, N. A. (2006). Differential susceptibility to synaptic plasticity reveals a functional specialization of ascending axon and parallel fiber synapses to cerebellar Purkinje cells. *J. Neurosci.* 26, 5153–5159.

Soteropoulos, D. S., and Baker, S. N. (2006). Cortico-cerebellar coherence during a precision grip task in the monkey. *J. Neurophysiol.* 95, 1194–1206.

Steuber, V., Mittmann, W., Hoebeek, F. E., Silver, R. A., De Zeeuw, C. I., Häusser, M., et al. (2007). Cerebellar LTD and pattern recognition by Purkinje cells. *Neuron* 54, 121–136.

Sugihara, I., Fujita, H., Na, J., Quy, P. N., Li, B. Y., and Ikeda, D. (2009). Projection of reconstructed single Purkinje cell axons in relation to the cortical and nuclear aldolase C compartments of the rat cerebellum. *J. Comp. Neurol.* 512, 282–304.

Sun, L. W. (2012). Transsynaptic tracing of conditioned eyeblink circuits in the mouse cerebellum. *Neuroscience* 203, 122–134.

Telgkamp, P., Padgett, D. E., Ledoux, V. A., Woolley, C. S., and Raman, I. M. (2004). Maintenance of high-frequency transmission at Purkinje to cerebellar nuclear synapses by spillover from boutons with multiple release sites. *Neuron* 41, 113–126.

Telgkamp, P., and Raman, I. M. (2002). Depression of inhibitory synaptic transmission between Purkinje cells and neurons of the cerebellar nuclei. *J. Neurosci.* 22, 8447–8457.

Teune, T. M., van der Burg, J., de Zeeuw, C. I., Voogd, J., and Ruigrok, T.

J. (1998). Single Purkinje cell can innervate multiple classes of projection neurons in the cerebellar nuclei of the rat: a light microscopic and ultrastructural triple-tracer study in the rat. *J. Comp. Neurol.* 392, 164–178.

Thach, W. T. (1968). Discharge of Purkinje and cerebellar nuclear neurons during rapidly alternating arm movements in the monkey. *J. Neurophysiol.* 31, 785–797.

Thach, W. T. (1970a). Discharge of cerebellar neurons related to two maintained postures and two prompt movements. I. Nuclear cell output. *J. Neurophysiol.* 33, 527–536.

Thach, W. T. (1970b). Discharge of cerebellar neurons related to two maintained postures and two prompt movements. II. Purkinje cell output and input. *J. Neurophysiol.* 33, 537–547.

Thier, P., Dicke, P. W., Haas, R., and Barash, S. (2000). Encoding of movement time by populations of cerebellar Purkinje cells. *Nature* 405, 72–76.

Toyama, K., Tsukahara, N., Kosaka, K., and Matsunami, K. (1970). Synaptic excitation of red nucleus neurones by fibres from interpositus nucleus. *Exp. Brain Res.* 11, 187–198.

Turner, R. S., and Anderson, M. E. (1997). Pallidal discharge related to the kinematics of reaching movement in two dimensions. *J. Neurophysiol.* 77, 1051–1074.

Uusisaari, M., and Knöpfel, T. (2008). GABAergic synaptic communication in the GABAergic and non-GABAergic cells in the deep cerebellar nuclei. *Neuroscience* 156, 537–549.

Uusisaari, M., Obata, K., and Knöpfel, T. (2007). Morphological and electrophysiological properties of GABAergic and non-GABAergic cells in the deep cerebellar nuclei. *J. Neurophysiol.* 97, 901–911.

Vervaeke, K., Lorincz, A., Gleeson, P., Farinella, M., Nusser, Z., and Silver, R. A. (2010). Rapid desynchronization of an electrically coupled interneuron network with sparse excitatory synaptic input. *Neuron* 67, 435–451.

Walter, J. T., Alviña, K., Womack, M. D., Chevez, C., and Khodakhah, K. (2006). Decreases in the precision of Purkinje cell pacemaking cause cerebellar dysfunction and ataxia. *Nat. Neurosci.* 9, 389–397.

Walter, J. T., Dizon, M. J., and Khodakhah, K. (2009). The functional equivalence of ascending and parallel fiber inputs in cerebellar computation. *J. Neurosci.* 29, 8462–8473.

Walter, J. T., and Khodakhah, K. (2006). The linear computational algorithm of cerebellar Purkinje cells. *J. Neurosci.* 26, 12861–12872.

Walter, J. T., and Khodakhah, K. (2009). The advantages of linear information processing for cerebellar computation. *Proc. Natl. Acad. Sci. U.S.A.* 106, 4471–4476.

Wang, X. J., and Buzsáki, G. (1996). Gamma oscillation by synaptic inhibition in a hippocampal interneuronal network model. *J. Neurosci.* 16, 6402–6413.

Welsh, J. P., Lang, E. J., Sugihara, I., and Llinás, R. (1995). Dynamic organization of motor control within the olivocerebellar system. *Nature* 374, 453–457.

Wise, A. K., Cerminara, N. L., Marple-Horvat, D. E., and Apps, R. (2010). Mechanisms of synchronous activity in cerebellar Purkinje cells. *J. Physiol.* 588, 2373–2390.

Wylie, D. R., De Zeeuw, C. I., DiGiorgio, P. L., and Simpson, J. I. (1994). Projections of individual Purkinje cells of identified zones in the ventral nodulus to the vestibular and cerebellar nuclei in the rabbit. *J. Comp. Neurol.* 349, 448–463.

Zhang, W., and Linden, D. J. (2006). Long-term depression at the mossy fiber-deep cerebellar nucleus synapse. *J. Neurosci.* 26, 6935–6944.

Zhang, W., and Linden, D. J. (2012). Calcium influx measured at single presynaptic boutons of cerebellar granule cell ascending axons and parallel fibers. *Cerebellum* 11, 121–131.

Zheng, N., and Raman, I. M. (2009). Ca currents activated by spontaneous firing and synaptic disinhibition in neurons of the cerebellar nuclei. *J. Neurosci.* 29, 9826–9838.

Zheng, N., and Raman, I. M. (2011). Prolonged postinhibitory rebound firing in the cerebellar nuclei mediated by group I metabotropic glutamate receptor potentiation of L-type calcium currents. *J. Neurosci.* 31, 10283–10292.

Conflict of Interest Statement: The authors declare that the research was conducted in the absence of any commercial or financial relationships that could be construed as a potential conflict of interest.

Received: 03 October 2012; accepted: 16 November 2012; published online: 11 December 2012.

Citation: Person AL and Raman IM (2012) Synchrony and neural coding in cerebellar circuits. Front. Neural Circuits ***6****:97. doi: 10.3389/fncir.2012.00097*

frontiers in
NEURAL CIRCUITS

REVIEW ARTICLE
published: 29 July 2013
doi: 10.3389/fncir.2013.00125

Linking oscillations in cerebellar circuits

Richard Courtemanche*, Jennifer C. Robinson and Daniel I. Aponte

Department of Exercise Science, Groupe de Recherche en Neurobiologie Comportementale/Center for Studies in Behavioral Neurobiology, Concordia University, Montréal, QC, Canada

Edited by:
Egidio D'Angelo, University of Pavia, Italy

Reviewed by:
Ken K. L. Yung, Hong Kong Baptist University, Hong Kong
David Parker, Cambridge University, UK

****Correspondence:***
Richard Courtemanche, Department of Exercise Science, Groupe de Recherche en Neurobiologie Comportementale/Center for Studies in Behavioral Neurobiology, Concordia University, SP-165-03, Richard J. Renaud Science Complex, 7141 Sherbrooke Street West, Montréal, QC H4B 1R6, Canada
e-mail: richard.courtemanche@concordia.ca

In many neuroscience fields, the study of local and global rhythmicity has been receiving increasing attention. These network influences could directly impact on how neuronal groups interact together, organizing for different contexts. The cerebellar cortex harbors a variety of such local circuit rhythms, from the rhythms in the cerebellar cortex *per se*, or those dictated from important afferents. We present here certain cerebellar oscillatory phenomena that have been recorded in rodents and primates. Those take place in a range of frequencies: from the more known oscillations in the 4–25 Hz band, such as the olivocerebellar oscillatory activity and the granule cell layer oscillations, to the more recently reported slow (<1 Hz oscillations), and the fast (>150 Hz) activity in the Purkinje cell layer. Many of these oscillations appear spontaneously in the circuits, and are modulated by behavioral imperatives. We review here how those oscillations are recorded, some of their modulatory mechanisms, and also identify some of the cerebellar nodes where they could interact. A particular emphasis has been placed on how these oscillations could be modulated by movement and certain neuropathological manifestations. Many of those oscillations could have a definite impact on the way information is processed in the cerebellum and how it interacts with other structures in a variety of contexts.

Keywords: oscillations, cerebellum, synchronization, sensorimotor interactions, network activity

INTRODUCTION

Oscillations are an important influence shaping local circuits in the brain (Buzsaki and Draguhn, 2004; Buzsaki, 2006). In recent years, various oscillatory phenomena have been identified as influential pattern synchronizers in the spinal cord, in the cerebral cortex, in the basal ganglia, and the cerebellum. Here, we will describe the various constitutive oscillatory phenomena in the cerebellar cortex, the main interactions that could take place in the cerebellar cortex between them, attempt to predict the resulting effects at the cerebellar output in the context of sensorimotor behavior, and then propose how oscillations in the cerebellum could contribute to pattern synchronizing across sensorimotor and cognitive systems.

The basic questions on neural coding that are current, in areas such as the cerebral cortex circuits, the hippocampal and parahippocampal structures, the olfactory system, and the amygdala (e.g., Collins et al., 2001; Perez-Orive et al., 2002; Harris et al., 2003; Glasgow and Chapman, 2007; Goutagny et al., 2009), are also key for the cerebellum. How do cerebellar cortex neurons shape into a population to form one of its many coherent representations at a given moment in time? What is the time-specific signature of cerebellar populations? Strong hints have been offered by the study of olivocerebellar interactions, showing that these ultimately produce intricate spatiotemporal patterns in Purkinje cell (PC) population coding to serve the task at hand (Welsh et al., 1995; Welsh, 2002). Considering the massively parallel modularity of the cerebellar cortex, we raise the question of how this complementarity could contribute to population coding via the various afferent systems and local circuit interactions. As has been demonstrated for olivocerebellar interactions, other existing oscillations are likely going to play a role in shaping cerebellar cortex population patterns. In addition, coherent long-range communication mechanisms are advantageous for a large structure such as the cerebellum, in order to coordinate its internal activity with other oscillatory sensorimotor networks. The temporal modulation of cerebellar population activity will certainly come into play in the capacity of the cerebellum to participate in sensorimotor transformations.

DIFFERENT TYPES OF OSCILLATIONS IN THE CEREBELLAR CORTEX

When studying oscillations in cerebellar circuits, a significant discovery was that harmaline administration produced hyperrhythmic olivocerebellar activity (De Montigny and Lamarre, 1973; Llinás and Volkind, 1973). This line of inquiry has led to a systematic exploration of population coding in olivocerebellar circuits (for an example of a recent review, see Llinás, 2009). In contrast with the study of olivocerebellar interactions, for a long time there was a silent echo to such oscillatory phenomena in the other components of the cerebellar circuitry. This became particularly more apparent considering the interest in peri-movement cerebral cortex oscillations (Sanes and Donoghue, 1993). These oscillations were not mirrored by similar comparable phenomena in the cerebellum: this had been noted by at least one voice (Bullock, 1997). The finding of granule cell layer (GCL)-specific oscillations (Pellerin and Lamarre, 1997; Hartmann and Bower, 1998) rekindled an interest in the diversity of the oscillatory phenomena in the cerebellum. However, as reported in the historical perspective of Isope et al. (2002), certain cerebellar oscillations had actually been discovered long ago. In this paper, with the recent reemergence of multiple oscillation patterns in the

cerebellar cortex circuitry (de Zeeuw et al., 2008; D'Angelo et al., 2009), we review the potential influences that these mechanisms and their interactions could have in the formation of cerebellar patterns of activity.

A quick graphical illustration of the oscillatory phenomena can be presented here, admittedly by staying in the context of our recordings, with mainly the (1) granule cell layer 4–25 Hz oscillations in the primate paramedian lobule – PM, (2) the similar oscillation patterns at 4–25 Hz in the rodent, and (3) the Purkinje-cell layer fast (∼150–300 Hz) oscillations being considered. **Figure 1** illustrates the local field potential (LFP) oscillations that can be recorded in the cerebellar cortex, here all recorded in the rhesus primate or laboratory rat *in vivo*. In the figure, it is apparent that the oscillatory phenomena in the primate cerebellar cortex GCL has a wide frequency band: already established in the range of 15–25 Hz, and recorded in the PM (see **Figure 2**), we also show that in the anterior lobe, certain sites show simultaneous oscillations at a higher frequency, in this case up to around 40 Hz (**Figure 1A**). This variety has not been much explored, and will warrant further investigation. The rodent version of these GCL oscillations has also been described, in the awake animal (∼5–12 Hz, **Figure 1B**), but has also been characterized around the same frequencies under urethane anesthesia (**Figure 1C**). Finally, fast oscillations around 200 Hz, a more recent phenomenon, have been described for the PC layer (PCL), here also recorded under anesthesia (see **Figure 1D**). A representation of the involved structures and circuitry involved in those recordings is shown in **Figure 2**.

A large component of the cerebellar literature concerning oscillations between 4 and 30 Hz has been characterized by the subthreshold oscillatory activity in the inferior olive (IO), with near 10 Hz frequencies. As these have been well studied, *in vivo* and *in vitro*, only a broad characterization will be given here, having been well reviewed by the authors [e.g., in motor control (Llinás et al., 1991; Welsh and Llinas, 1997; Llinás, 2009), and also in mechanistic terms (Llinás et al., 1981; Llinás and Sugimori, 1992; Jacobson et al., 2008)]. Additionally, in the past few years, additional rhythmic phenomena have appeared *in vivo* in the cerebellar cortex GCL, which have subsequently been investigated *in vitro*. We will describe some main points of olivocerebellar activity first, then the GCL oscillation at similar frequencies. Finally, in addition to these firmly established oscillatory phenomena, we will address the fast oscillations in the PCL (e.g., de Solages et al., 2008), the ultra-slow fluctuations in electrophysiological activity (Chen et al., 2009), and the slow cerebro-cerebellar membrane potentials (Ros et al., 2009). We will describe each of those oscillatory phenomena in quasi-chronological succession of their first report.

OLIVOCEREBELLAR RHYTHMICITY

The IO, located in the ventral brainstem, has long been studied for its powerful connection via climbing fibers (CFs) to contralateral PCs in the cerebellum. It is one of the strongest synaptic connections in the central nervous system (Llinás, 2009); an IO neuron may synapse with up to 10 PCs (Armstrong and Schild, 1970), but each PC only has one CF which intimately connects to its soma and dendritic arbor (see **Figure 2**). CF activation of PCs generates atypical action potentials, known as complex spikes (CS), that are characterized by having large amplitudes and subsequent wavelets. The timing of CF activation, under normal conditions firing at 1 Hz, is considered to be an important variable in determining cerebellar cortex information coding.

The IO has important intrinsic rhythm capabilities. Some of the first studies indirectly observed the IO as an oscillator using harmaline as a means to enhance the IO rhythmicity (Lamarre et al., 1971; De Montigny and Lamarre, 1973). Under normal conditions, the IO nucleus oscillates at a subthreshold 10 Hz (Devor and Yarom, 2002; Chorev et al., 2007). Animals receiving systemic harmaline, a psychoactive alkaloid, produced rhythmic CSs at ∼10 Hz, coming from CFs (Lamarre et al., 1971; De Montigny and Lamarre, 1973; Llinás and Volkind, 1973). These studies marked the beginning of a series of inquiries on the rhythmic properties of the olivocerebellar system. Typical spontaneous CS discharge at ∼1 Hz, but harmaline transforms the subthreshold oscillations into coherent and sustained firing at ∼10 Hz. This strong olivocerebellar rhythmic activation expresses itself as a systemic tremor of the animal [for a video of the phenomena, refer to Movie S1 from Park et al. (2010)]. Specifically, it was recently discovered that $Ca_V3.1$ T-type Ca^{2+} channels may be the molecular substrate allowing for the IO to oscillate. Park et al. (2010) effectively showed that mice lacking the $Ca_V3.1$ gene were not affected by systemic harmaline injections. This was confirmed electrophysiologically by recording the IO and deep cerebellar nuclei (DCN) *in vitro* in both wild-type and $Ca_V3.1^{-/-}$ mice. The cells of the IO have long been known to be electrically coupled together via gap junctions (Llinás et al., 1974), and therefore postulated to oscillate in clusters of neurons. Using voltage sensitive-dye technique to image populations of neurons, Leznik et al. (2002) demonstrated that clusters of IO neurons do oscillate in unison, at an average frequency of 1–7 Hz. Furthermore, external stimulation of the cell clusters consistently triggered an oscillatory reset; rather than change the frequency of oscillation, this external stimulation produced a phase shift in the subthreshold oscillations (Leznik et al., 2002). This could in turn synchronize CF activation of PCs in the cerebellum. The role of gap junctions in the IO is pivotal for the capacity to form clusters: blocking those gap junctions produces a disconnection of the IO clusters and virtually abolishes population oscillations without affecting the subthreshold oscillations of single cells (Leznik and Llinas, 2005).

In the same manner as thalamic and brainstem nuclei influence cortical systems via temporal patterns, it is interesting that a nucleus such as the IO can temporally influence a large neural sheet, such as the cerebellar cortex. IO rhythmicity could definitely contribute to the organization of network activity in the cerebellar cortex (Jacobson et al., 2008; Llinás, 2009). Recent models suggest that this network may be capable of influencing PCs at a much finer temporal resolution than 10 Hz (Jacobson et al., 2008, 2009). Their model posits that GABAergic input from the DCN, which decouples IO cells by acting on gap junctions (Lang et al., 1996), would set cells out of phase from each other. Since IO cells preferentially fire and optimize their influence on the PCs at the peaks of their subthreshold oscillations (Mathy et al., 2009), out of phase cells reaching threshold would do so staggered in time, greatly increasing their temporal resolution and influence on PCs. This could support the temporal detail needed for the timing of motor events (for full explanation, see Jacobson et al., 2008).

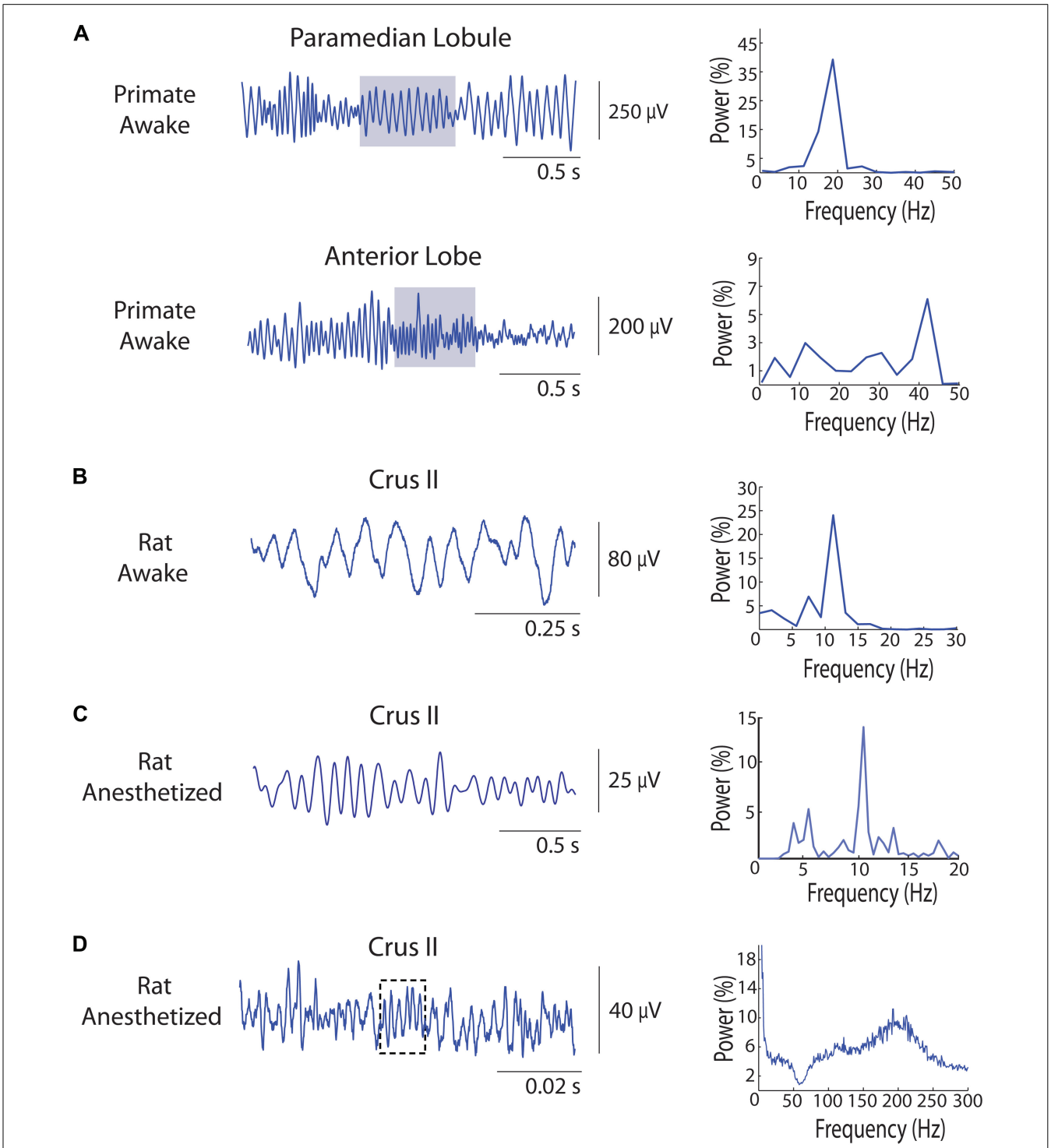

FIGURE 1 | A sample of oscillations recorded from cerebellar cortex *in vivo* local field potentials (LFPs) using metal microelectrodes. LFP example data located on the left, and corresponding Fast Fourier Transform (FFT) spectrum on the right. FFT shown in the form of %. **(A)** Simultaneous different types of LFP oscillations in the primate rhesus monkey cerebellum. Top: LFP oscillations from the PM GCL, around 19 Hz. Bottom: faster LFP oscillations recorded in the anterior lobe GCL, going up to 40 Hz. Gray shaded area corresponds to the time period for the FFT analysis. Notice the simultaneous co-existence of two different oscillatory phenomena. **(B)** Recording of LFP oscillations in the awake rat cerebellar cortex GCL. In this sample, the signal oscillates around 10.5 Hz, FFT on the whole trace. **(C)** Recording of LFP oscillations in the urethane-anesthetized rat cerebellar cortex GCL. Oscillations are here around the same frequency, at 11 Hz, FFT on the whole trace. **(D)** Recording of fast LFP oscillations in the urethane-anesthetized rat cerebellar cortex, using differential metal microelectrodes separated by 500 μm, with at least one tip located approximately in the Purkinje cell layer. A 312 Hz short 6-cycle episode is highlighted. FFT averaged on 120 2-s windows, so for the whole 2 min.

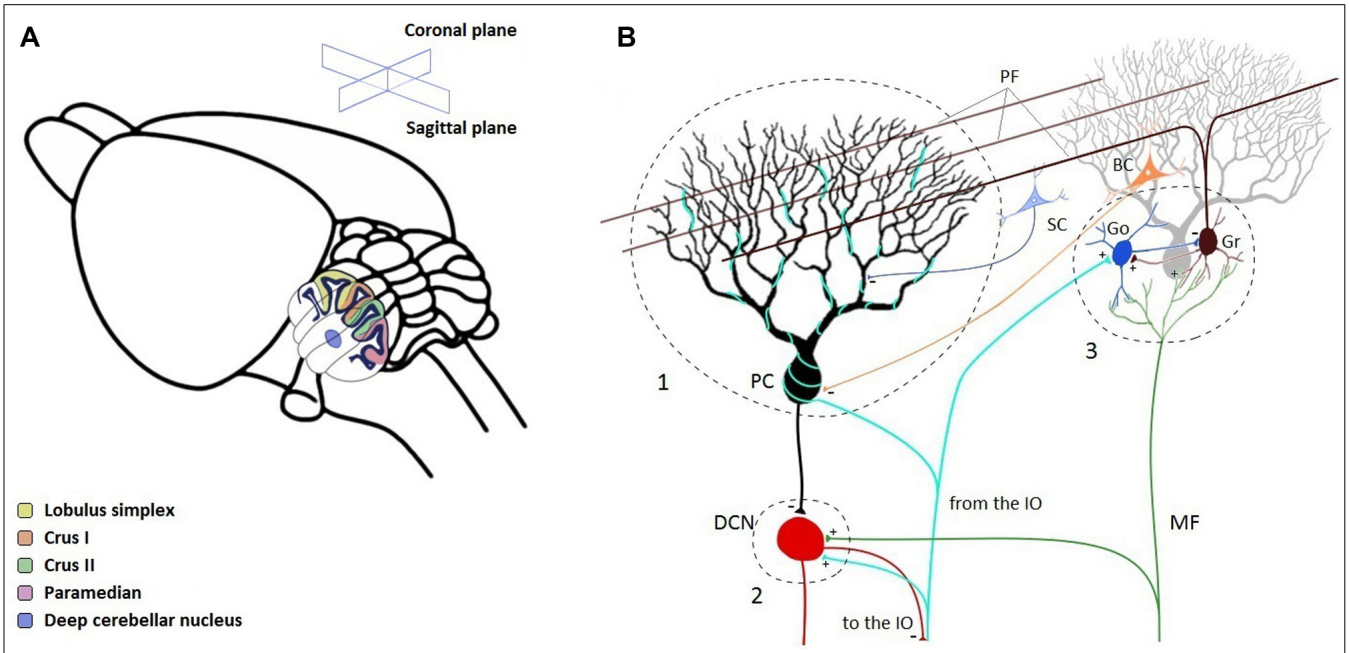

FIGURE 2 | Description of the cerebellar cortex substrate for local field potential oscillation interactions. (A) General cerebellar organization, here from a rodent brain. Potent LFP GCL oscillatory sites can be recorded from within the cerebellar cortex posterior lobe, including the crus lobules, Crus II and Crus I, and the paramedian lobule (PM). For both the primate and the rodent, the PM lobule is a common GCL LFP oscillation recording site, at the level where the virtual slice is taken. **(B)** Cerebellar circuitry, with an emphasis on the potential interaction sites between different oscillatory phenomena. Highlighted are the Purkinje cell (PC) afferent region (1), the deep cerebellar nuclei (2, DCN), and the Golgi cell (Go)–granule cell (Gr) circuits in the GCL (3). Interactions are discussed in the text. IO, inferior olive; MF, mossy fiber; PF, parallel fiber; SC, stellate cell; BC, basket cell, the latter two provided for context.

Functional roles of olivocerebellar oscillations

To evaluate the effects of these oscillations on cerebellar processing, a major technological advance was the creation of methods permitting the recording of CSs in arrays of PCs (Sasaki et al., 1989; Welsh et al., 1999), yielding population data in the awake behaving animal (Welsh et al., 1995). Recording CS activity in PCs provides an indirect confirmation of IO activity. This does not, however, inform on the nature of the organization of the IO network activity. Welsh et al. (1995) were able to correlate CS activity from matrices of PCs to animal behavior. Thus, the output of the IO system could be studied at a PC population level with regard to movement, informing on the effects of those connections to organize coherent cellular PC networks (Lang et al., 1996; Lang, 2002; Blenkinsop and Lang, 2006). In the awake animal, these olivocerebellar networks are organized under the influence of oscillations, namely in their parasagittal heightened synchrony (Lang et al., 1999). In the context of movement, these form organized networks, shaped as task-specific mosaics driven by oscillatory activity in the olivocerebellar system (Welsh et al., 1995).

Links have been made between this oscillatory activity and the IO working as a motor clock in health and disease (Welsh et al., 2005). However, there was resistance to the idea of the rhythmic activity of the IO working as a master motor clock (Keating and Thach, 1995, 1997). Recent additional evidence for the motor clock hypothesis came from tasks performed during brain imaging, where the IO functional magnetic resonance imaging (fMRI) activation can be related to the timing component of the tasks (Xu et al., 2006; Wu et al., 2011). There is also a role for the oscillations in olivocerebellar activity to modulate movement generation in the primary motor cortex (Lang et al., 2006b). However, while the timing of CS activity can be timed with movement parameters in the monkey (Kitazawa et al., 1998), in the context of rodent licking movements, certain CSs are not coherent with movement initiation in rhythmic licking (Bryant et al., 2010), somewhat different from Welsh et al. (1995). While the strict idea of a central clock is indeed difficult to prove or disprove, temporally constrained activity, more particularly rhythmic activity, should play an important role in timed sensorimotor or cognitive behavior (Steriade et al., 1993; Llinás, 2001; Paulsen and Sejnowski, 2006; Sejnowski and Paulsen, 2006).

Anatomically, olivocerebellar axons show a parasagittal plane orientation in their distribution (Oberdick et al., 1998; Apps and Garwicz, 2005), a motif matched by the patterns of specific protein expression such as zebrin (Hawkes and Leclerc, 1987; Leclerc et al., 1990; Hawkes et al., 1997). These anatomical patterns influence the flow of information across the cerebellar cortex (Apps and Hawkes, 2009; Ebner et al., 2012), and confer a sagittal modularity to the olivocerebellar activity, both confirmed in anesthetized and awake animals (Sasaki et al., 1989; Sugihara et al., 1995; Lang et al., 1999; Fukuda et al., 2001). This stripe of activity is spatiotemporally defined by the temporal exactness at which the afferent inputs come in: this is partly determined by the spatiotemporal organization within the IO (Llinás, 2009), and the isochronicity of the conduction time along the sagittal band (Fukuda et al., 2001;

but see Baker and Edgley, 2006a,b; Lang et al., 2006a). The final result is ultimately that sagittal bands of CSs respond preferentially at a frequency neighboring 10 Hz. This imposed rhythmicity onto the PCs would have important implications from the standpoint of spatiotemporal time encoding in the cerebellar cortex, favoring events separated by 100 ms (Welsh, 2002), but also a capacity to affect the cerebellar cortex network memory (Ito, 1989, 2006) at that frequency. This packaging of information using oscillatory activity has been identified within hippocampal and entorhinal systems (Jensen and Lisman, 2005; Buzsaki and Moser, 2013). In the cerebellum, while multiple synapses are likely to change with repeated circuit stimulation (Gao et al., 2012), oscillation with memory has scarcely been addressed, but are likely to play a role (D'Angelo et al., 2011). There is also evidence of cerebellar fMRI activity being linked to slow-wave oscillations during sleep, which was shown to have a role in memory processes (Dang-Vu et al., 2008).

GRANULE CELL LAYER 4–25 Hz OSCILLATIONS

While connectivity in the olivocerebellar pathway shows a direct and tightly interconnected system, the mossy fiber afferent system of the cerebellar cortex is strikingly different. Mossy fiber input interacts at multiple levels, connecting with many interneurons before reaching the final output layer, the PCs (Llinás et al., 2004; Ito, 2010). The main target of the mossy fiber pathway, the GCL, is a heavily interconnected network composed of the cell bodies of granule, Golgi, Lugaro, and unipolar brush cells. The Golgi–granule cell network, which acts to integrate the incoming signals from mossy input, is a very active and dynamic local network. Both granule and Golgi cells receive excitatory inputs from the mossy fibers. Golgi cells are inhibitory interneurons whose axonal projections mostly remain within the GCL, while granule cell axons extend up to the molecular layer where they bifurcate and synapse with the dendritic projections of the PC (Eccles, 1967; Kalinichenko and Okhotin, 2005; Ito, 2010). This connectivity is illustrated in **Figure 2**.

While the anatomy of the mossy fiber pathway is well-known (Eccles et al., 1967), the 4–25 Hz rhythmic oscillatory activity in the GCL was only recently reported. While exploring the cerebellar cortex for CS activity in the awake behaving monkey, Pellerin and Lamarre (1997) heard rhythmic "background" activity within the GCL when electrodes entered the PM of the monkey. The rhythmic activity which they heard was in reality a bursty multi-unit GCL discharge at ∼14 Hz: by adapting filters on the electrophysiological signal for the observation of LFPs, rhythmic oscillations were recorded in the form of waxing and waning spindles. This rhythmic signal was recorded while the rhesus monkey remained immobile but attentive to the environment; it decreased with the initiation of movement. This rhythmic activity was also affected by the level of arousal of the animal and was modulated in amplitude by both sensory events and motor output. In each situation, oscillatory power was shown to predictably diminish with reduced levels of arousal, input of a sensory stimulus, and the initiation of motor task. A similar oscillatory phenomenon was also reported shortly afterward in the rodent cerebellar cortex, at ∼7 Hz in the GCL of Crus II. These oscillations were present during immobility and were also stopped by the initiation of movement (Hartmann and Bower, 1998). Early accounts report certain slow field activity which could be related to GCL oscillations (Brookhart, 1960). As explained, this GCL rhythmic activity is tightly correlated with multi-unitary GCL activity, obvious from the LFP recordings. The oscillatory activity was found to be generally synchronous across separate recording sites in Crus II both within and across hemispheres in the GCL. These two papers marked the beginning of the identification of another rhythmic phenomenon in the cerebellar cortex, in this case rather than affecting the PCs through the CFs, the rhythms influence cerebellar output through the mossy fiber relay in the GCL.

Many similarities were evident in those two papers: (1) the LFP oscillations were clearly related to the GCL activity; (2) these oscillations were best recorded during periods of immobility of the animal; and (3) these oscillations were spindle-shaped and lasted several cycles. Thus, despite a difference in frequency band (monkey 14–20 Hz, rodent 7–8 Hz) and a minor difference in localization (monkey PM, rodent Crus II), the low-frequency rhythms were recorded optimally under similar conditions: the power of the oscillations was highest when animals were immobile, showing spindle-shaped oscillations that lasted over several cycles. Following these publications, unit activity in relation to the oscillatory LFPs in the cerebellar cortex was further defined in the primate showing: (a) the best cellular relationship being multi-unit granule cells; (b) second best being PC simple spikes; and (c) no obvious relationship between CF activation and beta-range LFPs (Courtemanche et al., 2002). One behavioral distinction here was that the animals were asked to perform several tasks, all of which essentially were related to the concept of active expectancy, or "waiting for the proper time to trigger the movement" (Courtemanche et al., 2002). In addition, with the potential that the 15–25 Hz GCL oscillations might need programmed movement to take place, we showed that GCL oscillations increase if the animal was in a state of passive expectancy, the spindles lasting as long as the waiting period (Courtemanche et al., 2002).

In the years since the Pellerin and Lamarre (1997) and the Hartmann and Bower (1998) papers, there have been several reports that have defined the rhythmic properties of the cellular components of the GCL, as well as the behavioral states which influence the development and efficiency of these rhythms. The cellular properties of the GCL components and their synaptic organization provide an ideal environment for the development and maintenance of rhythmic low-frequency activity. Granule cells possess specific slow potassium channels that enable 3–12 Hz bursting and resonance (D'Angelo et al., 2001). Golgi cells display specific firing properties that promote the rhythmic inhibition of granule cells, as demonstrated during both *in vitro* and *in vivo* recordings. Golgi cells possess intrinsic pacemaking and resonance, seen *in vitro* with the regular beating of Golgi cells at frequencies within the theta-band range (Dieudonn, 1998; Forti et al., 2006; Solinas et al., 2007). In addition, Dugué et al. (2009) showed in the rodent that Golgi cells could certainly be influenced by the oscillatory phenomenon in the GCL: by manipulating electrical synapse connectivity, they showed that Golgi cells could form a network capable of maintaining 4–25 Hz resonance in the GCL circuitry. These findings also complement *in vivo* recordings, where unitary activity shows spontaneous rhythmic firing found in both awake and anesthetized

animals (Edgley and Lidierth, 1987; Vos et al., 1999; Holtzman et al., 2006). Rodent GCL theta-range oscillations, under urethane anesthesia, show similar oscillatory frequencies as in the awake animal (Robinson et al., 2009), as is the case for urethane anesthesia and the hippocampal or entorhinal theta oscillations (Glasgow and Chapman, 2007; Zhang et al., 2010).

Golgi cells have many diverse synaptic connections with both granule and other Golgi cells; one of those types consists in Golgi–Golgi electrical synapses. Gap junction proteins connexin36 (Cx36) have been identified in the GCL and molecular layers of the cerebellar cortex, located primarily on apical dendrites of Golgi cells (Condorelli et al., 2000; Ray et al., 2006; Vervaeke et al., 2010). Cx36 gap junctions have been associated with the synchronizing of inhibitory networks (Deans et al., 2001) and may be a contributing factor to network synchrony within the GCL (Vervaeke et al., 2010). Functionally, electrical coupling between Golgi cells serves to promote synchronization of their rhythmic firing as a population, thus providing synchronous inhibition to granule cells. Dugué et al. (2009) showed that Golgi cells could maintain 4–25 Hz resonance in the GCL circuitry. In addition, Vervaeke et al. (2010) also demonstrated that in paired recordings of Golgi cells in the absence of mossy fibers, Golgi cells maintain synchronous signals, pointing to the capacity of the GCL to possibly develop or maintain low-frequency rhythms.

An additional cellular component, the Lugaro cell, may also act as a temporal coordinator in the GCL by modulating and synchronizing activity (Dieudonné and Dumoulin, 2000). Lugaro cells are inhibitory interneurons connected to Golgi cells that transversely connect different sites of the GCL (Lainé and Axelrad, 1996). Lugaro cells possess a myelinated axon, permitting them to connect sites with a faster response than the parallel fibers. An interesting property of Lugaro cells is that they produce oscillatory inhibitory post-synaptic current (IPSCs) in the membrane potential of Golgi cells following the administration of serotonin (Dieudonné and Dumoulin, 2000). This connection could thus potentially coordinate Golgi–granule local circuits in a coherent fashion. The Lugaro properties would make for a second mechanism by which a spatially defined, orthogonal network [sagittal for Golgi cells axons and Lugaro dendrites (Geurts et al., 2003), coronal for Lugaro axons], could influence the 4–25 Hz oscillations in the GCL. Intrinsically, the cell properties of both the granule cells (D'Angelo et al., 2001), and Golgi cells (Forti et al., 2006) could provide the underlying strong resonance around 4–25 Hz. These properties confer specific time windows for optimal GCL processing of information (D'Angelo, 2008; D'Angelo and de Zeeuw, 2009; D'Angelo et al., 2009). Overall, Lugaro, granule, and Golgi cells have all been reported to have distinctive properties that can facilitate rhythmicity, in which Golgi cells appear to play a pivotal role. One remaining question is whether this system can intrinsically generate these oscillations or is simply a cellular environment capable of maintaining externally driven rhythms.

Functional roles of 4–25 Hz GCL oscillations

To explore the functional role of the cerebellar rhythms with respect to sensorimotor systems, task-related cerebellar recordings have been compared to the rhythmic activity in other brain regions. O'Connor et al. (2002) found ∼7 Hz synchronized activity across the Crus II cerebellar cortex, the contralateral primary somatosensory cortex, and mystacial pad electromyography (EMG), addressing the potential interactions across extended somatosensory processing circuitry. One of their salient results is that this coherence was more pronounced when the animal was whisking weakly or not whisking at all. This finding seems to echo previous reports concerning optimal behavior for eliciting GCL LFP oscillations, namely the little or no obvious motor output; this information was now being related to a larger coherent network for whisking.

In primate recordings, Courtemanche and Lamarre (2005), also examined the link between GCL oscillations in the 10–25 Hz band range and sensorimotor processing. In the context of active expectancy, PM GCL LFP oscillations were highly synchronized with contralateral primary somatosensory cortex (SI) rhythms. This synchrony was particularly high during the waiting period before a learned lever press, when the monkey was just lightly touching the lever in anticipation of the right time to press. Synchronization between the two regions (PM–SI) was significantly higher in active expectancy than in passive expectancy or rest, hinting that the synchronization might be related to common functional processing. Primary motor cortex vs. PM GCL 10–25 Hz oscillations seemed less linked in the context of the tasks, though active expectancy also seemed to incite the greatest synchronization. Finally, an unreported 40 Hz cerebellar cortex anterior lobe oscillation also seemed to be related to primary motor cortex oscillations in the rest condition (see **Figure 1A**). More anterior lobe recordings, presumably in the GCL, would have to be performed to substantiate those oscillations further and describe their functional significance.

Courtemanche et al. (2009) reported data about the spatial organization of cerebellar cortex GCL oscillations by simultaneously recording with two electrodes in the rhesus monkey cerebellum. Anatomically and physiologically, the cerebellar cortex can be subdivided in many spatial modules (Hawkes et al., 1997; Herrup and Kuemerle, 1997; Ebner et al., 2012), and there are particular afferent patterns that will shape the inputs to the GCL. Specifically, the predominantly sagittal arrival of mossy fiber afferents (Scheibel, 1977; Heckroth and Eisenman, 1988), and the tendency of the Golgi cells to follow the sagittal axis (Sillitoe et al., 2008) could shape how local networks are constrained physiologically. These anatomical elements appear to anisotropically limit the extent of GCL rhythmicity. In Courtemanche et al. (2009), the modularity in the GCL synchronization was sought. The dual-GCL recordings showed a primarily parasagittal organization of the GCL oscillations when the animal was at rest, with strong parasagittal LFP synchrony, and much weaker coronal synchrony. However, during active expectancy, while the sagittal cross-correlation stayed, there was a strong increase of LFP synchronization in the coronal plane. Thus, there is potentially a widening of a putative sagittal module in the context of a sensorimotor task: this could be a hint of a recruitment mechanism in order to perform a task, originating in the GCL. This widening of the electrophysiological modulation of cerebellar cortical networks also appears in the context of synchronous firing in PCs (Heck et al., 2007).

Overall, these studies have shown that GCL 4–25 Hz oscillations can serve to spatiotemporally organize the communication (1) within the GCL through the organization of the cellular networks, (2) in the output from the GCL by influencing the PCs, (3) in the spatial patterns of GCL synchronization in time, as seen in the context of functional synchronization, and (4) between the cerebellum and cerebral cortex, as seen through the cerebrocerebellar LFP synchronization during task performance. There has been modeling of the oscillatory activity in the GCL that identifies its capacity to temporally organize the flow of inputs (Maex and De Schutter, 2005; Yamazaki and Tanaka, 2005; Ito, 2010). The GCL oscillations can thus help in the investigation of information flow throughout the cerebellar cortex and other communicating units along sensorimotor system pathways. This was shown in recent data (Courtemanche et al., 2009), adding nuance to what had already been predicted, namely that GCL oscillations at 4–25 Hz should have a patchy organization (de Zeeuw et al., 2008). Further recordings of GCL units with LFP signals will provide more information on the population specificity. Nonetheless, from the LFPs, a distinct dynamic modulation appears to exist in the GCL, with a task-related adjustment of the synchronous zones ultimately leading to optimal information processing in the cerebellar cortex.

A strategy that follows rhythmic synchronization between putative sagittal GCL-Purkinje modules could also be spatiotemporally optimal. From the standpoint of the GCL, the influence from 4 to 25 Hz rhythmicity (delays of 40–250 ms) provides the GCL sites with repeated "up-phases" lasting 50% of the rhythm cycle, amounting to periods lasting between 20 and 125 ms. These up-phases represent times when local groups of GCL neurons would be more easily excitable. This window corresponds well with certain demands imposed by the relatively slow conduction velocity of the parallel fibers (0.2–0.3 m/s; Bell and Grimm, 1969; Vranesic et al., 1994). If the objective was to simultaneously relay excitation at two cerebellar cortex sites along the parallel fibers, at these conduction velocities, the length of the parallel fiber (up to 6 mm; Brand et al., 1976) would be covered in a period of 20–30 ms. The up-states for excitation provided by the rhythmicity would thus have to last longer than 20–30 ms to provide an additional rhythmic advantage. From this calculation, a rhythm with a period of more than 20 ms, or frequencies less than 50 Hz would thus favor a spatiotemporal pattern of synchronization throughout the length of the parallel fibers.

FAST (>150 Hz) OSCILLATIONS IN THE PURKINJE CELL LAYER

Early in the study of cerebellar physiology, Adrian had recorded fast (150–250 Hz) oscillations from the ECoG (electrocorticographic) signal on the surface of the cerebellar cortex of the anesthetized cat and rabbit (Adrian, 1935; Isope et al., 2002). The presence of these oscillations was also confirmed in other species using a similar methodology (Brookhart, 1960). At the time, these oscillations were demonstrated to specifically originate from the cerebellar cortex (Dow, 1938). In a more recent series of studies, using microelectrodes to record from within cerebellar cortex of mutant mice, this type of fast activity (>150 Hz) was recorded by Cheron et al. (2008). In a mouse model of Angelman syndrome, they found prominent fast oscillations while recording LFPs, along with single unit activity (Cheron et al., 2004, 2008; Gall et al., 2005), and confirmed with precision the link of these oscillations with PC activity. In two other recent papers, the existence of these fast oscillations in normal animals has also been confirmed (de Solages et al., 2008; Middleton et al., 2008). Experiments *in vivo* showed fast (∼200–250 Hz) rhythms in normal rats (de Solages et al., 2008). The presence of such oscillations has also been confirmed by experiments *in vitro* (Middleton et al., 2008). *In vivo* experiments showed that these oscillations are robust, present mainly in the PCL, and are also affected by the recurrent PC collaterals (de Solages et al., 2008).

Functional specificity of fast oscillations

Fast oscillations could present a different modulatory pattern onto the cerebellar cortex circuitry. Via their localization in the PCL, they can more directly influence the motor output toward the DCN. Through recurrent collaterals, they can influence local neighboring zones and fine-tune spatially the output area (de Solages et al., 2008). However, they do not appear to show a sagittal or coronal pattern of coherence. This could be related to the restricted spatial extent of this coherence (on the order of 0.5 mm).

It is not known if these oscillations are specifically affected by movement initiation. However, they are affected by the neurophysiopathological disease state, as described below. They appear to be more pronounced in the case of specific diseases, such as Angelman syndrome, and in calretinin/calbindin knockout mice (Cheron et al., 2005). These conditions appear to exacerbate the oscillations, which will be described in section "Potential Interactions of These Oscillations in the Cerebellar Cortex: Perspectives from Movement."

SLOW OSCILLATIONS (≤1 Hz) IN THE CEREBELLAR CORTEX

Recently, a few research groups have identified slower oscillations in the cerebellar cortex circuitry. Specifically, one type involves slow oscillations (0.05–0.2 Hz) present in the ataxic tottering (*tg*) mouse, recorded with flavoprotein immunofluorescence (Chen et al., 2009). This mouse has defective $Ca_v2.1$ (P/Q-type) voltage-gated Ca^{+2} channel, and suffers from short bouts of dystonia/dyskinesia. These oscillations appear to be generated intrinsically, as they are not disturbed by blocking glutamate α-amino-3-hydroxy-5-methyl-4-isoxazolepropionic acid (AMPA) receptors, and affect the cerebellar cortex cells, including PCs. The slow oscillations, which seem to increase in activity, are spontaneously present in the cerebellar cortex active area during dystonic periods. The frequency increases to values of 0.15 Hz. These oscillations are coherent with the muscular activity triggered during dystonic episodes. The capacity to record such slow oscillations in normal animals does not appear to have been reported.

The McCormick group reported a slow oscillatory activity around 1 Hz in the cerebellar cortex of ketamine-anesthetized mice, driven by the neocortical oscillatory activity (Ros et al., 2009). This type of oscillation could influence cerebellar cortex coding on a slow timescale, in normal animals. This 0.5–1 Hz slow oscillation is similar to the up/down states seen in cortex and basal ganglia, which are thought to have a cortical origin (Stern et al.,

1998; Steriade, 2003). The pattern of activity seems similar to slow wave sleep activity recorded from neocortical and hippocampal sites (Clement et al., 2008). This slow cerebellar oscillation was shown to affect the multi-unit activity in the cerebellar cortex. In the awake mouse, this activity decreased in amplitude and accelerated to about 1.3 Hz. Tests showed a strong dependence of this locally generated cerebellar oscillatory activity to neocortical entrainment. The effects of these slow up/down states in the cerebellar cortex was to entrain granule cells and Golgi cells, but minimally PC simple spikes. However, the neocortical up-states seem to favor the emergence of PC CSs. Both of these recent sets of results, while coming from different phenotypes, appear to show how these slower oscillations could affect the cerebellar cortex circuitry.

POTENTIAL INTERACTIONS OF THESE OSCILLATIONS IN THE CEREBELLAR CORTEX: PERSPECTIVES FROM MOVEMENT

In this section, we will identify potential nodes of interaction for the oscillations presented in the previous sections. We will focus on certain contexts for inspecting spatiotemporal dynamics, namely how those oscillations relate to movement and motor neuropathology. There is more data available in the literature concerning the olivocerebellar and GCL oscillatory phenomena, both at frequencies within 4–25 Hz. However when appropriate, we will also cover the potential interactions of cerebellar cortex fast (>150 Hz) and slow (=1 Hz) oscillations. The identification of potential oscillatory interactions is largely unknown from the standpoint of the experimental data available. However, we attempt educated guesses in the case of two specific contexts: the immobility/movement interface, which is a standard sensorimotor context where it is possible to identify a phase transition in the circuits (Konig and Engel, 1995; Buzsaki, 2006; Courtemanche et al., 2009; Salazar et al., 2012), and also of select "neuropathological" activity in the circuits, such as during injection of harmaline, triggering symptoms of tremor (Llinás, 2009; Park et al., 2010), or in ataxic mouse models.

CROSSROADS AND POTENTIAL INTERACTIONS

By examining the anatomical intersections across the cerebellar circuitry, we have identified three potential interaction sites. These interaction sites constitute neuronal groups where the influence of more than one oscillatory phenomenon converges. We identified potential interactions at the following sites: at the level (1) of PCs; (2) of the DCN; and (3) at the GCL. Those sites and their connectivity are identified in the network diagram of **Figure 2**. Quite probably only for practical reasons in experimentation, many of the recordings of oscillations occurred in the posterior lobe, in the Crus II and PMs (see **Figure 2A**).

First we will describe some of the connectivity that could support these interactions. *(1) Level of the PCs.* One of the first potential sites of oscillatory interactions is at the level of the PCL (see "1" in **Figure 2B**). As a site, PCs receive, amongst other afferents, the CFs from the IO, the parallel fibers and the ascending axons from granule cells (Gundappa-Sulur et al., 1999; Bower, 2002; Ito, 2010). It is thus an area where the olivocerebellar oscillations and the GCL oscillations can converge, at similar frequencies. It is also a site where the 4–25 Hz oscillations can interact with the slow (<1 Hz) and fast (>150 Hz) oscillations. Specifically for the theta and beta bands, the way that oscillatory interactions would happen is via the convergence of the simple spike activity (influenced by the GCL oscillations – see Courtemanche et al., 2002), and the CS activity produced by the IO. *(2) Level of the DCN.* Another potential site of interaction are the cerebellar nuclei (see "2" in **Figure 2B**). The DCN receive connections mainly from PCs, but also receive collaterals from the IO and from mossy fibers (Llinás et al., 2004; Ito, 2010). The nuclei could thus be a site of interaction between the olivocerebellar and GCL oscillations. *(3) At the level of the GCL.* Along with local resonance mechanisms, another potential multi-oscillation site would be the GCL (see "3" in **Figure 2B**). The IO also send CF collaterals to the GCL (Geurts et al., 2003). Although less is known about these connections, there could be an interaction between the olivocerebellar and the GCL oscillations at this level.

FROM IMMOBILITY TO MOVEMENT

As was discussed previously, the GCL oscillations and the IO rhythmicity do not require movement in order to occur, as they can appear spontaneously during immobility or under anesthesia. However, when there is a switch from immobility to movement, multiple experimental results point to the interruption of the GCL oscillations (Pellerin and Lamarre, 1997; Hartmann and Bower, 1998; Courtemanche et al., 2002, 2009; Courtemanche and Lamarre, 2005). Looking at what happens at interaction site #1 (**Figure 2B**), this movement initiation (or the concomitant surge in sensory input) appears to limit the capacity of PCs to follow the oscillatory influence from the GCL. From a large set of studies, it has been established that simple spikes exhibit a variety of modulation patterns relative to movement, such as movement onset-timed increases or decreases in firing rate (Lamarre and Chapman, 1986; Medina and Lisberger, 2008; Ebner et al., 2011). At or just preceding movement onset, there is an important task-related change of state in the local neuronal network. This would modify how the oscillatory activity from the IO or the GCL could maintain their influence on the cerebellar cortex local circuits. In the case of an imminent movement, one could liken the interaction between the phasic sensorimotor information processing and the oscillatory processes to a neuronal tug-of-war, where these processes compete to influence the neuronal cerebellar cortex excitability. Indeed, the neuronal populations of PCs change state when going from immobility to movement, evidenced clearly in the case of the simple spikes. Other state-related changes, such as the bi-stability capacity of PCs, which differentiate neuronal responsivity (Loewenstein et al., 2005; Schonewille et al., 2006; Shin et al., 2007), could also affect the underlying measure with which baseline oscillations can exert influence on the PC neural sheet. As for the olivocerebellar CS activity, their rate is often increased after movement initiation, showing a change of state (Kitazawa et al., 1998; Medina and Lisberger, 2008). Again, this state change is likely an attractor that will affect and deter the PCs from following GCL oscillatory activity if the involved movement is phasic. In short, it appears that movement stops GCL oscillations, decreasing their oscillatory influence on PC simple spikes. At the same time, it appears that the phasic CS activity related to movement can monopolize olivocerebellar signaling. While the picture of olivocerebellar activity inferred by

CSs is not easy to identify due to their low firing rate ∼1 Hz, IO activity is directly related to movement initiation (Lang et al., 2006b).

In the context of going from immobility to movement, one could identify oscillatory interactions on the basis of sensorimotor spatiotemporal influences at the level of PCs (site #1). For example, the GCL oscillations, favoring a sagittal plane organization during immobility, expand their synchronization zone in a medio-lateral fashion, for a few millimeters, presumably to better synchronize the functional aspects of involved cerebellar zones (Courtemanche et al., 2009). In a similar manner, olivocerebellar CSs are better synchronized in the sagittal plane during immobility (Lang et al., 1999; Bosman et al., 2010), and re-organize this synchrony relative to movement (Welsh et al., 1995). This new organization specific for the task at hand produces a modified population code for the PCs, which were previously under the influence of both olivocerebellar and GCL oscillations. The olivocerebellar movement mosaic also appears to obey specific neural coding parameters, bringing together networks of PCs and resetting oscillations (Leznik et al., 2002), which would strongly signal movement initiation. One would expect that for specific GCL population codes going further up to PCs (Hartmann and Bower, 2001; Lu et al., 2005), the need to group together PCs pertaining to multiple receptive fields would require a networking mechanism such as oscillations, for the collection of information to produce an imminent movement. This is comparable to identifying a mechanism to bring together the multiple components of a cerebellar map (Apps and Hawkes, 2009), as is the case in other brain networks (Moser et al., 2010). However, when movement happens, it appears that the influence from the IO and GCL oscillations decreases its stronghold on the neuronal population, to make way for the phasic coding, which possibly acts as a reset. In a stimulus–response sensorimotor context, after the stimulus is given, the oscillations could then serve a network preparation role to optimize the neural populations that will serve to produce the upcoming response. For the case of phasic sensory activity, it appears that whisker sensory input favors the synchrony of simple spikes along the transverse plane, and that synchrony of CSs favor the sagittal plane (Bosman et al., 2010). Simple spikes seem to align better on-beam during movement, i.e., in the transverse plane and following the orientation of the parallel fibers (Heck et al., 2007). These quick and apparently information-specific changes of state in the networks would then favor more task-related information processing until the oscillatory stronghold on the networks resumes, similarly to the massive movement effect seen in the LFP synchrony (Courtemanche et al., 2009).

Finally, an interaction with faster and slower oscillations can be speculated with regards to movement. We already identified that fast (>150 Hz) oscillations are present under anesthesia, suggesting they do not require movement to be present. It is not known right now if in normal circuits, fast oscillations directly influence PCs during movement. However, as seen in the pathological circuits of knockout mice, they appear to be stopped by direct tactile stimulation (Cheron et al., 2005), in a manner similar to the slower oscillations in the GCL, or IO activity. Spatially, the faster oscillations seem to group together close-by PCs within a region less than 0.5 mm (de Solages et al., 2008), and maybe to a greater spatial extent in pathological models (Cheron et al., 2005). This spatial specificity for the higher frequency oscillations in the context of the cellular entrainment points to a capacity to have more localized change leading to a more information-specific involvement. This issue would have to be looked into further.

Evaluating the capacity of the DCN (site #2, **Figure 2B**) to entertain movement-related oscillatory interactions is a complex situation. Keating and Thach (1997) did not find strong evidence of rhythmicity in DCN unit firing. In a more recent report (Baumel and Cohen, 2012), there appears to be some rhythmic 7 Hz activity that can be recorded in the DCN; however, whether its source is from GCL or olivocerebellar activity cannot be determined yet. It also appears as though DCN activity could be related to rhythmicity in the electromyogram (Aumann and Fetz, 2004), playing a role in the way downward connections are affected by rhythmic efferent activity. There is a definitive advantage, though, for PC simple spikes to synchronize their activity onto common DCN target units, to increase the effectiveness of the connection (Person and Raman, 2012a,b). In this case, afferent oscillations could serve to provide the background for synchronous activity, increasing the likelihood of influencing DCN neurons via the synchronization of the PC firing. It is also known that the olivocerebellar activity can effectively influence the DCN neurons at a magnitude similar to the influence of simple spikes (Lang and Blenkinsop, 2011). This influence is beginning to be explored. It is clear, from recordings in IO units, that their rhythmic subthreshold oscillations, should they compound together, can provide the capacity to transmit rhythmic CSs to efferent targets (Chorev et al., 2007). Under the influence of harmaline, DCN neurons can be driven to fire in synchrony with the olivary activity (De Montigny and Lamarre, 1973; Lamarre, 1994). As for the olivocerebellar interactions affecting the GCL (site #3), in the same way that the IO can transmit rhythmic spikes to the PCs or to the DCN (Chorev et al., 2007), there is anatomical evidence that they can also influence the GCL, but a specific physiological relationship has not been reported or systematically studied.

NEUROPATHOLOGICAL ASPECTS

The link with oscillations and neuropathology for the cerebellar cortex is not as clear as is the case for the basal ganglia (Hutchison et al., 2004; Gatev et al., 2006). In Parkinsonian models, dopamine depletion leads to an increase in the oscillatory phenomena (Bergman et al., 1998; Hammond et al., 2007; Lemaire et al., 2012). Not all of the oscillations described in the above sections are primarily present in neuropathophysiological models; on the other hand, certain neuropathophysiological models appear to have enhanced types of oscillations. One interesting case, resembling essential tremor (Deuschl and Elble, 2000), is with the hyperrhythmicity in the olivocerebellar pathway produced by the administration of systemic harmaline to the animal, or directly in the IO. In these conditions, a strong IO population synchrony effect is produced by harmaline. The IO hypersynchrony increases the capacity to emit CSs and brings together much larger populations of PCs (see site #1, **Figure 2B**; Sugihara et al., 1995). The effect of this hypersynchrony on the GCL oscillations (relative

to site #2) is unknown. Such a hypersynchronous population pattern of activity could transmit rhythmic signals to the GCL, and drive the networks of the GCL (site #3) in a non-specific way (for example, triggering heightened diffuse synchrony in a manner out of the usual parasagittal plane dominance). This would have to be tested. Finally, with respect to oscillations in the cerebellar cortex at 4–25 Hz, Cheron et al. (2009) identified a role for BK (big potassium) calcium-activated potassium channels in PCs and Golgi cells. In mice where this channel has been knocked out, and consequently rendered ataxic, PC simple spikes show strong rhythmicity in the 15 Hz range. When comparing the LFPs with cell activity, the strong 15 Hz LFP component was tightly related to unit firing: PC simple spikes and CSs, and Golgi cells were phase-locked with the LFP. This model provides the opportunity to study multiple oscillatory interactions, both at the level of the PCL or the GCL. Another component is that the LFP oscillation synchrony appears to be less aligned with the sagittal plane than would be expected: the synchronization appears broad and strong in *both* transverse and sagittal orientations. This component would have implications on how the cerebellar cortex networks organize themselves relative to the sensorimotor maps, specifically by affecting DCN elements in a hypersynchronous mode, potentially removing the muscle/movement selectivity typically seen in ataxia.

Another disease which is related to the 4–25 Hz frequency range is the case of essential tremor, a disorder which is primarily characterized by a 4–12 Hz tremor (Lamarre, 1994; Pinto et al., 2003). A well-known clinical model of this disorder is the previously mentioned harmaline model. Harmaline-induced tremor is characterized by a strong, near 10 Hz tremor of the animal, very similar to the 4–12 Hz tremor observed in essential tremor patients (Lamarre, 1994). The mechanism of action of harmaline is thought to be a potentiation of $Ca_v3.1$ T-type Ca^{2+} channels in the IO that leads to strong subthreshold oscillations of IO cells and increase the probability of CF action potentials. Due to the strong CF–PC synapses, PCs are entrained to fire CSs at ∼10 Hz. This rhythmic activity, starting at the IO, spills over and then entrains the synchrony of upstream nodes of the Guillain–Mollaret triangle (rubral nucleus, olivary nucleus, and cerebellum), manifesting as tremor. This same basic mechanism is thought to be the cause of essential tremor, with a pathologically oscillating network comprising the IO, the cerebellum, the thalamus, and the motor cortex (Raethjen and Deuschl, 2012). Interestingly, deep brain stimulation of the ventral intermediate nucleus of the thalamus (Vim) is an efficacious treatment for essential tremor patients (Lozano and Lipsman, 2013). Although not monosynaptically connected to the IO, the Vim primarily receives input from the cerebellar nuclei, which receive input both directly and indirectly (through PCs) from the IO. With regard to the pathogenesis of essential tremor, the thalamus is considered to play an important role in coupling different regions of the nervous system (Buzsaki and Draguhn, 2004), with the olivocerebellar and primary motor cortex connections being of particular interest in essential tremor.

Schnitzler et al. (2009) found oscillatory coupling at tremor frequencies between brain areas, including subcortical areas such as the thalamus and cerebellum. Using magnetoencephalography (MEG), they showed cerebro-muscular and cerebro-cerebral coupling during a motor task. Additionally, Hanson et al. (2012) identified ensembles of Vim neurons that were oscillating at near-tremor frequencies between 2.5 and 7.5 Hz in essential tremor patients. However, there was no clear phase relationship between these oscillating units and tremor. Furthermore, Popa et al. (2013) found that repetitive bilateral transcranial magnetic stimulation of the posterior cerebellum of essential tremor patients improved all symptoms (e.g., tremor reduction, writing, pouring). The effects were progressive (ramping up over time), and persisted for up to 3 weeks after treatment (Popa et al., 2013). An additional benefit was that the functional connectivity of the cerebello-thalamo-cortical (CTC) network, evaluated using fMRI, was improved. When compared to controls, essential tremor patients had less functional connectivity within the CTC at baseline, but did show a partially re-established network connectivity of the CTC following the fifth day of treatment (Popa et al., 2013). With its neural and behavioral effects, this treatment seems promising. Although the pathophysiology of essential tremor remains elusive, the consensus remains that its genesis is related to a pathological synchrony of multiple areas, namely the olivocerebellum, thalamus, and motor cortex (Deuschl and Bergman, 2002).

Two other examples can be used to illustrate a neuropathological pattern at slower and faster frequencies. In the tottering mouse, the oscillations in the fluorescence measures (<1 Hz) seem to affect a large component of the cerebellar cortex circuits, including PCs (Chen et al., 2009). In this case, speculating on interactions of the oscillations at those nodes, a potential effect is that the PC output will again affect the DCN in a hypersynchronous fashion. This effect seems to be even more important during dystonic episodes, enough to trigger related rhythmic muscle contractions. Finally, in experiments on cerebellar mutant mice from the Chéron laboratory, faster oscillations seem to show heightened spatiotemporal synchrony. This is the case of the Angelman mouse model, where it appears like the fast (>150 Hz) oscillations in the cerebellar cortex are hypersynchronous for zones up to 1 mm (Cheron et al., 2005), a zone larger than normal fast coherence zones. Some of those fast oscillations are also seen in calretinin/calbindin mutant mice (Cheron et al., 2004, 2008), affecting the PC layer. In this model, the synchronization of fast oscillations appeared to follow the coronal plane, in line with the parallel fiber orientation, for a range up to 2 mm. For both these models, neural activity appears to show an increased synchrony at the level of the cerebellar cortex. This would also lead to a pattern of activity going to the DCN that lacks spatiotemporal selectivity.

In determining the effects of network oscillations in the cerebellar cortex, it appears that there are many different oscillatory phenomena that can coexist. At the same time, the potential for their interactions warrants that we define where and how they would influence one another, at the level of specific cells. We focused here on the PCL, the DCN, and the GCL. Finally, those interactions can be circumscribed in terms of certain behavioral conditions or circuit pathology. Future exciting research will firm up certain elements, but presently it appears that the immobility/movement interface is potentially influenced by the slow (<1 Hz), theta/beta rage (4–25 Hz), and fast (>150 Hz)

oscillations. Certain rodent models also permit the evaluation of a greater range of interactions and effects on movement, where hypersynchronous rhythmicity can adversely affect movement control.

GOING OUT OF THE CEREBELLUM, AND CONCLUSION

There is mounting evidence that cerebellar oscillations can interact with cerebral oscillations, potentially providing a long-range synchronization mechanism. These interactions have been identified in the rodent, the primate, and humans (O'Connor et al., 2002; Courtemanche and Lamarre, 2005; Soteropoulos and Baker, 2006; Kujala et al., 2007). More recent techniques for implantation of multiple microelectrodes over long periods of time are likely going to inform us about the role of the oscillations at various frequencies in triggering and modulating functional patterns of coherence in cerebro-cerebellar networks. Namely, in the context of this review, an important component is the temporal aspect of the flow of activity through and inside the cerebellum. What could be the potential roles that temporally patterned activity from the cerebellum would bring?

A first point of view is functional. A functional temporal aspect, focusing on oscillations, necessarily will rely on the structural aspects of the putative oscillators, basing interactions on the spatiotemporal properties of the neural activity. From many points of view, the cerebellum should provide accurate computations about the state of the world around us, and provide us with an enhanced capacity to further influence our environment by predicting our, and its, future state (Paulin, 1993; Bell et al., 1997, 2008; Courchesne and Allen, 1997). Oscillations in cerebellar circuits can certainly contribute to this time-dependent process, and help relate the cerebellar activity to other structures of the sensorimotor systems. Such rhythmicity could serve to synchronize its internal activity in a dynamic networks perspective but also ultimately to synchronize the activity of distant brain areas (Schnitzler and Gross, 2005). As such, with its long-range afferent input and long-range efferent penetration, the cerebellum, itself using oscillations and synchrony to coordinate its own components, could also act as a large-scale network synchronizer, via its synchronizing influences and buffering delay lines. This is akin to a role in helping to time neural operations in other structures (Llinás, 2011).

A second point of view when illustrating cerebro-cerebellar oscillatory interactions is more mechanistic. Cerebellar oscillations would influence the spatial and temporal patterns of activity in the cerebellar circuits, and the communications with the cerebrum. Cerebellar oscillations could also enhance communication with outside structures at precise times. One method to temporally control the flow of activity in a given structure is through oscillatory modulation of short periods of activity, separated by equally short silences (Sejnowski and Paulsen, 2006). Such activity has better temporal predictability. In the case of sensorimotor behavior, pre-movement oscillations in "motor" cerebral cortical areas have been identified for some time (Murthy and Fetz, 1992; Sanes and Donoghue, 1993). This corroborated, at the level of local recordings with electrodes having the capacity to resolve cells, certain elements that had been identified in earlier studies focusing on electroencephalographic (EEG) or ECoG signal (e.g., Bouyer et al., 1981; Pfurtscheller, 1981). The study of a more global sort of brain activity, from EEG to LFPs, and more recently MEG, brought a different perspective to researchers looking for cortical coding mechanisms of movement. These studies thus brought a new spin to traditional stories of information processing in sensorimotor circuits, adding a potential for oscillatory activity helping in the temporal control of the formation of neuronal circuits, a story already in full force for years in other brain areas such as the hippocampus (reviewed in Buzsaki and Draguhn, 2004; Buzsaki, 2006). The formation of systemic and local networks through their temporal properties is certainly an important component of the definition of task-related populations (Schnitzler and Gross, 2005). Such sensorimotor coding based on timed networks has been shown for cerebral mechanisms (Roelfsema et al., 1997; Singer et al., 1997; Buzsaki and Draguhn, 2004; Salazar et al., 2012), but temporal coding through oscillatory networks could even progress downward, affecting cerebral-to-spinal communications in LFP and EMG beta-range components (Baker et al., 1997), It has already been seen in MEG signals with gamma synchronization serving to organize corticospinal relationships (Schoffelen et al., 2005).

If oscillations play an important role in cerebellar circuitry, these rhythmicities need to serve to define co-active neural populations and to shape the modes of communication between those populations. While the anatomical connectivity must initially determine the way by which populations are defined, having been well studied by numerous researchers for cerebellar connectivity (Voogd, 1992; Parent, 1996; Voogd and Glickstein, 1998; Voogd and Paxinos, 2004) and cerebro-cerebellar relationships (Bloedel and Courville, 1981; Brodal et al., 1997; Schmahmann and Pandya, 1997; Middleton and Strick, 2000; Strick et al., 2009), the cerebellar circuits must also be defined spatiotemporally by the flow of neural activity at given points in time through the networks. Certain principles are often guides here: (1) the size of the interacting population is usually inversely proportional to the frequency of the oscillations, so the higher the frequency, the spatially smaller the involved circuits, while slower oscillations tend to integrate larger circuits through the loop delays (Buzsaki and Draguhn, 2004); and (2) networks with similar frequencies can more readily synchronize in a cooperative manner (Strogatz and Stewart, 1993; Strogatz, 2003).

Oscillations at slower frequencies thus appear to have a capacity to link together larger networks, or more distant components of larger networks. From this standpoint, oscillations at <1 Hz are likely to bring together the largest networks, as shown by Ros et al. (2009). However, a close second are the theta/beta-range oscillations (4–25 Hz), which appear to be coherent with cerebral cortex activity (O'Connor et al., 2002; Courtemanche and Lamarre, 2005). Finally faster oscillations (>150 Hz) appear less likely to have a cerebro-cerebellar role, potentially influencing more local circuit patterning. How oscillations help form a coherent network might also be as important as the oscillations' role in segmenting specific networks, both contributing to dynamic routing (Moser et al., 2010). Both of these effects could be beneficial for sensorimotor operations; the former could potentially unite cerebral and cerebellar populations into a coherent representation, the latter could potentially distinguish between different subpopulations

of the cerebellum and cerebrum for a more precise definition of a task-related (or operation-related) network.

ACKNOWLEDGMENTS

We gratefully thank Maxime Lévesque, Ettore Zucheroso, Carla Arasanz, Jonathan Bourget-Murray, and Andrew Chapman, for help and discussions. Some of the projects reported in this review were supported by fellowships and grants from the Natural Sciences and Engineering Research Council of Canada, and the National Alliance for Autism Research/Autism Speaks (U.S.A.), and by internal Concordia University grants, to Richard Courtemanche. This work also benefited from a Groupe grant from the Fonds de Recherche du Québec - Santé, to the Center for Studies in Behavioral Neurobiology.

REFERENCES

Adrian, E. D. (1935). Discharge frequencies in the cerebral and cerebellar cortex. *Proc. Phys. Soc.* 83, 32–33.

Apps, R., and Garwicz, M. (2005). Anatomical and physiological foundations of cerebellar information processing. *Nat. Rev. Neurosci.* 6, 297–311. doi: 10.1038/nrn1646

Apps, R., and Hawkes, R. (2009). Cerebellar cortical organization: a one-map hypothesis. *Nat. Rev. Neurosci.* 10, 670–681. doi: 10.1038/nrn2698

Armstrong, D. M., and Schild, R. F. (1970). A quantitative study of the Purkinje cells in the cerebellum of the albino rat. *J. Comp. Neurol.* 139, 449–456. doi: 10.1002/cne.901390405

Aumann, T. D., and Fetz, E. E. (2004). Oscillatory activity in forelimb muscles of behaving monkeys evoked by microstimulation in the cerebellar nuclei. *Neurosci. Lett.* 361, 106–110. doi: 10.1016/j.neulet.2003.12.091

Baker, M. R., and Edgley, S. A. (2006a). Reply from M. R. Baker and S. A. Edgley. *J. Physiol.* 573, 281–282. doi: 10.1113/jphysiol.2006.571102

Baker, M. R., and Edgley, S. A. (2006b). Non-uniform olivocerebellar conduction time in the vermis of the rat cerebellum. *J. Physiol.* 570, 501–506. doi: 10.1113/jphysiol.2005.099176

Baker, S. N., Olivier, E., and Lemon, R. N. (1997). Coherent oscillations in monkey motor cortex and hand muscle EMG show task-dependent modulation. *J. Physiol.* 501, 225–241. doi: 10.1111/j.1469-7793.1997.225bo.x

Baumel, Y., and Cohen, D. (2012). "DCN computation is compromised during harmaline-induced strong synchrony in *cerebellar Purkinje cells*," in *Society for Neuroscience Abstracts, p 580.517*, New Orleans, LA.

Bell, C. C., Bodznick, D., Montgomery, J. C., and Bastian, J. (1997). The generation and subtraction of sensory expectations within cerebellum-like structures. *Brain Behav. Evol.* 50, 17–31. doi: 10.1159/000113352

Bell, C. C., and Grimm, R. J. (1969). Discharge properties of Purkinje cells recorded on single and double microelectrodes. *J. Neurophysiol.* 32, 1044–1055.

Bell, C. C., Han, V., and Sawtell, N. B. (2008). Cerebellum-like structures and their implications for cerebellar function. *Annu. Rev. Neurosci.* 31, 1–24. doi: 10.1146/annurev.neuro.30.051606.094225

Bergman, H., Feingold, A., Nini, A., Raz, A., Slovin, H., Abeles, M., et al. (1998). Physiological aspects of information processing in the basal ganglia of normal and parkinsonian primates. *Trends Neurosci.* 21, 32–38. doi: 10.1016/S0166-2236(97)01151-X

Blenkinsop, T. A., and Lang, E. J. (2006). Block of inferior olive gap junctional coupling decreases Purkinje cell complex spike synchrony and rhythmicity. *J. Neurosci.* 26, 1739–1748. doi: 10.1523/JNEUROSCI.3677-05.2006

Bloedel, J. R., and Courville, J. (1981). "Cerebellar afferent systems," in *Handbook of Physiology. Section 1: The Nervous System.* Vol II. *Motor Control, Part 2*, ed. V. B. Brooks (Bethesda: American Physiological Society), 735–829.

Bosman, L. W., Koekkoek, S. K., Shapiro, J., Rijken, B. F., Zandstra, F., van der Ende, B., et al. (2010). Encoding of whisker input by cerebellar Purkinje cells. *J. Physiol.* 588, 3757–3783. doi: 10.1113/jphysiol.2010.195180

Bouyer, J. J., Montaron, M. F., and Rougeul, A. (1981). Fast fronto-parietal rhythms during combined focused attentive behaviour and immobility in cat: cortical and thalamic localizations. *Electroencephalogr. Clin. Neurophysiol.* 51, 244–252. doi: 10.1016/0013-4694(81)90138-3

Bower, J. M. (2002). The organization of cerebellar cortical circuitry revisited. *Ann. N. Y. Acad. Sci.* 978, 135–155. doi: 10.1111/j.1749-6632.2002.tb07562.x

Brand, S., Dahl, A. L., and Mugnaini, E. (1976). The length of parallel fibers in the cat cerebellar cortex. An experimental light and electron microscopic study. *Exp. Brain Res.* 26, 39–58. doi: 10.1007/BF00235248

Brodal, P., Bjaalie, J. G., de Zeeuw, C. I., Strata, P., and Voogd, J. (1997). "Salient anatomic features of the cortico-ponto-cerebellar pathway," in *Progress in Brain Research. The Cerebellum: From Structure to Function*, eds C. I. de Zeeuw, P. Strata, and J. Voogd (Amsterdam: Elsevier Science B.V.), 227–249.

Brookhart, J. M. (1960). "The cerebellum," in *Handbook of Physiology Section I: Neurophysiology II*, eds J. Field, and H. W. Magoun (Washington: American Physiological Society), 1245–1280.

Bryant, J. L., Boughter, J. D., Gong, S., LeDoux, M. S., and Heck, D. H. (2010). Cerebellar cortical output encodes temporal aspects of rhythmic licking movements and is necessary for normal licking frequency. *Eur. J. Neurosci.* 32, 41–52. doi: 10.1111/j.1460-9568.2010.07244.x

Bullock, T. H. (1997). Signals and signs in the nervous system: the dynamic anatomy of electrical activity is probably information-rich. *Proc. Natl. Acad. Sci. U.S.A.* 94, 1–6. doi: 10.1073/pnas.94.1.1

Buzsaki, G. (2006). *Rhythms of the Brain.* New York: Oxford University Press.

Buzsaki, G., and Draguhn, A. (2004). Neuronal oscillations in cortical networks. *Science* 304, 1926–1929. doi: 10.1126/science.1099745

Buzsaki, G., and Moser, E. I. (2013). Memory, navigation and theta rhythm in the hippocampal–entorhinal system. *Nat. Neurosci.* 16, 130–138. doi: 10.1038/nn.3304

Chen, G., Popa, L. S., Wang, X., Gao, W., Barnes, J., Hendrix, C. M., et al. (2009). Low-frequency oscillations in the cerebellar cortex of the tottering mouse. *J. Neurophysiol.* 101, 234–245. doi: 10.1152/jn.90829.2008

Cheron, G., Gall, D., Servais, L., Dan, B., Maex, R., and Schiffmann, S. N. (2004). Inactivation of calcium-binding protein genes induces 160 Hz oscillations in the cerebellar cortex of alert mice. *J. Neurosci.* 24, 434–441. doi: 10.1523/JNEUROSCI.3197-03.2004

Cheron, G., Sausbier, M., Sausbier, U., Neuhuber, W., Ruth, P., Dan, B., et al. (2009). BK channels control cerebellar Purkinje and Golgi cell rhythmicity in vivo. *PLoS ONE* 4:e7991. doi: 10.1371/journal.pone.0007991

Cheron, G., Servais, L., and Dan, B. (2008). Cerebellar network plasticity: from genes to fast oscillation. *Neuroscience* 153, 1–19. doi: 10.1016/j.neuroscience.2008.01.074

Cheron, G., Servais, L., Wagstaff, J., and Dan, B. (2005). Fast cerebellar oscillation associated with ataxia in a mouse model of Angelman syndrome. *Neuroscience* 130, 631–637. doi: 10.1016/j.neuroscience.2004.09.013

Chorev, E., Yarom, Y., and Lampl, I. (2007). Rhythmic episodes of subthreshold membrane potential oscillations in the rat inferior olive nuclei in vivo. *J. Neurosci.* 27, 5043–5052. doi: 10.1523/JNEUROSCI.5187-06.2007

Clement, E. A., Richard, A., Thwaites, M., Ailon, J., Peters, S., and Dickson, C. T. (2008). Cyclic and sleep-like spontaneous alternations of brain state under urethane anaesthesia. *PLoS ONE* 3:e2004. doi: 10.1371/journal.pone.0002004

Collins, D. R., Pelletier, J. G., and Pare, D. (2001). Slow and fast (gamma) neuronal oscillations in the perirhinal cortex and lateral amygdala. *J. Neurophysiol.* 85, 1661–1672.

Condorelli, D. F., Belluardo, N., Trovato-Salinaro, A., and Mudo, G. (2000). Expression of Cx36 in mammalian neurons. *Brain Res. Brain Res. Rev.* 32, 72–85. doi: 10.1016/S0165-0173(99)00068-5

Courchesne, E., and Allen, G. (1997). Prediction and preparation, fundamental functions of the cerebellum. *Learn. Mem.* 4, 1–35. doi: 10.1101/lm.4.1.1

Courtemanche, R., Chabaud, P., and Lamarre, Y. (2009). Synchronization in primate cerebellar granule cell layer local field potentials: basic anisotropy and dynamic changes during active expectancy. *Front. Cell. Neurosci.* 3:6. doi: 10.3389/neuro.03.006.2009

Courtemanche, R., and Lamarre, Y. (2005). Local field potential oscillations in primate cerebellar cortex: synchronization with cerebral cortex during active and passive expectancy.

J. Neurophysiol. 93, 2039–2052. doi: 10.1152/jn.00080.2004

Courtemanche, R., Pellerin, J. P., and Lamarre, Y. (2002). Local field potential oscillations in primate cerebellar cortex: modulation during active and passive expectancy. *J. Neurophysiol.* 88, 771–782. doi: 10.1152/jn.00080.2004

D'Angelo, E. (2008). The critical role of Golgi cells in regulating spatio-temporal integration and plasticity at the cerebellum input stage. *Front. Neurosci.* 2, 35–46. doi: 10.3389/neuro.01.008.2008

D'Angelo, E., and de Zeeuw, C. I. (2009). Timing and plasticity in the cerebellum: focus on the granular layer. *Trends Neurosci.* 32, 30–40. doi: 10.1016/j.tins.2008.09.007

D'Angelo, E., Koekkoek, S. K., Lombardo, P., Solinas, S., Ros, E., Garrido, J., et al. (2009). Timing in the cerebellum: oscillations and resonance in the granular layer. *Neuroscience* 162, 805–815. doi: 10.1016/j.neuroscience.2009.01.048

D'Angelo, E., Mazzarello, P., Prestori, F., Mapelli, J., Solinas, S., Lombardo, P., et al. (2011). The cerebellar network: from structure to function and dynamics. *Brain Res. Rev.* 66, 5–15. doi: 10.1016/j.brainresrev.2010.10.002

D'Angelo, E., Nieus, T., Maffei, A., Armano, S., Rossi, P., Taglietti, V., et al. (2001). Theta-frequency bursting and resonance in cerebellar granule cells: experimental evidence and modeling of a slow k+-dependent mechanism. *J. Neurosci.* 21, 759–770.

Dang-Vu, T. T., Schabus, M., Desseilles, M., Albouy, G., Boly, M., Darsaud, A., et al. (2008). Spontaneous neural activity during human slow wave sleep. *Proc. Natl. Acad. Sci. U.S.A.* 105, 15160–15165. doi: 10.1073/pnas.0801819105

Deans, M. R., Gibson, J. R., Sellitto, C., Connors, B. W., and Paul, D. L. (2001). Synchronous activity of inhibitory networks in neocortex requires electrical synapses containing connexin36. *Neuron* 31, 477–485. doi: 10.1016/S0896-6273(01)00373-7

De Montigny, C., and Lamarre, Y. (1973). Rhythmic activity induced by harmaline in the olivo-cerebello-bulbar system of the cat. *Brain Res.* 53, 81–95. doi: 10.1016/0006-8993(73)90768-3

de Solages, C., Szapiro, G., Brunel, N., Hakim, V., Isope, P., Buisseret, P., et al. (2008). High-frequency organization and synchrony of activity in the Purkinje cell layer of the cerebellum. *Neuron* 58, 775–788. doi: 10.1016/j.neuron.2008.05.008

de Zeeuw, C. I., Hoebeek, F. E., and Schonewille, M. (2008). Causes and consequences of oscillations in the cerebellar cortex. *Neuron* 58, 655–658. doi: 10.1016/j.neuron.2008.05.019

Deuschl, G., and Bergman, H. (2002). Pathophysiology of nonparkinsonian tremors. *Mov. Disord.* 17(Suppl. 3), S41–S48. doi: 10.1002/mds.10141

Deuschl, G., and Elble, R. J. (2000). The pathophysiology of essential tremor. *Neurology* 54(Suppl. 4), S14–S20. doi: 10.1212/WNL.54.4.14A

Devor, A., and Yarom, Y. (2002). Generation and propagation of subthreshold waves in a network of inferior olivary neurons. *J. Neurophysiol.* 87, 3059–3069.

Dieudonné, S. (1998). Submillisecond kinetics and low efficacy of parallel fibre-Golgi cell synaptic currents in the rat cerebellum. *J. Physiol.* 510, 845–866. doi: 10.1111/j.1469-7793.1998.845bj.x

Dieudonné, S., and Dumoulin, A. (2000). Serotonin-driven long-range inhibitory connections in the cerebellar cortex. *J. Neurosci.* 20, 1837–1848.

Dow, R. S. (1938). The electrical activity of the cerebellum and its functional significance. *J. Physiol.* 94, 67–86.

Dugué, G. P., Brunel, N., Hakim, V., Schwartz, E., Chat, M., Lévesque, M., et al. (2009). Electrical coupling mediates tunable low-frequency oscillations and resonance in the cerebellar Golgi cell network. *Neuron* 61, 126–139. doi: 10.1016/j.neuron.2008.11.028

Ebner, T. J., Hewitt, A. L., and Popa, L. S. (2011). What features of limb movements are encoded in the discharge of cerebellar neurons? *Cerebellum* 10, 683–693. doi: 10.1007/s12311-010-0243-0

Ebner, T. J., Wang, X., Gao, W., Cramer, S. W., and Chen, G. (2012). Parasagittal zones in the cerebellar cortex differ in excitability, information processing, and synaptic plasticity. *Cerebellum* 11, 418–419. doi: 10.1007/s12311-011-0347-1

Eccles, J. C. (1967). Circuits in the cerebellar control of movement. *Proc. Natl. Acad. Sci. U.S.A.* 58, 336–343. doi: 10.1073/pnas.58.1.336

Eccles, J. C., Ito, M., and Szentágothai, J. (1967). *The Cerebellum as a Neuronal Machine.* New York: Spinger-Verlag.

Edgley, S. A., and Lidierth, M. (1987). The discharges of cerebellar Golgi cells during locomotion in the cat. *J. Physiol.* 392, 315–332.

Forti, L., Cesana, E., Mapelli, J., and D'Angelo, E. (2006). Ionic mechanisms of autorhythmic firing in rat cerebellar Golgi cells. *J. Physiol.* 574, 711–729. doi: 10.1113/jphysiol.2006.110858

Fukuda, M., Yamamoto, T., and Llinás, R. (2001). The isochronic band hypothesis and climbing fibre regulation of motricity: an experimental study. *Eur. J. Neurosci.* 13, 315–326. doi: 10.1046/j.0953-816X.2000.01394.x

Gall, D., Roussel, C., Nieus, T., Cheron, G., Servais, L., D'Angelo, E., et al. (2005). Role of calcium binding proteins in the control of cerebellar granule cell neuronal excitability: experimental and modeling studies. *Prog. Brain Res.* 148, 321–328. doi: 10.1016/S0079-6123(04)48025-X

Gao, Z., van Beugen, B. J., and De Zeeuw, C. I. (2012). Distributed synergistic plasticity and cerebellar learning. *Nat. Rev. Neurosci.* 13, 619–635. doi: 10.1038/nrn3312

Gatev, P., Darbin, O., and Wichmann, T. (2006). Oscillations in the basal ganglia under normal conditions and in movement disorders. *Mov. Disord.* 21, 1566–1577. doi: 10.1002/mds.21033

Geurts, F. J., De Schutter, E., and Dieudonne, S. (2003). Unraveling the cerebellar cortex: cytology and cellular physiology of large-sized interneurons in the granular layer. *Cerebellum* 2, 290–299. doi: 10.1080/14734220310011948

Glasgow, S. D., and Chapman, C. A. (2007). Local generation of theta-frequency EEG activity in the parasubiculum. *J. Neurophysiol.* 97, 3868–3879. doi: 10.1152/jn.01306.2006

Goutagny, R., Jackson, J., and Williams, S. (2009). Self-generated theta oscillations in the hippocampus. *Nat. Neurosci.* 12, 1491–1493. doi: 10.1038/nn.2440

Gundappa-Sulur, G., De Schutter, E., and Bower, J. M. (1999). Ascending granule cell axon: an important component of cerebellar cortical circuitry. *J. Comp. Neurol.* 408, 580–596. doi: 10.1002/(SICI)1096-9861(19990614)408:4

Hammond, C., Bergman, H., and Brown, P. (2007). Pathological synchronization in Parkinson's disease: networks, models and treatments. *Trends Neurosci.* 30, 357–364. doi: 10.1016/j.tins.2007.05.004

Hanson, T. L., Fuller, A. M., Lebedev, M. A., Turner, D. A., and Nicolelis, M. A. (2012). Subcortical neuronal ensembles: an analysis of motor task association, tremor, oscillations, and synchrony in human patients. *J. Neurosci.* 32, 8620–8632. doi: 10.1523/JNEUROSCI.0750-12.2012

Harris, K. D., Csicsvari, J., Hirase, H., Dragoi, G., and Buzsáki, G. (2003). Organization of cell assemblies in the hippocampus. *Nature* 424, 552–556. doi: 10.1038/nature01834

Hartmann, M. J., and Bower, J. M. (1998). Oscillatory activity in the cerebellar hemispheres of unrestrained rats. *J. Neurophysiol.* 80, 1598–1604.

Hartmann, M. J., and Bower, J. M. (2001). Tactile responses in the granule cell layer of cerebellar folium crus IIa of freely behaving rats. *J. Neurosci.* 21, 3549–3563.

Hawkes, R., de Zeeuw, C. I., Strata, P., and Voogd, J. (1997). "An anatomical model of cerebellar modules," in *Progress in Brain Research. The Cerebellum: From Structure to Function*, eds C. I. de Zeeuw, P. Strata, and J. Voogd (Amsterdam: Elsevier Science B.V.), 39–52.

Hawkes, R., and Leclerc, N. (1987). Antigenic map of the rat cerebellar cortex: the distribution of parasagittal bands as revealed by monoclonal anti-Purkinje cell antibody mabQ113. *J. Comp. Neurol.* 256, 29–41. doi: 10.1002/cne.902560104

Heck, D. H., Thach, W. T., and Keating, J. G. (2007). On-beam synchrony in the cerebellum as the mechanism for the timing and coordination of movement. *Proc. Natl. Acad. Sci. U.S.A.* 104, 7658–7663. doi: 10.1073/pnas.0609966104

Heckroth, J. A., and Eisenman, L. M. (1988). Parasagittal organization of mossy fiber collaterals in the cerebellum of the mouse. *J. Comp. Neurol.* 270, 385–394. doi: 10.1002/cne.902700307

Herrup, K., and Kuemerle, B. (1997). The compartmentalization of the cerebellum. *Annu. Rev. Neurosci.* 20, 61–90. doi: 10.1146/annurev.neuro.20.1.61

Holtzman, T., Rajapaksa, T., Mostofi, A., and Edgley, S. A. (2006). Different responses of rat cerebellar Purkinje cells and Golgi cells evoked by widespread convergent sensory inputs. *J. Physiol.* 574, 491–507. doi: 10.1113/jphysiol.2006.108282

Hutchison, W. D., Dostrovsky, J. O., Walters, J. R., Courtemanche, R., Boraud, T., Goldberg, J., et al. (2004). Neuronal oscillations in the basal ganglia and movement disorders: evidence from whole animal and human recordings. *J. Neurosci.* 24, 9240–9243. doi: 10.1523/JNEUROSCI.3366-04.2004

Isope, P., Dieudonné, S., and Barbour, B. (2002). Temporal organization of activity in the cerebellar cortex: a manifesto for synchrony. *Ann. N. Y. Acad. Sci.* 978, 164–174. doi: 10.1111/j.1749-6632.2002.tb07564.x

Ito, M. (1989). Long-term depression. *Annu. Rev. Neurosci.* 12, 85–102. doi: 10.1146/annurev.ne.12.030189.000505

Ito, M. (2006). Cerebellar circuitry as a neuronal machine. *Prog. Neurobiol.* 78, 272–303. doi: 10.1016/j.pneurobio.2006.02.006

Ito, M. (2010). "Cerebellar Cortex," in *Handbook of Brain Microcircuits*, eds G. M. Shepherd and S. Grillner (New York: Oxford University Press), 293–300. doi: 10.1093/med/9780195389883.003.0028

Jacobson, G. A., Lev, I., Yarom, Y., and Cohen, D. (2009). Invariant phase structure of olivo-cerebellar oscillations and its putative role in temporal pattern generation. *Proc. Natl. Acad. Sci. U.S.A.* 106, 3579–3584. doi: 10.1073/pnas.0806661106

Jacobson, G. A., Rokni, D., and Yarom, Y. (2008). A model of the olivo-cerebellar system as a temporal pattern generator. *Trends Neurosci.* 31, 617–625. doi: 10.1016/j.tins.2008.09.005

Jensen, O., and Lisman, J. E. (2005). Hippocampal sequence-encoding driven by a cortical multi-item working memory buffer. *Trends Neurosci.* 28, 67–72. doi: 10.1016/j.tins.2004.12.001

Kalinichenko, S. G., and Okhotin, V. E. (2005). Unipolar brush cells – a new type of excitatory interneuron in the cerebellar cortex and cochlear nuclei of the brainstem. *Neurosci. Behav. Physiol.* 35, 21–36. doi: 10.1023/B:NEAB.0000049648.20702.ad

Keating, J. G., and Thach, W. T. (1995). Nonclock behavior of inferior olive neurons: interspike interval of Purkinje cell complex spike discharge in the awake behaving monkey is random. *J. Neurophysiol.* 73, 1329–1340.

Keating, J. G., and Thach, W. T. (1997). No clock signal in the discharge of neurons in the deep cerebellar nuclei. *J. Neurophysiol.* 77, 2232–2234.

Kitazawa, S., Kimura, T., and Yin, P. B. (1998). Cerebellar complex spikes encode both destinations and errors in arm movements. *Nature* 392, 494–497. doi: 10.1038/33141

Konig, P., and Engel, A. K. (1995). Correlated firing in sensory-motor systems. *Curr. Opin. Neurobiol.* 5, 511–519. doi: 10.1016/0959-4388(95)80013-1

Kujala, J., Pammer, K., Cornelissen, P., Roebroeck, A., Formisano, E., and Salmelin, R. (2007). Phase coupling in a cerebro-cerebellar network at 8–13 Hz during reading. *Cereb. Cortex* 17, 1476–1485. doi: 10.1093/cercor/bhl059

Lainé, J., and Axelrad, H. (1996). Morphology of the Golgi-impregnated Lugaro cell in the rat cerebellar cortex: a reappraisal with a description of its axon. *J. Comp. Neurol.* 375, 618–640. doi: 10.1002/(SICI)1096-9861(19961125)375

Lamarre, Y. (1994). "Central mechanisms of experimental tremor and their clinical relevance," in *Handbook of Tremor Disorders*, eds L. J. Findley and W. C. Koller (New York: Marcel Dekker Inc.), 103–118.

Lamarre, Y., and Chapman, C. E. (1986). Comparative timing of neuronal discharge in cortical and cerebellar structures during a simple arm movement in the monkey. *Exp. Brain Res. Ser.* 15, 14–27.

Lamarre, Y., De Montigny, C., Dumont, M., and Weiss, M. (1971). Harmaline-induced rhythmic activity of cerebellar and lower brain stem neurons. *Brain Res.* 32, 246–250. doi: 10.1016/0006-8993(71)90174-0

Lang, E. J. (2002). GABAergic and glutamatergic modulation of spontaneous and motor-cortex-evoked complex spike activity. *J. Neurophysiol.* 87, 1993–2008. doi: 10.1152/jn.00477.2001

Lang, E. J., and Blenkinsop, T. A. (2011). Control of cerebellar nuclear cells: a direct role for complex spikes? *Cerebellum* 10, 694–701. doi: 10.1007/s12311-011-0261-6

Lang, E. J., Llinás, R., and Sugihara, I. (2006a). Isochrony in the olivocerebellar system underlies complex spike synchrony. *J. Physiol.* 573, 277–279. doi: 10.1113/jphysiol.2006.571101

Lang, E. J., Sugihara, I., and Llinas, R. (2006b). Olivocerebellar modulation of motor cortex ability to generate vibrissal movements in rat. *J. Physiol.* 571, 101–120. doi: 10.1113/jphysiol.2005.102764

Lang, E. J., Sugihara, I., and Llinás, R. (1996). GABAergic modulation of complex spike activity by the cerebellar nucleoolivary pathway in rat. *J. Neurophysiol.* 76, 255–275.

Lang, E. J., Sugihara, I., Welsh, J. P., and Llinás, R. (1999). Patterns of spontaneous Purkinje cell complex spike activity in the awake rat. *J. Neurosci.* 19, 2728–2739.

Leclerc, N., Dore, L., Parent, A., and Hawkes, R. (1990). The compartmentalization of the monkey and rat cerebellar cortex: zebrin I and cytochrome oxidase. *Brain Res.* 506, 70–78. doi: 10.1016/0006-8993(90)91200-Z

Lemaire, N., Hernandez, L. F., Hu, D., Kubota, Y., Howe, M. W., and Graybiel, A. M. (2012). Effects of dopamine depletion on LFP oscillations in striatum are task- and learning-dependent and selectively reversed by L-DOPA. *Proc. Natl. Acad. Sci. U.S.A.* 109, 18126–18131. doi: 10.1073/pnas.1216403109

Leznik, E., and Llinas, R. (2005). Role of gap junctions in synchronized neuronal oscillations in the inferior olive. *J. Neurophysiol.* 94, 2447–2456. doi: 10.1152/jn.00353.2005

Leznik, E., Makarenko, V., and Llinas, R. (2002). Electrotonically mediated oscillatory patterns in neuronal ensembles: an in vitro voltage-dependent dye-imaging study in the inferior olive. *J. Neurosci.* 22, 2804–2815.

Llinás, R., Baker, R., and Sotelo, C. (1974). Electrotonic coupling between neurons in cat inferior olive. *J. Neurophysiol.* 37, 560–571.

Llinás, R., and Volkind, R. A. (1973). The olivo-cerebellar system: functional properties as revealed by harmaline-induced tremor. *Exp. Brain Res.* 18, 69–87. doi: 10.1007/BF00236557

Llinás, R. R. (2001). *I of the Vortex*. Cambridge: MIT Press.

Llinás, R. R. (2009). Inferior olive oscillation as the temporal basis for motricity and oscillatory reset as the basis for motor error correction. *Neuroscience* 162, 797–804. doi: 10.1016/j.neuroscience.2009.04.045

Llinás, R. R. (2011). Cerebellar motor learning versus cerebellar motor timing: the climbing fibre story. *J. Physiol.* 589, 3423–3432. doi: 10.1113/jphysiol.2011.207464

Llinás, R. R., Brookhart, J. M., and Mountcastle, V. B. (1981). "Electrophysiology of the cerebellar networks," in *Handbook of Physiology – The Nervous System II* (Bethesda: American Physiological Society), 831–876. doi: 10.1002/cphy.cp010217

Llinás, R. R., Humphrey, D. R., and Freund, H. J. (1991). "The noncontinuous nature of movement execution," in *Motor Control: Concepts and Issues* (Chichester: John Wiley and Sons), 223–242. doi: 10.1007/s00422-001-0307-9

Llinás, R. R., and Sugimori, M. (1992). "The electrophysiology of the cerebellar Purkinje cell revisited," in *The Cerebellum Revisited*, eds R. R. Llinás and C. Sotelo (New York: Springer-Verlag), 167–181.

Llinás, R. R., Walton, K. D., and Lang, E. J. (2004). "Cerebellum," in *The Synaptic Organization of the Brain*, ed. G. M. Shepherd (New York: Oxford University Press), 271–309.

Loewenstein, Y., Mahon, S., Chadderton, P., Kitamura, K., Sompolinsky, H., Yarom, Y., et al. (2005). Bistability of cerebellar Purkinje cells modulated by sensory stimulation. *Nat. Neurosci.* 8, 202–211. doi: 10.1038/nn1393

Lozano, A. M., and Lipsman, N. (2013). Probing and regulating dysfunctional circuits using deep brain stimulation. *Neuron* 77, 406–424. doi: 10.1016/j.neuron.2013.01.020

Lu, H., Hartmann, M. J., and Bower, J. M. (2005). Correlations between Purkinje cell single unit activity and simultaneously recorded field potentials in the immediately underlying granule cell layer. *J. Neurophysiol.* 94, 1849–1860. doi: 10.1152/jn.01275.2004

Maex, R., and De Schutter, E. (2005). Oscillations in the cerebellar cortex: a prediction of their frequency bands. *Prog. Brain Res.* 148, 181–188. doi: 10.1016/S0079-6123(04)48015-7

Mathy, A., Ho, S. S., Davie, J. T., Duguid, I. C., Clark, B. A., and Häusser, M. (2009). Encoding of oscillations by axonal bursts in inferior olive neurons. *Neuron* 62, 388–399. doi: 10.1016/j.neuron.2009.03.023

Medina, J. F., and Lisberger, S. G. (2008). Links from complex spikes to local plasticity and motor learning in the cerebellum of awake-behaving monkeys. *Nat. Neurosci.* 11, 1185–1192. doi: 10.1038/nn.2197

Middleton, F. A., and Strick, P. L. (2000). Basal ganglia and cerebellar loops: motor and cognitive circuits. *Brain Res. Brain Res. Rev.* 31, 236–250. doi: 10.1016/S0165-0173(99)00040-5

Middleton, S. J., Racca, C., Cunningham, M. O., Traub, R. D., Monyer, H., Knöpfel, T., et al. (2008). High-frequency network oscillations in cerebellar cortex. *Neuron* 58, 763–774. doi: 10.1016/j.neuron.2008.03.030

Moser, E. I., Corbetta, M., Desimone, R., Frégnac, Y., Fries, P., Graybiel, A. M., et al. (2010). "Coordination in brain systems," in *Dynamic Coordination in the Brain: From Neurons to Mind*, eds C. von der Marlsburg, W. A. Phillips, and W. Singer (Cambridge: MIT Press), 193–214.

Murthy, V., and Fetz, E. E. (1992). Coherent 25- to 35-Hz oscillations in the sensorimotor cortex of awake

behaving monkeys. *Proc. Natl. Acad. Sci. U.S.A.* 89, 5670–5674. doi: 10.1073/pnas.89.12.5670

Oberdick, J., Baader, S. L., and Schilling, K. (1998). From zebra stripes to postal zones: deciphering patterns of gene expression in the cerebellum. *Trends Neurosci.* 21, 383–390. doi: 10.1016/S0166-2236(98)01325-3

O'Connor, S., Berg, R. W., and Kleinfeld, D. (2002). Coherent electrical activity between vibrissa sensory areas of cerebellum and neocortex is enhanced during free whisking. *J. Neurophysiol.* 87, 2137–2148. doi: 10.1152/jn.00229.2001

Parent, A. (1996). *Carpenter's Neuroanatomy*, 9th Edn. New York: Williams and Wilkins.

Park, Y. G., Park, H. Y., Lee, C. J., Choi, S., Jo, S., Choi, H., et al. (2010). Ca(V)3.1 is a tremor rhythm pacemaker in the inferior olive. *Proc. Natl. Acad. Sci. U.S.A.* 107, 10731–10736. doi: 10.1073/pnas.1002995107

Paulin, M. G. (1993). The role of the cerebellum in motor control and perception. *Brain Behav. Evol.* 41, 39–50. doi: 10.1159/000113822

Paulsen, O., and Sejnowski, T. J. (2006). From invertebrate olfaction to human cognition: emerging computational functions of synchronized oscillatory activity. *J. Neurosci.* 26, 1661–1662. doi: 10.1523/JNEUROSCI.3737-05a.2006

Pellerin, J. P., and Lamarre, Y. (1997). Local field potential oscillations in primate cerebellar cortex during voluntary movement. *J. Neurophysiol.* 78, 3502–3507.

Perez-Orive, J., Mazor, O., Turner, G. C., Cassenaer, S., Wilson, R. I., and Laurent, G. (2002). Oscillations and sparsening of odor representations in the mushroom body. *Science* 297, 359–365. doi: 10.1126/science.1070502

Person, A. L., and Raman, I. M. (2012a). Synchrony and neural coding in cerebellar circuits. *Front. Neural Circuits* 6:97. doi: 10.3389/fncir.2012.00097

Person, A. L., and Raman, I. M. (2012b). Purkinje neuron synchrony elicits time-locked spiking in the cerebellar nuclei. *Nature* 481, 502–505. doi: 10.1038/nature10732

Pfurtscheller, G. (1981). Central beta rhythm during sensorimotor activities in man. *Electroencephalogr. Clin. Neurophysiol.* 51, 253–264. doi: 10.1016/0013-4694(81)90139-5

Pinto, A. D., Lang, A. E., and Chen, R. (2003). The cerebellothalamocortical pathway in essential tremor. *Neurology* 60, 1985–1987.

Popa, T., Russo, M., Vidailhet, M., Roze, E., Lehéricy, S., Bonnet, C., et al. (2013). Cerebellar rTMS stimulation may induce prolonged clinical benefits in essential tremor, and subjacent changes in functional connectivity: an open label trial. *Brain Stimul.* 6, 175–179. doi: 10.1016/j.brs.2012.04.009

Raethjen, J., and Deuschl, G. (2012). The oscillating central network of Essential tremor. *Clin. Neurophysiol.* 123, 61–64. doi: 10.1016/j.clinph.2011.09.024

Ray, A., Zoidl, G., Wahle, P., and Dermietzel, R. (2006). Pannexin expression in the cerebellum. *Cerebellum* 5, 189–192. doi: 10.1080/14734220500530082

Robinson, J., Ortiz-Pulido, R., Chapman, C. A., and Courtemanche, R. (2009). "Cerebellar cortex granule cell layer oscillations under urethane anesthesia, and inhibitory circuit manipulation," in *2009 Neuroscience Meeting Planner, Program No. 367.366.* (Chicago: Society for Neuroscience) Online.

Roelfsema, P. R., Engel, A. K., Kĥnig, P., and Singer, W. (1997). Visuomotor integration is associated with zero time-lag synchronization among cortical areas. *Nature* 385, 157–161. doi: 10.1038/385157a0

Ros, H., Sachdev, R. N., Yu, Y., Sestan, N., and McCormick, D. A. (2009). Neocortical networks entrain neuronal circuits in cerebellar cortex. *J. Neurosci.* 29, 10309–10320. doi: 10.1523/JNEUROSCI.2327-09.2009

Salazar, R. F., Dotson, N. M., Bressler, S. L., and Gray, C. M. (2012). Content-specific fronto-parietal synchronization during visual working memory. *Science* 338, 1097–1100. doi: 10.1126/science.1224000

Sanes, J. N., and Donoghue, J. P. (1993). Oscillations in local field potentials of the primate motor cortex during voluntary movement. *Proc. Natl. Acad. Sci. U.S.A.* 90, 4470–4474. doi: 10.1073/pnas.90.10.4470

Sasaki, K., Bower, J. M., and Llinás, R. (1989). Multiple Purkinje cell recording in rodent cerebellar cortex. *Eur. J. Neurosci.* 1, 572–586. doi: 10.1111/j.1460-9568.1989.tb00364.x

Scheibel, A. (1977). Sagittal organization of mossy fiber terminal system in the cerebellum of the rat: a Golgi study. *Exp. Neurol.* 57, 1067–1070. doi: 10.1016/0014-4886(77)90130-3

Schmahmann, J. D., and Pandya, D. N. (1997). Anatomic organization of the basilar pontine projections from prefrontal cortices in rhesus monkey. *J. Neurosci.* 17, 438–458.

Schnitzler, A., and Gross, J. (2005). Normal and pathological oscillatory communication in the brain. *Nat. Rev. Neurosci.* 6, 285–296. doi: 10.1038/nrn1650

Schnitzler, A., Munks, C., Butz, M., Timmermann, L., and Gross, J. (2009). Synchronized brain network associated with essential tremor as revealed by magnetoencephalography. *Mov. Disord.* 24, 1629–1635. doi: 10.1002/mds.22633

Schoffelen, J. M., Oostenveld, R., and Fries, P. (2005). Neuronal coherence as a mechanism of effective corticospinal interaction. *Science* 308, 111–113. doi: 10.1126/science.1107027

Schonewille, M., Khosrovani, S., Winkelman, B. H., Hoebeek, F. E., De Jeu, M. T., Larsen, I. M., et al. (2006). Purkinje cells in awake behaving animals operate at the upstate membrane potential. *Nat. Neurosci.* 9, 459–461. doi: 10.1038/nn0406-459

Sejnowski, T. J., and Paulsen, O. (2006). Network oscillations: emerging computational principles. *J. Neurosci.* 26, 1673–1676. doi: 10.1523/JNEUROSCI.3737-05d.2006

Shin, S. L., Hoebeek, F. E., Schonewille, M., De Zeeuw, C. I., Aertsen, A., and De Schutter, E. (2007). Regular patterns in cerebellar Purkinje cell simple spike trains. *PLoS ONE* 2:e485. doi: 10.1371/journal.pone.0000485

Sillitoe, R. V., Chung, S. H., Fritschy, J. M., Hoy, M., and Hawkes, R. (2008). Golgi cell dendrites are restricted by Purkinje cell stripe boundaries in the adult mouse cerebellar cortex. *J. Neurosci.* 28, 2820–2826. doi: 10.1523/JNEUROSCI.4145-07.2008

Singer, W., Engel, A. K., Kreiter, A. K., Munk, M. H., Neuenschwander, S., and Roelfsema, P. R. (1997). Neuronal assemblies: necessity, signature and detectability. *Trends Cogn. Sci.* 1, 252–261. doi: 10.1016/S1364-6613(97)01079-6

Solinas, S., Forti, L., Cesana, E., Mapelli, J., De Schutter, E., and D'Angelo, E. (2007). Fast-reset of pacemaking and theta-frequency resonance patterns in cerebellar Golgi cells: simulations of their impact in vivo. *Front. Cell. Neurosci.* 1:4. doi: 10.3389/neuro.03.004.2007

Soteropoulos, D. S., and Baker, S. N. (2006). Cortico-cerebellar coherence during a precision grip task in the monkey. *J. Neurophysiol.* 95, 1194–1206. doi: 10.1152/jn.00935.2005

Steriade, M. (2003). *Neuronal Substrates of Sleep and Epilepsy.* Cambridge: Cambridge University Press.

Steriade, M., Curro-Dossi, R., and Contreras, D. (1993). Electrophysiological properties of intralaminar thalamocortical cells discharging rhythmic (∼40 Hz) spike bursts at ∼1000 Hz during waking and rapid-eye movement sleep. *Neuroscience* 56, 1–9. doi: 10.1016/0306-4522(93)90556-U

Stern, E. A., Jaeger, D., and Wilson, C. J. (1998). Membrane potential synchrony of simultaneously recorded striatal spiny neurons in vivo *Nature* 394, 475–478. doi: 10.1038/28848

Strick, P. L., Dum, R. P., and Fiez, J. A. (2009). Cerebellum and nonmotor function. *Annu. Rev. Neurosci.* 32, 413–434. doi: 10.1146/annurev.neuro.31.060407.125606

Strogatz, S. H. (2003). *Sync: How Order Emerges from Chaos in the Universe, Nature, and Daily Life.* New York: Hyperion.

Strogatz, S. H., and Stewart, I. (1993). Coupled oscillators and biological synchronization. *Sci. Am.* 102–109. doi: 10.1038/scientificamerican1293-102

Sugihara, I., Lang, E. J., and Llinás, R. (1995). Serotonin modulation of inferior olivary oscillations and synchronicity: a multiple-electrode study in the rat cerebellum. *Eur. J. Neurosci.* 7, 521–534. doi: 10.1111/j.1460-9568.1995.tb00657.x

Vervaeke, K., Lorincz, A., Gleeson, P., Farinella, M., Nusser, Z., and Silver, R. A. (2010). Rapid desynchronization of an electrically coupled interneuron network with sparse excitatory synaptic input. *Neuron* 67, 435–451. doi: 10.1016/j.neuron.2010.06.028

Voogd, J. (1992). The morphology of the cerebellum the last 25 years. *Eur. J. Morphol.* 30, 81–96.

Voogd, J., and Glickstein, M. (1998). The anatomy of the cerebellum. *Trends Neurosci.* 21, 370–375. doi: 10.1016/S0166-2236(98)01318-6

Voogd, J., and Paxinos, G. (2004). "Cerebellum," in *The Rat Nervous System* (London: Elsevier Academic Press), 205–242.

Vos, B. P., Maex, R., Volny-Luraghi, A., and De Schutter, E. (1999). Parallel fibers synchronize spontaneous activity in cerebellar Golgi cells. *J. Neurosci.* 19:RC6.

Vranesic, I., Iijima, T., Ichikawa, M., Matsumoto, G., and Knopfel, T. (1994). Signal transmission in the parallel fiber-Purkinje cell system visualized by high-resolution imaging. *Proc. Natl. Acad. Sci. U.S.A.* 91, 13014–13017. doi: 10.1073/pnas.91.26.13014

Welsh, J. P. (2002). Functional significance of climbing-fiber synchrony: a population coding and behavioral analysis. *Ann. N. Y. Acad. Sci.* 978, 188–204. doi: 10.1111/j.1749-6632.2002.tb07567.x

Welsh, J. P., Ahn, E. S., and Placantonakis, D. G. (2005). Is autism due to brain desynchronization? *Int. J. Dev. Neurosci.* 23, 253–263. doi: 10.1016/j.ijdevneu.2004.09.002

Welsh, J. P., Lang, E. J., Sugihara, I., and Llinás, R. (1995). Dynamic organization of motor control within the olivocerebellar system. *Nature* 374, 453–457. doi: 10.1038/374453a0

Welsh, J. P., and Llinas, R. (1997). Some organizing principles for the control of movement based on olivocerebellar physiology. *Prog. Brain Res.* 114, 449–461. doi: 10.1016/S0079-6123(08)63380-4

Welsh, J. P., Schwarz, C., and Nicolelis, M. A. L. (1999). "Multielectrode recording from the cerebellum," in *Methods for Neural Ensemble Recordings*, eds S. A. Simon and M. A. L. Nicolelis (Boca Raton: CRC Press), 79–100.

Wu, X., Ashe, J., and Bushara, K. O. (2011). Role of olivocerebellar system in timing without awareness. *Proc. Natl. Acad. Sci. U.S.A.* 108, 13818–13822. doi: 10.1073/pnas.1104096108

Xu, D., Liu, T., Ashe, J., and Bushara, K. O. (2006). Role of the olivo-cerebellar system in timing. *J. Neurosci.* 26, 5990–5995. doi: 10.1523/JNEUROSCI.0038-06.2006

Yamazaki, T., and Tanaka, S. (2005). Neural modeling of an internal clock. *Neural Comput.* 17, 1032–1058. doi: 10.1162/0899766053491850

Zhang, H., Lin, S. C., and Nicolelis, M. A. (2010). Spatiotemporal coupling between hippocampal acetylcholine release and theta oscillations in vivo. *J. Neurosci.* 30, 13431–13440. doi: 10.1523/JNEUROSCI.1144-10.2010

Conflict of Interest Statement: The authors declare that the research was conducted in the absence of any commercial or financial relationships that could be construed as a potential conflict of interest.

Received: 17 January 2013; paper pending published: 15 March 2013; accepted: 11 July 2013; published online: 29 July 2013.

Citation: Courtemanche R, Robinson JC and Aponte DI (2013) Linking oscillations in cerebellar circuits. Front. Neural Circuits ***7****:125. doi: 10.3389/fncir.2013.00125*

frontiers in
NEURAL CIRCUITS

REVIEW ARTICLE
published: 22 February 2013
doi: 10.3389/fncir.2013.00001

Error detection and representation in the olivo-cerebellar system

Masao Ito*

Senior Advisor's Office, RIKEN Brain Science Institute, Wako, Saitama, Japan

Edited by:
Egidio D'Angelo, University of Pavia, Italy

Reviewed by:
Naoshige Uchida, Harvard University, USA
Yang Dan, University of California, Berkeley, USA

****Correspondence:***
Masao Ito, RIKEN Brain Science Institute, 2-1 Hirosawa, Wako, Saitama 351-0198, Japan.
e-mail: masao@brain.riken.jp

Complex spikes generated in a cerebellar Purkinje cell via a climbing fiber have been assumed to encode errors in the performance of neuronal circuits involving Purkinje cells. To reexamine this notion in this review, I analyzed structures of motor control systems involving the cerebellum. A dichotomy was found between the two types of error: sensory and motor errors play roles in the feedforward and feedback control conditions, respectively. To substantiate this dichotomy, here in this article I reviewed recent data on neuronal connections and signal contents of climbing fibers in the vestibuloocular reflex (VOR), optokinetic eye movement response, saccade, hand reaching, cursor tracking, as well as some other cases of motor control. In our studies, various sources of sensory and motor errors were located in the neuronal pathways leading to the inferior olive. We noted that during the course of evolution, control system structures involving the cerebellum changed rather radically from the prototype seen in the flocculonodular lobe and vermis to that applicable to the cerebellar hemisphere. Nevertheless, the dichotomy between sensory and motor errors is maintained.

Keywords: adaptation, error, internal model, microcomplex, motor learning

INTRODUCTION

Since the early discussions held around 1970 (see Ito, 2002), it has generally been assumed that climbing fibers emerging from the inferior olive convey error signals, which play a teacher's role in the learning mechanism of the cerebellum. However, where and how such error signals are derived and encoded in climbing fiber activities remains unclarified. In particular, problems regarding the sensory vs. motor nature of error signals and forward vs. inverse internal models have been debated (for example, Kobayashi et al., 1998; Winkelman and Frens, 2006; Ebner and Pasalar, 2008). Here, I attempt to clarify the problems by reexamining the control system structures of the cerebellum on the basis of recent experimental data on neuronal connections and signal contents of climbing fiber discharges in various cases of motor control involving the olivo-cerebellar system.

ADAPTIVE CONTROL SYSTEM MODEL OF THE CEREBELLUM

The errors that I am concerned with here are defined in terms of a basic scheme for adaptive control systems (**Figures 1A,B**). In this scheme, the controller converts instructions to motor commands, which in turn act on a controlled object that finally yields output responses to realize the instruction. An error is defined as the discrepancy between two lines of information, namely, instruction on the movement to be performed and information about the produced movement. Signals representing such an error then drive the adaptive mechanism attached to the controller.

There are two obvious ways to compute such an error as defined above. First, as shown in **Figure 1A**, when a control system performs feedforward control without an ongoing feedback, a comparator is required to compare between signals representing the desired movement and signals representing the performed movement received via respective pathways (red lines). These two lines of information are both represented in sensory coordinates as "kinematics" description of motion of the body or its parts in terms of position, velocity, acceleration, and direction. Errors derived from their comparison are also represented in sensory coordinates and are hence often called sensory errors.

In contrast, when a control system performs feedback control, the controller is driven by the difference between the desired and produced movements. In this situation, the controller itself acts as a comparator, as shown in **Figure 1B**. The sensory errors so derived at the inputs of the controller are readily converted by the controller to errors in motor commands, called motor errors. Motor errors are represented in motor-command coordinates in terms of "dynamics" description of motion such as force that causes motion. Kawato and his associates (Kawato et al., 1987; Kawato and Gomi, 1992a,b; Kawato, 1999) proposed an ingenious idea of feedback-error learning, that is, the motor errors derived by the primary motor cortex as a feedback controller play a crucial role in the learning mechanism of the cerebellum for arm movements (see below and **Figure 3B**). Based on these considerations, we here define sensory errors as detected by sensory systems and represented in sensory coordinates and motor errors as implied in motor commands and represented in motor command coordinates.

The microcomplex is the structural and functional unit module of neuronal circuits in the cerebellum derived from recent experimental studies (see Ito, 1984, 2006). It is a convenient biological concept corresponding to a block in control systems.

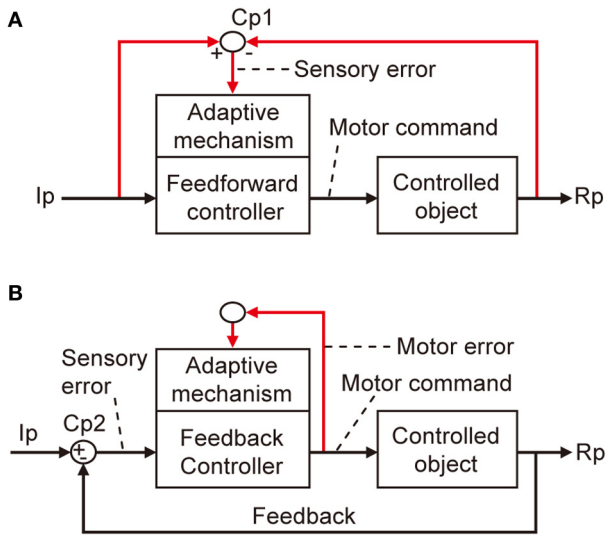

FIGURE 1 | Two types of adaptive control system. (A) Without online feedback. **(B)** With online feedback. Pathways for computing error signals are indicated by red lines.

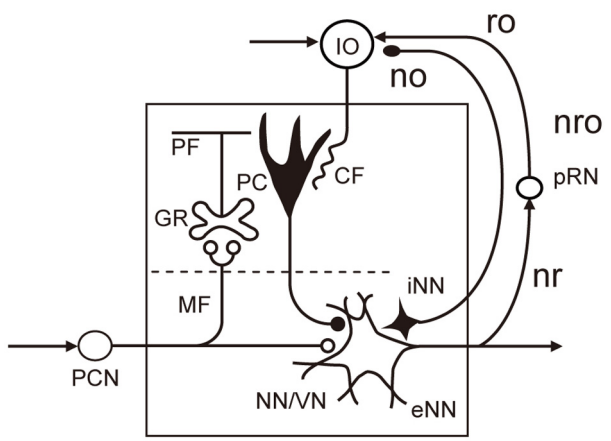

FIGURE 2 | Basic circuit structure of microcomplex. Abbreviations: CF, climbing fiber; GR, granule cell; IO, inferior olive; MF, mossy fiber; NN/VN, nuclear neuron/vestibular nuclear neuron; no, nucleoolivary pathway; nro, nucleorubroolivary pathway; PC, Purkinje cell; PCN, precerebellar neuron; PF, parallel fiber; pRN, parvocellular red nucleus; eNN, excitatory nuclear neuron; iNN, inhibitory nuclear neuron; ro, rubroolivary pathway; nr, nucleorubral pathway Inhibitory neurons are in black (others are excitatory).

As shown in **Figure 2**, each microcomplex consists of a microzone of the cerebellar cortex and associated cerebellar or vestibular nuclei. Each microcomplex receives major input signals via mossy fibers and converts them to an output of cerebellar or vestibular nuclear neurons. Each microcomplex also receives climbing fiber signals encoding errors for learning. (It also receives signals of beaded fibers for neuromodulation, but for simplicity, this will not be dealt with in this review). Climbing fibers originate from the inferior olive and pass the cerebellar cortex to supply strong excitatory synapses to Purkinje cells and other inhibitory interneurons. Collaterals of mossy fibers and climbing fibers also innervate cerebellar/vestibular nuclear neurons. Note that nuclear neurons, not Purkinje cells, are the output of the microcomplex.

The learning capability of a microcomplex is evident because microcomplex lesioning leads to the loss of adaptability in a relevant specific control function, as will be reviewed below. To discuss neural mechanisms of this learning capability in detail is beyond the scope of this review; hence, only two issues are mentioned here. One is that long-term potentiation/depression (LTP/LTD) as a neural substrate of memory is now located not only in the cerebellar cortex but also in the vestibular/cerebellar nucleus (see McElvain et al., 2010). Although synaptic plasticity is exhibited at many sites in the cerebellar tissues (D'Angelo et al., 1999; Hansel et al., 2001), LTD occurring at parallel fiber-Purkinje cell synapses conjunctively activated by climbing fibers has been considered to play a major role in fast adaptation, whereas LTP occurring at mossy fiber collateral-to-nuclear cell synapses accounts for slow adaptation (see below). These two types of adaptation are not parallel processes independent of each other, because cortical adaptation is required for initiation of nuclear adaptation (Kassardjian et al., 2005), as if memory trace shifts in time from the cortex to the nucleus (Okamoto et al., 2011). Another issue is that, although motor learning usually does not occur when LTD is impaired by pharmacological or genetic manipulation, the three types of mutant mouse generated by Schonewille et al. (2011) exhibit apparently normal motor learning even when LTD does not occur *in vitro* in cerebellar slices obtained from these mice. In another study, protein synthesis inhibitors readily blocked LTD induction *in vitro* (Karachot et al., 2001), but when injected into the cerebellar flocculus these inhibitors had virtually no effect on the fast optokinetic adaptation (see below), which has been related to LTD induction (Okamoto et al., 2011). This LTD-motor learning mismatch has been considered as being contradictory to the so-called Marr-Albus-Ito hypothesis, but I would like to point out that LTD is tested *in vitro* in slices, which function under fundamentally artificial conditions; slices are disconnected in electrical and chemical signaling from surrounding tissues and potential plasticity factors could be continuously washed out by perfusates. Moreover, to induce LTD in slices, artificial stimuli composed of electric pulses (repeated 300 times at 1 Hz) must be applied. It is possible that a disturbance could easily disrupt LTD induction *in vitro*, whereas LTD induction by natural stimuli under *in vivo* conditions might remain robust so that its blockade under similar conditions or perturbation could be relatively difficult. This possibility needs to be examined in future studies.

The microcomplex provides a neural substrate of internal models incorporated in the cerebellar control system (Kawato et al., 1987; Wolpert et al., 1998). Two types of internal model of the controlled object have been defined. The "inverse" model has the inputs and outputs corresponding to the outputs and inputs of a controlled object, and can serve by itself as an adaptive feedforward controller (**Figure 3A**). The forward model, in contrast, has the input and output corresponding to the input and output of a controlled object, and simulates the performance of the controlled object in feedback control (**Figure 3B**).

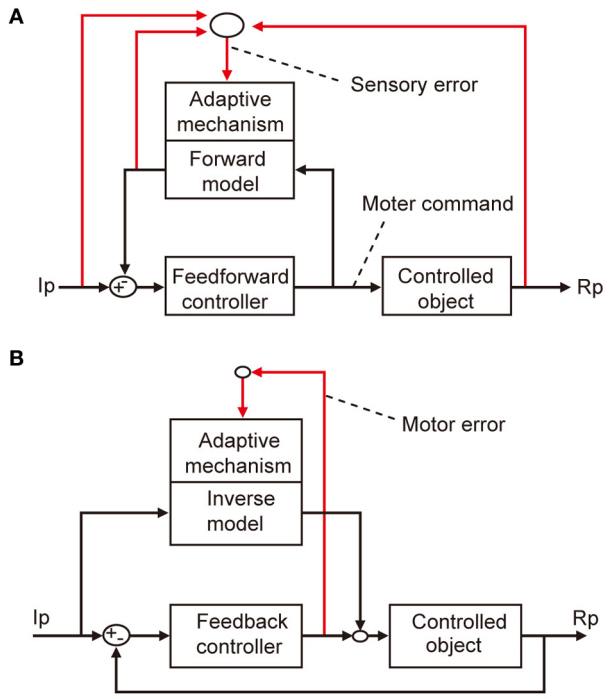

FIGURE 3 | Two types of internal model. (A) Forward model linked to feedforward controller. **(B)** Inverse model linked to feedback controller.

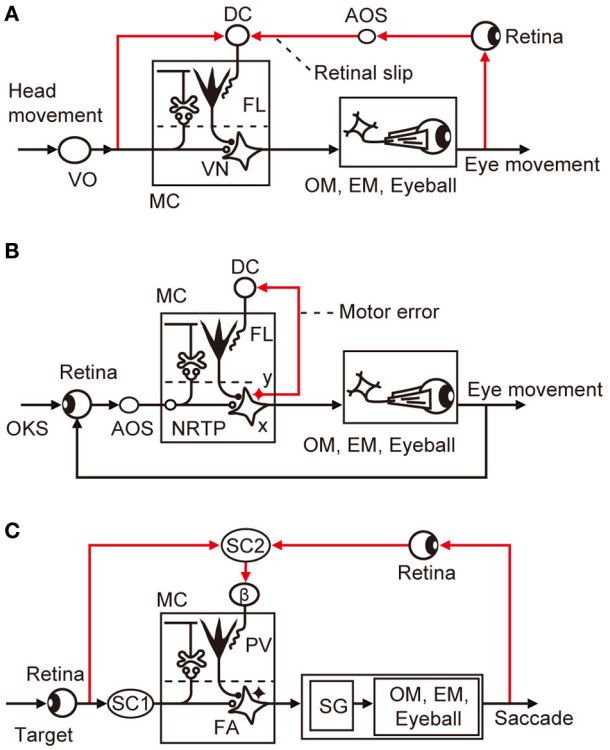

FIGURE 4 | Control system structure for three types of eye movement reflex. (A) VOR. **(B)** OKR. **(C)** saccade. Additional abbreviations: β, β subnucleus of inferior olive; DC, dorsal cap; EM, extraocular muscle; FA, fastigial nucleus; NRTP, nucleus reticularis tegmenti pontis; OKS, optokinetic stimulus; OM, oculomotor neurons; SC, superior colliculus; SG, saccade generator; AOS, accessory optic system; FL, flocculus; VN, vestibular nuclear neuron; MC, microcomplex; VO, vestibular organ; PV, posterior vermis; x, vestbuloocular relay neuron; y, vestibular nuclear neuron working in parallel with x.

VESTIBULOOCULAR REFLEX (VOR)

VOR has been explored as a model system of cerebellar control. As it is evoked by a head movement and causes a compensatory eye movement, VOR is a purely feedforward control lacking feedback (**Figure 4A**); hence, it should have a control system structure in which an adaptive mechanism is driven by sensory errors (**Figure 1A**). Note that VOR contains 14 component reflexes (Ezure and Graf, 1984) arising from six semicircular canals (three on each side) and four otolith organs (two on each side) and ending at different extraocular muscles (six on each side), but for simplicity, we focus on the horizontal canal-ocular reflex unless otherwise stated. When the head rotates ipsilaterally under illumination, the eyes rotate contralaterally to stabilize the retinal images of the external world. Here, the net discrepancy between the instruction given by head rotation via the vestibular organ and the information about the eye movements mediated by the retina represents sensory errors, which are called retinal slips.

Retinal slips can be manipulated by changing the relationship between head movements and movements of the visual environment using magnifying or minifying lenses, right-left converting prisms, or an inphase/outphase combination of head oscillation and screen oscillation. When an animal is continuously exposed to such manipulated retinal errors, the gain of VOR adaptively increases or decreases to minimize retinal slips. This paradigm causes the fast VOR adaptation that develops in 1 h and the slow adaptation that develops in 1 week (Kassardjian et al., 2005; Anzai et al., 2010). The fast VOR adaptation is mediated by the flocculus cortex, whereas the slow VOR adaptation is mediated by the vestibular nuclei.

Controller neurons for VOR are located in the vestibular nuclei; they receive excitatory inputs from vestibular afferents, which also project, directly or indirectly, to the flocculus as mossy fibers. VOR relay neurons also receive inhibitory innervation by Purkinje cells from a microzone in the flocculus (Sekimjak et al., 2003). Climbing fibers derived from the dorsal cap of the inferior olive project to floccular Purkinje cells. Dorsal cap neurons are activated by visual signals via the accessory optic system (AOS). The microcomplex so constructed constitutes an inverse model of the controlled object involving oculomotor neurons, extraocular muscles, and eyeballs, and is considered to serve as a feedforward adaptive controller for VOR (**Figure 4A**).

In **Figure 4A**, the dorsal cap is placed in the position for the comparator that computes retinal slips (compare with **Figure 1A**). It has been somewhat puzzling that floccular Purkinje cells receive climbing fiber signals during head rotation in darkness in the absence of vision to detect errors (Ghelarducci et al., 1975; Simpson et al., 2002). However, as seen in **Figure 4A**, vestibular signals represent an instruction on the extent to which the eyes should move to compensate for head movement, and are therefore important inputs to the comparator. How vestibular sensory signals reach the inferior olive is still unclear, but a likely

candidate of relay is the nucleus prepositus hypoglossi, which passes major inhibitory inputs to the dorsal cap (De Zeeuw et al., 1993). The nucleus prepositus hypoglossi contains neurons sensitive to horizontal head rotation (Lannou et al., 1984; McFarland and Fuchs, 1992).

These observations support the view that the dorsal cap acts as the comparator for VOR. If VOR works as shown in **Figure 4A**, involvement of motor errors in VOR adaptation is unlikely because there is no way to generate feedback errors in this purely feedforward control system. However, caution is needed regarding the interpretation of the finding that, under illumination, VOR operates jointly with the optokinetic eye movement response (OKR), which is a feedback control and may therefore introduce motor errors (see below).

OKR

OKR moves an eye to follow a relatively slowly moving visual environment. It is a feedback control system equipped with a visual feedback loop, and is a typical example in which a feedback controller generates motor errors. OKR exhibits an adaptive gain increase toward unity during prolonged sinusoidal oscillation of the visual environment around a stationary subject. Its short-term (fast) adaptation develops during a 1-h screen oscillation and diminishes throughout the subsequent 24 h. In contrast, long-term (slow) adaptation of OKR is established by repeated sessions of screen rotation for 7 days, and it persists for a week even after the flocculus is injected with locally acting lidocaine (Shutoh et al., 2006). Slow OKR adaptation is underlain by LTP in vestibular nerve-VOR relay neuron synapses. These lines of evidence suggest that the memory of fast OKR adaptation formed in the flocculus may subsequently induce the memory of slow adaptation in vestibular nuclear neurons (Okamoto et al., 2011).

In **Figure 4B**, we may assume that retinal slips are derived by comparing visually monitored eye movements with optokinetic stimuli at the inputs of the controller and are converted via the controller to motor errors. The motor errors so derived would drive the adaptive mechanism attached to the feedback controller as analyzed by Kawato and Gomi (1992b). Because there is no known recurrent collaterals of VOR relay neurons to the inferior olive, it is probable that a group of vestibular nuclear neurons, working in parallel to the VOR relay neurons, convey motor error signals to the dorsal cap (**Figure 4A**). A candidate for such neurons may also be found in the nucleus prepositus hypoglossi; it contains neurons not only sensitive to head velocity, as mentioned above, but also those sensitive to eye velocity (McFarland and Fuchs, 1992).

VOR and OKR share the same controller (microcomplex) and controlled object. The adaptive mechanism is also shared commonly so that VOR and OKR are simultaneously adapted even when exposed to adaptation separately. Indeed, sustained sinusoidal oscillation of a striped cylindrical screen around a stationary, alert pigmented rabbit for 4 h not only increased the OKR gain by 0.23, but also induced a simultaneous increase in the VOR gain by 0.18 (Nagao, 1989). Purkinje cell spikes recorded from the floccular areas related to horizontal eye movements (H-zone) normally exhibit modulation of simple spike discharges in phase with screen velocity and out of phase with turntable velocity. Sustained screen oscillation for 1 h enhanced the simple spike responses to not only the screen but also the turntable oscillation. These observations suggest that the adaptive mechanism of the controller is common to VOR and OKR.

Because of the overlap of neuronal circuits for VOR and OKR, it may be expected that the dorsal cap mediates both sensory and motor errors. However, it is generally difficult to isolate movement-related motor signals from stimulus-induced sensory signals because the stimulus causes movements that generate motor signals. Winkelman and Frens (2006) applied visual motion noise stimuli to a rabbit to break the tight relationship between instantaneous visual stimuli and eye movements. They found that climbing fiber signals contain motor signals two-fold the sensory signals. However, caution is needed in interpreting this finding because movement-related signals so detected may not always represent genuine motor errors (errors in motor commands); some of them may merely reflect visual perception of eye movements.

When evoked with a single moving dot pattern, climbing fiber signals are related to retinal slips. However, when Frens et al. (2001) applied two sets of patterns (one stationary and the other moving) in superposition, thereby generating two sets of differently moving retinal slips in superposition, the evoked climbing fiber discharges to floccular Purkinje cells were modulated by retinal slips generated by the moving dots, but not by the mixed retinal slips. Frens et al. (2001) interpreted this observation as negating the proposition that climbing fiber discharges represent retinal slips. Nevertheless, how rabbit AOS responds to such mixed retinal slips has not been clarified, and the possibility that two sets of retinal slips presented simultaneously interact nonlinearly with each other in the visual pathway mediated by AOS should be examined.

SACCADIC EYE MOVEMENT

A saccade is a quick, simultaneous movements of both eyes in the same direction to catch a visual target by small foveal areas of the retinas for high-acuity vision. Because of the very rapid (ballistic) eye movements in a saccade, it is not possible to control moving eyes by ongoing visual feedback; it is a purely feedforward control to which the sensory-error-learning scheme in **Figure 1A** should typically apply. Errors in a saccade are detected by comparison between the shift of the target spot in the retina that provokes a saccade and the shift of the eye position made by the saccade, both being projected to the map of the superior colliculus. The saccadic adaptation can be induced by repeatedly shifting the target while a saccadic movement is under way (for example, from 15° to 10° or 20°, the resultant eye position ending 5° long or short of the target). The saccade to the initial target position is followed by a corrective saccade to hit the shifted target position. After repeated trials, the eyes become able to catch the shifted position by only one saccade. This paradigm provides a favorable opportunity to explore the neuronal mechanism of error representation in climbing fibers (Soetedjo et al., 2008; Kojima et al., 2010).

Lesions in the posterior vermis permanently abolished this saccadic adaptation (McLaughlin, 1967). In most Purkinje cells

tested in this area by Soetedjo et al. (2008), the probability of complex spike firing increases in the "error interval" between the primary and corrective saccades. In most Purkinje cells, complex spikes occur around 100 ms after the error onset. The probability of complex spike occurrence depends on both error direction and size. These observations are in good agreement with the concept that complex spikes encode sensory errors (although some different observations and interpretations were reported by Catz et al., 2005). Kojima et al. (2007) located the pathway that conveys such errors in saccadic adaptation in the monkey midbrain tegmentum. Weak electrical stimulation of this pathway at ∼200 ms after a saccade in one horizontal direction produces changes in saccade gain, similar to changes induced by adaptation to real visual errors. This pathway appears to emerge from the superior colliculus and projects to subnucleus β of the medial accessory nucleus of the inferior olive, which in turn projects to the posterior vermis (Yamada and Noda, 1987; Kyuhou and Matsuzaki, 1991).

The microcomplex for control of saccade involves the posterior vermal cortex and caudal portion of the fastigial nucleus (Robinson et al., 1993). In depicting the entire control system structure for saccades in **Figure 4C**, the brainstem saccade generator circuit (Ramat et al., 2007) is placed within the control object that also includes the oculomotor system with eyeballs. The subnucleus β receives a strong input from the intermediate layer of the superior colliculus (Huerta and Harting, 1984), which contains neurons that discharge maximally for visual stimuli falling on a particular area of the contralateral hemifield (for review, see Sparks and Hartwich-Young, 1989). One may assume that these neurons could mediate the visual information of the target before and after saccades, from which error signals are produced at the β nucleus. The intermediate layer of the superior colliculus also contains many neurons that discharge prior to a saccade. This motor activity, however, seems irrelevant to climbing fibers because no complex spikes discharge to the dorsal vermis with a clear relationship to eye movements in the saccade (Soetedjo et al., 2008).

HAND REACH AND CURSOR TRACKING

In the hand-reach paradigm adopted by Kitazawa et al. (1998), the monkey saw its hand and fingers and the target before and after completion of the movement, but the movement itself was performed without visual feedback. In this case, Purkinje cells in cerebellar lobules HIV–HVI exhibited multiply timed climbing fiber responses at three different stages of the movement (first, second, and third responses). The third response occurred at the end point of the movement, apparently representing visually perceived deviations between the target and the reaching finger's end position. However, the first and second Purkinje cell responses appeared too early to be interpreted similarly.

On the other hand, in the visually guided wrist tracking movement adopted by Mano et al. (1986), a monkey followed a moving target with a cursor in the screen, which was driven with a handle moved by flexion or extension of the wrist. In this visually guided wrist tracking, Purkinje cells in the cerebellar hemisphere (lobules IV–VI) exhibited complex spikes related to movements, presumably reflecting motor errors. In another experiment by Wang et al. (1987), a monkey moved a manipulandum, the position of which is represented by a cursor on the screen. The monkey was trained to move the cursor from the start box to the target box, and the target box could be repositioned during movement. In this feedback control situation, climbing fiber discharges from Purkinje cells increased at various times of movement, apparently reflecting motor errors.

Control system models incorporating forward and inverse models have been proposed for voluntary arm movements, since the pioneering works by Kawato et al. (1987). In these models, the primary motor cortex is considered to play the role of the controller, whereas a microcomplex functions as a forward or inverse model of the controlled object that involves segmental circuits and skeletomuscular systems of the arm. In **Figure 5A**, a microcomplex provides a forward model, which forms a circular connection with the primary motor cortex, corresponding to the classic cerebrocerebellar communication loop. The internal feedback through the forward model is assumed to enable the motor cortex to predict consequences of the movement to be performed before the actual performance. In the situation in which the primary motor cortex operates in the feedforward manner, sensory errors should be processed by comparing the instruction, consequence, and prediction of movements, and passed to the forward model via the inferior olive (**Figure 5A**). The above-mentioned results of Kitazawa et al. (1998) can be explained on the basis of such a forward model. By contrast, in **Figure 5B**, a microcomplex provides an inverse model operating in parallel with the primary motor cortex. When the primary motor cortex functions as a feedback controller, it derives motor error signals, and passes them to the inverse model via the inferior olive. This inverse-model-based control explains well the above-mentioned experimental observations by Mano et al. (1986) and Wang et al. (1987). These model-based control systems will be considered later in comparison with the model systems postulated above for VOR, OKR, and saccade.

OTHER CASES OF CEREBELLAR CONTROL

In addition to VOR, saccade, and hand reaching examined above, the classical eye blink conditioning (see Thompson, 1988) and nociceptive withdrawal reflex (see Apps and Garwicz, 2005) are typical examples of a control system lacking feedback and receiving sensory errors to the inferior olive. The ocular following response (OFR) is an eye-movement reflex elicited by brief, unexpected movements of a visual scene such as 100 ms ramp changes (Kawano and Miles, 1986; Miles and Kawano, 1986). OFR may appear to operate by feedback, but in its early phase it is a feedforward mechanism because of its long loop time (0.1 s, Smith et al., 1969; Khan and Franks, 2003) for visual information processing across the retina. This mixture of feedforward and feedback control in OFR may explain the finding that climbing fibers to Purkinje cells in the ventral paraflocculus represent both sensory and motor errors (Kobayashi et al., 1998).

On the other hand, when feedback control is performed by OKR or cursor trackings, as described above, climbing fiber discharges represent motor errors. Smooth pursuit eye movements to follow a moving spot should be a feedback control, but the feedback is non-functional during the initial 100 m after the onset of movement of a target; here, eyes are driven in the

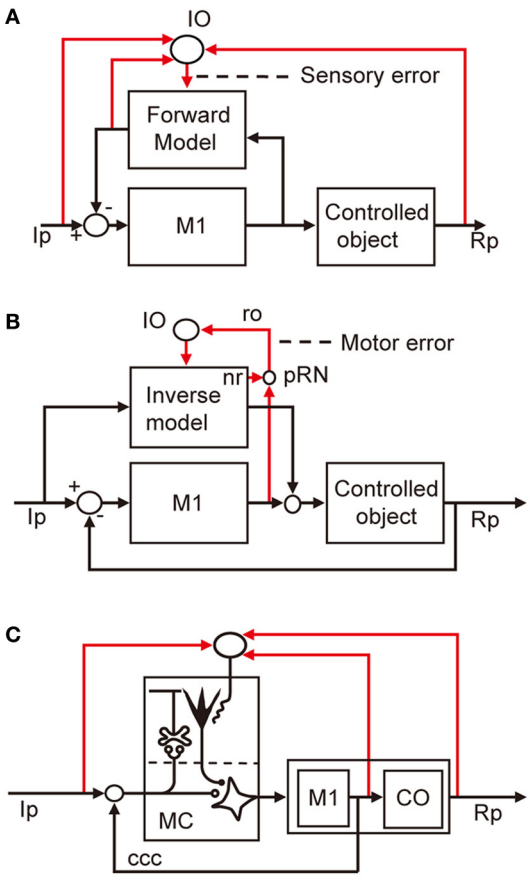

FIGURE 5 | Models for voluntary motor control. (A) Forward-model-based control of arm movement by primary motor cortex. **(B)** Inverse-model-based control. **(C)** Application of reflex control scheme. Additional abbreviations: ccc, cerebrocerebellar communication loop. CO, control object including segmental circuit and skeletomuscular system; MC, microcomplex, M1, primary motor cortex; IO, inferior olive; Ip, instructed performance; Rp, realized performance; ro, rubroolivary pathway; pRN, parvocellular red nucleus; nr, nucleorubral pathway.

feedforward manner because of the retinal delay (Smith et al., 1969). To manipulate motor errors independently of sensory errors, Yamamoto et al. (2007) trained monkeys to flex or extend the elbow by 45° in 400 ms under resistive and assistive force fields but without altering sensory measures of the movement such as velocity profiles. Unfortunately, the relationship of climbing fiber signals with muscle activities has not been reported.

It now appears that learning in a microcomplex is driven by either sensory or motor errors depending on the situation of whether a motor system performs the feedforward (or offline feedback) or feedback control. Both sensory and motor errors could access the inferior olive, but their representation would change depending on the circumstantial conditions.

SOURCES OF ERRORS

From the studies reviewed above, sensory errors are determined to be derived at various preolivary structures and finally converted to climbing fiber signals at the inferior olive. Typically, in VOR, retinal slip signals are derived by comparison between the vestibular and visual signals at the dorsal cap of the inferior olive (**Figure 4A**). In OKR, on the other hand, retinal slip signals are derived by comparison between the instructed and produced eye movements at the retina from which the retinal slip signals pass via AOS to the dorsal cap. For saccades, the superior colliculus detects errors and sends them to the β subnucleus of the inferior olive (**Figure 4C**).

On the other hand, when a feedback controller derives motor errors as feedback errors (**Figure 1B**), how are these motor errors conveyed to the inferior olive? A likely possibility is that involved in the classic dentatorubroolivary triangle (nro in **Figure 2**). There, large excitatory nuclear neurons mediating the outputs of a microcomplex project to certain midbrain structures including the parvocellular red nucleus, the nucleus of Cajal, and the nucleus of Darkschwitsch (Saint-Cyr and Courville, 2004; see also Glickstein et al., 2011). Neurons of these nuclei in turn project excitatory synapses to the inferior olive. In addition, the smaller inhibitory neurons in the cerebellar nuclei receive excitatory and inhibitory inputs in parallel with the larger excitatory nuclear neurons, and in turn send inhibitory connections to the inferior olive. A likely possibility (which is yet to be explored) is that these excitatory and inhibitory pathways mediate motor error signals to the inferior olive. However, a reservation must be made because this possibility does not fit the model for the internal model-based control of voluntary movement (see below).

For either sensory or motor errors, the inferior olive is the final station of the pathways along which errors are computed. The actual role of inferior olive neurons may be to recode the high-frequency information carried by their synaptic inputs into stochastic, low-rate discharges in their climbing fiber outputs (Schweighofer et al., 2004). Inferior olive neurons are mutually connected by gap-junction-mediated electrical synapses, and activation or inhibition of these synapses determines whether climbing fiber activity is rhythmic, random, or synchronous (Kitazawa and Wolpert, 2005), switching the efficacy of error signals in learning.

EVOLUTIONARY GAP

We have seen above that current models of the cerebellar control system have a gap between the phylogenetically old flocculonodular lobe and vermis (**Figure 4**) and the phylogenetically newer intermediate part of the cerebellar hemisphere (**Figure 5**). In particular, the microcomplex involved acts as a controller in the former, whereas it acts in the latter as an internal model linked to the controller in the primary motor cortex. Such a drastic change may not be impossible when one considers the remarkable evolutionary growth of the cerebellum in mammals; from the flocculonodular lobe/vermis linked with the brainstem, dominance shifts to the cerebellar hemisphere (intermediate and lateral parts) linked with the cerebral neocortex. The microcomplexes appear to be half-buried in the brainstem circuits in the former, whereas these appear to be free to be incorporated as internal models in the newly evolved controllers in the neocortex.

The internal-model-based control explains well the events in the cerebellum during voluntary arm movements. However, when these models are adopted, one must find a functional role of the

nucleorubroolivary pathway other than conveying motor errors. It has been suggested that motor errors generated by the primary motor cortex are passed to the parvocellular red nucleus to join the nucleorubroolivary pathway (Kawato et al., 1987). However, as yet, we have no idea about the possible function of the nucleorubral part of the pathway (**Figure 2**).

We also considered applying the adaptive control model for the flocculonodular lobe and vermis to the cerebellar hemisphere. We designated the microcomplex including the intermediate part of the cerebellar hemisphere and interpositus nucleus as the controller and the primary motor cortex as part of the controlled object (**Figure 5C**). To adopt this model, however, we need to clarify the role of the cerebrocerebellar communication loop linking the primary motor cortex with the cerebellar hemisphere. Obviously, more data on neuronal connections and signal contents of climbing fibers are required to fill the gap we face in demonstrating consistent neural designs of entire cerebellar control systems.

ACKNOWLEDGMENTS

The author thanks Dr. Soichi Nagao for valuable comments on the draft of this article.

REFERENCES

Anzai, M., Kitazawa, H., and Nagao, S. (2010). Effects of reversible pharmacological shutdown of cerebellar flocculus on the memory of long-term horizontal vestibulo-ocular reflex adaptation in monkeys. *Neurosci. Res.* 68, 191–198.

Apps, R., and Garwicz, M. (2005). Anatomical and physiological foundations of cerebellar information processing. *Nat. Rev. Neurosci.* 6, 297–311.

Catz, N., Dicke, P. W., and Their, P. (2005). Cerebellar complex spike firing is suitable to induce as well as to stabilize motor learning. *Curr. Biol.* 15, 2179–2189.

D'Angelo, E., Rossi, P., Armano, S., and Taglietti, V. (1999). Evidence for NMDA and mGlu receptordependent long-term potentiation of mossy fiber-granule cell transmission in rat cerebellum. *J. Neurophysiol.* 81, 277–287.

De Zeeuw, C. I., Wentzel, P., and Mugnaini, E. (1993). Fine structure of the dorsal cap of the inferior olive and its GABAergic and non-GABAergic input from the nucleus prepositus hypoglossi in rat and rabbit. *J. Comp. Neurol.* 327, 63–82.

Ebner, T. J., and Pasalar, S. (2008). Cerebellum predicts the future motor state. *Cerebellum* 7, 583–588.

Ezure, K., and Graf, W. (1984). A quantitative analysis of the spatial organization of the vestibulo-ocular reflexes in lateral- and frontal-eyed animals—II. Neuronal networks underlying vestibulo-oculomotor coordination. *Neuroscience* 12, 95–109.

Frens, M. A., Mathoera, A. L., and van der Steen, J. (2001). Floccular complex spike response to transparent retinal slip. *Neuron* 30, 795–801.

Ghelarducci, B., Ito, M., and Yagi, N. (1975). Impulse discharges from floccular Purkinje cells of alert rabbits during visual stimulation combined with horizontal head rotation. *Brain Res.* 87, 66–72.

Glickstein, M., Sultan, F., and Voogd, J. (2011). Functional localization in the cerebellum. *Cortex* 47, 59–80.

Hansel, C., Linden, D. J., and D'Angelo, E. (2001). Beyond parallel fiber LTD: the diversity of synaptic and non-synaptic plasticity in the cerebellum. *Nat. Neurosci.* 4, 467–475.

Huerta, M. F., and Harting, J. K. (1984). *Comparative Neurology of the Optic Tectum*, ed H. Vanegas (New York, NY: Plenum Press), 687–773.

Ito, M. (1984). *The Cerebellum and Neural Control.* New York, NY: Raven Press.

Ito, M. (2002). Historical review of the significance of the cerebellum and the role of purkinje cells in motor learning. *Ann. N.Y. Acad. Sci.* 978, 273–288.

Ito, M. (2006). Cerebellar circuitry as a neuronal machine. *Prog. Neurobiol.* 78, 272–303.

Karachot, L., Shirai, Y., Vigot, R., Yamamori, T., and Ito, M. (2001). Induction of long-term depression in cerebellar Purkinje cells requires a quickly turned over protein. *J. Neurophysiol.* 86, 280–289.

Kassardjian, C. D., Tan, Y.-F., Chung, J.-Y., Heskin, R., Peterson, M. J., and Broussard, D. M. (2005). The site of amemory shifts with consolidation. *J. Neurosci.* 25, 7979–7985.

Kawano, K., and Miles, F. A. (1986). Short-latency ocular following responses of monkey. II. Dependence on a prior saccadic eye movement. *J. Neurophysiol.* 56, 1355–1380.

Kawato, M. (1999). Internal models for motor control and trajectory planning. *Curr. Opin. Neurobiol.* 9, 718–727.

Kawato, M., Furukawa, K., and Suzuki, R. (1987). A hierarchical neural-network model for control and learning of voluntary movement. *Biol. Cybern.* 57, 169–185.

Kawato, M., and Gomi, H. (1992a). A computational model of four regions of the cerebellum based on feedback-error learning. *Biol. Cybern.* 68, 95–103.

Kawato, M., and Gomi, H. (1992b). The cerebellum and VOR/OKR learning models. *Trends Neurosci.* 15, 445–453.

Khan, M. A., and Franks, I. M. (2003). Online versus offline processing of visual feedback in the production of component submovements. *J. Mot. Behav.* 35, 286–295.

Kitazawa, S., Kimura, T., and Yin, P. B. (1998). Cerebellar complex spikes encode both destinations and errors in arm movements. *Nature* 392, 494–497.

Kitazawa, S., and Wolpert, D. M. (2005). Rhythmicity, randomness and synchrony in climbing fiber signals. *Trends Neurosci.* 28, 611–619.

Kobayashi, Y., Kawano, K., Takemura, A., Inoue, Y., Kitama, T., Gomi, H., et al. (1998). Temporal firing patterns of Purkinje cells in cerebellar ventral paraflocculus during ocular following responses in monkeys. II. Complex spikes. *J. Neurophysiol.* 80, 832–848.

Kojima, Y., Soetedjo, R., and Fuchs, A. F. (2010). Changes in simple spike activity of some purkinje cells in the oculomotor vermis during saccade adaptation are appropriate to participate in motor learning. *J. Neurosci.* 30, 3715–3727.

Kojima, Y., Yoshida, K., and Iwamoto, Y. (2007). Microstimulation of the midbrain tegmentum creates learning signals for saccade adaptation. *J. Neurosci.* 27, 3759–3767.

Kyuhou, S., and Matsuzaki, R. (1991). Topographical organization of the tecto-olivo- cerebellar projection in the cat. *Neuroscience* 41, 227–241.

Lannou, J., Cazin, L., Precht, W., and Le Taillanter, M. (1984). Responses of prepositus hypoglossi neurons to optokinetic and vestibular stimulations in the rat. *Brain Res.* 301, 39–45.

Mano, N., Kanazawa, I., and Yamamoto, K. (1986). Complex-spike activity of cerebellar Purkinje cells related to wrist tracking movement in monkey. *J. Neurophysiol.* 56, 137–158.

McElvain, L. E., Bagnall, M. W., Sakatos, A., and du Lac, S. (2010). Bidirectional plasticity gated by hyperpolarization controls the gain of postsynaptic firing responses at central vestibular nerve synapses. *Neuron* 68, 763–775.

McFarland, J. L., and Fuchs, A. F. (1992). Discharge patterns in nucleus prepositus hypoglossi and adjacent medial vestibular nucleus during horizontal eye movement in behaving macaques. *J. Neurophysiol.* 68, 319–332.

McLaughlin, S. C. (1967). Parametric adjustment in saccadic eye movements. *Percept. Psychophys.* 2, 359–362.

Miles, F. A., and Kawano, K. (1986). Short-latency ocular following responses of monkey. III. Plasticity. *J. Neurophysiol.* 56, 1381–1396.

Nagao, S. (1989). Role of cerebellar flocculus in adaptive interaction between optokinetic eye movement response and vestibulo-ocular reflex in pigmented rabbits. *Exp. Brain Res.* 77, 541–551.

Okamoto, T., Endo, S., Shirao, T., and Nagao, S. (2011). Role of cerebellar cortical protein synthesis in transfer of memory trace of cerebellum-dependent motor learning. *J. Neurosci.* 31, 8958–8966.

Ramat, S., Leigh, R. J., Zee, D. S., and Optican, L. M. (2007). What clinical disorders tell us about the neural control of saccadic eye movements. *Brain* 130, 10–35.

Robinson, F. R., Straube, A., and Fuchs, A. F. (1993). Role of the caudal fastigial nucleus in saccade generation. II. Effects of muscimol inactivation. *J. Neurophysiol.* 70, 1741–1758.

Saint-Cyr, J. A., and Courville, J. (2004). Sources of descending afferents to the inferior olive from the

upper brain stem in the cat as revealed by the retrograde transport of horseradish peroxidase. *J. Comp. Neurol.* 198, 567–581.

Schonewille, M., Gao, Z., Boele, H.-J., Veloz, M. F. V., Amerika, W. E., Simek, A. A. M., et al. (2011). Reevaluating the role of LTD in cerebellar motor learning. *Neuron* 70, 43–50.

Schweighofer, N., Doya, K., Fukai, H., Chiron, J. V., Furukawa, T., and Kawato, M. (2004). Chaos may enhance information transmission in the inferior olive. *Proc. Natl. Acad. Sci. U.S.A.* 101, 4655–4660.

Sekimjak, C., Vissel, B., Bollinger, J., Faulstich, M., and du Lac, S. (2003). Purkinje cell synapses target physiologically unique brainstem neurons. *J. Neurosci.* 23, 6392–6398.

Shutoh, F., Ohki, M., Kitazwa, H., Itohara, S., and Nagao, S. (2006). Memory trace of motor learning shifts transsynaptically from cerebellar cortex to nuclei for consolidation. *Neuroscience* 139, 767–777.

Simpson, J. I., Belton, T., Suh, M., and Winkelman, B. (2002). Complex spike activity in the flocculus signals more than the eye can see. *Ann. N.Y. Acad. Sci.* 978, 232–236.

Smith, K. U., Putz, V., and Molitor, K. (1969). Eye movement-retina delayed feedback. *Science* 166, 1542–1544.

Soetedjo, R., Kojima, Y., and Fuchs, A. F. (2008). Complex spike activity in the oculomotor vermis of the cerebellum: a vectorial error signal for saccade motor learning? *J. Neurophysiol.* 100, 1949–1966.

Sparks, D. L., and Hartwich-Young, R. (1989). The deep layers of the superior colliculus. *Rev. Oculomot. Res.* 3, 213–255.

Thompson, R. F. (1988). The neural basis of basic associative learning of discrete behavioral responses. *Trends Neurosci.* 11, 152–155.

Wang, J.-J., Kim, J. H., and Ebner, T. J. (1987). Climbing fiber afferent modulation during a visually guided, multi-joint arm movement in the monkey. *Brain Res.* 410, 323–329.

Winkelman, B. H., and Frens, M. A. (2006). Motor coding in floccular climbing fibers. *J. Neurophysiol.* 95, 2342–2351.

Wolpert, D. M., Miall, R. C., and Kawato, M. (1998). Internal models in the cerebellum. *Trends Cogn. Sci.* 2, 338–347.

Yamada, J., and Noda, H. (1987). Afferent and efferent connections of the oculomotor cerebellar vermis in the macaque monkey. *J. Comp. Neurol.* 265, 224–241.

Yamamoto, K., Kawato, M., Kotosaka, S., and Kitazawa, S. (2007). Encoding of movement dynamics by Purkinje cell simple spike activity during fast arm movements under resistive and assistive force fields. *J. Neurophysiol.* 97, 1588–1599.

Conflict of Interest Statement: The author declares that the research was conducted in the absence of any commercial or financial relationships that could be construed as a potential conflict of interest.

Received: 17 October 2012; accepted: 05 January 2013; published online: 22 February 2013.

Citation: Ito M (2013) Error detection and representation in the olivo-cerebellar system. Front. Neural Circuits ***7****:1. doi: 10.3389/fncir.2013.00001*

frontiers in
NEURAL CIRCUITS

HYPOTHESIS AND THEORY ARTICLE
published: 02 July 2013
doi: 10.3389/fncir.2013.00115

Beyond "all-or-nothing" climbing fibers: graded representation of teaching signals in Purkinje cells

Farzaneh Najafi [1] ***and Javier F. Medina*** [2] ***

[1] *Department of Biology, University of Pennsylvania, Philadelphia, PA, USA*
[2] *Department of Psychology, University of Pennsylvania, Philadelphia, PA, USA*

Edited by:
Egidio D'Angelo, University of Pavia, Italy

Reviewed by:
Egidio D'Angelo, University of Pavia, Italy
Henrik Jörntell, Lund University, Sweden

***Correspondence:**
Javier F. Medina, Department of Psychology, University of Pennsylvania, Solomon Labs Building, 3720 Walnut Street, Philadelphia, PA 19104, USA
e-mail: jmed@psych.upenn.edu

Arguments about the function of the climbing fiber (CF) input to the cerebellar cortex have fueled a rabid debate that started over 40 years ago, and continues to polarize the field to this day. The origin of the controversy can be traced back to 1969, the year David Marr published part of his dissertation work in a paper entitled "A theory of cerebellar cortex." In Marr's theory, CFs play a key role during the process of motor learning, providing an instructive signal that serves as a "teacher" for the post-synaptic Purkinje cells. Although this influential idea has found its way into the mainstream, a number of objections have been raised. For example, several investigators have pointed out that the seemingly "all-or-nothing" activation of the CF input provides little information and is too ambiguous to serve as an effective instructive signal. Here, we take a fresh look at these arguments in light of new evidence about the peculiar physiology of CFs. Based on recent findings we propose that at the level of an individual Purkinje cell, a graded instructive signal can be effectively encoded via pre- or post-synaptic modulation of its one and only CF input.

Keywords: complex spike, cerebellum, mossy fiber, motor learning, calcium, LTD, dendrite, motor learning

Marr's idea that cerebellar climbing fibers (CFs) play the role of "teachers" during motor learning was a stroke of genius. Like the rest of the hypotheses first introduced in his revolutionary "A theory of cerebellar cortex" (Marr, 1969), the idea that CFs provide instructive signals was built from the ground up, based on first principles and a deep understanding of the computational problems that need to be solved in motor control. In addition, Marr relied extensively on detailed knowledge about the wiring circuit and the physiology of the cerebellar cortex, which had been compiled just a few years before in a remarkable book by Eccles et al. (1967). We may never know with certainty what led to the aha moment that sparked the idea that CFs could act as "teachers"; but one can only imagine that in developing his pioneering theory, Marr must have been particularly intrigued by the unique properties of the CF input and the peculiar response it generates in the post-synaptic Purkinje cell.

"ALL-OR-NOTHING" INSTRUCTIVE SIGNALS

Climbing fibers are the axons sent by neurons in the inferior olive to the contralateral cerebellum (**Figure 1A**; red; Eccles et al., 1966; Desclin, 1974; Schmolesky et al., 2002; Ohtsuki et al., 2009). One of the most striking features of this olivo-cerebellar projection is that in the adult cerebellar cortex, each Purkinje cell is innervated by a single CF (Eccles et al., 1966; Schmolesky et al., 2002; Ohtsuki et al., 2009). This is one of the most powerful excitatory synapses in the brain (Eccles et al., 1966), comprising more than 1000 contacts distributed all along the proximal portion of the Purkinje cell dendritic tree (Palay and Chan-Palay, 1974; Strata and Rossi, 1998). As a result, activation of a single olivary neuron results in a large electrical event in the soma of the post-synaptic Purkinje cell, termed the "complex spike" (CS; Thach, 1967) because it consists of a fast initial spike followed by several slower spikelets of smaller amplitude separated from each other by 2–3 ms (**Figure 1B5**; asterisk; Eccles et al., 1966). The CS can be easily distinguished from the so called "simple spikes" (Thach, 1967), normal action potentials fired constantly by the Purkinje cells at high rates (**Figure 1B5**; thin lines). The cause of the spikelets in the CS was disputed for years (Armstrong and Rawson, 1979; Campbell et al., 1983b), but recent work has demonstrated that they are a result of the interaction between local resurgent sodium currents in the Purkinje cell soma (Raman and Bean, 1997, 1999a,b; Schmolesky et al., 2002), and the characteristic activation of the pre-synaptic CFs, which tend to fire in brief high-frequency bursts of 1–6 spikes (**Figure 1B1**; Crill, 1970; Armstrong, 1974; Mathy et al., 2009).

From the very beginning, the somatic CS was described as being "all-or-nothing" (Eccles et al., 1966), a label that has stuck to this day. This characterization of the CS is based on the finding that direct microstimulation of the inferior olive causes a seemingly binary response in the post-synaptic Purkinje cell (Eccles et al., 1966): "nothing" if the strength of stimulation is below a certain threshold, or a unitary ("all") CS for all strengths above threshold (**Figure 1B5**; same CS for weak or strong inferior olive stimulation). In other words, the CS evoked in an individual Purkinje cell is unaffected if additional CFs are activated by increasing the strength of stimulation in the inferior olive.

These groundbreaking experiments hold an important place in history, partly because in showing that the post-synaptic CF response does not depend on the number of stimulated cells in the inferior olive, they helped demonstrate that each Purkinje cell must receive input from one-and-only-one CF (Eccles et al., 1966). Importantly, the "all-or-nothing" quality of the post-synaptic CS also implies that the response of the sole pre-synaptic CF input

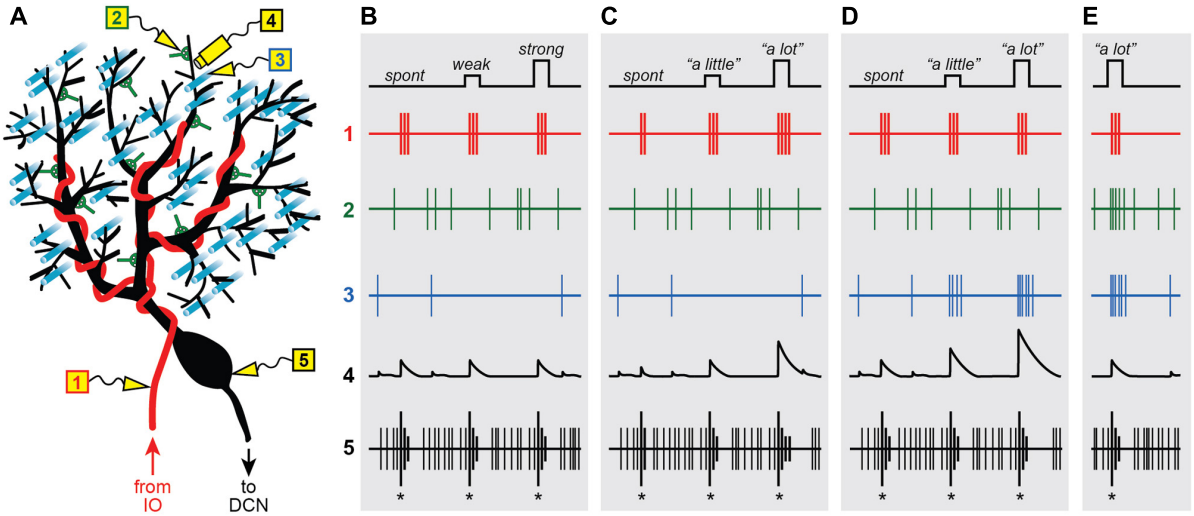

FIGURE 1 | Graded instructive signals in a Purkinje cell. (A) A schematic diagram of a Purkinje cell and its different synaptic inputs. Electrodes are placed in different locations to measure the extracellular spiking activity of the climbing fiber (1; red), a molecular layer interneuron (2; green), a parallel fiber (3; cyan) and the Purkinje cell axon (5; black). In addition, intracellular calcium signals are imaged in one of the Purkinje cell's distal dendrites (4; black), near electrodes 2 and 3. **(B–E)** Spikes and calcium signals measured in the five locations shown in **(A)**, under four different scenarios: when all climbing fiber signals are "all-or-nothing" whether firing is spontaneous (spont) or when the strength of stimulation in the inferior olive is weak or strong **(B)**, when instructive signals to lift the foot "a little" or "a lot" influence the number of spikes in the climbing fiber burst **(C)**, or when the instructive signals activate the climbing fiber simultaneously with parallel fiber inputs **(D)** and input from the molecular layer interneurons **(E)**.

is not graded with the strength of olivary stimulation, and must itself be "all-or-nothing" as well (**Figure 1B1**; same 3-spike burst for weak or strong IO stimulation). Later studies confirmed this prediction by recording directly from individual neurons in the inferior olive, and showing that their spiking response varies little with the strength of stimulation (Crill, 1970). This finding has far-reaching implications and is at the center of a heated debate about the functional role of the CF input.

SPONTANEOUS CLIMBING FIBERS AND THE SIGNAL-TO-NOISE PROBLEM

To Marr, the idiosyncratic properties of the olivo-cerebellar system could only mean one thing: each individual "all-or-nothing" CF input represents an "elemental" instruction that provides information about what the correct movement should be in a given context (Marr, 1969). It is important to remember that in the original theory, these instructive signals could be encoded in either motor or sensory coordinates (Marr, 1969). For example, if an obstacle is placed in front of the right foot causing the subject to trip while walking on a treadmill, the appropriate elemental instruction could be represented using motor commands coming from cerebral cortex (e.g., "lift right foot"), or sensory-related inputs coming from peripheral activation of cutaneous receptors (e.g., "the right foot hit an obstacle"). In either case, the idea was that the CF input would be providing an instructive signal to the Purkinje cell, triggering mechanisms of plasticity that would be used to correct subsequent movements (i.e., lift the right foot higher on the next step cycle and avoid the obstacle).

Almost 45 years after Marr's original proposal, his hypothesis remains controversial and the cerebellar field is still divided with regards to how CF signals are used to exert control over our movements (De Schutter and Maex, 1996; Simpson et al., 1996; Llinás, 2011). It appears that at least in some motor learning tasks, CFs are activated in a manner that is compatible with their presumed role as "teachers" (Gilbert and Thach, 1977; Raymond et al., 1996; Simpson et al., 1996; Kitazawa et al., 1998; Raymond and Lisberger, 1998; Ito, 2006, 2013; Medina and Lisberger, 2008; Rasmussen et al., 2008; Soetedjo et al., 2008). Further support comes from *in vitro* studies showing that CF inputs can trigger a variety of synaptic plasticity mechanisms in Purkinje cells (for reviews, see Hansel et al., 2001; Gao et al., 2012). However, a number of questions have been raised about the potential instructive role of CFs during motor learning, particularly with regards to the problems inherent in representing information with "all-or-nothing" signals from spontaneously active neurons (Llinás and Welsh, 1993; Llinás et al., 1997).

One argument against the idea that CFs act as "teachers" is that the "all-or-nothing" CF input is ambiguous from the point of view of an individual Purkinje cell, and suffers from the so-called "signal-to-noise" problem (Llinás et al., 1997). The trouble is that CFs are spontaneously active about once per second (Armstrong, 1974; Simpson et al., 1996), and at least in the prevailing view (**Figure 1B**), the post-synaptic Purkinje cell would have no way of distinguishing between these frequent spontaneous activations ("noise"), and the few which occur during motor learning and presumably encode elemental instructions ("signal"). Even if Purkinje cells were somehow able to discriminate between instructive and spontaneous CF inputs, the "all-or-nothing" character of the CF signal would put a hard limit on how much information can be encoded. At best, a CF could fire ("all") to signal "lift right foot" or remain silent ("nothing") to signal "do not lift right foot," but it would not be able to provide useful parametric information about

how far to lift it. These theoretical considerations call into question the ability of individual CFs to provide efficient instructive signals for motor learning. But are CFs really such "bad teachers?"

POOLING TOGETHER CF SIGNALS: THERE IS STRENGTH IN NUMBERS

Previous theoretical studies have suggested that even though a single "all-or-nothing" CF signal is ambiguous, an individual Purkinje cell could still solve the "signal-to-noise" problem by collecting information from its CF input across many trials (Sejnowski, 1977; Fujita, 1982; Kawato and Gomi, 1992; Gilbert, 1993; Mauk and Donegan, 1997; Mauk et al., 1997; Kenyon et al., 1998; Spoelstra et al., 2000; Dean et al., 2010). In these computational models, CF activity works as an equilibrium point signal: the CF fires ("all") to trigger plasticity when an error is made and the movement needs to be adjusted, but is silent ("nothing") if the movement is performed correctly. Because a single spontaneous CF input cannot be distinguished from a single error-related CF input, it is assumed that both types of CF signals are equally capable of inducing plasticity. However, only those CF signals that are repeatedly triggered with high probability in a specific learning context would lead to an enduring change in the Purkinje cell. This solves one problem, but leaves unanswered one important question: how can "all-or-nothing" CFs provide parametric information about the size of the error? After all, an effective instructive signal should indicate whether the movement requires just a small adjustment or a major overhaul.

An "all-or-nothing" CF signal cannot carry much information by itself, but instructive signals with details about error size could be encoded, at least in theory, by pooling together the activity of many olivary neurons. For example, the instructive signal "lift right foot" could be represented by activating any one of ten CFs, while at the same time graded information about how far to lift it could be encoded by modulating how many of the ten are simultaneously activated. The olivo-cerebellar system seems perfectly suited for this type of synchronous population coding: neighboring neurons in the inferior olive are electrically coupled by dendrodendritic gap junctions (Llinás et al., 1974; Sotelo et al., 1974; De Zeeuw et al., 1996, 1997; Marshall et al., 2007), and as a result, small groups of CFs converging on the same narrow parasagittal strip of cerebellar cortex have a tendency to fire synchronously (Bell and Kawasaki, 1972; Llinás and Sasaki, 1989; Sugihara et al., 1993; Simpson et al., 1996; Lang et al., 1999; Kitazawa and Wolpert, 2005). Furthermore, the level of co-activation in the CF population appears to encode sensorimotor-related information (Lou and Bloedel, 1992; Welsh et al., 1995; Wylie et al., 1995; Lang, 2002; Ozden et al., 2009; Schultz et al., 2009; Wise et al., 2010).

As pointed out by others (Ozden et al., 2009; Schultz et al., 2009; Bengtsson et al., 2011; Otis et al., 2012), the level of CF co-activation could potentially be read out and used as an instructive signal in downstream neurons of the deep cerebellar nuclei which receive convergent input from many Purkinje cells (Palkovits et al., 1977; Person and Raman, 2011). However, our concern here is with the representation of instructive signals at the level of an individual Purkinje cell, which receives input from a single CF (Eccles et al., 1966; Schmolesky et al., 2002; Ohtsuki et al., 2009), and therefore does not have easy access to information encoded in the population. Note that in theory, a Purkinje cell could receive information about activation of neighboring CFs through spillover mechanisms (Szapiro and Barbour, 2007; Mathews et al., 2012), but this possibility will not be considered further in this paper. Instead, we will discuss alternative ways to enhance the information capacity of individual olivary neurons, using mechanisms that challenge the conventional view that all CF signals are created equal.

MODULATION OF THE PRE-SYNAPTIC CLIMBING FIBER BURST

New discoveries about the spike-generating mechanisms of olivary neurons are challenging conventional wisdom about the way CFs encode information. As noted earlier, CFs fire in brief high-frequency bursts, comprising 1–6 spikes separated from each other by 2–3 ms (Crill, 1970; Armstrong, 1974; Mathy et al., 2009). The burst is generated in the olivary axon itself, as a result of an intrinsic positive feedback loop (Mathy et al., 2009): the first spike is initiated in the axon, but it also backpropagates into the dendrites where it opens high-voltage-activated calcium channels that cause a prolonged depolarization lasting up to 10 ms. When this depolarization reaches the axon, it triggers the rest of the spikes in the burst.

At first glance, this seemingly automatic and self-driven burst mechanism appears to fit well with the "all-or-nothing" character of the CF response to brief olivary stimulation (Crill, 1970), which was mentioned earlier and is characterized by a single burst of spikes that varies little whether the initial depolarization is just above threshold or much stronger (**Figure 1B1**). However, it is known that the processes underlying spike generation and dendritic depolarization are both influenced by a variety of factors, including the resting potential of the inferior olivary neuron (Llinás and Yarom, 1981; Ruigrok and Voogd, 1995). This opens up the possibility that information may be transmitted by modulating the number of spikes in the CF burst.

Indeed, the era of the "all-or-nothing" CF may be coming to an end. Recent studies have shown that the burst size, i.e., the number of spikes in the CF burst, is tightly regulated and provides extra information not available in the conventional binary signal (Maruta et al., 2007; Mathy et al., 2009; Bazzigaluppi et al., 2012; De Gruijl et al., 2012). For example, burst size is correlated with a number of critical parameters which together define the state of olivary neurons. These cells have a characteristic subthreshold membrane potential oscillation which is synchronized across neighboring olivary neurons via gap junctions (Lampl and Yarom, 1993, 1997; Devor and Yarom, 2002; Leznik and Llinás, 2005). It has been shown that the number of spikes in the CF burst varies systematically according to the phase of the oscillation *in vitro* (Mathy et al., 2009), the amplitude of the oscillation *in vivo* (Bazzigaluppi et al., 2012), and the extent of electrotonic coupling and synchrony in a computer model of the olivary network (De Gruijl et al., 2012). In addition, burst size can be used to distinguish between spontaneous and sensory-related CF signals evoked by sinusoidal whole-field visual stimulation (Maruta et al., 2007). This last study also found that the number of spikes in the CF burst varied systematically depending on the direction of the visual stimulus.

The findings of the studies mentioned in the preceding paragraph must be interpreted with some caution. As was also the case in previous experiments (Eccles et al., 1966; Armstrong and Rawson, 1979), the number of spikes per CF burst was quite variable from one burst to the next and always fell within the same limited range (1–6 spikes), regardless of condition or behavioral state. Therefore, the changes in burst size for any given situation were small (<1 spike per burst) and could only be detected in the average as a slight probability bias toward generating more bursts with many (>4) or few (1) spikes. It remains to be seen whether such a fickle modulation of the CF-burst signal could play a functional role during motor learning, perhaps by regulating the induction of plasticity in the post-synaptic Purkinje cell (Mathy et al., 2009). Nonetheless, these groundbreaking experiments have demonstrated that the number of spikes in the CF burst is not entirely random and can thus provide parametric information not available in a binary code.

Figure 1C illustrates a straightforward way to encode a graded instructive signal by systematically modulating the number of spikes in the CF burst, e.g., 2 spikes for "no instruction" due to spontaneous activation, 3 for "lift right foot a little," and 4 for "lift right foot a lot." Clearly, this example is an oversimplification. In reality, codes based on burst size would be inherently noisy because as mentioned above, the number of spikes in the CF burst is subject to stochastic variations within a limited range. However, the information capacity of an individual CF would still be enhanced under conditions in which burst size is probabilistic and only slightly biased one way or another depending on the parametric details of the instruction. A similar proposal for encoding parametric information in the CF system was formulated on theoretical grounds almost 40 years ago (Gilbert, 1974).

One advantage of the code in **Figure 1C1** is that it can be unambiguously read-out because a difference of just one spike in the CF burst has a substantial impact on the response evoked in the post-synaptic Purkinje cell. In the dendrites, burst size regulates the duration of the depolarizing plateau potential (Campbell et al., 1983a), the number of calcium spikes (Mathy et al., 2009), and the ability of the CF input to induce plasticity (Mathy et al., 2009; **Figure 1C4**). With regards to Purkinje cell output, burst size has a strong influence on both the number of CS-related spikes that are sent down the axon (Mathy et al., 2009), and the duration of the characteristic pause in simple spike activity that follows the CS (Mathy et al., 2009; **Figure 1C5**).

MODULATION OF THE POST-SYNAPTIC CLIMBING FIBER RESPONSE

It is often overlooked that the same groundbreaking paper that coined the term "all-or-nothing" to describe the Purkinje cell CS also made it very clear that the excitatory post-synaptic potential (EPSP) evoked after activation of the CF input could itself be graded (Eccles et al., 1966): the size of the EPSP was shown to depend critically on the membrane potential. This observation has important implications for the coding of instructive signals in Purkinje cells, particularly as it pertains to the regulation of CF-evoked calcium influx in the dendrites.

Activation of the CF input causes a massive depolarization of the proximal dendrites of the Purkinje cell (Eccles et al., 1966), triggering regenerative calcium spikes that propagate and cause calcium influx throughout the dendritic tree (Ross and Werman, 1987), including the terminal spiny branchlets (Konnerth et al., 1992; Miyakawa et al., 1992), where the excitatory parallel fiber (PF) synapses are located (**Figure 1A**; cyan). Dendritic calcium is the trigger for a wide variety of short-term (Batchelor and Garthwaite, 1997; Glitsch et al., 2000; Brenowitz and Regehr, 2003; Maejima et al., 2005; Rancz and Hausser, 2006) and long-term (Sakurai, 1990; Konnerth et al., 1992; Kano et al., 1996; Hansel and Linden, 2000; Miyata et al., 2000; Wang et al., 2000; Coesmans et al., 2004; Tanaka et al., 2007) mechanisms of plasticity in Purkinje cell synapses, and for this reason it is considered the neural implementation of behaviorally driven instructive signals at the most fundamental molecular level (for reviews, see Hansel et al., 2001; Gao et al., 2012).

What is important about the CF-triggered dendritic calcium signal from a neural coding perspective is that just like the evoked EPSP, its amplitude can be modulated *in vitro* (Miyakawa et al., 1992; Midtgaard et al., 1993; Callaway et al., 1995; Wang et al., 2000) and *in vivo* (Kitamura and Häusser, 2011) by a variety of factors that influence the membrane potential of the Purkinje cell. For example, activation of inhibitory synapses from molecular layer interneurons (**Figure 1A**; green) causes a conductance shunt that reduces the amplitude of the CF-triggered calcium signal (Callaway et al., 1995). Conversely, dendritic calcium influx is significantly enhanced if the CF input is preceded by stimulation of the excitatory PF pathway (Wang et al., 2000), which by itself causes a small graded calcium response via activation of voltage-gated calcium channels as well as metabotropic receptor-dependent release from intracellular stores (Eilers et al., 1995; Takechi et al., 1998).

Figure 1D illustrates a straightforward way to encode a graded instructive signal by systematically modulating the amplitude of the CF-triggered calcium response in the Purkinje cell dendrites. The three signals corresponding to "no instruction" due to spontaneous activation of the CF input, "lift right foot a little" and "lift right foot a lot" are associated with progressively increasing levels of PF excitation (**Figure 1D3**), and as a result, they are encoded in the dendrite as progressively larger calcium responses (**Figure 1D4**). Note that in this example there is a parallel systematic modulation of the characteristic post-CF pause in Purkinje cell activity (**Figure 1D5**), which is consistent with the recently described effect of extra dendritic calcium spikes on somatic spiking (Davie et al., 2008). On the other hand, the CS itself provides no parametric information about the instruction because it is the same regardless of the context in which the CF was activated (**Figure 1D5**). This is consistent with previous work demonstrating that the burst pattern of the CS is largely unaffected by dendritic events because the CF input causes a functional division between dendritic and axosomatic compartments (Davie et al., 2008).

We have made one key assumption in **Figure 1D**: the instructive signal that activates the CF input also activates some of the PF synapses on the same Purkinje cell. In other words, our proposal requires a high degree of spatial convergence in the cerebellar cortex: PF's and CFs inputs representing the same type of information must come together at the level of individual Purkinje cells.

The field is currently divided with regards to this "convergence" hypothesis (Apps and Garwicz, 2005). Previous studies have provided irrefutable evidence that the CF receptive field of an individual Purkinje cell matches that of the mossy fibers located in the granular layer directly underneath (Garwicz et al., 1998; Brown and Bower, 2001; Voogd et al., 2003; Odeh et al., 2005; Pijpers et al., 2006; Apps and Hawkes, 2009). What is less clear is whether this vertically aligned spatial organization would result in the Purkinje cell receiving the CF signal together with excitatory input from mossy fiber-driven PF's (Cohen and Yarom, 1998; Brown and Bower, 2001; **Figure 1D**), or with inhibitory input from mossy fiber-driven molecular layer interneurons (Ekerot and Jorntell, 2001, 2003; **Figure 1E**). Based on classic work (Eccles et al., 1967, 1972; Eccles, 1973), as well as more recent studies using *in vivo* imaging of peripherally evoked inhibitory responses in the cerebellar cortex (Gao et al., 2006) or patchy photostimulation of granule cells *in vitro* (Dizon and Khodakhah, 2011), we think both scenarios are possible. We suspect that the levels of local excitatory and inhibitory input may differ between groups of Purkinje cells, depending on their precise location relative to the activated PF's. This raises the intriguing possibility that the mossy fiber pathway may be used to set the membrane potential of the Purkinje cell, and in this way adjust the efficacy of CF-related instructive signals.

EPILOG: CF-DRIVEN PLASTICITY IN PURKINJE CELLS

Our paper highlights how graded modulation of individual CF inputs may be used for encoding parametric information about instructive signals. But to really understand the role of CFs in motor learning, we must first answer one fundamental question: if CFs are the "teachers," who might the students be and what do they learn? In "A theory of cerebellar cortex," Marr predicted that CFs would teach by modifying the strength of excitatory PF synapses (**Figure 1A**; cyan). Immediately after the publication of his revolutionary theory, Marr himself worked with Eccles on this topic, but "failed to discover any significant modification even after some hundreds of parallel fiber-climbing fiber inputs" (Eccles, 1973). This initial failure did not stop others from trying to induce plasticity by stimulating CFs with more physiological patterns. More than a decade later, Masao Ito would become the first person to demonstrate CF-dependent long-term depression (LTD) of PF synapses (Ito and Kano, 1982). Since then, research about cerebellar plasticity has exploded (Gao et al., 2012). We now know that CFs can trigger a variety of long-term modifications in PF synapses (**Figure 1A**; cyan; Ito and Kano, 1982), in molecular layer interneuron synapses (**Figure 1A**; green; Kano et al., 1992; Duguid and Smart, 2004; Mittmann and Häusser, 2007), and even in the CF synapse itself (**Figure 1A**; red; Hansel and Linden, 2000; Bosman et al., 2008; Ohtsuki and Hirano, 2008). The functional significance of these plasticity mechanisms remains largely unknown. We can only imagine that in contrast to the conventional "all-or-nothing" instructive CF input, the type of graded CF signals we have described here could provide an extra degree of flexibility for choosing carefully who the students are and what to teach them.

ACKNOWLEDGMENTS

We are grateful to K. Ohmae and J. Chin for help with the figure and to S. Wang for helpful discussion. Work supported by grant R01MH093727 from the National Institutes of Mental Health to Javier F. Medina.

REFERENCES

Apps, R., and Garwicz, M. (2005). Anatomical and physiological foundations of cerebellar information processing. *Nat. Rev. Neurosci.* 6, 297–311. doi: 10.1038/nrn1646

Apps, R., and Hawkes, R. (2009). Cerebellar cortical organization: a one-map hypothesis. *Nat. Rev. Neurosci.* 10, 670–681. doi: 10.1038/nrn2698

Armstrong, D. M. (1974). Functional significance of connections of the inferior olive. *Physiol. Rev.* 54, 358–417.

Armstrong, D. M., and Rawson, J. A. (1979). Activity patterns of cerebellar cortical neurones and climbing fibre afferents in the awake cat. *J. Physiol.* 289, 425–448.

Batchelor, A. M., and Garthwaite, J. (1997). Frequency detection and temporally dispersed synaptic signal association through a metabotropic glutamate receptor pathway. *Nature* 385, 74–77. doi: 10.1038/385074a0

Bazzigaluppi, P., De Gruijl, J. R., van der Giessen, R. S., Khosrovani, S., De Zeeuw, C. I., de Jeu, M. T. (2012). Olivary subthreshold oscillations and burst activity revisited. *Front. Neural Circuits* 6:91. doi: 10.3389/fncir.2012.00091

Bell, C. C., and Kawasaki, T. (1972). Relations among climbing fiber responses of nearby Purkinje Cells. *J. Neurophysiol.* 35, 155–169.

Bengtsson, F., Ekerot, C. F., and Jorntell, H. (2011). In vivo analysis of inhibitory synaptic inputs and rebounds in deep cerebellar nuclear neurons. *PLoS ONE* 6:e18822. doi: 10.1371/journal.pone.0018822

Bosman, L. W., Takechi, H., Hartmann, J., Eilers, J., and Konnerth, A. (2008). Homosynaptic long-term synaptic potentiation of the winner climbing fiber synapse in developing Purkinje cells. *J. Neurosci.* 28, 798–807. doi: 10.1523/JNEUROSCI.4074-07.2008

Brenowitz, S. D., and Regehr, W. G. (2003). Calcium dependence of retrograde inhibition by endocannabinoids at synapses onto Purkinje cells. *J. Neurosci.* 23, 6373–6384.

Brown, I. E., and Bower, J. M. (2001). Congruence of mossy fiber and climbing fiber tactile projections in the lateral hemispheres of the rat cerebellum. *J. Comp. Neurol.* 429, 59–70. doi: 10.1002/1096-9861(20000101)429

Callaway, J. C., Lasser-Ross, N., and Ross, W. N. (1995). IPSPs strongly inhibit climbing fiber-activated [Ca2+]i increases in the dendrites of cerebellar Purkinje neurons. *J. Neurosci.* 15, 2777–2787.

Campbell, N. C., Ekerot, C. F., and Hesslow, G. (1983a). Interaction between responses in Purkinje cells evoked by climbing fibre impulses and parallel fibre volleys in the cat. *J. Physiol.* 340, 225–238.

Campbell, N. C., Ekerot, C. F., Hesslow, G., and Oscarsson, O. (1983b). Dendritic plateau potentials evoked in Purkinje cells by parallel fibre volleys in the cat. *J. Physiol.* 340, 209–223.

Coesmans, M., Weber, J. T., de Zeeuw, C. I., and Hansel, C. (2004). Bidirectional parallel fiber plasticity in the cerebellum under climbing fiber control. *Neuron* 44, 691–700. doi: 10.1016/j.neuron.2004.10.031

Cohen, D., and Yarom, Y. (1998). Patches of synchronized activity in the cerebellar cortex evoked by mossy-fiber stimulation: questioning the role of parallel fibers. *Proc. Natl. Acad. Sci. U.S.A.* 95, 15032–15036. doi: 10.1073/pnas.95.25.15032

Crill, W. E. (1970). Unitary multiple-spiked responses in cat inferior olive nucleus. *J. Neurophysiol.* 33, 199–209.

Davie, J. T., Clark, B. A., and Häusser, M. (2008). The origin of the complex spike in cerebellar Purkinje cells. *J. Neurosci.* 28, 7599–7609.

Dean, P., Porrill, J., Ekerot, C. F., and Jorntell, H. (2010). The cerebellar microcircuit as an adaptive filter: experimental and computational evidence. *Nat. Rev. Neurosci.* 11, 30–43. doi: 10.1038/nrn2756

De Gruijl, J. R., Bazzigaluppi, P., de Jeu, M. T., and De Zeeuw, C. I. (2012). Climbing fiber burst size and olivary sub-threshold oscillations in a network setting. *PLoS Comput. Biol.* 8:e1002814. doi: 10.1371/journal.pcbi.1002814

De Schutter, E., and Maex, R. (1996). The cerebellum: cortical processing and theory. *Curr. Opin. Neurobiol.* 6, 759–764. doi: 10.1016/S0959-4388(96)80025-0

Desclin, J. C. (1974). Histological evidence supporting the inferior olive as the major source of cerebellar climbing fibers in the rat. *Brain Res.* 77, 365–384. doi: 10.1016/0006-8993(74)90628-3

De Zeeuw, C. I., Koekkoek, S. K., Wylie, D. R., and Simpson, J. I. (1997). Association between dendritic lamellar bodies and complex spike synchrony in the olivocerebellar system. *J. Neurophysiol.* 77, 1747–1758.

De Zeeuw, C. I., Lang, E. J., Sugihara, I., Ruigrok, T. J., Eisenman, L. M., Mugnaini, E., et al. (1996). Morphological correlates of bilateral synchrony in the rat cerebellar cortex. *J. Neurosci.* 16, 3412–3426.

Devor, A., and Yarom, Y. (2002). Generation and propagation of subthreshold waves in a network of inferior olivary neurons. *J. Neurophysiol.* 87, 3059–3069.

Dizon, M. J., and Khodakhah, K. (2011). The role of interneurons in shaping Purkinje cell responses in the cerebellar cortex. *J. Neurosci.* 31, 10463–10473. doi: 10.1523/JNEUROSCI.1350-11.2011

Duguid, I. C., and Smart, T. G. (2004). Retrograde activation of presynaptic NMDA receptors enhances GABA release at cerebellar interneuron-Purkinje cell synapses. *Nat. Neurosci.* 7, 525–533. doi: 10.1038/nn1227

Eccles, J. C. (1973). The cerebellum as a computer: patterns in space and time. *J. Physiol.* 229, 1–32.

Eccles, J. C., Ito, M., and Szentágothai, J. (1967). *The Cerebellum as a Neuronal Machine*. Berlin: Springer-Verlag. doi: 10.1016/j.pneurobio.2006.02.006

Eccles, J. C., Llinás, R., and Sasaki, K. (1966). The excitatory synaptic action of climbing fibres on the Purkinje cells of the cerebellum. *J. Physiol.* 182, 268–296.

Eccles, J. C., Sabah, N. H., Schmidt, R. F., and Taborikova, H. (1972). Integration by Purkyne cells of mossy and climbing fiber inputs from cutaneous mechanoreceptors. *Exp. Brain Res.* 15, 498–520. doi: 10.1007/BF00236405

Eilers, J., Augustine, G. J., and Konnerth, A. (1995). Subthreshold synaptic Ca2+ signalling in fine dendrites and spines of cerebellar Purkinje neurons. *Nature* 373, 155–158. doi: 10.1038/373155a0

Ekerot, C. F., and Jorntell, H. (2001). Parallel fibre receptive fields of Purkinje cells and interneurons are climbing fibre-specific. *Eur. J. Neurosci.* 13, 1303–1310. doi: 10.1046/j.0953-816x.2001.01499.x

Ekerot, C. F., and Jorntell, H. (2003). Parallel fiber receptive fields: a key to understanding cerebellar operation and learning. *Cerebellum* 2, 101–109. doi: 10.1080/14734220309411

Fujita, M. (1982). Adaptive filter model of the cerebellum. *Biol. Cybern.* 45, 195–206. doi: 10.1007/BF00336192

Gao, W., Chen, G., Reinert, K. C., and Ebner, T. J. (2006). Cerebellar cortical molecular layer inhibition is organized in parasagittal zones. *J. Neurosci.* 26, 8377–8387. doi: 10.1523/JNEUROSCI.2434-06.2006

Gao, Z., van Beugen, B. J., and de Zeeuw, C. I. (2012). Distributed synergistic plasticity and cerebellar learning. *Nat. Rev. Neurosci.* 13, 619–635. doi: 10.1038/nrn3312

Garwicz, M., Jorntell, H., and Ekerot, C. F. (1998). Cutaneous receptive fields and topography of mossy fibres and climbing fibres projecting to cat cerebellar C3 zone. *J. Physiol.* 512(Pt 1), 277–293. doi: 10.1111/j.1469-7793.1998.277bf.x

Gilbert, P. F. (1974). A theory of memory that explains the function and structure of the cerebellum. *Brain Res.* 70, 1–18. doi: 10.1016/0006-8993(74)90208-X

Gilbert, P. F. (1993). Theories of motor learning by the cerebellum. *Trends Neurosci.* 16, 177–178. doi: 10.1016/0166-2236(93)90144-B

Gilbert, P. F., and Thach, W. T. (1977). Purkinje cell activity during motor learning. *Brain Res.* 128, 309–328. doi: 10.1016/0006-8993(77)90997-0

Glitsch, M., Parra, P., and Llano, I. (2000). The retrograde inhibition of IPSCs in rat cerebellar Purkinje cells is highly sensitive to intracellular Ca2+. *Eur. J. Neurosci.* 12, 987–993. doi: 10.1046/j.1460-9568.2000.00994.x

Hansel, C., and Linden, D. J. (2000). Long-term depression of the cerebellar climbing fiber–Purkinje neuron synapse. *Neuron* 26, 473–482. doi: 10.1016/S0896-6273(00)81179-4

Hansel, C., Linden, D. J., D'Angelo, E. (2001). Beyond parallel fiber LTD: the diversity of synaptic and non-synaptic plasticity in the cerebellum. *Nat. Neurosci.* 4, 467–475. doi: 10.1038/87419

Ito, M. (2006). Cerebellar circuitry as a neuronal machine. *Prog. Neurobiol.* 78, 272–303. doi: 10.1016/j.pneurobio.2006.02.006

Ito, M. (2013). Error detection and representation in the olivo-cerebellar system. *Front. Neural Circuits* 7:1. doi: 10.3389/fncir.2013.00001

Ito, M., and Kano, M. (1982). Long-lasting depression of parallel fiber-Purkinje cell transmission induced by conjunctive stimulation of parallel fibers and climbing fibers in the cerebellar cortex. *Neurosci. Lett.* 33, 253–258. doi: 10.1016/0304-3940(82)90380-9

Kano, M., Fukunaga, K., and Konnerth, A. (1996). Ca^{2+}-induced rebound potentiation of gamma-aminobutyric acid-mediated currents requires activation of Ca^{2+}/calmodulin-dependent kinase II. *Proc. Natl. Acad. Sci. U.S.A.* 93, 13351–13356. doi: 10.1073/pnas.93.23.13351

Kano, M., Rexhausen, U., Dreessen, J., and Konnerth, A. (1992). Synaptic excitation produces a long-lasting rebound potentiation of inhibitory synaptic signals in cerebellar Purkinje cells. *Nature* 356, 601–604. doi: 10.1038/356601a0

Kawato, M., and Gomi, H. (1992). A computational model of four regions of the cerebellum based on feedback-error learning. *Biol. Cybern.* 68, 95–103. doi: 10.1007/BF00201431

Kenyon, G. T., Medina, J. F., and Mauk, M. D. (1998). A mathematical model of the cerebellar-olivary system II: motor adaptation through systematic disruption of climbing fiber equilibrium. *J. Comput. Neurosci.* 5, 71–90. doi: 10.1023/A:1008830427738

Kitamura, K., and Häusser, M. (2011). Dendritic calcium signaling triggered by spontaneous and sensory-evoked climbing fiber input to cerebellar Purkinje cells in vivo. *J. Neurosci.* 31, 10847–10858. doi: 10.1523/JNEUROSCI.2525-10.2011

Kitazawa, S., Kimura, T., and Yin, P. B. (1998). Cerebellar complex spikes encode both destinations and errors in arm movements. *Nature* 392, 494–497. doi: 10.1038/33141

Kitazawa, S., and Wolpert, D. M. (2005). Rhythmicity, randomness and synchrony in climbing fiber signals. *Trends Neurosci.* 28, 611–619. doi: 10.1016/j.tins.2005.09.004

Konnerth, A., Dreessen, J., and Augustine, G. J. (1992). Brief dendritic calcium signals initiate long-lasting synaptic depression in cerebellar Purkinje cells. *Proc. Natl. Acad. Sci. U.S.A.* 89, 7051–7055. doi: 10.1073/pnas.89.15.7051

Lampl, I., and Yarom, Y. (1993). Subthreshold oscillations of the membrane potential: a functional synchronizing and timing device. *J. Neurophysiol.* 70, 2181–2186.

Lampl, I., and Yarom, Y. (1997). Subthreshold oscillations and resonant behavior: two manifestations of the same mechanism. *Neuroscience* 78, 325–341. doi: 10.1016/S0306-4522(96)00588-X

Lang, E. J. (2002). GABAergic and glutamatergic modulation of spontaneous and motor-cortex-evoked complex spike activity. *J. Neurophysiol.* 87, 1993–2008. doi: 10.1152/jn.00477.2001

Lang, E. J., Sugihara, I., Welsh, J. P., and Llinás, R. (1999). Patterns of spontaneous Purkinje cell complex spike activity in the awake rat. *J. Neurosci.* 19, 2728–2739.

Leznik, E., and Llinás, R. (2005). Role of gap junctions in synchronized neuronal oscillations in the inferior olive. *J. Neurophysiol.* 94, 2447–2456. doi: 10.1152/jn.00353.2005

Llinás, R., Baker, R., and Sotelo, C. (1974). Electrotonic coupling between neurons in cat inferior olive. *J. Neurophysiol.* 37, 560–571.

Llinás, R., Lang, E. J., and Welsh, J. P. (1997). The cerebellum, LTD, and memory: alternative views. *Learn. Mem.* 3, 445–455. doi: 10.1101/lm.3.6.445

Llinás, R., and Sasaki, K. (1989). The functional organization of the olivo-cerebellar system as examined by multiple Purkinje cell recordings. *Eur. J. Neurosci.* 1, 587–602.

Llinás, R., and Welsh, J. P. (1993). On the cerebellum and motor learning. *Curr. Opin. Neurobiol.* 3, 958–965.

Llinás, R., and Yarom, Y. (1981). Electrophysiology of mammalian inferior olivary neurones in vitro. Different types of voltage-dependent ionic conductances. *J. Physiol.* 315, 549–567.

Llinás, R. R. (2011). Cerebellar motor learning versus cerebellar motor timing: the climbing fibre story. *J. Physiol.* 589, 3423–3432. doi: 10.1113/jphysiol.2011.207464

Lou, J. S., and Bloedel, J. R. (1992). Responses of sagittally aligned Purkinje cells during perturbed locomotion: synchronous activation of climbing fiber inputs. *J. Neurophysiol.* 68, 570–580.

Maejima, T., Oka, S., Hashimotodani, Y., Ohno-Shosaku, T., Aiba, A., Wu, D., et al. (2005). Synaptically driven endocannabinoid release requires Ca2+-assisted metabotropic glutamate receptor subtype 1 to phospholipase Cbeta4 signaling cascade in the cerebellum. *J. Neurosci.* 25, 6826–6835. doi: 10.1523/JNEUROSCI.0945-05.2005

Marr, D. (1969). A theory of cerebellar cortex. *J. Physiol.* 202, 437–470.

Marshall, S. P., van der Giessen, R. S., de Zeeuw, C. I., and Lang, E. J. (2007). Altered olivocerebellar activity patterns in the connexin36 knockout mouse. *Cerebellum* 6, 287–299. doi: 10.1080/14734220601100801

Maruta, J., Hensbroek, R. A., and Simpson, J. I. (2007). Intraburst and interburst signaling by climbing fibers. *J. Neurosci.* 27, 11263–11270.

doi: 10.1523/JNEUROSCI.2559-07.2007

Mathews, P. J., Lee, K. H., Peng, Z., Houser, C. R., and Otis, T. S. (2012). Effects of climbing fiber driven inhibition on Purkinje neuron spiking. *J. Neurosci.* 32, 17988–17997. doi: 10.1523/JNEUROSCI.3916-12.2012

Mathy, A., Ho, S. S., Davie, J. T., Duguid, I. C., Clark, B. A., and Häusser, M. (2009). Encoding of oscillations by axonal bursts in inferior olive neurons. *Neuron* 62, 388–399. doi: 10.1016/j.neuron.2009.03.023

Mauk, M. D., and Donegan, N. H. (1997). A model of pavlovian eyelid conditioning based on the synaptic organization of the cerebellum. *Learn. Mem.* 3, 130–158. doi: 10.1101/lm.4.1.130

Mauk, M. D., Steele, P. M., and Medina, J. F. (1997). Cerebellar involvement in motor learning. *Neuroscientist* 3, 303–313. doi: 10.1016/S1364-6613(98)01223-6

Medina, J. F., and Lisberger, S. G. (2008). Links from complex spikes to local plasticity and motor learning in the cerebellum of awake-behaving monkeys. *Nat. Neurosci.* 11, 1185–1192. doi: 10.1038/nn.2197

Midtgaard, J., Lasser-Ross, N., and Ross, W. N. (1993). Spatial distribution of Ca2+ influx in turtle Purkinje cell dendrites in vitro: role of a transient outward current. *J. Neurophysiol.* 70, 2455–2469.

Mittmann, W., and Häusser, M. (2007). Linking synaptic plasticity and spike output at excitatory and inhibitory synapses onto cerebellar Purkinje cells. *J. Neurosci.* 27, 5559–5570. doi: 10.1523/JNEUROSCI.5117-06.2007

Miyakawa, H., Lev-Ram, V., Lasser-Ross, N., and Ross, W. N. (1992). Calcium transients evoked by climbing fiber and parallel fiber synaptic inputs in guinea pig cerebellar Purkinje neurons. *J. Neurophysiol.* 68, 1178–1189.

Miyata, M., Finch, E. A., Khiroug, L., Hashimoto, K., Hayasaka, S., Oda, S. I., et al. (2000). Local calcium release in dendritic spines required for long-term synaptic depression. *Neuron* 28, 233–244. doi: 10.1016/S0896-6273(00)00099-4

Odeh, F., Ackerley, R., Bjaalie, J. G., and Apps, R. (2005). Pontine maps linking somatosensory and cerebellar cortices are in register with climbing fiber somatotopy. *J. Neurosci.* 25, 5680–5690. doi: 10.1523/JNEUROSCI.0558-05.2005

Ohtsuki, G., and Hirano, T. (2008). Bidirectional plasticity at developing climbing fiber-Purkinje neuron synapses. *Eur. J. Neurosci.* 28, 2393–2400. doi: 10.1111/j.1460-9568.2008.06539.x

Ohtsuki, G., Piochon, C., and Hansel, C. (2009). Climbing fiber signaling and cerebellar gain control. *Front. Cell Neurosci.* 3:4. doi: 10.3389/neuro.03.004.2009

Otis, T. S., Mathews, P. J., Lee, K. H., and Maiz, J. (2012). How do climbing fibers teach? *Front. Neural Circuits* 6:95. doi: 10.3389/fncir.2012.00095

Ozden, I., Sullivan, M. R., Lee, H. M., and Wang, S. S.-H. (2009). Reliable coding emerges from coactivation of climbing fibers in microbands of cerebellar Purkinje neurons. *J. Neurosci.* 29, 10463–10473. doi: 10.1523/JNEUROSCI.0967-09.2009

Palay, S., and Chan-Palay, V. (1974). *Cerebellar Cortex.* New York: Springer-Verlag. doi: 10.1007/978-3-642-65581-4

Palkovits, M., Mezey, E., Hamori, J., and Szentagothai, J. (1977). Quantitative histological analysis of the cerebellar nuclei in the cat. I. Numerical data on cells and on synapses. *Exp. Brain Res.* 28, 189–209. doi: 10.1007/BF00237096

Person, A. L., and Raman, I. M. (2011). Purkinje neuron synchrony elicits time-locked spiking in the cerebellar nuclei. *Nature* 481, 502–505. doi: 10.1038/nature10732

Pijpers, A., Apps, R., Pardoe, J., Voogd, J., and Ruigrok, T. J. (2006). Precise spatial relationships between mossy fibers and climbing fibers in rat cerebellar cortical zones. *J. Neurosci.* 26, 12067–12080. doi: 10.1523/JNEUROSCI.2905-06.2006

Raman, I. M., and Bean, B. P. (1997). Resurgent sodium current and action potential formation in dissociated cerebellar Purkinje neurons. *J. Neurosci.* 17, 4517–4526.

Raman, I. M., and Bean, B. P. (1999a). Ionic currents underlying spontaneous action potentials in isolated cerebellar Purkinje neurons. *J. Neurosci.* 19, 1663–1674.

Raman, I. M., and Bean, B. P. (1999b). Properties of sodium currents and action potential firing in isolated cerebellar Purkinje neurons. *Ann. N. Y. Acad. Sci.* 868, 93–96. doi: 10.1111/j.1749-6632.1999.tb11279.x

Rancz, E. A., and Hausser, M. (2006). Dendritic calcium spikes are tunable triggers of cannabinoid release and short-term synaptic plasticity in cerebellar Purkinje neurons. *J. Neurosci.* 26, 5428–5437. doi: 10.1523/JNEUROSCI.5284-05.2006

Rasmussen, A., Jirenhed, D. A., and Hesslow, G. (2008). Simple and complex spike firing patterns in Purkinje cells during classical conditioning. *Cerebellum* 7, 563–566. doi: 10.1007/s12311-008-0068-2

Raymond, J. L., and Lisberger, S. G. (1998). Neural learning rules for the vestibulo-ocular reflex. *J. Neurosci.* 18, 9112–9129.

Raymond, J. L., Lisberger, S. G., and Mauk, M. D. (1996). The cerebellum: a neuronal learning machine? *Science* 272, 1126–1131. doi: 10.1126/science.272.5265.1126

Ross, W. N., and Werman, R. (1987). Mapping calcium transients in the dendrites of Purkinje cells from the guinea-pig cerebellum in vitro. *J. Physiol.* 389, 319–336.

Ruigrok, T. J., and Voogd, J. (1995). Cerebellar influence on olivary excitability in the cat. *Eur. J. Neurosci.* 7, 679–693. doi: 10.1111/j.1460-9568.1995.tb00672.x

Sakurai, M. (1990). Calcium is an intracellular mediator of the climbing fiber in induction of cerebellar long-term depression. *Proc. Natl. Acad. Sci. U.S.A.* 87, 3383–3385. doi: 10.1073/pnas.87.9.3383

Schmolesky, M. T., Weber, J. T., de Zeeuw, C. I., and Hansel, C. (2002). The making of a complex spike: ionic composition and plasticity. *Ann. N. Y. Acad. Sci.* 978, 359–390. doi: 10.1111/j.1749-6632.2002.tb07581.x

Schultz, S. R., Kitamura, K., Post-Uiterweer, A., Krupic, J., and Häusser, M. (2009). Spatial pattern coding of sensory information by climbing fiber-evoked calcium signals in networks of neighboring cerebellar Purkinje cells. *J. Neurosci.* 29, 8005–8015. doi: 10.1523/JNEUROSCI.4919-08.2009

Sejnowski, T. J. (1977). Storing covariance with nonlinearly interacting neurons. *J. Math. Biol.* 4, 303–321. doi: 10.1007/BF00275079

Simpson, J. I., Wylie, D. R., and de Zeeuw, C. I. (1996). On climbing fiber signals and their consequence(s). *Behav. Brain Sci.* 19, 384–398. doi: 10.1017/S0140525X00081486

Soetedjo, R., Kojima, Y., and Fuchs, A. (2008). Complex spike activity signals the direction and size of dysmetric saccade errors. *Prog. Brain Res.* 171, 153–159. doi: 10.1016/S0079-6123(08)00620-1

Sotelo, C., Llinás, R., and Baker, R. (1974). Structural study of inferior olivary nucleus of the cat: morphological correlates of electrotonic coupling. *J. Neurophysiol.* 37, 541–559.

Spoelstra, J., Schweighofer, N., and Arbib, M. A. (2000). Cerebellar learning of accurate predictive control for fast-reaching movements. *Biol. Cybern.* 82, 321–333. doi: 10.1007/s004220050586

Strata, P., and Rossi, F. (1998). Plasticity of the olivocerebellar pathway. *Trends Neurosci.* 21, 407–413. doi: 10.1016/S0166-2236(98)01305-8

Sugihara, I., Lang, E. J., and Llinás, R. (1993). Uniform olivocerebellar conduction time underlies Purkinje cell complex spike synchronicity in the rat cerebellum. *J. Physiol.* 470, 243–271.

Szapiro, G., and Barbour, B. (2007). Multiple climbing fibers signal to molecular layer interneurons exclusively via glutamate spillover. *Nat. Neurosci.* 10, 735–742. doi: 10.1038/nn1907

Takechi, H., Eilers, J., and Konnerth, A. (1998). A new class of synaptic response involving calcium release in dendritic spines. *Nature* 396, 757–760. doi: 10.1038/25547

Tanaka, K., Khiroug, L., Santamaria, F., Doi, T., Ogasawara, H., Ellis-Davies, G. C., et al. (2007). Ca2+ requirements for cerebellar long-term synaptic depression: role for a postsynaptic leaky integrator. *Neuron* 54, 787–800. doi: 10.1016/j.neuron.2007.05.014

Thach, W. T. Jr. (1967). Somatosensory receptive fields of single units in cat cerebellar cortex. *J. Neurophysiol.* 30, 675–696.

Voogd, J., Pardoe, J., Ruigrok, T. J., and Apps, R. (2003). The distribution of climbing and mossy fiber collateral branches from the copula pyramidis and the paramedian lobule: congruence of climbing fiber cortical zones and the pattern of zebrin banding within the rat cerebellum. *J. Neurosci.* 23, 4645–4656.

Wang, S. S.-H., Denk, W., and Häusser, M. (2000). Coincidence detection in single dendritic spines mediated by calcium release. *Nat. Neurosci.* 3, 1266–1273. doi: 10.1038/81792

Welsh, J. P., Lang, E. J., Suglhara, I., and Llinás, R. (1995). Dynamic organization of motor control within the olivocerebellar system. *Nature* 374, 453–457. doi: 10.1038/374453a0

Wise, A. K., Cerminara, N. L., Marple-Horvat, D. E., and Apps, R. (2010). Mechanisms of synchronous activity in cerebellar Purkinje cells. *J. Physiol.* 588, 2373–2390. doi: 10.1113/jphysiol.2010.189704

Wylie, D. R., De Zeeuw, C. I., and Simpson, J. I. (1995). Temporal relations of the complex spike activity of Purkinje cell pairs in the vestibulocerebellum of rabbits. *J. Neurosci.* 15, 2875–2887.

Conflict of Interest Statement: The authors declare that the research was conducted in the absence of any commercial or financial relationships that could be construed as a potential conflict of interest.

Received: 20 March 2013; accepted: 12 June 2013; published online: 02 July 2013.
Citation: Najafi F and Medina JF (2013) Beyond "all-or-nothing" climbing fibers: graded representation of teaching signals in Purkinje cells. Front. Neural Circuits ***7****:115. doi: 10.3389/fncir.2013.00115*

frontiers in
NEURAL CIRCUITS

GENERAL COMMENTARY
published: 30 November 2012
doi: 10.3389/fncir.2012.00095

How do climbing fibers teach?

Thomas S. Otis*, Paul J. Mathews, Ka Hung Lee and Jaione Maiz

Department of Neurobiology and Center for Learning and Memory, Geffen School of Medicine at UCLA, Los Angeles, CA, USA
**Correspondence: otist@ucla.edu*

Edited by:
Chris I De Zeeuw, Erasmus Medical Center Rotterdam, Netherlands

A commentary on

A theory of cerebellar cortex
by Marr, D. (1969). J. Physiol. 202, 437–470.
A theory of cerebellar function
by Albus, J. S. (1971). Math. Biosci. 10, 25–61.

Four decades ago, Marr and Albus suggested that the climbing fiber (CF) pathway from the inferior olive (IO) to the cerebellum instructs the cellular changes necessary for motor learning (Marr, 1969; Albus, 1971). Subsequent work has confirmed that CFs can drive specific forms of associative motor learning (Gilbert and Thach, 1977; Mauk et al., 1986; Raymond et al., 1996; Jirenhed et al., 2007; Medina and Lisberger, 2008) and has detailed how CFs trigger learning-related forms of synaptic plasticity in Purkinje neurons (PNs) (Linden et al., 1991; Linden and Connor, 1995; Coesmans et al., 2004). Yet, it is widely believed that associative motor learning, such as eyeblink conditioning (Lavond and Steinmetz, 1989; Perrett et al., 1993; Medina and Mauk, 1999; Jorntell and Ekerot, 2002; Ohyama et al., 2006; Shutoh et al., 2006) and vestibulo-ocular reflex (VOR) adaptation (Miles and Lisberger, 1981; Boyden et al., 2004) result from distinct forms of synaptic plasticity that are coordinated at multiple sites within the cerebellar circuit, an idea formalized in several reviews (Raymond et al., 1996; Boyden et al., 2004; Gao et al., 2012). This raises a central question regarding how CFs coordinates plasticity at multiple sites. Simply stated, how do CFs teach?

To address this larger question it is useful to focus on three previously hypothesized sites of associative synaptic plasticity within the cerebellar circuit. At each, the CF is believed to instruct heterosynaptic forms of plasticity by driving changes in the strengths of other excitatory inputs, however, the direction of change triggered by CF activity, i.e., long-term depression (LTD) or long-term potentiation (LTP), is different at each site (**Figure 1A**). The best described example of CF teaching, and the main focus of the Marr/Albus hypothesis, occurs at the parallel fiber (PF)-to-PN synapse. In mature PNs the single CF input generates a salient and distinctive signal—a cell wide burst termed the complex spike (Eccles et al., 1964)—which instructs heterosynaptic LTD in those PFs that are coactivated with CFs [blue starburst, **Figure 1A**; (Wang et al., 2000; Hansel et al., 2001; Coesmans et al., 2004; Safo and Regehr, 2008)]. Albus also conjectured that CFs could drive plasticity at a second site, proposing heterosynaptic LTP of PF inputs to a subset of molecular layer interneurons [MLIs; red starburst in cortex, **Figure 1A**; (Albus, 1971)]. From the perspective of the PN, Albus considered CF enhancement of PF-to-MLI synapses as equivalent to "negative PF synaptic weights." Considering the fact that PNs spontaneously pacemake at rates up to ∼80 Hz (Hausser and Clark, 1997; Raman et al., 1997), PF-to-MLI LTP makes it possible to instruct learned pauses in PN spiking, something that PF LTD on its own cannot accomplish. Although this form of associative plasticity has yet to be demonstrated, there is evocative *in vivo* evidence that indirectly supports it (Jorntell and Ekerot, 2002). The final site at which CFs might instruct plasticity is at mossy fiber (MF)-to-deep cerebellar nucleus neuron (DCN) synapses (red starburst in the deep nuclei, **Figure 1A**). Much theoretical and experimental work supports the notion that MF-to-DCN synapses strengthen during associative learning (Miles and Lisberger, 1981; Lavond and Steinmetz, 1989; Perrett et al., 1993; Chen et al., 1996; Raymond et al., 1996; Garcia and Mauk, 1998; Medina and Mauk, 1999; Ohyama et al., 2006; Shutoh et al., 2006), and some of these studies indicate that plasticity in the cortex may precede or consolidate plasticity in the DCN (Ohyama et al., 2006; Shutoh et al., 2006; Wulff et al., 2009). The predicted consequence of all three forms of plasticity is to increase DCN excitability in response to particular patterns of MF/PF inputs. While it is generally accepted that CFs drive associative LTD of PFs, it is not clear whether CFs drive the associative forms of LTP during learning (i.e., PF LTP at the MLIs and MF LTP at the DCN). Perhaps relatedly, there is also some debate to whether any one of these forms of plasticity, including PF LTD (Schonewille et al., 2011), are necessary for motor learning.

In an effort to better understand the mechanistic details of how CFs participate in cerebellar learning, we have exploited optogenetic and pharmacological approaches to selectively manipulate CF signals. Using adeno-associated viral delivery of ChR2-eYFP to IO neurons we are able to transfect CFs with high efficiency and specificity in the rat (**Figure 1B**; Mathews et al., 2012). Optical activation then gives rise to "pure" CF signals generated at the key sites within the cerebellar circuit identified in **Figure 1A**. This approach shows that MLIs are cooperatively excited by several CFs, giving rise to a robust, CF-driven, feed-forward inhibition that can in turn lead to a transient, synchronous pause in multiple PNs (dashed line, **Figure 1A**). The CF excitation of MLIs shows cooperativity in part because it can result from the indirect spillover of glutamate from multiple CFs to an MLI, a phenomenon first described by Barbour and colleagues (Szapiro and Barbour, 2007). In this way our observations suggest that MLIs might read out population activity in many CFs (Bell and Kawasaki, 1972; Welsh et al., 1995; Lang et al., 1999; Marshall and Lang, 2009;

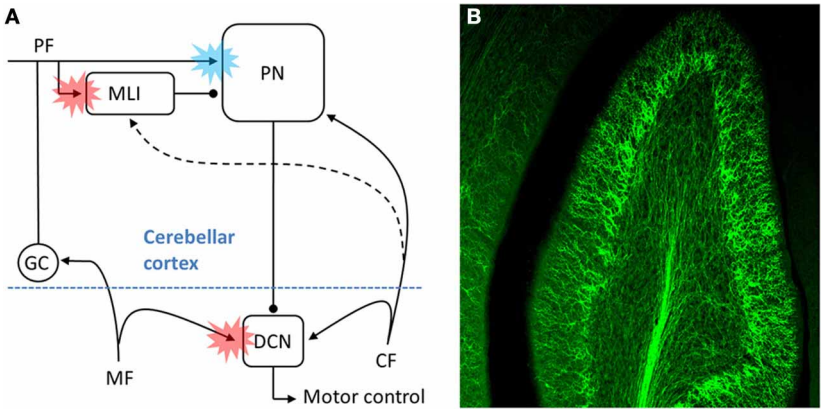

FIGURE 1 | The CF pathway and associative motor learning. **(A)** Schematic of the proposed sites (colored bursts) within the cerebellar circuit where CFs might teach during associative motor learning. The blue burst denotes CF driven LTD of PFs, while the red bursts denote CF-driven LTP of either PF inputs (at MLI) or inputs MF (at DCN). As discussed in the text, for at least two of the three sites the physiological details of the CF input, the underlying cellular mechanisms of plasticity, and the relative contribution to behavioral learning remain to be elucidated. **(B)** ChR2-eYFP expressing CFs are visible in this multi-photon microscopic image of part of folia X in a 300 μm thick rat brain slice.

Mukamel et al., 2009; Ozden et al., 2009), and that synchronous CF input to modules of PNs would result in synchronous pauses in PN spiking. In such a model, CF-dependent pauses in groups of PNs could then serve as proxy teaching signals in the DCN.

In complimentary experiments we have used specific pharmacological tools to manipulate a component of the CF signal, the post-complex spike pause in simple spike firing rate. Two very different compounds (1-EBIO, a positive modulator of calcium activated K^+ channels, or ZD 7288, an inhibitor of hyperpolarization activated cation channels) were each demonstrated to prolong the post-complex spike pause (Maiz et al., 2012). Either of these drugs infused into the cerebellar cortex during eyeblink conditioning resulted in markedly faster learning (Maiz et al., 2012). We hypothesize that prolongation of the CF-associated pause drives faster learning by facilitating associative LTP of MF inputs to DCN neurons (see **Figure 1A**). Considering the NMDA receptor dependence of MF to DCN plasticity, it is straightforward to imagine how a pause in descending PN inhibition could associatively drive the types of LTP that have been described *in vitro* (Pugh and Raman, 2006, 2009).

A critical step in understanding cerebellar learning is to explain how CFs, or other teaching signals, coordinate learning-related changes within the circuit. The experiments described here address important questions about the biology of the CF and how it might operate as a teaching signal. Related questions include whether CFs give rise to distinctive postsynaptic signals at those sites in the circuit where they have been hypothesized as teachers, and whether CFs trigger heterosynaptic, associative forms of plasticity that might contribute to learned motor behaviors. The striking anatomical organization of the cerebellar cortex coupled with the remarkable properties of the CF contact on PNs led to the insightful conjecture of Marr and Albus more than 40 years ago. Our observations are consistent with CFs exerting control over multiple sites within the cerebellar circuit, in part through indirect actions read out by MLIs or groups of PNs, a picture that brings to mind the aphorism from the Talmud, "*When you teach your son, you teach your son's son.*" Future experiments utilizing a wide breadth of classical and novel techniques, like those mentioned here will be required to determine just how paternalistic the CF is, and whether it broadens its influence in an analogous way.

REFERENCES

Albus, J. S. (1971). A theory of cerebellar function. *Math. Biosci.* 10, 25–61.

Bell, C. C., and Kawasaki, T. (1972). Relations among climbing fiber responses of nearby Purkinje Cells. *J. Neurophysiol.* 35, 155–169.

Boyden, E. S., Katoh, A., and Raymond, J. L. (2004). Cerebellum-dependent learning: the role of multiple plasticity mechanisms. *Annu. Rev. Neurosci.* 27, 581–609.

Chen, L., Bao, S., Lockard, J. M., Kim, J. K., and Thompson, R. F. (1996). Impaired classical eyeblink conditioning in cerebellar-lesioned and Purkinje cell degeneration (pcd) mutant mice. *J. Neurosci.* 16, 2829–2838.

Coesmans, M., Weber, J. T., De Zeeuw, C. I., and Hansel, C. (2004). Bidirectional parallel fiber plasticity in the cerebellum under climbing fiber control. *Neuron* 44, 691–700.

Eccles, J., Llinas, R., and Sasaki, K. (1964). Excitation of cerebellar Purkinje cells by the climbing fibres. *Nature* 203, 245–246.

Gao, Z., van Beugen, B. J., and De Zeeuw, C. I. (2012). Distributed synergistic plasticity and cerebellar learning. *Nat. Rev. Neurosci.* 13, 619–635.

Garcia, K. S., and Mauk, M. D. (1998). Pharmacological analysis of cerebellar contributions to the timing and expression of conditioned eyelid responses. *Neuropharmacology* 37, 471–480.

Gilbert, P. F., and Thach, W. T. (1977). Purkinje cell activity during motor learning. *Brain Res.* 128, 309–328.

Hansel, C., Linden, D. J., and D'Angelo, E. (2001). Beyond parallel fiber LTD: the diversity of synaptic and non-synaptic plasticity in the cerebellum. *Nat. Neurosci.* 4, 467–475.

Hausser, M., and Clark, B. A. (1997). Tonic synaptic inhibition modulates neuronal output pattern and spatiotemporal synaptic integration. *Neuron* 19, 665–678.

Jirenhed, D. A., Bengtsson, F., and Hesslow, G. (2007). Acquisition, extinction, and reacquisition of a cerebellar cortical memory trace. *J. Neurosci.* 27, 2493–2502.

Jorntell, H., and Ekerot, C. F. (2002). Reciprocal bidirectional plasticity of parallel fiber receptive fields in cerebellar Purkinje cells and their afferent interneurons. *Neuron* 34, 797–806.

Lang, E. J., Sugihara, I., Welsh, J. P., and Llinas, R. (1999). Patterns of spontaneous purkinje cell

complex spike activity in the awake rat. *J. Neurosci.* 19, 2728–2739.

Lavond, D. G., and Steinmetz, J. E. (1989). Acquisition of classical conditioning without cerebellar cortex. *Behav. Brain Res.* 33, 113–164.

Linden, D. J., and Connor, J. A. (1995). Long-term synaptic depression. *Annu. Rev. Neurosci.* 18, 319–357.

Linden, D. J., Dickinson, M. H., Smeyne, M., and Connor, J. A. (1991). A long-term depression of AMPA currents in cultured cerebellar Purkinje neurons. *Neuron* 7, 81–89.

Maiz, J., Karakossian, M. H., Pakaprot, N., Robleto, K., Thompson, R. F., and Otis, T. S. (2012). Prolonging the postcomplex spike pause speeds eyeblink conditioning. *Proc. Natl. Acad. Sci. U.S.A.* 109, 16726–16730.

Marr, D. (1969). A theory of cerebellar cortex. *J. Physiol.* 202, 437–470.

Marshall, S. P., and Lang, E. J. (2009). Local changes in the excitability of the cerebellar cortex produce spatially restricted changes in complex spike synchrony. *J. Neurosci.* 29, 14352–14362.

Mathews, P. J., Lee, K. H., Peng, Z., Houser, C. R., and Otis, T. S. (2012). Effects of climbing fiber driven inhibition on Purkinje neuron spiking. *J. Neurosci.* 32, (in press).

Mauk, M. D., Steinmetz, J. E., and Thompson, R. F. (1986). Classical conditioning using stimulation of the inferior olive as the unconditioned stimulus. *Proc. Natl. Acad. Sci. U.S.A.* 83, 5349–5353.

Medina, J. F., and Lisberger, S. G. (2008). Links from complex spikes to local plasticity and motor learning in the cerebellum of awake-behaving monkeys. *Nat. Neurosci.* 11, 1185–1192.

Medina, J. F., and Mauk, M. D. (1999). Simulations of cerebellar motor learning: computational analysis of plasticity at the mossy fiber to deep nucleus synapse. *J. Neurosci.* 19, 7140–7151.

Miles, F. A., and Lisberger, S. G. (1981). Plasticity in the vestibulo-ocular reflex: a new hypothesis. *Annu. Rev. Neurosci.* 4, 273–299.

Mukamel, E. A., Nimmerjahn, A., and Schnitzer, M. J. (2009). Automated analysis of cellular signals from large-scale calcium imaging data. *Neuron* 63, 747–760.

Ohyama, T., Nores, W. L., Medina, J. F., Riusech, F. A., and Mauk, M. D. (2006). Learning-induced plasticity in deep cerebellar nucleus. *J. Neurosci.* 26, 12656–12663.

Ozden, I., Sullivan, M. R., Lee, H. M., and Wang, S. S. (2009). Reliable coding emerges from coactivation of climbing fibers in microbands of cerebellar Purkinje neurons. *J. Neurosci.* 29, 10463–10473.

Perrett, S. P., Ruiz, B. P., and Mauk, M. D. (1993). Cerebellar cortex lesions disrupt learning-dependent timing of conditioned eyelid responses. *J. Neurosci.* 13, 1708–1718.

Pugh, J. R., and Raman, I. M. (2006). Potentiation of mossy fiber EPSCs in the cerebellar nuclei by NMDA receptor activation followed by postinhibitory rebound current. *Neuron* 51, 113–123.

Pugh, J. R., and Raman, I. M. (2009). Nothing can be coincidence: synaptic inhibition and plasticity in the cerebellar nuclei. *Trends Neurosci.* 32, 170–177.

Raman, I. M., Sprunger, L. K., Meisler, M. H., and Bean, B. P. (1997). Altered subthreshold sodium currents and disrupted firing patterns in Purkinje neurons of Scn8a mutant mice. *Neuron* 19, 881–891.

Raymond, J. L., Lisberger, S. G., and Mauk, M. D. (1996). The cerebellum: a neuronal learning machine? *Science* 272, 1126–1131.

Safo, P., and Regehr, W. G. (2008). Timing dependence of the induction of cerebellar LTD. *Neuropharmacology* 54, 213–218.

Schonewille, M., Gao, Z., Boele, H. J., Veloz, M. F., Amerika, W. E., Simek, A. A., et al. (2011). Reevaluating the role of LTD in cerebellar motor learning. *Neuron* 70, 43–50.

Shutoh, F., Ohki, M., Kitazawa, H., Itohara, S., and Nagao, S. (2006). Memory trace of motor learning shifts transsynaptically from cerebellar cortex to nuclei for consolidation. *Neuroscience* 139, 767–777.

Szapiro, G., and Barbour, B. (2007). Multiple climbing fibers signal to molecular layer interneurons exclusively via glutamate spillover. *Nat. Neurosci.* 10, 735–742.

Wang, S. S., Denk, W., and Hausser, M. (2000). Coincidence detection in single dendritic spines mediated by calcium release. *Nat. Neurosci.* 3, 1266–1273.

Welsh, J. P., Lang, E. J., Suglhara, I., and Llinas, R. (1995). Dynamic organization of motor control within the olivocerebellar system. *Nature* 374, 453–457.

Wulff, P., Schonewille, M., Renzi, M., Viltono, L., Sassoè-Pognetto, M., Badura, A., et al. (2009). Synaptic inhibition of Purkinje cells mediates consolidation of vestibulo-cerebellar motor learning. *Nat. Neurosci.* 12, 1042–1049.

Received: 16 September 2012; accepted: 11 November 2012; published online: 30 November 2012.

Citation: Otis TS, Mathews PJ, Lee KH and Maiz J (2012) How do climbing fibers teach? Front. Neural Circuits ***6****:95. doi: 10.3389/fncir.2012.00095*

frontiers in
NEURAL CIRCUITS

HYPOTHESIS AND THEORY ARTICLE
published: 28 May 2013
doi: 10.3389/fncir.2013.00094

Role of the olivo-cerebellar complex in motor learning and control

***Nicolas Schweighofer*[1,2]*, *Eric J. Lang*[3] *and Mitsuo Kawato*[4]**

[1] *Division of Biokinesiology and Physical Therapy, University of Southern California, Los Angeles, CA, USA*
[2] *Movement to Health Laboratory, Montpellier-1 University, Montpellier, France*
[3] *Department of Physiology and Neuroscience, New York University, New York, NY, USA*
[4] *Brain Information Communication Research Laboratory Group, Advanced Telecommuniction Research Institue International, Kyoto, Japan*

Edited by:
Chris I. De Zeeuw, Erasmus Medical Center, Netherlands

Reviewed by:
Yosef Yarom, Hebrew University, Israel
Jornt R. De Gruijl, Netherlands Institute for Neuroscience, Netherlands

***Correspondence:**
Nicolas Schweighofer, Division of Biokinesiology and Physical Therapy, University of Southern California, CHP 155, Los Angeles, CA 90089, USA.
e-mail: schweigh@usc.edu

How is the cerebellum capable of efficient motor learning and control despite very low firing of the inferior olive (IO) inputs, which are postulated to carry errors needed for learning and contribute to on-line motor control? IO neurons form the largest electrically coupled network in the adult human brain. Here, we discuss how intermediate coupling strengths can lead to chaotic resonance and increase information transmission of the error signal despite the very low IO firing rate. This increased information transmission can then lead to more efficient learning than with weak or strong coupling. In addition, we argue that a dynamic modulation of IO electrical coupling via the Purkinje cell-deep cerebellar neurons – IO triangle could speed up learning and improve on-line control. Initially strong coupling would allow transmission of large errors to multiple functionally related Purkinje cells, resulting in fast but coarse learning as well as significant effects on deep cerebellar nucleus and on-line motor control. In the late phase of learning decreased coupling would allow desynchronized IO firing, allowing high-fidelity transmission of error, resulting in slower but fine learning, and little on-line motor control effects.

Keywords: cerebellum, motor learning, inferior olive, electrical coupling, Purkinje cells, deep cerebellar nucleus, complex spikes, synchrony

EFFICIENT CEREBELLAR LEARNING AND CONTROL DESPITE SPORADIC INFERIOR OLIVE SPIKING

The inferior olive (IO) neurons, via the terminal portions of the axons called the climbing fibers, form a powerful input to the Purkinje cells of the cerebellar cortex (Szentágothai and Rajkovitz, 1959; Eccles et al., 1966; Desclin, 1974). Each Purkinje cell is innervated by only a single climbing fiber from which it receives hundreds of synapses (Llinas et al., 1969; Silver et al., 1998) that collectively provide such strong excitation that their action always triggers what is referred to as a "complex spike." Complex spikes are relatively sporadic, however, with a mean single cell firing rate of one to two spikes per second in awake animals, e.g., (Thach, 1968). Purkinje cells, which form the sole output of the cerebellar cortex, act primarily by inhibiting the deep cerebellar nuclear (DCN) neurons. The mossy fibers, via granule cells, provide the second excitatory input to Purkinje cells. In contrast to the massive input it receives from its one climbing fiber afferent, each Purkinje cell makes at most a few synapses with each of the ∼100,000–200,000 parallel fibers with which it synapses (Harvey and Napper, 1991). Thus, in contrast to the all-or-none nature of the climbing fiber input, the parallel fibers provide a graded input that helps modulate the Purkinje cell "simple spike" firing rate over a range that can span 0–200 Hz.

According to the motor learning theory of the cerebellum (Marr, 1969; Albus, 1971; Ito, 1982), these two classes of Purkinje cell inputs are those that are required by a supervised learning machine, i.e., a machine that learns to improve its performance by minimizing errors (Wolpert and Miall, 1996). Specifically, Purkinje cells learn the weighting of granule cell inputs to minimize the error signals conveyed by climbing fibers (Gilbert and Thach, 1977; Kitazawa et al., 1998), via plasticity in Purkinje cell synapses (Ito, 2001). In this way, the cerebellum can learn inverse models to refine motor commands from desired states (Kawato and Gomi, 1992a; Shidara et al., 1993; Schweighofer, 1998) or forward models to predict the consequences of movements from motor commands (Kawato et al., 1987; Miall et al., 2007; Tseng et al., 2007), or both.

The cerebellum has many features that appear to match those found in effective and efficient artificial learning machines that can learn inverse or forward models from errors, such as the cerebellar model articulation controller (CMAC, Albus, 1975). Like the cerebellum, these "supervised learning" machines recode multiple inputs into high dimensional patterns (the mossy fibers to granule projections), have modifiable synapses from the high dimension layer to the output (the granule cells to Purkinje cells synapses), and use a learning rule to minimize the errors in outputs (error signals carried via climbing fibers). Differences exist, however. One crucial difference that is bound to affect the learning performance of the cerebellum negatively is that the firing rates of IO neurons are very low, which implies that a single Purkinje cell will fire at most one or two complex spikes during a typical movement. Such low firing rates significantly decrease the error transmission rate capability of the system, and thus its learning efficiency, compared to an

artificial machine that is capable of high frequency transmission of errors.

To overcome this poor error transmission efficiency, the IO firing rate cannot simply be increased while maintaining good functioning of the cerebellum. One reason is that climbing fiber inputs are carried downstream by the Purkinje cells in the form of complex spikes. Assuming, for the sake of argument, that simple spikes are the only relevant output of the Purkinje cell, increases in complex spike firing rates would decrease the signal to noise ratio in the Purkinje cell output, interfering with the information being conveyed by simple spikes. In contrast, in artificial machines, because the error signal is only propagated to the level at which it is used to cause synaptic plasticity, and is not carried further downstream, it can carry any high frequency signals needed to minimize errors.

In addition to its role in motor learning, the olivo-cerebellar system may contribute directly to the on going motor commands issued by the cerebellum, and if so, complex spikes are then not simply noise, but a signal that likely needs to be distinguished from simple spikes. A long-standing argument for olivo-cerebellar activity contributing to motor commands directly is that abnormal complex spike activity patterns or lesions of the IO can cause problems in motor coordination and tremors (de Montigny and Lamarre, 1973; Llinas et al., 1975). For example, harmaline intoxication causes a tremor that is phase-locked to the highly synchronized olivo-cerebellar activity (Lamarre and Mercier, 1971; de Montigny and Lamarre, 1973; Llinas and Volkind, 1973). Olivo-cerebellar activity itself directly drives the cerebellar output that causes the tremor, rather than acting indirectly via modulation of simple spike activity because simple spikes are often absent when the tremor occurs (de Montigny and Lamarre, 1973). Further evidence that complex spikes are a significant part of Purkinje cell output comes from several studies that show that complex spikes can cause a significant inhibition of DCN activity, and that the strength of this inhibition is correlated with the level of synchrony (Bengtsson et al., 2011; Blenkinsop and Lang, 2011).

In addition, evidence exists for a direct contribution of olivo-cerebellar activity to cerebellar output under more physiological conditions. Changes in complex spike activity are associated with performance of well-learned movements. In particular, multi-electrode recordings have shown that increases in complex spike synchrony levels occur in relation to conditioned tongue licking movements (Welsh et al., 1995). Subsequent imaging studies have also found that complex spike synchrony increases during motor acts (Mukamel et al., 2009; Ozden et al., 2009). However, it is important to note that the definitions of synchrony used in the imaging studies was generally more relaxed, by an order of magnitude or more, than that used in the multielectrode experiments where typically a 1 ms definition has been used (i.e., the onset of two spikes must occur within 1 ms of each other to be considered synchronous). In contrast, a variety of time bins generally ranging from 20 to 256 ms were used in the imaging studies (Mukamel et al., 2009; Ozden et al., 2009; Schultz et al., 2009). As a result, imaging studies have reported higher absolute synchrony levels than the electrophysiological studies; however, this difference is likely apparent rather than real, as it disappears when a similar temporal definition for synchrony is used and other experimental factors are accounted for; see (Lang, 2009). In sum, both electrophysiological and imaging results are consistent with a direct role for olivo-cerebellar activity in motor coordination. Yet, just as was the case with motor learning, the low firing rates of complex spikes presents a problem for the direct participation of the olivo-cerebellar system in motor coordination. Specifically, that any Purkinje cell will, on average, only fire a single complex spike during a typical movement puts severe restrictions on the ability of the olivo-cerebellar system to code motor signals in terms of individual cell firing rates.

How can the olivo-cerebellar system solve the problem of contributing both to on-line motor control and to motor learning given the constraint of low firing rate? Moreover, how can the system perform its two proposed functions independent of each other, if needed? Here, we propose that the ability of this system to modulate the level of synchronization is central to answering these questions. We address this issue as follows. First, we review the anatomical and physiological organization of the olivo-cerebellar system, with emphasis on the electrical coupling between IO cells via gap junctions. Second, we discuss how moderate electrical coupling in the IO network can, somewhat counter-intuitively, desynchronize the activity of IO neurons, and as a result, influence the learning of fine motor commands without causing unwanted motor acts. Third, we concentrate on the possible function of the closed triangle circuit formed by the IO-Purkinje cell-DCN, in the dynamic modulation of the coupling strength between IO neurons, and suggest how this circuit can modulate the transmission of errors at different stages of learning. Finally, in the discussion, we speculate how a partial dissociation of the two roles of the Purkinje cell-DCN-IO circuit in both learning and control can be made possible by their differential dependence on synchrony levels, which are controlled by feedback from the cerebellum.

INFERIOR OLIVE NETWORK ANATOMY AND PHYSIOLOGY

The anatomical organization of the IO has two distinctive features. The first distinctive feature is that almost all (∼97%) IO neurons are projection cells (Fredette and Mugnaini, 1991) whose axons do not normally give off recurrent collaterals (see De Zeeuw et al., 1996 for a discussion of this issue). As a result, few of the chemical synaptic terminals within the IO arise from the IO neurons themselves. Instead, they originate from a variety of extrinsic sources. The majority can be grouped into two classes based on their origin and chemical nature: inhibitory, gamma-aminobutyric acid (GABA)ergic synapses arise from the DCN (for most IO regions) and a few other brainstem nuclei, and excitatory synapses, which arise from a variety of brainstem and spinal cord regions (de Zeeuw et al., 1989; Nelson and Mugnaini, 1989; Fredette and Mugnaini, 1991). The second distinctive feature is that IO neurons likely form the strongest gap junction coupled neuronal network in the adult human brain (De Zeeuw et al., 1995; Condorelli et al., 1998; Belluardo et al., 2000). Thus, because direct chemical synaptic interactions between IO neurons are limited, IO neurons interact strongly via electrical synapses. Indeed, electrical coupling between IO neurons and its dependence on gap junctions has been well-established (Llinas et al., 1974; Llinás and Yarom, 1981a; Long et al., 2001; Devor and Yarom, 2002; Leznik and Llinas, 2005).

The gap junctions mainly occur between the dendritic spines of neighboring IO neurons that form the core of a complex synaptic structure known as a glomerulus (Sotelo et al., 1974). Each glomerulus, in addition to its dendritic core, contains presynaptic terminals, which can control the efficacy of the electrical coupling between specific IO neurons by a current shunting mechanism (Llinas et al., 1974; Sotelo et al., 1974; Onizuka et al., 2013). Both GABAergic and non-GABAergic terminals are found within the glomeruli (de Zeeuw et al., 1989), indicating roles for both inhibitory and excitatory control over the effective coupling of specific IO neurons. In addition to intraglomerular synapses, excitatory and inhibitory synapses occur directly on the dendrites and somata of IO neurons (Sotelo et al., 1974; de Zeeuw et al., 1989), and thus likely exert a more global control over the excitability of each IO neuron. In sum, the activity of IO neurons is modulated by excitatory inputs (such as those carrying errors), gap junctions between other IO neurons, and inhibitory inputs from cerebellar nuclear neurons (Lang, 2003).

Electrical coupling of IO neurons and modulation of its efficacy is thought to underlie the patterns of synchronous complex spike activity that are observed in cerebellar Purkinje cells (Bell and Kawasaki, 1972; Sasaki et al., 1989; Lang et al., 1999). Before discussing this relationship, however, it is worth distinguishing electrical coupling of IO neurons from Purkinje cell complex spike synchrony, because even though the latter is often used as a measure of the former, and although the two phenomena are highly related, they are not identical. Electrical coupling refers simply to there being an electrical conductance between two neurons, and its strength may be measured by a coupling coefficient (e.g., see Devor and Yarom, 2002). In contrast, Purkinje cell complex spike synchrony reflects only the synchronized suprathreshold activity between two IO neurons, and will depend on both the strength of the coupling between the two IO cells and their membrane potentials relative to spike threshold. Thus, for example, if one of two coupled cells is more hyperpolarized, it may not fire an action potential, even when excited by current flowing from the other cell, and thus the complex spike activity in the Purkinje cells postsynaptic to these neurons will not be synchronized. Indeed, such a scenario has been postulated to explain some of the changes in synchrony distribution that occur following block of excitatory drive to the IO (Lang, 2001, 2002). Nevertheless, in most instances the level of complex spike synchrony is probably a good indicator of electrical coupling between IO neurons.

The patterns of synchronous complex spike activity that characterize the olivo-cerebellar system have been investigated *in vivo* during the past several decades using multielectrode recording. Consistent with the gap junction coupling of IO neurons underlying complex spike synchrony, both synchronous IO and complex spike activity is lost when IO gap junctions are blocked pharmacologically (Leznik and Llinas, 2005; Blenkinsop and Lang, 2006), and is absent in connexin36 knockout mice (Long et al., 2001; Marshall et al., 2007). Furthermore, gap junctions, together with cellular current dynamics, generate synchronized subthreshold oscillations in the membrane potential of IO neurons (Llinás and Yarom, 1981a,b; Manor et al., 1997; Schweighofer et al., 1999).

These studies showed that the spatial distribution of synchronous complex spike activity is rather restricted despite the extensive gap junction coupling of IO neurons. Complex spike synchrony can occur between specific widely separated regions of the cortex (De Zeeuw et al., 1996); however, the highest levels of synchronous activity are found mainly among Purkinje cells located in the same narrow (∼250–500 μm wide) cortical band, with the long axis of each band oriented parallel to the transverse axis of the folium in which it is located (Sasaki et al., 1989; Sugihara et al., 1993; Lang et al., 1999). Although the spatial resolution of most of these studies was only ∼250 μm (the spacing of the electrodes in the array), there is good reason to believe that finer grained patterns than the observed banding patterns are unlikely to exist, because recording with higher density multielectrode arrays (166 μm electrode spacing) failed to reveal any finer intraband structure (Fukuda et al., 2001), nor did studies with calcium imaging techniques, which, in theory, can record complex spikes from the entire local Purkinje cell population albeit with less temporal resolution (Mukamel et al., 2009; Ozden et al., 2009; Schultz et al., 2009). The synchrony bands are at least partly congruent with anatomically-defined compartments based on zebrin staining, as high synchrony levels are found mainly among cells within the same zebrin compartment (Sugihara et al., 2007), and thus reflect the topography of the olivo-cerebellar projection (Voogd and Bigaré, 1980).

However, complex spike synchrony is a dynamic entity as shown by changes in complex spike synchrony levels and patterns associated with movement (Welsh et al., 1995; Mukamel et al., 2009; Ozden et al., 2009). The control of the specific synchrony patterns reflects the activity of GABAergic and glutamatergic inputs to the IO. Intra-IO injection of picrotoxin (PIX), a GABA-A antagonist, or lesion of the GABAergic projection from the cerebellar nuclei, induces higher complex spike firing rates, and more widespread synchronization (Lang et al., 1996; Lang, 2002). Consistent with these *in vivo* findings, voltage-sensitive dye imaging results have demonstrated that PIX increases the size of coherently oscillating IO neuronal clusters in brainstem slice preparations (Lang et al., 1997). In contrast to blocking GABA, blocking glutamatergic activity produces lower firing rates and smaller, more discrete groups of Purkinje cells with synchronized activity (Lang, 2001, 2002).

That the GABAergic afferents to the IO largely arise from the DCN suggests that the cerebellum actively shapes its own inputs. Indeed, the topography of the connections between the IO and cerebellum allow functionally related Purkinje cells, DCN cells, and IO cells to be grouped into "microcomplexes" or modules (Ito, 1984; Schweighofer, 1998; Apps and Hawkes, 2009). That is, the connections between the IO and cerebellum are precisely aligned so that anatomically closed loops are formed between corresponding regions of the IO, cerebellar cortex and nuclei (Voogd and Bigaré, 1980; Sugihara and Shinoda, 2004; Apps and Hawkes, 2009; Sugihara et al., 2009; Ruigrok, 2010). Thus, the cerebellar cortex can be subdivided into numerous longitudinal zones, and Purkinje cells from anyone zone will target a specific region of the cerebellar (or in a few cases, the vestibular) nuclei, exerting an inhibitory influence on those neurons. In turn, about 30–50% of the cerebellar nuclear neurons from each regions end inhibitory projections to a particular IO region (de Zeeuw et al., 1989; Nelson and Mugnaini, 1989; Fredette and Mugnaini, 1991). Thus, a double- inhibitory feed back circuit

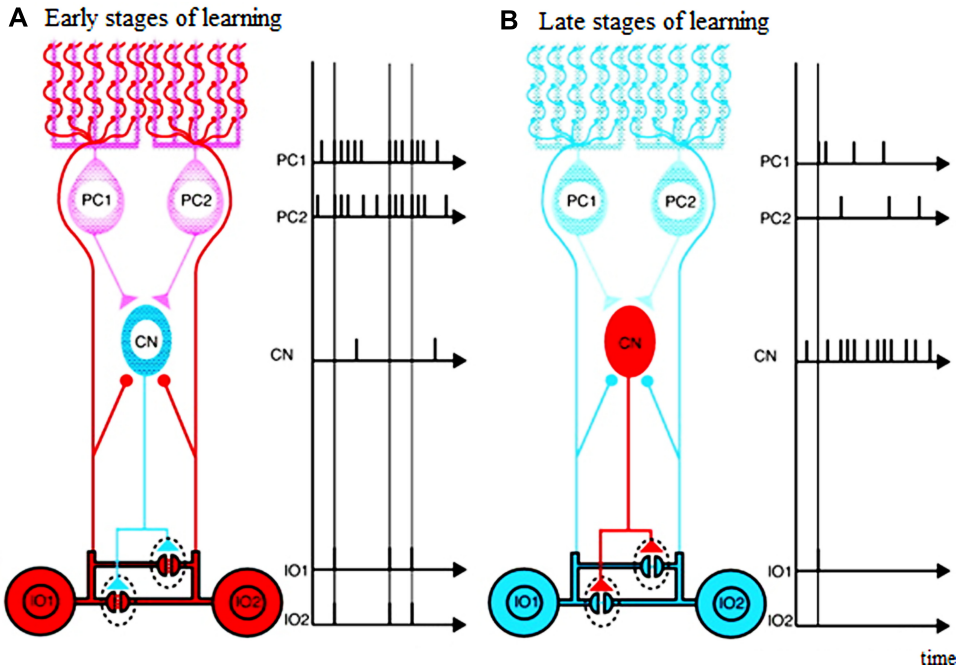

FIGURE 1 | Schematic diagram illustrating possible functions of closed triangle circuit consisting of inferior olive (IO) nucleus, Purkinje cells (PCs), and deep Cerebellar Nucleus (CN). (A) Early stages of learning. **(B)** Late stages of learning. Purkinje cells inhibit deep cerebellar nucleus cells. Inhibitory deep cerebellar nucleus cells innervate dendrites of inferior olive cells within glomeruli very close to gap junctions. The diagram does not include mossy-fiber inputs and their target granule cells, parallel-fiber inputs, inhibitory interneurons, excitatory deep cerebellar nucleus. Excitatory inputs to inferior olive cells are not shown either. Blue neurons are not excited, and red are excited. Excitatory synapses are shown by circles, and inhibitory synapses are shown by triangles. Horizontal lines show electrical gap junctions. Adapted from Figure 3 in Kawato et al. (2011), itself adapted from Figure 3 in De Zeeuw et al. (1998)

from Purkinje cells to the IO via the DCN exists, and enables each cerebellar cortical region to influence the activity of its own projection from the IO (see **Figure 1**). Consistent with this anatomical arrangement, complex spike synchrony bands appear to follow this modular organization (Sugihara et al., 2007), and the simple spike activity of each cortical region, via this feedback circuit, can regulate its own complex spike synchrony levels (Marshall and Lang, 2009).

In sum, it seems clear that synchrony is likely to be a physiologically important parameter of olivo-cerebellar function. However, there is less consensus on what its function or functions may be. This lack of consensus is certainly due to several factors, but in the following we will focus on the problems related to motor learning and specifically how electrical coupling of IO neurons can allow learning processes to occur at complex spike firing rates and synchrony levels that do not interfere with on-line motor coordination.

CHAOTIC RESONANCE ENHANCES LEARNING BY INCREASING INFORMATION TRANSMISSION

INTERMEDIATE COUPLING LEADS TO CHAOS AND INCREASE INFORMATIONTRANSMISSION VIA "CHAOTIC RESONANCE"

Coupled IO cells do not necessarily synchronize their firing, and indeed, although the system has the capability of generating widespread synchrony, it normally does not do so. Several results suggest that electrical coupling among IO neurons may allow other patterns of activity. First, in coupled oscillatory cell IO models, depending on coupling strength, the neurons can fire in phase or antiphase (Schweighofer et al., 1999). Antiphase firing of IO neurons has, in fact, been observed experimentally under *in vitro* conditions (Llinás and Yarom, 1986). Second, in networks of IO cells, coupling can induce chaos in subthreshold oscillations (Makarenko and Llinas, 1998). Moreover, in a model of IO neurons, a maximum chaotic regime of spiking activity was observed for intermediate levels of gap junction conductance (Schweighofer et al., 2004), whereas lower and higher coupling strengths induced more regular firing. Note that chaotic systems are deterministic, which means that their future behavior is fully determined by their initial conditions, with no randomness (noise) involved. However, small differences in initial conditions yield widely diverging outcomes, rendering long-term prediction impossible.

Our previous modeling study (Schweighofer et al., 2004) also indicated that such chaotic behavior can enhance information transfer in these neurons, via a "chaotic resonance" (Nishimura et al., 2000). We quantified the influence of electrical coupling on the low firing code of IO output by computing how much information about the input could be extracted from the IO output spike trains, i.e., the mutual information. The concept of chaotic resonance derives from that of stochastic resonance (see Wiesenfeld and Moss, 1995 for review), a phenomenon in which the presence of noise helps a non-linear system in amplifying a weak (under threshold) signal, as found in sensory neurons. Considering that

deterministic chaos resembles the feature of noise and provides a source of fluctuation, stochastic resonance-like behavior can be observed in deterministic dynamical systems in the absence of noise in two ways: either by substituting the stochastic noise source by a chaotic source, or directly via intrinsic chaotic dynamics, as we found in IO networks with intermediate coupling strengths.

In the chaotic regime of IO network, we have shown that the increase in information transmission in IO neurons is achieved via distributing-frequency components of the error inputs over the sporadic, irregular, and non-phase-locked spikes (Schweighofer et al., 2004). Desynchronization is indeed necessary for scattering the spike timings of each neuron to increase the time resolution of the population rate coding (Masuda and Aihara, 2002). Then, the complete continuous error signal can be reconstructed by spatial integration across Purkinje cells within a microcomplex and via temporal integration for each Purkinje cell via cumulative effects of long-term depression (LTD; see Figure 1 and associated text in Schweighofer et al., 2004 for an intuitive understanding).

Note that these results are robust to cell parameters and complexity and do not depend on the specificity of the cell model. In our original chaotic IO model, we used a rather complicated compartment model, and many physiological parameters were chosen rather arbitrarily, casting doubt on the generalizability of our results. In Tokuda et al. (2010), however, we showed that a simple, minimal, model of IO neurons also exhibits chaotic resonance for intermediate coupling.

INCREASED INFORMATION TRANSMISSION LEADS TO MORE EFFICIENT LEARNING

In Tokuda et al. (2010), we tested the prediction that efficient cerebellar learning is realized with an intermediate coupling strength. In these simulations, the IO neurons provide error signals to an idealized model of the cerebellar cortex that learns, via feedback error learning (Kawato et al., 1987; Kawato and Gomi, 1992b) to control a simplified model of the human arm in rapid reaching movements. As predicted, intermediate coupling levels, which allow chaotic resonance and increased information transfer of the error signals, accelerated motor learning models, despite the low IO firing rate (Tokuda et al., 2010).

Note that noise, ubiquitous in the nervous system, can have a similar effect to coupling in enhancing cerebellar learning via stochastic resonance (Tokuda et al., 2010). Indeed, we showed that noise and coupling are complementary and reinforce each other: the interplay between coupling and noise enlarged the parameter ranges of both coupling strength and noise intensity that provide efficient learning. However, chaos-induced desynchronization, possibly in addition to noise-induced desynchronization, is advantageous in two ways. First, from an energetics point of view, coupling generated chaos is a cheaper way of destroying the synchrony between cells, because noise in the nervous system is thought to arise mainly from synaptic noise (Hubbard et al., 1967). On the other hand, electrical coupling itself does not require energy expenditure. Second, although coupling could be modulated during learning by inhibitory inputs from the cerebellar nucleus, it is unclear how noise could be modulated during learning.

Experimental support for this role of electric coupling in cerebellar learning comes from mice mutants lacking electrotonic coupling between IO cells (Van Der Giessen et al., 2008). These mice have no prominent general motor deficits, but they do exhibit deficits in learning-dependent motor tasks such as locomotor or eye-blink conditioning. The IO neurons in these mice have altered subthreshold oscillations, resulting in more variable latencies of spikes, which lead to deficits in the timing of conditioned motor responses (Van Der Giessen et al., 2008). Similarly, humans with reduced IO coupling as a result of the anti-malaria drug mefloquine exhibit no general motor deficits but show motor learning impairments (van Essen et al., 2010).

DYNAMIC MODULATION OF IO ELECTRICAL COUPLING DURING LEARNING

MODULATION OF COUPLING VIA INHIBITION FROM NUCLEAR CELLS

In recent simulation work, we investigated whether inhibitory modulation of electrical coupling is indeed a major determinant of the IO firing dynamics (Onizuka et al., 2013). We specifically aimed at reproducing the IO firing dynamics of the PIX and carbenoxolone (CBX) experimental studies (Lang, 2002; Blenkinsop and Lang, 2006). The original model by Schweighofer et al. (1999) was modified by adding a model of the glomerulus comprised of dendritic spine necks that accommodate gap junctions and inhibitory synapses (see **Figure 1**).In this model, under simplifying assumptions, the effective coupling conductance $g_{\text{effective}}$ between connected IO cells is computed from the gap junction conductance g_{junction} and the conductance of inhibitory synapses $g_{\text{inhibitory}}$ and from the spine neck conductance g_{spine} as follows (Katori et al., 2010):

$$g_{\text{effective}} = \left(g_{\text{junction}} \cdot g_{\text{spine}}\right) / \left(2g_{\text{junction}} + g_{\text{spine}} + g_{\text{inhibitory}}\right)$$

Thus, if the inhibitory synaptic conductance is large, the effective coupling conductance decreases because of shunting inhibition. In (Onizuka et al., 2013), we determined the gap junction conductance $g_{junction}$ and the conductance of inhibitory synapses $g_{inhibitory}$ that minimize the fitting error between simulated IO firing from the model and the experimental complex spike data in three conditions: PIC, CBX, and control. We found that the inhibitory $g_{inhibitory}$ and gap junction $g_{junction}$ conductances roughly halved under the PIX and CBX conditions, respectively, supporting the role of a direct modulation of coupling strength via inhibitory inputs. Thus, because the inhibitory neurons controlling the strength of coupling between IO cells are located in the DCN, the strength of effective coupling, and thus the level of chaotic behavior, presumably depends on the modulation of the deep cerebellar neurons via plastic processes in the cerebellar cortex and nuclei.

Experimental support for a functional role of the inhibition near gap junctions was previously reported (Shaikh et al., 2010). It was argued that oculopalatal tremor may be due to the removal of inhibition near the electronic gap junctions in the IO. Interestingly, such patients with oculopalatal tremor show slower motor learning. This could be explained by the fact that only poorer error information can be transmitted when IO cells are strongly coupled and oscillate in-phase (Schweighofer et al., 2004).

DYNAMIC MODULATION OF IO ELECTRICAL COUPLING VIA THE PURKINJE CELL-DEEP CEREBELLAR NEURONS – IO TRIANGLE

The Purkinje cell-DCN -IO triangle may act as a circuit to satisfy the motor learning requirements of the cerebellar learning system (Kawato et al., 2011). That is, in the early phase of motor learning, when motor acts are clumsy and far from the desired ones and the executed movement trajectories are perturbed, the motor plans and commands both need to be grossly modulated. Conversely, in the late phase of the learning, when the motor acts become skillful and the movement trajectories are smooth and close to the desired ones, the motor plans and commands need only fine tuning.

The mosaic structures of the cerebellar system where the IO-Purkinje cell-DCN loop is topographically organized in "micro-complexes" may help such modulation of motor learning. The neural events to meet these motor learning requirements would be massive climbing-and mossy-fiber inputs to the Purkinje cells in the early phase of motor learning (leading to low DCN activity), and small mossy-and climbing- fiber inputs in the late phase. In the early phase of learning, highly effective coupling across the IO neurons due to low DCN activity would allow widespread synchronized IO firing in response to error signals, which could potentially lead to synaptic weight changes in many Purkinje cells. Cerebellar learning would be fast but coarse. Conversely, in the late phase of learning, if IO neuronal firing becomes less synchronized, synaptic changes would occur among more restricted Purkinje cell groups, which would allow more subtle modifications in the final learning stages (compare left and right panels in **Figure 1**).

In Tokuda et al. (2012), we conducted simulations to examine the advantage of the adaptive coupling strength over fixed coupling strength during motor learning. IO neurons transmitted error signals in a feedback-error learning scheme to learn the inverse dynamics of a two-dimensional arm. In the adaptive coupling condition, the coupling strength between the IO neurons was slowly decreased as learning proceeded. The error signals amplitudes were large early in learning because movements were mainly under feedback control. Feedback control in biological motor control is slow and inaccurate because of the low feedback gains necessary to avoid oscillations and divergence due the long feedback delays; see for instance (Schweighofer et al., 1998). As learning of the internal inverse model proceeded, the movements became straighter and the error signals became smaller. Since the small error signals provided only a weak influence on the IO neurons, weak coupling was needed to maintain the desynchronized neural activities. Results showed that adaptive coupling led to a more efficient learning process than with a fixed coupling strength.

DISCUSSION

We have reviewed experimental and computer simulations studies suggesting that the Purkinje cell-DCN -IO circuit may act as a self-regulating circuit that potentially has two functional roles, one in motor learning and one in on-line motor control. That is, the control of synchrony between IO complex spikes via modulation of electrical coupling could enhance cerebellar learning and on-line motor control. If the olivo-cerebellar system has two functional roles, then ideally it would be best if the performance of each function was controlled independently. Here, we suggest that modulation of the effective electrical coupling of IO neurons, and there by the levels of complex spike synchrony, may allow at least semi-independent control.

Specifically, the olivo-cerebellar system could contribute to motor commands primarily when it is operating in a relatively synchronized state. Synchronization, coupled with the convergence of the Purkinje cell to DCN pathway, would allow complex spikes to be distinguished from ongoing simple spike activity, and therefore they could alter the activity of DCN neurons in distinct ways from the latter signals. Thus, synchronous complex discharges would make a contribution to outgoing cerebellar motor commands distinct from that made by simple spike activity. In contrast, when complex spike activity is desynchronized it may not contribute significantly to motor commands, because in this state complex spikes may be less distinguishable from simple spike activity. It is possible that the burst nature of the complex spike may still allow the DCN neurons to distinguish them from simple spikes; however, the extent to which the secondary spikes of each complex spike are propagated is debated (Ito and Simpson, 1971; Campbell and Hesslow, 1986; Khaliq and Raman, 2005; Monsivais et al., 2005). Nevertheless, based simply on the firing rate superiority of simple spikes, it seems plausible that asynchronous complex spike activity would generally make a less significant direct contribution to shaping DCN activity. The olivo-cerebellar system may switch into an on-line motor control state for two causes, internal or external with respect to the cerebellum. On one hand, high synchrony states may be due to increased effective coupling levels among IO cells via low activity in the subset of DCN neurons that project to the IO. In this case, simple spikes would, via their action on the DCN, help in determining whether or not olivo-cerebellar activity will contribute to the upcoming motor command. On the other hand, large, highly synchronized volleys in excitatory afferent IO pathways could lead to synchronous complex spikes, which could also trigger a motor response.

In contrast to motor control, the potential for triggering motor learning exists regardless of synchrony level, because the ability of complex spikes to modulate synaptic plasticity at a single cell level are not affected by synchrony levels: plastic processes intrinsic to any one Purkinje cell caused by its firing a complex spike would be expected to be independent of the number of other Purkinje cells generating complex spikes at the same time (but see paragraph below). The overall speed of motor learning would be modulated by synchrony levels, however. In the early phases of learning, initially strong coupling would allow transmission of large errors to multiple functionally related Purkinje cells, resulting in fast but coarse learning (in addition to its significant effects on deep cerebellar nucleus and on-line motor control). In contrast, in the late phase of learning, decreased coupling would lead to desynchronized IO firing, allowing high-fidelity transmission of error, resulting in slower but fine learning, and little on-line motor control effects. We proposed that the desynchronized state arises via higher inputs from DCN activity. Thus, by modulating the effective coupling among IO cells, the DCN may control the characteristics of error signals sent to the cerebellum, once again acting in a self-regulating manner. Our proposal is at least in part coherent with data from (Milak et al., 1995) showing that the activity of DCN neurons increase above background activity during motor learning. However, our proposal, in its current form,

does not account for the additional results of Milak et al. (1995) showing that DCN activity progressively decreased as the task became well practiced. Perhaps excitatory and inhibitory inputs from the DCN to the IO control cellular activity and coupling in a non-linear manner, as suggested by our model of IO neuron, which is only firing for a limited range of inputs (see Figure 4 in Schweighofer et al., 1999). Additional work is needed to shed light on the effect of excitatory inputs on IO activity and coupling.

In addition to synchronized IO activity in the early phase of learning, learning can further be accelerated by IO neurons firing in bursts (Eccles et al., 1966; Crill and Kennedy, 1967). These bursts potentially allow the IO neurons to communicate in a more refined way than just binary, thereby increasing bandwidth (Maruta et al., 2007; Bazzigaluppi et al., 2012). The number of spikelets in a burst has been linked to the strength and type of long-term plasticity induced by climbing fiber activation (Mathy et al., 2009). Thus if synchronization of IO neuronal activity affected spikelet number, synchrony would be another possible mechanism by which the olivo-cerebellar system regulates learning processes in the cortex. However, the exact relationship of synchrony and spikelet number needs further study. The amplitude of subthreshold oscillations in IO neurons is an alleged surrogate for synchronization level of IO neuronal activity and simulations of IO networks, and *in vivo* recordings suggest that an inverse relationship exists between the amplitude of the subthreshold oscillation and IO spikelet number (Bazzigaluppi et al., 2012; De Gruijl et al., 2012). Thus, modulation of spikelet number is an intriguing possible mechanism for enhancing the control that the olivo-cerebellar system exerts over Purkinje cell plasticity, and in the role it plays in shaping motor commands sent to the DCN.

In any case, the above implies that by limiting synchrony levels, feedback from the cerebellum would enable the olivo-cerebellar system to allow modification of synaptic weights without causing movements. However, the separation of function is not complete, because synchronous complex spike activity would, in the currently proposed scheme, cause both generation of movements and synaptic plasticity. This implies that each time complex spikes contribute to movement generation, the circuitry generating the movement is altered, and thus the mapping of brain activity to movement is modified. This is in some ways analogs to the proposal that the process of memory retrieval may modify the memory trace itself (Sara, 2000). Indeed, it may partly explain the fact that even in highly skilled athletes and musicians the performance of highly practiced motor acts still retains some variability (e.g., as of 2013, the highest free throw percentage for a season by a player in the National Basketball Association is only 90.4% http://www.nba.com/statistics/default_all_time_leaders/AllTimeLeadersFTPQuery.html?top). Conversely, subtle modification of cerebellar circuits could underlie the efficacy of taking practice swings before hitting in baseball or similar warm up routines.

Finally, it is worth considering, in the context of the motor learning process, cases where truly high synchrony levels may occur. In the early phase of motor learning the motor plans and commands both need to be grossly modulated. Motor acts are clumsy and far from the desired ones and the executed movement trajectories are likely to be perturbed as a result. Consistent with this hypothesis, in motor learning of arm reaching under novel force fields, changes in motor commands are large for the first few trials, much more than the level of trajectory errors (Franklin et al., 2008). Such perturbations, if they resulted in a synchronous afferent volley to the IO, would be away to elicit widespread synchronous complex spike activity, and thus possibly elicit corrective movements, and perhaps more importantly to allow large-scale changes in synaptic connectivity. As the learning process continues, the motor acts become skillful and the movement trajectories become smooth and close to the desired ones. In this case, there is less likely to be major perturbations with highly synchronized complex spike activity resulting. Instead, motor plans and commands need only fine-tuning and the olivo-cerebellar system may generate relatively desynchronized activity that would drive such fine-tuning.

ACKNOWLEDGMENTS

Nicolas Schweighofer was supported by NSF BCS 1031899, Eric J. Lang was supported by NSF IOS-105858 and Mitsuo Kawato was supported by Japanese MEXT SRPBS.

REFERENCES

Albus, J. S. (1971). A theory of cerebellar function. *Math. Biosci.* 10, 25–61.

Albus, J. S. (1975). A new approach to manipulator control: the cerebellar model articulation controller (CMAC). *J. Dyn. Syst. Meas. Control* 97, 220–227.

Apps, R., and Hawkes, R. (2009). Cerebellar cortical organization: a one-map hypothesis. *Nat. Rev. Neurosci.* 10, 670–681.

Bazzigaluppi, P., De Gruijl, J. R., Van Der Giessen, R. S., Khosrovani, S., De Zeeuw, C. I., and De Jeu, M. T. (2012). Olivary subthreshold oscillations and burst activity revisited. *Front. Neural Circuits* 6:91. doi: 10.3389/fncir.2012.00091

Bell, C. C., and Kawasaki, T. (1972). Relations among climbing fiber responses of nearby Purkinje cells. *J. Neurophysiol.* 35, 155–169.

Belluardo, N., Mudò, G., Travato-Salinaro, A., Le Gurun, S., Charollais, A., Serre-Beinier, V., et al. (2000). Expression of connexin36 in the adult and developing rat brain. *Brain Res.* 865, 121–138.

Bengtsson, F., Ekerot, C. F., and Jorntell, H. (2011). In vivo analysis of inhibitory synaptic inputs and rebounds in deep cerebellar nuclear neurons. *PLoS ONE* 6:e18822. doi: 10.1371/journal.pone.0018822

Blenkinsop, T. A., and Lang, E. J. (2006). Block of inferior olive gap junctional coupling decreases Purkinje cell complex spike synchrony and rhythmicity. *J. Neurosci.* 26, 1739–1748.

Blenkinsop, T. A., and Lang, E. J. (2011). Synaptic action of the olivocerebellar system on cerebellar nuclear spike activity. *J. Neurosci.* 31, 14708–14720.

Campbell, N. C., and Hesslow, G. (1986). The secondary spikes of climbing fibre responses recorded from Purkinje cell axons in cat cerebellum. *J. Physiol.* 377, 225–235.

Condorelli, D. F., Parenti, R., Spinella, F., Salinaro, A. T., Belluardo, N., Cardile, V., et al. (1998). Cloning of a new gap junction gene (Cx36) highly expressed in mammalian brain neurons. *Eur. J. Neurosci.* 10, 1202–1208.

Crill, W. E., and Kennedy, T. T. (1967). Inferior olive of the cat: intracellular recording. *Science* 157, 716–718.

De Gruijl, J. R., Bazzigaluppi, P., De Jeu, M. T., and De Zeeuw, C. I. (2012). Climbing fiber burst size and olivary sub-threshold oscillations in a network setting. *PLoS Comput. Biol.* 8:e1002814. doi: 10.1371/journal.pcbi.1002814

de Montigny, C., and Lamarre, Y. (1973). Rhythmic activity induced by harmaline in the olivo-cerebello-bulbar system of the cat. *Brain Res.* 53, 81–95.

Desclin, J. C. (1974). Histological evidence supporting the inferior olive as the major source of cerebellar climbing fibers in the rat. *Brain Res.* 77, 365–384.

Devor, A., and Yarom, Y. (2002). Electrotonic coupling in the inferior olivary nucleus revealed by simultaneous double patch recordings. *J. Neurophysiol.* 87, 3048–3058.

De Zeeuw, C. I., Hertzberg, E. L., and Mugnaini, E. (1995). The dendritic lamellar body: a new neuronal organelle putatively associated with dendrodendritic gap junctions. *J. Neurosci.* 15, 1587–1604.

de Zeeuw, C. I., Holstege, J. C., Ruigrok, T. J., and Voogd, J. (1989). Ultrastructural study of the GABAergic, cerebellar, and mesodiencephalic innervation of the cat medial accessory olive: anterograde tracing combined with immunocytochemistry. *J. Comp. Neurol.* 284, 12–35.

De Zeeuw, C. I., Lang, E. J., Sugihara, I., Ruigrok, T. J., Eisenman, L. M., Mugnaini, E., et al. (1996). Morphological correlates of bilateral synchrony in the rat cerebellar cortex. *J. Neurosci.* 16, 3412–3426.

De Zeeuw, C. I., Simpson, J. I., Hoogenraad, C. C., Galjart, N., Koekkoek, S. K. E., and Ruigrok, T. J. H. (1998). Microcircuitry and function of the inferior olive. *Trends Neurosci.* 21, 391–400.

Eccles, J. C., Llinás, R., and Sasaki, K. (1966). The excitatory synaptic action of climbing fibers on the Purkinje cells of the cerebellum. *J. Physiol. (Lond.)* 182, 268–296.

Franklin, D. W., Burdet, E., Tee, K. P., Osu, R., Chew, C. M., Milner, T. E., et al. (2008). CNS learns stable, accurate, and efficient movements using a simple algorithm. *J. Neurosci.* 28, 11165–11173.

Fredette, B. J., and Mugnaini, E. (1991). The GABAergic cerebello-olivary projection in the rat. *Anat. Embryol.* 184, 225–243.

Fukuda, M., Yamamoto, T., and Llinas, R. (2001). The isochronic band hypothesis and climbing fibre regulation of motricity: an experimental study. *Eur. J. Neurosci.* 13, 315–326.

Gilbert, P. F., and Thach, W. T. (1977). Purkinje cell activity during motor learning. *Brain Res.* 128, 309–328.

Harvey, R. J., and Napper, R. M. (1991). Quantitative studies on the mammalian cerebellum. *Prog. Neurobiol.* 36, 437–463.

Hubbard, J. I., Stenhouse, D., and Eccles, R. M. (1967). Origin of synaptic noise. *Science* 157, 330–331.

Ito, M. (1982). Experimental verification of Marr-Albus' plasticity assumption for the cerebellum. *Acta Biol. Acad. Sci. Hung.* 33, 189–199.

Ito, M. (1984). *The cerebellum and neural control.* New York: Raven Press.

Ito, M. (2001). Cerebellar long-term depression: characterization, signal transduction, and functional roles. *Physiol. Rev.* 81, 1143–1195.

Ito, M., and Simpson, J. I. (1971). Discharges in Purkinje cell axons during climbing fiber activation. *Brain Res.* 31, 215–219.

Katori, Y., Lang, E. J., Onizuka, M., Kawato, M., and Aihara, K. (2010). Quantitative modeling of spatio-temporal dynamics of inferior olive neurons with a simple conductance-based model. *Int. J. Bifurcat. Chaos* 20, 583–603.

Kawato, M., Furukawa, K., and Suzuki, R. (1987). A hierarchical neural-network model for control and learning of voluntary movement. *Biol. Cybern.* 57, 169–185.

Kawato, M., and Gomi, H. (1992a). The cerebellum and VOR/OKR learning models. *Trends Neurosci.* 15, 445–453.

Kawato, M., and Gomi, H. (1992b). A computational model of four regions of the cerebellum based on feedback-error learning. *Biol. Cybern.* 68, 95–103.

Kawato, M., Kuroda, S., and Schweighofer, N. (2011). Cerebellar supervised learning revisited: biophysical modeling and degrees-of-freedom control. *Curr. Opin. Neurobiol.* 21, 791–800.

Khaliq, Z. M., and Raman, I. M. (2005). Axonal propagation of simple and complex spikes in cerebellar Purkinje neurons. *J. Neurosci.* 25, 454–463.

Kitazawa, S., Kimura, T., and Yin, P. B. (1998). Cerebellar complex spikes encode both destinations and errors in arm movements. *Nature* 392, 494–497.

Lamarre, Y., and Mercier, L. A. (1971). Neurophysiological studies of harmaline-induced tremor in the cat. *Can. J. Physiol. Pharmacol.* 49, 1049–1058.

Lang, E. J. (2001). Organization of olivocerebellar activity in the absence of excitatory glutamatergic input. *J. Neurosci.* 21, 1663–1675.

Lang, E. J. (2002). GABAergic and glutamatergic modulation of spontaneous and motor-cortex-evoked complex spike activity. *J. Neurophysiol.* 87, 1993–2008.

Lang, E. J. (2003). Excitatory afferent modulation of complex spike synchrony. *Cerebellum* 2, 165–170.

Lang, E. J. (2009). Functional imaging confirms principles of cerebellar functioning found with multisite recording [electronic response to Ozden, I., Sullivan, M. R., Lee, H. M., and Wang, S. S. H. Reliable Coding Emerges from Coactivation of Climbing Fibers in Microbands of Cerebellar Purkinje Neurons]. *J. Neurosci.* 29, 10463–10473.

Lang, E. J., Sugihara, I., and Llinás, R. (1996). GABAergic modulation of complex spike activity by the cerebellar nucleoolivary pathway in rat. *J. Neurophysiol.* 76, 255–275.

Lang, E. J., Sugihara, I., and Llinas, R. (1997). Differential roles of apamin- and charybdotoxin-sensitive K+ conductances in the generation of inferior olive rhythmicity in vivo. *J. Neurosci.* 17, 2825–2838.

Lang, E. J., Sugihara, I., Welsh, J. P., and Llinas, R. (1999). Patterns of spontaneous purkinje cell complex spike activity in the awake rat. *J. Neurosci.* 19, 2728–2739.

Leznik, E., and Llinas, R. (2005). Role of gap junctions in synchronized neuronal oscillations in the inferior olive. *J. Neurophysiol.* 94, 2447–2456.

Llinas, R., Baker, R., and Sotelo, C. (1974). Electrotonic coupling between neurons in cat inferior olive. *J. Neurophysiol.* 37, 560–571.

Llinas, R., Bloedel, J. R., and Hillman, D. E. (1969). Functional characterization of neuronal circuitry of frog cerebellar cortex. *J. Neurophysiol.* 32, 847–870.

Llinas, R., and Volkind, R. A. (1973). The olivo-cerebellar system: functional properties as revealed by harmaline-induced tremor. *Exp. Brain Res.* 18, 69–87.

Llinas, R., Walton, K., Hillman, D. E., and Sotelo, C. (1975). Inferior olive: its role in motor learing. *Science* 190, 1230–1231.

Llinás, R., and Yarom, Y. (1981a). Electrophysiology of mammalian inferior olivary neurones in vitro. Different types of voltage-dependent ionic conductances. *J. Physiol. (Lond.)* 315, 549–567.

Llinás, R., and Yarom, Y. (1981b). Properties and distribution of ionic conductances generating electroresponsiveness of mammalian inferior olivary neurones in vitro. *J. Physiol. (Lond.)* 315, 569–584.

Llinás, R., and Yarom, Y. (1986). Oscillatory properties of guinea-pig inferior olivary neurones and their pharmacological modulation: an in vitro study. *J. Physiol. (Lond.)* 376, 163–182.

Long, M. A., Deans, M. R., Patrick, S. L., Paul, D. L., and Connors, B. W. (2001). Connexin 36-dependent electrical coupling synchronizes subthreshold rhythmic activity of inferior olivary neurons. *Soc. Neurosci. Abstr.* 27, 70.13.

Makarenko, V., and Llinas, R. (1998). Experimentally determined chaotic phase synchronization in a neuronal system. *Proc. Natl. Acad. Sci. U.S.A.* 95, 15747–15752.

Manor, Y., Rinzel, J., Segev, I., and Yarom, Y. (1997). Low-amplitude oscillations in the inferior olive: a model based on electrical coupling of neurons with heterogeneous channel densities. *J. Neurophysiol.* 77, 2736–2752.

Marr, D. (1969). A theory of cerebellar cortex. *J. Physiol.* 202, 437–470.

Marshall, S. P., and Lang, E. J. (2009). Local changes in the excitability of the cerebellar cortex produce spatially restricted changes in complex spike synchrony. *J. Neurosci.* 29, 14352–14362.

Marshall, S. P., Van Der Giessen, R. S., De Zeeuw, C. I., and Lang, E. J. (2007). Altered olivocerebellar activity patterns in the connexin36 knockout mouse. *Cerebellum* 6, 287–299.

Maruta, J., Hensbroek, R. A., and Simpson, J. I. (2007). Intraburst and interburst signaling by climbing fibers. *J. Neurosci.* 27, 11263–11270.

Masuda, N., and Aihara, K. (2002). Spatiotemporal spike encoding of a continuous external signal. *Neural Comput.* 14, 1599–1628.

Mathy, A., Ho, S. S., Davie, J. T., Duguid, I. C., Clark, B. A., and Hausser, M. (2009). Encoding of oscillations by axonal bursts in inferior olive neurons. *Neuron* 62, 388–399.

Miall, R. C., Christensen, L. O., Cain, O., and Stanley, J. (2007). Disruption of state estimation in the human lateral cerebellum. *PLoS Biol.* 5:e316. doi: 10.1371/journal.pbio.0050316

Milak, M. S., Bracha, V., and Bloedel, J. R. (1995). Relationship of simultaneously recorded cerebellar nuclear neuron discharge to the acquisition of a complex, operantly conditioned forelimb movement in cats. *Exp. Brain Res.* 105, 325–330.

Monsivais, P., Clark, B. A., Roth, A., and Hausser, M. (2005). Determinants of action potential propagation in cerebellar Purkinje cell axons. *J. Neurosci.* 25, 464–472.

Mukamel, E. A., Nimmerjahn, A., and Schnitzer, M. J. (2009). Automated analysis of cellular signals from large-scale calcium imaging data. *Neuron* 63, 747–760.

Nelson, B. J., and Mugnaini, E. (1989). "Origins of GABAergic inputs to the inferior olive," in *The Olivocerebellar System in Motor Control*, ed. P. Strata (Berlin: Springer-Verlag).

Nishimura, H., Katada, N., and Aihara, K. (2000). Coherent response in a chaotic neural network. *Neural Process. Lett.* 12, 49–58.

Onizuka, M., Hoang, H., Kawato, M., Tokuda, I. T., Schweighofer, N., Katori, Y., et al. (2013). Solution to the inverse problem of estimating gap-junctional and inhibitory conductance in inferior olive neurons from spike trains by network model simulation. *Neural Netw.* doi: 10.1016/j.neunet.2013.01.006 [Epub ahead of print].

Ozden, I., Sullivan, M. R., Lee, H. M., and Wang, S. S. (2009). Reliable coding emerges from coactivation of climbing fibers in microbands of cerebellar Purkinje neurons. *J. Neurosci.* 29, 10463–10473.

Ruigrok, T. J. (2010). Ins and outs of cerebellar modules. *Cerebellum* 10, 464–474.

Sara, S. J. (2000). Retrieval and reconsolidation: toward a neurobiology of remembering. *Learn. Mem.* 7, 73–84.

Sasaki, M., Batsford, S., Thaiss, F., Oite, T., and Vogt, A. (1989). Ultrastructural studies in passive in situ immune complex glomerulonephritis. A rat model for membranous glomerulonephritis. *Virchows Arch. B Cell Pathol. Incl. Mol. Pathol.* 58, 173–180.

Schultz, S. R., Kitamura, K., Post-Uiterweer, A., Krupic, J., and Hausser, M. (2009). Spatial pattern coding of sensory information by climbing fiber-evoked calcium signals in networks of neighboring cerebellar Purkinje cells. *J. Neurosci.* 29, 8005–8015.

Schweighofer, N. (1998). A model of activity-dependent formation of cerebellar microzones. *Biol. Cybern.* 79, 97–107.

Schweighofer, N., Arbib, M. A., and Kawato, M. (1998). Role of the cerebellum in reaching movements in humans. I. Distributed inverse dynamics control. *Eur. J. Neurosci.* 10, 86–94.

Schweighofer, N., Doya, K., Fukai, H., Chiron, J. V., Furukawa, T., and Kawato, M. (2004). Chaos may enhance information transmission in the inferior olive. *Proc. Natl. Acad. Sci. U.S.A.* 101, 4655–4660.

Schweighofer, N., Doya, K., and Kawato, M. (1999). Electrophysiological properties of inferior olive neurons: a compartmental model. *J. Neurophysiol.* 82, 804–817.

Shaikh, A. G., Hong, S., Liao, K., Tian, J., Solomon, D., Zee, D. S., et al. (2010). Oculopalatal tremor explained by a model of inferior olivary hypertrophy and cerebellar plasticity. *Brain* 133, 923–940.

Shidara, M., Kawano, K., Gomi, H., and Kawato, M. (1993). Inverse-dynamics model eye movement control by Purkinje cells in the cerebellum. *Nature* 365, 50–52.

Silver, R. A., Momiyama, A., and Cull-Candy, S. G. (1998). Locus of frequency-dependent depression identified with multiple-probability fluctuation analysis at rat climbing fibre-Purkinje cell synapses. *J. Physiol.* 510(Pt 3), 881–902.

Sotelo, C., Llinas, R., and Baker, R. (1974). Structural study of inferior olivary nucleus of the cat: morphological correlates of electrotonic coupling. *J. Neurophysiol.* 37, 541–559.

Sugihara, I., and Shinoda, Y. (2004). Molecular, topographic, and functional organization of the cerebellar cortex: a study with combined aldolase C and olivocerebellar tracing. *J. Neurosci.* 24, 8771–8785.

Sugihara, I., Fujita, H., Na, J., Quy, P. N., Li, B. Y., and Ikeda, D. (2009). Projection of reconstructed single Purkinje cell axons in relation to the cortical and nuclear aldolase C compartments of the rat cerebellum. *J. Comp. Neurol.* 512, 282–304.

Sugihara, I., Lang, E. J., and Llinas, R. (1993). Uniform olivocerebellar conduction time underlies Purkinje cell complex spike synchronicity in the rat cerebellum. *J. Physiol.* 470, 243–271.

Sugihara, I., Marshall, S. P., and Lang, E. J. (2007). Relationship of complex spike synchrony bands and climbing fiber projection determined by reference to aldolase C compartments in crus IIa of the rat cerebellar cortex. *J. Comp. Neurol.* 501, 13–29.

Szentágothai, J., and Rajkovitz, K. (1959). Über den ursprung der kletterfasern des kleinhirns. *Z Anat. Entwickl-Gesch.* 121, 130–141.

Thach, W. T. (1968). Discharge of Purkinje and cerebellar nuclear neurons during rapidly alternating arm movements in the monkey. *J. Neurophysiol.* 31, 785–797.

Tokuda, I., Han, C. E., Aihara, K., Kawato, M., and Schweighofer, N. (2010). The role of chaotic resonance in cerebellar learning. *Neural Netw.* 23, 836–842.

Tokuda, I., Hoang, H., Schweighofer, N., and Kawato, M. (2012). Adaptive coupling of inferior olive neurons in cerebellar learning. *Neural Netw.* doi: 10.1016/j.neunet.2012.12.006 [Epub ahead of print].

Tseng, Y. W., Diedrichsen, J., Krakauer, J. W., Shadmehr, R., and Bastian, A. J. (2007). Sensory prediction errors drive cerebellum-dependent adaptation of reaching. *J. Neurophysiol.* 98, 54–62.

Van Der Giessen, R. S., Koekkoek, S. K., Van Dorp, S., De Gruijl, J. R., Cupido, A., Khosrovani, S., et al. (2008). Role of olivary electrical coupling in cerebellar motor learning. *Neuron* 58, 599–612.

van Essen, T. A., Van Der Giessen, R. S., Koekkoek, S. K., Vanderwerf, F., Zeeuw, C. I., Van Genderen, P. J., et al. (2010). Anti-malaria drug mefloquine induces motor learning deficits in humans. *Front. Neurosci.* 4:191. doi: 10.3389/fnins.2010.00191

Voogd, J., and Bigaré, F. (1980). "Topographical distribution of olivary and corticonuclear fibers in the cerebellum. A review," in *The Inferior Olivary Nucleus: Anatomy and Physiology*, eds J. Courville, C. De Montigny and Y. Lamarre (New York: Raven Press), 207–234.

Welsh, J. P., Lang, E. J., Sugihara, I., and Llinás, R. (1995). Dynamic organization of motor control within the olivocerebellar system. *Nature* 374, 453–457.

Wiesenfeld, K., and Moss, F. (1995). Stochastic resonance and the benefits of noise: from ice ages to crayfish and SQUIDs. *Nature* 373, 33–36.

Wolpert, D. M., and Miall, R. C. (1996). Forward models for physiological motor control. *Neural Netw.* 9, 1265–1279.

Conflict of Interest Statement: The authors declare that the research was conducted in the absence of any commercial or financial relationships that could be construed as a potential conflict of interest.

Received: 21 December 2012; accepted: 29 April 2013; published online: 28 May 2013.

*Citation: Schweighofer N, Lang EJ and Kawato M (2013) Role of the olivocerebellar complex in motor learning and control. Front. Neural Circuits **7**:94. doi: 10.3389/fncir.2013.00094*

frontiers in
NEURAL CIRCUITS

ORIGINAL RESEARCH ARTICLE
published: 09 October 2013
doi: 10.3389/fncir.2013.00159

Distributed cerebellar plasticity implements adaptable gain control in a manipulation task: a closed-loop robotic simulation

Jesús A. Garrido[1,2†]*, Niceto R. Luque[3†], Egidio D'Angelo[1,4]* and Eduardo Ros[3]

[1] *Neurophysiology Unit, Department of Brain and Behavioral Sciences, University of Pavia, Pavia, Italy*
[2] *A. Volta Physics Department, Consorzio Interuniversitario per le Scienze Fisiche della Materia, University of Pavia Research Unit, Pavia, Italy*
[3] *Department of Computer Architecture and Technology, University of Granada, Granada, Spain*
[4] *Brain Connectivity Center, C. Mondino National Neurological Institute, Pavia, Italy*

Edited by:
Chris I. De Zeeuw, Erasmus Medical Center, Netherlands

Reviewed by:
Christopher H. Yeo, University College London, UK
Guy Cheron, Université Libre de Bruxelles, Belgium

****Correspondence:***
Jesús A. Garrido and Egidio D'Angelo, Brain Connectivity Center, IRCCS Istituto Neurologico Nazionale C. Mondino, Via Mondino 2, Pavia, I-27100, Italy
e-mail: jesus.garrido@unipv.it; dangelo@unipv.it
† These authors have contributed equally to this work.

Adaptable gain regulation is at the core of the forward controller operation performed by the cerebro-cerebellar loops and it allows the intensity of motor acts to be finely tuned in a predictive manner. In order to learn and store information about body-object dynamics and to generate an internal model of movement, the cerebellum is thought to employ long-term synaptic plasticity. LTD at the PF-PC synapse has classically been assumed to subserve this function (Marr, 1969). However, this plasticity alone cannot account for the broad dynamic ranges and time scales of cerebellar adaptation. We therefore tested the role of plasticity distributed over multiple synaptic sites (Hansel et al., 2001; Gao et al., 2012) by generating an analog cerebellar model embedded into a control loop connected to a robotic simulator. The robot used a three-joint arm and performed repetitive fast manipulations with different masses along an 8-shape trajectory. In accordance with biological evidence, the cerebellum model was endowed with both LTD and LTP at the PF-PC, MF-DCN and PC-DCN synapses. This resulted in a network scheme whose effectiveness was extended considerably compared to one including just PF-PC synaptic plasticity. Indeed, the system including distributed plasticity reliably *self-adapted* to manipulate different masses and to learn the arm-object dynamics over a time course that included fast learning and consolidation, along the lines of what has been observed in behavioral tests. In particular, PF-PC plasticity operated as a *time correlator* between the actual input state and the system error, while MF-DCN and PC-DCN plasticity played a key role in generating the *gain controller*. This model suggests that distributed synaptic plasticity allows generation of the complex learning properties of the cerebellum. The incorporation of further plasticity mechanisms and of spiking signal processing will allow this concept to be extended in a more realistic computational scenario.

Keywords: cerebellar nuclei, long-term synaptic plasticity, gain control, learning consolidation, modeling

INTRODUCTION

The cerebellum plays a critical role in the precise control of movements, as is evident when studying patients with cerebellar malfunctioning and diseases (Thach, 1996). The cerebellum receives proprioceptive signals (Sawtell, 2010) and *copies* of motor commands (Schweighofer et al., 1998a) together with haptic information (Ebner and Pasalar, 2008; Shadmehr and Krakauer, 2008; Weiss and Flanders, 2011) through MFs. By means of these signals and its own internal circuitry, the cerebellum is able to learn and process sensorimotor information, and thereby regulate the initiation, intensity and duration of motor acts in an anticipatory manner (Spencer et al., 2005; Manto et al., 2012). This *gain control* operation is a fundamental aspect of motor control in animals, as it allows not only the rapid regulation of motor acts according to contextual cues, but also, through learning, adaptation of these acts to bodily and environmental changes. This *adaptable gain control* requires *closed-loop* interactions between command centers and effectors and is thought to involve the cerebellum embedded in the so-called *forward controller* loop (Schweighofer et al., 1998a; Wolpert et al., 1998; Wolpert and Ghahramani, 2000). In fact, the abstraction of models (kinematics and dynamics) of objects under manipulation (Shadmehr and Mussa-Ivaldi, 2012) is efficiently achieved thanks to close interaction between the cerebral and the cerebellar cortex (Middleton and Strick, 2000; Wang et al., 2008). However, two main issues remained unresolved. First, the adaptable gain controller localized in the cerebellum is thought to require suitable learning and memory mechanisms, whose nature is still debated. Secondly, it remains to be explained how a gain control system involving the cerebellum is able to optimize

Abbreviations: PF, parallel fiber; MF, mossy fiber; CF, climbing fiber; GC, granule cell; GoC, Golgi cell; PC, Purkinje cell; DCN, deep cerebellar nuclei; VN, vestibular nuclei; IO, inferior olive; MLI, molecular layer interneuron; EBCC, eye-blink classical conditioning; VOR, vestibule-occular reflex; MAE, mean average error.

its performance in the face of broad and varying operative ranges.

Several attempts have been made to understand how the cerebellum implements adaptable gain control. The original theories, based on analysis of network connectivity (Marr, 1969; Albus, 1971; Fujita, 1982), defined the cerebellum as a timing and learning machine. The granular layer was hypothesized to perform expansion recoding of input signals and the PF-PC synapse to learn and store relevant patterns under the control of the teaching signal provided by CFs. On the basis of electrophysiological determinations, it has been suggested that the inferior olive (IO), by comparing proprioceptive and predicted signals, is indeed able to provide quantitative error estimation (Bazzigaluppi et al., 2012; De Gruijl et al., 2012). Moreover, some authors, on the basis of eye-movement analysis, have advanced the hypothesis of a two-state learning mechanism (Shadmehr and Brashers-Krug, 1997; Shadmehr and Holcomb, 1997), wherein a fast learning process takes place in the cerebellar cortex (granular and molecular layer, possibly involving PF-PC plasticity) and a slow consolidation process takes place in deeper structures (possibly the DCN) (Shadmehr and Brashers-Krug, 1997; Shadmehr and Holcomb, 1997; Medina and Mauk, 2000). Clearly, in the development of an adequate model of adaptable cerebellar gain control, it has to be known where and how learning actually occurs. Long-term synaptic plasticity is thought to provide the biological basis for learning and memory in neuronal circuits (Bliss and Collingridge, 1993) and appears in various forms of potentiation (LTP) and depression (LTD). In the cerebellum, long-term synaptic plasticity was initially thought to occur only as LTD or LTP (Marr, 1969; Albus, 1971) at the PF-PC synapse, but now synaptic plasticity is known to be distributed and to occur also in the granular layer, molecular layer and DCN (Hansel et al., 2001; Gao et al., 2012). In particular:

(1) Synaptic plasticity in the granular layer is unsupervised and may serve to improve spatiotemporal recoding of MF input patterns into new GC discharges [expansion recoding (D'Angelo and De Zeeuw, 2009)].
(2) Synaptic plasticity in the molecular layer is supervised and may serve to store correlated granular layer patterns under the teaching signal generated by CFs. This plasticity is in fact composed of multiple mechanisms: PF-PC LTD may occur together with PF-MLI LTP, globally reducing PC responses, while PF-PC LTP may occur together with PF-MLI LTD and MLI-PC LTD, globally increasing PC responses (Gao et al., 2012).
(3) Synaptic plasticity in the DCN is supervised and may serve to store correlated granular layer patterns under the teaching signal generated by PCs (Hansel et al., 2001; Boyden et al., 2004; Gao et al., 2012). This plasticity is, in turn, composed of several mechanisms generating MF-DCN (Bagnall and du Lac, 2006; Pugh and Raman, 2006) and PC-DCN (Morishita and Sastry, 1996; Aizenman et al., 1998; Ouardouz and Sastry, 2000) LTP and LTD. On the one hand, it has been suggested that MF-DCN and PF-DCN plasticity are important in controlling cerebellar learning in the context of EBCC (Medina and Mauk, 1999, 2000) and that equivalent forms of plasticity in the VN are important in controlling cerebellar learning in the VOR (Masuda and Amari, 2008). On the other hand, it has been proposed that the nature of cerebellar cortical and nuclear plasticity and the involvement of extra-cerebellar plasticity sites are highly dependent on the task to be performed, e.g., EBCC or VOR (De Zeeuw and Yeo, 2005; Porrill and Dean, 2007; Lepora et al., 2010). In the present context, with the aim of developing a general computational scheme, we have not considered the potential task-dependence of the learning process.

We explored the impact of distributed cerebellar synaptic plasticity on gain adaptation using a robotic control task in a closed loop, starting from the assumption that there are three learning sites, one in the cerebellar cortex (PF-PC) and two in the DCN (MF-DCN and PC-DCN), all generating LTP and LTD. We found that simultaneous recalibration of weights at these multiple synaptic sites was required to implement self-adaptable gain control over a broad dynamic range involving manipulation of objects with different masses. Moreover, the model implied, due to the definition of the learning rules and the configuration of the learning parameters, that learning was faster in the molecular layer than in DCN, supporting adaptation mechanisms on different time scales. This result suggests that distributed synaptic plasticity is needed to generate the complex computational and learning properties of the cerebellum and to improve motor learning and control.

METHODS

A cerebellar model was constructed taking into account the major functional hypotheses concerning the granular layer, the PC layer and the DCN. The main synaptic connections between these structures (PF-PC, PC-DCN, and MF-DCN) were endowed with long-term synaptic plasticity mechanisms. The cerebellar model was embedded into a control loop designed to operate a simulated robotic arm manipulating different masses. The simulator of the robotic arm and the control loop were implemented in *Simulink* (Matlab R2011a), in accordance with previous models (Luque et al., 2011a,b,c; Tolu et al., 2013) (see Appendix B). The cerebellar model was implemented in C++ and was embedded in *Simulink* as an *S-function* block. The source code is available at: https://senselab.med.yale.edu/modeldb/ShowModel.asp?model=150067.

CEREBELLAR MODEL

The model provides a simplified representation of signal processing, while accounting for the main computational and learning properties of the cerebellar circuit. Each layer of the cerebellum was implemented as a set of parameter values corresponding to the firing rate of the neural population. Consequently, and since the interaction between neuronal layers in the model is linear, "synaptic strength" and "synaptic weight" correspond to gain factors describing the influence that firing frequency in the presynaptic cell group has on the postsynaptic cell group. Thus, like gain, "synaptic weights" are adimensional. An overview of the cerebellar circuit is shown in **Figure 1** and of computational features of the model is shown in **Figure 2**.

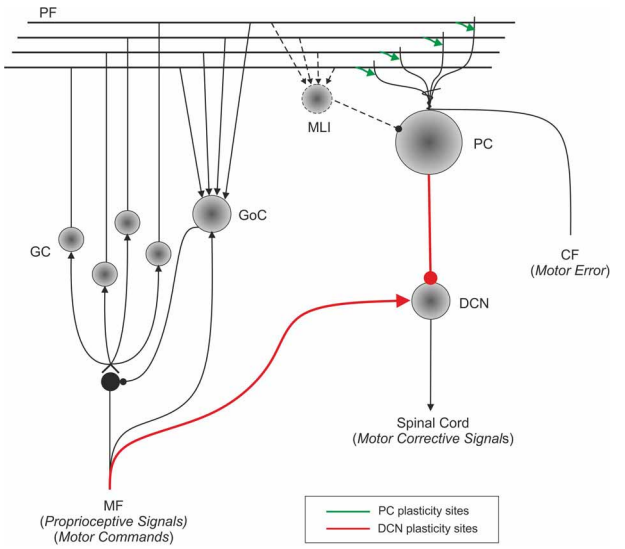

FIGURE 1 | Schematic representation of the main cell types in the cerebellum and of their connections. Suggestions about the nature of inputs signals are indicated [according to Schweighofer et al. (1998b)]. The pathways involved in long-term synaptic plasticity are drawn in green (for DCN afferents) and blue (for PC afferents). PF, parallel fiber; MF, mossy fiber; CF, climbing fiber; GC, granule cell; GoC, Golgi cell; PC, Purkinje cell; DCN, deep cerebellar nuclei; IO, inferior olive; MLI, molecular layer interneuron.

Signal coding in the cerebellar model

Previous models of cerebellar control of eyelid conditioning assumed that MFs convey spike sequences with a constant firing rate during presentation of the conditioned stimulus (Medina and Mauk, 1999; Yamazaki and Tanaka, 2007, 2009). Accordingly, in the present model, MF activity was represented by a constant firing rate. The MFs received constant signals (1) during the execution of each learning trial, and their input was set to 0 after the trial. It was assumed that, owing to internal dynamics, the granular layer circuit is capable of generating time-evolving states even in the presence of a constant MF input (Fujita, 1982). The CFs were assumed to transmit an error signal (0–1) representing the normalized difference between the desired and actual positions and velocities of each arm joint.

The onset of MF activity started the generation of the granular layer state sequence (see below) and also provided the excitatory drive to DCN cells (**Figure 2**). The DCN generated the cerebellar output by emitting positive (or zero) corrective torques that were added (with a positive or negative sign depending on whether it corresponded to agonist or antagonist muscles) to the crude inverse dynamic signal coming from the motor cortex.

The granular layer

The granular layer was implemented as a state generator (Yamazaki and Tanaka, 2005). When MF activity reaches the granular layer, it produces non-recurrent time patterns that are repeated exactly in each learning trial (**Figure 2A**). Thus, the relative time offset along the arm plant trajectory is represented by the correlative activation of 500 different states, mimicking the behavior of 500 PFs sequentially activated during movement execution. It should be noted that the procedure adopted here formally corresponds to a *labeled-line* coding scheme (**Figures 2A,B**).

The Purkinje layer

The PC layer has been suggested to correlate the PF input activity with the CF error-based teaching signal (Marr, 1969; Albus, 1971). Taking advantage of the state representation occurring in PFs, the PC layer was implemented by means of a look-up table, which associates each actual state with an output firing rate progressively learned along the trial (**Figure 2B**; see also below the synaptic plasticity section for a comprehensive description of mechanisms). The activity of the PC layer is defined as follows:

$$\mathrm{Pur}_i(t) = f_i\left(PF(t)\right), i \in 1,\ 2, \ldots \text{ Number of muscles} \quad (1)$$

where $\mathrm{Pur}_i(t)$ represents the firing rate of the PCs associated with the i-th muscle and f_i associates each granular layer state (i.e., one active PF) with a particular output firing rate at the i-th PC (**Figure 2B**). In the present 3-joint arm, there are six PCs accounting for the three pairs of agonist-antagonist muscles (one pair per joint).

DCN cells

The DCN cells integrate the excitatory activity coming from MFs and the inhibitory activity coming from PCs (**Figure 2C**). By linearly approximating the influence of excitatory and inhibitory synapses on DCN firing rate, the output of the DCN cell population was described as follows:

$$\mathrm{DCN}_i(t) = W_{MF-\mathrm{DCN}_i} - \mathrm{Pur}_i(t) \cdot W_{PC_i-DCN_i}, \quad i \in 1, 2, \ldots, \text{Number of muscles} \quad (2)$$

where $\mathrm{DCN}_i(t)$ represents the average firing rate of the DCN cell associated with the ith muscle, $W_{MF-\mathrm{DCN}_i}$ is the synaptic strength of the MF-DCN connection at the ith muscle, and $W_{PC_i-\mathrm{DCN}_i}$ is the synaptic strength of the PC-DCN connections at the ith muscle. Thus, the DCN layer was implemented as an *adder/subtractor* and the afferent activity coming from the MFs and PCs was scaled by synaptic strengths (MF-DCN and PC-DCN synapses, respectively). These synaptic weights were progressively adapted during the learning process, following the synaptic plasticity mechanisms explained below. It is important to note the absence of an MF activity term. As previously explained, we assume a constant input rate from MFs during the learning process. Thus, the excitatory component of the DCN firing rate is dependent only on the MF-DCN synaptic weight.

SYNAPTIC PLASTICITY

The cerebellar model included plasticity mechanisms at three different sites: the PF-PC, PC-DCN, and MF-DCN synapses. As a whole, this set of learning rules led the cerebellum

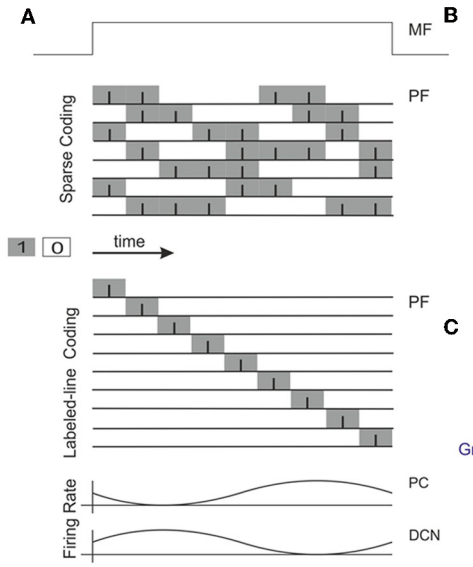

B

Time Bin	PF Sparse Code	PF Labeled-line Code	PC Output	DCN Output
0	1010010	10000000000	0.5	2
1	1101001	01000000000	0.2	3.2
2	0100101	00100000000	0	4
3	0010101	00010000000	0.2	3.2
4	0011110	00001000000	0.5	2
5	1001010	00000100000	0.8	0.8
6	1101000	00000010000	1	0
7	0110001	00000001000	0.8	0.8
8	0001101	00000000100	0.5	2

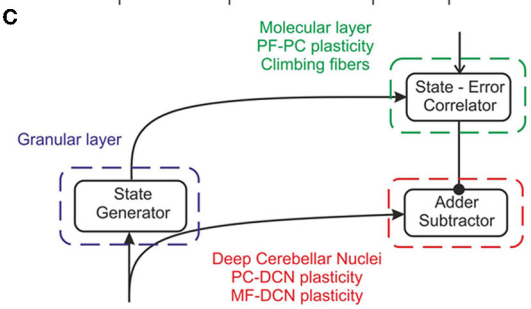

FIGURE 2 | Working hypothesis of cerebellar learning in a manipulation task. In our model, the system is further simplified by computing states without explicit spike representation. **(A)** During each manipulation trial, the onset of the movement initiates a *non-recurrent sequence of firing states* in the PFs (Yamazaki and Tanaka, 2007) due to the incoming activity in MFs. Each state is correlated with the error signal, representing the difference between the desired and actual positions of the robotic joint, and reaches the PCs through the CFs. This correlation is thought to occur through plasticity at the PF-PC synapses (Marr, 1969). After repeated pairing of *PF* states and CF error signals, an association is formed between the two; a learned corrective torque occurs and precedes the wrong movement. This association involves either reduction or increase of PC firing rate at different times. Finally, the temporally correlated signals from PCs are inverted (due to the inhibitory nature of the PC-DCN connection) and rescaled before reaching the motor neurons. The figure presents two alternative coding strategies: in our model, there are no spikes and the states correspond directly to the offset from movement onset indicated by the time bin. Formally, this corresponds to passing from a *sparse coding* to a *labeled-line coding*. **(B)** Binary representation of activity in a PF subset (1: active synapses, 0: inactive synapses) and firing rates in the corresponding PC and DCN neuron (in PCs the values are normalized in the range 0–1). A low PC firing rate corresponds to a high DCN firing rate. **(C)** Block diagram of the elements involved in the model. A *state generator* (which is reinitialized with the onset of a new trial) mimics the functionality of the cerebellar granular layer. A *state-error correlator* emulates the PC function: PF-PC long-term plasticity under supervision of CFs. Finally, an *adder/subtractor* receives the inputs coming from the MFs (multiplied by the MF-DCN synaptic weights) and subtracts the signal coming from the PCs (multiplied by the PC-DCN synaptic weights).

toward a relatively fast adaptation using PF-PC plasticity and a subsequent slow adaptation using MF-DCN and PC-DCN plasticity. This allowed the PF-PC synaptic weights to be kept within their optimum functional range through feedback coming from the actual movement. Importantly, the inclusion of the proposed learning rules allowed the cerebellar model to learn, independently, the timing (in the PF-PC synapses) and gain (in the MF-DCN and PC-DCN synapses) of the task.

PF-PC synaptic plasticity

This is the most widely investigated cerebellar plasticity mechanism and different studies have supported the existence of multiple forms of LTD (Ito and Kano, 1982; Boyden et al., 2004; Coesmans et al., 2004) and LTP (Hansel et al., 2001; Ito, 2001; Boyden et al., 2004; Coesmans et al., 2004). PF-PC plasticity was recently observed in alert animals (Márquez-Ruiz and Cheron, 2012). The main form of LTD is heterosynaptically driven by CF activity, and is therefore related to the complex spikes generated by CFs, while the main form of LTP is related to the simple spikes generated by PFs. The present model implements PF-PC synaptic plasticity as follows:

$$\Delta W_{PF_j - PC_i}(t) = \begin{cases} \frac{\mathrm{LTP_{Max}}}{(\varepsilon_i(t)+1)^{\alpha}} - \mathrm{LTD_{Max}} \cdot \varepsilon_i(t) & \text{if } PF_j \text{ is active at } t,\ i \in 1, 2, \ldots, \text{Num. of muscles} \\ 0 & \text{otherwise} \end{cases} \quad (3)$$

where $\Delta W_{PF_j - PC_i(t)}$ is the weight change between the jth PF and the target PC associated with the ith muscle, ε_i is the current activity coming from the associated CF (which represents the normalized error along the executed arm plant movement), $\mathrm{LTP_{Max}}$ and $\mathrm{LTD_{Max}}$ are the maximum LTP/LTD values, and α is the LTP decaying factor. It should be noted that in previous cases when a synaptic weight had to be modified according to a teaching signal, a linear function was used (Masuda and Amari, 2008). However, this implied that while LTD was generated proportionally to the incoming error signal through CFs, LTP was constantly generated

when spikes reached the target PC. In this way, plasticity was not able to fully remove the manipulation task error since LTD was always counterbalanced by "unsupervised" LTP. In order to avoid this problem, LTP_{Max} and LTD_{Max} were set to 0.01 and 0.02 and α was set at 1000. This led to a marked decrease of LTP (evolving with the change in ε) and prevented plasticity saturation (e.g., see **Figure 3**).

In accordance with the assumption that the granular layer operates as a state generator (Yamazaki and Tanaka, 2007), this synaptic plasticity rule modified the strength only of the active PFs. The synaptic weight variation was positive (LTP) when CF activity approached 0 (low error levels in the movement). Otherwise the weight variation was negative (LTD) and was linearly proportional to CF activity.

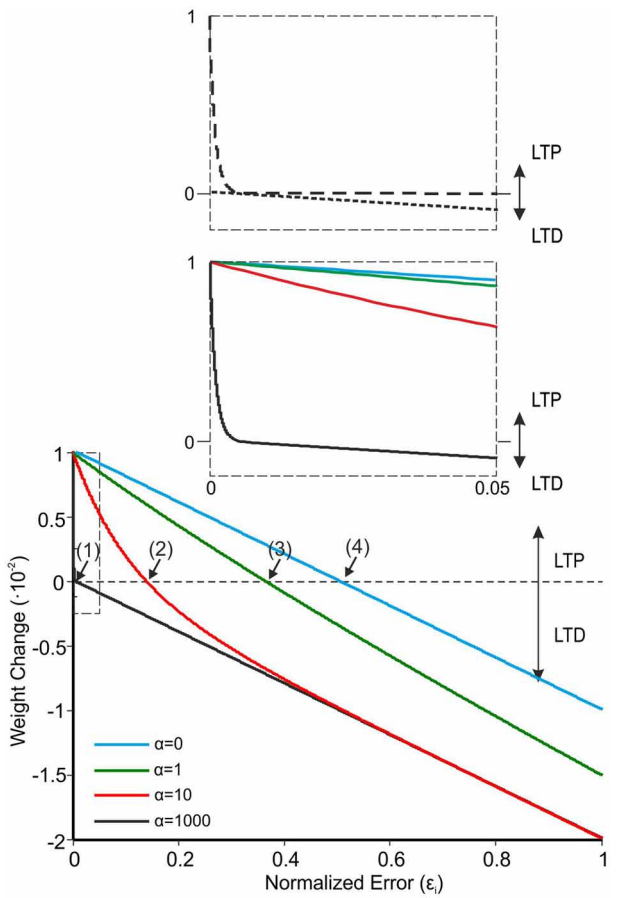

FIGURE 3 | The learning rule for PF-PC plasticity. Comparison of four different α values in Equation 3 (LTP_{Max} and LTD_{Max} were set at 0.01 and 0.02). Equation 3, which represents the synaptic weight change as a function of normalized error reaching the cerebellum through the CFs, shows better learning performances at high α values (black solid line). With $\alpha = 1000$, Equation 3 crosses the *X*-axis at a very low value (curve 1: $\varepsilon_i \approx 4.7 \cdot 10^{-3}$). When α is lowered, the curves cross the *X*-axis at progressively higher ε_i values (curve 2: $\alpha = 100$, $\varepsilon_i \approx 137.7 \cdot 10^{-3}$; curve 3: $\alpha = 1$, $\varepsilon_i \approx 366 \cdot 10^{-3}$; curve 4: $\alpha = 0$, $\varepsilon_i \approx 500 \cdot 10^{-3}$). The inset shows that with $\alpha = 1000$ there is a rapid decrease of LTP toward zero, while the LTD evolves linearly with the error.

MF-DCN synaptic plasticity

MF-DCN synaptic plasticity, which has been reported to depend on the intensity of DCN cell excitation (Racine et al., 1986; Medina and Mauk, 1999; Pugh and Raman, 2006; Zhang and Linden, 2006), was implemented as:

$$\Delta W_{MF-\mathrm{DCN}_i}(t) = \frac{\mathrm{LTP}_{\mathrm{Max}}}{(\mathrm{Pur}_i(t)+1)^{\alpha}} - LTD_{\mathrm{Max}} \cdot \mathrm{Pur}_i(t), \quad i \in 1, \ldots, \text{Number of muscles} \tag{4}$$

where $\Delta W_{MF-\mathrm{DCN}_i}(t)$ represents the weight change between the active MF and the target DCN associated with the *i*th muscle, Pur*(t)* is the current activity coming from the associated PCs, LTP_{Max}, and LTD_{Max} are the maximum LTP/LTD values, and α is the LTP decaying factor. In order to maintain the stability of the learning process, the LTP_{Max} and LTD_{Max} values had to be lower than those defined at the PF-PC synapse and were set at 10^{-3} and 10^{-4}, respectively. As in Equation 3, α was set at 1000, thus allowing a fast decrease of LTP and preventing early plasticity saturation (e.g., see **Figure 3**).

The MF-DCN learning rule, although formally similar to the PF-PC learning rule, bore two relevant differences. The first is due to the reduced ability of MFs, compared with PFs, to generate sequences of non-recurrent states (Yamazaki and Tanaka, 2007, 2009; Yamazaki and Nagao, 2012). The learning rule in Equation 4 would lead synaptic weights to their local maximum values (one activity value per different state) allowing plasticity to store temporally correlated information. In order to simplify the interpretation of the results, we used a single MF activity state, which was then associated by plasticity mechanisms with different gain values at MF-DCN synapses. The second difference concerns the connection driving LTD and LTP. While PF-PC plasticity was driven by CF activity, MF-DCN plasticity was driven by PC activity. This mechanism can optimize the activity range in the whole inhibitory pathway comprising MF-PF-PC-DCN connections: high PC activity causes MF-DCN LTD, while low PC activity causes MF-DCN LTP. This mechanism implements an effective cerebellar gain controller, which adapts its output activity to minimize the amount of inhibition generated in the MF-PF-PC-DCN inhibitory loop.

PC-DCN synaptic plasticity

PC-DCN synaptic plasticity was reported to depend on the intensity of DCN cell and PC excitation (Morishita and Sastry, 1996; Aizenman et al., 1998; Ouardouz and Sastry, 2000; Masuda and Amari, 2008) and was implemented as:

$$\Delta W_{PC_i-\mathrm{DCN}_i}(t) = \frac{\mathrm{LTP}_{\mathrm{Max}} \cdot \mathrm{Pur}_i(t)^{\alpha}}{(DCN_i(t)+1)^{\alpha}} - \mathrm{LTD}_{\mathrm{Max}} \cdot (1 - \mathrm{Pur}_i(t)), \quad i \in 1, \ldots, \text{Number of muscles} \tag{5}$$

where $\Delta W_{PC_i-\mathrm{DCN}_i}(t)$ is the synaptic weight adjustment at the PC-DCN connection reaching the DCN cell associated with the *i*th muscle. LTP_{Max} and LTD_{Max} are the maximum LTP/LTD values that this learning rule can apply at any time (as with the MF-DCN learning rule, these values were set at 10^{-3} and 10^{-4}

respectively), $Pur_i(t)$ is the current activity coming from the associated PC (in the range [0,1]), $DCN_i(t)$ is the current DCN output of the target DCN cell, and α represents the decaying factor of the LTP (again, it was set at 1000 as in MF-DCN and PF-PC learning rules). This learning rule led the PC-DCN synapses into a synaptic weight range appropriate to match the synaptic weight range at PFs. Equation 5 caused LTP only when both the PCs and their target DCN cell were simultaneously active.

CONTROL LOOP AND INPUT-OUTPUT ORGANIZATION

The brain can plan and learn the optimal trajectory of a movement in intrinsic coordinates (Houk et al., 1996; Nakano et al., 1999; Todorov, 2004; Hwang and Shadmehr, 2005). This operation consists of three major tasks: computation of the desired trajectory in external coordinates, translation of the task space into body coordinates, and generation of the motor command (Uno et al., 1989). In order to deal with dynamic variations, the system needs to incorporate a feedback error learning scheme (Kawato et al., 1987) in conjunction with a crude inverse dynamic model of the arm plant.

It was recently reported that multiple closed loops characterize the input-output organization of cerebro-cerebellar networks (Bostan et al., 2013). It has been proposed that the association cortices provide the motor cortex with the desired trajectory in body coordinates (**Figure 4A**). In the motor cortex, the motor command is calculated using an inverse dynamic arm model (for a review see Siciliano and Khatib, 2008). The *spinocerebellum-magnocellular red nucleus* system provides an accurate model of musculoskeletal dynamics, which are learned with practice by sensing motor command consequences in terms of executed movements (proprioception). The *cerebrocerebellum-parvocellular red nucleus system*, which projects back to the motor cortex, provides a crude inverse-dynamic model of the musculoskeletal system, which is acquired while monitoring the desired trajectory (Kawato et al., 1987). The crude inverse-dynamic model works together with the dynamic model, thus updating motor commands according to predictable errors occurring when executing a movement. In our control system, only the dynamic model involving cerebellar feedback to actual movement was implemented.

On the basis of these theories, we implemented a control loop using a forward architecture (see **Figure 4A**), in which only information about sensorial consequences of non-accurate commands was available (i.e., the difference between actual and desired arm plant joint positions). The natural error signal for learning was obtained as the difference between the actual movement and the motor command. This implies that if *M* muscles control a motor system endowed with *N* sensors, the *N* sensory errors must be converted into *M* motor errors (*MxN* complexity). How to use this sensory information to drive motor learning is the so-called *distal error problem* or *motor error problem* (Porrill et al., 2004; Haith and Vijayakumar, 2007). In order to circumvent this problem, the present cerebellar model used the adaptation mechanisms described above, which correlated the actual and desired states toward the generation of an accurate corrective motor command.

The system controller comprised different modules in accordance with studies indicating that the brain first plans the optimal trajectory in task-space coordinates, translates these into intrinsic-body coordinates, and finally generates the appropriate motor commands to achieve these transitions (Houk et al., 1996; Nakano et al., 1999; Todorov, 2004; Hwang and Shadmehr, 2005; Izawa et al., 2012). The system controller was composed of some pre-defined non-adaptive modules and a cerebellar model

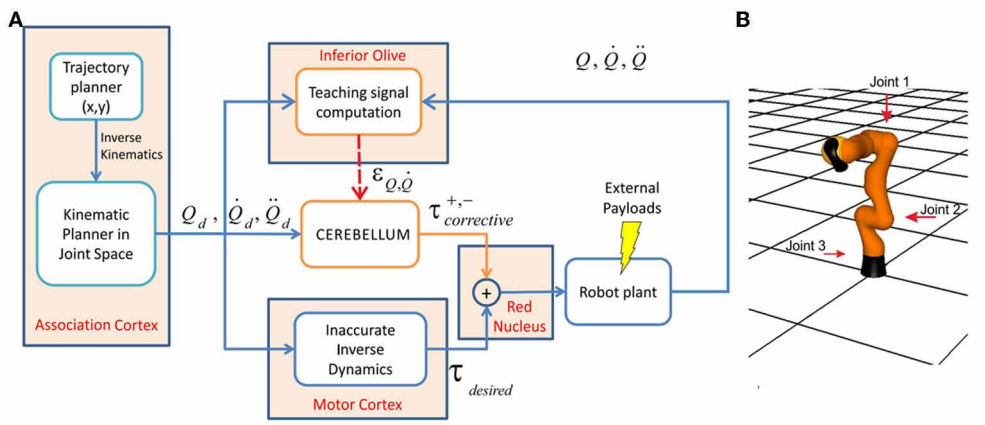

FIGURE 4 | Control scheme and robotic arm. (A) Essential control loop used for simulated manipulation tasks. The association cortex generates the desired trajectory (in terms of position, velocity, and acceleration) in body coordinates and the corresponding command signal is transmitted to both the motor cortex and to the cerebellum through the MFs. In the motor cortex command torques are calculated using an inverse dynamic arm model. The cerebellum generates corrective torques compensating for deviations from target trajectory (error) caused by the dynamic interaction of the arm with the object during manipulation. The signals from the motor cortex and cerebellum are added together in the red nucleus and then the output is delivered to the robot arm. The cerebellar corrective torques can be adapted in order to minimize the motor error. This requires a teaching signal generated by the IO. In the IO, the actual state is compared with the desired state in order to obtain the teaching error-dependent signal which reaches the cerebellum through the CFs. **(B)** The LWR arm. The three joints used in our experiments are indicated (red arrows); all the other joints were fixed (made rigid).

adapting over the learning trials (**Figure 4A**). The pre-defined modules, which maintained fixed parameters throughout the trials, independently of the load under manipulation, were the following:

- *Association cortex*. This module operated as a trajectory planner delivering desired positions and velocities of the target trajectory and it included an inverse kinematic model translating this trajectory from Cartesian into arm-joint coordinates.
- *Motor cortex*. This module, based on a recursive Newton-Euler algorithm (RNEA), generated crude step-by-step motor commands implementing the desired trajectory through an inverse dynamic model. The corresponding torque values could drive the robot arm along the desired trajectory in the absence of any external load, but failed to do so when loads were added during manipulation.
- *Red nucleus*. This module added the motor commands provided by motor cortex module to the corrective torques coming from the adaptive cerebellar module.

The cerebellar model is the only adaptive module in the system controller. This module learnt to correct the inverse dynamic model, pre-calculated for the desired trajectory in the absence of external load, in order to manipulate the actual load. The inclusion of three different learning rules allowed the cerebellar model to store the temporal properties of corrective torques in the PF-PC synapses and the gain of corrective torques in the MF-DCN and PC-DCN synapses.

The system integrated a lightweight robot (LWR) simulator within a feedforward control loop (Albu-Schäffer et al., 2011). The physical characteristics of the simulated robot plant were dynamically modified to match different contexts (e.g., the payload to be handled, which translated into a variation of the arm+object dynamics model). The LWR is a 7-degrees of freedom (7-DOF) arm composed of revolute joints. In our experiments, for simplicity, we only used the first, second and fifth joints, while the other joints were kept fixed (**Figure 4B**). The robot's dynamics were taken into account as indicated in appendix B.

MANIPULATION TASK AND EXPERIMENTAL PROTOCOL: TRAINING TRAJECTORY

Several reports in the literature have provided evidence of the role played by the cerebellum in complex manipulation-like tasks: (i) animal studies have shown that rapid target-reaching movements (Kitazawa et al., 1998) and circular manual tracking (Roitman et al., 2009) induced error encoding by PCs, (ii) imaging techniques have shown increased cerebellar activation in response to errors occurring during the execution of various tasks including tracking (Imamizu et al., 2000; Diedrichsen et al., 2005), and (iii) more specifically, prediction error has been shown to drive motor learning in saccades (Wallman and Fuchs, 1998) and reaching (Tseng et al., 2007). Thus, PCs are able to produce corrective signals in response to error signals (assumed to reach PCs through the CFs). The proposed model offers an explanation, based on evidence from complex learning tasks but also on theories proposed in relation to EBCC and VOR experiments, of how gain control (required for VOR and manipulation tasks) and timing control (also required for EBCC tasks) might occur in a plausible cerebellar model.

The model was tested in a smooth pursuit task (Luque et al., 2011a,b,c), in which the LWR targeted a repeated trajectory using its three revolute joints (**Figure 4B**). The benchmark *8-shape* trajectory (**Figure 5A**) was composed of vertical and horizontal sinusoidal components, whose equations in angular coordinates are given for each joint by:

$$q_1(t) = A_1 \cdot \sin(\pi t) + C_1 \tag{6}$$

$$q_2(t) = A_2 \cdot \sin(\pi t) + C_2 \tag{7}$$

$$q_3(t) = A_3 \cdot \sin(\pi t) + C_3 \tag{8}$$

where A_i and C_i are the amplitude and phase of the trajectories followed by each robot joint. The movement for the whole trajectory took just one second with masses requiring considerable corrective torques. This task was chosen to be sufficiently challenging to allow proper assessment of the learning capability of the cerebellar model. The corrective action driven by the cerebellum is especially relevant with respect to inertial components, Coriolis force and friction generated by movement (Schweighofer et al., 1998a). Changing the payload made it possible to assess the dynamics model abstraction capability of the cerebellum. As an example, **Figure 5B** shows the corrective torque values that the cerebellum should infer when manipulating a 10-kg payload. This corrective torque is calculated for each mass by means of the RNEA, which is able to solve the inverse dynamics problem.

In order to quantitatively evaluate movement performance, the mean absolute error (MAE) of each robot joint was calculated. This performance estimator was monitored in each trial and allowed evaluation of movement accuracy and of its improvement during the learning process.

RESULTS

As a first step in simulating the 8-shape task, the corrective torques needed for smooth manipulation of different masses (0.5, 1.5, 2.5, 6, and 10 kg) were calculated (**Figure 5B**). The maximum and minimum torque values for each joint and mass (see **Table A1** in Appendix A) were used to estimate the ideal weight values at DCN afferents. It was assumed that, as a consequence of learning, the maximum torque values corresponded to the MF-DCN synaptic weights, while the difference between the maximum and minimum torque values corresponded to PC-DCN synaptic weights. It should be noted that the PC-DCN synapse, by forming the only inhibitory pathway to the cerebellar nuclei, provides the only mechanism capable of reducing the output torques in the model.

NETWORK ACTIVITY AND MOTOR PERFORMANCE WITH FIXED WEIGHTS AT DCN SYNAPSES

In order to evaluate the impact, on the cerebellar circuit, of weights at synapses afferent to DCN, the PC firing rate was monitored after setting the MF-DCN and PC-DCN weights at their ideal values pre-calculated to handle different masses. The PF-PC weights were then allowed to change along a learning process

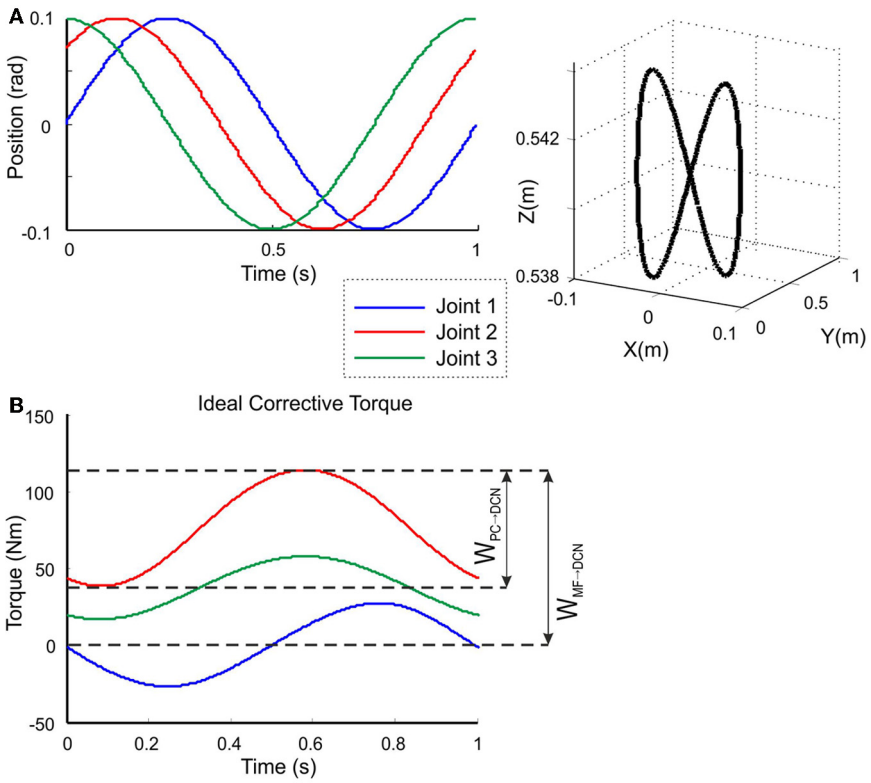

FIGURE 5 | Calculation of the target trajectory. Three-joint periodic trajectory defining an 8-shape movement [redrawn with permission from Luque et al. (2011c)] **(A)** Angular coordinates of each joint of the LWR *(left)*, and 3D view of the robot end-effector trajectory in Cartesian coordinates *(right)*. This 8-shape trajectory demands a movement difficult enough to allow robot arm dynamics to be revealed in fast movements (Hoffmann et al., 2007). **(B)** Ideal corrective signals that the cerebellar model had to infer for each of the three joints in order to correct the produced error when manipulating a 10-kg payload. According to the proposed hypothesis, the MF-DCN synaptic weights (W_{MF-DCN}) had to adapt to the gain of the maximum torque value at every joint, while the PC-DCN weight (W_{PC-DCN}) had to set the maximum inhibition (or torque value subtraction) needed.

composed of 1-s trial trajectories repeated 150 times. **Figure 6A** shows the normalized firing rate of one PC during a 1-s trial. The PC firing range changed clearly depending on the payload. It should be noted that in this configuration learning occurred only at the PF-PC synapse. As explained in the Methods, the change in PF-PC synaptic weights corresponds linearly to the change in PC firing rate.

Using the pre-calculated synaptic weight setting for a 1.5-kg payload allowed the PCs to operate over the whole range of firing rates producing, as a consequence, a fine adjustment of the DCN firing rate. This allowed the circuit to approach the ideal theoretical values of PC and DCN activity (**Figure 6B**) thus optimizing the learning corrective action in terms of stability and accuracy (**Figure 6C**). However, when DCN afferents were set at values pre-calculated for the manipulation of a heavier mass (10 kg), the PC activity was limited to a small frequency range in order to counteract the gain overscaling at DCN afferent synapses. Likewise, when DCN afferents were set at values pre-calculated for the manipulation of a lighter mass (0.5 kg), the learning process constrained PC activity to saturate to its minimum (no inhibition at DCN cells) along the trial (**Figure 6A**). These effects reduced the cerebellar output precision (**Figure 6B**) and made the corrective action unstable, decreasing the learning performance (**Figure 6C**). These experiments showed that synaptic weights at MF-DCN and PC-DCN connections were crucial to allow the cerebellar model to generate accurate and stable corrective motor outputs when manipulating different masses.

NETWORK ACTIVITY AND MOTOR PERFORMANCE WITH ADAPTABLE WEIGHTS AT DCN SYNAPSES

In order to investigate the effectiveness of learning rules regulating DCN synaptic weights, a simulation involving manipulation of a 10-kg payload was performed (**Figure 7**). The synaptic weights of MF-DCN and PC-DCN connections were allowed to self-adjust along a learning process composed of 1-s-trial trajectories repeated 1500 times.

Remarkably, the MF-DCN and PC-DCN synaptic weights tended to stabilize more slowly than those of the PF-PC synapse (**Figure 7A**) for two main reasons. First, the LTD_{Max} and LTP_{Max} parameters were higher in the PF-PC (10^{-2} and $2 \cdot 10^{-2}$ in Equation 3) than in MF-DCN and PC-DCN plasticity mechanisms (10^{-3} and 10^{-4} in Equations 4, 5). These LTD_{Max} and LTP_{Max} values were needed in order to stabilize the learning rules. Second, learning at the MF-DCN and PC-DCN synapses depended on PC normalized activity. Thus, the MF-DCN and PC-DCN synaptic weights changed only when some PF-PC

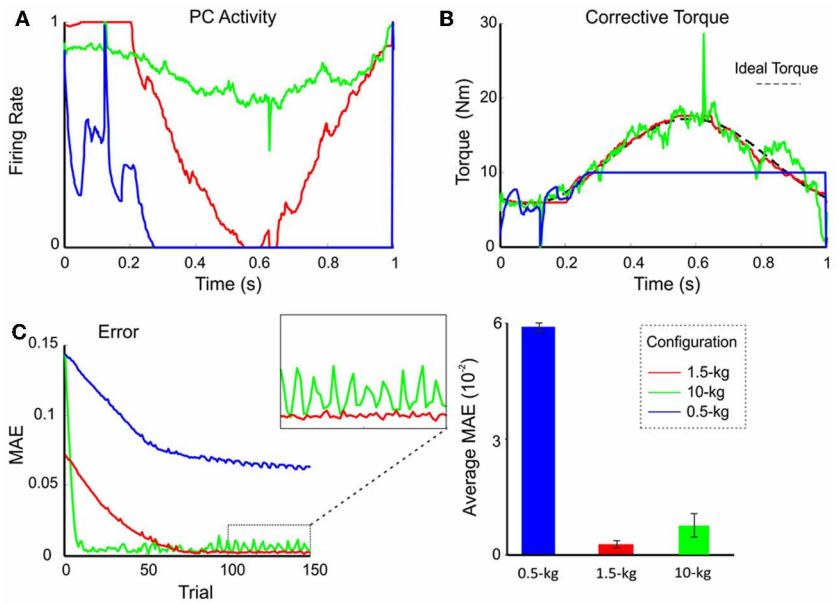

FIGURE 6 | Performance and learning with different weight configurations. Plasticity occurred only at PF-PC synapses, and was disabled at the MF-DCN and PC-DCN synapses. The synaptic weights were set at values appropriate for the manipulation of 0.5-kg (*blue lines*), 1.5-kg (*red lines*), and 10-kg (*green lines*) masses. In all three cases, 1.5-kg masses were actually manipulated. **(A)** Normalized activity of the PCs associated with the 2nd joint after 149 learning trials. For clarity, only the behavior of the second joint is shown, but similar results were found along the learning process also in joints 1 and 3. Note that by using the proper weight configuration *(red line)*, PC activity effectively ranged from 0 to 1. It should be noted that the time course of the PC firing rate corresponds to the synaptic weights at the PF-PC synapses (see Methods for explanation). **(B)** Corrective torque values provided by the DCN associated with the 2nd joint after 149 learning trials. **(C)** Evolution of the MAE during the learning process *(left)*. The box highlights the different stability of motor control during the last 50 trials. The histogram *(right)* shows the average MAE calculated over the last 50 trials for different payloads, revealing that smallest MAE values and variability occurred with the proper setting.

weights tended to saturate (toward 0 and 1, respectively; see above) (**Figure 7A**). Indeed, the evolution of weights was significantly slower at the PC-DCN than at the MF-DCN synapses. As exemplified for the agonist of joint 2, the MF-DCN weights stabilized in about 800 trials while the PC-DCN weights stabilized in more than 10,000 trials (for a comprehensive list of evolution of weights at the MF-DCN and PC-DCN synapses with different masses, see **Table A2** in Appendix A). This slow evolution was caused by the dependence of PC-DCN learning on DCN activity, which in turn depended on MF-DCN and PC-DCN adaptation (detailed information about the PC-DCN synaptic weights after the learning process is shown in **Table A3** in Appendix A). In parallel to the evolution of MF-DCN and PC-DCN synaptic weights, PF-PC weights evolved to stable values that were reached after 800 trials (**Figure 7A**).

After the DCN synaptic weight adaptation process, the cerebellum was able to provide corrective torques pretty similar to those theoretically calculated to solve the manipulation problem (**Figure 7B**; cf. **Figure 5C**). These torque values rapidly brought the MAE of the movement toward 0 (**Figure 7C**). When the synaptic weights were stabilized, the PC and DCN exploited their whole firing frequency range (**Figure 7D**). Thus, MF-DCN and PC-DCN plasticity allowed the system to efficiently self-rescale for optimal performance. Movies of learning simulations during manipulation of a 10-kg load are shown in the Supplemental Material.

DCN SYNAPTIC PLASTICITY IMPROVES PREDICTIVE MASS MANIPULATION

To further evaluate the effectiveness of the DCN learning rules, we considered how the difference between the *predicted* and *actual* manipulated mass influenced the accuracy of movement. To this end, learning trials with different payloads (0.5, 1.5, 2.5, 6, or 10 kg) were performed testing four different cerebellar model configurations. This made it possible to test the impact of adaptation occurring at multiple synaptic sites: (i) plasticity only at PF-PC synapses, (ii) plasticity at PF-PC and MF-DCN synapses, (iii) plasticity at PF-PC and PC-DCN synapses, and (iv) plasticity at PF-PC, MF-DCN, and PC-DCN synapses.

The synaptic weights that were not allowed to change were set at their theoretical values pre-calculated for the accurate manipulation of 10-kg masses. In this way both MFs and PCs were able to provide enough excitation and inhibition, respectively, in order to avoid saturation at DCN. These experiments allowed us to evaluate the complementary and cooperative role of the different plasticities.

For each combination of plasticities and masses, the learning process was simulated during 1500 trials, and the MAE at each joint was calculated at the end of the adaptation process. **Figure 8A** shows the average MAE during the last 100 trials. Plasticity at either MF-DCN or PC-DCN synapses reduced the average MAE, especially during the manipulation of lighter masses. Remarkably, enabling adaptation at just one of the two

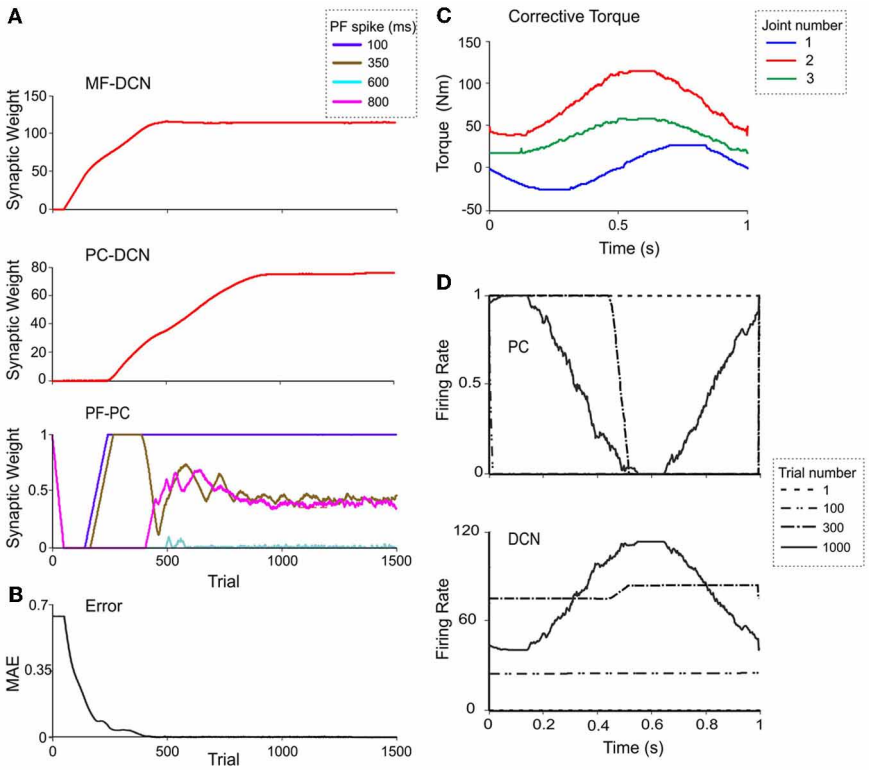

FIGURE 7 | Weight evolution in the cerebellar model with multiple plasticity mechanisms. Simulations were carried out using all the plasticity mechanisms (PF-PC, MF-DCN, and PC-DCN) for manipulation of a 10-kg external payload during 1500 trials. Initial synaptic weights allowed accurate movement of the arm without manipulation of any object (0-kg external payload). **(A)** Evolution of synaptic weights at MF-DCN *(top)*, PC-DCN *(middle)* and PF-PC *(bottom)* connections related to joint 2 *agonist* muscle. In PF-PC synapses, four different PFs that become active 100 ms *(purple)*, 350 ms *(brown)*, 600 ms *(cyan)*, and 800 ms *(pink)* after movement initiation are shown. **(B)** Corrective torques along a 1-s movement, provided by the cerebellar model at the 1500th trial in the learning process. Note the similarity of these values with the ideal ones calculated in **Figure 5C**. **(C)** Evolution of the average MAE of the three joints during the learning process. **(D)** Normalized PC firing rate *(top)* and DCN firing rate *(bottom)* during trials taken at different stages of the learning process: trial 1 *(red)*, trial 100 *(yellow)*, trial 300 *(gray)*, and trial 1000 *(green)*.

DCN afferent synapses was enough to improve manipulation precision. In line with this, plasticity at both MF-DCN and PC-DCN synapses simultaneously further increased the precision of manipulation. In order to obtain an objective evaluation of task performance independently of the manipulated mass, the "MAE reduction index" (MAE_{RI}) was defined:

$$MAE_{RI} = 1 - \frac{MAE_{C+}}{MAE_{C-}} \quad (9)$$

where MAE_{C+} is the MAE of the manipulation task when using the cerebellar model corrective action and MAE_{C-} is the MAE in the absence of cerebellar adaptation (1 is the perfect error correction by the cerebellar action and 0 represents lack of correction). Using MAE_{RI} it is possible to compare the adjustment capacity of the cerebellar model independently of the payload.

The effect of the different cerebellar models during the manipulation of different masses is shown in **Figure 8B**. In all the cerebellar models, the trajectory error decreased when manipulating heavier masses. However, only the models incorporating both MF-DCN and PC-DCN plasticity were able to improve lighter mass manipulation. These results could be explained by evaluating the variability of MAE (**Figure 8C**). On incorporating plasticity at all the synapses (PF-PC, MF-DCN, PC-DCN), the variability of MAE after learning was markedly reduced, thus enhancing the stability of movements.

Thus, the model, by adjusting the MF-DCN and PC-DCN synaptic weights, thereby causing the indirect adjustment of PC activity to its widest possible firing range, improved the smoothness of the robot arm trajectory during the manipulation of objects with different masses. This made it possible to produce an accurate and stable learning process irrespective of the manipulated payload, thus providing the cerebellar system with the capability to self-adapt in order to manipulate different objects.

IMPLICIT REPRESENTATION OF A DOUBLE LEARNING TIME SCALE

In order to verify whether the model supported the emergence of cerebellar learning consolidation, as indicated in recent behavioral and computational studies (Medina and Mauk, 1999; Ohyama et al., 2006; Xu-Wilson et al., 2009), the evolution of weight changes at DCN synapses was analyzed. During a 10-kg manipulation task (**Figure 9A**) the learning process was remarkably faster when DCN synaptic weights were pre-calculated. In this case, only the PF-PC synaptic weights, which stored the

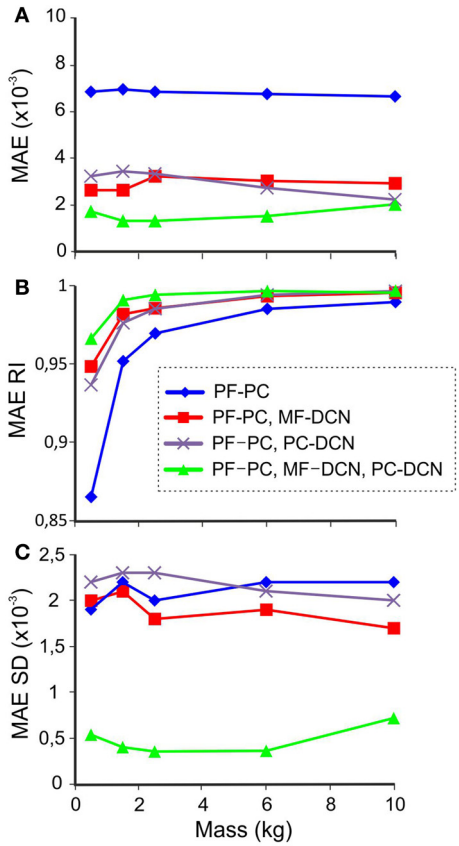

FIGURE 8 | Performance with different masses. In synaptic connections with fixed weights, the values correspond to the 10-kg set up to avoid saturation during manipulation of heavier masses. The last 100 of 1500 trials during learning processes were used for MAE estimation with different combinations of active learning rules at different masses. **(A)** MAE **(B)** MAE_{RI} (1 is perfect error correction by the cerebellar action and 0 is no correction), **(C)** MAE standard deviation (*SD*).

temporally correlated information, underwent adaptation, and learning was completed in around 50 trials. Otherwise, when weight changes at DCN synapses were enabled, learning required 200 trials (PC-DCN), 400 trials (MF-DCN), or 450 trials (PC-DCN and MF-DCN). In parallel, the MAE was remarkably reduced (**Figure 9B**).

Inspection of learning curves clearly showed that the learning process consisted of three different stages (**Figure 9**):

(i) The cerebellar model tried first to correct the initial error by using only PF-PC plasticity. This process took about 50 trials. When the MF-DCN or PC-DCN synaptic weights were not properly preconfigured, the PC activity saturated (**Figure 9C**).

(ii) When PC activity did not completely remove the error, the MF-DCN synaptic weights were slowly adjusted after the PF-PC synaptic weights became saturated. This process started after 50 trials and took about 480 trials to complete. After stabilization of MF-DCN synaptic weights, the error was highly reduced; nonetheless, object manipulation remained imprecise.

(iii) After about 300 trials, where the PC activity reached its maximum and in parallel with the MF-DCN weight evolution, the PC-DCN weights started increasing until the 1000th trial. Between 300 and 1000 trials the PC activity profile maintained a smooth shape and its trajectory remained close to the desired one.

Therefore, the model supported the existence of two different learning time scales consisting of: (i) a fast learning process, in which temporal information was inferred and stored at PF-PC synapses, and (ii) a slow learning process, in which the cerebellar excitatory and inhibitory gain values were adapted in the DCN and the manipulation precision increased. This second process was necessary only when the tool had never been manipulated before. During this process the MF-DCN and PC-DCN weights were simultaneously adapted at the same time as the PF-PC weights.

The fast and slow learning curves were fit to exponential decaying functions with time constants of 1–20 trials and 40–120 trials, depending on the object under manipulation (**Figure 9D**). The slow learning process could be further split into two components related to the MF-DCN and PF-PC connection with time-constants of 55–120 trials and 50–80 trials, respectively.

DISCUSSION

In this work, a theoretical model of the cerebellum is presented in the framework of a manipulation task, in which objects with different masses are moved along a desired trajectory. The main observation is that plastic mechanisms at DCN synapses effectively complement the learning capabilities of PF-PC synapses and contribute to the acquisition of the dynamics model of the arm/object plant. A proper synaptic weight adjustment at DCN synapses acts as a gain adaptation mechanism allowing the PFs to work within their most effective operative range, thus making the plasticity mechanisms between PFs and PCs more precise. This model, by incorporating distributed synaptic plasticity and by generating closed-loop simulations, allowed progressive error reduction based on feedback from the actual movement and accounted for three main theoretical aspects of cerebellar functioning.

First, the results support the principle that the cerebellum operates as a corrective inverse dynamic model (Schweighofer et al., 1996a,b, 1998b; Spoelstra et al., 2000). In the present model, the cerebellar granular layer was effectively implemented as a non-recurrent state generator (Yamazaki and Tanaka, 2007), in which the states correspond to the offset from stimulus onset implementing a *labeled-line coding* scheme. The granular layer states are then correlated with the error-based teaching signal received through the CFs. Thus, the model can be considered a particular case of an adaptive filter (Dean et al., 2009), in which the base functions in the granular layer are Dirac-deltas (impulse functions) with different delays for each granular cell or, in other words, a set of granular cells responding to different input stimuli along an arm trajectory trial (cf. D'Angelo and De Zeeuw, 2009).

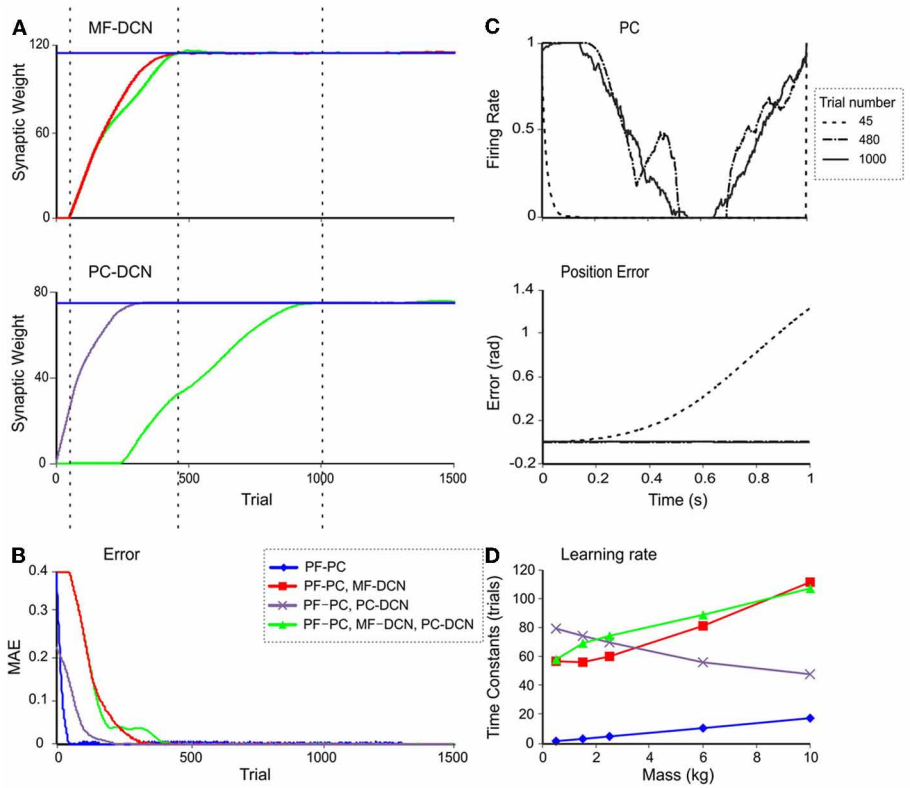

FIGURE 9 | Double time-scale learning. (A) Evolution of MF-DCN synaptic weight *(top)*, and PC-DCN synaptic weight *(bottom)* during the learning process when a 10-kg payload is being manipulated. **(B)** Evolution of MAE in the same trials as in A. **(C)** PC firing rate *(top)* and actual position error *(bottom)* in joint 2 at three different times: after 45 trials *(gray line)*, 480 trials *(yellow line)*, and 1000 trials *(green line)*. **(D)** Time constants of the fitted exponential functions of the MAE with different learning rule settings and masses. The MAE evolution during the learning process has been fitted to exponential decaying functions. The time constants are shown when enabling the use of plasticity only at the PF-PC synapses (blue line), at the PF-PC and MF-DCN synapses (red line), at the PF-PC and PC-DCN synapses (purple line), and at the PF-PC, MF-DCN, and PC-DCN synapses (green line).

Secondly, in the model, PF-PC plasticity temporally correlates the input state (or its representation in PFs) and the error estimation obtained during execution of the manipulation task. Instead, MF-DCN and PC-DCN plasticities store the excitatory and inhibitory gain of the neural network required to generate accurate correction of movement. Thus, the DCN afferent synapses infer the main properties of the object under manipulation, while the PF-PC synapses store the temporal characteristics of the task. As a consequence of this, plasticity at DCN synapses provides a homeostatic mechanism capable of keeping PC activity at its optimal range during learning. This effect can be observed in closed-loop simulations allowing progressive error reduction based on feedback from the actual movement.

Thirdly, the model supports the existence of a learning consolidation process, which has been demonstrated in behavioral experiments in human saccades (Brashers-Krug et al., 1996; Shadmehr and Brashers-Krug, 1997; Shadmehr and Holcomb, 1997; Xu-Wilson et al., 2009). While the cerebellar cortex plays a fundamental role at initial learning stages, the consolidation process seems to occur elsewhere. Our model provides a possible explanation of the learning consolidation process, locating it in the cerebellar nuclei. In our model, PF-PC plasticity evolves rapidly, while DCN plasticity evolves more slowly, because it depends on the previous evolution of plasticity at the PF-PC synapse itself. Therefore, our model naturally implements a double time-constant plasticity mechanism.

THE IMPACT OF PLASTICITY AT DCN SYNAPSES ON ADAPTABLE GAIN CONTROL

Several experimental studies have reported LTD and LTP in DCN neurons (Morishita and Sastry, 1996; Aizenman et al., 1998; Ouardouz and Sastry, 2000; Bagnall and du Lac, 2006; Pugh and Raman, 2006) and a few hypotheses have been advanced about the role they play in the whole network. In previous studies, (Medina and Mauk, 1999, 2000) it was suggested that MF-DCN plasticity provides a mechanism for consolidating time-correlated information in the cerebellum and proposed that PC activity could drive the DCN learning process. Our model extends this hypothesis to the process of gain consolidation. Moreover, our model includes the possibility, by using a PC-driven learning rule, of storing gain information at PC-DCN connections. A model proposed for the VOR suggested that combined plasticity at the MF-DCN and PC-DCN synapses plays an important role in learning consolidation (Masuda and Amari, 2008). Our model further suggests

that simultaneous MF-DCN and PC-DCN plasticity enhances movement precision in a manipulation task using a simulated robotic arm.

On the mechanistic level, our experimental approach allows different roles to be attributed to the different plasticity sites: PF-PC plasticity could act as a *time correlator* between the actual input state and the system error, while MF-DCN and PC-DCN plasticity together generated the *gain controller*. It is also possible that MF-DCN plasticity operates, at least in part, as a *state correlator*, as suggested previously (Masuda and Amari, 2008). Therefore, for improved performance, different aspects of computation have to be distributed over multiple adaptable network nodes.

BIOLOGICAL REALISM AND MODEL LIMITS

Before considering the further implications of this cerebellar model, its plausibility needs to be examined, analyzing the system design, learning rules, and coding strategies.

(1) In this model we implemented the PC as a table correlating granular layer states with output torques evolving through the learning process. This, in conjunction with the PF-PC learning rule, allows the PC to behave as a state-error correlator. However, PC recordings in awake animals (Lisberger and Fuchs, 1978; Van Kan et al., 1993; Escudero et al., 1996; Cheron et al., 1997; Medina and Lisberger, 2009) suggest that PCs are more complex than state-error correlators. In the present model, given the high level of abstraction, it is impossible to evaluate PC features in terms of spike patterns. Inferences about signal coding in PCs would probably require the incorporation of realistic cerebellar network models into the system controller.

(2) Since the learning rules used here at the MF-DCN and PC-DCN synapses depend only on PC and DCN activity, our model of gain control is compatible with different approaches to the distal error problem. Following the detailed descriptions provided on potential error detection mechanisms in the IO (Ito, 2013), the IO was assumed to receive both desired state information (encoding desired joint positions and velocities) conveyed by the motor cortex (Saint-Cyr, 1983) and actual state information (encoding actual joint positions and velocities) conveyed by the afferent sensory pathways, e.g., by the external cuneate nucleus concerning tactile and proprioceptive signals (Berkley and Hand, 1978; Molinari et al., 1996). This choice was supported by a computational model of the IO, which showed that the IO can indeed compare incoming signals (De Gruijl et al., 2012). It should be noted that alternative solutions to the distal error problem can be envisaged (Jordan and Rumelhart, 1992; Kawato, 1999), provided that PC activity saturates when the MF-DCN and PC-DCN weights are not properly tuned.

(3) We used cerebellar feedback to correct the actual movement and we assumed that the teaching signal comes only through the CFs. However, there are indications that cerebellar feedback is also reverberated to the motor cortex (Kawato et al., 1987; Siciliano and Khatib, 2008), and some investigations suggest that the teaching signal is also received and correlated at the granular layer level (Krichmar et al., 1997; Kistler and Leo van Hemmen, 1999; Anastasio, 2001; Rothganger and Anastasio, 2009). The introduction of these elements is expected to increase the level of flexibility in motor control and learning.

(4) We did not include the basal ganglia in our system controller. Recent evidence has suggested the existence of di-synaptic pathways connecting the cerebellum with the basal ganglia (Bostan et al., 2013). Both cerebellum (Swain et al., 2011) and basal ganglia (Bellebaum et al., 2008) have been suggested to contribute to reward-related learning tasks, but how these subsystems interact and reciprocally improve their operations remains an open issue.

(5) We assumed that PF-PC plasticity tends to saturate toward LTP and that salient codes are stored when the CFs drive plasticity toward LTD at specific synapses. This mechanism could correspond to classical postsynaptic LTD (Márquez-Ruiz and Cheron, 2012) coupled with presynaptic LTP (Gao et al., 2012). The effectiveness of this core plasticity mechanism could be extended through multiple forms of LTP and LTD occurring at the PF-PC synapses and could be integrated with the inhibitory role played by MLIs (Wulff et al., 2009). MF-DCN and PC-DCN plasticity is implemented according to principles set out elsewhere (Medina and Mauk, 2000; Masuda and Amari, 2008). In our model, MF-DCN LTD followed increased PC activity. The full mechanism would comprise a secondary DCN spike increase through a rebound mechanism (Pugh and Raman, 2006), but this was irrelevant at our spike-less modeling level. Similarly, other details about the mechanisms of plasticity have not been applied. It remains to be established whether a biologically precise representation of plasticity mechanisms (e.g., Solinas et al., 2010) might modify the core conclusion of this model.

(6) LTP and LTD between MFs and GCs have been shown to occur in slice experiments (D'Angelo et al., 1999; Armano et al., 2000; Maffei et al., 2002; Rossi et al., 2002; Sola et al., 2004; Gall et al., 2005; Mapelli and D'Angelo, 2007) and in vivo (Roggeri et al., 2008). However, the inclusion of granular layer LTP and LTD (Hansel et al., 2001) in a biologically realistic scenario would require (i) definition of the learning rules and teaching signals through the MFs (e.g., see D'Errico et al., 2009), (ii) definition of the spatiotemporal organization of the granular layer activity (D'Angelo, 2011; D'Angelo and Casali, 2012; D'Angelo et al., 2013; Garrido et al., 2013), and (iii) introduction of an explicit representation of spike timing (Nieus et al., 2006; D'Angelo and De Zeeuw, 2009). It has been suggested that MF-GC LTP and LTD, in conjunction with GC intrinsic plasticity and regulation of GoC–GC synaptic weights, could improve the learning capabilities of the system in target-reaching tasks (Schweighofer et al., 2001). In general, this hypothesis on the granular layer is compatible with the present model. Indeed, the labeled-line coding scheme that our model implements in the granular layer (**Figure 2**) can be seen as a particular case of sparse coding (although it is not very efficient in terms of the number of cells required to represent multiple states). Recent

discoveries have revealed that sparse coding in the granular layer is related to the amount of GCs available for a particular task (Galliano et al., 2013). Our model, in fact, represents an extreme case of this hypothesis in which the population of GCs is so extensive that each PF encoded a unique non-recurrent condition. Moreover, it has been shown that the same GC can receive convergent inputs from proprioceptive sensory pathways coming from the external cuneate nucleus and efferent motor copies coming from the cerebral cortex via the pontine nucleus (Huang et al., 2013). In previous studies we already predicted that multi-modal information in the GCs could improve state representation capabilities (and, as a consequence, manipulation performance) in a non-adaptive model of the granular layer (Luque et al., 2011a). The development of a cerebellar model accounting for all these discoveries in the granular layer would require the use of realistic models implementing synaptic plasticity mechanisms and managing spike information (Solinas et al., 2010; Luque et al., 2011b,c). The integration of the present model into a spike-timing computational scheme including MF-GC plasticity rule remains a future challenge.

THEORETICAL IMPLICATIONS

This model has been conceived in order to be simple enough to become mathematically tractable while, at the same time, including salient properties of the system so as to retain its links with biology. In this sense it lies halfway between a classical black-box model and a realistic biological model. A non-trivial consequence of the way the model is constructed is that of providing a theoretical explanation for DCN plasticity, which increases cerebellar adaptable solutions. Moreover, this model could be compared to prototypical cases elaborated for dynamic neural networks (Spitzer, 2000; Hoellinger et al., 2013). In these networks, learning of complex tasks is better accomplished when the number of hidden neurons increases, as they form complex categories that are needed to interpret the multi-parametric input space. In the cerebellar network, the hidden units could intervene at different levels, including that of GCs lying between extracerebellar neurons and PCs, PCs lying between GCs and DCN, and also GoCs or MLIs in their respective subcircuits. In fact, extrapolation from theoretical works is limited by several biological constraints. For example, category formation is probably much more efficient in PCs than in GCs given the 10^5 higher number of inputs in the PCs than in GCs, however there are many more GCs than PCs, and this results in a delicate balance between these cell types (the issue dates back to the seminal work of Marr, 1969). Conversely, GoCs and MLIs could implement exclusive-or (XOR) hidden layers, as suggested by experimental network analysis (Mapelli et al., 2010; Solinas et al., 2010). Moreover, PCs make synaptic connections with adjacent PCs through axonal collaterals suggesting that self-organizing properties might emerge in the molecular layer.

It should be noted that theoretical networks are oversimplified compared to the cerebellar model presented herein. For example, in Hoellinger's network plasticity can change the synapse from excitatory to inhibitory, connections are all-to-all, and gain and timing are stored in the same synapse (Hoellinger et al., 2013). A complementary step will be the inclusion of spiking dynamics, through the use of realistic network models (D'Angelo et al., 2009; Garrido et al., 2013). In this way, the implications of physiology (i.e., the role of the inhibitory PC collaterals, the complex structure of the PC dendritic tree and the operation of DCN cells with their characteristic postsynaptic rebounds) will be fully addressed.

CONCLUSIONS

This model proposes a plausible explanation on how multiple plasticity sites, including the PF-PC and the MF-DCN and PC-DCN synapses, may effectively implement cerebellar gain control. According to the proposed model, distributed synaptic plasticity implements a gain controller, which (i) is *self-adaptable*, i.e., automatically rescales as a function of the manipulated masses over a large dynamic range, (ii) operates over *multiple time scales*, i.e., accounts for fast learning of time correlations and for subsequent gain consolidation, and (iii) improves learning accuracy and precision. These functions can be partly separated: the PF-PC synapse is suggested to operate mostly as a time correlator, while gain is more effectively regulated in DCN afferent synapses under PC control. In this way, time correlation and gain can be partially processed and stored independently. This organization of learning could explain the impact of genetic mutations impairing plasticity at cerebellar synapses. Indeed, irrespective of the specific synaptic plasticity mechanism involved (be it in the granular layer, molecular layer or DCN), transgenic mice bearing LTP or LTD alterations show deficits in cerebellar-related behavior and learning. However, the learning of timing and gain appear to be differentially affected, revealing that processing of these two components of learning are at least partially segregated (for a review see Boyden et al., 2004; Gao et al., 2012). Finally, it should be noted that the coexistence of fast and slow learning mechanisms can be reconciled with the double time-scale phenomenological model of learning proposed by Shadmehr and Mussa-Ivaldi (2012), which has been proposed to depend on localization of a fast learning process in the PF-PC synapse and a slower one in the DCN afferent synapses (Medina and Mauk, 1999; Medina et al., 2000).

A controller with distributed plasticity is convenient from a system designer's point of view, since it allows efficient adjustment of the corrective signal regardless of the dynamic features of the manipulated object and of the way it affects the dynamics of the arm plant involved. It should be noted that the adaptation mechanism adopted herein is not constrained to any specific plant or testing framework, and could therefore be extrapolated to other common testing paradigms like EBCC and the VOR. In order to do so, further details may be added to the model accounting for specific synaptic plasticity mechanisms and circuits involved in the different learning processes.

ACKNOWLEDGMENTS

This work was supported by grants of European Union to Egidio D'Angelo (CEREBNET FP7-ITN238686, REALNET FP7-ICT270434) and by a grant of the Italian Ministry of Health to Egidio D'Angelo (RF-2009-1475845). We thank G. Ferrari and M. Rossin for technical support.

SUPPLEMENTARY MATERIAL

The Supplementary Material for this article can be found online at: http://www.frontiersin.org/journal/10.3389/fncir.2013.00159/abstract

Movie S1 | Learning simulation, joint-1-related activity and weight evolution during manipulation of a 10-kg load. Simulations were carried out using all the plasticity mechanisms (PF-PC, MF-DCN, and PC-DCN) along 1000 trials. Only 1 every 10 trials is shown. The movement has been recorded in real-time (each trial lasts 1 s) evidencing the difficulty of the task. *(top left)* 3D view of the actual *(black)* and desired *(red)* robot end-effector trajectory in Cartesian coordinates. *(medium left)* Ideal *(dotted lines)* and actual *(solid lines)* corrective torques during the current trial for joint 1 *(blue)*, 2 *(red)*, and 3 *(green)*. *(bottom left)* Evolution of the MAE. *(top right)* Evolution of four randomly chosen PF-PC synaptic weights. *(second to fifth rows right)* Evolution of PC activity, DCN activity, MF-DCN, and PC-DCN synaptic weights related to joint 1 *agonist (solid line)* and antagonist *(dotted line)* muscles. Note that, at the end of learning, joint-1 DCN neurons provided higher corrective torques to the antagonist muscle during the first half of the trial and to the agonist muscle during the second half of the trial.

Movie S2 | Learning simulation, joint-2-related activity and weight evolution during manipulation of a 10-kg load. Simulations were carried out using all the plasticity mechanisms (PF-PC, MF-DCN, and PC-DCN) along 1000 trials. Only 1 every 10 trials is shown. The movement has been recorded in real-time (each trial lasts 1 s) evidencing the difficulty of the task. *(top left)* 3D view of the actual *(black)* and desired *(red)* robot end-effector trajectory in Cartesian coordinates. *(medium left)* Ideal *(dotted lines)* and actual *(solid lines)* corrective torques during the current trial for joint 1 *(blue)*, 2 *(red)*, and 3 *(green)*. *(bottom left)* Evolution of the MAE. *(top right)* Evolution of four randomly chosen PF-PC synaptic weights. *(second to fifth rows right)* Evolution of PC activity, DCN activity, MF-DCN, and PC-DCN synaptic weights related to joint 2 *agonist (solid line)* and antagonist *(dotted line)* muscles. Differently from what observed for joint 1, at the end of learning, joint-2 DCN neurons provided higher corrective torques to the agonist muscle during the whole trial.

Movie S3 | Learning simulation, joint-3-related activity and weight evolution during manipulation of a 10-kg load. Simulations were carried out using all the plasticity mechanisms (PF-PC, MF-DCN, and PC-DCN) along 1000 trials. Only 1 every 10 trials is shown. The movement has been recorded in real-time (each trial lasts 1 s) evidencing the difficulty of the task. *(top left)* 3D view of the actual *(black)* and desired *(red)* robot end-effector trajectory in Cartesian coordinates. *(medium left)* Ideal *(dotted lines)* and actual *(solid lines)* corrective torques during the current trial for joint 1 *(blue)*, 2 *(red)*, and 3 *(green)*. *(bottom left)* Evolution of the MAE. *(top right)* Evolution of four randomly chosen PF-PC synaptic weights. *(second to fifth rows right)* Evolution of PC activity, DCN activity, MF-DCN and PC-DCN synaptic weights related to joint 3 *agonist (solid line)* and antagonist *(dotted line)* muscles. Similarly to what observed for joint 2, joint 3 corrective torques provided by DCN neurons were dominated by agonist muscle activity, but different gain values were provided with respect to joint 2.

REFERENCES

Aizenman, C. D., Manis, P. B., and Linden, D. J. (1998). Polarity of long-term synaptic gain change is related to postsynaptic spike firing at a cerebellar inhibitory synapse. *Neuron* 21, 827–835. doi: 10.1016/S0896-6273(00)80598-X

Albus, J. S. (1971). A theory of cerebellar function. *Math. Biosci.* 10, 25–61. doi: 10.1016/0025-5564(71)90051-4

Albu-Schäffer, A., Eiberger, O., Fuchs, M., Grebenstein, M., Haddadin, S., Ott, C., et al. (2011). Anthropomorphic soft robotics–from torque control to variable intrinsic compliance. *Rob. Res.* 70, 185–207. doi: 10.1007/978-3-642-19457-3_12

Albu-Schäffer, A., Haddadin, S., Ott, C., Stemmer, A., Wimböck, T., and Hirzinger, G. (2007). The DLR lightweight robot: design and control concepts for robots in human environments. *Ind. Rob. Int. J.* 34, 376–385. doi: 10.1108/01439910710774386

Anastasio, T. J. (2001). Input minimization: a model of cerebellar learning without climbing fiber error signals. *Neuroreport* 12, 3825. doi: 10.1097/00001756-200112040-00045

Armano, S., Rossi, P., Taglietti, V., and D'Angelo, E. (2000). Long-term potentiation of intrinsic excitability at the mossy fiber-granule cell synapse of rat cerebellum. *J. Neurosci.* 20, 5208.

Bagnall, M. W., and du Lac, S. (2006). A new locus for synaptic plasticity in cerebellar circuits. *Neuron* 51, 5–7. doi: 10.1016/j.neuron.2006.06.014

Bazzigaluppi, P., De Gruijl, J. R., van der Giessen, R. S., Khosrovani, S., De Zeeuw, C. I., and de Jeu, M. T. (2012). Olivary subthreshold oscillations and burst activity revisited. *Front. Neural Circuits* 6:91. doi: 10.3389/fncir.2012.00091

Bellebaum, C., Koch, B., Schwarz, M., and Daum, I. (2008). Focal basal ganglia lesions are associated with impairments in reward-based reversal learning. *Brain* 131, 829–841. doi: 10.1093/brain/awn011

Berkley, K., and Hand, P. (1978). Projections to the inferior olive of the cat II. Comparisons of input from the gracile, cuneate and the spinal trigeminal nuclei. *J. Comp. Neurol.* 180, 253–264. doi: 10.1002/cne.901800205

Bliss, T. V., and Collingridge, G. L. (1993). A synaptic model of memory: long-term potentiation in the hippocampus. *Nature* 361, 31–39. doi: 10.1038/361031a0

Bona, B., and Curatella, A. (2005). "Identification of industrial robot parameters for advanced model-based controllers design," in *Robotics and Automation, 2005. ICRA 2005. Proceedings of the 2005 IEEE International Conference on (IEEE)*, (Barcelona), 1681–1686.

Bostan, A. C., Dum, R. P., and Strick, P. L. (2013). Cerebellar networks with the cerebral cortex and basal ganglia. *Trends Cogn. Sci.* 17, 241–254. doi: 10.1016/j.tics.2013.03.003

Boyden, E. S., Katoh, A., and Raymond, J. L. (2004). Cerebellum-dependent learning: the role of multiple plasticity mechanisms. *Neuroscience* 27, 581–609. doi: 10.1146/annurev.neuro.27.070203.144238

Brashers-Krug, T., Shadmehr, R., and Bizzi, E. (1996). Consolidation in human motor memory. *Nature* 382, 252–255. doi: 10.1038/382252a0

Cheron, G., Dufief, M. P., Gerrits, N. M., Draye, J. P., and Godaux, E. (1997). Behavioural analysis of Purkinje cell output from the horizontal zone of the cat flocculus. *Prog. Brain Res.* 114, 347–356. doi: 10.1016/S0079-6123(08)63374-9

Coesmans, M., Weber, J. T., De Zeeuw, C. I., and Hansel, C. (2004). Bidirectional parallel fiber plasticity in the cerebellum under climbing fiber control. *Neuron* 44, 691–700. doi: 10.1016/j.neuron.2004.10.031

D'Angelo, E. (2011). Neural circuits of the cerebellum: Hypothesis for function. *J. Integr. Neurosci.* 10, 317–352. doi: 10.1142/S0219635211002762

D'Angelo, E., and Casali, S. (2012). Seeking a unified framework for cerebellar function and dysfunction: from circuit operations to cognition. *Front. Neural Circuits* 6:116. doi: 10.3389/fncir.2012.00116

D'Angelo, E., and De Zeeuw, C. I. (2009). Timing and plasticity in the cerebellum: focus on the granular layer. *Trends Neurosci.* 32, 30–40. doi: 10.1016/j.tins.2008.09.007

D'Angelo, E., Koekkoek, S. K. E., Lombardo, P., Solinas, S., Ros, E., Garrido, J., et al. (2009). Timing in the cerebellum: oscillations and resonance in the granular layer. *Neuroscience* 162, 805–815. doi: 10.1016/j.neuroscience.2009.01.048

D'Angelo, E., Rossi, P., Armano, S., and Taglietti, V. (1999). Evidence for NMDA and mGlu receptor-dependent long-term potentiation of mossy fiber-granule cell transmission in rat cerebellum. *J. Neurophysiol.* 81, 277.

D'Angelo, E., Solinas, S., Mapelli, J., Gandolfi, D., Mapelli, L., and Prestori, F. (2013). The cerebellar Golgi cell and spatiotemporal organization of granular layer activity. *Front. Neural Circuits* 7:93. doi: 10.3389/fncir.2013.00093

D'Errico, A., Prestori, F., and D'Angelo, E. (2009). Differential induction of bidirectional long-term changes in neurotransmitter release by frequency-coded patterns at the cerebellar input. *J. Physiol.* 587, 5843–5857. doi: 10.1113/jphysiol.2009.177162

De Gruijl, J. R., Bazzigaluppi, P., de Jeu, M. T., and De Zeeuw, C. I. (2012). Climbing fiber burst size and olivary sub-threshold oscillations in a network setting. *PLoS Comput. Biol.* 8:e1002814. doi: 10.1371/journal.pcbi.1002814

De Zeeuw, C. I., and Yeo, C. H. (2005). Time and tide in cerebellar memory formation. *Curr. Opin. Neurobiol.* 15, 667–674. doi: 10.1016/j.conb.2005.10.008

Dean, P., Porrill, J., Ekerot, C. F., and Jörntell, H. (2009). The cerebellar microcircuit as an adaptive filter: experimental and computational evidence. *Nat. Rev. Neurosci.* 11, 30–43. doi: 10.1038/nrn2756

Diedrichsen, J., Hashambhoy, Y., Rane, T., and Shadmehr, R. (2005). Neural correlates of reach errors. *J. Neurosci.* 25, 9919–9931. doi: 10.1523/JNEUROSCI.1874-05.2005

Ebner, T., and Pasalar, S. (2008). Cerebellum predicts the future motor state. *Cerebellum* 7, 583–588. doi: 10.1007/s12311-008-0059-3

Escudero, M., Cheron, G., and Godaux, E. (1996). Discharge properties of brain stem neurons projecting to the flocculus in the alert cat. II. Prepositus hypoglossal nucleus. *J. Neurophysiol.* 76, 1775–1785.

Fujita, M. (1982). Adaptive filter model of the cerebellum. *Biol. Cybern.* 45, 195–206. doi: 10.1007/BF00336192

Gall, D., Prestori, F., Sola, E., D'Errico, A., Roussel, C., Forti, L., et al. (2005). Intracellular calcium regulation by burst discharge determines bidirectional long-term synaptic plasticity at the cerebellum input stage. *J. Neurosci.* 25, 4813. doi: 10.1523/JNEUROSCI.0410-05.2005

Galliano, E., Gao, Z., Schonewille, M., Todorov, B., Simons, E., Pop, A. S., et al. (2013). Silencing the majority of cerebellar granule cells uncovers their essential role in motor learning and consolidation. *Cell Rep.* 3, 1239–1251. doi: 10.1016/j.celrep.2013.03.023

Gao, Z., van Beugen, B. J., and De Zeeuw, C. I. (2012). Distributed synergistic plasticity and cerebellar learning. *Nat. Rev. Neurosci.* 13, 619–635. doi: 10.1038/nrn3312

Garrido, J. A., Ros, E., and D'Angelo, E. (2013). Spike timing regulation on the millisecond scale by distributed synaptic plasticity at the cerebellum input stage: a simulation study. *Front. Comput. Neurosci.* 7:64. doi: 10.3389/fncom.2013.00064

Haith, A., and Vijayakumar, S. (2007). "Robustness of VOR and OKR adaptation under kinematics and dynamics transformations," in *Development and Learning, 2007. ICDL 2007. IEEE 6th International Conference on*, (London), 37–42.

Hansel, C., Linden, D. J., and Angelo, E. D. (2001). Beyond parallel fiber LTD: the diversity of synaptic and non-synaptic plasticity in the cerebellum. *Nat. Neurosci.* 4, 467–476.

Hoellinger, T., Petieau, M., Duvinage, M., Castermans, T., Seetharaman, K., Cebolla, A. M., et al. (2013). Biological oscillations for learning walking coordination: dynamic recurrent neural network functionally models physiological central pattern generator. *Front. Comput. Neurosci.* 7:70. doi: 10.3389/fncom.2013.00070

Hoffmann, H., Petkos, G., Bitzer, S., and Vijayakumar, S. (2007). "Sensor-assisted adaptive motor control under continuously varying context. Icinco 2007," in *Proceedings of the Fourth International Conference on Informatics in Control, Automation and Robotics, Vol Icso*, (Angers), 262–269.

Houk, J. C., Buckingham, J. T., and Barto, A. G. (1996). Models of the cerebellum and motor learning. *Behav. Brain Sci.* 19, 368–383. doi: 10.1017/S0140525X00081474

Huang, C. C., Sugino, K., Shima, Y., Guo, C., Bai, S., Mensh, B. D., et al. (2013). Convergence of pontine and proprioceptive streams onto multimodal cerebellar granule cells. *Elife* 2, e00400. doi: 10.7554/eLife.00400

Hwang, E. J., and Shadmehr, R. (2005). Internal models of limb dynamics and the encoding of limb state. *J. Neural Eng.* 2, S266. doi: 10.1088/1741-2560/2/3/S09

Imamizu, H., Miyauchi, S., Tamada, T., Sasaki, Y., Takino, R., Pütz, B., et al. (2000). Human cerebellar activity reflecting an acquired internal model of a new tool. *Nature* 403, 192–195. doi: 10.1038/35003194

Ito, M. (2001). Cerebellar long-term depression: characterization, signal transduction, and functional roles. *Physiol. Rev.* 81, 1143–1195.

Ito, M. (2013). Error detection and representation in the olivo-cerebellar system. *Front. Neural Circuits* 7:1. doi: 10.3389/fncir.2013.00001

Ito, M., and Kano, M. (1982). Long-lasting depression of parallel fiber-Purkinje cell transmission induced by conjunctive stimulation of parallel fibers and climbing fibers in the cerebellar cortex. *Neurosci. Lett.* 33, 253–258. doi: 10.1016/0304-3940(82)90380-9

Izawa, J., Pekny, S. E., Marko, M. K., Haswell, C. C., Shadmehr, R., and Mostofsky, S. H. (2012). Motor learning relies on integrated sensory inputs in ADHD, but over−selectively on proprioception in autism spectrum conditions. *Autism Res.* 5, 124–136. doi: 10.1002/aur.1222

Jordan, M. I., and Rumelhart, D. E. (1992). Forward models: supervised learning with a distal teacher. *Cogn. Sci.* 16, 307–354. doi: 10.1207/s15516709cog1603_1

Kawato, M. (1999). Internal models for motor control and trajectory planning. *Curr. Opin. Neurobiol.* 9, 718–727. doi: 10.1016/S0959-4388(99)00028-8

Kawato, M., Furukawa, K., and Suzuki, R. (1987). A hierarchical neural-network model for control and learning of voluntary movement. *Biol. Cybern.* 57, 169–185. doi: 10.1007/BF00364149

Khalil, W., and Dombre, E. (2004). *Modeling, Identification and Control of Robots*. Oxford: Butterworth-Heinemann.

Kistler, W. M., and Leo van Hemmen, J. (1999). Delayed reverberation through time windows as a key to cerebellar function. *Biol. Cybern.* 81, 373–380. doi: 10.1007/s004220050569

Kitazawa, S., Kimura, T., and Yin, P. B. (1998). Cerebellar complex spikes encode both destinations and errors in arm movements. *Nature* 392, 494–497. doi: 10.1038/33141

Krichmar, J., Ascoli, G., Hunter, L., and Olds, J. (1997). A model of cerebellar saccadic motor learning using qualitative reasoning. *Biol. Artif. Comput. Neurosci. Tech.* 1240, 133–145. doi: 10.1007/BFb0032471

Lepora, N. F., Porrill, J., Yeo, C. H., and Dean, P. (2010). Sensory prediction or motor control. Application of marr-albus type models of cerebellar function to classical conditioning. *Front. Comput. Neurosci.* 4:140. doi: 10.3389/fncom.2010.00140

Lisberger, S. G., and Fuchs, A. F. (1978). Role of primate flocculus during rapid behavioral modification of vestibuloocular reflex. I. Purkinje cell activity during visually guided horizontal smooth-pursuit eye movements and passive head rotation. *J. Neurophysiol.* 41, 733–763.

Luque, N. R., Garrido, J. A., Carrillo, R. R., Coenen, O. J., and Ros, E. (2011a). Cerebellar input configuration toward object model abstraction in manipulation tasks. *IEEE Trans. Neural Netw.* 22, 1321–1328. doi: 10.1109/TNN.2011.2156809

Luque, N. R., Garrido, J. A., Carrillo, R. R., Coenen, O. J., and Ros, E. (2011b). Cerebellarlike corrective model inference engine for manipulation tasks. IEEE Trans. Syst. Man Cybern. B Cybern. 41, 1–14. doi: 10.1109/TSMCB.2011.2138693

Luque, N. R., Garrido, J. A., Carrillo, R. R., Tolu, S., and Ros, E. (2011c). Adaptive cerebellar spiking model embedded in the control loop: context switching and robustness against noise. *Int. J. Neural Syst.* 21, 385–401. doi: 10.1142/S0129065711002900

Maffei, A., Prestori, F., Rossi, P., Taglietti, V., and D'Angelo, E. (2002). Presynaptic current changes at the mossy fiber–granule cell synapse of cerebellum during LTP. *J. Neurophysiol.* 88, 627.

Manto, M., Bower, J. M., Conforto, A. B., Delgado-García, J. M., da Guarda, S. N., Gerwig, M., et al. (2012). Consensus paper: roles of the cerebellum in motor control–the diversity of ideas on cerebellar involvement in movement. *Cerebellum* 11, 457–487. doi: 10.1007/s12311-011-0331-9

Mapelli, J., and D'Angelo, E. (2007). The spatial organization of long-term synaptic plasticity at the input stage of cerebellum. *J. Neurosci.* 27, 1285. doi: 10.1523/JNEUROSCI.4873-06.2007

Mapelli, J., Gandolfi, D., and D'Angelo, E. (2010). Combinatorial responses controlled by synaptic inhibition in the cerebellum granular layer. *J. Neurophysiol.* 103, 250. doi: 10.1152/jn.00642.2009

Márquez-Ruiz, J., and Cheron, G. (2012). Sensory stimulation-dependent plasticity in the cerebellar cortex of alert mice. *PLoS ONE* 7:e36184. doi: 10.1371/journal.pone.0036184

Marr, D. (1969). A theory of cerebellar cortex. *J. Physiol.* 202, 437–470.

Masuda, N., and Amari, S. (2008). A computational study of synaptic mechanisms of partial memory transfer in cerebellar vestibulo-ocular-reflex learning. *J. Comput. Neurosci.* 24, 137–156. doi: 10.1007/s10827-007-0045-7

Medina, J. F., Garcia, K. S., Nores, W. L., Taylor, N. M., and Mauk, M.

D. (2000). Timing mechanisms in the cerebellum: testing predictions of a large-scale computer simulation. *J. Neurosci.* 20, 5516–5525.

Medina, J. F., and Lisberger, S. G. (2009). Encoding and decoding of learned smooth-pursuit eye movements in the floccular complex of the monkey cerebellum. *J. Neurophysiol.* 102, 2039–2054. doi: 10.1152/jn.00075.2009

Medina, J. F., and Mauk, M. D. (1999). Simulations of cerebellar motor learning: computational analysis of plasticity at the mossy fiber to deep nucleus synapse. *J. Neurosci.* 19, 7140–7151.

Medina, J. F., and Mauk, M. D. (2000). Computer simulation of cerebellar information processing. *Nat. Neurosci.* 3, 1205–1211. doi: 10.1038/81486

Middleton, F. A., and Strick, P. L. (2000). Basal ganglia and cerebellar loops: motor and cognitive circuits. *Brain Res. Brain Res. Rev.* 31, 236–250. doi: 10.1016/S0165-0173(99)00040-5

Molinari, H. H., Schultze, K. E., and Strominger, N. L. (1996). Gracile, cuneate, and spinal trigeminal projections to inferior olive in rat and monkey. *J. Comp. Neurol.* 375, 467–480. doi: 10.1002/(SICI)1096-9861(19961118)375:3<467::AID-CNE9>3.0.CO;2-0

Morishita, W., and Sastry, B. R. (1996). Postsynaptic mechanisms underlying long-term depression of GABAergic transmission in neurons of the deep cerebellar nuclei. *J. Neurophysiol.* 76, 59–68.

Nakano, E., Imamizu, H., Osu, R., Uno, Y., Gomi, H., Yoshioka, T., et al. (1999). Quantitative examinations of internal representations for arm trajectory planning: minimum commanded torque change model. *J. Neurophysiol.* 81, 2140–2155.

Nieus, T., Sola, E., Mapelli, J., Saftenku, E., Rossi, P., and D'Angelo, E. (2006). LTP regulates burst initiation and frequency at mossy fiber–granule cell synapses of rat cerebellum: experimental observations and theoretical predictions. *J. Neurophysiol.* 95, 686. doi: 10.1152/jn.00696.2005

Ohyama, T., Nores, W. L., Medina, J. F., Riusech, F. A., and Mauk, M. D. (2006). Learning-induced plasticity in deep cerebellar nucleus. *J. Neurosci.* 26, 12656–12663. doi: 10.1523/JNEUROSCI.4023-06.2006

Ouardouz, M., and Sastry, B. R. (2000). Mechanisms underlying LTP of inhibitory synaptic transmission in the deep cerebellar nuclei. *J. Neurophysiol.* 84, 1414–1421.

Porrill, J., and Dean, P. (2007). Cerebellar motor learning: when is cortical plasticity not enough. *PLoS Comput. Biol.* 3:e197. doi: 10.1371/journal.pcbi.0030197

Porrill, J., Dean, P., and Stone, J. V. (2004). Recurrent cerebellar architecture solves the motor-error problem. *Proc. R. Soc. Lond. B* 271, 789–796. doi: 10.1098/rspb.2003.2658

Pugh, J. R., and Raman, I. M. (2006). Potentiation of mossy fiber EPSCs in the cerebellar nuclei by NMDA receptor activation followed by postinhibitory rebound current. *Neuron* 51, 113–123. doi: 10.1016/j.neuron.2006.05.021

Racine, R., Wilson, D., Gingell, R., and Sunderland, D. (1986). Long-term potentiation in the interpositus and vestibular nuclei in the rat. *Exp. Brain Res.* 63, 158–162. doi: 10.1007/BF00235658

Roggeri, L., Rivieccio, B., Rossi, P., and D'Angelo, E. (2008). Tactile stimulation evokes long-term synaptic plasticity in the granular layer of cerebellum. *J. Neurosci.* 28, 6354–6359. doi: 10.1523/JNEUROSCI.5709-07.2008

Roitman, A. V., Pasalar, S., and Ebner, T. J. (2009). Single trial coupling of Purkinje cell activity to speed and error signals during circular manual tracking. *Exp. Brain. Res.* 192, 241–251. doi: 10.1007/s00221-008-1580-9

Rossi, P., Sola, E., Taglietti, V., Borchardt, T., Steigerwald, F., Utvik, K., et al. (2002). Cerebellar synaptic excitation and plasticity require proper NMDA receptor positioning and density in granule cells. *J. Neurosci.* 22, 9687–9697.

Rothganger, F. H., and Anastasio, T. J. (2009). Using input minimization to train a cerebellar model to simulate regulation of smooth pursuit. *Biol. Cybern.* 101, 339–359. doi: 10.1007/s00422-009-0340-7

Saint-Cyr, J. (1983). The projection from the motor cortex to the inferior olive in the cat: an experimental study using axonal transport techniques. *Neuroscience* 10, 667–684. doi: 10.1016/0306-4522(83)90209-9

Sawtell, N. B. (2010). Multimodal integration in granule cells as a basis for associative plasticity and sensory prediction in a cerebellum-like circuit. *Neuron* 66, 573–584. doi: 10.1016/j.neuron.2010.04.018

Schweighofer, N., Arbib, M. A., and Dominey, P. F. (1996a). A model of the cerebellum in adaptive control of saccadic gain. I. The model and its biological substrate. *Biol. Cybern.* 75, 19–28. doi: 10.1007/BF00238736

Schweighofer, N., Arbib, M. A., and Dominey, P. F. (1996b). A model of the cerebellum in adaptive control of saccadic gain. II. Simulation results. *Biol. Cybern.* 75, 29–36. doi: 10.1007/BF00238737

Schweighofer, N., Arbib, M. A., and Kawato, M. (1998a). Role of the cerebellum in reaching movements in humans. I. Distributed inverse dynamics control. *Eur. J. Neurosci.* 10, 86–94. doi: 10.1046/j.1460-9568.1998.00006.x

Schweighofer, N., Spoelstra, J., Arbib, M. A., and Kawato, M. (1998b). Role of the cerebellum in reaching movements in humans. II. A neural model of the intermediate cerebellum. *Eur. J. Neurosci.* 10, 95–105. doi: 10.1046/j.1460-9568.1998.00007.x

Schweighofer, N., Doya, K., and Lay, F. (2001). Unsupervised learning of granule cell sparse codes enhances cerebellar adaptive control. *Neuroscience* 103, 35–50. doi: 10.1016/S0306-4522(00)00548-0

Shadmehr, R., and Brashers-Krug, T. (1997). Functional stages in the formation of human long-term motor memory. *J. Neurosci.* 17, 409–419.

Shadmehr, R., and Holcomb, H. H. (1997). Neural correlates of motor memory consolidation. *Science* 277, 821–825. doi: 10.1126/science.277.5327.821

Shadmehr, R., and Krakauer, J. W. (2008). A computational neuroanatomy for motor control. *Exp. Brain Res.* 185, 359–381. doi: 10.1007/s00221-008-1280-5

Shadmehr, R., and Mussa-Ivaldi, S. (2012). *Biological Learning and Control: How the Brain Builds Representations, Predicts Events, and Makes Decisions*. Cambridge, MA: Mit Press.

Siciliano, B., and Khatib, O. (2008). *Springer Handbook of Robotics; Part G. Human-Centered and Life-like Robotics*. New York, NY: Springer-Verlag New York Inc. doi: 10.1007/978-3-540-30301-5

Sola, E., Prestori, F., Rossi, P., Taglietti, V., and D'Angelo, E. (2004). Increased neurotransmitter release during long-term potentiation at mossy fibre-granule cell synapses in rat cerebellum. *J. Physiol.* 557, 843. doi: 10.1113/jphysiol.2003.060285

Solinas, S., Nieus, T., and D'Angelo, E. (2010). A realistic large-scale model of the cerebellum granular layer predicts circuit spatio-temporal filtering properties. *Front. Cell. Neurosci.* 4:12. doi: 10.3389/fncel.2010.00012

Spencer, R. M. C., Ivry, R. B., and Zelaznik, H. N. (2005). Role of the cerebellum in movements: control of timing or movement transitions. *Exp. Brain Res.* 161, 383–396. doi: 10.1007/s00221-004-2088-6

Spitzer, M. (2000). "Hidden layers," in *The Mind Within the Net: Models of Learning, Thinking and Acting*, ed M. Spitzer (Cambridge, MA: The MIT press), 115–136.

Spoelstra, J., Schweighofer, N., and Arbib, M. A. (2000). Cerebellar learning of accurate predictive control for fast-reaching movements. *Biol. Cybern.* 82, 321–333. doi: 10.1007/s004220050586

Swain, R. A., Kerr, A. L., and Thompson, R. F. (2011). The cerebellum: a neural system for the study of reinforcement learning. *Front. Behav. Neurosci.* 5:8. doi: 10.3389/fnbeh.2011.00008

Thach, W. (1996). On the specific role of the cerebellum in motor learning and cognition: clues from PET activation and lesion studies in man. *Behav. Brain Sci.* 19, 411–433. doi: 10.1017/S0140525X00081504

Todorov, E. (2004). Optimality principles in sensorimotor control (review). *Nat. Neurosci.* 7, 907–915. doi: 10.1038/nn1309

Tolu, S., Vanegas, M., Garrido, J. A., Luque, N. R., and Ros, E. (2013). Adaptive and predictive control of a simulated robot arm. *Int. J. Neural Syst.* 23, 1–15. doi: 10.1142/S012906571350010X

Tseng, Y. W., Diedrichsen, J., Krakauer, J. W., Shadmehr, R., and Bastian, A. J. (2007). Sensory prediction errors drive cerebellum-dependent adaptation of reaching. *J. Neurophysiol.* 98, 54–62. doi: 10.1152/jn.00266.2007

Uno, Y., Kawato, M., and Suzuki, R. (1989). Formation and control of optimal trajectory in human multijoint arm movement. Minimum torque-change model. *Biol. Cybern.* 61, 89–101. doi: 10.1007/BF00204593

van der Smagt, P. (2000). Benchmarking cerebellar control. *Rob. Auton. Syst.* 32, 237–251. doi: 10.1016/S0921-8890(00)00090-7

Van Kan, P. L., Houk, J. C., and Gibson, A. R. (1993). Output organization of intermediate cerebellum of the monkey. *J. Neurophysiol.* 69, 57.

Wallman, J., and Fuchs, A. F. (1998). Saccadic gain modification: visual error drives motor adaptation. *J. Neurophysiol.* 80, 2405–2416.

Wang, J., Dam, G., Yildirim, S., Rand, W., Wilensky, U., and Houk, J. C. (2008). Reciprocity between the cerebellum and the cerebral cortex: nonlinear dynamics in microscopic modules fop generating voluntary

motor commands. *Complexity* 14, 29–45. doi: 10.1002/cplx.20241

Weiss, E. J., and Flanders, M. (2011). Somatosensory comparison during haptic tracing. *Cereb. Cortex* 21, 425–434. doi: 10.1093/cercor/bhq110

Wolpert, D. M., and Ghahramani, Z. (2000). Computational principles of movement neuroscience. *Nat. Neurosci.* 3, 1212–1217. doi: 10.1038/81497

Wolpert, D. M., Miall, R. C., and Kawato, M. (1998). Internal models in the cerebellum. *Trends Cogn. Sci.* 2, 338–347. doi: 10.1016/S1364-6613(98)01221-2

Wulff, P., Schonewille, M., Renzi, M., Viltono, L., Sassoè-Pognetto, M., Badura, A., et al. (2009). Synaptic inhibition of Purkinje cells mediates consolidation of vestibulo-cerebellar motor learning. *Nat. Neurosci.* 12, 1042–1049. doi: 10.1038/nn.2348

Xu-Wilson, M., Chen-Harris, H., Zee, D. S., and Shadmehr, R. (2009). Cerebellar contributions to adaptive control of saccades in humans. *J. Neurosci.* 29, 12930–12939. doi: 10.1523/JNEUROSCI.3115-09.2009

Yamazaki, T., and Nagao, S. (2012). A computational mechanism for unified gain and timing control in the cerebellum. *PLoS ONE* 7:e33319. doi: 10.1371/journal.pone.0033319

Yamazaki, T., and Tanaka, S. (2005). Neural modeling of an internal clock. *Neural Comput.* 17, 1032–1058. doi: 10.1162/0899766053491850

Yamazaki, T., and Tanaka, S. (2007). The cerebellum as a liquid state machine. *Neural Netw.* 20, 290–297. doi: 10.1016/j.neunet.2007.04.004

Yamazaki, T., and Tanaka, S. (2009). Computational models of timing mechanisms in the cerebellar granular layer. *Cerebellum* 8, 423–432. doi: 10.1007/s12311-009-0115-7

Zhang, W., and Linden, D. J. (2006). Long-term depression at the mossy fiber–deep cerebellar nucleus synapse. *J. Neurosci.* 26, 6935–6944. doi: 10.1523/JNEUROSCI.0784-06.2006

Conflict of Interest Statement: The authors declare that the research was conducted in the absence of any commercial or financial relationships that could be construed as a potential conflict of interest.

Received: 04 June 2013; accepted: 17 September 2013; published online: 09 October 2013.

Citation: Garrido JA, Luque NR, D'Angelo E and Ros E (2013) Distributed cerebellar plasticity implements adaptable gain control in a manipulation task: a closed-loop robotic simulation. Front. Neural Circuits ***7****:159. doi: 10.3389/fncir.2013.00159*

This article was submitted to the journal Frontiers in Neural Circuits.

APPENDIX A. IDEAL TORQUE VALUES AND FINAL SYNAPTIC WEIGHTS

Table A1 | Theoretical torque values when manipulating different masses.

External masses	Torque (Nm) — Joint 1		Torque (Nm) — Joint 2		Torque (Nm) — Joint 3	
	Minimum	Maximum	Minimum	Maximum	Minimum	Maximum
0.5 kg	−1.40	1.45	1.8	5.85	0.72	3.05
1.5 kg	−3.95	4.07	5.75	17.16	2.51	8.7
2.5 kg	−6.7	6.9	9.55	28.64	4.15	14.56
6 kg	−16	16.5	23.15	68.5	10.15	34.76
10 kg	−26.66	27.46	38.68	114.08	17	57.85

The solution of the present manipulation problem required a continuous sinusoidal torque with different phases and amplitudes per each joint. The table shows the maximum and minimum corrective torques for each combination of joints and masses. Note that joint 1 includes both positive values (clockwise forces) and negative values (anti-clockwise) which should be applied by activating the pairs of agonist and antagonist muscles. Joints 2 and 3 required only the application of positive torques. Thus, most of the torques will be applied by the agonist muscles, requiring the antagonist muscles only for stabilization.

Table A2 | MF-DCN synaptic weights.

External masses	Weight — Joint 1		Weight — Joint 2		Weight — Joint 3	
	Agonist	Antagonist	Agonist	Antagonist	Agonist	Antagonist
0.5 kg	1.7	1.5	6	0	3.6	0
1.5 kg	4.2	4.1	17.4	0	9.3	0
2.5 kg	6.95	6.8	28.9	0	15.1	0
6 kg	16.3	16.9	68.9	0	35	0
10 kg	26.8	26.4	113.8	0	57.4	0

*The weights were obtained after a 10000-trial simulation involving manipulation of different masses with all learning rules enabled. After 10000 trials, the MF-DCN synaptic weights remained stable. Synaptic weights are represented for each muscle in the agonist/antagonist pairs. In joint 1, both clockwise and anti-clockwise corrective torques needed to be applied, so that agonist weights fitted the maximum torque and antagonist weights fitted the minimum torque values (ignoring the direction). In joints 2 and 3, the antagonist muscles were automatically disabled because only positive torques were required to achieve the desired correction (see **Table A1**).*

Table A3 | PC-DCN synaptic weights.

External masses	Weight — Joint 1		Weight — Joint 2		Weight — Joint 3	
	Agonist	Antagonist	Agonist	Antagonist	Agonist	Antagonist
0.5 kg	1.7	1.5	4.5	0	3.6	0
1.5 kg	4.2	4.1	11.9	0*	9.3	0*
2.5 kg	6.95	6.8	19.4	0*	11.71	0*
6 kg	16.3	16.1	45.8	0*	25.2	0*
10 kg	26.8	26.4	74.9	0*	40.1	0*

*The weights were obtained after a 10000-trial simulation involving manipulation of different masses with all learning rules enabled. After 10000 trials, some of the PC-DCN synaptic weights were stabilized. However, the weights marked with (*) slowly decreased and reached their convergence values after the 10000 trials (up to 30000 trials depending on the mass). Synaptic weights are represented for each muscle in the agonist/antagonist pairs. In joint 1, both clockwise and anti-clockwise corrective torques needed to be applied, so that inhibition coming from the PC-DCN connection completely inhibited MF-DCN activity and synaptic weight values became similar to those of the MF-DCN synapse (cf. **Table A2**). In joints 2 and 3, the antagonist muscle inhibition was automatically disabled because no excitation was needed (cf. **Table A2**).*

APPENDIX B. ROBOTIC ARM DESCRIPTION

The inverse dynamic equation defining the lightweight robot (LWR) is given by the expression:

$$\tau = M(Q)\cdot\ddot{Q} + C(Q)\cdot\left[\dot{Q}\dot{Q}\right] - D(Q)\cdot\left[\dot{Q}^2\right] + G(Q) + F(Q,\dot{Q}) \quad \text{(B1)}$$

where τ is the torque value vector to be applied by the robot joints, Q, $\dot{Q}$, and $\ddot{Q}$ are vectors representing the positions, velocities, and accelerations of the joints, $\left[\dot{Q}\dot{Q}\right]$ and $\left[Q^2\right]$ being vectors defined as follows:

$$\left[\dot{Q}\dot{Q}\right] = \left[\dot{Q}_1\cdot\dot{Q}_2,\ldots,\dot{Q}_1\cdot\dot{Q}_n,\dot{Q}_2\cdot\dot{Q}_3,\ldots,\dot{Q}_2\cdot\dot{Q}_n,\ldots,\dot{Q}_{n-1}\cdot\dot{Q}_n\right]^T \quad \text{(B2)}$$

$$\left[\dot{Q}^2\right] = \left[\dot{Q}_1^2,\dot{Q}_2^2,\ldots,\dot{Q}_n^2\right]^T \quad \text{(B3)}$$

where n represents the number of links included in the robotic arm, $M(Q)$ represents the inertia matrix (the mass matrix), $C(Q)$ is the Coriolis matrix, $D(Q)$ represents the matrix of centrifugal coefficients, $G(Q)$ is the gravity action on the joints and finally $F\left(Q,\dot{Q}\right)$ represents the friction term. The friction term is crucial in controlling LWR arms with high-ratio gear boxes since conventional methodologies fail to control these robots without a massive modeling (van der Smagt, 2000). At the same time, the friction term can be differentiated in two terms; dry and viscous friction components obtaining:

$$F(Q,\dot{Q}) = F_D(Q,\dot{Q}) \pm F_V(Q,\dot{Q}) \quad \text{(B4)}$$

where $F_D(Q,\dot{Q})$ and $F_V(Q,\dot{Q})$ are the dry/viscous friction matrices, respectively. The first four terms of Equation B1 mainly include the inherent robot dynamic parameters (inertia matrix, Coriolis/centrifugal matrix, and gravitational force vector). These parameters are up to eleven per joint (inertia matrix is symmetrical):

1. Inertia tensor terms: $(xx_j, xy_j, xz_j, yy_j, yz_j, zz_j)$
2. Center of Mass: (mx_j, my_j, mz_j)
3. Mass: (M_j)
4. Motor Inertia: (I_j)

where j ranges from 1 to the number of joints (3 in our model). These parameters are usually grouped according to these four categories in order to make the computational task easier (Khalil and Dombre, 2004). For our particular LWR (Albu-Schäffer et al., 2007), the nominal values obtained applying parametric methods (Bona and Curatella, 2005) are shown in **Tables B1–B3**.

Table B1 | Inertia tensor parameters ($kg\cdot m^2$).

Joint	xx_j	xy_j	xz_j	yy_j	yz_j	zz_j
1	0.0216417	0	0	0.0214810	0.0022034	0.0049639
2	0.0244442	0	0	0.0052508	0.0036944	0.0239951
3	0.0213026	0	0	0.0210353	0.0022204	0.0046970
4	0.0231668	0	0	0.0048331	0.0034937	0.0227509
5	0.0081391	0	0	0.0075015	0.0021299	0.0030151
6	0.0033636	0	0	0.0029876	0	0.0029705
7	0.0000793	0	0	0.0000783	0	0.0001203

Table B2 | Centers of masses (m), masses (kg) and motor inertias ($kg\cdot m^2$).

Joint	mx_j	my_j	mz_j	m_j	I_j
1	0.0	0.01698	−0.05913	2.7082	415.50e-6
2	0.0	0.11090	0.01410	2.7100	415.50e-6
3	0.0	−0.01628	−0.06621	2.5374	361.60e-6
4	0.0	−0.10538	0.01525	2.5053	138.50e-6
5	0.0	0.01566	−0.12511	1.3028	54.10e-6
6	0.0	0.00283	−0.00228	1.5686	60.08e-6
7	0.0	0.0	0.06031	0.1943	60.08e-6

Table B3 | Friction parameters: dry friction ($N\cdot m$) and viscous friction ($N\cdot m\cdot s/rad$).

Joint	F_{Dj}	F_{Vj}
1	∓0.35	2.0e-3
2	∓0.35	1.69800e-3
3	∓0.35	1.66000e-3
4	∓0.35	2.40000e-3
5	∓0.35	1.80000e-3
6	∓0.35	1.20000e-3
7	∓0.35	1.20000e-3

frontiers in
NEURAL CIRCUITS

REVIEW ARTICLE
published: 10 January 2013
doi: 10.3389/fncir.2012.00116

Seeking a unified framework for cerebellar function and dysfunction: from circuit operations to cognition

Egidio D'Angelo [1,2]* ***and Stefano Casali*** [1]*

[1] Department of Brain and Behavioral Sciences, Pavia, Italy
[2] IRCCS C. Mondino, Brain Connectivity Center, Pavia, Italy

Edited by:
Chris I. De Zeeuw, Erasmus Medical Center, Netherlands

Reviewed by:
Yosef Yarom, Hebrew University, Israel
Christian Hansel, Erasmus Medical Center, Netherlands

***Correspondence:**
Egidio D'Angelo and Stefano Casali, Department of Brain and Behavioral Sciences, Via Forlanini 6, I-27100 Pavia, Italy.
e-mail: dangelo@unipv.it; stefano.casali@unipv.it

Following the fundamental recognition of its involvement in sensory-motor coordination and learning, the cerebellum is now also believed to take part in the processing of cognition and emotion. This hypothesis is recurrent in numerous papers reporting anatomical and functional observations, and it requires an explanation. We argue that a similar circuit structure in all cerebellar areas may carry out various operations using a common computational scheme. On the basis of a broad review of anatomical data, it is conceivable that the different roles of the cerebellum lie in the specific connectivity of the cerebellar modules, with motor, cognitive, and emotional functions (at least partially) segregated into different cerebro-cerebellar loops. We here develop a conceptual and operational framework based on multiple interconnected levels (a *meta-levels hypothesis*): from cellular/molecular to network mechanisms leading to generation of computational primitives, thence to high-level cognitive/emotional processing, and finally to the sphere of mental function and dysfunction. The main concept explored is that of intimate interplay between timing and learning (reminiscent of the "timing and learning machine" capabilities long attributed to the cerebellum), which reverberates from cellular to circuit mechanisms. Subsequently, integration within large-scale brain loops could generate the disparate cognitive/emotional and mental functions in which the cerebellum has been implicated. We propose, therefore, that the cerebellum operates as a general-purpose co-processor, whose effects depend on the specific brain centers to which individual modules are connected. Abnormal functioning in these loops could eventually contribute to the pathogenesis of major brain pathologies including not just ataxia but also dyslexia, autism, schizophrenia, and depression.

Keywords: cerebellum, cognition, motor control, timing, prediction, autism, schizophrenia, dyslexia

INTRODUCTION

The cerebellum is classically thought to control movement coordination (Flourens, 1824; Luciani, 1891) and motor learning (Marr, 1969; Albus, 1972) but recent experimental evidence suggests that it may also play a key role in cognition and emotion (Schmahmann, 2004; Schmahmann and Caplan, 2006; Ito, 2008) [1]. This clearly raises broader questions: how can the same circuit cope with so many different tasks? Is signal processing in the cerebellar circuits always based on the same computational scheme? Is it conceivable that what underlies the different roles of the cerebellum is the specific connectivity of cerebellar modules, rather than specific microcircuit properties? In order to answer these questions, here we propose a conceptual and operational framework, or *meta-levels hypothesis*, based on four levels: (1) cellular/molecular, (2) network, primitives of circuit processing, (3) high-level cognitive/emotional processing, and (4) mental processing. We first review neuroanatomical, neuropsychological, neuropsychiatric, and neuroimaging studies in order to elucidate how the cerebellum might take part in cognitive and emotional functions, and how cerebellar damage could determine neurological and neuropsychiatric disorders. We then argue that the cerebellum carries out basic computational functions, timing, and learning, applicable in different cases. The cerebellum has been reported to assist brain operations by providing accurate timing of multiple series of signals coming from the cerebral cortex and the sensory systems [reviewed in Bower (1997, 2002); Jacobson et al. (2008); D'Angelo and De Zeeuw (2009); D'Angelo et al. (2009, 2010); D'Angelo (2010a,b, 2011); De Zeeuw et al. (2011)]. This could underlie the implementation of processes like sensory prediction, novelty detection, error detection, time matching, and sequence ordering (Ivry and Baldo, 1992; Ivry et al., 2002; Ghajar and Ivry, 2009). This multi-dimensional computation would allow the same circuit to contribute to functions

[1] We need to clarify the terminology used. We here treat brain functions on a "neurological" level, where cognition and emotion are kept distinct. This differs from the definition used in neuroinformatics, in which "cognitive processing" refers to computational primitives—like pattern recognition, generalization, and abstraction by artificial neural networks. These definitions, furthermore, should not be confused with the tenet of classic cognitive psychology, which maintained that emotion is a category of cognition (Spitzer, 1998).

as diverse as voluntary movement (a cognitive process, after all) and thought, provided that appropriate connections with different cortical and subcortical centers were established and that communication between these centers occurred over the appropriate frequency bands and using compatible codes (Ito, 1993, 2008; D'Angelo, 2011). We propose, therefore, that the cerebellum operates as a general co-processor, whose effect depends on the centers to which different modules are connected, affecting cognitive functions as well as sensory-motor processing.

BRAIN PROCESSING AND THE CEREBELLUM

The cerebellum has long been linked to the concept of motor control but now several observations indicate that it is also involved in cognitive/emotional processing. This extension of its role raises a key question: is there formal similarity between these two types of processing? A critical observation, in this regard, is that cognitive and sensory-motor processing should not, in principle, be very different. This prevents from a serious computational paradox: if the two processes were different, they may use different coding strategies. But then, how could the basic neuronal circuit of the cerebellum, which appears to be invariant across different areas, be able to process different signal codes? This would violate the idea that the cerebellum develops a single general algorithm. Indeed, different sections of the cerebral cortex (sensory, motor, and associative in nature) communicate with each other as well as with various cerebellar areas and so the neural codes are likely to be homogeneous. As a corollary of this, it is well-documented that motor planning means predicting the sensory consequences of a motor act: a motor plan is coded in terms of an anticipated sensory state (Blakemore et al., 1998a,b). This is akin to the general hypothesis of the "*prediction imperative*" that needs to be satisfied in order to allow brain processing (Llinás and Roy, 2009). Prediction processes are normally performed by "forward controllers," which use internal memory to represent the system state (Diedrichsen et al., 2010; Shadmehr and Mussa-Ivaldi, 2012).

IS THE CEREBELLUM A GENERALIZED FORWARD CONTROLLER?

On the basis of studies of the vestibulo-ocular reflex (VOR), eye-blink conditioning, and saccadic eye movements, and the fundamental theoretical concepts of motor learning (Marr, 1969), the cerebellum has been suggested to provide forward models of the motor system. These forward models can predict the posture or motion of body parts following a motor command and, by a further transformation, predict the sensory consequences of actions (Miall and Reckess, 2002). More precisely, a copy of motor commands generated by the motor cortex (*efference copy*) is sent to the cerebellum, which uses its internal forward model to predict their sensory consequences (*corollary discharge*). The sensory predictions are then compared to actual sensory feedback (Wolpert et al., 1998): in the presence of errors (or novelty, i.e., deviations from prediction), the cerebellum emits corrective signals. A fully characterized example of generation of predictions by cerebellar circuits is provided by electro-perception in weakly electric fishes, in which a cerebellar-like structure compares the expected electric field generated by the fish with the actual electric field sensed by the electroreceptors, thus gaining information on the structure of the environment through the changes that this latter has caused in the field itself (Bell et al., 2008).

In the presence of persistent deviations from prediction the cerebellum learns to modify the forward model itself. Learning appears to occur through two distinct processes, one faster and more labile, involving the cerebellar forward controller, the other, which may at least partly reside outside the cerebellum, slower and consolidated (Shadmehr and Mussa-Ivaldi, 2012). In fact, the cerebellar cortex is thought to process the faster component of memory, while the deep cerebellar nuclei may elaborate its slower component (Medina and Mauk, 2000). The cerebellum is thought to share its "predictor function" with the parietal lobes, in such a way that these two structures might work in parallel (Blakemore and Sirigu, 2003): the cerebellum as a whole is likely to generate faster but unconscious predictions, while the parietal lobes probably generate slower but conscious ones.

Given the anatomical connections of the cerebellum with associative areas (see below) and the similarity of motor planning and cognitive processing, it seems logical to generalize the forward controller role of the cerebellum to cognition. Indeed, Ito (2005) hypothesized that the cerebellum could operate as a generalized forward controller regulating cognition as well as sensory-motor control[2].

THE FORWARD CONTROLLER AND MENTAL ACTIVITY

The fundamental postulate about brain/mind functioning is that the brain generates a virtual reality (Churchland and Sejinowski, 1992; Churchland, 1998; Llinas and Paré, 1998), probably conferring an evolutionary advantage by predicting possible environmental configurations and allowing symbolic representation and communication. Several observations show that perception is not a copy of the external or internal energy patterns, but rather a mental elaboration endowed with quality and deformed by imperfect receptor sampling, adaptation, memories, and emotions. This makes conscious perception unique and subjective. At this point, one may speculate on how the cerebellum, being deeply interconnected with the cerebral cortex, might be involved in processing conscious percepts. We propose a somewhat provocative reflection.

A first issue is that whereas reality is perceived as *instantaneous*, computation in neurons and synapses actually takes time and the cerebral cortex needs hundreds of milliseconds to generate a conscious percept. This delay, in addition to violating the

[2]A conceptual obstacle is that sensory-motor processing is thought to be mostly automatic (and unconscious) while cognition and emotion are bound to consciousness. Akin with this, the thalamo-cortical circuit is usually thought of as the site of conscious processing and the cerebro-cerebellar circuit as the site of automatic control. Indeed, the cerebellum probably does not take part in conscious representations directly, given that abnormalities of the cerebellum do not seem to impair consciousness. In their hypothesis, Tononi and Edelman suggest that the ability of circuits to generate consciousness lies in the strength of their internal connectivity, which is quite high in the cortex but comparatively much poorer in the cerebellum (Tononi and Edelman, 1998). This would explain why the cortex is capable of developing conscious percepts, while the cerebellum is not. However, the cerebellum is deeply interconnected in closed loops with the cerebral cortex over multiple independent lines involving associative as well as sensory-motor areas (see below), so that the activity of the two structures is strongly integrated.

idea of the instantaneity of subjective perception, is far too long to allow movement and thought to be controlled in a purposeful, dynamic, and interactive manner. Therefore, the virtual reality generated by the brain has to be "anticipatory" and to occur somehow in advance of the elaboration of objective reality based on cortical processing of sensory signals. This anticipatory process may be based on the use of previous information and memory on various time scales, as would occur in a *forward controller*, which is exactly what the cerebellum is thought to be. A second issue is that reality is perceived as *continuous,* even though computational cycles during cerebro-cortical cognitive processing actually last about 25 ms (a γ-band cycle) and longer cycles about 100 ms (a θ-band cycle) (Buzsaki, 2006). The cerebellum, by exerting millisecond control of its output spikes, may help to maintain the *fast continuity* required for spatiotemporal integration of conscious percepts.

Thus, the fact that the cerebellum does not, clinically, appear to be needed to generate consciousness (Tononi and Edelman, 1998) does not mean that it is extraneous to the mechanisms controlling the relationship between objective reality and internal representation. Indeed, functional activation of the cerebellum has been revealed in relation to the conscious representation of time in tasks using internal memories (Addis et al., 2009; Nyberg et al., 2010; Szpunar, 2010, 2011). It should be noted at this point that one main theory on the working of the cerebellum is that it acts as a "comparator of intentionality with execution," which is precisely what the whole brain continuously does in order to relate neuronal activity to the world. On this basis, we conclude that it can hardly be considered surprising that the cerebellum takes part in cognition and emotion, that it can influence attention and intelligence (Cotterill, 2001), and that its dysfunction can affect "internal coherence" in dissociative diseases.

THE EXTENDED CEREBRO-CEREBELLAR LOOPS

The cerebellar cortex has, from the earliest studies, always been reported to have a similar structure in all its sections, and its circuit to show a regular "lattice"-like organization (Eccles et al., 1967) (**Figure 1**). The cerebellar circuit can be schematically described as follows: mossy fibers activate granule and Golgi cells in the granular layer. Granule cells emit parallel fibers and activate all the other neurons in the cerebellar cortex. Golgi cells are doubly activated by mossy and parallel fibers providing feedforward and feedback inhibition to granule cells. The granular layer also contains other interneurons, namely, Lugaro cells and unipolar brush cells (only in the flocculo-nodular lobe). In the molecular layer, parallel fibers activate Purkinje cells and also stellate and basket cells, which in turn inhibit Purkinje cells. Purkinje cells are also activated by climbing fibers generated by the inferior olive. Purkinje cells in turn project to the deep-cerebellar nuclei. In this context, the *modules* and the *cerebello-thalamo-cerebro-cortical* circuits (CTCCs) can be considered the main structural elements.

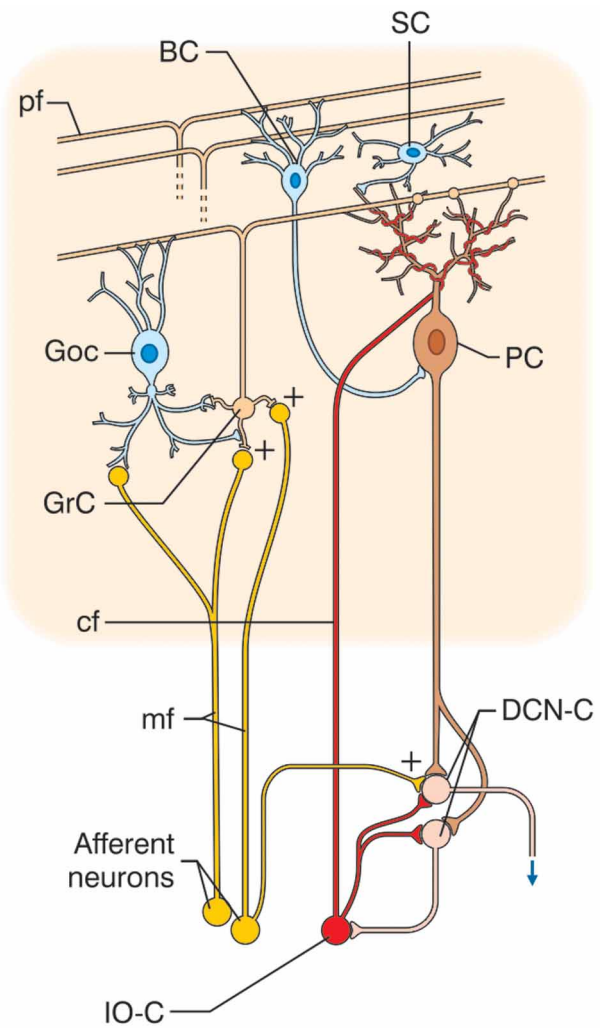

FIGURE 1 | Schematic representation of the cerebellar circuit. The cerebellar circuit consists of cortical and subcortical sections. At subcortical level, the *afferent fibers* activate DCN cells (DCN-C) and IO cells (IO-C). The DCN emits the output and at the same time inhibits the IO. In the cerebellar cortex, there are different types of neurons including granule cells (GrC), Golgi cells (GoC), Purkinje cells (PC), stellate and basket cells (SC, BC), Lugaro cells, and unipolar brush cells (not shown). The two main inputs are represented by mossy fibers (mf) originating in various brain stem and spinal cord nuclei, and by climbing fibers (cf) originating from the IO. Signals conveyed through the mossy fibers diverge to DCN and activate the granular layer (containing GrC and GoC). The ascending axon of the GrC bifurcates in the molecular layer (containing PC, SC, and BC) forming the parallel fibers (pf). The cerebellar cortical circuit is organized as a feedforward excitatory chain assisted by inhibitory loops: mfs excite GrCs, which activate all the other cortical elements. In the granular layer, inhibition is provided by GoC, in the molecular layer by SC and BC. Finally, PC inhibit DCN. The IO, which is also activated by brain stem and spinal cord nuclei, controls PC activity though a single powerful synapse. Thus, the whole system can be seen as a complex mechanism controlling the DCN output.

THE CEREBELLAR MODULAR ORGANIZATION

Macroscopically, the cerebellum consists of a tightly folded layer of cortex with white matter beneath in which deep nuclei are embedded. At microscopic level, each part of the cortex consists of the same small set of neuronal elements, laid out according to a highly stereotyped geometry. At an intermediate level, the cerebellum and its auxiliary structures can be broken down into several hundred or thousand *microzones* or *microcompartments*,

which are thought to represent effective cerebellar functional units (**Figure 2**). These can be further differentiated into *stripes*, *zones,* and *multizonal microcomplexes*, which are effective functional *modules* (Andersson and Oscarsson, 1978; Apps and Garwicz, 2005; Apps and Hawkes, 2009)[3].

A module is a conglomerate of several, non-adjacent parasagittal bands of Purkinje cells projecting to specific areas of deep cerebellar nuclei and gating segregated projections from the inferior olive (Cerminara, 2010; Oberdick and Sillitoe, 2011; Ruigrok, 2010). Likewise, the mossy fibers projecting to a certain group of Purkinje cells through the granular layer also project to the same deep cerebellar nucleus neuron receiving input from those Purkinje cells (Ito, 1984; Pijpers et al., 2006; Voogd, 2010). The modules have almost segregated inputs, since climbing fibers bifurcate on the parasagittal plane to as many as 10 not necessarily adjacent Purkinje cells (mossy fiber bifurcations spread across both planes). Thus, the majority of connections between neurons and interneurons in the cerebellar cortex occur within individual modules. The connections between modules occur almost exclusively via parallel fibers, which contact Purkinje cells and the other inhibitory interneurons (Lainé and Axelrad, 1998; Dieudonné and Dumoulin, 2000; Dean et al., 2004).

The modules have a very similar if not identical structure and do not show major differences in their neuronal properties, even though some variants have been reported. One of these concerns the vestibulocerebellum, which contains an additional cell type, the unipolar brush cell (Mugnaini et al., 2011), and may exhibit more sustained discharges to Purkinje cells (Kim et al., 2011). Another peculiar aspect is glycine feedback from the lateral cerebellar nuclei, which is sent only to the hemispheres and not to the vermis (Uusisaari and Knopfel, 2012). Finally, evident organization of genetic markers along the sagittal plane leads to a further "biochemical" compartmentalization[3]. These local properties do not undermine the general concept of a unified cerebellar computational algorithm, but they may bias certain modules toward specific functional states, as is thought to occur in other brain circuits in relation to neuromodulators and neuropeptides (e.g., LeBeau et al., 2005).

The cerebellar circuit appears to be organized in a feedforward manner, with information passing through the cortex without recurrent loops and with limited intermodular connectivity. This is in apparent contrast with the cerebral cortex, which shows zonal differences in thickness, in the proportion of granular and pyramidal neurons, in intracortical connectivity, in neuronal subtypes and spine distribution (Elston and DeFelipe, 2002; Douglas and Martin, 2004; Lubke and Feldmeyer, 2007). Moreover, while there is poor intermodular connectivity in the cerebellum, the cerebral cortex shows strong intercolumnar connectivity [the relevance of which has been commented above (Tononi and Edelman, 1998)]. Clearly, the different anatomo-functional organization of the two cortices implies different computational strategies. However, since the two cortices are deeply interconnected through serial parallel loops, the product of cerebro-cortical elaborations is continuously relayed to specific modules of the cerebellar cortex. Thus, in addition to the need to understand how cerebral and cerebellar cortical modules operate, it is essential to look in more detail at this interconnection of the two structures.

CEREBELLO-THALAMO-CEREBRO-CORTICAL CIRCUITS (CTCCs)

There is growing evidence that the *CTCCs* include several afferent and efferent cerebral cortical areas of a motor, sensory, or associative nature **(Figure 3)** (Strick et al., 2009). Most cerebro-cerebellar *afferent* projections pass through the basal (anterior or ventral) pontine nuclei and intermediate cerebellar peduncle, while most cerebello-cerebral *efferent* projections pass through dentate and ventrolateral (VL) thalamic nuclei. Some of these loops are here considered in more detail in relation to sensory-motor and cognitive-emotional functions: the *motor and somatosensory loops* (including those involved in oculomotor control), the *parietal loops*, the *prefrontal loops*, the *oculomotor loops*, and the loops formed with the basal ganglia and the limbic system. Cerebello-cerebral loops are highly segregated (Habas et al., 2009; Krienen and Buckner, 2009) and form complex interconnections also with the basal ganglia and subcortical areas. Interestingly, during phylogenesis, the cerebellar hemispheres evolve in parallel with the associative rather than the motor or sensory areas, which supports the progressive involvement of the cerebellum in cognitive processing.

Motor and somatosensory loops

The cerebellum projects both to motor and somatosensory areas. The output to the primary motor area (M1) is conveyed through the VL thalamic nuclei projecting to layers IV and V, while outputs to the primary somatosensory area (S1) pass through the intralaminar nuclei projecting to intragranular and superficial layers (Molinari et al., 2002). Through these projections to MI, the cerebellum can modulate motor cortex excitability in relation to the incoming sensory input (Luft et al., 2005). The cerebellum is also interconnected with premotor (Dum and Strick, 2003) and supplementary motor areas (Rouiller et al., 1994) involved in movement planning. Interestingly, transcranial magnetic stimulation (TMS) of the lateral cerebellum can strongly affect the contralateral cerebral motor cortex (Oliveri et al., 2005). Cerebellar TMS regulates the functional connectivity between Purkinje cells and deep cerebellar nuclei, modifying the excitability of interconnected motor areas, as shown by changes in motor-evoked potential amplitude and in short and long intracortical inhibition (Koch et al., 2009a).

[3]The cerebellum is made up of large compartments generally known as zones, which can be broken down into smaller compartments known as microzones. The demonstration, by microneurography, of cortical zones shows that each body part maps to specific points in the cerebellum, even though there are numerous repetitions of the basic map forming an arrangement that has been called "fractured somatotopy." A different indication of compartmentalization is obtained by immune staining for certain types of protein (e.g., zebrin, NOS etc.). This reveals stripes oriented perpendicular to the cerebellar folds. Different markers generate different sets of stripes, and the widths and lengths vary as a function of location, but they all have the same general shape. Oscarsson in the 1970s proposed that these cortical zones can be partitioned into smaller units called microzones. In 2005, Apps and Garwicz showed that several microzones can be organized into a multizonal microcomplex. All microzones in the microcomplex are connected to the same group of deep cerebellar nuclei and inferior olivary neurons and correspond to the cerebellar modules defined by Voogd.

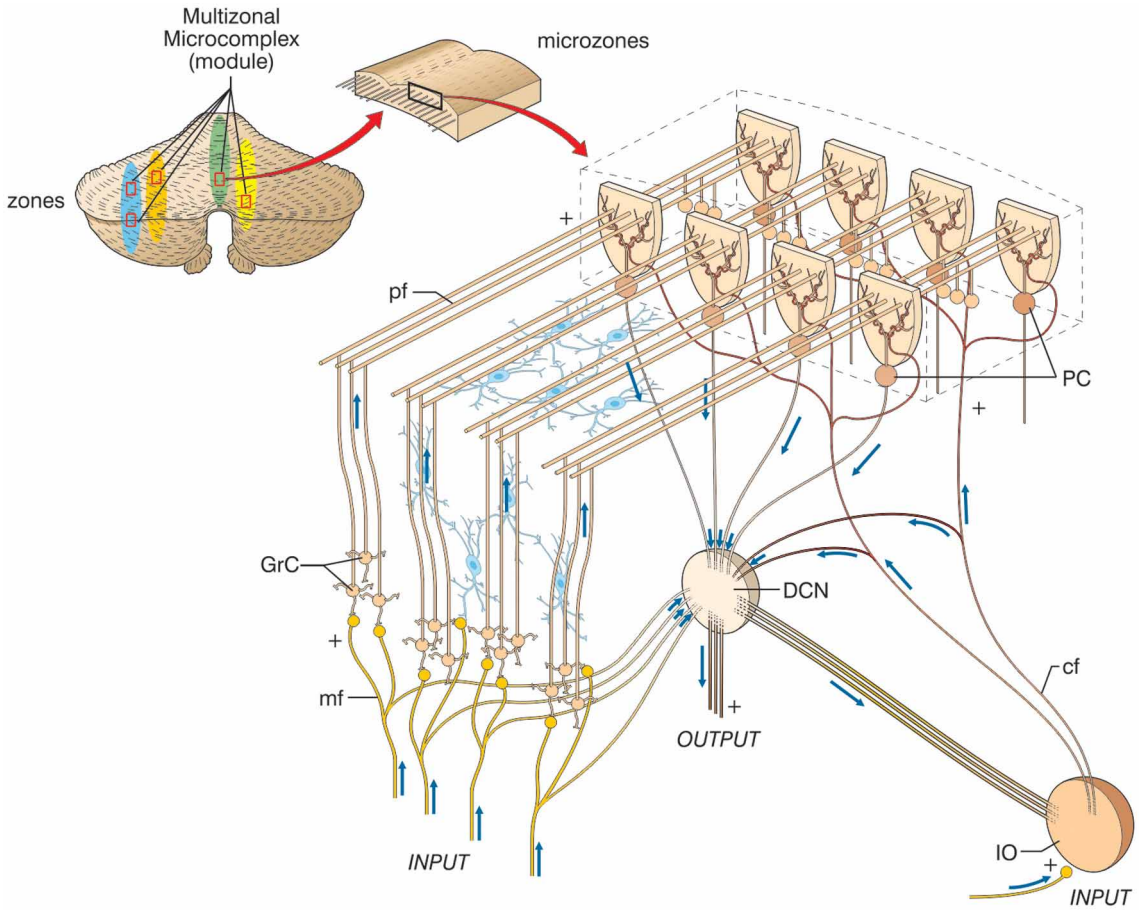

FIGURE 2 | The modular organization of the cerebellum. The picture shows a flattened view of the cerebellum. Four ideal *zones* are shown in color, each one containing *microzones* forming a *multizonal microcomplex*. The microzones have the basic structure reported in the expansion on the right (same symbols as in **Figure 1**, inhibitory interneurons are overlaid in blue). A microzone is defined as a group of the order of 1000 Purkinje cells all having the same somatotopic receptive field. These Purkinje cells are arranged in a long, narrow strip, oriented perpendicular to the cortical folds, so that Purkinje cell dendrites are flattened in the same direction as the microzones extend and are crossed by parallel fibers at right angles. The climbing fibers branches (about 10) usually innervate Purkinje cells belonging to the same microzone and the olivary neurons generating such climbing fibers tend to be coupled by gap junctions. This helps synchronizing Purkinje cells within a microzone on a millisecond time scale. The Purkinje cells belonging to a microzone all send their axons to the same small cluster of output cells within the deep cerebellar nuclei. Finally, the axons of basket cells are much longer in the longitudinal direction than in the mediolateral direction (not shown), causing them to be confined largely to a single microzone. Thus, cellular interactions within a microzone are much stronger than those between different microzones.

Parietal loops

The cerebellum is closely connected with the parietal lobes. The cerebellum sends input to area 7b of the inferior parietal lobe, in particular to the anterior intraparietal (AIP) area, through VL thalamic nuclei (Clower et al., 2001). AIP neurons are activated in response to the sight of an object, as well as to the act of grasping it, in reach-to-grasp arm movements (Tunik et al., 2005), and in the creation of crossmodal sensorial representations of objects (Grefkes et al., 2002). The cerebellar input to the AIP passes through a specific "output channel" of the dentate nucleus. The cerebellar-VL thalamic inputs to motor and premotor areas send secondary afferents to the AIP (Clower et al., 2005). The cerebellum also targets other parietal regions, namely the ventral lateral intraparietal area (vLIP) and medial intraparietal area (MIP) (Prevosto et al., 2010). Importantly, vLIP neurons can represent salient visual stimuli and are important for visual attentional control (Kusunoki et al., 2000), while the MIP is crucial for visual-motor coordinate transformation (Grefkes et al., 2004). In humans, the AIP is also connected to the ventral premotor cortex, while theMIP shows relatively strong projections to parahippocampal regions (Rushworth et al., 2006) forming complex loops involving multiple cortical areas, the thalamus, the cerebellum, and the basal ganglia.

Prefrontal loops

The cerebellum is reciprocally connected, through the thalamus (Middleton and Strick, 2001), with the medial prefrontal cortex (MPFC) (Watson et al., 2009), the dorsolateral prefrontal cortex (DLPFC) (Kelly and Strick, 2003), and the anterior prefrontal cortex (APFC) (Krienen and Buckner, 2009). The

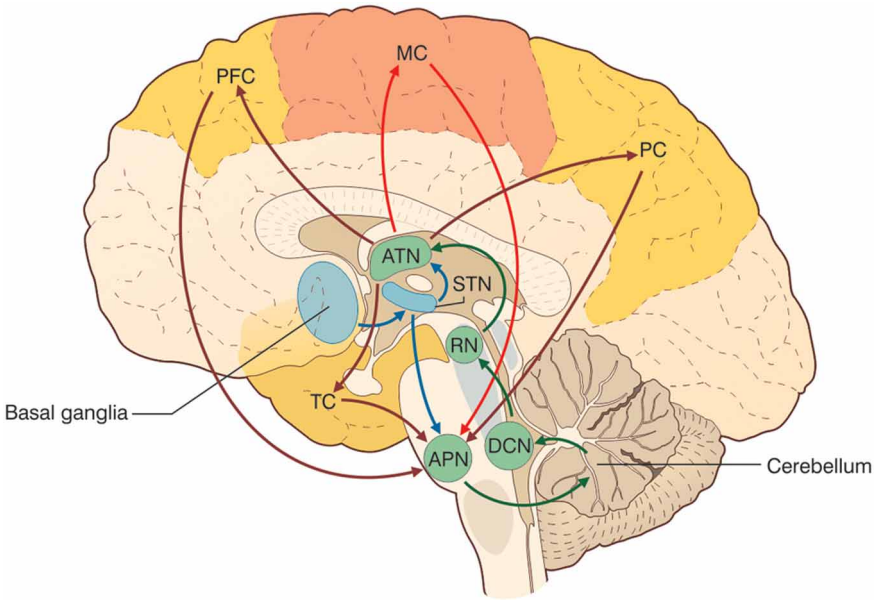

FIGURE 3 | The cerebello-thalamo-cerebro-cortical circuits (CTCCs). The figure represents schematically the bidirectional connectivity between the cerebellum and the telencephalon, in particular with the cereberal cortex. Telencephalic projections from the cortex and basal ganglia (through the subthalamic nucleus, STN) and limbic areas are relayed to the cerebellum through the anterior pontine nuclei (APN). The cerebellum in turn sends its output through the deep cerebellar nuclei (DCN), red nucleus (RN), and anterior thalamic nucleus (ATN) to various telencephalic areas including the motor cortex (MC), the prefrontal cortex (PFC), the parietal cortex (PC), and the temporal cortex (TC). These connections, which are supported by anatomical and functional data, forming several bidirectional cerebello-thalamo-cerebro-cortical circuits (CTCCs).

MPFC is important in saccadic movements and cognitive control (Ridderinkhof et al., 2004) and is strongly involved in determining behavior on the basis of expectations (Amodio and Frith, 2006). Moreover, this cortical area plays a key role in fear extinction processes (Morgan et al., 1993; Milad and Quirk, 2002). The DLPFC is particularly important in working memory control (Petrides, 2000), mental preparation of imminent actions (Pochon et al., 2001), and procedural learning (Pascual-Leone et al., 1996) and its functional alteration is involved in major psychoses (Weinberger et al., 1986, 1988; Dolan et al., 1993). The APFC is less understood (Ramnani and Owen, 2004) but its main function could be that of integrating multiple distinct cognitive processes during goal-directed complex behaviors.

Temporal loops

The exact nature of the connections between temporal areas—including the hippocampus and amygdala—and the cerebellum is still unclear. However, some studies have shown that the temporal cortex makes a "negligible" contribution to the corticopontine fiber tract (both in humans and in macaque monkeys) (Ramnani et al., 2006). This probably means that the cerebellum is unlikely to receive strong *direct* afferents from temporal areas. On the other hand, cerebellar fastigial nuclei seem to project to several temporal areas, like the hippocampus and amygdala (at least in monkeys and cats) (Heath and Harper, 1974). Accordingly, a recent human fMRI resting-state study found significant functional connectivity between the bilateral anterior inferior cerebellum and bilateral hippocampus and temporal lobes (He and Zang, 2004). Furthermore, dynamic causal modeling proved that, during a rhyming judgment task, the cerebellum and the lateral anterior temporal lobe are strongly and bidirectionally interconnected (Booth et al., 2007). More extensive studies are clearly required in order to elucidate the pattern of connectivity between the cerebellum and temporal areas; however, it seems reasonable to speculate that there exists some kind of functional interplay between these two structures.

Oculomotor loops

The cerebellum is also deeply involved in oculomotor regulation, which involves several cortical and subcortical areas participating in automatic and cognitive control processes. Besides the VOR, to which the cerebellar flocculo-nodular lobe is specifically devoted, the cerebellum is involved in the control of saccadic and smooth pursuit eye movements (Alahyane et al., 2008; Colnaghi et al., 2010; Panouillères et al., 2011). Both the lateral and posterior cerebellum, mainly the vermis, are involved in the control of ocular saccades (Robinson et al., 1993; Hashimoto and Ohtsuka, 1995; Goffart et al., 2003). The lateral cerebellum and the vermisare also involved in controlling the precision and velocity of smooth pursuit movements (Takagi et al., 1999). Saccades and pursuit, used in order to execute different cognitive-perceptual tasks (basically, saccades are required when searching for a static target, while pursuit is needed to track moving targets), are thought to be different outcomes of a single sensory-motor process aimed at orienting the visual axis (Xivry and Lefèvre, 2007). The cerebellum and the fastigial oculomotor region have been shown to play a major role both in controlling the execution of saccades and in elaborating the visuospatial information

concerning the target (Tilikete et al., 2006; Guerrasio et al., 2009). The oculomotor system comprises different areas. The retina projects to the superior colliculus (Lefèvre et al., 1998), which, in turn, sends afferents to the cerebellum and the lateral intraparietal area (LIP). The LIP is connected with the frontal eye field (FEF) and the basal ganglia and superior colliculus gate input from the FEF to the LIP (Straube and Buttner, 2007). A recent Diffusion Tensor Imaging (DTI) study (Doron et al., 2010) showed the cerebellum to be strongly connected with the precentral gyrus and the superior frontal gyrus, which take part in motor and oculomotor processes as well as the processing of spatial working memory (Boisgueheneuc et al., 2006). The cerebellum has thus been shown to be deeply integrated in processes controlling both the motor and cognitive components of eye movements.

Loops formed with the basal ganglia and limbic system

The cerebellum has recently been shown to form bidirectional connections with the basal ganglia. The cerebellum-basal ganglia pathway starts from the dentate nucleus, goes through the thalamus and reaches the striatum; the basal ganglia-cerebellum pathway starts from the subthalamic nucleus and ends in the cerebellar cortex, passing through the pontine nuclei (Bostan and Strick, 2010; Bartolo et al., 2011). The cerebellum is also thought to be connected with the limbic system, although few anatomical studies are available. Low-frequency stimulation of the cerebellar fastigial nucleus has an anti-epileptogenic effect when seizures are induced by amygdaloid kindling (Wang et al., 2008) and there exists evidence suggesting that the cerebellum may be connected with the amygdala, hippocampus, and septal nuclei (Snider and Maiti, 1976). The cerebellum is also connected with the hypothalamus (Haines et al., 1990) and, as indicated above, with limbic cortices like the DLPFC.

FUNCTIONAL ACTIVATION OF CEREBRO-CEREBELLAR LOOPS

One of the greatest recent achievements of neurophysiology has been to open a window on the mechanisms governing cognitive and emotional functions. Techniques like fMRI and Magnetoencefalography (MEG) have proved fundamental in this respect, since they provide information on the localization and correlation of active areas during controlled behavioral tasks. Moreover, the use of TMS has made it possible to intervene selectively on the CTCCs (by directly exciting or inhibiting or by modifying synaptic plasticity). In this way, neuroanatomy can be turned into functional connectivity, linking circuit organization with system functions and behavior, so that mental activity and major mental disorders can be explored on a physiological basis. In parallel with these developments, understanding of cerebellar functions is also improving greatly.

The close relationship between the cerebellum and cerebral cortex was first revealed by crossed cerebellar diaschisis, a reduction in metabolism and blood flow in the cerebellar hemisphere contralateral to a cerebral lesion (Beldarrain et al., 1997). Detailed investigations have since provided structural and functional evidence (see also below) of multiple cerebro-cerebellar loops processing, in concert, sensory-motor and emotional/cognitive tasks. In fMRI studies, cognitive and motor functions in human CTCCs appear segregated (Salmi et al., 2010). A non-verbal auditory working memory task was found to be associated with enhanced brain activity in the parietal, dorsal premotor, and lateral prefrontal cortices and in lobules VII–VIII of the posterior cerebellum. A sensory-motor control task activated the motor/somatosensory, medial prefrontal, and posterior cingulate cortices, and lobules V/VI of the anterior cerebellum. A purely cognitive task activated fronto-parietal cerebro-cortical areas and crus I/II in the lateral cerebellum. The tracts between the cerebral and the cerebellar areas exhibiting cognitive and sensory-motor activity are mainly projected via segregated pontine (input) and thalamic (output) nuclei. For example, crus I/II in the lateral cerebellum is linked with the DLPFC and is activated during cognitive tasks, whereas the anterior cerebellar lobe is not.

Functional imaging studies have helped to confirm the relationship between the specific activation of the latero-posterior lobe and cognitive processes during cerebellar damage, often associated with a frontal-like syndrome (see below) with memory deficits and aphasia, thought dysmetria, and incoordination between mental processing and motor execution (Arriada-Mendicoa et al., 1999). Moreover, malformations of or damage to the cerebellar vermis are commonly linked to affective alterations (Schmahmann and Sherman, 1998; Tavano and Borgatti, 2010). These observations support the view that cognitive/emotional and motor functions are at least partially segregated in the cerebellum, with cognitive functions localized in the lateral-posterior cerebellum.

FROM MOTOR CONTROL TO COGNITION AND EMOTION

Neurology classically considers the cerebellum in relation to *ataxia*, i.e., the motor consequences of cerebellar damage. Ataxia (from the Greekα–ταξισ, meaning "lack of order") is a neuropathological state consisting of gross lack of coordination of muscle movements. It is caused by dysfunction of those parts of the nervous system that coordinate movement and it includes forms of cerebellar, sensory, and vestibular origin. Cerebellar ataxia is expressed through a variety of elementary neurological deficits, such as antagonist hypotonia, asynergy, dysmetria, dyschronometria, and dysdiadochokinesia. How and where these abnormalities manifest themselves depends on which cerebellar structures have been damaged and whether the lesion is bilateral or unilateral. In very general terms, we can observe three main groups of symptoms[4]:

- impairment of body balance (Romberg test) and of eye movement control (saccade alterations, nystagmus) due to specific dysfunction of the vestibulocerebellum;

[4]According to a comparative anatomical, functional, and phylogenetic subdivision of the cerebellum, the vestibulocerebellum (archicerebellum) can be identified with the flocculo-nodular lobe, the spinocerebellum (paleocerebellum) with the rest of the vermis and para-vermal areas, and the cerebro-cerebellum (neocerebellum) with the cerebellar hemispheres. Hence, evolutionarily, there is a progressive increase in cerebro-cerebellar connections, which reach their maximum development in primates and humans, in parallel with the increased extension of the associative cortices.

- impairment of gait (wide-based, "drunken sailor" gait, characterized by uncertain starting and stopping, lateral deviations, and uneven steps) due to dysfunction of the spinocerebellum;
- difficulty executing voluntary, planned movements due to impairment of the cerebro-cerebellum. Disturbances include intention tremor (coarse trembling, accentuated on the execution of voluntary movements, possibly involving the head and eyes as well as the limbs and torso), peculiar writing abnormalities (large, uneven letters, irregular underlining), and a peculiar pattern of dysarthria (slurred speech, sometimes characterized by explosive variations in voice intensity despite a regular rhythm).

Quite apart from their undisputed clinical importance, these observations lend support to the idea that different motor functions are localized in specific cerebro-cerebellar loops and that the lateral cerebellum is involved, through cerebro-cerebellar loops, in the cognitive components of movement planning. In addition, on careful analysis, patients with focal cerebellar lesions have also been found to show cognitive-affective alterations (Schmahmann and Sherman, 1998) constituting a picture that might be called *dysmetria of thought*. The concept of "dysmetria of thought" or "cognitive dysmetria" has been proposed as a unitary neurocognitive framework of reference for schizophrenia symptoms [(Andreasen et al., 1998), see below] and involves a neural network with the main nodes in the prefrontal cortex (PFC), thalamus, and cerebellum. Cognitive dysmetria comprises:

- impairment of executive functions, such as planning, set-shifting, abstract reasoning, working memory, and verbal fluency;
- difficulties with spatial cognition, both in visuospatial organization and visuospatial working memory;
- personality change, with blunting of affect and/or disinhibited and inappropriate behavior;
- language deficits including agrammatism, dysprosodia, and mild anomia.

This constellation of symptoms, which is reminiscent of a prefrontal syndrome (Schmahmann, 2004; Schweizer et al., 2007), is called *cerebellar cognitive affective syndrome.* Clearly these symptoms are not exclusive to cerebellar damage; indeed, the aforementioned cognitive and affective alterations can also be found in patients with disorders of the cortical associative areas (especially prefrontal) and paralimbic areas, or with disorders of the subcortical areas to which the former are connected. It would be safe to say that these symptoms involve the whole CTCC loop. Anatomically, lesions of the posterior lobe are associated, in particular, with cognitive symptoms, while lesions of the vermis are consistently observed in patients with pronounced affective alterations. The anterior lobe seems to be less involved in the generation of these cognitive and behavioral deficits, while anterior lobe lesions are well-known to cause motor ataxia (Diener and Dichgans, 1992) **(Figure 3)**. Functional neuroimaging studies have consistently shown: (1) activation in the anterior lobe during motor learning and classical conditioning, (2) activation of the posterior lobe during several kinds of purely cognitive tests of executive functions (cognitive planning, set-shifting, working memory), language (verbal memory tasks, verb for noun substitution, synonym generation), mental imagery, and sensory discrimination, (3) activation of the vermal region during tests evaluating emotional modulation. Finally, (4) abnormal activation of the cerebellar vermis and posterior lobe has been observed in several primary psychiatric disorders, most notably schizophrenia, autism, and dyslexia, further discussed below.

THE EXTENDED COORDINATING AND PREDICTING ACTION OF THE CEREBELLUM

The cerebellum is assumed to contribute to sensory-motor processing in an automatic manner. After having received, analyzed, and recognized a sensory or a motor pattern (as a prediction of a future sensory state), the cerebellum produces gain and phase corrections that make it possible to regulate the force and activation of large sets of muscles[5]. The predicted and actual patterns are then compared; this is followed by the provision of appropriate correction sand thus the generation of movement *coordination*. As an extension of this, patterns coming from various cerebrocortical areas can be processed, allowing the "coordination" of higher cognitive functions. Once activated, the CTCC loops could be used not just for *automatic* but also for *controlled* functions. These can be set in the more general framework of *cognitive control* and *executive function*[6].

The cerebellum may take part in *cognitive control* by regulating executive functions, which it could do by manipulating different "objects." These can be considered parts of a set of virtual representations, given that they may be purely symbolic (e.g., thoughts) or applied to symbolic expression (e.g., speech) or voluntary movement (which, after all, is based on a virtual

[5]Motor controlis preprogrammed in a feed forward manner and is based on the coordination of elementary movements consisting of straight and curved segments. These "jerks" can be modulated in delay, duration, and strength. The analysis of a simple preprogrammed ballistic "jerk" movement, the saccadic movement needed to direct the eye toward a desired target, has shown that the cerebellum can indeed learn to control the beginning, the end, and the velocity of this elementary segment of movement.

[6]Cognitive control is the ability to direct mental processing toward complex targets. To achieve it, it is necessary to divert attention from actual sensory inputs, prioritize, and coordinate sequences of actions, and prolong this control until the target is achieved beyond immediate environmental interferences. Cognitive control allows regulation of executive functions, which can be automatic or controlled. Automatic executive functions are driven bottom-up through stimuli that activate internal behavioral modules, while the controlled executive functions operate in a top-down manner and imply choices based on general principles and experience. In general, once a controlled process is learned, it can be transformed into an automatic process, thereby accelerating its execution. The main properties of executive functions are that they are (1) goal-directed, (2) learned rather than innate, (3) multimodal; in addition, they (4) require generalization, (5) require working memory, (6) have limited capacity (only a few processes can be controlled at a time), and (7) require choices and selections to focus attention on a selected target. Executive control can associate, coordinate, and select multiple inputs and outputs, learning the procedure and generating behavioral flexibility and complexity. It should be noted that these aspects of cognitive control do not formally differ much from those of voluntary motor control.

representation of its sensory consequences—see above). The cerebellum then integrates these multiple internal representations (of a motor, sensory, or cognitive/emotional nature) with external stimuli and with voluntary (or self-generated) responses. Indeed, cognitive dysmetria, which is the loss of these functions, is characterized by difficulty in prioritizing, processing, and coordinating responses to incoming information (Andreasen et al., 1996; Crespo-Facorro et al., 1999). Importantly, the involvement of the cerebellum in *executive functions* becomes more prominent as the complexity of these functions increases (Gottwald et al., 2004). Deficits in semantic and phonemic fluency and poor performances reported in some memory tasks can be traced back to a deficit in executive functions. Moreover, performance on "basic" attentional tasks (e.g., Go/NoGo) is substantially normal, but performance on "high level" attentional tasks (e.g., the "divided attention" paradigm, where subjects have to respond simultaneously to multiple cognitive tasks) is impaired (Baddeley et al., 1984; Craik et al., 1996). Finally, patients with right-sided lesions are more impaired than those with left-sided lesions. This supports the idea of lateralization of cerebellar functions, with verbal deficits mostly occurring in the presence of right cerebellar lesions and visuospatial deficits tending to occur in left cerebellar lesions. Clearly, this lateralization replicates the division of cognitive competences between the two cerebral hemispheres, with which the cerebellum is cross-connected via the pontine nuclei and thalamus.

A similar role of the cerebellum in prioritizing, processing, and coordinating responses to incoming information could underlie cerebellar control of emotional experience[7]. Lesions of the cerebellum interfere with affective expectations from a given behavioral context. This is evident in fear conditioning paradigms, in which the relationship between a conditioning stimulus and a frightening unconditioned stimulus can be precisely controlled (Sacchetti et al., 2005). Vermal lesions can decrease reactivity to frightening stimuli, probably by controlling the output to the hypothalamus, amygdala, hippocampus, septal nuclei, and nucleus accumbens. Likewise, neuroimaging studies show that the cerebellum and the anterior cingulate cortex (ACC) are strongly activated when a painful stimulus is expected after a given cue (Ploghaus et al., 2003). While the cerebellum builds up the expectation of pain, the ACC, which is strongly connected with the cerebellum, plays an important role in several neurocognitive mechanisms capable of modulating pain perception, mainly attention, expectation, and reappraisal (Wiech et al., 2008). Moreover, the cerebellum, together with the ACC and the insula, is strongly activated when perceiving pain in others (Jackson et al., 2005), and these same structures (together with the primary and secondary somatosensory cortices, putamen, and thalamus) have been found to show activation that is related to the intensity of pain (Coghill et al., 1999). Finally, the cerebellum may also regulate the quality of emotional experience (Turner et al., 2007). Patients with cerebellar stroke report reduced pleasant feelings in response to happiness-evoking stimuli (while unpleasant experience to frightening stimuli was substantially similar to that recorded in controls).

The prefrontal cerebral cortex has classically been considered to be the main station exerting cognitive control and the limbic system cortices to be the ones primarily involved, together with amygdala and hippocampus, in affective control. Infact, signals processed in the cerebral cortex are continuously sent to subcortical structures, including the cerebellum, which then sends back to the cortex signals able to refine and control cerebro-cortical processing. This process resembles the control of movement planning occurring in the sensory-motor CTCC loops **(Figure 4)**.

META-LEVELS OF SIGNAL PROCESSING IN CTCC LOOPS

So far we have considered observations suggesting that the cerebellum, in addition to taking part in sensory-motor control, is also involved in cognitive/emotional functions. These observations are based on evidence of cerebellar activation during specific cognitive/emotional tasks and on the existence of connections between the cerebellum and relevant cerebro-cortical areas. Moreover, we have tried to make sense of all this by setting cerebellar activity within the general framework of brain functioning and cognitive control. But the question, now, is how can the cerebellum support these multiple operations? The basic hypothesis is that the cerebellum uses, throughout, the same circuit structure, and that different outcomes depend on the specific connections to different brain areas. This also implies that the same code is used for all the operations involving the cerebellum and that motor control and cognition/emotion have an equivalent structure at the level of spike coding.

On an operational level, in order to connect basic circuit functions with cognitive/emotional and mental processing, a series of meta-levels needs to be considered. Ideally, it should be possible, first, to demonstrate the connection between neighboring meta-levels, and thereafter to link the cellular/molecular mechanisms with cognitive/emotional processing and then with mental function and dysfunction.

1. *Cellular/molecular to circuit.* As regards the relationship between the cellular-molecular level and the circuit level of cerebellar operations, several specific hypotheses have been advanced, which are currently under investigation and have been discussed elsewhere (D'Angelo, 2011). The idea, basically, is that the cerebellum is able to exploit spike timing, neuronal dynamics and long-term synaptic plasticity in order to process incoming signals in the spatial, temporal, frequency, and phase domains. At circuit level, timing and plasticity in neurons and synapses can implement adaptable signal processing capabilities, which appear to be the prerequisites for the emergence of cerebellar processing (Hansel et al., 2001; D'Angelo and De Zeeuw, 2009). The outcome of circuit operations on cerebellar functions are themselves bound to signal timing and learning, in line with the original main theories of the cerebellum as a timing and learning device (Albus, 1972; Ivry and Keele, 1989).

[7]Emotional control, like cognitive control, has both a bottom-up and a top-down component. In the first case, a somato-visceral reaction (emotional response) is generated by detection of a significant pattern and the subject learns about it and subsequently elaborates an emotion (the James-Lange model). In the second case, the subject first elaborates an emotion and this then activates appropriate somato-visceral responses (the Cannon-Bard model).

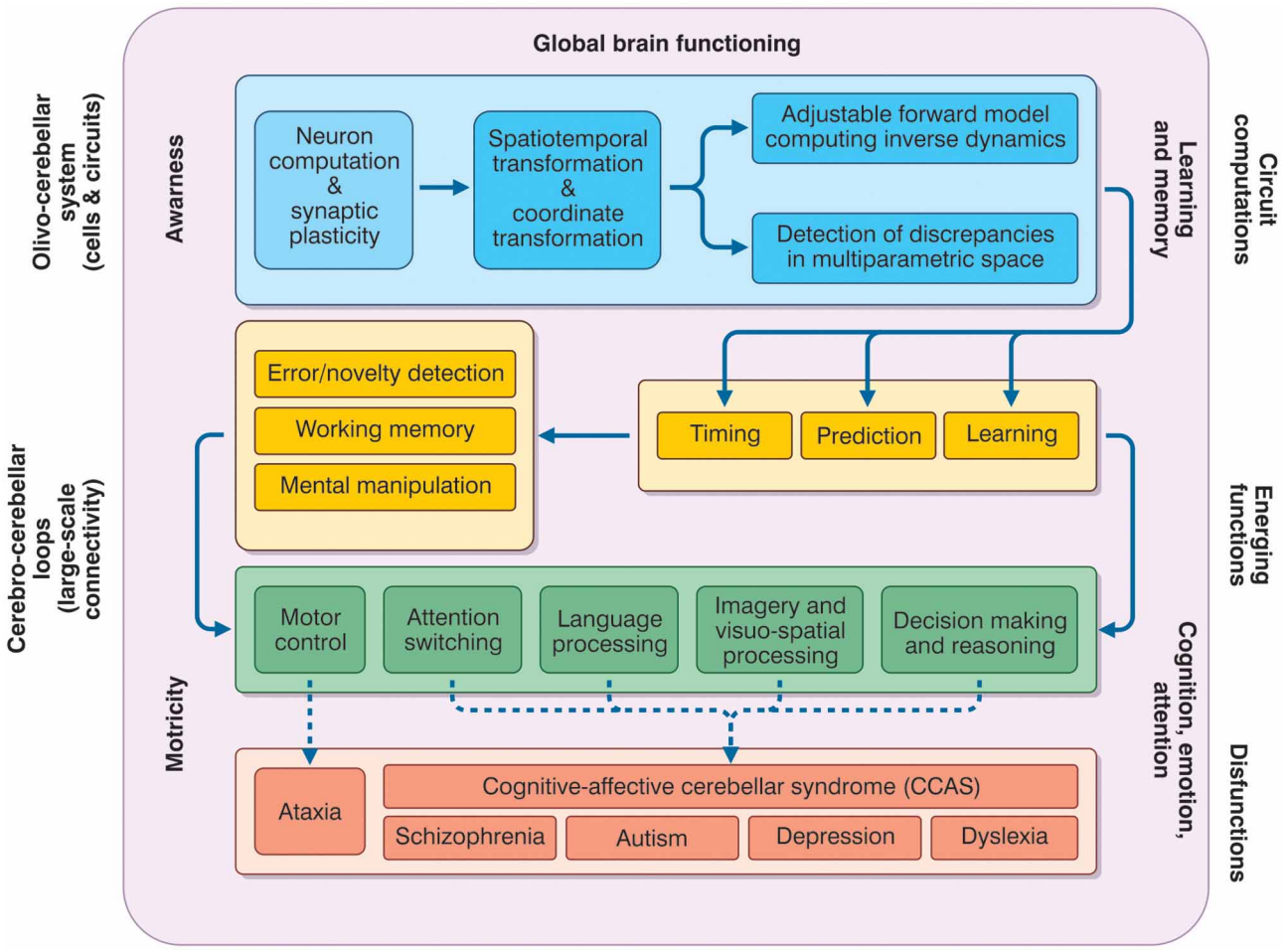

FIGURE 4 | The meta-levels of cerebellar activity. The figure depicts the causal relationships between the functions that the cerebellum is thought to play at different operative levels (meta-levels hypothesis) and between these same functions and brain pathologies. The *neuron and network* level lays in the blue box and is normally investigate using electrophysiological and imaging techniques. These combined with mathematical models, allow to infer the *computational functions of the circuit* (forward model, various parameter transformation and detection of discrepancies between predicted and actual signal patterns). Once integrated into the large-sale connectivity of the CTCC loops, circuit computations lead to emerging functions. At low-level (yellow boxes), these include *learning, prediction, and timing* (cerebellar processing primitives), which can implement structured cerebellar operations including forms of *working memory, error/novelty detection, and mental object manipulation.* The low-level functions lay at the basis of more complex high-level functions (green box) including *motor control, attention switching, language processing, imagery and visuospatial processing, decision-making, and reasoning.* Major aspects of brain pathology (red box) can be predicted on the basis of the low- and high-level functions. Emerging functions and dysfunctions are usually investigated using non-invasive recordings (fMRI, DTI, TMS etc.), neuropsychological and clinical assessments. As a whole, the cerebellar function can contribute to global brain operations not just of motricity but also of learning and memory, cognition, emotion, attention, and even awareness.

While connecting circuit operations to emergent behaviors is obviously a fundamental step in understanding how the cerebellum operates, cellular/molecular mechanisms pertain to a different realm and will not be covered here (D'Angelo, 2011).

2. *Processing primitives.* At a low-level of complexity, cerebellar circuit computations emerge in the operations of *timing, sensory prediction*, and *sequence learning.* These can be tested in simple experimental tasks and, once embedded in appropriate CTCCs and larger brain systems, may be regarded as a basis for explaining more complex sensory-motor cognitive-emotional operations.
3. *High-level cognitive processing.* The outcome of processing primitives, applied to complex behavioral operations and involving multiple interconnected brain areas, could lead to various high-level cognitive operations. These include *attention, language, working memory, visuospatial processing, imagery, reasoning, and decision-making.*
4. *Mental processing and psychiatric diseases.* At the highest level, cognitive/emotional functions can be integrated into mental processing. Dysfunction of the relative mechanisms emerges through complex pathological manifestations including *autism, schizophrenia, depression*, and *dyslexia.*

THE CEREBELLAR PROCESSING PRIMITIVES

Understanding how the cerebellum contributes to so many apparently disparate functions would be an enormous step forward as it would mean understanding the common *processing primitives* of the cerebellar circuit. The most plausible hypothesis is that the cerebellum has a predictive function, i.e., the ability to anticipate incoming information and thus to ensure that actions correctly anticipate changes in the environment (Moberget et al., 2008). This hypothesis has two parts. The *timing hypothesis* postulates that the cerebellum is critical for representing the temporal relationship between task-relevant events, while the *sensory prediction hypothesis* postulates that it is critical in generating expectancies regarding incoming information (Ivry et al., 2002). The two hypotheses are not mutually exclusive; rather, they seem to be set at two different hierarchical levels, with timing being more elementary than prediction. Indeed, whereas timing is merely the establishment of an ordered relationship between two elements, the ability to predict future patterns (as in *a forward controller*) requires, in addition, the ability to compare different incoming patterns and predict their consequences on the basis of internally stored memory. Computationally, timing requires only one processing line while sensory prediction requires several. In the Pellionisz and Llinas hypothesis (Pellionisz and Llinàs, 1982), this sensory prediction corresponds to a tensorial transformation in the spatiotemporal hyperspace of the cerebellar circuit. Finally, the cerebellum is likely to use internal memories to adapt its computational schemes. The meaning of cerebellar learning has been hotly debated, with controversy often arising over the role of long-term synaptic plasticity in motor learning. Nonetheless, compelling evidence suggests that learning helps to automate timing and sensory prediction with respect to specific motor and cognitive sequences.

TIMING

Motor coordination, which fails in cerebellar patients, is essentially a precise spatiotemporal sequence of movements of one or more body segments, which must show appropriate position, velocity, and acceleration. As Ivry underlines (Ivry, 2000), the cerebellum probably operates as an internal timing system providing a precise temporal representation for motor and non-motor tasks. Experiments of "irregularity detection," measuring cortical mismatch-negativity, have indicated that the cerebellum selectively contributes to processing the temporal properties of stimuli (Ivry, 2000). With regard to time estimation ability (timing), a recent review (Koch et al., 2009b) showed that the cerebellum is crucial when normal subjects are required to estimate the passage of brief time intervals and when time is computed in relation to given salient events. In turn, circuits involving the striatum and substantia nigra, which project to the PFC, are mainly implicated in processing supra-second time intervals in relationship with various cognitive functions.

One critical issue in physics and biology is velocity estimation, a process that could occur in different locations in the brain, such as the thalamo-cortical circuit (Ahissar et al., 2000; Szwed et al., 2003). As the cerebellum is a dedicated space-time processor, it is to be expected that it is also involved in velocity estimation. Indeed, a recent fMRI study (O'Reilly et al., 2008) identified a region in the posterior cerebellum (lobule VII crus 1) that is selectively activated during velocity judgment tasks (prospective spatiotemporal model). Conversely, when perceptual judgments are based only on the spatial (direction) characteristics of an object, this specific area is not significantly activated. Moreover, the functional connectivity between the posterior cerebellum and the anterior putamen (bilaterally), which is involved in timing (Matell and Meck, 2004), is enhanced during the velocity judgment task, which is essentially perceptual, with an only minimal motor component.

PREDICTION

As we have pointed out, the cerebellum has been considered to act as a forward controller (Miall and Reckess, 2002; Wolpert et al., 1998) implementing the contravariant transformations that are necessary in order to convert predictive sensory plans into motor representations. The involvement of the cerebellum is shown by the ability to predict the sensory consequences of one's own motor actions. Typically, in the absence of visual feedback, cerebellar patients have great difficulty in estimating the direction of pointing (Synofzik et al., 2008). The cerebellum signals discrepancies between predicted and actual sensory consequences of movements, triggering appropriate corrections. In a recent study, subjects were required to use their right hand to move a robotic arm; the motion of this arm determined the position of a second robotic arm, which made contact with subject's left palm. Computer-controlled delays were introduced between the movement of the right hand and the tactile stimulation on the left palm. Activity in the right lateral cerebellar cortex, measured with PET, showed a positive correlation with delay, i.e., with the time prediction error (Blakemore et al., 2001). This suggests that the cerebellum is less activated by a movement that generates a tactile stimulation than by a movement that does not (which signifies an error due to lack of sensorial feedback from the target). A similar phenomenon is seen with tickling, whose sensory effect is suppressed during self-stimulation (which signifies perfect cancellation of error) (Blakemore et al., 1998a). Accordingly, the somatosensory cortex is significantly more activated by an externally generated tactile stimulus than by a self-generated one, and the cerebellum has been shown to provide the signal needed to attenuate the sensory responses to self-generated tactile stimuli (Blakemore et al., 1998a, 1999; Blakemore and Sirigu, 2003).

LEARNING

Another basic function of the cerebellum is sequence learning. In a scenario simulating the absence of coordination in ataxia, Shin and Ivry (2003) showed that patients with cerebellar lesions were not able to learn simultaneously presented spatial and temporal sequences (conversely, patients with Parkinson's disease were able to learn these sequences, but not the relationship between them).

Along the same lines, cognitive sequencing functions can be selectively damaged in patients with cerebellar lesions; for example, patients with left-side cerebellar lesions perform poorly on script sequences based on pictorial material and patients with right-side cerebellar lesions on script sequences requiring verbal elaboration (Leggio et al., 2008). These deficits were not correlated with general intelligence, or with general

neuropsychological impairment. Furthermore, they were found both in patients with focal lesions and in subjects with degenerative cerebellar pathologies. It is noteworthy that when these patients were asked to order a set of cards representing several behavioral sequences, they were unable to work out the correct order, even though they could correctly describe and understand the meaning of the single cards. Interestingly, while cerebellar patients are not necessarily impaired in learning simple visual or spatial sequences, their ability to discriminate different durations of auditory stimuli is generally impaired. Indeed, learning sequences of auditory tones with different durations has been found to be rather difficult for cerebellar patients, even though the same patients can normally learn visual sequences and sequences of tones with different frequencies but not different durations (Frings et al., 2006; Ivry and Keele, 1989). These data are obviously consistent with the "timing hypothesis"; however, the impairment in script sequences could be related to more abstract cognitive processes and possibly to a lack of executive functions.

The role played by cerebellar structures in sequence learning depends on experience-related factors; in motor sequence learning tasks, the cerebellum shows prominent activation during early phases of learning; instead, after extended practice, the activation is located mainly at the level of the basal ganglia (Doyon et al., 2002). Notably, within the early phase of learning, the activation has been found to shift gradually from the cerebellar cortex to the deep cerebellar nuclei (Medina and Mauk, 2000; Shadmehr and Mussa-Ivaldi, 2012). Moreover, some researchers hypothesize that the cerebro-cerebellar loop is primarily involved in motor adaptation processes (e.g., adapting to environmental changes or perturbations), rather than in effective motor learning processes (e.g., learning new sequences of movements), which could be processed by cerebro-striatal circuits (Doyon et al., 2003; Debas et al., 2010). The cerebellum, coupled with the PFC, is particularly important in learning new visuomotor procedures by imitation (Petrosini, 2007) in the manner of *mirror neuron* effects. Finally, cerebellar damage can lead to severe impairment of non-motor associative learning independently of motor alteration (Drepper et al., 1999).

THE CEREBELLUM AND HIGH-LEVEL COGNITIVE PROCESSING

The timing, predictive, and learning properties of the cerebellum, once integrated within the circuits formed with the cerebral cortex, basal ganglia, and limbic system, can lead to control of more complex cognitive/emotional functions, including attention, language, memory, imagery, and reasoning.

ATTENTION

The cerebellar contribution to attentive functions has been revealed in several physiological and pathological conditions. Both autistic and cerebellar patients show a selective impairment in attention shifting from visual to auditory stimuli, although attention focusing is normal (Courchesne et al., 1994a). Moreover, the cerebellum, controlling the precision of saccades, probably plays an important role in orienting attention to a visual cue (especially in covert attention tasks). This role seems to be linked to procedural spatial learning functions, which are strongly related to the ability of the cerebellum to learn goal-directed trajectories, as recently supported by experimental results (Burguière et al., 2005) and computational modeling (Passot et al., 2009).

Indeed, patients with cerebellar lesions are able to correctly orient visual attention but their reaction times are rather slow (800 and 1200 ms) compared with those of normal control subjects (100 ms on average) (Townsend et al., 1999). Attention switching is reinforced when subjects have to reassign motor responses to different stimuli. In agreement with this "attentive hypothesis," some cerebellar areas show significant activation, measured with fMRI, during early phases of skill learning (both for motor and non-motor skills) and during pure visual attention tasks (Allen et al., 1997).

One theory is that the primary role of attention is to generate time-based expectancies of sensory information (Ghajar and Ivry, 2009). Essentially the suggestion is that, the higher the level of attention, the lower the performance variability, because the subject is less likely to be distracted by irrelevant information. The authors observe that the cerebellum is constantly activated after an attentional cue, independently of actual execution of movements, and even if the preparation of a potential motor response may be required. Accordingly, the cerebellum is bilaterally activated when a cue precedes the beginning of a motor task, whilst the primary motor cortex is activated only—and mainly contralaterally—during the execution of the task itself (Cui et al., 2000). Furthermore, it has been shown that PFC-projecting zones of the cerebellum process the symbolic content of sensory cues (Balsters and Ramnani, 2008). Ghajar and Ivry argue that the cerebellum may be actively involved in an attentional network comprising mainly the PFC, the inferior parietal lobule, and the cerebellum itself. The specialized role of the cerebellum might be to help encode the precise timing of sensory predictions. Cerebellar predictive activity probably works in a time frame of 2.5 s, so that events that fall within this window can be considered temporally bound.

Thus, according to Ghajar and Ivry's hypothesis, the predictive function of the cerebellum may be seen as a defining trait of attention. However, we can speculate that, in many tasks, attention is not necessarily closely bound up with sensory anticipation. The execution of visual search and feature match tasks, for example, may not rely on anticipatory mechanisms and may not involve the cerebellum directly. Nevertheless, cerebellar patients can fail in tasks of this kind, too, because impaired ocular movement control may lead to incomplete exploration of stimuli.

LANGUAGE PROCESSING AND VERBAL WORKING MEMORY

The cerebellum is deeply implicated in language, involving both motor and cognitive processing organized in the "phonological loop." Cerebellar pathology impairs acquisition of motor skills and primary articulatory abilities and the resulting reduced articulation speed impairs working memory for verbal material, reducing sensitivity to the onset, rime, and phonemic structure of language. This impairment of the phonological loop, in turn, leads to difficulty in language acquisition and dyslexia (Nicolson et al., 2001b) (see below).

Cerebellar damage can result in impairment of verbal working memory (Justus et al., 2005). Cerebellar patients demonstrate a reduction of the "phonological similarity effect" (normal subjects show more difficulties in memorizing phonologically similar words than phonologically dissimilar ones). Desmond et al. (1997) attempted to clarify the difference between the cerebellar contribution to phonological "rehearsal" mechanisms and to proper verbal working memory processes. During simple letter repetition tasks under fMRI, specific areas of the posterior vermis (lobules VI and VIIA) and of the cerebellar hemispheres (left superior HVIIA, right HVI) were activated. The same areas were activated together with an additional part of the right cerebellar hemisphere (HVIIB) during a sequential verbal working memory task. It was hypothesized that (1) HVIIA and HVI activations represent input from the frontal lobes (which are connected with the articulatory control processes of verbal working memory) and that (2) HVIIB reflects input from temporal and parietal areas (which, in turn, are probably the key areas of the phonological store), and that the function of the cerebellum during verbal working memory tasks could be to compare the output of subvocal articulation with the content of the phonological store. The verbal working memory deficit in cerebellar subjects is specific and is, both "forward and backward," independent of dysarthric symptoms, which suggests that the cerebellum is involved in the initial phonological encoding and, possibly, in strengthening memory traces (Ravizza et al., 2006). In normal subjects, single-pulse TMS delivered to the cerebellum during the encoding phase of a verbal working memory test does not affect the accuracy of the performance but lengthens the reaction times (Desmond et al., 2005). Clearly, the involvement of the cerebellum in linguistic processing reflects the role of this structure in timing, learning, prediction, and attention.

Cerebellar patients show poor performances on phonological verbal fluency tasks, but not on semantic verbal fluency tasks [(Leggio et al., 2000); but see Smet et al. (2007)], and therefore show a dissociation between their processing of phonological and semantic material. Patients with aright posterolateral cerebellar lesion are selectively impaired in verb-noun associations (Gebhart et al., 2002). This impairment is not observed when the task is to associate verbs with visual stimuli (pictures of objects) (Richter et al., 2004). It should be noted that cerebellar patients, unlike patients with Parkinson's disease, are normally able to perform category learning tasks (Maddox et al., 2005). When listening to disyllabic stimuli, subjects with bilateral cerebellar pathology do not show the phoneme-boundary effect generally shown by neurologically normal subjects. This may be due to their impaired ability to discriminate between intervals of different duration (Ackermann et al., 1997). Clinical studies also suggest that cerebellar pathology can play a causal role in prefrontal aphasic symptoms (Marien et al., 1996). Moreover, cerebellar activity switches hemispheres (from right to left) according to recruitment of right PFC, during linguistic tasks, in aphasia following a stroke of left cerebral hemisphere (Connor et al., 2006).

The (right) cerebellum is strongly activated during semantic disambiguation tasks (Bedny et al., 2008) and, bilaterally, during lexical decision tasks with semantic priming (Rissman et al., 2003). The cerebellum is activated during different kinds of verb-noun association tasks (Seger et al., 2000). Also, the cerebellum is strongly activated by semantic discrimination tasks and the intensity of the activation correlates positively with the difficulty of the task (Xiang et al., 2003). Finally, it should be noted that cerebellar theta-burst stimulation with TMS has been shown to selectively enhance associative priming, while semantic priming was unaffected (Argyropoulos, 2011).

IMAGERY AND VISUOSPATIAL PROCESSING

The cerebellum is involved in pure imagery processes, both motor (Ryding et al., 1993; Naito et al., 2002) and visual (Ishai et al., 2000; Mellet et al., 2000). Indeed, patients affected by unilateral cerebellar stroke show slowed or impaired motor imagery (González et al., 2005; Battaglia et al., 2006). Moreover, cerebellar patients are impaired in tests of mental rotation of objects (a typical example of a visual imagery process) while, at the same time, failing to show significant deficits in tasks evaluating basic perceptual functioning or sensory discrimination (Molinari et al., 2004). Some cerebellar patients show purer perceptual alterations, such as hemispatial neglect (Silveri et al., 2001), and there is evidence that the cerebellum could be involved in metric judgment processes, as tested in the line bisection task (Fink et al., 2000).

The neural networks involved in imagery processes show a strong inter-individual and inter-trial variability; for example, Gerardin et al. (2000) found the cerebellum to be constantly activated during actual execution of motor actions, whilst there emerged strong inter-individual differences in its degree of activation during the execution of motor imagery tasks. Along the same lines, Grealy and Lee recently described a cerebellar patient found to be more impaired in monitoring imagined simple actions than in controlling the actual execution of the same actions (Grealy and Lee, 2011). Conversely, a different study reported cerebellar activation only during actual execution of motor acts and not while imaging the same acts (Nair et al., 2003) and a further one reported reduced cerebellar activity during imagined movements compared with actual execution of the same movements (Lotze et al., 1999). These heterogeneous results may be explained by individual differences, differences in the nature of the cerebellar lesions, and in the complexity or novelty of the tasks involved. However, another possible reason for the aforementioned differences could be that the cerebellum is actively engaged in *manipulating and monitoring* mental images rather than in *generating* them. In the last two studies (Lotze et al., 1999; Nair et al., 2003), the subjects were asked to imagine themselves executing relatively simple finger-tapping movements. Conversely, in the other study (Grealy and Lee, 2011) the patient was asked to imagine himself doing a pointing movement toward a specific location in space and to guess the amount of time required to execute the complete movement. Thus, in this case, the subject (who showed no difficulties of any kind in generating mental images) needed to actively monitor his motor imagery process and to estimate specific spatiotemporal information. Similarly, in the other reported studies linking the cerebellum with motor imagery, subjects were required to extrapolate some specific information from their imagery processes and/or to mentally imagine rather complex activities, such as playing tennis. In the same way, visual imagery tasks often require subjects to infer some kind

of information from the mentally generated images and/or to actively manipulate these mental images (e.g., mental rotations). It is thus possible that the cerebellum is primarily engaged in manipulating mental images and in estimating spatiotemporal information related to dynamic motor imagery processes, whilst the pure generation of mental images probably does not rely primarily on cerebellar computations.

Furthermore, studies on hemicerebelloctomized rats, not displaying pure (declarative) spatial memory alteration, suggest that the cerebellum can play a major role in spatial navigation (Petrosini et al., 1998; Foti et al., 2010) and could be involved in developing procedural spatial search strategies.

DECISION-MAKING AND REASONING

The cerebellum is involved in decision-making under uncertainty (Blackwood et al., 2004) (probabilistic reasoning), which suggests that it can construct probabilistic models of external events. In a two-alternative forced-choice task condition, brain processing advances in four stages: processing of sensory information, option evaluation, intention formation, and, finally, action execution. In a recent MEG study (Guggisberg et al., 2007), the cerebellum and the inferior parietal cortex showed high frequency activity (gamma-band) during the intention formation and action execution stages (and, in some conditions, also during the option evaluation stage, mainly when all the options had the same value).

The cerebellum is also likely to be involved in reasoning processes of different types. For example, cerebellar activation has been observed during probabilistic and deductive reasoning (Osherson et al., 1998). Interestingly, deductive reasoning preferentially activates the left cerebellar hemisphere, while inductive reasoning activates the right cerebellar hemisphere (Goel and Dolan, 2004). Cerebellar activity in deductive reasoning seems to be independent of the presence/absence of semantic content (Goel et al., 2000), and also of its nature, concrete, or abstract (Goel and Dolan, 2001).

Although the meaning, if any, of cerebellar activation in reasoning is not fully understood, the cerebellum is thought to take part in creating and controlling adaptive working models of the environment, in cooperation with cortical structures, mainly the PFC (Vandervert, 2003; Vandervert et al., 2007). Indeed, there is interesting evidence that logical reasoning could be based on specific mental models and that, in turn, the internal structure of these models could directly influence the reasoning process (Johnson-Laird, 1980; Schaeken et al., 1996; Johnson-Laird, 2001). Therefore, the cerebellum could play an important role in manipulating the mental models required for logical reasoning.

MENTAL PROCESSING: CEREBELLAR INVOLVEMENT IN NEUROPSYCHIATRIC DISORDERS

Abnormal cerebellar processing can lead to alterations in mental functions. Cerebellar patients often show mood disorders, personality change, cognitive disorders, and dementia which may be integrated into the pathological frameworks of schizophrenia, depression, autism, and dyslexia. The rate of psychiatric morbidity associated with cerebellar degenerative diseases is about double that found in normal subjects (Leroi et al., 2002): 77% of patients with cerebellar degenerative diseases are affected by psychiatric disorders, compared with only 41% of neurologically healthy control subjects. Interestingly, the components of cognitive processing related to cerebellar activity also appear to be related to the pathogenesis of these diseases.

SCHIZOPHRENIA

Schizophrenia is a mental disorder characterized by a dissociation between internal representations and external reality. It is known that "cognitive dysmetria," typical of psychoses like schizophrenia, is also observed in cerebellar patients. A role of the cerebellum in early onset schizophrenia was recently reported in a DTI study which revealed reduced fractional anisotropy in the white matter of the parietal association cortex and in the left cerebellar peduncle (Kyriakopoulos et al., 2008). Moreover, neurological soft signs in schizophrenic patients are inversely correlated with volume of the right cerebellar hemisphere (Bottmer et al., 2005). The cerebellar dysfunction may impair the ability of schizophrenic subjects to recognize an action on the basis of a subject's intention. Indeed, schizophrenic patients are not able to correctly estimate the sensory consequences of their own actions (Synofzik et al., 2010), a deficit usually observed in cerebellar patients. In other words, this means that the consequences of their actions are not in agreement with the expected sensory results of these actions and with the subject's intentions. This is hardly surprising given the predictive function of the cerebellum.

Neuroanatomically, there is evidence showing that damage to a CTCC could be the primary pathophysiological alteration in schizophrenic patients (Konarski et al., 2005). Several imaging studies (CT, MRI) have reported abnormal volume of the cerebellar vermis (either hypoplasia orhyperplasia), while others have reported global cerebellar atrophy. Cerebellar hypoactivation (or even non-activation) has been measured with fMRI in cognitive tasks involving the prefrontal-cerebellar loop, tasks such as the (1) Wisconsin Card-Sorting Test, (2) working memory [n–back] task, and (3) periodic sequence-learning tasks. An ontogenetic substrate can be traced back to abnormalities in infant motor development (IMD) and executive function development (Ridler et al., 2006). IMD and executive function development are normally associated with increased gray matter density (GMD) in the premotor cortex, striatum, and cerebellum, reinforcing the fronto-cerebellar network. Schizophrenic patients have delayed IMD and deficits in executive functions correlating with disruption of the fronto-cerebellar network. In postmortem studies, reduction in the size of the anterior vermis in schizophrenic patients is associated with reductions in the density and size of Purkinje cells. Moreover, the synaptogenesis process could be impaired, both for excitatory and inhibitory neurons, and a core alteration may concern the NMDA receptors and synaptic plasticity (Stephan et al., 2009).

Overall, in view of the reported impairment of the cerebellum and Purkinje cells, it can be hypothesized that the neural basis of schizophrenia might partially overlap that of autism (Boso et al., 2010). Considering the general function of the cerebellum, it is possible that schizophrenic patients are impaired in switching from an egocentric frame of reference to an allocentric one (Yakusheva et al., 2007). In agreement with this hypothesis, when asked to imagine an object from another perspective,

schizophrenic individuals make more egocentric errors than do controls (Langdon et al., 2001; Shenton et al., 2001).

AUTISM

Autism is a developmental disorder defined by three core features: (1) impairment in social interaction, (2) impairment in communication, with a delay in language acquisition, and (3) repetitive, stereotyped behaviors. More specifically, autistic subjects show a selective difficulty in understanding intentions and beliefs (Frith et al., 1991). Cerebellar patients and autistic subjects have shown a similar impairment in shifting attention between auditory and visual stimuli (Courchesne et al., 1994a). It is possible, given the critical role of the cerebellum in revealing differences between predictions elaborated by the cortex and the objective reality conveyed by experience, that dysfunction of CTCCs may prevent the detection of novelty and impair attention switching (Boso et al., 2010).

The cerebellum and the brainstem (including the inferior olive) are significantly smaller in autistic patients than in healthy controls (Hashimoto et al., 1995; Bauman and Kemper, 2005). The Purkinje cells of the cerebellum are reduced, primarily in the posterior inferior regions of the hemispheres. In the limbic system (hippocampus, amygdala, and enthorinal cortex), neurons are small and show increased cell-packing density.

Decreased exploration of the environment in autistic children (a typical autistic behavioral trait) is correlated with the magnitude of cerebellar hypoplasia of the vermal lobules VI–VII. The rate of stereotyped behavior is negatively correlated with the size of cerebellar vermal lobules VI–VII and positively correlated with frontal lobe volume in the same autistic subjects (Pierce and Courchesne, 2000). Interestingly, two types of cerebellar pathology have been identified in autism (Courchesne et al., 1994b): *hypoplasia* of the posterior vermal lobules VI and VII and *hyperplasia* of the same lobules. This is particularly relevant if we consider that vermal hyperplasia has also been found in subjects affected by Williams syndrome, a genetic disorder characterized by hyper sociability, social disinhibition, deficits in general intelligence, and visuospatial abilities, in the presence of preserved facial processing and language ability (Schmitt et al., 2001). Conversely, autism is characterized by social withdrawal and isolation. From the perspective of "social cognition," these two pathologies can be seen as opposites (Riby and Hancock, 2008).

A neural response in the cerebellum, as in the visual cortex, is observable when processing a broad set of emotional facial expressions (happy, fearful, sad, angry, and disgusted faces) (Fusar-Poli et al., 2009). Conversely, the amygdala is selectively activated by happy, fearful, and sad faces, and the insula by disgusted and angry expressions. Alongside this evidence, an fMRI study has shown that the cerebellum is activated during implicit processing of facial expression, while temporal lobe regions are activated during explicit processing (Critchley et al., 2000a). Notably, when implicitly processing emotional expressions, subjects with high-functioning autistic disorders do not activate the left amygdala and the left cerebellum (Critchley et al., 2000b).

Abnormalities related to the autistic spectrum disorders have been found in spinocerebellar ataxia (SCA) patients (SCA3 and SCA6 patients), who show reduced performance on the Theory of Mind Test, in spite of showing normal attribution of social and emotional responses. These subjects also performed poorly in executive functions and memory tasks, but not in spatial and calculation tasks (Garrard et al., 2008). A previous study also found a specific cerebro-cerebellar network associated with "attribution of intention" tasks; this network is composed of the right medial and inferior parietal cortex, the temporal lobes, and the left cerebellum (Brunet et al., 2000).

DEPRESSION

According to the DSM-IV (APA, 1994), a depressive disorder is characterized by a depressed mood and a loss of interest in daily activities. Depression can also be characterized by the presence of cognitive symptoms, such as weak working memory processing and impairment in executive functions (Fales et al., 2008).

A recent paper (Savitz and Drevets, 2009) reviewed neuroimaging studies (MRI and PET) in major depressive disorder (MDD) and bipolar disorder (BP), a mood disorder defined by the presence of manic episodes with (or without) depressive episodes. In MDD and BP, frequent findings are: (1) hypermetabolism with volume loss in the hippocampus and in the orbital and ventral PFC, and (2) hypometabolism in the dorsal PFC. Another study in MDD patients (Fitzgerald et al., 2008) reported constant hypoactivity in the cerebellum, insula, and frontal and temporal cortices. An increase in the activity of these areas correlates with anti-depressant treatment. Similarly, a recent work reported reduced regional homogeneity in the right insula and the left cerebellum in MMD patients and their siblings (Liu et al., 2010).

The cerebellum is likely to play an important role in modulating depressive symptoms; for example, it has been reported that high-frequency repetitive TMS over the cerebellum can cause a mood improvement in normal subjects and a significant reduction of depressive symptoms (Schutter and Honk, 2005). This is particularly interesting if we consider that this effect is probably dopamine-mediated; thus, the cerebellum is likely to exert a strong influence on the basal ganglia, regulating mood. Moreover, patients affected by SCA often show mild depression (Klinke et al., 2010), especially those with SCA1 and SCA6. A voxel-based morphometry study (Peng et al., 2010) reported GMD reductions in the bilateral insular cortex and left cerebellum in first-episode MDD patients, associated with decreased GMD also in the right medial and left lateral orbitofrontal cortex, right DLPFC, bilateral temporoparietal cortex, right superior temporal gyrus, and left parahyppocampal gyrus. Moreover, in MDD patients, the cerebellum, dorsal ACC, and precuneus show reduced connectivity with the orbital frontal cortex (Frodl et al., 2009).

As already explained, the cerebellum is connected with brain areas involved in emotional control, including the PFC and the hypothalamus (Zhu et al., 2006); however, a clear functional mechanism able to account for cerebellar involvement in mood regulation remains to be identified. Remarkably, MDD patients with psychotic disorders, when compared with MDD patients without psychotic disorders, show reduced perfusion of the left cerebellum and right superior frontal cortex, as well as increased perfusion of the left inferior PFC and caudate nucleus (Gonul et al., 2004). In addition to the intriguing aspects raised by this

lateralization, these observations suggest that, in MDD, cerebellar activity correlates more closely with psychotic traits (e.g., delusions of control) than with "pure" depressive symptoms. The cerebellum is also involved in BP, with bipolar patients found to show poor emotional homeostasis, mania, and cognitive dysfunctions (Strakowski et al., 2005) and, on MRI scanning, a volume reduction in region V2 and V3 of the cerebellar vermis (Mills et al., 2005; Monkul et al., 2008).

DYSLEXIA

Developmental dyslexia (DD) is characterized by a selective difficulty in acquiring reading skills, in spite of normal general intelligence (Habib, 2000). There are three main hypotheses regarding the core deficit responsible for DD symptoms: the magnosystem deficit hypothesis (MDH) (Stein, 2001), the phonological deficit hypothesis (PDH) (Ramus, 2003), and the cerebellar deficit hypothesis (CDH). The MDH takes its name from the "magnocellular neurons" of the lateral geniculate nucleus, which mostly feed the visual "dorsal stream" dedicated to the analysis of movement (the "where" pathway). Normal magnocellular function is necessary for high motion sensitivity and stable binocular perception which, in turn, are essential for proper development of orthographic skills. Many dyslexics show poor visual localization and their motion sensitivity is impaired, which suggests that abnormal development of the magnocellular system could play a pathogenetic role in DD. The PDH postulates that DD is caused by an impaired ability to represent and process speech sounds. The CDH, on the other hand, is based on the observation that dyslexic children show deficits in motor coordination, motor skills, and automatic processing, which suggests that a cerebellar dysfunction constitutes the neurological basis of the disease (Fawcett and Nicolson, 2004). Indeed, in a PET study, dyslexic subjects learning a motor sequence showed abnormalities in cerebellar activation during both automatic processing and new learning. An early cerebellar deficit has been hypothesized to impair the development of articulatory and writing skills (Nicolson et al., 2001b), and non-fluent articulation would engage more attentional resources, thereby impairing sensory feedback processing. It can thus be hypothesized that a cerebellar impairment causes a marked phonological deficit which, coupled with an automation deficit, results in DD. Cerebellar dysfunction can also explain the specific impairment in time estimation tasks shown by dyslexic subjects (Nicolson et al., 2001a). On the whole, the PDH can be seen as a part of the CDH. Conversely, the CDH does not completely explain the MDH, even though there is a subtype of DD characterized by magnocellular impairment (Tallal et al., 2006).

Dyslexics show small right cerebellar anterior lobes on MRI (Eckert et al., 2003), suggesting that a fronto-cerebellar circuit impairment could indeed cause the symptoms of DD. The right cerebellum is the brain area that best discriminates dyslexics from healthy control subjects (Pernet et al., 2009). Moreover, dyslexic subjects have symmetric cerebellar (as well as parietal and temporal cortex) gray matter, while healthy controls show a greater asymmetry (Hier et al., 1978; Rae et al., 2002). Therefore, there is substantial evidence that the cerebellum takes part in the pathogenesis of DD.

DISCUSSION

Recently, an impressive amount of new data has revealed a disconcerting heterogeneity of functional roles attributed to the cerebellum. Here we propose a unified framework that might provide a logical explanation of the numerous operations in which the cerebellum is involved.

DIFFERENT INTERPRETATIONS OR DISPARATE OPERATIONAL PROCESSES?

Ito, highlighting that the cerebellum can acquire forward models of a controlled object (e.g., the arm) through practice, proposes that the cerebellum uses internal models in order to adapt motor acts and mental activities to contextual information (Ito, 1993, 2008). By virtue of these models, the cerebellum is able to exert fast, precise, and automated control of well-learned movements. If we also think of thoughts and cognitive processes as controlled objects, the logical conclusion is that these same internal models can be applied to cognitive processing as well. This is hardly surprising, as mental products are virtual objects and there may not be much difference between a "thought" and a "thought to move."

Along the same lines, Vandervert conjectures that the cerebellum is engaged in a dynamic interplay with working memory; his main idea is that repetitive working memory processes are actively adapted by the cerebellum and that this must result in better and faster attentional control and, consequently, in more precise and better timed cognitive processes (Vandervert, 2003, 2007; Vandervert et al., 2007).

Again, a comparable theoretical framework was advanced some years ago by Courchesne and Allen (1997). They hypothesized that the main function of the cerebellum is to predict the internal conditions required for different cognitive and motor activities and to rapidly and precisely set those conditions. Arguably, this "predict and prepare" function of the cerebellum must be implemented mainly unconsciously and automatically. Accordingly, the cerebellum is thought to be involved in implicit learning and, on the contrary, not to play a relevant role in declarative, explicit learning (Doyon et al., 1997). The cerebellum is likely to adopt a "trial-and-error" learning rule, unlike the cerebral cortex and basal ganglia, which seem to learn, respectively, through frequency-based and reward-based rules (Doya, 2000).

Finally, Ivry suggested that the cerebellum is involved in every task requiring precise timing processes (Ivry et al., 2002), including the production of skilled movements, eye-blink conditioning, duration discrimination of perceptual events, fast and precise regulation of attention and working memory, and some specific linguistic skills.

Other proposals are that the cerebellum is directly involved in cognitive/emotional processes, insofar as these are linked to some kind of motor or oculomotor activity (Doron et al., 2010), and that the main function of the cerebellum is to regulate the acquisition of sensory data across several sensory modalities, and thus to support various sensory, motor, and cognitive functions (Petacchi et al., 2005).

Clearly, although these frameworks are valid for interpreting data sets relative to specific experiments or methodologies, the link between these observations has remained largely speculative or unaddressed. Moreover, the involvement of the cerebellum

in some cognitive functions, like attention, language, mental imagery, and reasoning, as well as in neuropsychiatric disorders and emotion, has remained obscure.

A UNIFIED INTERPRETATION THROUGH THE META-LEVELS HYPOTHESIS

What we suggest in this paper is that, as a result of modular connectivity with the cerebral cortex, causal relationships exist between the low- and high-level cognitive functions that the cerebellum is thought to play. Finally, we conjecture that failure of this system can lead to mental pathologies. The identified low-level functions, *timing, prediction, and learning*, directly implement structured cerebellar operations including forms of *working memory, error/novelty detection, and mental object manipulation*. On the one hand, timing, prediction, and learning have been related to cellular and network operations [e.g., see Medina and Mauk (2000); D'Angelo (2011); D'Angelo et al. (2011)], even though there is, as yet, no precise understanding of the mechanisms involved. On the other hand, these same functions may lie at the basis of more complex functions including *motor control, attention switching, language processing, imagery and visuospatial processing, decision-making, and reasoning*. Finally, major aspects of brain pathology can be predicted on the basis of these same low- and high-level functions. In some cases, direct evidence of these relationships has been demonstrated, while in others these inter-dependencies are still implicit, providing scope for testing of the hypothesis of cerebellar functioning based on its organization into meta-levels (**Figure 4**).

Timing seems the most fundamental of all the low-level functions. Timing may be directly explained on the basis of circuit mechanisms, whose cellular and synaptic components have been partly revealed [e.g., see D'Angelo and De Zeeuw (2009); D'Angelo et al. (2009)]. Timing is reflected in the ordering of complex sequences ordinarily processed by the cerebellum and it is deeply integrated with prediction and learning.

Sensory prediction, or, more generally, *prediction*, has been shown to predominate in motor control, attention switching, working memory, and language processing (Shadmehr and Mussa-Ivaldi, 2012), but it is also thought to intervene during imagery and visuospatial processing (which are also components of motor planning) and during decision-making and reasoning. So-called fluid intelligence, a form of cognitive control involved in executive functions (e.g., in the Tower of Hanoi test), rests on a dynamic sequence of selective attention, planning, storage in the working memory, hypothesis updating, attention redirecting, and so on. It is thought that the cerebellum is involved, at least when the problem is unusual and unexpected, according to its error/novelty-detection function. The circuits underlying prediction are unclear. It can be supposed that different inputs collide in proper time frames generating patterns that can, at some level, be recognized by pattern detectors. A model based on timing control in the granular layer and pattern detection in the molecular layer has been proposed (D'Angelo, 2011).

Learning in the cerebellum, and the original concepts related to this, probably need to be revised and extended in the light of new cellular and system physiology data. On the one hand, the cerebellar cortex and nuclei are clearly endowed with numerous mechanisms of long-term synaptic plasticity and therefore probably undergo changes during activity not just at the parallel fiber-Purkinje cell synapse, but also at other synaptic sites (Hansel et al., 2001; Jorntell and Hansel, 2006; Ohtsuki et al., 2009; Gao et al., 2012). These distributed changes could have very different meanings, for example that of controlling the spatiotemporal dynamics of signal processing in the granular layer and perceptron operations in Purkinje cells. On the other hand, functional imaging shows that the cerebellum is primarily involved when unknown problems or circumstances are encountered. This suggests that the cerebellum can incorporate specialized forms of procedural memory that can be reconfigured and transmitted to other brain areas. This learning can modify cerebellar spatiotemporal processing in terms of timing, pattern recognition, and coincidence detection, ultimately affecting the internal forward model and the consequent predictive properties. Cerebellar learning could contribute to working memory.

A puzzling implication of all this is that cerebellar processing might, ultimately, take part in generating *conscious and coherent representations of the world*, a function typically ascribed to the thalmo-cortical loops. Indeed, rapid continuous cerebellar processing in the cerebellar circuit through feedforward independent modules could enhance the immediate and continuous representation of events, which is one of the key aspects of consciousness (Addis et al., 2009; Nyberg et al., 2010; Szpunar, 2010, 2011). Also worth noting is the specific involvement of the cerebellum in elaborating *problems of a statistical nature*. In this case, it can be imagined that, by imposing an internal dynamic model, the cerebellum helps to automatically elaborate the trend in a complex data distribution on the basis of its previous acquisition of the most probable data sets. Interestingly, many biologically relevant problems have a statistical nature and the role of the cerebellum in this sense should be further explored.

A dramatic translation of low-level into high-level functions is observed in mental processing and even more clearly in the related dysfunction occurring in certain brain diseases. In *schizophrenia*, there is major failure of prediction-based comparison between internal and external representations, and of coordinate transformation and therefore manipulation of mental models. Similarly, *autism* involves a failure in redirecting attention, which can either be locked into internal contents or be hyperfocused on selective objects. In *depression*, psychotic symptoms may be regarded as a loss of internal coherence between internally and externally generated signals, with consequent dysregulation of mood homeostasis. Finally, in *dyslexia*, a combination of failures in the phonological loop involving working memory and recognition and manipulation of mental objects could be involved.

CONCLUSIONS

The meta-levels hypothesis provides a key through which to order the multitude of manifestations of cerebellar physiology and pathology and reconcile the basic cerebellar functional mechanisms with the emerging properties of the network. The meta-levels hypothesis leads to testable predictions and opens the ways for new experimental designs. These can be broadly divided into those addressing (1) how the olivo-cerebellar system generates

its internal representations and operations, (2) how the emerging functions derive from connections of the cerebellum with other brain structures, and (3) how dysfunction of the system could lead to pathology. In general, tools like genetic engineering in experimental animals, large-scale mathematical modeling and non-invasive stimulation/recording technology (like TMS and fMRI) in humans could provide valuable information. For example, genetic mutations impairing LTP (Long-Term Potentiation) or LTD (Long-Term Depression) could be used to investigate the potential role of the various forms of long-term synaptic plasticity expressed by cerebellar synapses not just with respect to motor learning but also with respect to cognitive processing extending through the CTCCs. Moreover, the role of cellular properties on circuit and system computations could be analyzed using detailed mathematical models, the CTCCs could be investigated by DTI, and their functional activation during specific tasks identified by fMRI. These same techniques could improve brain disease analysis and therapy. For example, cerebellar TMS has an impact on different pathologies, including Parkinson's disease (Koch et al., 2009a), epilepsy (Brighina et al., 2006), and stroke (Webster et al., 2006). Ultimately, this analysis could contribute to the development of a theory on global brain functioning in which the cerebellum is considered an integral part and not just a structure purely devoted to motor control.

ACKNOWLEDGMENTS

This work was supported by the European Union (CEREBNET FP7-ITN238686 and REALNET FP7-ICT270434) and by the Italian Ministry of Health (RF-2008-1143418 and RF-2009-1475845) to Egidio D'Angelo.

REFERENCES

Ackermann, H., Gräber, S., Hertrich, I., and Daum, I. (1997). Categorical speech perception in cerebellar disorders. *Brain Lang.* 60, 323–331.

Addis, D. R., Pan, L., Vu, M. A., Laiser, N., and Schacter, D. L. (2009). Constructive episodic simulation of the future and the past: distinct subsystems of a core brain network mediate imagining and remembering. *Neuropsychologia* 47, 2222–2238.

Ahissar, E., Sosnik, R., and Haidarliu, S. (2000). Transformation from temporal to rate coding in a somatosensory thalamocortical pathway. *Nature* 406, 302–306.

Alahyane, N., Fonteille, V., Urquizar, C., Salemme, R., Nighoghossian, N., Pelisson, D., et al. (2008). Separate neural substrates in the human cerebellum for sensory-motor adaptation of reactive and of scanning voluntary saccades. *Cerebellum* 7, 595–601.

Albus, J. S. (1972). A theory of cerebellar function. *Math. Biosci.* 10, 25–61.

Allen, G., Buxton, R. B., Wong, E. C., and Courchesne, E. (1997). Attentional activation of the cerebellum independent of motor involvement. *Science* 275, 1940–1943.

Amodio, D. M., and Frith, C. D. (2006). Meeting of minds: the medial frontal cortex and social cognition. *Nature* 7, 268–277.

Andersson, G., and Oscarsson, O. (1978). Climbing fiber microzones in cerebellar vermis and their projection to different groups of cells in the lateral vestibular nucleus. *Exp. Brain Res.* 32, 565–579.

Andreasen, N. C., O'Leary, D. S., Cizadlo, T., Arndt, S., Rezai, K., Ponto, L. L., et al. (1996). Schizophrenia and cognitive dysmetria: a positron-emission tomography study of dysfunctional prefrontal-thalamic-cerebellar circuitry. *Proc. Natl. Acad. Sci. U.S.A.* 93, 9985–9990.

Andreasen, N. C., Paradiso, S., and O'Leary, D. S. (1998). "Cognitive dysmetria" as an integrative theory of schizophrenia: a dysfunction in cortical-subcortical-cerebellar circuitry? *Schizophr. Bull.* 24, 203–218.

APA. (1994). *Diagnostic and Statistical Manual of Mental Disorders 4*. Washington, DC: American Psychiatric Association.

Apps, R., and Garwicz, M. (2005). Anatomical and physiological foundations of cerebellar information processing. *Nat. Rev. Neurosci.* 6, 297–311.

Apps, R., and Hawkes, R. (2009). Cerebellar cortical organization: a one-map hypothesis. *Nat. Rev. Neurosci.* 10, 670–681.

Argyropoulos, G. P. (2011). Cerebellar theta-burst stimulation selectively enhances lexical associative priming. *Cerebellum* 10, 540–550.

Arriada-Mendicoa, N., Otero-Siliceo, E., and Corona-Vazquez, T. (1999). [Current concepts regarding the cerebellum and cognition]. *Rev. Neurol.* 29, 1075–1082.

Baddeley, A., Lewis, V., Eldridge, M., and Thomson, N. (1984). Attention and retrieval from long-term memory. *J. Exp. Psychol.* 113, 518–540.

Balsters, J. H., and Ramnani, N. (2008). Symbolic representations of action in the human cerebellum. *Neuroimage* 43, 388–398.

Bartolo, P. D., Gelfo, F., Burello, L., Giorgio, A. D., Petrosini, L., and Granato, A. (2011). Plastic changes in striatal fast-spiking interneurons following hemicerebellectomy and environmental enrichment. *Cerebellum* 10, 624–632.

Battaglia, F., Quartarone, A., Ghilardi, M. F., Dattola, R., Bagnato, S., Rizzo, V., et al. (2006). Unilateral cerebellar stroke disrupts movement preparation and motor imagery. *Clin. Neurophysiol.* 117, 1009–1016.

Bauman, M. L., and Kemper, T. L. (2005). Neuroanatomic observations of the brain in autism: a review and future directions. *Int. J. Dev. Neurosci.* 23, 183–187.

Bedny, M., McGill, M., and Thompson-Schill, L. S. (2008). Semantic adaptation and competition during word comprehension. *Cereb. Cortex* 18, 2574–2585.

Beldarrain, M. G., García-Moncó, J., Quintana, J., Llorens, V., and Rodeño, E. (1997). Diaschisis and neuropsychological performance after cerebellar stroke. *Eur. Neurol.* 37, 82–89.

Bell, C. C., Han, V., and Sawtell, N. B. (2008). Cerebellum-like structures and their implications for cerebellar function. *Annu. Rev. Neurosci.* 31, 1–24.

Blackwood, N., Ffytche, D., Simmons, A., Bentallc, R., Murray, R., and Howard, R. (2004). The cerebellum and decision making under uncertainty. *Brain Res. Cogn. Brain Res.* 20, 46–53.

Blakemore, S.-J., Frith, C. D., and Wolpert, D. M. (2001). The cerebellum is involved in predicting the sensory consequences of action. *Neuroreport* 12, 1879–1884.

Blakemore, S.-J., and Sirigu, A. (2003). Action prediction in the cerebellum and in the parietal lobe. *Exp. Brain Res.* 153, 239–245.

Blakemore, S.-J., Wolpert, D. M., and Frith, C. D. (1998a). Central cancellation of self-produced tickle sensation. *Nature* 1, 635–640.

Blakemore, S. J., Goodbody, S. J., and Wolpert, D. M. (1998b). Predicting the consequences of our own actions: the role of sensorimotor context estimation. *J. Neurosci.* 18, 7511–7518.

Blakemore, S.-J., Wolpert, D. M., and Frith, C. D. (1999). The cerebellum contributes to somatosensory cortical activity during self-produced tactile stimulation. *Neuroimage* 10, 448–459.

Booth, J. R., Wood, L., Lu, D., Houk, J. C., and Bitan, T. (2007). The role of the basal ganglia and cerebellum in language processing. *Brain Res.* 1133, 136–144.

Boso, M., Emanuele, E., Prestori, F., Politi, P., Barale, F., and D'Angelo, E. (2010). Autism and genius: is there a link? The involvement of central brain loops and hypotheses for functional testing. *Funct. Neurol.* 25, 15–20.

Bostan, A. C., and Strick, P. L. (2010). The cerebellum and basal ganglia are interconnected. *Neuropsychol. Rev.* 20, 261–270.

Bottmer, C., Bachmann, S., Pantel, J., Essig, M., Amann, M., Schad, L. R., et al. (2005). Reduced cerebellar volume and neurological soft signs in first-episode schizophrenia. *Psychiatry Res.* 140, 239–250.

Bower, J. M. (1997). Is the cerebellum sensory for motor's sake, or motor for sensory's sake: the view from the whiskers of a rat? *Prog. Brain Res.* 114, 463–496.

Bower, J. M. (2002). The organization of cerebellar cortical circuitry revisited: implications for function. *Ann. N.Y. Acad. Sci.* 978, 135–155.

Brighina, F., Daniele, O., Piazza, A., Giglia, G., and Fierro, B. (2006). Hemispheric cerebellar rTMS to treat drug-resistant epilepsy: case reports. *Neurosci. Lett.* 397, 229–233.

Brunet, E., Sarfati, Y., Hardy-Bayle, M.-C., and Decety, J. (2000). A PET investigation of the attribution of

intentions with a nonverbal task. *Neuroimage* 11, 157–166.
Burguière, E., Arleo, A., Hojjati, Mr., Elgersma, Y., Zeeuw, C. I. D., Berthoz, A., et al. (2005). Spatial navigation impairment in mice lacking cerebellar LTD: a motor adaptation deficit. *Nature* 8, 1292–1294.
Buzsaki, G. (2006). *Rhythms of the Brain*. New York, NY: Oxford University Press US.
Cerminara, N. L. (2010). Cerebellar modules: individual or composite entities? *J. Neurosci.* 30, 16065–16067.
Churchland, P. (1998). *Toward a Neurobiology of the Mind*. London, England: MIT Press.
Churchland, P., and Sejinowski, T. (1992). *The Computational Brain*. Cambridge, MA: MIT Press.
Clower, D. M., Dum, R. P., and Strick, P. L. (2005). Basal ganglia and cerebellar inputs to "AIP". *Cereb. Cortex* 15, 913–920.
Clower, D. M., West, R. A., Lynch, J. C., and Strick, P. L. (2001). The inferior parietal lobule is the target of output from the superior colliculus, hippocampus, and cerebellum. *J. Neurosci.* 21, 6283–6291.
Coghill, R. C., Sang, C. N., Maisog, J. M., and Iadarola, M. J. (1999). Pain intensity processing within the human brain: a bilateral, distributed mechanism. *J. Neurophysiol.* 82, 1934–1943.
Colnaghi, S., Ramat, S., D'Angelo, E., and Versino, M. (2010). Transcranial magnetic stimulation over the cerebellum and eye movements: state of the art. *Funct. Neurol.* 25, 165–171.
Connor, L. T., Braby, T. D., Snyder, A. Z., Lewis, C., Blasi, V., and Corbetta, M. (2006). Cerebellar activity switches hemispheres with cerebral recovery in aphasia. *Neuropsychologia* 44, 171–177.
Cotterill, R. M. (2001). Cooperation of the basal ganglia, cerebellum, sensory cerebrum and hippocampus: possible implications for cognition, consciousness, intelligence and creativity. *Prog. Neurobiol.* 64, 1–33.
Courchesne, E., and Allen, G. (1997). Prediction and preparation, fundamental functions of the cerebellum. *Learn. Mem.* 4, 1–35.
Courchesne, E., Townsend, J., Akshoomoff, N. A., Saitoh, O., Yeung-Courchesne, R., Lincoln, A. J., et al. (1994a). Impairment in shifting attention in autistic and cerebellar patients. *Behav. Neurosci.* 108, 848–865.
Courchesne, E., Townsend, J., and Saitoh, O. (1994b). The brain in infantile autism Posterior fossa structures are abnormal. *Neurology* 44, 214–223.
Craik, F. I., Govoni, R., Naveh-Benjamin, M., and Anderson, N. D. (1996). The effects of divided attention on encoding and retrieval processes in human memory. *J. Exp. Psychol.* 125, 159–180.
Crespo-Facorro, B., Paradiso, S., Andreasen, N. C., O'Leary, D. S., Watkins, G. L., Ponto, L. L. B., et al. (1999). Recalling word lists reveals "cognitive dysmetria" in schizophrenia: a positron emission tomography study. *Am. J. Psychiatry* 156, 386–392.
Critchley, H., Daly, E., Phillips, M., Brammer, M., Bullmore, E., Williams, S., et al. (2000a). Explicit and implicit neural mechanisms for processing of social information from facial expressions: a functional magnetic resonance imaging study. *Hum. Brain Mapp.* 9, 93–105.
Critchley, H. D., Daly, E. M., Bullmore, E. T., Williams, S. C., Amelsvoort, T. V., Robertson, D. M., et al. (2000b). The functional neuroanatomy of social behaviour changes in cerebral blood flow when people with autistic disorder process facial expressions. *Brain* 123, 2203–2212.
Cui, S.-Z., Li, E.-Z., Zang, Y.-F., Weng, X.-C., Ivry, R., and Wang, J.-J. (2000). Both sides of human cerebellum involved in preparation and execution of sequential movements. *Neuroreport* 11, 1–5.
D'Angelo, E. (2010a). Neuronal circuit function and dysfunction in the cerebellum: from neurons to integrated control. *Funct. Neurol.* 25, 125–127.
D'Angelo, E. (2010b). Rebuilding cerebellar network computations from cellular neurophysiology. *Front. Cell. Neurosci.* 4:131. doi: 10.3389/fncel.2010.00131
D'Angelo, E. (2011). Neural circuits of the cerebellum: hypothesis for function. *J. Integr. Neurosci.* 10, 317–352.
D'Angelo, E., and De Zeeuw, C. I. (2009). Timing and plasticity in the cerebellum: focus on the granular layer. *Trends Neurosci.* 32, 30–40.
D'Angelo, E., Koekkoek, S. K., Lombardo, P., Solinas, S., Ros, E., Garrido, J., et al. (2009). Timing in the cerebellum: oscillations and resonance in the granular layer. *Neuroscience* 162, 805–815.
D'Angelo, E., Mazzarello, P., Prestori, F., Mapelli, J., Solinas, S., Lombardo, P., et al. (2010). The cerebellar network: from structure to function and dynamics. *Brain Res. Rev*. 66, 5–15.
D'Angelo, E., Mazzarello, P., Prestori, F., Mapelli, J., Solinas, S., Lombardo, P., et al. (2011). The cerebellar network: from structure to function and dynamics. *Brain Res. Rev.* 66, 5–15.
Dean, P., Porrill, J., and Stone, J. V. (2004). Visual awareness and the cerebellum: possible role of decorrelation control *Prog. Brain Res.* 144, 61–75.
Debas, K., Carrier, J., Orban, P., Barakat, M., Lungu, O., Vandewalle, G., et al. (2010). Brain plasticity related to the consolidation of motor sequence learning and motor adaptation. *Proc. Natl. Acad. Sci. U.S.A.* 107, 17839–17844.
Desmond, J. E., Chen, S. H., and Perry, B., and Shieh, M. (2005). Cerebellar transcranial magnetic stimulation impairs verbal working memory. *Ann. Neurol.* 58, 553–560.
Desmond, J. E., Gabrieli, J. D., Wagner, A. D., Ginier, B. L., and Glover, G. H. (1997). Lobular patterns of cerebellar activation in verbal working-memory and finger-tapping tasks as revealed by functional, MRI. *J. Neurosci.* 17, 9675–9685.
De Zeeuw, C. I., Hoebeek, F. E., Bosman, L. W., Schonewille, M., Witter, L., and Koekkoek, S. K. (2011). Spatiotemporal firing patterns in the cerebellum. *Nat. Rev. Neurosci.* 12, 327–344.
Diedrichsen, J., Shadmehr, R., and Ivry, R. B. (2010). The coordination of movement: optimal feedback control and beyond. *Trends Cogn. Sci.* 14, 31–39.
Diener, H.-C., and Dichgans, J. (1992). Pathophysiology of cerebellar ataxia. *Mov. Disord.* 7, 95–109.
Dieudonné, S., and Dumoulin, A. (2000). Serotonin-driven long-range inhibitory connections in the cerebellar cortex. *J. Neurosci.* 20, 1837–1848.
Dolan, R. J., Bench, C. J., Liddle, P. F., Friston, K. J., Frith, C. D., Grasby, P. M., et al. (1993). Dorsolateral prefrontal cortex dysfunction in the major psychoses; symptom or disease specificity? *J. Neurol. Neurosurg. Psychiatry* 56, 1290–1294.
Doron, K. W., Funk, C. M., and Glickstein, M. (2010). Fronto-cerebellar circuits and eye movement control: a diffusion imaging tractography study of human cortico-pontine projections. *Brain Res.* 1307, 63–71.
Douglas, R. J., and Martin, K. A. (2004). Neuronal circuits of the neocortex. *Annu. Rev. Neurosci.* 27, 419–451.
Doya, K. (2000). Complementary roles of basal ganglia and cerebellum in learning and motor control. *Curr. Opin. Neurobiol.* 10, 732–739.
Doyon, J., Gaudreau, D., Laforce, R. Jr., Castonguay, M., Bédard, P. J., Bédardd, F., et al. (1997). Role of the striatum, cerebellum, and frontal lobes in the learning of a visuomotor sequence. *Brain Cogn.* 34, 218–245.
Doyon, J., Penhuneb, V., and Ungerleiderc, L. G. (2003). Distinct contribution of the cortico-striatal and cortico-cerebellar systems to motor skill learning. *Neuropsychologia* 41, 252–262.
Doyon, J., Song, A. W., Karni, A., Lalonde, F., Adams, M. M., and Ungerleider, L. G. (2002). Experience-dependent changes in cerebellar contributions to motor sequence learning. *Proc. Natl. Acad. Sci. U.S.A.* 99, 1017–1022.
Drepper, J., Timmann, D., Kolb, F. P., and Diener, H. C. (1999). Expand+Non-motor associative learning in patients with isolated degenerative cerebellar disease. *Brain* 122, 87–97.
Boisgueheneuc, F. D., Levy, R., Volle, E., Seassau, M., Duffau, H., Kinkingnehun, S., et al. (2006). Functions of the left superior frontal gyrus in humans: a lesion study. *Brain* 129, 3315–3328.
Dum, R. P., and Strick, P. L. (2003). An unfolded map of the cerebellar dentate nucleus and its projections to the cerebral cortex. *J. Neurophysiol.* 89, 634–639.
Eccles, J. C., Ito, M., and Szentagothai, J. (1967). *The Cerebellum as a Neural Machine*. Berlin, Heidelberg, New York: Springer-Verlag.
Eckert, M. A., Leonard, C. M., Richards, T. L., Aylward, E. H., Thomson, J., and Berninger, V. W. (2003). Anatomical correlates of dyslexia: frontal and cerebellar findings. *Brain* 126, 482–494.
Elston, G. N., and DeFelipe, J. (2002). Spine distribution in cortical pyramidal cells: a common organizational principle across species. *Prog. Brain Res.* 136, 109–133.
Fales, C. L., Barch, D. M., Rundle, M. M., Mintun, M. A., Snyder, A. Z., Cohen, J. D., et al. (2008). Altered emotional interference processing in affective and cognitive-control brain circuitry in major depression. *Biol. Psychiatry* 63, 377–384.
Fawcett, A., and Nicolson, R. (2004). Dyslexia: the role of the cerebellum. *Electron. J. Res. Edu. Psychol.* 2, 35–58.
Fink, G. R., Marshall, J. C., Shah, N. J., Weiss, P. H., Halligan, P. W.,

Grosse-Ruyken, M., et al. (2000). Line bisection judgments implicate right parietal cortex and cerebellum as assessed by fMRI. *Neurology* 54, 1324–1331.

Fitzgerald, P. B., Laird, A. R., Maller, J., and Daskalakis, Z. J. (2008). A meta-analytic study of changes in brain activation in depression. *Hum. Brain Mapp.* 29, 683–695.

Flourens, M.-J.-P. (1824). *Recherches Expèrimentales sur les Propriétés et les Fonctions du Système Nerveux dans les Animaux Vertébres*. Paris: Crevot.

Foti, F., Mandolesi, L., Cutuli, D., Laricchiuta, D., Bartolo, P. D., Gelfo, F., et al. (2010). Cerebellar damage loosens the strategic use of the spatial structure of the search space. *Cerebellum* 9, 29–41.

Frings, M., Maschke, M., Gerwig, M., Diener, H.-C., and Timmann, D. (2006). Acquisition of simple auditory and visual sequences in cerebellar patients. *Cerebellum* 5, 206–211.

Frith, U., Morton, J., and Leslie, A. M. (1991). The cognitive basis of a biological disorder: autism. *Trends Neurosci.* 14, 433–438.

Frodl, T., Bokde, A. L. W., Scheuerecker, J., Lisiecka, D., Schoepf, V., Hampel, H., et al. (2009). Functional connectivity bias of the orbitofrontal cortex in drug-free patients with major depression. *Biol. Psychiatry* 67, 161–167.

Fusar-Poli, P., Placentino, A., Carletti, F., Landi, P., Allen, P., Surguladze, S., et al. (2009). Functional atlas of emotional faces processing: a voxel-based meta-analysis of 105 functional magnetic resonance imaging studies. *J. Psychiatry Neurosci.* 34, 418.

Gao, Z., van Beugen, B. J., and De Zeeuw, C. I. (2012). Distributed synergistic plasticity and cerebellar learning. *Nat. Rev. Neurosci*. 13, 619–635.

Garrard, P., Martin, N. H., Giunti, P., and Cipolotti, L. (2008). Cognitive and social cognitive functioning in spinocerebellar ataxia. *J. Neurol.* 255, 398–405.

Gebhart, A. L., Petersen, S. E., and Thach, W. T. (2002). Role of the posterolateral cerebellum in language. *Ann. N.Y. Acad. Sci.* 978, 318–333.

Gerardin, E., Sirigu, A., Lehéricy, S., Poline, J.-B., Gaymard, B., Marsault, C., et al. (2000). Partially overlapping neural networks for real and imagined hand movements. *Cereb. Cortex* 10, 1093–1104.

Ghajar, J., and Ivry, R. B. (2009). The predictive brain state: asynchrony in disorders of attention? *Neuroscientist* 15, 232–243.

Goel, V., Buchel, C., Frith, C., and Dolan, R. J. (2000). Dissociation of mechanisms underlying syllogistic reasoning. *Neuroimage* 12, 504–514.

Goel, V., and Dolan, R. J. (2001). Functional neuroanatomy of three-term relational reasoning. *Neuropsychologia* 39, 901–909.

Goel, V., and Dolan, R. J. (2004). Differential involvement of left prefrontal cortex in inductive and deductive reasoning. *Cognition* 93, 109–121.

Goffart, L., Chen, L., and Sparks, D. (2003). Saccade dysmetria during functional perturbation of the caudal fastigial nucleus in the monkey. *Annu. N.Y. Acad. Sci.* 1004, 220–228.

Gonul, A. S., Kula, M., Bilgin, A. G., Tutus, A., and Oguz, A. (2004). The regional cerebral blood flow changes in major depressive disorder with and without psychotic features. *Prog. Neuropsychopharmacol. Biol. Psychiatry* 28, 1015–1021.

González, B., Rodríguez, M., Ramirez, C., and Sabaté, M. (2005). Disturbance of motor imagery after cerebellar stroke. *Behav. Neurosci.* 119, 622–626.

Gottwald, B., Wilde, B., Mihajlovic, Z., and Mehdorn, H. M. (2004). Evidence for distinct cognitive deficits after focal cerebellarlesions. *J. Neurol. Neurosurg. Psychiatry* 75, 1524–1531.

Grealy, M. A., and Lee, D. N. (2011). An automatic-voluntary dissociation and mental imagery disturbance following a cerebellar lesion. *Neuropsychologia* 49, 271–275.

Grefkes, C., Ritzla, A., Zillesa, K., and Fink, G. R. (2004). Human medial intraparietal cortex subserves visuomotor coordinate transformation. *Neuroimage* 23, 1494–1506.

Grefkes, C., Weiss, P. H., Zilles, K., and Fink, G. R. (2002). Crossmodal processing of object features in human anterior intraparietal cortex: an fMRI study implies equivalencies between humans and monkeys. *Neuron* 35, 173–184.

Guerrasio, L., Quinet, J., Büttner, U., and Goffart, L. (2009). Fastigial oculomotor region and the control of foveation during fixation. *J. Neurophysiol.* 103, 1988–2001.

Guggisberg, A. G., Dalal, S. S., Findlay, A. M., and Nagarajan, S. S. (2007). High-frequency oscillations in distributed neural networks reveal the dynamics of human decision making. *Front. Hum. Neurosci.* 1:14. doi: 10.3389/neuro.09.014.2007

Habas, C., Kamdar, N., Nguyen, D., Keller, K., Beckmann, C. F., Menon, V., et al. (2009). Distinct cerebellar contributions to intrinsic connectivity networks. *J. Neurosci.* 29, 8586–8594.

Habib, M. (2000). The neurological basis of developmental dyslexia. *Brain* 123, 2373–2399.

Haines, D. D. E., May, P. J., and Dietrichs, E. (1990). Neuronal connections between the cerebellar nuclei and hypothalamus in *Macaca fascicularis*: cerebellovisceral circuits. *J. Comp. Neurol.* 299, 106–122.

Hansel, C., Linden, D. J., and D'Angelo, E. (2001). Beyond parallel fiber LTD: the diversity of synaptic and non-synaptic plasticity in the cerebellum. *Nat. Neurosci.* 4, 467–475.

Hashimoto, M., and Ohtsuka, K. (1995). Transcranial magnetic stimulation over the posterior cerebellum during visually guided saccades in man. *Brain* 118, 1185–1193.

Hashimoto, T., Tayama, M., Murakawa, K., Yoshimoto, T., Miyazaki, M., Harada, M., et al. (1995). Development of the brainstem and cerebellum in autistic patients. *J. Autism Dev. Disord.* 25, 1–18.

He, Y., and Zang, Y. (2004). Detecting functional connectivity of the cerebellum using Low Frequency Fluctuations (LFFs). *Lect. Notes Comp. Sci.* 3217, 907–915.

Heath, R. G., and Harper, J. W. (1974). Ascending projections of the cerebellar fastigial nucleus to the hippocampus, amygdala, and other temporal lobe sites: evoked potential and histological studies in monkeys and cats. *Exp. Neurol.* 45, 268–287.

Hier, D. B., LeMay, M., Rosenberger, P. B., and Perlo, V. P. (1978). Developmental dyslexia. Evidence for a subgroup with a reversal of cerebral asymmetry. *Arch. Neurol.* 35, 90–92.

Ishai, A., Ungerleider, L. G., and Haxby, J. V. (2000). Distributed neural systems for the generation of visual images. *Neuron* 28, 979–990.

Ito, M. (1984). *The Cerebellum and Neural Control*. New York, NY: Raven Press.

Ito, M. (1993). Movement and thought: identical control mechanisms by the cerebellum. *Trends Neurosci.* 16, 448–450. discussion: 453–444.

Ito, M. (2005). Bases and implications of learning in the cerebellum—adaptive control and internal model mechanism. *Prog. Brain Res.* 148, 95–109.

Ito, M. (2008). Control of mental activities by internal models in the cerebellum. *Nat. Rev. Neurosci.* 9, 304–313.

Ivry, R. B. (2000). Exploring the role of the cerebellum in sensory anticipation and timing: commentary on tesche and karhu. *Hum. Brain Mapp.* 9, 115–118.

Ivry, R. B., and Baldo, J. V. (1992). Is the cerebellum involved in learning and cognition? *Curr. Opin. Neurobiol.* 2, 212–216.

Ivry, R. B., and Keele, S. W. (1989). Timing functions of the cerebellum. *J. Cogn. Neurosci.* 1, 136–152.

Ivry, R. B., Spencer, R. M., Zelaznik, H. N., and Diedrichsen, J. (2002). The cerebellum and event timing. *Ann. N.Y. Acad. Sci.* 978, 302–317.

Jackson, P. L., Meltzoff, A. N., and Decety, J. (2005). How do we perceive the pain of others? A window into the neural processes involved in empathy. *Neuroimage* 24, 771–779.

Jacobson, G. A., Rokni, D., and Yarom, Y. (2008). A model of the olivocerebellar system as a temporal pattern generator. *Trends Neurosci.* 31, 617–625.

Johnson-Laird, P. N. (1980). Mental models in cognitive science. *Cogn. Sci.* 4, 71–115.

Johnson-Laird, P. N. (2001). Mental models and deduction. *Trends Cogn. Sci.* 5, 434–442.

Jorntell, H., and Hansel, C. (2006). Synaptic memories upside down: bidirectional plasticity at cerebellar parallel fiber-Purkinje cell synapses. *Neuron* 52, 227–238.

Justus, T., Ravizza, S. M., Fiez, J. A., and Ivry, R. B. (2005). Reduced phonological similarity effects in patients with damage to the cerebellum. *Brain Lang.* 95, 304–318.

Kelly, R. M., and Strick, P. L. (2003). Cerebellar loops with motor cortex and prefrontal cortex of a nonhuman primate. *J. Neurosci.* 23, 8432–8444.

Kim, C. H., Oh, S. H., Lee, J. H., Chang, S. O., Kim, J., and Kim, S. J. (2011). Lobule-specific membrane excitability of cerebellar Purkinje cells. *J. Physiol.* 590, 273–288.

Klinke, I., Minnerop, M., Schmitz-Hübsch, T., Hendriks, M., Klockgether, T., Wüllner, U., et al. (2010). Neuropsychological features of patients with Spinocerebellar Ataxia (SCA) types 1, 2, 3, and 6. *Cerebellum* 9, 433–442.

Koch, G., Brusa, L., Carrillo, F., Gerfo, E. L., Torriero, S., Oliveri, M., et al. (2009a). Cerebellar magnetic stimulation decreases

levodopa-induced dyskinesias in Parkinson disease. *Neurology* 73, 113–119.

Koch, G., Oliveri, M., and Caltagirone, C. (2009b). Neural networks engaged in milliseconds and seconds time processing: evidence from transcranial magnetic stimulation and patients with cortical or subcortical dysfunction. *Philos. Trans. R. Soc. Lond. B Biol. Sci.* 364, 1907–1918.

Konarski, J. Z., McIntyre, R. S., Grupp, L. A., and Kennedy, S. H. (2005). Is the cerebellum relevant in the circuitry of neuropsychiatric disorders? *J. Psychiatry Neurosci.* 30, 178–186.

Krienen, F. M., and Buckner, R. L. (2009). Segregated fronto-cerebellar circuits revealed by intrinsic functional connectivity. *Cereb. Cortex* 19, 2485–2497.

Kusunoki, M., Gottlieb, J., and Goldberg, M. E. (2000). The lateral intraparietal area as a salience map: the representation of abrupt onset, stimulus motion, and task relevance. *Vis. Res.* 40, 1459–1468.

Kyriakopoulos, M., Vyasa, N. S., Barkerb, G. J., Chitnisb, X. A., and Frangoua, S. (2008). A diffusion tensor imaging study of white matter in early-onset schizophrenia. *Biol. Psychiatry* 63, 519–523.

Lainé, J., and Axelrad, H. (1998). Lugaro cells target basket and stellate cells in the cerebellar cortex. *Neuroreport* 9, 2399–2403.

Langdon, R., Coltheart, M., Ward, P. B., and Catts, S. V. (2001). Visual and cognitive perspective-taking impairments in schizophrenia: a failure of allocentric simulation? *Cogn. Neuropsychiatry* 6, 241–269.

LeBeau, F. E., El Manira, A., and Griller, S. (2005). Tuning the network: modulation of neuronal microcircuits in the spinal cord and hippocampus. *Trends Neurosci.* 28, 552–561.

Lefèvre, P., Quaia, C., and Opticana, L. M. (1998). Distributed model of control of saccades by superior colliculus and cerebellum. *Neural Netw.* 11, 1175–1190.

Leggio, M. G., Silveri, M. C., Petrosini, L., and Molinari, M. (2000). Phonological grouping is specifically affected in cerebellar patients: a verbal fluency study. *J. Neurol. Neurosurg. Psychiatry* 69, 102–106.

Leggio, M. G., Tedesco, A. M., Chiricozzi, F. R., Clausi, S., Orsini, A., and Molinari, M. (2008). Cognitive sequencing impairment in patients with focal or atrophic cerebellar damage. *Brain* 131, 1332–1343.

Leroi, I., O'Hearn, E., Marsh, L., Lyketsos, C. G., Rosenblatt, A., Ross, C. A., et al. (2002). Psychopathology in patients with degenerative cerebellar diseases: a comparison to Huntington's disease. *Am. J. Psichiatry* 159, 1306–1314.

Liu, Z., Xu, C., Xu, Y., Wang, Y., Zhao, B., Lv, Y., et al. (2010). Decreased regional homogeneity in insula and cerebellum: a resting-state fMRI study in patients with major depression and subjects at high risk for major depression. *Psychiatry Res.* 182, 211–215.

Llinas, R., and Paré, D. (1998). *The Brain as a Closed System Modulated by the Senses*. London, England: MIT Press.

Llinás, R. R., and Roy, S. (2009). The "prediction imperative" as the basis for self-awareness. *Philos. Trans. R. Soc. Lond. B Biol. Sci.* 364, 1301–1307.

Lotze, M., Montoya, P., Erb, M., Hülsmann, E., Flor, H., Klose, U., et al. (1999). Activation of cortical and cerebellar motor areas during executed and imagined hand movements: an fMRI study. *J. Cogn. Neurosci.* 11, 491–501.

Lubke, J., and Feldmeyer, D. (2007). Excitatory signal flow and connectivity in a cortical column: focus on barrel cortex. *Brain Struct. Funct.* 212, 3–17.

Luciani, L. (1891). *Il Cervelletto. Nuovi Studi di Fisiologia Normale e Patologica*. Firenze: Le Monnier.

Luft, A. R., Manto, M.-U., and Taib, N. O. B. (2005). Modulation of motor cortex excitability by sustained peripheral stimulation: the interaction between the motor cortex and the cerebellum. *Cerebellum* 4, 90–96.

Maddox, W. T., Aparicio, P., Marchant, N. L., and Ivry, R. B. (2005). Rule-based category learning is impaired in patients with Parkinson's disease but not in patients with cerebellar disorders. *J. Cogn. Neurosci.* 17, 707–723.

Marien, P., Saerens, J., Nanhoe, R., Moens, E., Nagels, G., Pickut, B. A., et al. (1996). Cerebellar induced aphasia: case report of cerebellar induced prefrontal aphasic language phenomena supported by SPECT findings. *J. Neurol. Sci.* 144, 34–43.

Marr, D. (1969). A theory of cerebellar cortex. *J. Physiol.* 202, 437–470.

Matell, M. S., and Meck, W. H. (2004). Cortico-striatal circuits and interval timing: coincidence detection of oscillatory processes. *Cogn. Brain Res.* 21, 139–170.

Medina, J. F., and Mauk, M. D. (2000). Computer simulation of cerebellar information processing. *Nat. Neurosci.* 3(Suppl.), 1205–1211.

Mellet, E., Tzourio-Mazoyer, N., Bricogne, S., Mazoyer, B., Kosslyn, S. M., and Denis, M. (2000). Functional anatomy of high-resolution visual mental imagery. *J. Cogn. Neurosci.* 12, 98–109.

Miall, R. C., and Reckess, G. Z. (2002). The cerebellum and the timing of coordinated eye and hand tracking. *Brain Cogn.* 48, 212–226.

Middleton, F. A., and Strick, P. L. (2001). Cerebellar projections to the prefrontal cortex of the primate. *J. Neurosci.* 21, 700–712.

Milad, M. R., and Quirk, G. J. (2002). Neurons in medial prefrontal cortex signal memory for fear extinction. *Nature* 420, 70–74.

Mills, N. P., DelBello, M. P., Adler, C. M., and Strakowski, S. M. (2005). MRI analysis of cerebellar vermal abnormalities in bipolar disorder. *Am. J. Psichiatry* 162, 1530–1532.

Moberget, T., Karns, C. M., Deouell, L. Y., Lindgren, M., Knight, R. T., and Ivry, R. B. (2008). Detecting violations of sensory expectancies following cerebellar degeneration: a mismatch negativity study. *Neuropsychologia* 46, 2569–2579.

Molinari, M., Filippini, V., and Leggio, M. G. (2002). Neuronal plasticity of interrelated cerebellar and cortical networks. *Neuroscience* 3, 863–870.

Molinari, M., Petrosini, L., Misciagna, S., and Leggio, M. G. (2004). Visuospatial abilities in cerebellar disorders. *J. Neurol. Neurosurg. Psychiatry* 75, 235–240.

Monkul, E. S., Hatch, J. P., Sassi, R. B., Axelson, D., Brambilla, P., Nicoletti, M. A., et al. (2008). MRI study of the cerebellum in young bipolar patients. *Prog. Neuropsychopharmacol. Biol. Psychiatry* 32, 613–619.

Morgan, M. A., Romanskib, L. M., and LeDoux, J. E. (1993). Extinction of emotional learning: contribution of medial prefrontal cortex. *Neurosci. Lett.* 163, 109–111.

Mugnaini, E., Sekerková, G., and Martina, M. (2011). The unipolar brush cell: a remarkable neuron finally receiving deserved attention. *Brain Res. Rev.* 66, 220–245.

Nair, D. G., Purcott, K. L., Fuchs, A., Steinberg, F., and Kelso, J. A. S. (2003). Cortical and cerebellar activity of the human brain during imagined and executed unimanual and bimanual action sequences: a functional MRI study. *Brain Res. Cogn. Brain Res.* 15, 250–260.

Naito, E., Kochiyama, T., Kitada, R., Nakamura, S., Matsumura, M., Yonekura, Y., et al. (2002). Internally simulated movement sensations during motor imagery activate cortical motor areas and the cerebellum. *J. Neurosci.* 22, 3683–3691.

Nicolson, R. I., Fawcett, A. J., and Dean, P. (2001a). Developmental dyslexia: the cerebellar deficit hypothesis. *Trends Neurosci.* 24, 508–511.

Nicolson, R. I., Fawcett, A. J., Dean, P., Zeffiro, T., and Eden, G. (2001b). A TINS debate – Hindbrain versus the forebrain: a case for cerebellar deficit dyslexia: the cerebellar deficit hypothesis. *Trends Neurosci.* 24, 508–511.

Nyberg, L., Kim, A. S., Habib, R., Levine, B., and Tulving, E. (2010). Consciousness of subjective time in the brain. *Proc. Natl. Acad. Sci. U.S.A.* 107, 22356–22359.

Oberdick, J., and Sillitoe, R. V. (2011). Cerebellar zones: history, development, and function. *Cerebellum* 10, 301–306.

Ohtsuki, G., Piochon, C., and Hansel, C. (2009). Climbing fiber signaling and cerebellar gain control. *Front. Cell. Neurosci.* 3:4. doi: 10.3389/neuro.03.004.2009

Oliveri, M., Koch, G., Torriero, S., and Caltagirone, C. (2005). Increased facilitation of the primary motor cortex following 1 Hz repetitive transcranial magnetic stimulation of the contralateral cerebellum in normal humans. *Neurosci. Lett.* 376, 188–193.

Osherson, D., Perani, D., Cappa, S., Schnur, T., Grassi, F., and Fazio, F. (1998). Distinct brain loci in deductive versus probabilistic reasoning. *Neuropsychologia* 36, 369–376.

O'Reilly, J. X., Mesulam, M. M., and Nobre, A. C. (2008). The cerebellum predicts the timing of perceptual events. *J. Neurosci.* 28, 2252–2260.

Panouillères, M., Neggers, S., Gutteling, T., Salemme, R., Stigchel, S., Geest, J., et al. (2011). Transcranial magnetic stimulation and motor plasticity in human lateral cerebellum: dual effect on saccadic adaptation. *Hum. Brain Mapp.* 33, 1512–1525.

Pascual-Leone, A., Wassermann, E. M., Grafman, J., and Hallett, M. (1996). The role of the dorsolateral prefrontal cortex in implicit procedural learning. *Exp. Brain Res.* 107, 479–485.

Passot, J.-B., Rondi-Reig, L., and Arleo, A. (2009). Cerebellum and

spatial cognition: a connectionist approach. *Adv. Comput. Intell. Learn*. 287–292.

Pellionisz, A. J., and Llinàs, R. (1982). Space-time representation in the brain the cerebellum as a predictive space-time metric tensor. *Neuroscience* 7, 2949–2970.

Peng, J., Liu, J., Nie, B., Li, Y., Shan, B., Wang, G., et al. (2010). Cerebral and cerebellar gray matter reduction in first-episode patients with major depressive disorder: a voxel-based morphometry study. *Eur. J. Radiol.* 80, 395–399.

Pernet, C. R., Poline, J. B., Demonet, J. F., and Rousselet, G. A. (2009). Brain classification reveals the right cerebellum as the best biomarker of dyslexia. *BMC Neurosci.* 10:67. doi: 10.1186/1471-2202-10-67

Petacchi, A., Laird, A. R., Fox, P. T., and Bower, J. M. (2005). Cerebellum and auditory function: an ALE meta-analysis of functional neuroimaging studies. *Hum. Brain Mapp.* 25, 118–128.

Petrides, M. (2000). The role of the mid-dorsolateral prefrontal cortex in working memory. *Exp. Brain Res.* 133, 44–54.

Petrosini, L. (2007). "Do What I Do" and "Do How I Do": different components of imitative learning are mediated by different neural structures. *Neuroscientist* 13, 335–348.

Petrosini, L., Leggio, M. G., and Molinari, M. (1998). The cerebellum in the spatial problem solving: a co-star or a guest star? *Prog. Neurobiol.* 56, 191–210.

Pierce, K., and Courchesne, E. (2000). Evidence for a cerebellar role in reduced exploration and stereotyped behavior in autism. *Biol. Psychiatry* 49, 655–664.

Pijpers, A., Apps, R., Pardoe, J., Voogd, J., and Ruigrok, T. J. (2006). Precise spatial relationships between mossy fibers and climbing fibers in rat cerebellar cortical zones. *J. Neurosci.* 26, 12067–12080.

Ploghaus, A., Becerra, L., Borras, C., and Borsook, D. (2003). Neural circuitry underlying pain modulation: expectation, hypnosis, placebo. *Trends Cogn. Sci.* 7, 197–200.

Pochon, J.-B., Levy, R., Poline, J.-B., Crozier, S., Lehéricy, S., Pillon, B., et al. (2001). The role of dorsolateral prefrontal cortex in the preparation of forthcoming actions: an fMRI study. *Cereb. Cortex* 11, 260–266.

Prevosto, V., Graf, W., and Ugolini, G. (2010). Cerebellar inputs to intraparietal cortex areas LIP and MIP: functional frameworks for adaptive control of eye movements, reaching, and Arm/Eye/Head movement coordination. *Cereb. Cortex* 20, 214–228.

Rae, C., Harasty, J. A., Dzendrowskyj, T. E., Talcott, J. B., Simpson, J. M., Blamire, A. M., et al. (2002). Cerebellar morphology in developmental dyslexia. *Neuropsychologia* 40, 1285–1292.

Ramnani, N., Behrens, T. E., Johansen-Berg, H., Richter, M. C., Pinsk, M. A., Andersson, J. L., et al. (2006). The evolution of prefrontal inputs to the cortico-pontine system: diffusion imaging evidence from Macaque monkeys and humans. *Cereb. Cortex* 16, 811–818.

Ramnani, N., and Owen, A. M. (2004). Anterior prefrontal cortex: insights into function from anathomy and neuroimaging. *Nature* 5, 184–194.

Ramus, F. (2003). Developmental dyslexia: specific phonological deficit or general sensorimotor dysfunction? *Curr. Opin. Neurobiol.* 13, 212–218.

Ravizza, S. M., McCormick, C. A., Schlerf, J. E., Justus, T., Ivry, R. B., and Fiez, J. A. (2006). Cerebellar damage produces selective deficits in verbal working memory. *Brain* 129, 306–320.

Riby, D. M., and Hancock, P. J. B. (2008). Viewing it differently: social scene perception in Williams syndrome and Autism. *Neuropsychologia* 46, 2855–2860.

Richter, S., Kaiser, O., Hein-Kropp, C., Dimitrova, A., Gizewski, E., Beckc, A., et al. (2004). Preserved verb generation in patients with cerebellar atrophy. *Neuropsychologia* 42, 1235–1246.

Ridderinkhof, K. R., Ullsperger, M., Crone, E. A., and Nieuwenhuis, S. (2004). The role of the medial frontal cortex in cognitive control. *Science* 306, 443–447.

Ridler, K., Veijola, J. M., Tanskanen, P., Miettunen, J., Chitnis, X., Suckling, J., et al. (2006). Fronto-cerebellar systems are associated with infant motor and adult executive functions in healthy adults but not in schizophrenia. *Proc. Natl. Acad. Sci. U.S.A.* 103, 15651–15656.

Rissman, J., Eliassen, J. C., and Blumstein, S. E. (2003). An event-related fMRI investigation of implicit semantic priming. *J. Cogn. Neurosci.* 15, 1160–1175.

Robinson, F. R., Straube, A., and Fuchs, A. F. (1993). Role of the caudal fastigial nucleus in saccade generation. II. Effects of muscimol inactivation. *J. Neurophysiol.* 70, 1741–1758.

Rouiller, E. M., Liang, F., Babalian, A., Moret, V., and Wiesendanger, M. (1994). Cerebellothalamocortical and pallidothalamocortical projections to the primary and supplementary motor cortical areas: a multiple tracing study in macaque monkeys. *J. Comp. Neurol.* 345, 185–213.

Ruigrok, T. J. H. (2010). Ins and outs of cerebellar modules. *Cerebellum* 10, 464–474.

Rushworth, M. F. S., Behrens, T. E. J., and Johansen-Berg, H. (2006). Connection patterns distinguish 3 regions of human parietal cortex. *Cereb. Cortex* 16, 1418–1430.

Ryding, E., Decety, J., Sjöholm, H., Stenberg, G., and Ingvar, D. H. (1993). Motor imagery activates the cerebellum regionally. A SPECT rCBF study with 99mTc-HMPAO. *Brain Res. Cogn. Brain Res.* 1, 94–99.

Sacchetti, B., Scelfo, B., and Strata, P. (2005). The cerebellum: synaptic changes and fear conditioning. *Neuroscientist* 11, 217–227.

Salmi, J., Pallesen, K. J., Neuvonen, T., Brattico, E., Korvenoja, A., Salonen, O., et al. (2010). Cognitive and motor loops of the human cerebro-cerebellar system. *J. Cogn. Neurosci.* 22, 2663–2676.

Savitz, J., and Drevets, W. C. (2009). Bipolar and major depressive disorder: neuroimaging the developmental-degenerative divide. *Neurosci. Biobehav. Rev.* 33, 699–771.

Schaeken, W., Johnson-Laird, P. N., and D'Ydewalle, G. (1996). Mental models and temporal reasoning. *Cognition* 60, 205–234.

Schmahmann, J. D. (2004). Disorders of the cerebellum: ataxia, dysmetria of thought, and the cerebellar cognitive sffective syndrome. *J. Neuropsychiatry Clin. Neurosci.* 16, 367–378.

Schmahmann, J. D., and Caplan, D. (2006). Cognition, emotion and the cerebellum. *Brain* 129, 288–292.

Schmahmann, J. D., and Sherman, J. C. (1998). The cerebellar cognitive affective syndrome. *Brain* 121, 561–579.

Schmitt, J. E., Eliez, S., Warsofsky, I. S., Bellugi, U., and Reissa, A. L. (2001). Enlarged cerebellar vermis in Williams syndrome. *J. Psychiatr. Res.* 35, 225–229.

Schutter, D. J., and Honk, J. (2005). A framework for targeting alternative brain regions with repetitive transcranial magnetic stimulation in the treatment of depression. *J. Psychiatry Neurosci.* 30, 91–97.

Schweizer, T. A., Levine, B., Rewilak, D., O'Connor, C., Turner, G., Alexander, M. P., et al. (2007). Rehabilitation of executive functioning after focal damage to the cerebellum. *Neurorehabil. Neural Repair* 22, 72–77.

Seger, C. A., Desmond, J. E., Glover, G. H., and Gabrieli, J. D. E. (2000). Functional magnetic resonance imaging evidence for right-hemisphere involvement in processing unusual semantic relationships. *Neuropsychology* 14, 361–369.

Shadmehr, R., and Mussa-Ivaldi, S. (2012). *Biological Learning and Control*. Cambridge: MIT Press.

Shenton, M. E., Dickey, C. C., Frumin, M., and McCarley, R. W. (2001). A review of MRI findings in schizophrenia. *Schizophr. Res.* 49, 1–52.

Shin, J. C., and Ivry, R. B. (2003). Spatial and temporal sequence learning in patients with Parkinson's disease or cerebellar lesions. *J. Cogn. Neurosci.* 15, 1232–1243.

Silveri, M. C., Misciagna, S., and Terrezza, G. (2001). Right side neglect in right cerebellar lesion. *J. Neurol. Neurosurg. Psychiatry* 71, 114–117.

Smet, H. J. D., Baillieux, H., Deyn, P. P. D., Mariën, P., and Paquier, P. (2007). The cerebellum and language: the story so far. *Folia Phoniatr. Logop.* 59, 165–170.

Snider, R. S., and Maiti, A. (1976). Cerebellar contributions to the papez circuit. *J. Neurosci. Res.* 2, 133–146.

Spitzer, M. (1998). *The Mind Within the Net: Model of Learning, Thinking and Acting*. Cambridge: MIT Press.

Stein, J. (2001). The magnocellular theory of developmental dyslexia. *Dyslexia* 7, 12–36.

Stephan, K. E., Friston, K. J., and Frith, C. D. (2009). Dysconnection in schizophrenia: from abnormal synaptic plasticity to failures of self-monitoring. *Schizophr. Bull.* 35, 509–527.

Strakowski, S. M., Adler, C. M., Holland, S. K., Mills, N. P., DelBello, M. P., and Eliassen, J. C. (2005). Abnormal fMRI brain activation in euthymic bipolar disorder patients during a counting stroop interference task. *Am. J. Psichiatry* 162, 1697–1705.

Straube, A., and Buttner, U. (2007). *Neuro-Ophthalmology. Neuronal Control of Eye Movements*. Magdeburg: Karger.

Strick, P. L., Dum, R. P., and Fiez, J. A. (2009). Cerebellum and nonmotor function. *Annu. Rev. Neurosci.* 32, 413–434.

Synofzik, M., Lindner, A., and Thier, P. (2008). The cerebellum updates predictions about the visual consequences of one's behavior. *Curr. Biol.* 18, 814–818.

Synofzik, M., Thier, P., Leube, D. T., Schlotterbeck, P., and Lindner, A. (2010). Misattributions of agency in schizophrenia are based on imprecise predictions about the sensory consequences of one's actions. *Brain* 133, 262–271.

Szpunar, K. K. (2010). Evidence for an implicit influence of memory on future thinking. *Mem. Cognit.* 38, 531–540.

Szpunar, K. K. (2011). On subjective time. *Cortex* 47, 409–411.

Szwed, M., Bagdasarian, K., and Ahissar, E. (2003). Encoding of vibrissal active touch. *Neuron* 40, 621–630.

Takagi, M., Zee, D. S., and Tamargo, R. J. (1999). Effects of lesions of the oculomotor cerebellar vermis on eye movements in primate: smooth pursuit. *J. Neurophysiol.* 83, 2047–2062.

Tallal, P., Miller, S., and Holly, F. R. (2006). Neurobiological basis of speech: a case for the preeminence of temporal processing. *Ann. N.Y. Acad. Sci.* 682, 27–47.

Tavano, A., and Borgatti, R. (2010). Evidence for a link among cognition, language and emotion in cerebellar malformations. *Cortex* 46, 907–918.

Tilikete, C., Koene, A., Nighoghossian, N., Vighetto, A., and Pélisson, D. (2006). Saccadic lateropulsion in Wallenberg syndrome: a window to access cerebellar control of saccades? *Exp. Brain Res.* 174, 555–565.

Tononi, G., and Edelman, G. M. (1998). Consciousness and complexity. *Science* 282, 1846–1851.

Townsend, J., Courchesne, E., Covington, J., Westerfield, M., Harris, N. S., Lyden, P., et al. (1999). Spatial attention deficits in patients with acquired or developmental cerebellar abnormality. *J. Neurosci.* 19, 5632–5643.

Tunik, E., Frey, S. H., and Grafton, S. T. (2005). Virtual lesions of the anterior intraparietal area disrupt goal-dependent on-line adjustments of grasp. *Nature* 8, 505–511.

Turner, B. M., Paradiso, S., Marvel, C. L., Pierson, R., BolesPonto, L. L., Hichwa, R. D., et al. (2007). The cerebellum and emotional experience. *Neuropsychologia* 45, 1331–1341.

Uusisaari, M. Y., and Knopfel, T. (2012). Diversity of neuronal elements and circuitry in the cerebellar nuclei. *Cerebellum* 11, 420–421.

Vandervert, L. R. (2003). How working memory and cognitive modeling functions of the cerebellum contribute to discoveries in mathematics. *New Ideas Psychol.* 21, 15–29.

Vandervert, L. R. (2007). Cognitive functions of the cerebellum explain how Ericsson's deliberate practice produces giftedness. *High Abil. Stud.* 18, 89–92.

Vandervert, L. R., Schimpf, P. H., and Liu, H. (2007). How working memory and the cerebellum collaborate to produce creativity and innovation. *Creat. Res. J.* 19, 1–18.

Voogd, J. (2010). Cerebellar zones: a personal history. *Cerebellum* 10, 334–350.

Wang, S., Wu, D.-C., Ding, M.-P., Li, Q., Zhuge, Z.-B., Zhang, S.-H., et al. (2008). Low-frequency stimulation of cerebellar fastigial nucleus inhibits amygdaloid kindling acquisition in Sprague–Dawley rats. *Neurobiol. Dis.* 29, 52–58.

Watson, T. C., Jones, M. W., and Apps, R. (2009). Electrophysiological mapping of novel prefrontal–cerebellar pathways. *Front. Integr. Neurosci.* 3:18. doi: 10.3389/neuro.07.018.2009

Webster, B. R., Celnik, P. A., and Cohen, L. G. (2006). Noninvasive brain stimulation in stroke rehabilitation. *NeuroRX* 3, 474–481.

Weinberger, D. R., Berman, K. F., and Illowsky, B. P. (1988). Physiological dysfunction of dorsolateral prefrontal cortex in schizophrenia, I. I. I. A New Cohort and Evidence for a Monoaminergic Mechanism. *Arch. Gen. Psychiatry* 45, 609–615.

Weinberger, D. R., Berman, K. F., and Zec, R. F. (1986). Physiologic dysfunction of dorsolateral prefrontal cortex in schizophrenia, I. Regional cerebral blood flow evidence. *Arch. Gen. Psychiatry* 43, 114–124.

Wiech, K., Ploner, M., and Tracey, I. (2008). Neurocognitive aspects of pain perception. *Trends Cogn. Sci.* 12, 306–313.

Wolpert, D. M., Miall, R. C., and Kawato, M. (1998). Internal models in the cerebellum. *Trends Cogn. Sci.* 2, 338–347.

Xiang, H., Lin, C., Ma, X., Zhang, Z., Bower, J. M., Weng, X., et al. (2003). Involvement of the cerebellum in semantic discrimination: an fMRI study. *Hum. Brain Mapp.* 18, 208–214.

Xivry, J.-J., and Lefèvre, P. (2007). Saccades and pursuit: two outcomes of a single sensorimotor process. *J. Physiol.* 584, 11–23.

Yakusheva, T. A., Shaikh, A. G., Green, A. M., Blazquez, P. M., Dickman, J. D., and Angelaki, D. E. (2007). Purkinje cells in posterior cerebellar vermis encode motion in an inertial reference frame. *Neuron* 54, 973–985.

Zhu, J.-N., Yung, W.-H., Chow, B. K.-C., Chand, Y.-S., and Wanga, J.-J. (2006). The cerebellar-hypothalamic circuits: Potential pathways underlying cerebellar involvement in somatic-visceral integration. *Brain Res. Rev.* 52, 93–106.

Conflict of Interest Statement: The authors declare that the research was conducted in the absence of any commercial or financial relationships that could be construed as a potential conflict of interest.

Received: 18 August 2012; accepted: 17 December 2012; published online: 10 January 2013.

Citation: D'Angelo E and Casali S (2013) Seeking a unified framework for cerebellar function and dysfunction: from circuit operations to cognition. Front. Neural Circuits ***6****:116. doi: 10.3389/fncir.2012.00116*

frontiers in
NEURAL CIRCUITS

MINI REVIEW ARTICLE
published: 23 April 2013
doi: 10.3389/fncir.2013.00072

The olivo-cerebellar system and its relationship to survival circuits

Thomas C. Watson[1], Stella Koutsikou[1], Nadia L. Cerminara[1], Charlotte R. Flavell[2], Jonathan J. Crook[1], Bridget M. Lumb[1] and Richard Apps[1]*

[1] School of Physiology and Pharmacology, Medical Sciences Building, University of Bristol, University Walk, Bristol, UK
[2] Queensland Brain Institute, The University of Queensland, Brisbane, QLD, Australia

Edited by:
Egidio D'Angelo, University of Pavia, Italy

Reviewed by:
Yosef Yarom, Hebrew University, Israel
Ilker Ozden, Brown University, USA

***Correspondence:**
Richard Apps, School of Physiology and Pharmacology, Medical Sciences Building, University of Bristol, University Walk, Bristol BS8 1TD, UK.
e-mail: r.apps@bristol.ac.uk

How does the cerebellum, the brain's largest sensorimotor structure, contribute to complex behaviors essential to survival? While we know much about the role of limbic and closely associated brainstem structures in relation to a variety of emotional, sensory, or motivational stimuli, we know very little about how these circuits interact with the cerebellum to generate appropriate patterns of behavioral response. Here we focus on evidence suggesting that the olivo-cerebellar system may link to survival networks via interactions with the midbrain periaqueductal gray, a structure with a well known role in expression of survival responses. As a result of this interaction we argue that, in addition to important roles in motor control, the inferior olive, and related olivo-cortico-nuclear circuits, should be considered part of a larger network of brain structures involved in coordinating survival behavior through the selective relaying of "teaching signals" arising from higher centers associated with emotional behaviors.

Keywords: cerebellum, inferior olive, periaqueductal gray, survival, modules

INTRODUCTION

A neural network of structures including, but not confined to, components of the limbic system (e.g., prefrontal cortex, amygdala, and hypothalamus) and closely linked brainstem structures (e.g., periaqueductal gray, PAG), are known to play a critical role in coordinating functions essential for survival, including a variety of emotionally related defensive behaviors triggered by aversive (e.g., fearful) or painful events (Bandler et al., 2000; Sokolowski and Corbin, 2012). Historically, considerable attention has been devoted to mapping activity within different components of these "survival circuits" in relation to a variety of sensory, emotional, or motivational stimuli (cf. LeDoux, 2012). In marked contrast, we know much less about how these circuits interact with the motor system to generate appropriate patterns of behavioral response. The aim therefore of this short review is to discuss evidence, including recent observations, which together suggest that the concept of survival circuits should be extended to include the olivo-cerebellar system. In particular, we will focus on cerebellar interactions with the PAG; a structure with a well characterized role in survival behaviors.

PAG AND SURVIVAL

The PAG is generally accepted to be a pivotal component of a central "survival network". It is a behaviorally important source of descending control that is activated in response to a variety of emotional and environmental stressors, such as fear, anxiety, and pain (Bandler et al., 1991), and is crucial in controlling the expression and co-ordination of responses in these contexts (Fanselow et al., 1991; Carrive et al., 1997; Walker and Carrive, 2003). These controls include cardiovascular regulation, sensory modulation and the generation of a variety of emotionally related motor behaviors, such as fight/flight or immobility/withdrawal from the environment (commonly known as *active* and *passive* coping, respectively).

Active coping enables an animal to escape a stressor (e.g., brief acute pain or encounter with a predator), and is elicited from a column of neurons situated in the dorsolateral/lateral (dl/l) functional column of the PAG. Activation of dl/lPAG increases arterial blood pressure, increases mobility (fight-or-flight responses) and elicits characteristic defense postures, e.g., the animal displays "reactive immobility" in that it is tense and ready for action but is temporarily motionless (Carrive, 1993; Lovick, 1993; Bandler and Shipley, 1994; Fendt and Fanselow, 1999; Keay and Bandler, 2001; Lumb and Leith, 2007). The dl/lPAG can be further divided into rostral and caudal segments with distinct defensive responses associated with upper and whole body movements, respectively (Bandler et al., 1991). By contrast, passive coping is characterized by a general disengagement from the environment when a stressor is inescapable (e.g., chronic pain) or when evading detection during close encounter with a predator. Passive coping is coordinated by a column of neurons located in ventrolateral (vl) PAG and is associated with a reduced responsiveness to external stimuli, and a general cessation in movements and a fixed (freezing) posture (Zhang et al., 1990; Bandler et al., 1991; Carrive, 1993; Lovick, 1993; Bandler and Keay, 1996). As part of these complex coping strategies, the PAG exerts descending control of spinal sensory processing that not only discriminates between noxious and non-noxious events but also between nociceptive inputs of different behavioral significance; C-nociceptor-evoked activity (mediating the slowly conducted, poorly localized and therefore distracting component of the nociceptive message) is depressed while A-nociceptor-evoked activity (the rapidly conducted component that encodes the intensity of the nociceptive signal; McMullan and Lumb, 2006b) is left intact or even enhanced. Indeed, previous

studies indicate that this pattern of effects could operate as part of both active and passive coping strategies that are co-ordinated by the dl/l- and vl-PAG, respectively. Therefore, in both situations differential control of A- vs C-fiber-evoked activity could preserve the detailed information of changes in the external environment that can drive motivational behaviors and accurately direct motor activity (A-fibers), whilst depressing those components of the nociceptive message (C-fibers) that are less useful in terms of survival (e.g., enabling escape behavior without the distraction of C-fiber mediated pain; Waters and Lumb, 1997; McMullan and Lumb, 2006a,b; Koutsikou et al., 2007; Heinricher et al., 2009; Leith et al., 2010).

In summary, outputs from the different functional columns in the PAG co-ordinate fundamentally different patterns of autonomic adjustment, sensory regulation and motor responses that are highly dependent on the behavioral significance of the environmental, emotional or sensory stimulus.

In terms of PAG function, attention to date has focused on neural pathways that underlie autonomic regulation and sensory control, and polysynaptic descending paths that modulate autonomic outflow and sensory processing at the level of the spinal cord are well described (Lovick and Bandler, 2005). In contrast, much less is known about the neural pathways and mechanisms that link PAG activity to distinct patterns of motor responses. Until recently (Cerminara et al., 2009; see below) we knew very little about whether descending control extends to sensory signals that feed into (and can modify) supraspinal motor circuits that co-ordinate movement. Furthermore, scant information is available on how sensorimotor structures, such as the cerebellum, can in turn, modulate activity within the PAG.

THE CEREBELLUM AND MODULAR ORGANIZATION

The cerebellum is involved in regulating a wide range of brain functions including autonomic and somatic reflexes, and voluntary movements (Ito, 1984). Recent neuroanatomical tracing, lesion and neuroimaging studies suggest that the cerebellum may also be involved in higher order processes (Schmahmann, 2004; Strick et al., 2009) including emotional behaviors. Anatomically and functionally, the cerebellum can be subdivided into a series of units termed "modules" that are highly conserved across mammalian species (Apps and Hawkes, 2009). Structurally, each module is defined by a specific climbing fiber input from a discrete part of the inferior olivary complex, which targets one or more longitudinal zones of Purkinje cells within the cerebellar cortex. In turn, the Purkinje cells within each zone project to a specific region of the cerebellar and vestibular nuclei (which themselves receive axon collaterals from the same olivary cells). Since all cerebellar cortical processing is forwarded to the cerebellar nuclei, the latter ultimately control cerebellar contributions to behavior. Cerebellar nuclear output is mainly excitatory (Batini et al., 1992) and projection neurons exert a powerful modulatory influence on a variety of ascending and descending pathways; including brainstem structures associated with the survival network (Ito, 1984; Armstrong, 1986).

Physiologically, olivo-cerebellar inputs, mediated by climbing fibers, are considered central (but not exclusive) to theories of cerebellar-dependent learning (Marr, 1969; Albus, 1971; Ito, 1972). In brief, it is thought that climbing fiber input acts as a teaching signal, which triggers plastic changes in synaptic efficacy in the cerebellar cortex (namely, long-term depression of parallel fiber synaptic transmission). Furthermore, these teaching signals are regulated or "gated" in a task dependent manner and it has been hypothesized that this ensures the transmission of only behaviorally relevant training signals (for review see Apps, 1999, 2000). However, currently we know relatively little about how gating relates to teaching signals arising from higher brain structures, including those involved in the survival network.

Many regard olivo-cortico-nuclear modules as a fundamental feature of cerebellar contributions to motor control and indeed many other functions such as cognition and autonomic regulation (Yeo and Hesslow, 1998; Nisimaru, 2004; Apps and Garwicz, 2005; Ramnani, 2006). Of particular relevance to the suggestion that the cerebellum should be considered part of a distributed survival network is the growing body of evidence that the cerebellar vermis (including the A module and associated output nucleus, fastigius), which has an established role in the regulation of posture, balance (e.g., Cerminara and Apps, 2011) and oculomotor control (Voogd and Barmack, 2006), also serves as a critical component of a network subserving emotionally related behaviors (Strick et al., 2009; Strata et al., 2011). Indeed, Sacchetti et al. (2004) have shown that brief, reversible tetrodotoxin (TTX) inactivation of vermis lobules V and VI impairs consolidation of fear memories and that cerebellar long-term synaptic plasticity is potentiated in fear-conditioned animals. Sacchetti and colleagues (2007) have also provided evidence that the cerebellar vermis (lobules V and VI) supports fear memory processing in the absence of the amygdala (the latter is generally regarded as a central component of the survival network). Collectively, these findings therefore suggest that the cerebellum, like the amygdala, is involved in the processing of fear related memory and associated defensive behaviors. However, the precise role of individual olivo-cortico-nuclear modules in survival networks remains to be established.

EVIDENCE OF A PAG – CEREBELLAR LINK

Given the key role of the PAG in survival circuits, interactions with the cerebellum may provide an important mechanism through which co-ordinated movements can be modulated to enhance survival behaviors in aversive or threatening situations. Anatomical mapping studies provide at least some evidence that interconnections exist between the PAG and cerebellum. Direct, bilateral projections from vlPAG to the cerebellar cortex were first described by Dietrichs (1983). The diffuse nature of the projection suggests the pathway most likely terminates as mossy fibers. In addition, several lines of anatomical evidence suggest that the PAG has links with the cerebellum via the inferior olive – climbing fiber system. Several studies have noted the presence of an ipsilateral projection from the PAG to the olive, including the caudal medial accessory olive (cMAO, Rutherford et al., 1984; Holstege, 1988). This region of the olive provides climbing fiber projections to the cerebellar vermis (Apps, 1990). The presence of such connectivity has been confirmed by using modern viral vector tracer techniques, which have the advantage over conventional tracers in that the

results are not confounded by tracer uptake by axons of passage (Flavell, 2008). In brief, by using targeted microinjections of green fluorescent protein (GFP) tagged adeno-associated virus-cytomegalovirus-enhanced GFP (AAV-CMV-eGFP) into vlPAG, Flavell, 2008 demonstrated a widespread but diffuse projection to all major subdivisions of the olive (see **Figure 1A**). Electrophysiological mapping studies have also shown that microstimulation in dorsal PAG elicits large field potentials localized to cerebellar vermis lobules VII/VIII – which have well defined roles in the control of oculomotor and cardiovascular functions (Noda and Fujikado, 1987; Nisimaru, 2004; Voogd and Barmack, 2006) – with a mean onset latency of 15.2 ± 0.8 ms ($n = 5$ rats, three trials per rat; Crook et al., unpublished observations; see **Figures 1B,C**). The waveform and trial-by-trial fluctuations in size of these evoked field potentials are typical of climbing fiber mediated responses (Armstrong and Harvey, 1968).

What role might the PAG link with the olivo-cerebellar system serve? In attempting to address this question there are two points worth noting. First, climbing fiber afferents, which terminate in a range of cerebellar cortical zones, are powerfully activated by nociceptive inputs (Ekerot et al., 1987). Second, climbing fiber pathways originating from the spinal cord (spino-olivocerebellar

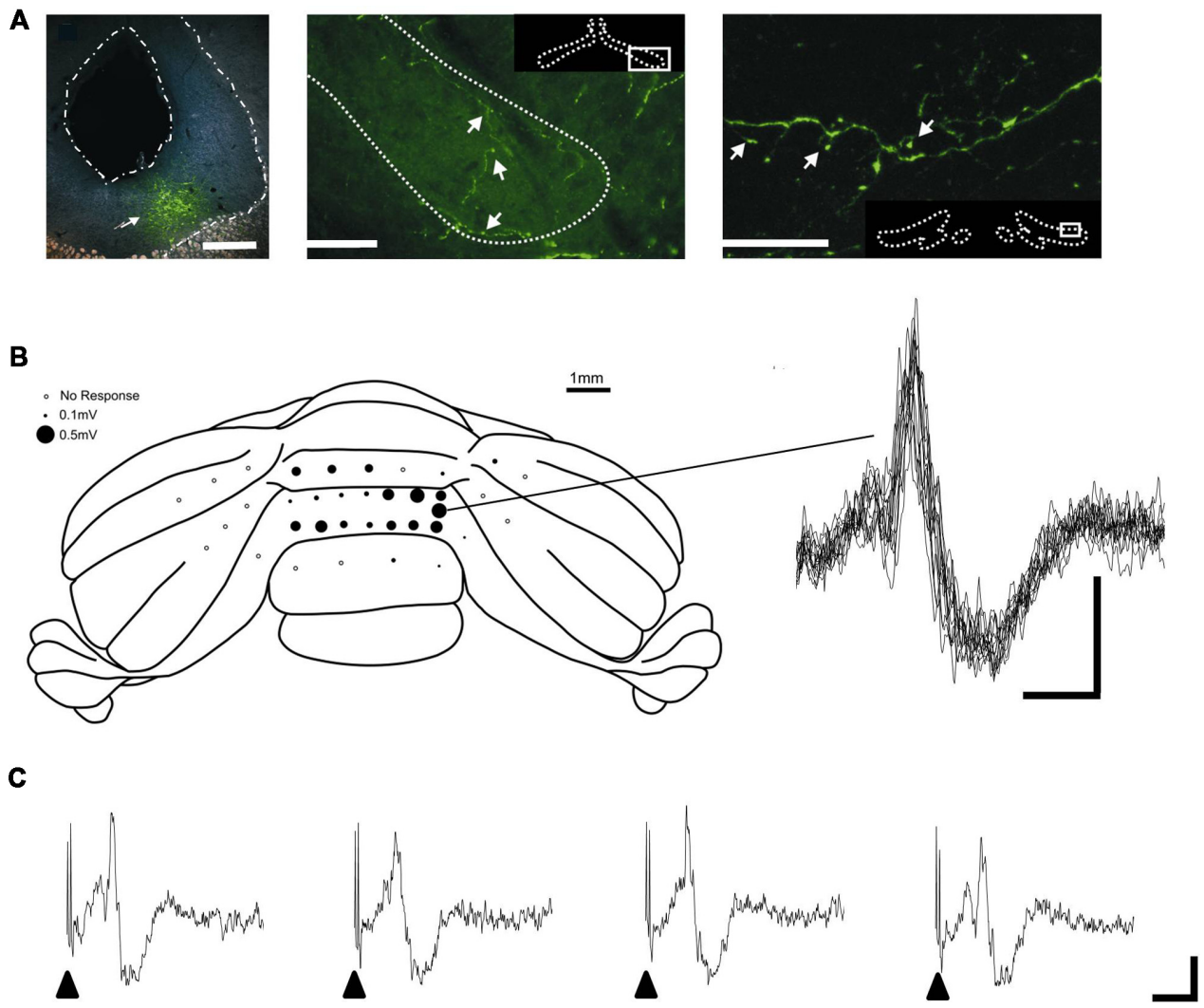

FIGURE 1 | PAG-olivo-cerebellar connectivity. (A) Microinjection of viral anterograde tracer (AAV-CMV-eGFP) into the vlPAG (left panel, injection site indicated by arrowhead; scale bar, 0.5 mm) leads to terminal labeling in the medial accessory olive (middle panel, indicated by arrowheads; scale bar, 100 μm) and dorsal accessory olive (right panel, indicated by arrowheads; scale bar, 30 μm) and also principal olive (not shown). **(B)** Left, posterior view of the rat cerebellum illustrating the distribution of responses evoked by stimulation of left dlPAG at intensity of 2x threshold in one experiment under sodium pentobarbital anasthesia (60 mg/kg administered intraperitoneally). Mean peak-to-trough amplitude (three trials) is represented by the size of filled circles. Right, example waveforms (superimposition of eight consecutive responses) obtained from the recording position indicated on the cerebellar schematic. Stimulus delivered at start of each trace. Scale bar, 15 ms and 0.2 mV. **(C)** Example of four consecutive responses recorded from the same position on the cerebellar cortex. Filled arrow heads indicate timing of PAG stimulation. Scale bars, 20 ms and 0.2 mV. Reproduced with permission from Flavell (2008) and Crook et al., unpublished.

paths, SOCPs) are subject to central modulation during motor learning and active movements (Apps, 1999). Given the well known role of the PAG in regulating transmission of nociceptive signals at the level of the spinal cord, this raises the possibility that the link with the olivo-cerebellar system serves a similar function.

To test this possibility Cerminara and colleagues (2009) electrically stimulated the hindlimb and recorded climbing fiber field potentials in the C1 zone of the ipsilateral copula pyramidis of anesthetized rats, and found that the size of the evoked cerebellar responses (generated as a result of transmission in SOCPs) could be significantly reduced by chemical neuronal activation of vlPAG (**Figure 2**). The climbing fiber responses evoked in this region of the cerebellar cortex are relayed by two SOCPs; one conveys ascending signals via the dorsal funiculus, the other via the ventral funiculus (Oscarsson, 1969; Armstrong et al., 1973; Oscarsson and Sjolund, 1977a,b,c). Importantly, responses evoked by electrical stimulation of the dorsal or ventral funiculus were also reduced by PAG activation (**Figure 2**). This demonstrates that modulation of SOCPs by the PAG must, at least in part, occur supraspinally. Since the ventral funiculus has direct projections to the inferior olive (Boesten and Voogd, 1975; Oscarsson and Sjolund, 1977a,b,c) this finding is consistent with the proposal that the PAG regulates transmission of ascending sensory signals at the level of the olive.

Direct anatomical projections from the PAG to the olive may have a role in this control, but this of course does not exclude the possibility that other (indirect) pathways are also involved. Descending connections to the PAG from higher structures such as the prefrontal cortex (Beitz, 1982; Keay and Bandler, 2001), may also be a route through which neocortical centers that are involved in emotionally related behavior can gain access to the olivo-cerebellar system. The finding that electrical stimulation of the prelimbic subdivision of rat prefrontal cortex powerfully drives activity in olivo-cerebellar pathways supports this hypothesis (Watson et al., 2009).

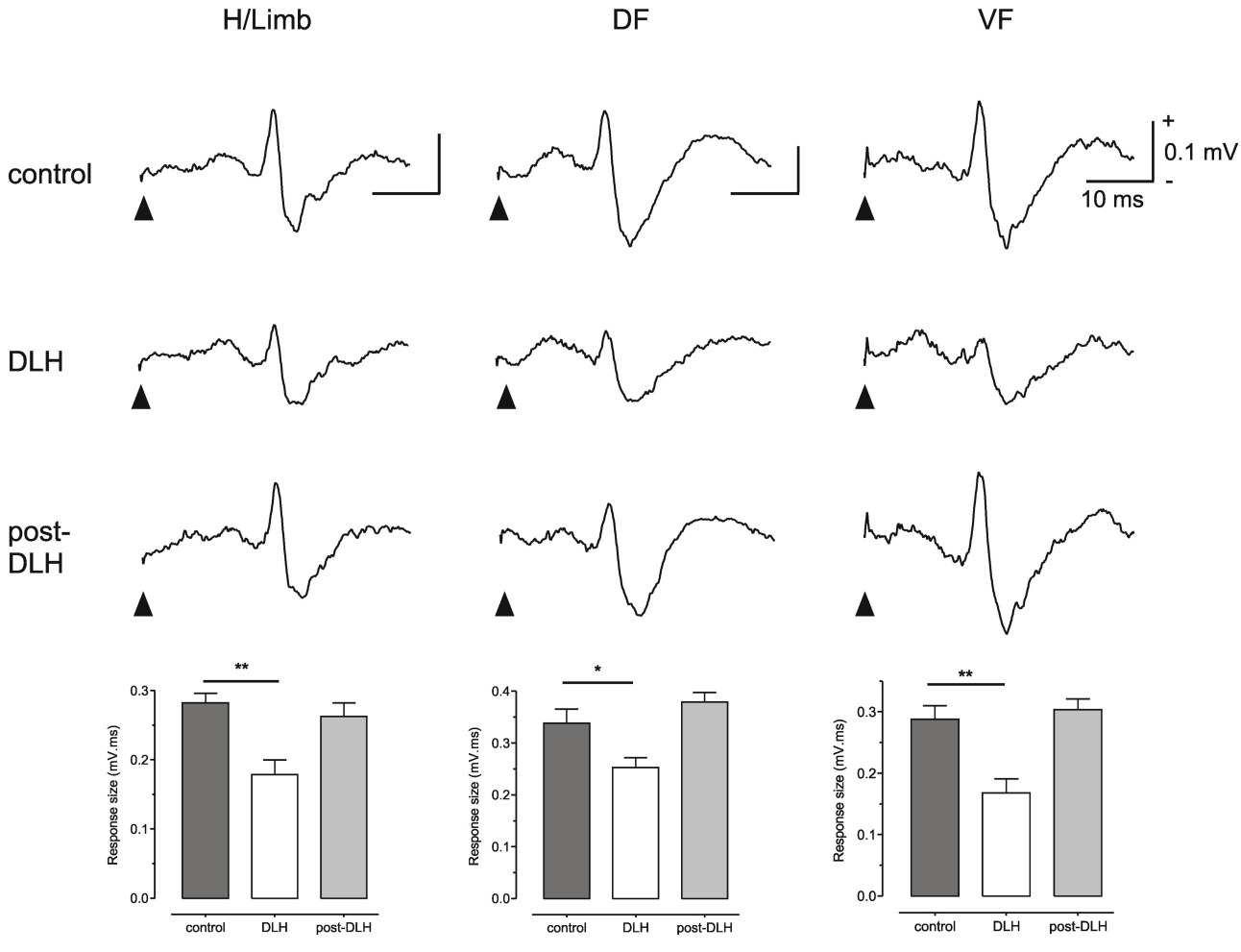

FIGURE 2 | The PAG can modulate SOCPs supraspinally. Climbing fiber fields evoked by stimulation of contralateral hindlimb (H/Limb), ipsilateral dorsal funiculus (DF) and contralateral ventral funiculus (VF) are all significantly suppressed following microinjection of an excitatory amino acid (D-homocysteic acid, DLH) into the vlPAG. Stimulation onset indicated by filled arrowheads. Each trace is an average of 15 trials. Each bar is the mean + SEM of $n = 15$ trials. $*P < 0.05$; $**P < 0.01$. Scale bar values are the same for each trace. Reproduced with permission from Cerminara et al. (2009).

CEREBELLAR OUTPUT TO SURVIVAL CIRCUITS

Important insights into cerebellar contributions to survival circuits can also be gained from anatomical/physiological analysis of cerebellar output (cf. Strick et al., 2009). In particular, several lines of evidence suggest the cerebellar fastigial nucleus has links with limbic structures involved in survival behaviors, such as the hippocampus, hypothalamus, ventral tegmental area (VTA), and amygdala (e.g., Snider and Maiti, 1976; Newman and Reza, 1979; Cao et al., 2013). In respect to cerebellar-PAG projections, Whiteside and Snider (1953) showed that electrical stimulation of vermal lobule VII in the anesthetized cat can evoke responses in the dorsal PAG with two distinct latencies (2–3 ms and 8–12 ms), which raises the possibility that multiple cerebello-PAG pathways exist. Consistent with a direct (short latency) projection, anatomical tracing studies have shown the existence of efferent fastigial projections to the PAG in a number of species (Martin et al. (1974) in the opossum; Beitz (1982); Gonzalo-Ruiz and Leichnetz (1987), Gonzalo-Ruiz et al. (1990) and Teune et al. (2000) in the rat, and Gonzalo-Ruiz et al. (1988) in monkey). Many of these studies have advanced the view that the projections subserve an oculomotor function. However, it is possible that functions of fastigial-PAG projections are more wide ranging and enable the powerful computational circuitry of the cerebellum to engage with circuits related to the expression of survival behaviors. Consistent with this proposal, clinical studies have shown that chronic stimulation of the cerebellar vermis can be used to regulate emotion and "correct behavior" in human patients suffering from intractable neurological disorders such as schizophrenia and epilepsy (Cooper, 1973a,b; Cooper et al., 1973a,b; Correa et al., 1980; Heath et al., 1980a,b, 1981). Furthermore, transmagnetic stimulation of the medial cerebellum in humans can also provide anti-depressive effects (Schutter and van Honk, 2005, 2009; Hoppenbrouwers et al., 2008; Schutter et al., 2009a,b) and can enhance the power of neuronal oscillations, within the theta and gamma frequency range, across regions of the frontal cortex that are thought to be essential to cognitive and emotional aspects of behavior (Schutter et al., 2003; Schutter and van Honk, 2005).

In experimental animals, lesion of the fastigius has a wide variety of behavioral effects such as drowsiness (Fadiga et al., 1968; Giannazzo et al., 1968a,b; Manzoni et al., 1968), aggression (Reis et al., 1973), and grooming behavior (Berntson et al., 1973; Reis et al., 1973). In addition, reductions in activity such as open-field exploratory behavior, and social interactions, independent of non-specific motor abnormalities, have been demonstrated following fastigial lesions in rat (Berntson and Schumacher, 1980). Finally, stimulation of the cerebellar vermis or the fastigial nucleus can elicit a variety of complex patterns of defense-like behavior such as sham rage and predatory attack (Zanchetti and Zoccolini, 1954; Reis et al., 1973). Given the links with PAG and other components of the survival network it seems reasonable to infer that the diverse effects of cerebellar manipulations are in part due to its interactions with survival circuits. The fact that the fastigial nucleus is the output for several cerebellar modules (A, AX, A2) raises the possibility that the range of different behaviors reported in the literature may be due to differential activation of one or more of these pathways.

CONCLUDING COMMENTS

The aim of this short review has not been to consider cerebellar interactions with every structure in the survival network; rather we have focused specifically on the cerebellar-PAG link as an illustrative example. Overall, the available neuroanatomical and physiological evidence suggests that the necessary interconnectivity exists to consider the inferior olive and cerebellum as additional components of a distributed "survival behavior network". The functional significance of olivo-cerebellar involvement in this network remains to be determined, but one influential theory of climbing fiber function is that they serve a teaching role (for a review see for example Yeo and Hesslow, 1998). The powerful climbing fiber mediated projection from PAG to the cerebellar vermis and gating of SOCPs by the PAG may be considered in relation to this theory. Under appropriate behavioral conditions in which survival circuits are engaged, the gating may reflect a switch from the usefulness of learning signals derived from the periphery, to allowing signals arising from higher centers to modify cerebellar function.

ACKNOWLEDGMENTS

We gratefully acknowledge the financial support of the Biotechnology and Biological Sciences Research Council, UK. We thank Louise Hickey and Lianne Leith for contributions to the viral tracing and electrophysiological mapping experiments.

REFERENCES

Albus, J. S. (1971). A theory of cerebellar function. *Math. Biosci.* 10, 25–61.

Apps, R. (1990). Columnar organisation of the inferior olive projection to the posterior lobe of the rat cerebellum. *J. Comp. Neurol.* 302, 236–254.

Apps, R. (1999). Movement-related gating of climbing fibre input to cerebellar cortical zones. *Prog. Neurobiol.* 57, 537–562.

Apps, R. (2000). Rostrocaudal branching within the climbing fibre projection to forelimb-receiving areas of the cerebellar cortical C1 zone. *J. Comp. Neurol.* 419, 193–204.

Apps, R., and Garwicz, M. (2005). Anatomical and physiological foundations of cerebellar information processing. *Nat. Rev. Neurosci.* 6, 297–311.

Apps, R., and Hawkes, R. (2009). Cerebellar cortical organization: a one-map hypothesis. *Nat. Rev. Neurosci.* 10, 670–681.

Armstrong, D. M. (1986). Supraspinal contributions to the initiation and control of locomotion in the cat. *Prog. Neurobiol.* 26, 273–361.

Armstrong, D. M., and Harvey, R. J. (1968). Responses to a spino-olivo-cerebellar pathway in the cat. *J. Physiol.* 194, 147–168.

Armstrong, D. M., Harvey, R. J., and Schild, R. F. (1973). Branching of inferior olivary axons to terminate in different folia, lobules or lobes of the cerebellum. *Brain Res.* 54, 365–371.

Bandler, R., Carrive, P., and Zhang, S. P. (1991). Integration of somatic and autonomic reactions within the midbrain periaqueductal grey: viscerotopic, somatotopic and functional organization. *Prog. Brain Res.* 87, 269–305.

Bandler, R., and Keay, K. A. (1996). Columnar organization in the midbrain periaqueductal gray and the integration of emotional expression. *Prog. Brain Res.* 107, 285–300.

Bandler, R., Keay, K. A., Floyd, N., and Price, J. (2000). Central circuits mediating patterned autonomic activity during active vs. passive emotional coping. *Brain Res. Bull.* 53, 95–104.

Bandler, R., and Shipley, M. T. (1994). Columnar organization in the midbrain periaqueductal gray: modules for emotional expression? *Trends Neurosci.* 17, 379–389.

Batini, C., Compoint, C., Buisseret-Delmas, C., Daniel, H., and Guegan, M. (1992). Cerebellar nuclei and the nucleocortical projections in the rat: retrograde tracing coupled to GABA and glutamate immunohistochemistry. *J. Comp. Neurol.* 315, 74–84.

Beitz, A. J. (1982). The organization of afferent projections to the midbrain periaqueductal gray of the rat. *Neuroscience* 7, 133–159.

Berntson, G. G., Potolicchio, S. J. Jr., and Miller, N. E. (1973). Evidence for higher functions of the cerebellum: eating and grooming elicited by cerebellar stimulation in cats. *Proc. Natl. Acad. Sci. U.S.A.* 70, 2497–2499.

Berntson, G. G., and Schumacher, K. M. (1980). Effects of cerebellar lesions on activity, social interactions, and other motivated behaviors in the rat. *J. Comp. Physiol. Psychol.* 94, 706–717.

Boesten, A. J., and Voogd, J. (1975). Projections of the dorsal column nuclei and the spinal cord on the inferior olive in the cat. *J. Comp. Neurol.* 161, 215–237.

Cao, B. B., Huang, Y., Lu, J. H., Xu, F. F., Qiu, Y. H., and Peng, Y. P. (2013). Cerebellar fastigial nuclear GABAergic projections to the hypothalamus modulate immune function. *Brain Behav. Immun.* 27, 80–90.

Carrive, P. (1993). The periaqueductal gray and defensive behavior: functional representation and neuronal organization. *Behav. Brain Res.* 58, 27–47.

Carrive, P., Leung, P., Harris, J., and Paxinos, G. (1997). Conditioned fear to context is associated with increased Fos expression in the caudal ventrolateral region of the midbrain periaqueductal gray. *Neuroscience* 78, 165–177.

Cerminara, N. L., and Apps, R. (2011). Behavioural significance of cerebellar modules. *Cerebellum* 10, 484–494.

Cerminara, N. L., Koutsikou, S., Lumb, B. M., and Apps, R. (2009). The periaqueductal grey modulates sensory input to the cerebellum: a role in coping behaviour? *Eur. J.Neurosci.* 29, 2197–2206.

Cooper, I. S. (1973a). Effect of chronic stimulation of anterior cerebellum on neurological disease. *Lancet* 1, 206.

Cooper, I. S. (1973b). Effect of stimulation of posterior cerebellum on neurological disease. *Lancet* 1, 1321.

Cooper, I. S., Amin, I., and Gilman, S. (1973a). The effect of chronic cerebellar stimulation upon epilepsy in man. *Trans. Am. Neurol. Assoc.* 98, 192–196.

Cooper, I. S., Crighel, E., and Amin, I. (1973b). Clinical and physiological effects of stimulation of the paleocerebellum in humans. *J. Am. Geriatr. Soc.* 21, 40–43.

Correa, A. J., Llewellyn, R. C., Epps, J., Jarrott, D., Eiswirth, C., and Heath, R. G. (1980). Chronic cerebellar stimulation in the modulation of behavior. *Acta Neurol. Latinoam.* 26, 143–153.

Dietrichs, E. (1983). Cerebellar cortical afferents from the periaqueductal grey in the cat. *Neurosci. Lett.* 41, 21–26.

Ekerot, C. F., Oscarsson, O., and Schouenborg, J. (1987). Stimulation of cat cutaneous nociceptive C fibres causing tonic and synchronous activity in climbing fibres. *J. Physiol.* 386, 539–546.

Fadiga, E., Manzoni, T., Sapienza, S., and Urbano, A. (1968). Synchronizing and desynchronizing fastigial influences on the electrocortical activity of the cat, in acute experiments. *Electroencephalogr. Clin. Neurophysiol.* 24, 330–342.

Fanselow, M. S., Kim, J. J., Young, S. L., Calcagnetti, D. J., Decola, J. P., Helmstetter, F. J., et al. (1991). Differential effects of selective opioid peptide antagonists on the acquisition of pavlovian fear conditioning. *Peptides* 12, 1033–1037.

Fendt, M., and Fanselow, M. S. (1999). The neuroanatomical and neurochemical basis of conditioned fear. *Neurosci. Biobehav. Rev.* 23, 743–760.

Flavell, C. F. (2008). *Nociceptive Processing in Cerebellar Pathways.* Ph.D. thesis, University of Bristol.

Giannazzo, E., Manzoni, T., Raffaele, R., Sapienza, S., and Urbano, A. (1968a). Changes in the sleep-wakefulness cycle induced by chronic fastigial lesions in the cat. *Brain Res.* 11, 281–284.

Giannazzo, E., Manzoni, T., Raffaele, R., Sapienza, S., and Urbano, A. (1968b). [Changes of the sleep-waking ccle following lesions of the cerebellar nuclei in the cat]. *Boll. Soc. Ital. Biol. Sper.* 44, 800–802.

Gonzalo-Ruiz, A., and Leichnetz, G. R. (1987). Collateralization of cerebellar efferent projections to the paraoculomotor region, superior colliculus, and medial pontine reticular formation in the rat: a fluorescent double-labeling study. *Exp. Brain Res.* 68, 365–378.

Gonzalo-Ruiz, A., Leichnetz, G. R., and Hardy, S. G. (1990). Projections of the medial cerebellar nucleus to oculomotor-related midbrain areas in the rat: an anterograde and retrograde HRP study. *J. Comp. Neurol.* 296, 427–436.

Gonzalo-Ruiz, A., Leichnetz, G. R., and Smith, D. J. (1988). Origin of cerebellar projections to the region of the oculomotor complex, medial pontine reticular formation, and superior colliculus in New World monkeys: a retrograde horseradish peroxidase study. *J. Comp. Neurol.* 268, 508–526.

Heath, R. G., Dempesy, C. W., Fontana, C. J., and Fitzjarrell, A. T. (1980a). Feedback loop between cerebellum and septal-hippocampal sites: its role in emotion and epilepsy. *Biol. Psychiatry* 15, 541–556.

Heath, R. G., Llewellyn, R. C., and Rouchell, A. M. (1980b). The cerebellar pacemaker for intractable behavioral disorders and epilepsy: follow-up report. *Biol. Psychiatry* 15, 243–256.

Heath, R. G., Rouchell, A. M., and Goethe, J. W. (1981). Cerebellar stimulation in treating intractable behavior disorders. *Curr. Psychiatr. Ther.* 20, 329–336.

Heinricher, M. M., Tavares, I., Leith, J. L., and Lumb, B. M. (2009). Descending control of nociception: specificity, recruitment and plasticity. *Brain Res. Rev.* 60, 214–225.

Holstege, G. (1988). Brainstem-spinal cord projections in the cat, related to control of head and axial movements. *Rev. Oculomot. Res.* 2, 431–470.

Hoppenbrouwers, S. S., Schutter, D. J., Fitzgerald, P. B., Chen, R., and Daskalakis, Z. J. (2008). The role of the cerebellum in the pathophysiology and treatment of neuropsychiatric disorders: a review. *Brain Res. Rev.* 59, 185–200.

Ito, M. (1972). Neural design of the cerebellar motor control system. *Brain Res.* 40, 81–84.

Ito, M. (1984). *Cerebellum and Neural Control.* New York: Raven Press.

Keay, K. A., and Bandler, R. (2001). Parallel circuits mediating distinct emotional coping reactions to different types of stress. *Neurosci. Biobehav. Rev.* 25, 669–678.

Koutsikou, S., Parry, D. M., Macmillan, F. M., and Lumb, B. M. (2007). Laminar organization of spinal dorsal horn neurones activated by C- vs. A-heat nociceptors and their descending control from the periaqueductal grey in the rat. *Eur. J. Neurosci.* 26, 943–952.

LeDoux, J. (2012). Rethinking the emotional brain. *Neuron* 73, 653–676.

Leith, J. L., Koutsikou, S., Lumb, B. M., and Apps, R. (2010). Spinal processing of noxious and innocuous cold information: differential modulation by the periaqueductal gray. *J. Neurosci.* 30, 4933–4942.

Lovick, T. A. (1993). Integrated activity of cardiovascular and pain regulatory systems: role in adaptive behavioural responses. *Prog. Neurobiol.* 40, 631–644.

Lovick, T. A., and Bandler, R. (2005). "The organisation of the midbrain periaqueductal grey and the integration of pain behaviours," in *The Neurobiology of Pain*, eds S.P. Hunt, and M. Koltzenburg (Oxford: Oxford UP), 267–287.

Lumb, B. M., and Leith, J. L. (2007). "Hypothalamic and midbrain control of C- versus A-fibre mediated spinal nociception: a role for COX-1 in the PAG," in *Neurotransmitters of Antinociceptive Decending Pathways*, eds S. Maione, and V. Dimarzo (Kerala: Reasearch Signpost), 37–57.

Manzoni, T., Sapienza, S., and Urbano, A. (1968). EEG and behavioural sleep-like effects induced by the fastigial nucleus in unrestrained, unanaesthetized cats. *Arch. Ital. Biol.* 106, 61–72.

Marr, D. (1969). A theory of cerebellar cortex. *J. Physiol.* 202, 437–470.

Martin, G. F., King, J. S., and Dom, R. (1974). The projections of the deep cerebellar nuclei of the opossum (Didelphis marsupiales virginiana). *J. Hirnforsch.*15, 545–575.

McMullan, S., and Lumb, B. M. (2006a). Midbrain control of spinal nociception discriminates between responses evoked by myelinated and unmyelinated heat nociceptors in the rat. *Pain* 124, 59–68.

McMullan, S., and Lumb, B. M. (2006b). Spinal dorsal horn neuronal responses to myelinated versus unmyelinated heat nociceptors and their modulation by activation of the periaqueductal grey in the rat. *J. Physiol.* 576, 547–556.

Newman, P. P., and Reza, H. (1979). Functional relationships between the hippocampus and the cerebellum: an electrophysiological study of the cat. *J. Physiol.* 287, 405–426.

Nisimaru, N. (2004). Cardiovascular modules in the cerebellum. *Jpn. J. Physiol.* 54, 431–448.

Noda, H., and Fujikado, T. (1987). Topography of the oculomotor area of the cerebellar vermis in macaques as determined by microstimulation. *J. Neurophysiol.* 58, 359–378.

Oscarsson, O. (1969). Termination and functional organization of the dorsal spino-olivocerebellar path. *J. Physiol.* 200, 129–149.

Oscarsson, O., and Sjolund, B. (1977a). The ventral spine-olivocerebellar system in the cat. II. Termination zones in the cerebellar posterior lobe. *Exp. Brain Res.* 28, 487–503.

Oscarsson, O., and Sjolund, B. (1977b). The ventral spino-olivocerebellar system in the cat. I. Identification of five paths and their termination in the cerebellar anterior lobe. *Exp. Brain Res.* 28, 469–486.

Oscarsson, O., and Sjolund, B. (1977c). The ventral spino-olivocerebellar system in the cat. III. Functional characteristics of the five paths. *Exp. Brain Res.* 28, 505–520.

Ramnani, N. (2006). The primate cortico-cerebellar system: anatomy and function. *Nat. Rev. Neurosci.* 7, 511–522.

Reis, D. J., Doba, N., and Nathan, M. A. (1973). Predatory attack, grooming, and consummatory behaviors evoked by electrical stimulation of cat cerebellar nuclei. *Science* 182, 845–847.

Rutherford, J. G., Anderson, W. A., and Gwyn, D. G. (1984). A reevaluation of midbrain and diencephalic projections to the inferior olive in rat with particular reference to the rubro-olivary pathway. *J. Comp. Neurol.* 229, 285–300.

Sacchetti, B., Sacco, T., and Strata, P. (2007). Reversible inactivation of amygdala and cerebellum but not perirhinal cortex impairs reactivated fear memories. *Eur. J. Neurosci.* 25, 2875–2884.

Sacchetti, B., Scelfo, B., Tempia, F., and Strata, P. (2004). Long-term synaptic changes induced in the cerebellar cortex by fear conditioning. *Neuron* 42, 973–982.

Schmahmann, J. D. (2004). Disorders of the cerebellum: ataxia, dysmetria of thought, and the cerebellar cognitive affective syndrome. *J. Neuropsychiatry Clin. Neurosci.* 16, 367–378.

Schutter, D. J., Enter, D., and Hoppenbrouwers, S. S. (2009a). High-frequency repetitive transcranial magnetic stimulation to the cerebellum and implicit processing of happy facial expressions. *J. Psychiatry Neurosci.* 34, 60–65.

Schutter, D. J., Laman, D. M., Van Honk, J., Vergouwen, A. C., and Koerselman, G. F. (2009b). Partial clinical response to 2 weeks of 2 Hz repetitive transcranial magnetic stimulation to the right parietal cortex in depression. *Int. J. Neuropsychopharmacol.* 12, 643–650.

Schutter, D. J., and van Honk, J. (2005). The cerebellum on the rise in human emotion. *Cerebellum* 4, 290–294.

Schutter, D. J., and van Honk, J. (2009). The cerebellum in emotion regulation: a repetitive transcranial magnetic stimulation study. *Cerebellum* 8, 28–34.

Schutter, D. J., Van Honk, J., D'Alfonso, A. A., Peper, J. S., and Panksepp, J. (2003). High frequency repetitive transcranial magnetic over the medial cerebellum induces a shift in the prefrontal electroencephalography gamma spectrum: a pilot study in humans. *Neurosci. Lett.* 336, 73–76.

Snider, R. S., and Maiti, A. (1976). Cerebellar contributions to the Papez circuit. *J. Neurosci. Res.* 2, 133–146.

Sokolowski, K., and Corbin, J. G. (2012). Wired for behaviors: from development to function of innate limbic system circuitry. *Front. Mol. Neurosci.* 5:55. doi: 10.3389/fnmol.2012.00055

Strata, P., Scelfo, B., and Sacchetti, B. (2011). Involvement of cerebellum in emotional behavior. *Physiol. Res.* 60(Suppl. 1), S39–S48.

Strick, P. L., Dum, R. P., and Fiez, J. A. (2009). Cerebellum and nonmotor function. *Annu. Rev. Neurosci.* 32, 413–434.

Teune, T. M., Van Der Burg, J., Van Der Moer, J., Voogd, J., and Ruigrok, T. J. (2000). Topography of cerebellar nuclear projections to the brain stem in the rat. *Prog. Brain Res.* 124, 141–172.

Voogd, J., and Barmack, N. H. (2006). Oculomotor cerebellum. *Prog. Brain Res.* 151, 231–268.

Walker, P., and Carrive, P. (2003). Role of ventrolateral periaqueductal gray neurons in the behavioral and cardiovascular responses to contextual conditioned fear and poststress recovery. *Neuroscience* 116, 897–912.

Waters, A. J., and Lumb, B. M. (1997). Inhibitory effects evoked from both the lateral and ventrolateral periaqueductal grey are selective for the nociceptive responses of rat dorsal horn neurones. *Brain Res.* 752, 239–249.

Watson, T. C., Jones, M. W., and Apps, R. (2009). Electrophysiological mapping of novel prefrontal - cerebellar pathways. *Front. Integr. Neurosci.* 3:18. doi: 10.3389/neuro.07.018.2009

Whiteside, J. A., and Snider, R. S. (1953). Relation of cerebellum to upper brain stem. *J. Neurophysiol.* 16, 397–413.

Yeo, C. H., and Hesslow, G. (1998). Cerebellum and conditioned reflexes. *Trends Cogn. Sci.* 2, 322–330.

Zanchetti, A., and Zoccolini, A. (1954). Autonomic hypothalamic outbursts elicited by cerebellar stimulation. *J. Neurophysiol.* 17, 475–483.

Zhang, S. P., Bandler, R., and Carrive, P. (1990). Flight and immobility evoked by excitatory amino acid microinjection within distinct parts of the subtentorial midbrain periaqueductal gray of the cat. *Brain Res.* 520, 73–82.

Conflict of Interest Statement: The authors declare that the research was conducted in the absence of any commercial or financial relationships that could be construed as a potential conflict of interest.

Received: 04 January 2013; accepted: 03 April 2013; published online: 23 April 2013.

Citation: Watson TC, Koutsikou S, Cerminara NL, Flavell CR, Crook JJ, Lumb BM and Apps R (2013) The olivocerebellar system and its relationship to survival circuits. Front. Neural Circuits 7:72. doi: 10.3389/fncir.2013.00072

frontiers in
NEURAL CIRCUITS

REVIEW ARTICLE
published: 13 March 2013
doi: 10.3389/fncir.2013.00035

The cerebellum: a new key structure in the navigation system

***Christelle Rochefort*[1,2†], *Julie M. Lefort*[1,2†] *and Laure Rondi-Reig*[1,2*]**

[1] *UPMC Univ Paris 06, UMR 7102, Paris, France*
[2] *CNRS, UMR 7102, Paris, France*

Edited by:
Chris I. De Zeeuw, ErasmusMC, Netherlands; Netherlands Institute for Neuroscience, Netherlands

Reviewed by:
Piergiorgio Strata, University of Turin, Italy
Mitchell Goldfarb, Hunter College of City University, USA
Dagmar Timmann, University Clinic Essen, Germany

****Correspondence:***
Laure Rondi-Reig, Laboratory of Neurobiology of Adaptive Processes, Navigation, Memory, and Aging Team, CNRS UMR7102, Université Pierre et Marie Curie, Bâtiment B-5ème étage, 9 Quai Saint-Bernard, 75005 Paris, France.
e-mail: laure.rondi@snv.jussieu.fr
† These authors have contributed equally to this work.

Early investigations of cerebellar function focused on motor learning, in particular on eyeblink conditioning and adaptation of the vestibulo-ocular reflex, and led to the general view that cerebellar long-term depression (LTD) at parallel fiber (PF)–Purkinje cell (PC) synapses is the neural correlate of cerebellar motor learning. Thereafter, while the full complexity of cerebellar plasticities was being unraveled, cerebellar involvement in more cognitive tasks—including spatial navigation—was further investigated. However, cerebellar implication in spatial navigation remains a matter of debate because motor deficits frequently associated with cerebellar damage often prevent the dissociation between its role in spatial cognition from its implication in motor function. Here, we review recent findings from behavioral and electrophysiological analyses of cerebellar mutant mouse models, which show that the cerebellum might participate in the construction of hippocampal spatial representation map (i.e., place cells) and thereby in goal-directed navigation. These recent advances in cerebellar research point toward a model in which computation from the cerebellum could be required for spatial representation and would involve the integration of multi-source self-motion information to: (1) transform the reference frame of vestibular signals and (2) distinguish between self- and externally-generated vestibular signals. We eventually present herein anatomical and functional connectivity data supporting a cerebello-hippocampal interaction. Whilst a direct cerebello-hippocampal projection has been suggested, recent investigations rather favor a multi-synaptic pathway involving posterior parietal and retrosplenial cortices, two regions critically involved in spatial navigation.

Keywords: cerebellum, hippocampus, navigation, LTD, self-motion, path integration, place cells, spatial representation

INTRODUCTION

Whilst the cerebellum has long been exclusively associated with motor function, its role in cognitive processes has, in the last decades, progressively become apparent. This review will first focus on the original work leading to the major hypothesis that long-term depression (LTD) at parallel fiber (PF)–Purkinje cell (PC) synapses underlies cerebellar motor learning. We then provide an overview of the arguments suggesting that cerebellar processing is also required in cognitive function such as spatial navigation and that it contributes to both hippocampal spatial map formation and optimal goal-directed navigation. The potential computation undertaken by the cerebellum for building hippocampal spatial representation is also discussed. Finally, the possible anatomical pathways involved in this cerebello-hippocampal association are explored.

CEREBELLAR LTD AND MOTOR LEARNING

LTD refers to an activity-dependent long lasting decrease in synaptic efficacy. This anti-hebbian form of synaptic plasticity was initially discovered in and thought to be unique to the cerebellum (Ito and Kano, 1982; but see Ito, 1989) until it was also described in many other brain areas [e.g., hippocampus (Stanton and Sejnowski, 1989) and cortex (Artola et al., 1990)]. Although Brindley was the first to propose plastic synaptic features to PC (Brindley, 1964), the Marr–Albus theory, which emerged after the fine description of the cerebellar circuitry (Eccles, 1965, 1967), was the one that historically inspired future research. According to this model, the cerebellum acts as a pattern classification device that can form an appropriate output in response to an arbitrary input (Boyden et al., 2004). This implies that the cerebellar circuitry allows adjustments of PF–PC synaptic efficacy, which would enable the storage of stimulus-response associations by linking inputs converging to the cerebellar cortex with appropriate motor outputs. Marr first developed this model by predicting the existence of long-term potentiation (LTP) at PF–PC synapses (Marr, 1969) and Albus modified it two years later by proposing LTD rather than LTP as the learning underlying cellular mechanism (Albus, 1971).

The experimental correlate of the Marr–Albus theory was discovered a few years later by Ito and Kano in 1982. The authors focused on a simple motor learning task and well-defined plastic system: the adaptation of the vestibulo-ocular reflex (VOR). The VOR enables the stabilization of images on the retina during head turns by eliciting eye movements in the opposite direction. Experimental adaptation of this reflex can be obtained by repeatedly displacing the visual stimulus during the head rotation.

By studying the VOR circuitry in the rabbit flocculus cerebellar region, Ito and Kano experimentally demonstrated the existence of LTD on PCs after conjunctive stimulation of parallel and climbing fibers (Ito and Kano, 1982; Ito, 1989). Since cerebellar architecture is composed of several uniform modules, it was then suggested that such signal processing may be similar along the entire cerebellum.

Following this work, the implication of LTD in motor learning has been suggested by the observed correlation between altered LTD and impaired motor learning. A series of mouse models lacking LTD has been studied in two main behavioral paradigms, the VOR adaptation and the eyeblink conditioning tasks. In the latter, for which the cerebellum has been shown to be essential (Clark et al., 1984; McCormick and Thompson, 1984a,b), the animal learns to associate a tone (conditioning stimulus) with a corneal air puff (unconditioned stimulus) leading to the eyelid closure. The analysis of mutant mouse models targeting signaling pathways involved in LTD such as the metabotropic glutamate receptor mGluR1 (Aiba et al., 1994), the protein kinase C (PKC) (De Zeeuw et al., 1998; Koekkoek et al., 2003) or the αCaMKII enzyme (Hansel et al., 2006) provided a strong support in favor of the hypothesis that cerebellar LTD is indeed related to cerebellar-dependent motor learning. Nevertheless, a further step to sustain this assertion would be to demonstrate that LTD is effectively induced after cerebellar motor learning.

The current view that cerebellar LTD underlies motor learning was recently challenged as the pharmacological inactivation of cerebellar LTD was not accompanied by a deficit in eyeblink conditioning and in the rotarod test (Welsh et al., 2005). Moreover using a fine behavioral approach designed to selectively eliminate the instructive signal from the climbing fiber (and thus the induction of heterosynaptic LTD) during a VOR adaptation task, it was shown that cerebellar motor learning was completely normal (Ke et al., 2009). In accordance with these findings, the use of three different mutant mouse models targeting specifically late events in the LTD signaling cascade confirmed the dissociation between LTD and simple motor learning tasks (Schonewille et al., 2011).

Interestingly, Burguiere et al. (2010) investigated the role of LTD in an aversive operant conditioning, using a Y-watermaze task in which mice had to learn to associate the correct turn with a stimulus presented before the turn. Inhibition of the PKC crucial for LTD induction did not prevent the animals from learning the stimulus-response "cue–direction" association. In the light of these recent findings, it thus appears that whereas some cerebellar synaptic transmission mechanisms are involved in motor learning, the LTD occurring at PF–PC synapses is not essential. In addition, another form of plasticity, the PF–PC LTP has been proposed to be important for motor learning (Schonewille et al., 2010). Taking into account the different plasticities of the cerebellar cortex including granule cells and PCs network, Gao et al. (2012a) proposed a new conceptual framework called "distributed synergistic plasticity." They suggest that many forms of synaptic and intrinsic plasticity at different sites combine synergistically to produce optimal output for behavior. This theoretical debate is still ongoing. These mutant mouse models were also an opportunity to extend the study of cerebellar plasticities in other forms of learning abilities, notably in relation to spatial navigation.

CEREBELLUM AND SPATIAL NAVIGATION

Spatial navigation is a cognitive function that can be defined as a dual process. Indeed it requires the integration of both self-motion (vestibular, proprioceptive, optic flow, or motor command efferent copy)[1] and external (visual, olfactory, auditory, or tactile) sensori-motor information to form an internal cognitive representation of the context in which the navigation takes place. This cognitive representation can then be used in order to elaborate an optimal goal-directed path adapted to the context (**Figure 1**).

Contribution of the cerebellum to cognitive functions such as navigation remains a controversial subject. Indeed, whilst an extensive range of cerebellar functions has been pointed out as early as 1950 (Snider, 1950) and since been completed and corroborated by more recent research, the current understanding of cerebellar functions in cognition suffers from great criticism. For instance, some findings providing important evidence in human that the cerebellum is involved in cognitive function has been refuted based on the general comments that reports of cerebellar activation during cognitive demands are not always replicated and might therefore "be related to actual or planned movements of the eyes, vocal apparatus, or finger" (Glickstein, 2007).

It can however be acknowledged that the view of the cerebellum in cognitive function has evolved with reports describing dysfunction of non-motor processes in patients with cerebellar pathology as well as findings from neuroimaging studies in normal adults (Schmahmann, 1991; Schmahmann and Sherman, 1998; Stoodley and Schmahmann, 2009). For instance, the role of the cerebellum in emotion has been suggested by the difference in the pattern of cerebellar activation induced by distinct types of emotion (Damasio et al., 2000; Baumann and Mattingley, 2012). Implication of the cerebellum in such function has also

[1] See Glossary.

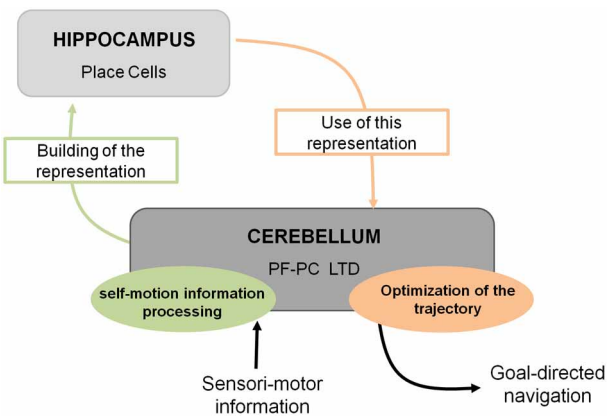

FIGURE 1 | Cerebello-hippocampal interaction for goal-directed navigation. The cerebellum contributes to spatial navigation at two levels, first in processing self-motion information to build spatial representation in the hippocampus at the level of place cells, and second in using this spatial representation to perform an optimal trajectory toward a goal. Studying L7-PKCI mice lacking LTD at PF–Purkinje cell synapses, this plasticity has been shown to be involved in both processes.

emerged from a series of investigations using associative fear learning paradigms in patient with cerebellar lesion (see for review Timmann et al., 2010). These results are further supported by studies in rodents, which clearly demonstrated that PF–PC LTP underlies associative memory processes related to fear behavior (for reviews see Sacchetti et al., 2009; Strata et al., 2011). Importantly it has been evidenced that cerebellar LTP was indeed induced by associative fear learning (Sacchetti et al., 2004; Zhu et al., 2007).

The earliest studies combining mental or virtual navigation tasks with brain imaging and focusing on hippocampal and cortical networks reported that cerebellum was also activated during these tasks (Maguire et al., 1998; Ino et al., 2002; Moffat et al., 2006). A few neuroimaging studies using driving simulators showed that a network of brain structures including the cerebellum was specifically activated during driving (Walter et al., 2001; Calhoun et al., 2002; Uchiyama et al., 2003; Horikawa et al., 2005). Findings emerging from patients with cerebellar damage led to diverging conclusions. A series of investigation in children who underwent a resection of cerebellar tumors points toward a role of the cerebellum in visuo-spatial skills (Levisohn et al., 2000; Riva and Giorgi, 2000; Steinlin et al., 2003), although discrepancies exist regarding the part of the cerebellum associated to it. Whereas impaired spatial abilities have been specifically associated to lesions of the left cerebellum in the study of Riva and Giorgi, others works did not find any lateralization (Levisohn et al., 2000). Several studies assessing visuo-spatial abilities in adult cerebellar patient reported that cerebellar lesion leads to an alteration in spatial function (Wallesch and Horn, 1990; Malm et al., 1998; Schmahmann and Sherman, 1998; Molinari et al., 2004), with for some reports a specific involvement of the posterior part of the cerebellum (Schmahmann and Sherman, 1998). However, other reports attribute the observed visuo-spatial deficits of cerebellar patient to unspecific attention impairment rather than spatial neglect (Frank et al., 2007, 2008, 2010). Moreover, in a study assessing the ability of adult subject to navigate without any visual input, patient with cerebellar ataxia displayed trajectories that were even more accurate than control (Paquette et al., 2011), although their angular motion was impaired (Goodworth et al., 2012). Based on the results emerging from both fMRI and cerebellar lesion studies, it has been recently suggested that the cerebellum is part of at least two distinct functional loops, one involved in motor processing and the other involved in cognitive processes (Strick et al., 2009; Ramnani, 2012). Whereas accumulating evidence support the idea that cerebellum participate in both motor and non-motor function, its specific involvement in human spatial navigation remains to be established.

In non-human primates, one of the first reports on the contribution of the cerebellum to spatial learning abilities emerged in the 80's. This study carried out on adult monkeys with experimental lesions of the deep cerebellar dentate nucleus revealed an impaired performance in the spatial parameter of a visuo-motor task involving a goal-directed movement of the arm (Trouche et al., 1979). These results represented a first step toward an enlarged view of cerebellar functions, encompassing more complex spatial learning task. The role of the cerebellum in spatial learning has also been investigated using water maze tasks in rodents given the reduced impact cerebellar lesions exert on swimming movements (see review in Lalonde and Strazielle, 2003). However, whilst several authors emphasized the navigation deficit in cerebellar mutant models, a recurrent problem has been to dissociate between the navigation process deficit *per se* and motor-related problems. Therefore, rodents were tested in cued or spatial learning paradigms of a water maze in order to evaluate their visuo-motor abilities or their spatial navigation abilities respectively (see **Figure 2** for more details about the paradigms). Several cerebellar mutant mice such as Grid2^{Lc}, Rorα^{sg}, reeler and weaver presented deficits in both cued and spatial learning (see review in Rondi-Reig and Burguiere, 2005). However, these natural mutations were relatively large and affected the whole cerebellar organization. Nevertheless, another cerebellar mutant mouse (Nna1^{Pcd}) which displays a postnatal specific degeneration of virtually all cerebellar PCs (Mullen et al., 1976) was able to perform the cued but not the spatial version of the task indicating that the severe spatial navigation deficit of this mutant was not simply due to motor dysfunction (Goodlett et al., 1992). Similarly, hemicerebellar lesions led to deficits in both spatial and cue version of the MWM (Petrosini et al., 1996), whereas more restricted lesions to the lateral cerebellar cortex, the dentate nucleus (Joyal et al., 2001; Colombel et al., 2004) or the Purkine cell layer (Gandhi et al., 2000) reveals a specific impairment in the spatial version of this task. Altogether, based on the specificity of the behavioral and neurobiological alterations, these data clearly supported the hypothesis that the cerebellum is involved in spatial learning (see reviews in Petrosini et al., 1998; Molinari and Leggio, 2007).

The accumulation of evidence supporting a role of the cerebellum in navigation raised the question of the potential roles of the two major cerebellar inputs, the olivo-cerebellar input (climbing fiber) and the mossy fiber–granule cells–PF input. Rondi-Reig et al. (2002) tested rats with lesion of climbing (CF) and/or PF inputs of the cerebellum in either the cued or the place protocol of the water maze. Rats with a lesion of CF associated with partial or total lesion of PF presented a deficit in the latency to find the platform in the spatial version of the task but not in the cued one. Interestingly a difference appeared between the CF and PF lesion in the initial body orientation relative to the platform. Animals presenting a lesion of the PF were unable to learn how to orient their body toward the non-visible platform and opted instead for a circling behavior, whereas animals with lesion of the CF were still able to reach control level. These results indicated a substantial role of the PF cerebellar inputs in navigation (Rondi-Reig et al., 2002) and pointed toward an underlying mechanism occurring at the PC synapse.

Recent use of the L7-PKCI transgenic model, in which the PKC dependent LTD that occurs at PF–PC synapses is altered, brought new insight regarding the process performed by the cerebellum (Burguiere et al., 2005, 2010; Rochefort et al., 2011) (**Figure 1**). Using this L7-PKCI model in an operant conditioning task, our team highlighted the idea that cerebellar LTD is not required for the learning of a stimulus-response association but is rather involved in the optimization of a motor response during a goal-directed navigation conditioning task (Burguiere et al., 2005, 2010). Using a behavioral protocol assessing specifically

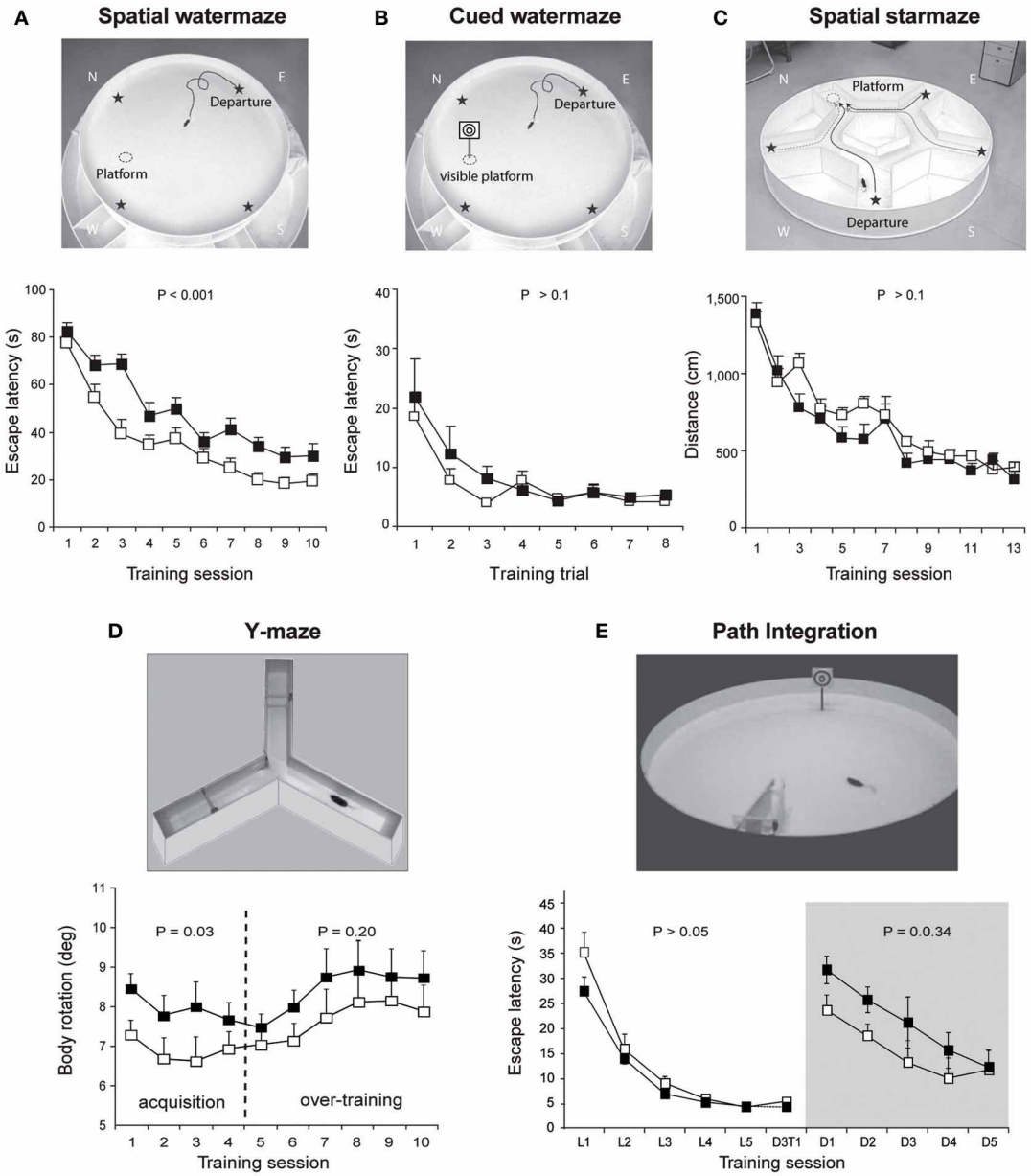

FIGURE 2 | Overview of the different paradigms used in L7-PKCI mice to assess their spatial navigation performances. (A) The spatial version of the Morris watermaze, in which a hidden platform can be found using the configuration of distal visual cues around the maze revealed spatial learning deficits in L7-PKCI mice. **(B)** These lower performances are not due to a deficit in visual guidance abilities, as revealed by subsequent training in the cued version of this maze. In this task, L7-PKCI mice correctly found the platform location indicated by a proximal visual cue. **(C)** The absence of deficit in the starmaze, in which alleys help to execute efficient trajectories toward an invisible platform, suggests that while L7-PKCI can learn to locate a goal using distal visual cues, they are unable to execute a direct trajectory toward it. **(D)** The use of a single intersection maze called the Y-maze enables analysis of trajectory quality. Trajectories optimization was quantified by the body rotation parameter which measures the angle between 3 successive points of the trajectory and is averaged over the whole path. Body rotation was specifically impaired in L7-PKCI mice during the acquisition of the task. **(E)** The inability of L7-PKCI mice to navigate in the dark (i.e., using self-motion information) was revealed in a path integration task, in which mice have to find a platform in a constant location and from a fixed departure point with an alley guiding the initial orientation of the body. In this task, mice first learn the path in the light and then reproduce it in the dark. **(A,B,C)** Data from Burguiere et al. (2005); **(D)** data from Burguiere et al. (2010); **(E)** data from Rochefort et al. (2011). N, W, E, S: North, West, East, and South, respectively. Stars on the pictures in **(A,B,C)** indicate each possible departure point.

path integration of the L7-PKCI mice (i.e., the ability to navigate using self-motion information only), we revealed an implication of cerebellar LTD in the formation of the self-motion based internal spatial map encoded in the hippocampus. Indeed, mice lacking this form of cerebellar plasticity presented impaired hippocampal place cell firing properties. Interestingly, the deficit in the hippocampal place code was observed only when mice had to rely on self-motion information. Subsequently, mice were

tested in a path integration task, in which they had to find a platform in a constant location and from a fixed departure point with an alley guiding the initial orientation of the body (**Figure 2**). Mice first learned the path in the light and then had to reproduce it in the dark. Consistently with their hippocampal place cell alteration, L7-PKCI mice were unable to navigate efficiently toward a goal in the absence of external information (**Figure 2**). Princeps studies on navigation in rats suggested that the cerebellum is not required for the retention of a learned path in a maze habit task with guiding alleys, even in the absence of vision (Lashley and McCarthy, 1926). It is possible that the fact that mice are overtrained and the presence of alleys guiding the animal movement had hidden a potential deficit. Likewise, L7-PKCI mice were also not deficient in the starmaze, a navigation task in which mice swim only within alleys (Burguiere et al., 2005).

The deficit in the spatial map observed in L7-PKCI mouse model brought the first evidence of a functional interaction between the cerebellum and the hippocampus in the acquisition of a spatial representation required to perform path integration (Rochefort et al., 2011). According to these findings, cerebellar LTD might participate in the mental construction of the representation of space whose seat is in the hippocampus, suggesting that the cerebellum takes part in the representation of the body in space. The next section is focused on describing the mechanisms by which the cerebellum might participate in navigation by processing and combining multimodal self-motion information and give pertinent information about body location in space.

CEREBELLAR CONTRIBUTION TO NAVIGATION INFORMATION PROCESSING

As previously explained, spatial navigation is an active process that requires the accurate and dynamic representation of our location, which is given by the combination of both external and self-motion cues. Vestibular information has been shown to be crucial for spatial representation (Stackman et al., 2002), spatial navigation (Stackman and Herbert, 2002; Smith et al., 2005), and specifically path integration (Wallace et al., 2002). However, vestibular information by itself does not provide sufficient information to properly locate in an environment. Coherent body motion information is indeed given by the combination of multiple sources of idiothetic information including vestibular, proprioceptive, optic flow, and motor command efferent copy signals. **Figure 3** suggests the role of the cerebellum in such integration.

Vestibular information is first detected in the inner ear by the otoliths organs for the linear component and by the semi-circular canals for the rotational component. As receptor cells are fixed to

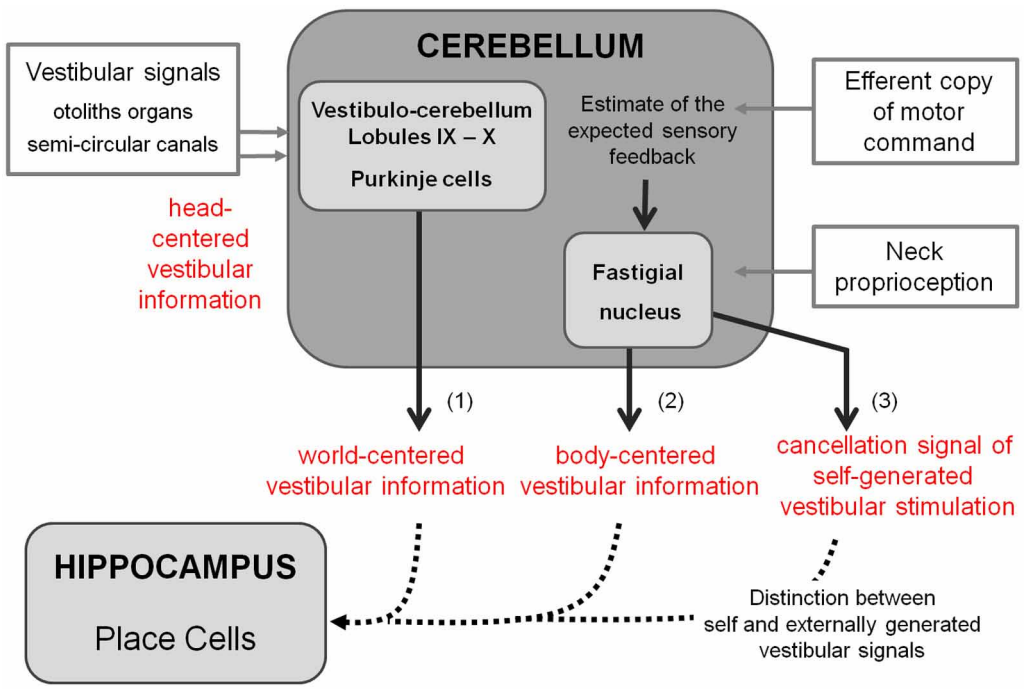

FIGURE 3 | Detailed cerebellar processing of self-motion information that can be used for building spatial representation. This figure represents the ascendant branch of **Figure 1** and highlights the cerebellar contribution to building spatial representation. Based on the existing literature, cerebellar processing of self-motion information could involve three different computations: **(1)** The combination of otolith and semi-circular signals to convert head centered vestibular information into world centered vestibular information. **(2)** The integration of neck proprioceptive information with head motion vestibular information to compute an estimate of body motion in space. **(3)** The hypothesis proposed by Cullen et al. (2011) of a possible production of a cancellation signal to suppress self-generated vestibular stimulation due to active movements. This computation implies using the efferent copy of motor command to predict expected sensory feedback and to compare it to the effective proprioceptive signal (Roy and Cullen, 2004). Such a cancellation allows distinguishing between self-and externally-generated vestibular signals. These transformations are required to provide the hippocampus with the appropriate self-motion information (dotted lines).

the head bone, vestibular signals are detected in a head reference frame (**Figure 4**). This means for example that based on semicircular signals only, a rotation of the head upright relative to the vertical axis cannot be distinguished from a rotation of the head horizontal relative to the horizontal axis. In other words, semicircular canal information alone does not discriminate vertical or horizontal body position. To compute the movement of the body in space, vestibular information needs to be integrated relative both to the body (taking into account the relative position of the head and the body, given by the neck curvature) and to the world, converting the signal initially in head-fixed coordinates into a signal in world-frame coordinates (taking into account gravity). These computations are not necessarily successive and result from the integration of different types of signals. Several recent studies showed that these two reference frame transformations occur in different cerebellar subregions. An elegant report recently pointed out that the cerebellar cortex computes the head-to-world reference frame conversion by combining semicircular and otolith organs inputs (Yakusheva et al., 2007). This computation takes place in the lobules 9 and 10 of the cerebellum and involves GABA transmission (Angelaki et al., 2010).

Head-to-body frame transformation seems to occur in the cerebellar fastigial nucleus. This region contains indeed a subpopulation of neurons (50%)—one synapse downstream the PCs—that has been shown to encode motion in body coordinates (Kleine et al., 2004; Shaikh et al., 2004). More recently, this idea has been further supported by the demonstration that fastigial neurons respond to both vestibular and neck proprioception, and specifically encode body movement in space (Brooks and Cullen, 2009). However, since head to body position has also been shown to modulate PC activity in the cerebellar anterior vermis in decerebrate cats (Manzoni et al., 1999), meaning that PCs also receive neck proprioceptive information, one cannot exclude that the head to body frame transformation might also take place in the cerebellar cortex.

Another implication of the cerebellum in the sensory processing involved in spatial navigation has been highlighted by studies on the cancellation of self-generated vestibular signals. During spatial navigation, displacement of the body in the environment undoubtedly generates stimulations of vestibular receptors. This includes translational stimulations corresponding to the displacement vector as well as rotational stimulations due to head and body reorientation. However, vestibular stimulations are not perceived, meaning that these self-generated signals have been canceled out, enabling reliable detection of stimuli from external sources. Crucial to navigation, the ability to distinguish self-generated vestibular signals coming from an active movement allows proper integration with other

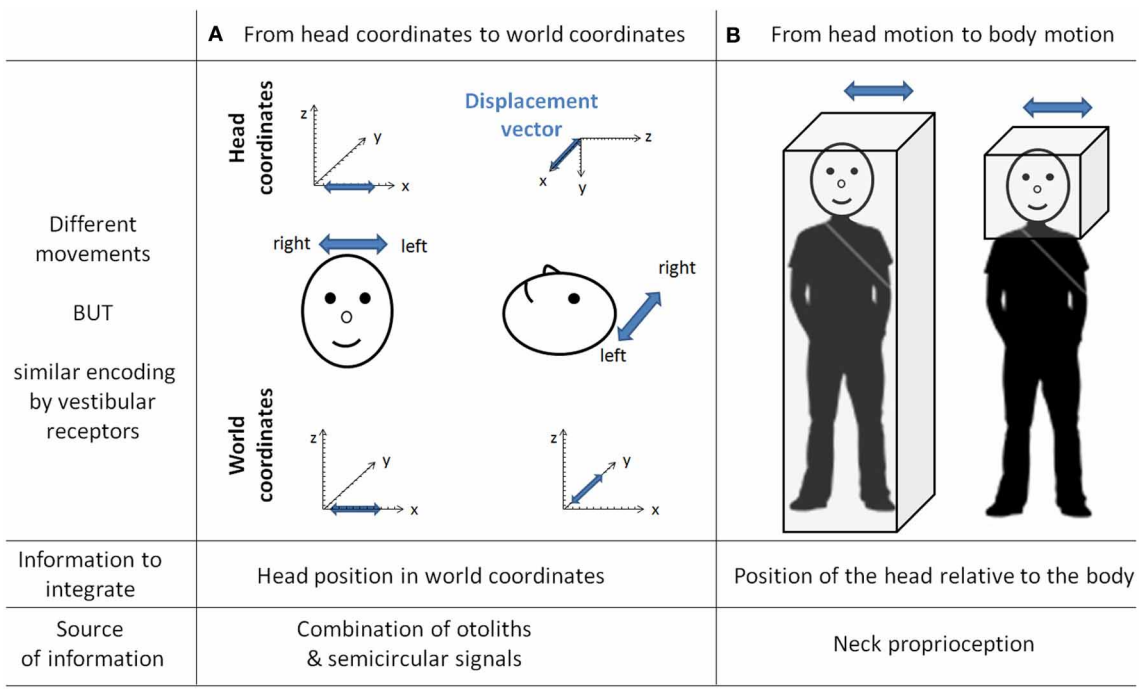

FIGURE 4 | The need for transformation of the vestibular signals. As the vestibular organs are located in the head, vestibular signal is detected in head coordinates. This implies several transformations of the vestibular signal to correctly compute body motion in space. This figure gives two examples of different movements similarly encoded by vestibular receptors. In column **(A)** is a linear displacement from left to right, with the head either vertical or horizontal. Indeed both movements are identical in the head reference frame [displacement vectors (in blue) project onto the x-axis] whereas they are different in the world coordinates (displacement vectors project either onto the x-axis or onto the y-axis). These two movements can be distinguished by taking into account the head position in space, which can be extracted from the combination of semicircular and otolith organs signals (Yakusheva et al., 2007). Column **(B)** illustrates two movements corresponding to the same head motion in space, but different body motions in space (i.e., on the right the body is stationary). These two movements can be distinguished by integrating information about the position of the head relative to the body (that is, the neck curvature, given by neck proprioceptors).

types of idiothetic signals to produce an accurate estimate of body movement, which forms the basic computation for path integration.

A particular population of neurons within vestibular nuclei termed Vestibular Only (VO) are selectively active during passively applied movements (McCrea et al., 1999; Roy and Cullen, 2001). The lack of response during active movements implies that self-generated vestibular signals are indeed canceled. Such cancellation requires knowledge about the currently performed movement provided by the combination of the different self-motion signals, and in particular the efferent copy of the motor command and proprioception. Because the VO neurons are modulated by neither proprioceptive inputs nor efferent copy of motor command when presented in isolation to alert animals, some authors suggested that a cancellation signal arrives from higher structures in the case of active movements (Roy and Cullen, 2003, 2004). Moreover, Roy and Cullen (2004) showed that during active movements, this cancellation signal occurs only if the actual movement matches the intended one. These authors proposed that, using the efferent copy of motor command, an internal model of proprioception is computed and compared to the actual proprioceptive signal. If it matches, a cancellation signal is generated and sent to the vestibular nuclei. The exact location of the cancellation signal generation remains to be determined. Such a region should receive proprioceptive signals, efferent copies of the motor commands or an estimate of the expected sensory consequences of actions, and vestibular signals. For these reasons Cullen et al. (2011) proposed that the cerebellar rostral fastigial nucleus would be a good candidate. Indeed it does receive inputs from the cerebellar cortex—whose function is thought to be (among others) the generation of sensory prediction—neck proprioception from the central cervical nucleus and the external cuneate nucleus and vestibular inputs from the vestibular nucleus (Voogd et al., 1996). Additionally, recordings in fastigial nucleus (Brooks and Cullen, 2009) strongly suggested that the integration of proprioceptive and vestibular information takes place in the rostral fastigial nuclei during passive movement. Whether this integration occurs during active movement and is used to generate a cancellation signal remains to be demonstrated.

Thus, the cerebellum is likely to act in a heterogeneous manner, involving several subregions in the cerebellar cortex and deep nuclei for the transformation of the reference frame adapted to navigation in space and for the cancellation of self-generated vestibular signals, enabling a focus on pertinent external stimulation for optimal path. The information, adequately transformed, is subsequently conveyed to the hippocampus (**Figure 3**).

The exact network and plasticities involved in this computation during navigation remains to be elucidated. Deficits observed in the L7-PKCI mice suggest that cerebellar PF–PCs LTD is involved in such computation and plays an important role in self-motion based hippocampal space representation.

ANATOMICAL AND FUNCTIONAL RELATION BETWEEN CEREBELLUM AND FOREBRAIN NAVIGATION AREAS

Demonstration that the cerebellum assists navigation at least in part by participating in the building of the hippocampal spatial map (Rochefort et al., 2011) implies that these structures are interconnected. Therefore, the cerebellum communicates either directly with the hippocampal system or with the forebrain navigation areas connected to it. Interestingly, a functional interaction between the hippocampus and the cerebellum has recently been supported by two studies conducted in rabbits using the hippocampal-dependent *trace* version of the eyeblink conditioning task (Hoffmann and Berry, 2009; Wikgren et al., 2010). Both investigations clearly demonstrate that during trace eyeblink conditioning, theta oscillation (3–7 Hz) occurs in the lobule HVI and the interpositus nucleus of the cerebellum and is synchronized with hippocampal theta oscillation. The cerebellar theta oscillations appeared to depend on the hippocampal theta rhythm. These data demonstrate that the hippocampus and the hemispheric lobule HVI of the cerebellum, which is involved in the stimulus-response association of the trace eyeblink conditioning, can synchronize their activity during specific cognitive demands. Whilst the data from Hoffmann and Berry (2009) suggest that this coordination enhances the associative learning abilities, Wikgren et al. (2010) did not observe a link between hippocampo-cerebellar synchronization and learning performances. Regardless, the latter investigations invite speculation on the possibility of multiple synchronization areas between the hippocampus and the cerebellum, which may be required for spatial navigation.

One important question raised by these findings is the anatomical circuitry underlying such functional interaction. Some evidence suggests a direct anatomical link between the hippocampus and the cerebellum. In cat and monkey, fastigial nucleus stimulation consistently evoked responses bilaterally in the rostro-caudal region of the hippocampus at delays indicating a monosynaptic connection (Heath and Harper, 1974; Snider and Maiti, 1976; Heath et al., 1978; Newman and Reza, 1979). Heath and Harper (1974) also found degenerated fibers in the hippocampus following lesion of the fastigial nucleus, meaning that these fibers could directly originate from the deep cerebellar nucleus. Hippocampal responses following posterior vermis stimulation were also reported (Heath et al., 1978; Newman and Reza, 1979) but not after stimulation of other cerebellar subregions. However, these observations have not, so far, been confirmed by anatomical investigations, possibly because of the potentially low number of implicated fibers.

Nevertheless, a recent study combining retrograde tracing and degeneration analysis after hippocampal lesion demonstrated a direct projection from the hippocampal formation to the cerebellum in chicken (folia VI–VIII) (Liu et al., 2012). The existence of a hippocampo-cerebellar projection does not imply a backward projection from the cerebellum to the hippocampus, which could explain the influence of cerebellar plasticity in shaping hippocampal place cell properties (Rochefort et al., 2011). However, tracing studies performed in the monkey in the last decade suggest a general organizational principle of the cerebello-cortical system where different areas of the neocortex are reciprocally connected to the cerebellum in closed loops (Clower et al., 2001; Middleton and Strick, 2001; Kelly and Strick,

2003; Prevosto et al., 2010). A direct cerebello-hippocampal projection remains to be discovered.

Alternatively, the cerebellum could interact with the hippocampus through multi-synaptic connections via the forebrain navigation circuit. Evidence from rat studies suggests that this interaction may take place via multiple pathways. The cerebellum reaches the forebrain mainly through the projection from the deep cerebellar nuclei toward the thalamus. Interestingly, substantial cerebellar inputs are found in the central-lateral thalamic nucleus (Haroian et al., 1981; Angaut et al., 1985; Aumann et al., 1994). The central lateral nucleus projects to both the posterior parietal and the retrosplenial cortices (Van der Werf et al., 2002), two cortical areas particularly involved in spatial navigation.

The posterior parietal cortex (PPC) is a multi-modal cortical area integrating self-motion and visuo-spatial information (Snyder et al., 1998; Save and Poucet, 2009). Its role in spatial navigation has been recently enlightened by the discovery of rat PPC cells the activity of which is tuned to self-motion and acceleration irrespective to the animal location or heading (Whitlock et al., 2012). The presence of cells encoding movement in an egocentric reference frame thus makes the PCC a primary candidate for the reception of cerebellar information and its transmission to other navigation areas. Such hypothesis is further supported by the close interaction between PPC and cerebellar lobule VIIa and Crus I and II showed in a human resting state functional connectivity study (O'Reilly et al., 2010). Moreover, combining anterograde and retrograde tracing, studies in both rat and primate confirmed that the PPC receives cerebellar input from the interposed and lateral nuclei via a thalamic relay in the central-lateral and ventro-lateral nuclei (Amino et al., 2001; Clower et al., 2001; Giannetti and Molinari, 2002; Prevosto et al., 2010). The existence of reciprocal connections from the parietal cortex to the cerebellum has not been documented so far in the rodent but cerebello-parietal interaction could follow the closed-loop architecture of cerebro-cerebellar interactions. Moreover in monkey, the homologous area to the rat PPC (the area 7) has indeed been shown to project to the cerebellar hemispheres via the pontine nucleus (Glickstein et al., 1985; Dum et al., 2002). Such projection could contribute substantially to multisensory integration (Glickstein, 2003).

The retrosplenial cortex is also thought to be involved in the allocentric-to-egocentric transformation process (Vann et al., 2009). Indeed, retrosplenial inactivation has been shown to impair allocentric navigation and path integration as well as field location of hippocampal place cells (Cooper et al., 2001; Cooper and Mizumori, 2001; Whishaw et al., 2001). This cortical area also contains head direction cells which are found in a network of structures (Taube, 2007) and were recently shown to underlie a rodent's sense of direction during path integration (Valerio and Taube, 2012). Head direction signal is prominently dependent on vestibular information (Stackman et al., 2002) and is believed to be generated subcortically and then processed by higher structures such as the retrospenial cortex (Taube, 2007).

Therefore, the cerebellum may contribute to two major circuits crucial for the representation of space in the hippocampal system (**Figure 5**): one comprising the retrospenial cortex more closely associated to the vestibulo-cerebellum, and the other involving the PPC receiving inputs from deep cerebellar nuclei and possibly involved in planning and execution of navigation behavior. Nevertheless the precise anatomical pathways between cerebellum and hippocampus activated during spatial navigation remain to be elucidated.

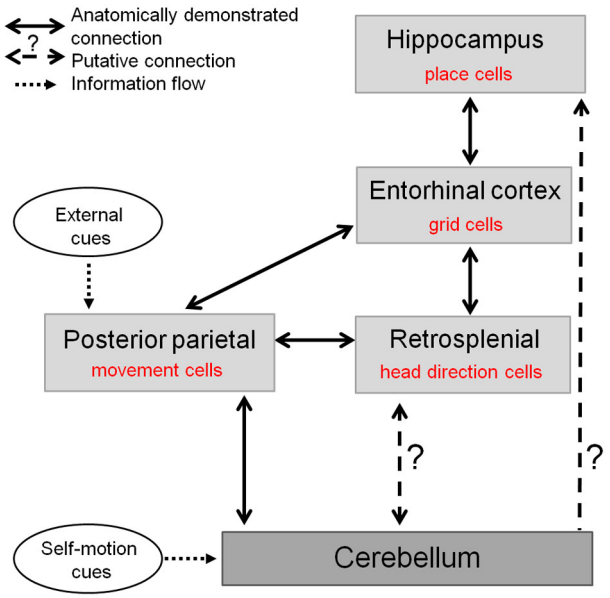

FIGURE 5 | The cerebellum in the anatomo-functional circuit underlying spatial navigation. Navigation system comprises a whole network of structures: (1) the hippocampus containing ≪place cells≫, which correlate with animal's location in space and underlie animal's spatial representation (O'Keefe and Dostrovsky, 1971), (2) the medial enthorinal cortex, containing ≪grid cells≫ which fire according to a grid-like pattern and are thought to constitute the metric system of the brain (Hafting et al., 2005), (3) a network of structures—among which the retrospenial cortex—containing ≪head direction cells≫, specific for a given direction of the head in space (Taube et al., 1990), and (4) posterior parietal cortex containing ≪movement cells≫, encoding self-motion and acceleration (Whitlock et al., 2012). The cerebellum takes part in this navigation system as it shapes hippocampal place cells properties (Rochefort et al., 2011). This contribution could occur either through a direct projection to the hippocampus or via a multi-synaptic connection involving a thalamic relay, to the posterior parietal cortex or the retrosplenial cortex.

CONCLUDING REMARKS

Recent converging evidence demonstrates the importance of the cerebellum in spatial navigation. Such implication in the navigation system at the hippocampal level or in forebrain navigation areas has been elucidated using electrophysiological, anatomical, and behavioral analyses in both human and animal models. Although the cerebellar network does not encode a spatial map of the environment, it does participate in map formation in the forebrain navigation areas by specifically encoding and computing self-motion information from different sources required to build the representation of the body in space. PF–PC LTD is implicated in this process, and other as yet to be determined modes of cerebellar plasticity may participate as well. The recent development of tetrodes multi-unit recordings in rat's cerebellum (de Solages et al., 2008; Gao et al., 2012b) opens new perspectives

to unravel the cerebellar computation occurring during goal-directed navigation. In order to unravel the precise contributions of the cerebellum to the processing of information during navigation, such technique will have to be combined with the use of mutant animals bearing specific cerebellar plasticity deficits.

ACKNOWLEDGMENTS

This is supported by the Fondation pour la Recherche Médicale DEQ20120323730, France, and National Agency for Research ANR-REG-071220-01-01, France. We are grateful to Glenn Dallérac and Pauline Obiang for helpful comments on the manuscript.

REFERENCES

Aiba, A., Kano, M., Chen, C., Stanton, M. E., Fox, G. D., Herrup, K., et al. (1994). Deficient cerebellar long-term depression and impaired motor learning in mGluR1 mutant mice. *Cell* 79, 377–388.

Albus, J. S. (1971). A theory of cerebellar function. *Math. Biosci.* 10, 25–61.

Amino, Y., Kyuhou, S., Matsuzaki, R., and Gemba, H. (2001). Cerebello-thalamo-cortical projections to the posterior parietal cortex in the macaque monkey. *Neurosci. Lett.* 309, 29–32.

Angaut, P., Cicirata, F., and Serapide, F. (1985). Topographic organization of the cerebellothalamic projections in the rat. An autoradiographic study. *Neuroscience* 15, 389–401.

Angelaki, D. E., Yakusheva, T. A., Green, A. M., Dickman, J. D., and Blazquez, P. M. (2010). Computation of egomotion in the macaque cerebellar vermis. *Cerebellum* 9, 174–182.

Artola, A., Brocher, S., and Singer, W. (1990). Different voltage-dependent thresholds for inducing long-term depression and long-term potentiation in slices of rat visual cortex. *Nature* 347, 69–72.

Aumann, T. D., Rawson, J. A., Finkelstein, D. I., and Horne, M. K. (1994). Projections from the lateral and interposed cerebellar nuclei to the thalamus of the rat: a light and electron microscopic study using single and double anterograde labelling. *J. Comp. Neurol.* 349, 165–181.

Baumann, O., and Mattingley, J. B. (2012). Functional topography of primary emotion processing in the human cerebellum. *Neuroimage* 61, 805–811.

Boyden, E. S., Katoh, A., and Raymond, J. L. (2004). Cerebellum-dependent learning: the role of multiple plasticity mechanisms. *Annu. Rev. Neurosci.* 27, 581–609.

Brindley, G. (1964). The use made by the cerebellum of the information that it receives from sense organs. *IBRO Bull.* 3:80.

Brooks, J. X., and Cullen, K. E. (2009). Multimodal integration in rostral fastigial nucleus provides an estimate of body movement. *J. Neurosci.* 29, 10499–10511.

Burguiere, E., Arabo, A., Jarlier, F., De Zeeuw, C. I., and Rondi-Reig, L. (2010). Role of the cerebellar cortex in conditioned goal-directed behavior. *J. Neurosci.* 30, 13265–13271.

Burguiere, E., Arleo, A., Hojjati, M., Elgersma, Y., De Zeeuw, C. I., Berthoz, A., et al. (2005). Spatial navigation impairment in mice lacking cerebellar LTD: a motor adaptation deficit? *Nat. Neurosci.* 8, 1292–1294.

Calhoun, V. D., Pekar, J. J., McGinty, V. B., Adali, T., Watson, T. D., and Pearlson, G. D. (2002). Different activation dynamics in multiple neural systems during simulated driving. *Hum. Brain Mapp.* 16, 158–167.

Clark, G. A., McCormick, D. A., Lavond, D. G., and Thompson, R. F. (1984). Effects of lesions of cerebellar nuclei on conditioned behavioral and hippocampal neuronal responses. *Brain Res.* 291, 125–136.

Clower, D. M., West, R. A., Lynch, J. C., and Strick, P. L. (2001). The inferior parietal lobule is the target of output from the superior colliculus, hippocampus, and cerebellum. *J. Neurosci.* 21, 6283–6291.

Cooper, B. G., Manka, T. F., and Mizumori, S. J. (2001). Finding your way in the dark: the retrosplenial cortex contributes to spatial memory and navigation without visual cues. *Behav. Neurosci.* 115, 1012–1028.

Cooper, B. G., and Mizumori, S. J. (2001). Temporary inactivation of the retrosplenial cortex causes a transient reorganization of spatial coding in the hippocampus. *J. Neurosci.* 21, 3986–4001.

Colombel, C., Lalonde, R., and Caston, J. (2004). The effects of unilateral removal of the cerebellar hemispheres on spatial learning and memory in rats. *Brain Res.* 1004, 108–115.

Cullen, K. E., Brooks, J. X., Jamali, M., Carriot, J., and Massot, C. (2011). Internal models of self-motion: computations that suppress vestibular reafference in early vestibular processing. *Exp. Brain Res.* 210, 377–388.

Damasio, A. R., Grabowski, T. J., Bechara, A., Damasio, H., Ponto, L. L., Parvizi, J., et al. (2000). Subcortical and cortical brain activity during the feeling of self-generated emotions. *Nat. Neurosci.* 3, 1049–1056.

de Solages, C., Szapiro, G., Brunel, N., Hakim, V., Isope, P., Buisseret, P., et al. (2008). High-frequency organization and synchrony of activity in the purkinje cell layer of the cerebellum. *Neuron* 58, 775–788.

De Zeeuw, C. I., Hansel, C., Bian, F., Koekkoek, S. K., van Alphen, A. M., Linden, D. J., et al. (1998). Expression of a protein kinase C inhibitor in Purkinje cells blocks cerebellar LTD and adaptation of the vestibulo-ocular reflex. *Neuron* 20, 495–508.

Dum, R. P., Li, C., and Strick, P. L. (2002). Motor and nonmotor domains in the monkey dentate. *Ann. N.Y. Acad. Sci.* 978, 289–301.

Eccles, J. (1965). Functional meaning of the patterns of synaptic connections in the cerebellum. *Perspect. Biol. Med.* 8, 289–310.

Eccles, J. C. (1967). Circuits in the cerebellar control of movement. *Proc. Natl. Acad. Sci. U.S.A.* 58, 336–343.

Frank, B., Maschke, M., Groetschel, H., Berner, M., Schoch, B., Hein-Kropp, C., et al. (2010). Aphasia and neglect are uncommon in cerebellar disease: negative findings in a prospective study in acute cerebellar stroke. *Cerebellum* 9, 556–566.

Frank, B., Schoch, B., Hein-Kropp, C., Hovel, M., Gizewski, E. R., Karnath, H. O., et al. (2008). Aphasia, neglect and extinction are no prominent clinical signs in children and adolescents with acute surgical cerebellar lesions. *Exp. Brain Res.* 184, 511–519.

Frank, B., Schoch, B., Richter, S., Frings, M., Karnath, H. O., and Timmann, D. (2007). Cerebellar lesion studies of cognitive function in children and adolescents - limitations and negative findings. *Cerebellum* 6, 242–253.

Gandhi, C. C., Kelly, R. M., Wiley, R. G., and Walsh, T. J. (2000). Impaired acquisition of a Morris water maze task following selective destruction of cerebellar purkinje cells with OX7-saporin. *Behav. Brain Res.* 109, 37–47.

Gao, Z., van Beugen, B. J., and De Zeeuw, C. I. (2012a). Distributed synergistic plasticity and cerebellar learning. *Nat. Rev. Neurosci.* 13, 619–635.

Gao, H., Solages, Cd., and Lena, C. (2012b). Tetrode recordings in the cerebellar cortex. *J. Physiol. Paris* 106, 128–136.

Giannetti, S., and Molinari, M. (2002). Cerebellar input to the posterior parietal cortex in the rat. *Brain Res. Bull.* 58, 481–489.

Glickstein, M. (2003). Subcortical projections of the parietal lobes. *Adv. Neurol.* 93, 43–55.

Glickstein, M. (2007). What does the cerebellum really do? *Curr. Biol.* 17, R824–R827.

Glickstein, M., May, J. G. 3rd., and Mercier, B. E. (1985). Corticopontine projection in the macaque: the distribution of labelled cortical cells after large injections of horseradish peroxidase in the pontine nuclei. *J. Comp. Neurol.* 235, 343–359.

Goodlett, C. R., Hamre, K. M., and West, J. R. (1992). Dissociation of spatial navigation and visual guidance performance in Purkinje cell degeneration (pcd) mutant mice. *Behav. Brain Res.* 47, 129–141.

Goodworth, A. D., Paquette, C., Jones, G. M., Block, E. W., Fletcher, W. A., Hu, B., et al. (2012). Linear and angular control of circular walking in healthy older adults and subjects with cerebellar ataxia. *Exp. Brain Res.* 219, 151–161.

Hafting, T., Fyhn, M., Molden, S., Moser, M. B., and Moser, E. I. (2005). Microstructure of a spatial map in the entorhinal cortex. *Nature* 436, 801–806.

Hansel, C., de Jeu, M., Belmeguenai, A., Houtman, S. H., Buitendijk, G. H., Andreev, D., et al. (2006). alpha-CaMKII Is essential for cerebellar LTD and motor learning. *Neuron* 51, 835–843.

Haroian, A. J., Massopust, L. C., and Young, P. A. (1981). Cerebellothalamic projections in the rat: an autoradiographic and

degeneration study. *J. Comp. Neurol.* 197, 217–236.

Heath, R. G., Dempesy, C. W., Fontana, C. J., and Myers, W. A. (1978). Cerebellar stimulation: effects on septal region, hippocampus, and amygdala of cats and rats. *Biol. Psychiatry* 13, 501–529.

Heath, R. G., and Harper, J. W. (1974). Ascending projections of the cerebellar fastigial nucleus to the hippocampus, amygdala, and other temporal lobe sites: evoked potential and histological studies in monkeys and cats. *Exp. Neurol.* 45, 268–287.

Hoffmann, L. C., and Berry, S. D. (2009). Cerebellar theta oscillations are synchronized during hippocampal theta-contingent trace conditioning. *Proc. Natl. Acad. Sci. U.S.A.* 106, 21371–21376.

Horikawa, E., Okamura, N., Tashiro, M., Sakurada, Y., Maruyama, M., Arai, H., et al. (2005). The neural correlates of driving performance identified using positron emission tomography. *Brain Cogn.* 58, 166–171.

Ino, T., Inoue, Y., Kage, M., Hirose, S., Kimura, T., and Fukuyama, H. (2002). Mental navigation in humans is processed in the anterior bank of the parieto-occipital sulcus. *Neurosci. Lett.* 322, 182–186.

Ito, M. (1989). Long-term depression. *Annu. Rev. Neurosci.* 12, 85–102.

Ito, M., and Kano, M. (1982). Long-lasting depression of parallel fiber-Purkinje cell transmission induced by conjunctive stimulation of parallel fibers and climbing fibers in the cerebellar cortex. *Neurosci. Lett.* 33, 253–258.

Joyal, C. C., Strazielle, C., and Lalonde, R. (2001). Effects of dentate nucleus lesions on spatial and postural sensorimotor learning in rats. *Behav. Brain Res.* 122, 131–137.

Ke, M. C., Guo, C. C., and Raymond, J. L. (2009). Elimination of climbing fiber instructive signals during motor learning. *Nat. Neurosci.* 12, 1171–1179.

Kelly, R. M., and Strick, P. L. (2003). Cerebellar loops with motor cortex and prefrontal cortex of a nonhuman primate. *J. Neurosci.* 23, 8432–8444.

Kleine, J. F., Guan, Y., Kipiani, E., Glonti, L., Hoshi, M., and Buttner, U. (2004). Trunk position influences vestibular responses of fastigial nucleus neurons in the alert monkey. *J. Neurophysiol.* 91, 2090–2100.

Koekkoek, S. K., Hulscher, H. C., Dortland, B. R., Hensbroek, R. A., Elgersma, Y., Ruigrok, T. J., et al. (2003). Cerebellar LTD and learning-dependent timing of conditioned eyelid responses. *Science* 301, 1736–1739.

Lalonde, R., and Strazielle, C. (2003). The effects of cerebellar damage on maze learning in animals. *Cerebellum* 2, 300–309.

Lashley, K. S., and McCarthy, D. (1926). The survival of the maze habit after cerebellar injuries. *J. Comp. Physiol. Psychol.* 6, 423–433.

Levisohn, L., Cronin-Golomb, A., and Schmahmann, J. D. (2000). Neuropsychological consequences of cerebellar tumour resection in children: cerebellar cognitive affective syndrome in a paediatric population. *Brain* 123(Pt 5), 1041–1050.

Liu, W., Zhang, Y., Yuan, W., Wang, J., and Li, S. (2012). A direct hippocampo-cerebellar projection in chicken. *Anat. Rec. (Hoboken)* 295, 1311–1320.

Maguire, E. A., Burgess, N., Donnett, J. G., Frackowiak, R. S., Frith, C. D., and O'Keefe, J. (1998). Knowing where and getting there: a human navigation network. *Science* 280, 921–924.

Malm, J., Kristensen, B., Karlsson, T., Carlberg, B., Fagerlund, M., and Olsson, T. (1998). Cognitive impairment in young adults with infratentorial infarcts. *Neurology* 51, 433–440.

Manzoni, D., Pompeiano, O., Bruschini, L., and Andre, P. (1999). Neck input modifies the reference frame for coding labyrinthine signals in the cerebellar vermis: a cellular analysis. *Neuroscience* 93, 1095–1107.

Marr, D. (1969). A theory of cerebellar cortex. *J. Physiol. (London)* 202, 437–470.1.

McCormick, D. A., and Thompson, R. F. (1984a). Cerebellum: essential involvement in the classically conditioned eyelid response. *Science* 223, 296–299.

McCormick, D. A., and Thompson, R. F. (1984b). Neuronal responses of the rabbit cerebellum during acquisition and performance of a classically conditioned nictitating membrane-eyelid response. *J. Neurosci.* 4, 2811–2822.

McCrea, R. A., Gdowski, G. T., Boyle, R., and Belton, T. (1999). Firing behavior of vestibular neurons during active and passive head movements: vestibulo-spinal and other non-eye-movement related neurons. *J. Neurophysiol.* 82, 416–428.

Middleton, F. A., and Strick, P. L. (2001). Cerebellar projections to the prefrontal cortex of the primate. *J. Neurosci.* 21, 700–712.

Moffat, S. D., Elkins, W., and Resnick, S. M. (2006). Age differences in the neural systems supporting human allocentric spatial navigation. *Neurobiol. Aging* 27, 965–972.

Molinari, M., and Leggio, M. G. (2007). Cerebellar information processing and visuospatial functions. *Cerebellum* 6, 214–220.

Molinari, M., Petrosini, L., Misciagna, S., and Leggio, M. G. (2004). Visuospatial abilities in cerebellar disorders. *J. Neurol. Neurosurg. Psychiatry* 75, 235–240.

Mullen, R. J., Eicher, E. M., and Sidman, R. L. (1976). Purkinje cell degeneration, a new neurological mutation in the mouse. *Proc. Natl. Acad. Sci. U.S.A.* 73, 208–212.

Newman, P. P., and Reza, H. (1979). Functional relationships between the hippocampus and the cerebellum: an electrophysiological study of the cat. *J. Physiol.* 287, 405–426.

O'Keefe, J., and Dostrovsky, J. (1971). The hippocampus as a spatial map. Preliminary evidence from unit activity in the freely-moving rat. *Brain Res.* 34, 171–175.

O'Reilly, J. X., Beckmann, C. F., Tomassini, V., Ramnani, N., and Johansen-Berg, H. (2010). Distinct and overlapping functional zones in the cerebellum defined by resting state functional connectivity. *Cereb. Cortex* 20, 953–965.

Paquette, C., Franzen, E., Jones, G. M., and Horak, F. B. (2011). Walking in circles: navigation deficits from Parkinson's disease but not from cerebellar ataxia. *Neuroscience* 190, 177–183.

Petrosini, L., Leggio, M. G., and Molinari, M. (1998). The cerebellum in the spatial problem solving: a co-star or a guest star? *Prog. Neurobiol.* 56, 191–210.

Petrosini, L., Molinari, M., and Dell'Anna, M. E. (1996). Cerebellar contribution to spatial event processing: Morris water maze and T-maze. *Eur. J. Neurosci.* 8, 1882–1896.

Prevosto, V., Graf, W., and Ugolini, G. (2010). Cerebellar inputs to intraparietal cortex areas LIP and MIP: functional frameworks for adaptive control of eye movements, reaching, and arm/eye/head movement coordination. *Cereb. Cortex* 20, 214–228.

Ramnani, N. (2012). Frontal lobe and posterior parietal contributions to the cortico-cerebellar system. *Cerebellum* 11, 366–383.

Riva, D., and Giorgi, C. (2000). The cerebellum contributes to higher functions during development: evidence from a series of children surgically treated for posterior fossa tumours. *Brain* 123(Pt 5), 1051–1061.

Rochefort, C., Arabo, A., André, M., Poucet, B., Save, E., and Rondi-Reig, L. (2011). Cerebellum shapes hippocampal spatial code. *Science* 334, 385–389.

Rondi-Reig, L., and Burguiere, E. (2005). Is the cerebellum ready for navigation? *Prog. Brain Res.* 148, 199–212.

Rondi-Reig, L., Le Marec, N., Caston, J., and Mariani, J. (2002). The role of climbing and parallel fibers inputs to cerebellar cortex in navigation. *Behav. Brain Res.* 132, 11–18.

Roy, J. E., and Cullen, K. E. (2001). Selective processing of vestibular reafference during self-generated head motion. *J. Neurosci.* 21, 2131–2142.

Roy, J. E., and Cullen, K. E. (2003). Brain stem pursuit pathways: dissociating visual, vestibular, and proprioceptive inputs during combined eye-head gaze tracking. *J. Neurophysiol.* 90, 271–290.

Roy, J. E., and Cullen, K. E. (2004). Dissociating self-generated from passively applied head motion: neural mechanisms in the vestibular nuclei. *J. Neurosci.* 24, 2102–2111.

Sacchetti, B., Scelfo, B., and Strata, P. (2009). Cerebellum and emotional behavior. *Neuroscience* 162, 756–762.

Sacchetti, B., Scelfo, B., Tempia, F., and Strata, P. (2004). Long-term synaptic changes induced in the cerebellar cortex by fear conditioning. *Neuron* 42, 973–982.

Save, E., and Poucet, B. (2009). Role of the parietal cortex in long-term representation of spatial information in the rat. *Neurobiol. Learn. Mem.* 91, 172–178.

Schmahmann, J. D. (1991). An emerging concept. The cerebellar contribution to higher function. *Arch. Neurol.* 48, 1178–1187.

Schmahmann, J. D., and Sherman, J. C. (1998). The cerebellar cognitive affective syndrome. *Brain* 121(Pt 4), 561–579.

Schonewille, M., Belmeguenai, A., Koekkoek, S. K., Houtman, S. H., Boele, H. J., van Beugen, B. J., et al. (2010). Purkinje cell-specific knockout of the protein phosphatase PP2B impairs potentiation and cerebellar motor learning. *Neuron* 67, 618–628.

Schonewille, M., Gao, Z., Boele, H. J., Veloz, M. F., Amerika, W. E., Simek, A. A., et al. (2011). Reevaluating the role of LTD in cerebellar motor learning. *Neuron* 70, 43–50.

Shaikh, A. G., Meng, H., and Angelaki, D. E. (2004). Multiple reference frames for motion in the primate cerebellum. *J. Neurosci.* 24, 4491–4497.

Smith, P. F., Horii, A., Russell, N., Bilkey, D. K., Zheng, Y., Liu, P., et al. (2005). The effects of vestibular lesions on hippocampal function in rats. *Prog. Neurobiol.* 75, 391–405.

Snider, R. S. (1950). Recent contributions to the anatomy and physiology of the cerebellum. *Arch. Neurol. Psychiatry* 64, 196–219.

Snider, R. S., and Maiti, A. (1976). Cerebellar contributions to the Papez circuit. *J. Neurosci. Res.* 2, 133–146.

Snyder, L. H., Grieve, K. L., Brotchie, P., and Andersen, R. A. (1998). Separate body- and world-referenced representations of visual space in parietal cortex. *Nature* 394, 887–891.

Stackman, R. W., Clark, A. S., and Taube, J. S. (2002). Hippocampal spatial representations require vestibular input. *Hippocampus* 12, 291–303.

Stackman, R. W., and Herbert, A. M. (2002). Rats with lesions of the vestibular system require a visual landmark for spatial navigation. *Behav. Brain Res.* 128, 27–40.

Stanton, P. K., and Sejnowski, T. J. (1989). Associative long-term depression in the hippocampus induced by hebbian covariance. *Nature* 339, 215–218.

Steinlin, M., Imfeld, S., Zulauf, P., Boltshauser, E., Lovblad, K. O., Ridolfi Luthy, A., et al. (2003). Neuropsychological long-term sequelae after posterior fossa tumour resection during childhood. *Brain* 126, 1998–2008.

Stoodley, C. J., and Schmahmann, J. D. (2009). Functional topography in the human cerebellum: a meta-analysis of neuroimaging studies. *Neuroimage* 44, 489–501.

Strata, P., Scelfo, B., and Sacchetti, B. (2011). Involvement of cerebellum in emotional behavior. *Physiol. Res.* 60(Suppl. 1), S39–S48.

Strick, P. L., Dum, R. P., and Fiez, J. A. (2009). Cerebellum and nonmotor function. *Annu. Rev. Neurosci.* 32, 413–434.

Taube, J. S. (2007). The head direction signal: origins and sensory-motor integration. *Annu. Rev. Neurosci.* 30, 181–207.

Taube, J. S., Muller, R. U., and Ranck, J. B. Jr. (1990). Head-direction cells recorded from the postsubiculum in freely moving rats. I. Description and quantitative analysis. *J. Neurosci.* 10, 420–435.

Timmann, D., Drepper, J., Frings, M., Maschke, M., Richter, S., Gerwig, M., et al. (2010). The human cerebellum contributes to motor, emotional and cognitive associative learning. A review. *Cortex* 46, 845–857.

Trouche, E., Beaubaton, D., Amato, G., and Grangetto, A. (1979). Impairments and recovery of the spatial and temporal components of a visuomotor pointing movement after unilateral destruction of the dentate nucleus in the baboon. *Appl. Neurophysiol.* 42, 248–254.

Uchiyama, Y., Ebe, K., Kozato, A., Okada, T., and Sadato, N. (2003). The neural substrates of driving at a safe distance: a functional MRI study. *Neurosci. Lett.* 352, 199–202.

Valerio, S., and Taube, J. S. (2012). Path integration: how the head direction signal maintains and corrects spatial orientation. *Nat. Neurosci.* 15, 1445–1453.

Van der Werf, Y. D., Witter, M. P., and Groenewegen, H. J. (2002). The intralaminar and midline nuclei of the thalamus. Anatomical and functional evidence for participation in processes of arousal and awareness. *Brain Res. Brain Res. Rev.* 39, 107–140.

Vann, S. D., Aggleton, J. P., and Maguire, E. A. (2009). What does the retrosplenial cortex do? *Nat. Rev. Neurosci.* 10, 792–802.

Voogd, J., Gerrits, N. M., and Ruigrok, T. J. (1996). Organization of the vestibulocerebellum. *Ann. N.Y. Acad. Sci.* 781, 553–579.

Wallace, D. G., Hines, D. J., Pellis, S. M., and Whishaw, I. Q. (2002). Vestibular information is required for dead reckoning in the rat. *J. Neurosci.* 22, 10009–10017.

Wallesch, C. W., and Horn, A. (1990). Long-term effects of cerebellar pathology on cognitive functions. *Brain Cogn.* 14, 19–25.

Walter, H., Vetter, S. C., Grothe, J., Wunderlich, A. P., Hahn, S., and Spitzer, M. (2001). The neural correlates of driving. *Neuroreport* 12, 1763–1767.

Welsh, J. P., Yamaguchi, H., Zeng, X. H., Kojo, M., Nakada, Y., Takagi, A., et al. (2005). Normal motor learning during pharmacological prevention of Purkinje cell long-term depression. *Proc. Natl. Acad. Sci. U.S.A.* 102, 17166–17171.

Whishaw, I. Q., Hines, D. J., and Wallace, D. G. (2001). Dead reckoning (path integration) requires the hippocampal formation: evidence from spontaneous exploration and spatial learning tasks in light (allothetic) and dark (idiothetic) tests. *Behav. Brain Res.* 127, 49–69.

Whitlock, J. R., Pfuhl, G., Dagslott, N., Moser, M. B., and Moser, E. I. (2012). Functional split between parietal and entorhinal cortices in the rat. *Neuron* 73, 789–802.

Wikgren, J., Nokia, M. S., and Penttonen, M. (2010). Hippocampo-cerebellar theta band phase synchrony in rabbits. *Neuroscience* 165, 1538–1545.

Yakusheva, T. A., Shaikh, A. G., Green, A. M., Blazquez, P. M., Dickman, J. D., and Angelaki, D. E. (2007). Purkinje cells in posterior cerebellar vermis encode motion in an inertial reference frame. *Neuron* 54, 973–985.

Zhu, L., Scelfo, B., Hartell, N. A., Strata, P., and Sacchetti, B. (2007). The effects of fear conditioning on cerebellar LTP and LTD. *Eur. J. Neurosci.* 26, 219–227.

Conflict of Interest Statement: The authors declare that the research was conducted in the absence of any commercial or financial relationships that could be construed as a potential conflict of interest.

Received: 07 October 2012; accepted: 22 February 2013; published online: 13 March 2013.

Citation: Rochefort C, Lefort JM and Rondi-Reig L (2013) The cerebellum: a new key structure in the navigation system. Front. Neural Circuits ***7****:35. doi: 10.3389/fncir.2013.00035*

GLOSSARY

Vestibular organs: Semicircular canals and otolith organs. The latter detect linear acceleration whereas the former are sensitive to angular acceleration.

Proprioception: Perception of the relative position of the different parts of one's body using information from proprioceptors (i.e., stretch receptors located in the muscles, tendons, and joints).

Efferent copy of motor command: It has been suggested that during an active movement, while the motor cortex sends a command to the periphery, a copy of the motor command is also generated and could be used to generate a prediction of the sensory consequences of the intended movement.

Optic flow: The displacement of images on the retina due to the relative motion between the observer and the scene. The displacement speed can be used to estimate one's proper acceleration.

Advantages of publishing in Frontiers

OPEN ACCESS
Articles are free to read, for greatest visibility

COLLABORATIVE PEER-REVIEW
Designed to be rigorous – yet also collaborative, fair and constructive

FAST PUBLICATION
Average 85 days from submission to publication (across all journals)

COPYRIGHT TO AUTHORS
No limit to article distribution and re-use

TRANSPARENT
Editors and reviewers acknowledged by name on published articles

SUPPORT
By our Swiss-based editorial team

IMPACT METRICS
Advanced metrics track your article's impact

GLOBAL SPREAD
5'100'000+ monthly article views and downloads

LOOP RESEARCH NETWORK
Our network increases readership for your article

Frontiers
EPFL Innovation Park, Building I • 1015 Lausanne • Switzerland
Tel +41 21 510 17 00 • Fax +41 21 510 17 01 • info@frontiersin.org
www.frontiersin.org

Find us on